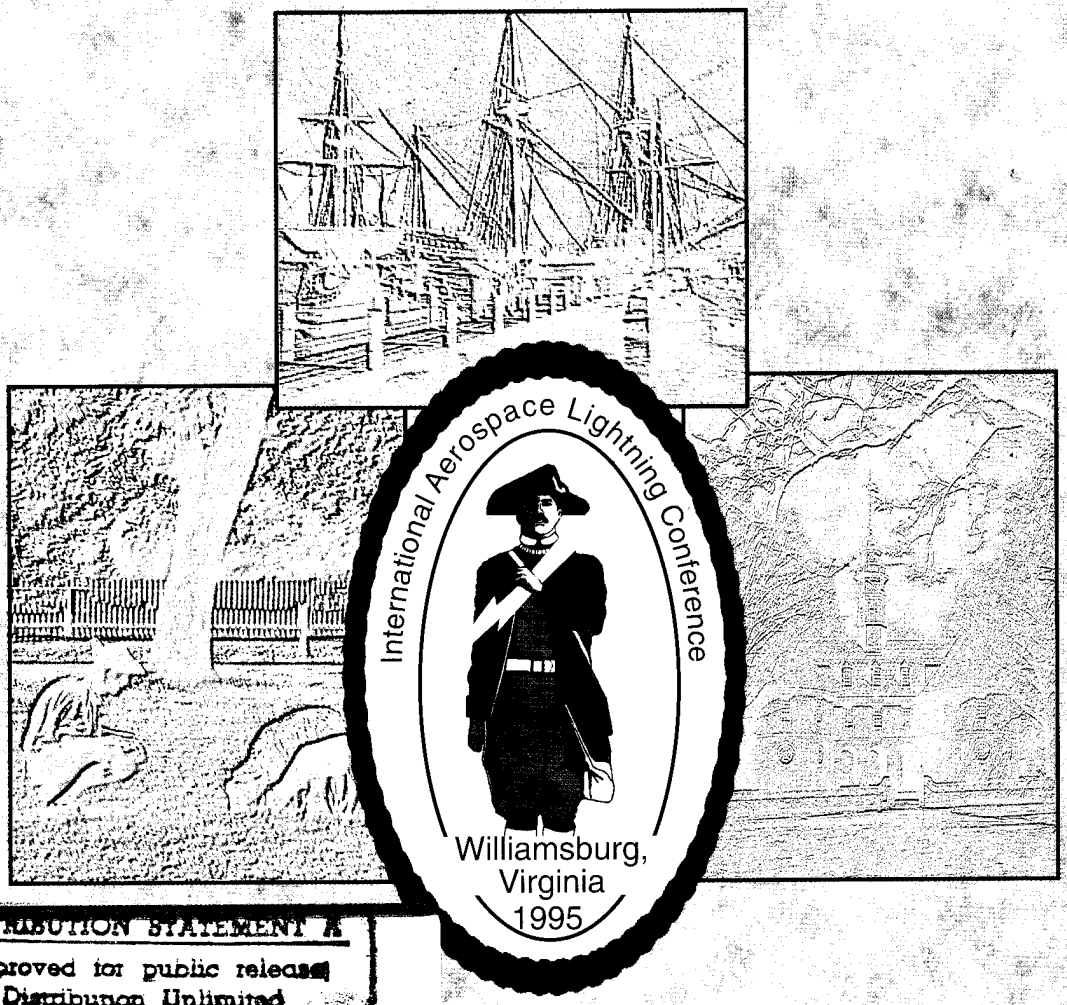
# International Aerospace and Ground Conference on Lightning and Static Electricity



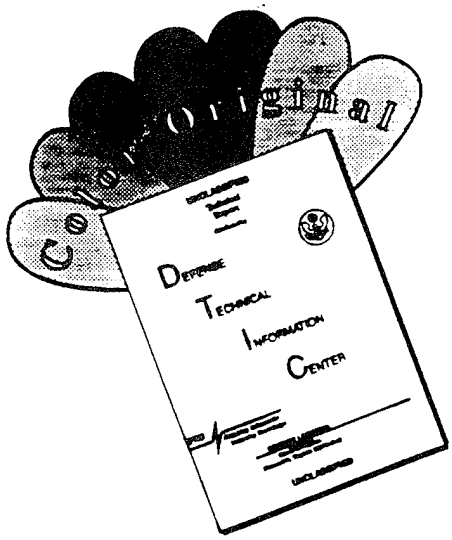

DISTRIBUTION STATEMENT A
Approved for public release
Distribution Unlimited

# BOOK OF PROCEEDINGS

Williamsburg, Virginia
September 26-28, 1995

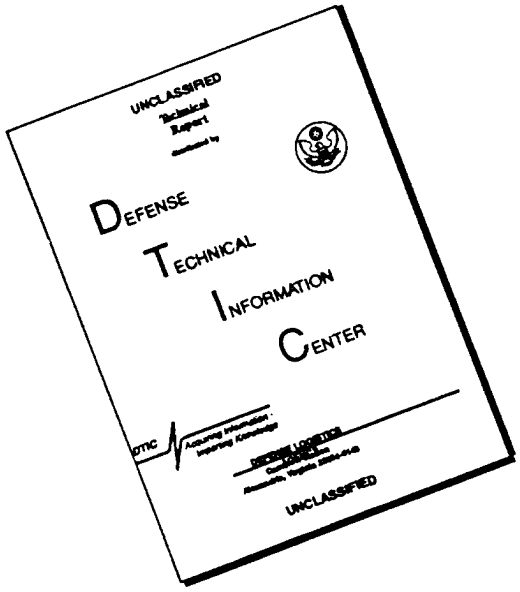
19960416 005

# DISCLAIMER NOTICE




THIS DOCUMENT IS BEST QUALITY AVAILABLE. THE COPY FURNISHED TO DTIC CONTAINED A SIGNIFICANT NUMBER OF COLOR PAGES WHICH DO NOT REPRODUCE LEGIBLY ON BLACK AND WHITE MICROFICHE.

# DISCLAIMER NOTICE




THIS DOCUMENT IS BEST QUALITY AVAILABLE. THE COPY FURNISHED TO DTIC CONTAINED A SIGNIFICANT NUMBER OF PAGES WHICH DO NOT REPRODUCE LEGIBLY.

NAWCADPAX--95-306-PRO

*Proceedings of the*

# 1995 International Aerospace and Ground Conference on Lightning and Static Electricity

September 26-28, 1995
Williamsburg
Virginia, USA



U.S. Navy
Naval Air Warfare Center Aircraft Division
Patuxent River, Maryland




DTIC QUALITY INSPECTED 1

# 1995 International Aerospace and Ground Conference on Lightning and Static Electricity 26-28 September 1995 - Williamsburg, Virginia, USA

## *TECHNICAL SPONSORSHIP*

National Interagency Coordination Group (NICG)

## *HOST ORGANIZATION*

Department of the Navy
Naval Air Systems Command
Naval Air Systems Command Headquarters
1421 Jefferson Davis Highway
Arlington, Virginia 22243

## *IN COOPERATION WITH*

Department of the Air Force
Department of the Army
Federal Aviation Administration
National Aeronautics and Space Administration
National Oceanic and Atmospheric Administration

## *IN ASSOCIATION WITH*

Florida Institute of Technology

## *1995 CONFERENCE CHAIRMAN*

Anthony J. Iacono
Naval Air Systems Command (AIR-4.1.7)
Naval Air Systems Command Headquarters
1421 Jefferson Davis Highway
Arlington, Virginia 22243
Phone (703) 604-6060
Fax (703) 604-2054

## *STEERING COMMITTEE*

Samuel Frazier
Michael Squires
Mike Whitaker
Dr. Andrew Revay, Jr.
Michael S. Glynn
David Albright
Donald MacGorman
John Madura
Lawrence C. Walko

## *TECHNICAL PUBLISHING TEAM*

Karen Brown
Sandy Biehler
Tara Gardner

## CHAIRMAN'S MESSAGE



I could not help but think how appropriate it is for this prestigious group to be brought together at this site for a Lightning and Static Electricity Conference. For it was in this town in 1756 that an American scientist named Benjamin Franklin was conferred an Honorary Degree from the College of William and Mary. During his long and useful life (1706-1790), Franklin concerned himself with many different matters: statesmanship and soap making, book printing and cabbage growing, and the rise of the tides and the fall of empires. All of which can be learned about here. He invented an efficient heating stove and what's more important, he proved lightning is electricity. We have all heard of his kite experiment and his later invention of the lightning rod. In fact, on Wednesday afternoon, I see there's a paper entitled "The Grounded Franklin Lightning Rod."

In this day and age, the subjects of lightning and static electricity have special significance. Over the ages, we have proven that lightning is not a weapon of the gods, but a flash of light in the sky caused by an electrical current. Today, we are blessed with advances in technology and instrumentation and have busied ourselves with every aspect of the phenomena. We have probed and measured lightning as it occurs and have photographed, measured, and recorded the voltages of a single strike. With this knowledge, we have been able to predict the effects lightning and static electricity will have on our daily life and take precautions to protect ourselves from the danger that electricity in this form presents.

Astronauts in space have observed the lightning flashes as a universal occurrence. From a global perspective, we are in this together. Conferences such as these aid our cause: to get a firmer grip on lightning phenomenology to meet our personal and national need.

Specifically, in Naval aviation, lightning and static electricity hold special significance. From the direct lightning strike to the aircraft or to the evidence of St. Elmo's fire as it dances on the wingtips or windscreen. We have a dual role: to prevent damage to hardware - aircraft and weapons systems - so we can perform the mission and to protect the aircrew from harm. In this regard, our statistics are pretty good. Yet, with the changes in aircraft designs to allow them to fly greater distances, carry additional ordnance, and to loiter in an area longer, we are faced with new problems. How conductive are the new lighter weight composite materials being used in newer aircraft designs? Is our bonding/grounding criteria adequate? What about our use of filter pin connectors to protect our systems? Questions such as these have to be answered, and I look to gatherings such as these to resolve some of these issues.

Lightning aside, we sometimes downgrade the effects that static electricity has on our air operations.

We have shocked personnel who unknowingly have reached to grasp helicopter hoists, hooks, safety collars, or cargo pallets. We have damaged micro-miniature circuit components and diodes due to poor packaging and procedures.

Aside from Naval aviation, all professions have a need to know more about the subject being discussed here this week. It affects us all!

The subject is a matter of political, economic, and social importance.

Politically - It is a matter that must be dealt with locally or on the international scene. Militarily, we must be able to operate in all types of conditions. Lightning is one of those conditions. In business, our standards and codes must be uniform, so that international trade may prosper and products and

construction are not degraded during inclement weather. The world has been getting smaller, and with the popularity of the Internet and the super highway, it will grow smaller still. We must have a common cause in investigating the lightning phenomena and rectifying problem areas.

Economically - To quote Ben Franklin after a lightning rod protected his wooden house from ruin after a direct strike, "An ounce of prevention is worth a pound of cure." So it goes today. It was cost effective to rectify the static electricity problems experienced by Naval aviation. We instituted separate training programs aimed at reducing the threats to personnel and micro circuits. To protect personnel, a static wand was developed and troops were trained in its use. To eliminate waste and high costs to government, micro miniature repair personnel were given wristlets and conductive mats and taught about the effects of static electricity to prevent damage to sensitive components. Proper packaging was also required of manufacturers to prevent loss during shipping and handling.

Socially - To assure the quality of life that we all strive to achieve, we must get in touch with our environment. Lightning and static electricity are a part of that environment. I need not elaborate to this crowd! Look around as you tour Williamsburg. The houses all have lightning protection, even the old trees about the town - notice the lightning grounding cables high in the branches and down the thick trunks. Knowing more about this phenomena has allowed us to enjoy life to the fullest. As we engage in sports - when there's lightning present we don't swim, grasp the mast on the boat, or swing a golf club. We've learned not to - or suffer the consequences.

I have looked forward to this week for over a year. Now that I am here, I cannot wait to attend the sessions outlined in the brochure. It appears to be an all-encompassing agenda and one that has something for all.

Allow me to end my presentation with a pertinent tale about Ben Franklin:

His experiments with electricity involved some personal risk and he knocked himself unconscious at least once. Being the inquisitive type, he tried to kill a turkey with an electric shock. The experiment got out of hand and Franklin, not the turkey took the jolt. When he regained consciousness he said, "I meant to kill a turkey and instead I nearly killed a goose."

I hope you all have a great academic and entertaining week, and I hope that no one's goose gets cooked!

Thank you.

**Anthony J. Iacono**
Conference Chairman

# TABLE OF CONTENTS

## SESSION 01P
## PLENARY SESSION
## CHAIRPERSON: ANTHONY J. IACONO

Submicrosecond Fields Radiated by First Return Strokes in Cloud-to-Ground Lightning ..... 1-1
*E. Krider, J. Willett, and C. Leteinturier*

## SESSION 02A
## MEASUREMENTS/STANDARDS
## CHAIRPERSON: JOHN DAWSON

Electromagnetic Environments and Test Methods for the Assessment of Indirect Hazards Due to Lightning Strikes ..... 2-1
*R. Evans and G. Odam*

A Review of Progress on the Joint Programme on Improving the Lightning and Static Protection of Radomes ..... 3-1
*R. Baldwin, C. Hardwick, J. Plumer, and J-P. Clerc*

Comparison of Electric Current Data from the FAA Research Electromagnetic Database with the Proposed Environment Standard ..... 4-1
*R. McDowall and M. Glynn*

## SESSION 02B
## POWER/COMMUNICATION DISTRIBUTION
## CHAIRPERSON: STANISLAW GRZYBOWSKI

Visualising the Correlation Between Telecommunication Faults and Lightning Activity ..... 5-1
*A. Grace and M. Bostock-Smith*

Lightning Measurement System Using Remote Control by Telephone Line and Electric Field Observations of Lightning in Winter ..... 6-1
*A. Wada and T. Shindo*

Lightning Protection System for Telecommunication Relay Station Design and Maintenance, A Field Experience in Tropical Country ..... 7-1
*R. Zoro and Z. Nawawi*

# TABLE OF CONTENTS (Cont'd)


**SESSION 03A**
**LIGHTNING PROTECTION**
**CHAIRPERSON: CHARLES GOLDBLUM**

Cost Benefit of an ABFM at KSC ..... 8-1
*A. Barnes, Jr. and J. Willett*

A Risk Management Approach to Lightning Safety ..... 9-1
*R. Kithil, Jr.*

Lightning Threat Probability for Space Launch Operations ..... 10-1
*T. Lie and R. Briët*

A Retest Criterion for Space Launch Processing Following Lightning Storms ..... 11-1
*J. Chai and T. Chin*

**SESSION 03B**
**MEASUREMENTS**
**CHAIRPERSON: JEFF CRAVEN**

Data Acquisition for System Level Indirect Effects of Lightning ..... 12-1
*E. Parimuha, M. Whitaker, S. Frazier, B. McClure, and P. Lumsden*

JRS Magnetic Lightning Current Detector ..... 13-1
*M. Brooks*

Scaling Algorithm for C-17A Simulated Lightning Test ..... 14-1
*J. Lippert and J. Schneider*

Lightning Energy Release Remote Measurement by Means of Radar ..... 15-1
*E. Dubovoy*

**SESSION 04A**
**METEOROLOGICAL**
**CHAIRPERSON: ARNOLD A. BARNES**

A Fractal Model of the Fine Structure of Lightning Radiation ..... 16-1
*G. Vecchi, D. Labate, and F. Canavero*

Three-Dimensional Lightning Structure in a Summer Florida Thunderstorm ..... 17-1
*L. Maier*

# TABLE OF CONTENTS (Cont'd)

Influence of Channel-Base Current and Current Reflections on the Initial and Subsidiary Lightning Electromagnetic Field Peak ..... 18-1
*F. Heidler and Ch. Hopf*

**SESSION 04B**
**TEST CRITERIA AND TECHNIQUES**
**CHAIRPERSON: KEITH CROUCH**

Susceptibility of Equipments to Multiple Strike Threats ..... 19-1
*V. Dunkley, R. Spencer, and C. Hardwick*

Lightning Protection for and Qualification Testing of Modular Avionics ..... 20-1
*O. Spiller*

EMC Specifications for Modular Avionics ..... 21-1
*P. Farfal and G. Chambert*

**SESSION 05A**
**SPECIFICATIONS AND STANDARDS**
**CHAIRPERSON: BILL WALKER**

Triggered and Intercepted Lightning Arcs on Aircraft ..... 22-1
*J. Boulay*

The Rationale of Proposed NATO STANAGS Describing the Lightning Environment for Land, Sea and Air Use and Defining Lightning Assessment Procedures for Munitions and Associated Systems ..... 23-1
*G. Odam and M. Richardson*

The Physics of Zoning ..... 24-1
*R. Perala, T. Rudolph, and G. Rigden*

Aircraft Fuel System Lightning Protection Design and Qualification Test Standard .. 25-1
*K. Crouch*

**SESSION 05B**
**ELECTROSTATICS**
**CHAIRPERSON: RICHARD C. ADAMO**

USN/USA/USAF Aircraft Lightning Strike Survey ..... 26-1
*T. Harwood*

# TABLE OF CONTENTS (Cont'd)

The Use of Magnetically Coupled Power Sources to Protect Ordnance and Electronics from Lightning and Static Electricity ..... 27-1
*K. Willis*

Inception Electric Field of a Laboratory Simulated Lightning Upward Leader Emitted from a Franklin Rod ..... 28-1
*G. Berger*

Charge Deposition on Ice Crystals and Drops After Lightning ..... 29-1
*T. Verma*

**SESSION 06A**
**TEST CRITERIA & TECHNIQUES**
**CHAIRPERSON: BRIAN KUHLMAN**

Detection of Fuel System Ignition Sources Using Hydrogen Vapor ..... 30-1
*K. Crouch*

Improvement of Lightning Attachment Tests ..... 31-1
*J. Clerc and M. Cantaloube*

Techniques for Producing Unipolar MIL-STD-1757A Waveforms Using Unique Resistor Banks ..... 32-1
*J. Press and M. Lehmann*

**SESSION 06B**
**ELECTROSTATICS**
**CHAIRPERSON: MIKE WHITAKER**

The Electrostatic Hazards Under an Hovering Helicopter ..... 33-1
*M. Cantaloube and C. Davoise*

E-6A Precipitation Static Assessments ..... 34-1
*J. Haines, M. Clelland, M. Whitaker, W. DePasquale, and B. Lubosch*

Methods of Determining the Electrostatic Potential and Charging Current of a Hovering Helicopter ..... 35-1
*G. Odam and R. Evans*

# TABLE OF CONTENTS (Cont'd)

## SESSION 07A
## STRUCTURES AND MATERIALS
## CHAIRPERSON: JERRY MCCORMICK


Stress Wave Visualisation in Aluminium and CFC Plates Subject to Simulated Lightning Strikes ..... 36-1
*J. Hardwick, N. Bourne, and Y. Mebar*

Electromagnetic Joint Integrity of the V-22 ..... 37-1
*J. Kuras and N. McClam-Brown*

Electrical Bonding Resistance Variations in CFC Panels ..... 38-1
*J. Calabria and W. Walker*


## SESSION 07B
## LIGHTNING PROTECTION
## CHAIRPERSON: THEODORE L. HARWOOD


Lightning-Induced Damage Phenomenology in Carbon Fiber Composite Materials.... 39-1
*A. Douay, D. Shockey, P. Gondot, and J-P. Avenet*

Reliable Simulation of Metal Surface Penetration by Lightning Continuing Currents ..... 40-1
*W. Zischank, F. Drumm, R. Fisher, G. Schnetzer, and M. Morris*

Fundamental Principles of Ground-Based Lightning Protection Systems ..... 41-1
*R. Briët*

A New Model of Cloud-to-Ionosphere Discharge - In Terms of a Ground-Cloud-Ionosphere Capacitor Derived from EHD (Electrohydrodynamics) on the Basis of New Physical Concepts of Critical Velocity and Electric Reconnection ..... 42-1
*H. Kikuchi*


## SESSION 08A
## PERSONNEL HAZARDS
## CHAIRPERSON: RONALD L. HOLLE


Chronic Pain Syndrome in a Lightning Victim ..... 43-1
*M. Cooper*

# TABLE OF CONTENTS (Cont'd)

Psychological Sequelae of Lightning Injury ..... 44-1
*M. Primeau, G. Engelstatter, and M. Cooper*

Recent Trends in the Number of Lightning Deaths and Injuries in the United States ..... 45-1
*R. López, R. Holle, and R. Passi*

**SESSION 08B**
**ORDNANCE AND EXPLOSIVES**
**CHAIRPERSON: JACK NIAL**

Lightning Coupling to EED Lines ..... 46-1
*A. Schaffar*

A Test Facility for Determining Weapon Systems Vulnerability from the Electrostatic Discharge (ESD) Phenomenon ..... 47-1
*N. Kaloterakis, J. Dulcey, J. Nial, and T. Ammons*

Explosion Proofing the "Explosion Proof" Vacuum Cleaner ..... 48-1
*R. Jones, K. Chen, and S. Holmes*

**SESSION 09A**
**MEASUREMENTS**
**CHAIRPERSON: VLADISLAV MAZUR**

Measured Environments Within 20 Meters of the Strike Points of Triggered Lightning ..... 49-1
*R. Fisher, G. Schnetzer, and M. Morris*

Statistics of Lightning Strikes to the CN Tower Observed During 1978-1994 ..... 50-1
*W. Janischewskyj, A. Hussein. J-X. Li, I. Rusan, and J-S. Chang*

Review of 15 Years LEMP Measuring Activities in the South of Germany ..... 51-1
*F. Heidler and C. Hopf*

Synchronized Multipoint Measurements of Lightning Electric Field Changes ..... 52-1
*T. Ushio, D. Wang, Z-I. Kawasaki, and K. Matuura*

# TABLE OF CONTENTS (Cont'd)

## SESSION 09B
## LIGHTNING PROTECTION
## CHAIRPERSON: EDWARD F. ROBERTS, JR.


Lightning Protection of RF-Systems ..... 53-1
*K. Borgeest, J. ter Haseborg, and F. Wolf*

Lightning Safety Evaluation of Launch Complexes for Personnel Safety ..... 54-1
R. Wojtasinski

Insured Property Damage Due to Lightning in Three Western US States ..... 55-1
*R. Holle, R. López, L. Arnold, and J. Endres*

Protection of a Computer Center ..... 56-1
*F. van der Hooft and P. Konings*


## SESSION 10A
## GROUND SITE LIGHTNING PROTECTION
## CHAIRPERSON: JACK R. LIPPERT


Rocket Triggered Lightning - Kennedy Space Center and Beyond ..... 57-1
*W. Jafferis*

Electromagnetic Responses of LV/SV Under the Catenary Wires Array Lightning Protection System to Near-By Lightning Strikes ..... 58-1
*J. Chai*

Probability Calculation of Direct Lightning Attachments to Structures at SLC40/41 ..... 59-1
*W. Jackson, H. Eley, J. Chai, and R. Briët*


## SESSION 10B
## LIGHTNING, GENERAL
## CHAIRPERSON: JOHN C. WILLETT


Comparison of Lightning Mapping with Operational Time-of-Arrival and Interferometric Systems ..... 60-1
*V. Mazur, E. Williams, R. Boldi, L. Maier, and D. Proctor*

The Measurement and Use of Lightning Ground Flash Density ..... 61-1
*L. Byerley III, K. Cummins, J. Tuel, D. Hagberg, Jr., and W. Bush*

# TABLE OF CONTENTS (Cont'd)

Evaluation of Lightning Performance of 115 kV Transmission Lines with Spline Ball Ionizers Based on Model Tests ..... 62-1
*S. Grzybowski*

**SESSION 11A**
**LIGHTNING PHENOMENOLOGY**
**CHAIRPERSON: WILLIAM JAFFERIS**

Fundamental Principles of Ground-Based Lightning Protection Systems ..... 63-1
*R. Briët*

Using Lasers to Trigger/Guide Lightning ..... 64-1
*A. Barnes, Jr. and M. Kozma*

Thunderstorm Localization Using MUSIC ..... 65-1
*T. Rynne, J. Robinson, K. Olszewski, C. Berthold, and L. Maier*

The Formation of Superbolts in Thunderclouds ..... 66-1
*A. Pühringer*

**SESSION 11B**
**LIGHTNING MODELING**
**CHAIRPERSON: ROD A. PERALA**

Influence of Tall Towers on the Return Stroke Current ..... 67-1
*F Heidler and T. Zundl*

Finite Difference Calculations of Lightning Effects at the Space Shuttle Launch Pad ..... 68-1
*R. Collier and G. Thomas*

MD-90 Transport Aircraft Lightning Induced Transient Level Evaluation by Time Domain Three Dimensional Finite Difference Modeling ..... 69-1
*B. Sherman, T. He, B. Nozari, and T. Rudolph*

Can a Transmission Line Model Predict the Lightning Current Pulse? ..... 70-1
*G. Vecchi and F. Canavero*

# TABLE OF CONTENTS (Cont'd)

## PROGRAM OF POSTER PRESENTATIONS


The Origin of Electric Charge ..... 71-1
*S. Alfas*

A Combined TOA/MDF Technology Upgrade of the U.S. National Lightning Detection Network ..... 72-1
*K. Cummins, E. Bardo, W. Hiscox, R. Pyle, and A. Pifer*

Test Requirements and Science of Determining the Electrostatic Discharge (ESD) Vulnerabilities of Weapons Systems ..... 73-1
*J. Dulcey and N. Kaloterakis*

Demonstration of the User-Friendly FAA Research Electromagnetic Database ..... 74-1
*D. Grush, E. Webb, and D. Evans*

Automatic Lightning Warning System for Indian Head Division, Naval Surface Warfare Center: A Case Study ..... 75-1
*C. Karabin*

The Selection of Parameter Values of Negative and Positive Lightning for Combination in the Composite Test Waveform ..... 76-1
*R. Evans and G. Odam*

Lightning Implications of Decreasing Circuit Card Trace Size and Spacing ..... 77-1
*S. Vakil*

Field Experiments on Laser Triggered Lightning ..... 78-1
*D. Wang, T. Ushio, Z-I. Kawasaki, S. Uchida, Y. Shimada, H. Yasuda, T. Yamanaka, C. Yamanaka, K. Matuura, Y. Ishikubo, and M. Adachi*

APPENDICES
A. CONFERENCE PARTICIPANTS ..... A-1
B. INDEX OF AUTHORS ..... B-1

# SESSION 01P
# PLENARY SESSION
# CHAIRPERSON: ANTHONY J. IACONO

# SUBMICROSECOND FIELDS RADIATED BY FIRST RETURN STROKES IN CLOUD-TO-GROUND LIGHTNING

E.P. Krider
Institute of Atmospheric Physics
The University of Arizona
Tucson, Arizona, USA
Telephone (520) 621-6831 FAX (520) 621-6833

J.C. Willett
Atmospheric Structure Branch, Phillips Laboratory (AFSC)
Hanscom AFB, Massachusetts, USA
Telephone (617) 377- 5954 FAX (617) 377-2984

C. Leteinturier
Institut de Physique et Chimie des Matériaux
Laboratoire des Plasmas et des Couches minces et Université de Nantes
2, rue de la Houssinière, 44072 Nantes – Cédex 03, France
Telephone (33) 4037-3963 FAX (33) 4037-3959

## ABSTRACT

Electric field, *E*, and *dE/dt* signatures have been measured during the initial onset of return strokes near Cape Canaveral, Florida. Values of the peak *dE/dt* for 63 first strokes were found to be normally distributed with a mean and standard deviation of 39 ± 11 V/m/μs, after they were range-normalized to 100 km. The full-width-at-half-maximum (FWHM) of the initial half-cycle of *dE/dt* had a mean and standard deviation of 100 ± 20 ns. The inferred peak current derivative at the source is 115 ± 32 kA/μs after correcting for the effects of propagation. The FWHM at the source is about 75 ± 15 ns.

## INTRODUCTION

Several experiments have recently shown that the electromagnetic fields that are radiated by return strokes in natural cloud-to-ground lightning contain large variations on a submicrosecond time-scale, when there is minimal distortion in the measurements due to ground wave propagation or the recording equipment (1–6). Similar submicrosecond variations have also been observed in the fields (and currents) produced by artificially initiated or triggered discharges to ground (7–15). Because submicrosecond field changes have important implications both for the physics of the discharge process and for the threat that lightning presents to a variety of complex systems (16), a new experiment was conducted during the summer of 1984 to obtain better statistics on the magnitude and duration of the initial, submicrosecond field that is radiated during the onset of natural first strokes.

In general, the shape of the field that is radiated by a return stroke depends on whether it is the first stroke in a flash, a subsequent stroke, or a subsequent stroke that is preceded by a dart-stepped leader (1, 17). Typically, the fields from first strokes begin with a relatively slow 'front' that rises for 2 to 8 μs to about half the peak field amplitude. This front is followed by a fast transition to peak, and the amplitude and duration of this fast transition are the parameters that are of primary interest in this report. We will first briefly describe the systematic biases that are necessarily present, both in this and in all other experiments that use a triggered recording system, and then we will discuss the results. A more complete discussion of the experiment and the data analysis is given by Krider et al. (18).

## EXPERIMENT

Lightning electric field, *E*, and field derivative, *dE/dt*, waveforms were recorded, together with the output of a wideband *RF* receiver, at an experiment site that was located on the eastern tip of Cape Canaveral, Florida. A map showing the location of the experiment is given in Figure 1. The recording systems could be triggered either on the *dE/dt* signal, on *E*, or on the output of the *RF* receiver, but only a single impulsive event could be stored for each discharge. Since many lightning processes produce large values of *dE/dt* with comparatively small values of *E*, the best samples of *dE/dt* were obtained with either a *dE/dt* or an *RF* trigger. The type of lightning process that produced a particular field impulse (*e.g.*, leader step, return stroke, or cloud pulse) was determined from the overall shape of the *E* signature.

The experiment trailer was located as close as possible to the Atlantic Ocean so that the fields produced by any discharge over the ocean would be detected with minimal distortion due to ground-wave propagation (19). The locations of the lightning strike points were obtained from a network of three gated, wideband magnetic direction finders[1] that was operated by the USAF Eastern Space and Missile Center and the NASA Kennedy Space Center. The locations of the direction-finder (DF) sites are shown by crosses in Figure 1. The principles of operation of the DFs and the lightning locating system have been described by Krider et al. (20, 21), and an estimated location accuracy of 1 km has been verified using rocket-triggered lightning at KSC (22).

Figure 2 shows an example of typical *dE/dt*, *E*, and *RF* waveforms that were produced by a first return stroke at a range of 36 km. Here, and throughout this paper, a positive signal is produced by a positive current moving upward; hence, it is an increase in potential gradient in the normal physics convention. All return strokes recorded in this experiment effectively lowered negative charge toward ground.

## RESULTS

Records similar to Figure 2 were obtained during four thunderstorms that were over

[1] Manufactured by Lightning Location and Protection Inc., Tucson, AZ 85705

the ocean and within 100 km of the experiment site. When these data were analyzed, however, it quickly became apparent that whenever the *dE/dt* signal was used to trigger the recording system, the distributions of the resulting peak *dE/dt* values were biased by the trigger threshold. To illustrate this problem, Figure 3 shows values of peak *dE/dt* plotted as a function of range for first return strokes and for return strokes subsequent to the first that were preceded by a dart-stepped leader. Here, and throughout this paper, the values have been normalized to a range of 100 km, assuming that these initial fields were entirely due to the radiation field term in the general field equations and hence that the measured amplitudes of *dE/dt* (and *E*) have an inverse distance dependence on range (17, 23). The sloping line in this figure shows the minimum signal that could be detected at the labeled value of the trigger threshold in the absence of noise. Note how most values of peak *dE/dt* are close to the range-normalized threshold signal at all ranges, and how the minimum signal that is detected has a strong range dependence.

In order to keep such biases to a minimum, the only results that we will discuss in detail are for one storm that occurred about 35 km east of the recording site on Sept. 5, 1984. During this storm, the recording system was triggered on the output of the *RF* receiver (tuned to 5 MHZ), and there were 63 first strokes that produced good values of *dE/dt*. The locations of these strokes are plotted as solid dots in Figure 1. The advantage of using an *RF* trigger is that the *RF* spectral amplitude tends not to be correlated with either the peak electric field, $E_p$, or the peak field derivative, $(dE/dt)_p$.

Values of $E_p$ from 65 first return strokes, range-normalized to 100 km, showed no evidence of a range-dependence and appeared to be log-normally distributed with a median value of 8.2 V/m and a mean and standard deviation of 8.5±2.5 V/m. Several other first strokes in this storm produced *E* fields that saturated the recording system; therefore, the above median and mean probably underestimate the true values. It should be noted that a median of 8.2 V/m is on the high side of the range of values that have been reported by other investigators, as summarized by Uman (17, 24).

A plot of the range-normalized values of $(dE/dt)_p$ for 63 first strokes is given in Figure 4 as a function of range. Here, it should be noted that there is a much more uniform population of low-amplitude signals than in Figure 3. There is also no indication of a range-dependence. Figure 5*a* shows a histogram of the values of $(dE/dt)_p$ in Figure 4, and Figure 5*b* shows the distribution of the full-width-at-half-maximum (FWHM) of the initial half-cycle of *dE/dt* [*i.e.*, $t_a + t_b$ in the notation of Weidman and Krider (3)]. Both distributions appear to be Gaussian, although that of FWHM fails the Chi-squared goodness-of-fit test. The left side of Table 1 gives the means and standard deviations of the data in Figure 5. Our mean $(dE/dt)_p$ is 17% larger than the 33 V/m/μs reported by Weidman and Krider (2) for first strokes, based on the initial slope of *E* signals, but is in good agreement with the 37 ± 10 V/m/μs reported by Weidman and Krider (3) for 13 *dE/dt* signatures. The mean FWHM is 37% larger than the 71 ns reported by Weidman and Krider (3).

The data in Figures 4-5 and Table 1 were obtained from lightning sources that were at ranges of 27 to 45 km, with a median of 36 km, where the field propagation from the source to the measuring equipment was almost entirely over sea water. At these distances, the effects of propagation should not affect the amplitude of $E_p$ by more than a few

percent (25–27), but the higher frequency components of *dE/dt* will be reduced, and the FWHM will be increased (23, 28, 29). Because of propagation, our measured values of $(dE/dt)_p$ and FWHM should be regarded as lower and upper limits, respectively, of the true values that are radiated by the source.

Zeddam et al. (28) have calculated the effect of propagation over a flat, finitely conducting surface on the *dE/dt* waveform radiated by a model return stroke. Making similar assumptions, Ming and Cooray (29) have computed the effects of propagation over a spherical, finitely conducting ocean, accounting for the effects of surface roughness due to waves. The results of Ming and Cooray (29) indicate that surface roughness increases both the attenuation and broadening, and the magnitude of this additional effect becomes comparable to that of finite conductivity alone at wind speeds between 20 and 30 knots (10 and 15 m/s). The roughness effect also depends on wind direction. Since we do not know the wind velocity at the ocean surface between the lightning and our observation site, but we believe it was less than 25 knots, we will ignore the effects of roughness and consider here only the effects of finite conductivity.

We have repeated the computations of Zeddam et al. (28) to estimate the effects of propagation over sea water on our measurements, and the relative attenuations and broadenings of a typical *dE/dt* signal are summarized in Table 2. The values for 35 km in Table 2 have been used to "correct" our estimates of the true means and standard deviations of $(dE/dt)_p$ and FWHM, and are shown on the right side of Table 1.

## DISCUSSION

The overall relationship between the current at the base of a lightning channel and the associated electromagnetic fields at various distances and times has been reviewed by Uman and Krider (30), Uman (17), Nucci et al. (31), and Thottappillil and Uman (32). If we assume that the initial field and field derivative produced by a natural first stroke can be described by the "transmission line model" in its simplest form (10,11,13,23), then this model can be used to estimate the peak current, $I_p$, and the peak rate of change of current, $(dI/dt)_p$, at the source:

$$I_p = \frac{2\pi\epsilon_0 c^2 D}{v} E_p \tag{1}$$

$$\left(\frac{dI}{dt}\right)_p = \frac{2\pi\epsilon_0 c^2 D}{v}\left(\frac{dE}{dt}\right)_p, \tag{2}$$

where $D$ is the distance to the discharge and $v$ is the upward velocity of the current front. With this model, the FWHM of the *dI/dt* signature is the same as the FWHM of *dE/dt*. This

model also assumes that the channel is straight and perpendicular to a flat, perfectly conducting ground and that the field is produced by a single current pulse propagating up a single channel at a constant velocity without dispersion. To assist the reader in evaluating these expressions, we note that equation (1) becomes

$$I_p = 5.0 \frac{E_p}{v} \quad kA \tag{3}$$

when $E_p$ is in V/m range-normalized to 100 km and $v$ is in units of $10^8$ m/s.

Since measured velocities of first strokes near the ground are typically between 1 and $3 \times 10^8$ m/s (33, 34), then a median $E_p$ of 8.2 V/m, a mean of 8.5 ± 2.5 V/m, and a mean $(dE/dt)_p$ of 46 ± 13 V/m/μs, all at 100 km after correction for propagation (see Table 1), imply that the associated median and mean $I_p$ and mean $(dI/dt)_p$ have the values shown in Table 3.

Willett et al. (11) have found that apparent velocities of $1.51 \times 10^8$ and $2.02 \times 10^8$ m/s provide the best fit to the ratios $E_p/I_p$ and $(dE/dt)_p/(dI/dt)_p$ for 28 rocket-triggered return strokes in Florida during 1987. These values of $v$ have been underlined in Table 3 because we believe that they represent the best estimates of the respective current parameters. Our preferred estimates of the median and average $I_p$ in Table 3 are close to the geometric means of 30 and 33 kA reported by Berger et al. (35) and Garbagnati and Lo Pipero (36), respectively, for the first strokes in strikes to instrumented towers that were initiated by downward propagating, negatively charged leaders. Our preferred estimate of the average $(dI/dt)_p$, 115 ± 32 kA/μs, is significantly larger than the geometric means reported by Berger et al. (35) and Garbagnati and Lo Pipero (36), 40 and 14 kA/μs, respectively, for strikes to towers, and our value is also larger than the geometric mean of the average rate of rise (from 10% to 90% of the peak current) of 28 kA/μs for rocket-triggered return strokes in Florida and Alabama that was reported by Fisher et al. (15).

The reasons for the lower values of the peak *dI/dt* in most of the tower data could be bandwidth limitations in the sensors and/or recording equipment or in reading these data (15, 37); or perhaps because towers, which are usually located on mountains, or the upward connecting leaders that originate from towers, limit the maximum *dI/dt* that can be measured with this technique. Similarly, we believe that the estimates of *dE/dt* and rise-time from the triggered-lightning measurements of Fisher et al. (15) may have been distorted by the relatively low bandwidth (2 or 6 MHz in Florida or Alabama, respectively) of their current-measuring instrumentation. It is also conceivable that our mean *dI/dt* is an overestimate because of remaining, undetected trigger biases, although we have argued that this is not the case. Finally, if the *dE/dt* signature that is radiated during a fast-field transition is produced by more than one current pulse propagating at the same time (10), then our inferred values of *dI/dt* will overestimate the true value for a single pulse by at most a factor of 2; otherwise, we expect that the above estimates of the mean $I_p$ and $(dI/dt)_p$ in natural first strokes will be within about 30% of the true values. This estimate assumes a residual uncertainty in propagation of 15%, calibration 10%, model 20%, and statistical biases 10%.

The best comparisons for our estimates of the FWHM of *dI/dt* (75 ± 15 ns, as corrected) are the Florida rocket-triggered lightning data of Leteinturier et al. (14). These authors report a mean of 91 ± 61 ns for 73 events recorded during 1987 and 1988, and this is in reasonable agreement with our estimate. Leteinturier et al. (14) also show a cumulative distribution of 10 to 90% risetimes that appears to be log-normal. This finding does not appear to be consistent with our distribution of FWHM.

Since the maximum *dI/dt* and its duration are important parameters in the design of lightning protection systems, and since an average of 115 kA/μs with a FWHM of 75 ns exceeds the specification of most lightning test standards or is regarded as extreme (16), we believe that the submicrosecond behavior of *E* and *dE/dt* signatures from natural lightning merits further study.

ACKNOWLEDGMENTS – The authors are grateful to Maj. P. Rustan of the U. S. Air Force for the use of his research vehicle, to W. Jafferis of the NASA Kennedy Space Center for his enthusiasm and support, to W. Hiscox of Lightning Location and Protection, Inc., for his assistance in computing the lightning locations, and to Margaret Sanderson Rae for assistance during preparation of the final manuscript. This research was supported in part by the NASA Kennedy Space Center, Grant NAG100092, and by the USAF Office of Scientific Research, Contract F49620-86-C-0013.

REFERENCES

1. C.D. Weidman and E.P. Krider, "The Fine Structure of Lightning Return Stroke Waveforms," Journal of Geophysical Research, Vol. 83, 1978, pp. 6239-6247. Also, "Correction," Journal of Geophysical Research, Vol. 87, 1982, p. 7351.

2. C.D. Weidman and E.P. Krider, "Submicrosecond Risetimes in Lightning Return Stroke Fields," Geophysical Research Letters, Vol. 7, No. 11, Nov. 1980, pp. 955-958.

3. C.D. Weidman and E.P. Krider, "Variations à l'Échelle Submicroseconde des Champs Électromagnétiques Rayonnés par la Foudre," Annales des Télécommunications, Tome 39, No. 5–6, Mai–Juin 1984, pp. 165-174.

4. V. Cooray, "A Novel Method to Identify the Radiation Fields Produced by Positive Return Strokes and Their Submicrosecond Structure," Journal of Geophysical Research, Vol. 91, 1986, pp. 7907–7911.

5. C. Leteinturier and J. Hamelin, "Experimental Study of the Electromagnetic Characteristics of Lightning Discharge in the 200 Hz-20 MHz Band," Electromagnetics, Vol. 7, 1987, pp. 423-439.

6. E.M. Thomson, P.J. Medelius, M. Rubinstein, M.A. Uman, J. Johnson, and J.W. Stone, "Horizontal Electric Fields from Lightning Return Strokes," Journal of Geophysical Research, Vol. 93, 1988, pp. 2429–2441.

7. R.P. Fieux, C.H. Gary, B.P. Hutzler, A.R. Eybert-Berard, P.L. Hubert, A.C. Meisters, P.H. Perroud, J. Hamelin, and J.M. Person, "Research on Artificially Triggered Lightning in France," IEEE Transactions on Power Apparatus and Systems, Vol. 97, 1978, pp. 725–733.

8. SPARG (Saint Privat d'Allier Research Group), "Eight Years of Lightning Experiments at Saint Privat d'Allier," Rev. Générale d'Électricité, Tome 9, 1982, pp. 561–582.

9. C.E. Baum, J.P. O'Neill, E.L. Breen, D.L. Hall, and C.B. Moore, "Electromagnetic Measurement of and Location of Lightning," Electromagnetics, Vol. 7, 1987, pp. 395–422.

10. J.C. Willett, V.P. Idone, R.E. Orville, C. Leteinturier, A. Eybert-Berard, L. Barret, and E.P. Krider, "An Experimental Test of the 'Transmission-Line Model' of Electromagnetic Radiation from Triggered Lightning Return Strokes," Journal of Geophysical Research, Vol. 93, 1988, pp. 3867–3878.

11. J.C. Willett, J.C. Bailey, V.P. Idone, A. Eybert-Berard, and L. Barret, "Submicrosecond Intercomparison of Radiation Fields and Currents in Triggered Lightning Return Strokes Based on the 'Transmission-Line' Model," Journal of Geophysical Research, Vol. 94, 1989, pp. 13,275–13,286.

12. D.M. LeVine, J.C. Willett, and J.C. Bailey, "Comparison of Fast Electric Field Changes from Subsequent Return Strokes of Natural and Triggered Lightning," Journal of Geophysical Research, Vol. 94, 1989, pp. 13,259–13,265.

13. C. Leteinturier, C. Weidman, and J. Hamelin, "Current and Electric Field Derivatives in Triggered Lightning Return Strokes," Journal of Geophysical Research, Vol. 95, 1990, pp. 811–828.

14. C. Leteinturier, J.H. Hamelin, and A. Eybert-Berard, "Submicrosecond Characteristics of Lightning Return-Stroke Currents," IEEE Transactions on Electromagnetic Compatibility, Vol. 33, 1991, pp. 351–357.

15. R.J. Fisher, G.H. Schnetzer, R. Thottappillil, V.A. Rakov, M.A. Uman, and J.D. Goldberg, "Parameters of Triggered-Lightning Flashes in Florida and Alabama," Journal of Geophysical Research, Vol. 98, 1993, pp. 22,887–22,902.

16. M.A. Uman, "Natural and Artificially Initiated Lightning and Lightning Test Standards," Proceedings of the IEEE, Vol. 76, 1988, pp. 1548–1565.

17. M.A. Uman, "Lightning Return Stroke Electric and Magnetic Fields," Journal of Geophysical Research, Vol. 90, 1985, pp. 6121–6130.

18. E.P. Krider, C. Leteinturier, and J.C. Willett, "Submicrosecond Fields Radiated During the Onset of First Return Strokes in Cloud-to-Ground Lightning." Submitted to Journal of Geophysical Research – Atmospheres, January 1995.

19. V. Cooray and Y. Ming, "Propagation Effects on the Lightning-Generated Electromagnetic Fields for Homogeneous and Mixed Sea-Land Paths," Journal of Geophysical Research, Vol. 99, 1994, pp. 10,641– 10,652.

20. E.P. Krider, R.C. Noggle, and M.A. Uman, "A Gated, Wideband Magnetic Direction Finder for Lightning Return Strokes," Journal of Applied Meteorology, Vol. 15, 1976, pp. 301–306.

21. E.P. Krider, R.C. Noggle, A.E. Pifer, and D.L. Vance, "Lightning Direction Finding Systems for Forest Fire Detection," Bulletin of the American Meteorological Society, Vol. 61, 1980, pp. 980–986.

22. M.W. Maier and W. Jafferis, "Locating Rocket Triggered Lightning Using LLP Lightning Locating System at the NASA Kennedy Space Center," Proceedings of the 10th

International Aerospace and Ground Conference on Lightning and Static Electricity, Paris, 1985, pp. 337-345.

23. V. Cooray, "Derivation of Return Stroke Parameters from the Electric and Magnetic Field Derivatives," Geophysical Research Letters, Vol. 16, 1989, pp. 61–64.

24. M.A. Uman, "The Lightning Discharge," Chapter 7, Academic Press, Orlando, FL, 1987, 377 pp.

25. M.A. Uman, C.E. Swanberg, J.A. Tiller, Y.T. Lin, and E.P. Krider, "Effects of 200-km Propagation on Lightning Return Stroke Electric Fields," Radio Science, Vol. 11, 1976, pp. 985-990.

26. V. Cooray and S. Lundquist, "Effects of Propagation on the Risetimes and Initial Peaks of Radiation Fields from Return Strokes," Radio Science, Vol. 18, 1983, pp. 409–415.

27. V. Cooray, "Effects of Propagation on the Return Stroke Radiation Fields," Radio Science, Vol. 22, 1987, pp. 757–768.

28. A. Zeddam, C. Leteinturier, and P. Degauque, "Influence of the Ground Conductivity on the Electric Field Derivative Measurements," Paper 6.2 in Proceedings of the 20th International Conference on Lightning Protection, Interlaken, Switzerland, Sept. 24-28, 1990.

29. Y. Ming and V. Cooray, "Propagation Effects Caused by a Rough Ocean Surface on the Electromagnetic Fields Generated by Lightning," Radio Science, Vol. 29, 1994, pp. 73–85.

30. M.A. Uman, and E.P. Krider, "A Review of Natural Lightning: Experimental Data and Modeling," IEEE Transactions on EMC, Vol. 24, 1982, pp. 79-112.

31. C.A. Nucci, G. Diendorfer, M.A. Uman, F. Rachidi, M. Ianoz, and C. Mazzetti, "Lightning Return Stroke Current Models with Specified Channel-Base Current: A Review and Comparison," Journal of Geophysical Research, Vol. 95, 1990, pp. 20,395–20,408.

32. R.Thottappillil and M.A. Uman, "Comparison of Lightning Return-Stroke Models," Journal of Geophysical Research, Vol. 98, 1993, pp. 22,903–22,914.

33. D.M. Mach and W.D. Rust, "Photoelectric Return-Stroke Velocity and Peak Current Estimates in Natural and Triggered Lightning," Journal of Geophysical Research, Vol. 94, 1989, pp. 13,237-13,247.

34. D.M. Mach and W.D. Rust, "Two-Dimensional Velocity, Optical Risetime, and Peak Current Estimates for Natural Positive Lightning Return Strokes," Journal of Geophysical Research, Vol. 98, 1993, pp. 2635-2638.

35. K. Berger, R.B. Anderson, and H. Kroninger, "Parameters of Lightning Flashes," Electra, Vol. 80, 1975, pp. 23–37.

36. E. Garbagnati and G.B. Lo Pipero, "Parameter von Blitzströmen," Elektrotechnische Zeitschrift, Vol. ETZ-A 103, 1982, pp. 61–65.

37. A. J. Eriksson, "Lightning and Tall Structures," Transactions of the South African Institute of Electrical Engineering, Vol. 69, 1978, pp. 2–16.

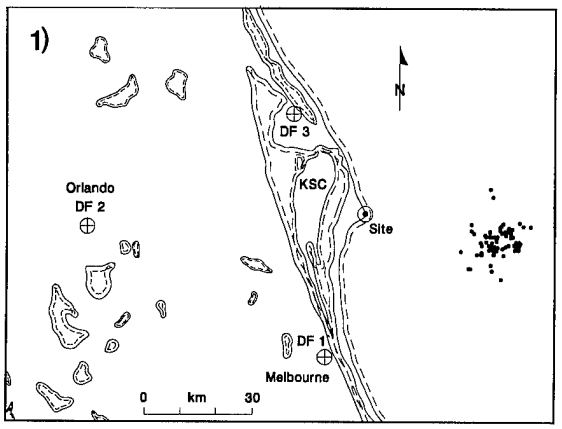



FIGURE 1. The location of the experiment site at Cape Canaveral, Florida, and the three magnetic direction-finder (DF) sites. The small dots show the locations of cloud-to-ground flashes that were analyzed between 20:37 and 21:15 UT on September 5, 1984.

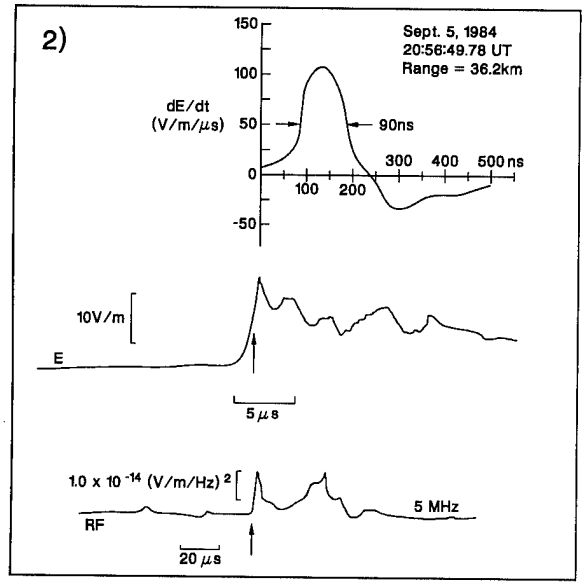



FIGURE 2. Examples of the *dE/dt* signature (top), *E* waveform (middle), and *RF* emission (bottom) produced by a first return stroke at 36.2 km range. The vertical arrows under the *E* and *RF* records show the time of the *dE/dt* trigger. The *RF* signal at this time peaked at a value of $1.6\times10^{-14}$ $(V/m/Hz)^2$.

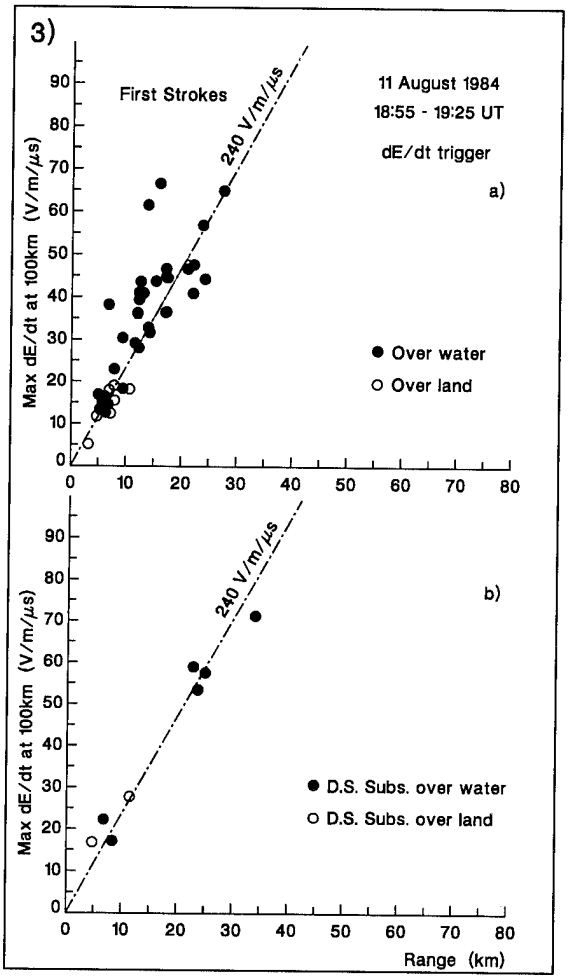



FIGURE 3. Values of the peak *dE/dt*, range-normalized to 100 km, that were radiated by (a) first return strokes and (b) subsequent return strokes produced by a dart-stepped leader as a function of range. Strokes over water are shown as solid dots, and those over or near land are shown as open circles. Note how the values tend to cluster along a line determined by the setting of the *dE/dt* trigger threshold.

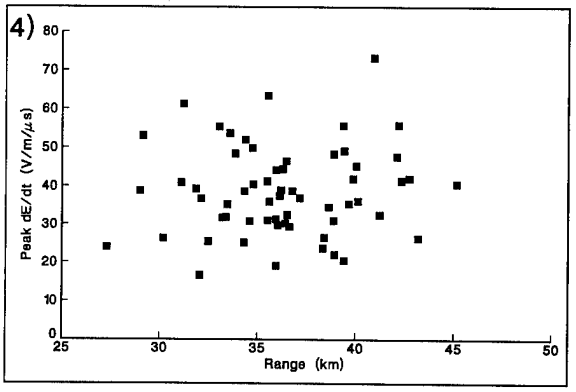



FIGURE 4. Values of peak *dE/dt*, range normalized to 100 km, as a function of range for 63 first return strokes.

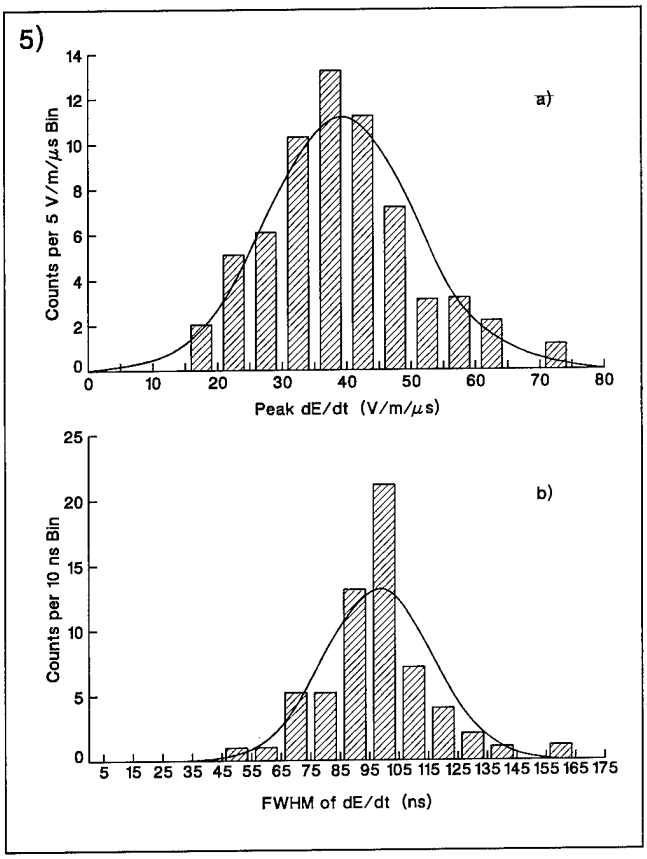



FIGURE 5. Histograms of (a) the measured peak *dE/dt* values, range-normalized to 100 km, for 63 first return strokes, and (b) the full-width-at-half-maximum (FWHM) of the initial half-cycle of the *dE/dt* signatures for 61 first strokes. A Gaussian probability-density function corresponding to the measured mean and standard deviation (Table 1) and scaled to produce the same total event count is shown as the solid curve on each histogram.

**TABLE 1.** Statistics of the initial peak *dE/dt* normalized to 100 km and the FWHM of the initial half-cycle of *dE/dt* for natural first return strokes. The corrected values are estimates after removing the effects of propagation over 35 km of sea water.

| | Measured | Corrected | Units |
|---|---|---|---|
| Peak *dE/dt* (N = 63) | Mean = 39<br>σ = 11 | Mean = 46<br>σ = 13 | V/m/μs |
| FWHM (N = 61) | Mean = 100<br>σ = 20 | Mean = 75<br>σ = 15 | ns |

**TABLE 2.** Effects of propagation over a flat surface of sea water ($\epsilon_r$ = 80, σ = 4 S/m) on a *dE/dt* waveform relative to a perfect conductor (σ = ∞).

| Distance (km) | Attenuation of $(dE/dt)_p$ | Increase of FWHM |
|---|---|---|
| 10 | 6% | 11% |
| 35 | 15% | 33% |
| 50 | 18% | 43% |

**TABLE 3.** Estimates of the median peak current, $I_{pm}$, the mean peak current and current derivative, $\overline{I_p}$ and $\overline{(dI/dt)_p}$, and their standard deviations for first return strokes derived from Eqs. (1) and (2) for various assumed velocities. The measured values of $E_{p_m}$, $\overline{E_p}$, and $\overline{(dE/dt)_p}$ at 100 km have been assumed to be 8.2 V/m, 8.5 ± 2.5 V/m, and 46 ± 13 V/m/μs, respectively.

| $v$ (× $10^8$ m/s) | $I_{pm}$ (kA) | $\overline{I_p}$ (kA) | $\overline{(dI/dt)_p}$ (kA/μs) |
|---|---|---|---|
| 1.0 | 41 | 42 ± 12 | 230 ± 65 |
| 1.5 | 27 | 28 ± 8 | 153 ± 43 |
| 2.0 | 20 | 21 ± 6 | 115 ± 32 |
| 2.5 | 16 | 17 ± 5 | 92 ± 26 |
| 3.0 | 13 | 14 ± 4 | 77 ± 22 |

# SESSION 02A
# MEASUREMENTS/STANDARDS
# CHAIRPERSON: JOHN DAWSON

# ELECTROMAGNETIC ENVIRONMENTS AND TEST METHODS FOR THE ASSESSMENT OF INDIRECT HAZARDS DUE TO LIGHTNING STRIKES

R H Evans and G A M Odam
GAO Consultancy, Barmouth, Gwynedd, UK
(Consultants, previously employed at RAE Farnborough)

## ABSTRACT

Electromagnetic environments relevant to indirect (Group II) effects for direct lightning attachments and nearby lightning flashes are compared for both airborne and ground materiel. Proposals are made for the definition of the electromagnetic environment for materiel on the ground when subjected to a nearby lightning strike, together with a discussion of possible analysis and test methods. The proposals are intended in particular to assist in the further development of the environments and assessment methods to be included in NATO STANAGS 4236 and 4327.

## INTRODUCTION

Various multi-nation military Standards concerning the definition of the lightning environment and assessment/test methods are being developed (1, 2, 3) as outlined in Reference 4. They are intended to take into account both existing military Standards and EUROCAE/AE4L/FAA civil documents. This paper, which is based on Reference 5, gives some supporting proposals relating to indirect (Group II) effects, and in particular discusses the relation between the effects of direct attachment and nearby flashes. Generally speaking the former are more severe and the latter therefore do not require separate assessment. However, there may be some ground-based weapons or other materiel which are required to survive a nearby strike to the ground but not a direct attachment; proposals are therefore made for defining the environment in this case, in terms of magnetic and electric fields and ground currents, together with a discussion of possible assessment/test methods.

## AIR APPLICATION

MAGNETIC FIELDS--For the purpose of estimating the magnitude of induced voltages it is usual, at least initially, to assume cylindrical geometry, that is, if we are considering an aircraft we assume the fuselage, wing etc to be a long structure whose cross-sections are the same throughout its length, and with the lightning current flowing axially. If the fuselage is taken to be a circular cylinder of radius r then the voltage induced per metre length for a wire in any given position inside may be expressed as:-

$$v = a\, dB/dt = a(\mu/2\pi r)\, di/dt \qquad (1)$$

where 'a' is a constant depending on the position of the wire (and having the dimensions of length), B is the magnetic flux density at the surface of the cylinder and $\mu$ is the permeability of air ($4\pi\ 10^{-7}$ H/m or 1.26 $\mu$H/m).

Nearby Flash--We wish to make a comparison with the case of a nearby lightning flash as distinct from an attachment. Figure 1 illustrates the case of maximum coupling, where the external lightning channel is treated as a long straight conductor parallel to the cylinder representing the aircraft fuselage and at a distance D from the centre of the cylinder, Eqn (1) then takes the form that the flux density at the centre of the cylinder (in the absence of the distorting effect of the cylinder) is $\mu i/2\pi D$ where i is the current in the lightning channel, but because we are considering early-time conditions (during the rising front of the current waveform) when no flux has penetrated the cylinder wall, the flux pattern is distorted as shown and at the poles the flux density is subject to an enhancement factor of 2. Thus the voltage per metre induced in the same wire as before is given by $2a\ (\mu/2\pi D)\ di/dt$. Hence for a given value of di/dt the ratio of nearby to attachment values of induced voltage is 2r/D.

ELECTRIC FIELD--For a cylinder, the electric field at the surface is:-

$$E = Q/2\pi kr \qquad (2)$$

where Q is the charge per metre of cylinder length and k is the permittivity of air ($10^{-9}/36\pi$ F/m).

For the effects of dE/dt we need to estimate the value of dE/dt at the cylinder surface. For the return current phase of the lightning flash we may relate dE/dt at the surface to di/dt by treating the fuselage as a cylinder acting as a uniform transmission line and the return current as a current wave travelling with a velocity 's'. At the surface of the cylinder we have, by differentiation of Eqn (2):-

$$dE/dt = (1/2\pi kr)\ dQ/dt \qquad (3)$$

But in a uniform transmission line:-

$$dQ/dt = di/dx = (di/dt)/(dx/dt) = (di/dt)/s$$

Hence

$$dE/dt = (1/2\pi ksr)\ di/dt = (60/r)\ di/dt \qquad (4)$$

since the propagation velocity s may be taken as $3 \times 10^8$ m/s for air. Thus for a cylinder of radius 1.5 m and di/dt of 100 kA/μs the value of dE/dt at the surface is $4 \times 10^{12}$ V/m/s.

Nearby Flash--We are mainly interested in the value of dE/dt during the return stroke phase of a flash at distance D, which is related to di/dt in a manner similar to that defined by Eqn (4) above, with D substituted for r. However, it is known that the velocity of propagation of a wavefront in a lightning channel is about $10^8$ m/s, which is one third of the velocity of propagation along a straight solid conductor in air. If we use this value for s then the expression connecting dE/dt and di/dt becomes:-

$$dE/dt = (180/D)\ di/dt \qquad (5)$$

so that the ratio of nearby to attachment values becomes 3r/D, compared with 2r/D obtained above for the magnetic field effects.

## GROUND APPLICATION - MAGNETIC AND ELECTRIC FIELD ENVIRONMENT

In the case of weapons or other materiel required to survive a nearby flash but not a direct attachment, it is necessary to specify a 'nearby lightning' environment. An assessment will be required of the likely effects of such an environment, possibly including tests.

Since materiel projecting above ground may divert an oncoming lightning leader towards itself, there must be some radius (R) within which a nearby strike cannot occur, the value depending on the geometry of the materiel and the surroundings. The value of R may be estimated making some assumptions and then the environment at the materiel calculated by substituting R in expressions which give the fields and their rates of change as functions of the distance from the strike point.

MAGNETIC FIELD DUE TO THE RETURN CURRENT--The magnetic environment is a substantially horizontal field due to the return stroke current flowing in the lightning channel, which for the purpose of standardised calculation may be supposed to be vertical. The simplest formula to employ is that for the magnetic field at distance D from a long (theoretically infinite) straight conductor carrying a current i, namely:-

$$H = i/2\pi D \quad A/m \tag{6}$$

The waveform of the magnetic field is the same as that of the lightning current. Usually we are interested in the voltage induced in a loop and this is proportional to the rate of change of field dH/dt. By differentiation this is seen to be:-

$$dH/dt = (di/dt)/2\pi D \quad A/m/s \tag{7}$$

Strictly, the magnetic field produced by the return current has two components, namely that due to the vertical part of the lightning channel above ground and that due to the current in the ground spreading out from the strike point, as sketched in Fig 3(a). If the ground is assumed to be a perfectly conducting plane then the total field at any point above the ground is that due to the combined effect of the lightning channel and its mirror image in the ground, that is, the field is the same as it would be if the current had continued vertically into the ground in the original straight line, and Eqns (6) and (7) would therefore apply. Even in practical circumstances there is evidence (Ref 6 for example) that in view of the many assumptions that have to be made in order to define a standard environment the use of Eqns (6) and (7) is reasonable. The maximum value of di/dt to be substituted in Eqn (7) is $10^{11}$ A/s.

ELECTRICAL FIELD DUE TO THE OVERHEAD LEADER--The electric field component of the environment is due to the overhead leader and is substantially vertical. For a negative cloud-to-ground flash the leader advances in zig-zag steps each about 50 m long and separated by pauses of 40-100 μs. In discussions of the final stage, when an answering streamer from the ground contacts the leader, thus completing the path along which the return stroke will flow, the conjunction height is typically taken to be 50 m, and certainly in the range 25-100 m, while the potential of the leader tip before junction takes place is considered to be in the range 10-100 MV (Ref 7). The vertical field on the ground under the leader will be a maximum just before a streamer from the ground travels up to meet the leader.

The maximum field may be calculated approximately by regarding the leader as a straight vertical line charge of Q coulomb/m, with its tip at a height h above the ground (assumed flat), the vertical length of the leader being large compared with h, as shown in Fig 2. The assumption of a vertical straight leader contrasts with the reality of a zig-zag stepped leader but it is one that is commonly made for reasons of simplicity and standardisation, when in any case accurate calculation is not possible. By integrating from zero to infinity the field due to an element δx of the lightning channel and its mirror image in the ground, it may be shown that at a point P on the ground (assumed flat) immediately below the leader the vertical electric field is given by:-

$$E_g = Q/2\pi kh = (Q/h)18 \times 10^9 \tag{8}$$

where k is the permittivity of air. If the leader velocity is 's' then the value of dE/dt on the ground is derived as follows:-

$$dE/dt = (dE/dh)(dh/dt) = dE/dh\ s$$

But $$dE/dh = Q/2\pi kh^2 = E/h$$

Hence on the ground $$dE/dt = sE_g/h \qquad (9)$$

As stated, we may take the height of the leader tip h to be 50 m. A reasonable value for charge per unit length of the leader Q is $10^{-3}$ coulomb/m, and for the leader velocity s is $10^8$ m/s, which is one third the velocity of light. We understand that a US Army Standard in a section on nearby lightning takes these values also. Substitution in (8) and (9) gives

$$E_g = 0.36 \times 10^6 \text{ V/m} \quad \text{and} \quad dE/dt = 0.72 \times 10^{12} \text{ V/m/s}.$$

As stated, the values for E and dE/dt at ground level given above are for perfectly flat ground and they are therefore not very relevant to a definition of the practical environment for the assessment of the effect of nearby lightning upon materiel. This is because the ground cannot be perfectly flat and the process of initiating streamers involves enhancement of the local field by projections on the ground (which may be quite small) until the field is limited by the breakdown value for air at ground level (3 MV/m). The enhancement factor needed to increase the flat-ground value of field (0.36 MV/m) to 3 MV/m is 8.3, which is easily possible for sharp points and edges.

From the above discussion it is considered reasonable to define the maximum field immediately below the leader as 3 MV/m. This is in agreement with the US Army document. It is thought that the value of dE/dt should be enhanced by the same factor as the field, namely to $6 \times 10^{12}$ V/m/s. An alternative way of looking at it is to assume that the field of 3 MV/m collapses in the time taken for the answering streamer to reach the leader and effect a junction, which is 0.5 μs for a leader height of 50 m. This method again gives $dE/dt = 6 \times 10^{12}$ V/m/s.

This recommended value of dE/dt is higher than the value of $1.3 \times 10^{12}$ V/m/s given in the US document but less than the value of $10^{13}$ V/m/s quoted in Reference 1 for general use for both air and ground/sea applications.

Reduction of Field with Horizontal Distance from the Strike Point--If we assume that the point on the ground immediately below the leader is also the strike point then in order to evaluate the effect of nearby lightning we need to calculate the field and dE/dt on the ground at various horizontal distances (of the order of the minimum distance R) from the strike point, where the field will still be substantially vertical. Again by integrating the field due to an element of the lightning channel and its mirror image (Fig 2) it may be shown that at a point P′ situated at a horizontal distance D, the field is equal to that on the ground immediately below the leader divided by the factor:-

$$(1 + D^2/h^2)^{1/2} \qquad (10)$$

The value of dE/dt is reduced by the same factor.

Expressions for Fields due to Nearby Lightning--Substitution of R for D and insertion of the maximum lightning parameter values proposed above gives the following expressions for the environment at the materiel:-

Rate of change of (horizontal) magnetic field (dH/dt) $1.6 \times 10^{10}/R$ A/m/s

Maximum (vertical) electric field (E) $3 \times 10^6 / (1 + R^2/50^2)^{1/2}$ V/m

Rate of change of electric field (dE/dt) $6 \times 10^{12} / (1 + R^2/50^2)^{1/2}$ V/m/s

GROUND APPLICATION - POTENTIAL GRADIENT IN THE GROUND

POTENTIAL GRADIENT IN THE ABSENCE OF CONDUCTING OBJECTS ON THE GROUND--If we assume that the lightning channel that makes contact with the ground is vertical and the ground itself has uniform resistivity in all directions, then the lightning current will spread out uniformly into the ground from the strike point as shown in Fig 3(a). Strictly this applies only to slowly changing currents since it neglects inductance and capacitance. The current flowing in the ground will produce a potential gradient at the surface which may cause potential differences between points on materiel which are nominally at the same (ground) potential.

In the absence of ionisation of the ground (see below), the potential gradient at radius r from the strike point is given by:-

$$\text{Potential gradient} = \rho i/2\pi r^2 \quad \text{V/m} \qquad (11)$$

where i is the total current in the lightning channel, which is of course a function of time, and $\rho$ is the resistivity of the ground in ohm-metres. By integration, the potential at radius r relative to a remote point is given by:-

$$\text{Potential} = \rho i/2\pi r \quad \text{volts} \qquad (12)$$

The numerical value of the resistivity of the ground can vary widely from place to place (say from 20 to 1000 ohm-metres) depending upon the nature of the terrain. In practice the above expressions hold only outside an ionised region whose radius (8, 9) is determined by the breakdown potential gradient $E_b$ at the ground surface, which is likely to be about 250 kV/m for soil at the lower end of the resistivity range and about 500 kV/m at the upper end. The soil on the ground surface will become ionised out to a radius (denoted by $r_o$) where the potential gradient given by Eqn (11) is equal to $E_b$, and within a circle of this radius the soil will be at a practically constant potential. Hence from (11) and (12):-

$$\text{Radius of ionised region} \quad r_o = (\rho i/2\pi E_b)^{1/2} \qquad (13)$$

and the potential of the ionised region is given by:- $(\rho i E_b/2\pi)^{1/2}$ (14)

Since these quantities are functions of the lightning current i they will rise and fall in time with the waveform of the current. In order to see what numerical values are likely to be involved for a severe lightning strike we may take the example: peak current=200 kA, $\rho$=100 ohm-m; $E_b$=250 kV/m. Then at the peak current the ionisation radius (Eqn 13) is 3.6 m and the potential of the ionised region (Eqn 14) is 0.9 MV. The potential gradient outside the ionised region is given in the following Table:-

| Radius m | 3.6 | 5 | 10 | 15 | 20 | 30 | 50 |
|---|---|---|---|---|---|---|---|
| kV/m | 250 | 128 | 32 | 14 | 8 | 3.6 | 1.3 |

POTENTIAL DIFFERENCE AND CURRENT IN CONDUCTING OBJECTS--The above Table gives the open-circuit value of the potential gradient, and estimating the voltage that would appear across a conducting object of finite resistance (or the current that would flow in an object of low resistance) placed on the ground requires a knowledge of the effective output impedance of the voltage source. In the case shown in Fig 3(b) the conducting body, which is assumed to have very high conductivity compared to that of the ground, is resting on the ground at a mean distance r from the lightning strike point and has a rectangular 'footprint' of length L in the direction of current flow and width W. The current flow lines (which in a small region may be taken to represent a constant current density in the absence of the conducting footprint) are sketched roughly, but in a particular example the flow lines could be computed by means of a program for solving three-dimensional electromagnetic field problems. Current will be `attracted` into the conductor over a cross-sectional area of nWL where n depends on the exact shape (the ratio L/W) but is probably in the region of 0.5. Since the current density at radius r from the strike point is $i/2\pi r^2$, the total current flow into the rectangle is given by $nWLi/2\pi r^2$. The open circuit potential drop over length L is given by $\rho Li/2\pi r^2$ and hence the effective output impedance of the voltage source for a rectangular footprint is given by:-

$$\text{Source impedance} = \rho/nW \qquad (15)$$

For n=0.5, $\rho$=100 ohm-metres and a footprint width W=1m this impedance is 200 ohm. If it is a square footprint (L=W=1m) situated at a radius of 10 m from the lightning strike point, the open circuit potential drop using the above Table would be 32 kV (at peak lightning current). With the conductor in place, assumed to be of low resistance compared with 200 ohm, the current flowing in it is 32000/200 A, which is 160 A.

The above estimates strictly apply only to slowly changing currents so that inductive effects may be ignored. In practice lightning currents change rapidly, and inductance in the load will mean that the potential difference across it will remain near the open-circuit value for a longer period, and that the current flowing in the load will be lower because of its inductive impedance.

Tests which simulate the conditions are not being proposed at present as it is considered that in most cases a theoretical assessment should be adequate.

## DISCUSSION OF POSSIBLE ASSESSMENT AND TEST METHODS FOR NEARBY LIGHTNING

GENERAL--For brevity we shall refer to the munitions and associated systems covered by Reference 2 as weapons. We are concerned with the effect on safety and suitability for service of weapons subjected to nearby lightning while on the ground. By definition therefore we are looking for Group II (indirect) effects, that is, essentially induced voltages and currents. As previously mentioned, nearby lightning needs to be specifically considered only in the case of those weapons where it is accepted that they could not be expected to survive a direct strike but which are required to survive a nearby strike.

New weapons in the above category would presumably be subjected to a Lightning Hazard Design Analysis as stipulated in Reference 2 and it would not be a great extension of the methods of transient prediction outlined in Ref 3 to include the effect of an external field instead of the usual assessment of the effect of lightning current flowing in the weapon itself due to a direct attachment. If such a preliminary assessment showed that the induced effects were well below the allowable level

then it would probably be decided not to proceed to any further analysis/tests for nearby lightning. If on the other hand such preliminary assessment predicted an excessive level of transient, or was inconclusive, then further assessment would be needed.

FORM OF FURTHER ASSESSMENT--It is unlikely that further analysis alone would be relied on, and testing of some form would therefore be part of the assessment. The method might be one of pure testing with no analysis (apart possibly for simple extrapolation), such as subjecting the weapon to a realistic form of field (but perhaps at an amplitude below full threat level) and measuring the induced transients at critical points in the weapon. Alternatively it might be a test/analysis method where measurements were made to obtain relevant data which facilitated further more accurate analysis.

MAGNETIC COUPLING, TESTING AND ANALYSIS--An example of test/analysis for magnetic coupling is some form of swept frequency CW test similar to that of Appendix C1 of Reference 2 for direct lightning attachment, in which the sinusoidal signals measured at selected points in the weapon are compared in amplitude, and preferably also in phase, over a range of frequencies with an external sinusoidal exciting current. The exciting current in the nearby case might be flowing in a vertical rod representing the lightning channel. Reference 2 stipulates a generator capable of being swept over the range 100 Hz to 50 Mhz, and a range not less than this is desirable to be sure of covering the whole relevant range including possible resonances.

If phase is measured as well as amplitude it is possible by means of the inverse Fourier transform to compute the time domain response to a current of any known waveform. The measurement of phase is often difficult but if only amplitude information is obtained it may still be possible to make useful calculations, such as the total specific energy of transients.

Such test/analysis methods assume that the response of the system is linear and that the acceptable transient level is known, since low level measurements with extrapolation do not stress the weapon to realistic levels.

MAGNETIC COUPLING, `REALISTIC` TESTS--For magnetic coupling these could be time domain tests where the correct shape of lightning current pulse would be passed down a rod representing the lightning channel and the corresponding transients recorded at selected points in the weapon. For a full theat test the pulse could be the standard lightning current waveform defined for transient assessment (Ground and Sea use) in Reference 1, which has a peak of 200 kA at 9.3 μs. It would probably be more practicable to employ a current waveform of the correct shape at a reduced amplitude so that an extrapolation factor would have to be applied to the resulting transients. This employment of reduced amplitude current would allow the generating equipment to be of lower power but the possibility of there being non-linear effects which might be undetected at lower test levels should be noted (this difficulty of course arises in lightning attachment tests also). If it was considered essential to achieve full-threat stresses in order to include any non-linearities and directly to confirm correct operation of all systems then of course full-threat level of exciting current would have to be employed. This would be necessary for example if the susceptibility levels of the equipments and components in the weapon were not known with certainty. Even when a full-threat test is applied, the limited confidence that can be placed on tests on only one specimen has to be recognised, as mentioned in Reference 3, paragraph 20.

Full-threat tests raise the question of safety and extensive damage and the possible need to provide a blast-proof enclosure for the weapon. It will need to be considered to what extent hazardous elements need to be removed and perhaps replaced with electrically similar dummies. For

example, can any or all of the igniters, detonators, fuzes, explosives and propellant be present? This matter is also mentioned in Paragraph 20 of Ref 3.

MAGNETIC COUPLING TESTS, FURTHER DETAILS--As mentioned, the most realistic way of producing the required magnetic field would be to pass the appropriate current down a vertical rod situated at the required distance. For a pulse test, the generator would be a capacitor charged to a high voltage and then rapidly discharged, as in whole aircraft attachment tests. In order to achieve maximum coupling to the various circuits in the weapon, the weapon would need to be placed in various orientations relative to the rod. Such an open field would present a high inductance to the current generator, and the current obtained for a given capacitance and voltage would be lower than in an attachment test, where it is possible to position return conductors around the test object so that a substantially coaxial system is created with a consequently low inductance. The return conductor from the vertical rod would probably be a metal bar running back from the foot of the rod to the generator; in which case the spreading out of lightning current into the ground would not be simulated.

In a swept frequency test the generator would probably consist of an oscillator and power amplifier.

The voltages and/or currents at selected points in the weapon would be sensed and transmitted to recording equipment in a well screened manner, probably by means of optical links.

ELECTRIC FIELD TESTS--As stated earlier in this paper, it is recommended that conditions should be taken to be $E = 3 \times 10^6$ V/m and $dE/dt = 6 \times 10^{12}$ V/m/s. A possible test, to be carried out in a high-voltage laboratory, could be to apply the field by means of an overhead flat plate connected to a high-voltage capacitor bank charged to a high voltage such as 1 MV from a Cockcroft-Walton dc generator, as sketched in Fig 4(a). The clearance between the plate and the top of the missile would be such as to produce intense corona on the missile. After an interval the rate of change of field would then be achieved by discharging the capacitor at the desired rate. Suitable equipment might be the 1 MV dc generator and 0.0165 μF capacitor stack employed in the attachment point location tests of Reference 10.

If the weapon to be tested is small, it might be possible to employ a similar arrangement to that for the dielectric puncture tests of Appendix C7 of Reference 2, which is based on Ref 10. The arrangement is shown in Fig 4(b), where the test object would be mounted on top of the capacitor stack, which is charged to a maximum of 1 MV from the dc generator. A flat plate is mounted above it, connected to a pulse generator whose output voltage is numerically equal to that of the dc generator but of opposite polarity. Before the pulse generator is triggered, the overhead plate is at ground potential and the test object is subjected to the dc field between the overhead plate and the capacitor stack. When the pulse generator is triggered, the voltage across the gap is doubled, the gap breaks down and discharge takes place; this could be a convenient way of achieving a high field followed by a collapse of field at a high value of dE/dt.

ACKNOWLEDGEMENT

This paper is based on work performed for the UK Ministry of Defence.

REFERENCES

1 NATO/CNAD 'Lightning Environmental Conditions Affecting the Design of Materiel for use by the NATO Forces', Second Draft STANAG 4236 Edition 2, February 1994.

2 NATO/CNAD 'Lightning, Munition Assessment and Test Procedures', Final Draft STANAG 4327, Edition 1, July 1994.

3 NATO/CNAD 'Rationale and Guidance Concerning STANAG 4327', Final Draft Allied Ordnance Publication 25, March 1995.

4 G A M Odam and M Richardson, 'The Rationale of Proposed NATO STANAGS Describing the Lightning Environment for Land, Sea and Air Use and Defining Lightning Assessment Procedures for Munitions and Associated Systems', Williamsburg Conference, September 1995.

5 R H Evans, 'Electromagnetic Environments and Test Methods for the Assessment of Indirect Hazards Due to Lightning Strikes, with Special Reference to Materiel on the Ground Exposed to Nearby Lightning', Tech Note in Preparation, DRA (Farnborough), UK.

6 A Ben Rhouma, A Eybert Berard et al, 'Nearby Lightning Electromagnetic Fields', publication source unknown.

7 P F Little, 'Models for Assessing Hazards Due to Lightning', Paper 5 in Atmospheric Electricity-Aircraft Interaction, AGARD Lecture Series 110, 1980.

8 E D Sunde, 'Earth Conduction Effects in Transmission Systems', New York, Dover Publications, 1968.

9 R A Perala, 'The Effect of Soil Conductivity and Insulation Dielectric Strength Upon Lightning Damage to Buried Insulated Cables', Lightning and Static Electricity Conference, Oxford, UK, 1982.

10 A W Hanson, 'Recent Experimental Work on Lightning Attachment Point Location Tests', Lightning and Static Electricity Conference, Oxford, 1982.

British Crown Copyright 1995/MOD
Published with the permission of the Controller of Her Britannic Majesty's Stationery Office

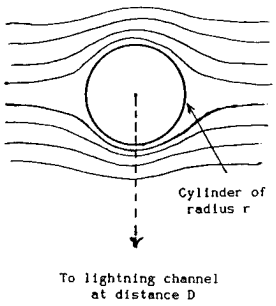



Figure 1 Magnetic Field Coupling to Nearby Lightning Channel

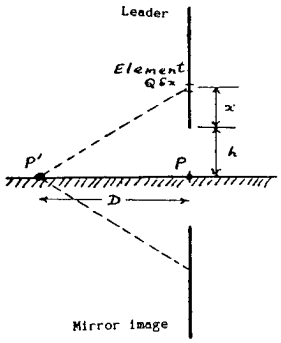
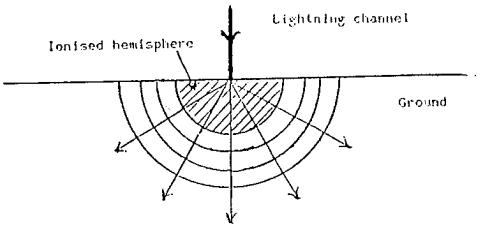
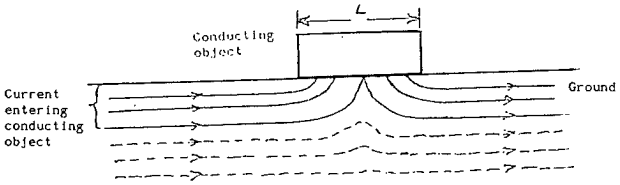



Figure 2 Electric Field Below Leader

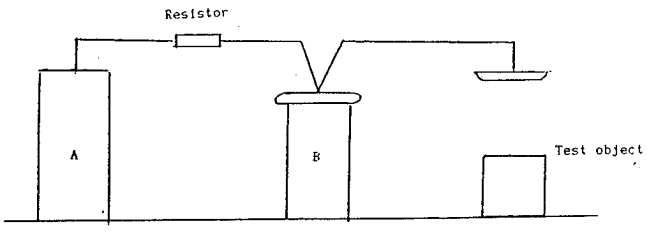



a) Spread of lightning current into the ground

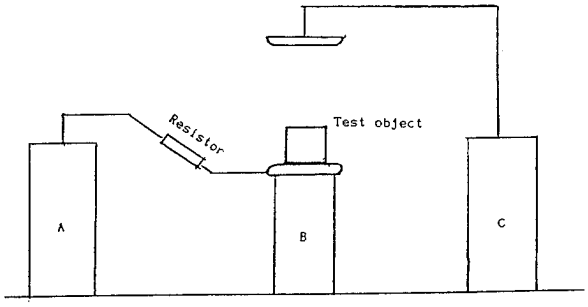



b) Current flow into a conducting object (length L, width W) resting on the ground

Figure 3 Current Flow Patterns Due to Lightning Strike to the Ground




a) Test for large test object




b) Possible test for small test object using generators of opposite polarity

A 1 MV Cockcroft Walton dc generator 0.004 μF

B 1 MV capacitor stack 0.0165 μF

C 9 x 165 kV Goodlet impulse generator 0.0167 μF

Figure 4 Possible Electric Field Tests

# A REVIEW OF PROGRESS ON THE JOINT PROGRAMME ON IMPROVING THE LIGHTNING AND STATIC PROTECTION OF RADOMES

R E Baldwin, C J Hardwick
Lightning Test and Technology, AEA Technology, Culham Science and Engineering Centre, Abingdon, Oxfordshire, OX14 3DB, UK
Telephone: (44)-1235-464278 Facsimile: (44)-1235-464325

J A Plumer
Lightning Technologies, Inc., 10 Downing Parkway, Pittsfield, MA 01201, USA
Telephone: +413-499-2135 Facsimile: +413-499-2503

J-P Clerc
Centre d'Essais Aéronautique de Toulouse(CEAT)/DGA, 23, Avenue Henri Guillaumet, F-31056 Toulouse, Cedex, France
Telephone: (33)-61-58-73-22 Facsimile: (33)-61-48-73-39

## ABSTRACT

The Joint Radome Programme, studying the problems of radome and fairing protection against lightning strikes started in 1993.

The rationale for the programme is reviewed, its aims presented and the status given as well as indications of some the findings. Further experimental work is currently underway to investigate the effects of icing, water and static electricity on diverter strip performance.

## 1 INTRODUCTION

The Joint Programme was formed in February 1993 to investigate and research the effects of lightning and static electricity on aircraft radomes and dielectric fairings. It is financed by a transatlantic consortium of Government Agencies and aerospace companies. The Programme is well under way and it is anticipated that it will be completed in 1996.

Radomes and fairings fitted with their chosen protection scheme are currently type tested to standards set some years ago, such as MIL STD 1757A and RTCA DO160C Section 23. Even though they pass these ground based tests, in some cases in service failures have occurred later. With the advent of wind shear radars it is likely that transmission requirements of radomes will be even higher in future placing further constraints on the amount of lightning protection that can be fitted.

The Joint Programme seeks to establish the difference between the in flight environment and the ground test environment and hence the cause of these in flight failures. This is being achieved by an extensive review of the in flight environment including electric field, icing and rain characteristics, in flight radome failures, dielectric breakdown mechanisms and the electrical characteristics of radome materials. This

review is being supplemented by computer modelling and experimental investigations of the characteristics of sponsor's radome materials and physical mechanisms of sponsor's protection devices and concepts. The information gained will be used to design a series of tests aimed at replicating in the laboratory all recognisable failure modes seen in service.

The final phase of the Programme will make recommendations as to updating of strike attachment test standards and to provide a guide handbook to aid the design of lightning protection of radomes and dielectric fairings. The Programme has been split into various Phases and Tasks and the progress of these will be reviewed.

## 2 THE PARTICIPANTS

Sponsors:-

| | |
|---|---|
| British Aerospace | UK |
| Ministry of Defence | UK |
| Chelton | France |
| CEAT | France |
| DGA | France |
| Northrop/Grumman | USA |
| Marion Composites (formerly Brunswick) | USA |
| Lightning Diversion Systems | USA |
| Dayton Granger | USA |
| Federal Aviation Administration | USA |
| United States Air Force | USA |
| United States Navy | USA |

Culham Lightning Club Members:-

| | |
|---|---|
| British Aerospace | UK |
| CASA | Spain |
| SAAB | Sweden |
| Short Brothers | UK (NI) |
| Civil Aviation Authority | UK |

The following research/test laboratories are participating:-

| | |
|---|---|
| Lightning Technologies Inc., Pittsfield MA | USA |
| AEA Technology Culham | UK |
| CEAT Toulouse | France |

# 3 THE WORK BREAKDOWN

## 3.1 PHASE 1 – ANALYTICAL STUDY OF ELECTRICAL BREAKDOWN PHYSICS & IN-SERVICE EXPERIENCE

- Task 1.1 – Aircraft Electrical Environment Data

**Objective**

To assimilate as much as possible of the available data on electric field conditions preceding and during the initial leader attachment. Data from programmes such as NASA F106, ONERA Transall, FAA CV-580 were studied.

**Results**

There are two scenarios for lightning attachments. Most strikes appear to be triggered by the aircraft itself when the aircraft enters a high field region in a cloud. Fields of about 100kV/m are necessary before leaders originate from the aircraft. For this scenario the rate of increase of field is determined by the aircraft velocity towards the charge centre of the cloud and is very modest.

For aircraft intercepting approaching leaders of a natural strike, the field at the aircraft can increase much more rapidly, being a function of the very fast leader velocity, dv/dt values of $10^8$ to $10^{10}$V/m/s are estimated.

These values are lower than those imposed by Component A of the HV waveform tests of MIL STD 1757A; these specify a voltage ramp of 1MV/μs over a 1m gap giving $\approx 10^{12}$V/m/s. Hence the slower voltage waveform Component D tests might be more appropriate especially if space charge and static electricity accumulation play an important role.

- Task 1.2 – Dielectric Breakdown Physical Data

**Objective**

To assemble pertinent physics of air and solid dielectric breakdown processes to aid understanding of the lightning/static charge interaction with such materials.

**Results**

Much data are available in the literature on air breakdown, however little data exist on specific materials used for radome manufacture which are often composite in nature. Moreover the radome problem is one of mixed dielectrics, viz., solid (or composite layers) radome material and air on either side, and the mechanism of breakdown will be a complex process of the interaction of electric arcs and materials. Therefore some testing has been necessary in Phase 2 to investigate this process.

- Task 1.3 – In Flight Experience Data

**Objective**

To document in-flight lightning and static charge experience of Radomes and other non-conductive components.

**Results**

Many strike records have been assessed and it is apparent that many incidents involve radomes and in about 40% of such cases radomes are damaged. Sometimes the cause of damage is trivial in that either no diverter strips, or solid diverters with too small a cross section have been installed. In the latter case a captured strike can explosively vaporise the strip fracturing the radome.

Nevertheless fractures of radomes with adequate solid strips, and segmented strips have been recorded.

Punctures have occurred on forward parts of the radome away from strip tips but paradoxically at the edges of the strips too. Sometimes segmented strips show no evidence of having gone into conduction, raising the question of what conditions occur when the radome is punctured without strip conduction.

This is one of the items investigated in Phase 2.

- Task 1.4 – Aircraft Surface Environment Data

**Objective**

To characterise the in-flight non-electrical environment such as rain, ice, and boundary layer air flow at the surfaces of non conducting composite components.

**Results**

From a survey of literature it is clear that both ice and water can build up on the radome, their effects are being investigated in Phase 2 of the programme.

- Task 1.5 – Electrostatic Charging Mechanisms and Data

**Objective**

To obtain data on static charging mechanisms and rates for exterior and interior surfaces of non-conducting composites under various flight environmental conditions.

This differs from Task 1.1 in that fields imposed from lightning conditions are excluded.

**Results**

The radome can be charged by both triboelectric effects on the exterior and internal corona. The magnitudes are sufficient to strongly modify the local fields that might be induced due to an external lightning threat at the radome, strip and antenna surfaces.

- Task 1.6 – Prepare Hypotheses and Models to Explain In-Flight Responses

**Objective**

Existing information available from lightning labs will be combined with test data generated under this programme to form hypotheses and models.

**Results**

Several important factors have been noted above which need further investigation. The temporal variation of the electric fields and the presence or otherwise of anti static paint, water and ice on the radome surface will affect the magnitude of charge that can build up modifying the local fields which may influence the development of arcs in the vicinity of the radome. Phase 2 investigates these factors.

## 3.2 PHASE 2 – EXPERIMENTAL EXAMINATION OF INTERACTION AND FAILURE MECHANISMS

Task 2.1 – Materials Electrical Properties Tests

**Objective**

To determine the electrical breakdown and surface flashover properties of composite materials used in aircraft non-conductive skins under flight environments.

**Results**

Radome manufacturers have provided sets of panels for assessing comparative dielectric strengths and relaxation times of various materials used in radome manufacture. New and moisture conditioned samples are available and materials have included quartz, glass, and Kevlar. The tests have to date not assessed the intrinsic dielectric strength, but surface flashover vs. breakdown as it is believed that this is a more important criterion (see 1.2). In general the breakdown is caused by the very high field strength present in the leader tips flashing over the surface and when this occurs

there is little difference between different materials. However some materials prove to be very weak dielectrics and were punctured before the surface flashover could begin.

- Task 2.2 – Examine Mechanisms of Protection Devices

**Objective**

To understand the protection mechanisms of protective devices that can be used on non-conducting composites, whilst retaining an acceptable degree of EM transparency. Devices include solid metal strips, segmented strips, dielectric films and anti static paint.

**Results**

While segmented strips are known to generally work well no study of the initiation of conduction mechanism under high voltage conditions or arc lift off under high current conditions ensuring survival of the strip have been made. This task has investigated both of these aspects with a variety of fast imaging techniques. The initiation of conduction appears to occur very early in the leader phase and after conduction is initiated, only small currents are necessary before the arc dissociates from the segments and lifts away.

Investigations of the modification of performance of the devices by ice and water is now under way.

- Task 2.3 – Continued Development of Computer Models

**Objective**

To use 2D modelling to gain an insight into the problem.

**Results**

It became apparent very quickly that simple electrogeometric models of the operation of protection are not valid; the puncture of the radome is very much associated with a dynamic development of electric fields and impinging arcs. Nevertheless simple 2D modelling allowed the significance of charge build up on external and internal surfaces to be quantified as well as the effect of dielectric on the field lines explaining some features of radome punctures noted in tests or flight (highest field in the dielectric is under the strip, field direction is generally parallel to the surface allowing tracking internal to the structure).

- Task 2.4 – Experimental Evaluation of Failure Modes

**Objective**

To replicate in the lab in flight punctures that have occurred due to both lightning and static.

**Results**

This phase is ongoing, in particular studies of the effects of anti static paint, water and ice on diverter strip performance are being undertaken.

The remainder of the programme will be undertaken after the completion of Phase 2.

3.3 PHASE 3 – FORMULATE IMPROVED TEST METHODS

- Task 3.1 – Formulate Improved Lightning and Static Charge Test Methods

Expected to include, electric field conditions and electrode configuration, environmental conditions, type of diagnostics.

- Task 3.2 – Demonstration Tests

Demonstration tests will be conducted to show the effectiveness of the improved methods proposed.

3.4 PHASE 4 – FORMULATE IMPROVED PROTECTION DESIGN METHODS

- Task 4.1 – Improved Protection Designs

Evaluate all the proposed improvements, in preparation for inclusion in the design guide and decide on any final tests required.

- Task 4.2 – Conduct Protection Method Evaluations

Carry out any final tests required from Task 4.1.

- Task 4.3 – Prepare Protection Design Handbook
- Task 4.4 – Review and Approval of Protection Design Handbook
- Task 4.5 – Print and Issue Protection Design Handbook

3.5 PHASE 5 – USER EVALUATIONS

- Task 5.1 – Tryout Laboratory Selection

At least one Laboratory in the US and one in Europe will be invited to try out the improved methods.

- Task 5.2 – Test Specimen Selection and Test Planning
- Task 5.3 – Tryout Tests

## 4 CONCLUSION

Failure mechanisms have been investigated, inflight data has been gathered, and materials characterised. Experimental programmes are being undertaken to establish the importance of anti static paint, icing and water on the radome surface. The programme is approaching the final phases in which the output from all tasks will be combined to give design information to the participants.

# COMPARISON OF ELECTRIC CURRENT DATA FROM THE FAA RESEARCH ELECTROMAGNETIC DATABASE WITH THE PROPOSED ENVIRONMENT STANDARD

Rosemarie L. McDowall
Galaxy Scientific Corporation
5906 Vine Drive
Mays Landing, New Jersey 08330
Telephone (609) 625-2360 FAX (609) 485-4005

Michael S. Glynn
FAA Technical Center
Atlantic City International Airport, New Jersey 08405
Telephone (609) 485-4138 FAX (609) 485-4005

## ABSTRACT

Airborne current measurements made under the Direct Strike Lightning (DSL) Characterization Program and the National Aeronautics and Space Administration (NASA) Langley Research Center Storm Hazards Program are compared with the environment proposed by the Society of Automotive Engineers (SAE) and the European Organization for Civil Aviation Equipment (EUROCAE). The data supporting the proposed environment were collected by ground-based sensors and are presented in "Aircraft External Lightning Environment and Test Waveform Standard" (hence forward referred to as the Environment and Test Standard).

There are only two categories in which the CV-580 data in the Federal Aviation Administration (FAA) Research Electromagnetic Database (FRED) support the ground-based data: the high end of the Charge Transfer for negative strokes and the low end of the Time to Peak.

An additional review of the actual waveforms in FRED needs to be conducted to verify that the Integration Start and Stop points are being correctly chosen. This verification would indicate that the values in the Environment and Test Standard may need to be reviewed and changed.

## INTRODUCTION

FRED contains data from the DSL Program during which a Convair 580 aircraft was flown into and around thunderstorms in Florida to collect lightning strike data. FRED also contains data from the NASA Storm Hazards Program during which an F-106 aircraft was flown into and around thunderstorms in the mid-Atlantic coast states to collect data on lightning strikes near the aircraft.

Both of these programs recorded analog and digital data from electric and magnetic field sensors as well as current sensors on the aircraft. This paper will only discuss the lightning current data.

## CV-580 DATA

During the summers of 1984, 1985, and 1987, an instrumented Convair 580 aircraft was flown into and around thunderstorms in Florida. The aircraft was instrumented with sensors which recorded lightning currents on the aircraft in addition to magnetic and electric fields induced by the lightning current (1). Analog data was recorded continuously on a Honeywell 101 analog recorder. A trigger channel served to pinpoint strikes on the tape. Digital data was digitized on a Tektronix 7612 digitizer and then stored on magnetic tape or floppy disk. There were 48 strikes recorded, providing 1248 analog and 126 digital waveforms.

The analog data was digitized by Electro Magnetic Applications, Incorporated (EMA) (2, 3). The analog records in FRED span 1 second of time with 100 ms of pretrigger data.

The digital data was also processed by EMA for entry into FRED. The digital records in FRED span 10.2 μs of time.

## F-106 DATA

During the summers of 1980 through 1986, an instrumented F-106 aircraft was flown through thunderstorms in Virginia. The aircraft was instrumented with sensors which recorded currents on the aircraft in addition to magnetic and electric fields (4, 5, 6, 7, 8). Analog data was recorded on a Honeywell 101 analog recorder. Digital data was collected with a Biomation or a LeCroy digitizer and recorded on the analog recorder.

Although both analog and digital measurements were made in the F-106 flights, only the digital data were available for entry into FRED. NASA processed the digital data from the analog tapes and then created digital tapes of digital data. However, these original NASA tapes were not available. As a result, the digital data had to be reread from the analog tapes.

The age of the analog tapes drastically affected the ability to retrieve the data. Oxide was shed from the older tapes every time they were handled or read, causing incomplete waveform data.

## ENVIRONMENT AND TEST STANDARD

EUROCAE Working Group 31 and the SAE AE-4L Committee are in the process of preparing a document entitled "Aircraft Lightning Environment and Test Waveform Standard" (9). This document presents lightning strike data collected on the ground by various researchers. It is the intent of this standard to present the natural lightning strike environment and then to determine an acceptable lightning environment to which aircraft will be tested during the certification process.

## COMPARISON OF DATA

Table 1 compares subsets of the FRED data with information contained in the draft standard proposed by EUROCAE and SAE AE-4L. The CV-580 data have been divided into analog (48 flashes) and digital (9 flashes) data. The F-106 data consists of 43 flashes. The digital waveforms (both the CV-580 and the F-106) contain less data and the durations are considerably less than the analog waveforms.

TABLE 1. COMPARISON OF FRED CURRENT DATA WITH THE DRAFT ENVIRONMENT AND TEST STANDARD

| | | Environment and Test Standard | | CV-580 Analog | CV-580 Digital | F-106 |
|---|---|---|---|---|---|---|
| | | Negative | Positive | | | |
| Peak Current (A) | Low | $1.4 \times 10^{4}$ | $4.6 \times 10^{3}$ | $2.50 \times 10^{2}$ | $1.56 \times 10^{3}$ | $1.57 \times 10^{-2}$ |
| | Typical | $3.0 \times 10^{4}$ | $3.5 \times 10^{4}$ | $1.50 \times 10^{3}$ | $2.54 \times 10^{3}$ | $1.06 \times 10^{-1}$ |
| | High | $8.0 \times 10^{4}$ | $2.5 \times 10^{5}$ | $2.23 \times 10^{4}$ | $1.13 \times 10^{4}$ | $2.44 \times 10^{4}$ |
| Peak Rate of Rise (A/s) | Low | $5.5 \times 10^{9}$ | $2.0 \times 10^{8}$ | $4.97 \times 10^{8}$ | $<5.9 \times 10^{10}$ | $2.4 \times 10^{6}$ |
| | Typical | $1.2 \times 10^{10}$ | $2.4 \times 10^{9}$ | $9.10 \times 10^{8}$ | $1.37 \times 10^{11}$ | $1.76 \times 10^{7}$ |
| | High | $3.2 \times 10^{10}$ | $3.2 \times 10^{10}$ | $5.64 \times 10^{10}$ | $>5.5 \times 10^{11}$ | $3.47 \times 10^{12}$ |
| Time to Peak (ns) | Low | $1.8 \times 10^{3}$ | $3.5 \times 10^{3}$ | $1.7 \times 10^{3}$ | <10 | 10 |
| | Typical | $5.5 \times 10^{3}$ | $2.2 \times 10^{4}$ | $1.55 \times 10^{4}$ | 140 | 120 |
| | High | $1.8 \times 10^{4}$ | $2.0 \times 10^{5}$ | $4.26 \times 10^{6}$ | >265 | $8.99 \times 10^{4}$ |
| Time to Half Value (ns) | Low | $3.0 \times 10^{4}$ | $2.5 \times 10^{4}$ | $1.15 \times 10^{3}$ | <5 | $2.64 \times 10^{4}$ |
| | Typical | $7.5 \times 10^{4}$ | $2.3 \times 10^{5}$ | $1.15 \times 10^{4}$ | 20 | 40 |
| | High | $2.0 \times 10^{5}$ | $2.0 \times 10^{6}$ | $1.73 \times 10^{6}$ | >140 | 5.38 |
| Charge (Coulomb) | Low | 1.3 | 10 | $1.49 \times 10^{-3}$ | $1.24 \times 10^{-5}$ | $7.43 \times 10^{-9}$ |
| | Typical | 7.5 | 80 | 3.16 | $9.71 \times 10^{-5}$ | $1.78 \times 10^{-6}$ |
| | High | 40 | 350 | 42.3 | $2.97 \times 10^{-3}$ | $2.05 \times 10^{-1}$ |
| Action Integral ($A^2s$) | Low | $6.0 \times 10^{3}$ | $2.5 \times 10^{4}$ | $2.91 \times 10^{5}$ | $2.76 \times 10^{-3}$ | $9.64 \times 10^{-10}$ |
| | Typical | $5.5 \times 10^{4}$ | $6.5 \times 10^{5}$ | $3.87 \times 10^{5}$ | .85 | $8.63 \times 10^{-6}$ |
| | High | $5.5 \times 10^{5}$ | $1.5 \times 10^{7}$ | $3.72 \times 10^{6}$ | 23.9 | $3.56 \times 10^{2}$ |

Five percent of the values in each data set are below the "Low" value, 50 percent are below the "Typical" value, and 95 percent are below the "High" value. Five percent of the CV-580 analog data is 2.4 flashes. Five percent of the CV-580 digital data is 0.45 flashes. Five percent of the F-106 data is 2.15 flashes.

The following assumptions were made in generating the data in table 1.

a. This table contains the Peak Current and Peak Rate of Rise values from the first stroke for negative strikes from the Environment and Test Standard.

b. The waveforms selected from FRED for the Time to Peak and Time to Half Max were the waveforms used in determining the Peak Current.

c. This table contains the Time to Peak from the first stroke for negative strikes from the Environment and Test Standard.

d. This table uses the Charge in Flash for the Charge Transfer for negative strikes from the Environment and Test Standard.

e. This table uses the Total Charge for the Charge Transfer for positive strikes from the Environment and Test Standard.

## DISCUSSION

All of the Peak Current values in FRED are below the Typical values of either negative or positive strikes in the Environment and Test Standard. Peak values in FRED are defined to be the point of a waveform with the greatest absolute value. These values in FRED, therefore, should not have been affected by computational errors.

The Peak Rate of Rise in FRED is the maximum instantaneous rate of rise. In other words, it is the greatest value of the derivative of the waveform taken between adjacent points. The mathematical definition of the Peak Rate of Rise is not given in the Environment and Test Standard. As a result, it may not be proper to compare the FRED data with the Environment and Test Standard for this parameter. It is interesting to note that the digital data in FRED shows much higher values for this parameter than would be expected. The analog data is, for the most part, lower than the data given in the Environment and Test Standard, although the High value for the CV-580 analog is almost twice the High value of either the Negative or Positive Environment and Test Standard data.

The Time to Peak, Time to Half Value, Charge, and Action Integral values in FRED are all calculated values. They are based on the Integration Start and Stop points which are calculated when the data is converted and entered into FRED. A computer algorithm was devised for determining these points. The algorithm is presented in the FRED Users Manual (10). Any error in this algorithm will produce errors of differing magnitudes in the derived parameters.

The Time to Peak, Time to Half Value, Charge, and Action Integral values for the digital data will not be compared with the Environment and Test Standard data since the digital waveforms are of such short duration. They are included in the table for completeness.

The Time to Peak for the Low value of the CV-580 data is essentially the same as the Environment and Test Standard Negative data. However, the remaining CV-580 data

is significantly higher than the Negative data and higher than the High value of the Positive data.

The span of data for the Time to Half Value in the CV-580 is two orders of magnitude greater than the span of data for the Negative Environment and Test Standard data. The Low value of the CV-580 is an order of magnitude lower than the Negative Environment and Test Standard data and the High value is an order of magnitude higher. The High value of the CV-580 is comparable to the High value of the Positive Environment and Test Standard data. However, the rest of the values are at least an order of magnitude lower.

The High value for Charge Transfer is comparable in the CV-580 analog and Negative Environment and Test Standard data. However, the remaining values are significantly lower. All of the CV-580 data values are lower than the Positive Environment and Test Standard data.

The span of Action Integral values for the Negative Environment and Test Standard data is two orders of magnitude. The span for the Positive Environment and Test Standard data is three orders of magnitude. While the span for the CV-580 data is only one order of magnitude. The High value of the CV-580 data is between the High values for the Negative and Positive Environment and Test Standard data. The Typical value of the CV-580 data is between the Typical values for the Negative and Positive Environment and Test Standard data, although it is much closer to the Positive. However, the Low value of the CV-580 data is an order of magnitude greater than the Low value for the Positive Environment and Test Standard data and two orders of magnitude greater than the Low value for the Negative Environment and Test Standard data.

## CONCLUSIONS

There are only two categories in which the CV-580 FRED data support the ground-based data: the high end of the Charge Transfer for negative strokes and the low end of the Time to Peak.

An additional review of the actual waveforms in FRED needs to be conducted to verify that the Integration Start and Stop points are being correctly chosen. This verification would indicate that the values in the Environment and Test Standard may need to be reviewed and changed. Given that a significant body of airborne data is now available, technical committees may need to rethink their reliance on ground-based data for certification of aircraft.

## REFERENCES

1. Rodney A. Perala, "A Program Plan for In-Flight Characterization of Cloud to Ground Lightning Strikes to Aircraft," EMA-84-R-14, February 1984.

2. J. R. Elliott and H.S. Weigel, "Digitization of CV-580 In-Flight Lightning Strike Data: Analog Data from 1984, 1985, and 1987," EMA-90-R-35, May 1990.

3. James R. Elliott and Poh H. Ng, "CV-580 Digital Data Processing for FRED Input: 1985 and 1987," EMA-91-R-38, September 1991.

4. Mitchell E. Thomas, "1983 Direct Strike Lightning Data," NASA-86426, August 1985.

5. Mitchell E. Thomas and Harold K. Carney, "1984 Direct Strike Lightning Data," NASA-97690, September 1986.

6. Mitchell E. Thomas and Felix L. Pitts, "1982 Direct Strike Lightning Data," NASA-84626, March 1983.

7. Klaus P. Zaepfel and Harold K. Carney, "1985 and 1986 Direct Strike Lightning Data," NASA Technical Memorandum 100533, Part 1, March 1988.

8. Klaus P. Zaepfel and Harold K. Carney, "1985 and 1986 Direct Strike Lightning Data," NASA Technical Memorandum 100533, Part 2, March 1988.

9. EUROCAE WG-31, "Draft Aircraft Lightning Environment and Test Waveform Standard," to be published.

10. DOT/FAA/AR-95/18, "Users Manual for the FAA Research and Development Electromagnetic Database (FRED) for Windows," FAA Technical Center, July 1995.

BIBLIOGRAPHY

Fisher, Bruce D. et al., "Final Results of the NASA Storm Hazards Program," 1988 International Aerospace and Ground Conference on Lightning and Static Electricity, April 1988, Oklahoma City, OK.

Ng, Poh H. and James R. Elliott, "F-106 Digital Data Processing for FRED Input: 1985 and 1986," EMA-92-R-16, January 1992.

Ng, Poh H. and James R. Elliott, "F-106 Digital Data Processing for FRED Input: 1982," EMA-92-R-22, March 1992.

# SESSION 02B
# POWER/COMMUNICATION DISTRIBUTION
# CHAIRPERSON: STANISLAW GRZYBOWSKI

# VISUALISING THE CORRELATION BETWEEN TELECOMMUNICATION FAULTS AND LIGHTNING ACTIVITY

Andrew Grace, Mike Bostock-Smith

BT Laboratories, Martlesham Heath,
Ipswich, Suffolk, IP5 7RE, UK

**ABSTRACT**

*Data visualisation techniques provide a powerful, yet simple way to extract valuable knowledge hidden within vast quantities of technical data. BT, the UK based telecommunications carrier, monitors its network 24 hours a day, 365 days a year, to improve customer service. Every day vast quantities of fault data is collected. For the past six years BT has also monitored all lightning activity recorded by the UK lightning mapping system.*

*In this paper we describe how lightning mapping data and large volumes of fault data is transformed by BT into valuable knowledge of lightning caused network 'hotspots' using suitable data visualisation and correlation techniques. These data visualisation techniques are now being used to measure the results of improvement programmes undertaken to improve the quality of service offered to BT customers through increased protection from the effects of lighting activity.*

## 1. Introduction

Within a telecommunications network, lightning activity can adversely affect the quality of service provided to customers. At one extreme, equipment can be destroyed as a result of direct lightning damage. More frequently, transient interruptions to service can be introduced into equipment or cables as a result of induced lightning activity.

Vast quantities of fault data is available from telecommunications network monitoring systems. Lightning activity data is also available from lightning mapping systems. In order to correlate the occurrence of lightning activity with network fault rates, it is first necessary to identify a suitable data analysis technique that is capable of handling the giga-byte quantities of data that need to be studied.

In this paper we describe the use of data visualisation techniques to correlate lightning activity with telecommunication network faults and hence quantify the impact of lightning activity upon the quality of service provided to customers.

In Section 2, we describe the effects that lightning activity can have upon a telecommunications network. In Section 3, we describe the lightning flash locator system that provides a record of lightning activity within the UK. In Section 4, the rational of using data visualisation techniques is presented. In Section 5, the visualisation techniques used to correlate lightning activity with fault data are introduced, together with two examples of the results obtained using these techniques. In Section 6, the application of these techniques to the quality improvement process is described.

## 2. Lightning effects upon telecommunications networks

It is well known that lightning activity and metallic conductors do not mix. Despite the massive investments made by BT in installing optical fibre into its core network, the vast majority of BT's customers are connected to their local telephone exchange by means of copper cables. These metallic conductors tend to act as an effective antenna during periods of lightning activity. As shown in Figure 1, on top of the effects of lightning activity introduced via the telecommunications network, the power supply to network equipment also provides a potential entry point for the effects of lightning activity.

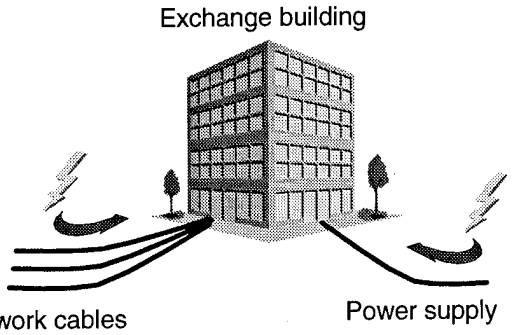



Figure 1. Points of entry for lightning activity into telecommunications networks.

Considerable effort and cost is already expended to protect BT's customers from the effects of lightning activity. Every new telephone line installed in the UK by BT contains a gas discharge device to protect the equipment connected to the network by customers. Dedicated data lines are also similarly protected with gas discharge devices. In addition to these 'business as usual' measures, during 1994 at least two million pounds was invested by BT in specific programmes to reduce the affect of lightning activity in areas where a lightning related weakness had been identified [1].

When the effects of lightning activity do enter the telecommunications network, a wide range of potential consequences can arise. At worst, cables and equipment are destroyed by direct lightning strike hits. In this case, service to the customer is lost and can only be restored by replacing the damaged component. Frequently, whilst no physical damage occurs, binary data errors are induced into data streams, as shown in Figure 2, which can produce synchronisation or signalling failures within switching units. In this case, service to the customer is temporarily lost but it automatically returns a short time later as the electromagnetic coupling effects of a lightning strike subside.

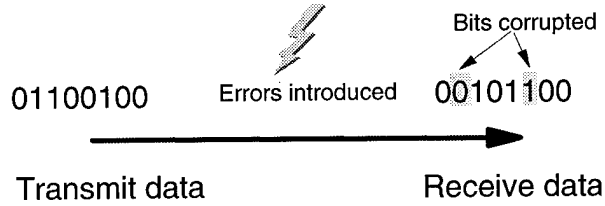



Figure 2. Digital transmission errors caused by lightning activity

As lightning does have an impact upon the Quality of Service offered by a telecommunications operator, it is therefore important to measure the overall impact of lightning activity upon their services and to then make decisions that will reduce or eliminate this impact. When faults occur as a result of a direct lightning strike hit, there is usually some physical evidence, such as heating or burn marks, which makes it possible to quantify the impact of lightning activity upon the destruction of equipment or cables. However, where there are no physical signs of damage, it is no longer possible to determine and quantify the link between

lightning activity and faults, be they long duration or transient in nature, by visual inspection of susceptible components.

BT monitors its network 24 hours a day, 365 days a year, to measure and to help improve the Quality of Service provided to its customers. The network monitoring systems provides data on the time and location of faults occurring throughout the BT network. With a network that serves in excess of 25 million customers in the UK, there is a massive quantity of fault data available for analysis. This data forms the starting point for quantifying the impact of lightning activity upon customer service.

## 3. UK lightning mapping service

Within the UK, data on the occurrence of lightning activity is available as a commercial service from a company called EA Technology. EA Technology have developed and installed a Lightning Flash Location System (LFLS) which provides a national service covering the whole of the UK [2]. This system was initially developed to provide the electricity supply industry with early warning of approaching storms and to assist with the identification of electricity outages caused by lightning strikes.

The LFLS uses radio direction finding techniques to locate individual lightning strikes and a national standard clock to record the time of their occurrence. As damage to the electricity distribution network is caused by cloud-to-ground strikes, the system discriminates between cloud-to-cloud strikes and cloud-to-ground strikes. At the frequencies used for direction finding, the radiation from a lightning strike propagates as two waves - the vertically polarised 'ground wave' and the horizontally polarised 'ground wave'. By choosing an extra low frequency of 1.1 kHz with a bandwidth of 350 Hz, only the 'ground waves' propagate the large distances to the LFLS direction finding aerials located across the British Isles. The position of the DF aerials are shown in Figure 3.




Figure 3. Position of Lightning Flash Location System direction finding aerials

For each lightning strike recorded by the LFLS, the following data is provided:

- position - latitude and longitude, and easting and northing grid references
- accuracy - quoted in terms of an error radius
- time - with milli-second resolution
- strength indicator

Using the data recorded by the LFLS it is possible to locate and track the movement of lightning activity across the UK, 24 hours a day, 365 days a year. The location of each lightning strike can be plotted on a map together with details of its strike time and location accuracy.

BT has taken the LFLS service since 1988. Initially the use of the service was evaluated with data supplied on an elapsed time basis via computer tape. Currently BT takes a 'live' feed from the LFLS and lightning strike data is displayed in real-time on a computer screen at BT Laboratories. In addition to the real-time display of lightning activity, all lightning strike data is loaded into a database for subsequent analysis. Over the past seven years at least 15 million lightning strikes have been logged into the BT lightning strike database.

## 4. Data visualisation

As described in the previous sections, data on both telecommunication network faults and lightning activity is available. The overriding problem with quantifying the link between lightning activity and faults is the sheer volume of data that needs to be analysed before any conclusions can be drawn. As shown in Figure 4, the main requirement of any suitable data analysis technique is to transform the mass of available data into valuable information from which knowledge can be determined [3].

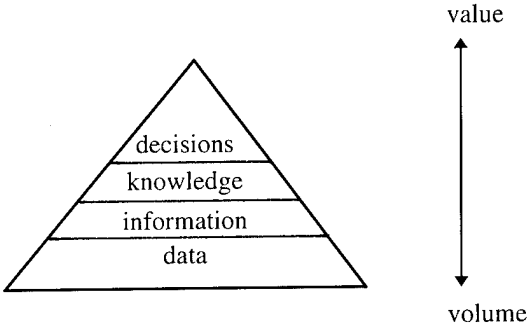



Figure 4. From volume to value.

Visualisation techniques are ideally suited to the analysis of the vast quantities of fault and lightning data [4]. These techniques make extensive use of computer graphics and increasing computer processing power to present vast quantities of data as a visual image. A visual image depicting lightning or fault activity can then provide a concise summary of the original data set. This visual summary provides the information from which knowledge of the correlation between lightning and faults can be determined.

## 5. Techniques for lightning and fault correlation

Visualisation techniques have been successfully used by BT to understand and quantify the impact of lightning activity upon faults. There are two data visualisation techniques used to analyse and correlate lightning strike data and fault data. The first type of analysis is used to understand the general impact of lightning activity across an entire network. The second type of analysis goes into much greater depth and provides specific knowledge as to the impact of lightning activity upon the behaviour of an individual item of equipment.

## 5.1 Visualisation of general lightning related fault trends

The technique used to show the general correlation between lightning activity and fault activity is based upon mapping, then comparing the location of lightning activity and fault activity. The passage of a thunderstorm is split into a sequence of time frames. For each time frame, the location of lightning strikes recorded by the LFLS are plotted onto a map. Also for each time frame, the location of faults recorded by the network monitoring system are plotted onto a separate map. When plotting the location of transient network faults, it is useful to suppress some types of faults that could mask the faults that might be correlated with lightning activity. This is achieved by applying a filtering algorithm to the original fault data set.

Figure 5 shows a number of one hour frames taken at two hour intervals from a sequence of lightning activity passing across the UK on one day during the summer of 1994

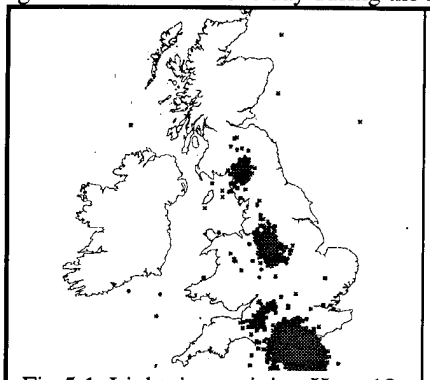


Fig 5.1. Lightning activity. Hour 18.

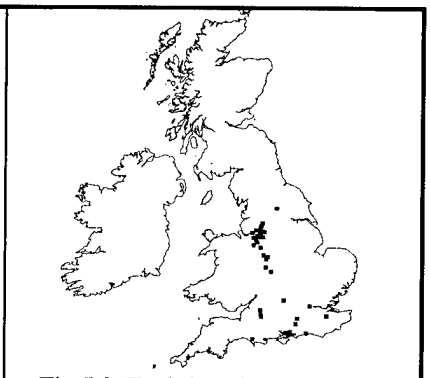


Fig 5.2. Fault locations. Hour 18

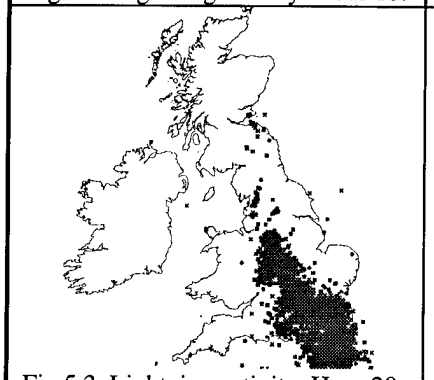


Fig 5.3. Lightning activity. Hour 20.

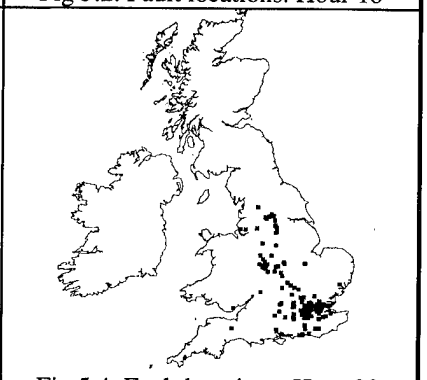


Fig 5.4. Fault locations. Hour 20

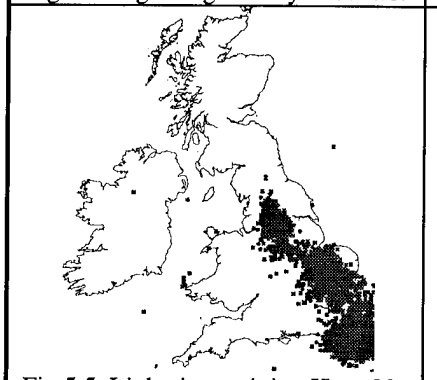


Fig 5.5. Lightning activity. Hour 22.

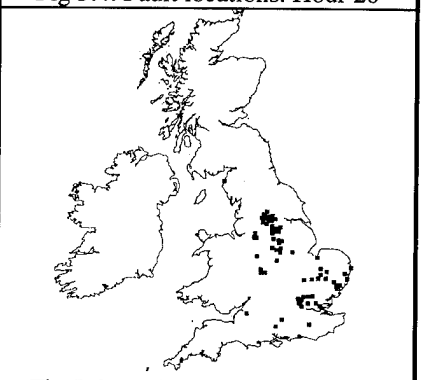


Fig 5.6. Fault locations. Hour 22.

For each frame, the location of lightning activity and faults has been mapped. A two stage filter was used with this data set to suppress faults lasting longer than two minutes and faults reported by equipment with an abnormally high fault report rate.

In Figures 5.1, 5.3 and 5.5, lightning activity can be seen to track from west to east across the UK. In Figures 5.2, 5.4 and 5.6, the location of faults can be seen to broadly fall within the footprint of the lightning activity. To provide a contrast to the sequence seen in Figure 5, Figure 6 shows a frame from earlier in the same day when, in the absence of lightning activity across the UK, no faults were recorded.

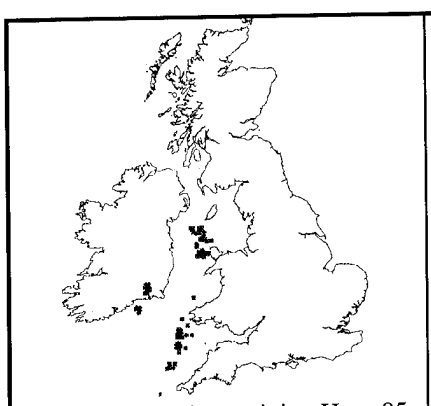


Fig 6.1. Lightning activity. Hour 05



Fig 6.2. Fault locations. Hour 05

## 5.2 Visualisation of specific lightning related faults

Having identified the general correlation between lightning activity and faults, it is also possible to study the fault history of an individual item of equipment to test for a specific correlation between the behaviour of that equipment and the occurrence of lightning activity. If a correlation does exist, it is then straightforward to identify the individual lightning strikes that were responsible for a series of faults reported by an item of equipment.

To test for a correlation between lightning activity and the fault history of an item of equipment, the number of instances where both a fault and a lightning strike were recorded simultaneously is calculated. To allow for potential, yet unknown timing differences between the fault and lightning strike timestamps, this test is repeated using a range of possible time-shift values so as to compensate for any potential clock synchronisation problem. The results obtained for a particular item of equipment being studied and a range of time-shift values are visualised as shown in Figure 7. If a correlation does exist, the resulting plot should contain a 'peak' at the point where clocks have effectively been re-synchronised, quite distinct from the 'noise' produced by random matches achieved using other time-shifts.

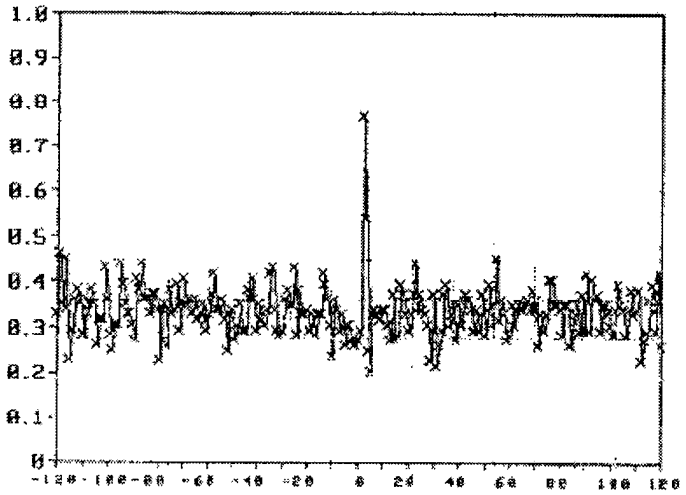



Figure 7. Correlation between lightning activity and an equipment fault history.
Y axis shows % match between lightning and faults. X axis shows time shift in seconds.

Using this visualisation technique, a correlation between a history of faults reported by an item of equipment and lightning activity can be proved. From all the lightning activity reported on a single day, shown in Figure 8.1, those lightning strikes that correlate with an equipment fault history can be identified. Figure 8.2 shows the actual location of those lightning strikes that caused the item of equipment under study to report a number of transient faults.

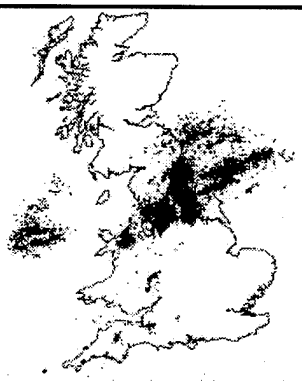


Figure 8.1. All lightning activity during 24 hour period



Figure 8.2. Lightning activity correlated fault during 24 hour period.

## 6. Quality improvement process

A telecommunications network operator needs to understand the behaviour of their networks in order to guarantee and improve the quality of service provided to their customers. Within BT, data from the LFLS and from network monitoring systems is studied using the visualisation techniques described in this paper. The conclusions drawn from applying these techniques are fed into the quality improvement process as shown in Figure 9.

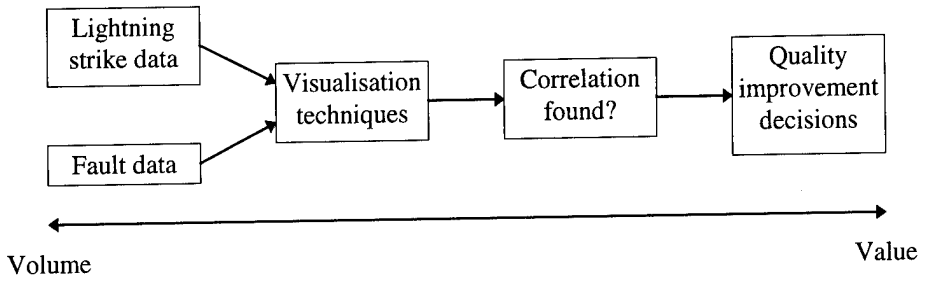



Figure 9. Visualisation input to the quality improvement process.

Where a lightning related quality weakness has been identified in the network, remedial activities can be initiated to improve the situation. Additional physical lightning protection can be applied to equipment, or earthing arrangements can be improved. Interestingly, for data communications, software can be altered to provide additional resilience to the effects of lightning. Communication protocols can be modified to reduce the impact of transient data corruption cause by lightning activity.

Having embarked upon a program of remedial work to correct a problem caused by lightning activity, after the work has been completed, these same visualisation techniques can be used to measure the success of the program. In this way it is possible to provide a feedback loop to the quality improvement process by being able to quantify a reduction in the impact of lightning activity upon fault rates.

# 7. Conclusion

In this paper we have shown how data visualisation techniques can be used to demonstrate a correlation between faults within a telecommunications network and lighting activity. Such techniques have been shown here to be capable of producing a visual summary of the vast quantities of data that need to be studied. Once a correlation has been identified, it is then possible to quantify the true impact of lighting activity upon telecommunication network fault rates.

In Section 5.1, we provided an example of a clear correlation between lightning activity and faults recorded on one day during the Summer of 1994. In Section 5.2, we provided an example of a clear correlation between lightning activity and the fault history of one specific item of equipment. These two examples demonstrate that data visualisation techniques allow a telecommunications network operator to quantify the impact of lightning activity upon the behaviour of their networks.

By using these data visualisation techniques, we have shown how value can be added to lighting mapping data within the telecommunications environment as part of the on-going process of improving the quality of service delivered to customers.

# 8. Acknowledgements

The authors wish to acknowledge the assistance given by their colleagues within BT who have provided the fault data visualised in this paper. The data from the UK lightning flash locator system was provided by EA Technology.

# 9. References


[1] Quality of Service report. April-September 1994. British Telecommunications PLC.

[2] Lightning Flash Location System. Product data sheet. EA Technology, Capenhurst, Chester, UK.

[3] Data mining applications in BT. R Shortland, R Scarfe. BT Technology Journal. October 1994.

[4] Visualisation of telecommunications network data. G R Walker, et al. BT Technology Journal. October 1993.

# LIGHTNING MEASUREMENT SYSTEM USING REMOTE CONTROL BY TELEPHONE LINE AND ELECTRIC FIELD OBSERVATIONS OF LIGHTNING IN WINTER

Atsushi Wada  Takatoshi Shindo
Central Research Institute of Electric Power Industry
Komae-shi, Tokyo 201 JAPAN
TEL(81-3)3480-2111  FAX(81-3)3488-6697

Abstract

In order to clarify the characteristics of lightning in winter, it is necessary to study not only striking events but also lightning physics in the thundercloud. It is expected that the characteristics of lightning will be clarified in more detail by simultaneous electromagnetic field measurement using several kinds of antennas.

In this paper, some results of electric field measurement using a remote control system are described and the characteristics of lightning in winter are discussed.

## 1. Introduction

Double-circuit faults of power transmission lines often occur in the coastal area of the sea of Japan in winter. The occurrence rate is larger than the value predicted by a prevailing calculation method based on the A-W theory. These faults cause a major problem because there are power plants of large capacity and will be constructed more in near future. One of the causes of such faults is thought to be the unusual characteristics of thunderclouds in winter of which altitude is low in comparison with that in summer. But the physical mechanism of the faults is still unclear.

In order to clarify the characteristics of lightning in winter, it is necessary to study not only striking events but also lightning physics in the thunderclouds. It is expected that the characteristics of lightning will be clarified in more detail by the simultaneous measurement of electromagnetic field by several kinds of antennas with the measurement of lightning current.

CRIEPI has been measuring the electromagnetic field by an automatic measuring system. But there sometimes were some troubles of data acquisition such as recording memory was overflown, and so on. To avoid these troubles and collect data effectively, we have developed a new measuring system.

The new system described in this paper enables us to check whether such troubles occur or not by using a telephone line. It is also possible to control a digital oscilloscope from a remote control site and to transfer a large amount of data using a telephone line from each measuring site to the control site.

By this system, the electric field and the electromagnetic field change have been measured with several kinds of antennas as follows. (1) a field mill network, (2) a slow antenna network, (3) a fast antenna, (4) a UHF antenna system.

In this paper, the new lightning measurement system is described, and some observation results of electric field change are presented. The characteristics of lightning in winter are discussed.

## 2. Remote control measurement system using a telephone line

### 2.1 Measurement system

The block diagram of the new measurement system is shown in Fig. 1. The characteristics of the system is summarized in Table 1. The measurement site consists of these components. (1) Lightning sensor ( for example, an antenna for measurement of electromagnetic field change ) (2) Digital oscilloscope (3) Computer (4) MO disk (5) Modem (6) GPS clock. The control site consists of these components. (1) Computer (2) Modem (3) Printer (4) MO disk.

The operation of the system is as follows.

(1) Recording of data

The data which is recorded in the digital oscilloscope is transferred to a MO disk automatically. The transfer time is 20 seconds in the case of 2 M word data. The capacity of MO disk is 230 MB and it is possible to record 110 data. The trigger time of the digital oscilloscope is recorded simultaneously in the memory of a GPS clock system with an accuracy of less than 100 ns. In the memory of the GPS clock system, 200 data is recorded and these data are transferred to a hard disk in the computer.

Table 1. Characteristic of remote control measurement system.

| |
|---|
| Measurement site ( Fukui ) |
| Digital oscilloscope: 10bit, 13ns, 1M word, 4ch<br>( Nicolet PPRO620 )<br>12bit, 50ns, 1M word, 2ch<br>( Nicolet PRO32 )<br>Computer: Compaq PC COM1<br>MO disk : 230 MB<br>Modem : 14.4 kbps<br>GPS clock: 100 ns ( Trak System GPS8812 ) |
| Control site ( CRIEPI, Tokyo ) |
| Computer: Compaq PC COM1<br>MO disk : 230 MB<br>Modem : 14.4 kbps |
| Control site ( Public telephone ) |
| Computer: IBM Think Pd 230cs<br>Modem : 14.4 kbps |

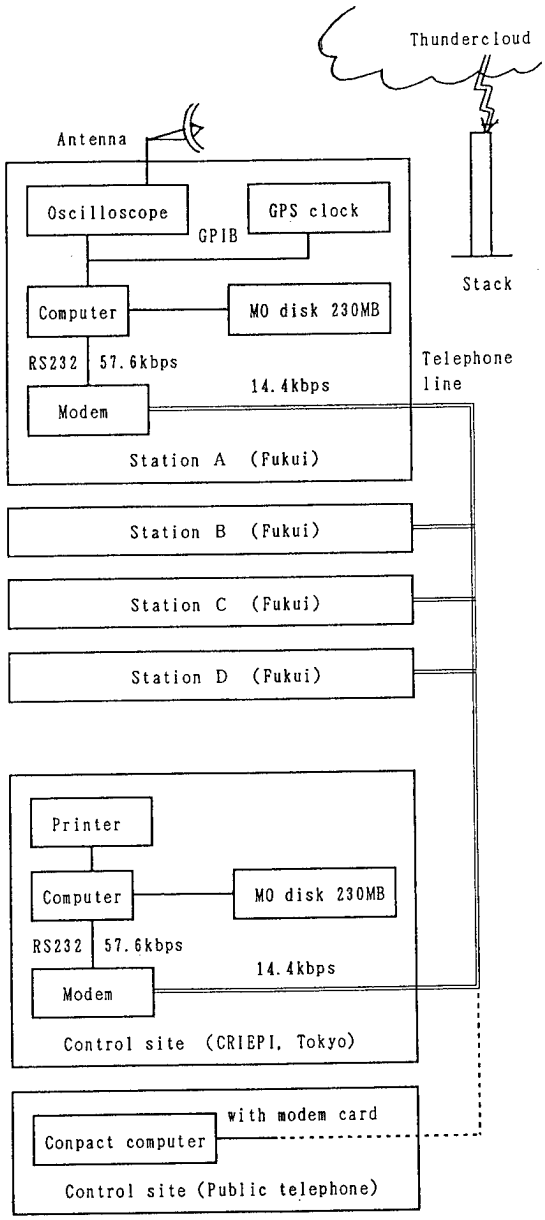



Fig. 1. Block diagram of the remote control measurement system using a telephone line.

(2) Check of data

The computer at the measurement site is controlled by a computer at the control site using a telephone line. The data which is recorded in the MO disk is recalled by a computer at the measurement site and the waveform is verified.

Even if lightning occurs during such operation, a data can be recorded automatically because a digital oscilloscope is always in a state of measurement. If the data acquisition has some problems, for example, no trigger, overflow of the data, and so on, measurement parameters such as trigger level, input range, sampling time, recording memory length are changed.

If the recorded data is useless such as a noisy one, it is eliminated from the memory of the MO disk for the effective use of the memory. It is therefore possible to continue to observe lightning for a long time without changing a MO disk or transferring of a large amount of data.

(3) Transfer of data

The data which is recorded in the MO disk at the measurement site is recalled and the data is transferred from the measurement site to the control site by remote control using a telephone line. The transferred data is recorded in the MO disk at the control site.

In the case of transferring of a large amount of data, a time which is taken to transferred a quality of transferred data are very important. To clarify these characteristics, an experiment of data transfer was done before starting of lightning measurement. As a result of comparison between the data which was recorded in a MO disk at the measurement site and the data which was transferred from the measurement site to the control site by using a telephone line, there was no difference between these data and validity of data transfer is confirmed. The transfer time of 2 M word data was about 20 minutes in the case of using a modem of 14.4 kbps speed.

2.2 Application to the measurement of lightning in the future

It is also possible to control the system at a public telephone station using a compact computer with a modem card ( See Fig.1.). Even if there is no telephone line in a measurement site such as a mountainous area, it is possible to apply our measurement system by connecting the measurement site to a place where we can use a telephone line with an optical fiber or a wireless phone.

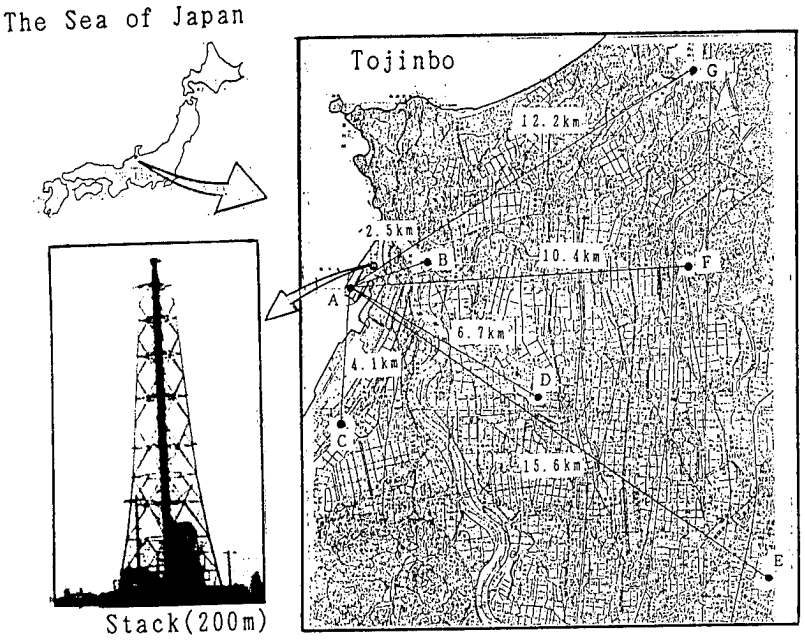
In the future, the usage of a satellite is considered for measurement of lightning in the wide area.

## 3. Measurement of electromagnetic field accompanied with lightning discharge

### 3.1 Antenna system of electromagnetic field

The elctromagnetic field accompanied with a lightning discharge have been measured by several kinds of antennas using a remote control measurement system in the Hokuriku area in Japan. The stations of lightning observation are shown in Fig.2. In the Hokuriku area in Japan, where IKL is about 40, there are many lightning strokes to a 200m stack in the Fukui thermal power plant in Winter.

Lightning currents have been measured by shunt-resistors at the top of the 200m stack in the Fukui thermal power plant /1/. The lightning progressing features have been measured by still cameras, a video camera, and ALPS ( Automatic Lightning Discharge Progressing Feature Observation System ) /2/.




| | | | |
|---|---|---|---|
| | Still camera | A and near stack | 1988-now |
| | Video camera | A | 1988-now |
| * | ALPS | A | 1988-now |
| | Shunt-resistor | Stack | 1988-now |
| | Field mill | A, B, C, D, E, F, G | 1991-now |
| | Slow antenna | A, B, C, D | 1994-now |
| | Fast antenna | A | 1993-now |
| | UHF antenna | A, C | 1994-now |

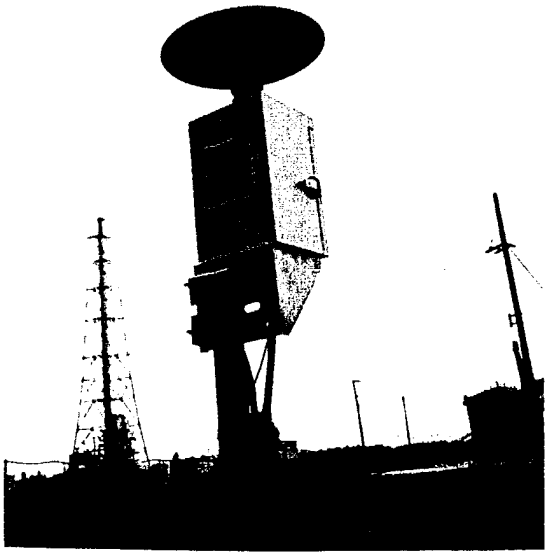
* ALPS : Automatic Lightning Discharge Progressing Feature Observation System /2/

Fig. 2. Stations of lightning observation on Hokuriku coast in winter in Japan.

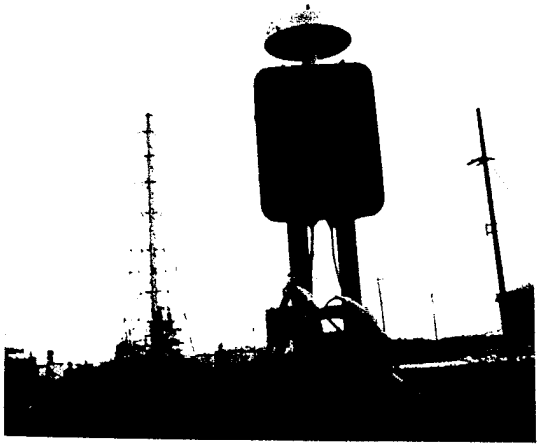
One of the purpose of lightning observation near the stack is to collect many data of simultaneous measurement of a lightning current, a lightning progressing feature, and electromagnetic field changes. By those measurements, it is expected that phenomena in the cloud before a lightning flash and between lightning strokes are known.

Several kinds of antennas which are used for measurement of electromagnetic field are shown in Fig. 3.

The characteristics of the antennas are summarized in Table 2. These antennas of different characteristics give information of different phase of lightning activity.



( a )



( b )



( c )

Fig. 3. Several kinds of antennas which are used for measurement of electromagnetic field. (a) Slow antenna. (b) Fast antenna ( At point A in Fig. 2 ). (c) UHF antenna ( At point C in Fig. 2).

Table 2. Characteristic of antenna.

| | Slow antenna | Fast antenna | UHF antenna |
|---|---|---|---|
| Frequency response | 50 ~ 3 MHz | 50 ~ 100 MHz | 330 MHz |
| Time constant | $\tau$ = 5 s | $\tau$ = 50 $\mu$s | (Interferometer) |

By the measurement of an electric field strength at several points on the ground using a field mill, it is possible to obtain information about lightning and thunderclouds as follows /3/. (1) Prediction of lightning flash. (2) Current polarity. (3) Movement of thunderclouds.

By the measurement of an electric field change at several points using a slow antenna, it is possible to obtain information about activity of thunderclouds as follows. (1) Position and quantity of a charge in a thundercloud /4/. (2) Striking point /5/.

By the measurement of the electric field changes using a fast antenna, it is possible to study the process of lightning discharge in more detail. For example, it detects pulse currents which are superimposed on a continuing current, because a fast antenna has a short time constant and high frequency response as compared with a slow antenna.

By the measurement of the electromagnetic wave using a UHF antenna at several points, it is possible to estimate sources of discharges in the thundercloud by using a time of arrival ( TOA ) method /6/ or a radio interferometry /7//8/.

We have been carrying out the simultaneous measurement of electromagnetic field by a field mill network, a slow antenna network, a fast antenna, and a UHF antenna network in order to understand the lightning in winter. Hereafter, the electric field measurements using a slow antenna are presented, and the characteristics of lightning in winter is discussed.

3.2 Electric field change in lightning ground flash in winter

A slow antenna which was used in 1994 has a frequency response of 50 Hz to 3 MHz and a time constant of 5 seconds as shown in Table 2. The data was recorded by a 12 bit digitizing oscilloscope with a 500 ns sampling time.

Fig. 4 shows one of the result of electric field change in a negative lightning ground flash using a slow antenna at point B in Fig. 2.

In this figure, it is considered that L is a field change accompanied with leader development in the thundercloud before the return stroke. The duration of L part is 3.1 ms and many pulses superimpose on the L part. It is also reported that UHF radiation increases very much when a leader starts to develop /9/. We infer that the origin of the pulses is a kind of streamers which progress into a charge region as a branch in the thundercloud. Further study is necessary to understand the phenomena in detail.

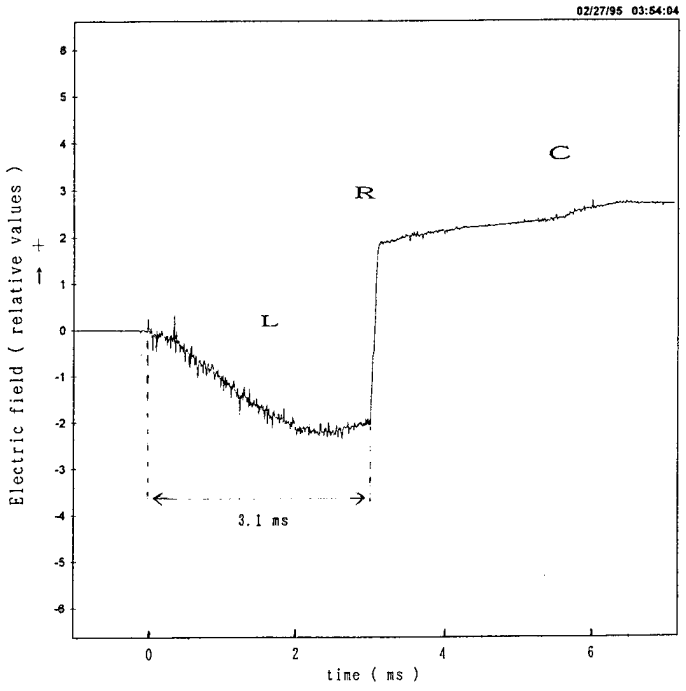



Fig. 4. Electric field change in negative lightning ground flash using a slow antenna at point B in Fig. 2. ( JST 03:54:04, 27th February, 1995 )

In the figure 4, it is considered that R is an electric field change corresponds to the return stroke and C is a part of continuing current by the facts that the electric field increase slowly. The electric field changes of L, R, and C have been measured with a slow antenna in the summer lightning /10/.

Table 3 shows statistics of electric field changes measured by a slow antenna at point B in Fig. 2.

A discrimination between a ground flash and a cloud discharge is based on the waveform of electric field change; the waveform of electric field change which is verified as a ground flash by a photo or a video picture is used as a reference of a ground flash. The records of a fast antenna and a UHF antenna were also used for the judgement whether a flash is to the ground or not.

Table 3. Statistics of electric field change observed by a slow antenna ( At point B in Fig. 2, from January to March in 1995 ).

| Thundercloud Polarity | Cloud to ground flash | | Cloud discharge |
|---|---|---|---|
| | Events | Multiplicity* | Events |
| Positive | 14 (42%) | 1 | 6 |
| Negative | 15 (45%) | 1.4 | 4 |
| Bipolar | 4 (12%) | | 10 |
| Total | 33(100%) | | 20 |

* Average number of lightning strokes in the 523 ms recording.

As shown in table 3, the characteristics of lightning in winter is as follows.

(1) The ratio of positive ground flashes to negative ground flashes is 1:1.

(2) The number of strokes per positive ground flash is one and that per negative flash are 1.4 in the 523 ms recording time.

(3) In the ground flashes, about 10 percent of them shows a bipolar change.

(4) Most of ground flashes include continuing currents.

In the characteristics described above, (1) is almost same characteristic in the reference /11/. (2) shows a similar tendency which the number of strokes per negative ground flash is large in comparison with positive ground flash /12/. It is considered that (3) is due to bipolar lightning /13/ or simultaneous lightning strokes at multi point /14/.

3.3 Simultaneous measurement of lightning progressing feature and electric field change

Fig. 5 shows one of the result of simultaneous measurement of a lightning progressing feature and an electric field change when a lightning strikes to the 200m stack. The striking point is not the lightning rod at the top of the stack because a lightning current is not recorded.

In the Fig. 5, (a) shows a lightning progressing feature observed by the ALPS. (b) is a magnification of (a). (c) is an electric field change observed by a slow antenna at point B 1.7 km away from the stack. The recording memory length of the ALPS is 0.4ms before the trigger point and 2.8 ms after the trigger point, and the total is 3.2 ms.

It is considered that the most bright part corresponds to a return stroke. The electric field change is recorded 7.5 ms before the return stroke, but no obvious luminosity is observed in the period of 0.4 ms before the return stroke. After that, in 12$\mu$s before the return stroke, an upward leader progresses from the top of the stack to the thundercloud.

We infer that a leader progresses from the thundercloud to the ground from the electric field change recorded before the return stroke. Furthermore, many pulses superimpose on the L part in the same way of L part in Fig. 4. We consider that these pulses are also radiated from streamers which progress into a charge region in the thundercloud.

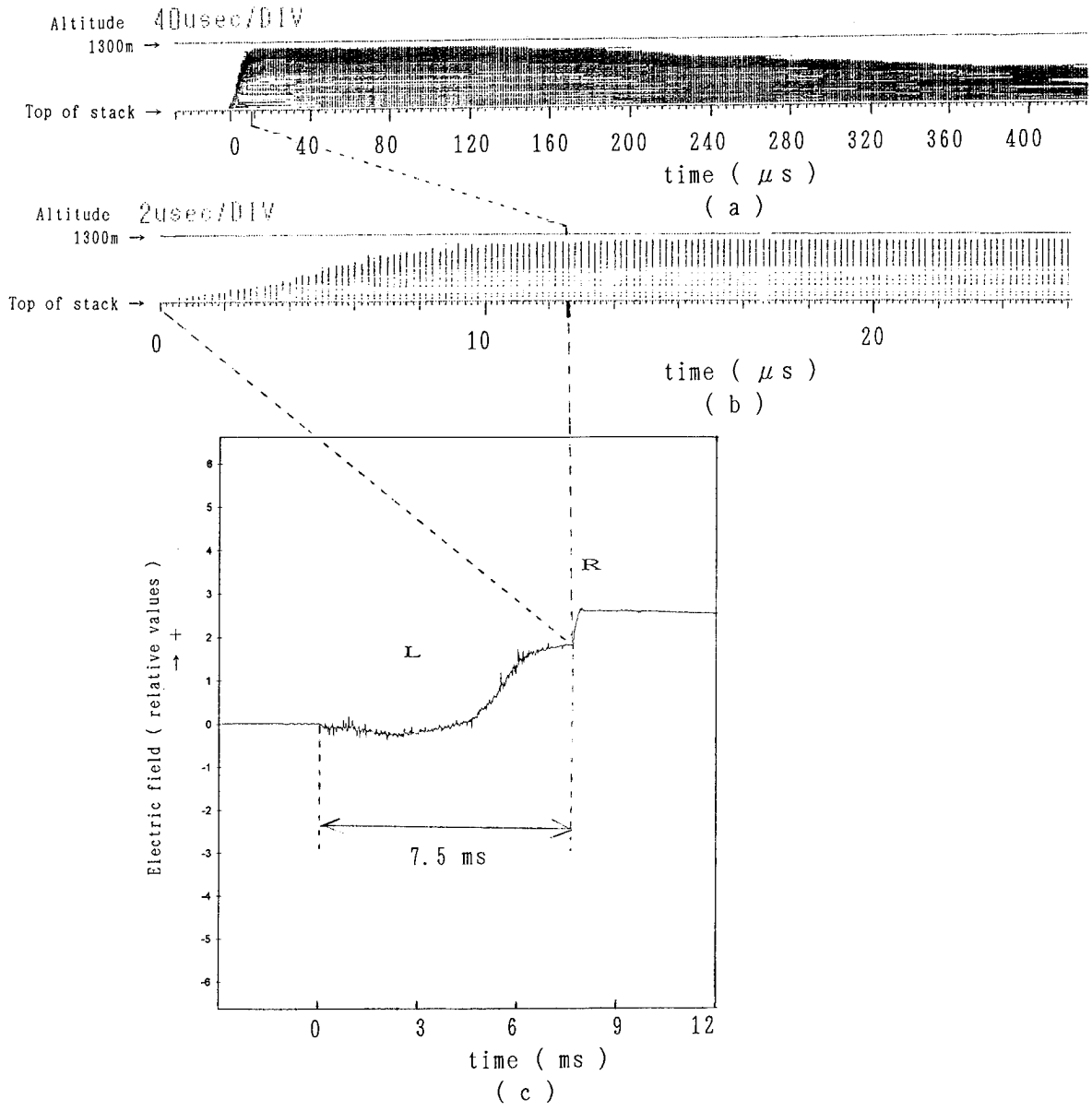



Fig. 5. Simultaneous measurement of lightning progressing feature and electric field change when lightning strikes to the 200m stack ( JST 03:52:03, 27th February, 1995 ). (a) shows a lightning progressing feature observed by the ALPS. The recording memory length of the ALPS is 0.4 ms before the trigger point and 2.8 ms after the trigger point, and the total is 3.2 ms. (b) is a magnification of (a). (c) is an electric field change observed by a slow antenna at point B 1.7 km away from the stack.

It has been considered that an upward leader progresses from a high structure when the electric field strength is great with approaching of thundercloud because the thundercloud base in winter season is low. After that, a return stroke occurs when the upward leader attaches to a charge region in the thundercloud. By the simultaneous measurement of the lightning progressing feature and electric field change when lightning strikes to the stack, however, it is considered that a downward leader which progresses from the thundercloud connects with an upward leader in the thundercloud or in the sky, and a return stroke occurs.

Observed electric field records suggest that a leader progressing from the thundercloud plays an important role to trigger an upward leader from a grounded object. It is necessary to study the condition of upward leader progressing.

Fig. 6 shows a photo at point A in Fig. 2 when lightning strikes to the stack. In fact, the lightning channel is almost vertical from a thundercloud to above the stack and it abruptly turns from above the stack to the top of the stack horizontally.

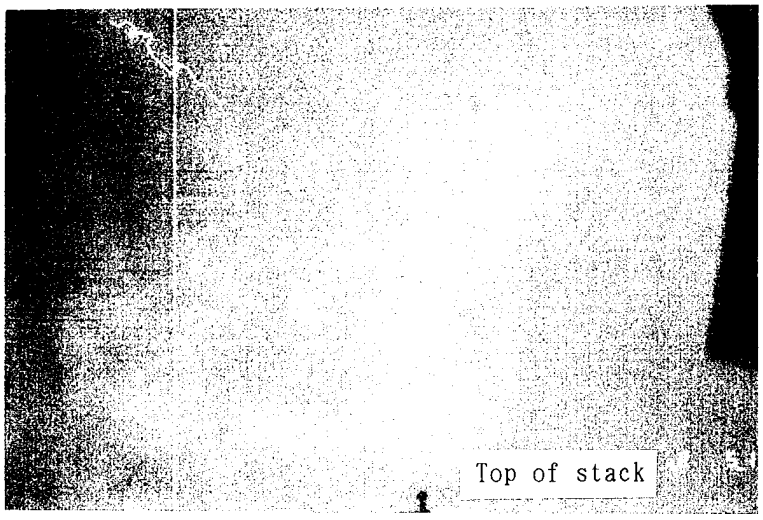



Fig. 6 Photo of lightning stroke to the stack ( JST 03:52:03, 27th February, 1995 ).

## 4. Conclusions

In this paper, first the lightning measurement system using a remote control by a telephone line is described. This is a new approach to the measurement of lightning. The system has several merits as follows.

(1) It is possible to check system operation remotely.
(2) It is possible to do remote control of a digital oscilloscope.
(3) It is possible to transfer a large amount of data.

It is very difficult to set up the device properly for measuring of lightning discharge, ( for example, trigger level, input range, sampling time, recording memory and so on ) because the physical quantity of lightning have a wide range for each lightning flash. With the remote control system, obtained data can be checked at once from a remote control site and the measurement system parameters can be readjusted if necessary. The system is very useful for lightning observation.

In addition to the measurement of a lightning current and a lightning progressing feature when a lightning strikes to the 200m stack in winter, the simultaneous measurement of electromagnetic field change using a field mill network, a slow antenna network, a fast antenna, and a UHF antenna network by the remote control system was started in 1994.

As a result of the measurement of electric field change using a slow antenna, the characteristics of lightning in winter are summarized as follows.

(1) The ratio of positive ground flashes to negative ground flashes is 1:1.

(2) The number of strokes per positive ground flash is one and negative flash is 1.4 in the 523 ms recording time.
(3) In the ground flashes, about 10 percent of them show bipolar changes.
(4) Most of currents of ground flashes include a continuing current.

By the simultaneous measurement of lightning progressing feature and electric field change, the characteristic of lightning in winter which strikes to a high structure was considered. As a result, it was shown that a leader which progresses from a thundercloud before a return stroke plays an important role in progressing of a upward leader from the ground.

## Acknowledgments

We thank Dr.T.Suzuki, Dr. S.Sasaki, Dr.S.Yokoyama, Dr.K.Miyake, Mr.S.Asakawa ( CRIEPI ), Mr. T. Wakai, and Mr.T.Sakai ( Hokuriku Electric Power Co.) for helpful support. We also thank Toyo-Technica Co. for valuable support to the remote control system.

## References

/1/ K. Miyake, et al., " Characteristics of Winter Lightning Current on Japan Sea Coast ", IEEE Transactions on Power Delivery, Vol.7, No.3, pp.1450-1457, 1992.
/2/ S. Yokoyama, et al., " Winter Lightning on Japan Sea Coast - Development of Measuring System on Progressing Feature of Lightning Discharge- ", IEEE Trans. on Power Delivery, Vol.5, No.3, pp.1418-1423, 1990.
/3/ A. Wada, et al., " Winter Thundercloud Observation on Hokuriku Coast in Japan ", 9th International Symposium on High Voltage Engineering, 1994
/4/ P. R. Krehbiel et al., " An Analysis of the Charge Structure of Lightning Discharges to Ground ", Journal of Geophysical Research, Vol.84, No.C5, pp.2432-2456, 1979.
/5/ T. Ushio et al., " Synchronized Multipoint Measurements of Lightning Electric Field Changes ", T.IEE Japan, Vol.114-B, No.11, pp.1160-1167, 1994.
/6/ D.E. Proctor, " VHF Radio Pictures of Cloud Flashes", Journal of Geophysical Research, Vol.86, No.C5, pp.4041-4071, 1981.
/7/ P. Richard, et al., Proc. of 7th Int. Conf. Atmos. Electr.,687, 1988.
/8/ C.T.Rhodes, et al., " Observations of Lightning Phenomena using radio interferometry", Journal of Geophysical Research, Vol.99, No.D6, pp.13059-13082, 1994.
/9/ Z-I. Kawasaki, et al., " Common Physical Processes in Natural and Triggered Lightning in Winter Storms in Japan ", J. G. R., Vol.97, No.D12, pp.12935-12945, 1992.
/10/ V. A. Rakov, et al.," Waveforms of First and Subsequent Leaders in Negative Lightning Flashes ", Journal of Geophysical Research, Vol.95, No.D10, pp.16561-16577, 1990.
/11/ M. Brook et al., " The Electrical Structure of the Hokuriku Winter Thunderstorms ", Journal of Geophysical Research, Vol.87, No.C2, pp.1207-1215, 1982.
/12/ T. Takeuti, et al., " On the Types of Thunderstorms Deduced from Cloud-to-Ground Discharges Observed in Sweden and Japan ", Journal of the Meteorological Society of Japan, Vol.55, No.6, pp.613-616, 1977.
/13/ K. Narita, et al., " Bipolar Lightning in Winter at Maki, Japan ", Journal of Geophysical Research, Vol.94, No.D11, pp.13191-13195, 1989.
/14/ H. Sugimoto, et al., " Observation of the winter lightning at transmission lines located at mountainous areas ", 22nd Int. Conference on Lightning Protection, R1a-05, 1994.

# LIGHTNING PROTECTION SYSTEM FOR TELECOMUNICATION RELAY STATION DESIGN AND MAINTENANCE A FIELD EXPERIENCE IN TROPICAL COUNTRY

**R.ZORO**
**Departement of Electrical Engineering**
**Institut Teknologi Bandung - Bandung**
**Indonesia**
**Telephone (62)(22) 250-7315 FAX (62)(22) 250-0918**

Z. NAWAWI
**Departement of Electrical Engineering**
**Universitas Sriwijaya - Palembang**
**Indonesia**
**Telephone (62) (711) 36-2959 Fax (62) (711) 36299**

## ABSTRACT

A Lightning Protection of Telecomunication Relay Station (TRS) at the Mount Tangkuban Perahu Indonesia which is located on high hill and was always hit by lightning, was designed and installed according to the IEC 1024-1 Standard

To keep the reliability of the this TRS, the maintenance of the Lightning Protection System (LPS) is carried out by measuring the peak lightning current which strike the tower. Is it measured by magnetic tape or Lightning Current Detector (LCD) and which is equipped with Lightning Current Counter (LCC), and the total lightning strikes and the distribution of lightning peak current per year can be monitored.

This paper describe the method to evaluate and to improve the performance of the LPS due to lightning strike to the Telecomunication Relay Station.

## INTRODUCTION

Telecomunication Relay Station at Mount Tangkuban Perahu in Indonesia are located at very high thunderstorm activity. Since it was build in 1990 more than 100 lightning strikes which damaged the equipments has been reported. Lightning Protection System was designed on 1994 by using the Lightning Protection Zone Concept according to IEC 1024-1 standard.
Several damaged was still reported after the TRS being protected, evaluation was carried out by installing the lightning current measuring system and current counter.
A simple lightning current detection by using commercial tape which is filled by 315 Hz sinusoidal, signal was put to a 30 cm fiber plate as tape carrier. This lightning current detector was installed perpendicular to the down conductor, Laboratory testing for calibration of this measuring system has been carried out to have the correlation between the length of erasement of sinusoidal signal and impulse peak current. Lightning current detector (LCD) was installed at the top of the tower and the bottom of the tower. Lightning current counter (LCC) was installed at down conductor to detect the lightning stroke to tower.

To investigate the lightning impulse current which flows to the equipment inside the building, a LCC was also installed at the grounding lead of lightning arrester of incoming power line.
On early 1995 lightning have hit the tower times, two times hit the top of the tower and three times hit the tower sides. The maximum lightning current of 30 kA was recorded on the LCD.

## CALIBRATION OF LIGHTNING CURRENT DETECTOR.

Correlation of peak impulse current and length of erasement of sinusoidal signal was expressed with the following equations :

$$\hat{I} = (2\,\pi\,Hp)/\gamma.(\,\gamma + (l/2)^2\,) \quad ; \quad \hat{I} \text{ in kA, } l \text{ in cm} \qquad (1)$$

Calibration was carried out at laboratory for High Voltage Engineering - TU Munich, Germany which gave the result :

$$\hat{I} = 1{,}49 + l^{1{,}343} \quad ; \quad \hat{I} \text{ in kA, } l \text{ in cm} \qquad (2)$$

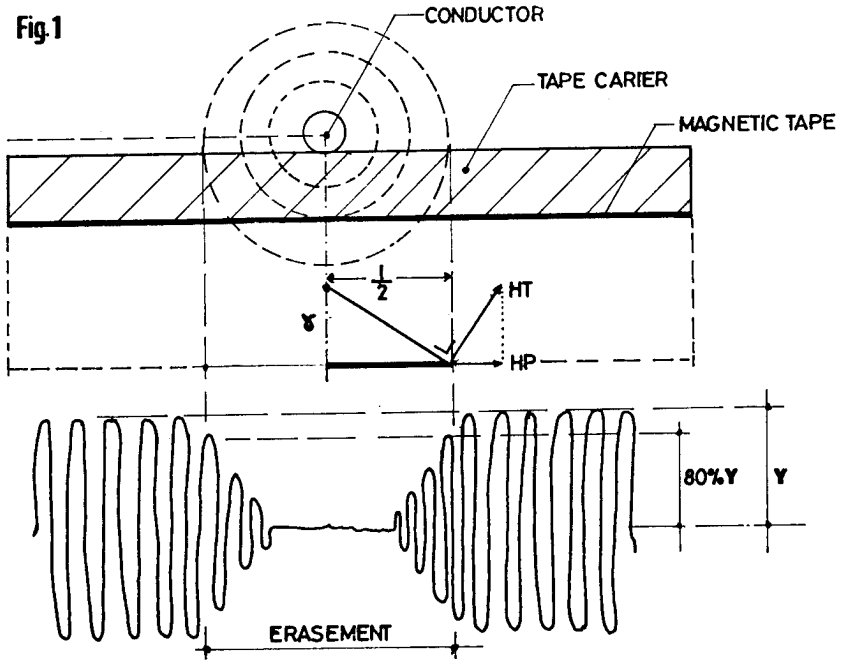



figure 1. Principal Meausrement Of Peak Lightning Current Detection (LCD)

LIGHTNING PROTECTION SYSTEM FOR
TELECOMUNICATION RELAY STATION (TRS)

TRS located at the 2076 m hill equipped with the radio inside 8 to 6 m building. The antenna was installed at 100 m high tower. The layout and side view of the TRS was shown on figure 2.

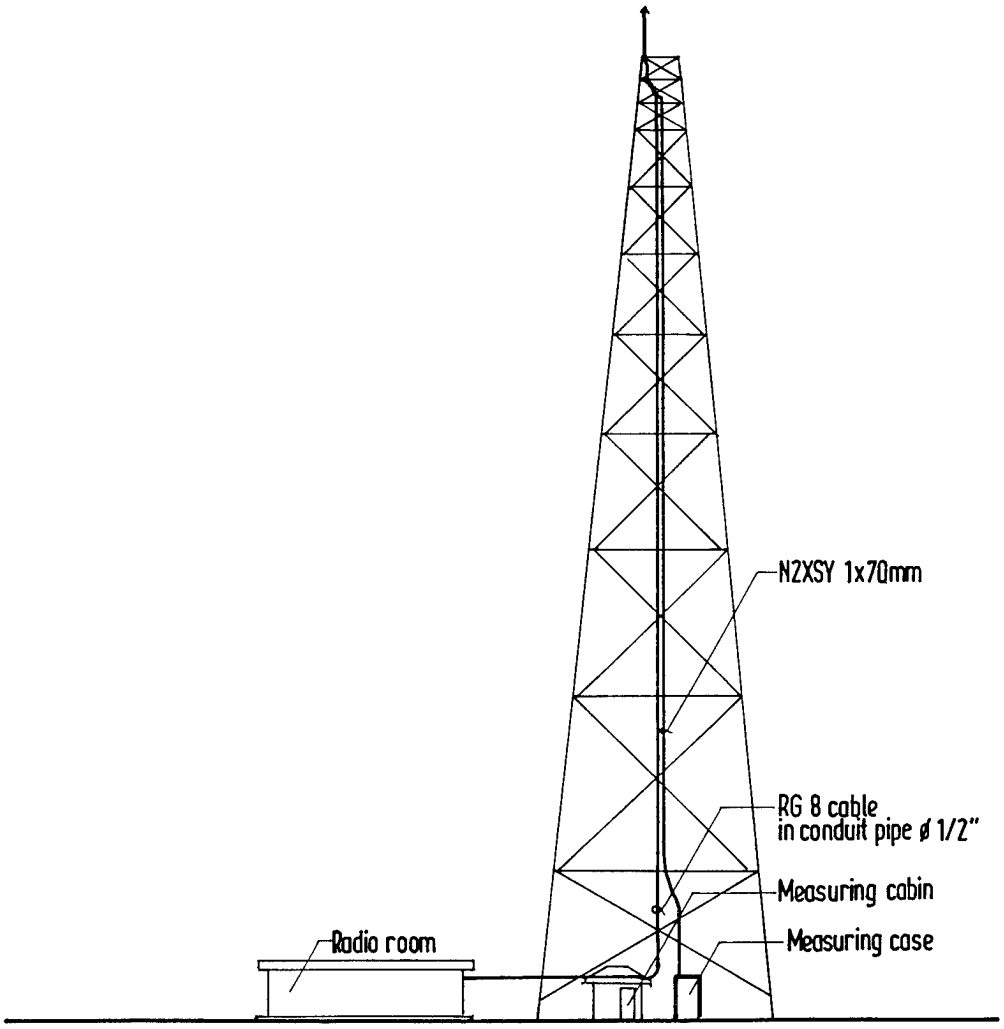



figure 2. Layout & Side View of TRS

Protection system was designed according to IEC standard 1024-1/1993 for electrical, and electronic equipment. Lightning arrester and grounding system was installed in order to get the minimum voltage difference at every equipment inside the building and prevent the lighnting impulse traveling from the electrical and electronic incoming lines.

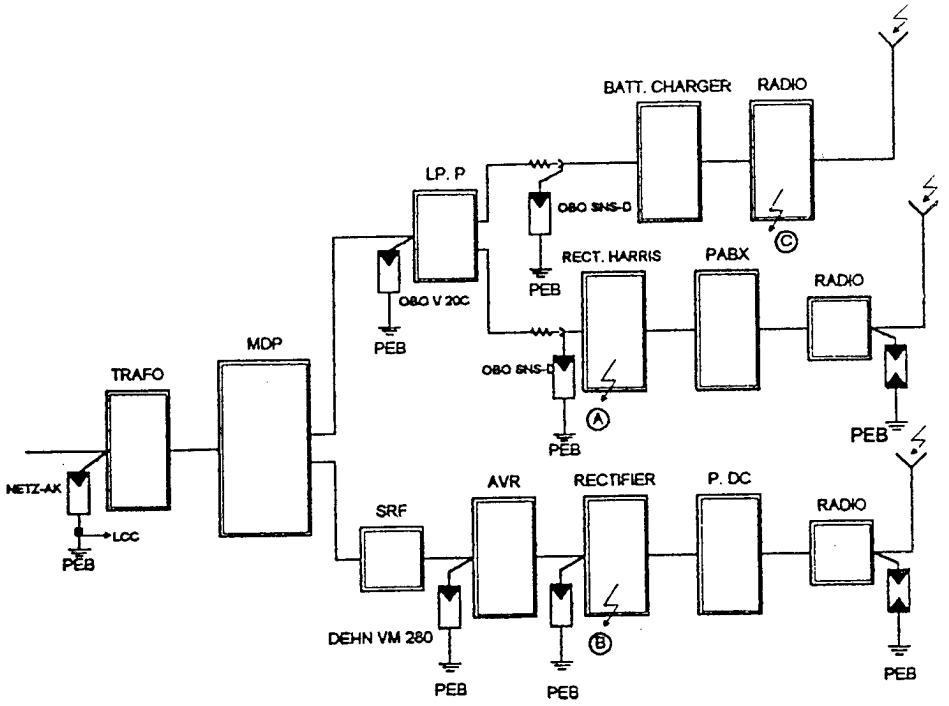



figure 3. LPS For Electrical & Electronic Equipment Inside The Building

Grounding system was designed by using combination of type A and type B standard of IEC 1024-1/1993 and Equipotential Bonding inside the building were connected as short as posible to the grounding system outside the building.

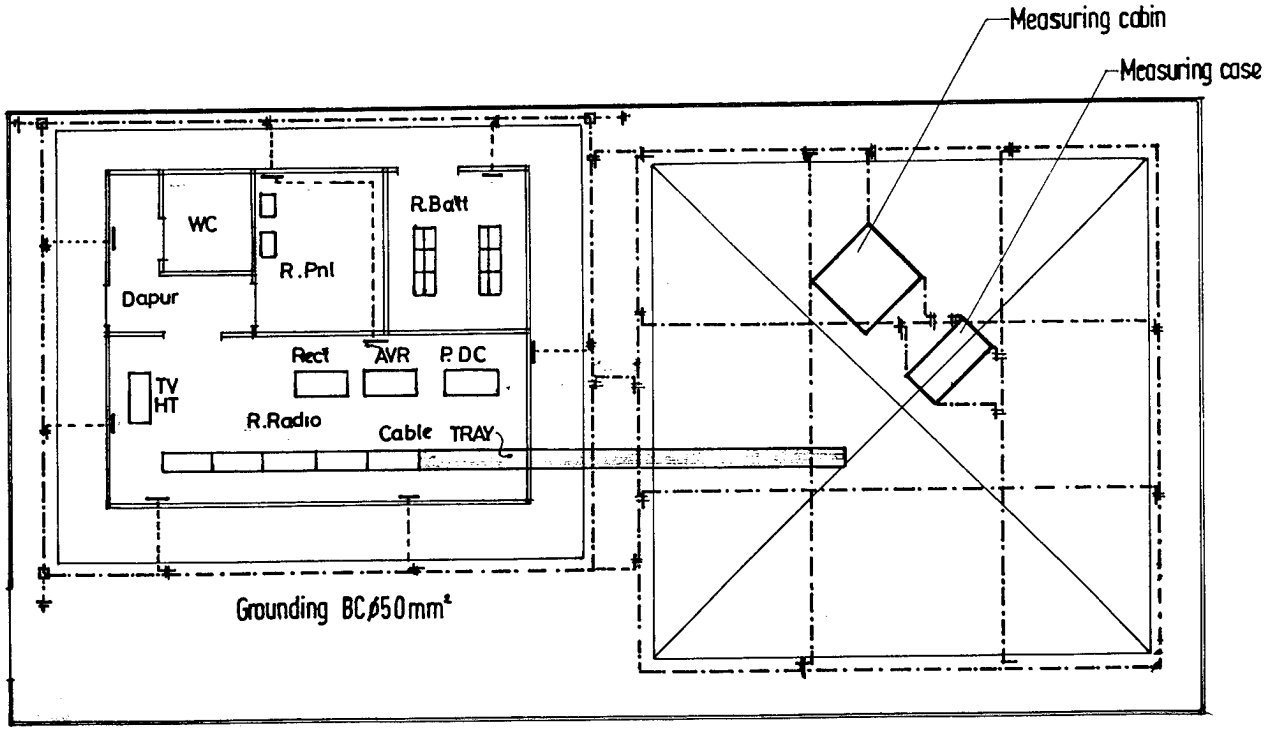



figure 4. Grounding System Of TRS With The Equipotential Bonding

MAINTENANCE OF LPS

On 1993 lightning was hit the tower more than 30 times and damaged the equipments inside the building. On November 1994 the LPS has already installed. The LCD measurement system which have already installed since 1993 was used to monitor the lightning strike to tower for maintenance purpose of LPS. To detect the lightning surge at the incoming power lines, the LCC was installed at the main panel (see fig.3)

On the beginning of December 1994 the lightning hit the tower and made some minor damaged on the equipment and also destroyed some arrester. Some modification was made by shorten the grounding lead from lightning arrester and by changing the equipotential bonding connection.

From the data of LCD, it was recorded that the highest lighnting current is 30 kA and three times the tower was hit from the side and the two times hit top of the tower.

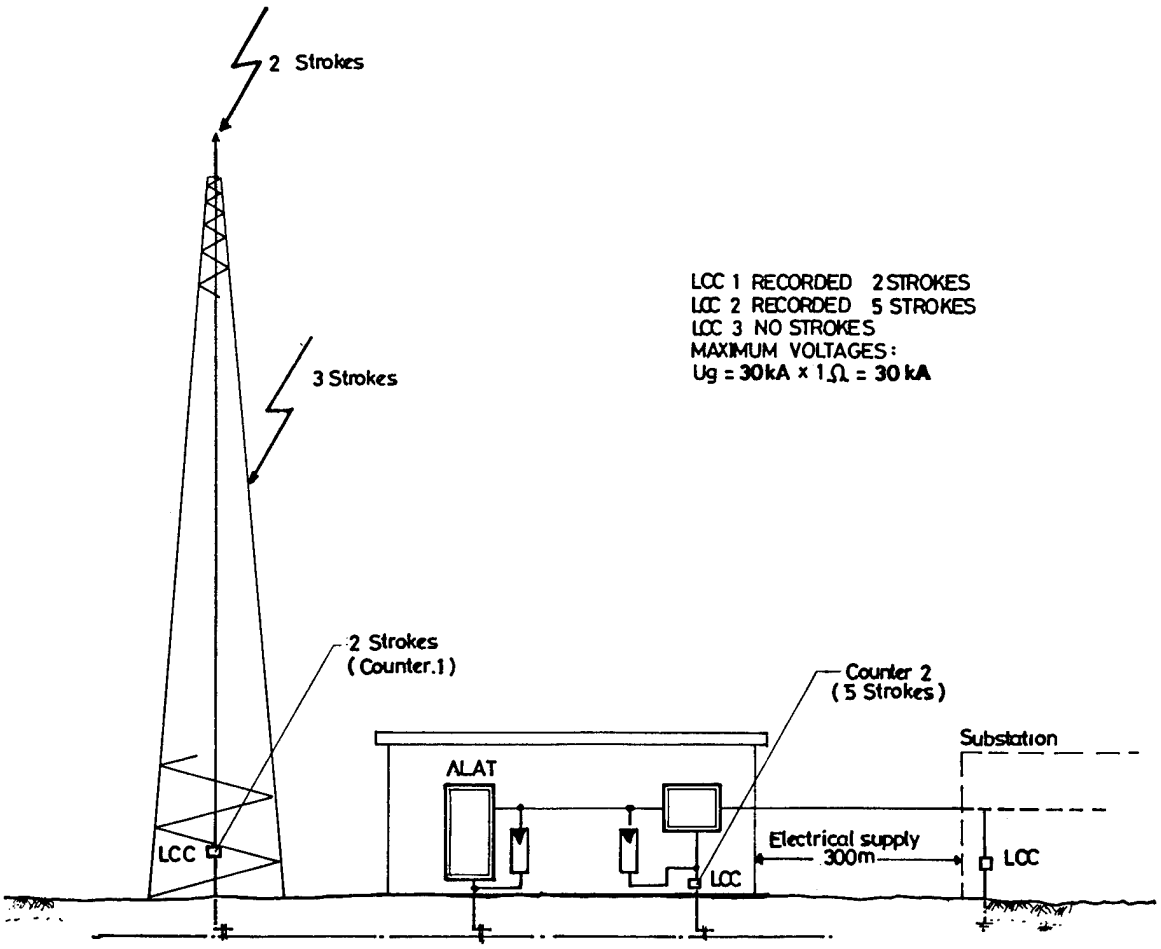



figure 5. Lightning Strike to the TRS

## CONCLUSION

TRS which is normally located on the high hill or at the highest object of the serrounding can be an easy target for direct lightning strikes. Due to these direct strike most of the damages was caused by elevation of the voltage at the grounding system. Carefull design of grounding system and the location of Equipotential Bonding will prevent the damages from the potential difference.
The LCD system on the tower and LCC on the incoming lines can give a valuable tools to evaluate the damages due to lightning strikes for the maintenance purposes.

## REFERENCES


1. Crouch, K.E, " Calibration Test On Magnetic Tape Lightning Current Detectors" Massachussets, NASA, 1980 (NASA Contactor Report 3270).
2. Altafein, RAC, et.al," LCD Direct Calibration For NOn Cylindrical Conductors" 20th ICLP, Switzerland, 1990.
3. Standard IEC- 1024-1/1993 - Part 1, "Protection Of Structures Against Lightning ".

# SESSION 03A
# LIGHTNING PROTECTION
# CHAIRPERSON: CHARLES GOLDBLUM

# COST BENEFIT OF AN ABFM AT KSC

Arnold A. Barnes, Jr.
Phillips Laboratory
Geophysics Directorate
Hanscom Air Force Base
Massachusetts, USA 01731-3010
Telephone (617) 377-2939 FAX (617) 377-8892

John C. Willett
Phillips Laboratory
Geophysics Directorate
Hanscom Air Force Base
Massachusetts, USA 01731-3010
Telephone (617) 377- 5954 FAX (617) 377-2984

ABSTRACT

Sixteen percent of the countdowns of Expendable Launch Vehicles (ELV) at Kennedy Space Center/Cape Canaveral AFS (KSC) are scrubbed or delayed due to lightning. These scrubs/delays are dictated by the lightning Launch Commit Criteria (LCC) which were rewritten after the loss of Atlas/Centaur 67 in 1989.

In a joint AF/NASA program, aircraft were fitted with field mills and were flown at KSC to obtain electric field data aloft in an effort to redefine the LCC and open more launch windows. Data obtained from these flights have been used to prepare modifications to three of the six lightning LCC rules. In addition, a new rule has been proposed to use an aircraft fitted with a suite of instruments to measure electric fields aloft {an Airborne Field Mill (ABFM)} to waive violations of three of these rules.

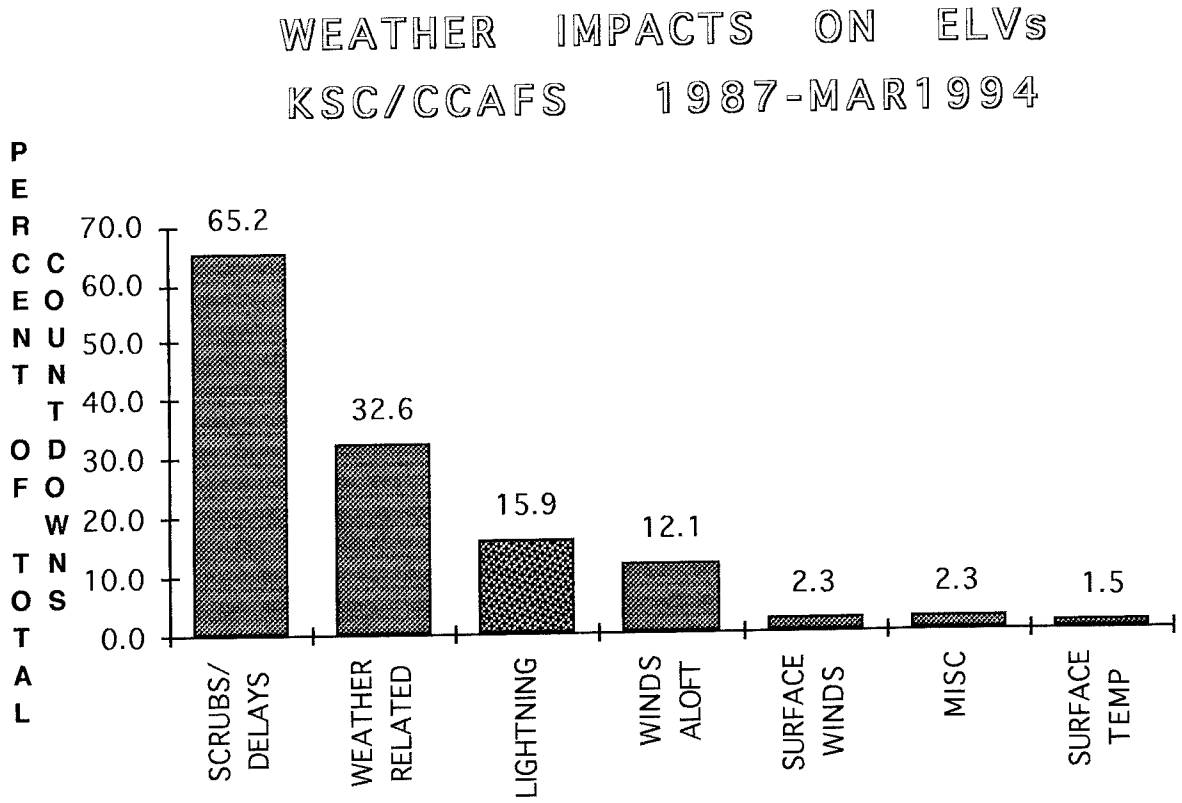
Using the statistics obtained from the joint Airborne Field Mill (ABFM) program and the weather data from scrubs/delays from 1987 through March 1994, we calculated the percentage of times that expendable launch vehicles (ELVs) could have been launched if an ABFM had been available to measure the electric fields in the clouds. The overall probability of unnecessary ELV delays was 3% and for ELV scrubs was 4%. If the same statistics are applied to the STS (Space Transportation System = Space Shuttle) as well as the ELVs, the projected yearly savings would amount to ~$640K.

Two of the other lightning LCC rules could be modified with the use of an ABFM, however the relevant data were not taken during the ABFM flight program. The small (5 minutes) launch windows for the STS to dock with the Space Station, coupled with a requirement for other than early morning launches, will make lightning a more relevant factor in the future. If we consider the probability that there will have to be more afternoon launches to re supply the Space Station and MIR and incorporate the use of the ABFM to relax these other two rules, we estimate the yearly savings would be in excess of $1M.

These savings would have to be offset by the cost of procuring, modifying, maintaining, and operating an operational ABFM.

## INTRODUCTION

Weather related scrubs and delays impact approximately one third of all missile countdowns on the Eastern Ranges. One-half of these are due to the conservative lightning Launch Commit Criteria (LCC). The chart below shows the percentage of scrubs/delays at KSC/CCAFS from 1987 through March 1994.




Improved forecasting of both natural and triggered lightning would open or expand launch windows. In addition, improved forecasting of natural cloud-to-ground lightning would provide safer ground handling and more time for ground handling.

This study was done for the Weather Integrated Product Team (WIPT) which is part of the Range Standardization and Automation (RSA) program. RSA is a joint Air Force Space Command (AFSPC) and Air Force Material Command (AFMC) program to standardize, modernize and automate the Air Force ranges. One of the WIPT objectives is to standardize, automate and improve lightning prediction techniques for all missile launches. Our approach has been to review equipment and techniques, to recommend changes to improve predictions of triggered lightning, and to provide

reports on methods to improve lightning prediction and cost savings. The ultimate Air Force application is to decrease launch window closures and ground handling stand-downs due to threat of lightning.

LAUNCH COMMIT CRITERIA

The following is an abbreviation of the present lightning LCC rules:

• THE LAUNCH WEATHER OFFICER MUST HAVE CLEAR AND CONVINCING EVIDENCE THAT THE FOLLOWING CONSTRAINTS ARE NOT VIOLATED:

• Rule A. Lightning within 10 nm within 30 minutes prior to launch.

• Rule B. Do not launch through:
1. CU (cumulus clouds) with tops higher than 5° C
2. or within 5 nm of CU with tops higher than -10°C
3. or within 10 nm of CU with tops higher than -20°C
4. or within 10 nm on nearest edge of CB or anvil.

•Rule C. GBFM (defined below) exceeds 1 kV/m within 5 nm of launch site unless:
1. there are no clouds within 10 nm of launch site
2. smoke or fog is causing abnormal readings.

•Rule D. Do not launch if flight path is through 4500 ft of cloud with any part between 0° and -20° C.

•Rule E. Do not launch if path is through cloud colder than 0°C associated with disturbed weather within 5 nm of path.

•Rule F. Do not launch through debris cloud, or within 5 nm of CB debris cloud not monitored by GBFM or producing radar returns greater than 10 dBz.

OBJECTIVE

Our objectives are to identify electric field measurements which would have the greatest cost-benefit potential for increasing launch opportunities at each range. We considered the following measurement alternatives for measuring electric fields aloft:

• 1. Ground Based Field Mills (GBFM)
• 2. Balloon borne instrumentation
• 3. Rocket borne instruments (REFS)
• 4. Radar detection of electric fields aloft in clouds
• 5. Radar detection of mixed-phase precipitation aloft
• 6. Remotely Piloted Vehicles (RPV)
• 7. Airborne Field Mills (ABFM).

Some of the reasons for choosing the Airborne Field Mill (ABFM) follow:

- GBFM do not provide information in the vertical
- Balloons impractical plus safety problems at the ranges
- REFS pose safety problems for the STS and the ELVs
- Range Safety is very leery of using remotely piloted vehicles on the ranges
- ABFM recommended by past studies and past experiments.

Previous ABFM experiments include (1) support to the Apollo-Soyez launch in 1975, (2) NASA/Ames Learjet flights over California, (3) flights with the New Mexico Institute of Mining and Technology (NMIMT) Special Purpose Test Vehicle for Atmospheric

Research (SPTVAR) over New Mexico and KSC, (4) jointly funded AF/NASA Learjet 28/29 flights in Florida, and (5) jointly funded AF/NASA Aeromet-SRI flights primarily in Florida.

ABFM DATA

Rules D, E and F were investigated on previous ABFM data missions because these rules were considered to have longer term variations and are considered to be the most troublesome for launch operations. Rule B has shorter term variations, and rule C was assigned a low priority for the data gathering missions.

Table 1 provides data on the occurrences of hazardous fields aloft during violations of lightning LCC rules D, E and F. Table 2 is a listing of violations of rules D, E, and/or F for STS and ELV delays and scrubs which were not due to non-weather causes or to rules A or B. These data were then combined to give table 3, the false-alarm frequencies and overall probability of unnecessary delays and scrubs for STS and ELV.

Next we obtained estimates of the costs for delays and scrubs from the AF and NASA and calculated the average cost per launch of unnecessary scrubs/delays for STS, Titan and Atlas/Delta.

| VEHICLE/COST | DELAY | SCRUB | COST/LAUNCH |
|---|---|---|---|
| STS | $80K | $1000K | $1.6K ($11.2K*) |
| TITAN | $80K | $800K | $33.6K |
| ATLAS/DELTA | $80K | $800K | $12.6K |

* assumes one scrub

Averaged anticipated annual launch scheduled were obtained as:

| | |
|---|---|
| STS | 10 |
| TITAN | 4 |
| ATLAS/DELTA | 7 |

From these data we calculated that the annual cost reduction for launches from the Eastern Range, assuming no STS scrubs, using the ABFM for rules D, E and F only would be $423K/year. If we assumed that the scrub/delay statistics for the STS were the same as for the ELV, then the annual cost reduction for using the ABFM for rules D, E and F only would be $637K/year.

DISCUSSION

Many of the STS launches have been purposely scheduled for the morning hours to avoid the afternoon showers and thunderstorms which build up over Kennedy Space Center. Future launches to re supply the Space Station or to join up with MIR will encounter significantly more launch delays due to afternoon thunderstorms and debris clouds. The small launch windows, approximately 5 minutes, will make weather even more of a critical factor. The recent two mid afternoon launch delays of the STS in order to dock with MIR are prime examples.

Data to be collected by the ABFM will also allow future modifications to rules B and C which will open more launch windows.

Of course the total cost effectiveness of an ABFM must take into account the cost of procuring, modifying, flying and maintaining the ABFM as well as the associated ground based equipment. There will also be political considerations.

We have looked at some preliminary data from Vandenberg AFB, where there is considerably less lightning, and we have the impression that the use of an ABFM at Vandenberg may not be cost effective, but more definitive data are needed to verify this.

Additional details of this study may be found in references (1 and 2).

## CONCLUSIONS AND RECOMMENDATIONS

There will be more launches from the Eastern Test Range during periods of potentially dangerous triggered lightning, and the use of an Airborne Field Mill aircraft will help to open launch windows presently closed by the conservative lightning Launch Commit Criteria.

More data are needed on the rule violations by hour of the day and by season. The data we used for this study were collected only at the time of launch attempts. The 45th Weather Squadron at Cape Canaveral Air Force Station, which supports all of the launches from the Eastern Test Range, has recently started routinely collecting data on rule violations in order to provide better statistics for studies such as this and for the planning of future launches.

This study considered only the impact of an ABFM on rules D, E and F. The ABFM could be used to verify GO launch conditions currently prohibited under rules B and C and to provide statistical information on the usefulness of an ABFM in modifying rules B and C.

The small (5 minutes) launch windows for the STS to dock with the Space Station, coupled with a requirement for other than early morning launches, will make lightning a more relevant factor in the future. If we consider the probability that there will have to be more afternoon launches to re supply the Space Station and MIR and incorporate the use of the ABFM to relax rules B and C, we estimate that the yearly savings would be in excess of $1M.

## REFERENCES

1. J. C. Willett, and A. A. Barnes, "Feasibility Analysis for Measuring Electric Field Aloft," Phillips Laboratory Technical Report, in editing, 1995.

2. A. A. Barnes, and J. C. Willett, "Expanding Launch Windows by Predicting Lightning," Poster paper presented at the 4th Annual Phillips Laboratory Technical Interchange Symposium, Albuquerque, New Mexico, 11 July 1995. Proceedings of this symposium are to be published and distributed in September 1995.

# Table 1 - ABFM Data on the Occurrence of Hazardous Fields Aloft During LCC Rule Violations

| ABFM STATISTIC | LCC (References Superscripted) | | | | |
|---|---|---|---|---|---|
| | RULE D | RULE E | RULE F (Age | | or Standoff) |
| | | | t = 0 | t > 1hr | Within 5nmi |
| Number of Cases | 863 | 524 | 150 | 28 | |
| Number "Hazardous" | 121a | 185c,e | 95n | 0m | ? |
| Hazardous Field | >3kV/m | >5kV/m | >1kV/m | >3kV/m | |
| Ratio: non-hazardous | .860 | .647 | .37 | 1.0 | |
| did not also violate Rule C | .88e | .63e | 1.0r | 1.0r | ? |

a Briefing to LCC "Peer Review Committee" by MSFC at KSC, 2/94
c Winter 1991 Deployment Report, MSFC, 2/25/92
e Winter 1992 Deployment Report, MSFC, 10/8/92
m Mailing to LCC "Peer Review Committee" from NASA/ME, 11/10/93
n D. Mach, personal communication, 9/7/94
r An educated guess

# TABLE 2 -- LCC Rule D, E, and/or F Violations for STS and ELV Delays and Scrubs that were Not also Due to Non-Weather Causes or LCC Rules A or B

| VEHICLE/IMPACT | DATE | INDIVIDUAL RULES | | | | RULE COMBINATIONS | | | |
|---|---|---|---|---|---|---|---|---|---|
| (Countdowns) | | D | E | F | C | D&E | E&F | D&F | D&E&F |
| STS Delays | 910605 | 1 | | | | | | | |
| (79) | 920625 | | | 1 | | | | | |
| | Totals | 1 | 0 | 1 | | 0 | 0 | 0 | 0 |
| | Q | .013 | 0 | .013 | | 0 | 0 | 0 | 0 |
| STS Scrubs | none | | | | | | | | |
| (79) | Totals | 0 | 0 | 0 | | 0 | 0 | 0 | 0 |
| | Q | 0 | 0 | 0 | | 0 | 0 | 0 | 0 |
| ELV Delays | 890510 | 1 | | | | | | | |
| (109) | 890925 | 1 | | | | | | | |
| | 900608 | 1 | | 1 | | | | 1 | |
| | 910107 | | | 1 | | | | | |
| | Totals | 3 | 0 | 2 | | 0 | 0 | 1 | 0 |
| | Q | .028 | 0 | .018 | | 0 | 0 | .009 | 0 |
| ELV Scrubs | 890609 | | | 1 | 1 | | | | |
| (109) | 890812 | 1 | | | 1 | | | | |
| | 891219 | 1 | | 1 | | | | 1 | |
| | 920218 | | | 1 | | | | | |
| | 940423 | 1 | | 1 | | | | 1 | |
| | Totals | 3 | 0 | 4 | | 0 | 0 | 2 | 0 |
| | Q | .028 | 0 | .037 | | 0 | 0 | .018 | 0 |

# Table 3 - False-Alarm Frequencies, P(Rule), and Overall Probability of Unnecessary Delays and Scrubs, P, for STS and ELV

| VEHICLE/IMPACT | INDIVIDUAL RULES | | | RULE COMBINATIONS | | | | OVERALL |
|---|---|---|---|---|---|---|---|---|
| | D | E | F | D&E | E&F | D&F | D&E&F | P |
| STS / Delays | .010 | 0 | .010 | 0 | 0 | 0 | 0 | .020 |
| STS / Scrubs | 0 | 0 | 0 | 0 | 0 | 0 | 0 | 0 |
| ELV / Delays | .021 | 0 | .014 | 0 | 0 | .005 | 0 | .030 |
| ELV / Scrubs | .021 | 0 | .029 | 0 | 0 | .011 | 0 | .039 |

1987 - March 1994

# A RISK MANAGEMENT APPROACH TO LIGHTNING SAFETY

Richard Kithil, Jr.
Lightning Safety Specialists,
Louisville, Colorado 80027-0778
Telephone: (303) 666 8817 Fax: (303) 666 8786

## ABSTRACT

Lightning is a random and unpredictable event. It may ignore whatever defenses mankind conceives. However, site-specific risk management programs can mitigate the lightning hazard. This paper describes recent personal and economic costs due to lightning, perception problems, risk management approaches, and a study of legal implications of the lightning hazard in recreation. The author calls for a National Lightning Safety Institute to coordinate, organize, and promote lightning safety.

## INTRODUCTION

Lightning safety has been little studied and less practiced. In ancient times thunder and lightning were audible and visible signs of the gods' displeasure: there was no defense whatsoever (1). In present times more than 45 different USA lightning protection codes (2) promulgate ambiguity and confusion concerning risk reduction. Current lightning studies are focused mainly upon its physical aspects. Atmospheric physicists, electrical engineers, meteorologists and other skilled disciplinarians probe the behavioral complexities of various sectors. At the same time, business enterprises (3) and trade organizations (4) offer proprietary protection designs. These may be incomplete, misleading or unsubstantiated. There is no Utopia in lightning safety.

The dearth of objective data about lightning safety contributes to accidents and injuries. Common misconceptions include: "*Lightning never strikes twice in the same place*" and "*Lightning rods prevent lightning strikes.*"

The ignorance and misinformation about lightning safety increase lightning's social cost in deaths and injuries and economic cost in electrical and electronic damage, explosions, fire, etc. A disciplined and systematic approach to lightning safety may result in better management of the hazard and reduced costs.

## LIGHTNING'S PERSONAL AND ECONOMIC COSTS

PERSONAL COSTS. Official US weather bureau lightning death and injury statistics have been challenged for two decades. Weigel's 1976 study put under-reporting at 50% (5). In 1993, Lopez, et al. examined *Storm Data* records for Colorado for a 12 year period and compared these with Colorado Health Department and Colorado Hospital Association information for the same duration. They found that *Storm Data* had under reported deaths by 28% and

injuries that required hospitalization by at least 42% (6). There is general agreement that lightning is one of the leading weather-related cause of deaths and injuries.

**Table 1. Annual average severe weather fatalities by decade from 1940-1991, National Weather Service, 1992. (7)**

| Year | Lightning | Tornado | Flood | Hurricane |
|---|---|---|---|---|
| 1940-1949 | 337 | 154 | 144 | 22 |
| 1950-1959 | 184 | 135 | 79 | 87 |
| 1960-1969 | 133 | 94 | 121 | 59 |
| 1970-1979 | 98 | 99 | 182 | 21 |
| 1980-1989 | 72 | 52 | 110 | 12 |
| 1990-1991 | 73 | 46 | 102 | 8 |
| Total (51 yrs.) | 8316 | 5731 | 5828 | 2031 |

Lightning claims 75 to 300 fatalities annually in the United States. Twice that number sustain serious injuries. Thirty percent of strike victims die and 70% of survivors suffer serious long-term after effects (8). Beyond this an unknown number of injuries do not require hospitalization.

Englestatter's 1994 definitive psychological study (see Table 2, below) describes some symptoms suffered by twenty five percent or greater of lightning strike victims (9).

**Table 2. Lightning strike victims sequelae, frequency 25% or greater.**

* Denotes Psychological ** Denotes Psychological or Organic
No Asterisk Denotes Organic

| | | | |
|---|---|---|---|
| Memory Deficits & Loss | 52% ** | Depression | 32% * |
| Attention Deficits | 41% ** | Inability to Sit Long | 32% |
| Sleep Disturbance | 44% * | External Burns | 32% |
| Numbness/Parathesias | 36% ** | Severe Headaches | 32% ** |
| Dizziness | 38% * | Fear of Crowds | 29% * |
| Easily Fatigued | 37% * | Storm Phobia | 29% * |
| Stiffness in Joints | 35% | Inability to Cope | 29% * |
| Irritability/Temper Loss | 34% * | General Weakness | 29% ** |
| Photophobia | 34% | Unable to Work | 29% ** |
| Loss of Strength/Weakness | 34% ** | Reduced Libido | 26% * |
| Muscle Spasms | 34% | Confusion | 25% ** |
| Chronic Fatigue | 32% * | Coordination Problems | 28% ** |
| Hearing Loss | 25% | | |

Despite the magnitude of lightning's effects on people, major federal disaster relief and safety organizations such as Federal Emergency

Management Agency (FEMA) and Occupational Safety and Health Agency (OSHA) have no provisions for personal lightning hazard education, standards, or training (10).

Conclusions from a 1989 public health study of lightning-related deaths were; "Making the public, particularly those in high-risk professions and those who are frequent users of high-risk recreational areas, aware of these [safety] measures through the media and publicity campaigns, is necessary to decrease the annual number of injuries and deaths from lightning strikes." (11)

ECONOMIC COSTS. Lightning-caused property loss statistics vary widely according to source. Different sources give different figures. *Storm Data* computed lightning-related property damage costs for the 1990-1992 period at $27 million annually (12). This data was obtained from newspaper clippings. The National Fire Protection Association (NFPA) reported direct annual structural lightning losses at $138.7 million as averaged over 1989-1993 (13). This information came from the nation's fire chiefs.

Holle et al. analyzed a major insurance company's lightning claim costs in Colorado, Wyoming and Utah. These were extrapolated to national figures. This finding showed there to be 307,000 separate claims totaling $332 million annually (14). A fourth source, the Insurance Information Institute, described national lightning damage amounting to nearly five percent of all paid insurance claims, with residential claims alone exceeding one billion dollars during 1990 (15).

Commercial claim costs are higher than those for residences. The Factory Mutual System reported 2,926 lightning claims in the 1973-1982 period, for a total cost of some $385 million. Average per claim cost was in excess of $13,000 (16). Statistical accuracy notwithstanding, the direct and indirect effects of lightning to electrical and electronic equipment are significant, and there is some recognition of the problem. Annual USA sales of Category A, B & C electrical surge protectors are about $800 million (17). Kessler describes an Oklahoma rural electric power cooperative (distribution only) that adopted widespread use of lightning arrestors, the cost of which amounted to some 5% of its' total asset value (18). Golde states that some 0.5% of all electric power investments for distribution and generating equipment are represented by lightning protection devices. These are estimated to reduce lightning damage by some 90% (19).

The insurance industry widely promotes policy cost discounts for use of deadbolt locks, fire extinguishers, security alarms, smoke detectors, etc. In contrast, for the most part there are no equivalent incentives for use of devices by the insured to protect sensitive electronic equipment.

A strong case can be made for reducing human and economic costs through the adoption of defensive measures. It is obvious that precise cost and loss figures are lacking. It also is apparent that the opportunity to achieve significant savings is overlooked.

## THE RISK PERCEPTION PROBLEM

A combination of limited information and ignorance can yield false conclusions . People respond to the lightning hazard as they perceive the risk. Thus, a faulty reaction might be: *"Lightning never strikes twice. It hit that tree during the last storm. I'll stand underneath it during this storm. It's a safe place."* Whereas an accurate reaction would be: "*The Red Cross brochure said an enclosed car is a safe place during lightning. I'll get into mine right now."*

Why is lightning underestimated as a hazard? Behavioral science has demonstrated that lay persons' risk analysis mostly is based upon anecdotal evidence, guesswork, hearsay, intuition, and personal experience instead of known facts (20, 21). Personal risk-weighing is a complex process. Some considerations are (22):

- *Is there a catastrophic potential?* Large scale events (floods and hurricanes) appear more threatening than random and isolated events (lightning).
- *Is it a familiar event?* "I do/do not know someone who was injured by lightning."
- *Is the hazard understood?* People have more fear about poorly understood subjects than well understood ones.
- *What are the effects on children?* Concern is higher where children are at risk.
- *What are the economic consequences?* The likelihood of incurring an unexpected financial burden such as an injury or loss of income increases concern.

These and other perceptions will influence individual decision-making regarding the lightning hazard. They also influence decision-makers such as architects and engineers who may or may not decide to include lightning safety and protection for their clients. A major Florida public school district provides a typical example of how lightning hazard risk decisions are made on a organizational or corporate level. The institution comprises 132 separate campuses. It is building seven or eight new schools per year. In early 1995 a lightning safety proposal recommended that the institution undertake design review, hazard identification, site inspections, facility analysis, risk assessment and personal exposure, overall safety evaluation and costs identification (23). The proposal outline was generated as a result of three random site inspections which showed:

- *Poorly grounded metal fences and gates at athletic fields;*
- *Improperly installed air terminals on high mast lighting stands;*
- *Use of ungrounded metal flagpoles at main entrances;*
- *Metal roofs with no bonding or grounding;*
- *Absence of transient voltage surge suppression and grounding to high voltage air conditioning, TV satellite dishes, closed circuit TV security cameras, and computer classroom equipment;*
- *Inconsistent use of protective equipment;*
- *Design and construction methods not in accord with NFPA*

*Lightning Protection Standard 780 or the National Electrical Code;*
- *Absence of any lightning safety training for teachers, athletic coaches, or administrative personnel. No lightning safety protocols in place;*
- *No awareness on the part of architectural or engineering consultants concerning lightning mitigation issues.*

The institution took no action in accepting, acknowledging, rejecting, or replying to the proposal. There was no interest in lightning safety.

Clearly a greater understanding of individual as well as organization risk perception is needed by safety educators. With this new knowledge, lightning safety information can be designed with more effectiveness.

## LIGHTNING SAFETY: A RISK MANAGEMENT APPROACH

Useful lightning detection tools tell us where lightning has struck. But the question remains: where will it strike next? The *prediction* of exact lightning strikes is not yet possible.

The highest threshold of lightning safety can be achieved by adopting a site-specific systems approach. Hardware and software should be integrated to this end. A single piece of equipment, such as a detector, will not in itself provide adequate risk reduction.

The goal is to construct focused defensive measures which collectively have the means of mitigating the lightning risk. What constitutes Risk in this environment? Risk is uncertainty. Risk is the possibility of loss. Risk is the probability of any adverse outcome (24). Risk management is a euphemism for present action to address a potential future problem. In this context, the are two basic choices: **do something** or **do nothing** to reduce the hazard.

A site-specific risk management program can be adopted for lightning hazards. In such programs adopting a "worst case" attitude is advised (25). The crisis scenario is described in Table 3.

**Table 3. Lightning Crisis Statement**

- We cannot stop lightning from striking.
- We will have lightning events in our area.
- We will experience equipment damage.
- We will have personal deaths and injuries.
- We will get sued.

Using the above gloomy hypothetical situation, what defensive measures can be adopted at reasonable cost? Five primary areas should be addressed:

- *Authentication.* In particular, senior management should recognize the hazard and issue a serious policy statement. Specialized equipment should be inspected and maintained to schedule. Record keeping should be detailed. Lightning awareness should be a part of the overall safety program

of the organization.

- *Information.* Post "Do's and Don'ts" safety stickers in creative locations such as on restroom mirrors and vending machines, as well as on bulletin boards and on maintenance equipment. Display posters and other educational signs. Conduct regular CPR training sessions for employees.
- *Detection.* Provide advance notice of lightning. Detectors are useful management tools: they assist in timely decisions to suspend operations and to resume operations. Credible detectors may use a variety of technologies including inferometry, network systems, optical cloud-to-cloud or cloud-to-ground, potential gradient, RF discharges and a combination of the preceding. Some models provide useful features such as battery backup, easy operator interpretation, internal surge protection, output ports for connected equipment, etc.
- *Notification.* Once lightning is detected, issue accurate and comprehensible warnings. Commercially available options to do this include public address systems, two way radios, dedicated alarm and siren systems using voice and/or visual messaging, and air horns. A procedure must be in place for timely notification which can be understood by all concerned.
- *Protection.* In brief:

  Provide safe shelter;
  Prepare an evacuation plan;
  Equip structures with air terminals, down conductors and low impedance grounding devices;
  Install appropriate power surge protection equipment to guard electrical and electronic components;
  Meet or exceed all Codes and Standards;
  Avoid equipment and vendor claims that are based upon pseudo-science.

No risk management program will prevent lightning from striking near or on a facility. But it is possible to have in place a protocol to maximize overall lightning safety.

## LEGAL IMPLICATIONS: A RECREATION EXAMPLE (26)

Recreation personnel should understand how to warn and to protect customers and employees against the lightning hazard. Families of lightning victims often bring suit against sports and recreation facilities (27). Most lawsuits from lightning events are based upon allegations of negligence---that is, that the defendants failed to take reasonable precautions to protect and/or to warn about foreseeable dangers.

When an activity has a risk of injury, and that risk can be reduced or eliminated by notifying the participant of that risk, strong legal considerations dictate that warnings be given to those people who might be injured. The Duty

To Warn concept routinely is observed on airline passenger in-flight information, on aspirin, beer and cigarette labels, fire and police vehicle sirens, on industrial safety signage, at railroad crossings, on step ladders, etc. Its theory and use applies to recreation situations as well.

With the development of reliable lightning detectors, it frequently is possible to learn of lightning hazards before they occur. By integrating detectors with other defenses such as air terminals, good grounding, management policies, safety signage, sirens, and surge protection the recreation facility can demonstrate it has mounted a "best efforts" defense against the hazards of lightning.

In contrast, failing to acquire the capability to detect/notify/protect may provide significant difficulties to a recreation facility which is being sued as the result of a lightning event. The threat might have been detected. Warning might have been given. Death or injury might have been avoided. It is a reasonable expectation that recreation facilities would try to manage this hazard.

There are in excess of 100,000 outdoor public and private recreation facilities in the USA, including parks, stadiums, and sports fields (golf, baseball, soccer, tennis, etc.) swimming pools, picnic sites, camping and boating areas, etc. At this writing, fewer than 1500 have installed lightning detection and warning devices (28). It is unfortunate that this safety concept is not well understood.

## CALL FOR A NATIONAL LIGHTNING SAFETY INSTITUTE

The failure to increase lightning safety awareness and to reduce lightning's social and economic costs is a consequence, in part, of the absence of cohesive and consistent national education.

Several specialized organizations are recent valuable contributors to the pool of lightning information studies. Works by Cherington, Yarnell et al. at the Denver-based Lightning Data Center have described considerable neurological research upon lightning victims (29, 30). The Lightning Strike and Electric Shock Victims Institute functions as a grief therapy center for lightning injured people and their families (31) These efforts notwithstanding, a unified national approach to the promotion of lightning safety is needed. There have been previous calls for national lightning safety boards (32). The author urges that one be established under the following general guidelines.

### National Lightning Safety Institute (NLSI)

(Preliminary Conceptual Design)

1. Mission Statement.

   A. NLSI promotes education and information about lightning safety and lightning hazard mitigation. Seminars and certification programs are provided for a broad base of employers, government agencies and non-profit groups.

B. NLSI is a lightning data resource center providing information for all interested private and public organizations.

C. NLSI maintains close relationships with concerned professional associations, the insurance industry, and public agencies such as FEMA, OSHA, National Oceanic and Atmospheric Administration (NOAA), Environmental Protection Administration (EPA), National Institute of Mental Health (NIMH), etc.

2. Organization.

NLSI is a non-profit corporation. It is overseen by a Board of Directors and officers. The Executive Director and staff run NLSI on a day- to-day basis. An appointed National Advisory Board recommends and reviews programs, policies and other activities of the Institute.

3. Proposed Initial Outreach Programs.

A. Lightning safety seminars.

B. Accreditation training for "Certified Lightning Safety Professionals."

C. Annual Workshop.

D. Monthly newsletter. World Wide Web home page.

E. Target Education Programs.

1. Youth groups such as Boy Scouts, Girl Scouts, 4H. National outdoor youth sports leagues such as baseball, golf, rodeo, soccer, swimming, tennis, etc.
2. State, county and city Parks & Recreation organizations.
3. Architectural and engineering (A&E) associations.

F. Media interaction and press releases.

G. Lightning incident investigations.

4. Financial support.

Financial support is solicited from industry, from professional associations, from the insurance community, and from government agencies. Income is generated from seminars and accreditation programs.

An adequately funded and pro-active lightning safety organization will provide national leadership and will promote awareness to mitigate lightning costs. It is an achievable goal.

ACKNOWLEDGMENTS.

The author acknowledges guidance and support from Dave Butler, Michael Cherington, MD., Bill Jafferis, and Warren Simmons. Appreciation also goes to members of the Denver-based Lightning Data Center. Finally, thanks to my wife and companion Lynda for aid and comfort.

## REFERENCES


1. Viemeister, P., "The Lightning Book." Cambridge, Mass.: MIT Press, 1961.
2. Information Handling Service. "Lightning Protection." Worldwide Standards Index, CD Rom, December, 1994.
3. Carpenter, R.B. ," Lightning and Surge Protection for Substations." IEEE Transactions on Industry Applications, Vol. 31, No. 1, Jan/Feb 1995.
4. "Encyclopedia of Associations." Detroit, MI: Gale Research, 1993.
5. Weigel, E.P., "Lightning: The Underrated Killer." NOAA, 6(2), 1976.
6. Lopez, R.E., Holle, R.L., Heitkamp, T.A., Boyson, M., Cherington, M., and Langford, K. "The Underreporting of Lightning Injuries and Deaths in Colorado, Bulletin of the American Meterological Society. November, 1993.
7. Vavrek, J. , Holle, R. L., and Allsop, J., "Flash To Bang." The Earth Scientist. Fall, 1993.
8. "Pediatric Basic Life Support." Journal of the American Medical Association, October 28, 1992.
9. Englestatter, G.H., "Psychological and Neuropsychological Sequelae to Lightning Strike and Electric Shock Injuries." Fourth Annual Meeting of Lightning Strike and Electric Shock Victims International, Maggie Valley, North Carolina, May 1994.
10. Review of FEMA and OSHA training programs by the author. July, 1995.
11. Duclos, P.J. and Sanderson, L.M., "An Epidemiological Description of Lightning-Related Deaths in the United States." International Journal of Epidemiology, Vol. 19, No. 3, Nov. 1989.
12. Holle, R., Lopez, R., Arnold, L., and Endres, J., "Insured Property Damage Due to Lightning in Three Western US States." 1995 International Aerospace and Ground Conference on Lightning and Static Electricity, Williamsburg, Virginia. September, 1995.
13. Author's correspondence with National Fire Protection Association. May, 1995.
14. Holle, et al. , op cit.
15. Insurance Information Institute, Consumer News, "Summer Storms Can Be Electrifying." Press Release. New York. August 11, 1989.
16. Byerly, L. and Reed, J., "Lightning Protection by Way of Thunderstorm Sensing and Automatic Electrical Isolation." International Aerospace and Ground Conference on Lightning and Static Electricity. October, 1992.
17. Author's correspondence with Jack O'Connell, VP, Zero Surge, Inc. Frenchtown, New Jersey.
18. Kessler, E., "The Thunderstorm in Human Affairs." Norman, OK: University of Oklahoma Press, 1983.

19. Golde, R.H. (ed.), "Lightning Protection." New York, New York: Academic Press, 1977.
20. Petak, W. J., "Natural Hazard Risk Assessment and Public Policy." New York, New York: Springer-Verlag, 1982.
21. Greening, L. and Dollinger, S.J., "Adolescents' Perceptions of Lightning and Tornado Risks." Journal of Applied Social Psychology, 1992, 22, 10.
22. Covello, V., "Social and Behavioral Research on Risk: Uses in Risk Management Decision making.", NATO Series, Vol. G4, Berlin, Germany:Springer-Verlag. 1985.
23. Business correspondence, author to client, April, 1995.
24. Whyte, A. V. and Burton, I., "Environmental Risk Assessment." Scientific Committee on Problems of the Environment (SCOPE), New York, New York:Wiley. 1980.
25. Seldner, B. and Cothrel, J.P., "Environmental Decision making for Engineering and Business Managers.", New York: McGraw Hill, 1994.
26. Adapted from an article by the author, " Warning Against Lightning by Golf Courses is Vital." Park/Grounds Management, January 1994.
27. Draper, J.M., "Personal Injury or Property Damage Caused by Lightning as a Basis of Tort Liability." 46 ALR4th Quick Index, American Law Review, 1994.
28. "Statistical Abstract, 1993" and author's correspondence with lightning detection manufacturers and distributors.
29. Cherington, M. , Yarnell, P.R. and London, S.F., "Neurologic Complications of Lightning Injuries." Western Journal of Medicine, 162. May, 1995.
30. Cherington, M. "Lightning Injuries." Annals of Emergency Medicine, 25. April 1995.
31. Lightning Strike and Electric Shock Victims International, Jacksonville, North Carolina.
33. Moore, C.B., Brook, M., and Krider, E.P., "A Study of Lightning Protection Systems.", Office of Naval Research, October 1981.

# LIGHTNING THREAT PROBABILITY FOR SPACE LAUNCH OPERATIONS

T. J. Lie
The Aerospace Corporation, M4/935
P.O.Box 92957
Los Angeles, CA 90009
Telephone (310)336-7274 FAX (310)336-5581

R. Briët
The Aerospace Corporation, M4/935
P.O.Box 92957
Los Angeles, CA 90009
Telephone (310)336-1912 FAX (310)336-5581

ABSTRACT

The present report formulates the lightning threat probability with application intended for space launch operations. If a launch operation is vulnerable to a lightning-induced electromagnetic pulse (LEMP) field greater than certain critical threshold, then the lightning threat probability predicts the likelihood that such damaging lightning strokes occur in the launch pad neighborhood in a given time period. It is also claimed that the lightning threat probability formalism is an indispensable tool for specifying lightning protection measures.

## Introduction

Lightning-induced electromagnetic pulse (LEMP) is a threat to every launch operation. One of the questions constantly asked is: what is the chance that LEMP can be damaging to the operation? This is the problem of predicting the lightning threat probability. The present report mathematically formulates this probability and applies it to a Titan launch system.

We suppose that the space launch system concerned is vulnerable to LEMP fields exceeding a critical threshold $H_c$:

$H_c$=critical LEMP field beyond which the system is vulnerable.

Following is an example problem. It was reported[1,2] that a lightning stroke of 20 kA current pulse could be damaging to a Titan launch system, if it occurred at 1 km away from the launch pad. The peak magnetic field of lightning was assumed to follow the Biot-Savart Law:

$$H_{pk} = I_{pk}/2\pi\rho \quad , \tag{1}$$

where $H_{pk}$=peak magnetic LEMP field

---

[1] Wilson, H. Z., and Heritage, H. A., "Lightning Evaluation, Eastern Space and Missile Center," Aerospace TOR-0088(3441-45)-1, The Aerospace Corp, 1 August 1988.

[2] Wilson, H. Z., "Lightning Effects at PAD-40 due to Nearby Strikes," Aerospace ATM 85(5447-03)-01, The Aerospace Corp, 19 June 1985.

$I_{pk}$ =lightning peak current
$\rho$ =horizontal distance from lightning.

The critical threshold $H_c$ for the Titan launch system is defined by the $H_{pk}$ of a 20 kA lightning at 1 km away, yielding $H_c$=3.183 A/m. One can thus pose the following question:

> Given a critical magnetic field $H_c$, what is the probability that the magnetic LEMP field at the launch pad exceeds this critical field due to lightnings in the neighborhood during a given cumulative time period of $t$, say, ten days?

A neighborhood is defined to be a perimeter of radius $R$, e.g., 10 km. The cumulative time $t$ is the accumulated time period during which the vulnerable components of the launch system are exposed to LEMP.

Conversely, suppose that the lightning survivability requirement of a launch system is specified to be, say, 99% for a period of 10 days. The natural question is:

> What is the electromagnetic (EM) field level to which the launch system needs to be hardened in order to meet the survivability requirement?

The lightning threat probability formalism is a useful tool for specifying the LEMP hardening.

The report is presented in the following order: In the next section, some mathematical notations are explained. In the third and fourth sections, the rate and probability of LEMP threats are formulated. The fifth section relates to a numerical application of the formulas to a Titan launch system. The LEMP hardening for lightning survivability requirements is discussed in the sixth section. The concluding summary is given in the last section.

## Definition of Mathematical Notations

Some mathematical notations need to be defined.

For the functional dependence of the peak magnetic field $H_{pk}$ on distance $\rho$, we assume, instead of Equation (1), the following generalized form:

$$H_{pk} = A I_{pk} / \rho^n , \tag{1A}$$

where the two constants $A$ and $n$ are empirically determined to fit the numerical calculation[3] of $H_{pk}$ in the near field of the lightning: $A$=0.105, $n$=1.15 (see Appendix A). Equation (1) is a special case of Equation (1A) with $A$=0.159 and $n$=1.

We define an average lightning density $D$ per 1985 data[1]:

$$\begin{aligned} D &= \text{average number of lightnings per day per square km} \\ &= 0.054 \ \text{(during summer months at Cape Canaveral).} \end{aligned} \tag{2}$$

---

[3] Lie, T. J., "Lightning-induced Electromagnetic Pulse (LEMP)," Aerospace TOR, The Aerospace Corp, (to be published).

Then, the rate of lightnings $\lambda(R)$ per day inside a neighborhood perimeter of radius $R$ (km) is

$$\lambda(R)=\pi R^2 D \quad \text{(daily rate of all lightnings per day in the neighborhood).} \tag{3}$$

The LEMP threat rate $\lambda(H_c;R)$, which is formulated in the next section, is defined:

$$\lambda(H_c;R)=\text{daily rate of LEMP threats of } H_{pk} \geq H_c \text{ in the neighborhood.} \tag{4}$$

Some formulas are expressed in terms of the normal distribution functions $P(z)$ and $Q(z)$:

$$\begin{aligned} P(z) &= \text{normal distribution function} = \int_{-\infty}^{z} \frac{ds}{\sqrt{2\pi}} e^{-s^2/2}, \\ Q(z) &= 1 - P(z) = \int_{z}^{\infty} \frac{ds}{\sqrt{2\pi}} e^{-s^2/2}. \end{aligned} \tag{5}$$

For instance, the lightning peak current distribution is described by the lognormal distribution[4]:

$$\begin{aligned} \text{Prob}(I_{pk} \geq I_c) &= \text{probability of lightning peak current } I_{pk} \text{ exceeding } I_c \\ &= P[ln(I_{pk}/I_m)/\sigma] \end{aligned} \tag{6}$$

where[5]

$$\begin{aligned} I_m &= \text{mean peak current} = 21.5\,kA, \\ \sigma &= \text{standard deviation} = 0.505. \end{aligned} \tag{6A}$$

**Rate of LEMP Threats** $\lambda(H_c; R)$

The mathematical formula for the daily rate of LEMP threats $\lambda(H_c;R)$ is derived below. The detailed calculations are deferred to Appendix A.

The average number per day of lightning strokes at a distance $\rho$ (km) from the launch pad within a width of $d\rho$ is given by $2\pi\rho D d\rho$, where $D$, as defined by Equation (2), is the average density of lightning strokes per day. We define the following probability:

$$\text{Prob}(H_{pk} \geq H_c|\rho) = \text{Probability for LEMP event of } H_{pk} \geq H_c \text{ under the condition that the lightning has struck at distance } \rho.$$

Then, the daily LEMP threat rate, $\lambda(H_c;R)$, of lightning strokes of $H_{pk} \geq H_c$ per day that strike within the launch pad neighborhood of radius $R$ is expressed as follows:

---

[4] Cianos, N,, and Pierce, E. T., "A Ground-Lightning Environment for Engineering Usage," Technical Report 1, Stanford Research Institute, August 1972.

[5] Chai, J. C., Private Communications, based on M. Maier's Memo for Computer Science Raytheon, dated 7 October 1991.

$$\lambda(H_c; R) = \int_0^R 2\pi\rho D \times \text{Prob}(H_{pk} \geq H_c|\rho)d\rho. \tag{7}$$

If we assume $H_{pk} = A I_{pk}/\rho^n$ and define the minimum critical current $I_c(\rho) = \rho^n H_c/A$ at distance $\rho$, then the event of $H_{pk} \geq H_c$ at distance $\rho$ is equivalent to the event of the lightning peak current $I_{pk}$ greater than $I_c(\rho)$:

$$\text{Prob}(H_{pk} \geq H_c|\rho) = \text{Prob}(I_{pk} \geq I_c(\rho)), \tag{8}$$

where $\text{Prob}(I_{pk} \geq I_c)$ is defined by Equation (6).

As it is shown in Appendix A, the integral of Equation (7), with insertion of Equation (8), can be expressed in terms of the normal distribution functions $P(z)$ and $Q(z)$ as follows:

$$\lambda(H_c; R) = \lambda(R)\left[Q(Z + \sigma_n) + P(Z - \sigma_n)e^{-2\sigma_n Z}\right], \tag{9}$$

where $$Z = \frac{1}{\sigma_n} ln\left(\frac{R}{R_m}\right) \text{ with } \sigma_n = \sigma/n \text{ and } R_m = \left(AI_m/H_c\right)^{1/n} exp(\sigma_n^2). \tag{9A}$$

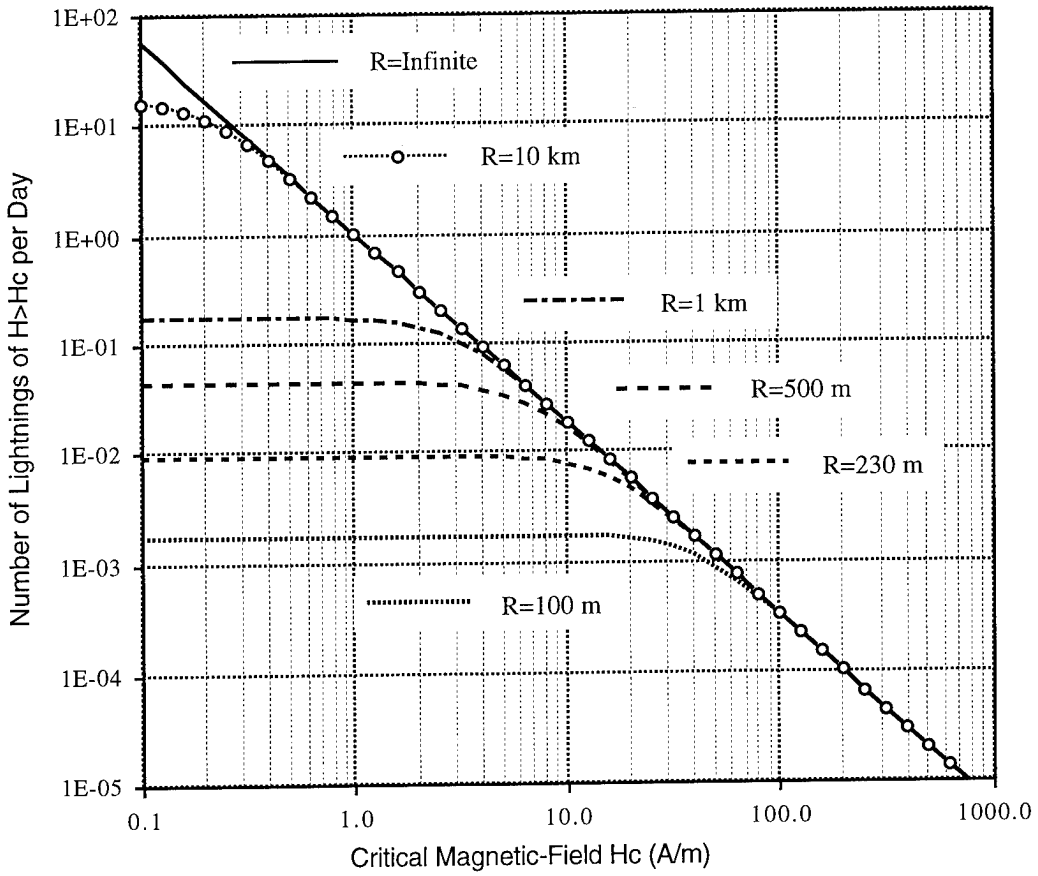



FIGURE 1: AVERAGE NUMBER OF DAMAGING LIGHTNINGS PER DAY
(FOR VARIOUS PERIMETER RADII *R*)

Figure 1 illustrates the LEMP threat rate $\lambda(H_c; R)$ as a function of $H_c$ for various perimeter radii $R$. It is noted that, as $R$ and $H_c$ go to infinity, Equation (9) reduces to:

$$\lambda(H_c; R) \xrightarrow[R, H_c \to \infty]{} \lambda_m(H_c) = \pi D R_m^2 = const / H_c^{2/n}, \tag{10}$$

and, in the limit as $R$ and $H_c$ go to zero, we obtain:

$$\lambda(H_c; R) \xrightarrow[R, H_c \to 0]{} \lambda(R) = \pi D R^2. \tag{10A}$$

**Lightning Threat Probability** $P_T(t, H_c; R)$

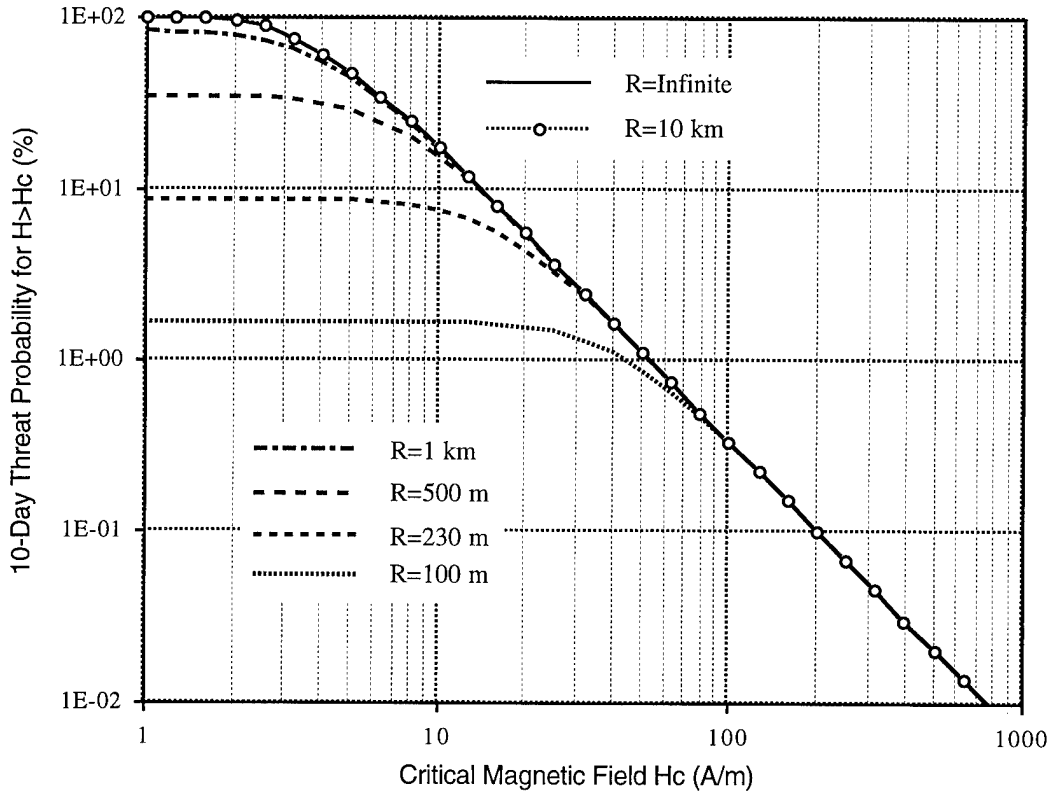



FIGURE 2: LIGHTNING THREAT PROBABILITY FOR 10 DAYS
(FOR VARIOUS PERIMETER RADII $R$)

With assumption of the Poisson process, the probability that the LEMP threats occur $k$ times† during a time period of $t$ is given by:

$$p_k(t, H_c; R) = \frac{[\lambda(H_c; R)t]^k}{k!} exp[-\lambda(H_c; R)t], \tag{11}$$

† $k$ is an arbitrary integer number ≥ 0.

and the lightning threat probability, i.e., the probability that the threat lightnings occur at least once in a time period of $t$, reads:

$$P_T(t, H_c; R) = 1 - exp[-\lambda(H_c; R)t]. \quad (12)$$

Figure 2 illustrates this lightning threat probability for $t$=10 days.

## Numerical Application to Titan Launch System

For the Titan launch system cited in the Introduction, the critical threshold magnetic field was $H_c$=3.2 A/m. For this case, the daily rate of LEMP threats and the 1- and 10-day lightning threat probabilities are listed in Table 1 for various perimeter radii $R$. This is the case without the catenary protection of the Titan launch complex.

TABLE 1: DAILY RATE OF THREAT LIGHTNING AND 1- AND 10-DAY LIGHTNING THREAT PROBABILITIES FOR THE TITAN LAUNCH SYSTEM FOR VARIOUS PERIMETER RADIUS $R$ (CRITICAL THRESHOLD MAGNETIC FIELD $H_C$=3.2 A/M)

| Perimeter Radius $R$ (km) | LEMP Threats per day: $\lambda(H_c; R)$ | 1-Day Prob $P_T(t, H_c; R)$ (%) | 10-Day Prob $P_T(t, H_c; R)$ (%) |
|---|---|---|---|
| 0.10 | 1.70E-03 | 1.70E-01 | 1.7 |
| 0.23 | 8.97E-03 | 0.89 | 8.6 |
| 0.50 | 3.98E-02 | 3.90 | 32.9 |
| 1.00 | 1.01E-01 | 9.61 | 63.4 |
| 10.00 | 1.39E-01 | 13.0 | 75.1 |
| Infinite | 1.39E-01 | 13.0 | 75.1 |

The presence of the catenary structure introduces two levels of critical field: one applicable to lightnings occurring outside the catenary tent, and the other inside the tent.

The catenary structure reduces[4] the electromagnetic fields by a factor of at least 30 when lightning strokes occur outside the catenary coverage area of 230 m radius. Hence, for lightnings occurring outside the catenary array, the critical field can be set at: $H_c$=95.5 A/m. Figures 1 and 2 show that, for $H_c$ of this high level, the contributions to the lightning threat probability for $H \geq H_c$ from all lightning events outside the 230m radius perimeter become negligible; only those lightning events striking inside the perimeter of radius $R$=230m are a concern for potential damage to the launch system.

For the cases of lightnings striking inside the catenary coverage area, some hit the catenary structure and the others land on the inside perimeter ground[6]. For those strokes hitting the catenary structure, the peak values of the scattered electromagnetic fields inside the catenary array do not

---

6 Jackson, W. M., Eley, H. E., Chai, J. C., and Briët, "Probability Calculation of Direct Lightning Attachments to Structures at SLC40/41," preprint paper submitted to the 1995 International Lightning Conference to be held in September 1995.

appear[7] to be reduced from the peak values of the fields without the catenary. *For these reasons and for the sake of conservatism, we assume that the catenary provides no shielding effects when the lightning events occur within the catenary perimeter.* This means that, with the catenary protection, the neighborhood perimeter radius $R$ is set to $R$=230m and the critical field $H_c$ remains $H_c$=3.2 A/m. For this case, the rate of threat lightnings and the threat probabilities are given by the 2nd row of Table 1 above.

## LEMP Hardening Levels for Lightning Survivability

Suppose that the lightning survivability of a launch system is required to be 99% for a cumulative time period of 10 days. What should be the LEMP hardening level to meet this requirement? The 99% survivability means that the lightning threat probability is 1%. From Figure 2, the critical threshold magnetic field $H_c$ is read to be 50 A/m. The near field pattern of lightning reveals (see Figure A of Appendix A) that the ratio of $E$-field to $H$-field is about 1000. Therefore, the critical threshold electric field $E_c$ corresponding to this $H_c$ is about 50 kV/m, which is comparable to that of the nuclear electromagnetic pulse (EMP). This is the LEMP level to which the launch system must be hardened.

An example case of lightning requirements cites a 99.9999% survivability for an electro-explosive device (EED) of a launch system with no indication of a time period. Suppose the time period is cumulatively $t$=1 day. One can find from the lightning threat probability formalism that the EED must be hardened to an extraordinarily high magnetic field of $H_c$=2.8 kA/m. This is an LEMP field at about 10 m distance from a 300 kA lightning. Thus, the 99.9999% survivability is requiring that the launch system must be hardened almost to a direct hit of 300 kA lightning, which can occur at most once in 1,600 years within a 10 km radius perimeter in Cape Canaveral.

The lightning threat probability formalism is a necessary tool for specifying lightning protection measures.

## Conclusions

The present report formulates the lightning threat probability for space launch operations. For a launch system that is vulnerable to an LEMP field greater than certain critical threshold $H_c$, the lightning threat probability yields the probability of having such threat lightnings in the neighborhood in a given period of time. The critical threshold field can be specified either by magnetic or electric field.

The report has chosen a sample case of a Titan launch system in Cape Canaveral that was diagnosed to be vulnerable to magnetic fields greater than $H_c$=3.2 A/m. With the critical threshold set at $H_c$=3.2 A/m and the neighborhood perimeter radius at $R$=10 km, the present report finds that the rate of LEMP threats in the neighborhood is 0.14 per day, and the lightning threat probability is 75% for 10 days, meaning that the lightning survival probability is 25% for 10 days. This is the case with no catenary protections. With the shielding effects of the catenary structure of the Titan

---

[7] Chai, J. C., Heritage, H. A., and Briët, R., "Electromagnetic Effects of the Four-Tower Supported Catenary Wires Array Lightning Protection System," Proceedings of the 1994 International Aerospace and Ground Conference on Lightning and Static Electricity, pp377-386, Bundesakademie für Wehrverwaltung und Wehrtechnik, Mannheim, Germany, May 1994.

launch complex, the lightning threat probability drops to 8.6% for 10 days, which means that the lightning survival probability is 91.4% for 10 days.

Conversely, if a system requirement specifies the lightning survival probability for a period of time, then, through the lightning threat probability formula, one can define the critical threshold $H_c$ to which the system under consideration must be hardened. Suppose that the survivability requirement is 99% for 10 days. Then, the critical threshold magnetic field is found to be $H_c \approx 50$ A/m, and the corresponding electric field to be $E_c \approx 50$ kV/m, which should be the required hardening specification to meet the 99% survivability requirement for 10 days. The lightning threat probability formalism is an indispensable tool for specifying lightning protection measures.

---

APPENDIX A: Mathematical Formulation of LEMP Threat Rate $\lambda(H_c;R)$

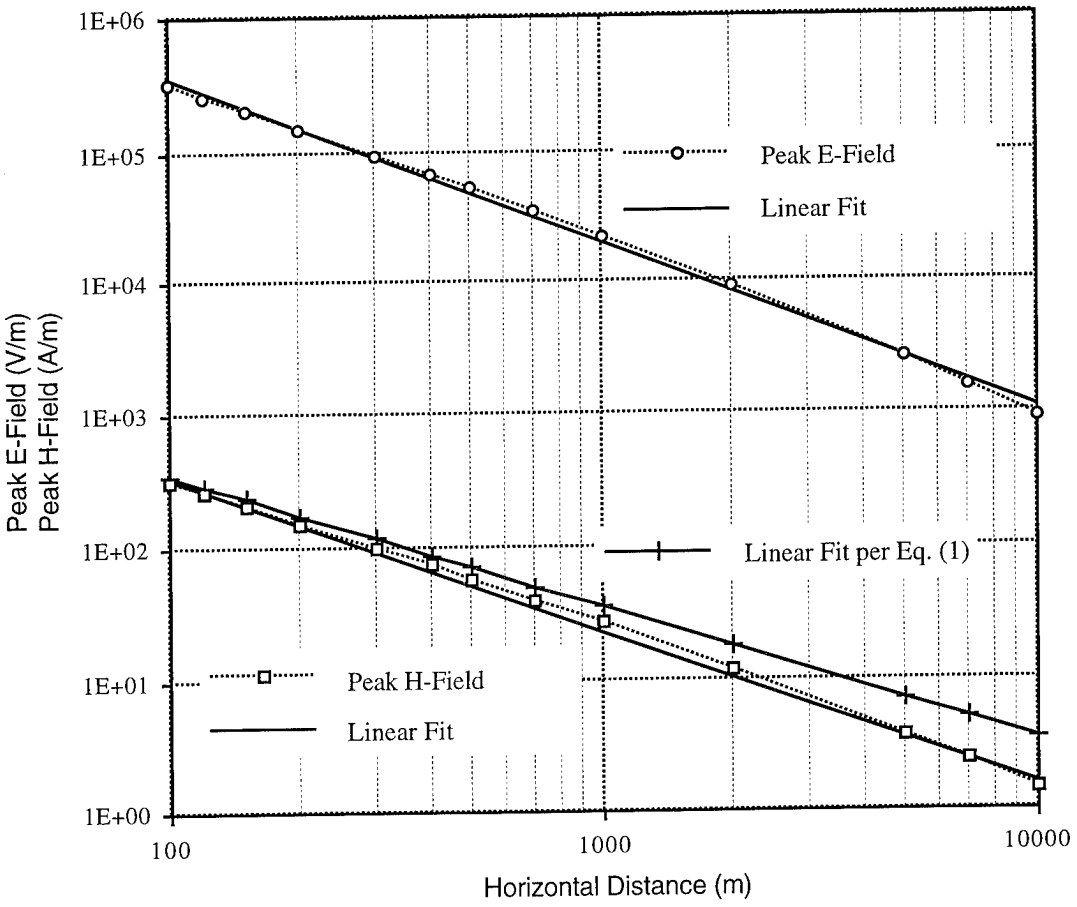



FIGURE A: LIGHTNING PEAK E AND H FIELDS AS FUNCTION OF DISTANCE AND APPROXIMATE POWER LAW FIT PER $(1/\rho^n)$

Figure A describes the peak electric and magnetic fields[3], $E_{pk}$ and $H_{pk}$, of lightning as observed at 150 ft above ground as functions of the horizontal distance $\rho$ for the case of the Component "A" lightning with a peak current of 220 kA as specified in MIL-STD-1795A.

As mentioned in the Introduction, the peak $H$-field, $H_{pk}$, is usually assumed[2] to follow the Biot-Savart law as given in Equation (1):

$$H_{pk} = I_{pk}/2\pi\rho \ , \tag{1}$$

where $I_{pk}$ =lightning peak current
$\rho$ =horizontal distance from lightning.

Figure A demonstrates[3] that it is better to assume the following more general form, instead of Equation (1):

$$H_{pk} = A I_{pk}/\rho^n , \tag{A1}$$

where the constant factor $A$ and the exponent $n$ are given empirically from Figure A:

$A$=0.105 (compared with 0.159 in case of Equation (1)),
and $n$=1.15 (compared with 1 in case of Equation (1)).

It is noted in Figure A that the peak $E$-field $E_{pk}$ in V/m is about 1000 Ω times the $H_{pk}$ in A/m† .

The rate of LEMP threat of $H_{pk} \geq H_c$ is given as follows (see Equations (7,8)):

$$\begin{aligned} \lambda(H_c; R) &= \int_0^R 2\pi\rho D \times \text{Prob}(H_{pk} \geq H_c|\rho) d\rho \\ &= \int_0^R 2\pi\rho D \times \text{Prob}(I_{pk} \geq I_c(\rho)) d\rho, \end{aligned} \tag{A2}$$

where $I_c(\rho)$ is defined $I_c(\rho) = \rho^n H_c/A$. The conditional probability $\text{Prob}(H_{pk} \geq H_c|\rho)$ is the probability of $H_{pk} \geq H_c$ under the condition that the lightning is at distance ρ, and $\text{Prob}(I_{pk} \geq I_c)$ is the probability that the lightning peak current $I_{pk}$ is greater than $I_c$.

With substitution of Equation (6) for $\text{Prob}(I_{pk} \geq I_c)$, we get:

$$\lambda(H_c; R) = \lambda(R) \int_0^R 2(\rho/R^2) d\rho \int_{x(\rho)}^{\infty} \frac{dy}{\sqrt{2\pi}} exp(-y^2/2), \tag{A3}$$

where $$x(\rho) = \frac{1}{\sigma} ln\left(\frac{\rho^n H_c}{A I_m}\right),$$

and $I_m$ is the mean peak current and $\sigma$ the standard deviation of the lightning peak current distribution (see Equations (6, 6A)).

By changing the integration variable from $\rho$ to $x$, we obtain, by defining $\sigma_n = \sigma/n$:

---

† $E_{pk} = A I_{pk}/\rho^n$ with $A = 90.9$, $n = 1.25$.

$$\rho = \left(\frac{AI_m}{H_c}\right)^{1/n} e^{\sigma_n x}, \qquad d\rho = \sigma_n \left(\frac{AI_m}{H_c}\right)^{1/n} e^{\sigma_n x} dx,$$

and $$\lambda(H_c; R) = 2\sigma_n \lambda(R) \left(\frac{AI_m}{R^n H_c}\right)^{2/n} \int_{-\infty}^{X} exp(2\sigma_n x) dx \int_{x}^{\infty} \frac{dy}{\sqrt{2\pi}} exp(-y^2/2),$$

where the integral upper limit $X$ is: $$X = \frac{1}{\sigma} ln\left(\frac{R^n H_c}{AI_m}\right).$$

Therefore,

$$\lambda(H_c; R) = 2\sigma_n \lambda(R) \int_{-\infty}^{X} exp[-2\sigma_n (X - x)] dx \int_{x}^{\infty} \frac{dy}{\sqrt{2\pi}} exp(-y^2/2), \tag{A4}$$

which reads, with the variable change from $x$ to $z = X - x$:

$$\begin{aligned}
\lambda(H_c; R) &= 2\sigma_n \lambda(R) \int_{0}^{\infty} exp(-2\sigma_n z) dz \int_{X-z}^{\infty} \frac{dy}{\sqrt{2\pi}} exp(-y^2/2) \\
&= 2\sigma_n \lambda(R) \int_{X}^{\infty} \frac{dy}{\sqrt{2\pi}} exp(-y^2/2) \int_{0}^{\infty} exp(-2\sigma_n z) dz \\
&\quad + 2\sigma_n \lambda(R) \int_{-\infty}^{X} \frac{dy}{\sqrt{2\pi}} exp(-y^2/2) \int_{X-y}^{\infty} exp(-2\sigma_n z) dz \\
&= \lambda(R) \int_{X}^{\infty} \frac{dy}{\sqrt{2\pi}} exp(-y^2/2) \\
&\quad + \lambda(R) \int_{-\infty}^{X} \frac{dy}{\sqrt{2\pi}} exp[(-y^2/2) - 2\sigma_n (X - y)].
\end{aligned} \tag{A5}$$

The integration can be carried out with the following notations:

$$\begin{aligned}
R_m &= \left(AI_m / H_c\right)^{1/n} exp(\sigma_n^2) \\
Z &= \frac{1}{\sigma_n} ln\left(\frac{R}{R_m}\right) = X + \sigma_n.
\end{aligned} \tag{A6}$$

Thus, $$\lambda(H_c; R) = \lambda(R)\left[Q(Z + \sigma_n) + P(Z - \sigma_n) e^{-2\sigma_n Z}\right], \tag{A7}$$

where $P(z)$ and $Q(z)$ are normal distribution functions (see Equation (5)).

# A RETEST CRITERION FOR SPACE LAUNCH PROCESSING FOLLOWING LIGHTNING STORMS

J.C. Chai
The Aerospace Corporation
P.O. Box 92957, M4-179, Los Angeles, CA 90009, USA
Telephone (310) 336-8341; FAX (310) 336-5581

T.S. Chin
Lockheed Martin Missiles & Space
P.O. Box 3504, Sunnyvale, CA 94088, USA
Telephone (408) 756-0117; FAX (408) 756-1656

## ABSTRACT

This paper proposes a lightning retest criterion which contains the essential physics of lightning and the system geometry. It also correlates all sensor readings into a simple rule of comparisons via the concept of retest indices. Therefore, it provides an instantaneous means for 'real-time' and 'on-the-spot' decision-making in launch processing operations following major lightning storms.

## INTRODUCTION/BACKGROUND

Ever since the AF/SMC began launching space vehicles into space from CCAS, Florida, a major recurring concern has been the potential damage to the launch vehicle/space vehicle (LV/SV) system induced by lightning. This concern is especially acute for launches taking place during the high lightning season in the summer months. Anyone who was involved in the actual launch activities can remember the hectic and sometimes chaotic atmosphere when a nearby lightning strike was reported during the critical path of a launch. Currently, the assessment of the potential damage to the LV/SV mainly depended on limited and primitive means. The decision to proceed with normal launch activities or to switch to retest/recertification procedures is a tough one. As more and more sensitive devices are used in the LV/SV, a more reliable lightning retest criterion is urgently needed. The retest criterion should be designed to help make a real-time decision. The purpose of such criterion is, on the one hand, to avoid unnecessary and costly tests/delays, and on the other hand, to avoid launching damaged/degraded satellites into space. A delicate balance between the two extremes must be achieved.

This paper formulates such a lightning retest criterion for space launch processing operations. It first lists the important parameters to be considered in a retest criterion, then outlines a way to formulate the criterion that includes all the essential lightning physics, and it concludes with an example of how the criterion can be applied in launch situations on a real-time basis.

## IMPORTANT PARAMETERS

A lightning retest criterion should include all the important parameters which affect the system under consideration. The first parameter is the *stress* induced by lightning on the system, and the second parameter is the intrinsic *strength* of the system to withstand the stress without suffering damage.

STRESSES-- Lightning, by virtue of transient electromagnetic field scattering from the system, will first induce electromagnetic stresses on the *external* surface of the system such as the payload fairing and umbilical cable sheath. The external stress (for example, in terms of induced electromagnetic fields or currents on the surface of the system) will then propagate through available paths to the circuits/devices in the *interior*, and deposit undesirable energies there, causing damage. A well-validated transient pulse monitoring system (TPMS) as installed for a particular payload will give the actual external stress, and analyses will complement it with a whole range of lightning threats. The stress at circuit levels is the true reason for damage concerns, and it is found in terms of stress energy and voltage waveforms by circuit coupling analyses such as SPICE code runs.

STRENGTHS-- However, stress *alone* will not indicate whether or not the circuit will be damaged. The strength of the circuit has to come into the picture. Even if the stress is very severe, for a circuit that has strength to withstand, say, ten times worse stress, it should not cause any damage concern.

The strength of a device/circuit is the intrinsic characteristic of such a device or circuit. A good example of the strength of a device/circuit is the burn-out damage threshold. Plenty of experimental data are available for various types of devices such as diodes, transistors, digital ICs, and other basic electronic/electrical components.[1] These data have been fitted to the Wunch-Bell-Jenkins-Durgins empirical failure models. Based on the footnote reference and other existing data, a conservative sample burn-out damage energy threshold is one micro-joule for some sensitive TTL, DTL and RTL digital ICs.

A comparison of the two in the susceptibility/vulnerability analysis yields the safety margin (SM), which is an indication of how well the circuit would fare in light of the given stress. A retest criterion can then be formulated with the desired safety margins included.

## FORMULATION OF RETEST CRITERION

In this paper, we are proposing to formulate the retest criterion based on a family of stress curves, which are expressed in terms of stress energy obtained from analyses and monitor readings from a high-fidelity on-line lightning monitoring system. The device at CCAS currently used to report lightning events is the Lightning Location and Protection System (LLPS). However, since the LLPS only gives the lightning current amplitudes, the range and the azimuth angle of the cloud-to-ground strokes to points of interest, mathematical models are used to translate the data into the electromagnetic (EM) environment. Moreover, because the response (i.e. electromagnetic stress) on the surface of the system depends on the property of the system, the EM environment

---

[1] For example, D.L. Durgin, et al., 'DEFT Handbook, (the Determinations of EMP Failure Thresholds)', DNA Report No. 9003-069, 10 August, 1983.

alone will not be sufficient to characterize the stress on the LV/SV system. To obtain the EM stress on the system due to lightning, further analyses or/and measurements need to be performed. The measurements will be taken by a proposed Hybrid On-line Lightning Monitoring System (HOLMS). Details of HOLMS are described elsewhere.

ANALYSES-- Figure 1 is a summary flow chart of the analyses discussed in this paper. Instead of waiting for nature to deliver lightning, parametric studies using mathematical models can be carried out to analyze many possible scenarios. *Field coupling* analyses, using scattering computer code for the launch complex with all significant structures included, will give the induced electromagnetic stress on all external surfaces in terms of current, E-field and time rate of change of H-field. These external stresses need to be propagated to the internal circuits/devices by various modes of penetrations where damage could occur. *Circuit coupling* analyses will use these internal stress drivers to obtain the stress energy at the most sensitive and/or critical circuit. From all these analyses a stress curve (see Figure 2) can be obtained for various levels of lightning threats.

On the other hand, the capability for the selected circuit to withstand the stress can be found in a concurrent *damage threshold analysis,* which combines mathematical models with empirical data. The strength of the circuit to tolerate the lightning stress can be expressed in terms of energy and be superimposed on the stress curve as shown later by the horizontal lines in Figure 3 (collectively known as the retest curve). Various safety margins can be incorporated into it to give additional levels of confidence, and also to account for the harder-to-define upset threshold.

MEASUREMENTS-- The *prerequisite* requirement for the retest criterion is that the HOLMS provides reliable data for a sufficient confidence level. This is necessary because in applying the stress curve for a retest decision, the stress in the x-axis must be the *actual* stress value 'seen' at the selected location. Therefore, an end-to-end calibration/validation of the HOLMS has to be performed before the retest criterion can be used with confidence. The HOLMS readings can also be used to verify the scattering model in the field coupling analysis, and lend confidence in our future ability to predict and understand the lightning-induced stress. This would help in the design of an appropriate mitigation scheme.

Ideally, a HOLMS should be able to provide readings at as many locations as needed. The present TPMS can only provide readings at six locations external to the SV. The 'Hi-Lo' limits for sensors to start printed records or to 'alert' the user are presently based on *external* stress estimates which need to be refined to correlate with the *internal* stress at the circuit level. Flow-down analyses are needed to propagate the external stress to the internal circuits, followed by circuit coupling analysis and susceptibility analysis. Ideally, some internal circuit lines can be monitored to provide direct readings at the circuit level, further eliminating some of the simplifying assumptions and uncertainties in the mathematical models.

COMBINED SENSOR READINGS-- The present TPMS provides three types of stress readings: sheath current on the umbilical cable, E-field on selected surfaces, and B-dot above the umbilical cable. Each type of reading presents a different mode of entry for the coupled lightning energy into the LV/SV system. These types must be coordinated to give a combined indication of the stress at the circuit level.

Primary & Secondary Retest Index (on a 10-scale)-- Due to the fact that lightning energy can enter the system in different ways, and the fact that HOLMS will deploy multiple sensors for higher fidelity and correlation, we propose a scheme, using

"Retest Indices" to account for different coupling mechanisms as recorded by multiple sensors' readings.

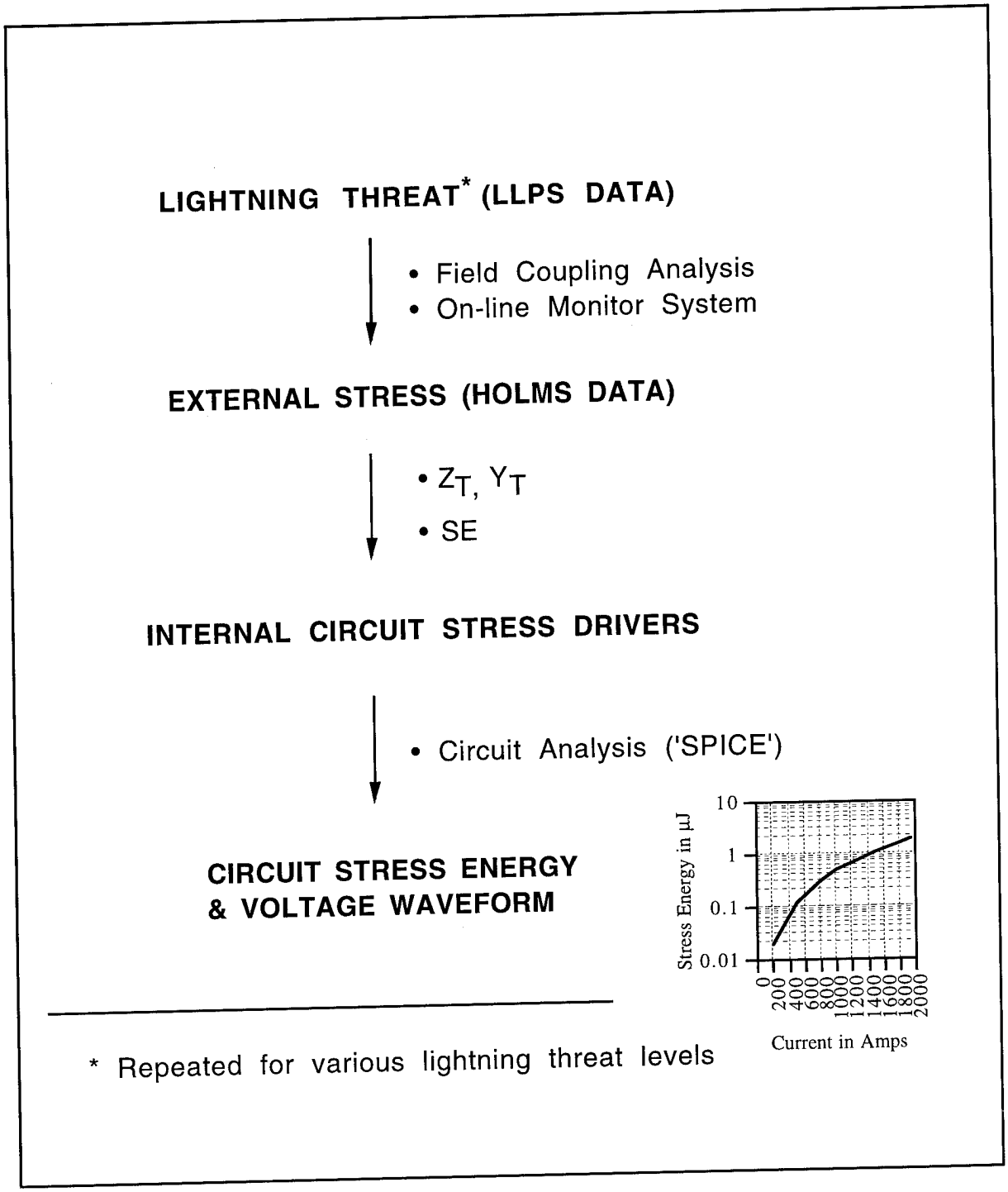



FIGURE 1. ANALYSES FLOW-DOWN FOR THE LIGHTNING-INDUCED EFFECTS ON SELECTED CIRCUITS.

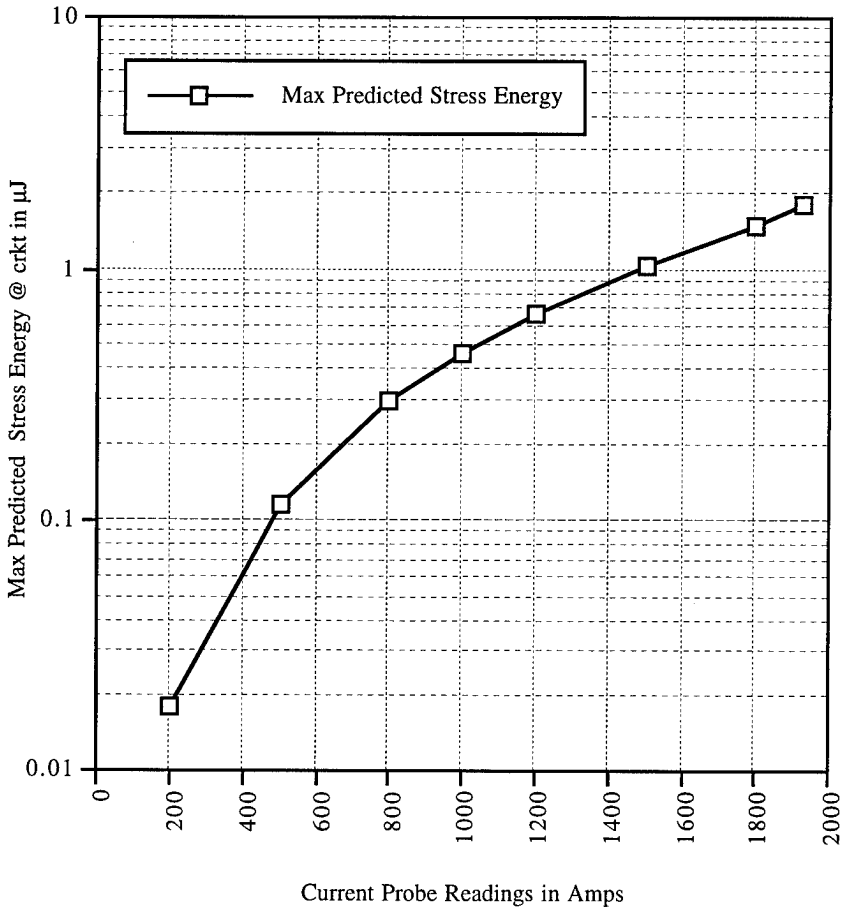



FIGURE 2. A SAMPLE CURRENT STRESS CURVE OBTAINED FROM ANALYSES.

All retest indices will be normalized. The primary retest index is defined as

$$rim_1 = \left[ \frac{m_1}{\max_1} \times 10 \right] \cdot w_1$$

and the subsequent and secondary indices (of lesser importance as compared to the primary retest index) are defined as

$$rim_2 = \left[ \frac{m_2}{\max_2} \times 10 \right] \cdot w_2, \quad \ldots$$

where the normalization to the factor of 10 is somehow arbitrary, yet without loss of generality; weights 'w' are dictated by lightning coupling mechanism and are given by expert analysts based on analyses and available data; 'm's are the *actual* monitor readings that are continuously updated; 'max's are *predicted* monitor values for the full-threat case known from pre-launch analyses; $w_1 > w_i$, $i > 1$, and $\sum_{i=1}^{n} w_i = 1$. Each point on each stress curve can now be related to a 'rim' value on the x-axis: its value can be easily obtained from the retest curve in Figure 3.

Combined Retest Index-- Therefore, the combined retest index, 'RIM', related to actual monitor readings through 'rim's, is defined by

$$RIM = \sum_{i=1}^{n} rim_i$$

The 'RIM' represents the actual stress as seen by selected circuits, from all n monitor readings.

Critical Retest Index-- The critical retest index, 'RIC', is designed to indicate the monitor's threshold reading levels at which potential damage can occur. This therefore involves the stress curves and the circuit damage threshold energy, with or without safety margins. It is defined as

$$RIC = \frac{\sum_{i=1}^{n} ric_i}{n}$$

where each 'ric' is obtained from the retest index axis at the point where the stress curve crosses the horizontal threshold line (see Figure 3). For illustration purposes, the '6dB'-line is used to define the intercept with the stress curve. Equal weights for damage are assumed once the energy reaches the circuit.

Depending on LV/SV contractors' needs, various stress curves with thresholds can be obtained for various types of circuits. Therefore, for a combined sensor reading, the type of circuits which will be stressed and the degree of stress can be easily identified.

Retest Decision-- Once the combined retest index of monitor readings (RIM) is determined for a particular event, it can be compared to the critical retest index

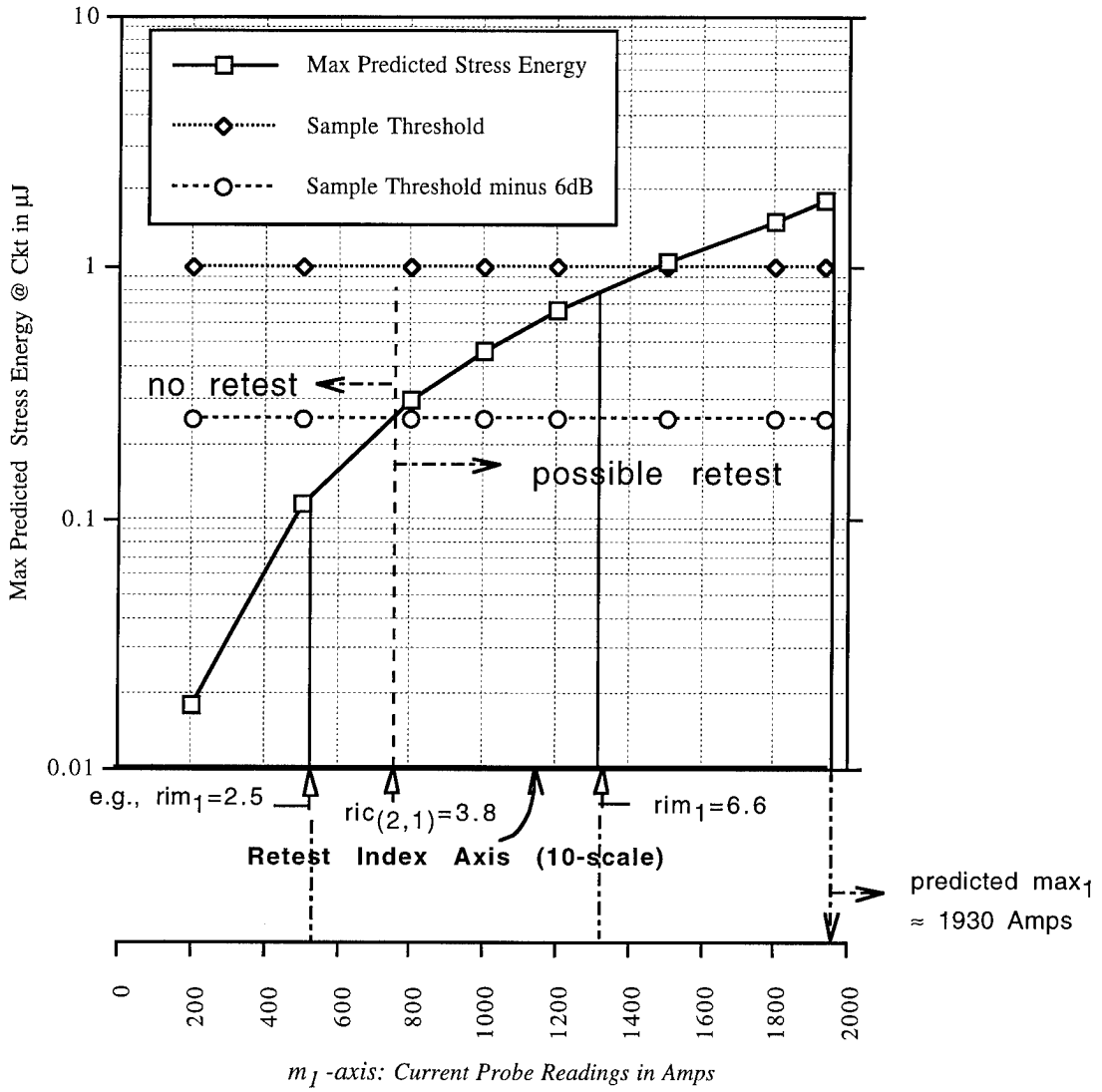



FIGURE 3. A SAMPLE RETEST CURVE: RETEST INDEX AND THE CURRENT STRESS CURVE WITH SAMPLE THRESHOLD LEVELS (SHOWN IN HORIZONTAL LINES) SUPERIMPOSED. NOTE THAT THESE CURVES ARE LV/SV-SPECIFIC.

(RIC) which has been found in pre-launch analyses. Testing and/or search for potential lightning-induced damage of selected circuits should be considered if

$$\boxed{RIM \geq RIC}$$

This result is almost instantaneous, and decisions can be made right on the spot where launch operations are in progress. The LV/SV contractors will also have the information for different types of circuits, enabling them to identify which circuit or device needs retest or repair.

## VERIFICATION OF RETEST CRITERION

For a retest criterion to be an effective tool for real-time decision making, it has to achieve the delicate balance mentioned earlier between too much and too little retest. It therefore involves a long term commitment of 'lessons learned' from accumulation of actual data. The process starts, firstly, with all hardware in HOLMS having been calibrated and validated, both in the controlled environment (in laboratories) and in actual lightning environment (at launch sites). These involve small-scale model testing, triggered lightning tests, in-situ measurements and comparison to existing databases. Secondly, the software implementation of the retest criterion algorithm can be verified by injecting known pulses into the algorithm stream, and monitor the responsiveness of the retest criterion to various stimuli. As time goes on, more data on the retests and damage found can be gradually incorporated into the retest criterion to gain more confidence in the tool for decision making.

## APPLICATION OF RETEST CRITERION

A whole set of sophisticated analyses and measurements has now been reduced to a simple comparison of two quantities: RIM and RIC, which contain as much lightning physics and other relevant information as one can reasonably demand at this time. Auxiliary stress curves with both actual monitor readings and retest indices are also made available for on- or off-site analysts' review. The application of the retest criterion as proposed in this paper can be best illustrated by a simple example which is given in a MATHCAD file as shown in Figure 4. The following quantities are first typed in:

-- The maximum monitor readings ('max') known from pre-launch full-threat case analyses.
-- The weights ('w') based on lightning coupling mechanisms & preliminary HOLMS data are entered.
-- The critical retest indices ('ric') for individual monitors from stress curves with various safety margins.

Then the combined critical retest index (RIC) is calculated. Note that in using the retest criterion, the only data updates are the monitor readings 'm's, and the only update calculations are the RIM for that set of 'm's and the comparison of RIM and RIC. Even these can be easily incorporated into the control software of the HOLMS, and the retest

Example: Application of Retest Criterion, with n=3 monitor readings

ORIGIN ≡ 1

(0) Range variables for this example

| | |
|---|---|
| $n := 3$ | number of monitors |
| $i := 1, 2.. n$ | range for monitors |
| $ism := 1, 2.. 4$ | range for safety margins |

(1) Max monitor readings from corresponding full-threat case analyses

| | |
|---|---|
| $max_1 := 1930$ | Amps; from the current probe |
| $max_2 := 35000$ | V/m; from the E-field sensor |
| $max_3 := 4.25 \cdot 10^7$ | A/m/s; derived from the B-dot sensor |

(2) Initial weights based on coupling mechanism for T-0 umbilical cable related circuits, & to be fine-tuned with HOLMS data

$w_1 := 0.5$ $w_2 := 0.25$ $w_3 := 0.25$

(3) Individual critical retest indices from stress curves obtained from pre-launch analyses!

| @SM=0dB | @SM=6dB | @SM=12dB | @SM=20dB |
|---|---|---|---|
| $ric_{(1,1)} := 7.4$ | $ric_{(2,1)} := 3.8$ | $ric_{(3,1)} := 2.0$ | $ric_{(4,1)} := 0.5$ |
| $ric_{(1,2)} := 5.7$ | $ric_{(2,2)} := 4.2$ | $ric_{(3,2)} := 3.0$ | $ric_{(4,2)} := 1.8$ |
| $ric_{(1,3)} := 6.3$ | $ric_{(2,3)} := 3.0$ | $ric_{(3,3)} := 1.8$ | $ric_{(4,3)} := 0.9$ |

(4) Composite Critical Retest Index - equal weights assumed once energy reaches circuits

$$RIC_{ism} := \frac{\sum_i ric_{(ism,i)}}{n}$$

(5) Update calculations of composite retest index on an arbitarily chosen scale of 10 , based on monitor readings --- the only inputs needed for updating actual data:

$m_1 := 458$ $m_2 := 2200$ $m_3 := 1.44 \cdot 10^7$ arb. examples for illustration

$$rim_i := \left(\frac{m_i}{max_i} \cdot 10\right) \cdot w_i \qquad RIM := \sum_i rim_i$$

(6) Retest Decision -- RIM > RIC ?

RIM = 2.191

| | $RIC_{ism}$ | |
|---|---|---|
| @ SM= 0dB | 6.467 | RIM=2.19 < RIC=6.47 --> no retest |
| @ SM= 6dB | 3.667 | 2.19 < 3.68 --> no retest |
| @ SM=12dB | 2.267 | 2.19 < 2.27 --> no retest: marginal |
| @ SM=20dB | 1.067 | 2.19 > 1.07 --> retest ! |

FIGURE 4. A MATHCAD FILE SHOWING THE EXAMPLE OF USING THE RETEST CRITERION.

decision can be almost instantaneous. Of course, if the launch director prefers to ship the data back to the factory for further consultation, he can certainty do so, although the retest criterion already includes pre-launch analyses conducted at the factory. The fact that he has the ability to make an instantaneous and well-founded decision can greatly streamline the launch operation, while reducing the risk, which will ultimately result in great long-term cost savings.

In the special case when there is only one stress curve (i.e., w=1) available from one monitor, the above retest criterion is still applicable, although with a somewhat reduced level of confidence. This situation can arise, for example, when only the susceptibility analysis for lightning coupling to circuits associated with the current on the T-0 umbilical cable is performed, while other modes of coupling, such as EM field penetrating through the payload faring, to other circuits are not included in the susceptibility analysis. An interim procedure, which still contains multiple sensors in the monitoring system and similar to what has been described above, can be adopted to increase the confidence of a retest decision. The procedure can be followed, with the other monitor readings utilized, in some pre-determined manner[2], as a means of quasi-quantitative confirmations. The best way to fully utilize the retest criterion is, of course, to generate a database of stress curves for all sensors in the monitoring system, with equal levels of circuit details, by performing susceptibility analyses for all identified circuits, with all modes of lightning coupling included in the analysis.

## CONCLUSIONS

A retest criterion for space launch processing following major lightning storms is described. It utilizes the concept of "retest indices" in the "retest curve" to combine major lightning coupling modes to selected circuits and/or devices, as recorded by a multi-sensor on-line monitoring system. If implemented into the launch operation procedures, it will provide a powerful tool for real-time decision-making.

---

[2] For example, E-field sensor readings inside known layers of enclosures can be compared to the Fourier transform, in the time domain, of the analytical E-field prediction for a certain threat level (e.g., 3 kV/m for a 200-kA lightning strike to the lightning rod on the overhead Catenary Wires Array Lightning Protection System at SLC40/41 @ CCAS), which satisfies the RS103 limits of MIL-STD-461D in the wide frequency domain. Other points can also be found for less severe threat levels to obtain the *shape* for the E-sensor stress curve. Note, however, by not performing a susceptibility analysis for the circuits, this curve only defines a generic shape for an allowable electric field *stress* level, which lacks the details and of the characteristics selected circuits involved, and, therefore, should be used with this limitation in mind.

# SESSION 03B
# MEASUREMENTS
# CHAIRPERSON: JEFF CRAVEN

# DATA ACQUISITION FOR SYSTEM LEVEL INDIRECT EFFECTS OF LIGHTNING

Ed Parimuha, Mike Whitaker and Sam Frazier
Naval Air Warfare Center Aircraft Division
Patuxent River, Maryland USA 20670

Bruce McClure and Pam Lumsden
United International Engineering, Inc,
Lexington Park, Maryland USA 20653

## ABSTRACT

The Naval Air Warfare Center Aircraft Division (NAWCAD), Patuxent River, Maryland is a U.S. Department of Defense Major Range and Test Facility Base, and Electromagnetic Environmental Effects ($E^3$) Center of Excellence. The NAWCAD has fielded a highly automated Data Acquisition and Processing System specifically designed to support large scale lightning and electrostatic tests. The system can collect data from 16 channels simultaneously with each channel controlling a fiber optic link with 8 inputs, allowing the measurement of a maximum of 128 test points without reinstrumenting the test object. Immediately upon test completion, the test data can be stored on a standard IBM PC CD-ROM for post-test analysis and archiving.

## INTRODUCTION

NAWCAD has had the need for a system for acquiring indirect effects lightning test response data. It is desirable to acquire this data quickly and efficiently, limiting the time test objects are under test and out of service, and also to limit their exposure to potentially harmful simulation environments. Previously, a portable, limited data acquisition system was housed in NAWCAD's first Electromagnetic Pulse (EMP) data acquisition enclosure, the EMPICS van. Time consuming pretest modifications to this system were necessary in order to support lightning tests, as this van was also used for EMP testing. In 1993, the Naval Surface Warfare Center transferred one of its data vans from the acquisition system for the EMPRESS II (Electromagnetic Pulse Radio Frequency Environment Simulator for Ships) to NAWCAD, where it was designated for the Lightning Data Acquisition and Processing System (LDAPS), Figures 1 and 2.

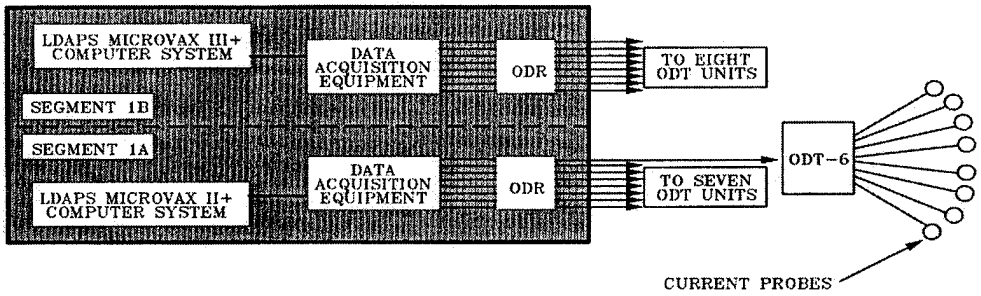



**Figure 1. Lightning Data Acquisition and Processing System (LDAPS) Block Diagram**

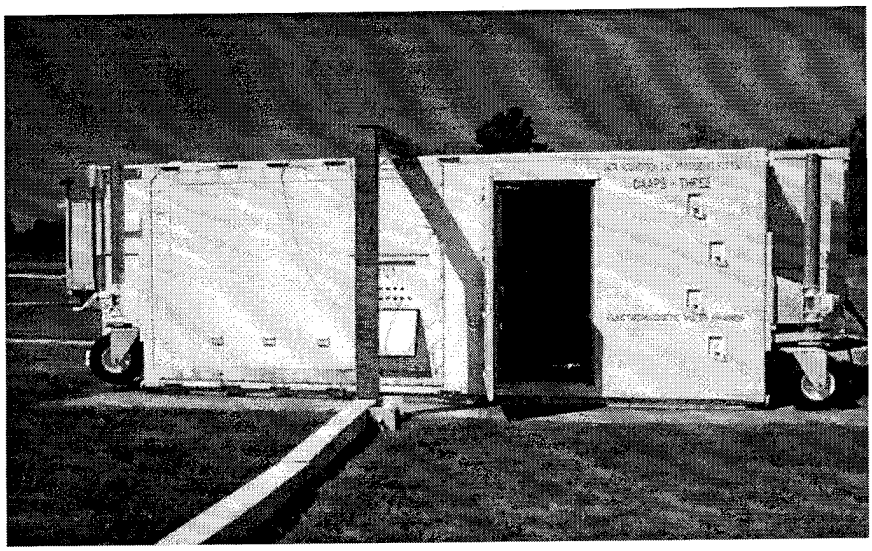


**Figure 2. LDAPS Module**

Because this EMPRESS II van contains a more sophisticated instrumentation suite than NAWCAD's old system, it can acquire a larger number of test point measurements for each time the aircraft is exposed to a lightning strike simulation.

Numerous adaptations were made to this EMPRESS van by the EMT Branch at NAWCAD, Code 5.1.7.2 to adapt the van for acquisition of stress response data from lightning tests. The system development effort is described in this paper.

## SPECIFIC LIGHTNING TESTING REQUIREMENTS

The requirements for the upgraded Lightning Data Acquisition and Processing System were driven by the use of LeCroy digitizers and the need to standardize electromagnetic transient data acquisition systems to minimize maintenance, training and operational issues. To meet these objectives, the EMT Branch established the following requirements:

a. Provide a dedicated LDAPS. The previous lightning data acquisition system had to be configured prior to a test using equipment from EMP DAPS modules.

b. Use LeCroy TR8828 series digitizers with EG&G fiber optic systems to maintain compatibility with present DAPS and to make maximum use of the equipment in the EMPRESS II van.

c. Provide the capability to use either LeCroy TR8828's (lightning testing) or 6880 digitizers (EMP testing).

d. Integrate the existing EMP/Lightning acquisition software to configure the LDAPS. This provides standard operating procedures for acquiring, processing and archiving test data.

e. Maintain the data storage capacity to at least that in the present DAPS modules, 150 Mbyte disk.

f. Provide within the LDAPS van two systems, each with 8 data channels using EG&G ODT-6 fiber optic systems and real time data display on video scopes instead of MicroVAX terminals. This would provide the capability to instrument up to 128 test points during one instrumentation cycle.

g. Transportable.

h. Hardened to prevent damage or upset to interior components due to electromagnetic simulation environment.

By integrating NAWCAD's existing lightning acquisition software to the new systems, it was possible to transfer NAWCAD's existing lightning acquisition capability. Since hardware IEEE addresses were set the same on the EMPRESS II and NAWCAD systems, integrating the software produced two new useable systems. It is noteworthy that the fiber optic transmitter controllers in the EMPRESS II van are made by a different company than those in NAWCAD's other vans. The different controllers came with their own software and are compatible with NAWCAD's acquisition systems.

## LIGHTNING SYSTEM DESIGNED TO PERFORM LIKE NAWCAD'S OTHER SYSTEMS

The LDAPS data van, like the other NAWCAD data acquisition vans, measures 8 x 8 x 20 feet. Its environmental control unit (ECU) extends its length to 26.3 feet. The LDAPS data van can be transported on a flat bed truck or towed short distances. With its 75,000 btu/hr capacity, the ECU can effectively maintain proper operating temperature. The hardness of these modules has been verified to prevent transient upset or damage to interior components in pulsed E fields of up to 50 kV/meter (1). This has been more than sufficient for any lightning test environment NAWCAD has experienced. This hardness is a necessity for acquiring data when the entire test object is illuminated by the simulated threat.

This lightning system was designed to function with identical operating procedures as NAWCAD's other systems. This facilitated the systems' sharing source code, thus aiding in NAWCAD's software configuration control. In addition, no special training is needed for system operators to acquire either EMP or lightning data. The measurement information stored by all these systems is similar in format and thus can be input to either NAWCAD's processing MicroVAX or its PC based processing and archiving systems, the Processing Language Using MATLAB (PLUM) and the Naval Air Electromagnetic Analysis System (NEMASYS).

The EMPRESS II van already contained hardware for checking test probe instrumentation circuits prior to data acquisition. These systems identify electrically shorted probe circuits, physically open probes, or probes different than entered in the computer for eight data channels (Acquisition operators will have already entered the probe being used on measurements for each transmitter input). Prior to acquisition, an operator can utilize the fiber optic controller to command fiber optically attached transmitters to send out calibration pulse signals sequentially to the probes on each of their inputs. The signal returning is modified according to the distinctive electrical properties of that probe, and is compared with the probe's known proper response. Identification of the transmitter and the transmitter input for failed probe comparisons are sent back to the acquisition computer and are shown as annotation on an oscilloscope overlay display of the actual signal and expected response. The system performs these functions automatically with no operator intervention, forming a queue of failures to view on the oscilloscope. Once a failed probe's transmitter input is in this queue, an operator can redo this test whenever he chooses continuing until the hardware problem on that input has been corrected. This system is incorporated as shown in Figure 3, showing the hardware configuration of a lightning acquisition system.

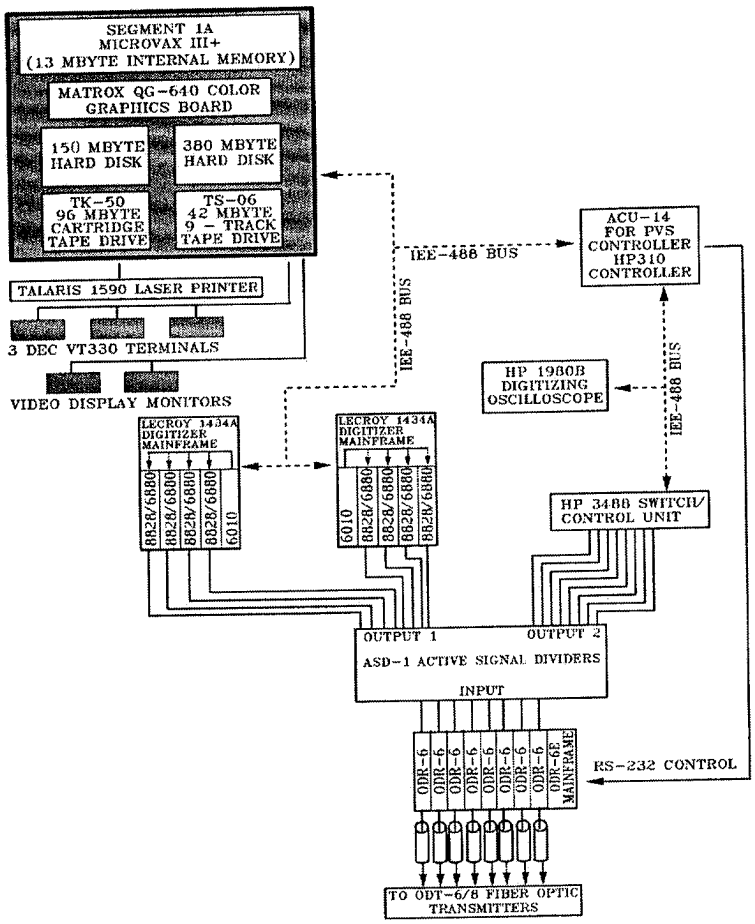



**Figure 3. Hardware Configuration of one LDAPS System**

The lightning system MicroVAX's perform calculations in the background during data acquisition. These include correcting raw data for effects of instrumentation used during acquisition, and extrapolating this corrected data to the specified threat.

The LDAPS uses the same relational databases in each phase of lightning testing that are used for NAWCAD's other EMP testing. The evolution of the test specific database from start to finish is shown in Figure 4. Descriptions of the points to be tested on the aircraft and their coded identifiers are the main database entries performed during the test planning phase. By the time the waveform data has been acquired, database records indicating all instrumentation used, parameter settings on these instruments, and all other information descriptive of the testing environment which are needed in calculating the final result, has been stored in that database. This information storage is represented by the middle two columns in Figure 4. The data processing and analysis phases which produce hard copies of acquired waveforms use this information and are represented by the last column in the figure.

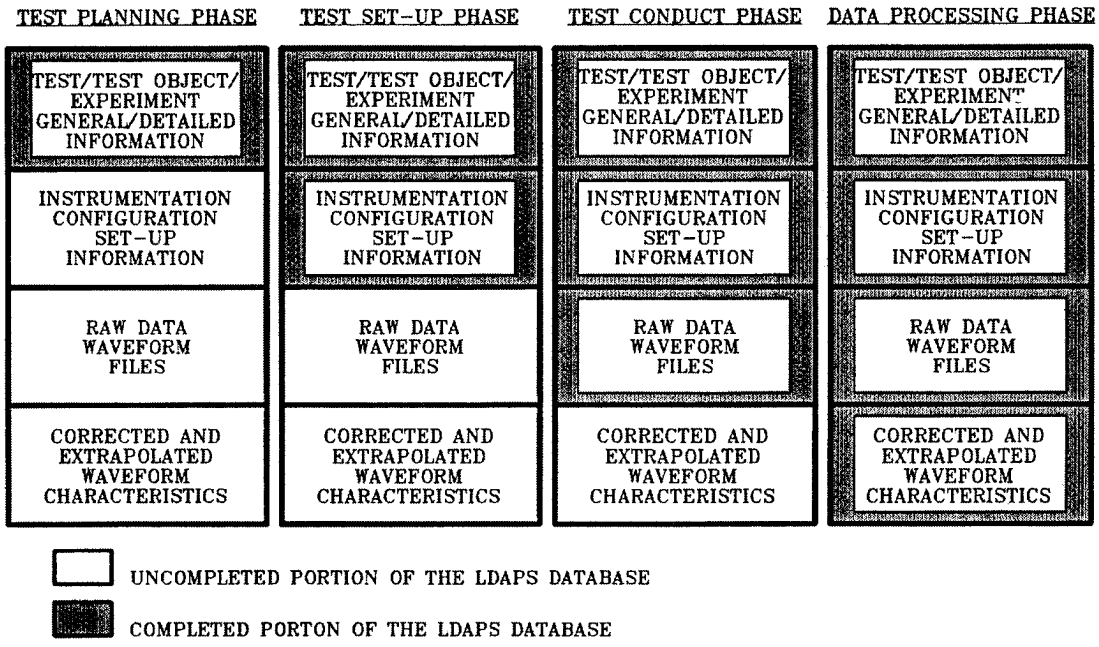



**Figure 4. Evolution of the Test Specific Database**

In addition, the database information can be output in the same way as that from NAWCAD's other systems for input to the PC based analysis systems, PLUM (2) and NEMASYS (3). PLUM is the U.S. Air Forces's signal processing tool developed by the Phillips Laboratory. It is built around the commercial numeric computational software, MATLAB of The Math Works, Inc. and has been modified for use in NEMASYS by NAWCAD. NEMASYS is NAWCAD's analysis package containing their own specific MATLAB based calculations, and extensive database analysis and reporting capabilities. NEMASYS contains Borland Intl.'s database manager PARADOX and produces hard copy output using Microsoft's EXCEL. It is automatically installable from floppy disk. The entire content of a user's test data can also be transported on similar media or CD ROM for analysis on remote NEMASYS systems. The waveforms measured by LDAPS are stored in the same file format as those acquired in NAWCAD's EMP testing, and both are convertible in the same way to the two PC-MATLAB based analysis packages.

The operating systems of NAWCAD's standard EMP acquisition MicroVAX's were transferred to the LDAPS MicroVAX's. This was significant in making the new lightning system operate as described above, as opposed to being like NAWCAD's previous lightning system. In the previous systems, there was a limited real-time QC capability, no internal data path calibration capability, and a non-standard windows display technique. Both the NAWCAD EMP systems and the LDAPS systems store their operating software on 150 MByte disk drives.

Changes were made to the old lightning system application software. The plotting of measurement waveforms following their capture is now output to Sony video scopes instead of to the operators' computer terminal screen. Also one of the two new MicroVAX's was designated as a 'master' which could arm the other system's digitizing oscilloscopes for data capture. This 'master' also can acquire the simulator output as a reference and calculate descriptive parameters for use by both systems. These changes, present in NAWCAD's EMP acquisition systems, also represent improvements over its previous lightning system.

The printer in the lightning acquisition van is networked to the two acquisition systems. Its controlling software can be loaded from either of the two MicroVAX's. Whereas NAWCAD previously had a one user Vaxstation system for acquiring lightning data, the new MicroVAX's III+s are networked to a server providing 15 terminal ports. Since the printer in LDAPS is connected from this networked terminal server, NAWCAD had to incorporate NSWC's controlling software. The software was copied from NSWC and used with NAWCAD's different version of operating system. There is also another terminal which can be manually switched between computers. In addition to a 95 Mbyte magnetic tape cassette with each system, the two lightning systems share a 9 track reel to reel tape drive which is switchable to either system needing that archiving capability.

SPECIFIC HARDWARE CAPABILITIES

LDAPS had been derived from NAWCAD's existing lightning and EMP data acquisition systems (DAPS's). The number of data channels has been increased from 6 to 8. Each data channel is able to control two types of Lecroy Corp. digitizing oscilloscopes for capturing transient response waveforms. The digitizer type which would be used for lightning testing acquisition, TR8828 series (4), captures 64 k samples at sample time intervals ranging from 5 nanoseconds up to 0.32 microseconds. The time interval is interactively selectable by the system operator as needed. These longer time intervals are sufficient for response measurements resulting from Mil-Standard lightning threats such as the double exponential waveform 1757. In its lightning system mode, calculations specific to lightning threat excitation are being made in near real time during acquisition.

Each of the two new systems housed in the LDAPS van is cabled for 8 channels of acquisition. Therefore, only hardware had to be added to provide 8 data channels. The hardware included two LeCroy digitizers, two additional fiber optic receiver modules, and two active signal divider components.

Two new sets of LeCroy 8828 type digitizers and memory modules were purchased for use with the new lightning system. Both NAWCAD's lightning and EMP acquisition systems can thus all be outfitted simultaneously with a complete suite of 8828 digitizers. The LDAPS data disks each hold 350 MBytes compared to 150 MBytes on the EMP systems. One of the MicroVAX's on the new system utilizes a CSP, Inc array processor which uses parallel processing at 20 MIPs to aid in processing the large 64 K point waveforms acquired in lightning testing. In addition to this array processor, data processing is greatly increased due to the increased speed of the MicroVAX's III+ over the VAXstation in the old system. NAWCAD has 50 Prodyn I-125-C type and 17 Pearson 5300 type current probes which have flat responses down past 1 Khz plus over 200 other current probes. In addition to having many one microsecond integrators, NAWCAD has 10 microsecond integrators for integrating signals from derivative field sensors in lower frequency lightning testing environments.

NAWCAD has numerous fiber optic data transmitters available for lightning acquisition. There are 21 EG&G ODT-6's (5) each having 8 individually selectable inputs. As this new van contains two systems having 8 channels each, probes on each of the inputs on each available channel mean that 8 x 8 x 2 test points could be readied for automatic computer controlled acquisition. The overview of the LDAPS system shown in figure 1 shows the available data paths. In practice, one channel would however be dedicated to collecting the pulser output reference only. Additional improvements due to these modifications are shown by the chart in Figure 5.

| | *OLD* | *NEW* |
|---|---|---|
| # Acquisition Channels | 8 | 16 |
| # of Test Points per Instrumentation | 64 | 128 |
| Processing Speed | X | >2X(1) |
| Testing Days Required | X | X/2(2) |

(1). 2 MicroVAX's III+s working in parallel plus the array processor rather than the VAXstation alone in the old system.

(2). Assuming personnel are capable of instrumenting twice as many test points in a day's instrumentation shift.

**Figure 5. Comparison Between Old NAWCAD Lightning Acquisition System Features and New**

The EG&G links vary by less than 3dB between 1 KHz and 150 MHZ. Four Nanofast, Inc. fiber optic links (6) having higher frequency ranges are also available for use. The MicroVAX remotely controls the EG&G links, specifying gains ranging from -64 to + 40 dB in 1 dB increments, while the Nanofast must be manually controlled when used in these systems.

Transmitter battery charging is done continuously 12 at a time in LDAPS, whereas NAWCAD previously had to utilize their EMP systems for this. In this lightning system, the Lecroy crates of digitizer outputs can be switched between controlling computers in the event of component failure.

## VERIFICATION OF THE NEW SYSTEMS' READINESS FOR DATA ACQUISITION

All features of the new system have to be verified before project completion. While the functionality of all cabling and devices will be checked, calibrations will be performed on all parts of the path of acquired data. For each of these data path components, this will be a permanently saved frequency domain profile of its effect. The significant components of data paths being calibrated in this way are shown in Figure 3. The overall system was tested by capturing a known waveform input and recording and processing it. NAWCAD's instrumentation calibrating software was installed in LDAPS to control an HP3577 network analyzer and create these calibration profiles (7). The calibration files that NAWCAD produces begin at 100 Hz. The previous lightning system had no such calibration recording system, a necessity for characterizing data paths in multi-component groups.

## SUMMARY AND CONCLUSIONS

1. NAWCAD quickly set up the hardware received from NSWC White Oak to function as a lightning acquisition system. The resulting system is fully compatible with NAWCAD's other transient waveform testing capabilities. The hardware in the NSWC van is functionally identical to the NAWCAD EMP vans down to the level of their component IEEE address settings.
2. The NSWC van conversion plan was effective, and the development project done within cost. All specific lightning capabilities previously developed by NAWCAD were incorporated. The

operating system and major software coding changes, except for the printer controller, were copied from NAWCAD's EMP acquisition systems. The printer controlling software that had run with NSWC's version of operating system was incorporated into NAWCAD's.

3. NAWCAD has a 16 channel lightning acquisition system capable of quickly acquiring large amounts of data. It operates identically to NAWCAD's EMP systems and produces compatible output. With its terminal server, numerous users can access the system simultaneously. The new system enables measurement of twice as many test points during an acquisition cycle, while subjecting the airplane to the same number of pulse simulations, and does this in less time due to increased computer speed, compared to the lightning acquisition system previously employed by NAWCAD.

# REFERENCES


1. J. Cafferky, "TACAMO EMP Simulator Data Acquisition and Processing System - DAS System Operator Manual", EG&G Special Projects, Inc., Volume I, December 1990.

2. "NAWCAD PLUM User's Manual",United International Engineering, Inc., under contract #N00421-90-D-0161, February 1995.

3. "NAVAIR Electromagnetic Analysis System (NEMASYS) User's Manual", NAWCAD, February 1995.

4. "Operators Manual TR8828 Series and MM8103A, MM8104, MM8105 Waveform Recording System", Lecroy Corporation, March 1987.

5. "ODT Optical Data Transmitters", EG&G Washington Analytical Services Center, Inc., Data Sheet 1230, May 1985.

6. "OP 300-2A Optical Analog Transmission System", Nanofast, Inc.

7. "Detailed Operating Procedures for the EMP Instrumentation Suite", BDM Engineering Services Company, Volume I, under contract #N00421-88D-0012, July 1991, p32-38.

# JRS MAGNETIC LIGHTNING CURRENT DETECTOR

Michael Brooks
I-NET, Inc.; Mail Stop INI-4
Kennedy Space Center, Florida 32899 USA
Telephone (407) 867-4879 FAX (407) 867-1087

## ABSTRACT

The concept of a magnetic lightning current detector originated by the late James R. Stahmann, Lightning Specialist at Kennedy Space Center (KSC), was proven feasible in 1991. Development testing of this concept continued into 1995. The device is a simple, durable, yes/no lightning strike indicator, readable with a portable gauss meter; a magnetic one bit memory device writeable by lightning. A lightning strike to a large conductive object causes negative or positive current to flow on the surface of the object. Lightning current flow creates a magnetic field perpendicular to the current. Significant magnetic field effects exist near the surface of the object during the rapid rise and decline of the current. The magnetic field will reorient some of the magnetic domains in an exposed device which has been previously magnetized with a specific vertical polarity. A simple, small permanent magnet can be used to apply a polarized, magnetic area on the device. A portable, handheld gauss meter can read the polarity. A simple flat plate device of magnetically soft material can be locally magnetized with a handheld permanent magnet such that the magnetic poles are oriented in a preferred direction. The magnetic polarity can be permanently marked on the simple plate device. The device can be attached to the surface of an object simply with adhesive or can be permanently mounted. The gauss meter (magnetometer) is used to read the device before and after suspected lightning strike to determine change or no-change in magnetic field strength or polarity. This paper describes the history and test results of the JRS Magnetic Lightning Current Detector (LCD).

## INTRODUCTION

In the three years prior to his death in late 1992, James R. Stahmann was working on lightning protection measures for Space Shuttle Solid Rocket Booster (SRB) segments while in transit and storage. As a consequence of these investigations, the need became apparent for a simple, inexpensive indication of a lightning strike to the segment . A strike to a segment would, at a minimum, cause it to be pulled from the vehicle processing flow and render it suspect to hidden grain separation. The segment would likely be sent back to the manufacturer for rework and recertification. These concerns led to the fabrication and testing of several conductive covers for these open-ended SRB segments. During these tests, Jim Stahmann originated and began the testing of a simple, inexpensive indicator of whether lightning had struck the SRB segment.

Since the author worked on lightning under Jim's direction for many years, the task of completing these tests fell to him at Jim's passing. Portions of Jim's technical notes on the subject lightning current detectors were found recently, and there are clear memories of his discussions of the tests. What follows is a description of what is believed to have been Jim's intentions and the testing performed by the author.

**BACKGROUND--**The concept of a magnetic lightning current detector is not new. Devices such as maglinks have been described by Foust and Keuhni (1) as well as others. Measurements of lightning current amplitude using pre-magnetized audio tape have been described by Darveniza (2) and Crouch (3) . The need in this case was to detect whether or not lightning had struck an SRB segment. Measurement of the amplitude of the lightning current was not required. What was needed was a discrete, yes-no indication .

**CONCEPT--**The original detector concept came in two forms: the first was a flat strip and the second was a strip made into a ring with a gap between the ends. The first detectors were made of a piece of a fruit juice can and the second of a piece of steel conduit. The flat strip juice can fragment was magnetized using a permanent magnet and taped to the side of an SRB segment. The north magnetic pole was oriented upward. At first it was thought that the upward pointing north magnetic field would be reoriented to 90 degrees to the downward current flow by the magnetic field due to the current. This was first done in 1991 during full scale tests of SRB segment covers using the Thiokol lightning simulator at Wendover, Utah. Both the strength and direction of the magnetic field in the juice can fragment was measured before and after firing the simulator. This measurement was performed using a modern, inexpensive, battery operated magnetometer. This magnetometer or gauss meter uses a gallium arsenide transverse Hall-Effect probe. These initial proof-of-concept tests reportedly showed a consistent measurable change in the magnitude of the residual magnetic field in the juice can fragment due to the lightning current flow. No records exist to indicate a complete change in direction of the magnetic north pole. Magnetizing and measuring a spot on the steel SRB casing was also tried. This method did not prove reliable and was abandoned.

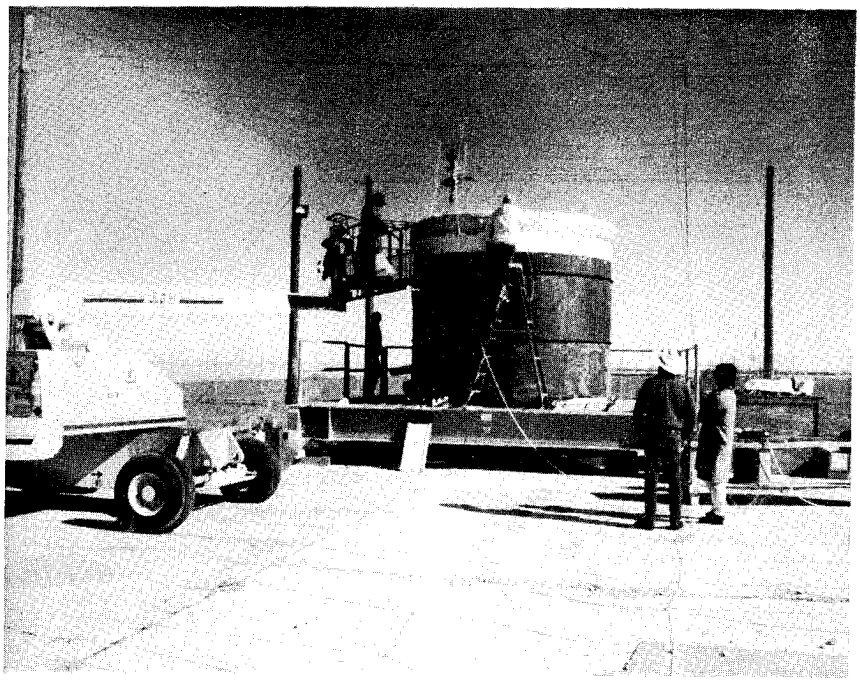
The second detector, the unmagnetized steel strip/ring, was placed around a simulator return conductor and taped in place. Before and after firing the simulator, the magnetometer probe was placed in the gap of the ring and the field measured. A consistent change in residual magnetic field was observed.

**TEST METHOD--**After Jim's passing, a new set of tests was planned on a conductive fabric cover for the SRB segments at the same Wendover facilities. These tests were conducted in November 1993 and are documented in a report by Steffan (4). Figures 1 and 2 are an overall view of the cover test setup. This new set of tests provided an opportunity to test and document Jim's original concept via the concurrent experiments described below. See Steffan(4) for details of the discharge waveforms.

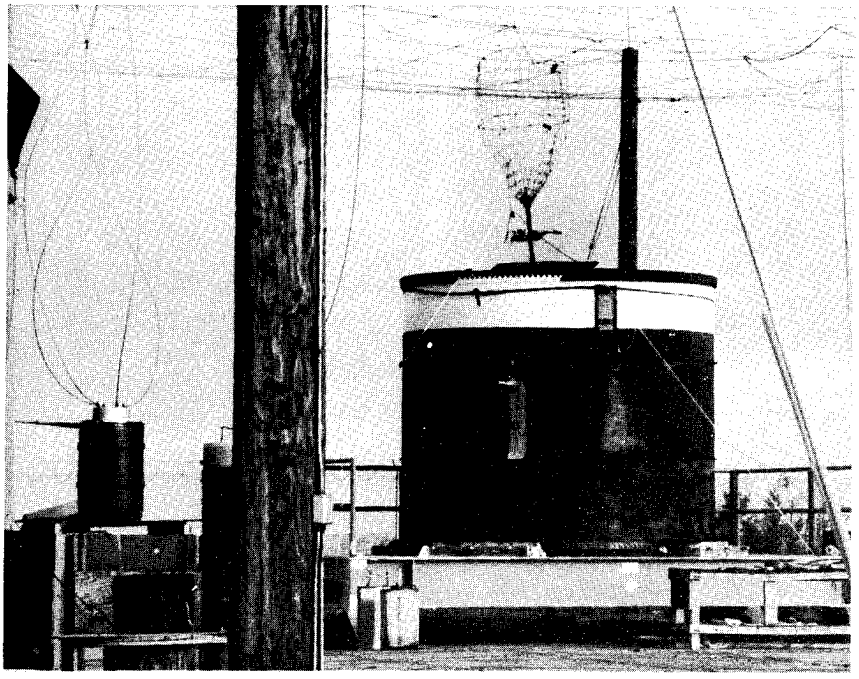
The first four discharges were considered as a warm-up for the simulator. These discharges were used to expose four KSC LCDs (Crouch, 3). This is a magnetic audio tape erasure device in common use at the Kennedy Space Center. The KSC LCD holder was connected directly to the primary discharge electrode as a control experiment. No other experimental detectors were exposed during these four discharges. The simulator provided current measurements. The KSC LCDs, though not calibrated for the electrode diameter, showed reasonable erasures.

Two detection methods were then simultaneously tested as follows. A set of ten test specimens of various steel strips (JRS LCDs) were numbered, marked and

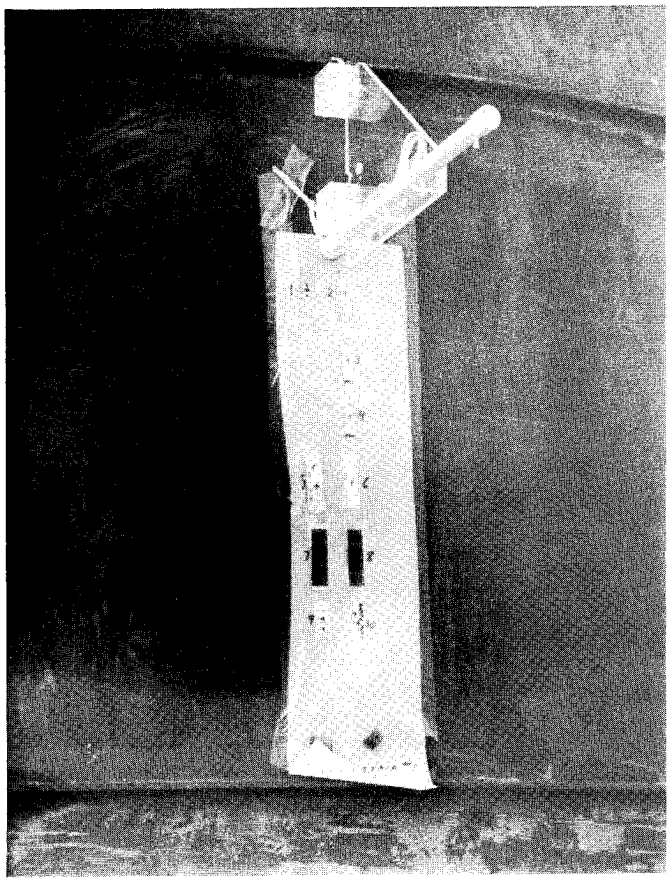
fastened to a sheet of 3 mil mylar. These are shown taped to the side of the SRB in figures 3 and 4. See table 1 for the size and type of steel. Numbers 1, 5, 7 and 9 were placed over a cardboard spacer approximately .060 inches thick for comparison.



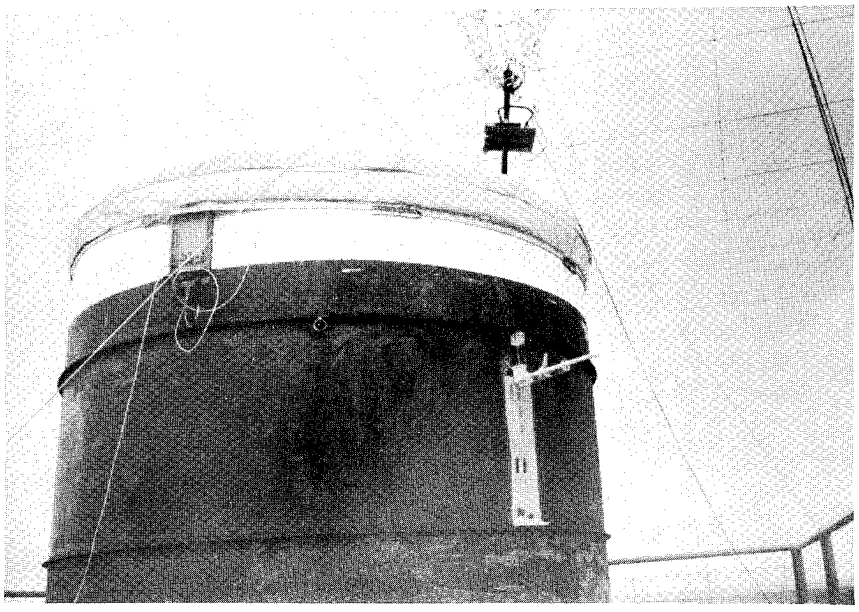
WENDOVER, UT. SRB COVER TESTS
FIGURE 1



WENDOVER, UT. SRB COVER TESTS
FIGURE 2



JRS LCDS AND KSC LCDS ON SRB CASING
FIGURE 3



JRS LCDS AND KSC LCDS ON SRB CASING
FIGURE 4

TABLE 1
JRS LCD TEST SAMPLES

#1. NETIC S3-6 High Permeability alloy .030" 1" x 3.5" over ~.060" spacer
#2. NETIC S3-6 High Permeability alloy .030" 1" x 3.5"
#3. cobalt tool steel .0625"x 2.5"x.75"
#4. cobalt tool steel .0625"x 2.5"x.75"
#5. common galvanized steel .014" x 1" x 3.5" over ~.060" spacer
#6. common galvanized steel .014" x 1" x 3.5"
#7. hot rolled carbon steel .054" x 1" x 3.5" over ~.060" spacer
#8. hot rolled carbon steel .054" x 1" x 3.5"
#9. original juice can fragment over ~.060" spacer
#10. new juice can fragment

The second experimental detection method was placing a KSC LCD at the top of the mylar sheet for comparative readings. This is the assembly of PVC pipe and acrylic sheet seen in figures 3 and 4. The magnetic tape is fastened around a long acrylic strip within the PVC pipe. The middle of the folded tape nearest the SRB is a known small distance from the SRB. This distance is taken into account in the KSC LCD calibrations when used with a wire or small known diameter lightning conductor.

Before each of the discharges, a fresh KSC LCD magnetic tape was loaded in the PVC pipe and each of the ten steel strips (JRS LCDs) was magnetized. The magnetizing was done in a consistent repetitive fashion as follows: A horseshoe magnet was placed over a marked spot touching the strip with the north pole pointing up. The magnet was then removed and the magnetometer probe placed perpendicularly on the mark with positive gauss=north=up. The gauss reading was recorded, the probe rotated 90 degrees clockwise and the gauss reading recorded again. This was for a basis to show directional change. The percent change in retained magnetic field was calculated by dividing the absolute value of the change in magnetic field (gauss) by the original gauss reading before the discharge. Up=north directional readings were used in the calculations, since not all samples showed a gauss reading at 90 degrees.

The next several discharges were Marx high rate of rise only and none exceeded 38 kiloamperes peak. The high current bank and the continuing current bank were not connected. The percent change in the residual magnetism of the JRS LCDs for one Marx discharge are shown in Table 2. Unfortunately, due to a last minute change in the cover test plan, circumstances prevented data being taken from additional Marx discharges.

TABLE 2
MARX HIGH RATE OF RISE DISCHARGE
(PERCENT CHANGE IN RETAINED MAGNETIC FIELD)

| Test Specimen Numbers | 1 | 2 | 3 | 4 | 5 | 6 | 7 | 8 | 9 | 10 |
|---|---|---|---|---|---|---|---|---|---|---|
| Discharge 1 | 42% | 23% | 15% | 1% | 46% | 36% | 46% | 0% | 10% | 46% |

The next twelve discharges were composite high current bank and continuing current bank. These discharges produced consistent changes in the residual magnetic

field in the JRS LCDs . The changes were decreases in the up=north direction and sometimes an increase in the left-right magnitude, but the changes were not consistent in this direction. The magnetometer only reads the net vector sum of all the magnetic domains in the sample. Reorienting part of the domains results only in a decrease in the sum. If the influence was sufficiently strong, the majority of the domains would be reoriented and the resulting north-south direction would be horizontal. The cobalt tool steel was the only material to fairly consistently have a non-zero gauss reading in the horizontal direction after the discharge. The best material for this application would have a high permeability and a high retentivity. Table 3 shows the percentage change in retained magnetic field for each of the ten samples over the course of twelve discharges. The bottom row is the average percentage change over the twelve discharges for each of the ten samples.

The tests of KSC LCDs at Wendover showed that the KSC LCD method is not effective on an SRB casing. Only one of the tapes exposed in this sequence showed any erasure, and it was in error by a factor of roughly ten in equivalent calibrated current through a wire. This was on the occasion of the largest high current bank discharge and closest proximity of the discharge electrode. In other words, the geometry of the SRB casing and the geometry of the current flow render this familiar conventional lightning magnetic current detector ineffective for this application.

TABLE 3
COMPOSITE DISCHARGES
(PERCENT CHANGE IN RETAINED MAGNETIC FIELD)

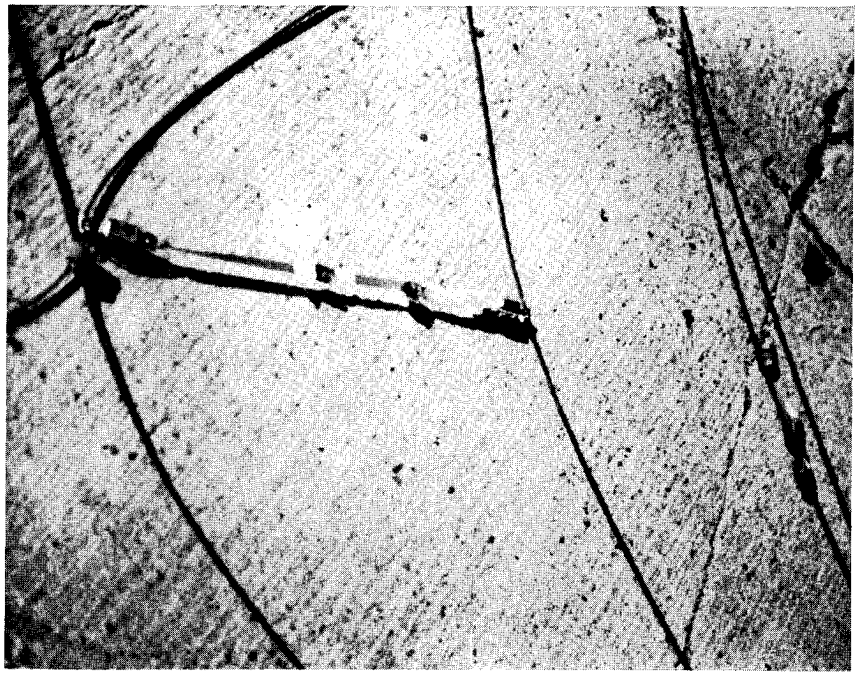
| Test Specimen Numbers | 1 | 2 | 3 | 4 | 5 | 6 | 7 | 8 | 9 | 10 |
|---|---|---|---|---|---|---|---|---|---|---|
| Discharge 1 | 88% | 71% | 36% | 29% | 92% | 53% | 84% | 74% | 73% | 51% |
| Discharge 2 | 56% | 53% | 24% | 39% | 88% | 47% | 60% | 53% | 71% | 49% |
| Discharge 3 | 100% | 100% | 67% | 66% | 120% | 106% | 75% | 71% | 100% | 98% |
| Discharge 4 | 73% | 29% | 13% | 13% | 71% | 23% | 55% | 24% | 63% | 38% |
| Discharge 5 | 70% | 36% | 12% | 17% | 82% | 39% | 123% | 53% | 68% | 41% |
| Discharge 6 | 43% | 43% | 17% | 21% | 27% | 27% | 72% | 44% | 63% | 40% |
| Discharge 7 | 47% | 47% | 13% | 17% | 20% | 30% | 69% | 37% | 58% | 33% |
| Discharge 8 | 38% | 38% | 13% | 20% | 25% | 22% | 53% | 29% | 62% | 93% |
| Discharge 9 | 30% | 30% | 26% | 24% | 31% | 22% | 40% | 32% | 50% | 25% |
| Discharge 10 | 68% | 68% | 33% | 26% | 35% | 39% | 63% | 32% | 64% | 36% |
| Discharge 11 | 12% | 12% | 8% | 15% | 17% | 22% | 44% | 32% | 48% | 16% |
| Discharge 12 | 38% | 34% | 15% | 17% | 30% | 25% | 58% | 32% | 51% | 36% |
| Avg % Change | 55% | 47% | 23% | 25% | 53% | 38% | 66% | 43% | 64% | 46% |

"C" SHAPE JRS LCD TESTS- The final series of tests at Wendover involved placing JRS LCDs around the simulator ground return grid wires and the SRB ground bonding wires. The JRS LCDs and KSC LCD were removed from the SRB segment and five of these JRS LCDs were used on the wires. The strips were formed into a "C" shape with a gap just sufficient to admit the magnetometer probe. They were held in place and shape by tape. This is shown in Figure 5. The current amplitudes and waveshapes were not known due to the multiple grid paths. Some of the test samples were placed around a clip-on ground strap jumper. This jumper was placed across two points in the ground grid. Current flowed in the jumper wire due to the inductive

gradient in the grid, and changed the field in the JRS LCDs. These tests were only looking for a reasonable change in retained magnetic field, and in that respect they succeeded. See table 4 for typical percent changes.

TABLE 4
MARX HIGH RATE OF RISE DISCHARGES
"C" SHAPE JRS LCD TESTS
(PERCENT CHANGE IN RETAINED MAGNETIC FIELD)

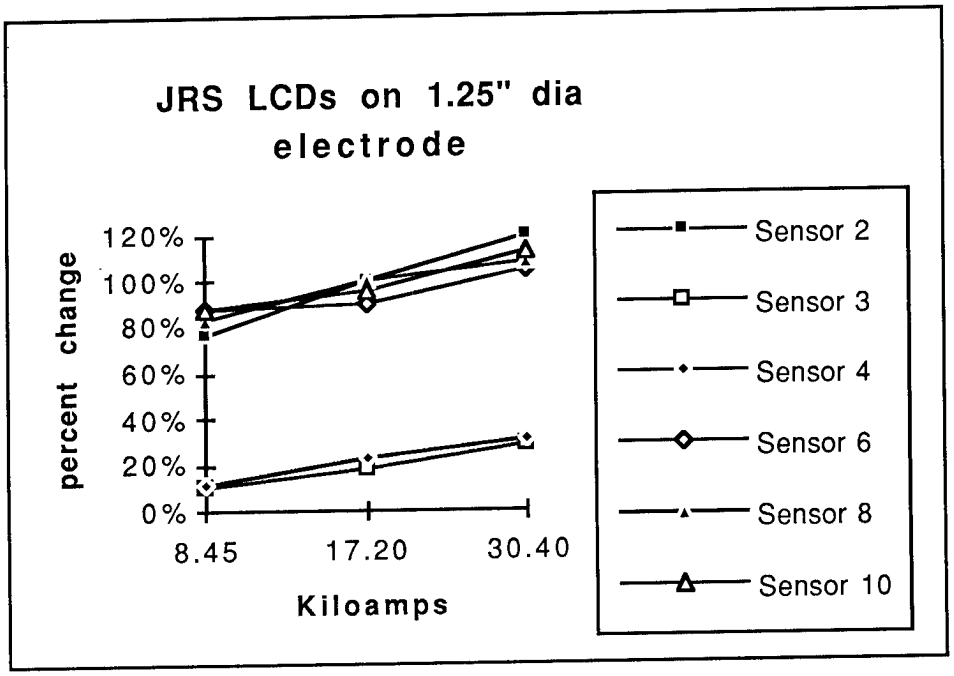
| Sensor Type | Sensor A Galvanized | Sensor B Galvanized | Sensor C NETIC | Sensor D HRCS | Sensor E HRCS |
|---|---|---|---|---|---|
| Discharge 1 | 82% | 45% | 56% | 55% | 30% |
| Discharge 2 | 133% | 149% | 149% | 147% | 149% |
| Discharge 3 | 100% | 30% | 53% | 36% | 35% |
| Discharge 4 | 50% | 66% | 0% | 14% | 104% |
| Discharge 5 | 3% | 0% | 34% | 44% | 27% |
| Discharge 6 | 9% | 9% | 55% | 48% | 92% |
| Discharge 7 | 209% | 209% | 136% | 7% | 7% |
| Avg % Change | 49% | 42% | 40% | 29% | 37% |



JRS LCD ON GROUND WIRE
FIGURE 5

FLAT SHAPE JRS LCD TESTS AT KSC In January 1994, a short series of tests were performed at KSC on six of the same JRS LCDs from Wendover. These tests were to look for a possible linear relationship between the flat JRS LCDs and the peak current, and to observe the effect of increasing the diameter of the electrode (SRB, etc.) to which the flat JRS LCD was attached. The simulator available was limited to

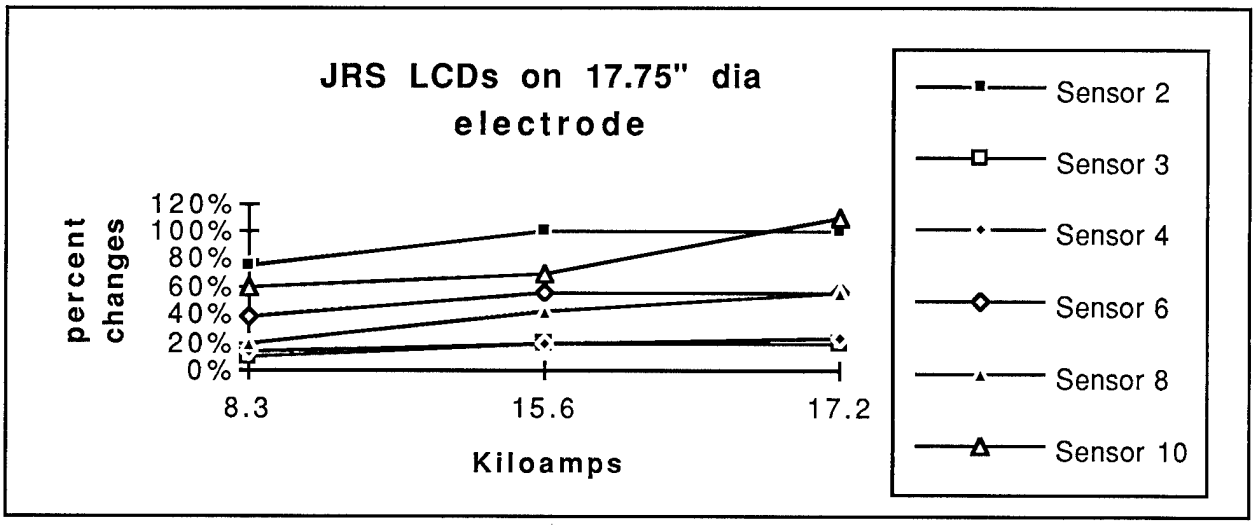
about 30 kiloamperes maximum. The current was discharged through a coaxial resistor on the surface of which were placed the JRS LCDs. The coaxial resistor has a terminal made of metal pipe of 1.25" diameter and a metallic body section whose diameter is 17.75". The JRS LCDs were first taped directly on the 1.25" diameter pipe for three discharges and then on the 17.75" diameter body for three discharges. The discharges were damped oscillatory with 3 to 6 rings. The sensors are the same as in table 1 and bear the same numbers as at Wendover, but no spacer was used under any of them. Figures 6 and 7 show the test results in percent change in retained magnetic field versus peak discharge current.




PERCENT CHANGE IN RETAINED MAGNETIC FIELD

| KAMPS | Sensor 2 | Sensor 3 | Sensor 4 | Sensor 6 | Sensor 8 | Sensor 10 |
|---|---|---|---|---|---|---|
| 8.45 | 77% | 10% | 12% | 88% | 83% | 88% |
| 17.2 | 100% | 19% | 23% | 90% | 100% | 96% |
| 30.4 | 120% | 29% | 31% | 105% | 109% | 113% |

FIGURE 6




PERCENT CHANGE IN RETAINED MAGNETIC FIELD

| KAMPS | Sensor 2 | Sensor 3 | Sensor 4 | Sensor 6 | Sensor 8 | Sensor 10 |
|---|---|---|---|---|---|---|
| 8.3 | 75% | 11% | 14% | 39% | 20% | 61% |
| 15.6 | 100% | 20% | 21% | 57% | 43% | 70% |
| 17.2 | 100% | 19% | 25% | 57% | 57% | 110% |

FIGURE 7

## CONCLUSIONS

The KSC LCDs were not effective as a detection method for lightning current on SRB segments. Flat JRS LCDs are effective as a go no-go detection method in the same application. A minimum acceptable percentage change must be established to avoid ambiguity. Five different types of steel were tested, one set directly on the mylar and one set on a cardboard spacer about .060 inches thick over the mylar. The cobalt tool steel averaged the lowest change in retained magnetic field in the vertical direction but was the only one of the five to show a partial change in direction of the field to horizontal. The lower response of the cobalt steel can be seen in figure 6. The remaining four steels all gave comparable results. None stood out as a best choice over the others. These four steels are not very different from one another in magnetic properties. Sensors 1, 5, 7 and 9 on the spacers yielded slightly higher retained field. This may be due to the casing acting as a magnetic shunt, or "keeper" on sensors 2, 6, 8 and 10. An astute choice of material perhaps would further optimize the performance, but even ordinary carbon steel or tinned steel food cans will yield satisfactory results. The use of these detectors could be extended to apply to other large flat or large diameter objects.

The "c" shaped form of the JRS LCD when starting with unmagnetized material yields the most marked change in field. If one or more of these detectors are placed around a grounding jumper that is in the presence of multiple parallel paths to ground a satisfactory reading can still be obtained.

Modern microprocessor based inexpensive, portable Hall effect gaussmeters have made this development possible. The beauty of this sensor is in its simplicity and low cost.

## REFERENCES

1. C. M. Foust and H. P. Kuehni, "The Surge-Crest Ammeter," General Electric Review, Vol. 35, No. 12, December, 1932, p. 644.

2. M. Darveniza, "Measurement of Impulse Currents Using Pre-Magnetized Tape," Journal of Electrical and Electronics Engineering, Australia - IE Aust. & IREE Aust., Vol. 6, No. 2, June 1986.

3. K. E. Crouch, "Calibration Tests on Magnetic Tape Lightning Current Detectors," NASA Contractor Report 3270 prepared under Contract CC82279A, Lightning Technologies, Inc., Pittsfield, Massachusetts, 1980.

4. D. A. Steffen, "SRM Lightning Protection Covers Test Program," EMA-94-R-005 Final Report, prepared for Thiokol Corporation, Contract No. 1RK010, January 1993.

## BIBLIOGRAPHY

Jiles, D., "Introduction to Magnetism and Magnetic Materials," Chapman and Hall, 1991, Bury Saint Edmunds, Suffolk, UK, ISBN 0412386305.

# SCALING ALGORITHM FOR C-17A SIMULATED LIGHTNING TEST

Jack R. Lippert and John G. Schneider
Computer Science and Applications, Inc.
2 Clifford Drive
Shalimar, FL 32579
(904) 651-4991 / FAX 904-651-2816

## ABSTRACT

The Air Force C-17A Lightning test consisted of injecting a scaled down but significant level current pulse waveform onto the skin of the whole aircraft and measuring the induced response on interior cable wiring and subsystems components, and later, scaled-up reinjection into the test point via a direct drive bulk cable current injection system. For this test, specified current rate-of-rise and decay times could not be achieved with the simulation hardware. These problems were overcome via a Fourier scaling algorithm used to modify the measured output by a transfer function to result in a representation of the output if originally stimulated with the desired input. This scaling technique is not complicated and allows for "correcting" a number of possible deficiencies that might occur in testing for whatever reason. The specifics of the scaling algorithm, the rationale behind it, and the limitations to its use is discussed in this paper.

## INTRODUCTION

The general methodology for assessing the C-17A susceptibility to lightning's induced effects is a best-compromise marriage of diverse requirements and real world test and operational limitations. The aircraft was subjected to simulated lightning threat impulses and systematically tested to verify functional capability and adequate safety margin for surviving the severe threat definition (200,000 amperes). Direct effects testing was not part of this effort.

The overall lightning testing consisted of two phases: 1) the Passive Systems Tests, where current waveform responses to a simulated lightning current pulse applied on the aircraft skin are measured on the interior wiring and bulk cables; and 2) The Active Systems Tests, where functional response and upset are monitored on powered-up subsystems when those same measured waveforms are scaled up and reapplied into the bulk cable via direct drive current injection. This approach reduces risk of catastrophic damage by limiting the excitation source applied to the entire aircraft, and incrementally increasing the threat severity to the individually tested in situ Line Replaceable Unit (LRU). It is normally accepted that functional upset will be observable before hardware damage will occur. Although the tests emphasis was placed upon the flight critical electrical/electronic line replaceable units (LRUs), the mission essential equipment was also of importance and included in the test points.

The passive systems tests utilized a Marx generator type capacitor bank to inject a current impulse into the aluminum skin of the aircraft. The standard waveform for induced effects testing, is the damped sinusoid Current Waveform E from MIL-STD-1757A, TO5. In general, a double-exponential waveform (based on Component "A" from either MIL-STD-1795A or 1757A) would also be acceptable, and at times preferable, as it would include the direct effect damage assessment at the same time. However, higher peak current amplitudes can be generated with less hardware if the damped oscillatory waveform format is used rather than the double-exponential. This issue was the determining factor for the C-17A tests since the large cargo aircraft presents a larger than usual inductive load that must be driven by the Marx generator. Even with the coaxial return path minimizing the apparent circuit inductance, the measured aircraft/return path load inductance ranged from a low of 13.5 mircoHenrys for the nose-to-tail configuration to over 19 microHenrys for the wing-to-wing configuration.

A total of three current path configurations were tested to expose the interior wiring runs to the coupling phenomena from the major possible lightning current distribution paths. In addition to the usual nose-to-tail and wing-to-wing configurations, a nose-to-(outboard) engine was selected as a potentially maximum coupling path for the flight critical full authority digital electronic engine controls. The measured response on the LRUs input cabling varied significantly, both in amplitude and waveshape components, depending upon the test configuration and specific wire routing to the LRU. In general, the largest response configuration example was used for the direct drive candidates. However, in a few instances where the waveshape was drastically altered when tested in a different configuration (e.g., derivative versus direct response) both waveforms were input for direct drive candidates. The number of direct drive points were disproportionally heavy with waveforms from the nose-to-engine configuration, accounting for almost half (38 out of 80) with nose-to-tail and wing-to-wing equally dividing the remainder.

## SCALING ALGORITHM

The peak current amplitude required to be consistent with Waveform E is 50,000 amperes, with a current rise rate of at least 25 kA/microsecond for the fastest 0.5 micro-second duration. This considerable amplitude represents an 80 percentile lightning stroke, meaning 80% of all lightning events' first return stroke would be less than or equal to 50,000 amperes.[1] The measured results from this significant input current only needs scaling by a factor of four to reach severe threat levels and avoids the risks of over-extrapolation of data/results which potentially could violate linearity assumptions. The linearity assumption is normally considered conservative because non-linear effects such as arcing should consume energy and reduce the remaining threat level, as evident by some test points that did not significantly increase. However, this general rule of thumb must be exercised with caution since an arc may precipitate a different current path and cause a larger impact elsewhere upon some local circuitry. Indeed, a small number of test points did show an increased response

significantly beyond the factor of two tested. However, the predominant response roughly agrees, within experimental tolerance, to the scaling of the current. Figure 1 is a charted example of responses from the 25kA to 50kA level for the nose-tail configuration. The apparently large ratio from the 34th test point is not due to high currents but rather to anomalously low current amplitude during the 25kA level test. The 50,000 ampere level was chosen as the most appropriate starting point for the extrapolation process for the active systems testing.

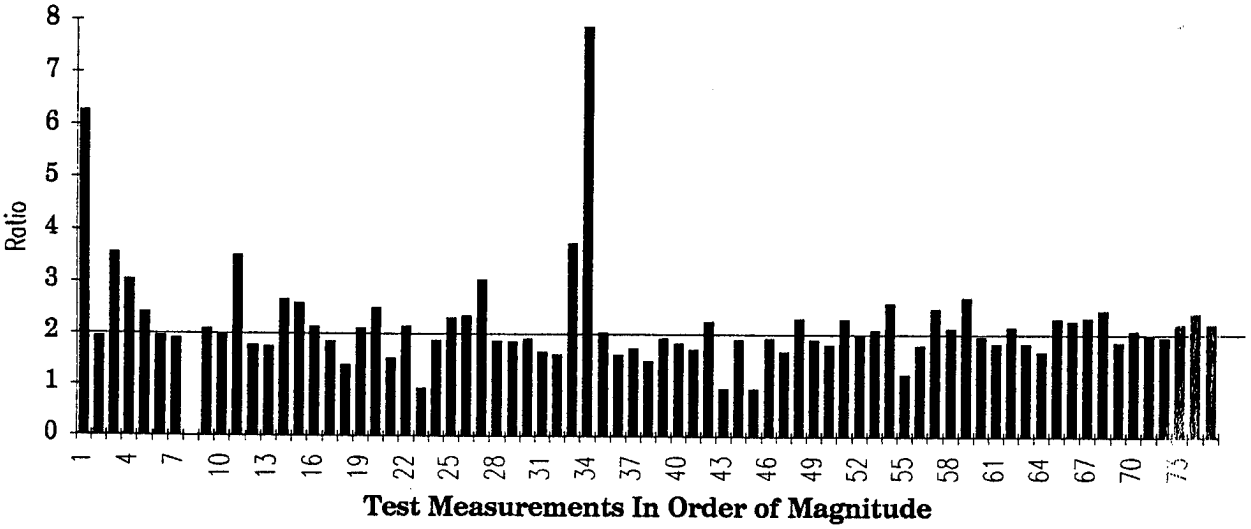



FIGURE 1. RATIO OF 50kA/25kA TEST MEASUREMENTS (NOSE-TAIL CONFIGURATION)

The active systems testing subjected the operating aircraft electrical/electronic equipment to a reproduced example of the passive system test measured waveform, directly injected into the bulk cable. The direct drive procedure incrementally increased the scaled waveform ultimately to the point of 6dB margin above the 200,000 amperes severe threat. At each incremental level a multiple pulse series of the threat waveform would be injected for approximately one minute. The aircraft active systems and control surfaces were monitored for evidence of sustained upset or uncontrolled flight conditions. At the conclusion of the direct drive testing phase, a thorough functional checkout assured that no damage occurred.

The factor of two safety margin accounts for the necessary non-realities and liberties that have to be taken with lightning simulation testing. For example, the coaxial return path which compensates for near ground field effects and reduces the load inductance for the Marx generator may artificially spread out the current attachment points possibly modifying current path distributions and the subsequent amount of coupling to elements in close proximity. Additionally, only a selected subset of the entire installed equipment can feasibly be tested. Still another limitation is subjecting only one active test point at a time via direct drive whereas the lightning

interaction would affect all of the systems simultaneously with potentially synergistic effects.

Ordinarily, the extrapolation technique to represent a more severe threat from a scaled simulated lightning impulse is direct and linear with current when the risetimes are consistent.[2] Since the C-17A large size presented a large inductive load to the simulation equipment, the resulting impulse current rate-of-rise fell short of the Waveform E specification, particularly in the wing-to-wing test configuration. This required each waveform to be scaled according to current rise rate as well as peak amplitude. The Naval Air Warfare Center (NAWC) data acquisition system stores the measured waveforms along with the corresponding input excitation (reference simulated lightning impulse). Both are required to perform a frequency convolution scaling algorithm upon each test point's stored waveform. This normalizes the responses from different configurations and pulse to pulse variance; and more importantly, results in a properly transformed signal with respect to both amplitude and frequency without overly conservative two point linear scaling.

The extrapolation algorithm uses a mathematical definition for the minimum acceptable frequency damped sine wave Waveform E scaled to peak at 200,000 amperes. Figure 2 presents this waveform. In preparation for direct drive testing, the candidate test point's measured response from the passive testing needs to be transformed for appropriate rise rate and amplitude. Using Fourier transforms in the frequency domain reduces the complex time domain convolution to simple multiple factors. Fourier transforms of the test point measured response, Y1(s), and its corresponding input reference, X1(s), are known and used to determine the aircraft transfer function for that test point, H(s), according to:

$$Y1(s) = H(s) * X1(s) \tag{1}$$

The response, Y2(s), from a different input driver can be analytically determined via:

$$\begin{aligned} Y2(s) &= H(s) * X2(s) \\ &= [Y1(s)/X1(s)] * X2(s) \end{aligned} \tag{2}$$

where X2(s) is the Fourier transform of the full scale mathematical expression for the threat mentioned above. This process is legitimate for any generic signal given the proviso that the overall system remains linear over that regime. This issue demonstrates the importance of, and another benefit from, using "substantial" current amplitude in the scaled threat input which is not likely to violate linearity assumptions when extrapolated only a few factors. Taking the inverse Fourier transform of the analytically determined Y2(s) now results in the time domain waveform that is appropriate for use as the direct drive input for that test point.

Figures 3 and 4 help explain the application of this algorithm to a test point measurement example. The first figure shows the corrected time domain waveform measured from the passive testing along with its associated spectral density plot. The Marx generator dominated frequency of about 50kHz is clearly notable. The latter

figure is the algorithm transformed time and frequency plots for the same test point. The generator peak has been shifted to the faster Waveform E specification while the aircraft configuration components (around 650kHz) is unchanged. The time domain waveform not only has the proper frequency content but the resulting amplitude reflects the impact from both the linear peak scaling (factor of four) as well as the rate of rise increase since this signal is from a derivative based response. Other response measurements, evident of diffusion or direct current sharing, would be properly transformed in their own right by this technique. For example, the resulting response from a double-exponential impulse could be "constructed" from the aircraft transfer function, obtained by an easier to simulate sinusoidal impulse, and transformed via this algorithm. The strength of this process offers the testing community a significant tool for increased capability.

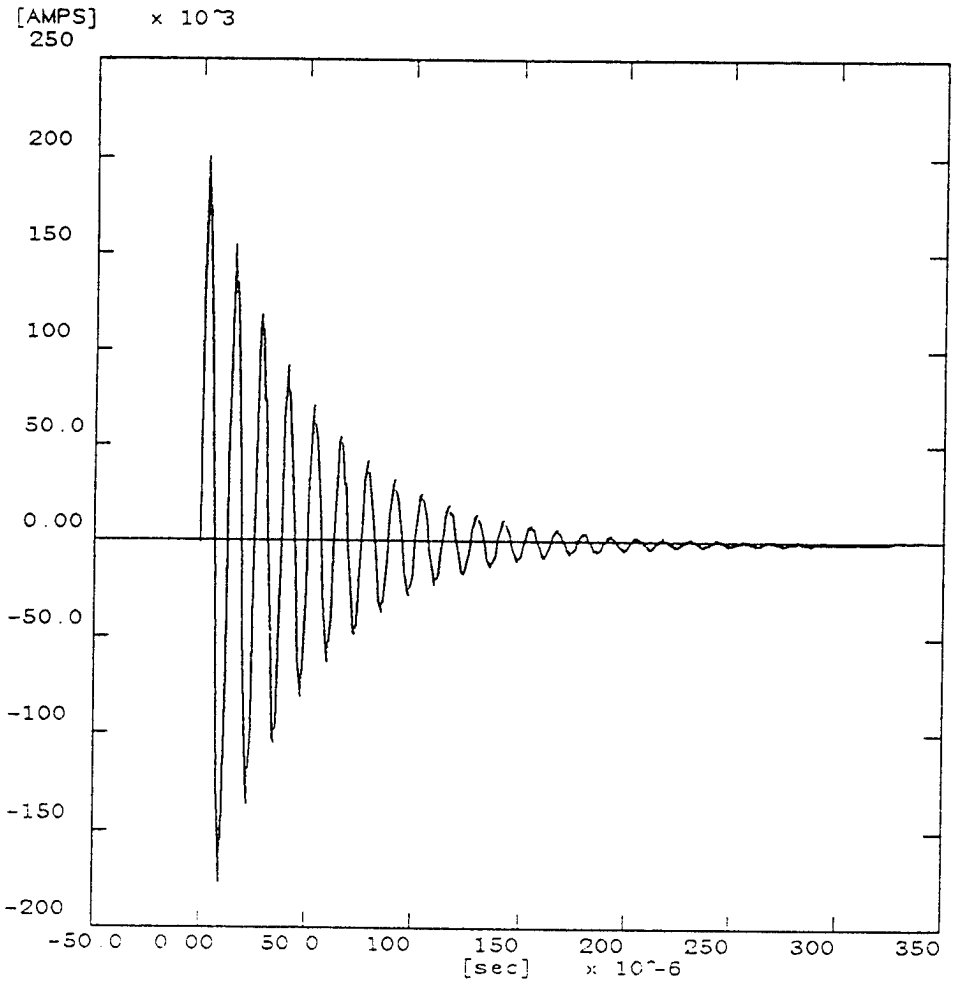
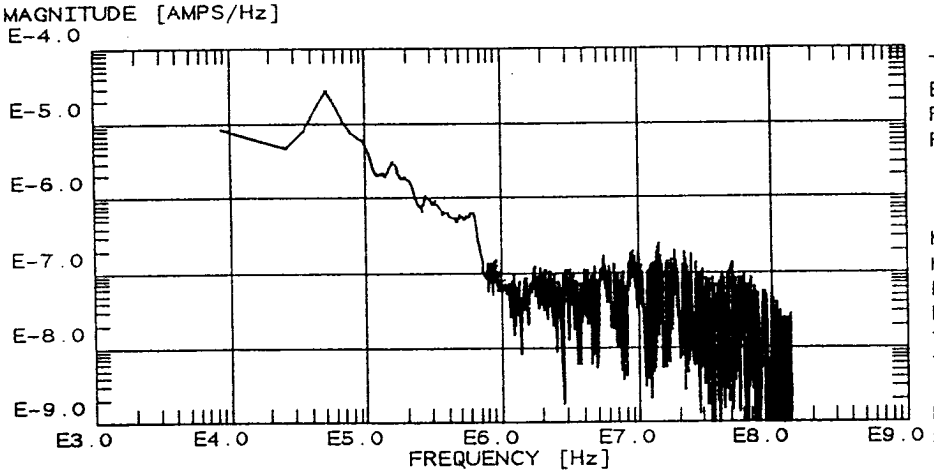
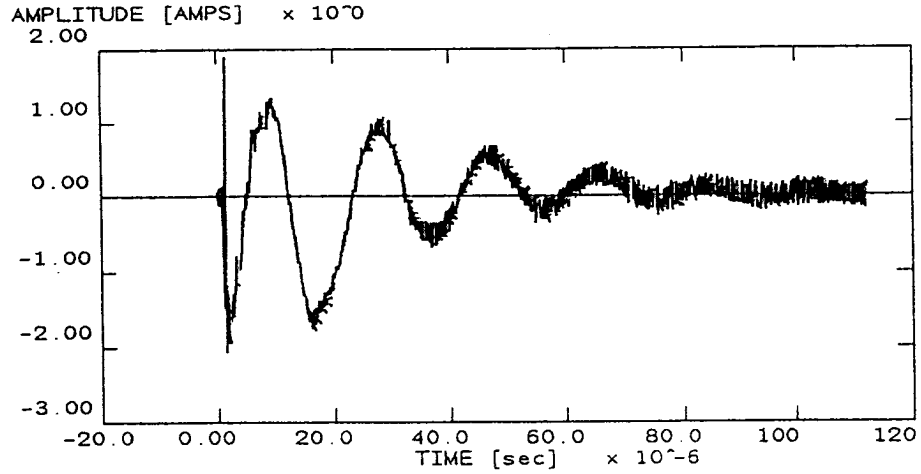



FIGURE 2. SCALED-UP WAVEFORM E TO SEVERE THREAT

30-JUN-93 17:26:14 FILE: DAS_DATA:BSG00605_0001_02_2.RAW



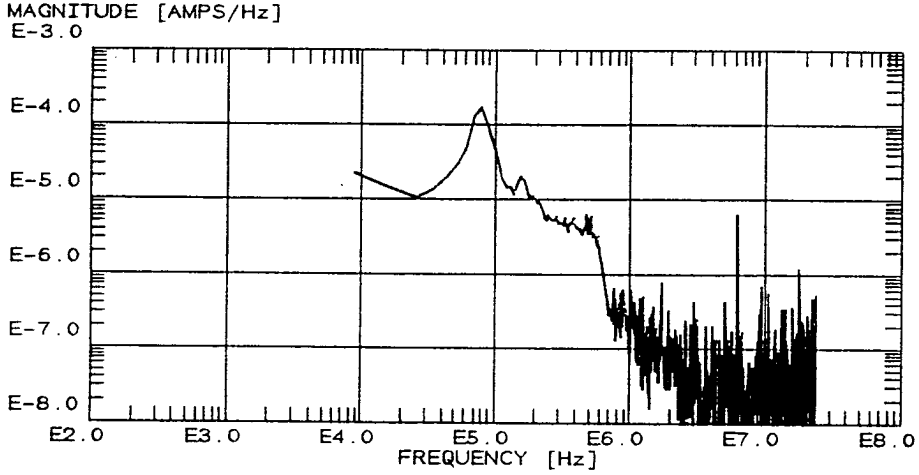



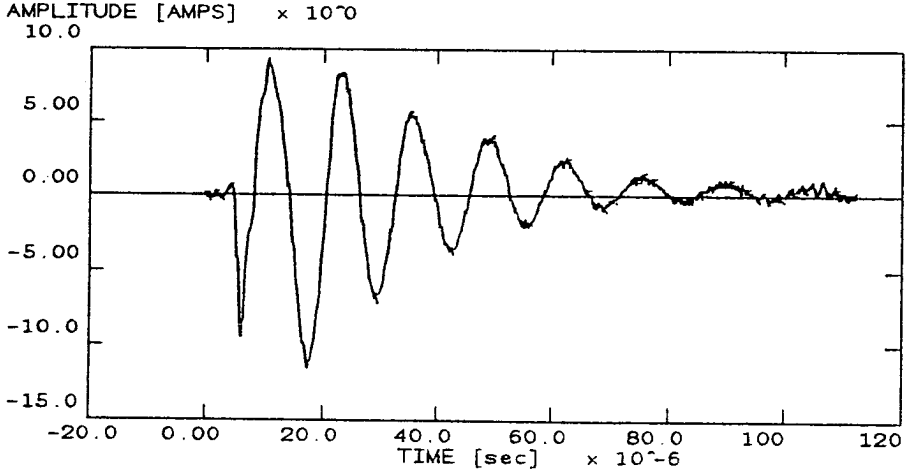

| | |
|---|---|
| Test ID | C-17 LIGHT |
| Experiment Number | 2 |
| Pulse Number | 905 |
| Pulse Date | 15-JUN-1993 11:53:29 |
| Ref Field [kV/m] | 50.32 E+03 |
| Rise Time [sec] | 4.441 E-06 |
| Measurement Type | IS |
| Measurement Priority | B |
| Probe type | I-125-2C |
| Probe Eu Conv. factor | 1 000 |
| Transmitter Gain [db] | -18 |
| Total Scalar Gain [db] | -18 |
| Peak [AMPS] | -2.043 |
| Signal/Noise Ratio [dB] | 30 |
| Action Integral [(AMPS)^2*sec] | 33.15 E-06 |
| Total Charge [Coulombs] | 39.62 E-06 |
| Derivative Peak [Amps/Sec] | 220.2 E+06 |
| Derivative at .5us [Amps/Sec] | 532.1 E+03 |
| 10-90% of pk slope [Amps/Sec] | 94.78 E+06 |
| Risetime to pk [sec] | 30.95 E-09 |
| Decay Time (1/2) PK [sec] | 48.76 E-09 |
| Signal/Reference ratio in Db | -87.83 |
| Extrapolated Pk [Amps] | 8.117 |

FOR OFFICIAL USE ONLY

FIGURE 3. BSG00605 REPEAT 1, CORRECTED DATA

30-JUN-93 17:28:14 FILE: DAS_DATA:BSG00605_0001_02_2.RAW




| | |
|---|---|
| Test ID | C-17 LIGHT |
| Experiment Number | 2 |
| Pulse Number | 905 |
| Pulse Date | 15-JUN-1993 11:53:29 |
| Ref Field [kV/m] | 50.32 E+03 |
| Rise Time [sec] | 4.441 E-06 |
| Measurement Type | IS |
| Measurement Priority | B |
| Probe type | I-125-2C |
| Probe Eu Conv. factor | 1.000 |
| Transmitter Gain [db] | -18 |
| Total Scalar Gain [db] | -18 |
| Peak [AMPS] | -11.57 |
| Signal/Noise Ratio [dB] | 37 |
| Action Integral [(AMPS)^2*sec] | 1.315 E-03 |
| Total Charge [Coulombs] | 0.249 E-03 |
| Derivative Peak [Amps/Sec] | 14.94 E+06 |
| Derivative at .5us [Amps/Sec] | 4.698 E+06 |
| 10-90% of pk slope [Amps/Sec] | 3.598 E+06 |
| Risetime to pk [sec] | 3.205 E-06 |
| Decay Time (1/2) PK [sec] | 5.268 E-06 |
| Signal/Reference ratio in Db | -72.76 |
| Extrapolated Pk [Amps] | 11.57 |

| %E | Freq (Hz) | Amplitude | Q | Delay |
|---|---|---|---|---|
| 132.2 | 79.86 E+03 | -20.44 | 4.2 | 1.7E-05 |

FOR OFFICIAL USE ONLY

FIGURE 4. BSG00605 REPEAT 1, EXTRAPOLATION REPORT

REFERENCES:

1. B.G. Melander, "Atmospheric Electricity Hazards Threat Environment Definition," AFWAL-TR-85-3052, August 1985.

2. W. McCormick, K. Maxwell, and R. Finch; "Analytical and Experimental Validation of the Lightning Transient Analysis Technique," AFFDL-TR-78-47, March 1978.

3. J.R. Lippert, and J.G. Schneider; "C-17A Lightning Test and Analysis." final report for UIE subcontract under Navy contract N00421-90-D-0161, September 1993.

# LIGHTNING ENERGY RELEASE REMOTE MEASUREMENT BY MEANS OF RADAR.

E.I.Dubovoy
Academician Mints Radiotechnical Institute
8th of March 10, 125083, Moscow, Russia
Telephone (095) 212-9987, (095) 311-5957

## ABSTRACT

According to the theory that has been developed by author previously the radar echo signal from the lightning has a duration dependent only from lightning energy release E and independent from other characteristics of the lightning. This paper contains theoretical arguments and the first experimental verification of this method of the remote determination of lightning energy release in synchronously measurements of the radio-wave reflection at 35 cm and electric field impulses of lightning return strokes.

## INTRODUCTION

The determination of a lightning physical characteristics - a current, its duration t, energy release E per one length unit of discharge channel is one of the fundamental problem of the atmospheric physics. This problem has simultanously practical meaning for aviation, naval transport, aeronautic, protecting of forests and energy nets.

For this time didn't exist the remote method of these characteristics determination for lightning with arbitrary position in space. Only for vertical lightning discharge cloud-to-ground may be used the transmission-line or more complicated model of Uman et al. (1,2). This theoretical and practicale model permit with help of measurement of the lightning electromagnetic field impulse (EFI) intensivity to determine the current and other physical characteristics in vertical lightning.

In the author's papers (3, 4, 5) the method is developed for the energy release E determination in a lightning with help of impulse radar radiation, measurement of the radio-reflection intensity from discharge channel and its duration $\tau$. This method can be used without direct visibility of a lightning on the distance upto some hundred kilometer. This method is not dependent from the other characteristics of the lightning, including its orientation in space. Therefore it is clear the important meaning of the new remote method. The review of the theoretical papers (3,4) and the first experiment in using of this method is made in (5, 6).

THEORETICAL ARGUMENTS.

In this paragraph we bring forward arguments on behalf of the proposed method. Earlier in (3) was adduced, that the energy release E in return stroke is determined practically without any model supposition only on the basis of a knowledge of the current in return stroke and its duration. After that in (4,5) was be shown that for a solution of radiation gas dynamic equations for discharge channel expansion it is enough to know only the energy input E. This solution enable possible to calculate the gas extension in the discharge channel, temperature, radius, air and electron density Ne and to solve the problem of radio-wave reflection on the channel. This system was solved in (4). The channel's evolution was received by the numerical integration of radiation gas dynamic equations, taking into accounting Joule's heat sources, own magnetic field, electron and molecular air thermoconductivity, and energy transfer by radiation. The washing out the border and cooling of the widened ionized channel is determined, principally, by the molecular diffusion process. It brings partly to radiowave absorption in discharge channel and to decrease radio-wave reflection intensity.

The formula for the radiowave reflection intensity S(t) taking into account a lightning zigzag and different angles of incidence is deduced in (7,8). S(t) and impulse radioreflection duration for each return stroke are dependent only from the energy release E per one length unit and not dependent on current and its duration $t$ separatly.

The values of the radio-reflection duration $\tau$ are represented in table 1 for impulse radar wave length $\lambda$=35 cm in dependence from energy release E per one length unit of channel.

Table 1. The duration $\tau$ in msec of radioreflection intensity S(t) for different E.

| E G/m | 250 | 300 | 400 | 500 | 600 | 700 | 800 | 1000 |
|---|---|---|---|---|---|---|---|---|
| $\tau$ ms | 11 | 14 | 19 | 23 | 25 | 31 | 33 | 40 |

The in-time falling rates of this function $S$ differ strongly from the results of (9). It is supposed in (9) that the lightning channel reflects ideally when the central part of the channel is highly ionized, dielectric permittivity $\varepsilon<0$ there, high-frequency case takes place and electron concentration in the critical point $\varepsilon=0$ strongly depends on the wavelength: $Ne \sim 1/\lambda^2$. However, the high-frequency case does not occure. The hot lightning channel partly absorbs radar waves in the reflecting layer soon after the return stroke. According to the formula of kinetics the electron concentration at a critical point $\varepsilon=0$ depends weakly on wavelength $\lambda$. Hence the dependends of the reflection intensity on $\lambda$ is not so strong as it was

stated in (9).

So in table 2 the duration $\tau$. is represented for two values energy release E=2000 G/m and E=6000 G/m in dependence from wave length $\lambda$ =3, 10, 35 and 200 cm.

Table 2. The duration $\tau$ msec of radioreflection intensity S(t) for different $\lambda$ and E.

| $\lambda$ cm / E G/m | 3 | 10 | 35 | 200 |
|---|---|---|---|---|
| 2000 | 40 | 50 | 60 | 80 |
| 6000 | 60 | 80 | 100 | 150 |

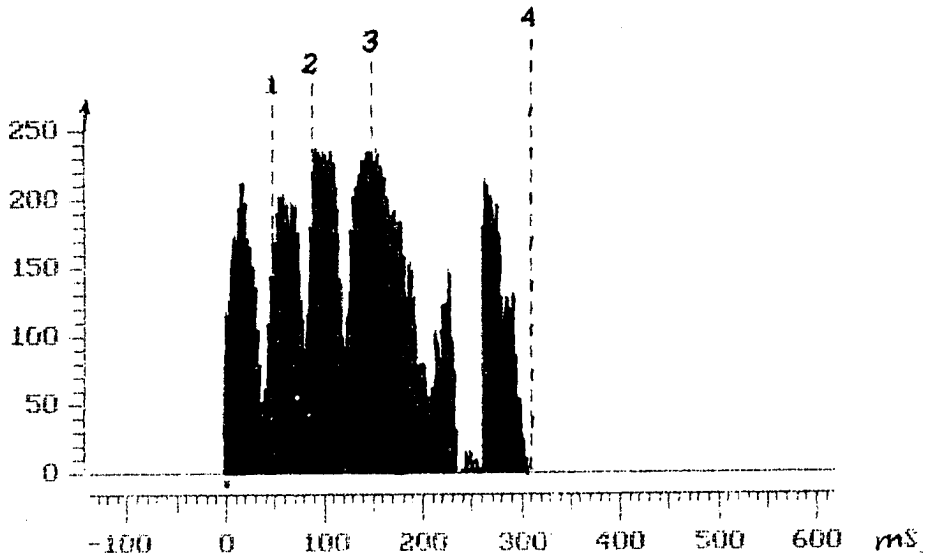
This method may be verifyed experimentally with full truth if synchronously with radiolocation electromagnetic field impulse to measure in each return stroke for vertical discharges as is made in experiments of Uman et al. (2). Transmission-line model (1) for this discharge channel make it possible to calculate current and then energy release E. If to compare E measured by these two methods - of Uman and of radiolocation - it is possible to verify the radiolocation method of energy determination for vertical discharge. That comparison was made in the synchronous experiment of last years by Dubovoy et al. (5, 6).

## EXPERIMENT

In the summer 1993 synchronous measurements of the radar echo signal and intensity of the electric field impulse (EEI) associated with return strokes in lightning discharge were carried out. The radar wavelength was 35 cm, 2 $\mu$s pulse width, pulse repetition frequence of 570 Hz, the antenna beam width of $4.5^{\circ}$ in horizontal plane and $22^{\circ}$ in a vertical plane.

The radio wave reflection have been measured on the distance of 50-80 km for 32 lightning flash observed over Elbrous in the Caucasus. This mountain has 6 km in the altitude. The signals of echo pulses passed from the radar to special analog-digital convertor and then to interface board in PC AT computers. Synchronously with the radio wave reflection measurement the own electromagnetic radiation pulses from lightning return strokes have been measured and recorded by notable oscillograph. The vertical component of the electric field intensity was measured in a bandwidth from 100 Hz to 1 MHz.

The example of the radio wave reflection measurement is presented on the histogram.




The radio reflection intensity is shown versus the time in msec from the beginning of the lightning discharge. The EFI signal from each return stroke came during the radio reflection are represented on fig.1 by dotted line.

One can see on the histogram that in accordance with the theory (4,6) the EFI from each return stroke coincide with the radio reflection peak values. By this experiment (5) it was shown that EFI came from the different part of the lightning channel. The energy release have been found from the duration of radar echo for each return stroke of the lightning discharges with arbitrary space position. The energy release was over a range of 240 to 1000 G/m.

CONCLUSION.

If we would know, that a lightning is a vertical cloud-to-ground discharge then from the intensity EFI we could determine the current and its duration by use the transmission-line model of Uman et al. (1) or more complex model. The theory (3) would make it possible to calculate energy input E by EFI measurement and to compare its value with value of E measured by radar. But with help of a radar or with a measurement EFI for remote unvisible discharge it can't be known with full truth is the discharge vertical or not. From the radar measurements we select only those discharges with maximum possibility that they were vertical lightnings. They have the smallest projection of the reflective part of lightning on radar beam and maximum of radioreflection intensity. Therefore in table 3 the calculated from EFI values E are compared with E determined from duration of radioreflection only statiscally.

Table 3. The comparison energy release E values from two different measurements

| Radar echo duration t, msec | E from radar measurement G/m | E from EFI measurement G/m |
|---|---|---|
| 10 ± 5 | 240 ± 60 | 300 ± 50 |
| 25 ± 5 | 600 ± 200 | 400 ± 10 |

The value of energy release per one length unit E in both type of experiments don't contradict statistically one to the other. By the theory (3, 4, 5) a coincidation must be not only in statistical sense, but for every vertical lightning. Therefore it can't to speak about full adequace one to the other means of the determination of E for vertical cloud-to-ground discharges. These uncertainty can be removed if to compare these two value of E in sinchronous experiment by radar and EFI measurements only after vertical lightnings as is in classical experiments of Uman et al. (2) by stroke the lightning to tower.

Nevertheless the radar method is now the only remote method of a measurement an energy release of E per one length unit independenly from the lightning position (orientation) in space.

Acknowlegments. This research was supported by the Russian Foundation of Fundamental Investigations.

REFERENCES

1. M.A. Uman, D.K. McLain, R.J. Fisher, and E.P. Krider, "Electric Field Intensity of the Lightning Return Stroke", J. Geophys. Res., vol. 78, 1973, p. 3523-3528

2. M.A. Uman, "The Lightning Discharge", New York: Academic Press, 1987.

3. E.I. Dubovoy, V.I. Pryazhynsky, and G.I. Chitanava, "Computation of Energy Input to a Lightning Channel" (in Russian), Meteorol. Hidrol. vol. 2, 1991, p.40-45.

4. E.I. Dubovoy, V.I Pryazhinsky and V.E. Bondarenko, "Numerical Modeling of the Gasodynamic Parameters of a Lightning Channel and Radio-sounding Reflection" (in Russian), Izv. Russ. Acad. Sci. Atmos. oceanic Phys., vol.27, 1991, p.194-203

5. E.I. Dubovoy, M.S. Mikhailov, A.L. Ogonkov and V.I. Pryazhinsky, "Measurement and Numerical Modeling of Radio Sounding Reflection from a Lightning Channel", J. Geophys. Res., vol. 100, 1995, p.1497-1502.

6. E.I. Dubovoy, A.L. Ogonkov, "The Synchronous Measurement of the Electromagnetic Field and Radioreflection Impulses from

a Lightning and Experimental Verification of the Numerical Modeling Results" (in Russian), Moscow, preprint N941 of the Mints Radiotechnical Inst., 1994.

7. L.I. Divinsky, "The Effective Reflection Surface of the Lightning Channel" (in Russian), Atmospheric Electricity, St. Petersburg, Gidrometeoizdat, 1976

8. T.H. Van Vleck, F. Block and M. Hamermest, "Theory of Radar Reflection from Wires or Thin Metalic Strips", J. Appl. Phys., vol. 18(3), 1947, p.274-294

9. G.A Dawson, "Radar as a Diagnostic Tool for Lightning", J. Geophys. Res., vol. 77, 1972, p.4518-4528.

# SESSION 04A
# METEOROLOGICAL
# CHAIRPERSON: ARNOLD A. BARNES

# A FRACTAL MODEL OF THE FINE STRUCTURE OF LIGHTNING RADIATION

G.Vecchi, D.Labate and F.Canavero
Dipartimento di Elettronica, Politecnico, I-10129 Torino
fax: 39 11 5644015; e-mail: vecchi@polito.it

**Abstract.** We investigate the fine structure of field radiated by a lightning return stroke on a tortuous, lossy discharge channel. The analysis is carried out using a fractal description of the channel and of the graph of the time history of the field. The effect on the radiated field of the base current pulse shape, and of channel losses are considered. A parametric model of these effects is introduced, that allows the reconstruction of the channel fractal dimension from the field waveform. The effect of noisy data is discussed, and an efficient fractal-based filtering illustrated, that makes the reconstruction robust.

## 1 Introduction and motivations

The time history of the electromagnetic field radiated by lightning discharges exhibits a jagged shape with remarkable spectral content in several bands of practical importance for communication, control, and generally consumer electronics. It is therefore desirable to have a simple model of the fine structure of discharge radiated field. In order to bypass the difficulties of the complex, non-linear analysis at the microscopical level of the discharge process, a simple model should be *macroscopical* (phenomenological). At this macroscopical level, fractals should be appropriate descriptors: fractal geometry has been proven very effective in the description of chaotic phenomena [1], and of many complex, random natural phenomena that exhibit non-stationary statistics and $1/f$ power spectrum, [2], as is the case of the electromagnetic field radiated by lightning. The fractal nature of discharge paths has already been established [4], [9].

Here, the problem of finding the field radiated by a fractal-modeled, three-dimensionally tortuous lightning channel is addressed, analyzing such a field from the fractal point of view, in order to assess the fractality of the temporal field and seek the relationship between the fractal parameters of the model of the discharge and those of the field.

In a recent work by the authors [5] a similar analysis has been carried out: there, the channel was assumed lossless, and the current on it approximated by the usual transmission line (TL) assumption; the ground was assumed flat and perfectly conducting and the current waveform assumed in the simulation was the standard model proposed by Uman and modified by LeVine and Meneghini. From that analysis, the graph of the field radiated by a fractal channel appears to be a fractal itself, for a convenient time interval.

In order to further proceed towards the development of a fractal model of discharges, that could eventually be based on measured field data, that analysis is now extended to ascertain

the effect of some of the employed approximations. Here, we will consider a more realistic channel model, analyzing the effects of "kink" discontinuities (at the channel bends), of the base current pulse shape, and of channel losses. The presence of noise on the field waveform is is also considered, since noise will be present in any practical measurement, and the issue of fractal-based filtering will be addressed.

Because of space constraints, the reader is warned that only a fraction of the vast related literature about base current and channel loss models will be cited; further reference (often back to seminal works) can be found in the cited works.

# 2 Transient radiation from a fractal channel

**Fractal Dimension.** The fractal dimension $D$ is a quantitative measure of the space-filling property of a curve [3, Ch. 5]. A fractal curve has a fractal dimension $1 < D < 2$, as contrasted to a standard (euclidean) curve that has $D = 1$, and to a two-dimensional surface that has $D = 2$. Throughout this paper the fractal dimension has been estimated applying the "variation" algorithm introduced by Dubuc et al. [7], which has been proven to be reliable and robust. Its description is omitted here. Like in all fractal estimation algorithm, the fractal dimension of the curve will be estimated as the slope of a straght line connecting a set of points on a doubly logarithmic graph; because in practice these points do not lie exactly on a straight line, the confidence interval in the least squares linear fit yields the uncertainty on the estimation, and therefore in all the reported results the fractal dimension will be expressed as $D \pm \Delta D$, where $\Delta D$ is the uncertainty range on the dimension estimation.

**Fractal model of the channel.** The lightning channel is described as a function of the altitude $z$, i.e., $\mathbf{r}_c(z) = x(z)\hat{x} + y(z)\hat{z} + z\hat{z}$, where $\mathbf{r}_c(z)$ describes paramerically the point on the channel and the functions $x(z)$ and $y(z)$ are two fractal curves. In particular $x(z)$ and $y(z)$ are chosen to be two statistically independent random fractals, in order to account for the random nature of the channel formation. The fractal curves are generated as attractors of an *Iterated Function System* (IFS), [3, Ch. 3]. There is nothing critical about choosing the IFS algorithm for the generation of the fractal channel. One can equally well use another fractal generation algorithm. We compared the results with the IFS method and the (widely used, also in our precedent work [5]) random midpoint displacement algorithm [2, Ch. 2] finding negligible differences. In this work, we have assumed that the fractal curves $x(z)$ and $y(z)$ have the same fractal dimension, which results to be the dimension of the entire (three-dimensional) channel, $D_c$. This has been done in order to reduce the number of parameters to be considered when comparing the fractal properties of channel and field.

Although the fractal dimension $D_c$ of the channel is set during the generation process of the fractal curves $x(z)$ and $y(z)$, it has been evaluated using the fractal dimension estimation algorithm, in order to assess the intrinsic uncertainty in the estimation algorithm that will be employed in the analysis of the fractal properties of the radiated field.

**Radiation from a tortuous lossy channel.** The return stroke channel is modeled as piecewise linear, composed of $N$ straight segments. The ground is assumed flat and perfectly conducting: at ground level the vertical component of the electric field will be twice as much its free-space counterpart. Corrections due to lossy earth could be inserted as detailed in [8].

The return stroke is assumed to propagate up the channel with constant speed $v$, regardless of the channel kinks, starting at ground level, $z = 0$, at $t = 0$. According to the so-called modified TL (MTL) model (eg. [6]), the shape of the current pulse remains unchanged along the channel, but in order to account for channel losses the an altitude-dependent attenuation is included:

$$i(s,t) = i(0, t - s/v)\exp(-s/L_c) \tag{1}$$

In the equation above, $s$ is the total length along the (piecewise linear) channel path. Radiation is calculated without considering the discontinuities at junctions between segments; this effect will be discussed later in Sec. 3. We will use the results derived in [5]; the employed approximations include the Fraunhofer (far-field) assumption, and the assumption that the distance $r_i$ between the observer to the center of the $i-$th segment is $r_i \gg \lambda$ over the entire band of interest. Retaining only the vertical ($z$) component of the (total) electric field at ground, at a location $\mathbf{r}$ from the channel foot one finds

$$E_z(\mathbf{r},t) \approx \frac{Z_0}{2\pi r}\left\{C_1\, i(s_1, t - t_1) + \sum_{i=2}^{N-1}(C_i - C_{i-1})\, i(s_i, t - t_i) - C_N\, i(s_N, t - [t_N + \tau_N])\right\} \tag{2}$$

where $c$ is the speed of light, $Z_0 = \sqrt{\mu_0/\epsilon_0}$, $C_i \equiv (\hat{z}\cdot\hat{s}_i)e^{-s_i/L_c}/(c/v - a_i)$, $\hat{s}_i$ is the direction along the $i-$th segment, and:

$$t_i = r_i/c + s_i/v - \tau_i/2, \quad \tau_i = (1 - a_i v/c)L_i/v, \quad s_i = \sum_{n=1}^{i-1} L_n + \frac{L_i}{2}, \tag{3}$$

From equation (2), one sees that each term in the sum appears as a contribution originating at the junction between two segments ("kink"), and each contribution to the field is a replica of the current waveform at that junction, whose amplitude is a function of the change in direction of the channel at the junction of two segments ($C_i$), and of the altitude-dependent local pulse strength ($i(s_i)$).

# 3 Kink discontinuities

Two different approches have been considered to model the effect of the kink discontinuities.

In the first approach each kink is modeled as a circular bend joining two straight sections of the discharge path. The current along the channel kink has been left unchanged, but the geometry has been taken into account in the radiation process, letting the current pulse to travel also along the circular bends. A simple analysis of the the radiation from the (partial) turn reveals that the radiated electric field is proportional to the first two time derivatives of the current travelling along the wire, and the effect of a bend appears as an additional narrow spike.

In the second approach the curved bend effect is neglected in the radiation, but the current is modified in order to account for the transmission line discontinuities. This can be done by modelling the kinks as lumped networks according to the transmission line model of the return stroke process. Regardless of the accuracy in the modeling of the discontinuity, the general result (energy conservation and Parseval theorem) is that to a low-pass filtering effect in the transmission across the kink always corresponds the complementary high-pass effect in the reflection from the kink, and this generates narrow spikes in the radiated field.

In conclusion, both approaches lead to the result that the kinks generate additional narrow spikes in the radiated field. Since we could not find any evidence of such effect in the *measured* fields reported in the literature, for the time being we have considered them "unphysical" and consistently they have been discarded from our model.

# 4 Effect of base current pulse shape

**Base current model.** We are interested in considering the fine structure of the radiated field and we want to assess what parameters of the current pulse essentially affect the fine structure of the field, i.e. the fractal dimension of the field $D_f$. Therefore, the base current is approximated by a simple double exponential pulse:

$$i_0(t) = I_0[e^{-t/T_d} - e^{-t/T_r}]. \tag{4}$$

A typical radiated field waveform obtained with this base current and the approximation described above is shown in Fig. 1. This approximation fails to correctly reproduce the initial time derivative, and the late time decay. However, as it will be shown later, only the *rise* time affects the fine scale of the field, and neither the derivative in the origin, nor the late time behaviour affect the former. To check this, we have compared the field obtained using the base current in [6] with that obtained by the double exponential in (4). It appears that this approximation does not affect the fine-scale structure of the waveform, as is intuitive from the graphs of Fig. 1, and as emerges more precisely from the evaluation of the fractal dimensions, that turn out to be equal.

The time constants $T_d$ and $T_r$ differ from the decay-time $t_d$ and rise-time $t_r$ of the current pulse for a multiplicative constant, but for the sake of conciseness in the following we will shortly refer to $T_r$ and $T_d$ as rise- and decay-time.

**Results.** In order to separate effects, the fractal dimension $D_f$ of the field radiated by a channel with no attenuation ($L_c \to \infty$) has been studied first as a function of the pulse shape parameters $T_r$ and $T_d$. The effect of the decay length $L_c$ will be considered in Sec. 5. The fractal dimension of the channel $D_c$ has been let to vary between 1.1 and 1.6, a range that includes the typical measured values of fractal dimension of lightning channels (see [9]).

We have observed that the effect of the decay time on the radiated field fine-structure is negligible: for a fixed $T_r$, and $T_d$ ranging between the extremal (and unphysical) cases of delta-like pulse (when $T_d \to 0$) and of step-like function (when $T_d \to \infty$), the field waveforms

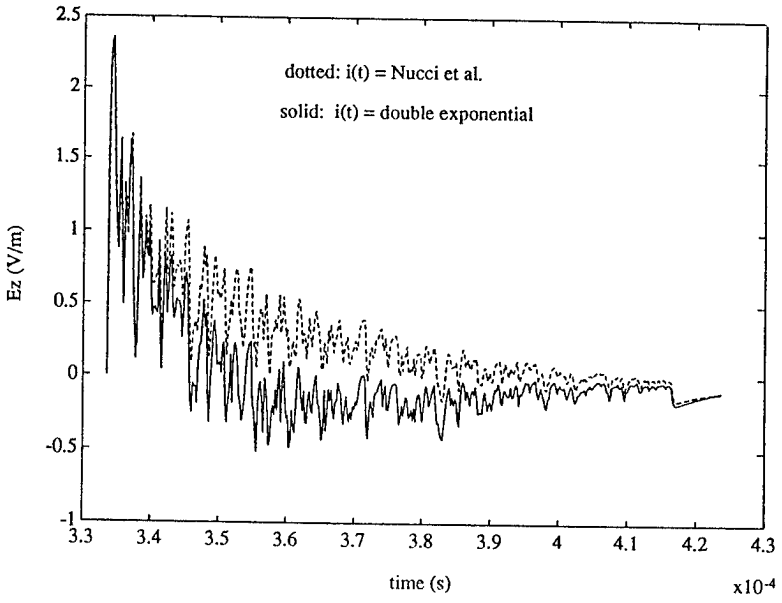



Figure 1: *Comparison between the radiated field waveforms obtained using the double exponential pulse shape in (4) (solid line) and the more accuarate form in [6] (dashed). Here* $r = 100\,km$, $L_c = 2000\,m$.

(not shown here) are different, but they still show the same fractal dimension. Accordingly, no further discussion will consider $T_d$.

$T_r$ has been let to vary between $10^{-8}$ s and $10^{-4}$ s, a range that let our approximation (4) adapt to the different models found in the literature. A typical form of the resulting relationship $D_f$ vs. $T_r$ is shown in Figure 2 for the case $D_c = 1.20$, whence it is apparent that $D_f$ is inversely proportional to $T_r$; this trend agrees with the findings of Cooray and Orville [10], who observed that a reduction in rise-time results in increasing the irregularity of the radiated field waveform. The graph exhibits an approximately linear central region and two extremal saturation regions, where $D_f$ tends to $D_{f0} \approx 1$, and to $D_{f\infty} \approx 1.8$. Since the employed estimation algorithm is known to underestimate the actual values when $D_f > 1.6$, (as described by *Dubuc* and as confirmed by extensive checks conducted by the authors), the estimated asymptotic value $D_{f\infty}$ (for small $T_r$) should be replaced by $D_f \approx 2$. Although these extremal cases are of scarce practical importance by themselves, they are helpful to understand the dependance of $D_f$ on $T_r$. To this aim, it is useful to define the average transit time $\tau_{av}$ of the current pulse along the channel; we observe that for $2T_r \approx \tau_{av}$, that is $t_r \approx \tau_{av}$, then $D_f \approx D_c$, while in the extremal cases $T_r \ll \tau_{av}$ and $T_r \gg \tau_{av}$, $D_f$ tends to 2 and to 1 respectively.

In the case $T_r \ll \tau_{av}$ the radiated field is approximately a sequence of isolated spikes, each generated by a channel kink. In fact, the traveling pulse generates a spike when crossing a kink (see Sec 2) and they are isolated since, being the risetime of the current pulse very samll, each spike is unaffected by the preceding one; it can be proved that the fractal dimension of this sequence of spikes approaches 2.

On the other hand, in the case $T_r \gg \tau_{av}$, the current rise front is "too slow" to follow the

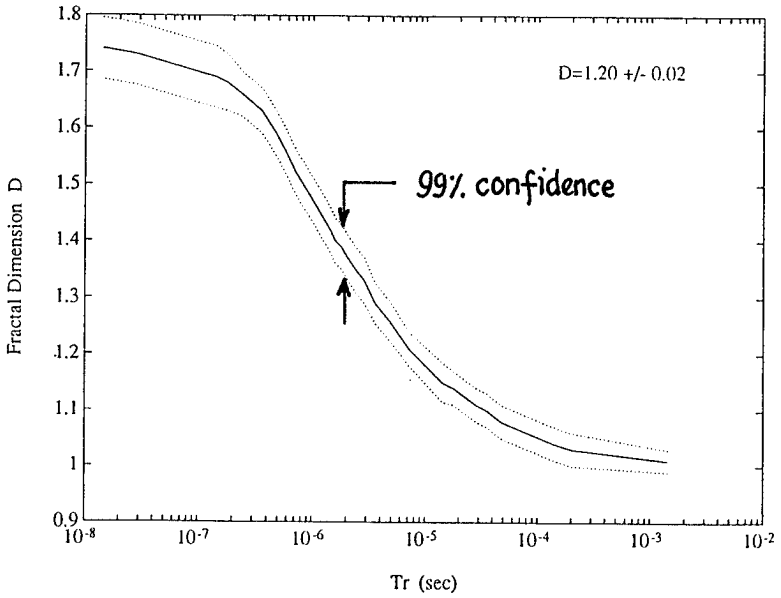



Figure 2: *Effect of the rise time $T_r$ on the field fractal dimension $D_f$, for a lossless channel and for the case of $D_c = 1.20$.*

channel irregularities, thus the radiated field is a smooth curve and $D_f$ tends to 1.

At last in the case $T_r \simeq \tau_{av}$ the kink contributions "stay on" and sum up so that the radiated field closely follows the fractal nature of the channel. In this case: $D_f \approx D_c$. This condition is satisfied, with our choice of parameters, at $T_r \approx 5.0 \cdot 10^{-6}$ $s$ (as one can see in Fig. 2).

As we will see in Sec. 5, the graph $D_f$ vs. $T_r$ exhibits qualitatively the same behavior for any value of the fractal dimension of the channel $D_c$.

# 5 Combined effect of pulse risetime and channel attenuation

$L_c$ has been let to vary between $10^2$ m and $10^6$ m; typical values of $L_c$ in the literature range from 500 m to 3000 m according to [6]. Typical results are reported in Figs. 3 and 4, for varying channel dimension and attenuation, respectively. It appears that $D_f$ is directly proportional to $L_c$, i.e. inversely proportional to the channel pul attenuation. In fact, the altitude-dependent attenuation $\exp(-s/L_c)$ (see (1)) reduces the strength of the contributions radiated by the higher (from channel foot) kinks, which results in reducing the irregularity of the field waveform, and therefore reducing the field fractal dimension.

On the other hand, the smoothing effect due to increasing the rise time $T_r$ cumulates to the smoothing effect of decreasing the decay length $L_c$. The results in Fig. 4 show that the effect of $T_r$ appears as a vertical displacement of the $D_f$ vs. $L_c$ graphs and that the shape of the curves is only slightly affected by $T_r$; on the other hand the effect of $D_c$ appears just as a vertical displacement of the curves in Fig. 3.

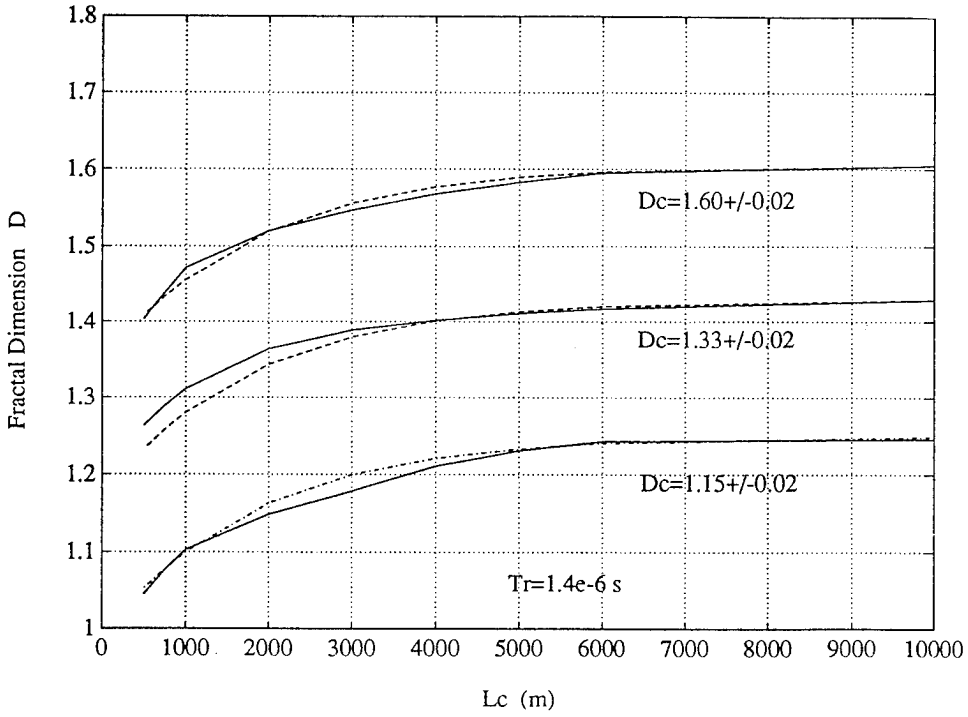



Figure 3: *Effect of the attenuation length $L_c$ and of the channel fractal dimension $D_c$ on the radiated field dimension $D_f$ for the case $T_r = 10^{-4}$ s. Solid line: actual values, dashed line: approximation in (5).*

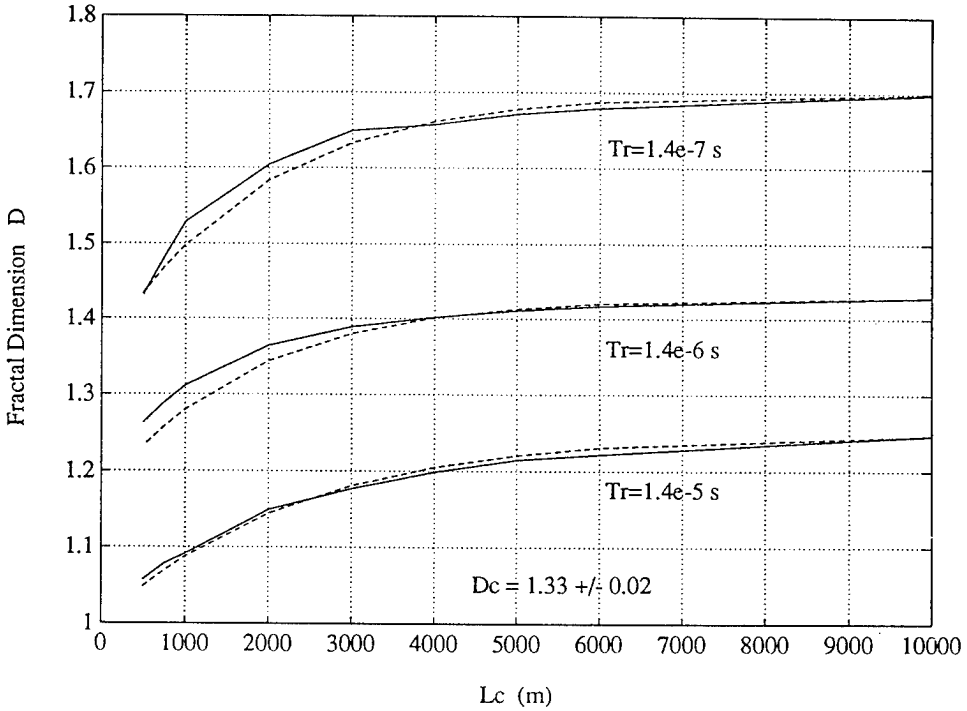



Figure 4: *Effect of the attenuation length $L_c$ and of the current pulse rise time $T_r$ on the radiated field dimension $D_f$ for the case $D_c = 1.33$. Solid line: actual values, dashed line: approximation in (5).*

These considerations, along with extensive checks, suggested the following model to fit these dependences:

$$D_f(L_c, D_c, T_r) \approx \alpha(T_r)[1 - \exp(-\gamma(T_r)L_c)] + \beta_0(T_r) + \beta_1(T_r)D_c \tag{5}$$

where the functions $\alpha$, $\beta_0$, $\beta_1$ and $\gamma$ can be obtained through separate (least square) fits holding all but one parameters constant. We can thus obtain $D_c$ as a function of the remaining parameters:

$$D_c \approx \frac{1}{\beta_1(T_r)} \{D_f - \alpha(T_r)[1 - \exp(-\gamma(T_r)L_c)] - \beta_0(T_r)\} \tag{6}$$

# 6 Channel Reconstruction

We now investigate the possibility of getting information on the discharge path geometry (as its fractal dimension) from the knowledge of the field time waveform. i.e. to estimate the fractal dimension of the channel $D_c$.

According to the conclusion of Sec 5 we can obtain $D_c$ if we can estimate the parameters $D_f$, $T_r$ and $L_c$. We observe that the value of $D_f$ is obtained by a direct fractal dimension estimation over the time series radiated field at least in absence of noise. As shown below, the estimation of $T_r$ and $L_c$ can be done from the field waveform as well. As in any reconstruction, the robustness in presence of noisy data has to be assessed: this will issue will be addressed later on.

As to the rise time, both the simulated and the experimental data of the (far-field) radiated field show a "clean" peak in the early part of the time waveform. Also, the damping effect ($L_c$) is negligible on the early part of the field time waveform, and thus the early part of the radiated field time history exhibits the same risetime of the current traveling pulse. This allows the estimation of $T_r$ from the initial part of the field waveform.

As to the decay length $L_c$, we observe that the local (in time) fluctuation in the amplitude on the field waveform is due to the changing direction of the channel (see (2)), that "modulates" the pulse amplitude as it passes through the channel irregularities. Therefore, the temporal amplitude irregularity is proportional to the local geometrical irregularity of the the channel (about the location that gives rise to the contribution that reaches the observer at time $t$), *and* to the pulse strength there. We assume that the channel is "uniformly" (geometrically) irregular throughout. Therefore if we find that the amplitude irregularity on the field time-history is not constant, but decreasing, this can be attributed to the damping in the propagation of the current pulse travelling along the discharge path. This suggests to extract the irregularities from the field time-history (which can be done by subtracting the radiated field by its smoothed version) and study their envelope: the decreasing in the envelope vs. time will be related to the attenuation of the travelling current pulse along the channel, and the decay length $L_c$ can be inferred by (least squares) fitting the envelope of the irregularities to the model $\exp(-z/L_c)$. The application of this tecnique to some numerically generated radiated field time series shows that the decay length can be inferred with good approximation (a few percent).

# 7 Effect of measurement noise on the field

Noise is introduced in any actual measurement, and it is important to check whether the actual fractal dimension of the field can be correctly estimated in the presence of the corrupting noise; likewise, one has to assess the robustness of the parametric inversion outlined in the Sec. 5 and 6 in order to reconstruct the fractal description of the geometry of the channel from the radiated field.

The effect of noise has been studied by adding a zero-mean white additive gaussian noise to a numerically evaluated radiated field time history assuming a signal-to-noise ratio $S/N$ ranging from 0 dB to 50 dB. The noise is initially obtained as white noise by a random number generation algorithm, and the data are then low-pass filtered (by an ideal digital low-pass filter) to account for a realistic cut-off frequency (500 MHz) of the measuring equipment. Since the frequencies corresponding to the time-scale range over which the simulated field waveforms appear to be a fractal are below this limit, the low-pass filtering does not affect the fractal geometric properties of the waveforms.

Since we are interested in considering the corruption of only the fine-scale structure of the radiated field, we define an effective, *high frequency* signal-to-noise ratio, and denote it as $(S/N)_{HF}$, by considering as signal not the whole radiated field time history, but only the high-frequency part estimated by subtracting the waveform to its smoothed version (which is equivalent to applying an high-pass filtering). The ratio $(S/N)_{HF}$ appears to be about 10 dB less than the $S/N$ defined over the entire spectrum of the waveform for the typical radiated field waveforms.

As discussed in Sec. 5, the geometry of the channel (i.e. $D_c$) may be estimated from the knowledge of the radiated field time-history through the parameters $D_f$, $L_c$ and $T_r$. The tecniques employed for the estimation of $T_r$ and $L_c$ (described in Sec. 6) are not significantly affected by the presence of noise; in fact the estimation of $L_c$ (Sec. 6) is based on the analysis of the envelope of the irregularities of the field waveform vs. time, obtained as a global least squares fit. Since the noise is a zero-mean signal, its effect on the (least squares) fit of the irregularities of the field is negligible and it only affects the uncertainty range. The estimation of $T_r$ is based on a macroscopical analysis (see Sec. 6), and this is intrinsically noise-insensitive. On the other hand the intuitive noise effect of increasing the global fractal dimension $D_f$ of the radiated field (by increasing the space-filling property of the waveform) is confirmed. It turns out that the corrupting effect of the noise on $D$ is inversely proportional to the ratio $S/N$, and is negligible for $S/N$ greater than 40 dB (i.e. $(S/N)_{HF} > 30$ dB). We need thus to filter out the noise effect in order to restore the "true" $D_f$ of the curve, but the standard frequency filtering cannot be applied since by filtering out all the high frequency events we would also loose the fractal information on the curve. Therefore we need a different approach.

We can apply a *local fractal* analysis by defining the *local fractal dimension* of a waveform $f(t)$ as the fractal dimension estimated over a sliding time window, and applying the so-called *fractal filtering* [11]. This is a digital nonlinear filtering that discriminates signals having different fractal dimensions. If a signal is the sum of two (or more) signals having different fractal dimension, say $D_1$ and $D_2$, and the fractal dimensions are sufficiently separated, it is possible to assess a threshold value $D_T$, with $D_1 < D_T < D_2$, and apply a fractal filtering to

filter out the signal components having (local) fractal dimension $D > D_T$. We have applied a simple first-order lag recursive filter, as described in [11], with the filter parameter being proportional to the difference between the threshold $D_T$ and the local dimension $D$. An important feature of this filtering is that it preserves peak heights and the vertical transitions to a high degree. The performances of the fractal filtering are very good in general, unless the obvious case in which the ratio $(S/N)_{HF}$ is negative, i.e. the power of the noise is greater than the power of the high-frequency signal. In Table 1 the results are reported of the application of the fractal filtering to some noise-added radiated field waveforms, for the case of dB $(S/N)_{HF} =$ 0 dB.

| **Actual Signal** | **Noisy Signal** | **Filtered Signal** |
|---|---|---|
| $D = 1.53 \mp 0.02$ | $1.69 \mp 0.02$ | $1.52 \mp 0.02$ |
| $D = 1.37 \mp 0.01$ | $1.67 \mp 0.02$ | $1.36 \mp 0.02$ |
| $D = 1.25 \mp 0.01$ | $1.72 \mp 0.02$ | $1.24 \mp 0.02$ |
| $D = 1.20 \mp 0.02$ | $1.73 \mp 0.02$ | $1.20 \mp 0.01$ |
| $D = 1.18 \mp 0.02$ | $1.72 \mp 0.02$ | $1.17 \mp 0.02$ |

Table 1: *Effect of noise on fractal dimension of field and performance of fractal filtering for for* $(S/N)_{HF} = 0\,dB$

# References


[1] Grassberger, Procaccia, "Measuring the strangeness of strange attractors", *Physica 9D*, p. 189, 1983

[2] Peitgen, H. O., and D. Saupe, *The Science of Fractal Images*, 312 pp., Springer-Verlag, New York, 1988

[3] Barnsley, M., *Fractals everywhere*, 396 pp., Academic Press, San Diego, CA, 1988.

[4] Femia, N., L. Niemeyer, and V. Tucci, Fractal characteristics of electrical discharges: experiments and simulations, *J. Phys. D: Appl. Phys.*, *26*, 619-627, 1993.

[5] G.Vecchi, D.Labate, F.Canavero: "Fractal approach to lightning radiation on a tortuous channel", *Radio Science* vol. 29, No. 4, pp. 691-704, July-August 1994.

[6] Nucci, C.A., G. Diendorfer, M.A. Uman, F. Rachidi, M. Ianoz, and C. Mazzetti, "Lightning return stroke current models with specified channel-base current: A review and comparison", *J. Geophys. Res.*, *95*, 20,395-20,408, 1990.

[7] Dubuc, B., J. F. Quiniou, C. Roques-Carmes, C. Tricot, and S. W. Zucker, "Evaluating the fractal dimension of profiles", *Phys. Rev. A*, **39**, no. 3, 1500-1512, 1989.

[8] Gardner, R. L. (Ed.), *Lightning Electromagnetics*, 540 pp., Hemisphere, New York, 1990.

[9] Tsonis, A. A., "A Fractal Study of Dielectric Breakdown in the Atmosphere", in *Non-Linear Variability in Geophysics*, edited by D. Schertzer, and S. Lovejoy, pp. 167-174, Kluwer Academic Publisher, The Netherlands, 1991.

[10] Cooray, V., and R. E. Orville, "The Effects of Variation of Current Amplitude, Current Risetime, and Return Stroke Velocity Along the Return Stroke Channel on the Electromagnetic Fields Generated by Return Strokes", *J. Geophys. Res.*, **95**, no. D11, 18617-18630, 1990.

[11] Strahle, W. C., "Adaptative Nonlinear Filter Using Fractal Geometry", *Electronics Letters*, **24**, 1241-1248, Sept. 1988.

# THREE-DIMENSIONAL LIGHTNING STRUCTURE IN A SUMMER FLORIDA THUNDERSTORM

Launa Maier
NASA
TE-ISD-3A
Kennedy Space Center, Florida 32899
(407) 867-4409

Paper unavailable for publication.

# INFLUENCE OF CHANNEL-BASE CURRENT AND CURRENT REFLECTIONS ON THE INITIAL AND SUBSIDIARY LIGHTNING ELECTROMAGNETIC FIELD PEAK

F. Heidler and Ch. Hopf

Federal Armed Forces University Munich
ET 7, Werner-Heisenberg-Weg 39
D-85577 Neubiberg, GERMANY
Telephone +49/89/60043736 FAX +49/89/60043723

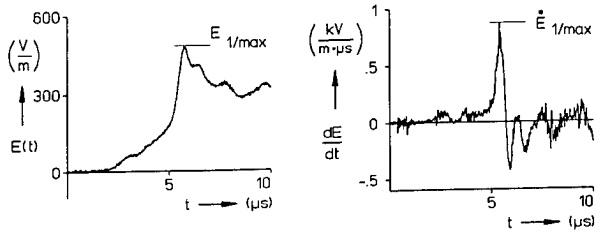
## ABSTRACT

Considering the fundamentals of the so-called TCS (travelling current source) model a method is presented taking into account the current reflections at the striking point as well as at the current source. Although the current in the striking point results from the superposition of the reflected and non-reflected current portions, a procedure was found considering a channel-base current. For far distances a field approach was developed enabling the calculation of the channel-base current directly from the field data. With this far field approach the maximum current and the maximum current steepness can be calculated even from near distant fields having typical initial peaks, which are often followed by so-called subsidiary peaks.

## 1. INTRODUCTION

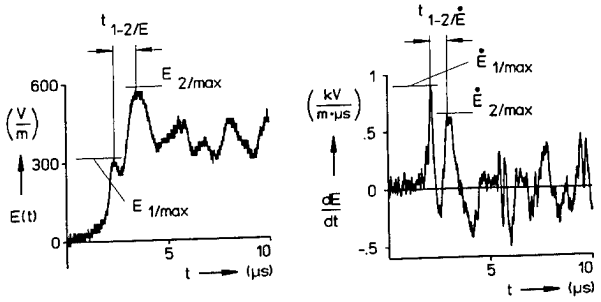
Since about 15 years the so-called lightning electromagnetic impulses (LEMP) are measured at the High Voltage Institute of the Federal Armed Forces University Munich. Normally the electric field of negative return strokes to earth has an initial peak $E_{1/max}$ (fig. 1a) and the corresponding field derivative has a bipolar waveform with a time on half value of about $T_{50}$ = 0,2...2 $\mu$s (fig. 1b). Sometimes the initial peak is followed by a subsidiary peak $E_{2/max}$, which may be even higher than $E_{1/max}$ (fig. 2a). If a subsidiary peak is present the field derivative has two characteristic maxima (fig. 2b) /1,2,3/.

Current reflections are well-known from measurements at tall towers /4, 5/. They are also expected from return strokes to earth, because the characteristic impedance of the return stroke channel is normally much higher than the earth resistance. In /6, 7/ by ***Heidler*** and ***Hopf*** a fundamental new method was introduced taking into account current reflections at the striking point. The method bases on the assumptions of the TCS - model, which was extended considering a downward and an upward propagating current wave moving on the return stroke channel with light velocity $c_o$. Their sum results in the total current, which is responsible for the LEMP generation. Since the current is generated at the top of the lightning channel, opposite to the original TCS-model the current at the top of the increasing lightning channel is considered to be known. To enable the direct use of the current data, the return stroke model was extended operating optionally with a channel-base current as input parameter. As shown by ***Heidler*** and ***Hopf*** in /8/ with this method and using power functions the initial as well as the subsidiary peak can be explained satisfactorily. Because the initial and subsidiary peaks are dominated by the so-called far field component, in the following a method is presented to simplify the analysis by neglecting the near and intermediate field components.




a) Electric field E(t) b) Field derivative Ė(t)

Fig. 1: Electric field of a negative return stroke with an initial peak




a) Electric field E(t) b) Field derivative Ė(t)

Fig. 2: Electric field of a negative return stroke with an initial and a subsidiary peak

## 2. THE TCS-MODEL FOR THE CURRENT REFLECTION

The TCS-model /3/ describes the lightning discharge during the return stroke period. The thermo-ionized return stroke channel is assumed to be a transmission line, where the current propagates with light velocity $c_o$. At the top of the increasing return stroke channel a current source is considered starting from earth level and travelling with the velocity $v < c_o$ toward the thundercloud. From the current source the current $i_Q$ is fed into the lightning channel having a vertical orientation to the earth's surface. In opposite to the original TCS-model defined for a given current at the striking point here the source current $i_Q$ is assumed to be known. Fig. 3 shows the fundamental considerations, where the earth reflections are described by the earth reflection factor ϱ and the reflections at the top of the return stroke channel by the top reflection factor R, respectively. The arrows indicate the propagation direction. The total current i(z,t) results from the sum of the downward and upward propagating currents $i_d(z,t)$ and $i_u(z,t)$:

$$i(z,t) = i_u(z,t) + i_d(z,t). \tag{1}$$

In /6,7/ it is shown by ***Heidler*** and ***Hopf***, that the top reflection factor R depends only on the speed of light $c_o$ and the velocity of the increasing return stroke channel v. For v = const. it is given by:

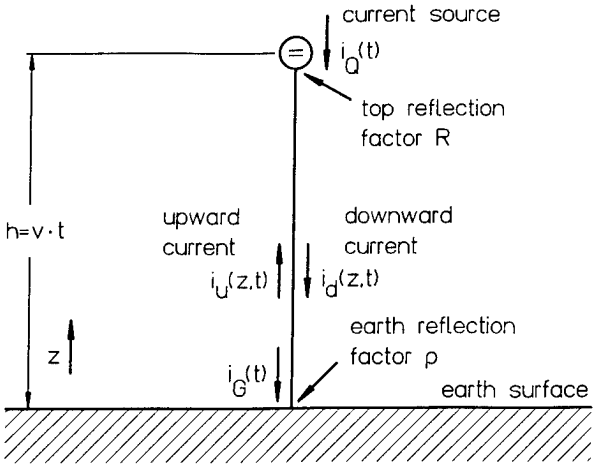



Fig. 3: Reflections on the return stroke channel.

$$\frac{i_d}{i_u} = R = -A\,, \quad with \quad A = \frac{c_o - v}{c_o + v}\,. \tag{2}$$

The real current source $i_Q$ is replaced mathematically by a new fictive current source $i_o$ located at the same place on the channel top and being equal to the downward propagating current at the channel top. For v= const. and R = -A (equation (2)) the relationship between $i_Q(t)$ and $i_o$ is given by:

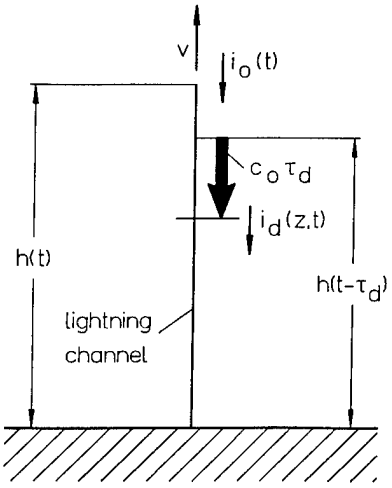
$$i_o(t) = i_Q(t) + \sum_{\nu=1}^{\infty} (-\varrho A)^{\nu} \cdot i_Q(A^{\nu} t). \tag{3}$$

The downward and upward propagating currents $i_u(z,t)$ and $i_d(z,t)$ result from the new fictive current source $i_o(t)$ by the use of the propagation times $\tau_u$ and $\tau_d$ /6, 7/:

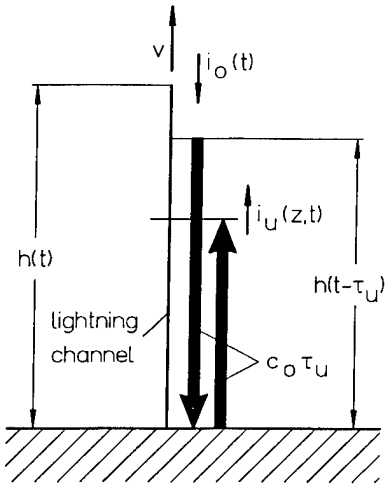
$$i_d(z,t) = i_o(t_d^*) \;, \qquad with \quad t_d^* = t-\tau_d \tag{4a}$$

$$i_u(z,t) = \varrho i_o(t_u^*), \qquad with \quad t_u^* = t-\tau_u \tag{4b}$$

The propagation distance of the downward propagating current between $h(t-\tau_d)$ and z is identical to $c_o\tau_d$. In fig. 4a the distance is marked by a thick arrow. The propagation time $\tau_d$ results in:




a) Downward propagating current $i_d$




b) Upward propagating current $i_u$

$$\tau_d = \frac{h\{t-\tau_d\}-z}{c_o} = \frac{v\cdot(t-\tau_d)-z}{c_o} \tag{5}$$

Hence follows

$$(t-\tau_d) = t_d^* = \frac{c_o t+z}{c_o+v} \;. \tag{6}$$

With fig. 4b and substituting z by -z analogously the propagation time of the upward propagating current can be derived:

$$(t-\tau_u) = t_u^* = \frac{c_o t-z}{c_o+v} \;. \tag{7}$$

Fig. 4: Definition of the propagation times $\tau_d$ and $\tau_u$

Now the current in the striking point $i_G(t) = i(z=0,t)$ is assumed to be given. The basic idea is to calculate the real source current $i_Q$ from the given current at ground level $i_G$. The current $i_G$ is split up in the downward and the upward propagating current $i_{G/d}$ and $i_{G/u}$. With $i_G = i_{G/d} + i_{G/u}$ and $i_{G/u} = \varrho i_{G/d}$ the downward propagating current follows to:

$$i_{G/d}(t) = \frac{i_G(t)}{1+\varrho}. \tag{8}$$

From equation (4a) and (6) and with $z = 0$ the relationship between the source current $i_o(t)$ and the downward propagating current $i_{G/d}(t) = i_d(z=0,t)$ results in:

$$i_{G/d}(t) = i_o\left(\frac{t}{k}\right) \;, \qquad k = 1+\frac{v}{c_o}. \tag{9}$$

With $i_{G/d}(kt) = i_o(t)$ and from equation (3) it follows:

$$i_Q(t) = i_{G/d}(kt) - \sum_{\nu=1}^{\infty}(-\varrho A)^\nu \cdot i_Q(A^\nu t). \tag{10}$$

Equation (10) can be written as

$$i_Q(t) = i_{G/d}(kt) - \varrho R i_Q(At) - \sum_{\nu=2}^{\infty} (-\varrho A)^{\nu} \cdot i_Q(A^{\nu} t). \tag{11}$$

or

$$-\varrho R \cdot i_Q(At) = -\varrho R \cdot i_{G/d}(Akt) + \varrho R \cdot \sum_{\nu=1}^{\infty} (-\varrho A)^{\nu} \cdot i_Q(A^{\nu+1} t). \tag{12}$$

From equation (12) it follows

$$-\varrho R \cdot i_Q(At) = -\varrho R \cdot i_{G/d}(Akt) + \sum_{\nu=2}^{\infty} (-\varrho A)^{\nu} \cdot i_Q(A^{\nu} t). \tag{13}$$

Summarizing the equations (11) and (13) the source current is given by:

$$i_Q(t) = i_{G/d}(kt) - \varrho R \cdot i_{G/d}(Akt) \; . \tag{14}$$

Finally with equation (8) the relationship between the currents from the current source $i_Q$ and in the striking point $i_G$ is /8/:

$$i_Q(t) = \frac{1}{1 + \varrho} \left[ i_G(kt) - \varrho R \cdot i_G(Akt) \right] \; . \tag{15}$$

## 3. FAR FIELD APPROACH OF THE TCS - MODEL CONSIDERING REFLECTIONS

For the field propagation the earth's surface is considered to be an ideal conducting plane. The return stroke channel acts as a vertical antenna increasing with the velocity v = const.. The far distant field component radiated from an antenna element with the length dz is given by /3, 9/:

$$d\vec{E}_f(t) = - \frac{1}{2\pi\varepsilon_o} \frac{\sin^2\theta}{c_o^2 r} \frac{\partial i(z, t - r/c_o)}{\partial t} d\vec{z} \tag{16}$$

For an far distant observer in point X (fig. 5) the field retardation can be neglected: $(t - r/c_o) \rightarrow t$. With $r \approx s$, $\sin\theta \approx 1$ and $E(t) \rightarrow E_f(t)$ equation (16) becomes:

$$d\vec{E}_f(t) = - \frac{a}{c_o} \frac{\partial i(z,t)}{\partial t} d\vec{z}, \qquad with \quad a = \frac{1}{2\pi\varepsilon_o c_o s} \tag{17}$$

Fig. 6 shows schematically the current distribution on the lightning channel. In the height h the downward propagating current is given by $i_d(z = h,t) = i_o(t)$ and the upward propagating current by $i_u(z = h,t) = \varrho\, i_o(At)$. With $i_o(t) = i_{G/d}(kt) = [i_G(kt)]/(1 + \varrho)$ the total current in the height h = z follows to:

$$i(h,t) = i_d(h,t) + i_u(h,t) = \frac{1}{1+\varrho} \left[ i_G(kt) + \varrho i_G(Akt) \right] \tag{18}$$

The electric field $E_f(t)$ is given by the the sum of $E_f(t)_{z \le h}$ and $E_f(t)_{z=h}$. For $z \le h$ the field component $E_f(t)_{z \le h}$ is generated by the current variation on the return stroke channel:

$$\vec{E}_f(t)_{z \le h} = - \frac{a}{c_o} \int_{z=0}^{z=h=vt} \frac{\partial i(z,t)}{\partial t} d\vec{z} = - \frac{a}{c_o} \int_{z=0}^{z=h=vt} \frac{\partial i_d(z,t)}{\partial t} d\vec{z} - \frac{a}{c_o} \int_{z=0}^{z=h=vt} \frac{\partial i_u(z,t)}{\partial t} d\vec{z} \tag{19}$$

The upward propagating current is given by: $\partial i_u/\partial t \cdot dz = \partial i_u \cdot dz/dt = c_o \cdot di_u$. The direction of the downward propagating current is opposite to the z - direction: $\partial i_d/\partial t \cdot dz = \partial i_d \cdot dz/dt = - c_o \cdot di_d$. Equation (19) becomes:

$$E_f(t)_{z \le h} = - \frac{a}{c_o} \int_{i_{G/d}(t)}^{i_o(t)} -c_o \, di_d - \frac{a}{c_o} \int_{i_{G/u}(t)}^{\varrho i_o(At)} c_o \, di_u = \frac{a}{1+\varrho} \left[ i_G(kt) - i_G(t) - \varrho i_G(Akt) + \varrho i_G(t) \right] \quad (20)$$

In the height z=h the current discontinuity is given by $i(z=h,t) = i_o(t) + \varrho i_o(At)$ and $i(z>h) = 0$. With $\partial i(h,t)/\partial t \cdot dz = v \cdot di$ it follows:

$$E_f(t)_{z=h} = - \frac{a}{c_o} \int_{h/-}^{h/+} \frac{\partial i(z,t)}{\partial t} \, dz = - \frac{a}{c_o} \int_{i(h,t)}^{o} v \, di = \frac{a}{1+\varrho} \frac{v}{c_o} \left[ i_G(kt) + \varrho i_G(Akt) \right] \quad (21)$$

With $Ak = 1 - v/c_o$ and sumarizing equation (20), (21) the total far distant electromagnetic field results in:

$$E_f(t) = \Gamma_o H_f(t) = \frac{a}{1+\varrho} \left[ k \cdot i_G(kt) - (1-\varrho) \, i_G(t) - \varrho Ak \cdot i_G(Akt) \right] \quad (22)$$

The far distant magnetic field is given by the relationship $H_f(t) = E_f(t)/\Gamma_o$ (resistance of free space: $\Gamma_o \approx 377\ \Omega$). The time-derivation of the far distant electromagnetic field follows to:

$$\frac{dE_f(t)}{dt} = \Gamma_o \frac{dH_f(t)}{dt} = \frac{a}{1+\varrho} \left[ k^2 \frac{di_G(kt)}{dt} - (1-\varrho) \frac{di_G(t)}{dt} - \varrho (Ak)^2 \frac{di_G(Akt)}{dt} \right] \quad (23)$$

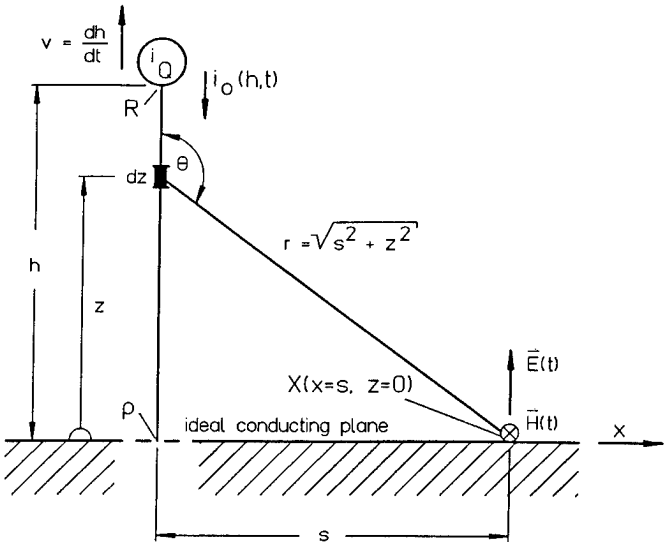



Fig. 5: Geometry of the return stroke channel

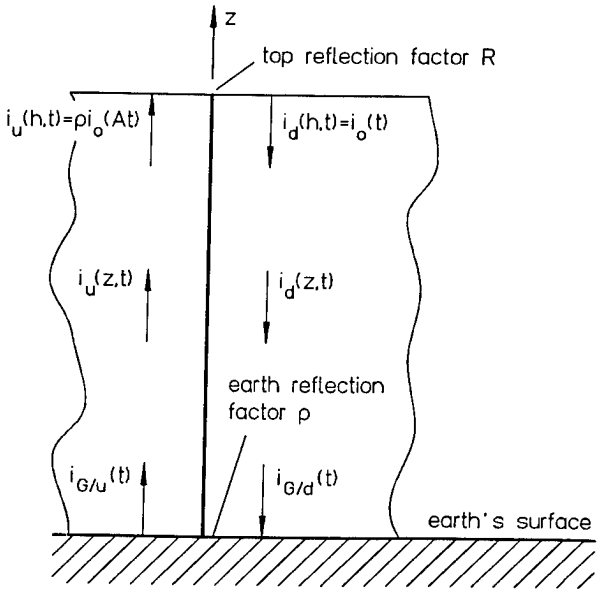



Fig. 6: Current on the return stroke channel ($h \gg s$)

## 4. DERIVATION OF THE LIGHTNING CURRENT FROM THE FAR FIELD APPROACH

First the solution is derived for $\varrho = 0$ and $\varrho = 1$. Then an arbitrary earth reflection factor is discussed. Because the far distant magnetic field can be substituted via the relationship $E_f = \Gamma_o \cdot H_f$, only the electric field is considered.

### 4.1 Earth reflection factor ϱ = 0 : No reflection

Neglecting earth reflections (ϱ = 0) equation (22) becomes /10/:

$$E_f(t) = a\,[k \cdot i_G(kt) - i_G(t)] \quad , \qquad a = \frac{1}{2\pi\epsilon_0 c_0 s} \tag{24}$$

Considering times $t/k^1$, $t/k^2$, $t/k^3$, ... the following expression can be deduced from equation (24):

$$\frac{1}{k^1}E_f(\frac{t}{k^1}) = a \cdot [i_G(t) - \frac{1}{k^1} i_G(\frac{t}{k^1})]$$

$$\frac{1}{k^2}E_f(\frac{t}{k^2}) = a \cdot [\frac{1}{k^1} i_G(\frac{t}{k^1}) - \frac{1}{k^2} i_G(\frac{t}{k^2})] \tag{25}$$

$$\frac{1}{k^3}E_f(\frac{t}{k^3}) = a \cdot [\frac{1}{k^2} i_G(\frac{t}{k^2}) - \frac{1}{k^3} i_G(\frac{t}{k^3})]$$

⋮ ⋮

Summarizing the right and left sides of equation (25) the following formula results:

$$\frac{1}{k^1}E_f(\frac{t}{k^1}) + \frac{1}{k^2}E_f(\frac{t}{k^2}) + \frac{1}{k^3}E_f(\frac{t}{k^3}) + \ldots = a \cdot i_G(t) \tag{26}$$

Finally the current at the striking point is given by (compare /11,12/):

$$i_G(t) = 2\pi\epsilon_0 c_0 s \sum_{j=1}^{\infty} \frac{1}{k^j} E_f(\frac{t}{k^j}) \tag{27}$$

The first time-derivation of the current follows to:

$$\frac{di_G(t)}{dt} = 2\pi\epsilon_0 c_0 s \sum_{j=1}^{\infty} \frac{1}{k^{2j}} \frac{dE_f(\frac{t}{k^j})}{dt} \tag{28}$$

### 4.2 Earth reflection factor ϱ = 1 : Total current reflection

In the case of total current reflection (ϱ = 1) equation (22) becomes:

$$E_f(t) = \frac{ak}{2}[i_G(kt) - A i_G(Akt)] \quad , \qquad a = \frac{1}{2\pi\epsilon_0 c_0 s} \tag{29}$$

Considering times $A^0t/k$, $A^1t/k$, $A^2t/k$, ... from equation (29) it follows:

$$A^0 E_f(\frac{A^0 t}{k}) = \frac{ak}{2}[A^0 i_G(A^0 t) - A^1 i_G(A^1 t)]$$

$$A^1 E_f(\frac{A^1 t}{k}) = \frac{ak}{2}[A^1 i_G(A^1 t) - A^2 i_G(A^2 t)] \tag{30}$$

$$A^2 E_f(\frac{A^2 t}{k}) = \frac{ak}{2}[A^2 i_G(A^2 t) - A^3 i_G(A^3 t)]$$

⋮ ⋮

Summarizing the right and left sides of equation (30) the following formula results:

$$A^0 E_f(\frac{A^0 t}{k}) + A^1 E_f(\frac{A^1 t}{k}) + A^2 E_f(\frac{A^2 t}{k}) + \ldots = \frac{ak}{2} i_G(t) \tag{31}$$

Finally the current at the striking point is given by:

$$i_G(t) = \frac{4\pi\epsilon_0 c_0 s}{k} \sum_{j=0}^{\infty} A^j E_f(\frac{A^j t}{k}) \tag{32}$$

The first time-derivation of the current follows to:

$$\frac{di_G(t)}{dt} = \frac{4\pi\epsilon_0 c_0 s}{k^2} \sum_{j=0}^{\infty} A^{2j} \frac{dE_f(\frac{A^j t}{k})}{dt} \tag{33}$$

### 4.3 Arbitrary earth reflection factor

The electric field of equation (22) is split up into the two components

$$E_f(t) = E_{f/1}(t) - E_{f/2}(t) \tag{34}$$

with

$$E_{f/1}(t) = \frac{a}{1+\varrho}[k \cdot i_G(kt) - (1-\varrho)\, i_G(t)] \tag{35}$$

$$E_{f/2}(t) = \frac{a}{1+\varrho} \cdot \varrho A k \cdot i_G(Akt) \tag{36}$$

For the component $E_{f/1}$ times $t/k^1$, $t/k^2$, $t/k^3$, ... are considered:

$$\frac{(1-\varrho)^0}{k^1} E_{f/1}(\frac{t}{k^1}) = \frac{a}{1+\varrho} \cdot [i_G(t) - \frac{(1-\varrho)^1}{k^1} i_G(\frac{t}{k^1})]$$

$$\frac{(1-\varrho)^1}{k^2} E_{f/1}(\frac{t}{k^2}) = \frac{a}{1+\varrho} \cdot [\frac{(1-\varrho)^1}{k^1} i_G(\frac{t}{k^1}) - \frac{(1-\varrho)^2}{k^2} i_G(\frac{t}{k^2})] \tag{37}$$

$$\frac{(1-\varrho)^2}{k^3} E_{f/1}(\frac{t}{k^3}) = \frac{a}{1+\varrho} \cdot [\frac{(1-\varrho)^2}{k^2} i_G(\frac{t}{k^2}) - \frac{(1-\varrho)^3}{k^3} i_G(\frac{t}{k^3})]$$

⋮ ⋮ ⋮ ⋮

Summarizing the right and left sides of equation (37) the following formula results:

$$\frac{(1-\varrho)^0}{k^1}E_{f/1}(\frac{t}{k^1}) + \frac{(1-\varrho)^1}{k^2}E_{f/1}(\frac{t}{k^2}) + \frac{(1-\varrho)^2}{k^3}E_{f/1}(\frac{t}{k^3}) + \ldots = \frac{a}{1+\varrho}i_G(t) \tag{38}$$

Finally the current at the striking point is given by:

$$i_G(t) = 2\pi\epsilon_0 c_0 s(1+\varrho)\sum_{j=1}^{\infty}\frac{(1-\varrho)^{j-1}}{k^j}E_{f/1}(\frac{t}{k^j}) \tag{39}$$

The first time-derivation of the current follows to:

$$\frac{di_G(t)}{dt} = 2\pi\epsilon_0 c_0 s(1+\varrho)\sum_{j=1}^{\infty}\frac{(1-\varrho)^{j-1}}{k^{2j}}\cdot\frac{dE_{f/1}(\frac{t}{k^j})}{dt} \tag{40}$$

To obtain the current the following iteration algorithm was applied:

Step 0 : $E_{f/1}(t) = E_f(t)$ is chosen
Step 1 : $i_G(t)$ is calculated with equation (39)
Step 2 : $E_{f/2}(t)$ is calculated with equation (36)
Step 3 : The component $E_{f/1}$ is corrected by: $E_{f/1}(t) = E_f(t) + E_{f/2}(t)$
Step 4 : Go to Step 1 and repeat the procedure until the iteration is ended

In the same way with equation (40) instead of equation (39) the current derivative can be deduced using

$$\frac{dE_{f/2}(t)}{dt} = \frac{a}{1+\varrho}\cdot\varrho A^2k^2\frac{di_G(Akt)}{dt} \tag{41}$$

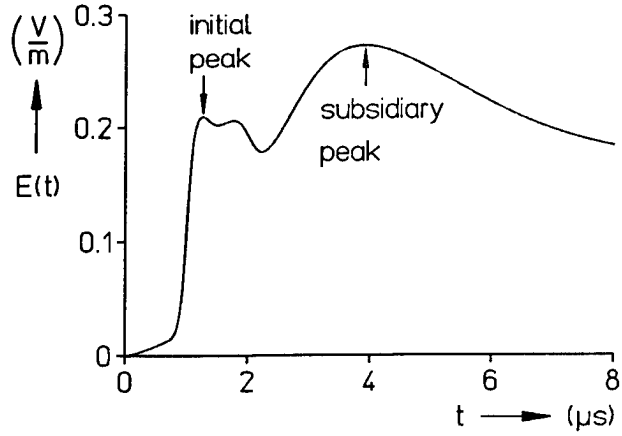
The algorithm was tested calculating first the electric field and the electric field derivative from the given current via the TCS - model. Fig. 7 shows an example, where the current is discribed by:

$$i(t) = \frac{i_{max}}{\eta}\cdot[\,C\cdot X + (1-C)\cdot Y\,]\cdot e^{-\frac{t}{\tau_2}} \tag{42}$$

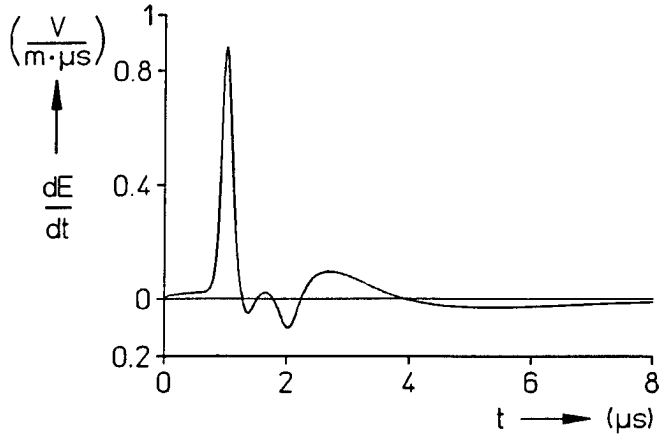
$$Y = \frac{A\cdot k_1^n + k_1^m}{1+k_1^m}\;;\; X = \frac{k_2^l}{1+k_2^l}\;;\quad k_1 = \frac{t}{\tau_1}\;;\; k_2 = \frac{B\cdot t}{\tau_1}$$

The current parameters are chosen to m = 6, n = 1,3, l = 18, $\tau_1$ = 4,0 $\mu$s, A = 0,4, B = 3,0, C = 0,4, $\tau_2$ = 75,0 $\mu$s and $i_{max}$ = 10 kA. The current and the current time-derivative are marked 'original' in fig. 7b and fig. 7c.

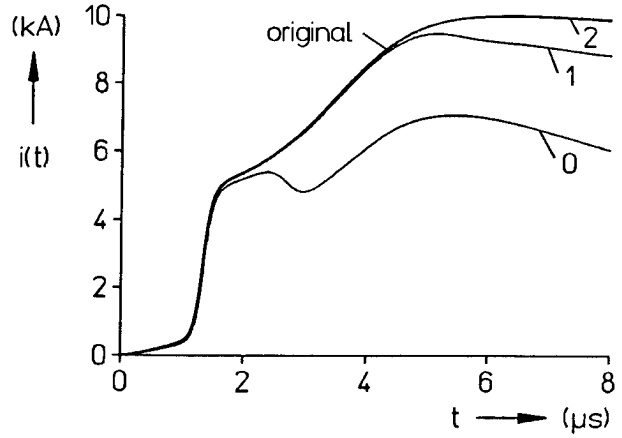
Considering $\varrho$ = 0,8 and v = 100 m/$\mu$s the electric field (fig. 7a) and its time-derivative (fig. 7b) were calculated with the TCS - model in the unrealistic far distance s = 1000 km to avoid the influence of the near and intermediate distant field components. Without iteration marked by '0' in fig. 7c,d only the fast current rise could be calculated satisfactorily. After one iteration marked by '1' the agreement of the current steepness is rather good, whereas for the calculation of the current maximum two iterations or more should be applied.



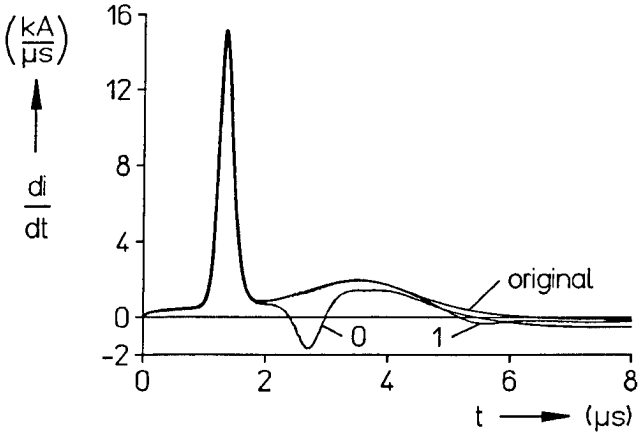

a) Electric field E(t)




b) Electric field derivative dE(t)/dt




c) Current i(t)




d) Current derivative di(t)/dt

Fig. 7: Accuracy of the iteration algorithm
(0: no iteration; 1: 1 iteration; 2: 2 iterations)

## 5. CONCLUSION

The return stroke channel has a characteristic impedance of about $\Gamma = 500...1000\ \Omega$ /4/. Opposite that the earth resistance of buildings is normally in the order up to some $\Omega$. In /13/ experimental results are presented, where the earth resistance is lowered by breakdown processes along the earth surface. Hence follows, that even for lightning strikes to earth the current might be significantly reflected. This hypothesis is validated by triggered lightning experiments over salt water and earth. In both cases the lightning currents had approximately the same amplitudes /14/.

If current reflections are taken into account, the current on the return stroke channel consists of the superposition of the different reflected current portions. Nevertheless a procedure was found considering a channel-base current. For far distances an approach was found, which is also valid for near distant fields ($s \geq 1$ km) during the first microseconds. Basing on this approach an algorithm was deduced enabling the calculating of the lightning current from the far field data. Even if the electric field has an initial as well as an subsidiary peak, by this method the maximum current and the maximum current steepness could be calculated satisfactorily.

## REFERENCES


/1/ Hopf, Ch.: dE/dt-measurements and simultaneous all sky video camera observations. 9th Intern. Symposium on EMC (1991), Zurich, H3.

/2/ Heidler, F.: Results of simultaneous dE/dt- and dH/dt- measurements. 22nd Intern. Conf. on Lightning Protection (1994), Budapest, R1c-04.

/3/ Heidler., F.: Lightning electromagnetic impulse - Theorie und Messungen. Diss. Universität der Bundeswehr München, 1987.

/4/ Beierl, O.: Elektromagnetische Verträglichkeit beim Blitzeinschlag in ein Gebäude. Diss. TU München, 1991.

/5/ Anderson, R.B.; Eriksson, A.J.: Lightning parameters for engineering application. Electra 69 (1980), p. 65 - 102.

/6/ Heidler, F.; Hopf, Ch.: Lightning current and lightning electromagnetic impulse considering current reflection at the earth's surface. 22nd Intern. Conf. on Lightning Protection (1994), Budapest, R 4-05.

/7/ Heidler, F.; Hopf, Ch.: Influence of the lightning channel termination on the lightning current and lightning electromagnetic impulse. 16th Intern. Aerospace and Ground Conf. on Lightning and Static Electr. (1994), Mannheim, p. 65-74.

/8/ Heidler, F.; Hopf, Ch.: Initial and subsidiary peak of lightning electromagnetic fields considering channel-base current and reflections at the return stroke channel. 9th Intern. Symp. on High Voltage Engineering ISH (1995), Graz, paper to be presented.

/9/ Uman, M.A.; McLain, D.K.; Krider, E.P.: The electromagnetic radiation from a finite antenna. AJP (1975), vol.43, P. 33-38.

/10/ Heidler, F.: Some deductions from the Travelling Current Source model. 8th Inter. Wroclaw Symp. on EMC (1986), Wroclaw, S. 245 - 252.

/11/ Heidler, F; Hopf, Ch.: LEMP calculation and lightning current function. 8th ISH (1993), Yokohama, vol. 4, rep. 7.13, p. 237 - 240.

/12/ Rachidi, F.; Thottappillil, R.: Determination of lightning currents from far electromagnetic fields. JGR (1993), vol. 98, D10, p. 18315 - 18321.

/13/ Fisher, R.J.; Schnetzer, G.H.; Morris, M.E.: Measured Fields and earth potentials at 10 and 20 meters from the base of triggered lightning channels. 22nd Intern. Conf. on Lightning Protection (1994), Budapest, R1c-10.

/14/ Fisher, R.J.; Schnetzer, G.H.; Thottappillil, R.; Rakov, V.A.; Uman, M.A.; Goldberg, J.D.: Negative subsequent strokes. Natural versus triggered lightning. 22nd Intern. Conf. on Lightning Protection (1994), Budapest, R1c-2.

# SESSION 04B
# TEST CRITERIA AND TECHNIQUES
# CHAIRPERSON: KEITH CROUCH

# SUSCEPTIBILITY OF EQUIPMENTS TO MULTIPLE STRIKE THREATS

V P Dunkley, R W Spencer, C J Hardwick
Lightning Test and Technology (LTT), AEA Technology, Culham Science and Engineering Centre, Abingdon, Oxfordshire, OX14 3DB, United Kingdom
Telephone: +44-1235-463246, Facsimile: +44-1235-464325

## ABSTRACT

Although avionics systems are being tested for immunity to the multiple burst and stroke threats of AC20-136, no standard test procedures are defined yet. We report investigations on a 1553 data bus using multiple burst pulses having fixed and random spacing.

The inherent hardness of the 1553 bus system means that data corruption could only occur where the level of signal induced on the cabling is very high.

When data corruption occurs we find that the error rate is affected by the test method. Fixed pulse spacings near the data rate produce higher error rates than randomly spaced pulses.

## INTRODUCTION

The multiple burst and stroke environments were introduced into the external lightning threat definition contained in the FAA Advisory Circular AC20-136 in 1990. The multiple burst wave train defined in that document consists of 24 separate bursts of 20 pulses, each burst occupying up to 1 millisecond (the inter pulse and burst spacings and the total number of bursts were revised in 1993); the multiple stroke wave train consists of 24 single pulses. Both events have a total duration of up to 2 seconds. The concern with these threats is that because of the repetitive nature and large number of pulses generated during each event, they could cause upset in full authority digital control systems due to the pulses coinciding with particular parts of the system operating cycle.

Although generators are available to produce trains of pulses at equipment test levels with the required pulse spacings, no standard gives a defined test methodology for performing these tests. AC20-136 merely defines the external environment and RTCA DO160C only gives test methods for single pulses. There is a need for a well-defined test methodology based on knowledge of the way that the multiple burst and multiple stroke wave trains corrupt digital data. The result of a system test could be highly dependent on the coincidence of wave train and software cycle timing.

A Culham Lightning Club research programme was set up to investigate possible test methodologies.

This paper presents the results of part of the programme in which we investigated the effects of different multiple burst pulse trains on MIL STD 1553 data.

The paper briefly describes the format of 1553 data; then describes the implementation of the system used for assessing data corruption and presents results

obtained from tests carried out using the multiple burst waveform. Finally suggestions are made for other work under this programme.

## 1553 DATA STANDARD

Although it is accepted that the physical configuration of the 1553 bus (i.e., a balanced transformer coupled system) suggests that it is inherently 'hard' against EMC disturbance, it was chosen as a suitable target for investigation because of its wide adoption as a data transmission standard. Also modes of upset might be generic to serial data systems. However the test system was produced in a way that allows the use of other interface hardware standards and different data formats.

The 1553 system transmits serial data along screened twisted pair cabling of 70→85Ω characteristic impedance. Data is coupled onto and off the bus using transformer coupling.

The data on the bus is Bi-phase Manchester encoded data that is transmitted at a rate of 1Mb per second. Bi-phase Manchester encoding means that the data is sent as two anti-phase signals along the two signal lines. The Manchester encoding method defines a logic 1 as being a transmission from 1 to 0 during the clock period and logic 0 as a 0 to 1 transition (this is demonstrated in figure 1). A complete message occupies 20 bits. The first 3 bits are used as a SYNC pulse which is one cycle of a square wave; the phase of this defines whether the proceeding information is a 'COMMAND', 'STATUS' or 'DATA' message. In the example in figure 1 the SYNC signifies a DATA message, a SYNC of opposite phase would signify that the following message was either STAT or COMM. The following 16 bits form the message and the last bit is a parity bit.

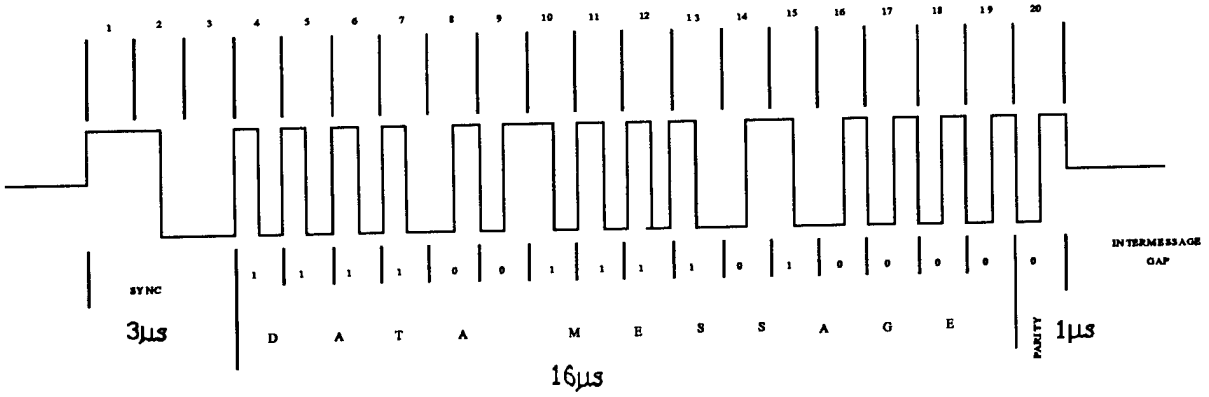



FIGURE 1 EXAMPLE OF A COMPLETE 1553 MESSAGE

The 1553 standard requires the insertion of 'Intermessage Gaps' during data communication, and these gaps must have a minimum duration of 8µs. During an

'Intermessage Gap' the bus is in an idle condition, with both data lines at a potential midway between the positive and negative voltage levels.

## TEST SET UP FOR ASSESSING DATA CORRUPTION

The overall test arrangement is shown in figure 2. All of the coding/decoding and 1553 data processing is done in the 1553 processor module, which communicates with the Receive and Transmit modules using fibre optic links. The Receive and Transmit modules are connected to a terminated bus onto which the interfering multiple burst pulses were injected.

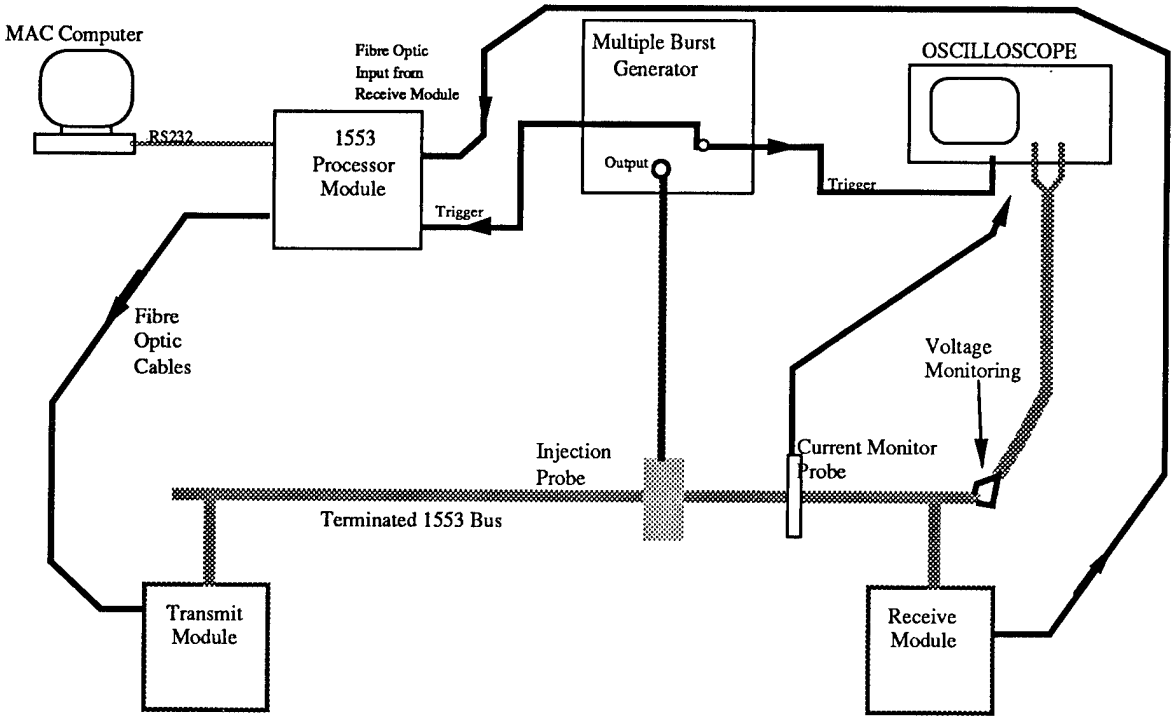



FIGURE 2 DIAGRAM OF TEST SET-UP USED FOR ASSESSING DATA CORRUPTON

A high speed digitising oscilloscope was used to monitor either the cable current , or the voltages on the twisted pair wires.

1553 BUS CONFIGURATION – For these tests the bus configuration simulated a single bus – approximately 1.5m long – with two LRU's (Receive and Transmit modules) connected as 'Direct Coupled Stubs'. Direct coupling means that the LRU's are wired directly onto the main bus as opposed to being connected by an additional coupling transformer (each LRU still has a transformer internally). The cable used was a commercial grade screened twisted pair cable with a $Z_0$ of around 75–80Ω.

Early testing showed that the signal levels available from the Multiple Burst generator were not sufficient to cause corruption of the message data with the normal screening offered by the cable. Therefore the interference rejection properties of the cable were degraded, by parting the screen (which on the cable used is simply twisted and not lapped) and forming a 30mm by 200mm loop between the two inner wires. This allowed much larger differential interference signals to be induced onto the bus.

OPERATION OF ERROR ANALYSIS SYSTEM – In operation a text 'message' file is written on the MAC computer; this file contains the information to be transmitted on the bus. Optionally it contains commands to set the time window around each burst that is used for data capture; and the number of bursts that are analysed on each experimental run. The system analyses data for 1ms prior to each interfering burst, plus 1, 2, 4, 8, 16 or 32ms afterwards. The number of bursts that are processed for each run is 1, 2, 4, 8, 16 or 32, (the maximum number is inversely proportional to the length of the data capture window).

The 'message' file is sent to the processor module where the information is encoded and stored in a large RAM (Random Access Memory) ready for transmission. The information in the message file is simply repeated as many times as is necessary to fill the RAM.

Upon command from the MAC, the Processor Module starts sending the data from the RAM, via the fibre optic links to the Transmit Module which then transmits the data onto the bus. Data received by the Receive Module is sent via fibre optics back to the Processor Module. The Processor Module samples this data at 16MHz (this emulates the functioning of standard 1553 receiver/decoder hardware).

At the start of each burst of pulses from the MBG, a trigger pulse is generated and this is sent to the oscilloscope and Processor Module. The Processor Module uses this pulse to indicate the start of the post trigger sample window and after the pre-defined period stops sampling and stores the received data in memory, before re-starting sampling ready for the next burst. This process is repeated until the required number of burst trigger signals has been received.

After the specified number of trigger signals, the received data is available for processing, by comparison with the transmitted data. The processing is performed in the Processor Module and the results sent to the MAC.

All communications between the Processor Module and the MAC can be stored in a LOG file for future reference.

ERROR ANALYSIS – The 1553 data is checked for differences between the received and corresponding transmitted data. For these tests the logic state of each $^1/_2$ bit of received data is determined simply by taking a majority vote on the 8 samples taken during the time of the $^1/_2$ bit. (The data rate is 1Mbit per second, but it is sampled at 16MHz; therefore 8 samples represent $^1/_2$ bit.) If ≥50% of the samples are a 'high', then the logic state for this $^1/_2$ bit is classed as 'high'. This value is compared to the data that was transmitted, if they are not equal then an error is logged. This is done for each $^1/_2$ bit in each sample window. The Processor Module reports the time (in terms of Transmit bit number after the start of data transmission) of the error, the type and start time of the data message in which the error occurs; and the 1553 data word bit number for the error.

## ASSESSMENT OF INDUCED SIGNALS IN FULLY SCREENED CABLE

As noted earlier corruption of the 1553 data could not be achieved when injecting transients on fully screened cable and it was considered important to determine the levels that would be required. To do this we measured the levels of differential signal induced on fully screened cable, to compare with the levels of signal required to cause corruption of data.

Actual 1553 cable was not available for the tests and so the normal aircraft standard screened, twisted pair cable was used.

Each end of a 1.5m length of cable was terminated at a metal box. The inner cables passed through the walls of the boxes and were terminated with 75Ω resistors. Approximately 0.5m lengths of cable were used to connect from these terminating boxes, to the 1553 Receive and Transmit Modules; 360° screening was maintained throughout. The Receive and Transmit Modules and one of the terminating boxes were bonded to the ground plane. With this arrangement the length of cable subjected to the multiple burst pulses was 2m. The voltages appearing on the inners of the cable at the terminating resistor were measured using the digitising oscilloscope.

Using this arrangement, with 1MHz pulses having a peak amplitude of 21A, we measured a common mode voltage – $V_{CM} \approx 680V$,
and a differential voltage – $V_{DIFF} \approx 10mV$.

This gives a Common Mode Rejection of 37dB.

Thus the differential induced voltage expressed in mV per amp of peak current, per meter length of cable screen is:-

$$\mathbf{V_{DIFF} = 0.23mVA^{-1}m^{-1}}.$$

## DETERMINATION OF 1553 CORRUPTION THRESHOLD

Determination of the induced signal levels that were required to produce errors in the 1553 data was done using the cable with degraded screening as described earlier. It was found that there were two distinct levels that caused corruption of data.

The first (lower) level results in the 'Intermessage Gap' being corrupted with what appear as odd logic pulses. This initially occurs with an interference signal having a peak value of approximately 650mV ($V_{DIFF}$). With standard aircraft cable this would require a peak screen current of:

$$650mV \div 0.23mVA^{-1}m^{-1} = \mathbf{2.8kAm} \text{ – a high level.}$$

A much higher level is required to corrupt the actual 1553 messages - causing $^1/_2$ bits to have the wrong value. The level of signal required to produce this corruption is approximately 4.3V corresponding to **18.7kAm** on fully screened cable!

It seems unlikely that this level of induced signal will appear in an aircraft installation and even the lower level of 2.8kAm seems very high. Even if this level were present it would be relatively simple to filter out the induced errors since they do not constitute a recognised 1553 message.

ERROR ASSESSMENT – While it would appear unlikely that a standard 1553 bus would be at risk of corruption, the degraded system was used to assess and

compare the responses to random and fixed pulse spacing (within each burst of the multiple burst).

This was done using a sequence of messages containing a range of different data with each word separated from the next by an 8μs Intermessage Gap. The Processor Module was set to process 16 bursts with a 2ms window (i.e., 1ms post trigger). With the message format used there are between 35.6 and 36 data words in 1ms, depending on where the start of the 1st data word is with respect to the start of the 1ms time window. Thus there are between 712 and 720 data bits in 1ms which for 16 bursts amounts to 11,456 ±0.56% data bits.

The Multiple Burst Generator was configured to produce randomly spaced bursts and the pulse spacing was optionally selected as random spacing (between 10μs and 50μs) or fixed spacing of 27μs. 27μs was chosen because this is 1μs less than the 'message plus gap' time of the 1553 data and it was expected that errors would appear sequentially 1 bit earlier in successive data words, which in fact they did. The pulse spacings used were those from the original multiple burst definition and not from the revised definition.

Two pulse levels were applied; firstly a level just slightly above the threshold level and then at a significantly higher level using the waveform shown in figure 3. Figure 4 shows the recorded oscilloscope trace of corrupted data.

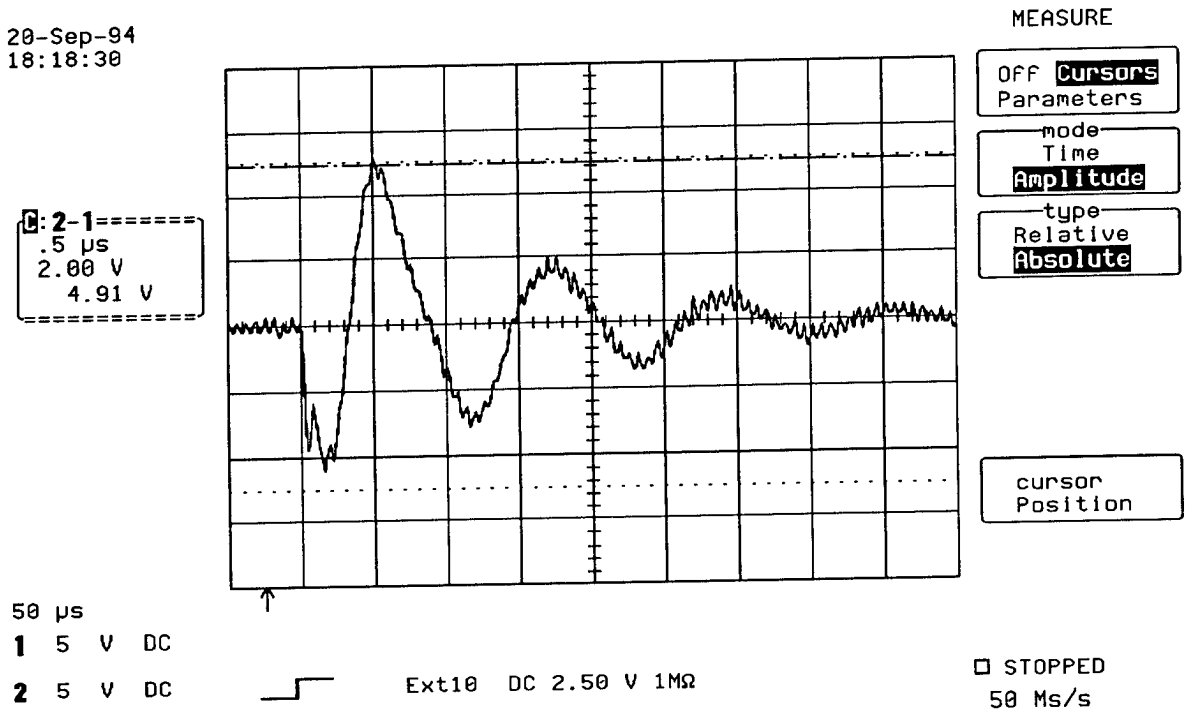



FIGURE 3 HIGHER LEVEL WAVEFORM INTERFERENCE PULSE

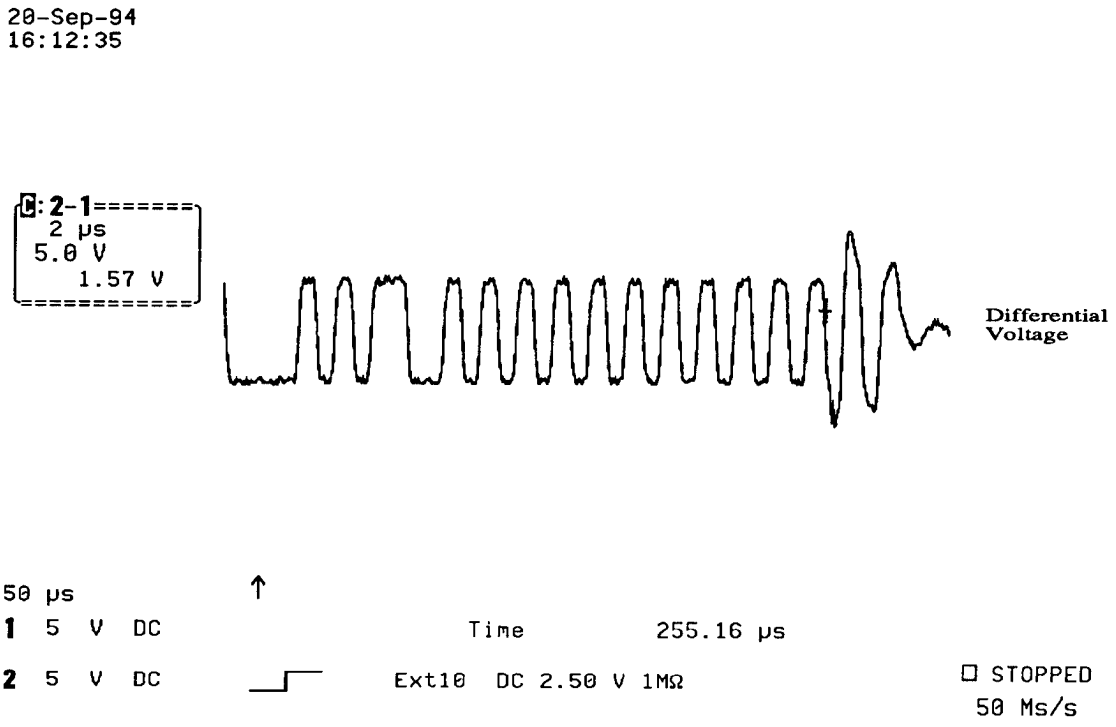



FIGURE 4 SCOPE TRACE OF CORRUPTED DATA USING HIGHER LEVEL INTERFERENCE PULSES

Approximately 70 test runs were recorded and analysed for errors, 39 at the threshold level and 33 at the higher level. To avoid effects that might be due to long term drifting, the pulse sequences were applied using fixed and random pulse spacings alternately.

Corruption of either a 1/2 bit or the whole 1 bit, was counted as an error.

At the lower level of interference the total number of errors was less, but the spread in error counts was greater than at the higher pulse level.

This might be expected since the time for which the pulse is at or above a level to cause corruption is short and therefore the coincidence between the data pulse and interfering pulse needs to be much closer than it needs to be at the higher level. The number of corruptions to complete data bits in comparison to total errors, also increases with the higher pulse level. Again this might be expected because the interference is at a sufficiently high level for a longer period of time.

Figures 5 and 6 compare the results from the fixed pulse and random pulse runs. The histogram data is arranged to show the results in order of increasing error rate. Clearly the fixed pulse spacing resulted in more errors. This is probably because the fixed spacing was deliberately chosen to be slightly shorter than the word repetition rate, although there may also be a generator effect. The MBG uses pulse circuits that are re-charged between pulses and with the random pulse spacing there is a risk of pulse amplitude variation caused by the differences in re-charge times.

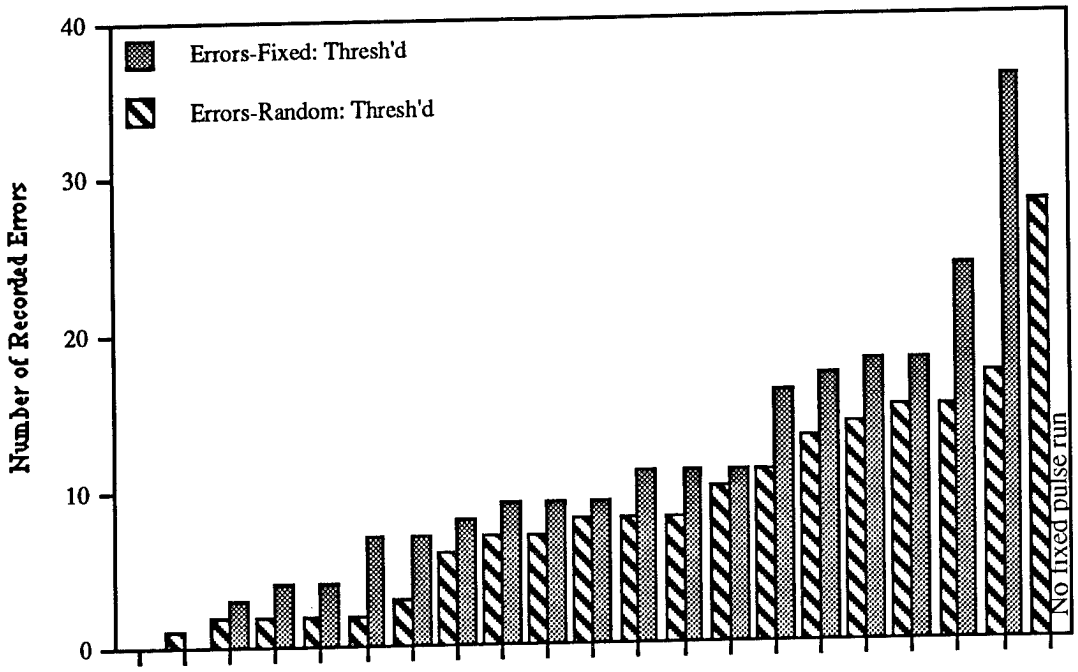



FIGURE 5 COMPARISON OF ERRORS INDUCED BY FIXED AND RANDOM SPACED PULSES AT UPSET THRESHOLD PULSE LEVEL

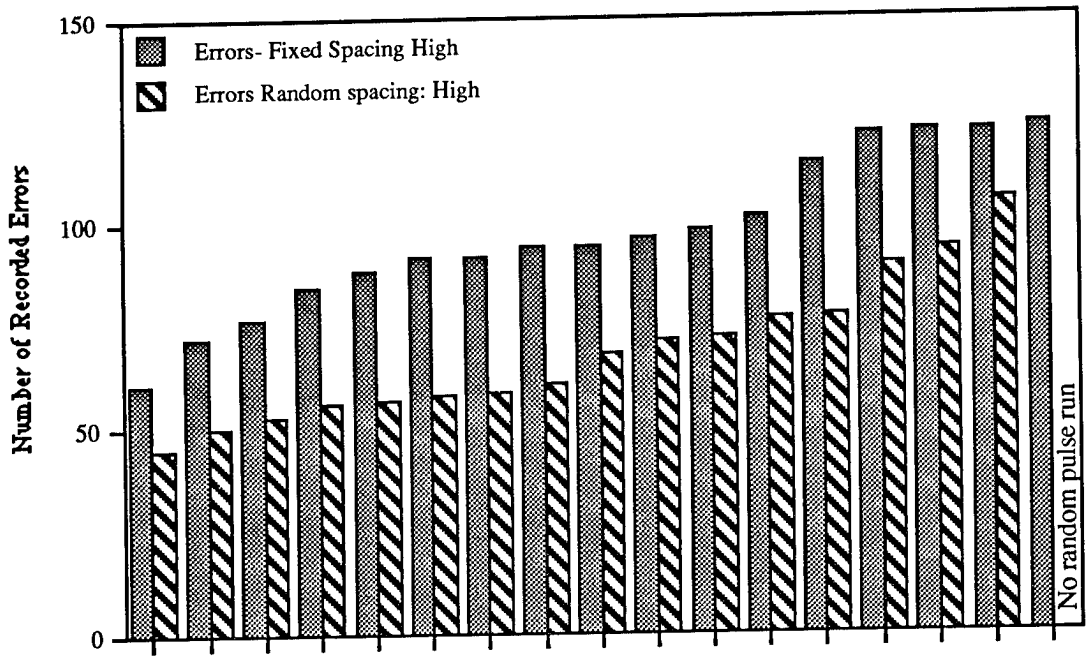



FIGURE 6 COMPARISON OF ERRORS INDUCED BY FIXED AND RANDOM SPACED PULSES AT HIGHER PULSE LEVEL

Future investigations will cover:-

- Verifying the statistical data on random versus fixed pulse spacing by adjusting the MBG to produce pulse spacings in the range required by the revised standard and ensuring that all pulses are the same amplitude.
- Checking the effects of the Long Wave multiple stroke pulses on the 1553 data. These could create many more errors since the waveform is much longer and the available current levels are also higher. We have a generator that will produce both fixed and random spaced pulses.
- Modifying the Transmit and Receive Modules, and the software to look at upset on a different data bus system.

## CONCLUSIONS

- The tests have shown that the 1MHz interference pulses need to be of similar magnitude to the 1553 data signals before the data is corrupted. To generate this level of signal on standard screened twisted pair cable would require screen currents of around 19kAm which is an unreasonably high level. Corrupting just the intermessage gap in the 1553 data would require around 3kAm. Even if this level of signal is available in an aircraft, this type of corruption might not seriously impair the operation of the 1553 bus since it should be relatively easy to identify the corruption as interference. However, this greatly depends on the 1553 error checking and correction, and whether or not the intermessage gap is an essential part of the transmission.
- For the 1553 data transmission system studied, pulses applied with a fixed spacing of slightly less than the data word repetition time, produced higher error rates than pulses applied with random spacing.

## ACKNOWLEDGEMENT

The author wishes to acknowledge the help of Mr P A Kellet, who wrote de-bugged and modified the Analyser software - on several occasions at short notice.

This work was sponsored by the Culham Lightning Club, comprising British Aerospace, CAA (UK), CASA (Spain), Rolls Royce, Saab Scania AB (Sweden), Short Brothers (NI)

# LIGHTNING PROTECTION FOR AND QUALIFICATION TESTING OF MODULAR AVIONICS

Olaf Spiller
Daimler-Benz Aerospace Airbus GmbH
Bremen, Germany

## ABSTRACT

The concept of modular avionics is the latest step in the avionics design philosophy for commercial aircraft. It is not surprising that one of the main driving forces for the introduction of modular avionics is the benefit of reduced costs for manufacturers and users alike. As part of fully taking advantage of these and technology benefits, the implementation of the protection against indirect effects of a lightning strike to the aircraft, and its qualification, have to be looked at from both a technological and an economic point.

This paper will look at the impact of the lightning protection within a line replaceable module (LRM) and discusses other solutions, as well as looking at the implications of either with respect to flexibility and modifications. The qualification of the system or equipment also has various aspects.

## 1. INTRODUCTION

Until now, the controller or computer in most avionics structures is designed to carry out one or several specific functions. Any standardization is only with respect to a given function, packaging, connectors and some signals. This results in a wide variety of equipment and the associated cost penalties for purchase and maintenance.

The introduction of modular avionics strives to bring a higher level of standardization and integration. With the aim of reduced cost for development, equipment price and cost of ownership, also protection against indirect effects of a lightning strike and EMI must be optimized to meet that goal. The possibilty to include several different functions in one cabinet opens up the question on how and where to include the lightning and EMI protection for the hardware. Distributing the protection elements within a cabinet/LRM leads to the necessity to carefully define the qualification procedure for the various hardware components not only for the initial qualification, but also to minimize the necessary effort in the case of future modifications.

With the ARINC specifications for integrated modular avionics (IMA), standardized testing is proposed, without being specified any further for lightning induced transients susceptibility testing.

## 2. EQUIPMENT PROTECTION

The protection on equipment level complements the protection offered by the aircraft structure or dedicated protection schemes like conduits or similar. There are various basic technologies used in transient protection (MOV, TVS diodes etc.) within an equipment. The difficulty often is to find a device with the necessary energy handling capability in an economically sized package. Until today, each interface to the outside world (other equipment) was protected as necessary by a dedicated protection element depending on the design level as given in the equipment specification. For a piece of equipment with many connections to other systems, this could mean that a considerable portion of its volume is taken up by lightning and EMI protection.

### 2.1. Protection Schemes

2.1.1. ARINC Design Guidelines

The ARINC specification addresses the distribution of protection within the modular avionics cabinet and modules, without being specific. The application of the protection should "provide reductions in life-cycle costs in terms of first costs, weight and maintainability" [1]. The overall aim is to be able to install a LRM in any cabinet, independent of the environmental conditions the cabinet is subjected to. The cabinet shall provide a standard environment for the LRM.

Nevertheless, the question remains in how far LRMs will have to be designed to withstand lightning strike indirect effects, when the cabinet already provides protection. According to ARINC 650 [2], for both cabinet and LRM the environmental condition "Lightning Induced Transient Susceptibility" shall be considered. An example for the installation of the cabinet in the avionics bay is given in Table 1 below.

| DO-160 C Section | Cabinet (Avionics Bay) | LRM |
|---|---|---|
| 22. Lightning Induced Transient Susc. | **J / M** | **J** |

**Table 1: IMA Environmental Considerations**

**Note:** ARINC 650 and 654 do not yet reference categories in accordance with DO-160 C Change 2 (Section 22) [3]!

Any inputs/outputs which are protected at the cabinet level would usually not require any further protection on LRM level, since especially the use of transient voltage suppression diodes offers a low clamping voltage. Those inputs/outputs which are only protected at the entrance to the LRM would bypass the protection offered by the cabinet and possibly cause

problems by coupling to other wiring on the backplane of the cabinet. The ARINC specification 654 acknowledges the analogous problem with respect to RF interference. There it says that "conducted interference should be eliminated before it contaminates the backplane"[1]. Therefore, any protection against lightning induced transients should be located where the wiring enters the IMA cabinet, but this implies that no dedicated protection within a LRM is needed. This however, has to be further considered when looking at the qualification process.

2.2. Alternative Scheme

As mentioned before, the ARINC specification 654 suggests to filter and protect against electromagnetic interferences before any disturbance enters the cabinet with its LRMs. The specification opens up the possibility of additional printed circuit boards (PCBs) or dedicated modules (LRM). Though this is given in the context of protection against RF interference, it only seems to be logical to apply this principle to the lightning protection as well.

A module containing the complete range of lightning protection, and as far as is practical EMI protection, would be situated directly behind the connector to the aircraft wiring. Additional measures, also given in the ARINC specifications, would divide the cabinet into a "dirty" and "clean" area, with the filter/protection module separating the two. This configuration makes the IMA cabinet and the LRMs therein look like a large, multi-function black box of "classic" design.

## 3. QUALIFICATION TESTING

As mentioned in chapter 2 above, cost reduction in all aspects is a prime target for the introduction of modular avionics. Qualification testing should be no exception. However, it remains to be seen, whether the testing of both the LRM (though reduced) and the populated cabinet still leaves an overall cost advantage.

### 3.1 Test Procedures

3.1.1. Damage Tolerance Test

Test procedures for the assessment of the damage tolerance of an equipment are given in RTCA DO-160 C Section 22 [3] chapter 22.5. In many cases the requirements for the pin injection tests will be those driving the design of the lightning protection on the equipment level. The actual values for this test are given in Table 2 below.

When using a ptotection scheme as described in chapter 2.1.1 above, there is the possibility to test the measures applied to the LRM independently of those applied to the cabinet. Nevertheless, it will be necessary to perform complementary testing for the LRM when installed in the cabinet, to verify the adequacy of the overall design. While this applies to the pin injection test, the situation is different for cable bundle tests, since the interaction with the rest of the installation in the cabinet has to be considered as well. This way of qualification procedure is a double effort, which from a technical point of view is unnecessary, as both pin injection and cable bundle tests can be done with the fully configured cabinet, thus eliminating testing of the LRM.

| Level | Waveforms 3 | 4 | 5 |
|---|---|---|---|
| | $V_{oc}/I_{sc}$ | $V_{oc}/I_{sc}$ | $V_{oc}/I_{sc}$ |
| 1 | 100/4 | 50/10 | 50/50 |
| 2 | 250/10 | 125/25 | 125/125 |
| 3 | 600/24 | 300/60 | 300/300 |
| 4 | 1500/60 | 750/150 | 750/750 |
| 5 | 3200/128 | 1600/32 | 1600/1600 |

**Table 2: DO-160 C Section 22 Pin Injection Test Levels**

When considering an IMA equipment that has a dedicated lightning protection module, for obvious reasons the testing is only to be performed with the cabinet and the installed LRMs together. This eliminates the need to define the apportioning of the protection elements and splitting of the verification effort. This does not exclude that precompliance testing of the LRM components for damage tolerance will be beneficial, in order to fine tune the protection.

3.1.2. Functional Upset Tests

A requirement of equal importance for an equipment or system is the functioning during and after a lightning strike to an aircraft. In this context only equipment/systems are considered, which are classified as "critical" or "essential" for airworthiness purposes.

As given in DO-160, for this purpose cable bundle tests are performed as either cable induction or ground injection tests, depending on the required waveform/test level. They must be performed on a fully configured equipment, with a representative interconnecting wiring and external loads and equipment either as real components or representative simulations. Depending on the complexity of the equipment/system under test, it may be necessary to have tests with the simultaneous injection into more than one cable bundle. Furthermore, in recent years airworthiness authorities have required multiple burst and multiple stroke tests for certification. These tests can be performed in a similar way as described in chapter 22.5.2 in DO-160 C. Not given in this document are test levels. Guidance to define waveforms, test levels etc. can be found in the Advisory Circular AC 20-136 [4].

In Figure 1, a setup used for a previous test program is given. The equipment under test only performs a specific control function. The tests were performed using several different frequencies and pulse spacings for both multiple stroke and multiple burst tests.

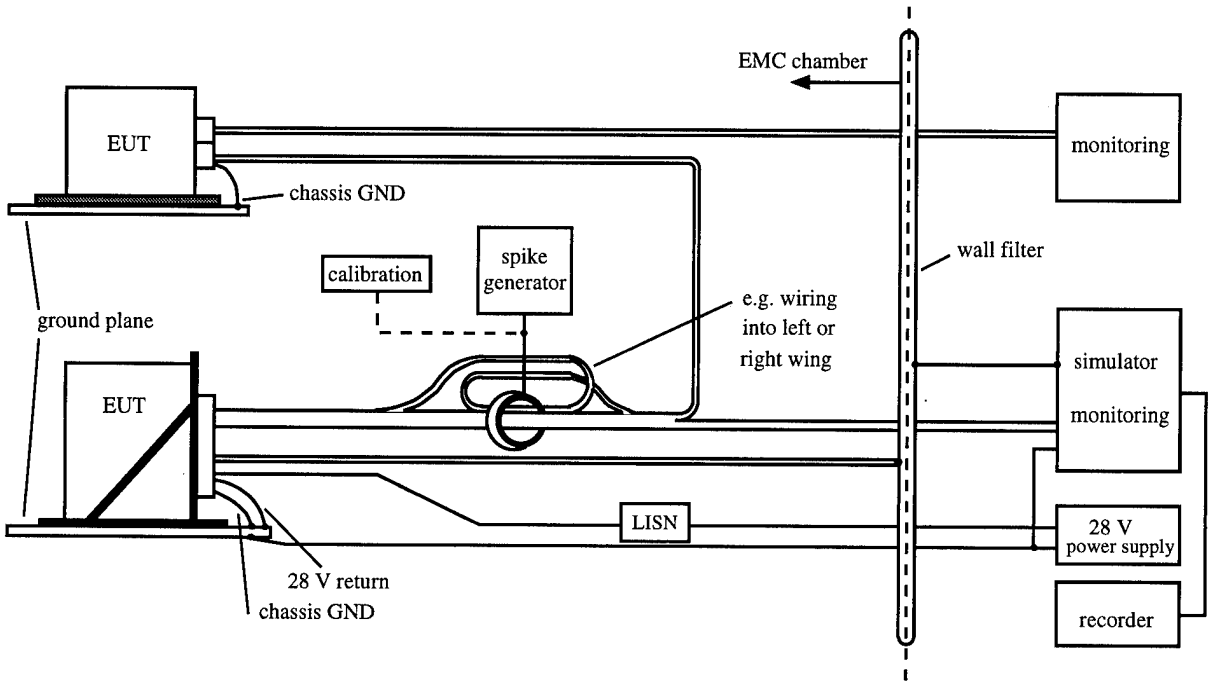



**Fig. 1: Multiple Stroke/Burst Test Setup for non-IMA Avionics**

For modular avionics the situation is more complex. Within a given cabinet modules are installed that possibly perform several different functions, having interconnecting wiring into different areas of the aircraft, while also sharing common resources (e.g. sensors) and having different airworthiness criticality. Therefore, the test procedure has to define as far as necessary the different test levels simultaneously e.g. to be injected into a certain cable bundle, as well as the specific pulse spacing if needed. In Figure 2 a basic test setup is shown.

It may well prove to be more complicated to set up the loads and equipment connected to the IMA cabinet, as well as monitor their function in a practical test environment, than to generate and induce the necessary test conditions. While it can be discussed whether the differences in the test levels can be limited, the interaction of the LRMs in the cabinet with each other through shared resources makes it necessary to have them all tested together. Accordingly, the test effort gets further increased, should it prove to be necessary to test one or more LRMs in different operating modes. Under these circumstances the qualification testing for a given number of functions will be at least as extensive as with the same functions distributed over several "black boxes".

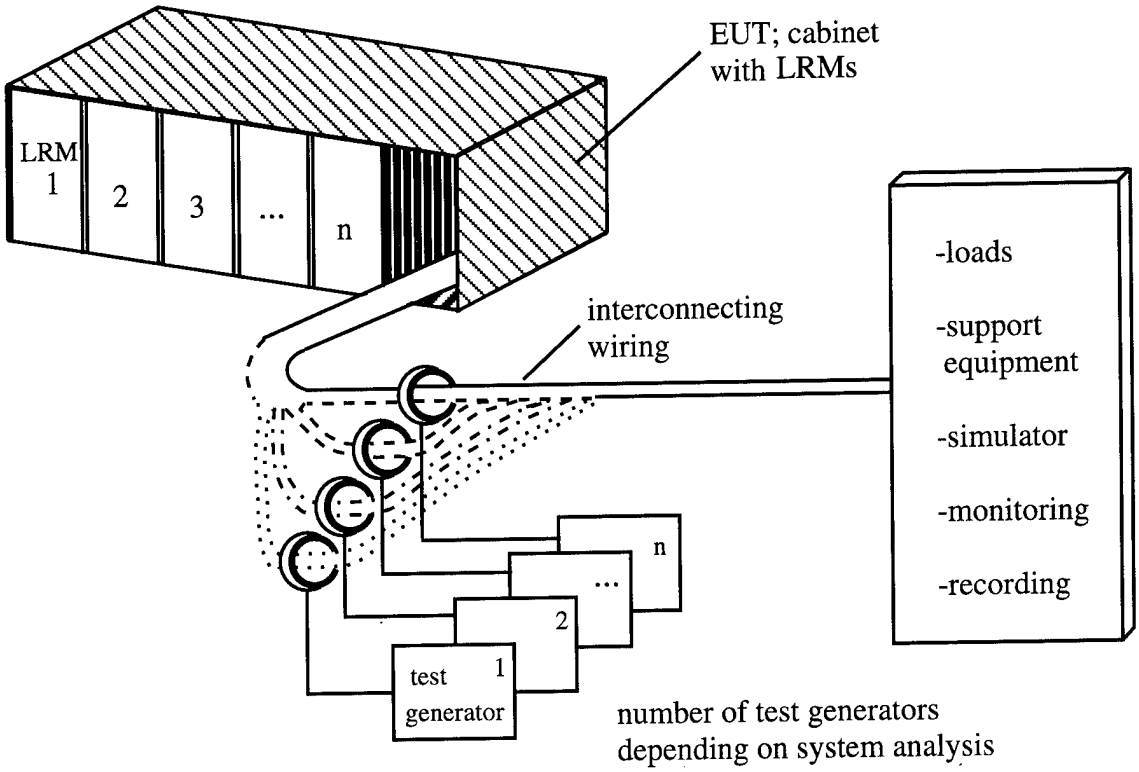



**Fig. 2: Setup for IMA Functional Upset Test**

### 3.2. Modifications

Any modification to an equipment will have to be assessed for its impact on the validity of the initial qualification. Integrated modular avionics are not exempt from this. An advantage could be the level of standardization on the LRM level together with the use of spare hardware. While it may be possible for the damage test portion to have a qualification by similarity to an identical protection-LRM hardware combination, for the functional upset tests this may not be possible. Accordingly, it will be difficult to maintain the cost advantage gained in other areas by the introduction of modular avionics, because in the case of a certain level of modifications, the qualification effort will be higher than with former avionics structures.

## 4. DISCUSSION

This paper wants to point at areas of the lightning protection for, and qualification testing of modular avionics that are not yet well defined.

The proposal to distribute the equipment protection devices between cabinet and LRM is problematic since it may introduce an electromagnetic disturbance into the backplane area of the cabinet. Furthermore, this type of lightning protection does not significantly (if at all) reduce the effort and cost of qualification testing.

Accordingly, a dedicated protection/filter module at the interface to the aircraft wiring provides the desired separation and a clean backplane for the cabinet. It may however pose problems in the case of modifications of the equipment and interfaces external to the IMA cabinet.

Though multiple stroke/burst functional upset testing is not explicitly defined in DO-160 C, together with the Advisory Circular [4] test conditions can be drawn up for a qualification test procedure. More problematic seems to be the suggestion in [4] to use test levels derived from the internal environment and to select pulse spacing and possibly the frequency of the waveform 3 after an analysis for a system susceptibility associated with this. This is deemed to be overly severe and not well supported by the random nature of the lightning event. Where needed, the airframe and wiring resonance frequencies can be used. As the equipment has to be tested for damage tolerance anyway, it seems possible to use test levels, which only in unusually severe cases are related to the internal environment. Otherwise some arbitrary level can be determined that is high enough to stress the protection, but otherwise only aims at inducing a functional upset in susceptible system components.

With respect to the open questions of qualification and certification, it seems doubtful that in the area of lightning protection and qualification testing, modular avionics offer a significant cost benefit over the currently used avionics.

## 5. REFERENCES


[1] ARINC Specification 654
"Environmental Design Guidelines for Integrated Modular Avionics Packaging and Interfaces"

[2] ARINC Specification 650
" Integrated Modular Avionics Packaging and Interfaces"

[3] RTCA DO-160 C
"Environmental Conditions and Test Procedures for Airborne Equipment"
Change 2 promulgates Section 22: "Lightning Induced Transient Susceptibility"

[4] Advisory Circular 20-136
"Protection of Aircraft Electrical/Electronic Systems Against the Indirect Effects of Lightning"

# EMC SPECIFICATIONS FOR MODULAR AVIONICS

Patrick Farfal
AEROSPATIALE - Espace & Défense
Boîte postale n° 2
78133 Les Mureaux Cedex, FRANCE
Telephone (33) 1 34.92.23.70 FAX (33) 1 34.92.13.11

Georges Chambert
AEROSPATIALE - Espace & Défense
Boîte postale n° 2
78133 Les Mureaux Cedex, FRANCE
Telephone (33) 1.34.92.31.06 FAX (33) 1 34.92.17.34

## ABSTRACT

Modular avionic equipment, or Multi-Manufacturer Boxes, result from a major trend in some avionics applications. These boxes include Sub-assemblies made by several Manufacturers, on the responsibility of the Prime Contractor.

In order to prevent conflicts which might occur during the integration stage, EMC specifications must be adapted to this type of box.

Near-field and conduction environments, including lightning and nuclear environments, can be specified; simple models allow a quantified approach.

Simple test procedures can be defined.

An overall approach for the implementation of these new specifications is proposed, considering the responsibilities of each Manufacturer.

## INTRODUCTION

This paper deals with the EMC Specifications for lightning and other electromagnetic environments applied to on-board electronic boxes which include functional modules or printed circuit (PC) boards made by several Manufacturers, on the responsibility of the Prime Contractor. This type of electronic box is an example of **modular avionics** (or racked package), called **"Multi-Manufacturer Box"**.

Such a box comprises a case which delimits an electromagnetic area shared by the modules or PC boards.

Common EMC Specifications refer to electronic boxes with well materialized electromagnetic boundaries, and whose industrial responsibility is assigned to one Manufacturer (at least from the Prime Contractor's point of view).

It is not the same for Multi-Manufacturer Boxes, in which the coexistence of modules and PC boards from several sources may induce conflicts that system level specifications can and must prevent.

So, the Prime Contractor, responsible for the EMC of his system, has to adapt the methods of management and control of EMC, while assigning clear responsibilities to each Manufacturer. Then, it is necessary to:

• determine the items to be dealt with: emission/susceptibility, conduction/radiation, protection against external stresses,
• define the related specifications,
• propose a checking approach,
with a clear assessment of industrial responsibilities.

It will be pointed out, from a few examples, that this problem has a solution.

## MULTI-MANUFACTURER BOXES

### A - CONCEPT

So far, the most commonly met architectures of on-board subsystems have been "exploded" ones, i.e. shared in several separate boxes, for example inertial measurement unit, guidance or flight control computers, ordnance subsystem... For a few years, a trend towards gathering electrical and electronic functions into one box (or a limited number of boxes) has appeared. This type of architecture results in a simplified system, weight spare and easier operational use.

So, a Multi-Manufacturer Box consists of a case housing electronic modules and PC boards, arranged side by side, without materialized electromagnetic boundaries (in order to take advantage of the concept by simplifying the mechanical design and reducing size and weight), and designed and delivered by several Manufacturers, according to their capabilities.

### B - GENERAL DESIGN

Every preliminary design of a system starts with the definition of a functional and physical architecture:
• functional and physical partition of the system, defining the functions and their materialization,
• internal functional and physical links: nature of the information transferred, data media, electrical and mechanical interfaces.

The basic part of a Multi-Manufacturer Box can be a **Receiving Sub-assembly** which at least consists (see figure 1) of:
• a **case**, which is the mechanical boundary of the box, therefore the mechanical interface with the vehicle; it comprises the standard locations dedicated to the various modules from several origins, the internal wiring and connectors, the external connectors;
• an **internal power distribution system** (inverter) delivering, from the vehicle power supply, the standard voltages to the functional modules,
• **a standardized data distribution system** (bus and bus controller).

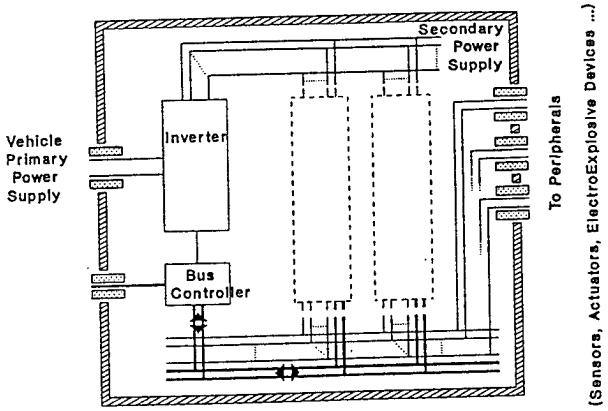



FIGURE 1
RECEIVING SUB-ASSEMBLY

## PROBLEMS RELATED TO THE MULTI-MANUFACTURER BOX CONCEPT

### A - GENERAL

The main technical problem is the development which proves to be more critical than in the case of an "exploded" (or multi-box) architecture, because of the mixing of various functions, particularly through the "link functions" (power supply, data transmission, mechanical links). Obviously, this problem immediately appears coupled to an industrial one, since several Manufacturers are closely involved in the development of the box.

These drawbacks are not, by nature, different from those met in a multi-box architecture, but they get sharper there, in case of changes, either from the evolution of system requirements or, above all, from difficulties met during the integration phase (internal environment for example).

Then, the solution lies in reinforcing the technical and industrial management by the Prime Contractor. Electromagnetic Compatibility is an example of that, in order to control the internal electromagnetic environment, regarding the responsibilities of everyone.

### B - EMC OF A MULTI-MANUFACTURER BOX

The control of EMC between all the **Sub-assemblies** of the box (from now on this term will include all the internal constituents: modules or PC boards, electronic Receiving Sub-assembly) needs:

- a preliminary analysis of the electromagnetic features of their interfaces,
- the definition of a method for checking these interfaces,
- a specification, so as to guarantee electromagnetic margins.

This problem is not different from the one met by every Manufacturer who has to assemble a box in a usual manner; but in that case, the Manufacturer is fully responsible for the internal EMC of his box, whereas in a Multi-Manufacturer Box this responsibility rises to the system level; so this system level responsibility involves the Prime Contractor, who has to prevent potential conflicts, which might only occur during the integration stage, therefore late in the development.

### C - EMC CONCERNS

EMC generally considers two environment areas: Radiation (R) and Conduction (C) and two specifications areas: Emission (E) and Susceptibility (S), which leads to four types of specifications (see MIL-STD 461):

RE = Radiated Emission
RS = Radiated Susceptibility
CE = Conducted Emission
CS = Conducted Susceptibility

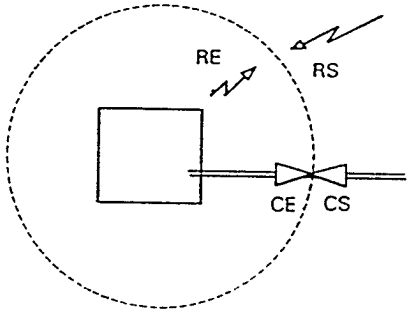



FIGURE 2
EMC CONCERNS

Radiation

The radiation interface between two Sub-assemblies is an immaterial surface located at most within a few centimeters of each Sub-assembly; its field-characterization cannot be deduced from usual tests performed at a 1 meter's distance: specifications and procedures must

be adapted. It will be shown that the near-field level is mostly dominated by the compatibility between Sub-assemblies, whereas external specifications are less severe at the Sub-assembly level.

On the other hand, the radiation interface with other parts of the vehicle (outside the box) is relevant to existing specifications and procedures.

Conduction

External links (vehicle primary power supply, command and control links to and from outside the box), each type of which generally regards only one Sub-assembly, are relevant to the EMC of a traditional box (CE, CS, see figure 3).

On the other hand, the Receiving Sub-assembly comprises some resources which are shared by several Manufacturers:

- data distribution (bus), usually standardized,
- secondary power supply with no general specification, but some existing standards which can help the Prime Contractor make up the "secondary" specifications (see figure 3):

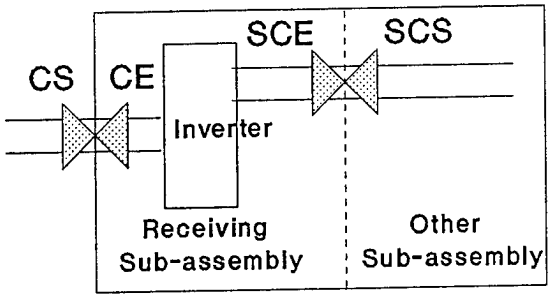



FIGURE 3
CONDUCTION SPECIFICATIONS

SCE = Secondary Conducted Emission
SCS = Secondary Conducted Susceptibility

Obviously, the inverter shall meet the external specifications in order to contribute to the overall compatibility of the box. It can be seen that the Manufacturer in charge of the Receiving Sub-assembly and those in charge of other Sub-assemblies do not have the same responsibilities, since they do not deliver according to the same specifications.

Lastly, the Prime Contractor has to take into account the need for hardening against lightning or nuclear electromagnetic pulses (L EMP and N EMP). For these types of threats, the aggressions against the electronic boxes are mostly dominated by the conducted signals generated by the coupling on the cable harnesses.

Specific protection devices must be introduced in order to meet the requirements of good behaviour of the box, which is a complete system.

## NEAR-FIELD CHARACTERIZATION

### A - PREPONDERANCE OF CONSTRAINTS BETWEEN SUB-ASSEMBLIES OVER EXTERNAL CONSTRAINTS FOR THE NEAR-FIELD ENVIRONMENT

We will show that the requirements of MIL-STD-461 (RE 101, RE 102, RS 101, RS 103) are less constraining that those induced by the closeness of the Sub-assemblies.

After giving a summary of the MIL-STD specifications, we will estimate:

- the amplitudes of currents on the Sub-assembly PC boards necessary for generating the fields specified by RE 101 and RE 102 outside the box,
- the amplitudes of voltages induced onto the Sub-assembly PC boards when the box has to undergo the RS 101 and RS 103 fields,

taking into account a typical case attenuation.

Summary of the MIL-STD-461 of interest (for each specification, the most constraining one has been chosen, even if the whole is unconsistent)

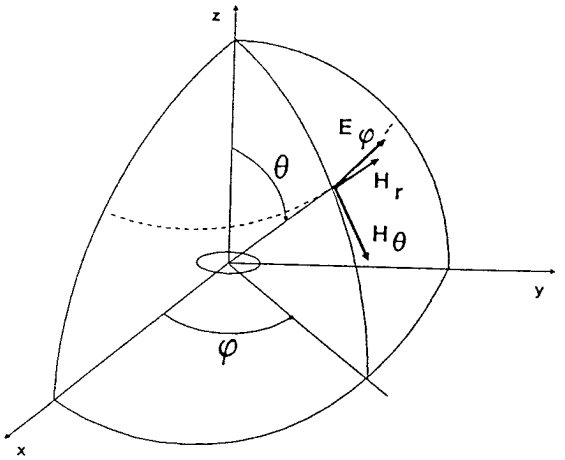
| | Field Component | Distance from box faces | Limits |
|---|---|---|---|
| RE 101 (Navy) | B | 7 cm | from 165 dBpT @ 60 Hz<br>155 dBpT @ 400 Hz<br>112 dBpT @ 2 KHz<br>to 78 dBpT @ 100 KHz |
| RE 102-2 (Aircraft and Space Systems | E | 1 m | from 60 dBµV/m @ 10 KHz<br>to 28 dBµV/m @ 1 MHz (†) |
| RS 101-2 (Army) | B | | from 180 dBpT @ 60 Hz<br>to 116 dBpT @ 100 KHz and above |
| RS 103 (Space) | E | | 20 V/m 10 KHz-40 GHz (†) |

TABLE 1

(†) The study will be limited to 1 MHz.

Modeling of radiating sources and susceptible circuits

The radiating components of a piece of equipment are small compared with the wavelength, taking account of their sizes and the frequencies of the fields. Then, they behave like radiating doublets. As the voltages and circuits impedances are rather low, conduction currents are the main emitting sources, so they can be modelled as magnetic doublets, which generate the following fields:




$$\begin{cases} H_r = \frac{k^3}{2\pi} M \cos\theta \left[ \frac{1}{(kr)^2} - \frac{i}{(kr)^3} \right] e^{-ikr} \\ H_\theta = \frac{k^3}{4\pi} M \sin\theta \left[ \frac{1}{kr} - \frac{i}{(kr)^2} - \frac{1}{(kr)^3} \right] e^{-ikr} \\ H_\varphi = 0 \end{cases}$$

$$\begin{cases} E_r = 0 \\ E_\theta = 0 \\ E_\varphi = 30 k^3 M \sin\theta \left[ \frac{1}{kr} - \frac{i}{(kr)^2} \right] e^{-ikr} \end{cases}$$

$M = S\,I$ = loop area x current $\qquad k = \frac{2\pi}{\lambda}$

FIGURE 4
FIELDS GENERATED BY A MAGNETIC DOUBLET

The 1/kr components are relevant to RE 102 and RS 103 specifications, the $1/(kr)^2$ components to RE 101 and RS 101; the $1/(kr)^3$ components will be relevant to near-field specifications (1 to 2 cm).

We assume that the fields are generated by loops whose sizes will be represented by parameters as follows:

| Loop | Sizes (cm) | Area ($cm^2$) |
|---|---|---|
| 1 | 16 x 24 | 384 |
| 2 | 8 x 12 | 96 |
| 3 | 4 x 4 | 24 |
| 4 | 2 x 3 | 6 |

Loop 1, for example, could represent a power supply link around a PC board inside a usual piece of equipment.

The same sizes of loops will be used for susceptibility estimates.

Attenuation of box case

We use a typical law given in figure 5 for H-field:

The following estimates are limited to 1 MHz; above this limit, results are meaningless because of the large attenuation, and in addition, above 1 GHz, models are not sufficient.

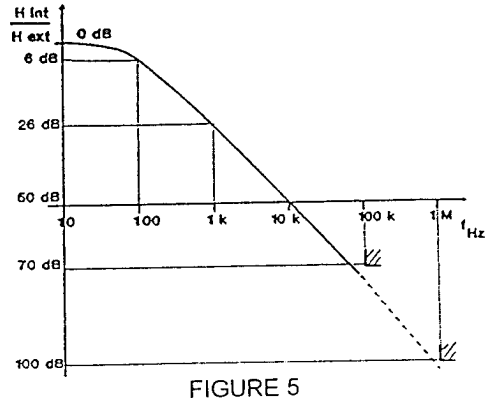



FIGURE 5
CASE H-ATTENUATION

Comparison between functional currents or voltages and those resulting from emission or susceptibility specifications

- With respect to RE 101-1:

let us assume an emitting loop close to the wall of the box, in order to meet the 7 cm distance requirement; the internal currents capable of generating specified fields ($H_r$ component) are given by table 3:

| Frequency (Hz) | 60 | 400 | 2 K | 10 K | 100 K | Loop type |
|---|---|---|---|---|---|---|
| Maximum allowed current (A) | 71 | 125 | 0.440 | 0.710 | 0.710 | 1 |
| | 93 | 164 | 0.580 | 0.930 | 0.930 | 2 |
| | 222 | 393 | 1.40 | 2.22 | 2.22 | 3 |
| | 760 | 1340 | 4.8 | 7.6 | 7.6 | 4 |

TABLE 3

Evidence for potential conflicts appears inside the dotted line, since the maximum allowed currents are of the same order of magnitude as functional currents met in on-board applications. But it must be pointed out that in many cases RE 101 limits can be exceeded without nuisance for next boxes, and in many programs the specification can be alleviated.

• With respect to RE 102-2:
the component specified in RE 102 is the E-field, so $E\varphi$ must be estimated; this component is maximum in the direction $\theta = 90°$, where $H_r$ is worth zero but $H_\theta$ is maximum. The maximum allowed currents will be estimated from $H_\theta$, through the wave impedance $E_\varphi/H_\theta$ in the direction $\theta = 90°$, whose low value (less than 1 ohm to a few ohms) clearly shows the magnetic feature of the wave at this distance.
Even for the largest loop (1), the calculations result in hundreds of amperes; such amplitudes of disturbing currents are quite unrealistic, so the RE 102-2 cannot induce any constraint onto near-field specifications.
To understand these surprising results, it must be noticed that the specifications are applied to boxes with their cables, whose sizes lead to magnetic moments of the same order of magnitude, with currents lower than in the case of internal loops.
• With respect to RS 101 and RS 103:
the voltages induced by the specified fields onto the largest loop (1) only rise to a few mV at very low frequencies, and more often to hundreds of µV or less.
Then, RS 101 and RS 103 requirements cannot induce constraints onto near-field specifications, which shall be limited far below these values.

B - NEAR-FIELD REQUIREMENTS CONSIDERING INTRA-BOX COMPATIBILITY

The aim is to estimate the voltages induced by the listed emitting sources (bus signals, pulsed control signals, ...) by means of coupling models, and to compare the resulting values with the susceptibility thresholds of electronic functions considered as receivers of these emissions.

Coupling approach

Assuming that the only couplings to be taken into account are those between two Sub-assemblies at a distance of 15 mm from each other (average distance between PC boards from different Manufacturers), the parameter of this study is the mutual inductance between an emitting and a receiving loop, whose sizes have been defined above.

The open-circuit voltage $\upsilon_{20}$ is related to the receiving loop (its value is a susceptibility level):
$\upsilon_{20} = M\ di1/dt$ (time domain)
$V_{20} = jM\omega I_1$ (frequency domain),
whereas $i_1$ is the disturbing current. So, M can be specified, given the susceptibility threshold (loop 2) and the operating current (loop 1).

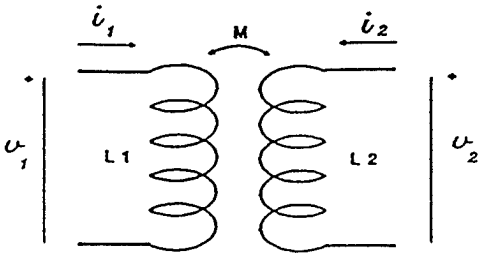



FIGURE 6
COUPLING MODEL
1: EMITTING LOOP
2: RECEIVING LOOP

For loops at a distance of 15 mm from each other, M is given (nH) by table 4:

| Loop | 1 | 2 | 3 | 4 |
|---|---|---|---|---|
| 1 | 213<br>[95] | | | |
| 2 | 53<br>[26] | 98<br>[68] | | |
| 3 | 13<br>[8] | 24.5<br>[24] | 37<br>[32] | |
| 4 | 3.3<br>[3.5] | 6.1<br>[6.3] | 9.2<br>[9.0] | 8.6<br>[8.2] |

TABLE 4

The values inside brackets are measured values, but on loops inside a metallic box; the difference with free-space values can reach a factor of 2 for the largest loops.

It must also be pointed out that the coupling is the largest when both loops have the same size.

Estimate of allowed mutual inductances

Restricting to the time domain, we consider the following signals:

| | Typical characteristics | | | Limits of disturbance |
|---|---|---|---|---|
| Control signal (relay, ordnance, ...) | 0/28 V | 500 mA | tr = 10 µs | 5 V |
| Bus signal | ± 7 V | 100 mA | tr = 100 ns | 50 mV (†) |

TABLE 5

(†) arbitrary value; depends on the allowable bit error rate.

These values result in allowed mutual inductances as follows (without margins):

| | | Receiver | |
|---|---|---|---|
| | | Control | Bus |
| Source | Control | 100 µH | 1 µH |
| | Bus | 5 µH | 50 nH |

TABLE 6

The bus distribution system may lead to a critical situation, first due to its large susceptibility (which could be lower if a higher bit error rate was allowed), but above all because of its wide spectrum.

The same approach is applicable to the frequency domain.

C - NEAR-FIELD LIMITS ASSESSMENT

Test procedure

Specifying a magnetic field (in dBpT or dBµA/m) or the current which generates it through a given circuit is equivalent. It is even easier to implement the coupling with a given loop at a given distance than to measure a field with a near-field probe.

The test loop, either in a susceptibility or in an emission test, is the loop 1 (16 x 24 = 384 cm²), located at a distance of 15 mm from the PC board of the Sub-assembly under test (size to be confirmed by an experiment at high frequencies).

Susceptibility specification

Let us deal with the transient susceptibility, assuming that 50 nH is the maximum allowed coupling.

The tightest coupling is obtained with loops of equal size (see table 4). A 50 nH coupling is realized by two 55 cm² loops at a distance of 15 mm from each other. With a 384 cm² test loop, the same 55 cm² critical loop offers a 30 nH mutual inductance. So, by impressing a current multiplied by 50/30 in the test loop, the result on the loop under test will be identical.

Referring to tables 5 and 6, the 50 nH limit guarantees immunity, in the loop under test, from current variations of 100 mA in 100 ns, which leads to 100 x 50/30 = 170 mA in 100 ns in the test loop, without margin. The recurrence of the current in the test loop is that of the functional bus signal (1 MHz for example).

This approach can be applied to continuous wave susceptibility requirements, and to narrow or wide-band emission limits.

## CONDUCTION CHARACTERIZATION: SECONDARY POWER SUPPLY NETWORK

This problem, like the near-field characterization problem, also has a solution, but unlike the previous one, it cannot have a theoretical solution, as emitting sources and susceptibility thresholds depend on of too many uncontrolled parameters.

Referring to figure 3, we can define, for **Secondary Conducted Emission**:

$SCE_S$ as Secondary Conducted Emission from Source (i.e. Receiving Sub-assembly)
$SCE_L$ as Secondary Conducted Emission from Load (i.e. other Sub-assembly)

illustrated by figure 7:

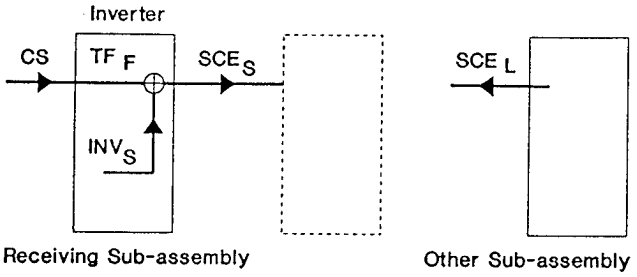



FIGURE 7
SECONDARY CONDUCTED EMISSION

where:

- $INV_S$ is the Inverter noise on a resistive load (steady-state noise)
- $TF_F$ is the Forward Transfer Function of the Inverter.

A Sub-assembly is considered as a simple load, with traditional $SCE_L$ specifications, whereas, for the Receiving Sub-assembly, the following symbolic equation can be written:

$$SCE_S = INV_S + CS \times TF_F \quad (1)$$

Then, the two types of Sub-assemblies do not play identical roles as regards EMC requirements.

For **Secondary Conducted Susceptibility** we define:

$SCS_S$ as Secondary Conducted Susceptibility towards Source (i.e. Receiving Sub-assembly)

$SCS_L$ as Secondary Conducted Susceptibility towards Load (i.e. other Sub-assembly)

These specifications can be derived from the emission specifications by adding the desired margins:

$$SCS_L = SCE_S + n\ dB\ (2)$$
$$SCS_S = SCE_L + n\ dB\ (3)$$

where n = 6 in the lower part of the spectrum whereas 20 to 30 is better in the higher part. It should be noted that these relations are symbolic, since $SCS_L$ and $SCS_S$ do not have the same units ($SCE_L$ is defined as a current variation).

The two types of Sub-assemblies do not either play the same roles there: the susceptibility test of the Receiving Sub-assembly shall add a reinjection measurement so as to meet the CE specification of the complete box (see figure 8):

$$CE = INV_P + SCS_S \times TF_R\ (4)$$

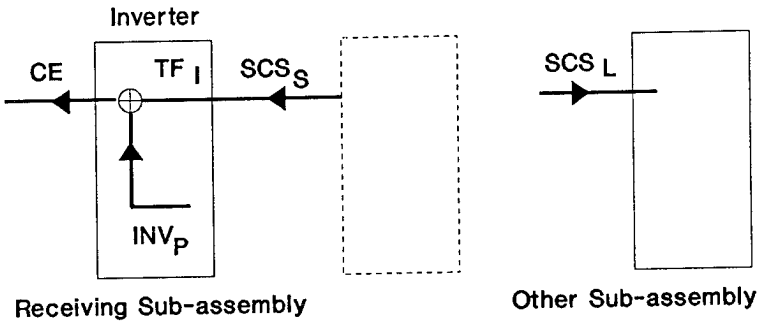



FIGURE 8
SECONDARY CONDUCTED SUSCEPTIBILITY

where:

- $INV_P$ is the noise reinjected by the Inverter only towards the primary power network,
- $TF_R$ is the Reverse Transfer Function of the Inverter.

$SCE_S$, $SCE_L$, $SCS_S$, $SCS_L$ requirements will be deduced from CE and CS requirements through equations (1) to (4), given the characteristics of the inverter ($INV_S$, $INV_P$, $TF_F$, $TF_R$); these characteristics can only be known from experience by means of statistical experiments which can previously be performed on Inverters and PC boards of the same type as in the Multi-Manufacturer Box.

This approach amounts to establishing standards for the transfer functions, for example.

If this experimental data is missing, specifications can be drawn from some existing standards.

For example, the perturbations emitted by Sub-assemblies may be adapted from VXI bus specifications (see figure 9)

Test procedures may be drawn from MIL-STD-462.

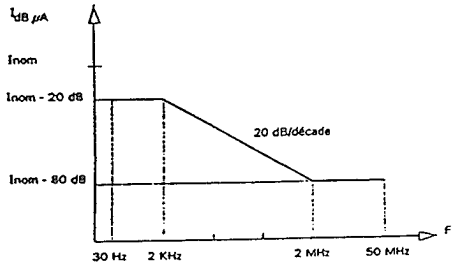



FIGURE 9
$SCE_L$ LIMITS

## CONDUCTION CHARACTERIZATION: L EMP AND N EMP REQUIREMENTS

These environments are mainly expressed in terms of conduction specifications, as cable bundles are the main penetration way to the electronic boxes.

Protection devices, in general surge suppressors and filters, are defined from the specifications, and implemented according to state-of-the-art rules which prescribe efficient grounding and possibly an electromagnetic separation of the filtering area from the rest of the box (clean area). So these protections must be located immediately behind the case connectors, as they are attached to a well materialized electromagnetic boundary.

Under these conditions, the residual signals which could be reinjected into a Sub-assembly do not need any specific protection at the inputs/outputs of the Sub-assembly, as it could be in a usual electronic box.

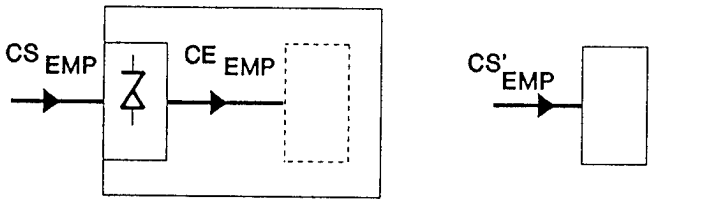



FIGURE 10
EMP REQUIREMENTS

All the inputs/outputs of a Sub-assembly will need a processing of EMP signals in the Receiving Sub-assembly; this processing is done by protection devices, whose definition is derived from $CS_{EMP}$ and $CE_{EMP}$ (therefore $CS'_{EMP}$) specifications; the Receiving Sub-assembly thus appears to be responsible for the overall good behavior of the Multi-Manufacturer Box.

Then the Receiving Sub-assembly, in addition to the above-mentioned basic functions has to comprise the L EMP and N EMP protection devices.

Test procedures are usual ones.

## VERIFICATION APPROACH

The bottom-up-type verification phase, complementary to the top-down-type specification phase, must contribute to the proof of overall EMC, taking in account the industrial responsibility of each Manufacturer involved in the design and delivery of the Sub-assemblies.

It is the responsibility:

- of the designer and manufacturer of a Sub-assembly to prove that his product meets the internal requirements,
- of the box integrator, who will probably be the designer and manufacturer of the Receiving Sub-assembly, to prove that his product meets the EMC internal and external requirements, and to characterize the electromagnetic interfaces between Sub-assemblies,
- of the Prime Contractor to prove the EMC of the whole box.

For example, qualification tests in radiation comprise the following proofs:

| | RE | RS | Near-field RE | Near-field RS |
|---|---|---|---|---|
| Receiving Sub-assembly | X | X | X | X |
| Sub-assembly | | | X | X |
| Whole box | X | X | | |

## CONCLUSION

We have listed the EMC problems to be solved in a Multi-Manufacturer Box, example of modular avionics, whose standard resources are shared among several designers and Manufacturers of Sub-assemblies.

These problems have quickly proved to be quite different from those usually set by traditional boxes, and moreover coupled with an industrial responsibility problem; new problems must be solved by the Prime Contractor, since no Manufacturer has the whole responsibility for the EMC of the box:

- control of the internal radiated environment (near-field requirements),
- guarantee of good behavior of Sub-assemblies connected to the secondary power network (shared among several Manufacturers),
- protections against lightning and nuclear EMP.

From a few examples, it has been shown that a solution exists:

- near-field compatibility, with simple coupling models resulting in simple specifications and test implementation,
- conduction compatibility, needing an experimental approach but likely to be preliminarily solved by means of existing standards,
- lightning and nuclear EMP, for which protection devices can be implemented in the same way as in a usual piece of equipment.

The capability of specifying, defining test procedures and establishing a verification approach, while regarding everyone's industrial responsibilities, is a guarantee for the Prime Contractor to control the ElectroMagnetic Compatibility of the Multi-Manufacturer Box.

## REFERENCES


1 - MILITARY STANDARD 461
Requirements for the control of electromagnetic interference
Emissions and Susceptibility - 11 January 1993

2 - MILITARY STANDARD 462
Measurement of electromagnetic interference characteristics - 11 January 1993

3 - H. JAEGER, MBB-Deutsche Aerospace,
"Study note on HERMES Space Vehicle Avionic Bay Module EMC Requirements (1992)"

4 - IEEE Standard for VME bus Extensions for Instrumentation: VXI bus
IEEE STD 1155 - 1992

# SESSION 05A
# SPECIFICATIONS AND STANDARDS
# CHAIRPERSON: BILL WALKER

# TRIGGERED AND INTERCEPTED LIGHTNING ARCS ON AIRCRAFT

J.-L. Boulay

Office National d'Etudes et de Recherches Aérospatiales
BP 72, 92322 Châtillon Cedex, France
Telephone 46.73.48.55

## SUMMARY

Triggered and intercepted lightning events on aircraft can be perfectly defined by their electrostatic and electromagnetic signatures. A number of electromagnetic signatures were recorded during the lightning experiments conducted with the FAA CV580 and the DGA TRANSALL aircraft.

The two kinds of electromagnetic signatures are strongly related to the atmospheric electric field properties; critical values of the E-field are now identified for triggered and intercepted lightning events.

In the present paper, the electromagnetic signatures corresponding respectively to triggered and intercepted lightning flashes are described with associated lightning currents.

A global analysis of the physical processes involved in the two configurations is proposed; for the triggered lightning flash attachment phase, the theory of the bidirectional leader seems to be correctly validated. Some experiments carried out in laboratory are presented and discussed briefly in the light of this new model.

For the intercepted lightning event, the electromagnetic signature gives some qualitative indications about the nature of the electric discharges which occur around the aircraft. Hypothesis about the corresponding physical phenomena are presented and analyzed.

We conclude the paper by giving some indications about the zoning problem which seems to be one the most important problems to be solved after these in flight lightning programs.

## INTRODUCTION

When an aircraft flies nearby or through clouds, it may be affected by phenomena involving electrical or electromagnetic processes: The electrostatic discharges (ESD) and the lightning discharges. The former are relatively frequent in a cloud environment, but they are not really dangerous except under some very specific conditions; the latter are not so common but are more severe and may sometimes lead to catastrophic accidents.

ESD discharges on aircraft essentially disturb radio communication and radio navigation equipment [1] [2]. Under certain conditions, strong ESD discharges may occur on dielectric frontal surfaces of the airframe, such as radomes, windshields

and antenna covers, leading to more severe effects and sometimes to the equipment destruction. The aircraft's ESD protection is relatively simple in principle: Static dischargers or antistatic treatments on nonconductive surfaces considerably reduce ESD interference [3]. But applying these protection systems is more delicate in practice. New optimized methods and new controlling equipment were developed in this domain over recent years and their applications are now just starting.

Lightning discharges, depending on their current amplitude, are generally considered as more severe than ESD. The discharge current passing through much of the airframe gives rise to strong electromagnetic fields which can penetrate the airframe skin by diffusion or by aperture coupling. The resulting fields inside the airframe may be sufficient to yield strong current pulses at the inputs of sensitive internal equipment. These pulses may create disturbances and equipment failures. When the lightning phenomenon is very severe, direct current effects may leave holes or even completely destroy external systems. Until now, aircraft were protected against the direct effects of a lightning flash, and more particularly certain essential components like radomes, antenna covers, wing tips, and fuel tanks. Because of the conductive properties of the essential parts of the airframe and the relatively low susceptibility of electronic equipment, the indirect effects of lightning were not considered to be as dangerous as the direct effects.

With today's new structural materials, like composites and epoxy panels, combined with the increasing role of the electronics and the greater susceptibility of electronic components, aircraft engineers now have to consider the electromagnetic effects of the lightning [4].

When these new considerations appeared ten years ago, most experts arrived at the conclusion that only a few characteristics concerning lightning interactions on aircraft were known. Most of the knowledge was in fact coming from actual lightning stroke data and analysis of ground observations by different laboratories. No measurements were available for aircraft struck by lightning.

This led the lightning research community to decide in favor of in-flight research. From 1980 to 1988, three main experiments were carried out:

- Two were undertaken in the USA by NASA [5, 6] and the USAF [7, 8, 9].
- The third was conducted in France under the auspices of the French DGA (General Delegation for Armament) [10, 11, 12].

Briefly speaking, these three programs yielded essentially the same general results, and the data is very important because, after in-flight result analysis, our view of the lightning interactions with an aircraft changed completely. In particular, we now know that the lightning flashes are usually triggered by the aircraft itself. The idea of an aircraft intercepting a pre-initiated natural discharge is not rejected, but its occurence probability is low.

New characteristics of the lightning threat were found, in particular the multiple burst phenomena at the beginning of the event and the multiple stroke mechanism during the permanent phase of the lightning flash. Specific processes, like the sweeping mechanism, were validated in flight and observed by accurate instrumentation.

In this paper, we focus on data obtained in flight with the TRANSALL aircraft; we describe in detail the triggered and intercepted lightning arcs by their electrostatic and electromagnetic signatures; we present the physical mechanisms associated with the two configurations and we conclude by some remarks concerning the aircraft zoning problem.

## AIRCRAFT INSTRUMENTATION

ELECTROSTATIC MEASUREMENTS--It is obvious that a lightning flash can be obtained on an aircraft in a very active electrified cloud such as a cumulo-nimbus. In fact, it is not necessary that an aircraft fly inside the cloud to be struck by a lightning discharge. Lightning phenomena may be encountered in the vicinity of a storm region or of cloud debris after a storm dissipation period.

In most cases, we observe that the lightning flash is triggered by the aircraft itself, which means that no lightning activity would occur in the absence of aircraft. Under these conditions, two parameters are essential in defining the triggering conditions:

- The external atmospheric E-field.
- The aircraft potential.

As an aircraft is isolated in the air, the only way of measuring these two parameters is with surface electrostatic field sensors. With the only external field $E_0$, the aircraft structure considerably changes the configuration of the external E-field lines, which depends on the aircraft geometry and the orientation of the E-field axis versus the airframe reference axis. On a point A of the aircraft structure, the resulting local induced field $\vec{E}_A$ is given by:

$$\vec{E}_A = k_{A,i}\,\vec{E}_i + k_{A,j}\,\vec{E}_j + k_{A,k}\,\vec{E}_k$$

where $\vec{E}_i$ $\vec{E}_j$ and $\vec{E}_k$ are the three components of the external E-field $\vec{E}_0$ in the airframe reference axis; $k_{A,i}$ are the local aircraft geometry coefficients and represent the local enhancement of the induced field. At some place on the airframe there is a neutral line with no locally induced charge.

With the hypothesis of only an aircraft potential V, the E-field lines converge towards the airframe and the surface induced E-field on a point A is given by the equation:

$$\vec{E}_A = k_{A,v} \cdot V \cdot \vec{n}_A$$

where $k_{A,v}$ is a geometric coefficient depending on the location of the point A and $\vec{n}_A$ is the vector normal to A.

The superposition of two previous electrical configurations represents the general case of a global electrostatic equilibrium on the aircraft. The resulting E-field in a particular point A is given by:

$$\vec{E_A} = \sum_i k_{A,i} \vec{E_i} + k_{A,v} \cdot V \cdot \vec{n_A}$$

To find the solution for the three components of the external field $\vec{E_0}$ and for the aircraft potential, at least four different sensors are needed at four different points on the airframe. The unknown parameters are then solved by a four-equations system as follows:

$$\begin{pmatrix} E_A \\ \\ \\ E_D \end{pmatrix} = \begin{pmatrix} k_{Ai} \\ \cdots \\ \cdots \\ k_{D,v} \end{pmatrix} \begin{pmatrix} E_i \\ E_j \\ E_k \\ V \end{pmatrix}$$

or

$$\begin{pmatrix} E_i \\ E_j \\ E_k \\ V \end{pmatrix} = [k]^{-1} \ (E)$$

$[k]^{-1}$ is a fourth-order matrix of enhancement factors k, and (E) is a fourth-order vector given by the four different sensors.

All the "k" coefficients may be obtained either by numerical codes solving the Poisson equation or by laboratory measurements carried out on a representative conductive mock-up of the airframe.

Due to accuracy problems in the solution of the previous four equations system, five simultaneous measurements are needed to solve the problem in all flight conditions. A view of the implementation of the five E-field sensors is given in figure 1. The location of the five units is also defined in order to obtain the better measurements accuracy [13].

ELECTROMAGNETIC MEASUREMENTS--In a lightning flash, the airframe is connected at two points A and B by two lightning channels which maintain the electrical contact between the aircraft and the two regions of the cloud with negative and positive charges.

In principle, only one current sensor at A or B is sufficient to measure the global variation of the lightning discharge current. In fact there are at least two physical reasons why this first hypothesis is not valid:

- First is that the two points A and B are not unique. The lightning arcs may be connected at these two points at the event beginning, but one of the root channels may later move along the airframe (sweeping process) due to aerodynamic and magnetic forces.

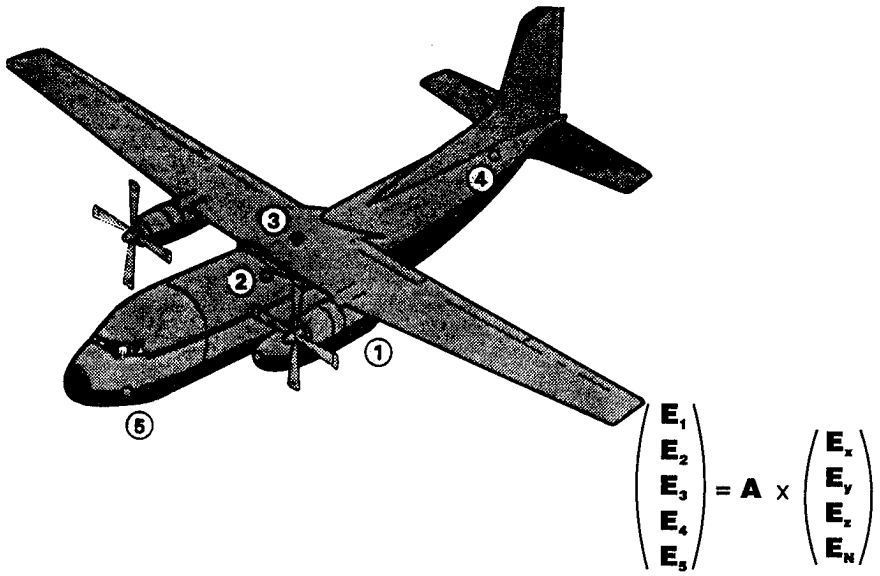



Figure 1. Sensor implementation for electrostatic signature.

- The second reason is related to the interaction of a nearby lightning discharge, with no connection between the discharge process and the aircraft.

The solution to this problem is to measure the electromagnetic interactions at several locations on the airframe at the same time as the lightning current. For a given configuration of the two lightning channels, there is a unique relationship between the current in the lightning arc and the electromagnetic field measured at a given point on the structure. The electromagnetic field is detected by its two components: The electric component E normal to the local airframe surface, and the magnetic component H, which is perpendicular to the current direction.

The relationship between the current and the electromagnetic field is determined in two ways:

1) By a 3D numerical code solving the Maxwell equations. The aircraft structure is represented numerically at the center of the calculation volume, and the two lightning channels are simulated by thin wires connecting the airframe to the boundary layers of the calculation volume. A given current waveform is applied to the wires and the global distribution of the E and H fields is calculated [14].
2) By real-scale with instrumentation of the aircraft. This has to be conducted in a "quasi coaxial configuration", which means that the aircraft is located inside and along the axis of a cylindrical wiring system. A current pulse is applied, by

a Marx HV generator, between an entry point on the aircraft and the return path of the coaxial system. The entry and exit points of the current may be modified in order to represent all the lightning situations encountered in flight.

For the TRANSALL experiment, we used seven $\vec{E}$ and $\vec{H}$ sensors located in different regions of the aircraft structure as shown in figure 2. The implementation of these seven couples of sensors results also from a theoretical approach in order to analyze different situations of the lightning arcs attachment on the airframe.

A complete lightning characterization requires cameras to observe the situation of the lightning arcs on the airframe; six cameras are installed in the cockpit, in the fuselage, and in special enclosures at the wing tips. Special arrangements for I and $\frac{dI}{dt}$ sensors are also installed on the radome, the tail, and at the wing tips.

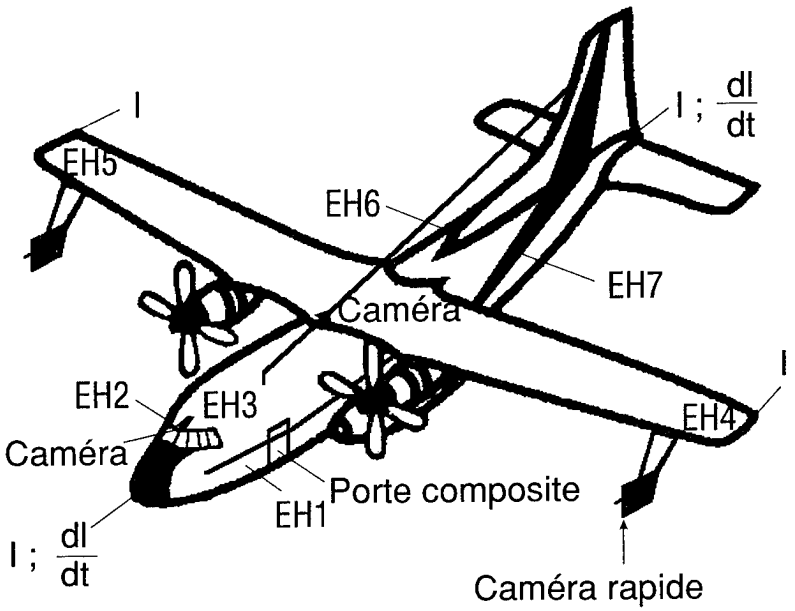



Figure 2. Sensor implementation for electromagnetic signature.

## SIGNATURES OF THE LIGHTNING FLASH

GENERAL OBSERVATIONS--During the CV580 and TRANSALL experiments, 65 lightning flashes were obtained.

Among these 65 events, 60 are triggered flashes (T) and 5 are intercepted flashes (I) giving a ratio $\frac{T}{T + I} = 92{,}3\ \%$.

Most of these lightning flashes are cloud-to-cloud flashes and we consider that the probability to obtain a cloud-to-ground flash is very low even with an aircraft flying at low altitude.

Typical E-field recordings show three successive phases defined as follows:

- A preparatory phase.
- An attachment phase.
- A permanent phase.

a) The preparatory phase

This phase covers all the processes which exist before the first lightning breakdown.

For the triggered lightning flash, this phase lasts sometimes more than 10 s; the outside E-field is observed to increase from 0 and rising to 100 $kV.m^{-1}$. At the end of this phase breakdown triggering is observed.

For the intercepted lightning flash, this preparatory phase does not exist, which means that the external E-field and the aircraft potential remain below the threshold of the E-field sensors.

b) The attachment phase

This phase covers all the existing processes which exist between the first lightning breakdown and the thermalization of the two lightning channels.

This phase has a very short duration: 10 ms for the T flash and 70 ms for the I flash, this phase exhibits very fast variations in the E-field with peak to peak variations of $\pm$ 2 $MV.m^{-1}$. The E-field signatures are totally different for the triggered and intercepted flashes.

For the triggered event, we observe during the attachment phase a repetition of current pulses now known as the MB process (multi burst); for the intercepted event no bursts are observed.

c) The permanent phase (identical for T and I events)

This phase covers all the processes involving the aircraft between the thermalization of the two lightning channels and the extinction of the lightning channels (sometimes the separation of these channels from the airframe).

Following the attachment processes, the permanent phase corresponds to the configuration of the aircraft completely connected by two lightning arcs. The permanent phase may have a duration of 1 s (on rare occasions less than 0.2 s or more than 1.5 s). During this phase, a permanent current is crossing the airframe, and sweeping processes of the two arcs may be observed. At intervals of roughly 100 ms strong current pulses are observed giving the MS process (multi-stroke phenomena).

As a preliminary conclusion and for the T and I flashes, the distinction between the different phases may be resumed as follows:

| | PREPARATORY PHASE | ATTACHMENT PHASE | PERMANENT PHASE* |
|---|---|---|---|
| Triggered lightning flash | - 10 s duration<br>- external field reaches 50 to 100 kV/m before lightning | - 10 to 15 ms duration<br>- same EM signature for all sensors<br>- no induced field effects<br>- burst of pulses (MB) | - 1 s duration<br>- permanent current<br>- repetition of current pulses multistrokes (MS) |
| Intercepted lightning flash | - no evidence of a preparatory phase<br>- low external field | - 60 to 80 ms duration<br>- EM signature depends on sensor location<br>- strong induced field effects<br>- no MB | - 1 s duration<br>- permanent current<br>- repetition of current pulses: (MS) |

* same phase characteristics for T and I events.

We focus now our presentation on electrostatic and electromagnetic signatures which are observed during the preparatory and the attachment phases.

THE TRIGGERED LIGHTNING FLASH

Preparatory Phase - ES Signature--For the T lightning flash, a typical electrostatic signature which occurs during the preparatory phase is given in figure 3. The three recordings correspond to the output of the three E-field sensors located as shown on the aircraft drawing. The evolutions of the three signals indicate clearly the induced effect of an external E-field; During the first period $T_1$ $T_2$, the cockpit and the tail sensors vary in opposite directions, the fuselage sensor showing a moderate variation.

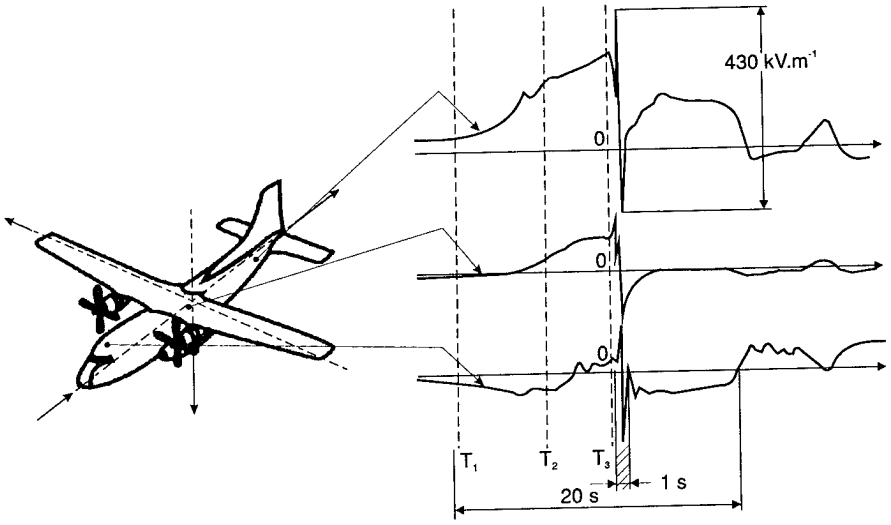



Figure 3. Electrostatic signature for a T lightning flash.

At time $T_2$, space charge effects due to corona discharges around the vehicle become more and more important and change locally some E-field measurements; phase space charge effects are clearly observed on the cockpit sensor output. At time $T_3$, one electrical field on a particular point on the airframe reaches a critical value which gives the first development of a positive streamer discharge. If the general configuration of the external E-field permits a sufficient propagation of the positive streamer and the transition to a positive leader, a complete lightning flash may occur.

The triggering conditions in terms of external E-field and aircraft potential are more observable on the two first curves given in figure 4. The first curve gives the variations of the aircraft potential during a period of 2 seconds; for this test, the value of the aircraft potential at the instant of the breakdown is 675 kV; the second curve corresponds to the variation of the external E-field along the wing to wing axis; its critical value is of the order of 100 $kV.m^{-1}$. We may observe that the component of the external E-field along the aircraft trajectory remains at a very low value. This situation, very common during the TRANSALL experiment, corresponds to a flight path around the storm-cloud, and not in the direction of the cloud.

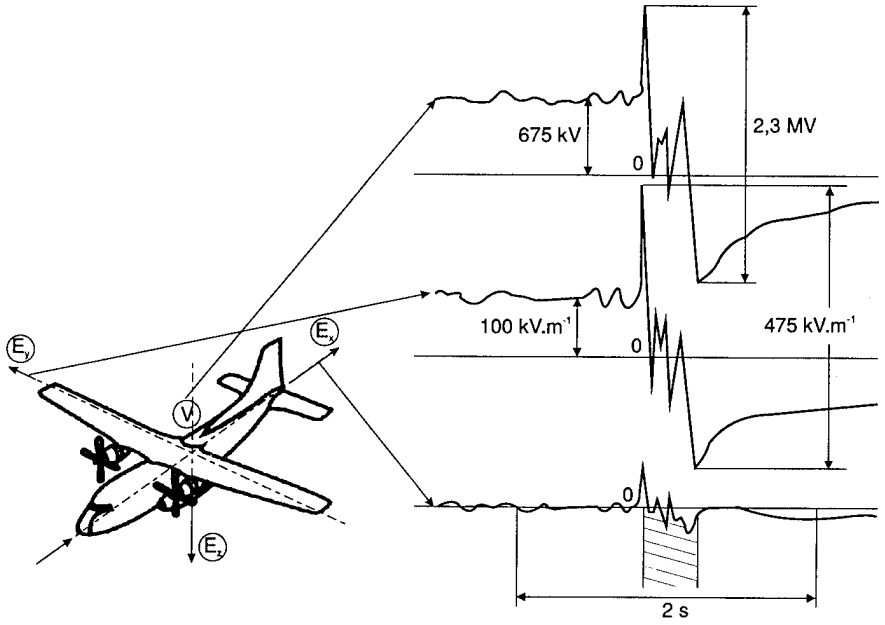



Figure 4. Critical E-field and aircraft potential.

Taking into account the characteristics of the electrostatic signatures corresponding to triggered lightning flashes, we arrive to the two following important conclusions:

a) The external E-field has to reach values between 50 kV/m to 100 kV/m over a distance of about 1 km (or more).
b) The aircraft potential at the instant of the breakdown may vary from several kVolts to MVolts; the aircraft potential is not critical for the initiation of the lightning event; we observe in fact that the evolution of the aircraft potential is

a consequence of all the positive and negative corona which take place around the aircraft due to strong induced field effects.

Attachment Phase - EM Signature--All the E-field signals observed during the attachment phase of a triggered lightning flash are characterized by the same typical signature (same data for the TRANSALL and the CV580 aircraft). This "unique" signature seems to prove that the physical mechanisms responsible for the lightning connection on the aircraft are always the same, independently of the atmospherical parameters and the aircraft geometries.

Figure 5 represents the variation of the E-field signal and of the discharge current detected on a sensor in connection with the lightning channel, for the same period of time.

The attachment signature is perfectly divided into three successive sub-phases:

- The first AB which exhibits a steady negative increase in the static E-field. The duration of this phase is roughly 4 to 5 ms. With the sensors used on the aircraft, no discharge current can be detected during this first sub-phase.
- The second phase, BC, occurs at B, where the E-field reaches a critical negative value. This phase lasts 1 to 2 ms and corresponds to the beginning of a sequence of generally 4 to 5 successive current pulses.
- A third phase, CD, starts when the static E-field reaches a critical positive value. This phase continues for 5 to 6 ms and is associated with the beginning of a steady current with superimposed discrete current pulses.

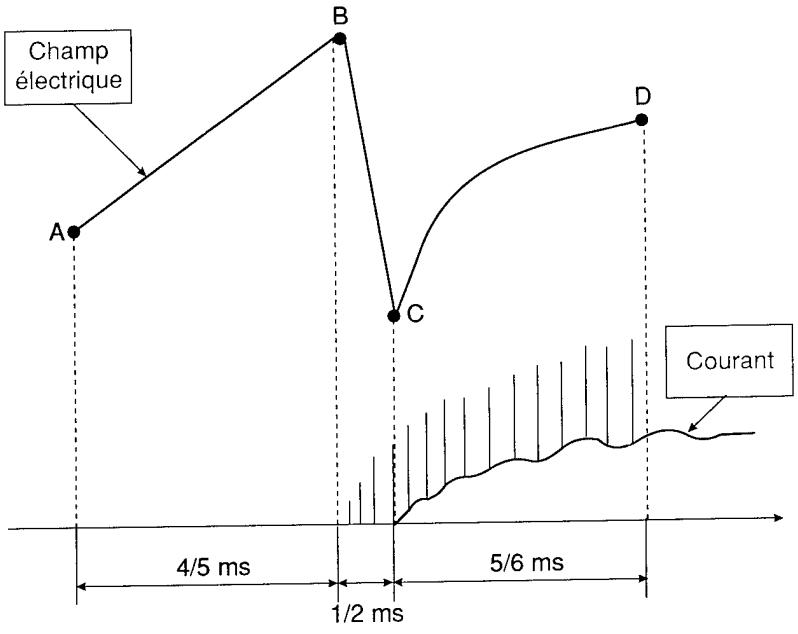



Figure 5. Electromagnetic signature for a T lightning flash.

In the lightning simulation test procedure, this attachment phase is known as the first burst of the "multiple burst" sequence. We now know that a second attachment process may occur during a complete lightning flash, and that it is possible for a third attachment process to occur within a particularly long event.

It is accepted today that a multiple burst sequence consists of:

1) Three successive current pulses bursts. These three bursts can occur in a period of 1 s with a mean duration of 0.5 s between them.
2) Each burst consists of an average 20 successive current pulses with a constant period between 50 and 200 μs.
3) Each current pulse has a peak amplitude of 10 kA, a rise time of 300 ns, and a fall time of 3 μs.

THE INTERCEPTED LIGHTNING FLASH

Preparatory Phase - ES Signature--As mentioned previously, we have a few intercepted lightning flashes with good and valuable data.

For an I event, one ES signature is presented on figure 6 in terms of external E-field ($E_x$, $E_y$ and $E_z$) and aircraft potential. It is evident that no electrostatic activity occurs before the lightning flash which starts at time 0.

The aircraft potential is certainly less than 50 kV and the external E-field probably less than 20 $kV.m^{-1}$; these two values indicate that the aircraft is flying in a low electrical activity zone (no corona discharges).

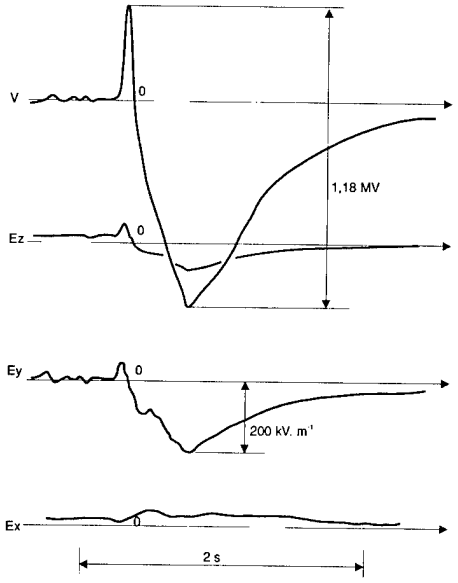



Figure 6. Electrostatic signature for an I lightning flash.

Attachment Phase - EM Signature--This EM signature is shown on figure 7 where 6 simultaneous E-field recordings are presented.

For a better understanding of the different E-field variations, the locations of the sensors on the airframe are also given. We observe first, the same global evolution of sensors 7 and 4 for one hand and sensors 6 and 5 for the other hand showing clearly an induced response of the sensors to an outside E-field; the difference between amplitudes of sensors 7 and 4, for instance, is due to the different enhancement factors at the location of the sensors (wing and fuselage in this case).

Sensors 1 and 3, located in front of the aircraft show a complex variation which can be explained only by using numerical techniques.

The different points A, A', A" and B will be explained in section 4. The portion following the point B is represented with more details in figure 8. Obviously, B is a singular point for all the sensors recordings; region BC and region CD seem to be very comparable to the same region BC and CD of the triggered lightning attachment phase. In conclusion, for the I event, the following remarks can be made:

- During a first sub phase AB, a strong induced E-field effect is observed.
- During a second sub phase BCD, all the sensors have the same evolution which is also comparable to the sub phase BCD of the T event.

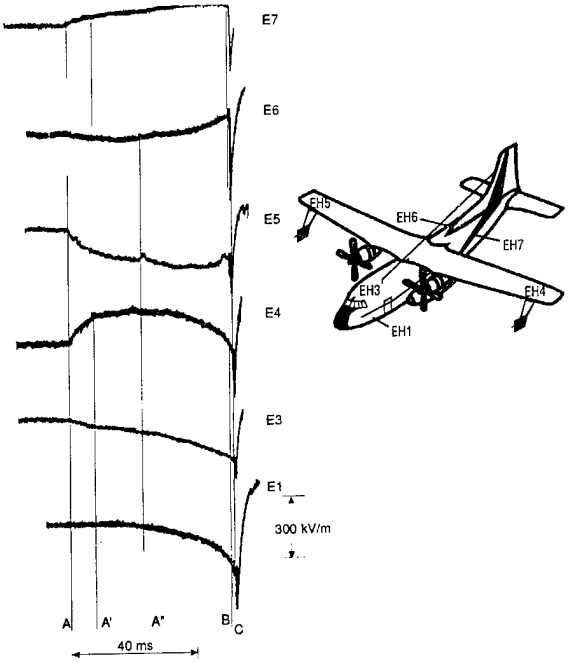



Figure 7. Electromagnetic signature for an I lightning flash (first period).

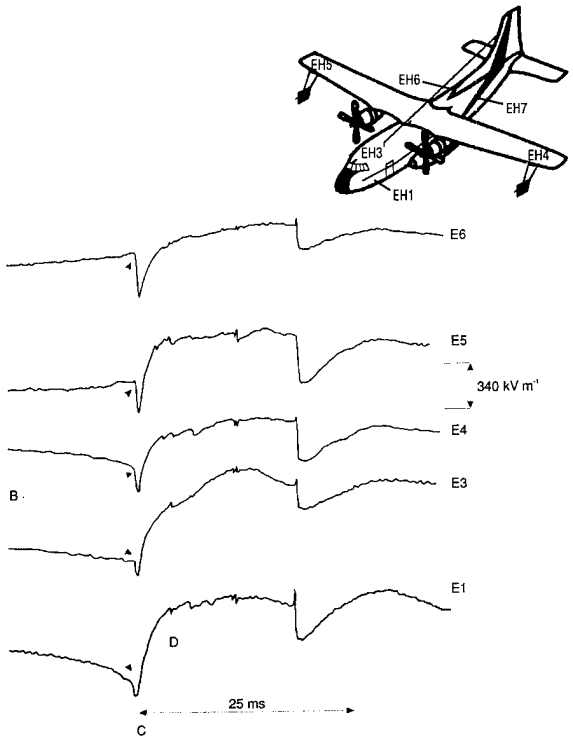



Figure 8. Electromagnetic signature for an I lightning flash (second period).

PHYSICAL MECHANISMS ASSOCIATED WITH THE ATTACHMENT PHASE TRIGGERED LIGHTNING PROCESSES--The physical mechanism associated with the attachment phase is now known as the "bi-leader discharge process". Although the theory is still being developed by different groups worldwide, the concept of the bi-leader mechanism is validated and accepted.

This concept can be summarized as follows (see the three diagrams in figure 9):

- During sub-phase AB, a positive leader $L_+/S_+$ starts out from a particular region of the aircraft (radome, wing and tail tips). This discharge propagates from the aircraft towards a negative region of the cloud at a velocity of about $10^4$ $ms^{-1}$ and over distances of more than one kilometer. The current in this positive leader is of the order of 1 to 10 A, and of course is not detectable by the current sensors on the aircraft structure, it becomes more and more negative, and the E-field normal to the surface also increases towards the negative values.

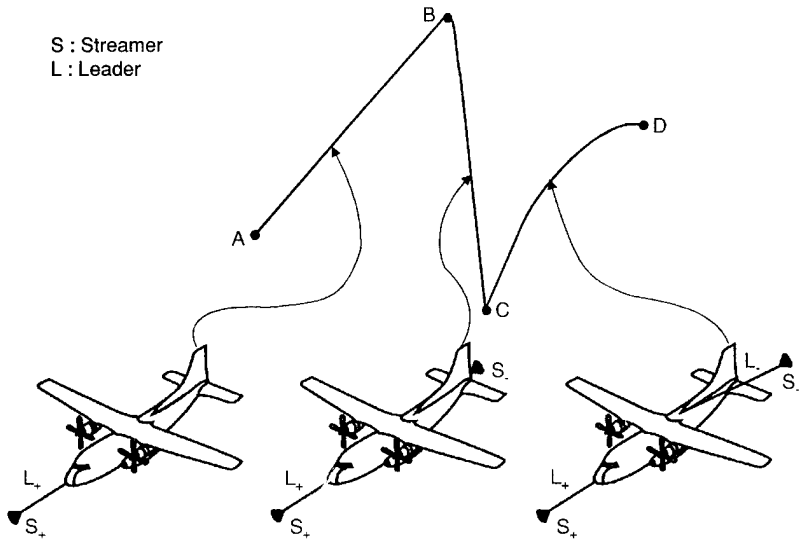



Figure 9. Physical mechanisms for a T lightning flash attachment.

- At point B, the E-field reaches a critical value, which triggers a negative streamer. This negative streamer has an unstable propagation giving a succession of current pulses which are clearly detected by the sensors. During the phase BC, the E-field varies considerably from high negative to positive values.
- At point C, the negative and positive leaders have now propagated over long distances, the ionization processes in both channels are very efficient, the temperatures in the core channels are higher than 10 000 K, and the conductivity is ever increasing. A permanent current can now pass through the aircraft structure, which means that charges can be transferred from the two charged regions of the space now connected by the lightning arcs.

- **SURFACE DISCHARGE**
- **HV DISCHARGE**
- **TRIGGERED LIGHTNING**

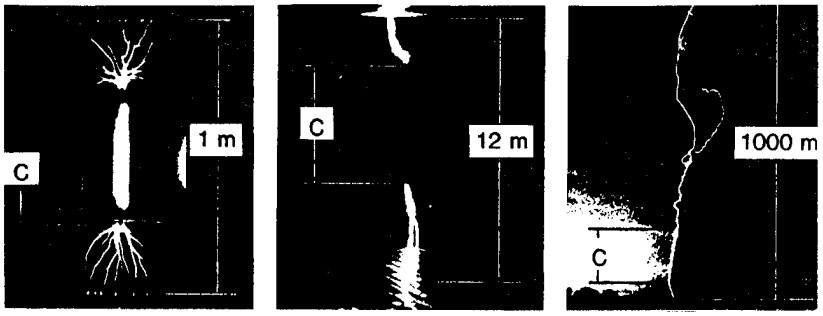



Figure 10. Experimental validation of the bi-leader concept.

In the attachment phase of a triggered lightning flash, the aircraft itself acts as a switch making contact between the positive and negative poles of a generator. The external E-field is sufficient to start and control globally the entire process.

This new concept, which is now basically understood [15] was experimentally validated. Three different experiments were carried out (see photographs in figure 10).

- The first was a laboratory experiment applying the concept of electrical surface discharge [16]. A small conductor C of 1 cm length, was introduced between two dielectric plates, one charged positively, the other negatively. The distance between the plate tips is 1 m. By switching the initial floating potential of conductor C to ground, a bi-leader process can be triggered developing first a positive leader followed by a negative leader.
- A second experiment [17] was carried out at the High Voltage Laboratory of *Electricité de France* at les Renardières. The aircraft was simulated by a cylindrical conductor, 4 m long, installed in an electrical floating configuration at the middle of a 15 m gap. The gap consisted of a very large flat electrode (25 x 25 m) overhead the model and the floor of the laboratory underneath. A 5 MV pulse voltage was suddenly applied in the gap and the discharge process was followed by an image converter and by E-field sensors located on the cylinder and on the ground. The bi-leader mechanism was established perfectly well, yielding first a positive leader propagating towards the negative electrode and then a negative one advancing towards the ground. The measurements performed during these tests were used extensively to verify the theoretical bi-leader model.
- Lastly, a third experiment was undertaken at the Kennedy Space Center by ONERA, CENG, NASA, and the University of New York at Albany, to develop a bi-leader in a real environment [18]. The technique consisted in firing small rockets trailing a long conductive wire (100 m), in very active storm situations characterized by a static E-field on the ground of 6 $kV.m^{-1}$. When the rocket reached an altitude of about 200 m, a positive leader started out from the rocket nose and propagated up in the direction of the cloud base. This first propagation was followed, a few milliseconds later, by a strong negative stepped leader, initiated at the end of the trailing wire and propagating down to the ground.

INTERCEPTED LIGHTNING PROCESSES--The physical mechanisms associated with the attachment phase of an intercepted lightning flash are not completely understood at present time. More experiments in laboratory have to be carried out for validation and a theoretical model which is in preparation has to be tested by numerical simulations.

Nevertheless some mechanisms, expected to occur, are summarized by the five diagrams in figure 11:

- During sub phase AA', a natural negative discharge S_/L_ is propagating and is approaching the vehicle; this discharge induces a large separation of charges on the airframe. This separation of charges depends on the geometry and the direction of the approaching discharge: The sensors outputs are, of course, different in this situation.
- At point A', there is a first emission of a positive corona followed by the propagation of a positive streamer $S_+$; some positive charges are leaving the aircraft reducing the induced effect of the outside propagation S_/L_.

- Zone A"B corresponds to the propagation of a complete positive discharge $S_+/L_+$ starting from the aircraft in the direction of the previous negative discharge; point B is the instant of contact between the two opposite discharges.
- During BC, the aircraft is connected to the initial negative discharge; a preliminary negative streamer S_ starts from the aircraft followed by a negative leader L_ at point C.
- During CD, the aircraft is inside the lightning channel and we arrive to the permanent phase of the lightning flash.

As an illustration, the photography presented in figure 12 gives an idea of the mechanisms which exist during the period between A to B. This picture was taken during an attachment test carried out at *Electricité de France* on a specific grounded system with a 5MV generator.

A negative discharge propagates primarily towards the ground; this propagation is suddenly completely modified at a given point I when an opposite positive discharge is initiated from a ground point J.; the contact between the two channels occurs just at the middle between points I and J.

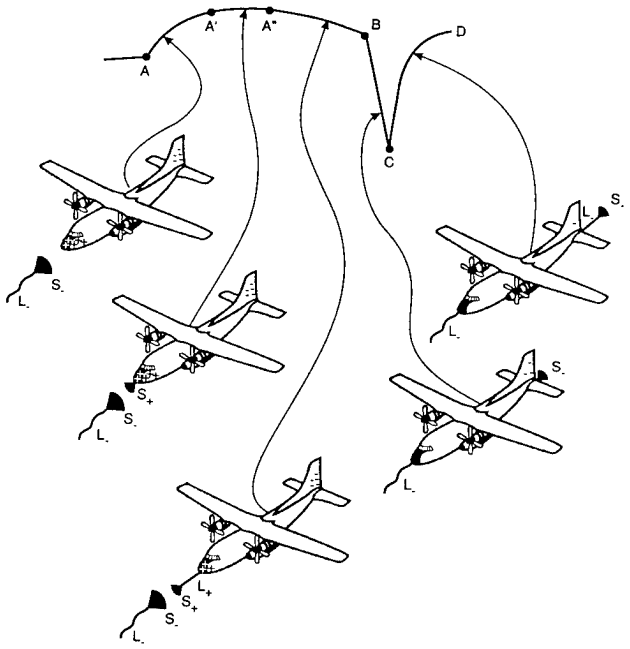



Figure 11. Physical mechanisms for an I lightning flash attachment.

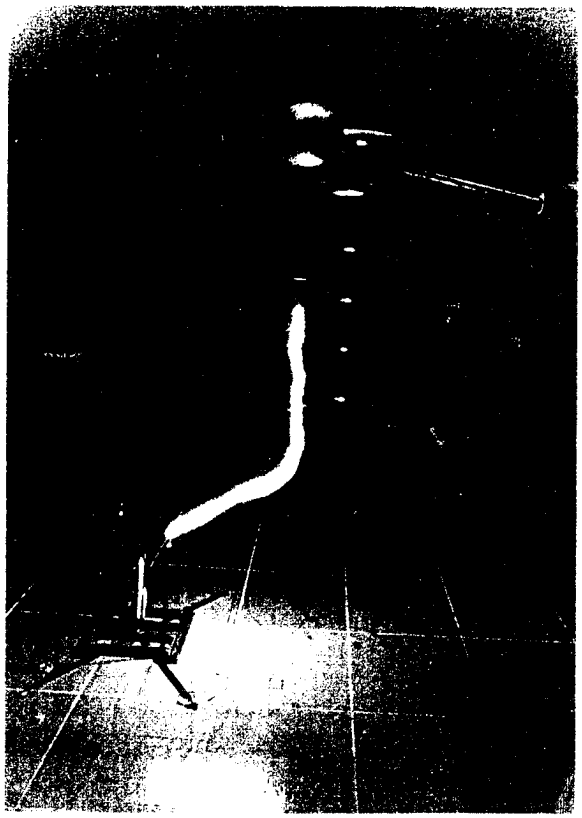


Figure 12. Experimental validation of an intercepted discharge.

## CONCLUSIONS

Progress was noticeable over the past decade concerning lightning flashes affecting aircraft in flight. In light of the experiment campaigns carried out in flight on different aircraft, and after analysis and interpretation of the data, we arrive at a very high level of knowledge of the general mechanisms involved in such a phenomena.

This new knowledge can be summarized as follows:

a) Most of the lightning discharges affecting aircraft are triggered discharges. The aircraft itself is responsible for it. The outside atmospheric field, resulting from charge separation inside the cloud, is sufficient to create the process and to maintain a complex discharge propagation over distances of several kilometers. The critical E-field is around 100 $kV.m^{-1}$.

b) A triggered lightning discharge occurs in two phases. The first is an attachment phase, which consists of the initiation of two separate discharge processes on the aircraft. This bi-leader propagation is associated with the "multiburst waveform" now applied for equipment certification. The other phase is a "permanent" one consisting of successive sequences of current impulses. This phenomena is not understood for the moment, but its characteristics are perfectly documented by flight data validated by measurements made on three different aircraft [19, 20]. This phase is associated with the "multistroke waveform" which is also recommended for equipment certification.

c) An intercepted lightning discharge also occurs in two main phases. The first is an attachment phase consisting of an approaching negative discharge, creating an opposite discharge from the airframe. These two discharges propagate in such a way as to make a contact; after this contact, the second phase is again a permanent phase. The mechanisms associated with the intercepted lightning flash are not completely understood. Numerical simulations and high voltage tests are necessary to clarify these mechanisms.

d) All this data and the related analysis are very recent. We know that work is continuing to understand thoroughly some of the complex interactions between an aircraft and a lightning arc in greater depth. One of these interactions, for example, is the arc-sweeping mechanism of the lightning channel on the aircraft structure. We are just beginning to analyze this; But the consequences for aircraft lightning protection are essential. Broad discussions are getting under way, with aviation authorities (FAA, EUROCAE, CAA, DGAC) to propose international rules in this field. Effort is still needed to develop numerical tools, define protection techniques, and prepare control equipment.

e) More specifically, at the light of this recent knowledge, a new zoning definition must be undertaken. Even if the existing rules, possibly modified, have to be applied during a certain period, experts in this domain have to engage discussions to propose a zoning definition more adequate and in agreement with the physics of lightning. As a preliminary step, and in accordance with the inflight

observations the generic drawing given in figure 13 shows the possibly four zones which have to be defined:

- Attachment zone (zones A).
- Sweeping zones (zones B) connecting two attachment zones.
- hanging zones (zones C) included in zones B.
- conducting zones (if they may exist).

All these zones can be defined by numerical investigations; it is not sure for the moment whether experimental definition may be achieved and more work has to be done also in this way.

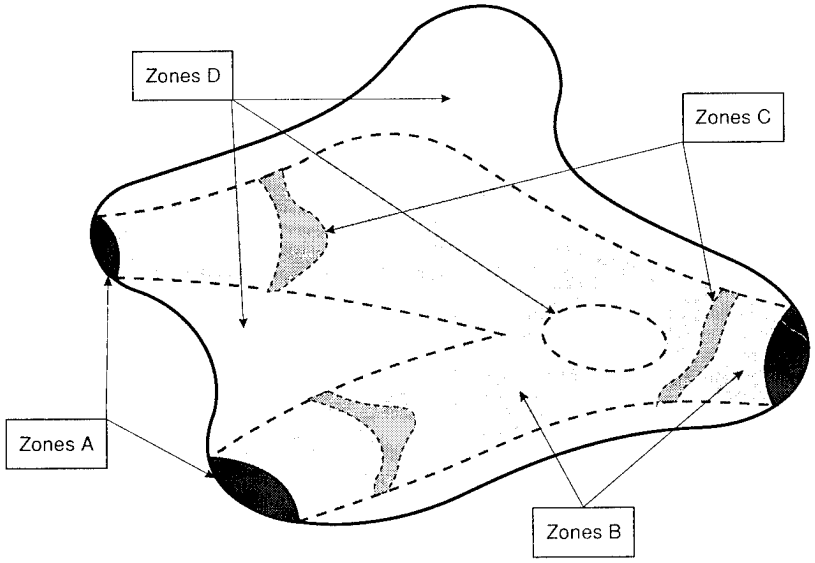



Figure 13. Suggested new aircraft zoning.

REFERENCES

1. J.L. Boulay, "Elimination des perturbations radioélectriques d'origine électrostatique sur avions", La Recherche Aérospatiale, 1979-2, pp. 101-120, 1979.
2. R.L. Tanner and J.E. Nanevicz, "An analysis of corona generated interference in aircraft", Proceedings of the IEEE, 52, 1, 1964.
3. J.E. Nanevicz and R.L. Tanner, "Some techniques for the elimination of corona discharge noise in aircraft", Proceedings of the IEEE, 52, 1, 1964.
4. F.A. Fisher, J.A. Plumer, R.A. Perala, "Lightning protection of aircraft", Lightning Technologies Inc., Pittsfield, MA 01201, USA, 1990.
5. F.L. Pitts, "Electromagnetic measurements on lightning strikes to aircraft", AIAA 19th Aerospace Science Meeting, 1981.
6. F.L. Pitts, "F106 data summary and model results relative to threat criteria and protection design analysis", ICOLSE, Dayton (USA), 1986.
7. P.L. Rustan et al., "Airborne measurements of the rise-time in lightning return stroke fields", ICOLSE, Forth Worth (USA), 1983.

8. P.L. Rustan, J.P. Moreau, "Aircraft lightning attachment at low altitudes", ICOLSE, Paris (France), 1985.
9. V. Mazur, "A physical model of lightning initiation on aircraft in thunderstorms", J. Geophys. Res., *4*, D3, 1989.
10. J.P. Moreau, J.C. Alliot, "Analysis of the first milliseconds of aircraft lightning attachment", ICOLSE, Dayton (USA), 1986.
11. J.L. Boulay et al., "Analysis of recent in-flight lightning measurements on different aircraft", ICOLSE, Oklahoma (USA), 1988.
12. J.P. Moreau et al., "Transall 88. Lightning characterization program", ICOLSE, Bath (USA), 1989.
13. J.L. Boulay and P. Laroche, "Aircraft potential variations in-flight", ICOLSE, Oxford (UK), March 1982.
14. J.C. Alliot et al., "3D computer codes developed at ONERA in time-domain and in frequency-domain to model electromagnetic interaction with a vehicle", 2nd ESA Workshop on Electromagnetic Compatibility, Noordwijk (Netherlands), december 1990.
15. V. Mazur and J.P. Moreau, "Aircraft-triggered lightning: processes following strike initiation that affect aircraft", J. Aircraft, *29*, 4, pp. 575-580, july-august 1992.
16. S. Larigaldie et al., "Lightning leader laboratory simulation by means of rectilinear surface discharges", J. Appl. Phys., 1982.
17. B. Hutzler and I. Taudière, "Attachment process of lightning on aircraft in the light of laboratory simulations", ICOLSE, Bath (UK), 1989.
18. P. Laroche et al., "Observations of bi-directional leader development in a triggered lightning flash", ICOLSE, Cocoa Beach (USA), april 1991.
19. J.L. Boulay, "Current waveforms observed during lightning strikes on aircraft", ICOLSE, Cocoa Beach (USA), april 1991.
20. J.P. Moreau and S. Larigaldie, "Description and interpretation of aircraft lightning attachment from electric and magnetic field measurements and video observation", ICOLSE, Cocoa Beach (USA), april 1991.

# THE RATIONALE OF PROPOSED NATO STANAGS DESCRIBING THE LIGHTNING ENVIRONMENT FOR LAND, SEA AND AIR USE AND DEFINING LIGHTNING ASSESSMENT PROCEDURES FOR MUNITIONS AND ASSOCIATED SYSTEMS

G A M Odam
GAO Consultancy, Barmouth, Gwynedd, UK
(Consultant, previously employed at RAE Farnborough)

M Richardson
Ordnance Board, Ministry of Defence, UK

## ABSTRACT

The organisation CNAD (Conference of National Armament Directors) are responsible within NATO for design requirements and test methods for all materiel, be it for use on land, sea, or in the air. The AC310 Group of CNAD are tasked to prepare STANAG 4236 'Lightning Environmental Conditions Affecting the Design of Materiel for use by the NATO Forces'. Group AC310 have also prepared Draft STANAG 4327 'Lightning, Munition Assessment and Test Procedures' which will soon be circulated for ratification. The rationale for these two documents is given together with an outline of their contents.

## INTRODUCTION

If there are no acceptable International Standards, members of NATO must use STANAGS if available. Such documents take precedence over National Standards. UK MOD are custodians of 3 STANAGS concerning lightning:-

| | |
|---|---|
| STANAG 4236 - | Lightning Environmental Conditions affecting the Design of Materiel, for use by the NATO Forces (1) |
| STANAG 4327 - | Lightning, Munition Assessment and Test procedures (2) |
| STANAG 3855 - | Lightning Qualification Test Techniques for Aircraft and Hardware ( 3) |

Currently 4236 is published at Edition 1 but 2nd Draft Edition 2 is being discussed by AC310. Draft Edition 1 of 4327 is about to be offered for ratification; 4327 has an advisory 'handbook' (AOP 25, Ref 4) giving background and rationale.

This paper is primarily concerned with 4236 and 4327 but passing mention is given to 3855. Much of the content of 4327 is very similar to that proposed for a revision of the lightning content of a UK Aircraft Standard (5). Source material for the latter document and the STANAGS has been drawn from a DRA Farnborough Technical Memorandum (6), taking due note of EUROCAE/RTCA Civilian Standards together with the relevant US MIL Standards.

The main purpose of this paper is to draw the Lightning Community's attention to what is going on within NATO regarding standardisation concerning lightning hazards. The rationale for 4236 and 4327, with its AOP, is given below.

## RESPONSIBLE AUTHORITIES AND TERMS OF REFERENCE FOR THE LIGHTNING STANAGS

There are 3 NATO committees which develop STANAGS concerning lightning. Two of those committees, AC301 and AC310, report to CNAD (Conference of National Armament Directors) and the other, the Air Electrical Working Party, to MAS (Military Agency for Standardisation). MAS has been in existence longer than CNAD and the former is responsible for all standardisation regarding operational matters, one consequence of which is that it has an interest in design requirements and supports certain standards concerning that aspect. This causes some conflict with the responsibilities of CNAD who are responsible for the design requirements and test methods for all materiel. AC301 are responsible for standardisation of all environmental matters and test methods for all materiel, except that they do not have a responsibility for design requirements and test methods for munitions (only the environment for munitions). AC301 delegated their responsibility for Climatic, Mechanical and Electrical (RF, ESD and Lightning) environmental STANAGs to Sub Group III of AC310, hence STANAG 4236 is the responsibility of AC310 SG III.

As noted above, Draft STANAG 3855 is the responsibility of the Air Electrical Working Party of MAS. It was originally in the custodian-ship of the US Air Force and started life in 1978 at a closed conference sponsored by ONERA at Chatillon, France. During the 1980s the Custodian-ship changed to UK. Attempts to get the project moving met with considerable lack of interest. Consequently Draft STANAG 3855 has not progressed as far as STANAGs 4236 and 4327. It should be noted, however, that the lightning environments given in 4236 will include air environments when 4236 Edition 2 is ratified.

An outline of the contents of 2nd Draft STANAG 4236 Ed 2 and draft STANAG 4327 is given in Appendix 1.

## SOME AREAS COMMON TO 4236 AND 4327

DEFINITIONS AND TERMINOLOGY--Both documents have a glossary of terms and definitions which recognise four groups of lightning effects, namely:-

| | |
|---|---|
| Group I | (direct effects) |
| Group II | (indirect effects) |
| Group III | (far-field effects) |
| Group IV | (leader phase effects) |

ZONING--The zoning definitions are the same in both documents and generally agree with the intentions of those given by EUROCAE/AE4L. The wording in some cases is somewhat different but is thought to be preferable. Both documents recognise the swept leader effect and define a transition Zone 1C, although the parameters of that zone are to be taken as those of Zone 1A unless otherwise agreed with the relevant National Authority. The changes that have been made to the zoning definitions are as follows; Zone 1 now applies to both the leader and return stroke, whilst that for Zone 2 emphasises that it applies only to a return stroke. The Zone 3 definition has been reworded to make it more precise.

The latest draft of AC20-53B seen by the authors, defines Zones 2A and 2B as areas which have a high probability of a subsequent stroke attachment, and Zones 1A and 1B as areas with a high probability of initial stroke attachment. This, at first sight, implied that a subsequent stroke was necessary for an attachment in a swept stroke area, excluding attachments due to continuing currents. Obviously that is not so and it was not the intention of those who drafted the new definitions to imply that. It is understood that the definitions were necessary to allow a leader attachment in a Zone 1A and the possibility of a swept leader. It is doubtful, however, that the probability of a reattachment occurring in a Zone 2 area due to a subsequent stroke is greater than that due to a continuing current swept into it. The definitions proposed for AC20-53B are not necessary in STANAGs 4236 and 4327 as a Zone 1C is defined in those documents.

Both D0160C and draft AC20-53B talk about low and high probabilities of flash hang-on, as also did Reference 6 and earlier issues of Reference 2. What those documents should really be talking about are low and high probabilities of long flash hang-on; such changes are incorporated into the STANAGs.

LIGHTNING ENVIRONMENTS AND TEST WAVEFORMS--As is noted above, 4236 provides the lightning environments to be used in all other STANAGs. These environments and the test waveforms derived from them, discussed below, are therefore common to 4327. They are repeated in that document as 4236 Ed 2 has yet to be agreed.

## RATIONALE AND CONTENT OF 4236

NATURAL AND DERIVED ENVIRONMENTS--Edition 1 of 4236 was biased towards munitions. That has been corrected at Draft Edition 2. As noted above, the lightning environments given in 4236 apply to all materiel used by NATO, if that materiel can be exposed to a lightning threat. The environments derived from our knowledge of natural lightning and its interaction with objects in the air, on the ground, or at sea, have to be tailored to the particular class of materiel being considered. Some difficulties do arise as the multiple burst is said not to apply to ground and sea based materiel, although there is some controversy over whether or not that is true (see below). Again the charge content and action integral are enhanced for ground and sea based systems to cater for the higher values of those parameters which have been observed in Europe.

MULTIPLE BURST AND MULTIPLE STROKE ENVIRONMENTS--There is a difference of opinion amongst UK experts concerning whether or not the Multiple Burst environment applies to ground and sea based materiel. One school of thought says that the environment is due to a relaxation process that only applies to an isolated body in space and consequently it cannot occur with a body in contact with the ground or sea. The other opinion holds that the phenomena is not caused by such a process and that the environment applies just as much to materiel for use on land and at sea as it does to materiel used in the air. There is obviously need for further discussion but until a consensus is obtained, References 1 and 2 hold that the Multiple Burst will not apply to ground and sea based materiel.

NEARBY ENVIRONMENT--A ground environment for nearby strikes is given in Annex D of the STANAG. The background to that environment is detailed in Reference 7.

TEST WAVEFORMS--Test waveforms resulting from the derived environments are given in Annex E of the STANAG, which recognises the presently accepted 4 component Composite Test Waveform, as given, for example, in AC20-53B.

COMPONENT C LEVELS AND DURATION--There has been comment and discussion in UK, about an apparent anomaly regarding the Component C levels and duration specified for swept stroke zones, inasmuch as the 400-800 A level for a swept stroke area seemed inconsistent with the 200-800 A of the full duration Component C; and, perhaps more importantly, there seemed to be a conflict with D0160C Section 23 which states that an average level of 400 A for 45 ms is needed. The reason for the latter document quoting 45 ms was said to be that 5 ms was allowed for Component B.

It is our view, supported by others within the UK, that Component B is rather pointless for most tests and generally may be neglected. It is felt important that a level of 400 A be specified as the lower limit of a short duration Component C for a swept stroke area, as otherwise, for example, in a burn through test a lower level could be used which would be below the burn through asymptote (see Fig 1 and Ref 8). If an average 400 A is specified, there is a danger that a test house might use a much lower current rising to a much higher current, or vice versa. A range of currents from 200-800 A to give 200 coulombs may or may not be a good representation of continuing current, but there is not really an anomaly in choosing a 400 A level in that range for burn through tests.

RATIONALE AND CONTENT OF 4327 AND AOP 25

CONTENT OF 4327 AND AOP 25--The content of 4327 is outlined in Appendix 1. AOP 25 explains the background and rationale of the STANAG and gives advice concerning assessment and test methods. At the moment there is some overlap between AOP 25 and STANAG 4236. In the second editions, this will be reduced and harmonised.

ASSESSMENT PROCEDURES GIVEN IN 4327--STANAG 4327 calls for an on-going Lightning Hazard Design Analysis (LHDA) to be made within the framework of a Lightning Protection Plan (LPP). The LPP has to provide:-

i The Lightning Hazard Design Analysis.

ii A statement defining the general environmental conditions (Climatic, Mechanical and Electrical) in which any lightning protection device must be capable of operation.

iii The relevant Test Plans, if testing is required.

iv The relevant Test Schedules if Test Plans are prepared.

v Reports of all tests made with analysis, conclusions and recommendations, including a risk analysis if full protection has not been achieved.

The LHDA must be started at the beginning of the project and it, in effect, provides a check list of areas for attention, also calling for a detailed Lightning Transient Assessment and an Explosives Hazards Assessment. The LHDA also has to determine the need for testing as decided by and in addition to the transient and explosion hazard assessments.

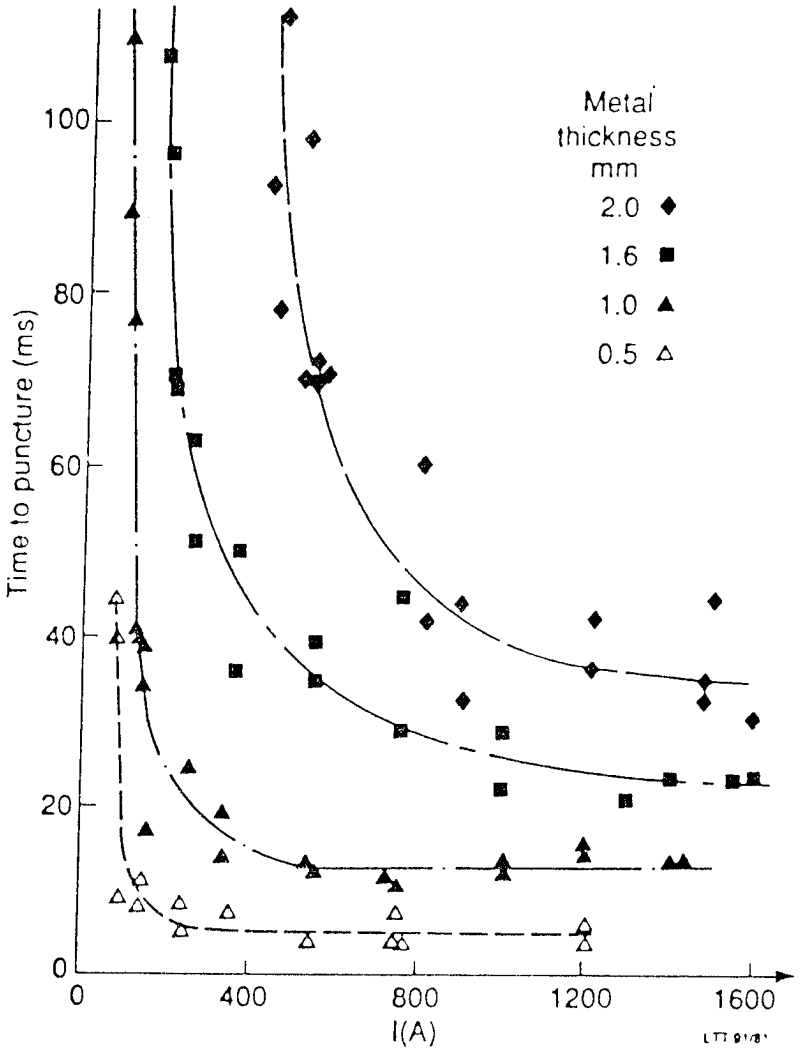



FIG 1 ALUMINIUM PUNCTURE THRESHOLD AS A FUNCTION OF CURRENT AND DWELL TIME

THE LIGHTNING ENVIRONMENT--The lightning environment in 4327 is identical with that proposed for 4236 Edition 2. When the latter document is ratified, 4327 Edition 2 will call up 4236 rather than stating the environment in detail.

ZONING--Zoning is discussed and explained in AOP 25 and zoning definitions are noted in both 4236 and 4327. The LHDA requires that a statement should be given noting the applicability of zoning as determined according to the rules given in AOP 25, as applicable.

GROUP II (INDIRECT) EFFECTS EVALUATIONS--Reflecting UK views concerning the clearance of military aircraft against Lightning Indirect effects, the LHDA requires that a lightning transient assessment shall be made to include an evaluation of shock excitation and ground voltage transient protection and the verification that induced voltages cannot cause voltage flashover or insulation breakdown.

The evaluation of shock excitation and ground voltage protection is made by a combination of modelling, Low Level Swept CW and pulse tests to establish Weapon Transient Levels (WTLs) for

comparison with Equipment Transient Test Levels (ETTLs) obtained from equipment tests as discussed below. There is a school of thought which says that there should always be a full threat upset test, either on a system rig with multipoint injection, or preferably during a whole weapon pulse test. With regard to the latter preference it is argued that only by testing on the weapon at full threat will the correct environment due to lightning occur, with appropriate amplitude and phase of voltages and currents on cables and electromagnetic fields in equipment bays. The opposing view is that even such a test cannot reproduce the actual excitation that occurs in practice and that all the variables and imponderables can be swept up by applying an adequate margin between levels obtained from validated analysis and the bench test levels to which equipment is cleared. STANAG 4327 adopts the latter position and at the moment requires a margin of 12 dB, although lower margins may be used by agreement with the National Authority.

EQUIPMENT TESTS--The Damped Sinewave and Ground Voltage Equipment Tests are essentially those of DEF STAN 59-41 (9), tests DCSO8 and DCSO9 respectively.

GROUP I (DIRECT) EFFECTS TEST PROCEDURES--The Direct Effects Test Procedures given in Reference 6 included the need for fast rise time Components A and D for mechanical effects tests. At the moment that requirement has been dropped in 4327 pending the outcome of research by LTT, who maintain that test houses will be unable to provide Component A with a rise time less than 10 μs. The UK MOD viewpoint is that tests should not be tailored to specific test equipment.

With regard to the Composite Test Waveform, and especially considering Group I effects, the philosophy that has been followed is that it is not necessary to use all the waveform components relevant to a particular attachment zone in a test but only those that affect the particular damage mechanism under investigation. For example, if failure is only action integral dependent then Component A is essential but there is little point in using Component C. The selection of the waveforms given for the Group I test methods adopts this position.

GROUP IV (LEADER PHASE EFFECTS) TEST PROCEDURES-- STANAG 4327 does not recognise the validity of high voltage model tests to decide strike point location. The test procedures given are to be used when an assessment of puncture/flashover characteristics are required.

The physical processes are taken to be that charge will be deposited, both by the high ambient 'quasi dc' E field which often exists before the strike and by the rapidly increasing field (above the quasi dc level when present) as the leader approaches. That charge, together with the rise time of the E field pulse at leader attachment, can significantly influence the probability of puncture or flashover of the dielectric. Consequently when assessing the risk of dielectric puncture, a slowly rising waveform is required to allow the surface charge to develop. Such a waveform would favour flashover rather than puncture. A convenient way, however, of getting both the surface charge and the correct rise time for puncture studies is to superimpose the test pulse on a dc voltage applied to the test electrode, which is the test method recommended by Reference 10.

EXPLOSIVE HAZARDS EVALUATION-- STANAG 4327 gives requirements for 'Energetic Materiel Hazard Assessment Tests, Liquid Explosives, Propellants and Fuels', based on the fuel hazard evaluation recommended in Reference 5. Appendix C4 of 4327 is the requirement for energetic materiel assessment tests for solid explosives (Whole System Tests); these are in effect 'zap it and see if it goes bang' tests, where the preparation of a special round with solid explosives removed would invalidate the electrical characteristics of the test object. Part System Tests are included when bulk explosives/propellant can be removed without invalidating the electrical characteristics but the fuzes/electro explosive devices have to be in place.

## CONCLUSIONS

STANAG 4236 is being developed which will define the lightning environments applicable to all materiel used by NATO. Those environments take note of, and generally will be in agreement with, those being developed for International Civilian Standards. STANAG 4327 has been developed which prescribes assessment and test methods applicable to munitions. That STANAG is about to be offered to NATO for ratification.

## REFERENCES:


1 NATO/CNAD, 'Lightning Environmental Conditions Affecting the Design of Materiel, for use by the NATO Forces', Second Draft STANAG 4236 Edition 2, February 1994.

2. NATO/CNAD, 'Lightning, Munition Assessment and Test Procedures', Final Draft STANAG 4327 Edition 1, July 1994.

3. NATO/MAS, 'Lightning Qualification Test Techniques for Aircraft and Hardware', First Draft STANAG 3855.

4. NATO/CNAD, 'Rationale and Guidance concerning STANAG 4327 Lightning, Munition Assessment and Test Procedures', Fnl Draft Allied Ordnance Publication 25, March 1995.

5. UK MOD(PE), 'Design and Airworthiness Requirements for Service Aircraft, Volume 1 Aeroplanes, Volume 2 Rotorcraft', DEF STAN 00-970.

6. G A M Odam, A W Hanson and R H Evans, 'Lightning Protection Requirements for Aircraft, a Proposed Specification', RAE Tech Memo FS(F)632 Revised Issue 1, May 1991.

7. R H Evans and G A M Odam, 'Environments and Test Methods for the Assessment of Indirect Hazards Due to Lightning Strikes', Williamsburg Conference, September 1995.

8. UK AEA, Culham Short Course Notes.

9. UK MOD(PE), 'Electro Magnetic Compatibility', DEF STAN 59-41.

10. A W Hanson, Private communication to G A M Odam.

## APPENDIX 1

## OUTLINE CONTENTS OF FIRST DRAFT STANAG 4236 EDITION 2

ANNEX A Definitions and Terminology

ANNEX B Lightning Discharges and Interactions with Materiel

ANNEX C Natural Lightning Parameters

ANNEX D Derived Lightning Environment (Lightning Threat Levels) to be used as Design Criteria

ANNEX E Waveforms for Test and Analysis

## OUTLINE CONTENTS OF FINAL DRAFT STANAG 4327 EDITION 1

ANNEX A Definitions and Terminology

ANNEX B Requirements for the Assessment of the Capability of Munitions and Associated Systems to Withstand Lightning Effects
- APPENDIX B1 Lightning Environment and Design Aim Parameters
- APPENDIX B2 Evaluation of Shock Excitation and Ground Voltage Transient Protection
- APPENDIX B3 Explosives and Fuel Hazards Assessment
- APPENDIX B4 Lightning Test Waveforms for use with the Test Methods given in Appendices C1 to C7

ANNEX C Lightning Test Methods
- APPENDIX C1 Requirements for Group II Tests on Whole Weapons
- APPENDIX C2 Requirements for Group II Tests on Parts of Weapons
- APPENDIX C3 Requirements for Equipment Tests
- APPENDIX C4 Requirements for Energetic Material Hazard Assessment
- APPENDIX C5 Requirements for Energetic Material Hazard Assessment Tests, Liquid Explosives, Propellants and Fuels
- APPENDIX C6 Group I Test Methods
- APPENDIX C7 Group IV Test Methods
- APPENDIX C8 Methods of Detecting Sparking

British Crown Copyright 1995/MOD
Published with the permission of the Controller of Her Britannic Majesty's Stationery Office

# THE PHYSICS OF ZONING

Rodney A. Perala
Terence H. Rudolph
Greg J. Rigden

Electro Magnetic Applications, Inc.
P.O. Box 260263
Denver, CO 80226
Phone (303) 980-0070 Fax (303) 980-0836

## ABSTRACT

Zoning is an important topic of current interest because it defines locations on aircraft where test currents are to be applied for protection and validation purposes. For example, both the SAE-AE4L and the EUROCAE WG31 committees are presently engaged in producing a zoning document. The existence of these activities testifies to the fact that it is generally recognized that previous zoning prescriptions do not seem accurate or complete, and sometimes are not consistent with observable data.

Zoning is a difficult subject because it is probably impossible to perform well controlled experiments in this area. For example, experiments would need to involve research aircraft flying in a thunderstorm environment, and observing when and where attachments occur. But one would also require simultaneous observations of thunderstorm conditions such as the ambient electric field and its spatial variation, particle densities and charges, humidity, altitude, and aircraft net charge. Also, aircraft parameters such as thrust, attitude and velocity should be observed. In order to fully understand zoning for aircraft, the full parameter space of the preceding factors should be explored. Then one would have to repeat these observations with various other aircraft in order to parameterize aircraft factors. Because these types of experiments are not likely to occur, three other sources of information can be used: in-flight experience data, laboratory experiments, and analysis. The objective of this paper is to describe the physics involved in aircraft attachment so that proper laboratory experiments and analysis can be done. Application of these physical processes to airborne vehicles is demonstrated. The scope of this paper is limited to initial attachment only.

## INTRODUCTION

In this paper we are concerned with one aspect of zoning, namely initial attachment. Historically, there have been several methods to determine where this will occur. First of all, scale model tests have been done. These typically involve construction of a small scale model of an aircraft and applying to the model a large electric field from a nearby electrode. The field is large enough to cause arcs to attach to the model. The electrode is moved to various positions around the aircraft so that fields of many orientations are included in the process.

The second approach involves analysis of some kind. One method is to use a rolling sphere to determine locations and associated probabilities of attachment (1,2). Another method is to perform electric field modelling (3,4), in which air breakdown locations are determined for an applied uniform E-field of various angles of polarization. The angles are stochastically varied so that a probabilistic determination of attachment locations can be made.

The thesis of our paper is that the approaches mentioned above may not include all the relevant physics. Our objective is to clearly define the electrostatic problem for an aircraft in flight in a thunderstorm environment. Application of these factors is illustrated by considering a rocket in flight. Specifically, it is shown that for a rocket in flight, initial attachment to the nose tip is not expected, but is instead predicted to occur perhaps 40 cm downstream from the rocket nose tip. This is expected because the dynamic air pressure combined with the local electric field results in the largest electric field to air density ratio at the downstream location. The effects of the exhaust are also shown to be important in defining the proper electrostatic state of the vehicle prior to attachment.

## DEFINITION OF THE APPROPRIATE ELECTROSTATIC PROBLEM

In this section, we attempt to define the electrostatic problem for an aircraft in flight in a thunderstorm environment. This is necessary to provide a definition of the physics including the necessary initial conditions. If one has a clear understanding of this electrostatic problem, then appropriate tests and analyses could possibly be implemented.

It is well known that most lightning experienced by an aircraft is triggered by the aircraft itself (5-12). The basic requirement is that the local electric field exceed the air breakdown level at some location on the vehicle and that the total field near the aircraft attachment point is large enough over a sufficiently large distance to create and propagate a leader. In fact, this process probably happens for all lightning, even for the case of an approaching stepped leader, because its fields will also cause arcs to begin on the aircraft and to eventually connect to the leader itself.

There are many factors which affect the triggering of lightning by aircraft. These factors are illustrated in Figure 1 and are listed as follows:

1. Ambient thunderstorm field and its spatial variation
2. Net static charge on the aircraft
3. Exhaust effects
4. Dynamic air density around the aircraft
5. Thunderstorm particles
6. Microphysics of air breakdown
7. Aircraft geometry and materials

THE AMBIENT THUNDERSTORM ELECTRIC FIELD - The ambient thunderstorm electric field is defined as the field that exists in the absence of the aircraft. This field is caused by the thunderstorm charge density. If an observer (i.e. the aircraft) is far from the charge locations, then the field may be regarded as uniform over the dimensions of the aircraft. If the aircraft is close to the charge, then the fields are non-uniform over the aircraft dimensions.

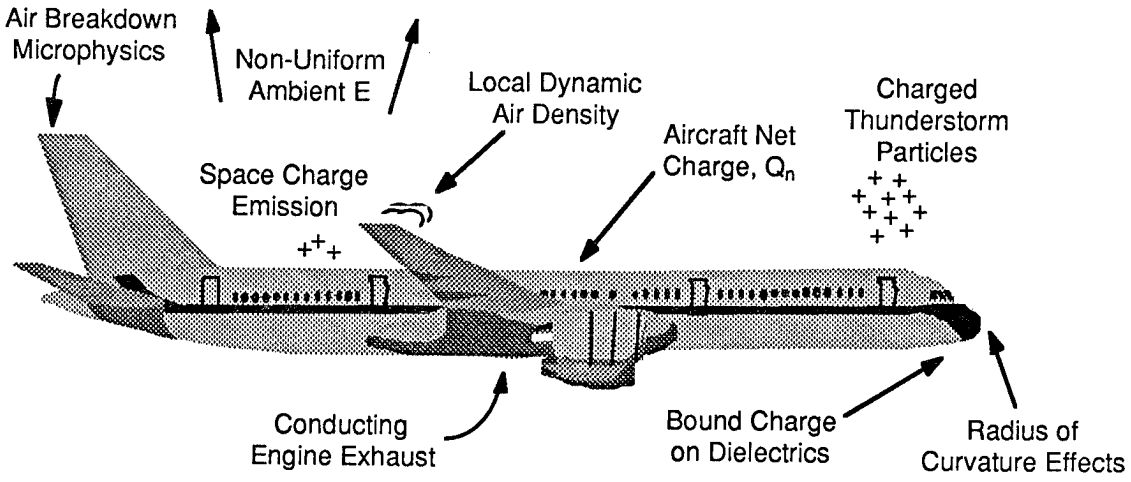



FIGURE 1 SUMMARY OF TRIGGERING ISSUES

The ambient electric field induces a polarization charge density on the aircraft. The integral of this charge density over the aircraft is zero, that is, no net charge is present.

NET AIRCRAFT CHARGE - The net charge on the aircraft also contributes to the total local electric field on the aircraft surface. This charge must arise from some charging mechanism, such as static dischargers, triboelectrification (i.e., contact with particles) or engine charging. The net charge is defined as the result of integrating the local charge density over the entire aircraft surface.

EXHAUST EFFECTS - Exhaust effects have been studied extensively and reported in previous conferences (12-15). The exhaust of a vehicle in flight can have two electrostatic effects.

First, the exhaust can create a charging mechanism. Basically, the exhaust is conductive enough so that an electric field causes conduction currents to flow, which act as a current source driving the aircraft, causing a non-zero net charge. This charging might be on the order of a few microamperes, so it is small compared to other possible sources which may be on the order of 1 ma. However, it is possible that engine charging may be the only charging source in some conditions. It has been found in this case that the aircraft reaches a steady state condition where the total local electric field at an aircraft extremity is large and is a scalar multiple of the ambient field, and the total electric field at some point in the exhaust is zero (12).

The second effect is by virtue of the exhaust conductivity, a portion of the exhaust becomes an electrostatic extension of the aircraft, so that any electrostatic modelling or testing of an aircraft must include a portion of the exhaust, which is treated as a perfect conductor. Previous experiments and analyses have shown that the portion of the exhaust to be included in the aircraft model are those portions for which the conductivity is larger than $3 \times 10^{-10}$ mho/m (12, 13). Note that this value corresponds to a dielectric relaxation time of about .03 seconds.

Although the above described exhaust effects were derived from studies of the exhaust on solid rocket motors, the same principles also apply to aircraft engine

exhaust. For example, electric field charging of a helicopter by its exhaust has been observed, and exhaust conductivities on the order of $3 \times 10^{-9}$ mho/m have been measured (16, 17). This is an order of magnitude larger than the critical value determined from the solid rocket experiments and analysis.

AIR DENSITY EFFECTS - The local air density on and near the surface of an aircraft is important because the value of the electric field required for air breakdown is proportional to the air density.

The air density is a function of the local air pressure on the aircraft's surface, which in turn depends upon the ambient air pressure and aircraft aerodynamics. The air pressure depends upon the aircraft shape, speed, attitude, and altitude.

THUNDERSTORM PARTICLES - Thunderstorm particles include ice crystals, hail, graupel, rain and snow. These particles may have two effects. First, they are sufficiently conducting so that they can enhance ambient electric fields and thereby create triggered discharges. Many think these particles may play such a role in the initiation of natural lightning, because measurements of fields in clouds have not exceeded about 400 kV/m, well below air breakdown level. They may play such a role in the aircraft triggered lightning process as well.

The second effect is that they can create a non-uniform electric field in the vicinity of the aircraft, thereby initiating discharges from aircraft locations which would not be evident from uniform field considerations.

AIR BREAKDOWN MICROPHYSICS - The microphysics of air breakdown includes processes such as ionization, attachment, and recombination rates. It also includes the availability of free trigger electrons, usually caused by cosmic rays, whose flux density is a function of altitude. Although the electron avalance rate is a strong function of the electric field and thereby determines the air breakdown level, most of these processes relate to the physics of what occurs after a discharge is initiated. However, it is the microphysics which describes corona and arc development, which is important for the radius of curvature effect described in the next section.

AIRCRAFT GEOMETRY AND MATERIALS - The aircraft geometry and materials are important in two ways:

- They determine the electric field enhancement factors
- They determine the possibility of either initial corona or arc discharges

There are really two aircraft enhancement factors, one which accounts for the polarization charge ($k_p$), and one which accounts for the aircraft net charge ($k_n$). These can be defined by:

$$E_t = E_p + E_n \tag{1}$$

$$E_p = k_p E_a \tag{2}$$

$$E_n = k_n Q_n$$

where $E_t$ is the total electric field at a location on the aircraft surface, $E_p$ is the field at that location caused by the polarization charge, $E_n$ is the field at that location caused by the net charge $Q_n$, and $E_a$ is the ambient thunderstorm field. In words, the total electric field anywhere on the aircraft is caused by both the ambient field and the aircraft net charge.

One should note that because of the exhaust effects described earlier, the values of $k_p$ and $k_n$ must also depend upon a portion of the exhaust included as part of the overall aircraft geometry.

Also, the discussion so far has assumed an aircraft whose material conductivities are rather large, such as metal or carbon fiber composites. If good dielectric materials are present (those with relaxation times on the order of a fraction of a secord or larger), such as radomes or fairings, charge bound on them may also affect the polarization charge density on the aircraft.

Finally, it is frequently thought that when $E_t$ is greater than the ambient air breakdown level, at a particular location, arc attachment will occur. This is not always the case, however, because of two factors.

First, as discussed previously, local air density is a factor because as air density increases, the breakdown electric field also proportionally increases. Thus, the important physical parameter is not the electric field itself, but the ratio of electric field to air density. The local air density is a function of the vehicle aerodynamics, including speed, attitude, and altitude for a given aircraft.

The second factor concerns the radius of curvature of aircraft extremities. It has been found that if the radius of curvature is less than a certain value, then corona will occur at ambient field levels lower than that for which a propagating arc will occur. This is because at points of small radii of curvature, the local field drops off rapidly as one moves away from the point, and there is not sufficient energy in the local field to propagate an arc. This effect is related to the spatial derivative of the electric field $\frac{\partial E}{\partial s}$; $\frac{\partial E}{\partial s} \leq$ minimum value for arc formation.

The minimum value has been found experimentally for both two electrode geometries (18) and three electrode geometries (19) (i.e., one electrode is floating between the other two), with similar results.

The minimum value is found to be about $2.5 \times 10^8$ (volts/m)/m, which is also the value one obtains for the largest field on the surface of a sphere of radius 2 cm inserted into a uniform field of $\frac{1}{3}$ x 2.6 MV/m, which is just enough to cause breakdown on the sphere at sea level. The factor $\frac{1}{3}$ arises from the fact that the enhancement factor of a sphere in a uniform field is 3.

The result is that locations on an aircraft having a radius of curvature less than 2 cm may go into corona before an arc discharge would occur. This would also create a space charge that could shield part of the aircraft and/or flow around the rest of the aircraft, if say, perhaps, the sharp point of concern were a pitot tube. This space charge could also influence the local field on other parts of the aircraft, causing the initial attachment to occur at locations not evident from simple considerations.

The reader should note that this radius of curvature effect is a non-linear effect, which cannot be properly accounted for in a scale model test in which all dimensions are scaled.

## SUMMARY OF THE AIRCRAFT ELECTROSTATIC PROBLEM

Our suggested aircraft electrostatic problem for initial attachment is summarized by the existence of the following factors:

- The presence of an ambient generally non-uniform thunderstorm electric field
- The presence of a net charge on the aircraft
- A portion of the engine exhaust included as a perfectly conducting extension of the aircraft
- Local dynamic air pressure effects upon the local breakdown field
- Radii of curvature at aircraft extremities affects on the creation of corona or propagating arcs
- Space charge emitted from sharp points affecting aircraft electric field distribution
- Bound charge on dielectric materials

We are not saying at this point that all of the above factors are important all the time. We do not believe enough research has been done to evaluate many of these factors. We are merely stating our view of what the relevant physical processes may be.

## AN EXAMPLE: THE TITAN IV ROCKET

We now present an example of some of the previously described principles applied to a rocket in flight. The factors which are included in the example are:

- Exhaust effects on enhancement factors
- Exhaust charging
- Dynamic air pressure distribution
- Uniform ambient field
- Radius of curvature effects
- Net static charge

The geometry of the Titan IV rocket is shown in Figure 2. The complete analysis of this problem is too lengthy and complex to fully describe here; for more information, the reader is referred to (20). Only the main points are given here.

The rocket was analyzed in a uniform ambient thunderstorm field polarized parallel to the rocket axis. The exhaust was assumed to charge the vehicle in the manner previously described (12, 13). The portions of the exhaust which are more conductive than $3 \times 10^{-10}$ mho/m were included as a perfectly conducting extension of the vehicle. The electrostatic boundary value problem was such that the polarization charge density and the net charge density sum to zero at the lower extremity of the exhaust. The local air density profiles for the vehicle in flight were obtained by a combination of scale model experiments and fluid dynamics analysis. We now summarize the final results which provide the locations on the rocket where an initial attachment is expected to occur. This is presented in Figure 3.

The most probable locations on the rocket surface from which arcs are initiated are those points where the local electric field exceeds the air breakdown value, which is to say that the ratio of the electric field to the local air density is a maximum. Exploring the electrostatic field distribution and the air density distribution over the entire vehicle reveals the electric field to air density ratio is a maximum near the rocket tip, far exceeding the ratio at other locations. Further observations near the tip indicate the most likely breakdown points on the rocket surface to be located in an annular ring

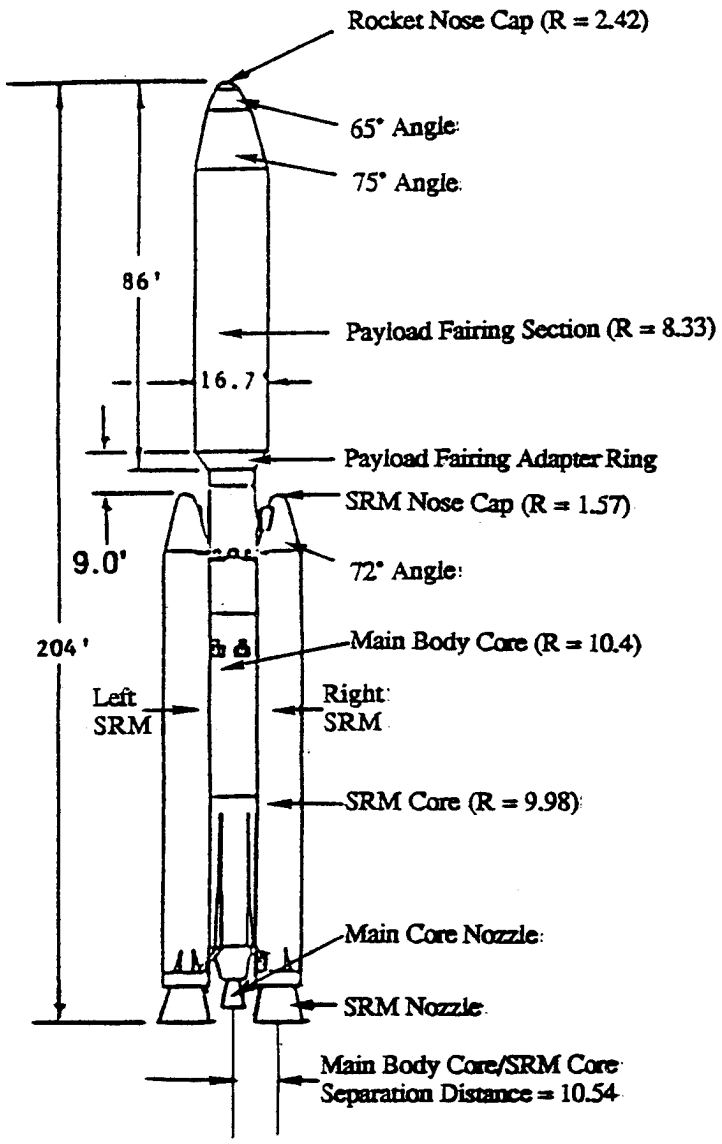
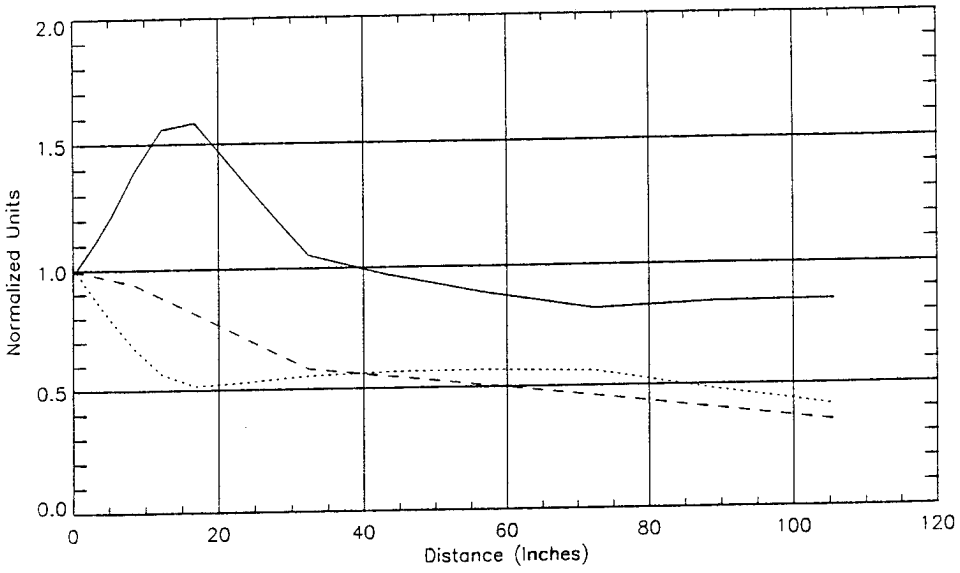
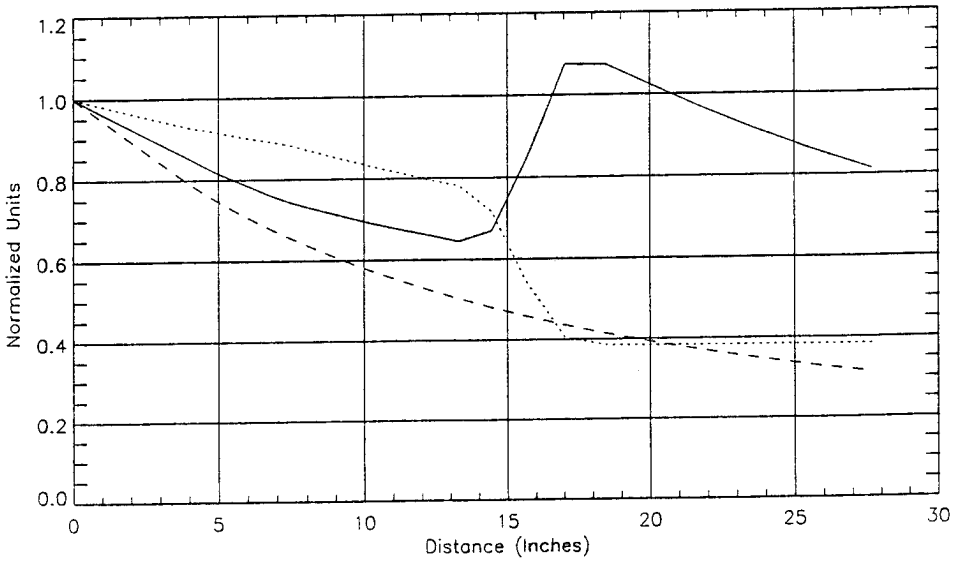



FIGURE 2 TITAN IV CENTAUR/SRMU ROCKET (R IS THE RADIUS OF CURVATURE, ALL DIMENSIONS ARE IN FEET)




(A) THE NORMALIZED VALUES ALONG THE ROCKET SURFACE AS A FUNCTION OF THE AXIAL DISTANCE FROM THE ROCKET TIP




(B) THE NORMALIZED VALUES ON THE ROCKET AXIS FROM THE TIP ON OUTWARD

FIGURE 3 THE NORMALIZED ELECTRIC FIELD (PLOT 1), THE NORMALIZED AIR DENSITY (PLOT 2), AND THE ELECTRIC FIELD TO AIR DENSITY RATIO (PLOT 3). THE VALUES ARE NORMALIZED WITH RESPECT TO THE VALUES AT THE ROCKET TIP

around the rocket tip behind the large air densities associated with the shock wave. At Mach 1.6, the annular ring exists at an axial tip distance between 12 and 17 inches as shown in Figure 3A, which plots the electrostatic field, the normalized air density, and the field to density ratio on the rocket surface as a function of axial distance from the tip. All quantities in Figure 3 are normalized with respect to the associated rocket tip values. The shock wave is evident in the abrupt fall-off of the air density. This fall-off results in a field to density ratio at 12 to 17 inches that is approximately 60% higher than the value at the rocket tip.

Another plot of interest is shown in Figure 3B which graphs the same quantities as in Figure 3A, except along the rocket axis from the tip out forward to a distance of approximately 28 inches. The normalized electric field decreases in an approximately inverse distance squared manner. The air density remains relatively large due to the shock front, out to a distance of approximately 14 inches where an abrupt fall-off is observed. As a consequence, the field density ratio achieves a maximum on the rocket axis at a location between 17 and 18 inches from the tip as observed in the figure. At this point, the ratio is approximately 10% higher than the tip value, but lower than the ratio on the annular ring.

The main point of this example is it illustrates initial attachment may not occur at the tip of an airborne vehicle, but instead some distance away from it because of the effects of the local air density distribution caused by vehicle aerodynamics.

REFERENCES

1. C.C.R. Jones, "The Rolling Sphere as a Maximum Stress Predictor for Lightning Attachment Zoning". Paper presented at 1989 International Conference on Lightning and Static Electricity, University of Bath, UK, September 26-28, 1989.

2. C.H. King and T.P. Ogden, "Analysis Technique for Lightning Attachment Zoning of Aircraft". Paper presented at 1989 International Conference on Lightning and Static Electricity, University of Bath, UK, September 26-28, 1989.

3. P. Bonamour, P. Gondot, and B. Lepetit, " Applications of the Finite Elements Method in the Frequency Domain to the Simulation of Lightning Effects". Paper presented at the Proceedings of the 1994 International Aerospace and Ground Conf. on Lightning and Static Electricity, Mannheim, Germany, May 24-27, 1994.

4. C.J. Hardwick and V.K. Thompson, "Zoning of Aircraft by Electric Field Modelling". Presented at 1992 International Aerospace and Ground Conference on Lightning and Static Electricity, Atlantic City, New Jersey, October 6-8, 1992.

5. T. Rudolph and R.A. Perala, "Linear and Non-linear Interpretation of the Direct Strike Lightning Response of the NASA F-106 Thunderstorm Research Aircraft". NASA CR-3746, December 1983.

6. T. Rudolph, R.A. Perala, P.M. McKenna, and S.L. Parker, "Investigations into the Triggered Lightning Response of the F-106 Thunderstorm Research Aircraft". NASA CR-3902, June 1985.

7. T.H. Rudolph, R.A. Perala, C.C. Easterbrook and S.L. Parker, "Development and Application of Linear and Nonlinear Methods for Interpretation of Lightning Strikes to Inflight Aircraft". NASA CR 3974, 1986.

8. T.H. Rudolph, et al., "Experimental and Analytical Studies of the Triggered Lightning Environment of the F-106B". EMA-87-R-37, April 1987.
9. F.L. Pitts, L.D. Lee, R.A. Perala and T.H. Rudolph: "New Results for Quantification of Lightning/Aircraft Electrodynamics". J. of Electromagnetics, Vol 7, 1987, pp. 451-485.
10. V. Mazur, "A Physical Model of Lightning Initiation on Aircraft in Thunderstorms". J.G.R., Vol. 94, n. D3, March 1989.
11. G. Labaune, F. Issac, J.P. Moreau, A. Bondiou, J.C. Alliot, B. Hutzler, and F. Morillon, "Experimental Study of the Connection Between a Long Spark and an Aircraft Mock Up". IX Int. Conf. on Gas and their Applications, Venezia, Sept. 1988.
12. R.A. Perala, et.al., "A Model for Predicting Triggering of Lightning by Launch Vehicles, Missiles, and Aircraft". Presented at 1994 International Aerospace and Ground Conference on Lightning and Static Electricity, Mannheim, Germany, May 24-27, 1994.
13. R.A. Perala, H. Pergament, G.J. Rigden, T.H. Rudolph, D.A. Steffen and H.S. Weigel, "Measurements of the Electrostatic Properties of Rocket Plumes". Presented at the Proceedings of the 1994 International Aerospace and Ground Conference on Lightning and Static Electricity, Mannheim, Germany, May 24-27, 1994.
14. F.J. Eriksen, T.H. Rudolph and R.A. Perala, " The Effects of the Exhaust Plume on the Lightning Triggering Conditions for Launch Vehicles". Published in Proceedings of the 1991 International Aerospace and Ground Conference on Lightning and Static Electricity, Cocoa Beach, FL, April 16-19, 1991.
15. R.A. Perala, T.H. Rudolph, C.C. Easterbrook and D.A. Steffen, "Development of Models for Predicting the Triggering of Lightning by Launch Vehicles". Paper presented at 1992 International Aerospace and Ground Conference on Lightning and Static Electricity, Atlantic City, New Jersey, October 6-8, 1992.
16. C.B. Moore and M. Brook, "Electrification of Hovering Helicopters". Presented at 1991 International Aerospace and Ground Conference on Lightning and Static Electricity, Cocoa Beach, Florida, April 16-19, 1991.
17. C.B. Moore, J.J. Jones and S.J. Hunyady, "Charge Control Experiments on a CH-53E Helicopter in a Dusty Environment". Presented at 1991 International Aerospace and Ground Conference on Lightning and Static Electricity, Cocoa Beach, Fl., April 16-19, 1991.
18. W. Hermstein, "Die Stromfaden-Entladung und ihr Ubergang in das Flimmen". Archiv fur Electrotechnik, XLV Band, Heft 3, 1960.
19. H.S. Weigel, "Corona/Arc Experiment Test Report". Final report under Contract No. F04701-91-C-0085, EMA-94-R-002, October 1993.
20. R.A. Perala, T.H. Rudolph, D.A. Steffen, G.J. Rigden and H.S. Weigel, "A Model for Predicting the Triggering of Lightning by Launch Vehicles". Final report under Contract No. F04701-91-C-0085, EMA-93-R-035, January 31, 1994.

# AIRCRAFT FUEL SYSTEM LIGHTNING PROTECTION DESIGN AND QUALIFICATION TEST STANDARD

K. E. Crouch
Lightning Technologies, Inc.
10 Downing Parkway
Pittsfield, Massachusetts, USA
Telephone (413)499-2135 FAX (413)499-2503

## ABSTRACT

SAE Committee AE4L published the first aircraft lightning test procedures document (1). Those procedures were incorporated into MIL-STD-1757 (2) and referenced in AC 20-53 (3). These documents provide information on ignition detection techniques, but do not address the establishment of pass/fail criteria or methods of determining pass/fail margins.

The need for work in both of these areas has long been recognized and has been the subject of research over the past decade. As part of that research, Lightning Technologies, Inc. under contract to the FAA Technical Center, developed a proposed revision for fuel system lightning protection requirements (4). The proposal includes a procedure for assessing lightning related fuel system design failure rates and determining an appropriate pass/fail criteria based on an acceptable risk. It also includes a procedure for evaluating multiple tests. Under present practice, one failure out of two tries is treated the same as one failure out of multiple tries. This provides little incentive to conduct more than one test during a certification program.

Examples of the proposed procedures and some applications of them are given in the following paragraphs to elicit responses from the community. It is anticipated that several discussions will take place before a consensus is attained and the procedures are incorporated into procurement documents.

## INTRODUCTION

The following paragraphs are proposed to supplement or replace paragraphs in the present test documents. Since the proposal deals only with fuel system evaluations, only paragraphs involved with fuel system testing are included. The paragraph numbering is similar to that used in the original SAE document, reference 1.

The first opportunity for incorporating these proposals will be in a revision presently under consideration by SAE AE4L and EUROCAE WG-31. The following paragraphs were submitted for consideration in the EUROCAE and SAE AE4L Testing Standard Working Draft.

PROPOSED TEST STANDARD FOR AIRCRAFT FUEL SYSTEMS

4.1.3 High Current Tests - Fuel System Components

BACKGROUND

Past experience has shown that many catastrophic aircraft lightning incidents have involved the fuel system. It is doubtful that future experience will differ greatly from the past.

There are four basic approaches to protecting the aircraft from lightning related fuel vapor ignition hazards:

1. Containment - Design the structure to be capable of containing the resulting over pressure without rupture.

2. Inerting - Control the atmosphere in the fuel system to ensure that the atmosphere cannot support combustion.

3. Foaming - Fill the fuel system volumes with a material which prevents the propagation of a flame front.

4. Elimination of Ignition Sources - Design the structure to ensure that no ignition sources are caused by lightning currents.

The first option utilizes the fuel system structure as a pressure vessel capable of withstanding the internal pressure resulting from an explosion. This approach is impractical for most systems and is mainly used for some external drop tanks.

Inerting, foaming and/or flame suppression systems are used on fighter-type aircraft, mainly to protect against gunfire hazards. These approaches are generally not applied to larger, longer range aircraft.

The procedures and techniques which follow establish the test requirements for verifying the protection design of fuel systems for all approaches, but apply mostly for designs using the fourth and most common approach, elimination of ignition sources.

The accomplishment of a "spark-free" (ignition source free) design is quite challenging considering that tens of thousands of amperes of current are conducted by the structure during a lightning strike and a voltage spark of 200 $\mu$J can ignite the vapor space in a tank.

SCOPE--These procedures are intended to provide a means for showing that an aircraft fuel system design meets the requirements for protection against lightning initiated, fuel vapor ignition hazards for conventional designs as well as for those involving advanced composite structures or any other new techniques.

Ignition hazards include those due to direct effects (on fuel tank structures and plumbing) as well as indirect effects on wires or circuits in a fuel vapor cavity (such as

fuel quantity probes). These procedures apply to fuel tanks and systems which are a part of the structure of an aircraft, as well as externally mounted tanks on wing tips, fuselage or other parts of the aircraft. The procedures apply to systems included in the initial design as well as modifications to existing fuel system components.

The procedures do not address the indirect induced effects (upset or damage) on either analog or digital electronic or electrical systems except as they relate to fuel ignition hazards.

The procedures are applicable to aerospace vehicles and parts or assemblies thereof. When these procedures are in conflict with the lightning test requirements found in the specifications, the requirements of this document govern, unless specifically deleted by the specification. (Note: The term "aerospace vehicles" includes fixed/variable wing aircraft, helicopters, missiles and spacecraft).

REQUIREMENTS--Aerospace vehicle fuel system protection designs verified using these procedures shall be shown to be protected against the hazards of lightning related ignitions for both direct and indirect effects. The lightning protection design shall be verified by similarity, test or analysis in accordance with the requirements listed below.

Containment Designs--Fuel systems and/or components designed to provide containment of the explosion shall be shown to be capable of withstanding an internal explosion. The system shall be filled with an explosive fuel/air mixture (1.2 stoichiometric propane air or equivalent) and ignited with an internal auxiliary spark source. Partial pressure or flow mixing techniques shall be used to introduce the fuel/air mixture. The system shall withstand the test without damage that would prevent continued safe flight and landing or exceed that called out in the system specifications.

Inerting and Foam Designs--Fuel systems and/or components designed to contain inerting, flame suppressants, or foams shall be shown to be capable of preventing combustion in the system. Testing shall consist of the introduction of an auxiliary ignition source into a system filled with a combustible mixture to verify that combustion will not occur and/or that combustion cannot be supported after being initiated.

Elimination of Ignition Sources--Fuel systems and/or components designed to be "spark-free" shall be shown to withstand the applicable lightning currents for the lightning zone of the aircraft in which they are located without introducing ignition sources in fuel vapor areas. Testing shall be the preferred method of verification. Engineering design tests on subelement and subassembly (coupon samples) structures should be conducted during the early design phase of the program to evaluate materials, fasteners, joints, interfaces, access doors, fuel caps, vent pipes, couplers, etc. Qualification tests should be conducted on coupon-size samples. Tests may also be conducted on subassemblies (up to and including the full tanks) to verify the system capability. System tests will require the injection of test currents at many locations to ensure that all potential ignition sources have been stressed. Since observations inside such systems are difficult, and an ignition source may be hard to identify, coupon samples are preferred.

All tests conducted (design and verification) shall be evaluated to determine the margin of safety provided by the design. Each test must consider potential ignition by voltage sparks, hot spots, and thermal sparks. These sources are defined as follows:

Voltage Spark - An electrical breakdown of the fuel/air mixture between two separated conductors.

Hot Spot - A surface in contact with fuel/air mixtures which is heated by the conduction of lightning currents to a temperature which will ignite the mixtures.

Thermal sparks - Burning particles emitted by rapid melting and vaporization of conductive materials carrying current through a point contact.

The use of fuel tank sealant materials (installed to prevent fuel leaks) to suppress and/or cover sparking in the fuel system shall be discouraged and be restricted to providing safety margin only.

4.1.3.1 Objective

Tests are conducted to determine the probability of ignition due to skin or component puncture, hot spot formation, or sparking in a region containing fuel vapors. The ignition hazard may be caused by lightning strikes attaching to the skin of the fuel system or being conducted through the area due to entry and exit points near or remote to the component.

4.1.3.2 Test Set-Up

The test setup requirements are basically the same as those described in paragraph 4.1.2 for structural damage tests.

The combustible vapor ignition detection technique (CVIDT), with the ignition sensitivity adjusted to the pass/fail criteria specified, shall be used to detect all ignition sources.

The CVIDT uses still and motion picture (video) cameras to view the test item which aids in identifying the location of potential ignition sources. The test item is immersed in a mixture with the required sensitivity, and cameras are mounted behind a glass barrier. Further information on the CVIDT with application and calibration information are given in Appendix C of reference 4.

4.1.3.3 Waveforms

The same test current waveform(s) should be applied as are specified for structural damage tests in paragraph 4.1.2 for the appropriate zone(s) in which the test specimen is located.

4.1.3.4 Measurements and Data Recording

Test current measurements are to be taken and recorded as specified in paragraph 4.1.2 for structural damage testing. The minimum data to be collected/recorded would be as follows:

- Description and photographs of test set-up
- Photographs of test specimens before and after testing
- Descriptions of damage (close-up photographs may be useful)
- Test current waveform(s) and magnitudes
- Sensitivity of fuel mixture
- Environmental data - temperature, air pressure, and humidity
- Date, test personnel, witnesses, and location
- Deviations from test plan

4.3.1.5 Test Procedure

The following procedures are generic for a typical test conducted in a laboratory environment. The actual steps required will depend on the particular test equipment and test item. Each laboratory will have steps unique to their operations which will be followed during their tests.

a) Setup high current generator(s), discharge circuit, return conductors, test chamber, gas flow system, measurement and recording equipment.

b) Insert dummy test specimen or connect shorting straps to the circuit so that approximate waveform and generator verifications can be made without damaging the test specimen.

c) Inspect test area, safety interlocks, test generators and connections to insure safe operation.

d) Clear test area as required, charge and initiate discharge of generator(s) into dummy test specimen or straps to verify test generator operation. Verify waveforms, magnitudes, and operation of measuring equipment.

e) Remove dummy test specimen or shorting straps, adjust the electrodes or conducted entry leads for the actual tests as required.

f) Take background photographs of test specimen in test chamber. Install blow-out panels on chamber. Fill with test gas mixture, allowing time to achieve proper concentration. Ignite with auxiliary spark gap at level prescribed.

g) Replace blow-out panels and refill chamber. Open camera lenses, start video camera.

h) Charge generator(s) and initiate discharge into test specimen.

i) Ground the generator output or otherwise insure that the test specimen is safe to work on, close camera shutters, and stop video camera. Ignite mixture if it did not ignite during test.

j) Record appropriate data and prepare for next test as required.

4.1.3.6 Data Interpretation

The still and video camera films should be viewed to determine if any light was emitted during the tests, even if the mixture did not ignite. The cause of any light noted should be determined. If thermal sparks are observed, then more tests will probably be needed. Even under the most ideal conditions, it is almost impossible to get thermal sparks of equal levels. Several identical samples must be tested to insure that the thermal sparks will not ignite during a subsequent test.

PASS/FAIL CRITERIA SELECTION

It is the responsibility of the manufacturer, in conjunction with the appropriate procuring or regulatory agency, to establish the pass/fail criteria for the fuel system. The selection requires that an analysis of risks be made, since it is not possible to design a risk-free system. The analysis will need to consider the aircraft strike rate, the probability of a strike to the area which would affect the component under test, and the probability of an explosive mixture being present in the void.

The voltage spark ignition energy levels of propane, JP-4, JP-5, and JP-8, in the most sensitive mixtures, are very nearly identical. This means that 1.2 stoichiometric propane/air represents the fuel system threat.

Propane/air will ignite 50% of the time at 550 $\mu$J, 99% of the time at 900 $\mu$J, and 1% of the time at 330 $\mu$J. A 200 $\mu$J voltage spark will result in an ignition of propane/air less than 1 time in 10,000 tries.

Suppose the strike incidence rate for an aircraft was 1 in 2000 hours, and the fuel system component was in an area where 10% of the strikes could attach to or be swept across. The rate for the component is 1 in 20,000 hours or $50 \cdot 10^{-6}$ per flight hour (pfh). During a normal flight, with the most volatile fuel expected during service (JP-4 for example), a flammable vapor may be present during 10% of the time. This lowers the incidence rate to 1 in 200,000 hours or $5 \cdot 10^{-6}$ pfh. The lightning strike test levels (200 kA) are predicated on an incidence rate of 0.5%, so the test represents an incidence rate of $25 \cdot 10^{-9}$ pfh.

If the pass/fail criteria for the system is set at 900 $\mu$J (all sparks, occurring during tests, are 900 $\mu$J or less), then the risk of a lightning strike resulting in an ignition would be $25 \cdot 10^{-9}$ pfh. If a 550 $\mu$J criteria were selected, the rate (and risk) would drop to $12 \cdot 10^{-9}$ pfh. At 330 $\mu$J, the rate would be $2.5 \cdot 10^{-10}$ pfh. However, if 200 $\mu$J were selected, the rate would be $2.5 \cdot 10^{-12}$ pfh.

The relative importance of these numbers depends on the total system risk analysis. In some parts of the system, $10^{-5}$ may be the best attainable and must be accepted. In other areas, $10^{-15}$ may be attainable with reasonable effort. This example is not intended to provide any guidance on what risk may be acceptable.

Once the pass/fail criteria has been selected, then a fuel mixture sensitivity can be selected. If it is desired to be 90% confident that a test passes the criteria, then the test gas must exhibit a 90% probability of ignition at that level.

## EVALUATING MULTIPLE TESTS

Qualification tests, and some design tests, are often conducted on a single test specimen and may involve a single test. When the required test margins greatly exceed the environment, or the test response is very repeatable, a single test may be appropriate. In testing fuel systems, the detection vapor and the structure tend to respond statistically and the need for more than one test becomes much more important. Unfortunately, qualification testing criteria does not usually address evaluating multiple test results. If one test fails, the item fails, if one out of ten fails, the item still fails. Under such a requirement, there is no incentive to conduct more than one test.

The solution involves establishing a confidence level for the criteria, for which statistical calculations can be made. In terms of fuels testing, the criteria selected could be a 90% confidence that no sparks exceeding 550 $\mu$J were present during the test.

To verify that such a criteria has been met, two assumptions must be made when conducting multiple tests. First, the ignition vs. energy characteristics of the detector mixture must be well established and known to at least a 99% confidence. This requires that a substantial number of tests have been conducted and used in computing the relationship between ignition probability and energy.

Second, and probably more difficult to verify, the repeated tests must be essentially identical. When thermal sparks are involved, which are present in a large portion of fuel system sparking, this assumption may not be easy to justify. However, without this assumption, no matter how flawed the assumption may be, no conclusions regarding multiple tests can be made.

If a mixture with known ignition probabilities is used in the chamber, and no ignition occurs during the first test, then the following conclusions can be drawn. Since no ignition occurred, it can be concluded with 90% confidence that the energy level representing 90% ignitions was not exceeded. Similarly, there would be a 50% confidence that the 50% ignition energy level was not exceeded and only a 1% confidence that the 1% ignition energy level was not exceeded.

Suppose that the pass/fail criteria for the system is a 90% confidence that no sparks exceeding 550 $\mu$J are created by the test. If the detection mixture used during the test has a 50% probability of ignition at the 550 $\mu$J level, the criteria can not be met by a single, non-ignition test result. There are two possibilities for proceeding. Retest with another mixture that has a 90% or greater probability of ignition at 550 $\mu$J or retest several times with the same mixture.

Retesting with the same mixture will probably be easier than developing a new mixture since new formulations will require extensive testing to verify the ignition energy level probabilities. Table 1 gives some examples of how additional tests will increase the confidence that sparks developed during the tests do not exceed the specified energy level.

In the first example, the mixture selected has a 90% probability of ignition at the pass/fail energy level specified. After the first test (no ignition), there is a 10% chance (confidence) that a spark occurred during the tests that exceeded the energy level and a 90% chance (confidence) that the spark was less than the energy level. After a second test with no ignition, assuming that the second test resulted in a spark identical to that of the first test, there is an even greater confidence that the spark was lower than the 90% probability energy. Since the results of the result of the second test was the same as the first, the two probabilities of the spark being greater than the level are multiplied. This squaring of the probability, as shown in the table, gives a 1% chance that the spark was greater than the level or a 99% chance that the spark is less than the ignition energy of the detection mixture. As the number of tests resulting in no ignitions increase, so does the confidence that the energy of the spark did not exceed the selected level.

The lower the probability of ignition for the detector mixture at the selected energy level (criteria), as in example 2, the greater will be the number of non-ignition tests needed to achieve the same confidence that the sparking is below the selected ignition energy level.

Example 3 shows the confidence levels associated with obtaining ignitions. It is interesting to note that after one test, what can be concluded about the energy of the spark is the same whether or not an ignition occurred.

Example 4 considers the problem where both ignitions and non-ignitions occur during the tests. With both occurring, it is possible to estimate the actual energy level of the spark. If one ignition occurs in two tries, it may be the 50% level. Two out of three indicates the 66% level. The confidence of those estimates can be calculated using statistical formulas appropriate for the distribution.

A mathematical formulation of above logic is no doubt possible, but is beyond the limited statistical experience of this author.

### 4.1.4 High Voltage Streamer Tests

Tests and theoretical calculations have shown glow discharges (corona) are not sufficient to ignite fuel/air mixtures. The standard voltage spark source uses a corona source to stabilize the gap break down, and that corona source (100 $\mu$A) cannot ignite even sensitive hydrogen/argon mixtures. The test as described and as carried out can not produce anything other than corona discharges. The entire paragraph must be deleted.

TABLE 1 - DETERMINING CONFIDENCE OF SELECTED IGNITION PROBABILITY LEVELS AS A FUNCTION OF REPEATED TESTS CONDUCTED IN KNOWN VAPOR MIXTURES

| Test No. | Ignition | Confidence that Spark was | |
|---|---|---|---|
| | | Greater than Level | Less than Level |
| Example 1 - Detection mixture ignites 90% of the time at the pass/fail energy level | | | |
| 1 | n | 10% (P=.1) | 90% |
| 2 | n | 1.0% ($P^2$=.01) | 99% |
| 3 | n | 0.1% ($P^3$=.001) | 99.9% |
| Example 2 - Detection mixture ignites 40% of the time at the pass/fail energy level | | | |
| 1 | n | 60% (P=.6) | 40% |
| 2 | n | 36% ($P^2$=.36) | 64% |
| 3 | n | 21% ($P^3$=.21) | 79% |
| Example 3 - Detection mixture ignites 40% of the time at the pass/fail energy level | | | |
| 1 | y | 60% | 40% (P=.4) |
| 2 | y | 84% | 16% ($P^2$=.16) |
| 3 | y | 94% | 6% ($P^3$=.06) |
| Example 4 - Probable spark energy level | | | |
| 1 | n | | |
| 2 | y | 50% | |
| 3 | n | 33% | |
| 4 | n | 25% | |
| 5 | y | 40% | |

REFERENCES

1. SAE Committee AE4L, "Lightning Test Waveforms and Techniques for Aerospace Vehicles and Hardware," June 20, 1978.

2. Department of Defense, U.S.A., Military Standard "Lightning Qualification Test Techniques for Aerospace Vehicles and Hardware," MIL-STD-1757A, 20 July 1983.

3. Federal Aviation Administration, "Protection of Airplane Fuel Systems Against Fuel Vapor Ignition Due to Lightning," Advisory Circular No. 20-53A, April 12, 1985.

4. K. E. Crouch, "Aircraft Fuel System Lightning Protection Design and Qualification Test Procedures Development," FAA Report No. DOT/FAA/CT-94/74, September 1994.

# SESSION 05B
# ELECTROSTATICS
# CHAIRPERSON: RICHARD C. ADAMO

# USN/USA/USAF AIRCRAFT LIGHTNING STRIKE SURVEY 1973 - 1994

Theodore L. Harwood
Computer Sciences Corporation
1215 Jefferson Davis Hightway, Suite 1209
Arlington, Virginia 22202
Telephone (703) 416-0966 FAX (703) 416-0885

## ABSTRACT

This paper reports on one of many ongoing efforts by participants a joint international civilian and military program to compile lightning data on aircraft and to evaluate existing aircraft radome lightning protection design strengths and weaknesses. U.S. Navy, U.S. Army and U.S. AirForce lightning data has been compiled over a twenty year period and analyzed to determine lightning attachment locations and aircraft altitudes when struck by lightning. Strike rates for U.S. Navy aircraft are also presented.

## INTRODUCTION

Lightning strikes on military aircraft are not an infrequent event. Navy, Army and Air Force pilots have reported that their aircraft have been struck by lightning at least 1570 times since 1974. Many strikes to military aircraft are not reported because the lightning attachment to the aircraft is not felt or seen by the aircrew and no damage occurs. Military aircraft are largely manufactured with aluminum, which is an excellent conductor of electricity. Current densities at any single point between entry and exit points on a metallic structure seldom cause damage. The direct effects of the lightning interaction with metallic surfaces of the aircraft at the entry and exit points are normally evidenced by pitting of the metal surface. If the surface trailing edge experiences a flash hang-on, the metal surface can experience melt-through. Direct effects on nonmetallic surfaces include pinholes and delamination. Other damage mechanisms are the result of resistive heating of conductors, lightning channel shock wave and over-pressure and over-voltages induced on electronics.

Lightning statistics for military aircraft compiled over this 20 year period indicate that the nose of the aircraft is struck more than 48%, with radome damage cited in more than 36% of the strikes. Civilian aircraft lightning statistics also indicate an inordinate number of radomes damaged due to interaction with the lightning environment. Additionally, the European military and civilian aircraft community have also been subject to significant lightning induced radome damage. A high reported rate of lightning strikes to the nose of aircraft is not surprising. The flash occurs in the aircrew field of view, often causing temporary flash blindness lasting from a few seconds to a few minutes. Additionally,

radomes are more susceptible to damage from the lightning current than other parts of the aircraft.

Typical lightning induced radome damage ranges from burn marks and pin holes in the radome, to complete destruction of the entire radome and radome loss in flight. These findings are disturbing in that there is a lightning test standard for radomes that the majority of the aircraft have passed and have been judged to be "lightning hard." Additionally, the effect of the loss of a radome in flight for transatlantic two-engine aircraft such as the AIRBUS A320 and the Boeing 767 could result in a significant loss of life if the radome were to be injested into one or both engines.

## BACKGROUND

Lightning interaction with aircraft is a complex event. It consists of phenomena associated with lightning attachment to the object, interaction of lightning induced electric fields and currents with the airframe and systems, movement of the aircraft through the established lightning channel, meteorological conditions at the time of strike and various other factors. The interaction of the aircraft with the lightning environment is categorized into the two effects previously discussed: (1) direct effects; and, (2) indirect effects.

Direct Effects. Lightning direct effects are associated with the physical damage at the attachment points where the lightning channel interacts with the structure of the aircraft. The direct effects lightning environment is generally divided into four separate components: (1) initial stroke; (2) intermediate current; (3) continuing current; and, (4) restrike. MIL-STD-1757A "Lightning Qualification Test Techniques for Aerospace Vehicles and Hardware" defines the representative direct effects waveforms. Lightning can also attach (or reattach) to the fuselage, wings, vertical and horizontal stabilizers. These direct effects (physical interaction of lightning channel with structure and components) can penetrate metal or composite materials and ignite fuel or cause catastrophic failure of flight control systems.

Indirect Effects. Indirect effects damage is associated with the damage, either electrical or physical, as a result of the coupled currents and waveforms on the airframe and its systems while the aircraft is a part of the lightning channel. Indirect effects damage can also be associated with a near-by lightning strike where there is no physical attachment to the airframe. Lightning produces radiated electric and magnetic fields that couple to electrically conductive components of the aircraft. MIL-STD-1757A defines these as waveforms as well.

Aircraft Lightning Protection and Validation Efforts. Military aircraft standards normally require that aircraft be protected to lightning effects in accordance with MIL-B-5087B and MIL-STD-1757A. MIL-B-5087B specifies that protection for lightning require that bonding allow discharge current to be carried between the extremities of an aircraft without risk of damage to flight controls or producing sparking or voltages within the vehicle in excess of 500 volts. These requirements are based on a lightning current waveform of 200,000 amps peak, a pulse width of 5 to 10 microseconds and a rate of rise of at least 100,000 amps per microsecond. It gives guidance on bonding jumper size, resistance of control surface hinge attachments, bonding of protrusions, rivet spacing for riveted skin construction, lightning test requirements and corrosion control techniques.

## DISCUSSION

This paper presents the results of a survey of reported lightning strikes to U.S. Navy U.S. Army and U.S. Air Force aircraft during the period of 1974 to 1993. The data was compiled from reports from the Navy Safety Center, Norfolk, VA, and the Air Force Safety Agency, Norton AFB, CA. An overview of the lightning strikes to Navy, Army and Air Force aircraft is presented in Tables 1, 2 and 3.

TABLE 1. US NAVY LIGHTNING DATA

| A/C | STKS | A/C | STKS | A/C | STKS | A/C | STKS |
|---|---|---|---|---|---|---|---|
| A-3 | 5 | E-2 | 9 | S-3 | 1 | T-2 | 3 |
| A-4 | 38 | E-6 | 1 | C-9 | 3 | T-34 | 1 |
| A-5 | 8 | F-4 | 8 | C-12 | 25 | T-39 | 5 |
| A-6 | 16 | F-14 | 9 | C-118 | 2 | T-44 | 6 |
| A-7 | 11 | F-18 | 12 | C-130 | 7 | | |
| EA-6 | 10 | P-3 | 163 | C-131 | 2 | | |

TABLE 2. US ARMY LIGHTNING DATA

| A/C | STKS | A/C | STKS | A/C | STKS |
|---|---|---|---|---|---|
| A200 | 1 | U-3 | 1 | UH-1 | 2 |
| C-12 | 37 | U-8 | 1 | UH-60 | 1 |
| OV-1 | 2 | U-21 | 19 | CH-47 | 3 |

TABLE 3. US AIR FORCE LIGHTNING DATA

| A/C | STKS | A/C | STKS | A/C | STKS | A/C | STKS |
|---|---|---|---|---|---|---|---|
| A-7 | 8 | F-4 | 149 | C-119 | 1 | C-20 | 1 |
| A-37 | 1 | F-5 | 2 | C-124 | 8 | C-21 | 7 |
| A-10 | 5 | F-15 | 39 | C-130 | 208 | C-22 | 1 |
| F-100 | 4 | F-16 | 9 | C-131 | 17 | C-5 | 12 |
| F-102 | 4 | B-52 | 107 | C-135 | 99 | C-9 | 2 |
| F-101 | 4 | B-57 | 2 | C-140 | 1 | T-29 | 14 |
| F-105 | 3 | C-47 | 1 | C-141 | 34 | T-39 | 8 |
| F-106 | 17 | C-97 | 2 | C-10 | 1 | | |
| F-111 | 64 | C-118 | 2 | C-12 | 4 | | |

The tables provide lightning strike data for 48 individual type aircraft, however, the strike data (62%) is dominated by just five aircraft (P-3, C-130, F-4, B-52 and C-135). Lightning strikes to aircraft that perform similar missions are as follows:

| Aircraft Mission | Number of Strikes | % of Total Strikes |
|---|---|---|
| Attack | 99 | 6.3% |
| Bomber | 122 | 6.0% |
| Cargo | 702 | 44.7% |
| Special Mission | 21 | 1.3% |
| Fighter | 394 | 25.1% |
| Patrol | 163 | 10.4% |
| Trainer | 90 | 4.4% |
| Utility | 23 | 1.1% |
| Helicopter | 6 | 0.3% |

The nose of the aircraft was the most frequently reported attachment point for all aircraft. Wing tips, pitot probes, vertical stabilizers, antennas and external fuel tanks also show some percentage of lightning attachments. Figure 1-1 presents the reported points of lightning attachment to all aircraft. The UNK value indicates that there was a lightning event on the aircraft, but the attachment point was not reported in the lightning file.

The majority of lightning strikes reported were below 15,000 feet. The data was usually reported in altitude above Mean Sea Level (MSL). The actual elevation above ground level (AGL) can be less by 1,000 feet to 5,000 feet, dependent on the height of the ground below the aircraft (i.e., an aircraft altitude of 15,000 feet MSL above Denver, Colorado will be only 10,000 feet AGL). This can place the aircraft in the more severe cloud-to-ground lightning environment. Figure 1-2 shows the percentage of strikes that occur as related to aircraft altitude.

The 20 year flight hour history of operational Navy aircraft is shown in Table 3. The hours flown by the Fleet Replacement Squadrons (FRSs) average 35% of total flight hours. These hours were not taken into account when calculating operational aircraft lightning strike rates as the training commands rarely fly in bad weather conditions. The reported strike rate (i.e., total strikes per flight hour) of Navy aircraft is also shown in Table 3. Flight hour data for U.S. Air Force and U.S. Army aircraft was not available.

These strike rates are not significantly different than those reported by Corbin [1] for U.S. military aircraft. They are considerably different than Corbin reported for commercial aircraft. Corbin identified that Plumer [2] and Anderson [3] reported rates of from one strike in 2941 flight hours to one strike in 7752 hours. Only the P-3 exhibited rates comparable to commercial aircraft.

Reported strike rates for military aircraft vary by over an order of magnitude from that of civilian aircraft. This raises questions concerning military aircraft lightning experience. This situation has sometimes been attributed to the military aircraft "see-and-avoid" capability. This may be the case for war time operations, however, the 20 year history reported in this paper has been peace time flight. Military aircraft are under the same flight restrictions as commercial aircraft while enroute to the restricted training area. The "see-and-avoid" argument cannot wholly be responsible for the strike rate discrepancy.

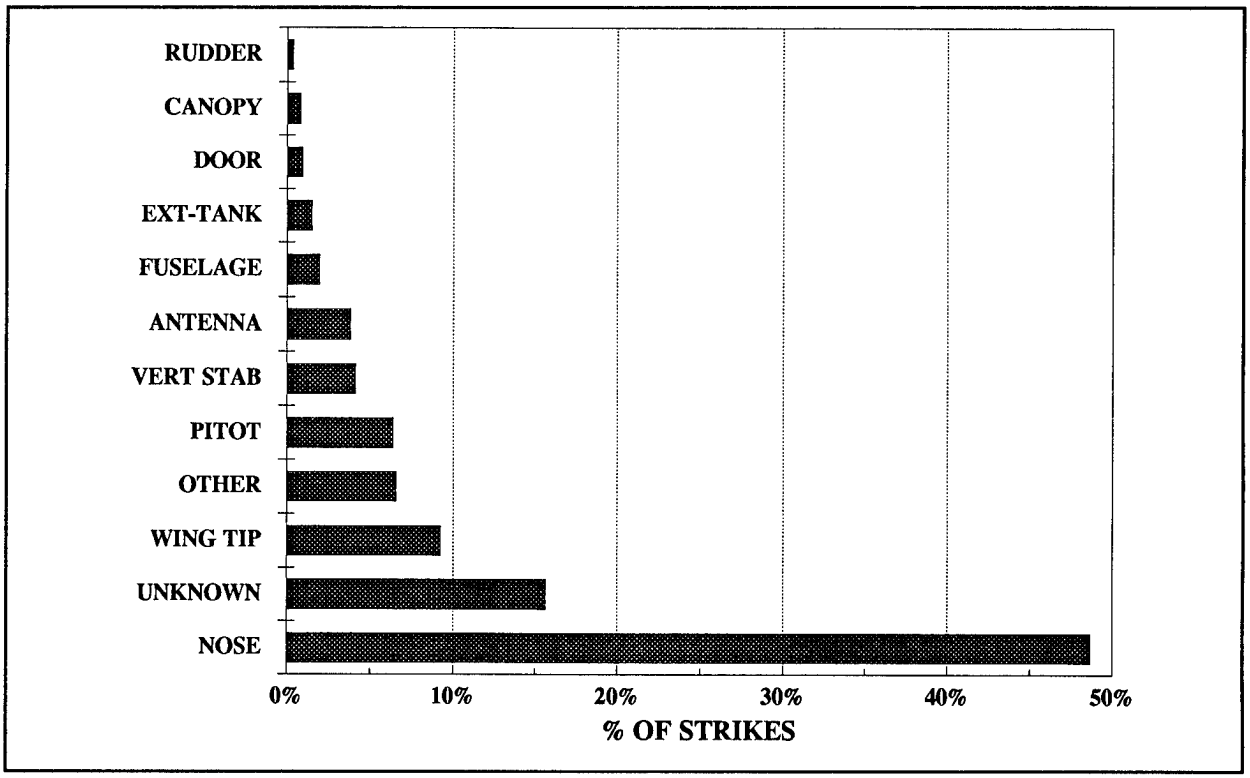



FIGURE 1-1. REPORTED STRIKE LOCATIONS, ALL AIRCRAFT.

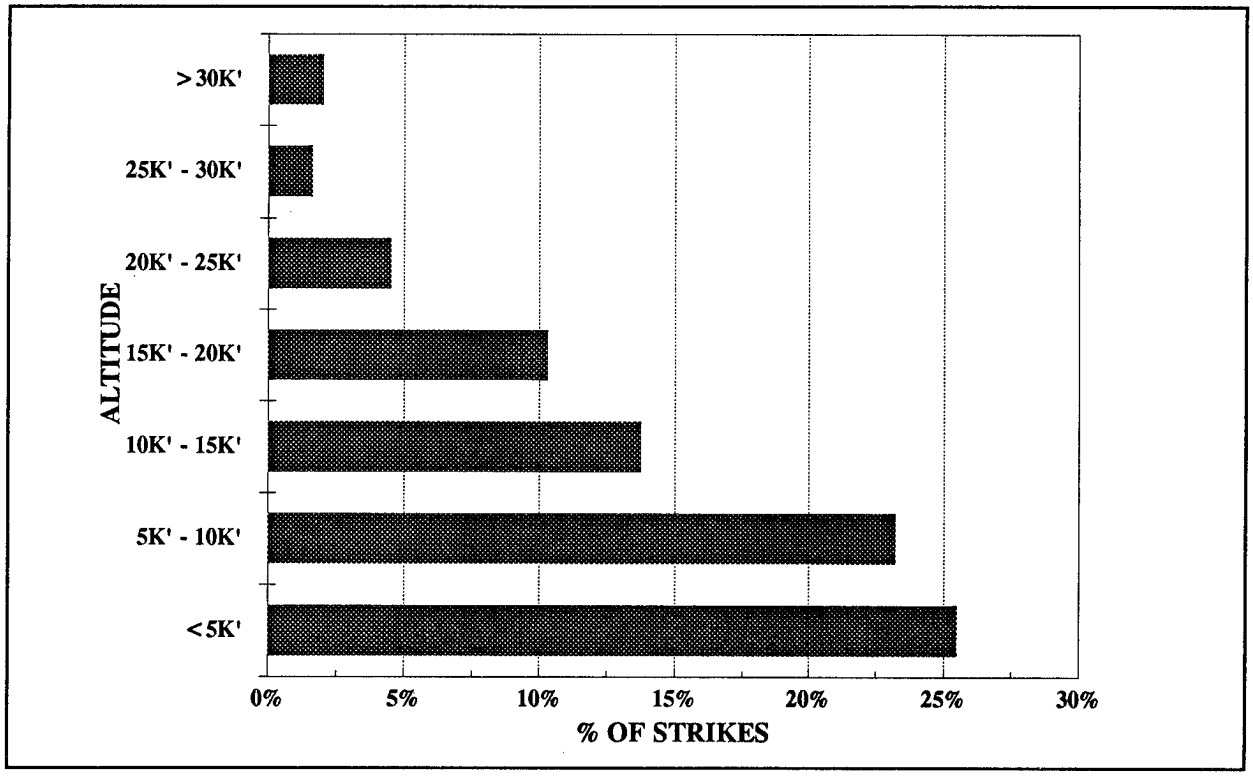



FIGURE 1-2. ALTITUDE OF AIRCRAFT WHEN STRUCK BY LIGHTNING.

TABLE 3. U.S. NAVY OPERATIONAL AIRCRAFT STRIKE RATES.

| A/C | TOTAL REPORTED STRIKES | TOTAL HOURS | FRS HOURS | TACTICAL HOURS IN ENVIRONMENT | REPORTED STRIKE RATE |
|---|---|---|---|---|---|
| P-3 | 163 | 1,216,782 | 425,874 | 790,908 | 4,852 |
| A-6 | 18 | 2,658,724 | 930,553 | 1,728,171 | 96,009 |
| E-2 | 9 | 847,089 | 296,481 | 550,608 | 61,179 |
| EA-6 | 10 | 532,736 | 186,458 | 346,278 | 34,628 |
| F-14 | 11 | 1,659,121 | 580,692 | 1,078,429 | 98,039 |
| F/A-18 | 13 | 1,416,085 | 495630 | 920,455 | 70,804 |
| TOTAL | 224 | 8,330,537 | 2,915,688 | 5,414,849 | 24,173 |

Other factors are involved. For example, discussions with the manufacturer of the F/A-18 aircraft indicate that their technicians have detected over 30 strikes to the Navy F/A-18 (vice the 13 reported). Many of the strikes reported by the manufacturer did little or no damage to the aircraft. U.S. military aircraft do not report on strikes that result in little-to-no damage unless safety-of-flight is compromised. Additionally, scale model testing of the A-6 aircraft indicates that strikes to the nose area should occur about 17% of all strikes. Strikes to the nose area were experienced over 55% of the time. The strikes to the nose area often impact safety-of-flight due to aircrew momentary blindness. Allthese strikes are probably reported, even though little or no damage occurs in the majority of strikes. This would result in a three-to-one ratio of actual strikes to reported strikes. An adjusted average Navy aircraft peace time strike rate of one in 8000 flight hours is more reasonable, taking non-reported strikes into account.

REFERENCES

1. J. C. Corbin, "Lightning Interaction With USAF Aircraft," Proceedings of the 1983 International Aerospace and Ground Conference on Lightning and Static Electricity, Fort Worth, Texas, 21-23 June 1983, paper 61.
2. J. A. Plumer, and B. L. Perry, "An Analysis of Lightning Strikes in Airline Operation in the USA and Europe," Proceedings of the 1975 International Aerospace and Ground Conference on Lightning and Static Electricity, Culham Laboratory, England, 14-17 April 1975.
3. R. B. Anderson, H. Kroniger, and M. Smith, "Lightning Strikes to Aircraft - An Analytical Study," Proceedings of the 1982 International Aerospace and Ground Conference on Lightning and Static Electricity, Oxford, England, 23-25 March 1982.

# THE USE OF MAGNETICALLY COUPLED POWER SOURCES TO PROTECT ORDNANCE AND ELECTRONICS FROM LIGHTNING AND STATIC ELECTRICITY

*BY*

**Kenneth E. Willis**
**Quantic Industries, Inc.**
**990 Commercial Street**
**San Carlos, CA 94070**
**Phone: 415-637-3074**
**Fax: 415-637-3093**

## ABSTRACT

If a pyrotechnic material, explosive device or electronic circuit is completely surrounded by an electrically conducting "Faraday cage", then they are immune to the effects of lightning or electrostatic discharge. This paper describes a technology which couples electrical energy to an electroexplosive device or electrical circuit within a Faraday cage by an oscillating, highly divergent magnetic field which can penetrate a conducting but magnetically permeable membrane used to separate the primary and secondary of a transformer. The transformer secondary is within the Faraday cage, and provides an electrical power source within.

## INTRODUCTION

Many methods have been used to protect electroexplosive devices (EED's) from inadvertent initiation from electromagnetic radiation (EMR):

- Low impedance bridgewires that dissipate some thermal energy generated by EMR.
- Capacitive and inductive elements used as filters.
- Faraday cage shielding of power source, connecting wires and the EED.
- Spark gaps or transorbs to "clamp" voltage spikes.
- Switches and relays used to disconnect and shunt the EED.

These techniques vary in effectiveness, cost, added weight and reduced reliability. The ideal, lowest cost method is to surround the device in a conducting shell, or Faraday cage. All external EMR is excluded from the interior. The only problem is how to get the functioning energy into the device when needed unless a battery or other power source is contained in the Faraday cage. The invention of the RFAC solved the problem with a method for transferring electrical energy into a Faraday cage while excluding other external EMR.

This paper describes an effective method of protecting electroexplosive devices and electronic circuits from the effects of externally generated electrostatic discharges and

radiofrequency radiation. This technology has been in use for several years by NATO weapon systems to protect electroexplosive devices against inadvertent initiation. The technology was transferred to the United States in 1990 and qualified for use with electroexplosive devices by the Navy (NSWC - Indian Head). More recent applications include an all electronic ignition safety device for rocket motors and protection of laser diode drive circuits in laser ordnance initiation systems.

## TECHNOLOGY DESCRIPTION

The Radio Frequency Attenuation Coupler (RFAC) technology was originally developed in the UK for the protection of electroexplosive devices from HERO (Hazards of Electromagnetic Radiation to Ordnance), ESD (Electrostatic Discharge) and EMP Electromagnetic Pulse). Figure 1 describes the RFAC concept. An electrical circuit converts incoming DC power into an alternating current wave form with a primary frequency of approximately 100 KHz. The RFAC electronics will not turn on until the input voltage is within proper limits for a specified period of time. By assuring the voltage is in a proper range and has been applied for a few milliseconds, the circuitry prevents the device from responding to transients on the input line. The AC power drives the primary of a transformer as depicted in Figure 1. A thin foil (CuNi alloy) of conducting, but magnetically permeable material is placed between the primary and the secondary **E** cores of the transformer. A shield of highly conductive material (Faraday cage) is constructed around the electronics assembly, or electroexplosive device, to be protected. Thus the interior of the Faraday cage is isolated from any incident EMR. Energy is transferred from the primary to the secondary of the transformer through the coupling of a highly divergent magnetic field, created by the **E** core, which permeates the foil. If intense magnetic fields are generated near the coupler, they become sufficiently non-divergent (or planar) at the transformer interface so as to be highly attenuated by the transformer itself. In this manner the interior of the Faraday cage has a source of electrical power which is immune from external EM fields created by RF transmitters, electrostatic discharges or EMP.

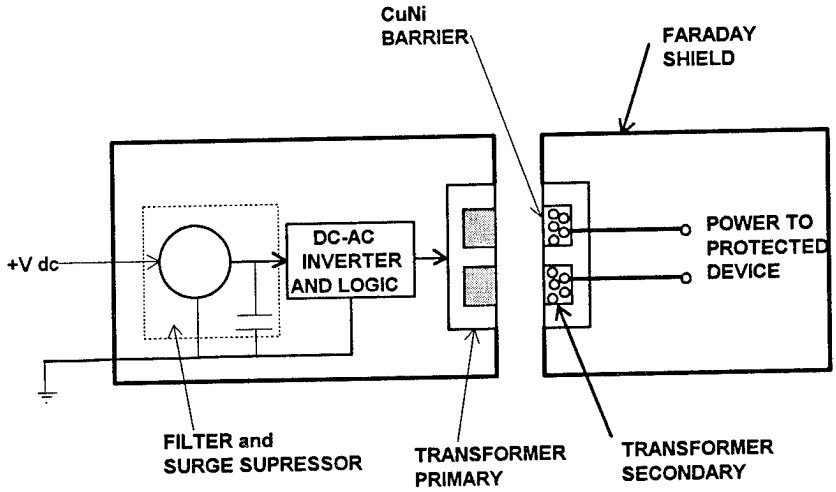



Figure 1 - The RFAC Concept

A major factor in providing safety is the limited amount of energy that can be transferred during each cycle of current. As current increases in the primary coil, the transformer saturates and no further energy can be transferred until the current is reversed. Approximately 100-1000 cycles are required to function the EED. Thus, a single pulse, regardless of the current and voltage, cannot cause inadvertent function; at most it will simply melt the transformer primary coil. The primary circuit does have a transorb and inductor to protect the circuitry from spikes or surges. These components are not related to the *safety* of the device, but are there to enhance *reliability.*

The physics upon which the RFAC is based has been around a long time. Applying the concept to the protection of EED's was apparently first proposed by Wing Commander Reginald Gray of the Royal Air Force in 1957. In the mid- to late 1970's Mr. Raymond Sellwood in the UK, applied the concept to a practical device and called it the RFAC. Mr. Sellwood was granted several patents on this implementation, including a US patent in 1979.

## QUALIFICATION TESTING

The Indian Head Division of the Naval Surface Warfare Center evaluated the RFAC under a foreign Weapons Evaluation/NATO Comparative Test Program. This test used the RFAC technology to protect a standard Navy EED, the Mark 23 Mod 0 impulse cartridge. The cartridge was considered "susceptible" when exposed to HERO environments. Design verification tests were conducted that considered electrical (MIL-I-23659) and functional (MIL-D-21625F) characteristics. The results were successful and published in an Indian Head Technical Report in 1989. Shortly thereafter the technology was licensed for North American applications.

An application specific integrated circuit (ASIC) was developed to replace the hybrid electronic module used in the UK implementation. This ASIC provided some additional safety functions and lowered the cost of the device. This new version was implemented in a connectorized format that had the same pyrotechnic functions as the Mark 23 Mod 0; this cartridge was designated the CCU-119/A. The CCU-119/A was then subjected to a full qualification test sequence at Indian Head. The test results were positive and the test report published in 1993. The qualification tests included:

- VISUAL
- X-RAY
- BRIDGEWIRE INTEGRITY
- ESD
- STRAY VOLTAGE
- FORTY FOOT DROP
- SIX FOOT DROP
- TEMPERATURE FIRINGS (-65°, 70°, 200° F)
- TH&A CYCLING
- SALT-FOG
- COOK-OFF

- HIGH TEMPERATURE EXPOSURE
- HIGH TEMPERATURE STORAGE
- SHOCK
- VIBRATION

The qualification test report was published as IHTR-1714 dated 8 April 1994. The qualification testing also included exposure to the MIL-STD-1385B HERO environments. When an EED is tested for HERO susceptibility, a fiber optic sensor is mounted near the bridgewire in order to measure the temperature rise due to the RF heating. When the initiator of the RFAC was so instrumented, there was no temperature rise detectable within the accuracy of the instruments, a phenomena which disturbed the testers. It is difficult to obtain a quantitative measure of attenuation provided by the RFAC, but it appears to be in excess of 60-80 dB over the frequencies defined in MIL-STD-1385B.

## APPLICATIONS

Several NATO weapon systems are equipped with RFAC:

- Chevaline SLBM
- Airfield attack Dispenser (Tornado)
- Spearfish and Stingray Torpedoes
- Stores Ejection Systems
- ASDIC (Cormorant)

The first US application was, as mentioned earlier, the CCU-119/A. This was a connectorized RFAC which allowed the cartridge to be replaced and reuse the more expensive primary electronics assembly. Figure 2 is a picture of the CCU-119/A. The upper left insert is the microelectronics module and the two transformer halves compared to a dime. The cut-away shows the placement of the secondary transformer and the bridgewire in the EED. The lower right photograph is the secondary EED (left) and the connecterized primary (right).

The next application used the RFAC to protect an electronic circuit. A diode laser was used to initiate pyrotechnics in a motor arm fire device. The RFAC circuitry is modified to add an additional enabling switch. This switch is a FET (field effect transistor) which must be activated before the firing power can be transferred to the drive circuit. Since laser diodes can be activated with currents under one amp, and can be excited by RF radiation, the diode drive circuit must be protected as if it were an EED. This all-electronic arm fire device can directly initiate Boron Potassium Nitrate (an insensitive pyrotechnic) since the diode laser energy density is very high. The diode laser arm-fire device was packaged in a cylinder one inch in diameter and 4 inches long.

Recently, the RFAC has been modified to perform the functions of a rocket motor ignition safety device as defined in MIL-STD-1901 using a conventional hot wire EED protected against inadvertent initiation by the RFAC. As in the diode laser arm-fire, a

separate enable signal is required before the fire signal can function the EED. This device has been qualified to the requirements of a tactical missile specification.

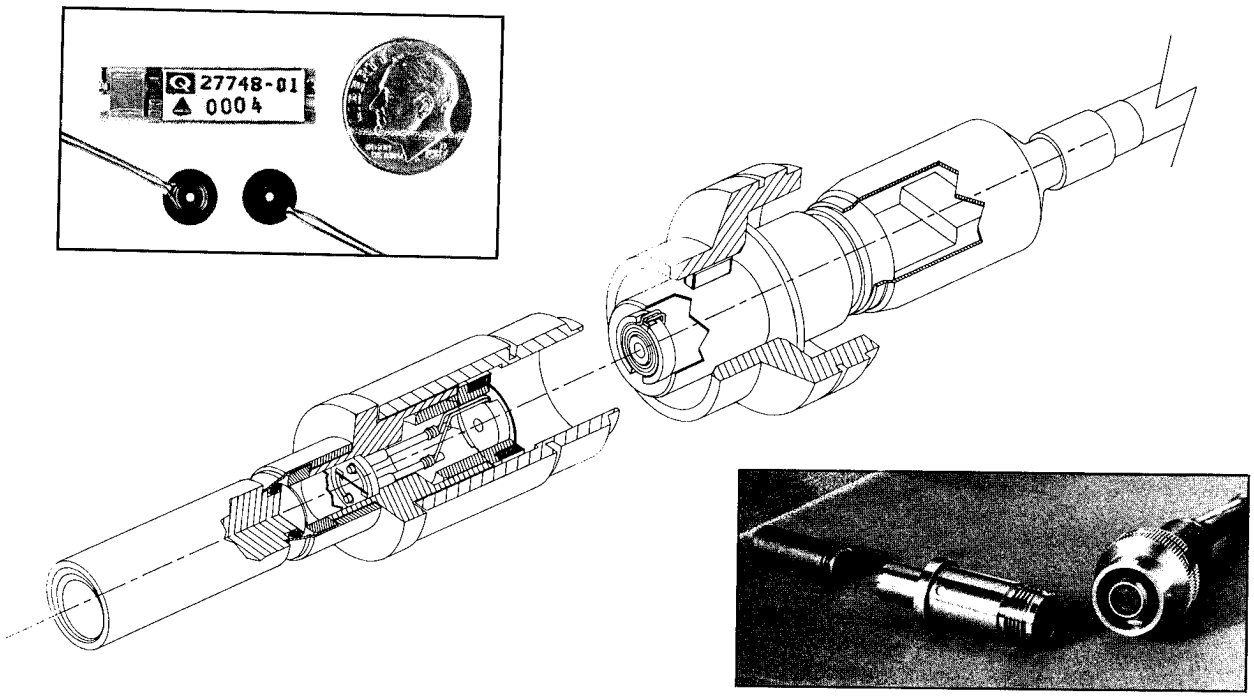



Figure 2 - The CCU-119/A

If future applications require the transfer of more power, the ASIC RFAC circuit can support larger transformers up to 19mm in diameter. The typical dual bridgewire EED requires only 10-20 watts for a few milliseconds. The laser diode drive circuits required more power, and hence larger transformers.

## SUMMARY

The RFAC technology has proven capable of protecting electroexplosive devices and sensitive electronic circuits against inadvertent function in the most severe EMR and ESD environments. The technology has found wide use in NATO weapon systems, but is not used in the US for similar applications. The first production application in the US was for a rocket motor arm-fire device. The attenuation of EMR and ESD is far higher than can be achieved with filters or low impedance bridgewires. When used as an arm-fire device, the EED is protected from inadvertent initiation even after the device is armed or enabled, a characteristic not found in electromechanical, "out-of-line" systems.

# INCEPTION ELECTRIC FIELD OF A LABORATORY SIMULATED LIGHTNING UPWARD LEADER EMITTED FROM A FRANKLIN ROD

**Gérard Berger**
Laboratoire de Physique des Gaz et des Plasmas
Décharges Electriques et Environnement, CNRS-SUPELEC
Plateau de Moulon, 91190 GIF sur YVETTE, France
Telephone (33) 169851777 FAX (33) 169410334

## ABSTRACT

The inception field of the continuous positive upward lightning leader $E_i$ has been firstly investigated in high voltage laboratory. A simple lightning rod conductor has been set under field conditions close to those experienced at ground level during the propagation of a negative downward leader. From light and current recordings, experimental values of $E_i$ have been deduced. They have been successfully compared with theoretical $E_i$ intensities derived from a purposely modified version of Rizk's model fitting our experimental set-up. This leads to predict $E_i$ for any Franklin rod. Experiments at natural scale are under progress to check the likely extrapolation of the model to natural conditions.

## INTRODUCTION

Lightning protection by means of simple rod conductor is well known since the middle of the eighteenth century, according to the first concepts of Benjamin Franklin. Since this era, one of the most fascinating problems offered to scientists has been to assess the extension of the area protected by using a vertical Franklin rod. Up to now, the universal paradigm has been to use the models of the rolling sphere, the protective angle or more generally the electrogeometric model. This approach of lightning interception is not enough physical and very often fails in actual conditions. The need of a more physical model of lightning interception has been felt by the international experts of lightning protection and this is the task devoted to an ad hoc working group working under the auspices of the CIGRE. Several leader progression models have been elaborated in the recent years. Among them, the model of Dellera and Garbagnati (1) and the model of Gallimberti (2) offer a semi-empirical approach to calculate the so-called striking and lateral interception distances provided that an incoming negative downward leader is well described by a set of line and point charges. These models are built from the knowledge of long air sparks in high voltage laboratory. They give way to complex numerical simulations and have not already been validated under real conditions. Starting from another viewpoint, Rizk (3), (4), (5) has developed a new model allowing to predict the continuous leader inception field. This concept leads to predict the threshold field $E_i$ (initiation field) generated by the negative lightning downward leader at which the positive upward leader starts its continuous propagation from the tip of a lightning rod conductor the height h of which being known. In order to check the validity of this physical model, and because no such values of $E_i$ are up to now available under natural conditions, we have simulated the conditions of the initiation of the positive upward discharge in a high voltage laboratory, as previously reported (6), (7), (8). After a short summary of the experimental set-up and testing procedure, we shall remind the salient features of Rizk's model and describe how to modify it to take the geometry of our test gap into account. Experimental and theoretical results then will be compared before their tentative extrapolation towards the natural scale.

## UPWARD CONNECTING DISCHARGE SIMULATION IN HIGH VOLTAGE LABORATORY

The natural electric field at ground level presents two superimposed components : "permanent" and "impulse" components. The permanent field is due to the charge distribution inside the lowering cloud whereas the impulse field is generated by the distribution of charge along the negative downward leader channel when propagating towards the Earth's surface. It can be shown from field measurements that the permanent electric field can reach up to 50 $kV.m^{-1}$ and sometimes more (generally between 5 and 20 $kV.m^{-1}$). Such an electric field may induce a spontaneous corona discharge around the lightning rod.

A simple model of the leader charge distribution allows to compute the fast-rising electric field at ground level during the downward leader propagation as a function of the total charge and altitude of the leader above ground . The general shape and time constants of the field increase have been confirmed by field measurements in nature, which gives consistence to the simulated field profile.

In high voltage laboratory, the negative leader is too weak to trigger a sufficiently strong positive discharge. It is however possible to study the formation and early propagation of the ascending discharge by creating a volume as large as possible inside which the quasi-uniform field varies in time such as the electric field generated by the propagating downward leader. We thus simulate only the positive upward discharge initial formation and propagation. The test gap comprises of an upper plate of large size hung over a conducting ground. The upper plate is energized from two power supplies, one under negative direct voltage (permanent field up to 20 $kV.m^{-1}$), one under negative impulse voltage (impulse field up to 300 $kV.m^{-1}$). In practice, the impulse field is produced using a negative switching impulse, the risetime of which being between 300 and 1000 $\mu s$, the crest voltage being fitted so that in the range of field where ionization processes take place (100-300 $kV.m^{-1}$, field at flat ground, not perturbated by the presence of the rod), natural and simulated field intensities coincide. Thus, the natural and simulated fields will be close in time and in their rate of growth. The impulse voltage is delivered from a Marx generator. We have to notice that apparently similar experiments performed using lightning voltage impulses of the standard shape 1.2/50 $\mu s$ (unfortunately very common) are not at all representative of lightning attachment processes, too short for convenient ionization processes to build up.

The test gap arrangement is shown in figure 1. The electric field between the plate and the ground is quasi-uniform and varies with time as the sum of the permanent and impulse components. Depending on the availability of space and on the performances of the two high voltage generators, the gaplength was equal to some 3 meters (Bazet experiments) and 13 meters (Les Renardières experiments). Similar experiments performed in 1987 (10) by researchers of Electricité de France (EdF) will be refered to for the sake of comparison. The lightning rods are placed along the plate symmetry axis, linked to the ground. The arrangement used for the largest experiments was made of a rectangular upper plate of 15x20 m surrounded by a tore and having four large spheres at the corners to prevent any corona discharge.

In order to analyse the main features of the discharge development, the electric current flowing through the rod conductor, the light emitted from the vicinity of the rod tip and from the whole gap are recorded as function of the time elapsed since the impulse voltage has been switched on. Using an image converter, the space and time evolution of the discharge has been photographically recorded at Les Renardières Laboratory. The elaboration of the current and light pictures (see figure 2) leads to the typical following results. When a Franklin rod is tested, the discharge issued from it exhibits some distinct steps (here 4 ionization steps) before the final continuous propagation of the leader starts. The corresponding current measured through a coaxial shunt presents related pulses followed by a relatively smooth increase when the leader propagates continuously . The initial velocities of the leaders are ranging from 1.5-2 $cm.\mu s^{-1}$. The streamers preceding the leader increase rapidly in length as soon as the conductivity of the leader channel increases, moving quickly towards the upper plane.

Such experiments allow to determine the continuous leader inception field $E_i$. For 1 m high rods (Bazet experiments), it has been derived from measurements that the mean field for an upward continuous leader to occur is 285 $kV.m^{-1}$ if the gaplength between the upper plate and the ground is 3 m. For 3.5 m high rods (Les Renardières experiments, gaplength = 13 m), the corresponding value is 202 $kV.m^{-1}$ . For EdF experiments, performed in 1987, the gaplength is 4 m, the rod being either 1 m or 0.5 m high ( $E_i$ is 304 and 353 $kV.m^{-1}$ respectively).

## THEORETICAL APPROACH OF THE INITIATION FIELD

In the case of a conventional downward negative lightning, the following stages of a lightning stroke incidence have been considered by Rizk in the formulation of his model. The lightning rod is assumed to correspond to a free standing structure maintained at ground potential. Following the initiation of corona streamers, a streamer-positive leader transition takes place under appropriate conditions, the positive leader seeking an encounter with the descending negative leader. In case of occurence of a final jump, breakdown eventually occur. The core of the model aims to determine the physical conditions of the initiation of the continuous leader.

GENERAL FORMULATION OF LEADER INCEPTION CRITERION-- Rizk's model (3) first assumes that the leader inception field is greater or equal to the corona inception field. Let us notice that these ambient fields correspond to the fields induced from the negative leader, that is to say that they are supposed unperturbated by the presence of the rod conductor. Let us consider first the basic configuration of a positive rod-plane gap. The positive leader grows as an extension of an ionized zone, in the vicinity of the highly stressed rod tip, where a multitude of streamer-stems converge. For the initiation of sustained leader growth, Rizk assumes that the difference between the applied field $E_{lc}$ and the opposing streamer space charge field $E_{in}$, at the tip of the streamer stem zone, must equal or exceed a critical gradient $E_c$, defined by :

$$E_{lc} - E_{in} = E_c \quad (1)$$

These fields can be related to corresponding potentials through an equivalent radius $r_{eq}$, characterizing the ionized streamer-stem zone, which is smaller than the distance from the tip to an equivalent center of the streamer space charge. Setting $\alpha$ a proportionality constant which in general is function of the ratio between $r_{eq}$ and the distance from the stem zone to the center of the space charge. The previous expression for fields can be translated in terms of potentials :

$$U_{lc} - U_{in} = U_c \quad (2)$$

The induced voltage $U_{in}$ at the tip of the ionized streamer-stem zone due to streamer space charge under critical conditions may be split into two components :

$$U_{in} = U_{ia} - U_{ib} \quad (3)$$

where $U_{ia}$ is the induced potential due to the critical space charge $Q_0$ placed at a center of charge within the streamer zone at a distance s from the high voltage electrode and $U_{ib}$ represents the absolute value of the potential induced at P (tip of the streamer-stem zone situated at a distance $s_0$ from the high voltage electrode) by image charges induced on the opposite electrode and other nearby objects, due to space charge $Q_0$ and whatever significant charge that $Q_0$ induces on the highly stressed electrode. Hence, $U_{ia}$ and $U_{ib}$ are defined by :

$$U_{ia} = Q_0 / 4\Pi\epsilon_0(s-s_0) \text{ and } U_{ib} = Q_0 / 4\Pi\epsilon_0 R \quad (4)$$

where R is only a function of the geometry and can be computed by means of charge simulation. $Q_0$ is proportional to $U_{lc}$. A simple expression of $U_{lc}$ may be derived from the above expressions :

$$U_{lc} = U_{c\infty} / \left(1+ \frac{A}{R}\right) \quad (5)$$

From the conditions prevailing during the final jump, $U_{c\infty}$ and A may be identified : $U_{c\infty}$ = 1556 kV and A = 7.78 m.

APPLICATIONS TO LIGHTNING ROD CONDUCTORS--Let us now consider a lightning rod conductor (4) for which the various geometric parameters are defined in figure 3. This situation differs from the rod-plane configuration as far as leader inception is concerned. First, the tip of the streamer-stem zone is practically at earth potential. Moreover, the gap distance d and the approximate height h above ground of the equivalent streamer space charge $Q_0$ are completely different. In this case, R = 2h, independently of the length of the gap d.

The test gap studied in paragraph 1 is slightly different from the case just above, since the upper plate is set at a finite height d above the conducting ground. A computation of R is needed using image charges both with respect to the plate and ground. An infinite number of image charges have to be set along the vertical axis passing through $Q_0$. The full computation leads to :

$$\frac{2}{R} = \Sigma\,(h - nd)^{-1} - \Sigma\,(d(m))^{-1} \quad (6)$$

n and m being relative integers, m differing from 0. The previous expression may be transformed into :

$$\frac{1}{R} = \frac{1}{2h}\left(1+ 2\,a^3\,\Sigma\,(n(n^2 - a^2))^{-1}\right) \quad (7)$$

where $a = \frac{h}{d}$ and n varying from 1 to $\infty$.

The continuous leader initiation electric field $E_i$, if taking account for the ambient ground field $E_g$ due to cloud charges (the permanent field in high voltage laboratory), is thus given by :

$$E_i = E_g + 1556 / h\left(1+ \frac{7.78}{R}\right) \quad (8)$$

where $E_i$ is in $kV.m^{-1}$.

## VALIDATION OF THE THEORY IN LABORATORY

The following table 1 exhibits the comparison between experimental and theoretical values of the initiation field $E_i$ obtained in paragraph 1. An error of less than 2% can be observed between those values, which gives consistency to the theoretical model developed by Rizk and modified as shown just above.

When the plate-ground distance tends to infinite, as for the case of natural lightning, $E_i \rightarrow E_g + 1556\ (h + 3.89)$. This might be valid in nature for the case of negative downward lightning.

**Table 1 Continuous leader inception field $E_i$**

| | Experimental | Theoretical |
|---|---|---|
| Bazet : d = 3.03 m h = 1.05 m | 285 | 289 |
| EdF : d = 4 m h = 0.5 m | 353 | 353 |
| EdF : d = 4 m h = 1 m | 304 | 308 |
| Renardières : d = 13 m h = 3.46 m | 202 | 206 |
| Renardières : d = 13.5 m h = 3.5 m | 205.5 | 205.7 |

## APPLICATION TO LIGHTNING ATTACHMENT PROCESS

A first look to the previous results points out that the upward leader is initiated for electric fields notably lower than 500 $kV.m^{-1}$, which shows a first limitation of the classical electrogeometric model. Breakdown of large gaps in laboratory occurs around 250 $kV.m^{-1}$, even though the applied field rate of growth is continuously decreasing. The further propagation of the upward leader under natural conditions will depend on the field profile generated by the downward leader. For upward leaders longer than 15-20 m, recent observations of Yokoyama et al (11) exhibit that the upward leader propagation is stepped. From their data, leader step mean velocity can be measured equal to 1.6 $10^6$ $m.s^{-1}$ (see figure 4). Berger's values reported by Golde in 1977 were ranging from 2 to 12 $10^5$ $m.s^{-1}$. Due to inherent working conditions in laboratory (lack of available space for free propagation), these values are not attainable, which emphasizes the need of further investigations in nature.

## CONCLUSIONS

It is now available to predict the initiation electric field of the propagating upward positive leader $E_i$ in laboratory knowing only the geometry of the test gap and the tested lightning rod conductor. A further step of the application of this theoretical approach is to validate the model to natural conditions since a very simple of expression of $E_i$ has been established when d tends to infinite. That is the purpose of a current program performed in nature and using natural or triggered lightning for which field measurements at the rod vicinity and electrical current flowing through the rod are simultaneously recorded. Perhaps after next summer season such data will be available. Preliminary validation of Rizk's model by comparison to Japanese data on triggered lightning (9) has shown that we may be confident in that respect. Moreover, we are under progress to complete the model during the connecting leader propagation so that the scaling factor problem would be solved.

## REFERENCES

(1) L. Dellera, E. Garbagnati, "Lightning stroke simulation by means of the leader progression model", IEEE Trans. on Power Delivery, pp. 2009-22, october 1990
(2) A. Bondiou, I. Gallimberti, "Theoretical modelling of the development of the positive spark in long gaps", Journal of Physics D : Applied Physics, 27, 6, pp. 1252-66, june 1994
(3) F.A.M. Rizk, "Switching impulse strength of air insulation : leader inception criterion", IEEE Trans. on Power Delivery, 89 WM 116-5 PWRD, pp. 2187-95, october 1989
(4) F.A.M. Rizk, "Modeling of transmission line exposure to direct lightning strokes", IEEE Trans. on Power Delivery, 90 WM 084-4 PWRD, pp. 1983-97, october 1990
(5) F.A.M. Rizk, "Modeling of lightning incidence to tall structures", IEEE Trans. on Power Delivery, 93 WM 081-0 PWRD and 93 WM 082-8 PWRD, october 1993
(6) G. Berger, "The Early Streamer Emission lightning rod conductor", 15th Int. Aerospace and Ground Conf. on Lightning and Static Electricity, paper 38, Atlantic City, october 1992
(7) G. Berger, "Determination of the inception electric field of the lightning upward leader", 8th Int. Symp. on High Voltage, paper 70.01, Yokohama, august 1993
(8) G. Berger, "Formation of the positive leader of long air sparks for various types of rod conductor", 22nd Int. Conf. on Lightning Protection, Budapest, september 1994 and also in Lightning and Mountains Conf., Chamonix Mont-Blanc, june 1994
(9) K. Horii, H. Sakurano, "Observation of the final jump of the discharge in the experiment of artificially triggered lightning", IEEE Trans., PAS-**104**, 10, pp. 2910-7, october 1985
(10) B. Hutzler et al, "Etude de la formation et du développement de décharges ascendantes", EdF internal report, published CIGRE 33-88 WG-01 IWD, Stockholm, 1988
(11) S. Yokoyama, K. Miyake, T. Suzuki, S. Kanao, "Winter lightning on Japan Sea coast - Development of measuring system on progressing feature of lightning discharge", IEEE Trans. on Power Delivery, 5, 3, p. 1418-25, july 1990

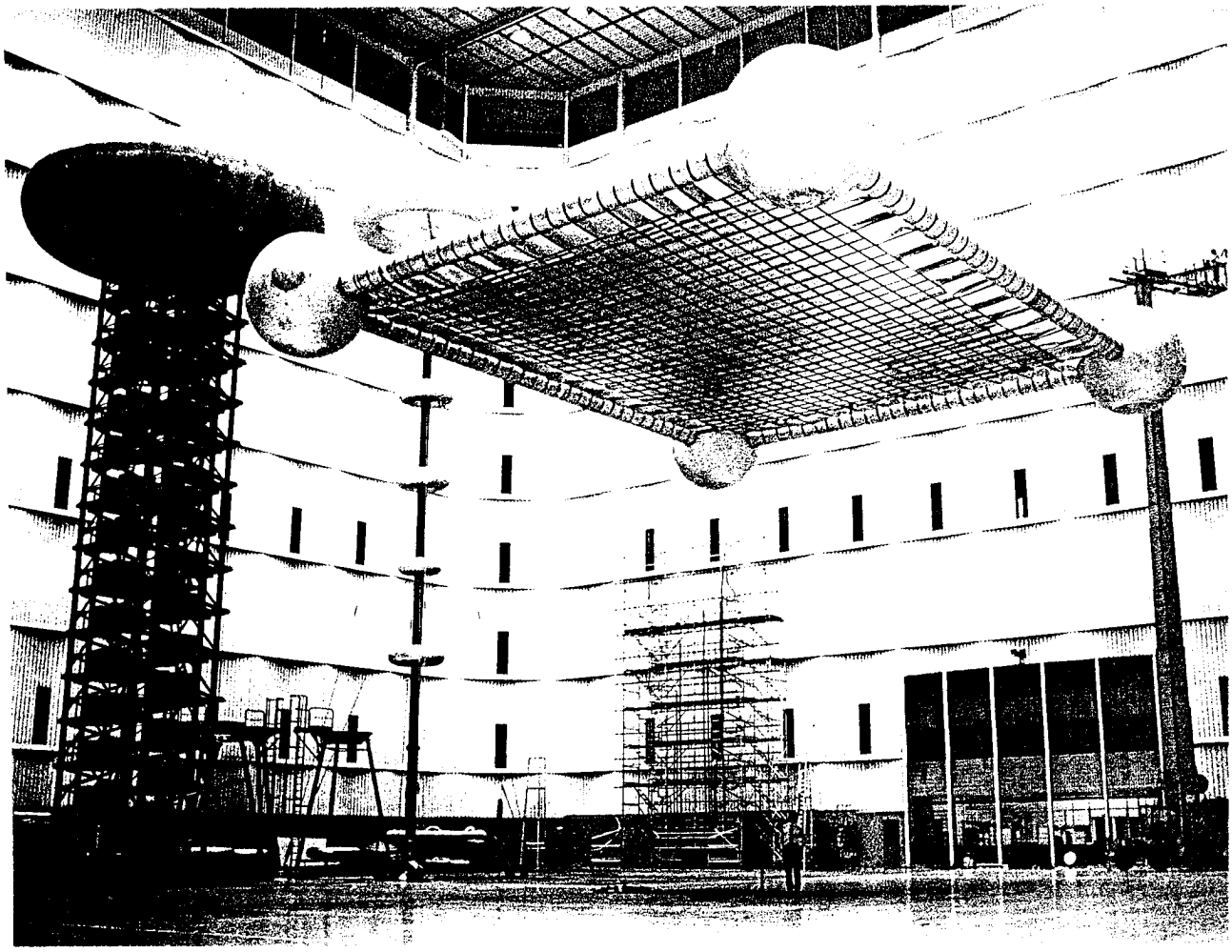


Figure 1 Experimental set-up

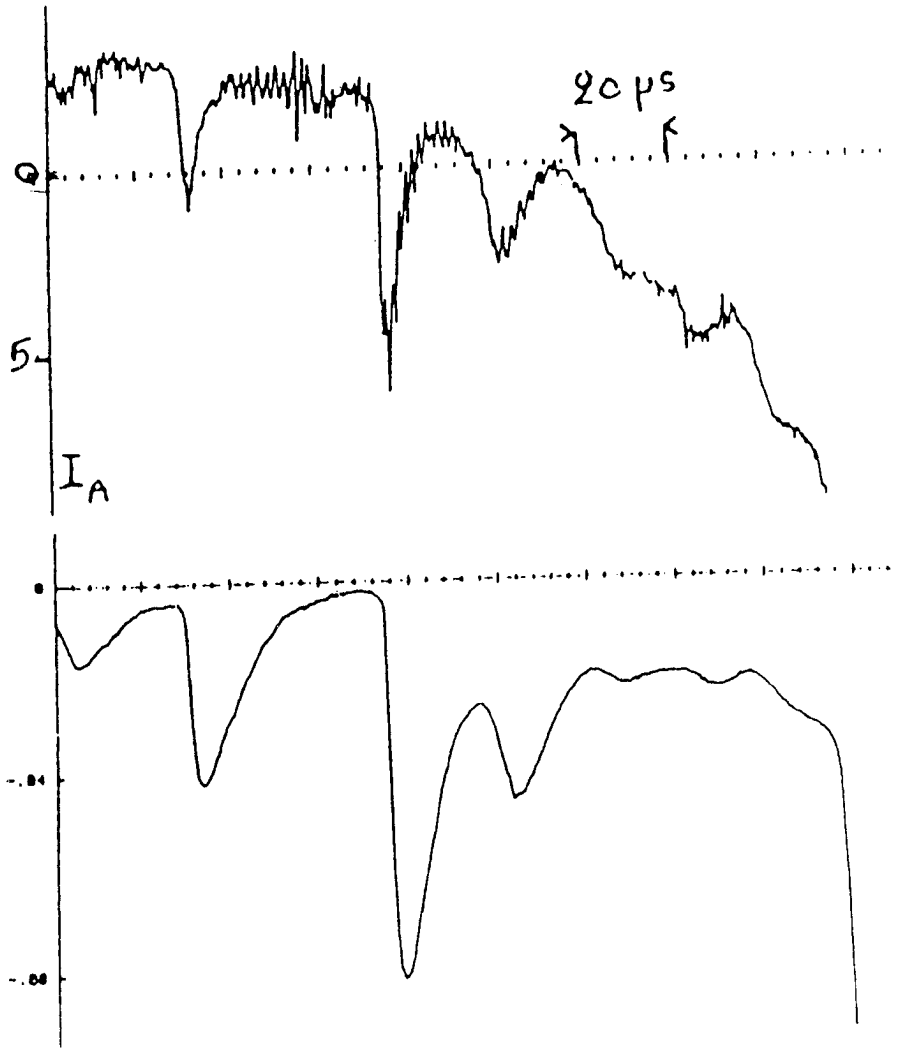



Figure 2 Current and light at a Franklin rod tip

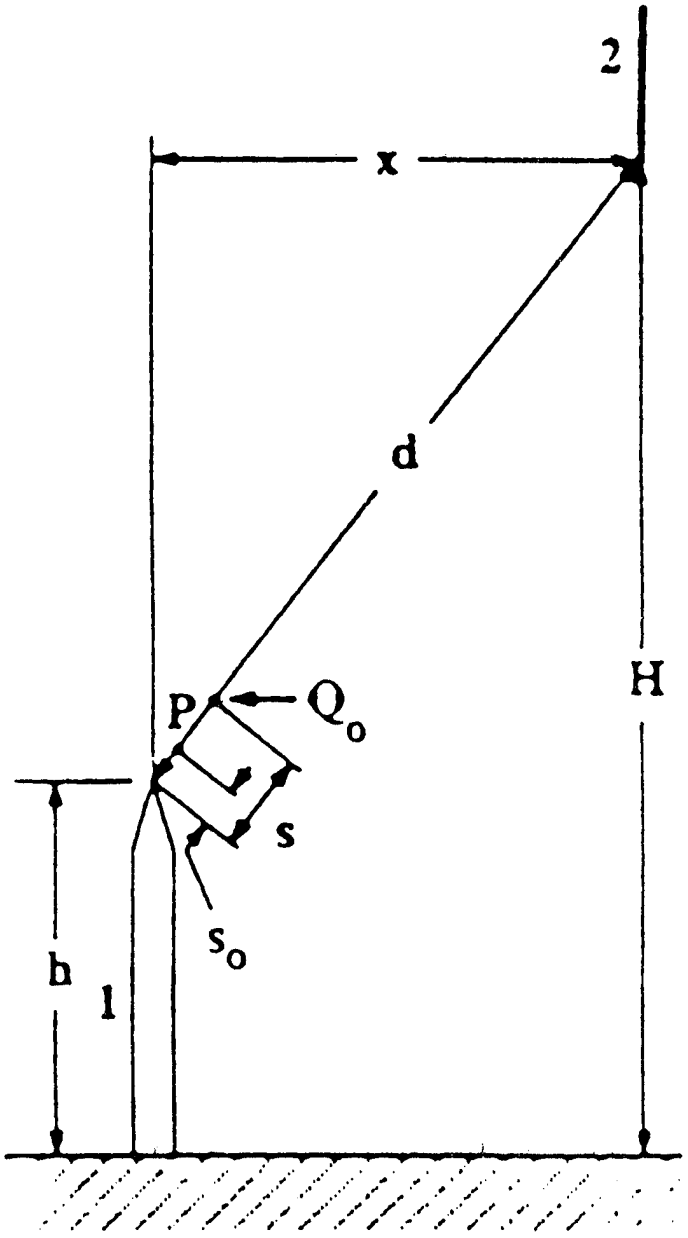



Figure 3 Definitions of parameters involved in $E_i$ computation

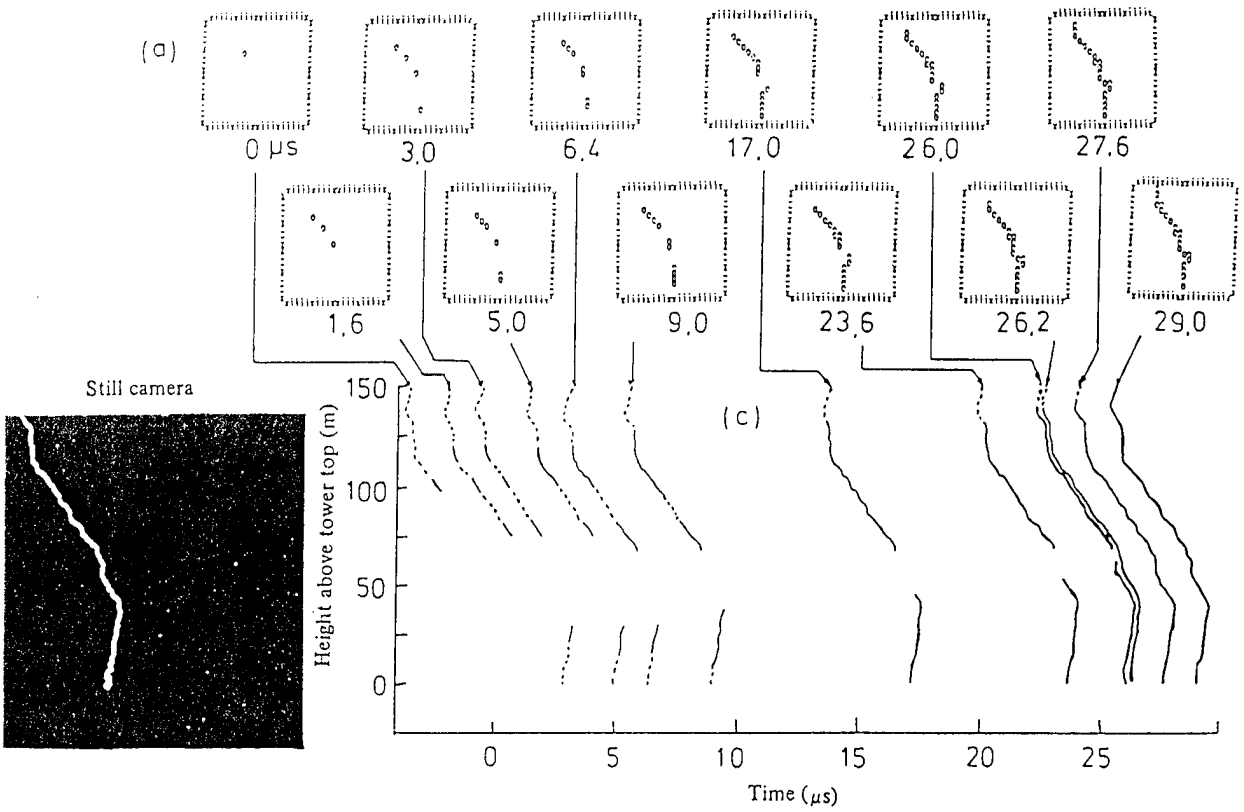



Figure 4 Lightning interception from Yokoyama's experiments

# CHARGE DEPOSITION ON ICE CRYSTALS AND DROPS AFTER LIGHTNING

T.S. Verma
Department of Physics, University of Roorkee,
Roorkee -247667 India

**INTRODUCTION :**

The ground based measurements suggest that in a cloud to ground flash, a large quantity of negative charge is lowered from cloud to earth. Thus the return stroke can be thought of as introducing an equal but opposite (Positive) charge (of order 10 Coulomb) into the lower region of the cloud, where an excess negative charge can be expected to reside on hydrometeors. it is speculated (Moore et al, 1964) that this enormous charge spreads over a significant volume of the cloud by a network of channels forming a tree-like pattern.

This sudden (50 micro-seconds) introduction of positive charge (10 coulomb) gives rise to a high transient electric field which may consequently set many hydrometeors into corona discharge. The observed UHF noise before and after lightning stroke (Brook and Kigagawa, 1964) are indicative of presence of such discharges. A burst of high frequency radiation immediately after the return stroke was also reported. These radiation are likely to originate from the charge drainage processes occurring within the cloud. Corona discharges of positive streamer type have been extensively studied because of their unique property of a long range propagation over a few hundred meter distance within the cloud provided the

requirement of a critical ambient field is fulfilled. The critical field at normal atmospheric pressure has been experimentally found to be 4 KV $cm^{-1}$ (Phelps, 1974). On applying the laboratory results to thundercloud, Griffiths and Phelps (1976), taking the overall effect of pressure and humidity into account, estimated this critical field to be 2.5 - 3.5 KV $cm^{-1}$.

The positive streamers in their voyage within the cloud are expected to interact with drops and ice particles, and deposit charge onto them, which will consequently lead to a modification in the charge distribution within the cloud.

## SECTION – I

### THE EXPERIMENTAL ARRANGEMENT

The layout of the apparatus is shown in Figure 1, where the ice crystal understudy, deposited on the tip of finely drawn glass fibre, was suspended into the chamber. The chamber comprises of a pair of circular and smooth-edged metal electrodes. A sharp metal point, passing through a PTFE stud which was well fitting into a circular hole in one of the two electrodes, acted as a live-electrode, and was used to produce streamers. The electric field required for their sustained propagation was derived from the same high voltage pulse, which was applied to the point. This was done by connecting the point

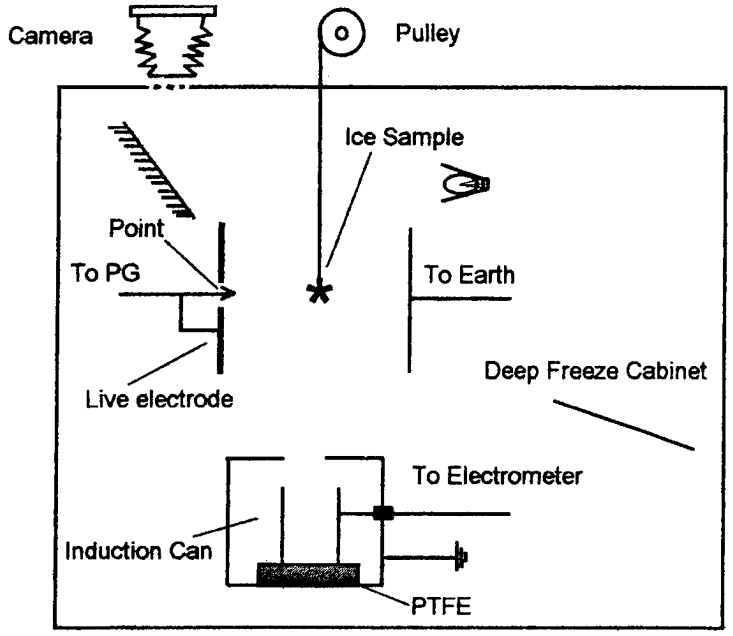



Fig. 1 Schematic diagram of the apparatus used for this experimental study.

Table 1 Charging by Streamers

| Sample | Description | Longest dim.(mm) | Mass (mg) | Q range (pC) |
|---|---|---|---|---|
| A | Irregular pellet | 5 | 7 | 13.2-19.9 |
| B | Lump of ice | 3 | 5 | 9.9-20.4 |
| C | Plance w/dendries | 5 | 9 | 14.9-24.8 |
| D | Thick plane | 4 | 10 | 19.9-34.8 |
| E | Sector plate | 3 | 6.7 | 13.2-29.8 |
| F | Column w/spikes | 3 | 4.6 | 24.8-38.0 |
| G | Needle | 2 | 0.8 | 3.3- 4.9 |
| H | Sector plate | 3 | 2.6 | 21.0-28.4 |
| I | Column | 2.5 | 1 | 8.9-15.4 |
| J | Plate | 2 | - | 15.4-21.0 |
| K | Plate | 2 | - | 18.6-25.9 |

with the live-electrode. The gap between the electrode was adjustable by varying the position of the earthed electrode.

A subsidiary experiment in the dark was performed to determine the conditions for positive streamers to cross over the electrode-gap. This was done by manoeuvering the gap distance, the position of the point and its geometry. Using the dark adapted eye 'best estimates' of the required settings were found. Another subsidiary experiment, to determine the degree of non-uniformity of the electric field between the electrodes and the point was performed. It was found that up to 2 cm from the live-electrode the present fractional change in the field values was less than 10%. Thus it was concluded that the ambient electric field in which the streamers propagated was sufficiently uniform for the experiment to proceed.

The chamber was installed in deep-dreeze cabinet. The crystal was raised up or lowered down by the use of a motor-driven pulley, the arrangement of which was assembled on the top of the cabinet. The glass fibres were drawn as fine as possible and then glued to the nylon thread. Before the crystal was transferred, the fibre was rinsed in the alcohol to remove any static charges. A tiny drop of distilled and deionised water was placed at the top of the fibre with the help of a micro-syringe. When the drop was super-cooled, the pre-selected crystal was brought into contact with it, and they were

instantly cemented together.

It was found that due to the twists present in the thread and mechanical vibrations, the crystal did not remain at one particular orientation. Therefore a modification to this arrangement was made. To provide a rigid support, a 1 cm long PTFE rod of diameter 4 mm was gued to a 50 cm long metal rod of the same diameter. A fine hole was made in the cross-sectional part of PTFE, so that one end of the glass fibre could be fixed in. To minimise the problem of static charges which the PTFE might retain, it was sliver-painted on the sides. This ensured electrical contact with the metal rod which was earthed. The rod could gradually be moved in or out, and could be fixed at any desired position. An additional advantage of this arrangement was the capability to rotate the face of the ice-sample. The temperature in the chamber was determined by taking the mean of the readings of two thermometers, one placed near the top of the chamber and the other near the bottom.

The ice samples grew on the walls of the deep freeze. Their habit and growth depended upon the prevailing conditions in the cabinet, mainly temperature and humidity, which could be varied. Crystals were selected and preserved for use. For our experiments, the samples were irregular pellets, this planes, thick plates with dendritic extensions, needles, columns and assemblage of sector plates.

## THE PROCEDURE AND RESULTS

The crystals at the tip of the glass fibre, for all these measurements, unless otherwise specified, were positioned at about 3.5 cm from the live-electrode (i.e. 3 cm from the protruding point), and the electrode gap was dept at 5.8 cm. A high voltage pulse, of magnitude +30 kV and of duration of 100 micro-seconds, was applied to the point to produce positive streamers. After the exposure to streamers the crystal was slowly lowered into the induction can which was connected to the electrometer, as shown in Figure 1, to determine the deposited charge, Q. Care was taken to avoid any contact of the ice sample with the induction can. The crystal was then raised and the process was process was repeated. About ten observations were taken with randomly varying the face of the crystal exposed to streamers. To ensure that the crystal had not retained any charges from its previous exposure, after each measurement it was raised out of the can and discharged by the use of a radioactive source; this was checked using the electrometer. Finally, the crystal was photographed, its longest dimension was noted, and its mass was determined with a micro-balance.

The results of these experiments are listed in Table 1, where the range (min.-max.), of charge, Q, deposited on the crystals together with their description, longest dimension and mass are shown. For most of the measurements the average temperature in the chamber was about -12°C. This temperature

was chosen in order to maintain almost similar conditions as were in experiment of Griffiths and Latham (1974) where investigations of corona discharge from ice particles were made. They found below temperature -18°C the electrical properties of ice crystals were such as to inhibit the corona discharge. It was found that frost formation on the electrode produced problems, and therefore efforts were made to complete each run as early as possible. Before the next run, a hot stream of air was used to remove the icing.

**DISCUSSION AND POSSIBLE IMPLICATIONS**

As seen from Table 1, where charges deposited on the various ice samples as a result of streamer interactions are shown. there is a wide scatter in the measured values. Despite the usual errors in the measurements, the statistical nature of streamer process may be a main source of this observed scatter. The charges in the streamer tips are subjected to high degree of variability, and even if other conditions remain unchanged, we cannot be specific about the interacting streamer tip. The random orientation of the crystals may be an additional source of variability.

The factors mentioned in the preceding paragraph led us to express the results, Table 1, as a range of charges (min.-max.) instead of their average values. The Needle (G) and Column (I) collected charges ranging from 3.3 to 4.9, and 8.9 to 15.4 pC respectively, whereas a high value of charge on the typical column with spikes (F) was from 24.8 to 38 pC. The plate

crystals (D, J, K and H) acquired charges on an average, from 20 to 30 pC. The irregular pellet (A) and lump of ice (B) had charges from 10 to 20 pC. These observations indicate that ice crystals of longest dimension 2-5 mm should acquire charges lying between 15 to 30 pC.

## SECTION – II

### PLAN OF THE EXPERIMENT

The basic plan of our experiment was to inject a system of streamers into a cloud of droplets, and to measure the charges deposited upon the drops as a consequence of streamer-drop interactions. A high voltage pulse of positive polarity when applied on a metal point gives rise to positive streamers which will propagate over a large distance in a uniform ambient electric field if it exceeds a critical value. These conditions which were fulfilled in our experiments simulate to a great extent what happens in a natural thundercloud where a sustained propagation of positive streamers over a few hundred meters can be expected.

In order to investigate interactions of streamers with drops of various sizes, this experimental study (Verma, T.S. 1979, A Laboratory Study of Rain-gush, Ph. D. Thesis, University of Manchester, England) was divided into three parts where different techniques of drop production were used.

1. Droplets of radii 12 to 30 μm were produced using a spinning top apparatus [May (1949)] and sized by a technique developed by May (1950).

2. Drops having radii between 35 to 85 μm were obtained by a drop generating device first developed by Abbott and Cannon (1972).

3. Drops of radii 200 to 950 μm were produced by the technique described by Atkinson and Miller (1965).

The cloud of droplets or stream of drops was allowed to fall freely through a chamber where they were exposed to a system of streamers which were produced by the application of high voltage pulses to a sharp metal point. The high voltage pulses of short duration were obtained from a pulse generator. The charge deposited on the drops as result of interactions, which was much higher than their initial charges, was measured by a charge amplifier/electrometer.

## DATA AND DISCUSSION OF RESULTS

The major errors in these experiments lay in the measurement of the charge and the size of the drops. The charge pulses were measured with an error less than ± 15%, and the dispersion in small droplet-size, as mentioned earlier, varied from ± 10- ± 15%. In addition, the statistical nature of the streamer system could be an additional source of variability. The charges on large drops were measured with a variation of ±10%, and the dispersion in drop-size was ± 2- ± 7% for medium-

sized drops and ± 2 % for precipitation drops.

Figure 2 illustrates a complete finding of these three different sets of experiments where deposited charges on the drops, as a result of positive streamer interactions, have been plotted against drop radius, In these measurements the peak pulse voltage used to produce positive streamers was + 30 kV and the pulse was of 100 $\mu$s duration. In these conditions the streamers were propagating. The results of the experiment of Phelps and Vonnegut (1970) have also been shown in the figure. The present results suggest that there exists a consistent tendency for charge deposition to increase with drop-size.

According to Phelps and Vonnegut (1970) and Phelps (1972) the smaller drop ($r < 50$ $\mu$m) are expected to be charged by an indirect mechanism, and the larger drops by a direct mechanism. The surface charge density in the direct process was more, by one order of magnitude, than that of the indirect charging mechanism. Our experiments did not reveal evidence for two distinct charging processes. Our measurements show that the charges on medium and large drops are quite close to those expected on the basis of Phelps' copper sphere experiment ; on the other hand, our smaller droplets acquired charges approximately one order of magnitude higher than Phelps observed.

References :

Brook, M. and Kitagawa, N., J. Geophys. Res. 69 No.12 ( 1964).

Griffiths, R.F. and Phelps, C.T; Q.J. Roy.Met. Soc. (1976). 102, 419-426.

Moore et al. J. Atmos. Sci. 646-665 (1964).

Phelps, C.T. J. Atmos. Terr. Phys. 36 P 103 -111 (1974)

Verma, T.S. J. Met. Soc. JAPAN Vol. 60 No. 4 (1982).

Verma, T.S. J. Annales Geophysical Vol.1 No.4.5 PP 345-352 (1983).

Verma, T.S. et al. Q.J.R. Met. Soc. Vol 109 PP 631-644 (1983).

# SESSION 06A
# TEST CRITERIA & TECHNIQUES
# CHAIRPERSON: BRIAN KUHLMAN

# DETECTION OF FUEL SYSTEM IGNITION SOURCES USING HYDROGEN VAPOR

K. E. Crouch
Lightning Technologies, Inc.
10 Downing Parkway
Pittsfield, Massachusetts, U.S.A.
Telephone (413)499-2135 FAX (413)499-2503

## ABSTRACT

The present fuel system lightning-related ignition detection techniques, ignition of propane/air and photography of test specimens, are both subject to significant interpretation. Neither gives any information on the margin by which a specific design passes or fails a test. These deficiencies have long been recognized and have been the subject of research over the past decade.

Hydrogen gas, or other gases with more sensitive voltage spark energy ignition levels, can be mixed in proportions that will yield variable ignition energy levels and reduced combustion energy release. Tests show that proper mixtures can give both pass/fail margin information as well as produced less violence during an ignition.

## INTRODUCTION

Early researchers assumed any spark that could be seen was probably energetic enough to cause an ignition. The first tests were conducted with John Robb of Lightning and Transient Research Institute (LTRI) sitting inside a darkened test chamber watching for sparks on the test specimen. The story continues that John was called away to a meeting one day during a test series, and none of the rest of the crew was willing to sit in the chamber. Since the testing had to be completed, the crew put a polaroid camera on John's chair and the tests continued. The largest opening in the camera was f/4.7 and 3000 speed film was all that was available at the time. It is believed that this was the origin of the photographic ignition detection technique.

Regardless of the actual origins of the photographic technique, it is well documented that pictures of incendiary voltage sparks (200 $\mu$J) are nearly impossible to find on the photographs (1). On the other hand, non-incendiary levels of thermal sparks, and hot spots are clearly visible in photographs. Other drawbacks of the photographic detection technique are also well known. They include translucent structures and ignition sources that are hidden from view.

The ignition of a 1.2 stoichiometric propane/air mixture represents the actual threat present in an aircraft fuel system. For those situations where the photographic detection technique could not be used, a propane and air mixture was used. Propane/air mixtures when ignited in a confined space can develop overpressures of greater than 150 psi and temperatures exceeding 1500°C. For most tests and specimens, confinement is not an

option and the test system must be vented. This results in a significant flame released into the laboratory. For these reasons, many laboratories are reluctant to make use of combustible vapor detection techniques.

Another significant drawback to the propane/air detection technique is the statistical nature of the ignition probability (2). For most detection applications, ignition probability has been ignored. Lewis and von ELbe (3) published data showing that the minimum voltage spark ignition level of hydrocarbon fuels was on the order of 200 $\mu$J. Many investigations have relied on this information to infer that successfully passing a combustible vapor test verified the design to a 200 $\mu$J criteria. As shown in figure 1, the probability of ignition for a 200 $\mu$J voltage spark is between 1 in 1000 to 1 in 10,000. As can be determined from the figure, one successful test in a propane/air mixture yields a 50% confidence that the spark energy did not exceed 550 $\mu$J. If a higher confidence is required, then the test must be repeated many times, or a more sensitive fuel mixture with a lower ignition energy must be used.

## SENSITIVE FUELS

More sensitive fuels, ones that have voltage spark ignition energy levels lower than propane, do exist. Mixing these fuels at lower or higher stoichiometric concentrations will raise the energy level necessary to ignite. If lower concentrations were used, the energy available in the mixture will be reduced resulting in lower overpressures and temperatures. It would appear possible to adjust a fuel/air mixture that would have higher sensitivity (lower voltage spark ignition energies) and less combustion energy available for release during an ignition.

Three fuels meet the above requirements:

Hydrogen
Ethene (Ethylene)
Ethyne (Acetylene)

Minimum ignition data on the last two is not readily available, but Lewis and von Elbe have published extensive data on the ignition of hydrogen in various mixtures. Figure 2, taken from Lewis and von Elbe (4) shows ignition energies of hydrogen for various inerting gases and concentrations. These curves were used as a starting point for low overpressure ignition detectors.

From the curve, it appears that a mixture of 7% hydrogen, 21% oxygen, and 72% argon would have a minimum ignition energy of 100 $\mu$J. The energy released burning a 7% hydrogen mixture should be significantly less than in a propane/air mixture.

Several sets of tests were conducted using the 7% hydrogen mixture (5). Table 1 shows the probability of ignition of the hydrogen mixture. A plot of the data is shown in figure 3. Using the plot in figure 3, ignition probabilities are listed in table 2.

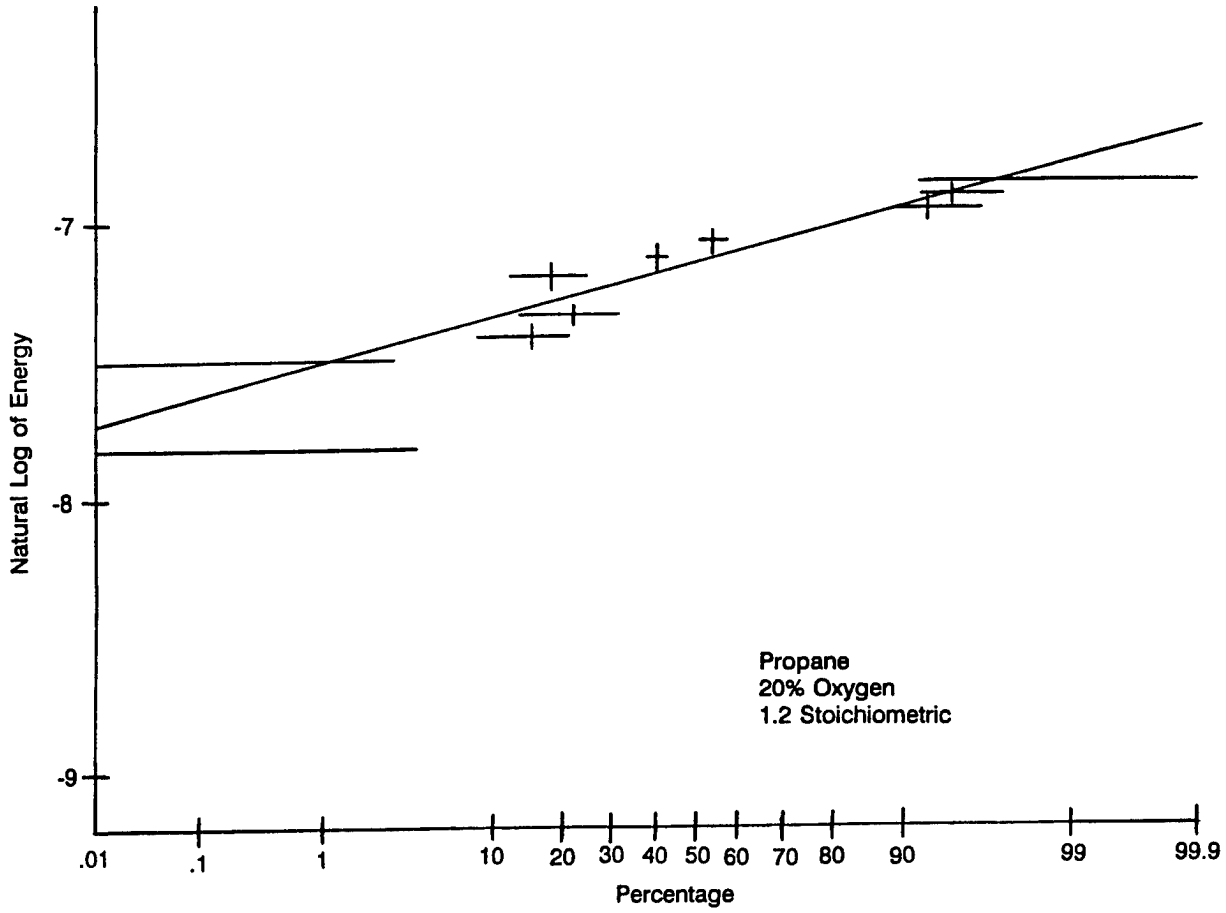



FIGURE 1 - NADC-86100-20, FIGURE 12, PROBABILITY OF IGNITION VS. SPARK ENERGY

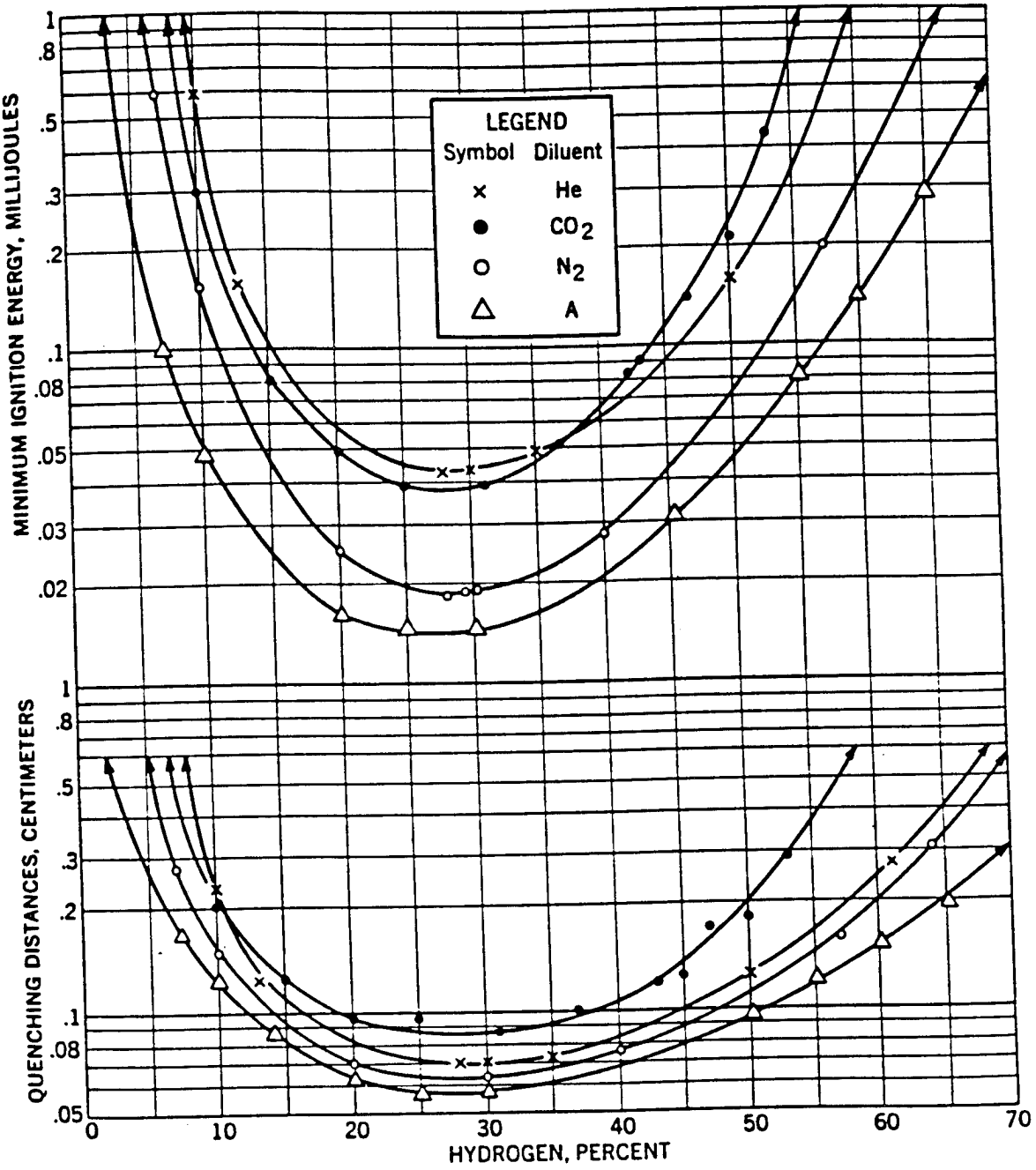



FIG. 173. Minimum ignition energies and quenching distances for hydrogen–oxygen–inert gas mixtures at atmospheric pressure. $O_2/(O_2 + \text{inert gas}) = 0.21$.

FIGURE 2 - FROM LEWIS AND VON ELBE

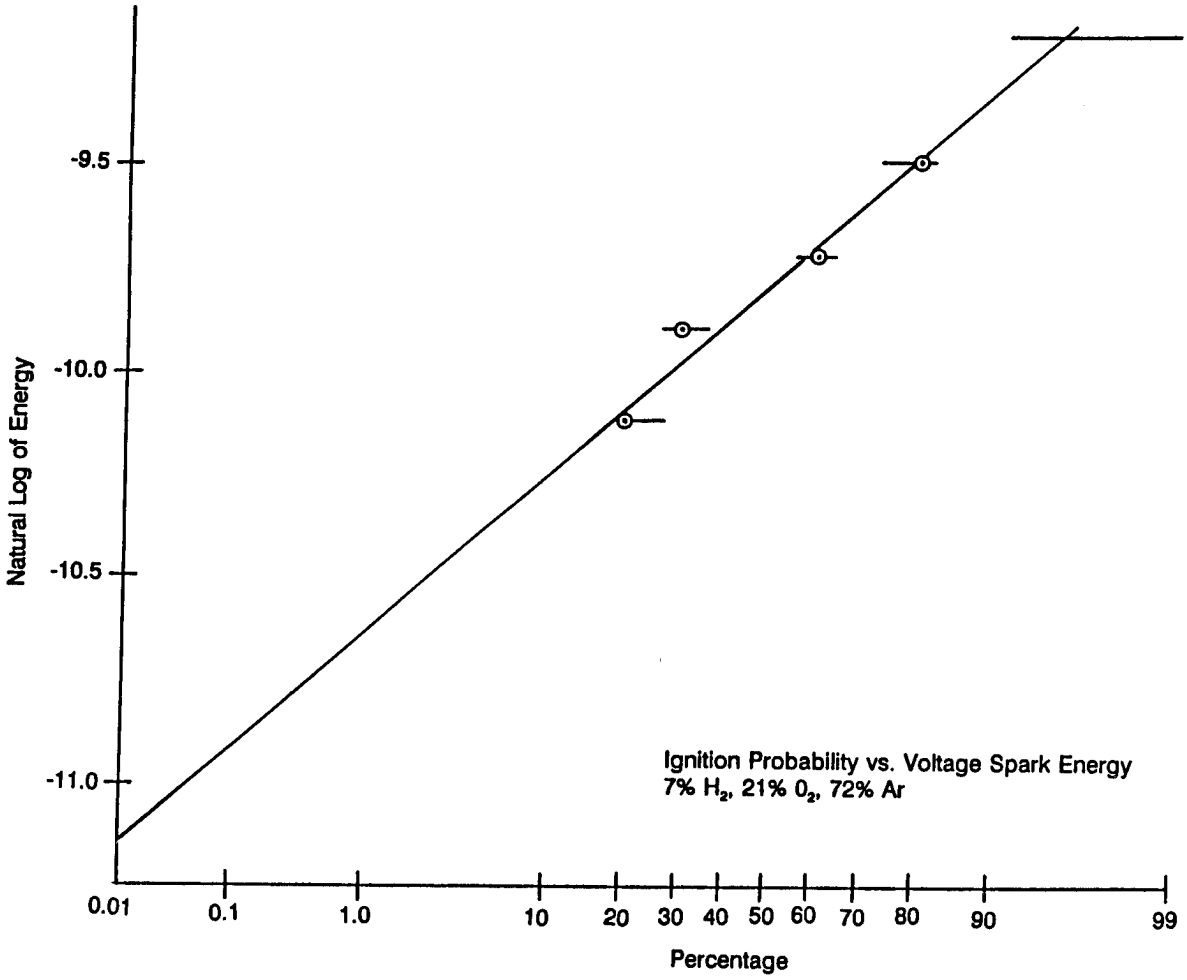



FIGURE 3 - IGNITION PROBABILITY PLOT OF $H_2$ - $0_2$ - AR DATA,
(7% $H_2$, 21% $0_2$, 72% AR)

TABLE 1 - IGNITION PROBABILITY OF HYDROGEN (7%), OXYGEN (21%) AND ARGON (72%) AS A FUNCTION OF VOLTAGE SPARK ENERGY

| Energy $\mu$J | Ln (E) | Attempts (No.) | Ignitions (No.) | % Ignitions (Including Range) |
|---|---|---|---|---|
| 40 | -10.13 | 10 | 2 | 18-**20**-27 |
| 50 | -9.90 | 10 | 3 | 27-**30**-36 |
| 60 | -9.72 | 10 | 6 | 55-**60**-64 |
| 75 | -9.50 | 10 | 8 | 73-**80**-82 |
| 100 | -9.21 | 10 | 10 | 91-**100** |

TABLE 2 - IGNITION PROBABILITIES TAKEN FROM PLOT (FIGURE 3)

| 0.01% ($\mu$J) | 0.1% ($\mu$J) | 1.0% ($\mu$J) | 10% ($\mu$J) | 50% ($\mu$J) |
|---|---|---|---|---|
| 15 | 20 | 25 | 35 | 55 |

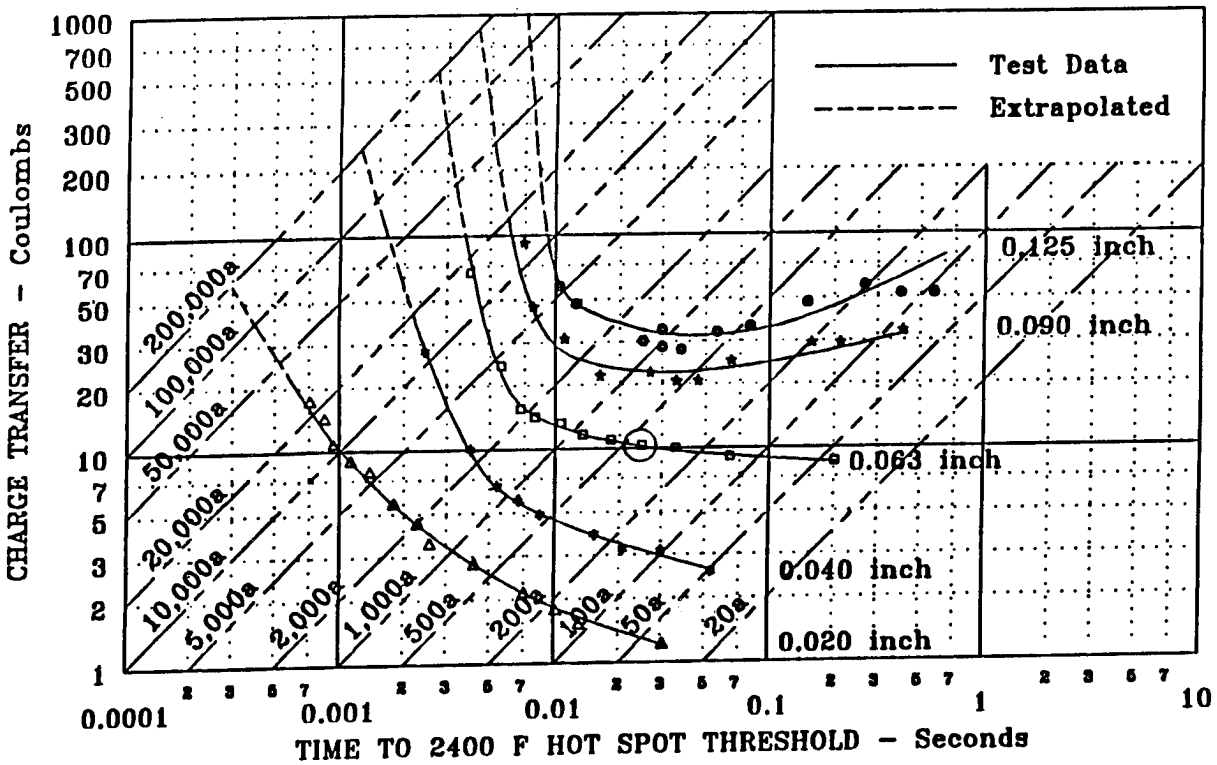
Table 3 shows a comparison of propane ignition energies taken from figure 1 and hydrogen data taken from the Lewis and von Elbe curve, figure 2. Although the curve indicates that 7% hydrogen in argon has a minimum ignition level of 100 $\mu$J, the test data (table 2) resulted in a much lower level, about 15 $\mu$J.

Two observations were made during the hydrogen vapor tests. First, the burn time was long, characteristic of lean burning vapors, and the overpressure was so very low that it often did not rip the aluminum foil covering the vent hole. Second, burning hydrogen emits no light in the visible range so sparks causing the ignition can be photographed during the test.

Some hot spot ignition tests were also conducted using titanium sheet materials and the hydrogen vapors. The data was compared to that of Oh and Schneider (6) and is shown in figure 4. The hydrogen data point falls on the data produced by Oh and Schneider. It appears that hydrogen is no more sensitive than propane to hot spots. This conclusion is consistent with the NADC hot spot data that indicated that the 900°C ignition temperature was not dependent on the fuel mixture.

TABLE 3 - PROBABILITY OF IGNITION AS A FUNCTION OF GAS MIXTURE AND SPARK ENERGY

| Fuel | % by Vol. | 0.01% | 0.1% | 1.0% | 10% | 50% |
|---|---|---|---|---|---|---|
| | | (microjoules) | | | | |
| | | In Air (Nitrogen-Oxygen) | | | | |
| Propane | 4.8 | 435 | 480 | 555 | 645 | 785 |
| Hydrogen | 28.0 | 20 | | (TBD) | | |
| | 15.0 | 50 | | | | |
| | 12.0 | 100 | | | | |
| | 9.0 | 200 | | | | |
| | 7.0 | 200 | | | | |
| | | In Argon-Oxygen | | | | |
| Hydrogen | 28.0 | 15 | | (TBD) | | |
| | 18.0 | 20 | | | | |
| | 10.0 | 50 | | | | |
| | 7.0 | 100 | | | | |
| | 5.5 | 200 | | (TBD) | | |
| | 4.5 | 500 | | | | |




Coulomb hot spot and ignition thresholds for titanium skins (6AL4V).

◯ Demonstration Test Data Point

FIGURE 4 - FROM OH & SCHNEIDER

## CONCLUSION

The tests demonstrate that hydrogen, and probably other gases with voltage spark ignition energies less than propane can be mixed to ignite at preselected energy levels which are less than propane/air. With appropriate mixtures, both an improvement in the pass/fail margin and a reduction in the violence associated with an ignition can be attained.

## REFERENCES


1. K. E. Crouch, "Development and Verification of a Standardized Spark Ignition Source," Proceedings of the 1989 International Conference on Lightning and Static Electricity, Addendum, University of Bath, UK, 26-28 September 1989.

2. K. E. Crouch, "Aircraft Fuel System Lightning Protection Design and Qualification Test Procedures Development: Investigation of Fuel Ignition Sources," NADC Report No. NADC-86100-20, August 1986.

3. B. Lewis and G. von Elbe, et al., "Ignition of Explosive Gas Mixtures by Electrical Sparks," Third Symposium on Combustion & Flame & Explosion Phenomena," Baltimore, MD, Williams & Wilkins Co., 1949.

4. B. Lewis and G. von Elbe, "Combustion, Flames, and Explosions of Gases," Third Edition, Academic Press, 1987, p. 347.

5. K. E. Crouch, "Aircraft Fuel System Lightning Protection Design and Qualification Test Procedures Development," FAA Report No. DOT/FAA/CT-94/74, September 1994.

6. L. L. Oh and S. D. Schneider, "Lightning Strike Performance of Thin Metal Skins," Proceedings of the 1975 Conference on Lightning and Static Electricity, Culham Laboratory, England, 3-5 December 1975.

# IMPROVEMENT OF LIGHTNING ATTACHMENT TESTS

J.P. Clerc and M. Cantaloube

Délégation Générale pour l'Armement
Centre d'Essais Aéronautique de Toulouse
Toulouse, FRANCE

Telephone 61.58.73.22 FAX 61.58.73.39

## ABSTRACT

The test set-up described in DO 160 C - ED 14 C for lightning attachment tests has not always been able to duplicate in flight failures of radomes. One of the reasons may be the presence of water on the surface of the radome which impedes the formation of an arc above the radome, leading to its puncture. Other reasons for the discrepancies between the laboratory tests and the in-flight damages may be the use of a fast impulse voltage waveform (1.2 µs rise time) and of rod electrode. Some tests were performed at CEAT laboratory in order to know the pertinence of each of these hypotheses. The different results obtained with various test set-up are described and modifications of the standard test procedure are proposed.

## I - INTRODUCTION

Some radomes, qualified with the usual standards (DO 160C ED 14 C chap 23) have behaved very poorly when submitted to real in flight lightning. These facts, which occurrences are not rare, clearly demonstrate that the compliance to the current standards is not sufficient. Thus, a revision of the tests methods is necessary.

A group of lightning tests laboratories, governmental organisations , radome manufacturers and lightning diverter manufacturers has initiated a study in order to improve the attachment tests methods and the protection of radome.

This paper will present some tests, performed in the CEAT lightning test facility, with a simple test set-up. These tests will compare the break down voltages between an electrode and a diverter strip in different configurations. In particular, the influence of the polarity, of the electrode shape, of the weather conditions (mainly rain), of the diverter position and of the diverter type will be analysed. This paper will not propose a new test procedure (work which is going on within the group mentioned before), but will demonstrate the need to a revision of current standards and should present the difficulty to choose the correct procedure, difficulty resulting from the great diversity of results. This work should also be of some help in the comprehension of the attachment process on lightning diverters.

## II - TEST SET-UP

The diverter strip is placed in the middle of a PVC panel. The strip is as long as the panel and its top is also at the top of the panel. The panel can be placed vertically or at an angle of 45° from the vertical (figure 1).

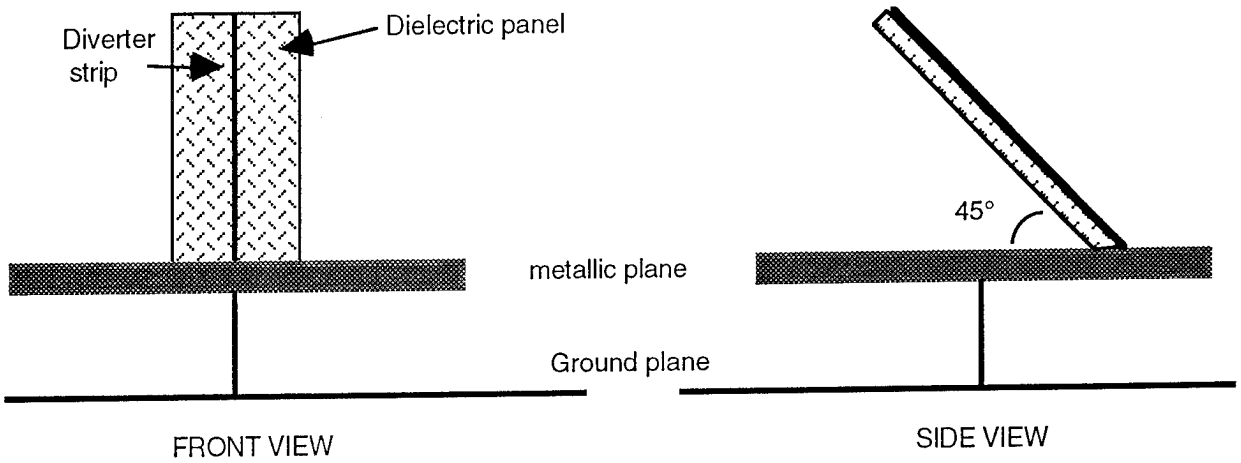
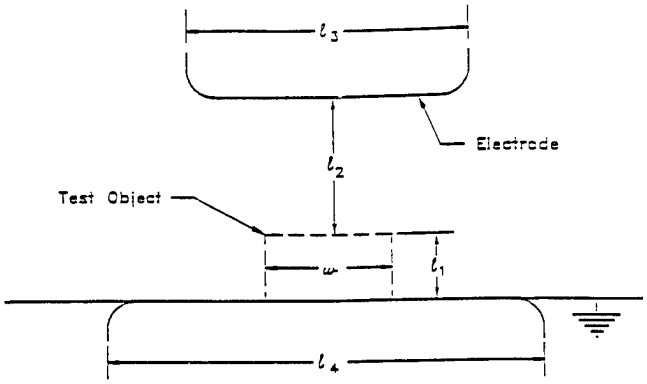



FIGURE 1
Diverter set-up

The test arrangement described in DO 160 C - ED 14C is the following :




Note: The ground plane may be either a very broad, flat one, or one with a profiled edge of width $\ell_4$.

| Test Set up Dimentions | For $\omega$ and $\ell$ <100mm | For $\ell_1>\omega$ and $\ell_1$>100mm | For $\omega>\ell_1$ and $\omega$>100mm |
|---|---|---|---|
| $\ell_2$ | 150mm | $\geq 1.5\ell_1$ | $\geq 1.5\omega$ |
| $\ell_3$ | $>2\ell_2$ | $>2\ell_2$ | $>2\ell_2$ |
| $\ell_4$ | $\geq\ell_3$ | $\geq\ell_3$ | $\geq\ell_3$ |

Gap and Electrode Dimensions for High Voltage Tests

NOTES: The tolerance for $\ell_2$ is 20 percent.

The values for $\ell_3$ and $\ell_4$ are minimum values.

FIGURE 2

This test arrangement has several drawbacks :

- The electrode is plane, while in many cases a rod electrode is useful (more directional)
- the ground plane is very large compared with the aircraft diameter at the place where the radome are mounted (when nose radome are tested).

DO 160 C -ED 14C authorises three waveforms (short impulse (1.2/50 μs), long impulse (50 to 200 μs rise time) and a ramp (1 MV/μs). The short impulse is recommended.

The arrangement used during the tests at CEAT is slightly different (figure 7) :

The diverter strip is placed above a metallic plane (dimensions 1.5 m * 1.5 m) which is placed 0.82 m above the ground plane. The metallic plane is grounded. This set-up better simulates the available ground plane of the aeroplane. The diverter strip is 80 cm long and its top is then 1.62 m above the ground.

The bottom of each electrode used is placed 2 meters above the top of the diverter strip. Three electrodes were used :

- a plane electrode, dimensions 10m X 5m with anti corona on its edges,
- a sphere electrode with a diameter of 25 cm,
- a rod electrode with a pointed tip ( diameter of the rod : 5 cm)

The electrode is connected to the CEAT 5 MV Marx generator which can provide the short impulse and the long impulse (switching impulse).

Two types of diverter strips are used :

- a usual solid bar diverter with a sharp edge at its top,
- a segmented diverter with diamonds (~3 mm side), resistivity = 2 MΩ/m.

Two measurements are performed :

- The voltage of the electrode measured with a capacitor divider,
- The current in the electrode measured with a current transformer.

Optical fibre links are used between the sensors and the digitizer placed in a faraday cage, minimizing the "noise".

## III - THE ELECTRIC FIELD CONFIGURATION

Before any testing, the electric field mapping obtained with the three electrodes should be analysed.

Using the axi-symmetry of the test set-up (except for the diverter strip which has a rectangular section and which will be approximated by a cylinder), a 2-D finite elements numerical code can be used (with an axi-symmetrical solution). The electrode is at the potential 100 V and the ground at the 0V potential. The diverter strip and the metallic plane are also forced at the ground potential. The solution is only a static solution but it is well representative of the field configuration during the tests, in particular with the long waveform.

With the plane electrode, the resulting electric field is presented figure 3 (the norm of the electric field is represented).The "average" electric field is 100 V / 2 m = 50 V/m. The real field is slightly lower (40 V/m) in the major part of the space between the electrode and the diverter strip. High values of field are present in the close proximity of the strip. One should also mentioned the fairly high values of field at the extremity of the metallic plane. It will be much easier to obtain an arc starting from the diverter than from the electrode, but the diverter will compete with the edge of the metallic plane.

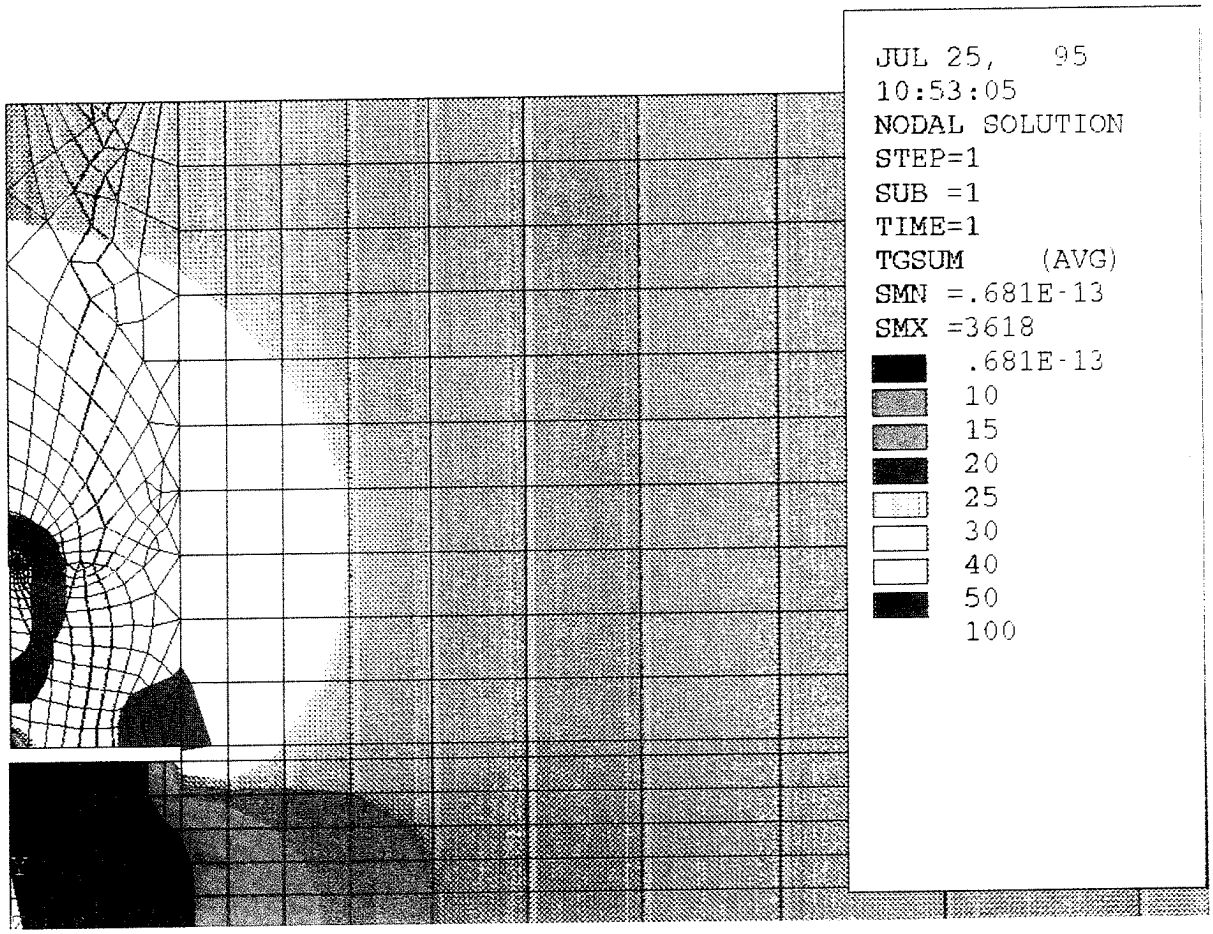



FIGURE 3
Electric field configuration - Plane electrode

With the sphere electrode, the results are presented figure 4. The electric field is concentrated around the sphere and along the diverter strip. Fields above 260 V/m are present around the electrode. In the middle of the space between the electrode and the diverter strip, there is a region of low electric field (lower than 25 V/m). The field on the edge of the metallic plane is lower than with the plane electrode (30 V/m instead of 80 V/m). The arc can start either from the electrode or from the diverter strip but, in both cases, the diverter provides a good protection.

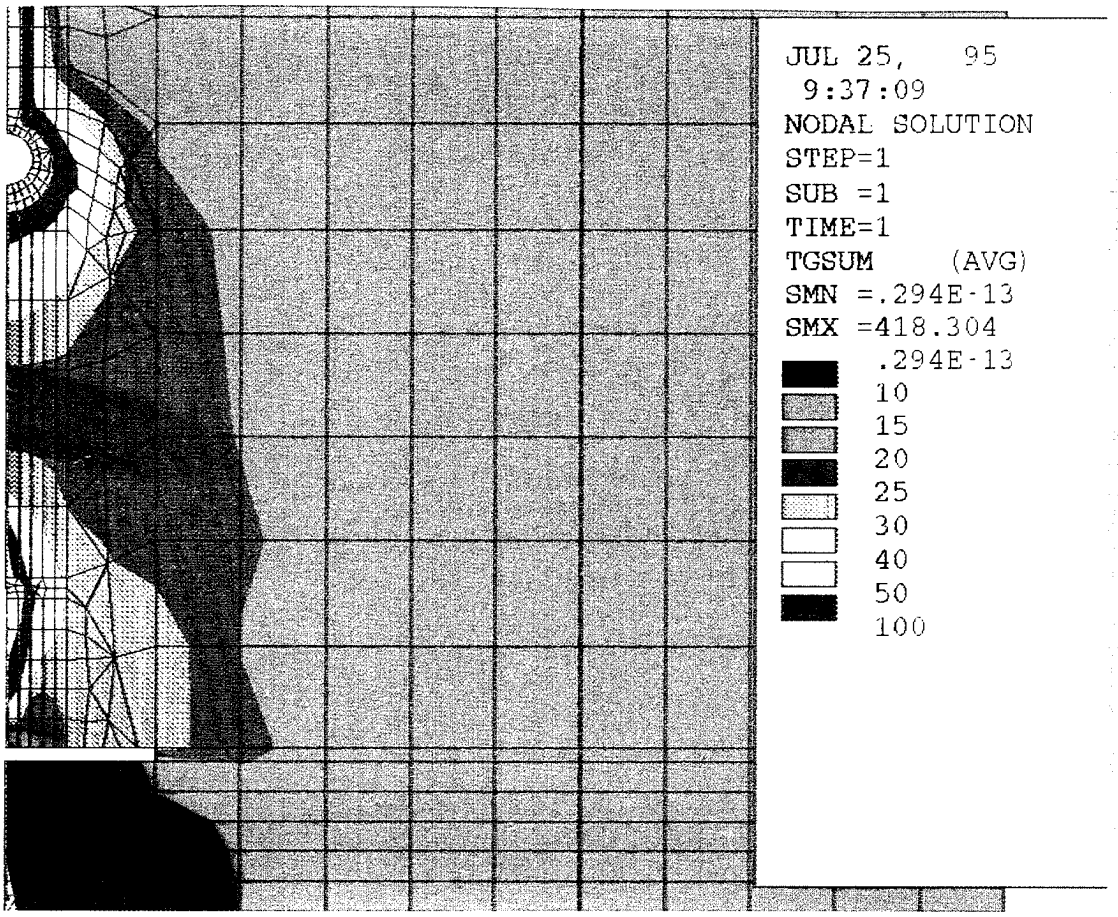



FIGURE 4
Electric field configuration - Sphere electrode

With the rod electrode, the electric field configuration obtained is presented figure 5. The results are very similar than those obtained with the sphere electrode, but the electrostatic energy is stored rather near the diverter strip than near the electrode while, with the sphere electrode, the sharing is even. The edge of the metallic plane is slightly more stressed than with the sphere electrode (35 V/m instead of 30 V/m). The diverter strip remains the main point of attachment (or of start) of an arc.

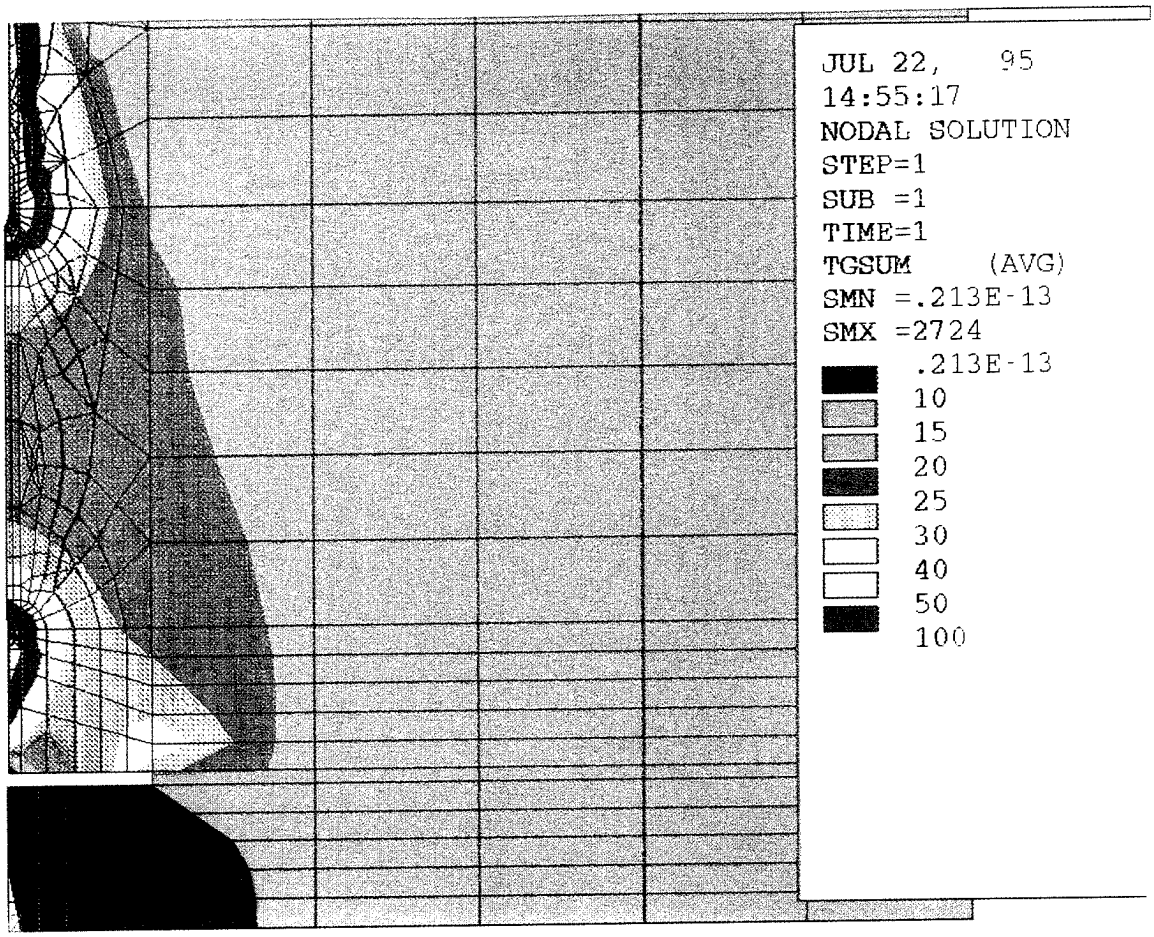



FIGURE 5
Electric field configuration - Rod electrode

## IV - RAIN SIMULATION

The segmented diverters are suspected to behave differently when they are dry and when they are wet. When the aircraft enters into a region with precipitation, its skin (included the nose radome) is covered with a layer of ice or of water. The ONERA has numerically estimated the thickness of ice and of water in some typical flight situations (1). The following curves give the thickness of water on an AIRBUS A320 radome when the aircraft is flying at Mach 0.3 at the flight level 100. The liquid water content of the air is 2.5 $g/m^3$ , which corresponds to a 50 mm/hour shower. The outside air temperature is +15° C. The droplets are supposed to be 2 mm in diameter.

As it is very difficult to reproduce the real in flight conditions (in particular the speed of the water droplets), the ONERA has also estimated the resulting water thickness on the same radome, with laboratory parameters (speed of the droplet of 1 m/s or 10 m/s and water flow of 0.1, 0.25 and 0.5 Kg/(s.m$^2$)).

The following figure (6) gives the results of the ONERA calculations. The X axis is the distance along the radome, the origin being at the top. The Y axis is the thickness of water.

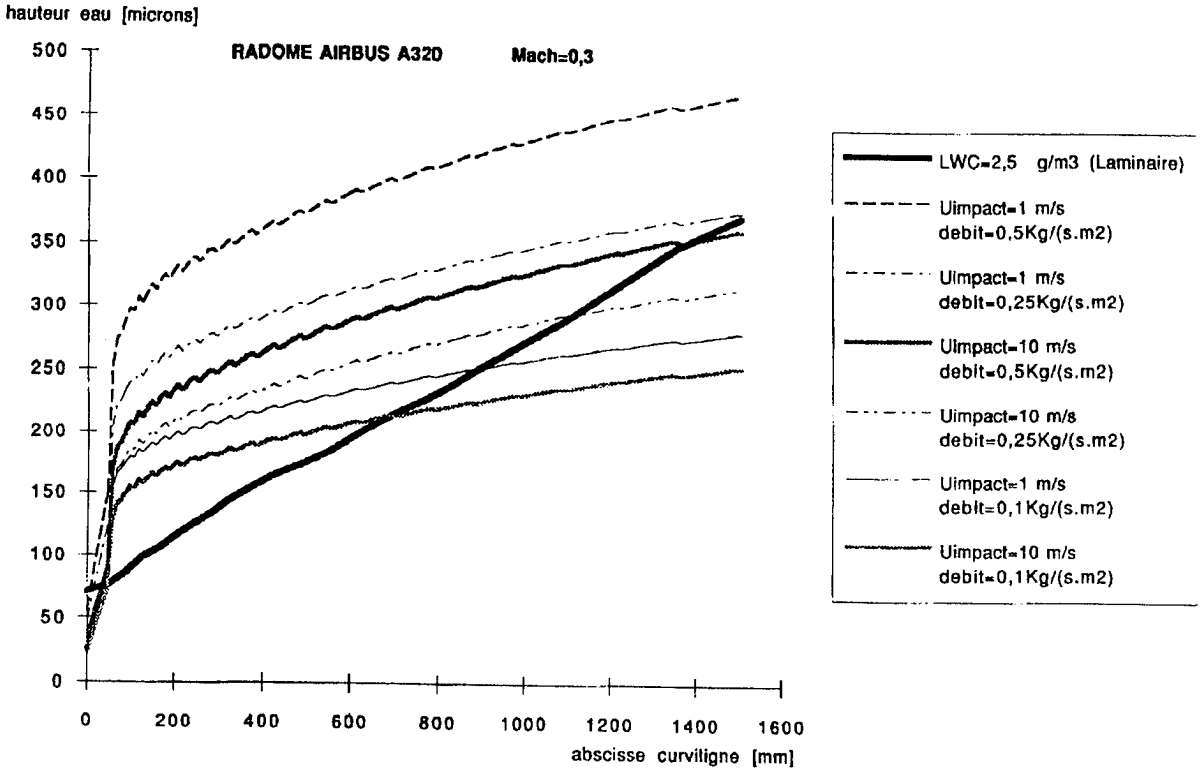



FIGURE 6
Water thickness on a A320 radome

Two different laboratory water conditions were chosen :

H1 : Speed of the droplet : 10 m/s Water flow : 0.1 Kg/(s.m$^2$)
H2 : Speed of the droplet : 10 m/s Water flow : 0.5 Kg/(s.m$^2$)

The thickness of the water layer is bigger with H2 than with H1. In both cases, the layer is thicker than in flight at the top of the radome, but correctly simulates the in flight conditions, where the diverter strip are usually placed.

In order to achieve the H1 and H2 parameters, the water is sprayed with air under pressure. A correct setting of the water flow and of the airflow allows good results.

## V - MEASUREMENTS

The results are summarised in the following table :

| ELECTRODE | | | HUMIDITY | | | POSITION | | WAVEFORM | | DIVERTER STRIP | | VOLTAGE (kV) | |
|---|---|---|---|---|---|---|---|---|---|---|---|---|---|
| Plane | Sphere | Rod | Dry | H1 | H2 | 90° | 45° | Short | Long | Solid | Segments | + | - |
| | | ••• | ••• | | | ••• | | | ••• | ••• | | 910 | -1400 |
| | | ••• | ••• | | | ••• | | | ••• | | ••• | 992 | -1400 |
| | ••• | | ••• | | | ••• | | | ••• | ••• | | 900 | -1400 |
| | ••• | | ••• | | | ••• | | | ••• | | ••• | 870 | -1450 |
| | | ••• | ••• | | | | ••• | | ••• | ••• | | 930 | -1340 |
| | | ••• | ••• | | | | ••• | | ••• | | ••• | 880 | -1250 |
| | ••• | | ••• | | | | ••• | | ••• | ••• | | 830 | -1350 |
| | ••• | | ••• | | | | ••• | | ••• | | ••• | 890 | -1450 |
| | | ••• | | ••• | | | ••• | | ••• | ••• | | 830 | -1430 |
| | | ••• | | ••• | | | ••• | | ••• | | ••• | 900 | -1530 D |
| | | ••• | | | ••• | | ••• | | ••• | ••• | | 730 | -1350 |
| | | ••• | | | ••• | | ••• | | ••• | | ••• | 940 | -1700 |
| | | ••• | ••• | | | | ••• | ••• | | ••• | | 930 | -1100 |
| | | ••• | ••• | | | | ••• | ••• | | | ••• | | -1180 |
| | | ••• | | ••• | | | ••• | ••• | | ••• | | 930 | -1120 |
| | | ••• | | ••• | | | ••• | ••• | | | ••• | 1100 | |
| | | ••• | | | ••• | | ••• | ••• | | ••• | | 950 | -1120 |
| | | ••• | | | ••• | | ••• | ••• | | | ••• | 990 | -1180 D |
| ••• | | | | ••• | | | ••• | ••• | | ••• | | 1250 | -1130 |
| ••• | | | | | ••• | | ••• | ••• | | ••• | | 1310 | -1060 |
| ••• | | | | ••• | | | ••• | | ••• | ••• | | | -830 |
| ••• | | | | | ••• | | ••• | | ••• | ••• | | Ground | -830 |

"D" means that the diverter strip was destroyed after one of the ten shots

In the "Voltage" cells are given the voltages at which the flashes occurred in the positive polarity and in the negative polarity (in kV). These voltages are slightly lower than the charging voltage of the Marx generator because, with the fast waveform, the flash occurs after the maximum voltage and, with the slow waveform, it occurs before the maximum.

According to DO 160 C - ED 14 C procedure, the charging voltage of the generator is slightly increased (5%) until the arc flashes. Ten shots are done at the same level. The lowest value at which the arc occurs is then recorded.

## VI - ANALYSE

POSITIVE / NEGATIVE-- The breakdown voltages are lower in the positive polarity than in the negative polarity excepted with the plane electrode. This can be well understood if one considers that the positive corona is easier to obtain than the negative one. The positive corona starts in a region of low field (the positive energised plane electrode) and thus needs an higher value of charging voltage. In the negative polarity the corona starts from the diverter strip which greatly enhances the field.

ELECTRODE SHAPE-- In the positive polarity the breakdown voltages are lower with the sphere electrode than with the rod electrode. This is consistent with the results of the electric field modelling.

With the plane electrode, the long waveform and in the positive polarity, the arc attaches to the metallic plane instead of the diverter, which is consistent with the results of the electric field modelling.

VERTICAL / INCLINED-- The inclination of the diverter strip is of little effect on the breakdown voltage.

DRY / WET-- In dry conditions the segmented diverter behaves as well as the solid bar diverter (even better in some cases).

With rain simulation the results are different :

The solid bar diverter need, in the positive polarity with the long waveform, lower voltages to function as the humidity increases (930 kV dry , 830 kV with H1 and 730 kV with H2). It is roughly insensitive to water in the negative polarity (long waveform) and with the short waveform in both polarities.

The segmented diverter needs higher voltages to function as the water layer increases. This fact is true in both polarities with the long waveform (880 kV/-1250 kV dry, 900 kV/-1530 kV with H1 and 940 kV/-1700 kV with H2).With the short waveform, we are missing some measurements to give a clear conclusion, but the results do not show any precise trend. During the tests performed with water spray, the segmented strips were often destroyed, which may indicate that the current flowed inside the strip instead of above.

## VII - CONCLUSION

Even if all cases have not been tested, these tests have confirmed the lower efficiency of the segmented diverters when the radome is wet. They have also underlined that the choice of a geometry of electrode is crucial. For the shots performed in the axis of a radome, a rod or sphere electrode will force the attachment to the diverter while a plane electrode will allow the arc to attach to other points of the structure.

Attachment tests on objects protected with solid diverters should not be done with rain simulation, the dry conditions being conservative. On the contrary, tests on objects protected with segmented diverters should be done with rain simulation.

The present standards, which describe the attachment test procedure, need to be modified in order to take into account the observations mentioned before. Other parameters than those studied here should also be analysed. For instance, the influence of a floating test set-up (bi-leader simulation) or of an ice layer on the radome could be determined. The use of a streak camera would be really useful for such studies.

FIGURE 7 Test set-up - Sphere electrode

**REFERENCE**

**(1)** - ONERA, Direction de la physique générale
"Détermination des épaisseurs d'eau et de givre sur deux radômes"
Rapport n° 8/7766 PY Août 1994

# TECHNIQUES FOR PRODUCING UNIPOLAR MIL-STD-1757A WAVEFORMS USING UNIQUE RESISTOR BANKS

James L. Press and Monty Lehmann
R&B Enterprises, Division of EMC Science Center, Inc.
20 Clipper Road
West Conshohocken, PA 19428, USA
Telephone (610) 825-1960 FAX (610) 825-1684

## INTRODUCTION

MIL-STD-1757A details a set of standard test waveforms and techniques for the lightning qualification testing of aircraft. The document illustrates waveforms intended to represent different phases of an actual lightning strike. For qualification testing, four current waveforms, designated Components A, B, C and D, are used to determine direct effects. An additional Component E is used to determine indirect effects. Test Method TO2 of the standard applies to structures and components in zones of the aircraft for which there is a high probability of initial lightning flash attachment, and to structures and components in the zone to which a flash will likely be swept (1). RTCA/DO-160C, Section 23 (2), specifies the same waveforms and procedures except that it does not address the Component E waveform.

A full threat lightning test facility has been developed to meet the requirements of these two standards. Its design is based upon available capacitors, power supplies, and additional hardware that allow the requirements to be met. The pulser is designed to supply the desired action integral without undue strain to the components. Additional safety items, such as large-volume dump resistors and heavier connections, are incorporated into the pulser design so that it can better withstand the heating effects of the Component A waveform. After initial testing, it was determined that the high voltage current resistors were a major cost driver in terms of maintenance and reliability. A unique resistor bank was developed and proved to significantly reduce the costs of operation. The pulser was tested and numerous MIL-STD-1757A and DO-160C, Section 23, tests have been performed with reliable and repeatable results.

The Component A pulser, powered by a Marx generator, is capable of driving 200 kA at 80% peak rating. The pulse is fired by pneumatic switches and arc-over spark gaps to produce a waveform whose action integral meets or exceeds the requirements of MIL-STD-1757A Component A (Figure 1). The output waveform is reproducible and is designed to perform with minimum overshoot to increase reliability and minimize maintenance. Component B is achieved using a small discrete pulser, and Component C is achieved using a standard dc power supply. Component D is achieved with an easily installed modification to the Component A Marx generator.

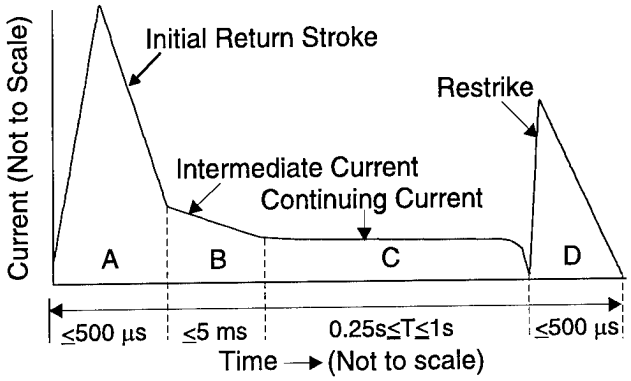



FIGURE 1. CURRENT WAVEFORMS.

## MIL-STD-1757A REQUIREMENT

COMPONENT A - INITIAL HIGH PEAK CURRENT — Component A has a peak amplitude of 200 kA ±10% and an action integral of 2 x $10^6 A^2$ seconds ±20%, with a total time duration not exceeding 500 µs. These values represent a stroke whose intensity is known to be exceeded by only 0.5% of the known strikes at the time of the promulgation of MIL-STD-1757A (20 July 1983). A unidirectional waveform is preferred but oscillatory waveforms are acceptable. For maintenance and reliability reasons, a Marx generator design is used for a unipolar pulse. Since component A is responsible for the blast, magnetic force, and acoustic shock effects on structures and components, these physical constraints were considered in the design.

COMPONENT B - INTERMEDIATE CURRENT — Component B has an average amplitude of 2 kA ±10% flowing for a maximum duration of 5 ms and a maximum charge transfer of 10 coulombs (C). The waveform is required to be unidirectional. An exponential decay waveform was utilized for its simplicity. The effects of the intermediate current are primarily thermal and can result in the melting of metals and the burning of nonmetallic components. The main severity factor of Component B lies in the deposition of energy in a relatively short time to simulate one lightning attachment point on a swept stroke path.

COMPONENT C - CONTINUING CURRENT — Representing the continuing current in a severe lightning flash, Component C transfers a charge of 200 C ± 20% in a time span between 0.25 and 1 second. The waveform is required to be unidirectional. A dc power supply was selected as a source of Component C due to the ability to control and regulate the waveform using this method.

Component C can cause the melting of metals and the burning of composites. The average rate of charge delivery is less than Component B; therefore, the amount of damage per unit of time is less than that produced by the intermediate current. This

implies that Component C is more damaging to structures or components in aircraft zones 1B or 2B than elsewhere, since only the trailing edges have sufficient dwell time for the full 200 C of charge to enter the aircraft.

COMPONENT D - RESTRIKE CURRENT — Component D has a peak amplitude of 100 kA ±10% and an action integral of 0.25 x $10^6 A^2$ seconds (±20%). This component may be unidirectional or oscillatory with a total time duration not exceeding 500 μs. As stated, the unidirectional waveform is most desirable. Component D represents a severe restrike, and its parameters are based upon data available when MIL-STD-1757A was released.

## GENERATOR DESCRIPTION

The unique resistor bank is utilized for Components A and D. The following description details the Components A and D generators only. Details for the other generators can be found in the literature (3).

DESIGN CONCEPTS — Forty-eight 500-μF, 10-kV Maxwell Model No. 32259 capacitors, along with twenty 2-μF Aerovox, 50-kV Model PX190D21 capacitors and two power supplies rated at 100 kV, 0.3 A and 10 kV, 2 A, were available. With this equipment, a Marx generator capable of an output of 200,000 A requires an erected voltage of 51 kV into the estimated circuit inductance. A design was developed in accordance with MIL-STD-1757A. After completion of the initial design, an inventory of existing equipment indicated that only a few other items needed to be modified or reconfigured. Once the Component A generator was designed, the Component D generator would essentially be the Component A generator with modified capacitance and output resistance. The Component B generator was designed using two 500-μF capacitors charged to the desired voltage and discharged through an air gap. The Component C generator was essentially a Sorensen 1200-A dc power supply with appropriate switches and timing circuits.

COMPONENT A GENERATOR DETAILS — The main objective of the circuit design of the 200-kA Component A pulser is to protect and extend the useful life of the high energy capacitors. In particular, it is important to keep the maximum charge of each capacitor at 10 kV or less and to limit the output voltage reversal during pulsing to less than 10%. If these capacitors were used to develop an oscillatory waveform, the useful life of the capacitors would be dramatically reduced. Since the replacement cost of each capacitor is approximately $1,500, and since replacement would contribute to the overall maintenance cost and operational capability of the pulser, an oscillatory waveform was ruled out during the early design phase of the generator.

Once the oscillatory waveform was eliminated, the next design criteria to be examined was the peak current rating of the Model 32259 capacitors. Each capacitor had a maximum rating of 100 kA. Using six capacitors in parallel for each stage of a Marx generator effectively divides the erected current by a factor of six. Therefore,

each capacitor is subjected to a level of 34 kA, well below its maximum rated current. This level extends the useful life of the capacitor and reduces maintenance costs.

Based on the Component A parameters, the Marx generator produces a unidirectional pulse that rises quickly to 200 kA and then decays in less than 500 μs. The estimated inductance for the six-stage Marx generator was taken into account and additional resistance was added to prevent the waveform from overshooting.

The selected charge voltage on each Marx stage is 8.5 kV to produce an erected voltage of 51 kV. Calculations showed that the action integral of this setup is 2.6 x $10^6 A^2$ seconds. The PSpice output is shown in Figure 2 and the overall schematic is shown in Figure 3. The pulser is triggered by a pneumatic switcher built out of existing hardware.

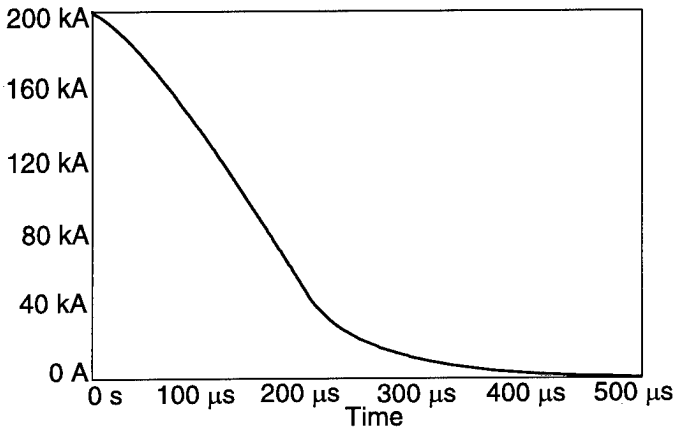



FIGURE 2. COMPUTER SIMULATED OUTPUT FOR MARX.

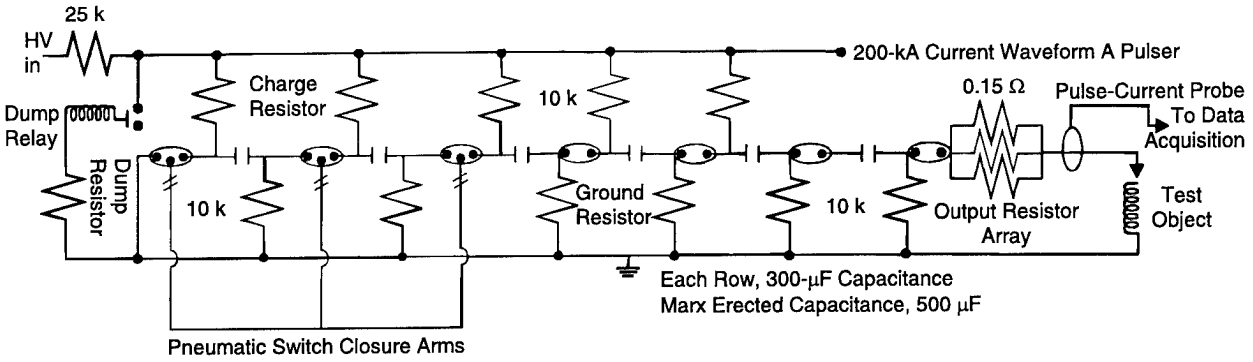



FIGURE 3. COMPONENT A MARX GENERATOR.

COMPONENT D GENERATOR DETAILS — It was initially decided that the Component D generator would essentially be the Component A generator, modified and charged to a lower voltage, and equipped with proper resistors to meet the action integral requirement. After preliminary testing, it was determined that the Component D requirement could be met using the modified design of the Marx stages instead of the

Component A configuration. This reduces the capacitance of each stage, and the erected capacitance of the Marx generator is thereby reduced. Figure 4 shows a schematic of the Component D Marx generator.

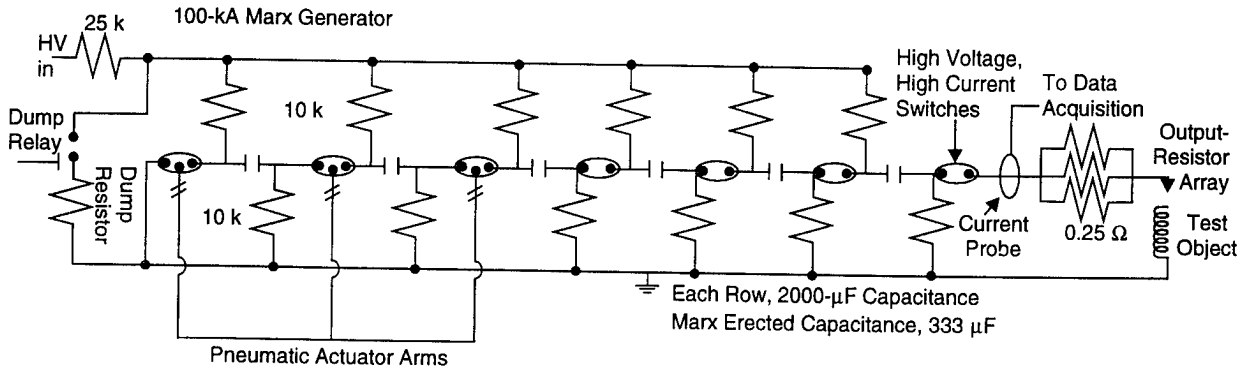



FIGURE 4. COMPONENT D MARX GENERATOR.

## RESISTOR DEVELOPMENT

Numerous high voltage/high current carbon resistors were available when the initial evaluation of the Components A and D generators was performed. However, initial test shots of the generators showed that the carbon resistors could not handle the rapid charging of the Marx generator. The 10kV, 2A Hipotronic supply was capable of charging the Marx in less than four minutes but the rate was slowed to 20 minutes to avoid damage to the resistors. After damaging a number of resistors, alternative resistors were investigated.

WATER RESISTORS (RUBBER ENDCAPS) — The first attempt at an alternative was to manufacture a water resistor consisting of a plastic tube cut to a length of approximately one meter. The diameter of the tube was 5 cm and the total volume was 7800 cubic cm. By mixing the proper amount of copper sulfate with distilled water in the tube, high-power resistors were produced at a significantly lower cost than the cost of carbon resistors. The resistance range was limited to 50 - 200 kilo-ohms but was acceptable for our application. Figure 5 shows a photograph of a resistor. The endcaps are sealed with rubber stops containing a metal electrode (1/4-inch bolt) that extends through the rubber stop to provide an electrical connection point and allow the conduction of energy into the copper sulfate/water solution. The endcaps are secured by hose clamps tightened around the rubber endcap.

Evaluation of these water resistors allowed the charging of the Marx in 10 minutes. However, with a delay of approximately 5 minutes between charging, the

resistors would heat up to a point where the water solution would begin to seep out around the rubber endcap. In addition, air pockets would form within the resistor and had to be removed manually by tapping on the resistor. After five to ten charging events, the rubber endcaps began to deteriorate and contaminate the water/copper sulfate solution. This led to the use of a parallel combination of resistors as shown in Figure 6. These parallel combinations were difficult to handle and led to unacceptable delays in the attempt to remove air pockets from all resistors.

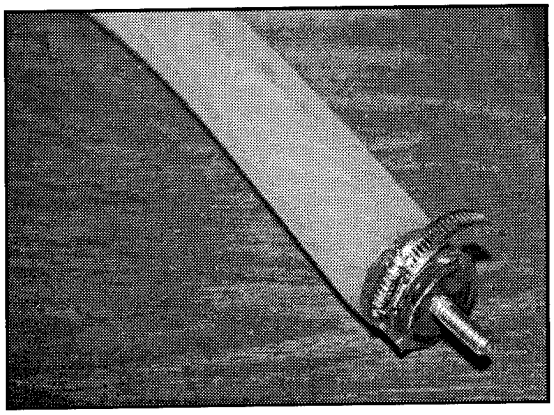


FIGURE 5. RESISTOR.

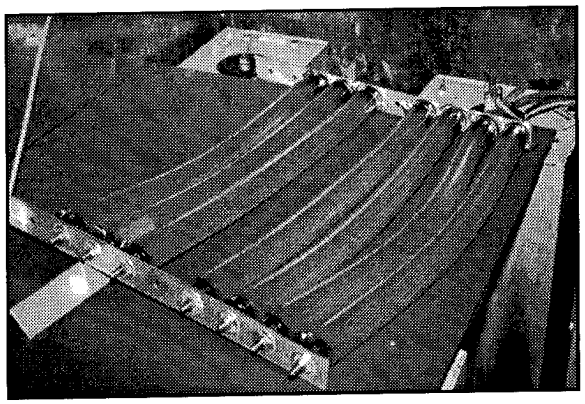


FIGURE 6. PARALLEL COMBINATION OF RESISTORS.

WATER RESISTORS (METALLIC ENDCAPS) — Since the rubber endcaps contaminated the resistors, forcing replacement of them every 15 to 20 charging cycles, alternative endcaps were investigated. Monel endcaps were designed as shown in Figure 7. The design allowed sealing of the resistor by placing a groove ring around the outer edge as a seating for the plastic tubing. A hose clamp was used to secure the monel endcap.



FIGURE 7. MONEL ENDCAP.

This re-designed resistor eliminated the requirement to use many parallel combinations since the monel endcap did not deteriorate after charging. However, the resistor still developed air pockets if the charging cycles were less than 8 - 10 minutes and the tapping of each resistor was required. Charging time for the Marx generator remained at approximately 10 minutes using these resistors, but the maintenance requirement of replacing resistors every five to ten charging cycles was eliminated. These resistors were marginally acceptable in terms of maintenance and facility cost.

TRAY RESISTORS — The copper sulfate/water solution resistors proved to be cost-efficient and allowed for flexible resistance values with high wattage. However, the development of air pockets due to heating still required using parallel combinations of resistors. After discussions between test engineers and technicians, it was decided that a large tray resistor could replace the series of parallel resistors. Large volume resistors were designed using 15-gallon trays with resistance values of 15 kilo-ohms. A single tray resistor was built and is shown in Figure 8. Three electrodes (1/4-inch bolts) were attached to each side of the tray resistor for electrical connection. The trays were then sealed to keep dirt and dust from contaminating the solution. Initial evaluation showed no indication of heating problems or changes in resistance values. Three additional tray resistors were built and incorporated into the Marx system as shown in Figure 9. These resistors allow maximum charging of the Marx (2 minutes) without the build up of air pockets during charging cycles and eliminate the concerns of heating the charging resistors. During one test requirement when the customer requested an evaluation of his equipment to Component A at a level of 50 kA, we performed over 70 charge cycles in a 8-hour period. The resistors showed no adverse response to this rapid and almost continuous charging of the Marx.

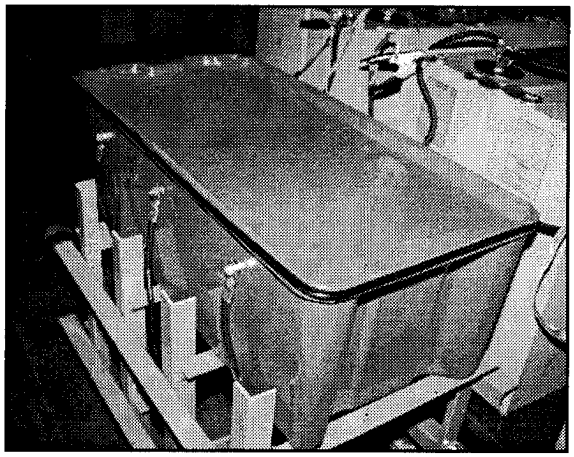


FIGURE 8. SINGLE TRAY RESISTOR.

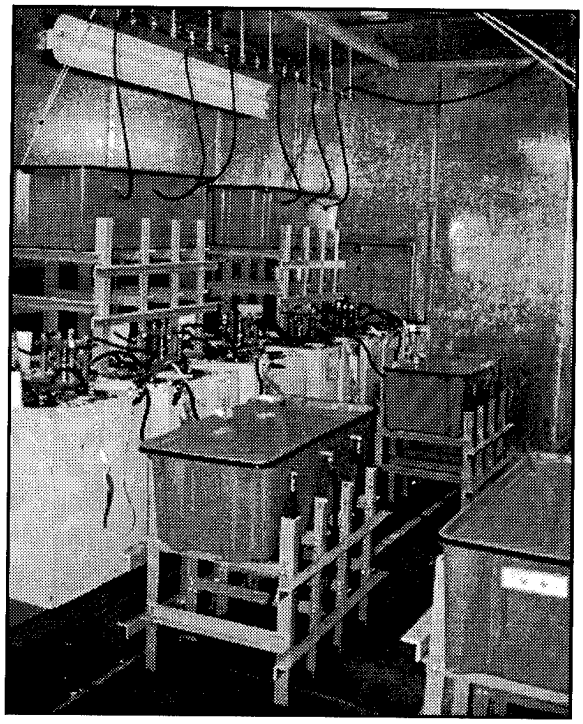


FIGURE 9. MARX SYSTEM TRAY RESISTORS.

The tray resistors have been in place at the R&B Lightning Test Laboratory for 15 months and are checked regularly for resistance changes, physical damage, and solution contamination. At this writing, the original tray resistors are still in operation with no problem and only minimum maintenance which consists of a monthly visual inspection and resistance measurement. In addition to the charging resistors, a 90-ohm emergency dump resistor was constructed. This resistor is capable of dissipating 1 MJ of energy in less than 5 seconds. The emergency resistor consists of 2.5 cubic feet of a copper sulfate and water solution. This emergency dump resistor is used if any emergency shut-down button is pushed or if unauthorized entry is made into the pulser area. A second dump resistor was manufactured and placed on wheels to discharge the Marx in the unlikely (and unwanted) event of a fully charged Marx and a non-functional discharge switch.

## CONCLUSION

To reduce both material and maintenance costs, a unique large-volume water/copper sulfate solution resistor has been developed and tested. The resistors have increased the testing capability of the R&B Lightning Test Lab and have reduced the overall facility costs. This facility meets all the requirements of MIL-STD-1757A, DO-160C, and various platform specific specifications such as V-22. The use of the unique resistor allows for efficient lightning test with a minimum time between test shots and a minimum maintenance cycle. The Marx generator can be assembled at a customer site for long-term testing due to the robust components.

## REFERENCES

1. MIL-STD-1757A, "Lightning Qualification Test Techniques for Aerospace Vehicles and Hardware," DoD, June 17, 1990.

2. RTCA/DO-160C, "Environmental Conditions and Test Procedures for Airborne Equipment," Section 23- Lightning Direct Effects:September 27, 1990.

3. James L. Press and Monty Lehmann, "Producing Unipolar Lightning Waveforms to Satisfy MIL-STD-1757A," ITEM Update 1994, pp. 75-80, 84.

# SESSION 06B
# ELECTROSTATICS
# CHAIRPERSON: MIKE WHITAKER

# THE ELECTROSTATIC HAZARDS UNDER AN HOVERING HELICOPTER

**Maurice CANTALOUBE and Christian DAVOISE**

**CENTRE D'ESSAIS AERONAUTIQUE DE TOULOUSE**
23, avenue Henri Guillaumet
31056 - TOULOUSE FRANCE

## ABSTRACT

Helicopters hovering above the earth are often charged with static electricity and this can cause operational problems for ground personnel or ammunitions when contact with the helicopter is required. Voltage, current and electric field measurements were made on two large helicopters hovering over two types of soil. Data about the charging voltage, energy level ($1/2\ CV^2$), discharging pulse current and polarity of the helicopter were recorded and some results are given to ascertain the electrical hazard to ground personnel attaching cargo to helicopters and to crew member being winched down a cable.

## 1) GENERAL BACKGROUND

It is well know that aircraft in flight may acquire an electrostatic charge, the main charging mecanisms being the engine exhaust, precipatation and tribo-electric effects and induction in a cloud electric field. This charge may be an important hazard to crew and ground workers with an hovering helicopter.This problem has been studied since 1960 by many investigators [1] [2] [3] [4]

Recent measurements on two CH 53 E helicopters [2] hovering over clean aluminium runway and over the desert sand gave potential thresholds up to + 90 KV, with a charging time constant of few seconds.

The last STANAG drafts 4239 and 4235 of NATO define the electrostatic environment by helicopter transport and the test procedures to be used for determining the safety for munitions and associated systems. In these documents, helicopter can be represented by an electrical circuit equivalent to capacitance of 1000 pF $\pm$ 20% charged to 300 kV in an 1 ohm series resistance and 20 u H series inductance. So it is interesting to compare these standard values to real values.

In other parts, some incidents were reported by the R.A.E. [3] in search and rescue operations. In France, some ground workers handling cargo, complained electric shocks, but fortunately no lethal incident were reported.

## 2) DESCRIPTION OF EXPERIMENTS

Two series of experiments have been made, the first at FONSORBES (near TOULOUSE) in october 1994 and the second at BOUCAU (Atlantic ocean beach near BAYONNE) in March 1995. Both experiments were carried out with two large french helicopters:

- a "COUGAR", military model of SUPER-PUMA manufactured by AEROSPATIALE, with and without a cargo hang by dielectric ropes. This helicopter was equipped with 16 passive dischargers on the horizontal stabilizotor (experiment at FONSORBES)
- a second helicopter of quite similar dimensions -PUMA-. This one was not equipped of passive dischargers (older model of helicopter). The experiment took place at BOUCAU

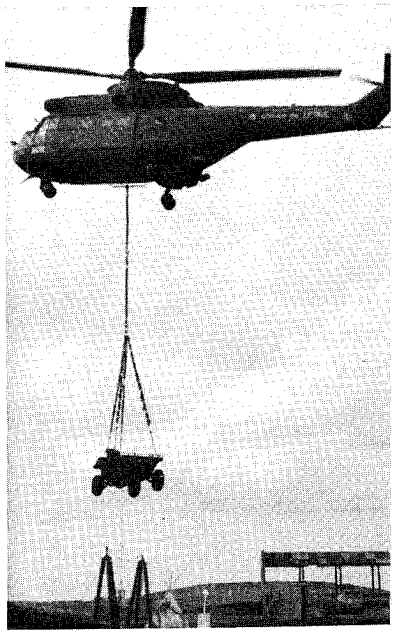


**Fig. 1 - photography of "PUMA" helicopter hovering above the measurement set-up.**

### 2.1. Type of measurements

At each campaign, the measurements were performed in many sessions, starting in the morning and ending one day later. The atmopheric conditions were recorded : Temperature, humidity, wind speed and helicopter altitude (from the helicopter instruments)

### 2.1.1. Charging current

By shorting the helicopter to the ground through a short circuit or resistor, a current measurement is recorded by an ammeter. This value determines the effective resistance of the helicopter (electric resistance in Ohm of an airbone helicopter to the ground). This number combined with the helicopter capacitance determines the charging and discharging time constant.

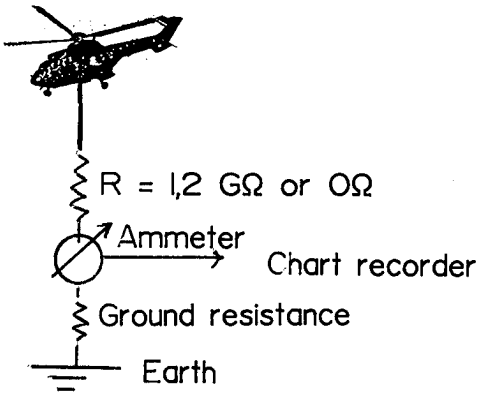



**Fig. 2 - schematic diagram of current measurement.**

### 2.1.2. Charging voltage of the helicopter (Vh) and the cargo (Vc)

The classic method using a high resistive dividor and a D.C. voltmeter does not permit to measure the "open circuit voltage" because of the very high value of the source resistance (>> $10^9 \Omega$) compared to the resistance leakage of dividor. So by using a capacitive dividor, we recorded the peak value of capacitive discharge voltage (the switching time of helicopter connection is low) after each flight.

**Capacitive dividor : ROSS model VD 240**
- input resistance 480 MΩ
- input capacitance 5 pF
- voltage ratio ≃ 1/1000

**Fiber optic link :**
- bandwith 0 - 1,5 MHz

**Ground resistance :**
- 28 Ohm at FONSORBES Location
- 380 Ohm at BOUCAU Location

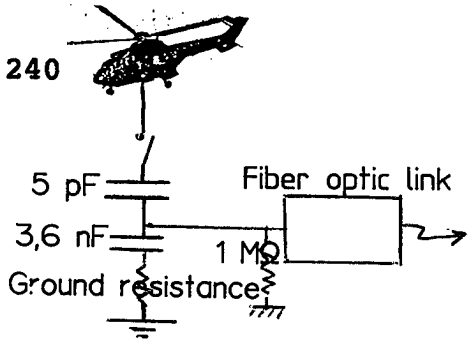



**Fig. 3 - schematic diagram of voltage measurement.**

### 2.1.3. Discharge current impulse

Two circuits of helicopter discharge, were analysed for simulating the main cases of operating usual conditions :

. Rs = 1000 (representative of simple model of human body) . Cargo handling or rescue operations

. Rs = 0 : Ground resistance (loading or unloading munitions cargo)

Current sensor : Pearson model 411

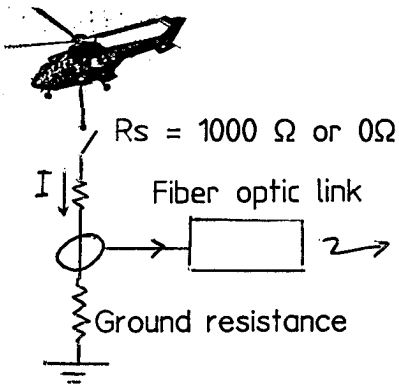



**Fig. 4 - schematic diagram of current measurement discharges**

**2.1.4._ Ground electric_field**

Near the voltage sensor (2-1-2), a field mill sensor manufactured by DIMENSIONS (patent ONERA) records the vertical electric field (Ev) in two different conditions :

. Without helicopter : Ev = E atmospheric

. With hovering helicopter: Ev = E atmospheric + E induced by the helicopter

**3) MAIN RESULTS**

**3.1._Charging current by_shorting the helicopter_to ground**

The different phases of helicopter flight are clearly seen on the record of figure 5 : engine starting, rotor turning and engine stopping with their comparative currents flowing from the ground to helicopter. The level of current is very low, resulting the atmospheric conditions at BOUCAU (salt and humid air), however two charging process can be noticed : engine running and blades triboelectric effects.

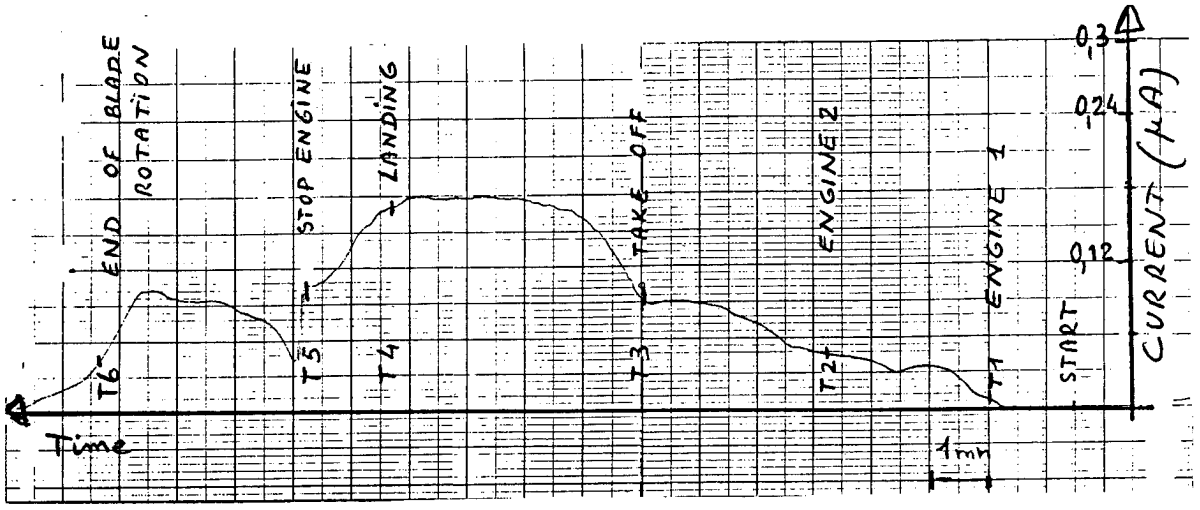



**Fig. 5 : The charging current by shorting the helicopter to ground during hovering conditions (h = 0 m to 5 m and to 0 m)**

## 3.2. Potential relative to earth. Discharge current impulse

Table 1 give some results recorded during the two experiments.

| TEST | Location | Date and test number | Flight conditions | Helicopter altitude | Helicopt. voltage | Ambiant field | Discharge current (peak level) | Weather conditions (ground) |
|---|---|---|---|---|---|---|---|---|
| COUGAR + Winch | Fonsorbes (land) | 04.10.94 15H17 ① | Hovering | 12 m | -22,5 kV | -190 V/m | -- | P = 996 Hpa<br>T = 15 to 17°C |
| " " | " " | 04.10.94 16H06 ② | Hovering | 32 m | - 3,8 kV | -- | -- | Hr = 65 to 75%<br>V = 1 to 3 m/s |
| " " | " " | 04.10.94 17H51 ③ | 7.800 feet | 12 m | + 11,7 kV | -- | -- | |
| " " | " " | 05.10.94 11H03 ④ | 60 Kts | 12 m | +20,7 kV | -250 V/m | -- | |
| COUGAR + Winch + Ropes + vehicule | " " | 05.10.94 11H20 ⑤ | Hovering | 19 m | +12,2 kV | -250 V/m | -- | P = 1000Hpa<br>T = 10 to 12°C |
| COUGAR + Winch | " " | 05.10.94 11H30 ⑥ | " | 12 m | -- | -240 V/m | 520 A | |
| COUGAR + Winch + Ropes + vehicule | " " | 05.10.94 11H31 ⑦ | 60 Kts | 12 m | +14,9 kV | -250 V/m | -- | Hr = 77 to 83%<br>V = 2 to 3 m/s |
| COUGAR + Winch + Ropes (10m) | " " | 05.10.94 12H08 ⑧ | Hovering | 16 m | + 4,1 kV | -- | -- | |
| PUMA + Winch | BOUCAU (beach) | 28.03.95 10H38 ⑨ | Hovering | 10 m | + 1,3 kV | -280 V/m | -- | |
| "" "" | " " | 28.03.95 10H46 ⑩ | Hovering | 5 m | + 0,85 kV | -- | -- | T = 19 to 20°C |
| "" "" | " " | 28.03.95 14H24 ⑪ | -- | -- | -- | +270 V/m | 4,9 A | Hr = 50 to 55% |
| "" "" | " " | 28.03.95 15H03 ⑫ | 60 kts | 5 m | + 1,56 kV | -- | -- | windy |
| PUMA + Winch+ Ropes + vehicule | " " | 28.03.95 15H50 ⑬ | Hovering | 16 m | + 2,51 kV | +200 V/m | -- | |

**TABLE 1 : Main results recorded during the two experiments [5]**

Therefore we can note appendice):

. at FONSORBES, levels are higher (about 20 KV) and the polarity of the potential is positive or negative. The impulse current through a short circuit (or a man) can reach a peak level of 500 A (oscillating discharge)

* at BOUCAU, current and voltage measurements are very low but in coherence with the charging current (0,3 uA-see & 3.1.) These results are surprising because measurements took place over a sand beach, but perhaps fog and salt air wind prevented the helicopter from stocking charges.

## 3.3. Vertical electric field and helicopter polarity

| TEST Number | Ground electric field (without helicopter) $E_a$ | Ground electric field (with hovering helicopter) $E_v$ | helicopter Polarity | Voltage measurement (see § 3.2.) | Voltage deduced from E values. ($V \simeq -E \times h$) |
|---|---|---|---|---|---|
| | | | | | $V_H = -(E_v - E_a).h$ |
| ① | E = -190 V/m | E = +1500 V/m | Négative | -22,5 kV | 1690 X 12 ≃ - 22 kV |
| ④ | E = -250 V/m | E = -2080 V/m | Positive | + 20,7 kV | 1750 X 12 ≃ 22 kV |
| ⑨ | E = -280 V/m | E = -140 V/m | Positive | + 1,38 kV | 140 X 10 ≃ 1,4 kV |
| ⑫ | E = 200 V/m | E = 10 V/m | Positive | + 2, kV | 190 X 16 ≃ 3 kV |

**TABLE 2 : Prediction of the helicopter potential from electric field measurement at ground**

**From the measurements of ground electric field, it seems possible to deduced the polarity of helicopter voltage and perhaps more, an approximate value of its relative potential to earth (table 2)**

## 4) EQUIVALENT CIRCUIT OF DISCHARGING PROCESS

A simple model of the helicopter discharging process is given by the equivalent circuit shown in figure 6. The circuit parameters are deduced from measurements by PSPICE calculations.

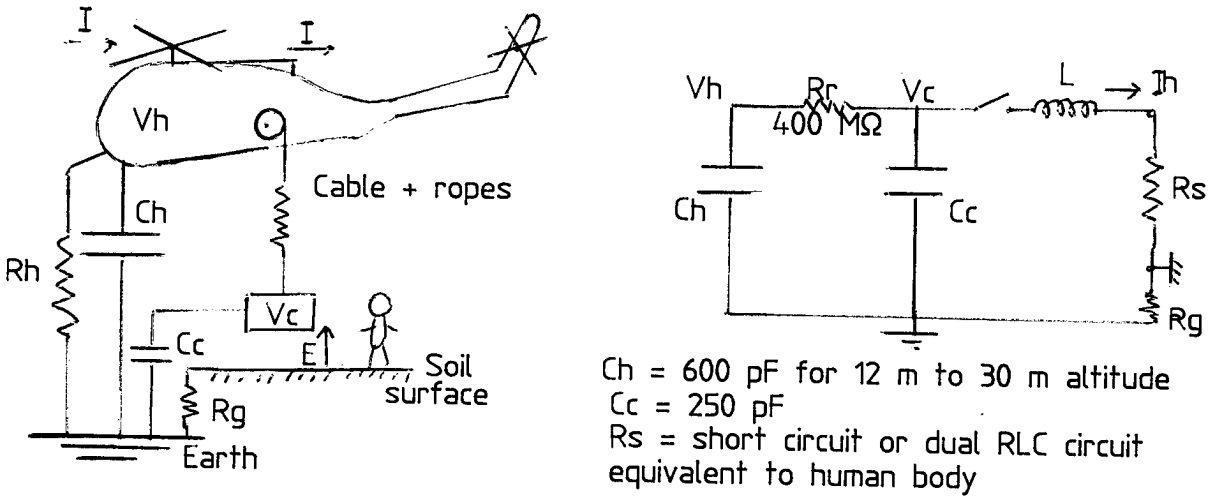



**Fig. 6 : Equivalent circuit of discharging process**

## 5) PERSONEL OR SYSTEMS SAFETY

From these experiments, some partial conclusions can be noted :

- Helicopter and cargo acquire the same potential, despite the use of dielectric ropes. The recorded values were lower than published or STANAG data, perhaps due to the passive discharger for the "COUGAR" and the atmospheric conditions for the "PUMA". The maximum recorded levels are :

  Vh = + 22 KV, - 19 KV
  Ih = 500 A (peak)
  Qh = 12 µC
  Wh ≃ 150 mJ.

This last value can be compared with physiological response of the human body (100 mJ = shock in fingers. DALZIED data) or minimum ignition energy for hydrocarbon gases at stochiometric conditions (200 µ J) or electro-explosive devices ( EEDs ) suceptibility.

## 6) CONCLUSIONS

The electrostatic hazards of transport by helicopter can be resumed :

- injury to ground personnel ; handling cargo or touching helicoter (150 mJ on "COUGAR")
- possible damage to the cargo as a result of impulse discharge current passing through it (peak of 500 A recorded)
- arcs and radiated fields when ground contact is made.

The measured values are lower compared to published or STANAG values but the following methods to reduce the possible hazards would be systematically applied, even in France.

- grounding technique. The helicopter should be continuously held at ground when explosives are loaded or unloaded. For ground personnel, it is advisable that the first contact with soil surface (wet or dry) be made through a resistive link ( 1 MΩ seems to be good) in order to limit the peak current.
- limitation potential:

Passive dischargers should be installed to decrease the electrostatic potential of helicopter (and cargo), mainly on the large helicopters.

The measurement technique used during these 2 experiments have provided comprehensive results. The measurement of ground electric field should allow to predict the value and the polarity of the hovering helicopter potential before handling or rescue operations (to be confirmed)

## REFERENCES :

[1] Passive potential equalization between the cargo handler and a hovering helicopter by J.E. DOUGLAS and J.E. NANEVICZ ICOLSE 1975 England

[2] Measurement of the electrostatic charging on large helicopters and control of the shock hazard by R.E. PECHACEK and D.P. MURPHY - ICOLSE 89 - NAVAL RESEARCH LABORATORY

[3] Electrostatics hazards in helicopter search and rescue operations by G. ODAM and R. EVANS - RAE England

[4] Electrical safety evaluation of a helicopter static charge grounding wand by J.L. DAWSON - NAVAL AIR TEST Center PATUXENT RIVER.

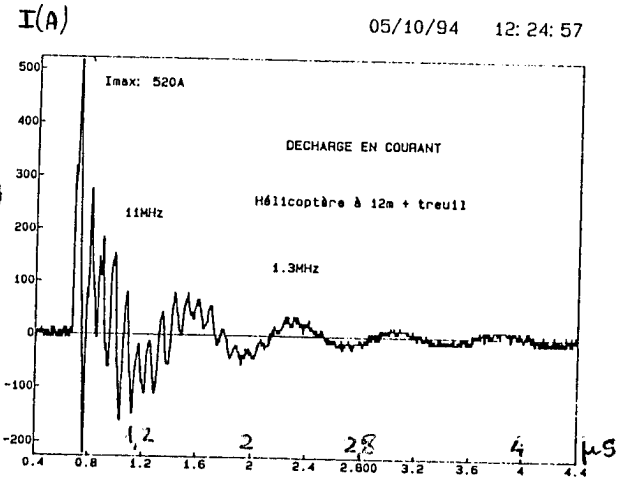
[5] Mesure du potentiel electrostatique sur helicoptere - C.E.A.T. P.V. n° E 94/62 37 00 par C. DAVOISE Février 1995.

# A N N E X E

- Helicopter discharge current impulse (through a short circuit)

  500 A peak

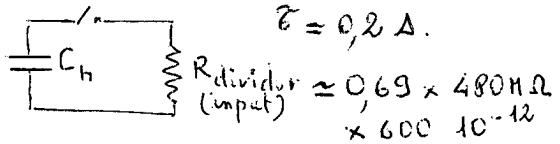
  (test number : (6))

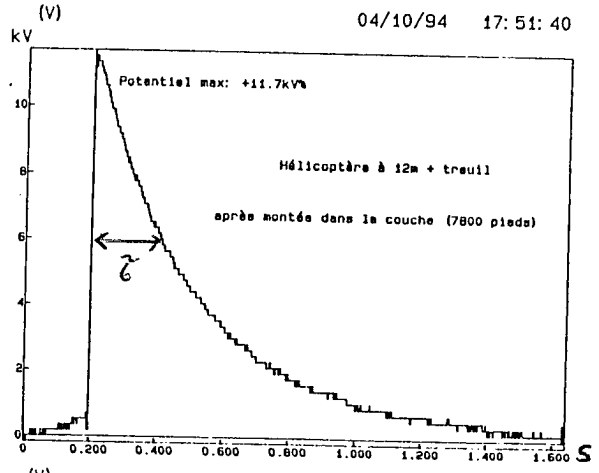



- Helicopter voltage

  V h = 11 kV

  (test number : (3))

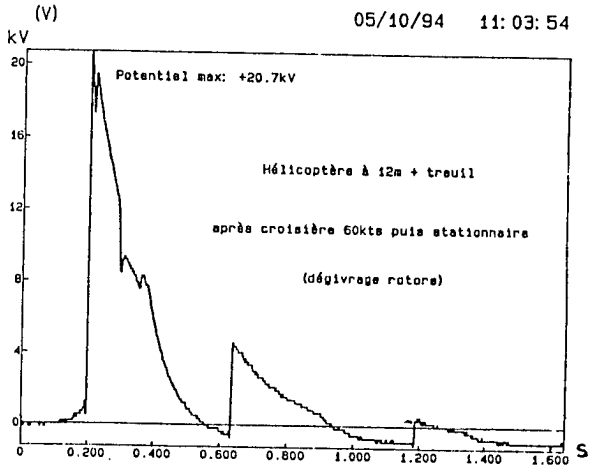



- Helicopter voltage

  V h = 20 kV

  (test number : (4))




**Typical records of voltage and current on "COUGAR" helicopter at "FONSORBES" location**

# E-6A
# PRECIPITATION STATIC ASSESSMENTS

Joel Haines, Mike Clelland, and Mike Whitaker
Naval Air Warfare Center Aircraft Division
Code 5.1.7.2
Patuxent River, Maryland 20670-5304

William DePasquale
Dual, Incorporated
745C Great Mills Road
Lexington Park, Maryland 20653

Bernd Lubosch
Dual, Incorporated
5600 Liberty Parkway
Midwest City, Oklahoma 73110

Electromagnetic Environmental Effects ($E^3$) is a serious concern in today's Navy. As part of the $E^3$ life-cycle effort, P-Static Assessments of TACAMO Fleet aircraft are being conducted. These assessments are used to monitor aircraft bonding integrity and maintenance procedures throughout the aircraft life-cycle. To minimize the problems associated with $E^3$, aircraft bonding integrity must be maintained.

A P-Static assessment is a quick-look method for finding bonding inconsistencies on the skin of the aircraft. Working hand in hand with the Fleet, problem areas can be identified and maintenance actions initiated to correct them. In the future, the P-Static assessments will be incorporated into the Enhanced Phase Maintenance (EPM) procedures.

The P-Static assessments consist of power off testing along with dc bonding measurements of the static discharging system. The Fleet receives a brief report describing problems found during the assessment with recommended fixes. A database will be developed to document all problem areas and note any similarities between aircraft.

## INTRODUCTION

To ensure that the level of electromagnetic pulse (EMP) hardening will be maintained throughout the life of the E-6A aircraft, the Hardness Maintenance/Hardness Surveillance (HM/HS) program was implemented. HM is a set of comprehensive procedures to ensure that Fleet operations, logistic support, and/or maintenance do not degrade the designed EMP hardness. HS includes system level and field surveillance tests and inspections performed throughout the aircraft life-cycle to monitor hardness integrity. As part of the HM/HS plan, Precipitation Static (P-Static) assessments of the Take Charge and Move Out (TACAMO) Fleet aircraft are being conducted.

P-Static testing is performed by using a high voltage test set to deposit a charge onto the aircraft with a high voltage ion discharge wand. Any unbonded panels, screws, rivets, doors, etc. can contribute to electromagnetic interference (EMI). This EMI can disrupt aircraft communications equipment and, in turn, impede the mission of the E-6A. Panels can become unbonded through the normal course of operations. Proper bonding of panels to the airframe can alleviate a high percentage of P-Static problems.

Standard test methods and equipment will give the Fleet the ability to protect the E-6A aircraft and its systems from P-Static problems. Early detection will preclude the necessity for a major test program to fix P-Static related problems. P-Static testing can identify electrically isolated areas, evaluate static wick performance, measure static wick parameters, test lightning diverter strips, and identify affected avionics.

The E-6A mission is primarily communications. A major P-Static problem could adversely affect the ability of the aircraft to perform its mission. Further mission communication upgrades to the E-6A, like the E-6A Avionics Block Upgrade (ABU) and the E-6B Airborne National Command Post (ABNCP), require that EMI caused by P-Static be kept at a minimum. For this reason, a P-Static assessment program is being put into place at the Fleet maintenance level.

The E-6A $E^3$ Hardness Maintenance / Surveillance (HM/S) Integrated Product Team (IPT) is responsible for performing system level hardness assurance and surveillance tests, evaluating and developing test equipment capable of monitoring and detecting EMP hardness degradation, providing on-site life-cycle $E^3$ HM/HS technical and engineering support to the Fleet, as well as integrating P-Static into the Enhanced Phase Maintenance (EPM) plan. The scope of this paper is to discuss the HM/S IPT's current plans on P-Static.

Since 1990, all E-6A aircraft have undergone EMP HS field. All testing performed by the HM/S IPT is done on a not to interfere basis with the Fleet. P-Static testing is performed in the same manner. One HM/S IPT member and one Fleet maintenance personnel conduct the test in one 10 hour shift. Standard test methods and equipment give the TACAMO Fleet the ability to protect the aircraft and its systems from P-Static problems.

## TEST RESULTS

Currently, P-Static evaluations have been performed on three E-6A aircraft (BuNo 164387, 164388, and 164408). Evaluations on each aircraft produced similar results. Several panels on the engine struts were not bonded properly to the aircraft. Also, panels on the vertical stabilizer were not properly bonded. The following table is an example of some of the problem areas found during these assessments.

| LOCATION | THRESHOLD $\mu A/ft^2$ | SUGGESTED FIXES |
|---|---|---|
| TWO HINGES ON AFT SIDE OF THE FLIGHT RECORDER PANEL (#10/96), BOTTOM OF VERTICAL STABILIZER | 10 | BOND HINGES AND PANEL TO AIRCRAFT |
| HF LIGHTNING ARRESTOR PANEL (#911-01), TOP OF VERTICAL STABILIZER | 10 | BOND PANEL TO AIRCRAFT |
| #1 ENGINE STRUT ACCESS PANEL L10133-05 | 15 | BOND PANEL TO AIRCRAFT |

When the problem area list is given to Fleet maintenance personnel, the process of correcting the problems is initiated. Generally, these fixes are uncomplicated. Installation of a bonding strap is a typical fix for bonding problems.

The P-Static test set can be used as an EMI trouble shooting tool as well. For example, E-6A BuNo 164408, was having such severe EMI problems that its VHF/UHF radios were virtually unusable. Using the P-Static test set, it was discovered that a lightning diverter strip on the nose radome was improperly installed, leaving it unattached to the aircraft. With the electrical charge buildup, arcing across the gap between the lightning diverter strip and the aircraft began. This arcing was being picked up by the VHF/UHF communication system, raising the noise floor of the radios so high that voice communication was impossible. A bonding strap was installed as a quick fix for the next flight. A metal plate was later installed as a permanent fix.

A baseline of all Fleet E-6As, including the ABU and ABNCP aircraft, is planned.

## TEST METHODOLOGY

Currently, ground testing of aircraft at Tinker Air Force Base is performed using widely accepted test methods in the electrostatic field. Testing is performed by using a high voltage test set to deposit a charge onto an aircraft with a high voltage ion discharge wand. The wand is comprised of a high voltage dish with electrostatic dischargers attached, which enables the wand to "spray" a simulated P-Static charge onto the aircraft.

Each area of the aircraft is sprayed at 40 kV and approximately 50 $\mu A/ft^2$ current while sensitive hand-held receivers are monitored for any electromagnetic interference (EMI) generated by P-Static. Because the wand is comprised of electrostatic dischargers, P-Static noise generated by the wand itself is almost nonexistent, thus enabling a very effective test method for aircraft. EMI is generally produced due to arcing between

isolated sections of the aircraft. However, problems have also occurred due to corona discharge from the aircraft and streamering effects.

Noise generated on the receivers can be heard in the form of popping, motorboating or squealing, depending on the severity of the P-Static problem.

After the entire aircraft has been sprayed, the areas with the most serious P-Static problems will be identified. Then the actual aircraft radios or equipment to be tested for P-Static interference can be monitored while each problem area is resprayed at 20 $\mu A/ft^2$ current. This current level has been determined to be severe for inflight P-Static induced on Navy aircraft. However, because the design of the high voltage test set is dynamic, testing can be performed at any voltage level up to 40 kV and any current level up to 200 μA. Also, because each problem area can be examined closely, a solution can readily be determined (such as installing a bonding strap).

Testing for P-Static interference is not the only use of the high voltage test set and wand. Additionally, specific checks can be performed on each aircraft static discharger to examine proper discharging capability. A poorly performing discharger will generally begin arcing and generate noise on the hand-held receivers. Also, the wand can be used to find dischargers which may be installed on isolated panels (thereby becoming less effective for dissipation of electrostatic charge from the aircraft). Finally, the wand can be used to test a fix installed on a problem area to ensure that P-Static no longer presents a problem in that area.

During a standard P-Static evaluation, other instrumentation is used to augment testing. A Digital Low Resistance Ohmmeter (DLRO) is used to check bonding of the aircraft. Bonding checks can be made of installed electrostatic dischargers, fuel tank cap or vent areas (for safety), and also between isolated sections of the aircraft's surface. Bonding checks can be made to determine if the aircraft discharging system functions are in compliance with MIL-B-5087B (1), the current bonding specification for Naval aircraft.

Also, a digital megohmmeter (megger) can be used to check the tip to base resistance of electrostatic dischargers to be used on aircraft, whether installed or not. This will determine compliance with MIL-D-9129D (2), which gives the current specification limits for Naval aircraft dischargers. This can be used to determine if the discharger has internal damage and may need to be replaced.

All of these test methods are relatively simple to accomplish. However, for the testing to be accomplished correctly and consistently, standard documentation will also be necessary. These will include standard test procedures, detailed operating procedures and equipment maintenance documents. Currently, all three types of documents are available for P-Static testing of aircraft at Patuxent River. However, this documentation can be tailored for testing at the Fleet level.

If this test methodology can be incorporated into EPM, then the Fleet will have the capability and expertise to test the E-6A aircraft for problems related to P-Static, without the need for a large test program.

Currently, the Naval Air Warfare Center at Patuxent River is tasked to provide Fleet support and has distributed a P-Static equipment and documentation package to the E-6A Fleet at Tinker Air Force Base, Oklahoma City, OK.

## SUMMARY

By incorporating standard test methods and equipment into the Fleet, a reliable system of Precipitation Static ground testing of Fleet aircraft can be established. It will provide a relatively simple means of evaluating the E-6 aircraft and its systems for P-Static effects during maintenance phases. Also, the need for a large test program to maintain the E-6A aircraft's operability under P-Static weather conditions will be greatly reduced.

# METHODS OF DETERMINING THE ELECTROSTATIC POTENTIAL AND CHARGING CURRENT OF A HOVERING HELICOPTER

G A M Odam and R H Evans
GAO Consultancy, Barmouth, Gwynedd, UK
(Consultants, previously employed at RAE Farnborough)

## ABSTRACT

Methods are given for determining the electrostatic charging current and aircraft potential to ground of a hovering helicopter. The limitations of using a field mill to give aircraft potential are described. One method, using in turn EHT generators of both polarities to artificially charge the aircraft, gives an accurate measurement of aircraft potential to ground with the ability to distinguish the component due to ambient field. The method was used to enable a comparison to be made of different arrangements of passive dischargers at the extremities of Sea King main rotor blades, to control the aircraft potential under benign ambient field conditions.

## INTRODUCTION

It is well known that aircraft including helicopters can acquire a static charge in flight. It is important to know the charging characteristics of a helicopter, especially when the aircraft is carrying under-slung fuel or ordnance loads or when it is engaged in search and rescue operations. This paper puts on record measurement methods used by the writers since the mid-1960s when in post at the Royal Aircraft Establishment, Farnborough (now Defence Research Agency, Farnborough), as members of the Electrostatic and Lightning Hazards Section. It was this early helicopter research which led to the interest in lightning and the formation of the Culham Lightning Studies Unit. Helicopter potentials to ground can range from a few kV in benign atmospheric conditions up to several hundred kV in bad weather conditions. In some Sea King electrostatic shock incidents reported to Farnborough, it was estimated that the aircraft potential was as high as 1 MV. Methods of measuring these potentials and the associated charging currents and the limitations of the methods are given below.

## CHARGING MECHANISMS

AN AIRCRAFT AS A CHARGED BODY - -An aircraft in flight may be regarded as a body having capacitance surrounded by an air dielectric. All the normal considerations for such a system apply. For example the dielectric has a leakage resistance which, if the capacitor is charged, allows a certain current to leak away. This resistance is obviously dependent on the aircraft shape and size (surface area) and the conductivity of the air. The resistance can be considerably lowered by processes which increase the ion density in the air, such as thermal dissociation and corona. For example the use of afterburners has been known to completely discharge a previously charged aircraft, doubtless due to the vast increase in thermal ionisation in the engine exhaust efflux.

Also a marked change occurs when field stresses exceed the breakdown stress for air and the aircraft extremities go into corona. It may be noted that the object of all dissipative devices is to lower the effective leakage resistance.

GENERAL COMMENTS - -As is well known an aircraft can acquire charge in one or more of three possible ways. These are by engine charging, induction charging and precipitation charging. Engine charging is of course an internal effect of the aircraft whilst induction and precipitation charging are the result of external influences. The first and last mechanisms mentioned above impart a nett charge to the aircraft whilst induction charging only results in charge separation.

ENGINE CHARGING - -This results when an unbalance of ions produced during the combustion process are carried away by the exhaust gases. Helicopter charging currents are generally less than 1.0 μA and in general do not produce any serious hazard, although on some aircraft (Whirlwind 10 and Sea King) voltages up to 90 kV have been measured.

INDUCTION CHARGING - -This is a process arising from the induction effects of external charge concentrations, resulting in charge separation across the airframe. Atmospheric potential gradients of one polarity or another are always present. Their magnitudes rarely achieve values sufficient to cause airframe corona discharges except in close proximity to active thunderstorms, but they do have a wide effect on helicopter operation, since values of aircraft voltage well below those required for corona could prove dangerous. However in the absence of cloud the atmosphere potential gradient is typically 100 V/m and thus for helicopters flying below 20 metres altitude voltages would be less than 2 kV and available discharge energy levels less than 1.0 mJ. Clouds with little vertical development cause gradients within ±250 V/m, whilst cumulo-nimbus can produce very large disturbances up to ±20 kV/m. Thus in the proximity of shower or thunderstorms type clouds voltages of the order of 5 to 100 kV might be found on a helicopter, merely due to the ambient field alone.

PRECIPITATION CHARGING - -Two types are important - that due to tribo-electric or frictional effects of dry particles in the air and that due to the impact of rain or wet snow.

Rain precipitation charging is a form of splash or spray electrification resulting from the break up of water droplets on impact with the airframe. Two separate charging mechanisms may be involved (1) but in practice only induction spray charging has significance.

The latter effect results from the shattering of water droplets in the presence of an applied electric field, the polarity of the small ions released to the air being controlled by the polarity of the field. Because impact energies with high speed aircraft or rotor blades are very high and the field intensities at the leading edges will generally be much higher than ambient field gradients, this mechanism can give rise to very high charging currents.

## REVIEW OF MEASUREMENT METHODS

### BASIC PARAMETERS

Aircraft Capacitance - -This is dependent on aircraft shape, size and, for altitudes of less than 30 m, proximity to ground. Rogers and Minihan (2) using models have shown that the variation of capacitance with altitude is given by:-

$$C = (k_o + k_1/h) \quad (1)$$

where h = height above ground and $k_o$ and $k_1$ are constants.

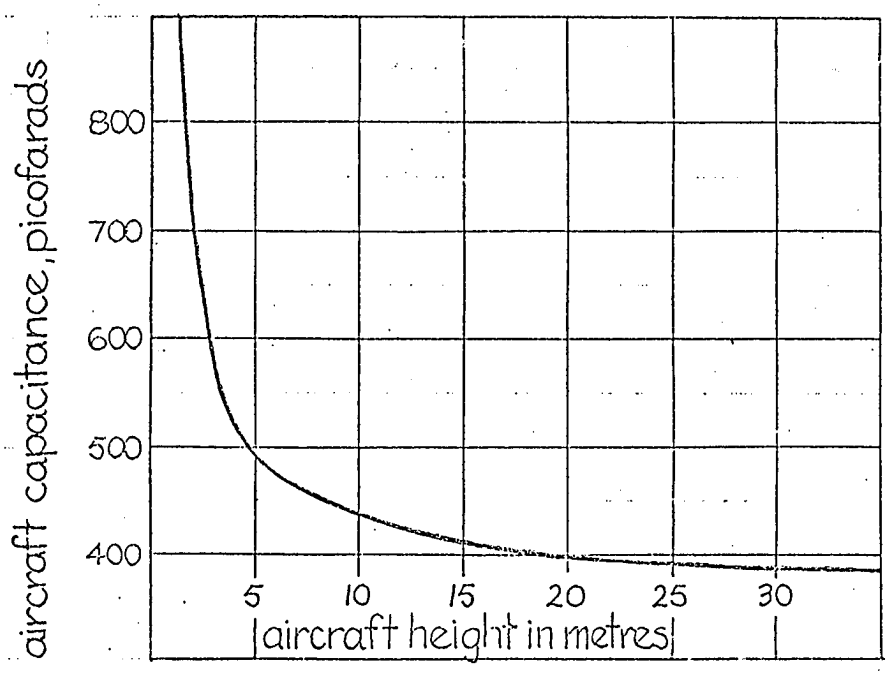



FIG 1 VARIATION OF AIRCRAFT CAPACITANCE WITH ALTITUDE FOR HELICOPTERS WEIGHING APPROXIMATELY 4000 KG

Fig 1 shows the variation and typical values for helicopters of approximately 4000 kg gross weight. Most helicopters in service today when hovering above 3 m will have capacitance values of less than 1000 pF.

Charging Current ($i_c$) - -This is the rate at which charge is incident upon the aircraft. If $i_L$ is the instantaneous leakage current (a voltage dependent term) then the effective charging current $i_c'$ is

$$i_c' = (i_c - i_L) \qquad (2)$$

In the steady state condition, that is when the aircraft has reached its equilibrium voltage, $i_c'$ falls to zero and the leakage current exactly balances the incident charging current. The object of charge dissipation devices is to achieve this balance at lower aircraft voltages by modifying the voltage dependency of the leakage term.

Aircraft Voltage - -By this we usually mean the steady state or equilibrium voltage as defined above. Since voltage implies a potential difference, confusion often arises as to the reference level. For helicopter work it is convenient to refer voltage to earth potential, since this readily permits the calculation of energy available for discharge.

This voltage V is related to the charging current by the expression

$$V_{(t)} = 1/C \int_0^t (i_c - i_L)\, dt \qquad (3)$$

$$\text{or} \quad V = Q/C \qquad (4)$$

where Q is total charge.

Since $dv/dt = (i_c - i_L)/C$ the low values of capacitance quoted above give very rapid charging times. Peak current, and hence voltage, is an important parameter when considering induced transients resulting from discharges to earth.

Stored Energy - -This is important in the helicopter case as it is the energy available for discharge when the aircraft is earthed and is then the parameter most frequently used in assessing the degree of hazard to personnel or underslung fuel or armament loads. The energy stored is given by the usual expression

$$E = 1/2\ CV^2 \qquad (5)$$

MEASUREMENTS

Charging Current - -When the aircraft voltage is zero $i_L$ is zero. Therefore, in the case of a hovering helicopter a simple way of measuring the charging current is to connect the aircraft to the ground and measure the current flowing in this connection.

Aircraft Voltage - -Again in the helicopter case this is easily measured by connecting an electrostatic voltmeter with suitable range extension capacitors between the airframe and ground, either from within the aircraft or by probing from the ground. This is essentially a charge sharing method and relies on a knowledge of the aircraft capacitance. Simplistic and more advanced methods of measuring charging current and aircraft voltage are discussed below.

Field Intensity - -A knowledge of field intensity gives a very useful indication of the state of charge of an aircraft. A device known as a field-mill is used to measure field intensity and is described elsewhere, for example in Reference 3. Obviously it can only measure the field intensity at the particular part of the aircraft surface where it is installed, but this is not a serious limitation if the parameters under investigation can be correlated to this field. With suitable recording, continuous records can be made of the electrostatic charging activity encountered by an aircraft. A field mill fitted to a hovering helicopter may be calibrated in terms of aircraft voltage at a given height by applying known voltages from a ground high voltage supply unit but this method has limitations as discussed below.

The Royal Aircraft Establishment developed an experimental field mill for aircraft use, with a logarithmic scale to measure field strengths of either polarity in the range 400 V/m to 300 kV/m (4).

## SIMPLE CHARGING CURRENT AND AIRCRAFT VOLTAGE MEASUREMENTS

As is noted above, charging current can be measured at any hover altitude by connecting a micro-ammeter between airframe and ground. With a knowledge of aircraft capacitance, voltage to ground can be measured to an acceptable accuracy by 'charge sharing' methods whereby a capacitor of known value in parallel with an electrostatic voltmeter is connected between the aircraft and ground. Both current and voltage measurements can be made on the ground, by probing to a weighted and conducting drop line as shown in Figure 2. Measurements can be made more conveniently, from within the aircraft, whereby a weighted insulated drop line making contact with the ground is connected to one side of the measuring equipment, the other side of which is connected to airframe, as shown in Figure 3. The measuring equipment can be simple and robust, and that used by Farnborough was mounted in a perspex box which could easily be rested on the observer's knees. The same equipment was used on the ground and it is diagrammatically shown in Figure 4. Analogue instruments were used which had to be allowed to settle down to steady readings before values were noted.

With modern technology, the equipment could easily be digital with read-out and recording facilities. When making current measurements the micro-ammeter had initially to be set at a high range to accommodate the initial discharge current when the aircraft was earthed.

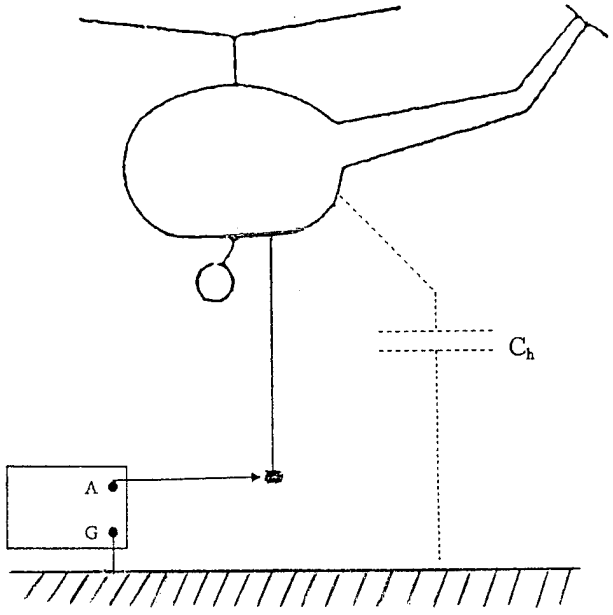



FIG 2 MEASUREMENTS MADE ON THE GROUND

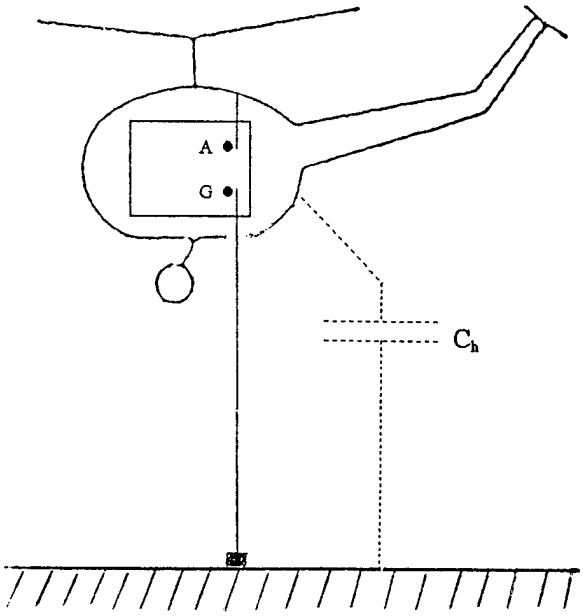



FIG 3 MEASUREMENTS MADE IN THE AIR

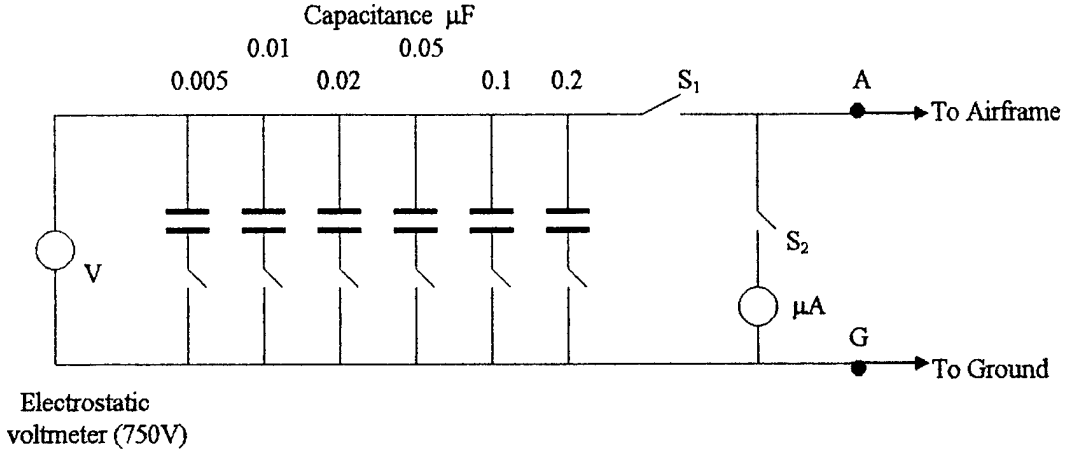



FIG 4 CIRCUIT DIAGRAM OF EQUIPMENT USED FOR THE MEASUREMENTS OF FIGS 2 & 3

The charge sharing method of estimating aircraft potential to ground and measuring the charging current with a micro-ammeter are quick and easy ways of determining the charging characteristics of a helicopter and do not require an expensive aircraft 'trials fit', as an aircraft can be prepared in a few minutes.

Sometimes when measurements are made on the ground on a number of aircraft, particularly in inclement weather, the measuring equipment may be put in a covered vehicle with a length of about 30 m of HT cable supported on insulated stakes about 1 m high between the vehicle and the measurement point, as was done in the trial reported in Reference 5. In that trial the cable was arranged cross wind and the end remote from the instruments terminated in a copper ring provided to make good electrical contact with a 12 m drop line suspended from the helicopter cabin floor and terminated with a weight. During the tests the weight was about 1.5 m above the ground. Potential measurements were made by picking up the end of the cable with an insulated rod and probing for a short time on to the weight. During the current readings, which were usually made immediately after a potential probe, the cable was connected to the weight until the meter indicated a steady reading.

In the measuring circuit of Figure 4, potential readings were taken with switch $S_2$ open but $S_1$ and the appropriate shunt capacitor switch closed. During the time that contact was made with the helicopter the charge stored in the helicopter capacitance $C_h$ was shared with the shunt capacitance $C_s$, so that if $V_m$ is the reading of the voltmeter then the original helicopter potential was:-

$$V_h = (C_h + C_s) / C_h \times V_m \qquad (6)$$

The six shunt capacitors gave a measurement range of about 1.7 kV to 300 kV for a helicopter capacitance of 500 pF and proportionally less for higher capacitance. The advantage of this charge sharing method is that it permits a selective range of measurements with simple robust equipment not involving the use of high voltage instruments. Strictly, the capacitance of the HT cable and the voltmeter should be added to $C_s$ but it was found that their neglect did not introduce an error of more than 5% in the worst case. The overall errors of the method were estimated to be less than 15%. The charging current was measured on a sensitive micro-ammeter with switch $S_1$ open and $S_2$ closed. As is noted above, the charge sharing method requires a knowledge of the helicopter capacitance. Reference 2 has shown that at heights greater than 9 m a helicopter has the same capacitance as a conducting sphere of radius equal to the overall helicopter length divided by 5.2. Various formulas for the capacitance of a sphere of radius r at height h (to the centre of the sphere) have been derived, such as the series:-

$$C = 4\pi kr\,(1 + n + n^2 + \text{ -- terms in higher powers of n}) \qquad (7)$$

where $n = r/2h$ and k is the permittivity of air (8.8 pF/m). As in the measurements on model helicopters (2), the capacitance reduces as the height increases (n becoming small), approaching the value for an isolated sphere, namely $4\pi kr$.

The measured potential $V_h$ is due not only to the nett charge but may also have a component $hE_a$ where $E_a$ is the earth's ambient field; similarly the measured current may have a component required to cancel the potential due to the earth's field when the helicopter is earthed through the micro- ammeter. These effects may be allowed for by measuring the earth's field prevailing at the time of the trial, using a field mill mounted near the ground.

If it is assumed that the ambient field is sufficiently low to be neglected, the measured current is equal to the charging current $i_c$ and the ratio $V_h/i_c$ represents the 'leakage' resistance $R_L$ between the helicopter and earth, although of course this is not an accurate representation because in fact $R_L$ is voltage dependent.

Approximately the time constant $C_hR_L$ governs the rate at which the helicopter recharges after having been earthed. For example, the results of one trial at a hover height of 12 m were

$C_h = 433$ pF, $V_h = 29$ kV, $i_c = 0.45$ μA, $R_L = 6.4 \times 10^{10}$ ohm, time constant = 28 s.

When the shunt capacitor is connected, the total capacitance will be $C_h + C_s$ and the system will start to climb up to $V_h$ on a time constant of $(C_h + C_s) R_L$, which in the case quoted above would have been 1300 s. Obviously the value of $V_m$ must be noted (after the meter has settled down to a steady reading) before the system voltage starts climbing to $V_h$.

The above method measures the natural charging condition at the time of the trial. To explore the characteristics over a wide range the helicopter may be artificially charged by connecting the drop line through a micro-ammeter to a high voltage power supply of reversible polarity on the ground, as described below.

## MORE ADVANCED MEASUREMENTS OF CURRENT AND VOLTAGE

A method, originally used by Granger Associates (6), of determining charging current and aircraft voltage by artificially charging the aircraft was successfully used to determine the advantages of fitting passive dischargers to Sea King main rotor blades. The results of the trial are fully described in Reference 7. The discharge characteristics of the aircraft were obtained for various discharger configurations by connecting a conducting drop-line from the aircraft hovering at 18 m, to a ground-line which in turn was connected either to a negative or positive 100 kV EHT generator housed in the trials caravan. The current arriving at the aircraft from the power supply for a given EHT voltage was measured by a micro-ammeter in the aircraft. Values of current for discrete levels of voltage up to 100 kV for both positive and negative polarities were relayed to the caravan by a radio link.

On 3 different airframes it had been found that under benign atmospheric conditions Sea King aircraft charged positively with natural charging currents between 0.5 and 2.5 μA; this was attributed to an engine charging effect which with an ambient field contribution had been found to give aircraft voltages up to 100 kV. Both drop-line and ground charging measurements made on the trials aircraft confirmed natural charging currents in the above range and of positive polarity. The currents measured ranged between 1.2 and 2.4 μA, the drop-line measurements agreeing with the values given by the ground charging method.

Figure 5 shows the voltage/current characteristics for different discharger fits. Figure 5a shows the measured V/I curve of the helicopter when unprotected (no dischargers), with the original wick dischargers, and with configuration (A). Figure 5b indicates that the addition of rotorblade dischargers achieved a substantial modification of the characteristic, the outboard position (A + C) being the most effective. Before and after each flight, with the helicopter away from the trials area, the ambient E field was measured by means of a field mill mounted on the roof of the trials caravan and calibrated in that position. The field was nearly always positive, generally in the region of 150 to 350 V/m, with a maximum of 480 V/m, corresponding at a hover height of 20 m to potentials of 3 to 7 kV (9.6 kV maximum).

In Figure 5a, the natural charging conditions revealed by the measurements of the preceding section are represented by the points 'x' and 'y'. Intercept 'x' corresponds to the current that flows when the helicopter is earthed, and intercept 'y' to the helicopter voltage.

The latter follows as there must be zero current in the drop-line when the ground power supply is adjusted to exactly equal the equilibrium voltage of the aircraft due to whatever natural charging processes are taking place.

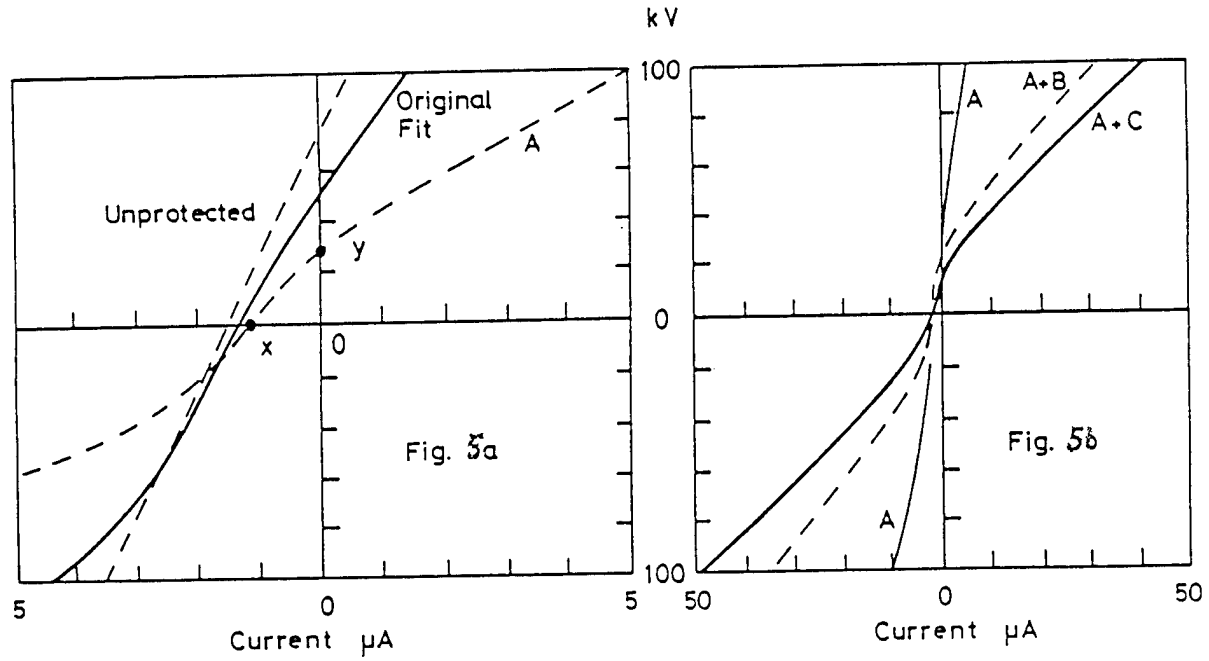



FIG 5 POTENTIAL VS CURRENT CHARACTERISTICS OF SEA KING HELICOPTER WITH VARIOUS STATIC DISCHARGER CONFIGURATIONS

## AIRBORNE MEASUREMENTS OF POTENTIAL TO GROUND USING A FIELD MILL

An indication of the state of charge during flight may be obtained by fitting a field mill to the underside of the helicopter. This indicates the electric field in that location, which is made up of a component $F_1V_c$ due to the charge and a component $F_2E_a$ due to the ambient field, where $V_c$ is the potential due to the charge, $E_a$ is the ambient field and $F_1$, $F_2$ are calibration factors for the installation, being constant for a given height but reducing with height, tending to a constant above a height of about 30 m. The total potential $V_t$ is $V_c + hE_a$ and the total mill reading $E_{mt}$ in terms of total potential is therefore $F_1(V_t - hE_a) + F_2E_a$ or:-

$$E_{mt} = F_1V_t - (F_1h - F_2)E_a \qquad (8)$$

The field mill installation was calibrated by connecting the hovering helicopter through a drop line to a high voltage power supply on the ground and plotting the mill reading against the potential for various hover heights, so obtaining a set of straight lines, as shown in Fig 6. The slope of each line is $F_1$, so we may plot $F_1$ as a function of height for that particular installation. The calibration factor $F_2$ is only weakly dependent on height and may be assumed constant. The intercept of each line on the $E_{mt}$ axis is $(F_1h - F_2)E_a$ and plotting this intercept against $F_1h$ yields the values of ambient field $E_a$ during the trial and also the value of $F_2$. If the ambient field is also measured by a separate field mill on the ground this acts as a check on the value of $E_a$

obtained from the intercept measurements. Use of the installation during flight to measure the total potential $V_t$ requires a knowledge of $E_a$ possibly measured on the ground and relayed to the helicopter, since:-

$$V_t = E_{mf}/F_1 + (h - F_2/F_1)E_a \quad (9)$$

Alternatively, in fair weather the effect of $E_a$ might be ignored or a value of say 100 V/m assumed.

It may be of interest to note the values of the factors $F_1$ and $F_2$ for a conducting sphere of radius r, with the field mill mounted on the lowest point looking vertically down, namely:-

$$F_1 = (1/r)(1 + n + 3n^2 + \text{--- higher powers}) \quad (10)$$

$$F_2 = 3(1 + 2n^3 + \text{--- higher powers}) \quad (11)$$

where $n = r/2h$. These reduce with increasing height, approaching the limiting values 1/r and 3 respectively. A field mill has a zero error, usually between 10 and 100 V/m. The latter could be comparable to the reading due to the ambient field in fair weather.

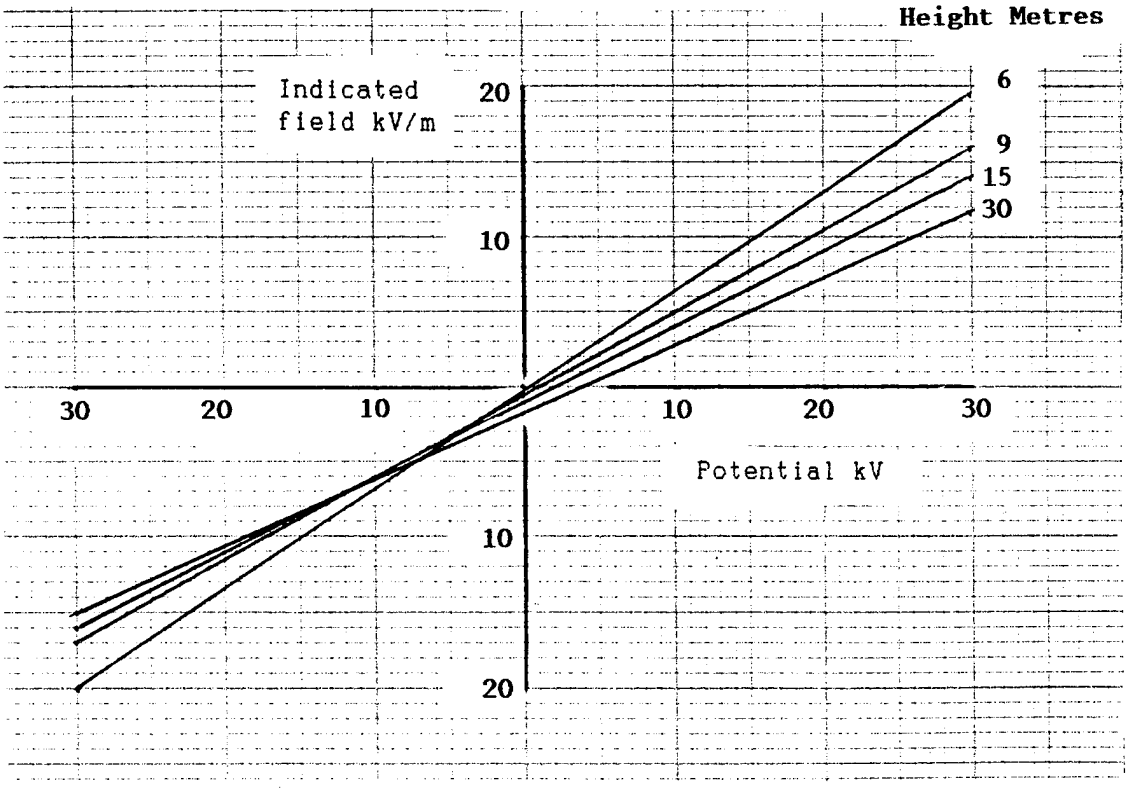



FIG 6 CALIBRATION OF FIELD MILL INSTALLATION BY CONNECTION OF HT POWER UNIT TO HOVERING HELICOPTER

REFERENCES

1. G A M Odam : Electrostatic Charging of Aircraft in Flight, First International Conference on Static Electricity, Vienna, 1970.

2. M E Rogers, E B M Minihan : Variation of Helicopter Capacitance with Altitude. RAE Technical Note I.E.E. 43 1964.

3. J A Chalmers : Atmospheric Electricity, Pergamon Press, London.Second Edition, p 143 1967.

4. G A M Odam, R H Forrest : An Experimental Automatic Wide Range Instrument to Monitor the Electrostatic Field at the surface of an Aircraft in Flight. RAE Technical Report 69218 1969.

5. G A M Odam, H V Willis and M E Rogers : Static Electricity Measurementsmade on Whirlwind 10, CH37, CH34 and UH1B Helicopters, at RAF Old Sarum, on 24 May 1967, RAE Tech Memo IEE 189, Oct 1967.

6. Granger Associates : Loran D Electrostatic RF1 and Null Field Discharger Flight Tests I, 1967.

7. G A M Odam, R H Evans, P F Little and J Butterworth : Electrostatic Hazards in Helicopter Search and Rescue Operations, Lightning and Static Electricity Conference, Oxford 1982.

British Crown Copyright 1995/DERA
Published with the permission of the Controller of Her Britannic Majesty's Stationery Office

# SESSION 07A
# STRUCTURES AND MATERIALS
# CHAIRPERSON: JERRY MCCORMICK

# STRESS WAVE VISUALISATION IN ALUMINIUM AND CFC PLATES SUBJECT TO SIMULATED LIGHTNING STRIKES

John Hardwick
Lightning Test and Technology, AEA Technology, Culham Science and Engineering Centre, Abingdon, Oxfordshire, OX14 3DB
Telephone: +44-1235-464264, Facsimile: +44-1235-464325
Neil Bourne, Yoav Mebar
Shock Physics, PCS, Cavendish Laboratory, Madingley Road, Cambridge, CB3 0HE
Tel 44-1223-337205 Fax 44-1223-350266

## ABSTRACT

Both thermal and mechanical damage can be imparted to structures by the attachment of lightning current arcs. In addition to the mechanical impulse imparted by the magnetic interaction lightning specialists have been concerned by so called acoustic shock effects.

Measurements of stress on panels using both electrical transducers and optical means have been employed to study the phenomenon.

Whilst no stress waves were observed with aluminium panels they were seen with CFC panels early on in the current pulse; possibly due to local explosive vaporisation of fibres within the panel at the initial arc attachment point.

## 1 INTRODUCTION

Direct effect thermo-mechanical damage to aircraft structures is associated with the severe parameters of the lightning return stroke. The return stroke can be considered to consist of two phases; a high amplitude short duration phase, Component A (200kA for about 100μs) and a lower amplitude continuing current phase, Component B and C (<2kA for hundreds of milliseconds).

Damage to traditional aluminium panelling in the form of melted holes is largely accounted for by the significant charge transfer in the continuing current phase (1). The high amplitude component causes little Joule heating on account of the excellent conductivity of aluminium and only minor surface pitting occurs. However significant mechanical effects can occur in this phase; the magnetic interaction between current flow in the arc and in the structure surface exerts an impulsive force on the surface. This force is proportional to the square of the current amplitude and is thus by far the largest in the Component A phase. During this phase there will also be radial pressure waves from the expanding arc channel (thunder), this may have a significant longitudinal component due to the tortuosity of the arc channel. The net mechanical effect is also a function of the mechanical response time of the structure (2). In addition to elastic displacement, thin aluminium panels can also be dented by the mechanical forces imparted by the arc.

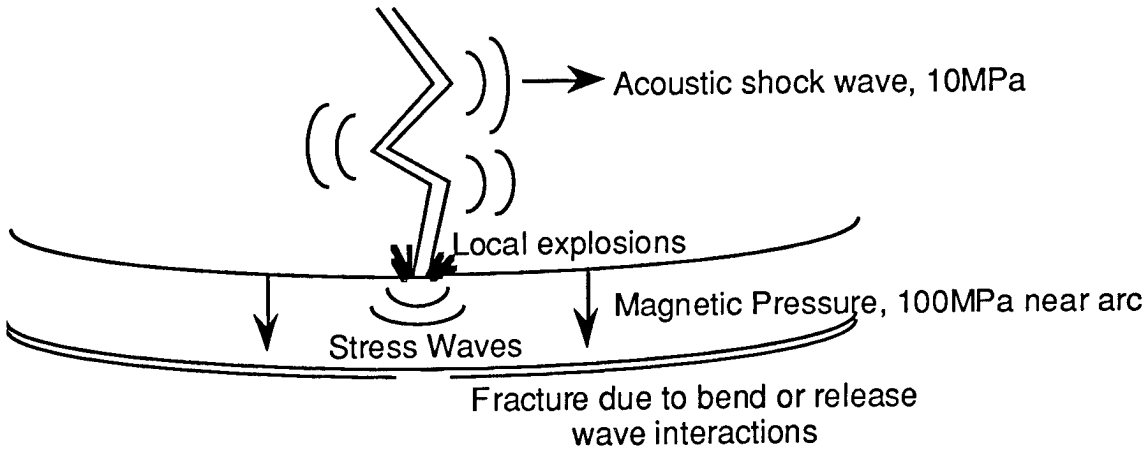
As well as significant damage imparted by the continuing current phase, carbon fibre composite (CFC) structures, on account of their significant resistance are also

damaged by Joule heating deposited by Component A. Damage consists of surface ply delamination, tufting of fibres and epoxy resin vaporisation at the attachment site (3).

This type of damage can be minimised by coating the CFC with surface metalisation. However delamination diametrically opposite the strike point has sometimes been observed even when the CFC has had some surface protection and has suffered little surface damage. This type of debonding has also been observed on the reverse side of honeycomb panels and the effect has been attributed to "acoustic shock" and/or stress wave interactions. Moreover rise time requirements to cover such effects have been suggested for Component A simulation in recent draft STANAGS (4). An analysis of this effect was earlier presented by Robb et al. (5) and is also the topic of the present study. Section 2 reviews possible mechanical damage mechanisms, Section 3 describes the experimental arrangement, Section 4 the results and Section 5 gives a summary.

## 2 POSSIBLE INTERPRETATIONS OF THE OBSERVED RESULTS ATTRIBUTED TO STRESS WAVES

The geometry of a strike attachment to a panel is shown in figure 1.




(i) The surface of the sample could be thermally and mechanically shocked when the lightning arc forms at the panel. It is expected that these forces will peak at relatively late times (at or later than the time of peak current, typically 6μs); Joule heating will be greatest then as will the maximum vertical component of a pressure wave from the arc (thunder).

(ii) For unprotected or poorly protected CFC, conduction in the surface fibres causes explosive heating and vaporisation of the epoxy matrix. The rapidly expanding plasma around the fibre site could drive a strong shock wave through the material which reflects from the rear surface of the sample spalling material at this point. This could explain the observed front and rear surface damage.

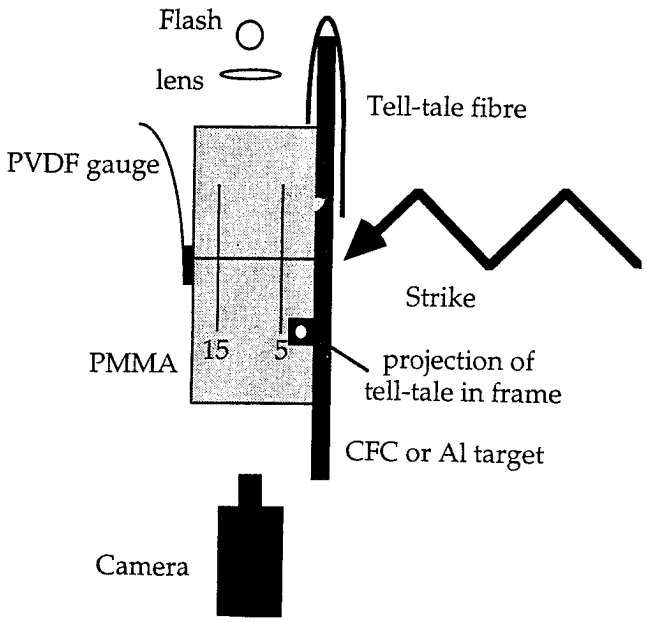
(iii) While the magnetic interaction can account for the gross displacement of structures at late timescales it is regarded as unlikely that it can generate shock waves in the thin samples since the driving force at the sample surface rises on too slow a time

scale. It is possible that coalescing stress waves within the material would steepen into a shock but this is likely to take several tens of mm. Thus it is more probable that this impulsive force will only cause plate bending. This however could result in failure at the rear surface of the plate from the tensile stresses there on bending. Moreover for composite sandwich panels, the last layer of the sandwich if weakly bonded could act as a momentum trap and become delaminated.

## 3 EXPERIMENTAL TECHNIQUE

In order to explore these possible damage mechanisms a time resolved measurement of the mechanical response of the sample was attempted. This is important since several of these proposed schemes occur over very different time scales. These involved electrical and optical methods to a polymethylmethacrylate (PMMA) plate attached to the rear of the panel.

The experimental set-up is described in figure 2.




The current arc was generated from the LTT A/D bank which comprises a two stage 387.5μF capacitor bank that can be charged to a maximum of 40kV per stage. The arc was initiated with a fine copper fuse wire from an arc jet diverting electrode. A polythene mask restricted the initial arc attachment point movement. The high-speed camera used in these studies was the Ultranac FS501 programmable image converter camera. This camera is capable of framing at variable rates up to 50 million frames per second. In this work the exposure time of each frame was set to be 20ns, whilst the interframe time was varied in order to make measurements of wave speeds and of dynamic failure events. The sequence was lit with a QCA5 Xenon discharge tube. It delivered about 100J of energy in 100μs. The light was collimated using a lens so that the sequences were taken using the shadowgraph technique. Changes in density in the PMMA material caused by passage of stress waves will result in changes in the

refractive index which register as a dark line at the position of the wave on the photographic record. In order to enhance the sensitivity of the optics to small density variations the schlieren technique was employed in some shots. The field of view of the camera was set so as to view a region to the rear of the strike and covers an area of about 20×30mm. Marks were placed on the surface of the PMMA backing down the central axis beneath the impacting strike at 5mm and 17mm from the impact surface. A fibre optic tell-tale was fed from the impacted plate around to the rear of the PMMA backing block in order that light from the strike might appear in each frame giving a fiducial marker for temporal correlation.

The experiment was triggered by using an output from the trigger pulse to the bank. The signal from the bank was fed into a three channel delay generator with an immediate output to trigger the flash source, an output after 20μs to trigger the camera and one after 25μs to trigger the strike. This ensured the PMMA block was fully illuminated during the exposure window set for the period of interest. In all experiments the electrode was positive with respect to the earthed target.

The targets were 2mm aluminium sheet bare or painted and 4.3 or 2.9mm painted CFC. In all cases 50mm thick 100mm square polished PMMA blocks were glued with epoxy to the rear of the targets ensuring good acoustic coupling in the case of the CFC.

It is practically difficult in such a noisy electrical environment to adequately screen a transducer to allow in-material stress measurements. Of the available transducers only the polyvinylidene difluoride (PVDF) type was regarded as suitable for this application since they produce large voltages.

In later experiments a specially designed PVDF gauge was used in order to measure the stress signal introduced by the strike. The operation of the gauge is described in detail in Reference 6. In order to remove the effects of induced voltages in the short leads, a dummy gauge was constructed as close as possible to the PVDF gauge. The leads of the gauge were kept as close as possible to one another and were fed through copper piping into the inputs of high frequency optical links. These were DC-20MHz Nicolet Isobe 3000 fibre optic links.

The gauge was placed 25mm from the rear surface of the target embedded within the PMMA. The differential output of the gauge was integrated by the input impedance of the link and the capacitance of cabling to yield a voltage proportional to the stress.

## 4 RESULTS AND DISCUSSION

For most tests a current pulse with a rise time of about 12μs with 160kA peak current and an action integral of $5.4 \times 10^5 A^2s$ was applied to the plates.

No high amplitude or rapidly rising stress waves were observed for the aluminium targets despite increasing the sensitivity of the visualisation technique used. However, for the CFC targets stress waves were observed.

Figure 3 shows an example taken using the more sensitive schlieren technique with a CFC panel. Correlation with the strike was confirmed by the fibre optic tell-tale (see figure 2) in which the light can clearly be seen increasing through the selected frame sequence. The arc attachment is timed to occur just before frame 1. A wave can be seen in frame 2 propagating across the PMMA block to frame 5. The time between frames is 1μs giving peak current at about frame 13. There is more than one wave front

visible in the picture suggesting that there is a train of wavelets propagating through the target. The development of the wavefronts is consistent with an acoustic velocity in PMMA of 2.7mm/μs. The point of attachment is symmetrically in the centre of the frame. However, the wavelets propagate from a point 15mm below this. This suggests that the waves result from some secondary mechanism perhaps operating within the plate such as fibre and matrix explosion.

The stress transducer data were reduced according to the following scheme. Figure 4a shows the raw data for a shot to a CFC panel. The dummy signal is subtracted from the PVDF signal to yield the difference signal.

The PVDF difference traces for a shot to the CFC panel are plotted with the current trace in figure 4b.

The current and stress traces are offset since the compression pulse induced takes time to travel from the arc to the gauge position 25mm from the target rear surface and the time delay is consistent with a wave speed of 2.7mm $\mu s^{-1}$. Hence the deduced wave speed from the measurement and the optical measurements are consistent and no shock fronts are observed. The general shape of the stress pulse is analogous to the current pulse. The signal oscillates after the current pulse had dropped to zero consistent with the pulse rebounding within the PMMA backing block. It is believed some hardware integration of the pulses occurred due to the capacitance of the readout wiring and it is not possible at this stage to put reliable stress values to these traces. However, the general shapes and trends are clear. An interesting feature of figure 4b is the spike observed at about 10μs at the start of the difference signal which is seen with the CFC panels but not with the aluminium. This is consistent with the observed fast rising wavelets in the case of CFC. The fact that this feature is not apparent for aluminium targets suggests that this effect does not result from the vaporisation of the fuse wire that initiates the strike but is a direct result of different mechanisms operating in the case of CFC panels.

The surface damage to CFC was extensive and typical of arc root damage to such material. Results of a micro-structural examination of the struck plate are shown in figure 5, this shows micro-graphs of the back surface at 90°. It is clear that extensive cracking has occurred in the first 0° laminate layer from the back surface. A higher magnification view of the same area shows that the cracks have propagated through the epoxy matrix around the fibres, which seem to be unbroken themselves. This can be confirmed by examining the equivalent area in the 0° view, where no such fracture has been observed.

The presence of cracks so close to the back surface suggest that they have been produced by a release wave interaction producing a large tensile stress that exceeds the tensile strength of the material in this region. Away from the back-surface, in the centre of the plate the material again appears to be undamaged, as was seen in the 0° orientation.

Robb et al. (5) have estimated the total amplitude of stress waves in CFC panels to be of order 10 MPa. They calculated the origin of these waves by assuming that the stress within the panel was of the order of that in the incident air shock (thunder) and added to it a component due to rapid heating (thermal shock). Measurement of the acoustic impedance of the CFC can be compared with that of air to yield a transmission coefficient $\alpha$ across the air/panel interface given by the well-known formula:

$$\alpha = \frac{2Z_1}{Z_1 + Z_2}$$

where Z1 and Z2 are the impedances of air and specimen respectively. The calculated coefficient of about $10^{-4}$ is sufficiently small to neglect transmission of air shocks. Any thermally induced shock waves can only rise with the increase in current. Such waves rise sufficiently slowly that the wave is not a shock and the panel does not experience rapid gradients of stress that would result in failure of the composite. We thus reject these two mechanisms in favour of explosive vaporisation since this will efficiently couple large stresses into the material that can rise in fractions of a microsecond. It is this last criteria that is especially important if failure is to occur, since it is high strain-rate as well as amplitude that is required to fail the composite. The stress within the CFC will be obtained by reflection of part of the pulse superposed with the remaining incident pulse. Pulses rising with the current will not damage the composite since the strain-rate is low. However, the large amplitude, microsecond precursor seen in figure 4b (and only with the CFC) may be expected to induce tensile stresses several times those required to spall the composite since the strains will be induced across the weak fibre/matrix interfaces. In our geometry, this pulse will partially reflect at the PMMA interface leading to tensile stresses back from the interface in the CFC which, as we have seen, lead to cracks opening. When the PMMA backing is removed, this effect would become more severe.

These results are preliminary and it is hoped to verify these tentative conclusions when further work has been undertaken.

## 5 SUMMARY

The stress wave propagation from lightning strike on aluminium and CFC plates has been investigated. Within the pulse shape constraints of the Culham bank it has been found that no large amplitude or fast rising stress waves were propagated into the transparent backing in the case of aluminium target plates whilst stress waves were observed in the case of CFC plates.

A novel PVDF gauge was designed and constructed. These transducers observed a signal which followed the current pulse qualitatively as would be expected from stresses resulting from the magnetic interaction. Painting of the aluminium surface did not result in any increase of the stress recorded. The stress induced in the PMMA blocks appeared similar with a CFC target but in this case a transient at the start of the stress pulse was observed probably correlated with the optically observed stress waves.

The appearance of multiple stress wavelets away from the point of attachment is indicative of the quantity of damage introduced and suggests that multiple explosions of current carrying fibres may be a dominant damage mechanism in CFC. This may also explain the variability of the source of such disturbances noticeable in the sequences.

Micro structural examination showed cracks within a laminate of the back surface possibly the result of a release wave interaction near the back surface.

Faster rising current pulses may well induce sharper wave fronts which increases the strain rate that a material would have to support thus increasing its likelihood of failure. This remains a priority for further investigation.

The fact that the stress waves appear to be associated with exploding fibres and are not observed with aluminium panels suggests that protected CFC panels will not exhibit stress waves either and any delaminations on protected composite structures would probably be due to plate bending and conventional mechanical effects. More tests would be required to confirm this.

## 6 ACKNOWLEDGEMENTS

We thank Professor J E Field of PCS, Cavendish Laboratory, Cambridge for his encouragement and permission to loan the high-speed cameras. We also thank Tetsuro Obara and Jeremy Millett of PCS for experimental work. The CFC panels were kindly provided by Barry Pridham of BAe Warton. The work was funded by the Culham Lightning Club comprising British Aerospace, Civil Aviation Authority, CASA (Spain), Rolls Royce, Saab-Scania (Sweden) and Short Brothers.

## 7 REFERENCES

1. Little et al., "Arcs on Metal Sheet in Simulated Lightning Discharges." IEEE International Symposium on EMC, Seattle, 1977.
2. Jones et al., "Magnetic Force and Shock Damage Resulting from Lightning Strikes." 59-1 ICOLSE, Forth Worth, 1983.
3. Reid, "Investigations into Damage for Various Types of Unprotected CFC with a Variety of Lightning Arc Attachments." ICOLSE, Cocoa Beach, April 1991.
4. Odam, "Lightning, Munition Assessment and Test Procedures." Ninth draft STANAG 4377, 1994.
5. Robb et al., "Combined Mechanical-Electrical Ignition Hazards to Carbon-Reinforced Composite Fuel Tanks." 32-1 ICOLSE, Orlando, 1984.
6. Obara et al., "The Construction and Calibration of an Inexpensive PVDF Stress Gauge for Fast Pressure Measurements." Meas. Sci. Technol, 6, 345-348, 1995.

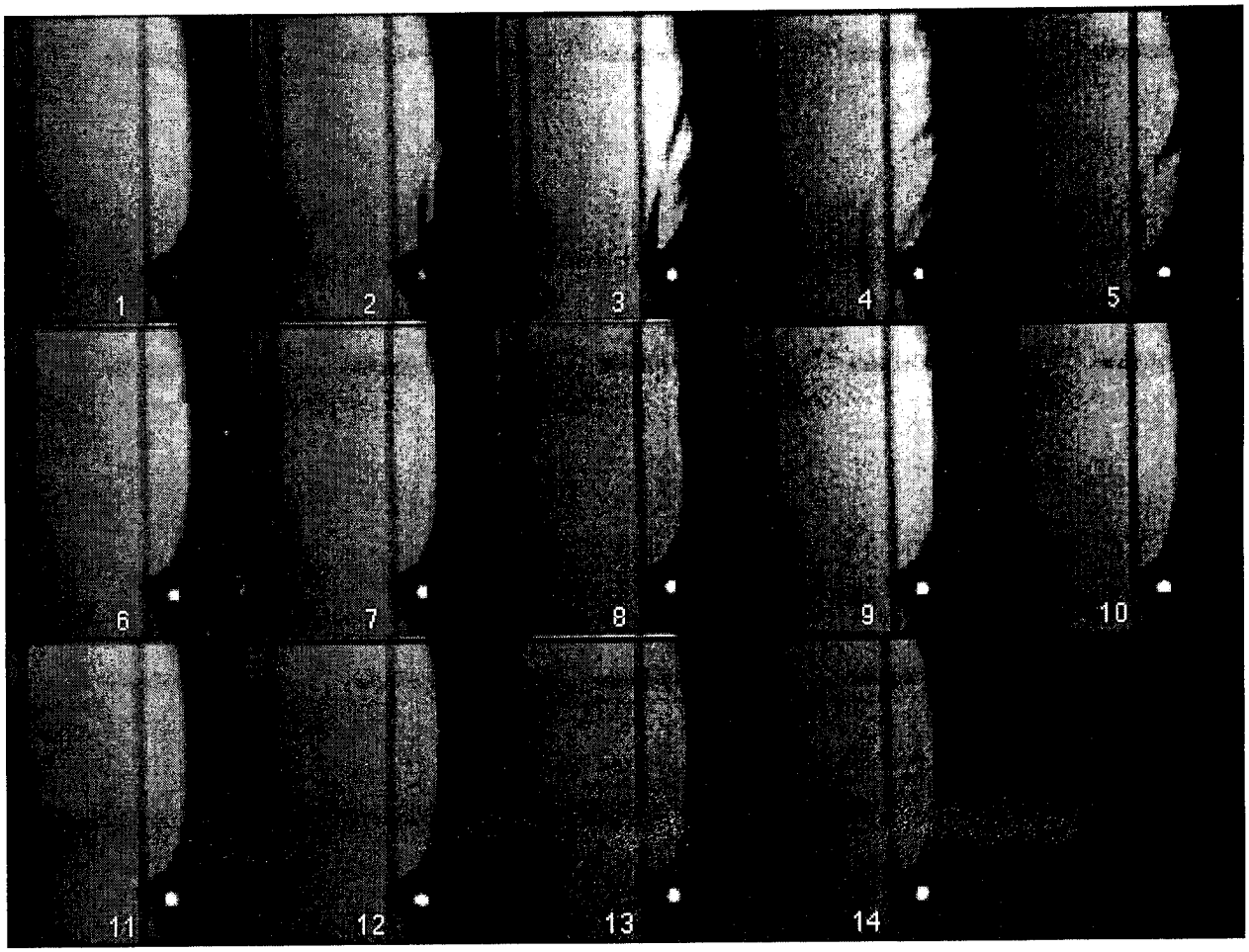



FIGURE 3 FAST FRAMING CAMERA SEQUENCE FOR ARC ATTACHMENT TO CFC PANEL USING SCHLIEREN TECHNIQUE. INTERFRAME TIME 1μs

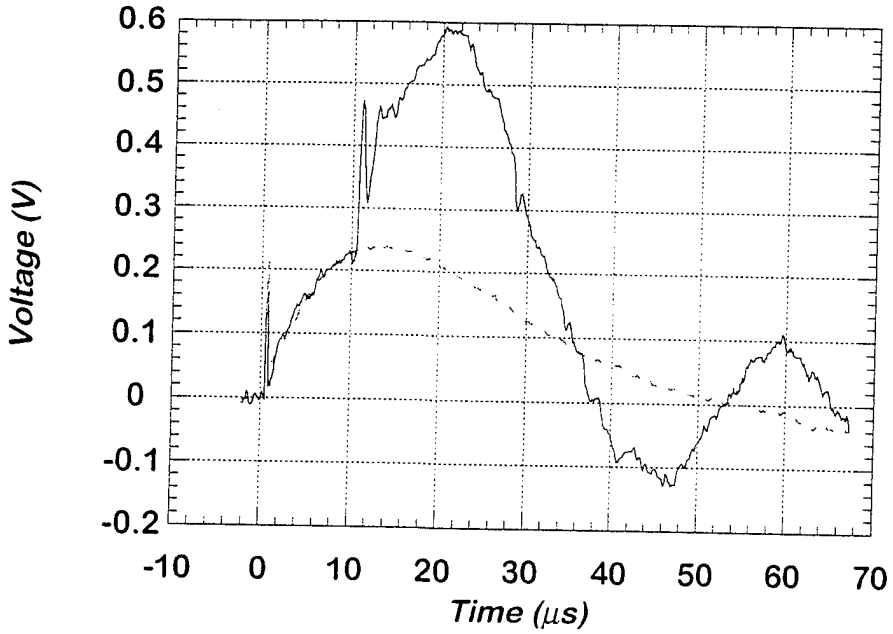



FIGURE 4A RECORDED PVDF (SOLID) AND DUMMY (DOTTED) SIGNALS FOR STRIKE TO CFC PANEL. THE WAVEFORMS ARE SIMILAR UNTIL ABOUT 10μS WHEN THE STRESS SIGNAL APPEARS

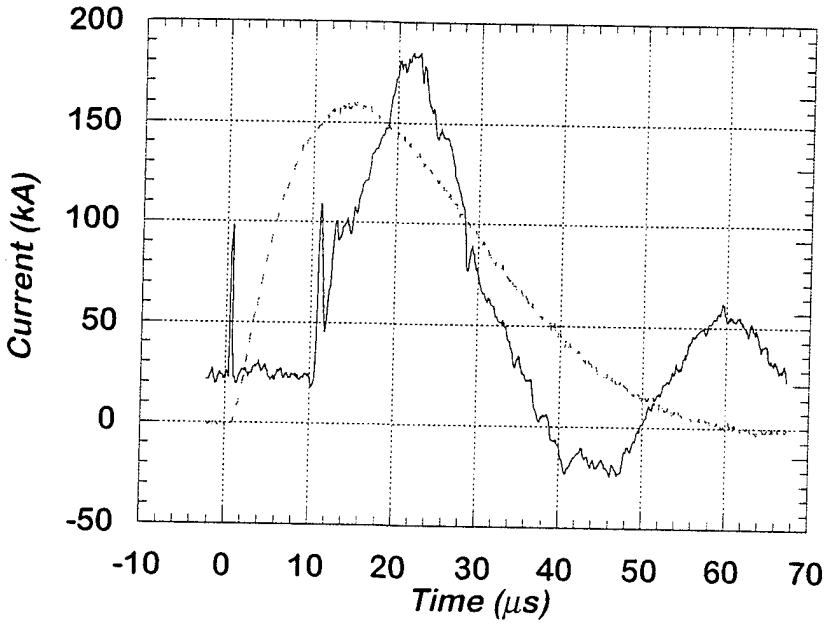
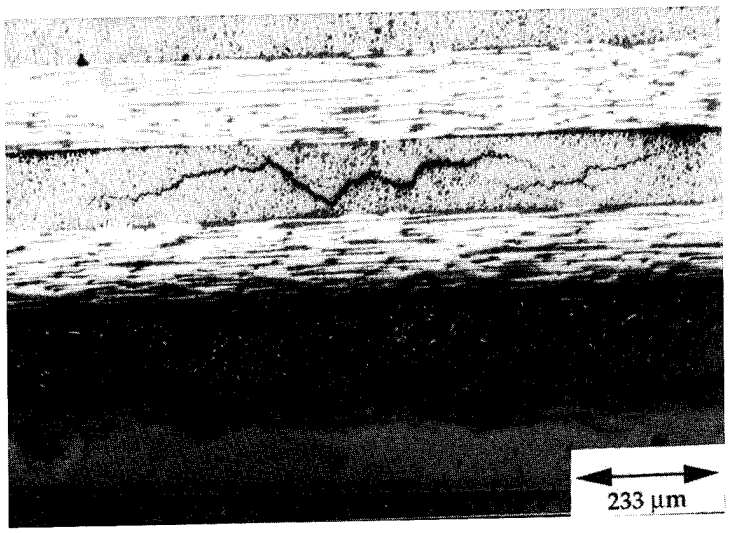
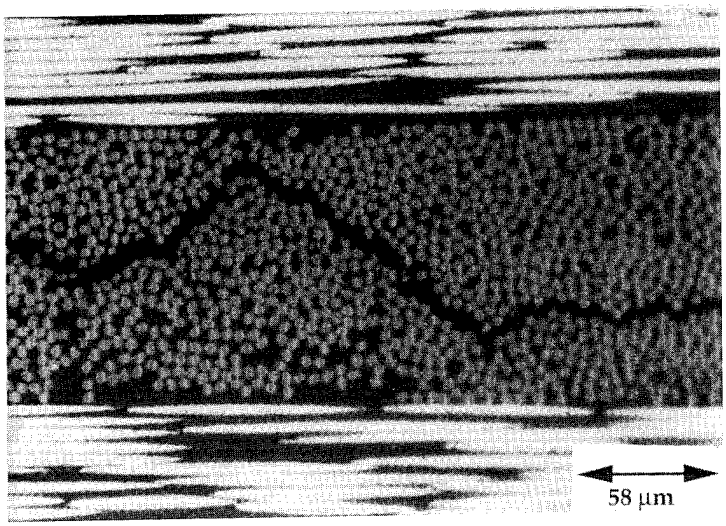



FIGURE 4B DIFFERENCE SIGNAL OBTAINED BY SUBTRACTING THE DUMMY SIGNAL FROM THE PVDF SIGNAL COMPARED TO THE CURRENT PULSE (DOTTED). THE TIME DELAY BETWEEN THE DIFFERENCE SIGNAL AND THE CURRENT PULSE IS DUE TO THE TRANSIT TIME OF THE STRESS PULSE IN THE PMMA BLOCK




A. LOW MAGNIFICATION OVERVIEW




B. HIGHER MAGNIFICATION VIEW OF ABOVE

FIGURE 5 MICROGRAPHS OF CRACKS AT BACK SURFACE, VIEWED AT 90°

# ELECTROMAGNETIC JOINT INTEGRITY OF THE V-22

John C. Kuras
The Boeing Company
Boeing Defense & Space Group
Helicopters Division
Mail Stop P24-16
P.O. Box 16858
Philadelphia, PA 19142
Telephone (610) 591-2384 FAX (610) 591-9286

Nadine McClam-Brown
The Boeing Company
Boeing Defense & Space Group
Helicopters Division
Mail Stop P24-24
P.O. Box 16858
Philadelphia, PA 19142
Telephone (610) 591-9896 FAX (610) 591-8238

## ABSTRACT

This paper describes the V-22 structural skin joint design and presents the results of joint admittance, and lightning direct effects testing. An analytical model of the joint's electrical properties is proposed.

The U.S. Navy V-22 Osprey is a fly-by-wire aircraft constructed of graphite composite skin over a mostly aluminum internal frame. Due to the combination of its construction and operational environment, it is challenging to assure the electromagnetic integrity of the V-22.

One of the most critical electromagnetic design issues during V-22 development was how to provide electrical conductivity between the composite skin panels. A multi-discipline "Integrated Product Team" approach was used to develop a cost effective skin panel joint design which meets the electromagnetic, corrosion, structural, weight, aerodynamic, maintainability, and producibility requirements of the V-22.

## INTRODUCTION

Due to the unique nature and mission of the V-22, the electromagnetic integrity of its structure is both more critical, and yet more challenging to assure than on most systems (airborne or otherwise) that have been fielded previously. Its stringent (and usually conflicting) system requirements confound the application of traditional electromagnetic design practices: First, the combination of graphite/aluminum construction and the salt spray environment in which the V-22 will be based necessitates exceptionally strict

corrosion protection measures. These measures inherently electrically isolate the conductive components of the aircraft. Second, the V-22 is an "all weather" weapons system. It must be able to survive a 200 KA (peak) lightning strike (i.e., MIL-B-5087 waveform) without causing a category 1 event. This requires careful electromagnetic shielding of the vehicle's fly-by-wire flight control system. Finally, the V-22 must take off vertically. In order to minimize weight, the electromagnetic shielding of the vehicle's structure must be utilized wherever possible. This requires electrical bonding between the conductive structural components. Most of the time, these same components are required to be electrically isolated due to corrosion considerations. These conflicting design requirements have necessitated several innovative approaches to electrical bonding on the V-22. This paper describes the development and testing of one such instance: the electrical bonding of fuselage skin panels.

## BACKGROUND

The electromagnetic integrity of the V-22 is provided by a two tier integrated shielding design. The first tier shielding is provided by the structural components of the aircraft. However, due to the large amount of composite structure, the tier 1 shielding by itself is insufficient to provided the total required LEMP shielding. Thus, all electrical sub-systems require some degree of tier 2 shielding(1,2). The second tier utilizes shielded enclosures, avionics bays, and wireways. Line replaceable units located outside the avionics bays are shielded by their metal cases. The wiring to these remote units is shielded using high quality metal overbraid. All of these second tier components are electrically bonded together to form a continuous Faraday shield surrounding the circuitry and wiring. Since the shielding for the second tier tends to be parasitic weight (i.e., has no other design requirements, such as structural strength, sizing its weight), minimizing its shielding effectiveness requirement saves weight. By maximizing the utilization of first tier shielding, the shielding effectiveness requirements for the second tier is reduced.

Except for parts of the cockpit and the avionics bays (just aft of the cockpit), the V-22 fuselage skin is constructed entirely of graphite/epoxy composite. Because the V-22 is an un-pressurized aircraft, most of the fuselage skin is required to react relatively low out-of-plane loads. Thus, the skin gauge in most of the composite areas of the fuselage is relatively thin. In some areas it is as little as 38 thousandth of an inch. Lightning direct effects tests performed on representative skin panels during early phases of the V-22 development demonstrated that even swept stroke (100 KA) attachments could produce unacceptable damage to these thin skins(3). Trade studies were performed which determined that (for the V-22) a 0.040 pound per square foot expanded copper foil mesh embedded in an adhesive provides the optimum combination of direct effects protection, indirect effects shielding[1], and maintainability, durability, producibility, surface

[1] The conductivity of the skin panels plus copper mesh is roughly 1 to 2 mΩ/□. Although lighter weight expanded copper mesh products can provide the required direct effects protection, it was determined(5) that the increased LEMP shielding effectiveness of the heavier mesh would minimize the overall combined weight of tier 1 and 2 shielding.

smoothness, etc.(4) The areas of the fuselage which are protected by this copper foil mesh are illustrated in figure 1.

The fuselage design of the V-22 aircraft which were built in the late 1980's utilized considerably more composite construction than the current V-22 design. Because both the skin and the structural framework of the fuselages of these vehicles were constructed of graphite/epoxy, phosphate fluoride coated titanium fasteners (which have relatively good electrical conductivity) were used to fasten the skin joints. Even though these fasteners were wet installed using a non-conductive sealant, the electrical conductivity through these structural joints was sufficient (roughly 200 mhos/meter) to cause negligible reduction in the overall tier 1 shielding effectiveness(6).

Most of the internal frames in the forward and center sections of the current V-22 design are aluminum. Due to the galvanic incompatibility of aluminum and graphite, they must be electrically isolated when electrolytes (such as salt water) are present. Since sealants and paint cannot sufficiently assure the exclusion of electrolyte from within these structurally critical joints, it is necessary to (also) electrically isolate the graphite skins from the aluminum frames. This is accomplished (see figure 2) by incorporating a thin ply of fiber glass into the composite lay-up on the frame side of the skin panel edges. In addition, the entire frame (including the side facing the graphite skin) is anodized, primed, and painted. Finally, the frames are attached to the skins using K-coated titanium fasteners. K-coat is an aluminum-pigmented coating used on titanium fasteners to reduce galvanic corrosion when installed in aluminum. This coating is non-conductive. The electrical conductivity across skin panel joints constructed in this manner is roughly 2 mhos/meter. If left untreated, this low joint conductivity would have essentially eliminated tier 1 low frequency shielding. This would have been unacceptable electromagnetically. The remainder of this paper describes the findings of a multi-discipline team of V-22 engineers that were tasked with identifying a design solution which would satisfy all of the various requirements imposed on these joints.

## REQUIREMENTS

The electromagnetic requirements which the V-22 skin panel joints must satisfy are: 1) They must provide a minimum of 200 mhos/meter (DC) joint conductivity. 2) The joint must be able to conduct zone 3 lightning current with a peak of 200 KA divided by the local circumference of the aircraft without causing damage sufficient to require maintenance to the joint. This includes damage to the shielding effectiveness, i.e., the joint must continue to provide a minimum conductivity of 200 mhos/meter. It also applies to damage to the corrosion protection features. 3) A lightning attachment to the joint (with a waveform appropriate to the lightning zone at that joint) must not cause a category 1 event. 4) Any form of lightning damage to the structure must be repairable at the "Organization" level of maintenance.

Other design requirements imposed on the joint include: 1) The joint must incorporate the corrosion protection features outlined above. 2) It must satisfy aerodynamic smoothness and discontinuity (step/gap) requirements. 3) It must be maufacturable and repairable. 4) It must withstand maximum structural static and vibration

loads without degrading electromagnetic performance. and 5) Cost and weight must be kept to a minimum.

## DESIGN SOLUTIONS ON OTHER AIRCRAFT

A survey of the electrical bonding approaches utilized on other composite aircraft was performed. None of the design approaches surveyed were found to be adequate for use on the V-22.

The designs which were the most similar to the V-22 construction were the F-22, the B-2, the 777 empennage, and the F-18. However, the lightning protection architectures of each of these aircraft rely on electrical conductivity between the composite skin and the aluminum or titanium sub-structure to enhance the vehicle's low frequency shielding effectiveness (i.e., reduce structural voltage drop). On the V-22's fuselage, electrical bonding between the composite skin (specifically, the copper foil) and the aluminum structure is provided only at the avionics bays and at the main landing gear wheel wells. All other aluminum structure has a high electrical resistance (~ohms per fastener) to the copper mesh. None of the designs surveyed had the requirement to simultaneously electrically isolate the aluminum sub-structure and provided electrical continuity across the joint.

## OTHER DESIGN SOLUTIONS EVALUATED

The following skin panel joint design alternatives were considered:

1) Do nothing: Attempt to conduct through the fasteners: This alternative was tested. It was ruled out due to inadequate joint conductivity.

2) Using conductive fasteners and standard MS jumper cables, jumper the skin panels from the inside: This alternative was ruled out due to weight, installation cost, and maintenance considerations.

3) Using thin (.040 lb./sq. ft.) copper mesh, provide an electrical path around the edge of the panel to the inside of the joint. Electrically bond the thin mesh to the aluminum substructure: This alternative was ruled out for maintenance reasons. The high current levels produced by a lightning strike would tend to damage the mesh at creases as well as stress the free hanging mesh due to magnetic forces. The right angle turn in the mesh where it wraps around the inner panel edge could not be repaired without removing the skin panel from the aircraft.

4) Use a conductive filler or sealant material in the gap: This alternative was ruled out for manufacturing and maintenance reasons. There is currently no conductive sealant available which has sufficient working life to be usable between the skin and sub-structure. It is not feasible to use a different sealant in the gap vs. between the skin and sub-structure, as this would require careful cleaning and routing of the skin panel gap after the skins were installed on the aircraft. This routing would require special tooling to prevent accidental damage to the aircraft.

5) Add a conductive sheet of mesh or foil material across the gap by embedding it within the joint between the skin panels and the sub-structure: This was tried during a

previous V-22 development phase and found to be impractical for manufacturing reasons. An experiment was conducted which determined that it was not feasible to slip a thin sheet of conducting foil between the skin and sub-structure after the skin panel was in place, but prior to fastener installation. This approach would also cause maintenance prcblems, because the skin panels would have to be removed to repair the joint if the conductive path were lost due to lightning damage. In addition, since this approach would rely on fastener contact to the foil to provide conductivity, it is not an electromagnetically acceptable solution for the current V-22 design, because the current design uses a non-conducting fastener finish.

6) Add a conductive sheet to the outside (airflow side) of the joint by cold bonding it to the skin: This approach was tested(7) and found to be unacceptable for electromagnetic reasons. Since the non-conductive copper mesh adhesive was not removed to permit metal-to-metal contact between the copper mesh and the additional conductive sheet, there was little electrical conductivity through the added sheet. In addition, after passing a very low level lightning pulse through the test joint, the additional sheet was partially dis-bonded from the panel. A post-test resistance measurement indicated that the sheet was electrically open circuited by the pulse.

7) Remove sufficient adhesive material to expose the copper mesh. Apply a layer of conductive adhesive across the gap: This approach was tested(7) and found to be unacceptable for electromagnetic reasons. The test panel joint resistance was about 50% higher than the requirement. In addition, after passing a very low level lightning current through the joint, there was considerable charring of the adhesive and the resistance increased to about an order of magnitude beyond the requirement.

8) Remove sufficient adhesive material to expose the copper mesh. Apply a layer of conductive paint across the gap: This was tested(7) and found to provide acceptable electrical conductivity. In addition, after passing a very low level lightning pulse through the test panel, the joint showed no visible signs of damage. However, the electrical resistance of the joint increased to levels comparable to the post-strike resistance of the conductive adhesive joint (see item #7 above).

9) Remove sufficient adhesive material to expose the copper mesh. Cold bond a sheet of copper mesh across the gap: This approach was tested and found to be acceptable. The following is a detailed description of the process:

## THE V-22 DESIGN

The outermost layer of the composite lay-up for the V-22 fuselage is a thin copper mesh. The mesh is pre-impregnated with an adhesive material and co-cured with the structural graphite and matrix components. The adhesive material is non-conductive and contains a non-conductive (fiber glass) scrim mat. During the cure cycle, the adhesive flows and envelopes the copper mesh, totally encasing it in adhesive. After cure, the copper mesh is both physically and electrically isolated from the outer (air-flow side) of the skin panel by cured adhesive as well as the scrim mat. This is done purposefully to protect the thin copper mesh from mild impact damage and corrosion. The adhesive will partially isolate the copper mesh from the underlying graphite. Because there is no scrim mat

between the copper and graphite layers, the amount of electrical isolation between these two layers will vary from panel to panel.

Since the copper mesh is intended to provide lightning protection, the ideal electrical "bridge" scheme would provide a low resistance path between the copper mesh in adjacent skin panels, rather than bridge between the graphite layers. Although conducting between the graphite layers would be electrically sufficient, such an electrical path may tend to see higher (but acceptable) damage when stressed by lightning currents. Thus, if all other design considerations are equally satisfied, preference should be given to the copper mesh to copper mesh bridge over the graphite to graphite bridge. A schematic of the V-22 joint design is illustrated in figure 2. However, the approach used on the V-22 is applicable for any structural joint between skin panels constructed of composite materials with embedded electromagnetic shielding where the various components of the joint structure has been protected from Galvanic corrosion by electrically isolating the parts. An electric path across the joint can be provided as follows:

1) Remove any non-conductive material from the airflow side of the skin panels near the joint so that the embedded electromagnetic shielding material is exposed.

2) Obtain a strip of conductive mesh material of appropriate length and width to cover the exposed electromagnetic shielding in the skin panels. This material will act as the electric path across the gap between the skin panels. This conductive mesh material must have the following properties:

a) It must be chemically compatible with the other materials used in the joint construction.

b) It must be porous enough to permit un-cured resin material to readily flow through it.

c) It must be plastic (flexible) and durable enough to withstand:
   1. handling and shaping during construction
   2. vibration and fatigue loads throughout the life of the aircraft
   3. magnetic field stresses caused by lightning induced currents

d) It must be constructed in such a manner so as to permit sufficient direct conductor to conductor contact between the conductive mesh and the exposed embedded shielding material during the resin cure process.

e) It must be conductive enough to provide the required shielding effectiveness or conductivity.

f) It must have sufficient current carrying ability to survive a low level lightning pulse with minimal degradation in conductivity.

Boeing uses a medium duty expanded copper mesh (0.080 lb./sq. ft.) which has not been rolled flat after expansion. The twisting of the connecting strands of the mesh caused by the stretching (expanding) process forces the intersections of the strands to bow outward from the plane of the mesh. The heavier weight of the copper mesh provides additional strength to these bowed intersections, and causes them to resist compression (normal to the surface). This allows the mesh to be pressed into contact with the underlying skin panel when surface pressure is applied and permits uniform contact between the mesh and the shielding material embedded in the skin panels without impeding the tangential flow of resin material. If the mesh were flat or compressible, it

could float in the resin when surface pressure is applied, and would not necessarily uniformly contact the shielding material in the skin panel.

3) Obtain a room temperature curing thermo-set resin system. This system must have the following properties:

a) It must be chemically compatible with the other materials used in the joint construction.

b) When cured, it must be non-porous enough to protect the exposed embedded shielding material in the skin panels as well as the conductive mesh material specified in item #2 above from mild impact damage and corrosion.

c) The material must be non-conductive so as to minimize the amount of heating within the resin when lightning current flows through the conductive mesh material.

d) During the cure cycle, the material must flow and envelope the conductive mesh, totally encasing it in resin. After cure, the conductive mesh will be both physically and electrically isolated from the outer (air-flow side) of the skin panel by cured resin.

e) After cure, the resin must be strong enough to maintain a high pressure contact between the conductive mesh and the embedded shielding material in the skin panels.

Boeing uses Hysol EA 956.

4) Apply the un-cured resin to the exposed embedded shielding material. While the resin is readily fluid, press the conductive mesh into the resin and apply a uniform surface pressure of sufficient magnitude to assure good electrical contact between the mesh and the shielding material embedded in the skin panels. Maintain the uniform surface pressure until the resin is cured.

Boeing uses a 20 lb. per square inch vacuum bag to apply surface pressure to the mesh/resin.

## TEST RESULTS

Several 16 inch square test panels representative of various skin joints on the V-22 were constructed, and the electrical bonding process outlined above was applied to each. The width of the thick copper strip, as well as the applied thickness of the resin was varied to determine optimum values. These panels were tested for lightning direct effects, DC resistance, low frequency joint admittance, and microwave shielding effectiveness(7,8,9). Figure 3 is a close-up photo of the damage caused by a zone 1A simulated lightning strike to a point roughly 3 inches from the joint, and is typical of the results obtained. The damage to the thin mesh within a few inches of the attachment point is typical of the damage that occurred to similar test panels without joints. The damage to the externally applied thick copper strip is localized to within 0.75 inch of the edge of the strip, and extends roughly 8 inches along its length. The DC resistance across the joint was 1.7 mΩ before the strike and 1.9 mΩ after. The joint admittance of the panel was measured over the frequency range of 100 KHz to 100 MHz both before and after the simulated lightning

strike. The results are illustrated in figures 4 and 5. As can be seen from the plots, there is essentially no effect on joint admittance.

## ANALYSIS

A plot of the admittance data (from reference 6) for a joint with conductive fasteners and no conductive splice strip is illustrated in Figure 6. The joint admittance data indicates that in the 10 KHz to 100 KHz range, the joint admittance decreases by 20 dB per decade (roughly). The 20 dB per decade decrease in admittance implies that the joint conduction mechanism over this frequency band is inductive.

There are two possible causes for this inductance: a) the inductance between the fasteners' shafts and b) the inductance of the slot formed by the gap in the copper foil between the panels and the edges of the panel test fixture. Based on the measured admittance at 10 KHz, the inductance of the joint appears to be about 3.5 nH for a 1 meter joint. By modeling a pair of fasteners on either side of the joint as a two wire transmission line, the estimated per length inductance due to the fasteners would be about 0.07 nH•m, which is insufficient to account for the observed inductance.

The input impedance of a slot antenna can be calculated from its dual, the electric dipole, by interchanging E with H and $\mu$ with $\varepsilon$. The input impedance of the slot will then be related to the impedance of the electric dipole dual by:

$$Z_s = \frac{1}{4}\eta_0^2 \frac{1}{Z_d}$$

where,

$Z_s$ = the impedance of the slot

$Z_d$ = the impedance of the electric dipole

$\eta_0$ = the impedance of free space = $120\pi$

According to Jasik(10), the input impedance of a short electric dipole is given by:

$$Z_d = 20(kl)^2 - j\frac{120}{kl}\left(\log\left(\frac{2l}{a}\right) - 1\right)$$

where,

$k$ = wave number = $\frac{2\pi}{\lambda}$

$l$ = length of the dipole

a = radius of the dipole $\cong \frac{\text{slot width}}{2}$

The slot that was measured was .125 inch wide and 12.5 inch long, so the 10 KHz impedance of the slot in a perfectly conducting infinite ground plane will be approximately:

$$Z_s = j3.944x10^{-3}$$

Which yields an inductance of 20 nH•m. This is considerably higher than the measured value. The fasteners on the test panel were on 4.17 inch centers along the gap,

and directly across from one another. The 10 KHz impedance of a 4.17 by .125 inch slot will be approximately:

$$Z_s = j1.68x10^{-3}$$

Which yields an inductance of 2.83 nH•m. This is within 25% of the measured value. Thus, it appears that the inductance is due primarily to the series of "slots" formed by the panel edges and fasteners. Since the joint protection method outlined above both eliminates this inductance and significantly reduces the DC resistance of the joint, it can be presumed that most of the LEMP current flows through the added copper strip, rather than the fasteners.

## SUMMARY/CONCLUSIONS

A process has been developed for electrically bonding the V-22's expanded copper mesh at skin panel joints without compromising the system's corrosion protection scheme. This process is easy to apply and maintain. The design has been verified via test to provide excellent lightning protection for the joint. At LEMP frequencies, the protected joints are electromagnetically indistinguishable from surrounding aircraft skin. An analytical model was presented which appears to agree well with the measured reactance of (unprotected) V-22 joints.

## REFERENCES


1. W. Gjertson, R. Carney, "Electromagnetic Environmental Effects ($E^3$) Control Plan V-22.", Bell/Boeing document 901-970-663 Rev. A, January 1995.
2. J. Kuras, R. Carney, "V-22 Lightning Protection and Analysis Report.", Bell/Boeing document 901-970-665 Rev. C, October 1995.
3. J. Bogard, T. Sharpe, "Test Report for Zones 1A, 2A, and 3 Simulated Lightning Strike Testing of Composite Skin Panels.", Bell/Boeing document 901-970-644, June 1988.
4. D. Coder, et. al., "Early Aircraft Design Cost Savings Analysis.", Bell/Boeing document 901-970-632, 1986.
5. D. Coder, et. al., "V-22 Stage II Electromagnetic Environment Assessment Analysis.", Bell/Boeing document D901-99230-1, July 1985.
6. J. Bogard, D. Coder, "Joint Electromagnetic Integrity test Report.", Bell/Boeing document 901-970-642, July 1989.
7. D. Coder, "Joint Electromagnetic Integrity Test Report Volume I, Lightning Direct Effects Test.", Bell/Boeing document 901-970-680, May 1995.
8. D. Coder, "Joint Electromagnetic Integrity Test Report Volume II, Panel Joint Admittance Test.", Bell/Boeing document 901-970-681, May 1995.
9. "Twenty-Sixth/EMD-7 V-22 Electromagnetic Compatibility Advisory Board (EMCAB) Meeting Minutes of 22 February 1995", Naval Air Warfare Center, Aircraft Division, Warminster, PA, May 22, 1995.
10. H. Jasik, "Antenna Engineering Handbook.", New York, New York: McGraw-Hill Book Company, 1961.

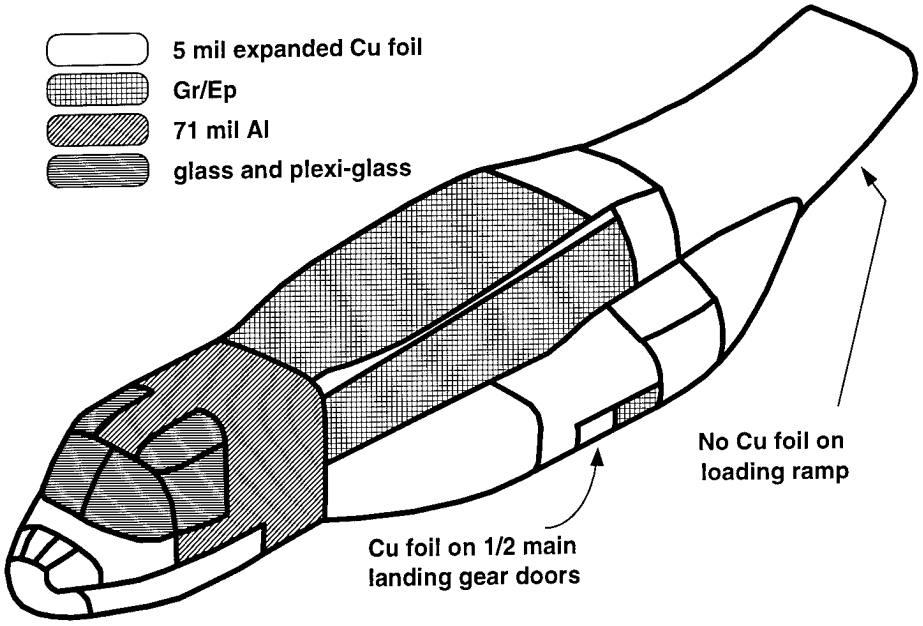



FIGURE 1 : LOCATION OF EXPANDED COPPER MESH ON THE V-22 FUSELAGE

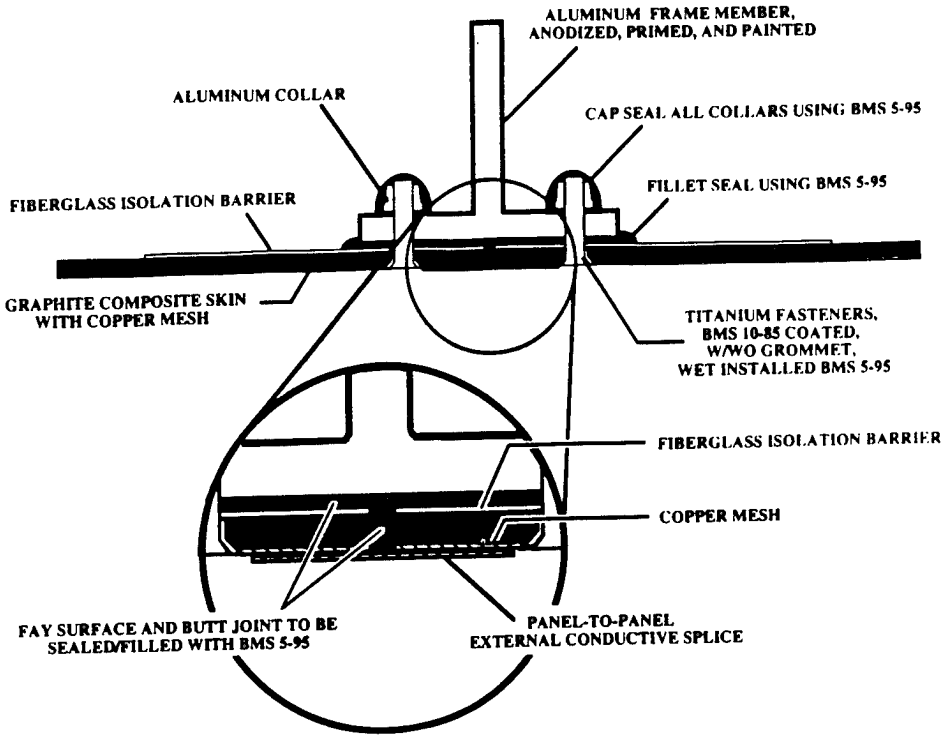



FIGURE 2 : CONSTRUCTION OF V-22 COMPOSITE SKIN JOINTS

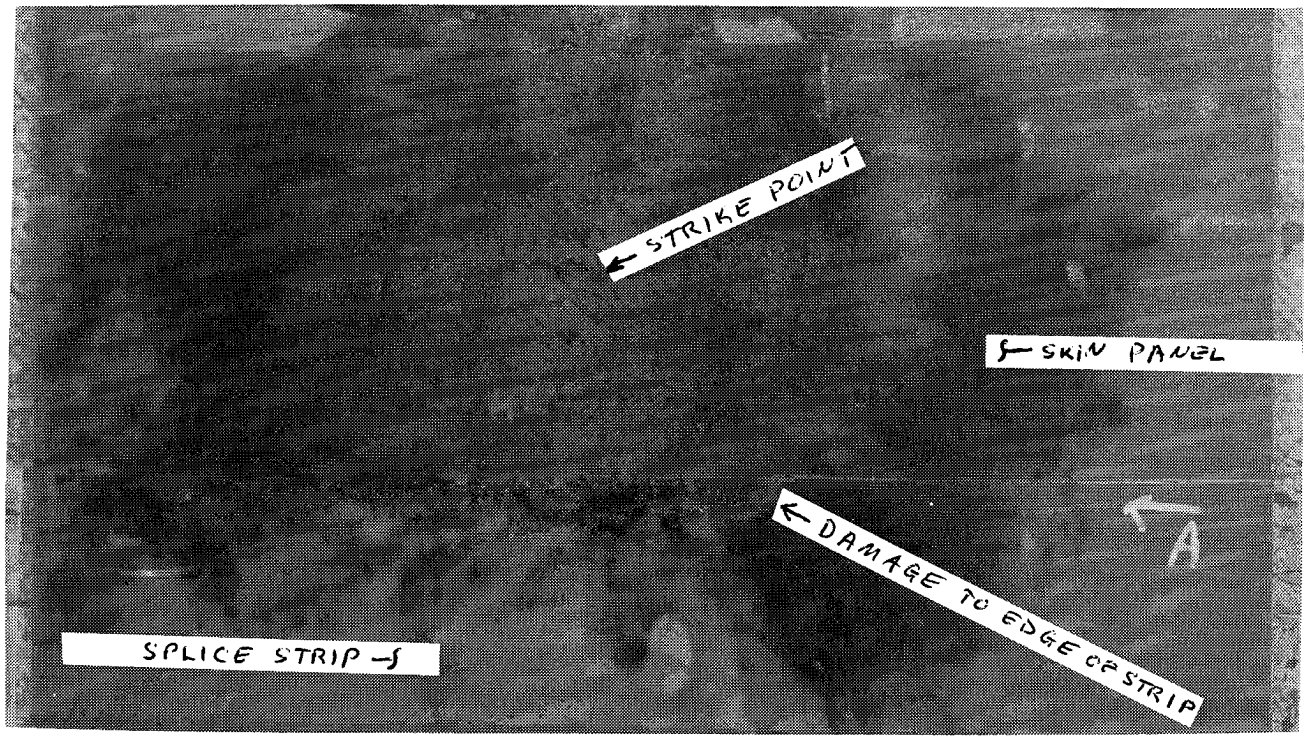



FIGURE 3 : SIMULATED ZONE 1A LIGHTNING DAMAGE TO V-22 COMPOSITE SKIN JOINT

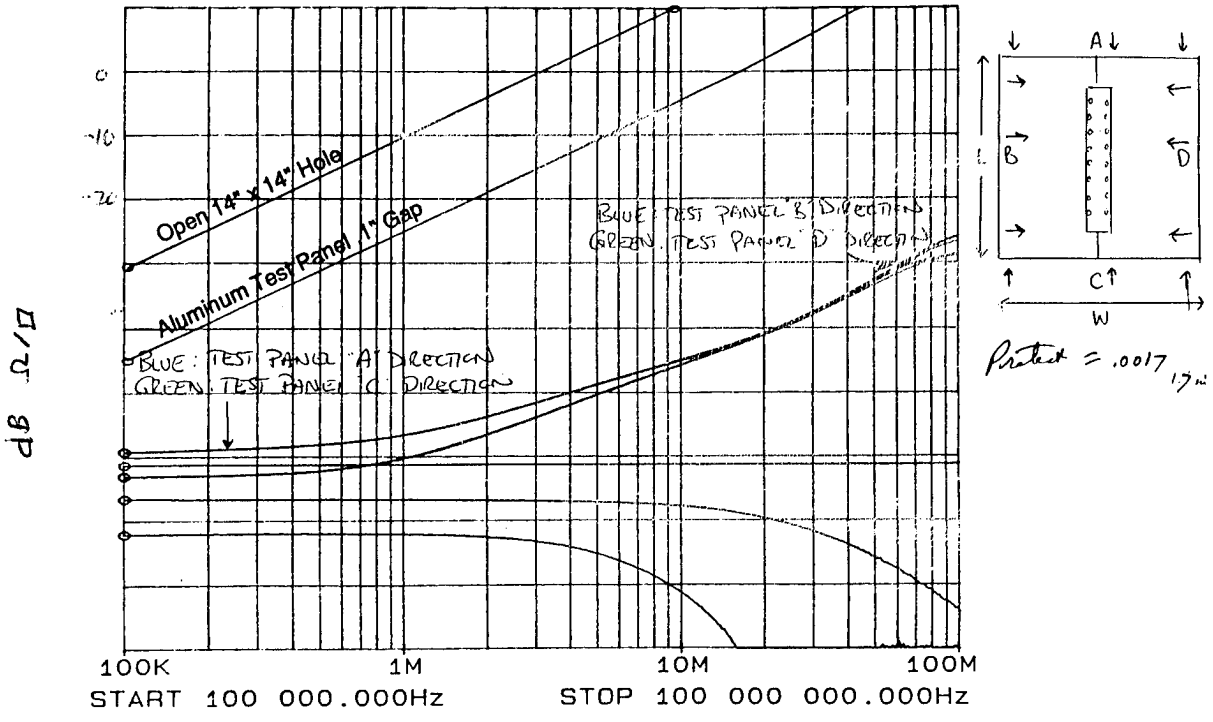



FIGURE 4 : TRANSFER IMPEDANCE OF PROTECTED V-22 JOINT BEFORE ZONE 3 LIGHTNING TEST

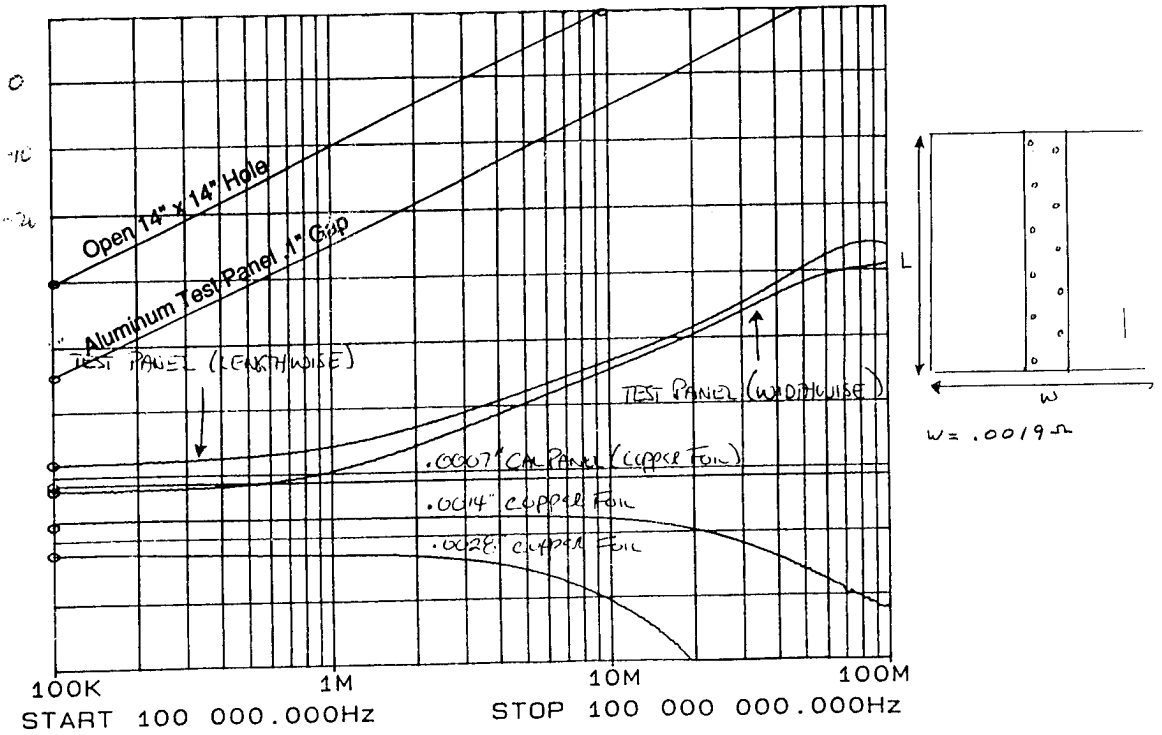



FIGURE 5 : TRANSFER IMPEDANCE OF PROTECTED V-22 JOINT AFTER ZONE 3 LIGHTNING TEST

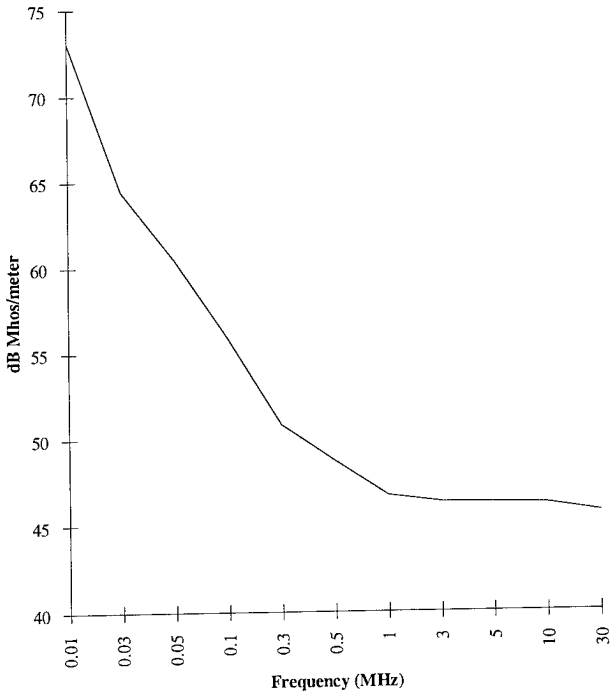



FIGURE 6 : JOINT ADMITTANCE FOR AN UNPROTECTED JOINT WITH CONDUCTIVE FASTENERS

# "ELECTRICAL BONDING RESISTANCE VARIATIONS IN CFC PANELS"

Joseph A. Calabria, NCE
Computer Sciences Corporation

William T. Walker, NCE
VEDA, Inc.

## ABSTRACT

Twenty-six, 24 inch-by- 24 inch fuselage coupons were evaluated for end-to-end DC electrical resistance measurements prior to and immediately following full stroke (200kAmp) Zone 1B lightning currents and tailored (21.2kAmp) Zone 3 lightning continuing current in accordance with MIL-STD-1757A waveforms.

The panels were composed of fiberglass (FG) and carbon-fiber-composite (CFC) materials with varying surface treatments of conductive silver paint (0-, 15-, 30-, 45-mil), expanded copper foil (0-, 4-mil) and sealer paint topcoat (3-mil). The silver paint evaluated was a water-based, polyurethane mixture containing silver coated magnetic ceramic microballoons (SCMCM) manufactured by Spectro Dynamics Systems, Inc.

Lightning test results showed an increase in coupon damage with the application of silver paint and a decrease in end-to-end DC bonding resistance on coupons containing expanded copper foil (with or without SCMCM paint).

A recommendation is made to evaluate alternate techniques to satisfy the MIL-B-5087B criteria for lightning integrity of: 1) fuselage coupons comprised of CFC/foil/sealer paint with CFC joints and seams; and 2) fuselage coupons with a repair to the CFC substrate.

## INTRODUCTION

The use of non-metallic materials for vehicle skin and structural members is receiving increasing attention by aircraft manufacturers due to the combined advantages of stiffness and weight savings of these materials. The replacement of aluminum surfaces and structures with Carbon-Fiber-Composite (CFC) material on modern aerospace vehicles complicates lightning protection by introducing high impedance paths between lightning current entry and exit points. A high impedance will force the lightning currents to seek lower resistance exit paths via internal metal structures, hydraulic lines, fuel lines or wire cable bundles. Any one of these paths (by direct or indirect

means) can induce catastrophically high voltages on sensitive flight critical cables and systems and/or introduce dangerous current paths to operators within the vehicle.

Reference 1 provides a comprehensive tutorial on aircraft lightning protection and the use of materials for aircraft structure, including carbon-fiber-composites (CFC) and fiberglass (FG). Reference 2, which is used by the military and others as the lightning requirements document, provides little flexibility for non-aluminum aircraft structures. Nonetheless, the 500 volt Class L requirement of (2) remains the desired requirement for aircraft lightning hardness.

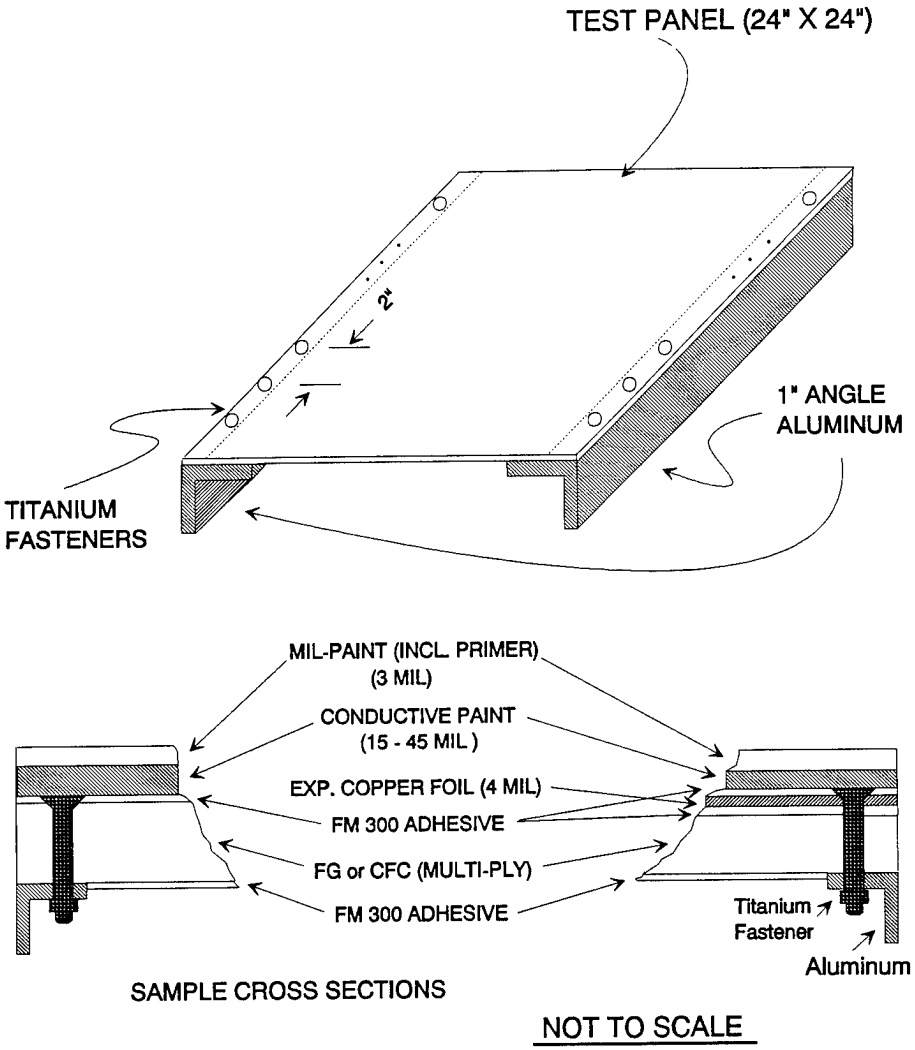
The purpose of this paper is to characterize aerospace type coupons composed of Carbon Fiber Composite (CFC) before and after exposure to simulated direct attachment lightning currents. The results are compared with the end-to-end DC resistance value of a bare CFC coupon.

## TEST ARTICLE DESCRIPTION

**CARBON FIBER COMPOSITE (CFC) COUPON** - The CFC coupons were made of ten (10) plies of AS-4 unidirectional fiber, laid up with (+/-45, +/-45, 0, 90, -/+45, -/+ 45) orientations as shown in **figure 1.** The fibers were separated by a matrix of FM 300 adhesive which also formed the external "jell coat" layer. A cross-section of the CFC coupon is shown in **figure 2.** A 24 inch coupon was selected to represent a fuselage panel for the underbelly area of a modern helicopter. The aluminum angle is a test artifact used to permit currents to exit or enter the coupon. It is attached at the bottom of the coupon with a Titanium fastener; a one-inch wide strip of the panel was sanded to remove the jell coat layer and enhance carbon fiber contact with the aluminum. An aluminum collar is used to permit the lightning current to penetrate the layers of CFC material.

The baseline CFC coupon received no top surface treatment. Variations from the baseline are listed below, and include conductive and non-conductive top coat treatments.

- Carbon Fiber Composite (CFC)
  - CFC Unpainted Baseline (CFC)
  - CFC with MIL-STD Paint (CFC/P2)
  - CFC with Silver Loaded Paint (P1) and P2 (CFC/P1/P2)
  - CFC Expanded Copper Foil and P2 (CFC/Foil/P2)
  - CFC with Expanded Copper Foil, P1 and P2 (CFC/Foil/P1/P2)
- Fiberglass (FG) with P1 and P2 (FG/P1/P2) - Information Only




NOTE:
- 1" aluminum angle is for direct attachment of lightning generator
- 1" aluminum angle is used on opposite ends when zone 3 current transfer tests are involved
- Fastener spacing, 2" is to optimize current distribution, i.e. eliminate current concentration at a single point

FIGURE 1 - COUPON CROSS-SECTION

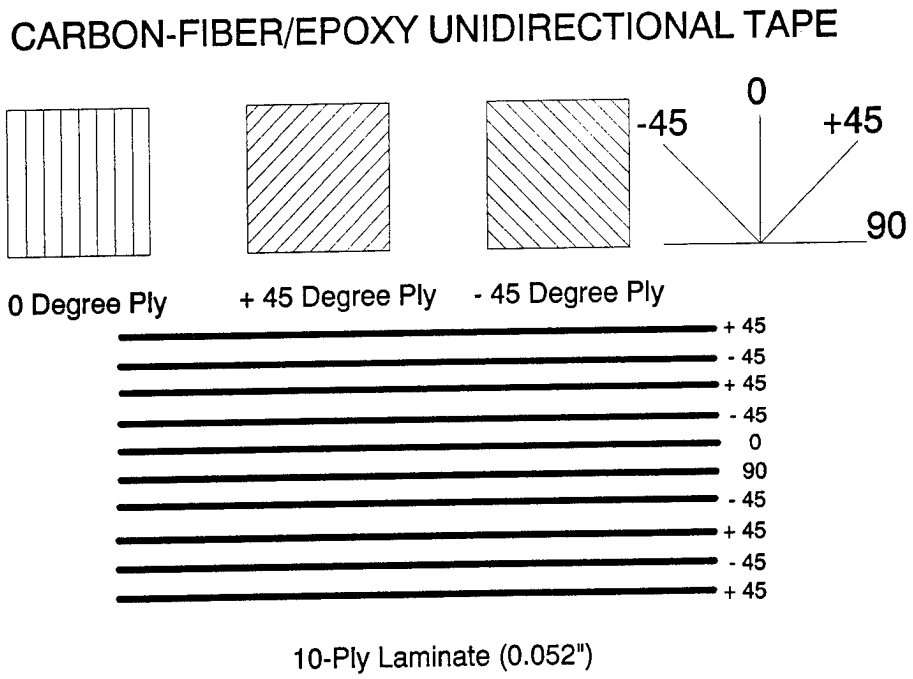



**FIGURE 2** - CARBON-FIBER-COMPOSITE (CFC) COUPON LAY UP

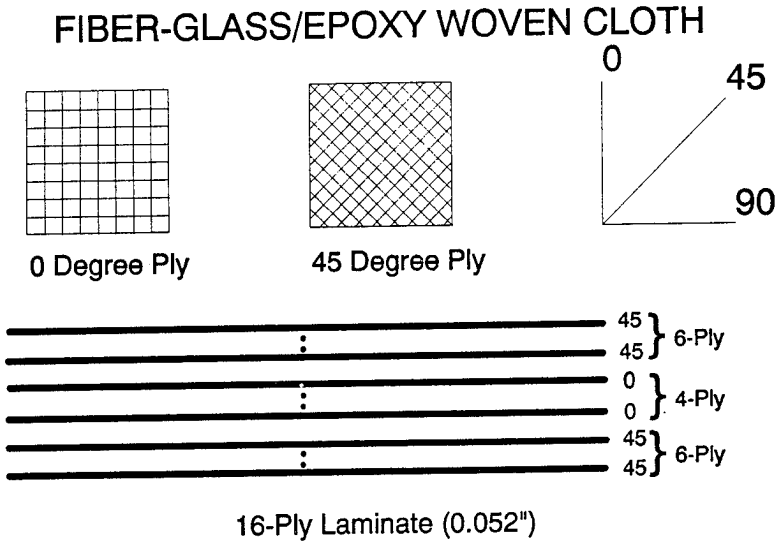



**FIGURE 3** - FIBERGLASS (FG) COUPON LAY UP

**FIBER GLASS (FG) COUPON** - The FG coupons were made of sixteen (16) plies of woven cloth fiber, laid up with ($-45_6$, $0_4$,$+45_6$) orientations as shown in **figure 3**. The fibers were separated by a matrix of FM 300 adhesive which also formed the external layer. A 24 inch coupon was selected to represent a fuselage panel for the underbelly area of a helicopter. The aluminum angle is a test artifact used to permit currents to exit or enter the coupon. The only coupon type for this study included a conductive top coat treatment as listed above, since the lightning properties of a non-conductive FG panel is well documented (1).

**TOP COAT TREATMENTS**

**Expanded Copper Foil** - a 4-mil layer of expanded copper foil was used as a means of distributing lightning currents across the CFC coupons. The characteristics of this layer are:

- Surface Resistivity: < 1.0 milliohms/square (Ω/□)
- Size: 24 inch x 24 inch x 0.004 inch (4 mils)
- Weight: $4.13 \times 10^{-2}$ lb/ft$^2$

**Silver Loaded Conductive Paint (P1)** - A layer of conductive paint of varying thicknesses (and resistances) was applied to coupons of CFC and FG. The water-based urethane conductive paint, known as Silver Coated Magnetic Ceramic Microballoon (SCMCM), was applied for lightning protection in one, two and three layers of paint yielding thicknesses of 15-, 30- and 45-mils. The characteristics of the paint are listed below.

- Surface Resistivity: 80 milliohms/□
- Conductive Coating: 0.025 micron (1 microinch) silver over a 50 micron diameter hollow ceramic sphere
- Density: 0.7 g/cm$^3$
- Weight: $2.5 \times 10^{-2}$ lb/ft$^2$ (@ 15 mil)

**MIL-STD Aircraft Paint (P2)** - All but three of the coupons were overcoated with 1-mil of MIL-P-23377 epoxy primer and 2-mils of MIL-C-85285 polyurethane topcoat (3-mils total thickness). The paints were cured for one-week at room temperature.

**TEST METHODOLOGY**

**ELECTRICAL BOND RESISTANCE** - This test measured the end-to-end direct current electrical bond resistance (Rdc) using a four (4)-probe BIDDLE Digital Low Resistance Ohmmeter (DLRO), Model 24700 milliohmmeter, having a minimum range of zero to six milliohms with a resolution of 1 micro-ohm. Each coupon was measured before and after exposure to the lightning current.

**Test Measurements** - End-to-end resistance measurements were conducted on each panel before and after the Zone 3 or Zone 1B tests at three sets of probe locations: top-top (A-X); middle-

middle (B-Y); and bottom-bottom (C-Z), where A,B,C were locations on the left aluminum angle and X,Y,Z were corresponding locations on the right aluminum angle. The measurements were rounded down at the third decimal to account for resistance between the aluminum-titanium interface (typically 0.5 milliohm).

**Rdc Setup** - Each coupon was inverted and laid flat on 2 wooden beams (2x4's) on a wooden table. One twin probe of the milliohmmeter was placed at the left aluminum angle and the other twin probe was placed on the right aluminum angle for each measurement.

**SIMULATED LIGHTNING WAVEFORMS**

The Zone 3 waveform elements (A and C) correspond to Zone 3 current waveform Test Method T02 of (3). The Zone 1B waveform elements (A, B, C and D) correspond to Zone 1B current waveform Test Method T02 of (3). They are supplied sequentially in one test but not necessarily as one continuous discharge.

**TEST SETUP** - For each test, a 6 inch x 24 inch aluminum sheet was clamped to the aluminum angles on opposite sides of the test article to facilitate a uniform current distribution across the test article.

For the Zone 3 current test, separate capacitor banks for the A and C waveforms were used. Each coupon was mounted vertically to the test fixture. The test current pulse for Zone 3 lightning consists of the discharge of the "A" component, followed sequentially by the "C" component.

Component A has a peak amplitude of 21,200 Amp (± 10%) and an action integral of $2.4 \times 10^4$ $A^2.s$ (± 20%). The peak amplitude is scaled from the 200,000 Amp peak of a Zone 1 attachment by equation (1):

$$Iz_3 = Iz_1 \times L/\pi D \qquad (1)$$

where: $Iz_1$ = 200,000 Amp (A) or 200-800 Amp (C)
L = coupon length (2 ft)
D = fuselage diameter at Zone 3 (6 ft)

Component C is also scaled by equation (1) to 20-80 Amps, and transfers a charge of 27 coulombs (+/- 20%) in a pulse time from 0.25 to 1.0 second.

For the Zone 1B current test, separate capacitor banks for the A, B, C, and D waveforms were used. Each coupon was mounted horizontally to the test fixture. The discharge probe was placed at the center of the coupon's top surface. Component A has a peak amplitude of 200,000 Amps (± 10%) and an action integral of $2.0 \times 10^6$ $A^2.s$ (± 20%). Component B has an average amplitude of 2,000 Amps (± 10%) and transfers 10 Coulombs of charge (± 10%). Component C has an amplitude between 200 and 800 Amps and transfers 200 Coulombs of charge (± 20%). Component D has a peak

amplitude of 100,000 Amps (± 10%) and an action integral of 0.25 x $10^6$ $A^2$.s (± 20%).

**TEST RESULTS**

The results showed a change in end-to-end DC electrical resistance, Rdc, after conduction of the Zone 1B or Zone 3 lightning currents. Coupons with the silver paint treatment showed an increase in Rdc after conduction of the Zone 1B or Zone 3 lightning currents when compared to the baseline. Coupons with Copper foil treatment (with and without silver paint) showed a decrease in Rdc after conduction of the Zone 1B or Zone 3 lightning currents when compared to the baseline.

**Table 1** details the DC electrical resistance, Rdc, measurements conducted on each panel before and after the Zone 3 and Zone 1B tests. The tabulated values indicate the average resistance of at least three measurements taken from the aluminum angle located on 2 opposite sides of each panel, using the Biddle milliohmmeter. The results are plotted in **figures 4A and 4B.**

**PRETEST RESULTS** - The following results are listed in **table 1** under the column labelled "Pretest". Note that the paired (A-X, B-Y, C-Z) measurements described above showed a sensitivity to the fiber layup as discussed in (4). The largest sensitivity however, was measured on coupon I1, 0.08 milliohm out of 11.65 milliohms, or less than 1%.

1. The application of military paint (E1/F1) did not change to the pretest DC resistance of the CFC-baseline coupons (C1/C3/D1).
2. As shown for coupons E1/F1 vs G1 through H3, the application of silver paint (P1) decreased the electrical bonding resistance, Rdc, of the CFC coupons to 32 milliohms (from 41 milliohm average - CFC baseline).
3. The application of expanded copper foil (Foil) decreased the pretest DC resistance to 12 milliohms for coupons I1 and J1, vice 41 milliohms average for E1 and F1. Coupon I2 was measured at 36 milliohms and appeared to have a fabrication problem with the fastener top interface.
4. For coupons K1 through L3, the application of silver paint (P1) increased the pretest DC resistance to 16 milliohms from 12 milliohms average for I1/J1 (CFC/Foil/P2).
5. The application of silver paint (P1) to the fiberglass panels, coupons A1 through B3, created a conductive surface of 1.2 ohms average from a non-conductive fiberglass surface. Coupon A3 was measured at 13.250 ohms and appeared to have a fabrication problem with the fastener top interface.

**POST-TEST RESULTS**

<u>CFC Material</u> - 1. The electrical bonding resistance, Rdc, measured approximately 40 milliohms for the baseline (coupons C1/C3/D1) prior to the lightning test.

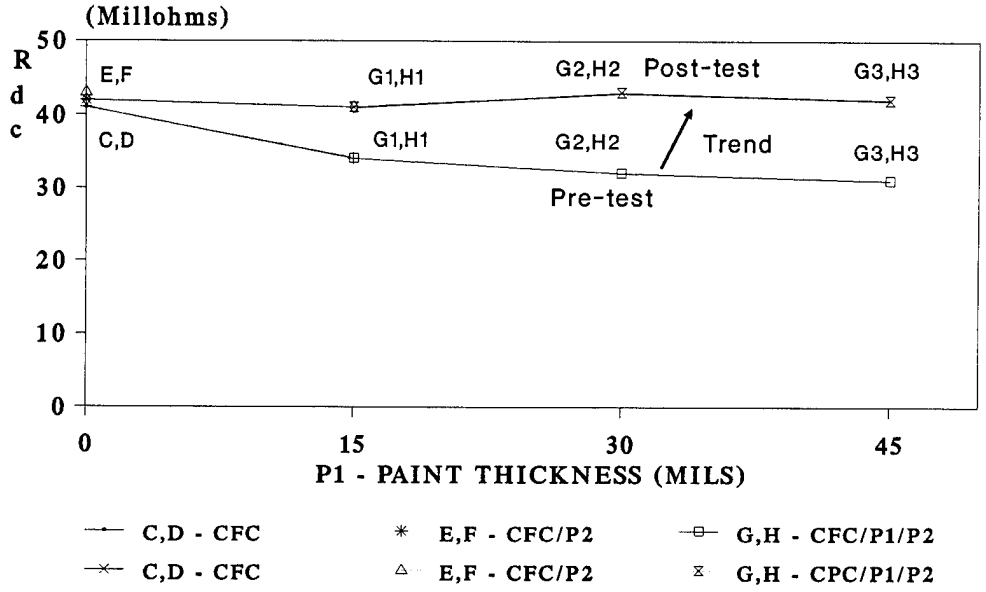
2. No change in Rdc was measured after the Zone 3 lightning test (on coupons C1/C3), while an increase in Rdc to 44 milliohms was measured as a result of the Zone 1B lightning test on coupon D1, probably due to a loss of carbon at the CFC-fastener interface.

**TABLE 1** END-TO-END ELECTRICAL RESISTANCE TEST RESULTS

| COUPON TYPE | | COUPON ID | PRETEST Rdc (Ohms) | POST-TEST Rdc (Ohms) | COMMENT |
|---|---|---|---|---|---|
| FG/P1/P2 | Zone 3 Current | A1 | 0.550 | Open >14MΩ | Increased |
| | | A2 | 0.932 | Open >14MΩ | Increased |
| | | A3 | 13.250(1) | Open >14MΩ | Increased |
| | Zone 1 Current | B1 | 1.950 | Open >14MΩ | Increased |
| | | B2 | 0.243 | Open >14MΩ | Increased |
| | | B3 | 2.383 | Open >14MΩ | Increased |
| CFC-Baseline | Zone 3 Current | C1 | 0.039 | 0.039 | No Change |
| | | C3 | 0.040 | 0.040 | No Change |
| | Zone 1 Current | D1 | 0.042 | 0.044 | Increased |
| CFC/P2 | Zone 3 Current | E1 | 0.041 | 0.041 | No Change |
| | Zone 1 Current | F1 | 0.042 | 0.043 | Increased |
| CFC/P1/P2 | Zone 3 Current | G1 | 0.036 | 0.040 | Increased |
| | | G2 | 0.031 | 0.040 | Increased |
| | | G3 | 0.031 | 0.039 | Increased |
| | Zone 1 Current | H1 | 0.032 | 0.041 | Increased |
| | | H2 | 0.032 | 0.046 | Increased |
| | | H3 | 0.030 | 0.045 | Increased |
| CFC/Foil/P2 | Zone 3 Current | I1 | 0.012 | 0.003 | Decreased |
| | | I2 | 0.036(1) | 0.014 | Decreased |
| | Zone 1 Current | J1 | 0.012 | 0.005 | Decreased |
| | | I1 | 0.003 | 0.005 | (2) |
| CFC/Foil/P1/P2 | Zone 3 Current | K1 | 0.013 | 0.005 | Decreased |
| | | K2 | 0.014 | 0.004 | Decreased |
| | | K3 | 0.014 | 0.004 | Decreased |
| | Zone 1 Current | L1 | 0.013 | 0.006 | Decreased |
| | | L2 | 0.011 | 0.006 | Decreased |
| | | L3 | 0.016 | 0.006 | Decreased |

**NOTE:** (1) possible fabrication error at fastener top interface
(2) Coupon I1 tested for Zone 1B after Zone 3 test

## (A) CFC COUPON RESISTANCE VS SILVER PAINT THICKNESS (NO FOIL)




## (B) CFC COUPON RESISTANCE VS SILVER PAINT THICKNESS (WITH CU FOIL)

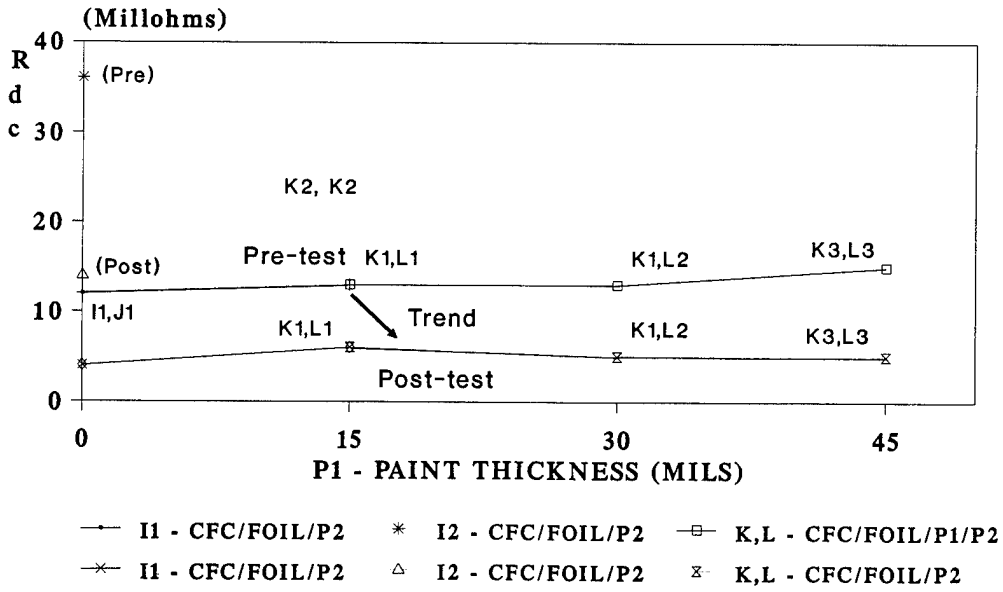



**FIGURE 4** END-TO-END RESISTANCE (Rdc) TEST RESULTS

**CFC With Surface Treatment** - Various surface treatments to the CFC-Baseline (coupons C1/C3/D1) as shown by the coupon variations in **table 1** produced varied results for Rdc in both pretest and post-test measurements.

1. The application of non-conductive military paint (P2) increased the pretest Rdc from 40 milliohms (coupons C1/C3/D1) to 41 milliohms average (coupons E1/F1). Comparing across **table 1**, no change in Rdc occurred after the Zone 3 test, but an increase in Rdc was measured after the Zone 1B test for coupon F1.

2. The application of silver paint to CFC substrate (coupons G1/H1; G2/H2; G3/H3) decreased Rdc to 34, 31, and 30 milliohms average before the lightning test.

3. For coupons with Copper foil (I1/J1/K1-L3), the value of Rdc decreased to 5 milliohms average after the lightning test. This resistance decrease is indicative of a resistance drop at the copper foil-titanium fastener interface probably caused by arcing at the interface and resulting deposit of copper material at the surface nonconformities.

4. Also, for coupons with Copper foil (I1/J1/K1-L3), no advantage was observed by the presence of silver paint, since the post-test value of Rdc for these coupons averaged 5 milliohms. However, the coupon integrity for coupons K1-L3 was severely compromised by the silver paint layer as discussed below.

**FG Material** - The evaluation of the FG coupons was primarily academic and yielded expected results.

1. The addition of silver paint provided a relatively low resistance path (approximately 1.2 ohm) over the FG substrate.

2. Upon conduction of the lightning currents (Zone 3 or Zone 1B), silver paint was lost from the coupon surface and electrical continuity was destroyed especially at the silver-titanium interface resulting in an open circuit condition (Rdc > 14 Megohms).

## DISCUSSION OF RESULTS

**SURFACE RESISTANCE** - Using a lumped-parameter equation (Eq. 2) for the coupon resistance, Rdc, as a parallel current distribution (5), one can solve for the surface resistance, R1 (Eq. 3):

$$Rdc = Rc//R1 = (Rc \times R1)/(Rc + R1) \quad (2)$$

$$R1 = \left|(Rc \times Rdc)/(Rc - Rdc)\right| \quad (3)$$

where: Rc = 41 milliohms (CFC);
R1 = Conductive Surface Resistance (paint, foil, etc.)

1. As shown in **table 2**, calculated values of the surface resistance ranging from 119 to 295 milliohms for the silver paint layers. These values of Rdc are much higher than the advertised resistivity of 80 milliohms/square, but includes contact

**TABLE 2** CONDUCTIVE SURFACE RESISTANCE VALUES (R1) FOR CFC COUPONS

| COUPON TYPE | COUPON ID | SILVER PAINT (mils) | CFC-BASELINE (C1/D1) Rc (ohms) | BEFORE | | AFTER | | COMMENT |
|---|---|---|---|---|---|---|---|---|
| | | | | Rdc (ohms) | R1 (ohms) | Rdc (ohms) | R1 (ohms) | |
| CFC/P2 | E1 | 0 | 0.041 | 0.041 | N/A | 0.041 | N/A | No Silver Paint |
| | F1 | 0 | 0.041 | 0.042 | N/A | 0.043 | N/A | No Silver Paint |
| CFC/P1/P2 | G1 | 15 | 0.041 | 0.036 | 0.295 | 0.040 | 1.640 | - |
| | G2 | 30 | 0.041 | 0.031 | 0.127 | 0.040 | 1.640 | - |
| | G3 | 45 | 0.041 | 0.031 | 0.127 | 0.039 | 0.800 | - |
| | H1 | 15 | 0.041 | 0.032 | 0.146 | 0.041 | Open | - |
| | H2 | 30 | 0.041 | 0.032 | 0.146 | 0.046 | Open | 1" Dia Hole |
| | H3 | 45 | 0.041 | 0.030 | 0.119 | 0.045 | Open | 1" Dia Hole |
| CFC/Foil/ P2 | I1 | 0 | 0.041 | 0.012 | 0.017 | 0.005 | 0.006 | Foil Layer |
| | J1 | 0 | 0.041 | 0.012 | 0.017 | 0.005 | 0.006 | Foil Layer |
| CFC/Foil/ P1/P2 | K1 | 15 | 0.041 | 0.013 | 0.019 | 0.005 | 0.006 | - |
| | K2 | 30 | 0.041 | 0.014 | 0.021 | 0.004 | 0.004 | - |
| | K3 | 45 | 0.041 | 0.014 | 0.021 | 0.004 | 0.004 | - |
| | L1 | 15 | 0.041 | 0.013 | 0.019 | 0.006 | 0.007 | 2" Dia Hole |
| | L2 | 30 | 0.041 | 0.011 | 0.015 | 0.006 | 0.007 | 6" Dia Hole |
| | L3 | 45 | 0.041 | 0.016 | 0.026 | 0.006 | 0.007 | 4" Dia Hole |

resistance of the silver-titanium fastener surface, electrical coupling to the CFC substrate, and multiple paint layers.

2. The application of expanded copper foil to the CFC substrate (coupons I1/J1) decreased Rdc to 12 milliohms before the lightning test. Using the above lumped-parameter calculation for resistance and solving for R1 yields a value of 17 milliohms for the copper foil surface resistance. This value for R1 appears high, but includes the contact resistance of the copper foil-titanium fastener interface and electrical coupling to the CFC substrate.

**COUPON INTEGRITY** - The use of 2.5 milliohms (DC) as an equivalent requirement for MIL-B-5087B, Class L bond for joints or surface interfaces does not provide useful engineering data as to the integrity of the CFC coupon to withstand a lightning strike (see **table 2 - COMMENT**).

1. The DC electrical resistance values for CFC coupons after exposure to the Zone 1B currents remained unchanged from pretest readings. This was true for coupons with severe damage to the surface treatments and CFC substrate.

2. The Copper foil treatment layer on J1 vaporized in the area surrounding the Zone 1 attachment point, but the loss of Copper was not evident from the resistance measurement. In fact, Rdc decreased to 5 milliohms from 12 milliohms and the calculated R1 value decreased to 6 milliohms from 17 milliohms.

3. Similar results are shown in **table 2** for the Copper foil coupons with the silver paint application (L1/L2/L3). With damage to the CFC and loss of copper foil and silver paint, the measured values of Rdc decrease to 6 milliohms from approximately 15 milliohms, and R1 decreased to 7 milliohms from approximately 20 milliohms (average).

4. The DC resistance (Rdc) can be used as a figure of merit for structural and surface interfaces for CFC coupons, as well as to identify poorly constructed or repaired coupons. However, it can not indicate the ability of the interface to survive the lightning current densities.

**RECOMMENDATIONS**

1. The silver coated magnetic ceramic microballoon (SCMCM) paint should not be used where structural lightning protection is a requirement. No further investigation of this paint for lightning protection is recommended.

2. A non-destructive method and figure of merit (FOM) is needed to evaluate the ability of repaired CFC coupons and joints to survive MIL-STD-1757A lightning current densities.

3. The DC resistance (Rdc) can be used as a FOM for coupon and joint integrity, once the item has been qualified to withstand the lightning current densities by other means.

**REFERENCES**


1. DOT/FAA/CT-89/22, "Aircraft Lightning Protection Handbook", September, 1989.
2. MIL-B-5087B (ASG), Amendment 1, Military Specification, "Bonding, Electrical, and Lightning Protection for Aerospace Systems", 6 February 1968.
3. MIL-STD 1757A, Military Standard, "Lightning Qualification Test Techniques for Aerospace Vehicles and Hardware", 20 July 1983.
4. P. F. Little, "Lightning Hazards Due To Composite Materials in Aircraft", Proceedings IEEE 1983 International Symposium on Electromagnetic Compatibility, p.166.
5. ADA124016, "Composite Material Aircraft Electromagnetic Properties and Design Guidelines", DTIC, February 2, 1983.

# SESSION 07B
# LIGHTNING PROTECTION
# CHAIRPERSON: THEODORE L. HARWOOD

# LIGHTNING-INDUCED DAMAGE PHENOMENOLOGY IN CARBON FIBER COMPOSITE MATERIALS

A.C. Douay* and D.A. Shockey
SRI International
333 Ravenswood Avenue, Menlo Park, California 94025, USA
Telephone: +1-(415) 859 2587 Fax: +1-(415) 859 2260

P. Gondot and J-P. Avenet
Aerospatiale, Centre Commun de Recherches
12, rue Pasteur B.P. 76, 92152 Suresnes Cedex, France
Telephone: +33-(1) 46 97 33 79 Fax: +33-(1) 46 97 30 08

## ABSTRACT

Four carbon fiber composite plates protected by a bronze mesh were tested against direct effects of lightning. The damage was analyzed with the help of a binocular microscope and a scanning electron microscope. Damage modes affecting the bronze mesh, the resin layer in which it is embedded and the carbon fiber plies were identified and could be associated with specific testing conditions and loadings, namely a conduction or an attachment test, and a pulse or a continuous component of lightning. Finally, interpretations are presented to explain the damage phenomenology for most of these identified damage modes, thus improving the physics understanding of direct effects of lightning to help design models and simulation tools.

## INTRODUCTION

Aircraft manufacturers must protect their products against direct effects of lightning and they comply in doing so with aircraft certification authorities regulations. Direct effects may be described as all types of thermomechanical material damage resulting from the attachment of the lightning arc onto the structure. To achieve safety goals regarding direct effects, all major aircraft manufacturers acquired some ability to design proper protections. Nowadays designing protections against direct effects is done almost exclusively by experimentation. Reid's article (1) gave an overview of direct effects summarizing most of the physical understanding of those. A few researchers like Little (2) made some simulations of damage on metal sheets, and a few others (3,4,5) even made a few simulations on carbon/epoxy composites. All these models proposed were macroscopic.

However, the physics of direct effects on composite materials is not well understood. Safety standards and regulations regarding lightning are consequently chosen with conservatism. The same limits on our comprehension of direct effects resulted in the exclusive development of experimental design techniques, as opposed to theoretical tools.

* Present address: Aerospatiale, 12, rue Pasteur B.P. 76, F-92152 Suresnes Cedex, France, Tel: +33-1-46 97 31 76

If it were possible to improve the scientific understanding of direct effects, then, safety standards, regulation regarding lightning, protection design and validation methods could be also improved.

This article describes a research effort aimed at understanding the physics of direct effects in carbon fiber composites (CFCs). The ultimate goal is to develop simulation tools using adequate damage models. This paper brings a new light on the phenomenology of direct effects. Laboratory experiments were conducted on CFC plates. Surface damage was carefully examined on each plate with a binocular and a scanning electron microscope. Consequently 1) different surface damage modes were identified, 2) damage modes could be correlated with different types of loadings, and 3) the phenomenological development of several damage modes could be understood. Deeper modes of damage found in the core of the material such as interply delamination are not treated in this paper.

## EXPERIMENTS

Four CFC plates were examined. A description and loading summary for these 4 plates is given in table 1. Plates #1 and #2 are 4mm thick composite laminates made of 14 woven T300 carbon fiber plies embedded in a 914 epoxy resin. The stacking sequence is $[((0,90)/(-45,+45))_3/(0,90)]_s$. Plates #3 and #4 are 4mm thick composite laminates made of 32 unidirectional T300 carbon fiber plies embedded in a 914 epoxy resin. The stacking sequence is $[(0/90/-45/+45)_4]_s$. All four plates are covered on one side by a protective bronze mesh ($80g/m^2$) embedded in the same 914 epoxy matrix. This mesh is made of woven 0° and 90° bronze wires 0.1mm in diameter and regularly spaced at 1mm intervals. None of the plates was painted.

TABLE 1 DEFINITION OF PANELS

| Number | Ply Type | Ply Orientation | Loading |
|---|---|---|---|
| 1 | woven | $[((0,90)/(-45,+45))_3/(0,90)]_s$ | $A_c + A_a$ |
| 2 | woven | $[((0,90)/(-45,+45))_3/(0,90)]_s$ | $A_c + (D+C^*)_a$ |
| 3 | unidirectional | $[(0/90/-45/+45)_4]_s$ | $A_c + A_a$ |
| 4 | unidirectional | $[(0/90/-45/+45)_4]_s$ | $A_c + (D+C^*)_a$ |

Loading indexes: c: conduction loading (figure 1a), a: attachment loading (figure 1b)

All plates were tested at Aerospatiale's lightning test facility using the standard lightning waveform defined in FAA Advisory Circular 20 53 A. The loading sequence was unusual: it was intended to show the possible extent of damage of a single part of the aircraft submitted to 2 strikes throughout the life of an aircraft: First plates were predamaged in conduction, as if a lightning strike had occured a first time in some other location on the aircraft. In this instance, plates are predamaged by a type A lightning component in a conduction test ($A_c$ in table 1), as shown in figure 1a. Second, the plates were damaged in attachment mode, as if lightning had struck this material directly on a subsequent occasion. They were damaged through an attachment test by either another component A, or by a component D followed by a component C* ($A_a$ or $(D+C^*)_a$ in table 1). The test setup for the attachment test is shown in figure 1b. The A component is a short (~200μs), intense (200kA) pulse. The component D is half as short (~100μs), half

as intense (100kA) as the component A. Finally, component C* is a much longer (50ms), much weaker (400A) current waveform.

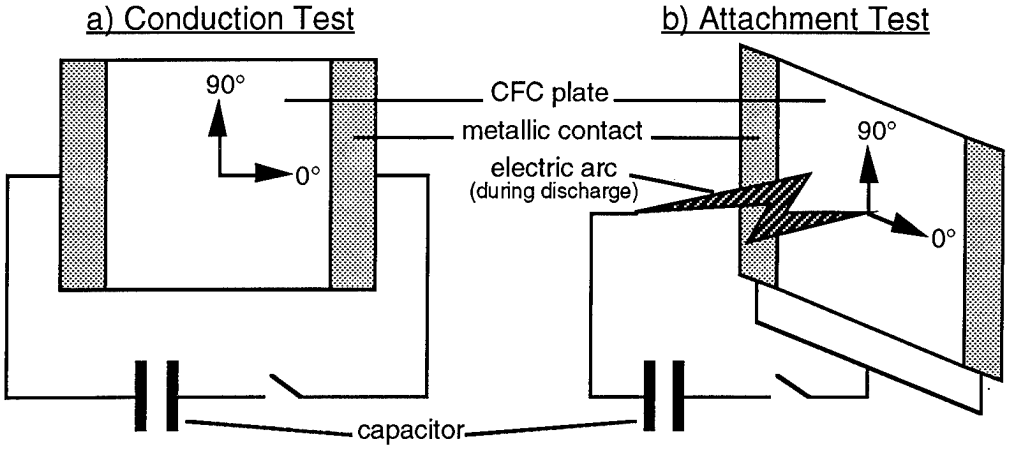



FIGURE 1 TEST SETUP

DAMAGE MODES

BRONZE MESH DAMAGE -- 0° bronze wires have disappeared all over each plate. 90° wires have vanished to various extents around the center of damage where the simulated arc struck the panel. The area where 90° wires disappeared forms 2 ellipses as shown on the topview of an impacted plate in figure 2a.

PROTECTION LAYER MATRIX FRAGMENTATION -- Looking closer and closer to the impact point (typically within 2-3cm from the impact point), the surface protection layer matrix in which the bronze wires are embedded is more and more damaged. From the craters left in this layer, it can be deduced that fragments have disappeared. Several types of fragmentations can be identified in this damaged zone, based on the location and aspect of the fragments prints in the matrix.

Type 1 Fragmentation -- This fragmentation is the most common one: it was observed on all 4 panels. It occurs at bronze mesh nodes where 0° wires overlap 90° wires. These nodes will be referred to as 0/90 nodes. Based on the observation of the craters left behind in the matrix, fragments forming at 0/90 nodes, or fragments of type 1, vary in shape and size around the impact point, and they vary with distance from the impact point as well. They may be very elongated or almost circular, and measure up to 1mm in width. Their thickness is typically that of the surface layer, about 0.2mm.

Type 2 Fragmentation -- This fragmentation is the mirror image of fragmentation of type 1. It occurs at nodes of the woven bronze mesh where 90° wires overlap 0° wires. These nodes will be referred to as 90/0 nodes. Fragments forming at 90/0 nodes, or fragments of type 2, are different from fragments of type 1 since they occur only in a confined zone close to the impact point. As deduced from the craters left in the surface layer, their shape and size is often different from those of fragments of type 1, even though they vary as well in shape and size depending on their location around the impact point. Their size is up to 1mm like for fragments of type 1.

Type 3 Fragmentation -- Finally, fragmentation of type 3 is specific to CFC plates made of woven carbon fiber plies, like panels #1 and #2. Fragments of type 3 form at the

nodes of the (0,90) top fiber ply where 90° fiber bundles overlap 0° bundles. Based on the observation of the craters left in the surface layer, These fragments are usually quite large in comparison to fragments of type 1 or 2, up to 2mm in width, and unlike these they cannot be correlated with specific nodes of the bronze mesh.

In all types of fragmentations, the surface layer matrix has completely disappeared locally, and the carbon fibers are fully visible underneath. The resin in which those fibers were embedded mostly vanished too, and fibers are often damaged themselves: broken, bent, swollen or consumed.

CENTRAL DAMAGE MODES-- Examining panels close to the impact point reveals on plates #2 and #4 a locally heavily damaged area within 1cm of the impact point. The protection layer has completely disappeared there. On the boundaries of this zone fibers are intact but the resin was melted. Inside this central zone, most of the fibers now visible are loose, the resin has completely disappeared, and most fibers are broken. The second or even third ply is then visible at the very center of damage. Several small areas (less than 1mm in diameter) inside this region are heavily damaged: fibers are badly swollen and cracked, if not shredded. Such small areas sometimes look as if a chunk of fibers had been scooped out.

## DAMAGE CAUSES

0° BRONZE WIRES-- These wires completely disappeared all over the surface of each panel. 0° is the direction of current in the conduction test, where currents pass homogeneously across each plate. Hence the straightforward correlation between the conduction test and the 0° wire damage.

90° BRONZE WIRES-- These have disappeared around the center of each plate, forming a pattern made of 2 ellipses (figure 2d). The hypothesis is that the damage was caused by the 90° component of the current density distributed around the impact point. Figure 2c shows the approximate current lines from a macroscopic standpoint, however, most of the current component flowing in the 90° directions flows into the bronze wires, and only this component will significantly contribute to wire damage.

This hypothesis can be confirmed by a simple theoretical analysis. The analysis consists in making the simplifying assumption where the arc attaching in the center of the plate generates an isotropic current density distribution around the impact point as shown in figure 2a. It is shown that a resulting isolevel of 90° current density component is a double circle as shown in figure 2b.

In fact the current density distribution is not isotropic since currents flow out of the plates only by 2 opposite edges as shown in figure 1b, and since the material itself is orthotropic. Qualitatively the current lines are therefore as shown in figure 2c where they turn to be parallel to the 0° direction. As a result the isolevels of 90° current density will not be so extended in the 90° direction, so that the isolevel will appear as a flattened ellipse as shown in figure 2d.

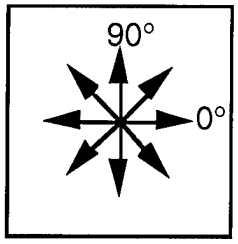
Furthermore, the addition or withdrawal of the C* current waveform did not result in the appearance or disappearance of the damage to the 90° wires.

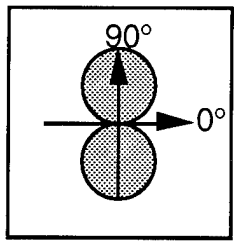
Finally, the same hypothesis of isotropic current density shows that twice the current intensity in the arc implies that the same level of current density, hence a similar damage level, occurs at twice the distance from the impact point. By switching from a D component to an A component, an equivalent current density will therefore be found at

twice the distance in the second case. A comparison between plates #1 and #2, and between plates #3 and #4, shows that the diameter of the damaged area where 90° wires have vanished is halved, just as the pulse loading has been halved.

Damage expected from an isotropic current distribution:

a) simplified current distribution

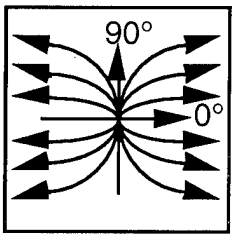


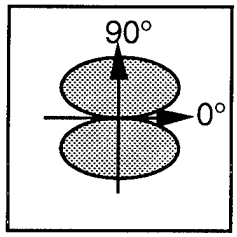




b) 90° wire damage pattern resulting from a)

Current distribution deduced from the observed damage:

c) real current distribution




d) 90° wire observed damage pattern

FIGURE 2 PANELS' TOPVIEW: 90° BRONZE WIRE DAMAGE

The coherence of all those arguments indicates that the degradation of bronze wires results from the current density flowing through them, and that the A and D pulse waveforms in particular are the ones from which sufficient density levels are reached to damage the bronze wires.

FRAGMENTS OF TYPE 1, 2 & 3 -- All fragment types are more or less isotropically distributed around the center of damage. They are occasionally slightly more spread out at 90° rather than at 0°.

The extent of the areas where these forms of damage are observed follow the same patterns as for the areas where 90° wires are damaged. Fragmentation zones are indeed roughly twice as large when the pulse component in the attachment test is twice larger, i.e. an A component as opposed to a D component.

Just like for 90° wires, the long, low intensity C* current waveform apparently does not play a role in this damage mode.

Consequent to these arguments, all types of fragmentation most likely originate from the pulse components in the attachment test.

CENTRAL DAMAGE MODES-- Central damage modes described as fusion, fiber fracture and arc attachment spots are observed only on panels #2 and #4. These damage modes were not observed on panels #1 and #3 which were struck exclusively by the A pulse component. Panels #2 and #4 are the only ones submitted to a C* component during the attachment test. Furthermore, these forms of damage are confined to a small area near the center of damage (within a 1cm radius of the impact point as opposed to 2 to 8 cm for wire damage and fragmentation modes). These two arguments indicate that the long duration, low intensity C* waveform is the origin of these damage modes.

All damage modes and their respective testing and loading conditions are summarized in table 2:

TABLE 2 DAMAGE MODES SUMMARY

| test setup | loading | damage |
|---|---|---|
| 0° conduction | component A | 0° bronze wire damage |
| attachment | component A or D | 90° bronze wire damage |
| attachment | component A or D | fragmentation-1, -2 & -3 |
| attachment | component C* | resin fusion |
| attachment | component C* | carbon fibers fracture |
| attachment | component C* | thermal damage of carbon fibers |

DAMAGE PHENOMENOLOGY

An important hypothesis was made concerning the chronology of loading and damage modes. For pulse waveforms, loading durations are of the order of 100μs and loading rise times of the order of 10-20μs. Consequently, this type of loading is considered to be very fast in comparison to damage evolution characteristic times. In the case of a continuous waveform, loading times are of the order of a few 10ms and therefore damage modes attributed to this lightning component are assumed to happen progressively throughout the loading, if not beyond.

BRONZE WIRE DAMAGE-- On one hand the vanishing of 0° and 90° bronze wires looks identical. On the other hand the origin of these two forms of damage is identical, namely the current density which flows through those wires during a pulse waveform. The damage phenomenology should consequently be identical, and will be presented once for both damage modes.

Basic observations were made with a binocular microscope, which has a limited magnification (40x), and which allows some chromatic observations through the thickness of the surface epoxy layer. More observations were made using a scanning electron microscope (SEM), which allows surface examination only.

Based on these observations, a probable bronze wire damage phenomenology is proposed. It is explained here for 90° bronze wires, and illustrated by figure 3, representing a section of the plate in the 90° direction and along a 90° bronze wire:

1) - Decohesion between the bronze wires and the resin in which they are embedded probably occurs first (along the 90° wire, item a in figure 3). Recalling that fast transient current densities concentrate near the surface of a conducting material, this is most likely due to the resistive heating in the bronze wire resulting in the sublimation of the resin in contact with the wire.

2) - Occasional fractures of the 90° bronze wire at the 90°/0° node of the bronze mesh (item b in figure 3) is another early event in the damage process. This might be due to an explosive sublimation of the resin in contact with the wire, which would result in flexion stresses at this type of location, and/or the strong thermal stresses resulting from the bronze heating itself, and resulting in buckling.

3) - Heavy degradation of the bronze cohesion, where the bronze is dissociated into irregular grains roughly 5μm in diameter. This might have resulted from the very fast

resistive heating of the bronze wire and/or from thermal stresses as well. This damage stage occurs all along the 90° wire (item a in figure 3).

4) - Wire fractures were seen at 0°/90° bronze mesh nodes. Joule effect and thermal stresses in particular must be higher in these locations in comparison to what happens at 90°/0° nodes. However, those wires are only carrying the current in the 90° direction, since 0° wires have disappeared during the initial conduction test. Current is transferred from 90° wire to 90° wire by jumps in the carbon fiber plies between wires. The current indeed must find its way from the center of the plate to the metallic contacts on its sides in the 0° direction (figure 1a). Current flows between carbon fibers and bronze wires will be essentially limited to those areas where wires are in contact with fibers, i.e. at 0°/90° nodes. Hence the increased energy deposit at these locations. (see item c in figure 3).

5) -Partial ejection of a bronze wire section. Whole sections of bronze wires are ejected starting from 0°/90° nodes and exiting from the epoxy resin in which they are embedded through the openings at 90°/0° nodes (item d in figure 3). This indicates that forces pushing on the bronze wire to eject it are strong. These observations remain consistent with the hypothesis of pressures flexing it and contributing to the wire's fracture at 90°/0° nodes, and with the hypothesis that additional pressure occurs at 0°/90° nodes.

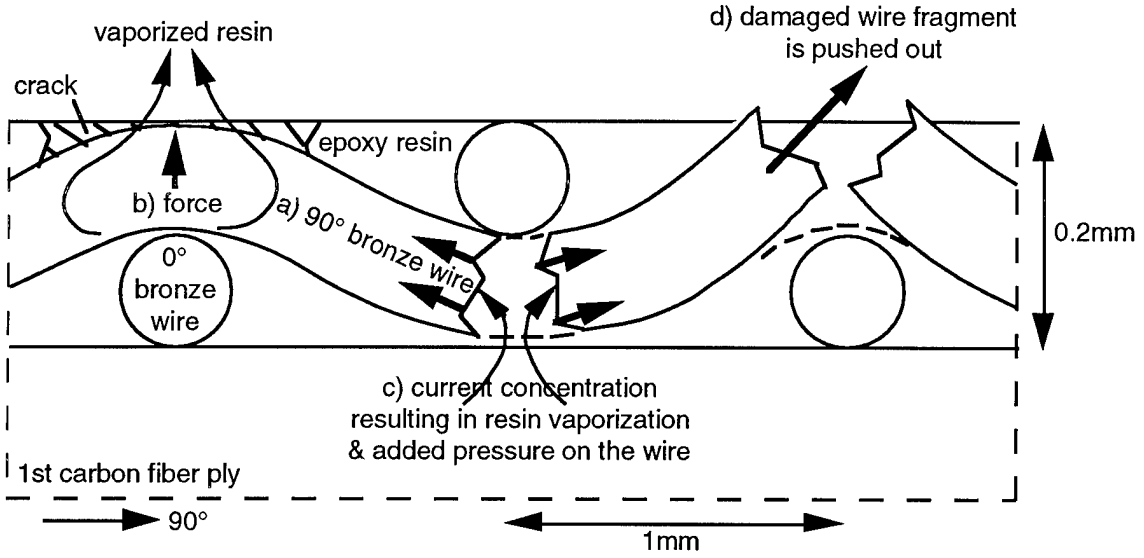



FIGURE 3 BRONZE WIRE DAMAGE PHENOMENOLOGY

FRAGMENTATION OF TYPE 1 -- Several key observations allow to reconstruct the probable fragment formation process. It is illustrated in figure 4, which represents a section of the plate in the 90° direction and along a 90° bronze wire:

1) - Fragments of type 1 are all centered on 0°/90° nodes. This is where the energy must have been deposited which formed this fragment. The source of this energy will have been the current density concentration explained in 4) of the previous section entitled "BRONZE WIRE DAMAGE". (see item a in figure 4). Where fragments were ejected the carbon fiber ply underneath is visible. The resin has been vaporized, while the carbon fibers themselves are often broken and bent, and sometimes consumed, indicating that current densities must have been quite high.

2) - Fragments edges are surfaces inclined by more or less 45° w.r.t. the plane of the plate. (See item b in figure 4). These are fracture surfaces. Patterns on these surfaces indicate that cracks originate near the center and propagate outwards through the thickness of the protective layer.

3) - Finally, the whole fragment thus formed is ejected by the same pressure forces from the vaporized resin. (See item c in figure 4).

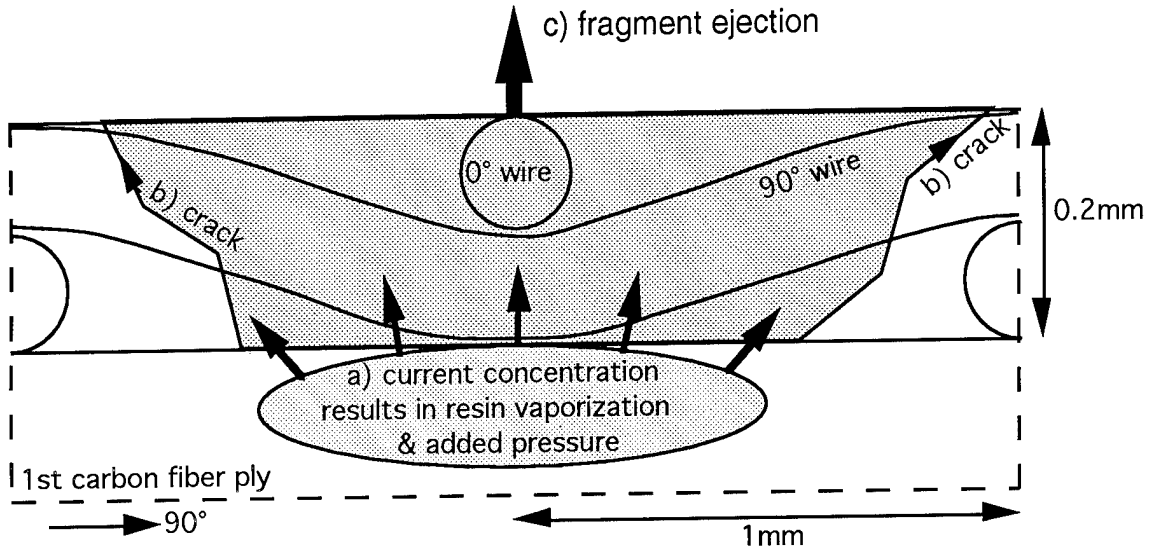



FIGURE 4 DAMAGE PHENOMENOLOGY OF FRAGMENTS OF TYPE 1

FRAGMENTATIONS OF TYPES 2 & 3 -- Phenomenological interpretations of fragmentations of type 2 and 3 were studied as well but have not been substantiated by enough observations to be presented with a reasonable degree of certainty. However, their existence contributes to demonstrate how complex the details of the damage are. Their different aspects and the different environments in which they occur indicate a still more complex damage phenomenology than presented in this paper.

CENTRAL DAMAGE -- Between panels #3 and #4, all damage modes caused by the pulse current waveform were not modified by the additional lightning component C* on panel 4. However, it is not possible to determine to which extent the additional damage caused by the continuous current waveform was modified by the previous loadings and resulting damage modes. It will be simply assumed in the present study that previous damage modes occur quickly in comparison to the time period over which the continuous component C* is applied.

In the present case, it means that nothing of the bronze mesh remains in the center and that the resin in which it was embedded is fragmented. When the C* lightning component is then applied, the electric arc attaches directly onto the carbon fibers. Since total current density is much lower (400A) than for pulse components (100-200kA), the current density is high only within a small radius around the impact point. The several damage modes described in this central zone are interpreted within this frame. The 3 damage modes are in fact 3 damage levels of the same phenomena illustrated in figure 5 showing a section of the plate's first carbon fiber ply near the central zone where the protective layer (not represented) has completely disappeared:

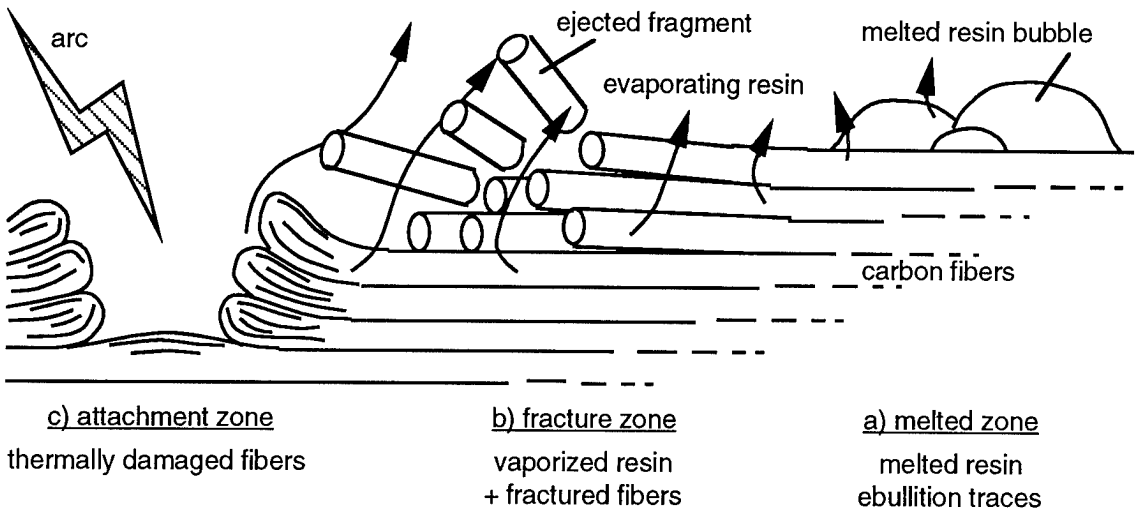



FIGURE 5 CENTRAL DAMAGE PHENOMENOLOGY

1) - The boundary of this central damage zone is shaped by melted resin with traces of ebullition, as witnessed by frozen bubbles' remains. Along this boundary current density was high enough to melt the resin but not to vaporize it. This zone is represented by item a in figure 5.

2) - Closer to the center of damage, the current density increases. The result is a zone called "fracture zone" because of the omnipresence of fractured fibers there. The resin is almost completely vaporized, and fibers are clean but broken across a large area (up to 1cm in radius) within which attachment zones are found. These fractures most likely occurred as the vaporizing resin deeper in the fiber ply blew across its thickness and broke the now loose fibers. This zone is represented by item b in figure 5.

3) - The lightning arc attached to the material all over this central zone in small spots characterized by:

- small, well bounded dimensions (up to 1mm in diameter)
- heavily damaged fibers: they are swollen, longitudinally cracked, even shredded
- occasional traces of constriction of a fiber bundle where the arc attached. This is a typical effect of electromagnetic pressure forces acting on a soft conducting path (2)

Such a zone is represented by item c in figure 5.

## ASSESMENT OF RECENT MODELIZATION WORKS

The present work already enables us to assess the validity of the hypothesis of recent modelization efforts by Avrootskij (3) and Hardwick (4): Avrootskij linked the delamination between carbon fiber plies to the pressure build-up resulting from the resin vaporization. The present study showed that this pressure build-up plays an important role in the bronze grid damage process and in the process of fragmentation of type 1. As a result we may confirm that assuming the same phenomenon could play a role in delamination is a reasonable hypothesis.

Hardwick's model (4) was implemented in a coupled thermal / electromagnetic code. Simulation results were not satisfactory when model cells are assumed to be destructed once the resin is vaporized. The resulting computed damage is too deep and too narrow. The hypothesis that the resin vaporizes is actually a reasonable one in view of the present study, but the investigation of the central damage modes showed that fibers survived the agression well beyond the resin vaporization and that the lightning arcs attached directly to those fibers. As a consequence the currents continue to flow along the top plies of the composite much longer than assumed. For this reason Hardwick's model gave better results when damaged cells were not removed from the computation.

## CONCLUSION

Several types of damage modes for protected CFC plates and their origins were clearly identified in this work. The damage mechanisms could be understood for most of these damage modes. In particular 0° and 90° bronze wire damage was shown to be due to A or D pulse components of lightning, and that under those loadings current flowing in the bronze wires triggered both the wire's fracture, the resin vaporization, and eventually the ejection of the whole wire by large fragments.

Fragmentation of type 1, another damage mode affecting the protective layer, occurred under A or D pulse component loading, and resulting current concentrations in the carbon fiber ply at 0°/90° bronze mesh nodes triggered resin vaporization which in turn triggered the ejection of the chunk of protective layer located directly above. Fragmentations of type 2 and 3 of the protective layer were described as well but were not fully explained.

The continuous C* component in an attachment test results in a very local damage where several damage modes of increasing severity can be observed. First the resin only melts, then, closer to the energy source, it vaporizes fast enough and breaks surrounding carbon fibers as it flows out of the plate. Finally, the damage is most important in small spots where the arc had directly attached, and where even carbon fibers are severely damaged.

Both damage mode identification and phenomenological interpretation showed that the whole damage evolution is very complex. These results already enable us to understand the results of past modelization studies. They also suggest a route to develop a comprehensive thermomechanical damage simulation capability, although additional observations are necessary to gain a more complete understanding of the physics of direct effects particular to different materials and different protection strategies.

## ACKNOWLEDGEMENTS

This work has been possible thanks to a cooperation between Aerospatiale - Centre Commun de Recherche, and SRI International - Poulter Laboratory who provided financial and experimental support, and material and scientific support, respectively. Special thanks to Mr. Bruno Lepetit and Mr. Franck Uhlig for their fruitful suggestions regarding this work and this paper.

REFERENCES

1. G.W. Reid, "Mechanical Damage to Aircraft Structures from Lightning Strikes". Proceedings of the Institution of Mechanical Engineers, Part G - Journal of Aerospace Engineering, Vol. 207, no G1, pp1-14, 1993.

2. P.F. Little, A.W. Hanson, and J.A. Dobbing, "Arcs on Metal Sheets in Simulated Lightning Discharges". Proceedings, IEEE International Symposium on EMC, Seattle, USA, pp. 375-380, 1977.

3. V.A. Avrootskij, I.M. Sergievskaya, E.G. Sobolevskaya, "Electrical Characteristics of Graphite Epoxy Composites and their Lightning Protection". Proceedings, 20th International Conference on Lightning Protection, Interlaken, Switzerland, pp5.3/1-5.3/3, 1990

4. N. Jennings, C.J Hardwick, "A Computational Approach to Predicting the Extent of Arc Root Damage in CFC Panels". Proceedings' Addendum, 15th International Aerospace and Ground Conference on Lightning and Static Electricity, Atlantic City, USA, pp41.1-41.8, 1992.

5. P. Gondot, J-P. Avenet, R. Haug, G. Hartmann, P. Levesque, "Experimental and Theoretical Analysis of Thermal Sparks in Composite Fuel Tanks". Proceedings, 16th International Aerospace and Ground conference on Lightning and static Electricity, Mannheim, Germany, pp161-168, 1994.

# RELIABLE SIMULATION OF METAL SURFACE PENETRATION BY LIGHTNING CONTINUING CURRENTS*

W. Zischank and F. Drumm
Universität der Bundeswehr München
Fakutät für Elektrotechnik, ET/7
D-85577 Neubiberg
Germany
Telephone: ++49 89 6006 3721 FAX: ++49 89 6004 3723

R. J. Fisher, G.H. Schnetzer, and M.E. Morris
Sandia National Laboratories
Electromagnetic Analysis and Test Department
P.O. Box 5800-0865
Albuquerque, NM 87185, USA
Telephone: 505-845-8647 FAX: 505-844-7857

## ABSTRACT

A program with the ultimate aim of quantifying the fidelity of laboratory test techniques used to simulate the penetration of metallic surfaces by lightning continuing currents has been undertaken. Descriptions of the program methodology, dominant factors found to influence test results, and data obtained so far are given. Based on considerations of fundamental arc phenomenology and on the acquired experimental data, a standard test configuration has been established, which has been demonstrated at two independent laboratories to produce consistent results that are generally corroborative of techniques suggested elsewhere in the lightning literature.

## INTRODUCTION

Of specific interest to Sandia National Laboratories is the assessment and reduction of the potential safety threat posed by the penetration of metallic casings of munitions due to the direct attachment of lightning strikes. Laboratory tests using the Sandia Lightning Simulator (SLS) (1) have resulted in the complete penetration of even relatively thick materials, such as 3.8-mm stainless steel, using severe but credible lightning continuing currents. Of fundamental importance in the interpretation of such test results is the degree of simulation fidelity inherent in the test technique *vis-à-vis* corresponding natural lightning currents of the same magnitude and waveshape. The degree of damage produced at the interface of an electrical arc and a metallic surface is a complicated function of many physical factors. At the first order level, these include electrode and test surface materials, condition, and geometry; arc length and polarity; ambient pressure; and arc current parameters. Since the SLS replicates both typical stroke and continuing current components of natural lightning exceptionally well, it was felt that the uncertainties regarding test fidelity were dominated by the other listed factors.

To asses the validity of the Sandia test results, an attempt was made to quantify the correspondence of the laboratory test technique to the process of the attachment of natural lightning to metallic surfaces. To this end, during 1989 an extensive literature review was conducted (2). While this effort provided considerable insight into the major factors that are involved and revealed several aspects of Sandia's then currently employed test technique that deviated from those being used at other test facilities, no adequate audit trail quantitatively linking accepted test practices to real lightning arcs

*This work was partially supported by the U.S. Department of Energy under Contract DE-AC04-94AL85000.

was discovered. As a result, experiments were then designed and fielded during 1990 (3) and 1991 (4) in which aluminum, ferrous and stainless steel, copper and titanium samples were exposed to triggered lightning strikes. The acquired damage spots, correlated with the measured stroke and continuing currents that produced them, established a set of benchmark data points produced by real lightning arcs. The next step was an attempt to reproduce the same current waveforms in the SLS and compare results obtained in the laboratory using various combinations of test electrode geometries and spacings with those of the benchmark lightning damage samples. Several important results reported earlier (eg., 5, 6) were confirmed, and additional quantitative data were obtained. The main conclusions at the time were as follows: damage is a very strong function of the waveform of the applied current, and total charge transfer is a completely inadequate test specification for lightning assessments; at least over the range of continuing currents of peak amplitudes of 200 to 700 A, results are qualitatively independent of the electrode geometry (pointed tungsten or tungsten with an electrode jet diversion feature, hereafter referred to as an *indirect electrode*) but are more consistent on a shot-to-shot basis using the indirect electrode; over the same current range, which represents the limits of the Sandia continuing current generator, the results are qualitatively independent of interelectrode spacings from 1.3 to 2.5 cm; and, finally, qualitatively good to excellent replication of the triggered lightning damage spots were obtained for Al, Cu, ferrous and stainless steel in terms of radius and appearance of the corresponding damage spots. A tentative "standard" test configuration using the jet diversion electrode, a dielectric arc spot restricting aperture over the test surface, and an interelectrode gap of 2.5 cm was established on the basis of the preliminary results.

Unfortunately, during these experiments it became immediately evident that, for any given test electrode configuration and spacing, the waveshape of the applied current was the dominant factor controlling damage. Limitations of the Sandia continuing current generator, which produces an exponentially decaying current with an approximately 0.5-s decay constant, would not allow a close enough reproduction of the recorded triggered lightning currents to permit the desired direct calibration of laboratory results vs. real lightning damage spots.

A collaborative effort was then initiated with the University of the Armed Forces in Munich (UAFM) in which a systematic series of tests was performed by them using their laboratory capability for producing constant current waveforms of up to 1-s duration over a range of 50 to 1000 A. The specific objectives of these tests included the independent confirmation of the earlier results related to electrode geometry and spacing, and the development of a detailed data set against which an advanced two-dimensional thermal transport model of lightning spot damage could be subsequently validated. If this validation is achieved for the constant current data spots, the model will then be driven by the measured triggered lightning current, thereby being further validated against the benchmark spots produced by real lightning. The final step will be to compare results from the (presumably) validated model driven by time varying current waveforms realizable in the laboratory against test results acquired with those same currents. In this way, an indirect quantification of the uncertainty bounds on the fidelity of laboratory test results obtained with any arbitrary specified current waveform will be achievable.

The remainder of this paper represents the first report of the data and overall conclusions obtained so far from the constant current experiments carried out by the UAFM. In effect, we present here a snap-shot report of an on-going effort.

## ELECTRODE JET PHENOMENON

Due to the limited source voltage available in laboratory simulations of continuing currents, in order to sustain an arc it is necessary to position a test electrode, referred

to hereafter as a *counter electrode*, close to the specimen under test. This represents a major departure from a natural lightning attachment to such a surface. As has been documented earlier (e.g., 5, 7), the interaction of jets of ions and vaporized material originating from the surfaces of the counter electrode and specimen surface can cause shot-to-shot inconsistencies and either over- or undertesting with respect to effects produced by natural lightning of the same current parameters.

An explanation of the electrode jet was first given by Maecker (8) based on magnetic self compression in an arc and the development of a strong net longitudinal pressure gradient in the vicinity of the arc root on an electrode surface. Since this explanation has not been found elsewhere in the lightning technical literature, it is summarized here.

Current flowing in a straight conductor is surrounded by an azimuthal magnetic field **H.** A volume element of this conductor carrying a current density **j** undergoes a perpendicular force **F** ($N/m^3$) given by the Lorentz relationship

$$\mathbf{F} = \mathbf{j} \times \mathbf{B} \tag{1}$$

where **B** is the magnetic flux density given by $\mathbf{B} = \mu\mathbf{H}$. The force **F** and the resultant magnetic pressure on the conductor is everywhere radially inward. For a solid conductor, it is of negligible significance. In the case of an arc burning in a compressible gas, however, this force works in a direction to constrict the arc channel until an equilibrium point is reached between the inward magnetic force and the internal kinetic pressure p of the heated gases within the column; that is:

$$\text{grad } p = \mathbf{j} \times \mathbf{B}. \tag{2}$$

For a symmetric arc (Figure 1) carrying a constant current density $j = i/(\pi R^2)$, the inward pressure as a function of the radius r from the center of the arc can be calculated (8) as

$$p(r) = p_o \cdot \left(1 - \frac{r^2}{R^2}\right), \quad p_o = \frac{\mu_o \cdot i^2}{4\pi^2 R^2} \tag{3}$$

with $p_o$ being the pressure in the arc center, where r = 0. From Eqn. 3 it is seen that the magnetic pressure is inversely proportional to the cross sectional area ($\pi R^2$) of the arc.

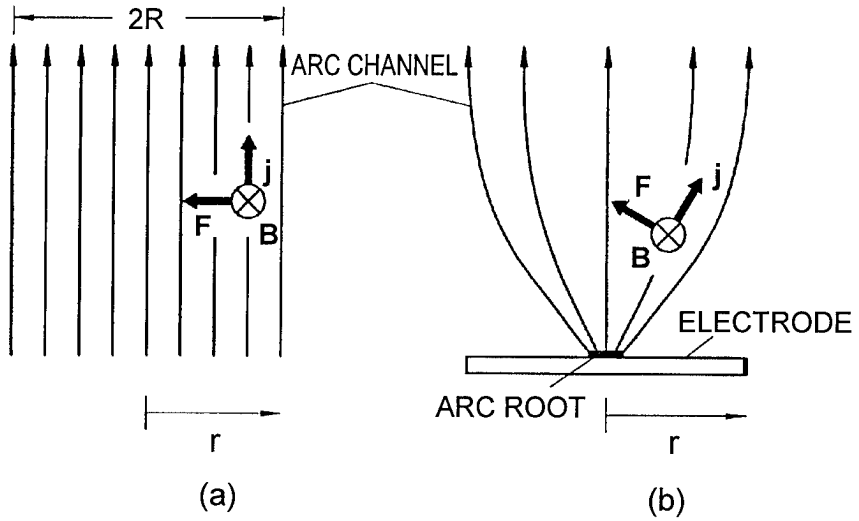



Figure 1. (a) Symmetric arc with constant current density; (b) constriction of arc root at an electrode spot

This relationship plays a crucial role in cases in which the radius changes along the length of the arc, such as in the vicinity of the attachment point at the electrode surface, where from experimental observations, it is well known that the arc root radius is very much smaller than the body of the arc column elsewhere. This behavior is shown in Figure 2 for a 200-A arc to a flat electrode. The constriction of the arc root is consistent with the *minimum principle* (9) known for arcs: Conditions in an arc, like temperature and radius, adjust to minimize arc voltage and thermal losses. The temperature on a metallic surface under a fully developed electrode spot is slightly above the boiling point of the electrode material (approximately 2600°C for aluminum, for example); while that within the arc column away from the surface is of the order of 10,000°C. To minimize thermal losses from the channel into the electrode material, the arc root constricts, thereby reducing the contact area (10). This constriction reaches a limit set by the maximum ion density carried by the arc (9).

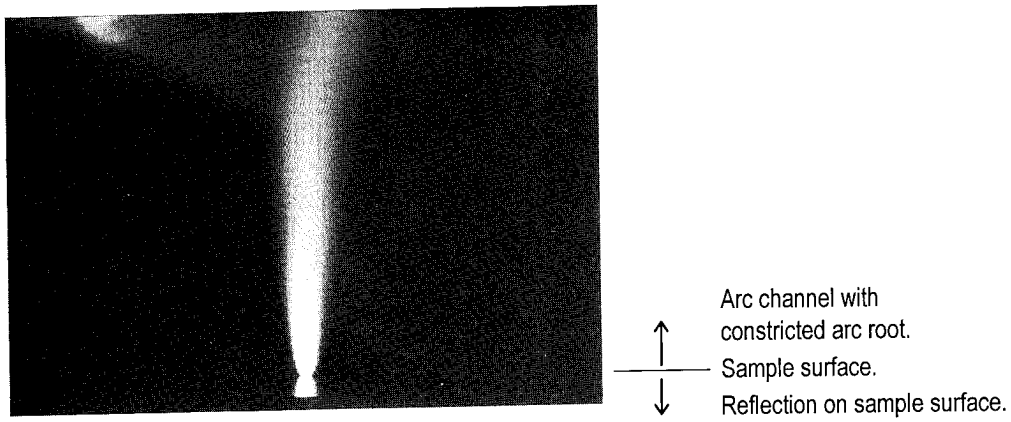



Figure 2. Arc root behavior at a copper electrode surface of a fully established 200-A arc burning in air at atmospheric pressure

## TEST EQUIPMENT

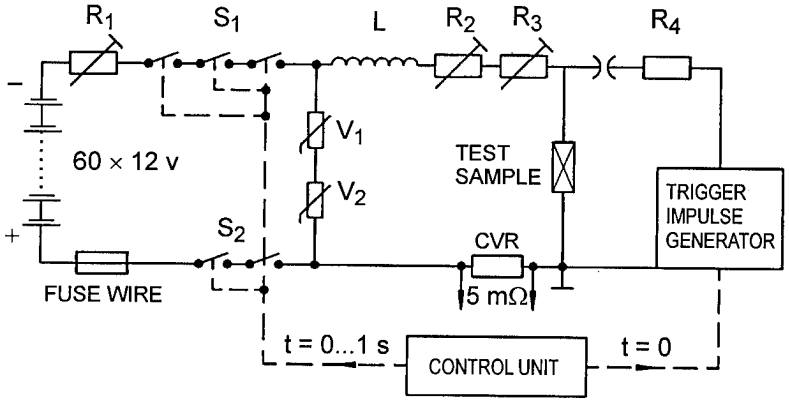
CONSTANT CURRENT GENERATOR–In addition to many other factors, erosion of metal surfaces is a strong function of the amplitude and waveform of the applied current. In the process of validating a thermal spot damage model, it is therefore advantageous to employ initially data produced under constant current conditions. The design of the UAFM constant current generator is shown in Figure 3. It consists of a set of 60 12-V car batteries connected in series. The current flow is initiated by a low energy impulse generator. The current amplitude is set between the limits of about 50 and 1000 A by adjustable damping resistors ($R_1$, $R_2$, $R_3$). An inductor L is used to decouple the trigger pulse from the batteries and to stabilize the arc current. The duration of the current (up to 1 s) is set by a control unit, which opens the circuit breakers $S_1$ and $S_2$. $S_1$ is a commercial DC circuit breaker (Siemans 3WE 13) with its three poles connected in series. $S_2$ is a pneumatically operated two-pole switch. An example of the resulting current is given in Figure 4.

TEST SETUP–The samples were all tested in the horizontal plane to eliminate the effects of gravity on the molten metal pools produced on the test specimens. The test setup was arranged with six symmetric quasi-coaxial current return conductors (Figure 5) to balance magnetic force effects on the arc. The specimens were fixed in a sample holder as shown in Figure 6. Each sample had a diameter of 70 mm and a thickness of 5 mm. To enhance the stability of the arc root, a restricting aperture of dielectric material was laid directly onto the surface of the sample. From preliminary tests with different dielectric materials, it was found that 1-mm-thick Micarta™

performed best for this purpose. Other candidate materials such as mylar and Teflon exhibited a tendency to burn away and produce turbulent gases, which rather than helping to stabilize the arc root at a fixed spot sometimes resulted in just the opposite.

## TEST RESULTS

The UAFM constant current generator was employed in three test series to investigate the following issues related to melting of metal surfaces: the influence of the electrode/gap configuration, the influence of the electrode jet on the arc root, and the achievable test-to-test repeatability under fixed conditions. To permit eventual comparison with the benchmark samples exposed to negative triggered lightning flashes, polarity was chosen such that the test samples formed the anode; that is, the counter electrode was connected to the negative output terminal of the current generator.




$R_1$ = 0...1 Ω : NiCr resistor
$R_2$ = 0...4 Ω : NiCr resistor
$R_3$ = 0...12 Ω: Carbon resistor
$R_4$ = 200 W
L = 5 mH
$V_1$, $V_2$: Varistor, 30 mm disc, 550 V

Figure 3. Square-pulse, constant amplitude current generator employed in the present experiments

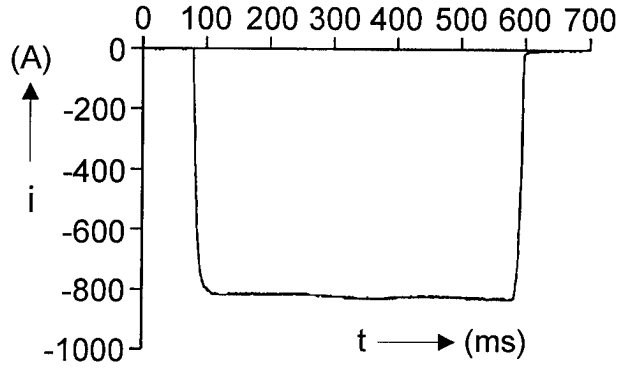



Figure 4. Example output current from the generator shown in Figure 3

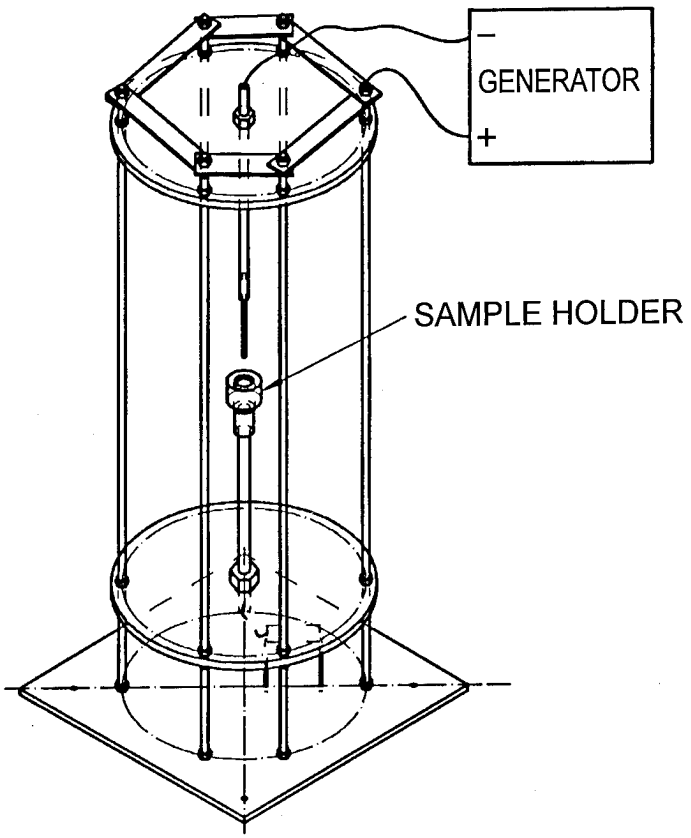



Figure 5. Simulated lightning continuing current test arrangement

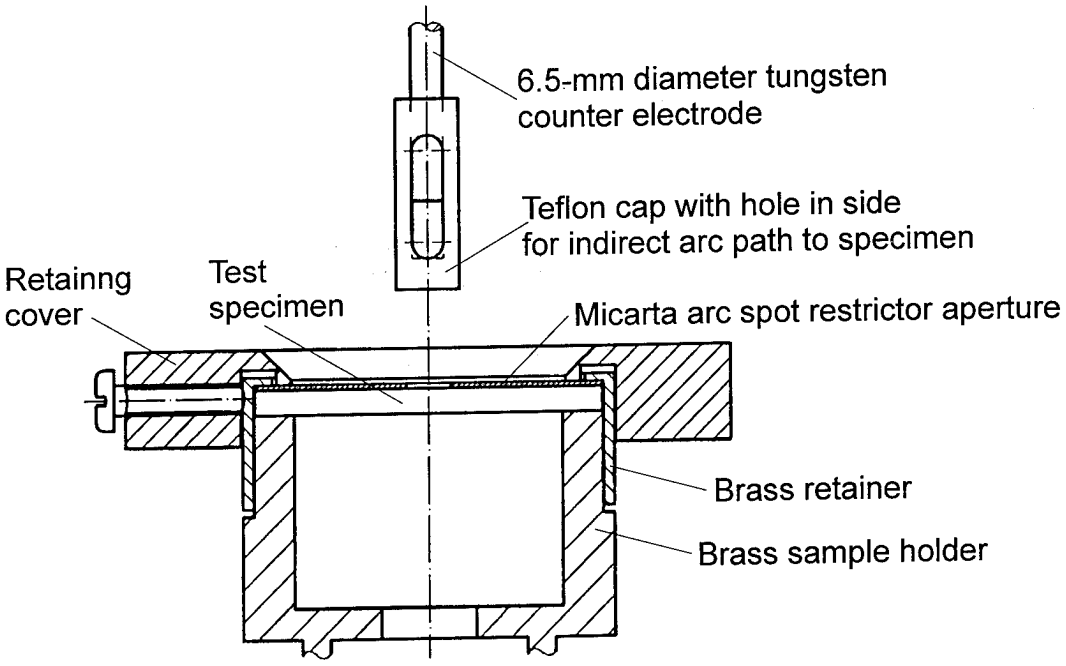



Figure 6. Cross-sectional detail of metallic disk sample holder and jet diverting electrode used during the present experiments

INFLUENCE OF ELECTRODE AND GAP CONFIGURATION–From earlier experiments (eg., 5, 6) it was well known that the interaction of electrode jets from the test specimen and the counter electrode can significantly influence test results. In principle, these effects can be minimized by either increasing the gap spacing or using an indirect counter electrode designed to divert its jet away from the sample. These alternatives were evaluated by examining the resulting melted pool diameters they produced on four materials: aluminum, copper, ferrous steel, and stainless steel. (Depth of the melt front is also being determined from the sectioned samples, but these data are not as yet available.)

Two types of counter electrodes were investigated: a bare 6.5-mm diameter, flat tipped tungsten rod, and an indirect electrode of the design illustrated in Figure 6. For each type, the gap spacing was varied between 0.5 cm and 6 cm. Tests were conducted at nominal current levels of 200 and 800 A, in each case with a 0.5-s square pulse waveshape. After initial trials, the diameter of the restricting aperture was chosen to be 15 mm for the tests at 200 A and 20 mm for those at 800 A, the larger diameter having been selected for the latter case to avoid the piling up of molten material at the rim of the restrictor. Test results are presented in Figure 7, showing the molten area on the metal surface as a function of the gap spacing for both types of electrodes at each of the two test current levels. In each case, the area was determined by manually

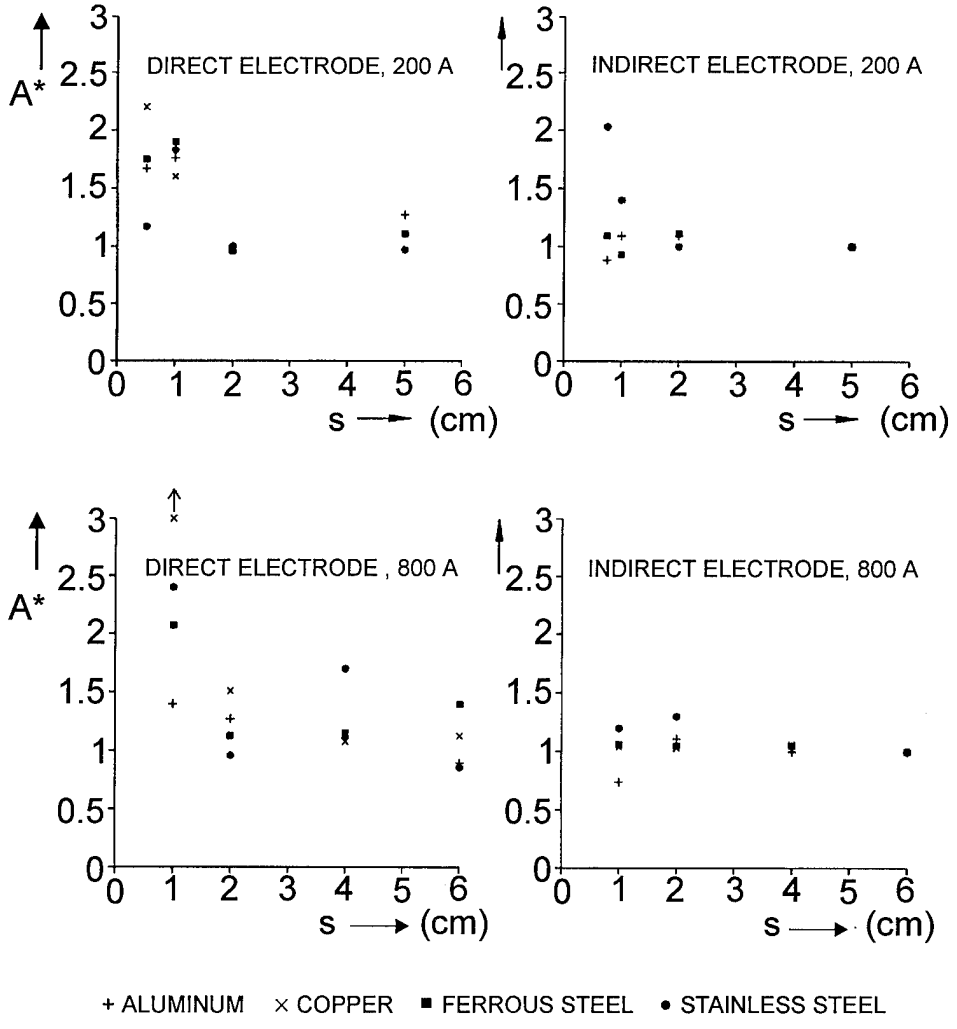



Figure 7. Normalized molten spot areas as a function of interelectrode gap length

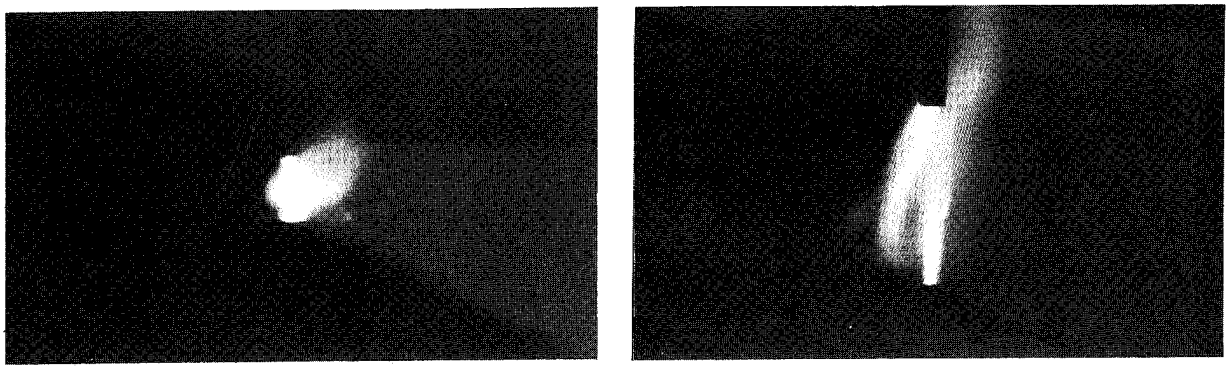
measuring the long and short axes of the spot with a capillar rule and then estimating the total area based on the relationship for the area of an ellipse. More precise determinations are in the process of being generated, but they are not as yet available. In Figure 7, the values of the molten area for the four materials are normalized in each case to the area resulting from the indirect electrode at the maximum gap spacing employed. All aluminum samples were fully penetrated at the 800-A level.

From the data of Figure 7, it can be concluded that at 200 A the spot size becomes independent of the electrode spacing for gaps of about 2 cm and greater for both the direct and indirect counter electrode types. At 800 A, however, the spot size for the direct electrode is still dependent on the gap spacing at 6 cm, while for the indirect electrode, the spot size stabilizes at 2 cm or greater.

INFLUENCE OF THE ELECTRODE JET ON THE ARC ROOT–During the first test series described above it was found that in a significant number of cases the arc root was unstable on the surface of the sample. Visual inspection revealed that the arc either jumped around on the surface, resulting in two or more separate spots (especially for copper), or wandered around leaving a continuous track rather than a discrete spot. It was therefore decided to investigate the arc root behavior under the influence of the interaction of the electrode jets in a second test sequence using a VHS video recording system. The camera was operated in a stroboscopic mode, yielding a 1-ms image every 20 ms. These qualitative tests were performed on copper samples at a current of 200-A amplitude and 0.5-s duration.

From the initial video images, it was observed that for a gap spacing of more than 2 cm the arc did not originate at the center of the test sample, but rather at the rim of the restricting aperture, presumably due to electric field distortion at the edge of the dielectric material. Later, under the influence of the symmetric magnetic field within the test volume, the arc would migrate to the center of the sample leaving a track of molten material behind. To avoid this in the following tests, a *guide wire* of 0.1-mm diameter copper was used. This wire was carefully aligned over the center of the sample, terminating about 10 mm above its surface.

From the video records made under these conditions, it was found that there are two major implications of the interaction of the electrode jets from the counter electrode and the specimen surfaces. First, the interaction can result in a more-or-less symmetric disk-like formation between the two electrodes (Figure 8a). Such a disk usually occurs in very short gaps (10). The resulting strong jet in the radial direction can blow out a significant amount of molten material from the pool. If this same material were to



(a) (b)

Figure 8. Observed behavior of jets involving a direct counter electrode (a) disk-like formation with strong radial jet; (b) interaction of jets forcing each other out of the center of the gap

remain in the pool, it would be further heated and ultimately vaporized. However, the energy needed to accomplish this is about an order of magnitude more than that required for melting alone (11). Hence, if the molten material is removed artificially by the jet action, a larger spot size results for a given amount of energy input to the surface; that is, an overtest results.

Secondly, for longer gaps of a few centimeters or so, the disk formation no longer occurs. Rather, the two electrode jets interact in a manner in which they tend to force each other out from the center of the gap volume (10). This results in severe turbulence of the arc column (8), causing the arc root to skip around erratically on the surface of the sample. This dispersion of the incident energy over multiple spots reduces the depth of maximum penetration that would have occurred had the arc remained stationary in a single spot, and an undertest results. In either case, it is evident that elimination of electrode jet interaction is a fundamental requirement for improving the fidelity of lightning penetration simulations in the laboratory. The effectiveness of the indirect electrode configuration in diverting the jet from the counter electrode, thereby suppressing this undesirable behavior, is demonstrated in Figure 9.

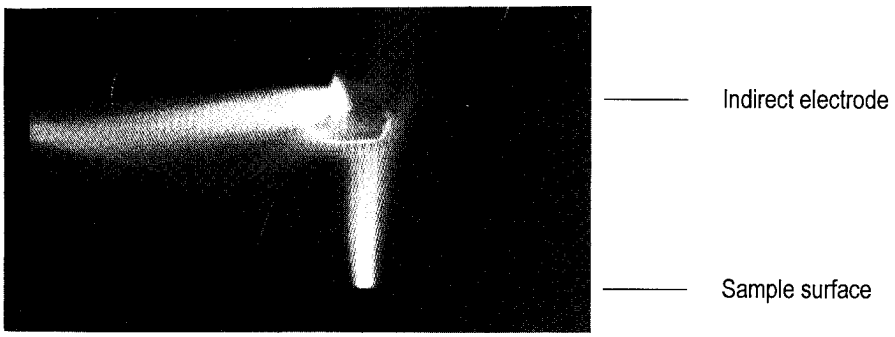



Figure 9. Diversion of jet from an indirect counter electrode configuration

STANDARD TEST CONFIGURATION–On the bases of the measured spot sizes as functions of electrode type and gap spacings and on the video records of electrode jet behavior, the following "standard test configuration" was established. All samples were tested in a horizontal position to avoid gravity effects on the pool of melted material. To avoid electrode jet interactions, the use of an indirect electrode with an interelectrode spacing of 5 cm was chosen. To suppress arc root migration and keep it stabilized at a single attachment point on the surface, the use of a heat resistant dielectric restrictor aperture, having a diameter of about 10-mm greater than the expected spot size, was employed. Finally, to enhance the probability of the development of a single, stabilized attachment point at the center of the specimen, a fine copper guide wire of 0.1-mm diameter was used, which terminated 10 mm above the sample.

CONSISTENCY OF TEST RESULTS–To evaluate consistency of the test results achieved with the above defined standard test configuration, ten consecutive tests were performed at both 200 and 800 A on samples of each of four materials: aluminum, copper, ferrous steel, and stainless steel. To avoid full penetration of the aluminum at the 800-A level, the duration of the current was reduced to 160 ms. The pulse width of the current in all the other tests was 500 ms to allow maximum time for possible arc root movement. The mean values of the resulting molten areas, their standard deviations over the ten tests, and the corresponding maximum and minimum spot sizes are given in Tables 1 and 2, which correspond to the two different test current amplitudes. At 200 A, the arc root wandered on the surfaces of two of the copper samples, the data from which are excluded from Table 1. For ferrous steel at 800 A, only five samples were tested.

Table 1. Consistency of molten spot sizes at 200 A

| Material | Mean value ($mm^2$) | Standard Deviation | Maximum | Minimum |
|---|---|---|---|---|
| Aluminum | 29.4 | 7.9% | +16% | -10% |
| Copper | 6.35 | 8.0% | +10% | -13% |
| Ferrous steel | 40.7 | 5.1% | +7.1% | -5.5% |
| Stainless steel | 34.9 | 13% | +27% | -18% |

Table 2. Consistency of molten spot sizes at 800 A

| Material | Mean value ($mm^2$) | Standard Deviation | Maximum | Minimum |
|---|---|---|---|---|
| Aluminum | 51.3 | 7.2% | +13% | -9.3% |
| Copper | 56.2 | 2.3% | +3.4% | -3.8% |
| Ferrous steel | 134 | 5.3% | +5.0% | -7.3% |
| Stainless steel | 143 | 6.9% | +7.3% | -14% |

REFERENCES


1. White, R.A., "Lightning Simulator Circuit Parameters and Performance for Severe-Threat, High-Action-Integral Testing," Int. Conf. on Lightning and Static Electricity, Orlando, June 1984.

2. Fisher, R.J. and M.A. Uman, "Simulation Fidelity in Lightning Penetration Studies," SAND89-3051, February 1990.

3. Fisher, R.J. and G.H. Schnetzer, "Damage to Metallic Samples Produced by Correlated Measured Lightning Currents," Int. Conf. on Lightning and Static Electricity, Cocoa Beach, April 1991.

4. Schnetzer, G.H. ad R.J. Fisher, "1991 Rocket-Triggered Lightning Test of the DoD Security Operations Test Site (SOTS) Munitions Storage Bunker, Ft. McClellan, Alabama," SAND91-2343, February 1992.

5. Dobbing, J.A., A.W. Hanson, and P.F. Little, "Simulated Lightning Attachments to Aircraft Skins," IEEE Gas Discharge Conf., 1978.

6. Little, P.F., A.W. Hanson, and J.A. Dobbing, "Arcs on Metal Sheets in Simulated Lightning Discharges," IEEE Int. Symposium on EMC, Seattle, 1977.

7. Kern, A., "Simulation and Measurement of Melting Effects on Metal Sheets Caused by Direct Lightning Strikes," Int. Conf. on Lightning and Static Electricity, Cocoa Beach, April 1991.

8. Maecker, H., "Plasmaströmungen in Lichtbögen infolge eigenmagnetischer Kompression," Zeitschrift für Physik, Vol. 141, 1955 pp. 198-216.

9. Rieder, W., "Plasma und Lichtbogen," Vieweg Verlag Braunschweig, 1967.

10. Burkhard, G., "Schaltgeräte der Elektrotechnik," VDE Verlag Berlin Offenbach, 1985.

11. Zischank, W., "Funkenstrecken zur Überspannungsbegrenzung bei direkten Blitzeinschlägen," Dissertation, Universität der Bundeswehr München, 1983.

# FUNDAMENTAL PRINCIPLES OF GROUND-BASED LIGHTNING PROTECTION SYSTEMS

## PART I

## The Grounded Franklin Lightning Rod

**Richard Briët, Ph.D.**
**LT-MP Applications**
5661 Citrus Court
Cypress, CA 90630
Phone/Fax: (714)-826-8490

ABSTRACT

The widely accepted concept of lightning protection zones around the foot of tall structures[1] is based on direct observations of natural, and simulated lightning. Until now, the physics that explains the size and the shape of protection zones is not well understood. We note that both the Lightning Protection Code[2] in NFPA 780, and the International Standard, IEC 1024, ignore the electrical properties of the structures that attract lightning.

This is the first of two companion papers about the theory of lightning protection systems. It introduces the proven principle of Least Action (due to Euler and Lagrange, and applied by Fermat as the principle of least time) as the governing principle of the propagation of a lightning step leader. When combined with the statistical interpretation of the physical world around us, we discover a new principle, or perhaps found just a different way to look at physics. We have called it: "the **L**east **T**ime - **M**aximum **P**robability (**LT-MP**) principle".

In this paper we introduce the key elements for the fundamental theory of lightning propagation, and we claim that the theory correctly describes lightning interactions with nearby structures. It is the basis for the development of new lightning analysis tools. Following a brief description of the fundamental concepts, we write the general expression for all possible channels of a step leader, and we show that the **LT-MP** principle is a selection rule for finding the most probable lightning channel, and the most probable attachment point on the ground, or on nearby structures! In particular, we will demonstrate that the theory reveals the existence of lethal zones, and that these are inseparable companions of the protection zones near the base of standing structures.

Of particular interest is the introduction of (1) an effectiveness coefficient, in terms of which the quality of a lightning protection system is quantified, and (2) the subsequent discovery, and stern warning to the community that there are protection systems that are not as effective as conventional wisdom says they are. To conclude this paper, we show what makes Lightning Protection Zones collapse. In the companion paper we generalize the theory, and apply the tools introduced in this paper to (1): perform trade studies, (2): to evaluate the effectiveness of existing lightning protection systems, and (3): to show how new designs are optimized before they are constructed.

---

[1] See "The Lightning Protection Code," in NFPA 780, Section 3-10, 1992, or the International Standard, CEI/IEC 1024-1: 1990, "Protection of Structures," Part 1: General Principles.

[2] NFPA 780, USA, implements the Franklin LPS; IEC 1024, rest of the world, implements the Faraday Cage LPS. Ref.: Norman H. Davis, Deputy Technical Advisor for TC 81, private correspondence, 8/8/95.

THE FUNDAMENTAL PRINCIPLE OF LIGHTNING PROPAGATION

***Lightning follows the path of Least Time***
***because***
***It is the path of Maximum Probability***

This is the fundamental principle which governs the propagation of lightning: We have called it "**the LT-MP** principle." The LT-MP principle combines Fermat's Principle of **L**east **T**ime[1] with the statistical interpretation of the laws of physics, according to which any outcome of a physical measurement, such as an observation, shows statistical behavior. In nature, all is possible, but all is not equally likely. The LT-MP principle states that:

*The proportionate number of similar outcomes in a large number of measurements,* including the simple acts of observing a phenomenon, *is inversely proportional to the time it takes to complete the process that makes the phenomenon observable* (i.e. measurable).

This is a tautology that simply states: "**What is seen most often, is what occurs most often, and vice versa[2]".** The first half of the LT-MP principle takes us to classical statistics; the second half relates to the proven[3] Euler/Lagrange principle of least action, or Fermat's principle of least time. In lightning the process is the transport of an ensemble of charged particles from a source region (that is the region where lightning originates) to a drain region (that is the region of its destination): *the process involves many channels.* Amongst these, the main channel is the channel which conducts the majority of the particles: it is the channel through which the transport of charged particles is completed most often. Some particles move slowly, others move much faster than average in the aggregate of particles. However, for any velocity distribution function, most particles propagate near the average velocity. Therefore, the minimum time for the majority of particles to complete the journey between the source and the drain region is found by dividing the minimum distance by the average velocity of propagation, i.e.:

$$\tau_j(p)_{\min} = \frac{minimum \cdot distance \cdot traveled}{average \cdot velocity} \quad . \qquad (01)$$

The index, *"j"*, identifies a specific channel, and the parameter *"p"* allows us to apply the variational principle to identify the most likely channel. Thus, the LT-MP principle is a selection rule for finding the main lightning channel, and the **maximum probability** that lightning strikes a specific target in the region is given by:

$$P_j(p)_{\max} = \frac{\left[1/\tau_j(p)_{\min}\right]}{\sum_{allk}\left[1/\tau_k(p)_{\min}\right]} \quad , \qquad (02)$$

where the normalization factor, $N$ , counts all other targets in the region. It is given by:

$$N = \sum_{allk}\left[1/\tau_k(p)_{\min}\right] \qquad (03)$$

---

[1] Fermat's Principle of Least Time is one representation of the Principle of Least Action.

[2] An alternate statement for the LT-MP principle is: *"What is seen most often is what is there most often, and vice versa."* When something already exists, then the time to complete the process to put it at its fixed location is zero, and according to **Equation (02)** the probability that we will find it at its fixed location is arbitrarily close to one, which implies certainty.

[3] With "proven", we mean that the outcome of most observations in physics are consistent with Fermat's principle

## THE EFFECTIVENESS COEFFICIENT, $E_{bf}$

We introduce the concept of a *"relative probability"* to compare the probability of a lightning channel passing through a structure *"b"* with the probability that it follows an *other* channel by way of a different structure *"f"*. It is given by:

$$E_{bf}(p) = \frac{P_b(p)}{P_f(p)} = \frac{\tau_f(p)}{\tau_b(p)} \qquad (04)$$

For the special case where *"b"* refers to a lightning protection structure, and *"f"* refers to the ground (like in cloud-to-ground lightning), the relative probability measures the effectiveness of that structure to attract nearby lightning onto itself. For this special case, the relative probability is called the **effectiveness coefficient**. Where the effectiveness coefficient is greater than one, the probability that an object is struck by lightning is better than 50%, and the region is called a "lethal zone". Likewise, where the effectiveness coefficient is less than one, the probability that the object is struck by lightning is *less* than 50%, and the zone is called a "safe zone". If relative safety is provided by a nearby structure, the "safe zone" is called a "zone of protection", and the structure that provided the protection is called the "primary structure". All nearby structures that are protected by a primary structure are called "secondary structures". A LPS is called *"Effective"* if its effectiveness coefficient, $E_{12}$, is greater than one: it is called "ineffective" (or *"defective"* ) if $E_{12}<1$. On the basis of these concepts we can derive expressions for the shape and size of lethal zones: the results show that *lethal zones and protection zones are inter-dependent*, i.e., one cannot exist without the other.

## PARAMETRIC EQUATION OF THE LETHAL ZONE

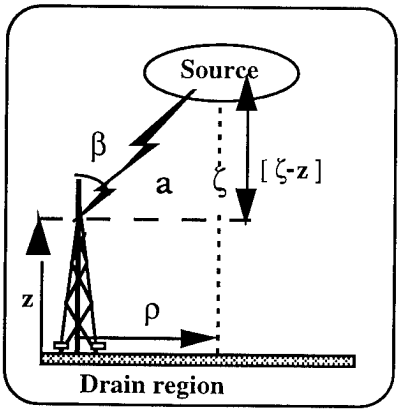



FIGURE 1 . TALL STRUCTURE ON FLAT TERRAIN.

In **Figure 1,** let $u_0$, and $u_s$ be the average velocities of propagation in air, and in the structure of a lightning protection system, respectively. We imagine a tower *"b"* standing on flat terrain, and assume that over the striking distance, (1) the atmospheric electric field is constant, and (2) the perturbation of this field by a step leader is negligible[1]. Let us further assume that a source region exists at an elevation, $\zeta$, above a point on the ground, which is located at a horizontal distance $\rho$ from the foot of the tower. The ground on which the tower stands is a homogeneous drain region. Let the electrical length of the tower be **z**, and let the length of the air channel be **a**. Then the travel time via the tower is:

$$\tau_b(z) = \frac{z}{u_s} + \frac{a}{u_o} = \left(\frac{1}{u_o}\right) \bullet \left(z \bullet \frac{u_o}{u_s} + \sqrt{(\zeta - z)^2 + \rho^2}\right) \qquad (05)$$

Using the variational technique to find the minimum time, where z is the variable , we find:

---

[1]This assumption guarantees that the acceleration of the charged particles in the atmospheric electric field, $\mathbf{a_E}$, is constant, and therefore, the distance traveled, $D$, is the average velocity, u, multiplied by the travel time, $\tau$, i.e.: $D = u_o \cdot \tau + \frac{1}{2} \cdot a_E \cdot \tau^2 = u \cdot \tau$, where $u = \frac{1}{2}\left(u_o + u_f\right)$, and $u_f = u_o + a_E \cdot \tau$.

$$\tau_b(z)_{\min} = \frac{\left(\zeta - \left(1-\cos^2\beta\right)\bullet z\right)}{u_o \bullet \cos\beta} \qquad (06)$$

where the constant angle of incidence, $\beta$, can be calculated from:

$$\cos\beta = \frac{u_o}{u_s} = \frac{(\zeta - z)}{\sqrt{(\zeta - z)^2 + \rho^2}} \qquad (07)$$

Similarly, the minimum travel time for a cloud-to-ground strike is given by:

$$\tau_0(\zeta)_{\min} = \tau_o = \frac{\zeta}{u_o} \qquad (08)$$

From **Equations (06)** and **(08)**, we find the critical height, $\mathbf{z_x}$, of tower *"b"*:

$$\mathbf{z_x} = \frac{\zeta}{(1+\cos\beta)} \qquad (09)$$

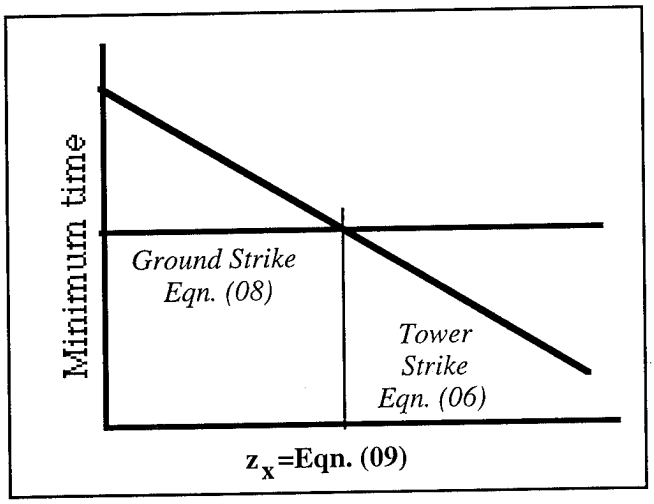



**FIGURE 2.** PLOTS OF EQN. (06) AND EQN. (08): LIGHTNING FOLLOWS THE PATH OF LEAST-TIME.

The corresponding critical distance is found from the substitution of **Equation (09)** into **Equation (07)**. It is given by:

$$\rho_x = \mathbf{z_x} \bullet \sin\beta = \frac{\zeta \bullet \sin\beta}{(1+\cos\beta)} \qquad (10)$$

These results paint the complete picture of what will happen, if a lightning storm passes over a flat area that supports a single, tall tower[1].

OBSERVING A PASSING LIGHTNING STORM

According to the **L T - M P** principle, *"lightning follows the path of Least Time, because it is the path of Maximum Probability"*. This is the selection rule for finding the most probable lightning channel. When lightning strikes a tower, *"b"*, **Equation (06)** shows that the minimum time is a linear function of its height, **z**. The minimum time for a cloud-to-ground stroke is given by **Equation (08)**: it is constant. Both equations are plotted in **Figure 2**. They intersect at $\mathbf{z=z_x}$, which is given by **Equation (09)**. **Figure 2** shows that tall structures are struck more often than short structures. This is what the LT-MP principle dictates. In other words, tall structures appear to attract lightning better than short structures. The effectiveness coefficient in **Equation (04)** enables us to say exactly how much better. For a tower that reaches the critical height, $\mathbf{z_x}$, the effectiveness coefficient, $E_{bo}(\mathbf{z_x})=1$, when the source region is at $\rho_x$. These results are consistent with actual observations. However, there is something special: **Equation (07)** tells us that *the angle of incidence is constant.* The interpretation is shown in **Figure 3**. According to the theory, when a storm

[1] When we say "tall", we mean "**h** is taller than $\mathbf{z_x}$."

approaches an erect tower, lightning will initially find its way directly to ground, and ignore the tower until it reaches the *critical distance*, $\rho_x$, given by **Equation (10)**. At this point, lightning may strike the tower, or the ground with equal probability. By definition, at this range the effectiveness coefficient is one. When the source region is inside the critical range, we find it inside the *cone of attraction*, and lightning will strike the tower above the critical height, $z_x$, at a constant angle of incidence, $\beta$, until the source is close enough to strike the tip of the tower. This occurs when the radius of attraction is $\rho_h$. Inside this range, the source region is said to be inside the *tracking cone*. As the storm passes through the tracking cone, the point of attachment will remain at the highest point of the tower. It will begin to creep down the tower, when the source region leaves the tracking cone. At the critical range, $\rho_x$, the attachment point is again located at the critical height, $z_x$. Outside the critical range, lightning seems to ignore the tower more than half of the time. Using **Equation (02)**, we can estimate the maximum probability of a direct strike to the tower. With a laser beam it is possible to create an ionized path in the atmosphere. Lightning is triggered when such a conducting path runs between a source region and a drain region. According to theory, when such an artificial lightning channel enters the cone of attraction, it will be deflected, and, to follow the path of least time, lightning must strike the tower at the critical angle of incidence, $\beta$. Researchers at the Osaka University in Japan said they often saw this effect. Ed Vance of SRI[1] told me that he observed the same effect years ago, using copper wire as the medium to conduct high amplitude arc discharges.

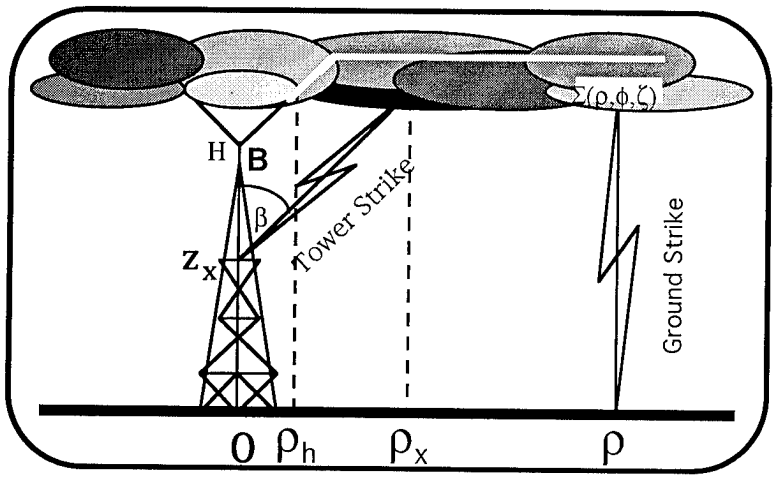



FIGURE 3. LIGHTNING STORM OVER AN ERECT TOWER.
The inverted cone with its apex at $z_x$ is the "Cone of Attraction". At the tip of the tower, the inverted cone is the "Tracking Cone". Superimposed on the diagram is a horizontal white trace in the clouds, which suddenly droops down to end up at "B". This trace represents LASER-triggered lightning discussed at the end of this section, and in Scientific American, Feb., 1993, p. 105.

## HOW TO FIND THE ZONE OF PROTECTION

The above description of a lightning storm passing through a region where a single tower stands in an open field is consistent with direct observations. But what we really need to know is how lightning propagates in an area that is populated with more than one structure. Until now, we have shown that lightning strikes a tall tower at a point $z_x$ above the foot of the tower, if the source region is at the critical range, $\rho_x$, from the base of the tower. In this case, the effectiveness coefficient is one. The question is: "could there be other structures for which the relative striking probability is the same?" Of course, the answer is "Yes!" All targets with equal effectiveness coefficients have by definition an equal chance of a direct strike from a fixed source region. To find these towers, we equate **Equation (08)** with **Equation (05)**. When we do this, we obtain the equation of an ellipse:

[1]Personal communications, Bordeaux, France, June, 1994.

$$\left(\frac{\rho}{\rho_x}\right)^2+\left(\frac{\zeta-z}{z_x}\right)^2=1 \qquad (11)$$

where $z_x$, and $\rho_x$ are given by **Equations (09)**, and **(10)**. This ellipse separates the space into the region inside the ellipse, where the relative probability of a direct strike to a single tower is greater than 50%, and a region outside the ellipse, where it is less than 50%. Based on these probabilities, we call these the **lethal region**, and the **safe region**, respectively. The ellipse in **Equation (11)** is called "the critical ellipse." Since a lightning storm could enter into the region from any direction, the plane of the ellipse could be oriented in any direction, and therefore, the interior of the solid of revolution of the critical ellipse about its vertical axis defines the **lethal zone**. The space outside the lethal zone is a relatively **safe zone**. Likewise, the solid of revolution of a quadrant of a tangent critical ellipse about a tall tower defines the **zone of protection**. They are all shown in **Figure 4.**

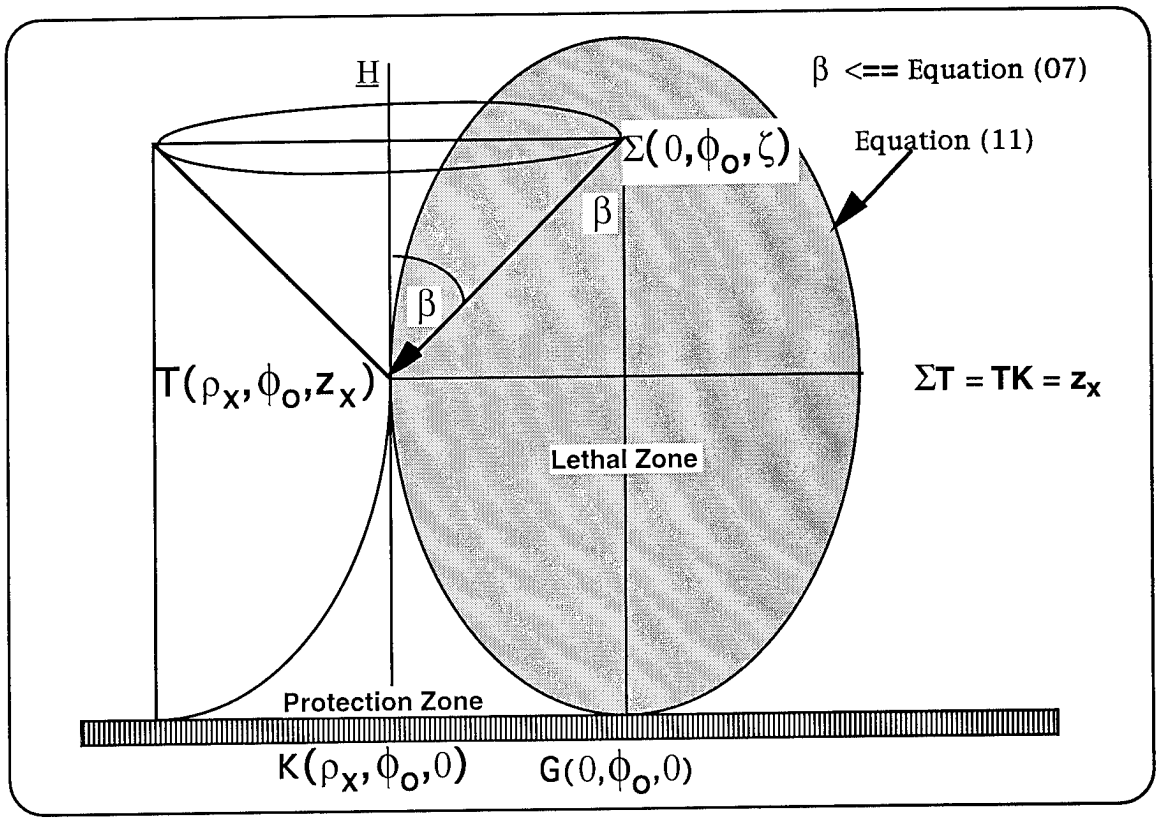



FIGURE 4. THE THEORETICAL LIGHTNING LETHAL ZONE.
The most probable lightning attachment point on a tall, erect tower whose base is located at $\mathbf{K}(\rho_x,\phi_o,0)$, and whose height, **H**, exceeds $z_x$, will occur at a point $T(\rho_x,\phi_o,z_x)$, provided that the lightning bolt originated from a source at $\Sigma(0,\phi_o,\zeta)$, where $\rho_x$=GK is the critical range, and $\zeta$ is the elevation of the source region above the ground. The solid of revolution of the shaded elliptical area about ΣG is the lethal zone; the volume inside the solid of revolution of arc (TG) about TK is the protection zone provided by the tower .

## COMPARISON WITH CONVENTIONAL ZONES OF PROTECTION

Concepts of protection zones date back at least four thousand years, but the conventional concepts of protection zones are just over one hundred years old.

There are many references that describe lightning protection zones. Representative ones are the following: "LIGHTNING, Vol. 2, Lightning Protection," R.H. Golde, ed., Academic Press, New York; 1977, p. 547; and "The Lightning Protection Code," NFPA 780, Section 3-10, 1992 edition[1], which is published by the National Fire Protection Association. **Figure 5** compares the LT-MP protection zone with two representative zones of protection. Whereas one may initially think that there is little difference between the spherical, and the ellipsoidal lethal zones, the diagram clearly shows that a rocket that is well within the conventional zone of protection, is in fact exposed, according to the new LT-MP theory! This result could be very disturbing. To say the least, a direct strike to a rocket on a launch complex may cause an explosion on the ground. Such an explosion may bring about a catastrophe that would not only destroy the rocket, but also the launch complex, all support structures, and surrounding areas within a radius of several miles! We even cannot begin to estimate the political fallout from such a disaster, but venture to say that the Challenger disaster would be small in comparison.

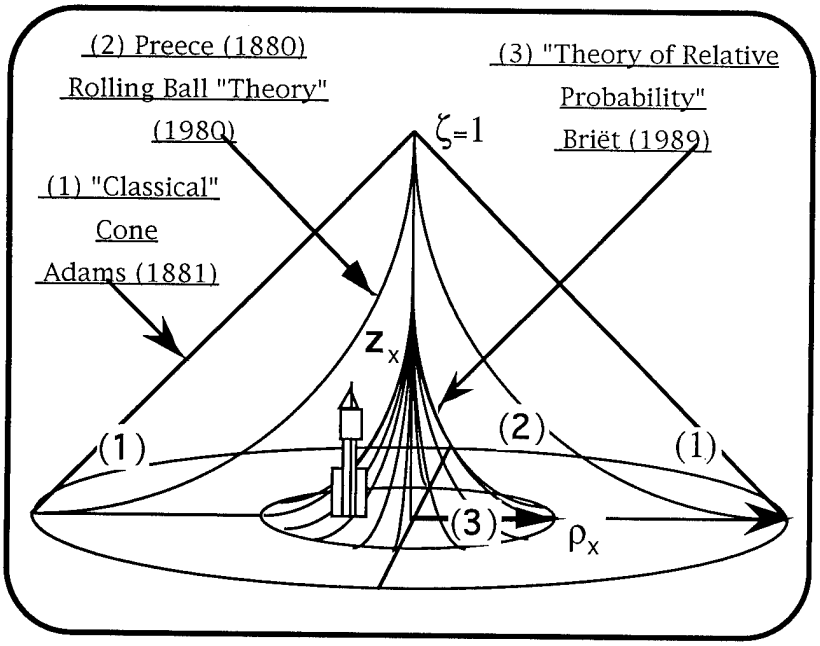



**FIGURE 5.** COMPARISON OF LIGHTNING PROTECTION ZONES:
1): Adams, 1881, and 45-degree cone in NFPA #78, 1945,
2): Preece, 1880, and Rolling Ball Theory in NFPA #780, 1992,
3): Lightning Protection Zone according to LT-MP Theory.
(Briët, 24 July, '89): β=45 degrees. Note the exposed rocket !!

## REVIEW OF LT-MP RESULTS

The *proven* principle of **L**east **T**ime, and classical statistics lead to the **L**east **T**ime-**M**aximum **P**robability principle. The LT-MP principle explains many lightning phenomena, in particular reveals the existence of lightning zones. In all of the above, we tried to shift the focus from the zones of protection to the lethal zones, because from this perspective it is easier to explain how lightning selects a most favorite target on the ground. The explicit expressions for the maximum probability, $\mathbf{P_{max}}$, and the effectiveness coefficient, $\mathbf{E_{12}}$, is the hub for new analytical tools to do trade studies, and for optimization algorithms for Lightning Protection Systems. Even at this early stage we showed that a flaw in the definitions of conventional protection zones may result in a preventable disaster. **Figure 6** is an illustration of this concern.

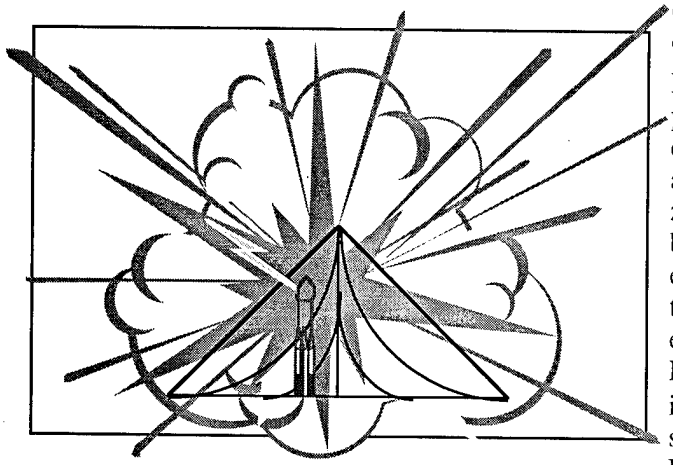


**FIGURE 6.** LT-MP CONSEQUENCES. Some lightning protection systems may leave secondary structures exposed to lightning because the conventional zones of protection are overly optimistic.

[1] NFPA # 780, 1992 supersedes all earlier versions of NFPA #78.

INTRODUCING THE COLLAPSING ZONE OF PROTECTION

We have defined the lethal zone as the solid of revolution of the critical ellipse about its vertical axis: the solid of revolution of a tangent quarter segment of the critical ellipse about the axis of an erect tower defines the zone of protection near the base of the tower. A comparison of the LT-MP protection zone with conventional protection zones showed that the quality of protection of most lightning protection systems is less than what is commonly believed. **Figure 6** shows what could happen, if we continue to build lightning protection systems on the basis of the conventional concepts of lightning protection zones. This problem is even worse for inclined structures. Moreover, we will show that an inclined, grounded lightning rod will completely lose its ability to attract lightning onto itself, when the angle of inclination, $\theta$, measured with respect to the vertical direction, equals $\beta$.

THE INCLINED, GROUNDED LIGHTNING ROD.

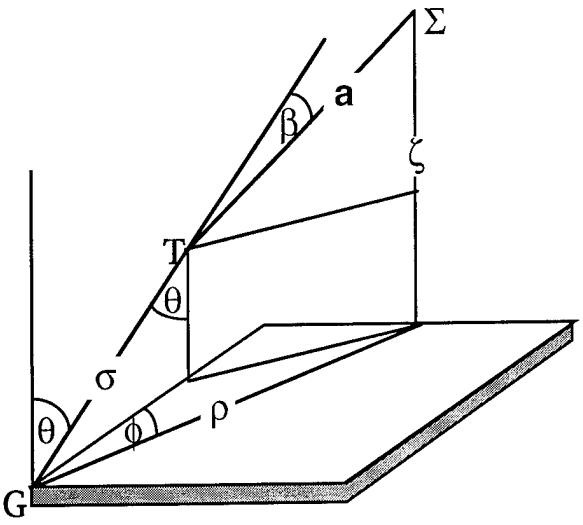



FIGURE 7. INTERACTION OF LIGHTNING WITH AN INCLINED TOWER. GT=σ; ΣT=a; inclination angle =θ; angle of incidence =β.

Consider a tall, inclined, and grounded rod rising up from the ground at a point **G** on flat terrain. For analysis purposes, we assume that the rod is perfectly rigid, i.e. we will ignore sagging. (See **Figure 7**.) We will also assume that a source region exists at $\Sigma$: it is located at an elevation of $\zeta$ above the ground, at a distance, $\rho$, from the foot of the rod, which is grounded at **G**. The inclination angle of the rod with the vertical is $\theta$. If a direct strike occurs, then lightning strikes the inclined structure at a point, **T**, where **GT** is $\sigma$. Let the vertical plane through the inclined tower be the reference plane, and let its intersection with the ground plane be the reference axis for a cylindrical coordinate system: its origin is located at **G**. Thus, in this coordinate system, the source region is at $\Sigma(\rho, \phi, \zeta)$. On the basis of the **LT-MP** principle we will determine the shape of the zone of protection, and the rod's critical length, $\sigma_x$. The horizontal, and vertical components of the air channel, **a**, are easily found from **Figure 7**. Its horizontal component follows from the cosine rule, applied in the ground plane, and its vertical component is $(\zeta-\sigma.\cos\theta)$. Thus, the magnitude of **a** is given by:

$$a(\sigma) = \sqrt{(\zeta - \sigma\cdot\cos\theta)^2 + \rho^2 - 2\cdot\rho\cdot\sigma\cdot\sin\theta\cdot\cos\phi + (\sigma\cdot\sin\theta)^2} \qquad (12)$$

and the transit time by way of the grounded inclined rod is:

$$\tau(\sigma) = \left(\frac{1}{u_o}\right)\left(a(\sigma) + \sigma\cdot\cos\beta\right) \qquad (13)$$

The minimum time is found by letting $d\tau/d\sigma=0$, solving for $\mathbf{a_x}$, and substituting the result into **Equation (13)**. It is a standard procedure that yields both the constant angle of incidence, $\beta$, and the minimum time, which are given by:

$$\cos\beta = \frac{\zeta \cdot \cos\theta + \rho \cdot \sin\theta \cdot \cos\phi - \sigma}{a_x(\sigma)} = \frac{u_o}{u_s} \qquad (14)$$

and

$$\boxed{\tau(\sigma)_{min} = \left(\frac{1}{u_o \cdot \cos\beta}\right) \cdot \left(\zeta \cdot \cos\theta + \rho \cdot \sin\theta \cdot \cos\phi - \left(1 - \cos^2\beta\right) \cdot \sigma\right)}, \qquad (15)$$

respectively. We find the critical length, $\sigma_x$, by equating **Equation (15)** with **Equation (08)**. The critical length of an inclined rod depends explicitly on $\theta$, and $\phi$. It is given by:

$$\boxed{\sigma_x = \frac{(\cos\theta - \cos\beta)}{(1 - \cos^2\beta)} \cdot \zeta + \frac{\sin\theta \cdot \cos\phi}{(1 - \cos^2\beta)} \cdot \rho} \qquad (16)$$

As expected, the result for the erect tower, $z_x$, is recovered from **Equation (16)** if the inclination angle, $\theta$, is set equal to zero, i.e.:

$$\sigma_x[\theta = 0] = \frac{\zeta}{(1 + \cos\beta)} = z_x \qquad (17)$$

Likewise, **Equation (06)** is recovered from **Equation (15)**, by setting $\theta = 0$. This correspondence gives us confidence in **Equations (14), (15),** and **(16),** but what is really useful is the visualization of the changing zone of protection as a function of the angle of inclination. We will now show how easy it is to visualize the collapsing zone of protection.

PROCEDURE TO CONSTRUCT THE ZONE OF PROTECTION

In **Figure 4**, we described the zone of protection around an erect tower as the solid of revolution of a quarter segment of a tangent critical ellipse around the symmetry axis of the tower. An alternate operational definition of the zone of protection is the following:

*"The zone of protection is the residual space outside the lethal zone, and inside the critical range, when the lethal zone traces the critical contour surrounding a structure."*

This definition prescribes a procedure for constructing the zone of protection at the base of an inclined lightning rod. The construction of a zone of protection calls for a three step procedure:

(a) Find the critical contour that circumscribes the foot of a lightning protection structure.
(b) Use the appropriate lethal zone to trace the critical contour at the base of a structure.
(c) Retain the residual space outside the lethal zone, and inside the critical contour:

These steps are illustrated in **Figure 8**. Note that the "appropriate lethal zone" is the solid of revolution of the critical ellipse associated with an erect structure that is constructed of the same materials as those used in the construction of the inclined structure.

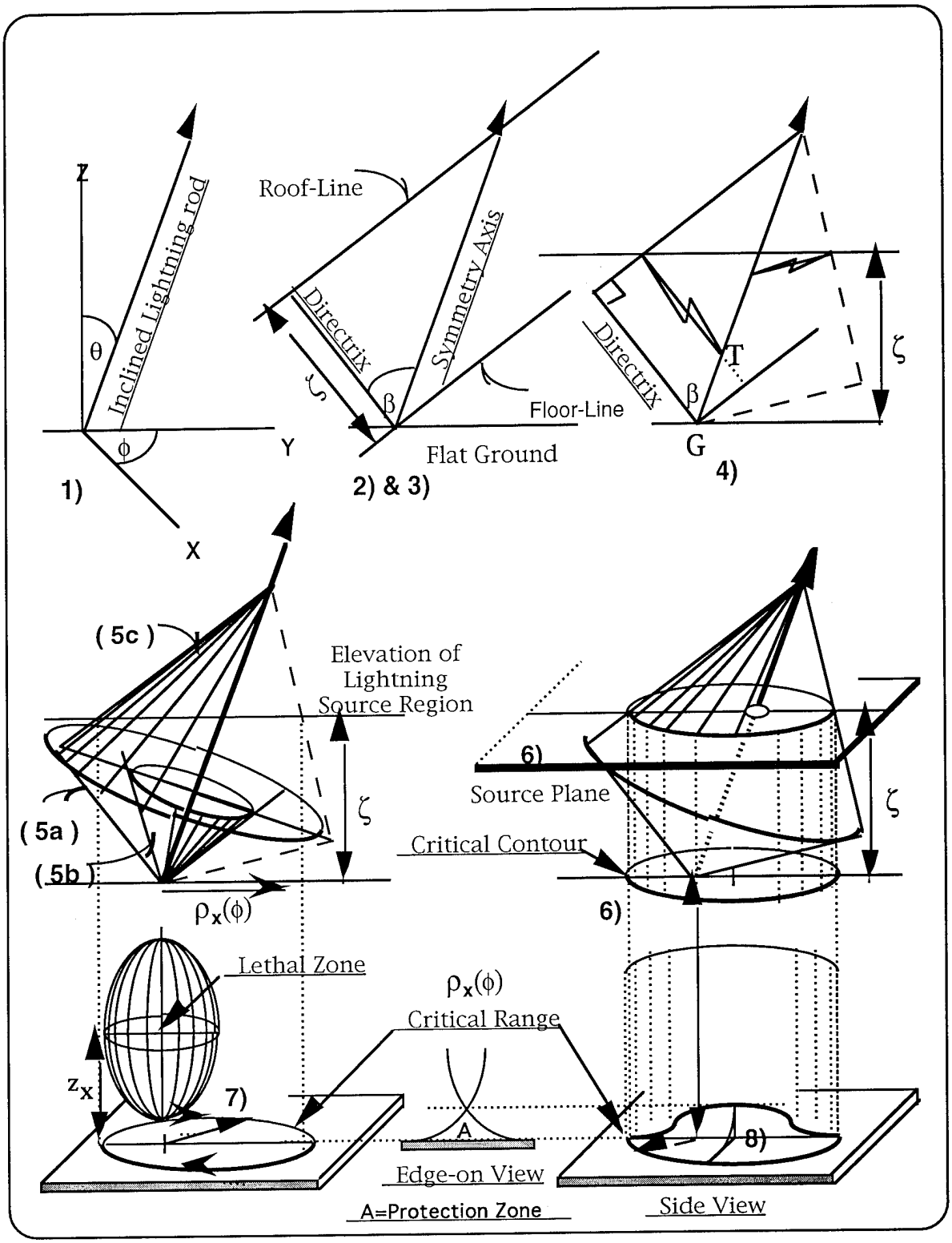



**FIGURE 8.** STEP-BY STEP PROCEDURE TO CONSTRUCT THE LIGHTNING PROTECTION ZONE NEAR AN INCLINED GROUNDED LIGHTNING ROD. THE NUMERALS IN EACH DIAGRAM REFERENCE THE STEPS OUTLINED IN THE TEXT. NOTE THAT THE VOLUME OF THE PROTECTION ZONE VANISHES AS THE INCLINATION ANGLE, θ, APPROACHES β.

**(a) Find the critical contour.**

1) In the reference plane, draw an inclined lightning rod, where $\theta$ is the angle of inclination, measured from the vertical direction.

2) At the foot of the rod, draw a line segment whose length is $\zeta$. The angle between this line and the rod is the critical angle, $\beta$. Let us call this line the "Directrix."

3) Draw perpendicular lines at both ends of the directrix: the one at the foot of the directrix, we call "the floor-line", and the one at the top end, we call "the roof-line".

4) Draw a horizontal source-line at an elevation $\zeta$ above the ground. When a step leader originates from a point at the intersection of the roof-line with the source-line, then the most likely lightning channel is the one which initially runs parallel to the directrix, strikes the rod at the point, **T**, and finally follows the rod into the ground at **G**. This is the path given by **Equations (13)**, and **(15)**.

5) Group the directrix with the roof-line, and the floor-line, and generate a solid of revolution about the inclined rod: the latter thus becomes the symmetry axis. The result is a solid whose shape is that of a top: the base region shows a directrix-cone, (**5a**), which encloses a floor-cone, (**5b**). The roof-cone, (**5c**), completes the top.

6) At the elevation $\zeta$, construct a horizontal source plane: the source line is now in the source plane. The intersection of the roof-cone with the source-plane is a conical cross section: if $0 < \theta < \beta$, it is an ellipse, and its projection on the ground is the critical contour. It can be shown that the semi-major-, and semi-minor axes of the critical contour, are given by:

$$\textbf{Semi}-\textbf{Major}\cdot\textbf{axis} = \left(\tfrac{1}{2}\right)\cdot\zeta\cdot\cos\beta\cdot\left(\frac{1}{\cos\beta}-\frac{1}{\cos\theta}\right)\cdot\left(\frac{1}{\sin(\beta+\theta)}+\frac{1}{\sin(\beta-\theta)}\right) \qquad (18)$$

and

$$\textbf{Semi}-\textbf{Minor}\cdot\textbf{axis} = \zeta\left(\frac{1}{\cos\beta}-\frac{1}{\cos\theta}\right)\cdot\cot\beta\ . \qquad (19)$$

This completes the construction of the critical contour around the base of an inclined tower.

**(b) Use the appropriate lethal zone to trace the critical contour.**

7) Imagine a lathe with a cutting tool, whose cross section is the critical ellipse. With the cutting tool touching the ground, and spinning about the vertical major axis, trace the critical contour, which was obtained in **step (6)**.

**(c) Retain the zone of protection.**

8) According to the operational definition, the residual space outside the lethal zone, and inside the critical range is the zone of protection. In **Figure 8** the numeral **(7)** labels the procedure: the final product carries the label **(8)**. The zone of protection looks like a hill with a ridge straddling the vertical reference plane, that cuts through the major axis of the elliptical critical contour.

**Figure 9** on the next page shows that the attachment point moves down the incline when the rod bends away from the source region (See **L1** through **L5** in diagrams **(a)** and **(b)**). It moves up the incline when the rod bends towards the source (See **R1** through **R5** in diagrams **(a)** and **(b)**). When we leave the reference plane, and imagine the source region to be located at a critical range from the inclined rod, the attachment point moves up and down the incline when the source region follows the critical contour around the rod. This is shown in diagrams **(c)** and **(d)**. This is a legitimate procedure for finding lightning attachment zones on ground-based structures: the attachment zones are the segments on a structure where lightning attachment points are most likely to occur. Although this result was obtained for structures on the ground, the procedure for finding lightning attachment

zones on aircraft is essentially the same. This is of interest to airplane manufactures who must protect their aircraft against lightning. Thus, the LT-MP principle also serves the aircraft industry by providing them with a new analysis tool to calculate the most probable locations of lightning attachment zones. Until now, the allocation of lightning attachment zones on aircraft[1] is almost exclusively based on experimental data.

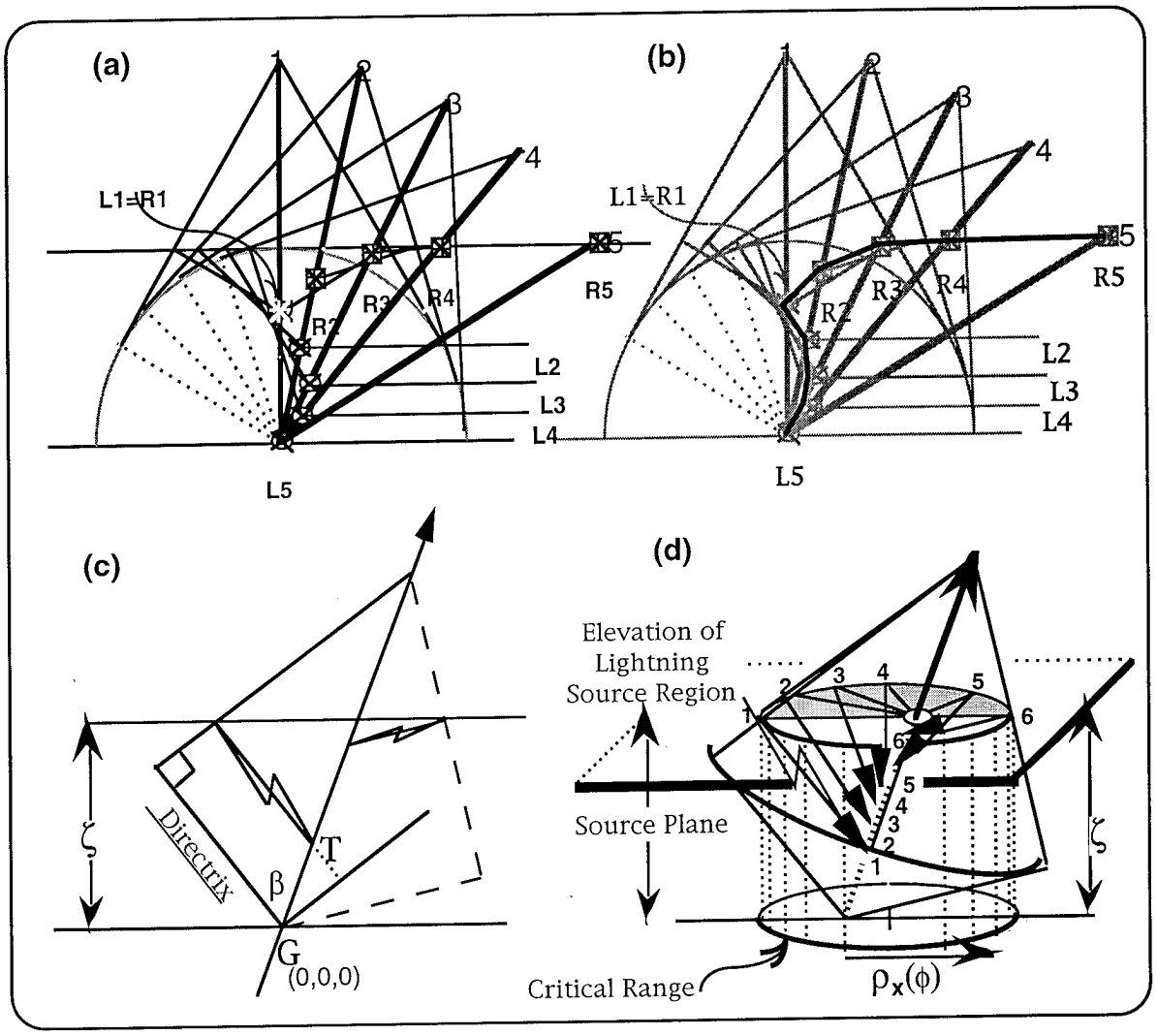



FIGURE 9. STEP-BY STEP PROCEDURE TO FIND THE LIGHTNING ATTACHMENT POINT TO AN INCLINED ROD. Diagrams ( **a** ) and ( **b**) show that with increasing $\theta$, the attachment point for lightning coming in from the left drops [see **L1** through **L5** ], while the attachment point for lightning coming in from the right moves up [see **R1** through **R5**]. The solid line in diagram (**b**) shows the locus of attachment points in the vertical plane as a function of inclination angle, $\theta$. Diagram ( **c**) shows a cross section of the lightning interaction cone, with one representative lightning stroke from the left, and another coming from the right hand side of the rod. Diagram (**d**) shows how for a fixed inclination angle, $\theta$, the position of the attachment point moves up the incline as the source region moves along the edge of the critical range from point 1 to point 2, and on to point 6. It returns to its original position when the critical contour is traced completely.

---

[1]See Chapter 3 in "Lightning Protection of Aircraft," F.A. Fisher, and J.A. Plumer, Lightning Technologies Inc., and R.A. Perala, Electro Magnetic Applications Inc., 1990, published by Lightning Technologies Inc., 10 Downing Parkway, Pittsfield, MA 01201, USA.

## SUMMARY AND CONCLUSIONS

We started this paper with the introduction of the **LT-MP** principle. When applied to lightning, the principle asserts that *"lightning follows the path of Least Time, because it is the path of Maximum Probability"*. This principle is deceptively simple, and one may easily overlook the fact that it is as powerful as its origins, which are (1) the *proven* principle of Least Action, and (2) *classical* statistics (We could extend the concept to include the field of quantum statistics). The principle contains an explicit expression for the probability of a lightning path (or channel). The introduction of an effectiveness coefficient enabled us to quantify the quality of a Lightning Protection System. We then showed that the effectiveness coefficient divides the airspace into separate lightning regions, which revealed the existence of lethal zones, and their associated zones of protection.

In this paper we showed that the physical configuration of a structure has a profound effect on the quality of a Lightning Protection System (LPS). In particular, we showed how the zones of protection near an inclined structure collapse as a function of inclination angle. To simplify the mathematical analysis, we provided a geometrical solution, and in **Figures 8,** and **9** we showed how one can visually determine the most likely lightning attachment points on a tall structure. In conclusion, we assert that the LT-MP principle and Ohm's Law are alternate descriptions of the same physical law. Thus, the LT-MP statement:

*"Lightning follows the path of Least Time,*
*because it is the path of Maximum Probability"*

is equivalent to the statement of Ohm's Law:

*"Lightning follows the path of Least* ***Impedance,***
*because it is the path of Maximum Probability".*

The second part in the statement of Ohm's Law is not normally taught in introductory physics courses, because classical physics is rarely taught from the perspective of classical statistics: We took liberty to complete the statement of Ohm's Law on the basis of the lessons learned from the LT-MP principle.

*The conclusion that the effectiveness of protection zones may be compromised as a result of the common engineering practice to terminate grounding cables at remote locations is an important result: It obliges us to warn all users of lightning protection systems that their protection system may not be effective! There is an urgent need to assess the vulnerability of protected assets under existing LPSs.*

The special theory introduced in this paper is generalized in the second of two companion papers, in which we will present one example of a trade study and demonstrate the adverse effect from the common practice of grounding cables at remote locations.

## RECOMMENDATIONS

The lightning protection zones described in **(1):** Golde's book (See "LIGHTNING, Vol. 2, Lightning Protection," R.H. Golde, ed., Academic Press, New York, 1977, p. 547), **(2):** Lightning Protection Code in NFPA 780 and its derivatives (See "The Lightning Protection Code," NFPA 780, Section 3-10, 1992 edition[1], and also the International Standard in IEC 1024-1), and **(3):** in other publications, are sometimes not consistent with fundamental principles of physics. In this paper we introduced the **L**east **T**ime-**M**aximum **P**robability

[1] NFPA # 780, 1992 supersedes all earlier versions of NFPA #78.

principle, which appears to explain some of the previously unsolved problems, and inconsistencies between conventional wisdom, and direct observations of the lightning phenomenon. Perhaps the most visible example of the successful application of the LT-MP principle to lightning phenomenology is its description of the lethal zone, and its companion protection zone near tall structures.

We hope that this paper motivates the reader to re-evaluate her, or his thoughts about the theory of lightning propagation, and in particular about its application to lightning protection systems' designs: the theory presented here explains why people can be struck by lightning when they are believed to be protected by nearby tall structures. We strongly recommend that the reader independently tests our theory, and in particular our claim that some lightning protection systems are inadequate.

The application of the theory in trade studies to evaluate existing designs, and to optimize new designs of Lightning Protection Systems will be presented in **Part II** of this series.

REFERENCES

"The Lightning Protection Code," in NFPA 780, Section 3-10, 1992., issued, and periodically updated by the National Fire Protection Association.

The International Standard, CEI/IEC 1024-1: 1990, "Protection of Structures," Part 1: General Principles.

Chapter 3 in "Lightning Protection of Aircraft," F.A. Fisher, and J.A. Plumer, Lightning Technologies Inc., and R.A. Perala, Electro Magnetic Applications Inc., 1990, published by Lightning Technologies Inc., 10 Downing Parkway, Pittsfield, MA 01201, USA.

ACKNOWLEDGMENT

I thank Dr. Ramez Atiya, and Dr. Eugene Robl, both of Salt Lake City, Utah; Dr. Sherman Wei, of Chicago, Illinois; Mr. Harry Z. Wilson, and Mr. John R. Walker, both of Los Angeles, California, for their critical reviews, and for their support and encouragement to go ahead, and allow others to independently judge the value of this work. Mr. Harry Z. Wilson in particular is credited for teaching me the rudimentary art of lightning protection technology, and for telling me strange stories about "lightning zones of protection," for which neither he, nor acknowledged, and well published experts in the field had an explanation. I credit Dr. Carl Baum for assuring every one in the room at a technical interface meeting in Albuquerque, NM, in May of 1988 that "Nobody understands the propagation of lightning, or the existence of so-called zones of protection!" I was bothered by his strong statements, and out of respect, I accepted Dr. Baum's challenge to find the answers. I thank Mr. Norman H. Davis for broadening my vision, and for raising my awareness about lightning protection activities in the rest of the world. My special thanks go to my wife and family for their patience and understanding, and for their tolerance of the long hours I spent away from them, mentally and physically, behind a desk computer, pursuing this obsession about lightning, and the LT-MP concept, which is so simple, I find it beautiful.

Richard Briët,
July 24, 1995.

GLOSSARY ... DEFINITIONS

**Attraction cone:** an inverted cone, centered about the symmetry axis of a tower, with a half-apex angle less than or equal the *characteristic angle*, $\beta$. See also *"tracking cone."*

**Characteristic angle, $\beta$:** the critical angle of incidence at the point where lightning strikes a tall tower. See also *"attraction cone,"* also called the *"cone of attraction."*

**Critical contour**: the locus of points, focused about the base of a support tower, whose distance from the focal point is the *critical distance*. For an erect tower, it is a circle.

**Critical distance** or "range", $\rho_x$: the maximum *radius of attraction* of a lightning protection system.

**Critical ellipse**: an vertical ellipse, touching the ground, whose vertical semi-major axis is the *critical height*, and whose horizontal semi-minor axis is the *critical distance*.

**Critical height, $z_x$**: the minimum height of the tip of an air terminal on top of a lightning protection system, when the *lethal zone* touches the ground at a point that is located at the critical distance, $\rho_x$, from the base of the support tower. For a grounded Franklin rod, the critical height, $z_x$, equals the semi-major axis of the corresponding critical ellipse, $\zeta/(1+\cos\beta)$, and the *critical range* $\rho_x = z_x.\sin\beta$.

**Critical range**, $\rho_x$: See "critical distance."

**Drain region:** the end of a step leader. For the last step in cloud-to- ground lightning, it is the ground.

**Effectiveness coefficient, $E_{12}$**: the comparison of the probability of a direct strike to a primary structure, $P_1$, with the probability of a direct strike to a secondary structure, $P_2$, expressed as the ratio $P_1/P_2$. When compared with the probability of a cloud-to-ground strike, $P_0$, the ratio, $E_{10}$, is the effectiveness of a primary structure to attract lightning onto itself.

**Electrical length**: the equivalent path-length of the segment of a structure, that is part of the over-all lightning channel between a lightning source region (origin), and a lightning drain region (destination). For an electrically homogeneous rod, it is the impedance of the conducting part of the rod, divided by its impedance per unit length.

**Interaction mode 1, 2, or 3:** When lightning strikes a lightning protection system at **(1)** a point on an air terminal of length **"s"**, also called the lightning rod; at **(2)** a point on a grounding cable of an air terminal, at a distance "$\sigma$" from the grounding point; or at **(3)** a point on an interconnecting cable between two air terminals, at a distance "$\xi$" from a reference tower, it is called a "mode 1", "mode 2", or a "mode 3" interaction, respectively.

**Lethal zone**: the solid of revolution of the critical ellipse about its vertical axis.

**Lightning protection system (LPS)** Any system of stand-alone, or connected structures that serve as an electrical decoy to attract lightning towards itself, and away from other structures. A complete lightning protection *system* may include lightning diverters (shielding enclosures included), transient protection devices, and lightning monitors. (Note: One could separate internal- from external LPSs).

**Optimal design** A lightning protection system is optimally designed, if its radius of attraction is $\rho_x$, while its height is kept to a minimum, without compromising its effectiveness as a lightning diverter.

**Primary structures** Any structure, whose primary function is to prevent direct strikes to other structures, by attracting lightning towards itself, is called a primary structure.

**Protection zone** When the lethal zone traces the *critical contour* around the base of a lightning protection structure, then the residual volume of the space outside the *lethal zone*, and inside the *critical contour* is called the zone of protection. For a grounded Franklin rod, the zone of protection is a cusped cone: the solid of revolution of a tangent quadrant of the *critical ellipse* about the rod generates the cone.

**Radius of attraction:** the horizontal distance between the base of a reference support tower, and the bottom of a critical ellipse, where the critical ellipse touches the support tower.

**Relative Probability:** A term used for the ratio of the probabilities of two events, to compare their relative frequency of occurrence. See also "Effectiveness coefficient."

**Secondary structures** Any structure that by design is protected against direct lightning strikes by one or more primary structures, is called a "secondary structure."

**Source region:** the region from where lightning is seen to originate.

**Striking distance:** the travel distance of a step leader: the last step defines the striking distance, $S_d$.

**Tracking cone.** A cone of attraction attached to the highest point of a grounded lightning rod, whose half apex angle, $\alpha$, is less than, or equal to the critical angle, $\beta$.

**Type I, II, or III structures:** When the structure of a lightning protection system shows only self-standing support towers; at least two support towers in a string-configuration; or at least three support towers in a ring-configuration, it is a "Type I", a "Type II", or a "Type III" structure, respectively.

# A NEW MODEL OF CLOUD-TO-IONOSPHERE DISCHARGE — IN TERMS OF A GROUND-CLOUD-IONOSPHERE CAPACITOR DERIVED FROM EHD (ELECTROHYDRODYNAMICS) ON THE BASIS OF NEW PHYSICAL CONCEPTS OF CRITICAL VELOCITY AND ELECTRIC RECONNECTION

Hiroshi Kikuchi
Nihon University, College of Science and Technology
8, Kanda Surugadai, 1-chome, Chiyodaku, Tokyo 101, Japan

## ABSTRACT AND SUMMARY

In recent ground spacecraft-based video observations performed in the United States, it has been shown that the cloud-to-ionosphere electrical discharge can occur on the topside of clouds rather than or in addition to the conventional cloud-to-ground or cloud-to-cloud discharges. Based on these observations, the present paper attempts to provide an explanation for this striking phenomenon on the basis of a new universal model of a ground-cloud-ionosphere capacitor taking into account global charge and electric field distributions, and other meteorologico-electric data available for both top and bottom sides of the clouds with the aid of new physical concepts of critical velocity and electric reconnection by using a new set of EHD (electrohydrodynamic) equations. For the case of thundercloud formation, the cloud-to-ionosphere electric field is usually upward, producing positive charge at the top of the cloud and negative charge at the bottom of the cloud and inducing negative charge at the bottom of the ionosphere and positive charge on the ground. However, in portions of the topside of the cloud, the opposite situation may occur, producing downward electric field between negative charge at the top of the cloud and positive charge at the bottom of the ionosphere. According to a new model, thewhole processes for cloud-to-ionosphere discharge is thought to be following. The first corona and positive streamers are initiated from the top of the positive cloud when the local electric field reaches a threshold value. Then, positive leaders with positive space charge-layer head elon. .ted from positive streamers tend to propagate upward toward the ionosphere with the ion critical ionization velocity estimated to be $(1.2\text{-}1.4)\times10^{4}$ m/s, slightly depending on atmospheric constituents. When positive leaders reaches a lower edge of the ionosphere, say 40 to 100 km in altitude and forms a discharge channel to the ionosphere, it is most likely that dart leaders will be descending towards the cloud from the ionosphere, establishing a discharge channel sheet between the ionosphere and the cloud with or without main discharge. In portions of the topside of the clouds with negative charge, negative streamers may be initiated, transferring into negative leaders that tend to propagate upwards towards the ionosphere with the electron critical ionization velocity estimated to be $2\times10^{6}$ m/s. When approaching the

ionosphere, atmospheric pressure is rapidly decreasing down to $10^{-2} \sim 10^{-5}$ kPa, and electric discharge tends to form aurora-like beam plasma discharge rather than lightning discharge, involving or accompanying airglows at the lower edge of the ionosphere. Explanation for possible transition from lightning to aurora due to a pressure decrease is attempted on the basis of a unified concept of critical ionization velocity proposed by the present author. A model predicts a sequence of triggered discharges, cloud-to-cloud, cloud-to-ground, or cloude-to-ionosphere, that might have occurred by an electric merging -reconnection process when charge group or cloud distributions formed an electric cusp. Detailed analyses are required, based upon observations obtained so far.

## INTRODUCTION

In recent thunderstorm observations conducted by several groups in the United States, spacecraft-based video images revealed a number of upper atmospheric optical flashes above thunderstorms with a duration ranged from 10 to 283 ms, occurring over a period of 100∼410 minutes (1∼7). The luminous structures, generally not visible to the naked, dark-adapted eye, exhibited on video a wide variety of brightness levels and shapes including streaks, aurora-like curtains, smudges, fountains, and jets (7). The structures were 10∼50 km, wide, brightness 10∼50 kR, roughly that of bright aurorae, and their upper portions extended to 30∼100 km.

Boeck et al. (8) described an enhanced airglow luminosity at the altitude of the airglow or the D-layer (about 95 km) in coincidence with a lightning flash in a tropical oceanic thunderstorm directly beneath it. This luminous event in the ionosphere was the only one of its kind observed during an examination of several thousand images of lightning recorded under suitable viewing conditions with Space Shuttle cameras.

These two kinds of event provide new evidence of direct coupling between lightning and ionospheric events.

Based on these observations, the present paper attempts to provide an explanation for such a striking phenomenon of thunderstorm-ionosphere coupling on the basis of a new model of a capacitively coupled ground-ionosphere system or circuit, taking into account global charge and electric field distributions, and other meteorologico-electric data available for both top and bottom sides of the clouds with the aid of new physical concepts of critical ionization velocity and electric reconnection on the basis of a new electrohydrodynamics (EHD).

## CHARGE AND ELECTRIC FIELD IN A GROUND-CLOUD-IONOSPHERE SYSTEM

The classic model for the charge structure of a thundercloud was developed in the 1920s and 1930s from ground-based measurements of thundercloud electric fields (9, 10). In this model, the thundercloud forms a positive dipole or vertical double layer as shown in "Figure A-1"; that is, a positive charge region above a negative charge region. By the end of the 1930s. Simposon and co-workers (11) had verified this overall structure from measurements made with sounding balloons inside clouds and had also identified a small localized region of positive charge at the base of the cloud. Subsequent measurements of electric fields both inside and outside the cloud have confirmed the general validity of this double-dipole structure as shown in "Figure A-2" (e.g. 12).

For the classical positive dipole model, positive charge is induced at the surface of the ground, causing upward electric fields between the bottom of the cloud and the ground, while on the topside of the cloud, electric fields are initiated from positive charge at the top of the cloud, being directed upwards, and terminating at the bottom of the ionosphere, as shown schematically in "Figure A-1a". Its equivalent electric circuit may be reprented by "Figure A-1b".

In the modern double dipole model, a small amount of positive charge localized at the base of the cloud forms a small negative electric dipole, being accompanied by a main positive dipole, as shown schematically in "Figure A-2a". Consequently, the electric field configuration on the bottom side of the cloud does change, inducing a small amount of negative charge in a local region of the ground right beneath the negative dipole, and the field configuration on the topside of the cloud also changes, inducing a small amount of positive charge in a local region of the ionosphere right above the negative dipole.

## ELECTRIC CUSP FOR A DOUBLE-DIPOLE CLOUD

The double-dipole model described in the preceding section indicates the existence of points, lines or sheets of zero electric field, around which electric field several occurs and a region of low electric field is formed, may be termed "electric cusp" or "electrically neutral point, line or sheet" (13-17) analogous to magnetic cusp familiar to plasma and geo-astro physicists. The shaded area in "Figure A-2" represents an electric cusp across which there exist two regions of opposite polarity. The areas right underneath and above the negative dipole between the ground and the ionosphere possess downward electric fields and are separated by the electric cusp from the region of upward electric field lines right underneath and above the positive dipole.

Such an electric cusp can be a source-origin of "chaos" leading to a process of

electric reconnection and capable for triggering or initiating lightning discharges, as discussed for triggered lightning by a rocket with trailing wire grounded (13~17) and for the statistics that the occurrence rate of lightning strokes becomes maximum in the region of electric field reversal or electric cusp (18). In other words, it can be stated in general that electric cusp and reconnection be involved in bipolar and/or multiple flashes of lightning and play important roles in causing them. This may also be true without an exception for the case of upper atmospheric optical flashes when recalling their bipolar nature observed and their correlation with positive cloud-to-ground flashes (7). Based on such an idea, we now attempt to explain upper atmospheric flashes and to draw a conceptional model for global ground-cloud-ionosphere coupling.

## CLOUD-TO-IONOSPHERE DISCHARGES BY ELECTRIC RECONNECTION

We are interested in a number of recent observations of upper atmospheric optical flashes that are thought to have been caused by electric discharges at the top of cloud clusters towards the ionosphere as a result of multiple coupling between cloud-to-ground, cloud-to-cloud, and cloud-to-ionosphere discharges. In particlar, we notice the following remarkable features observed for upper atmospheric flashes:

1. a large horizontal extent of flashes as wide as 50 km;
2. their bipolar nature with much higher occurrence rate to positive cloud-to-ground flashes than to negative cloud-to-ground flashes;
3. their correlation with positive cloud-to-ground flashes;
4. their anti-correlation with negative-cloud-to-ground flashes;
5. their correlation with "spider lightning" intracloud discharges.

These observations indicate that cloud shape and charge distribution are thought to be inclined and extended rather horizontally with a sequence of cusped charge distribution or horizontal double-layers, as illustrated schematically in "Figure A-3". Such a horizontal extent of cloud clusters might be due to stratospheric jet streams on the topside of the clouds in a way similar to cloud and charge distributions in a costal region of the Sea of Japan during winter, although this requires some meteorological evidence.

Once one assumes such a model of electric field and charge configurations for upper atmospheric optical flashes, though somewhat oversimplified, the following general principle applies to such luminous events: a region of electric cusp becomes the source-origin of whole processes and any relevant perturbation to the cusp region tends to trigger electric reconnection leading to cloud-to-ground, cloud-to-cloud, and/or cloud-to-ionosphere discharges. In principle, there are two possibilities of the cloud-to-ionosphere discharges:

(i) The first positive cloud-to-ground discharge is triggered by electric reconnection in a cusp region right beneath a positive polarity, involving intracloud and/or cloud-to-ionosphere discharges. Such processes can be explained in terms of an equivalent circuit in "Figure A-3b".

(ii) The first negative cloud-to-ground discharge induces intracloud discharges, then leading to the second but positive cloud-to-ground discharge through cloud-to-cloud and cloud-to-ground channels established for the first negative stroke. At the same time, intracloud discharges tend to reconnect the electric field lines in the opposite direction on the topside of the clouds at the cusp boundary, leading to positive upper atmospheric discharges. Accordingly, positive discharges are thought to occur, on both bottom and top sides of cloud clusters towards the grou d and the ionosphere.

Taking these into account, cloud-to-ionosphere discharges are thought to be accompanied by positive cloud-to-ground strokes and/or spider lightning intracloud discharges, as observed by upper atmospheric luminous events.

## LIGHTNING-TO-AURORA TRANSITIONIN TERMS OF CRITICAL VELOCITY AND ITS RELATION TO CLOUD-TO-GROUND AND CLOUD-TO-IONOSPHERE DISCHARGES

Lightning is usually considered an electric discharge in a natural environment under the atmospheric pressure, while aurorae are observed at high-latitude ionosphere-magnetosphere boundaries on the nightside and are thought to be a kind of electric discharges in low pressure gases, the so-called "beam-plasma discharge" manifested in space. Accordingly, it is inferred that lightning discharges may transfer to aurorae with decreasing pressure. It seems that this viewpoint may have been demonstrated by simultaneous observations of cloud-to-ground lightning and cloud-to-ionosphere discharge in sky. In fact, a unified view of lightning and aurora as electric discharges in higher and lower pressure gases, respectively can be done in terms of "critical ionization velocity" by introducing the E/P (E: electric field, P: pressure) dependence of electron and ion drift velocities in gases as shown in "Figures A-4 and A-5".

Electron and ion critical velocities can be defined, respectively, regardless of gas pressure, as

$$\frac{1}{2} m_- v^2_{-c} = e V_i \qquad (1)$$

and

$$\frac{1}{2} m_+ v^2_{+c} = e V_i \qquad (2)$$

where $e$, $m_-$, and $m_+$ are the electric charge, mass, and the ion mass, $V_i$ is the ionization potential of a background gas, $v_{-c}$ and $v_{+c}$ are electron and ion critical velocities at which velocities collective avalanche ionization takes place. The leader velocity of cloud-to-ground lightning and the propagation velocity of a luminous front of upper atmospheric flashes can be estimated by either Eq. (1) or Eq. (2).

## REFERENCES


1. R.C. Franz et al. Science, 249, 48, 1990.
2. W.L. Broeck et al. EOS Trans. AGU, 72, 171, 1990
3. O.H. Vaughan et al. Mon. Weather Rev., 120, 1459, 1992
4. W.L. Broeck et al. Geophys. Res. Lett. 19, 99, 1992
5. J.R. Winkler, J. Geophys. Res. 98, 8775, 1993
6. D.D. Sentman et al. Geophys. Res. Lett. 20, 2857, 1993
7. W.A. Lyons, Geophys. Res. Lett. 21, 875, 1994
8. W.L. Boeck et al. Geophys. Res. Lett. 19, 99, 1992
9. C.T.R. Wilson, Proc. R. Soc. London A92, 556, 1916
10. C.T.R. Wilson, J. Franklin Inst. 208, 1, 1929
11. G.C. Simpson et al. Proc. R. Soc. London A161, 309, 1937
12. W.J. Koshak et al. J. Geophys. Res. 94, 1165, 1989.
13. H. Kikuchi, in Proc. 6th EMC Zürich Symp., ed. T. Dvorak, ETH-IKT, Zürich, 1985, p.47
14. H. Kikuchi, in Laboratory and Space Plasmas, ed. H. Kikuchi, in Environmental and Space Electromagnetics, ed. H. Kikuchi; Springer-Verlag, Tokyo, 1989, p.331
15. H. Kikuchi, in Environmental and Space Electro-magnetics, ed. H. Kikuchi, Springer-Verlag, Tokyo, 1991, p.561
16. H. Kikuchi in Proc. of XX ICPIG-Invited Papers Issue, 1991, p.32
17. H. Kikuchi, in Dusty and Dirty Plasmas, Noise, and Chaos in Space and in the Laboratory, Plenum, New York, 1994, p.535
18. H. Kikuchi, presented at 6th Workshop on Physics of Dusty Plasmas, Univ. of Calif., San Diego, March 22-24, 1995.

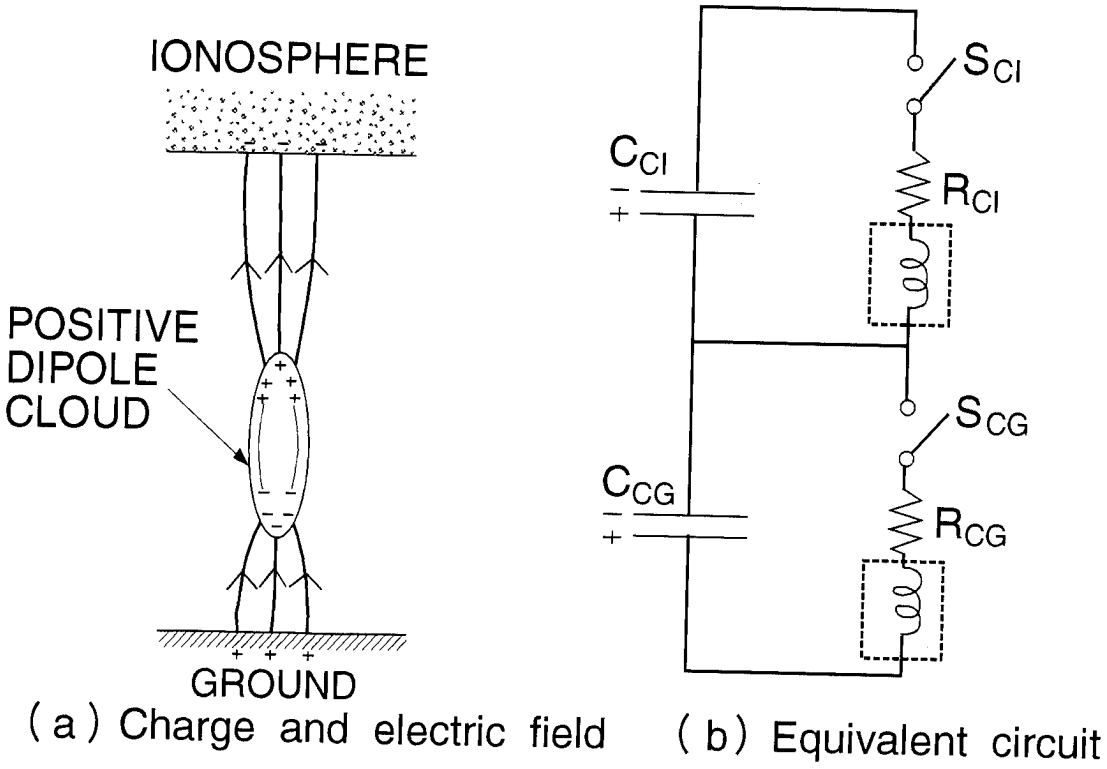



Fig. A-1. Ground-cloud-ionosphere system for a positive dipole cloud.

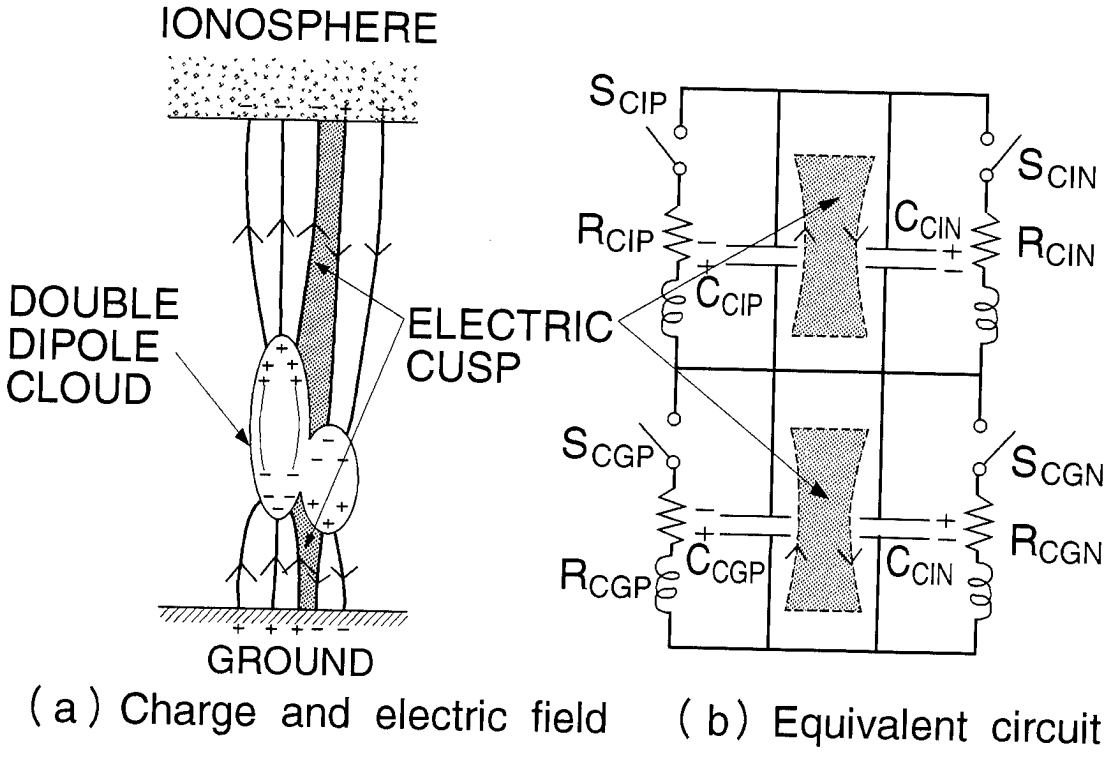



Fig. A-2. Ground-cloud-ionosphere system for a double dipole cloud.

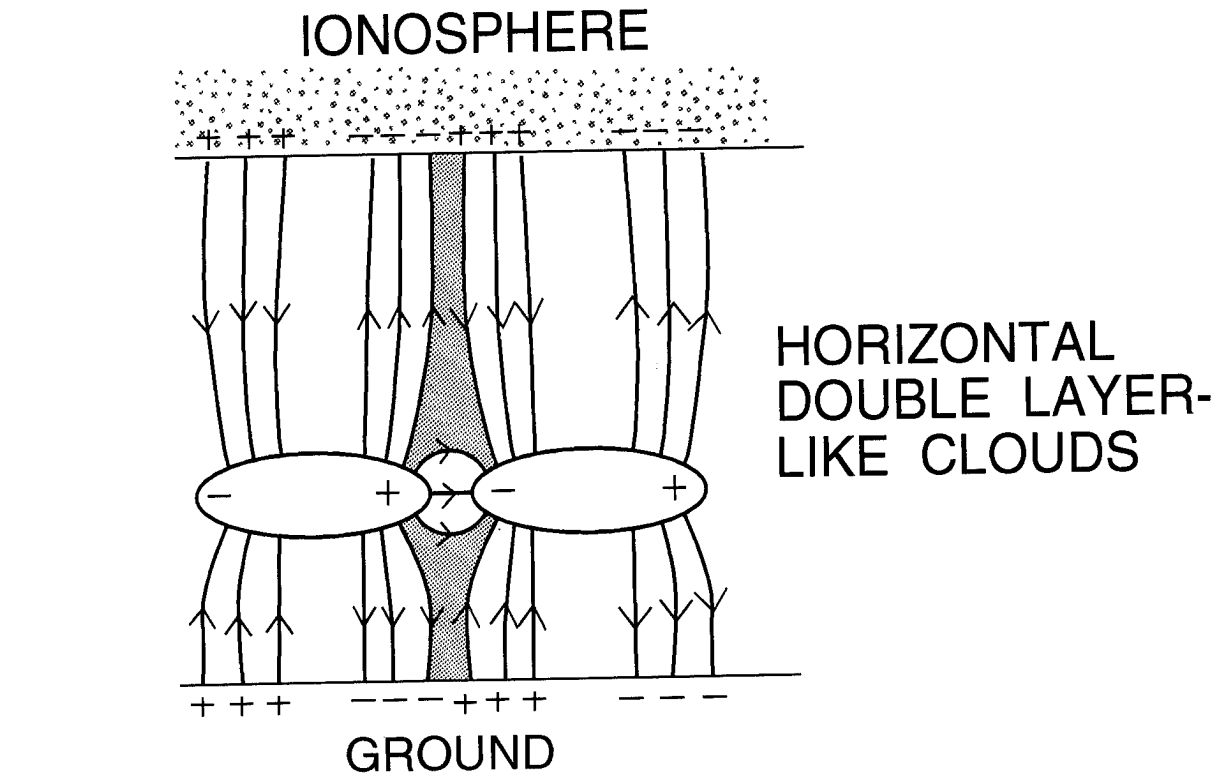



Fig. A-3. Ground-cloud-ionosphere system for a sequence of horizontal double layer-like clouds

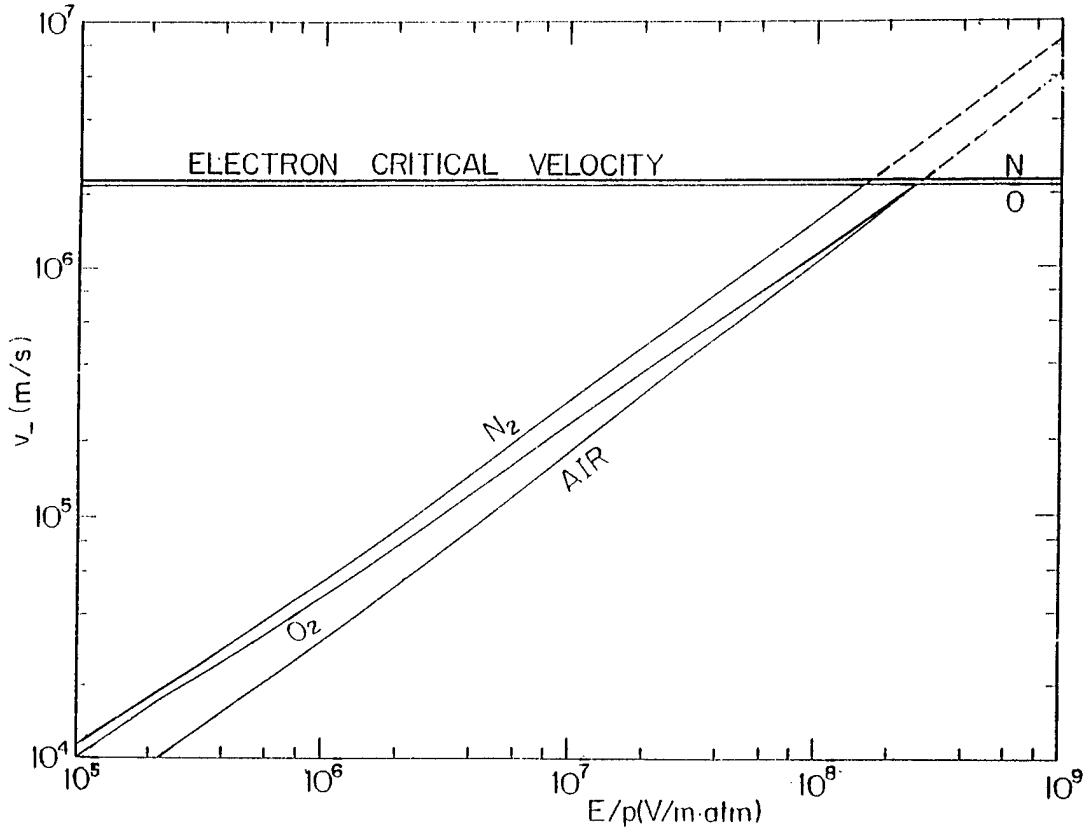



Fig. A-4. Electron drift velocity and electron critical velocity in gases.

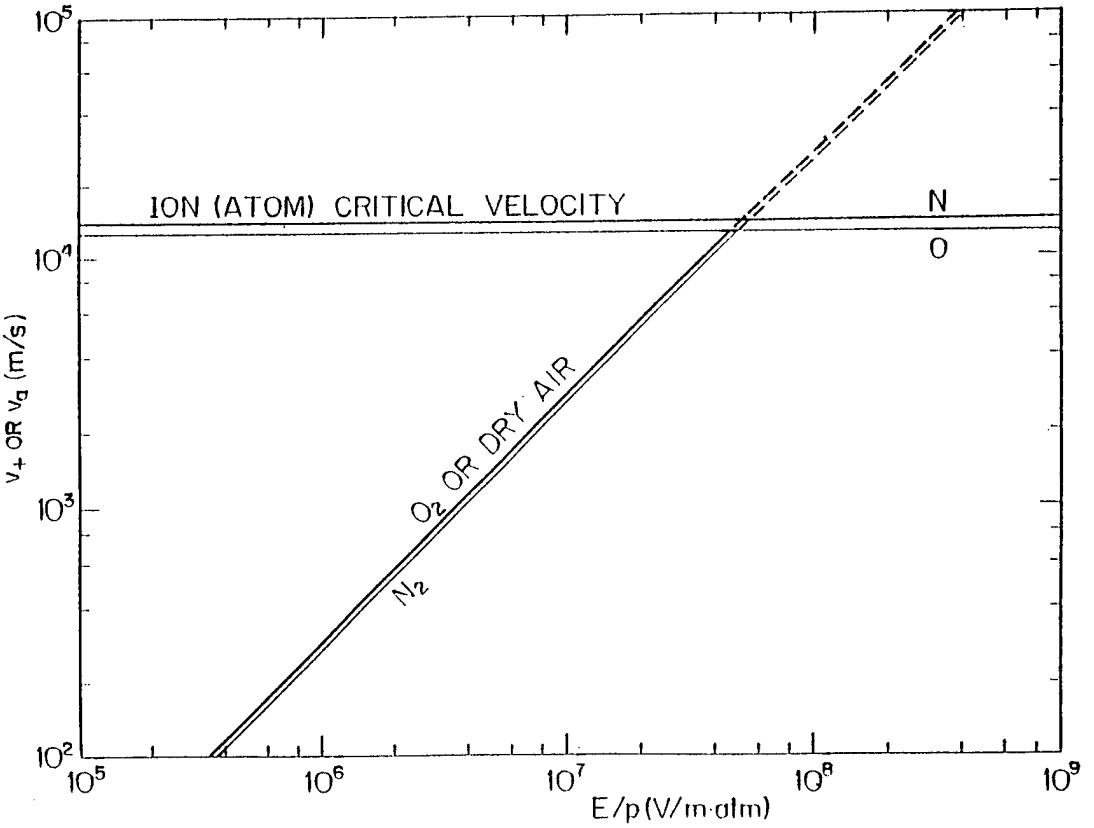



Fig. A-5. Ion drift velocity and ion critical velocity in gases.

# SESSION 08A
# PERSONNEL HAZARDS
# CHAIRPERSON: RONALD L. HOLLE

# CHRONIC PAIN SYNDROME IN A LIGHTNING VICTIM

Mary Ann Cooper, M.D., FACEP
Department of Emergency Medicine
University of Illinois
Telephone (312) 413-7489 FAX (312) 413-0289

## ABSTRACT

While most victims of lightning injury in the United States survive each year, many will have permanent sequelae. One of the prominent but hard to document complaints is that of chronic pain. A case history is used to illustrate a chronic pain syndrome that is more easily documented.

## CASE REPORT

On June 4, 1994, a 32 year old female sheriff's deputy working as an Emergency Medical Systems dispatcher in Louisiana during a thunderstorm was using her left arm in an extended fashion to press the transmitter button. At approximately 7:30 pm lightning presumably hit the tower and was transmitted through the equipment to her arm. She recalls hearing a "loud train sound" and experiencing a "real bad sting" in her left hand. Sounds became muted as she lost consciousness but she recalls her sergeant picking her up from the console and lying her on the floor. Subsequently she experienced heaviness, weakness, and discoloration of her lower extremities which improved after ten days. Although she was seen in the emergency department of local hospital she was released when her initial testing was normal. The next day she returned for pain and numbness in her left neck and arm severe enough to require treatment with narcotics. All subsequent testing, including MRI, has been essentially normal.

The left upper extremity has continued to be stiff and painful. The patient has developed a dystrophic posture, holding the arm close to her body and is unable to use the arm both because of pain, numbness, and lack of ability to grip and do fine motor movements. The extremity exhibits both color and temperature changes as well as increased sweating. She has developed sleep disturbance and headaches. These changes are consistent with Reflex Sympathetic Dystrophy (RSD), an injury of the autonomic nervous system (ANS).

## AUTONOMIC NERVOUS SYSTEM

The autonomic nervous system (ANS) controls aspects of our body functions

which we take for granted and which are not routinely under our control: pupillary dilatation, heart rate, thermoregulation (through sweating and vasodilation/ vasoconstriction), digestion and other gastrointestinal functions, genitourinary function, and blood pressure. The ANS is divided into two components: sympathetic and parasympathetic which generally have opposite effects on the body. The sympathetic nervous system (SNS) may be thought of as the "fight of flight" system. The ANS traverses the entire neural system, having components in both the central (brain and spinal cord) and peripheral nervous systems. Injuries to both the central nervous system (brainstem) and peripheral nervous systems may cause ANS injury.

Acute damage to the nervous system has been described in numerous case reports that were summarized in Cooper's early work (1) as usually temporary paralysis of the lower and sometimes upper extremities. These patients present to the emergency department with a flaccid paralysis of the extremities marked by cold pulseless mottled extremities probably caused by intense sympathetic nervous system stimulation. Ten Duis has described this further as "keraunoparalysis" (2). Hypertension and tachycardia (rapid heart beat) may also occur (1, 3-7). All of these usually disappear within hours and the prognosis is usually good (1,8).

Cardiac and EKG changes have also been described (1, 3-11). These changes may take weeks to months to resolve and may be due to either central injury to the cardiac centers (12), direct effects on the heart or its conduction system, or through ANS dysfunction (6, 9-11).

## REFLEX SYMPATHETIC DYSTROPHY

Reflex sympathetic dystrophy is a composite term for several previously reported pain syndromes such as causalgia, Sudeck's atrophy (wasting), hand-shoulder syndrome, phantom limb (13-15). It may occur from trivial injury and classically is heralded by pain beginning within hours to days of the injury. This pain is often out of proportion to the trauma, may spread beyond the injury area, and is characterized as 'burning' in nature although the patients may use other terms to describe it such as aching, throbbing, gnawing, or sharp. It is often exacerbated by emotional or physical stress.

RSD is divided into three stages although not all the symptoms may be present in any given patient (13-15):

Stage I -- The Acute Stage: This may last up to six months and is characterized by burning pain with hyperpathia (abnormal pain to normal stimulus), allodynia (pain on the side of the body opposite of the injury), and hyperalgesia (increased sensitivity to pain). The skin may appear to

be warm and red and there may be increased hair and nail growth. The involved extremity may exhibit excessive sweating and swelling and may be difficult to move secondary to pain and stiffness.

Stage II -- The Dystrophic Stage: This usually begins six months after the initial onset and is characterized by spread of the swelling, pain and edema, trophic changes (changes in form -- muscle wasting, hair and nail loss, joint contractures) appear and osteoporosis (bone thinning) becomes evident probably from disuse secondary to pain. The patient will invariably have sleep disruption, anxiety, and depression.

Stage III -- The Atrophic Stage: This occurs about one to two years after the injury and is characterized by cool, pale and cyanotic (dusky, bluish) skin. The pain may have spread to other parts of the body. The trophic changes now appear as smooth glossy skin and there may be joint stiffness. These changes are usually permanent and may be disabling. Patients may develop abnormal motor movements, spasms, tremor, and increased reflexes late in this phase (16).

RSD has been reported after electrical injury and may be quite prominent in lower voltage injuries, if only because many of the other symptoms are minor and disappear rapidly compared to high voltage injuries (17-21). Only one author has reported RSD in lightning injury (23). In his report two telephone operators were affected were struck by lightning that entered through their headphones. Both were successfully treated and able to return to work after repeated sympathetic intrapleural blocks, physical therapy, occupational therapy and biofeedback training.

## DIAGNOSIS

The diagnosis is usually made on a clinical basis from the patient's description of the pain and the findings of hyperpathia, cutaneous vasoconstriction, sweating and swelling (13-15, 22). Routine laboratory tests are usually normal. However, skin temperature and blood flow studies may show decreased flow. Thermography is controversial. Bone scans may show early periarticular activity (increased uptake) around the affected joints. Plain X-rays may show bone thinning later in the course of the syndrome.

Sympathetic blockade involves injection of the sympathetic chain with an anesthetic agent. This may provide some relief in the early stages, is diagnostic, and may predict permanent relief if a sympathectomy is performed. Unfortunately, if the RSD is allowed to progress to State III or if it is the type with no hyperalgesia, sympathetic blockage may be ineffective (13-15, 22).

## TREATMENT

Non-steroidal anti-inflammatory drugs (NSAIDS) such as Motrin and Naprosyn are the first line treatment. Splinting or casting of the extremity should be avoided if possible. Physical therapy should be started early and is important for mobility and pain control although some patients will not tolerate it well. A transcutaneous nerve stimulator may be helpful. If NSAIDS are ineffective, a variety of anticonvulsants, tricyclic antidepressants, and steroids may be effective. Permanent sympathetic blockade of the cervical or thoracic ganglia may be helpful in earlier stages. Calcium-channel blockers or sympatholytics may be added for increased effect or should be considered if permanent sympathetic blockade is contraindicated (13-15,21).

## DISCUSSION

The particular patient described in this case report was unresponsive to sympathetic blockade, has recently entered a pain clinic program and there is a good prognosis for her withdrawal from pain medication, acceptance of her pain, and return to work in the next few months.

While this may be one of the first case reports of reflex sympathetic dystrophy in a lightning victim, over the years I have received many patient calls with similar types of complaints of chronic pain after a lightning or electrical injury. At the time, I did not know of this syndrome. In correspondence with Dr. Andrews of Australia, he was relieved to find that a number of his patients with similar complaints fit into a recognized complex.

Lightning victims frequently complain of pain syndromes as well as neuropsychological problems after their injuries (24-27). Often the objective tests that are available do not show abnormalities, in large part because the lesions suffered are at the cellular level rather than gross lesions seen with more typical types of trauma. Because the victims find physicians, friends, and family unfamiliar and sometimes unsympathetic to their injuries, they tend to become isolated for the first few months after their injuries, leading to even more inability and willingness to cope with their injuries.

Patients with chronic pain often exhibit the same kind of isolation and depression because pain is very difficult to test for objectively (28, 29).

## REFERENCES

1. MA Cooper, "Lightning Injuries: Prognostic Signs for Death." Annals of Emergency Medicine, 9:134-38, 1980.

2. HJ ten Duis, KJ Klassen, PE Reenalda, "Keraunoparalysis, a 'Specific' Lightning Injury." Burns, 12:54-7, 1985.

3. SR Craig, "When Lightning Strikes, Pathophysiology and Treatment of

Lightning Injuries." Postgraduate Medicine, 79:109-24, 1986.

4. AA Cwinn, SV Cantrill, "Lightning Injuries." Journal of Emergency Medicine, 2:379-88, 1985.

5. GC Hanson, GR McIlwraith, "Lightning Injury: two case histories and a review of the management." British Medical Journal, 4:271-4, 1973.

6. JP Kleiner, JH Wilkin, "Cardiac effects of Lightning stroke." Journal of the American Medical Association, 240:2757-9, 1978.

7. TS Weeramanthri, IB Puddy, LJ Beilin, "Lightning Strike and Autonomic Failure--Coincidence or Causally Related?" Journal of the Royal Society of Medicine, 84:68708, 1991.

8. MA Cooper MA, CJ Andrews, "Lightning Injuries." In Auerbach P, eds: Wilderness medicine, 3rd ed, St. Louis, CV Mosby, pp 261-89, 1995

9. SHD Jackson, DJ Parry, "Lightning and the Heart." British Heart Journal, 43:454-7, 1980.

10. R Lichtenberg, D Dries, K Ward, W Marshall, P Scanlon, "Cardiovascular Effects of Lightning Strikes." Journal of the American College of Cardiologists, 21:531-6, 1993.

11. CJ Andrews, DM Colquhoun, M Darveniza, "The QT Interval in Lightning Injury With Implications for the 'Cessation of Metabolism' Hypothesis." Journal of Wilderness Medicine, 4:155-66, 1993.

12. CJ Andrews, "Srudies in Aspects of Lightning Injury." Dissertation, Department of Electrical Engineering, University of Queensland, 1993.

13. SN Raja, N Hendler, "Sympathetically Maintained Pain." Current Practice in Anesthesiology, 2:421-25, 1990.

14. N Hendler, SN Raja, "Reflex Sympathetic Dystrophy and Causalgia." Chapter 39, Handbook of Pain Management, eds CD Tollison, JR Satterwaite, JW Tollison, Baltimore, Williams and Wilkins, pp 484-96, 1994.

15. RJ Schwartzman, "Causalgia and Reflex Sympathetic Dystrophy." Current Diagnosis in Neurology, E Feldman, ed. St. Louis, Mosby, pp 258-60, 1994.

16. RJ Schwartzman, J Kerrigan, "The Movement Disorder of Reflex Sympathetic dystrophy." Neurology, 40:57-61, 1990.

17. (10) JA Aldrete, R Ghaly, "Delayed Sympathetically Maintained Pain Caused by Electrical Burn at the Current's Entry and Exit Sites." Journal of Pain Symptomatology and Management. 541-3, 1994.

18. (12) EM Denum, JL Redd, KA Buchanan, TJ Brennan, JL Rowlingson, HN Himel, RF Morgan, RF Edlich, "Reflex Sympathetic Dystrophy after a Minor Electric Shock." Journal of Emergency Medicine, 11:393-6, 1993.

19. (14) A Eldad, A Newman, A Weinberg, P Benmeir, M Rotem, M Chavoat, JM Gomori, MR Wexler, "Late Onset of Extensive Brain Damage and Hypertension in a Patient with High-Voltage Electrical Burns." Journal of Burn Care and Rehabilitation, 12:214-7, 1992.

20. (15) H Hooshmand, F Radfor, E Beckner, "The Neurophysiological Aspects of Electrical Injuries." Clinical Electroencephalography, 20:111-20, 1989.

21. HJ ten Duis, "Acute Electrical Burns." Seminars in Neurology, Vol 15, in press.

22. JA Cohen, "Autonomic Nervous System Disorders and Reflex Sympathetic Dystrophy in Lightning and Electrical Injuries." Seminars in Neurology, Vol 15, in press.

23. TR Shantha, "Causalgia Induced by Telephone-Mediated Lightning Electrical Injury and Treated by Intrapleural Block." Anesthesia and Analgesia, 73:507-8, 1991.

24. M Primeau, GH Engelstatter, MA Cooper, "Psychological Sequelae of Lightning Injury." International Aerospace and Ground Conference on Lightning and Static Electricity, 1995.

25. M Primeau, GH Engelstatter, KK Bares, "Behavioral consequences of lightning and electrical injury." Seminars in Neurology, Vol. 15, in press.

26. D Shaw, ME York-Moore, "Neuropsychiatric sequelae of lightning stroke." British Medical Journal, 2:1152-55, 1957.

27. MA Cooper, CJ Andrews, "Lightning Injuries." Chapter 11, Wilderness Medicine, Auerbach ed, st. Louis, Mosby year Book, 1995

28. N Hendler, S Talo, "Chronic Pain Patient Versus the Malingering Patient." in Foley, Payne, eds, Current Therapy of Pain. Philadelphia, BC Decker, pp 14-22, 1989.

29. N Hendler, "Depression Caused by Chronic Pain." Journal of Clinical Psychiatry, 45(3):30-36, 1994.

wmsbrgtx.chapters4

# PSYCHOLOGICAL SEQUELAE OF LIGHTNING INJURY

Margaret Primeau, Ph.D.
Department of Psychology
Finch University of Health Sciences/The Chicago Medical School
North Chicago, IL, USA
Telephone (708) 578-3305 FAX (708) 578-3015

Gerolf H. Engelstatter, Ph.D.
Carolina Psychological Health Services
Jacksonville, NC, USA
Telephone (910) 347-3010 FAX (910) 347-6137

Mary Ann Cooper, M.D.
Department of Emergency Medicine
University of Illinois at Chicago
Chicago, IL, USA
Telephone (312) 413-7480 FAX (312) 413-0289

## ABSTRACT

At least 1000 persons survive injury by lightning in the U.S. each year. Our understanding of the psychological consequences is based on a handful of case reports and a few cohort surveys. This literature and some original findings are discussed in order to characterize patterns of outcome and make recommendations for evaluation and management. Research on mechanisms of injury and on predictors of outcome is needed.

## INTRODUCTION

There are many anecdotal reports of the initial effects of lightning injury (1). For example, in Chicago recently, a 30-year-old man and his 13-year-old nephew were struck by lightning in front of their house. Both were knocked to the ground; the man remained conscious and just had cuts on his forehead from the fall, but the boy lost consciousness and suffered cardiac arrest. A bystander resuscitated him and he was hospitalized in serious condition (2).

In another incident, when lightning struck a rifle range at Fort Polk in 1960, 16 of the 67 soldiers training there were injured (3). Of two who were directly hit, one suffered loss of consciousness, skull fracture, rupture of the right tympanic membrane, multiple first and second degree burns, and pulmonary hemorrhage. He was disoriented and incoherent as well as pale and cold on admission. By the next day he was bright and alert, but remained hospitalized for several weeks. The second man did not lose consciousness at first, and reported seeing a tremendous flash of light and experiencing violent muscular contractions and rigidity of his entire body. He was unable to move and felt himself fall backwards. He thought he was dead. Then he was aware of smoke rising from his body, and a bitter taste in his mouth. He could not move his legs or his left arm, but raised his right arm to gesture

for help. His clothes were torn to shreds and he had superficial burns from his left arm to his right leg. At the hospital he was also pale and cold, but alert and well-oriented, and, unlike most victims, was able to remember the experience. He was discharged the next day after resting and receiving local treatment for the burned areas. The other 14 soldiers were knocked down and complained of soreness, headache, or back pain, but did not require treatment.

Thus, some people who are struck by lightning not only live to tell about it, but seem to show no lasting signs of it. Others experience injuries that may significantly alter cognitive and emotional functioning. Central nervous system (CNS) damage from lightning injury can impair higher order functions such as memory, judgment, and personality, as well as regulatory functions such as those of the endocrine and autonomic systems. Peripheral and systemic injuries may be disabling and, in turn, affect psychological functioning. According to case reports, CNS and peripheral dysfunction may resolve, persist, or even worsen with time.

Lightning injury is puzzling because of both the variability of sequelae across cases and the difficulty in making inferences about the organic basis of the symptoms. Neurobehavioral problems may be the only sequelae, and yet damage to the nervous system may not be evident on ordinary tests. Cognitive and emotional problems interact, and it is hard to say which is primary.

Our understanding of the later psychological sequelae of lightning injury is limited. Empirical studies are few, and we are not as yet able to characterize the prevalence of various psychological outcomes, nor to predict outcome from the specifics of the lightning incident. Prospective studies of survivors from a variety of sources are needed so that intervention and compensation can be provided appropriately. This information should also be useful in education and prevention.

## LITERATURE

CASE STUDIES--Several published case studies illustrate the neuropsychological outcomes that survivors experience. Troster and Ruff (4) did serial evaluations of a college student who experienced an indirect strike with no burns or loss of consciousness. Initially he showed poorer concentration, attention, and verbal memory and learning than expected for his education. Five months after the injury, cognitive functioning had improved, and by two years postinjury, it had normalized. At that point, emotional status was good except for "a sense of loss and frustration."

Two cases with good outcome were described by Frayne and Gilligan (5). In the first, a farmer injured by telephone-mediated lightning initially suffered loss of consciousness, a ruptured tympanic membrane, and a superficial burn . Computed Tomography (CT) of the brain was normal. Over the next two weeks he exhibited a personality change and periods of complete disorientation. Memory for new verbal material was also impaired. These sequelae resolved within one month of injury.

The second case was a student struck on the head while playing football. Initially he suffered a convulsion and was subsequently agitated and aggressive, with bilateral deafness. Brain injury (a right posterior parietal infarct) was evident on CT. Concentration, problem-solving, and coordination were impaired. Over six weeks, the CT abnormality and left-ear deafness resolved; the cognitive deficits gradually resolved.

Persistent deficits may also occur. A young man working as a lineman was hit while in contact with his truck (6). He experienced cardiac and respiratory arrest as well as convulsions. Confusion, headaches, and seizures continued after the acute period. The CT was normal. An evaluation 16 months later revealed moderately severe deficits in verbal learning, problem-solving, psychomotor speed, and right-hand sensorimotor function. Psychological distress was severe and included thoughts of suicide. Although this man also had a premorbid history of depression and learning disability, these factors did not account for the severity of his current problems.

Another young man was struck while working under his vehicle (6). He did not lose consciousness but had burns and disorientation at first. Subsequently he complained of severe headaches, back pain, and depression. Two years after the injury, evaluation indicated mild deficits in verbal learning and problem-solving. Psychological testing revealed depression and preoccupation with chronic pain. He had not worked since the injury.

COHORT STUDIES--There are three studies of cohorts in the literature. Six months after the Ascot incident in England in 1955 in which 50 people were injured by lightning, Shaw and York-Moore (7) sent out questionnaires to which 28 survivors responded. The authors reported "late neuropsychiatric sequelae" in 39% of these cases, including depression (7%), "anxiety or hysterical states" (11%), and pain (18%).

In a retrospective study of telephone-mediated lightning injury in Australia, Andrews and Darveniza (8) analyzed reports of 132 persons. Many said they experienced anxiety (20%) and emotional shock (25%) at first; about 13% reported persisting emotional aftereffects such as anxiety and depression, although only 6% said that these lasted more than one week postinjury. In a subsequent study involving 10 new incidents investigated at the time they occurred (9), these researchers found that while 6 persons initially experienced anxiety, marked psychological disturbance persisted in 2 cases.

These cohort studies give us the best estimate to date of the prevalence of psychological dysfunction after lightning injury, which is 10-20%. The literature indicates that cognitive dysfunction typically consists of amnesia for the event, initial disorientation, and difficulties with attention, concentration, verbal memory, and new learning. Although recovery of cognitive function was reported to be complete in the published cases described above, the actual frequency of good outcome is not known.

## OUR STUDY

SURVEY FINDINGS--We examined the self-reports of late sequelae in 100 survivors of lightning injury (10). The frequencies of their symptoms are shown in table 1. It is noteworthy that many of the complaints are referable to the nervous system, such as cognitive problems, sleep disorder, headaches, autonomic dysfunction, pain, weakness, mobility problems, and sensory disturbances. Emotional aftereffects were common, namely, depression, phobias, and personality change. In fact, four of the eight most frequent complaints are also symptoms of depression.

TABLE 1. FREQUENCIES OF COMMON AFTEREFFECTS REPORTED BY 100 SURVIVORS OF LIGHTNING INJURY.

| SYMPTOM | % OF RESPONDENTS |
|---|---|
| Neurobehavioral | |
| Memory Deficit | 52 |
| Sleep disturbance | 44 |
| Attention deficit | 41 |
| Dizziness | 38 |
| Low endurance | 38 |
| Muscle spasms | 34 |
| Decreased grip strength | 34 |
| Irritability | 34 |
| Inability to sit for long | 32 |
| Chronic fatigue | 32 |
| Headaches | 30 |
| Inability to work | 29 |
| Inability to cope | 29 |
| Weakness | 29 |
| Incoordination | 28 |
| Reduced libido | 26 |
| Communication problems | 25 |
| Confusion | 25 |
| Chronic pain | 21 |
| Pinched nerves | 17 |
| History of coma/loss of consciousness | 15 |
| Seizure disorder | 12 |
| Paralysis | 11 |
| Inability to walk | 11 |
| Aphasia | 6 |
| Out of body experience | 5 |
| Ataxia | 5 |
| Sensory | |
| Paresthesias | 40 |
| Numbness | 36 |
| Photophobia | 34 |
| Tinnitus | 33 |
| Hearing loss | 25 |
| Visual acuity loss | 20 |
| Deafness | 13 |
| Sjogren's sign | 9 |
| Emotional | |
| Depression | 32 |
| Agoraphobia | 29 |
| Storm phobia | 29 |
| Emotional problems | 24 |
| Flashbacks | 20 |
| Personality change | 19 |
| Nightmares | 12 |
| Random fears | 11 |
| Suicidal thoughts | 6 |

TABLE 1, continued.

| SYMPTOM | % OF RESPONDENTS |
|---|---|
| Other | |
| Stiffness in joints | 35 |
| External burns | 32 |
| Back problems | 25 |
| Hyperhidrosis | 25 |
| Bowel problems | 23 |
| Internal burns | 21 |
| Arthritis | 19 |
| Bladder problems | 17 |
| Heart problems | 12 |
| Skin problems | 11 |
| History of heart attack | 10 |
| Kidney problems | 10 |

In order to determine whether subtypes of late outcome could be described, we compared this group to 65 survivors of electrical injury who responded to the same questionnaire (11). The average interval since injury across groups was 4.5 years. Factor analysis was used to characterize symptom intercorrelation, and cluster analysis was used to identify subgroups. In addition, discriminant analysis was used to see whether lightning and electrical injury differed in outcome.

The analyses identified several symptom factors and 4 clusters of cases. For lightning injury, 64% of the survivors were characterized by the prominence of multiple, neurobehavioral complaints suggestive of mild to moderate organic brain syndrome coupled with affective disorder (see table 2). Two additional clusters consisted of cases with more circumscribed symptoms conforming to gross CNS insult (12%), and cases with primarily systemic problems (e.g., cardiac; 21%). Compared to electrical injury, however, late sequelae of lightning injury appeared to be milder; discriminant analysis correctly classified 70% of cases in each group on the basis of higher scores for the electrical injury group on the factor of multiple neurobehavioral and emotional symptoms; and more frequent auditory deficit in lightning injury ($p < .01$).

TABLE 2. SUBGROUP CHARACTERISTICS: CLUSTER ANALYSIS OF 87 LIGHTNING INJURY SURVIVORS .

| CLUSTER (N) | MEAN AGE | CHARACTERISTICS |
|---|---|---|
| 1 (33) | 38.1 | Multiple neurobehavioral symptoms and anxiety |
| 2 (23) | 50.8 | Multiple neurobehavioral symptoms |
| 3 (11) | 21.0 | Severe CNS insult |
| 4 (20) | 67.2 | Primarily systemic problems |

CONCLUSIONS FROM SURVEY DATA--Since the respondents were self-selected, these results may not reflect distributions of outcome in the population of lightning survivors. Also, since we did not have systematic information on initial severity, duration of symptoms, status of compensation claims if any, or premorbid adjustment, the role of these factors in predicting outcome could not be considered. However, we believe the results indicate that when recovery does not occur in the

short term, risk is high for chronic sequelae of a global, neurobehavioral and emotional character.

Whether or not these persons are typical of lightning survivors, they are likely to be the ones who seek medical attention and get involved in compensation claims. Thus it is important to address questions of differential diagnosis and management for cases with persistent symptoms.

## EVALUATION AND MANAGEMENT

EVALUATION--Comprehensive neuropsychological and psychiatric evaluation is recommended for purposes of a) quantifying and tracking cognitive impairments, b) identifying current psychological disorders, c) characterizing personality and premorbid adjustment, and d) assessing secondary gain and the likelihood of malingered deficits (12).

The neuropsychological evaluation should emphasize assessment of attention, concentration, memory, and problem-solving as these are more sensitive to brain dysfunction than IQ scores. Psychological disorders such as depression, post-traumatic stress disorder (PTSD), or anxiety disorders warrant treatment and may account for or exacerbate cognitive problems such as memory deficit. The possibility of psychogenic (as opposed to neurogenic) impairment should also be considered. Conversion disorder has been discussed in the literature (7,13,14) and may underlie neurobehavioral complaints, although this tends to be the default diagnosis when conventional tests are negative. The base rate of conversion disorder in lightning injury is not known.

Personality characteristics such as coping style, and premorbid factors such as health history and achievement in work and school, are also relevant to outcome (15). Since the occurrence of lightning injury is a function of occupation, lifestyle, and risk-taking behavior (16,17), some survivors have traits that do not facilitate adjustment.

DIAGNOSIS--When conventional neurodiagnostic tests like CT scan are positive, the presence of behavioral deficits is not questioned. However, when tests do not reveal organic injury, behavioral deficits are suspect. It is helpful to consider the example of mild traumatic brain injury, or postconcussion syndrome, for three reasons. First, the constellation of typical symptoms resembles that in lightning injury, i.e., impaired concentration and memory, headaches, dizziness, irritability, depression, and fatigue (15,18). Second, the neurological examination, CT scan, and other objective tests may be negative. Nevertheless, recent studies have demonstrated neurophysiological abnormalities in mild traumatic brain injury by such means as measurement of regional cerebral metabolism and evoked potentials (18). Finally, psychiatric disorders have been described after concussion in persons who do not have premorbid histories of emotional or adjustment problems, suggesting that the "mild" CNS insult is sufficient to account for psychological disorders (19). The case of the farmer with a normal CT scan after lightning injury who exhibited transient personality disturbance also illustrates this point (5). Comprehensive evaluation of survivors of lightning injury is needed to make a proper diagnosis.

MANAGEMENT--Some clinicians recommend counseling from the beginning to explain complications, reassure patients, and facilitate adjustment (15,16). If neuropsychological deficits persist beyond the acute period, cognitive retraining should be offered. Psychiatric disorders as well as pain and dysesthesias may require medication such as antidepressants or anticonvulsants (16). Depression, anxiety, and PTSD are also amenable to cognitive-behavioral forms of psychotherapy.

## SUMMARY

The psychological outcomes of lightning injury appear to be bimodally distributed, with the majority of survivors experiencing recovery from behavioral effects within the first several weeks. In contrast, we estimate that 10 to 20% of survivors experience persistent cognitive and psychological problems. Individuals in this latter group tend to report multiple neurobehavioral and emotional symptoms which resemble sequelae of traumatic brain injury. However, the potential interaction of psychological factors and neurological dysfunction make the evaluation and treatment of this group challenging. Community-based followup studies of lightning incidents, and further research with sensitive diagnostic tests such as functional neuroimaging, are needed to improve patient care and help resolve compensation claims fairly.

## REFERENCES

1. C.J. Andrews and M.A. Cooper, "Clinical presentation of the lightning victim." In C.J. Andrews, M.A. Cooper, M. Darveniza, and D. Makerras, eds., "Lightning injuries: electrical, medical, and legal aspects." Boca Raton, LA: CRC Press, 1992,47-70.

2. C.L. Tan, "Two struck by lightning hospitalized, but alive." Chicago Tribune, July 27, 1995, sec. 2, p. 3.

3. H.A. Buechner and J.C. Rothbaum, "Lightning stroke injury--A report of multiple casualties resulting from a single lightning bolt." Military Medicine, Vol. 126, 1961, 755-762.

4. A.I. Troster and R.M. Ruff, "Accidental high-voltage electrocution: Neurobehavioral sequelae in three cases." Presented at National Academy of Neuropsychology meeting, Chicago, Nov., 1987.

5. J.H. Frayne and B.S. Gilligan, "Neurological sequelae of lightning stroke." Clinical and Experimental Neurology, Vol. 24, 1987, 195-200.

6. N.H. Pliskin, personal communication, July, 1995.

7. D. Shaw and M.E. York-Moore. "Neuropsychiatric sequelae of lightning stroke." British Medical Journal, Vol. 2, 1957, 1152-1155.

8. C.J. Andrews and M. Darveniza, "Telephone-mediated lightning injury: an Australian survey." Journal of Trauma, Vol. 29, 1989, 665-671.

9. C.J. Andrews and M. Darveniza, "Special aspects of telephone-mediated lightning injury: An Australian perspective." In C.J. Andrews, M.A. Cooper, M. Darveniza, and D. Makerras, eds., "Lightning injuries: electrical, medical, and legal aspects." Boca Raton, LA: CRC Press, 1992, 163-189.

10. G.H. Engelstatter, "Neuropsychological and psychological sequelae of lightning and electric shock injuries." Presented at the Fourth Annual Meeting of the Lightning Strike and Electric Shock Victims, International, Maggie Valley, NC, May, 1994.

11. M. Primeau. G.H. Engelstatter, and K.K. Bares, "Behavioral consequences of lightning and electrical injury." Seminars in Neurology, Vol. 15, 1995, in press.

12. N.H. Pliskin, G.J. Meyer, M.C. Dolske, R.L. Heilbronner, K.M. Kelley, and R.C. Lee, "Neuropsychiatric aspects of electrical injury. A review of neuropsychological research." Annals of the New York Academy of Science, Vol. 720, 1994, 219-223.

13. K.M. Kelley, N. Pliskin, G. Meyer, and R.C. Lee, "Neuropsychiatric aspects of electrical injury. The nature of psychiatric disturbance." Annals of the New York Academy of Science, Vol. 720, 1994, 213-218.

14. M. Critchley, "Neurological effects of lightning and electricity." Lancet, Vol., 1, 1934, 68-72.

15. R.L. Heilbronner, "Rehabilitation of the neuropsychological sequelae associated with electrical trauma." Annals of the New York Academy of Science, Vol. 720, 1994, 224-229.

16. M.A. Cooper and C.J. Andrews, "Lightning injuries." In P.S. Auerbach and E.C. Geehr, eds., "The management of wilderness and environmental injuries," 3rd. ed., St. Louis: Mosby Year Book, 1995, in press.

17. P.F. Mellen, V.W. Weedn, and G. Kao, "Electrocution: A review of 155 cases with emphasis on human factors." Journal of Forensic Sciences, Vol. 37, 1992, 1016-1022.

18. S.J. Brown, J.R. Fann, and I. Grant, "Postconcussional disorder: time to acknowledge a common source of neurobehavioral morbidity." Journal of Neuropsychiatry and Clinical Neuroscience, Vol. 6, 1994, 15-22.

19. K.D. Cicerone and K. Kalmar, "Persistent postconcussion syndrome: the structure of subjective complaints after mild traumatic brain injury." Journal of Head Trauma Rehabilitation, Vol. 10, 1995, 1-17.

# RECENT TRENDS IN THE NUMBER OF LIGHTNING DEATHS AND INJURIES IN THE UNITED STATES

Raúl E. López and Ronald L. Holle
National Severe Storms Laboratory, NOAA
Norman, Oklahoma

Ranjit M. Passi
Center for Marine Sciences, University of Southern Mississippi
Stennis Space Center, Mississippi

## ABSTRACT

Time fluctuations in the number of lightning deaths and injuries from 1959 to 1990 have been examined for the contiguous United States. After taking into account the population increase, there was a decreasing trend in casualties during this period resulting in an overall reduction of 30%. This trend probably resulted from improved forecasts and warnings, increased public education efforts, and socio-economic changes.

In addition, there was a 40% reduction in the number of deaths. This additional reduction in deaths was probably due to improved medical attention given to lightning victims and a wider knowledge of cardiopulmonary resuscitation techniques among the public. Improved medical care would increase the chances of a person surviving a lightning strike but would not affect the total number of casualties.

Superimposed on the overall downward trend there appear to be cyclical variations of a period of the order of a decade. From 1959 until 1968 there was a sharp reduction in the number of casualties, but starting in 1969 and continuing until the present, there was an overall increase. It appears that these oscillations are climatologically related. The patterns of these fluctuations were parallel to nationwide changes in thunder-day frequencies, cyclone frequencies, and surface temperature values, representing thunderstorm, synoptic, and continental scales.

A simple conceptual model has been devised to identify the principal factors contributing to the number of lightning casualties. The model indicates that the number of casualties is directly proportional to the flash density, the population, and the fraction of the population exposed to the lightning threat.

## INTRODUCTION

The principal source of information for lightning deaths and injuries in the United States is *Storm Data* and is the basis for the annual natural hazard statistics and 20-year normals issued by the Warning and Forecast Branch of the National Weather Service. *Storm Data* is a monthly National Oceanic and Atmospheric Administration (NOAA) publication that describes damaging and severe weather during the year and it includes reports of deaths and injuries attributed directly to lightning.

When the number of lightning fatalities for the last few years reported by *Storm Data* is compared to those of 20 or 30 years ago, a drastic reduction in numbers is evident. This has been variously attributed to improvements in forecasts and warnings, and to changes in the reporting and compilation of lightning casualties by the National Weather Service. We have adressed many of these issues in a series of papers that consider death and injury statistics at the state and national levels (1, 2, 3, and 4). In this paper, we report on the nature of the nationwide changes in the number of lightning deaths and injuries reflected in *Storm Data* during the period of 1959 to 1990.

## OVERALL NUMBER OF CASUALTIES

*Storm Data* reported 2983 deaths and 8233 injuries directly due to lightning over the US during the period of 1959 to 1990. That gives an average number of 93 deaths and 257 injuries per year. The yearly values, however, fluctuated considerably during the period. The minimum yearly number of deaths was 63 during 1979, and the maximum 210 during 1963. Injuries fluctuated from 145 in 1967 to a maximum of 399 in 1975.

## TIME VARIATION OF LIGHTNING CASUALTIES

Figure 1 portrays the time series of yearly lightning deaths for the contiguous US (solid line) and the corresponding US population (dotted line). As can be seen, the yearly deaths show a significant decrease with time. The national population, however, shows an almost linear increase. Therefore, the drop in the number of deaths due to lightning relative to the population is even greater. Superimposed on this overall downward trend, there appear to be 3 distinct periods, each about a decade in duration: 1959 to 1967, 1968 to 1979, and 1980 to 1990. The first period (1959-1967) contains the highest number of deaths in the entire record but shows a drastic decrease from 210 to 70 deaths in the latter part of the period. During the second period (1968-1979), the number of deaths rises to, and stays around, 100 deaths per year until 1979 when the lowest number in the record of 63 deaths occurs. The third period (1980-1990) is characterized by about 70 deaths per year. All three periods show considerable interannual variability which reflects the probabilistic component of lightning casualties.

Figure 2 shows the time series of yearly lightning injuries for the contiguous US (solid line) and the corresponding US population (dotted line). There is a large difference between this and the lightning fatality time series of Fig. 1. The injury graph shows a considerable overall increase with time compared to deaths. A comparison with the population curve, however, indicates that the injuries have not kept up completely with the population increase. The three periods described above for the yearly number of deaths can also be recognized in the injury time series.

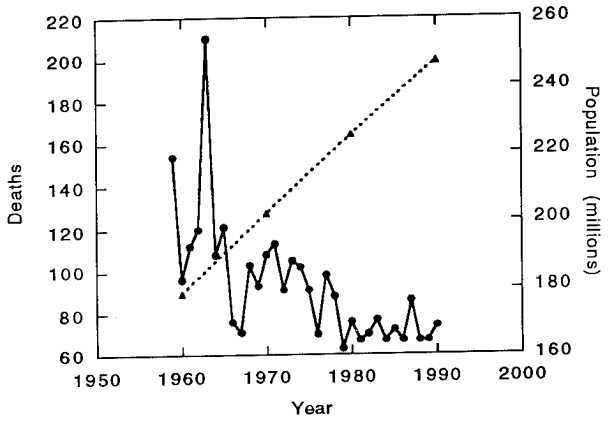



*FIGURE 1. Time series of yearly lightning deaths for the contiguous US (solid line) and the corresponding US population (dotted line).*

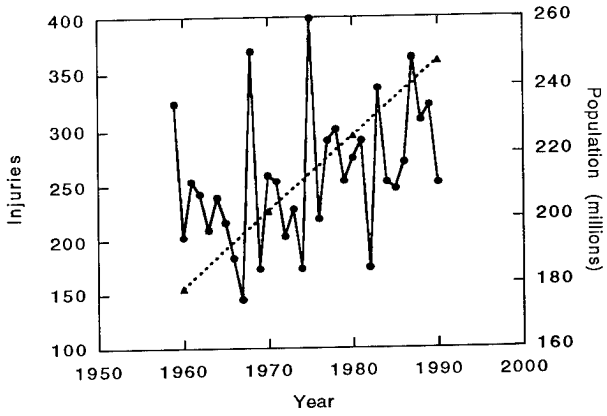



*FIGURE 2. Time series of yearly lightning injuries for the contiguous US (solid line) and the corresponding US population (dotted line).*

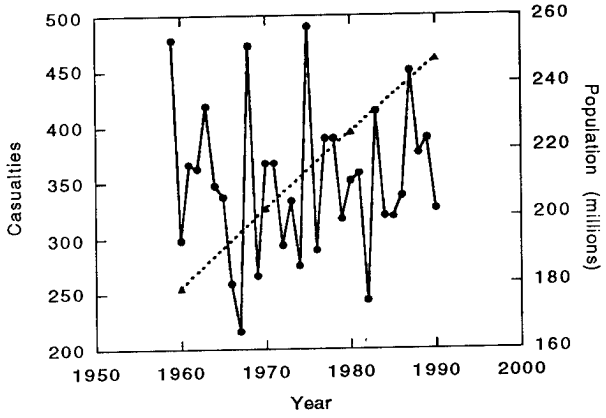



*FIGURE 3. Time series of yearly lightning casualties (deaths and injuries combined) for the contiguous US (solid line) and the corresponding US population (dotted line).*

Deaths and injuries have been combined in Fig. 3. Again, the time series of yearly

lightning casualties for the continental US (solid line) is accompanied by the corresponding US population (dotted line). Notice that although a general increase in the total number of lightning victims is indicated, there is a drop with time relative to the population. As expected, this tendency lies between that of deaths and injuries.

## OVERALL TRENDS OF CASUALTIES

The effect of the population increase can be taken into account by dividing the yearly number of deaths and injuries by the corresponding population. Figure 4 shows a plot of the resulting normalized series for deaths (solid curve). The dashed line represents a linear fit to the normalized data. If the number of deaths had kept up with the population increase, the dashed line would have been parallel to the abscissa. There is, however, a linear drop of 70% relative to the population during the period. Figure 5 is the corresponding graph for injuries. The line fitted to the normalized yearly number of injuries is nearly horizontal but still represents a drop of 8% with respect to the population increase during the 32-year period. The combined normalized casualty series (Fig. 6) shows a linear trend relative to the population that represents a decrease of 30% during the period, intermediate between that of deaths and injuries.

Two questions immediately arise: Why is there a linear downward trend in the number of population-normalized deaths and injuries? And, why should there be such a marked difference between the two? One possible explanation for the trend is that a combination of improvements in thunderstorm forecasts and warnings, as well as community education of the lightning threat and changes in socio-economic patterns (see López et al. (3)) have caused a drop in lightning casualties with time. If this was the only cause, however, it would be very difficult to explain why a much larger reduction has occurred in deaths than in injuries. It is likely that, in addition, a significant portion of the reduction in deaths is due to the improved medical attention given to lightning victims such as a faster response of emergency medical services, better life support technology, and wider knowledge of cardiopulmonary resuscitation among the

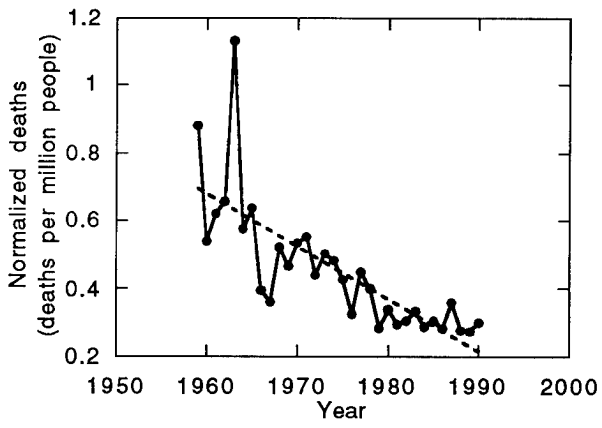



*FIGURE 4. Time series of yearly lightning deaths normalized by population for the contiguous US (solid line). A linear function has been fitted to the data (dashed line).*

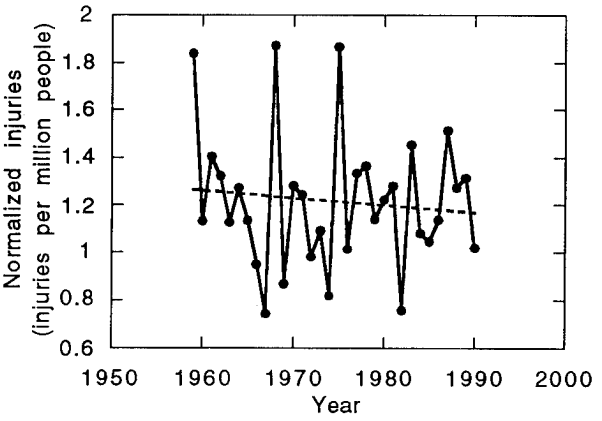



*FIGURE 5. Time series of yearly lightning injuries normalized by population for the contiguous US (solid line). A linear function has been fitted to the data (dashed line).*

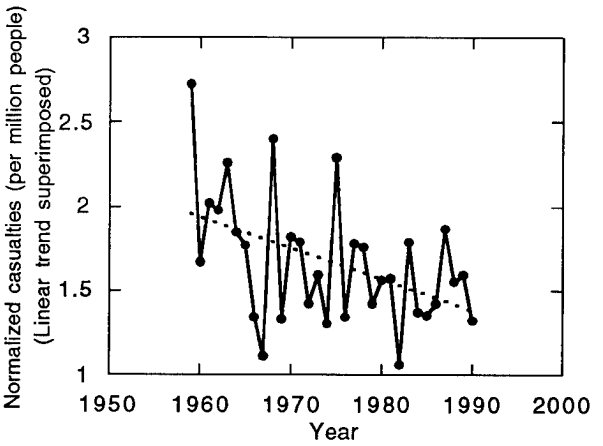



*FIGURE 6. Time series of yearly lightning casualties normalized by population for the contiguous US (solid line). A linear function has been fitted to the data (dashed line).*

public. This improved medical care could reduce the number of deaths from lightning strikes but not the number of injuries. Actually, an increase in the number of injuries would result because potential deaths would now become only injuries. For the same reason, the number of total casualties would not be affected by improved medical attention. Thus, it is reasonable to hypothesize that:

- the linear drop in the number of normalized total casualties of 30% could be due to improved warnings, public education, and socio-economic changes,
- a similar drop is present in the number of normalized deaths and injuries separately,
- but the number of deaths is further decreased by 40% to a total drop of 70% due to improved medical care, while the injuries are increased because of the conversion of potential deaths into just injuries, resulting in a combined drop of only 8%.

## DECADAL FLUCTUATIONS OF CASUALTIES

A five-year running average has been computed for the normalized casualty series of Fig. 6 to smooth out some of the high frequency interannual variability. Figure 7 shows the resultant series. The linear trend indicated by the dashed line of Fig. 6 can also be eliminated by taking normalized casualty departures from the fitted line. The resultant series is portrayed in Fig. 8, where both the trend and the interannual variability have been filtered out.

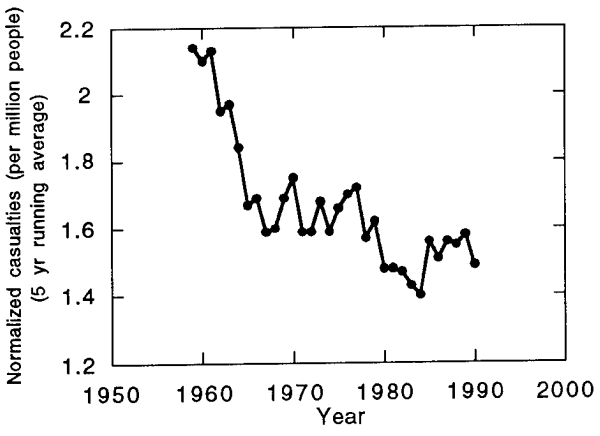



*FIGURE 7. Time series of yearly lightning casualties normalized by population for the contiguous US. A 5-year running average has been applied to the data.*

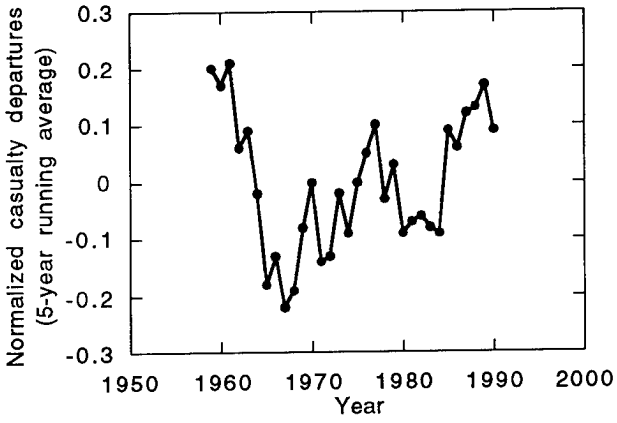



*FIGURE 8. Time series of normalized casualty departures from the linear trend of normalized casualties for the contiguous US. A 5-year running average has been applied to the data.*

It is evident from Fig. 8 that besides the population and socio-economical trends, there are fluctuations of one or two decades in duration. Notice that from the beginning of the period in 1959 until 1968 there was a very sharp reduction in the casualty departures. Starting in 1969 and continuing until the present time, however, there has been an overall increase in the casualty departures. This general increase appears to have been modulated by an oscillation from low to high to low values from 1967 to 1980. The question now remains as to the nature of these fluctuations. López and Holle (1) explored this question by comparing the series of lightning casualty departures with series of different climatological variables. Their results suggest that these fluctuations may be due to climatological factors.

Figure 9 shows the time series of mean 5-year frequency of thunder days obtained from Changnon (5) (solid line) and the normalized lightning casualty departures from Fig. 8 (dashed line). The thunder-day series shows a drop in the number of days with thunder from 1950 to 1970. From the minimum at the end of that period, the number rose considerably during the first 5 years of the 1970s, dropping again during the next 5 years. The casualty departures follow closely those same oscillations, except that the relative amplitudes are somewhat different.

Similarly, Figure 10 shows the yearly numbers of July cyclones from 1959 to 1977 obtained by Zishka and Smith (6) (solid line)

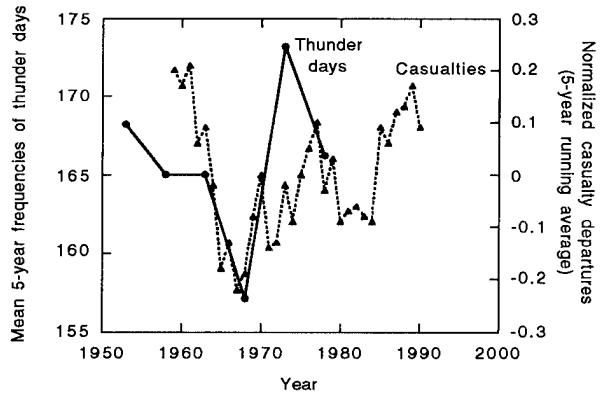



*FIGURE 9. Time series of mean 5-year frequency of thunder days obtained from Changnon (5) (solid line) and the normalized lightning casualty departures from the linear trend from Fig. 8 (dashed line). A 5-year running average has been applied to the casualty departures.*

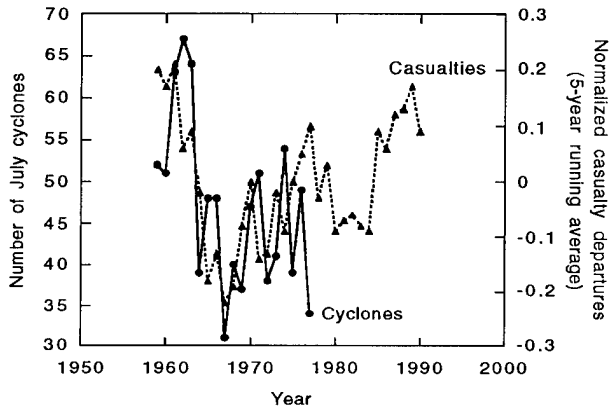



*FIGURE 10. Time series of the yearly number of July cyclones obtained from Zishka and Smith (6) (solid line) and the normalized lightning casualty departures from the linear trend from Fig. 8 (dashed line). A 5-year running average has been applied to the casualty departures.*

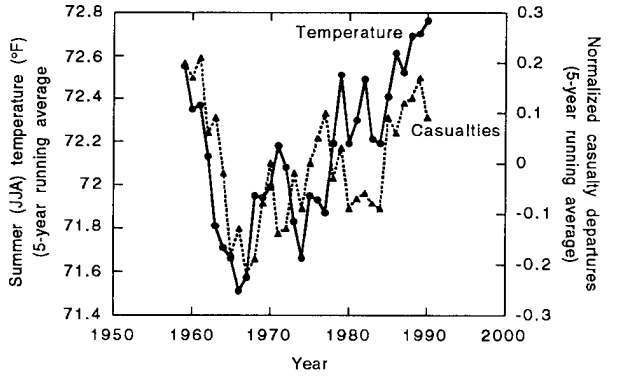



*FIGURE 11. Time series of the summer (June, July, and August) surface temperatures for the contiguous United States obtained from Heims et al. (7) (solid line) and the normalized lightning casualty departures from the linear trend from Fig. 8 (dashed line). A 5-year running average has been applied to both series.*

with the normalized casualty departures superimposed (dashed line). The number of cyclones shows a dramatic drop from the early to the late 1960s. The minimum number was reached in 1967. This drops matches very closely the drop in normalized casualty departures. After that, the number of cyclones has gradually risen, notwithstanding the considerable interannual variability. This subsequent rise is also matched closely by the casualty departures.

Figure 11 shows the temperature series derived from Heim et al. (7) for the contiguous 48 states, for the period corresponding to the lightning casualty data (1959-1990), and during the months of June, July, and August when most of the lightning casualties occurred (solid line). The normalized casualty departure series has been superimposed (dashed line). A 5-year running average has been applied to both series. The temperature series indicates a rapid drop of about 2°C from 1959 to 1967 which is followed very closely by the drop in lightning casualties. From 1968 on there has been a more gradual overall increase both in temperatures and in casualties. The average relative increase in temperatures has been slightly larger than the relative overall increase in casualties.

## A CONCEPTUAL MODEL FOR LIGHTNING CASUALTY CHANGES

The results of this paper indicate that there are time fluctuations in the number of lightning casualties that appear to correspond to climatic variations. These fluctuations are superimposed on trends produced by demographical, socio-economical, and medical changes. It would be useful to have a conceptual model that quantifies the relationships between the different factors responsible for the variations in the number of lightning casualties. A first attempt is presented in this section.

The number of casualties in a given region and during a given period of time depends on the population vulnerable to lightning strikes, the number of flashes, and the area of the region. Numerically, one can pose the following question: Is there a functional relationship between the number of lightning casualties $N_c$, the number of flashes $N_f$, the population $N_p$, and the area A, of a particular

region during a given period of time? Specifically, we are interested in large areas (e.g., country or state scale) and long periods of time (at least a year).

If we assume that the population vulnerable to a lightning strike is uniformly distributed over the given area, then each flash has the same probability $P_h$ of hitting a person. In terms of the Binomial Probability Law: If the probability of success is p, and the number of trials is n, then the expected number of successes is n x p. In our context: $P_h$ = probability of a success and $N_f$ = number of trials. So,

$$N_c = N_f \, P_h. \qquad (1)$$

Now we need to determine $P_h$ in terms of the known parameters.

The probability of one flash of lightning hitting a person in an area can be expressed as

$$P_h = e \, N_p \, P_{h'} \qquad (2)$$

where

$N_p$ = total population of the area,
e = exposure factor (the fraction of the population exposed to lightning), and
$P_h$ = probability of one flash of lightning hitting a particular person.

Lightning can be considered to hit a person if any part of the person lies within the area of influence of the flash. It can be assumed that the area that can be affected by an average flash and the area an average person occupies are circles of radii $r_f$ and $r_p$, respectively. As shown in Fig. 12, the total area of success (hit) is then

$$A_h = \pi (r_f + r_p)^2. \qquad (3)$$

And the probability of lightning hitting a particular person is

$$P_h = A_h / A. \qquad (4)$$

Substituting into Eqn. 1 yields the desired relationship

$$N_c = N_f \, N_p \, e \, \pi (r_f + r_p)^2 / A. \qquad (5)$$

That is, the number of casualties is directly proportional to the flash density over the area, the population, and the exposure factor. The radii of influence $r_f$ and $r_p$ can be assumed to be basically constant for all regions, and can be taken as the averages for all sizes of people and types of flashes.

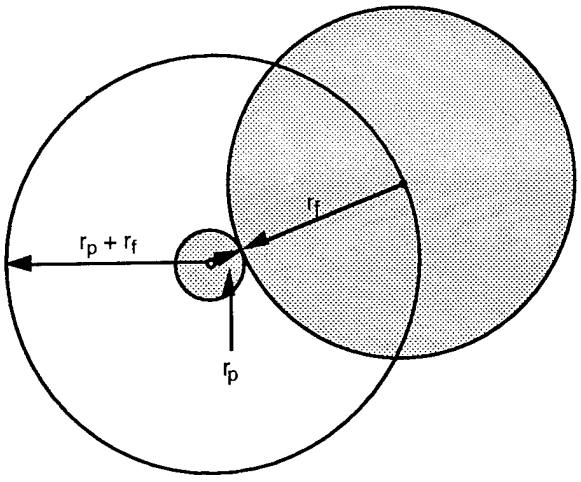



*FIGURE 12. Schematic representation of the area affected by a flash and the area occupied by a person (shaded circles of radii $r_f$ and $r_p$, respectively). The total area of success (clear circle of radius $r_p+r_f$) represents all possible locations of the flash that would produce a hit.*

According to this model, gradual changes with time in $N_p$, the population of the region, would cause a demographic trend in $N_c$, the number of casualties. Population changes have been basically linear for the nation as a whole and for most states during the last 40 years. Therefore, the trend in the number of casualties produced by the population change would also be linear. Dividing the number of casualties occurring each year by the corresponding population would produce a series of yearly normalized casualties that would not contain this trend.

Equation 5 also indicates that changes in the exposure factor e, the fraction of the population vulnerable to being hit by lightning, would be responsible for trends in the normalized casualties. This factor varies gradually with time in accordance to socioeconomic changes in the population. Thus, as (1) better forecasts and warnings are produced, (2) people are better educated on the nature of the lightning threat and safety precautions, and (3) occupational changes away from outdoor employment take place, the fraction of the population exposed to the lightning threat gradually diminishes.

Therefore, the number of normalized casualties would drop accordingly. In the previous analyses we have assumed that the changes in e were linear in time and have extracted the linear downward component present in the normalized casualty series to produce departure series that would not contain this socioeconomic factor.

The model also indicates that changes with time in $N_f/A$, the flash density over the region, would produce fluctuations in the departure series of normalized casualties. Changes in flash density are indicative of variations in the thunderstorm activity of the region. These variations are in turn due to changes in the synoptic situation which correspond to large-scale changes in surface temperature distributions. The residual fluctuations in the departure series of lightning casualties from our data appear to, indeed, be related to fluctuations in thunderstorm activity, synoptic situation, and surface temperature.

## SUMMARY AND CONCLUSIONS

Time fluctuations in the number of lightning deaths and injuries from 1959 to 1990 have been examined by analyzing time series of lightning casualties derived from the NOAA publication *Storm Data* for the contiguous United States. The effect of the population increase during the period was removed by dividing the yearly values of casualties by the corresponding yearly population. The resulting population-normalized series revealed the presence of an overall linear trend in the number of total casualties per million people amounting to a decrease of 30% during the 32 years of data. It is possible that this downward trend in casualties resulted from a combination of improvements in thunderstorm forecasts and warnings, increased efforts in the education of the public about the lightning threat, and changes in socio-economic patterns.

In addition to this overall trend, there was a 40% reduction in the number of population-normalized deaths (but not of non-fatal injuries) during the period of record. It appears that this additional reduction in deaths was due to improved medical attention given to lightning victims such as a faster response of emergency medical services, better life support technology, and wider knowledge of cardiopulmonary resuscitation techniques among the public. This improved medical care would increase the chances of a person surviving a lightning strike but would not affect the number of total casualties.

Superimposed on the overall downward trend there were fluctuations of one or two decades in duration. From the beginning of the period in 1959 until 1968 there was a very sharp reduction in the casualty departures from the trend. Starting in 1969 and continuing until the present time, however, there has been an overall increase in the casualty departures. This general increase was modulated by an oscillation from low to high to low values from 1967 to 1980. From a comparison of the series of lightning casualty departures from the linear trend with series of different climatological variables, it appears that these oscillations are climatologically related. The patterns of these fluctuations were parallel to nation-wide changes in thunder-day frequencies, cyclone frequencies, and temperature values.

A simple conceptual model shows which are the principal factors responsible for the variations in the number of lightning casualties. The model indicates that the number of casualties is directly proportional to the flash density over the area, the population, and the fraction of the population exposed to the lightning threat. The effect of these different factors is to produce demographic and socio-economic trends, as well as climatological fluctuations in the number of casualties.

*Acknowledgments.* The work of R.M. Passi was supported by ONR Grant No. N00014-95-1-0069.

## REFERENCES

1. R.E. López and R.L. Holle. "Fluctuations of lightning casualties in the United States: 1959-1990." Journal of Climate (Submitted), 1995.

2. R.E. López, R.L. Holle, T.A. Heitkamp, M. Boyson, M. Cherington, and K. Langford. "The underreporting of lightning injuries and deaths in Colorado." Bulletin of the American Meteorological Society, Vol. 74, 2171-2178, 1993.

3. R.E. López, R.L. Holle, and T.A. Heitkamp. "Lightning casualties and property damage in Colorado from 1950 to 1991 based on Storm Data." Weather and Forecasting, Vol. 10, 114-126, 1995.

4. R.L. Holle, R.E. López, R. Ortiz, C.H. Paxton, D.M. Decker, and D.L. Smith. "The local meteorological environment of lightning casualties in central Florida." Preprints, 17th Conference on Severe Local Storms and Conference on Atmospheric Electricity, St. Louis, MO, American Meteorological Society, Boston, 779-784, October, 1993.

5. S.A. Changnon. "Secular variations in thunder-day frequencies in the twentieth century." Journal of Geophysical Research, Vol. 90, 6181-6194, 1985.

6. K.M. Zishka and P.J. Smith. "The climatology of cyclones and anticyclones over North America and surrounding ocean environs for January and July, 1950-77." Monthly Weather Review, Vol. 108, 387-401, 1980.

7. R.R. Heim, Jr., C. Garvin, and L. Nicodemus. "State, regional, and national monthly and annual temperature weighted by area for the United States, January 1931 - December 1991." Historical Climatology Series 4-1. National Climatic Data Center, Asheville, North Carolina, 77pages, 1993.

# SESSION 08B
# ORDNANCE AND EXPLOSIVES
# CHAIRPERSON: JACK NIAL

# LIGHTNING COUPLING TO EED LINES

André SCHAFFAR
AEROSPATIALE - Espace & Défense
Boîte postale n° 2
78133 Les Mureaux Cedex - FRANCE

Téléphone (33) 1.34.92.27.45 FAX (33) 1.34.92.17.34

## ABSTRACT

The topic of this paper is to present a method allowing the analysis of the ignition risk of Electro Explosive Devices (EED) integrated in a launch vehicle or rocket when it is struck by lightning.

Three types of EED have been considered: low and mean energy hot wire and exploded wire.

The first step consisted in establishing an electrical model of each type of EED, derived from differential mode impedance measurement on real devices.

On the other hand, tests of hot wire EED susceptibility to various lightning pulses were performed.

In a third step the whole control line was modelized in order to compute the interference induced in EED filament.

The ignition risk has been found to be very low for a 10 kA lightning threat.

The remaining work consists in modelling validation by global test.

Finally, a system tool which is able to deal with every threat and coupling configuration will be available.

## INTRODUCTION

In the development of launch vehicles or rockets, there is a permanent need of assessment of lightning coupling to EED, in order to build a vehicle the design of which minimizes the ignition risk in case of ligthning threat on ground or in flight.

The need is due to the lack of representative mock-up on which tests can be performed in the early phases of programs.

So a coupling assessment method has been set-up. It is based on elementary tests on EED and cables whose results contribute to electrical model construction, and modelling in order to compute EED filament response to ligthning pulse flowing along vehicle structure.

Modelling requires two types of tools:

- harness electromagnetic environment calculation is performed by 3D code solving Maxwell's equations,
- cable or harness coupling is treated by a transmission line code.

## REFERENCE CONFIGURATION

A very simple configuration has been choosen for the study (see figure 1).

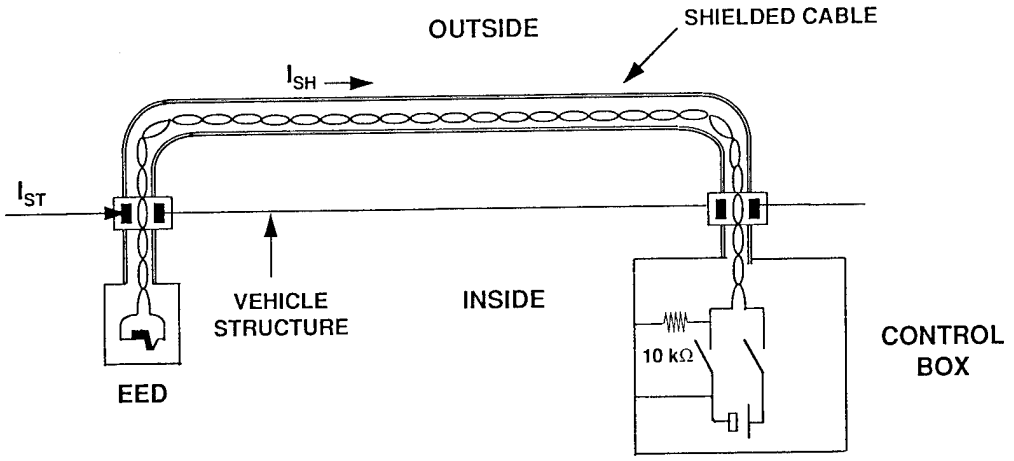



FIGURE 1 - CONFIGURATION

EED is fired by a Control Box enclosing battery, Control relay and EED grounding resistor. Control Box real design is generally more complex. Both devices are integrated inside vehicle structure. They are interconnected through a twisted and shielded double wire cable; the shield is grounded a both ends. Cable routing is mainly located outside vehicle structrure.

EED can be of three types:

- hot wire-low energy,
- hot wire-mean energy,
- exploded wire,

Control Box design applies only on hot wire EED.

## MAIN STEPS OF METHOD

The main steps of method to process the reference configuration are listed herunder.

1. Cable shield current computation by 3D FDTD code (input for cable response calculation).

## CABLE SHIELD CURRENT COMPUTATION

The cable shield current computation process is described in figure 2. The example refers to ARIANE 5 on launch table.

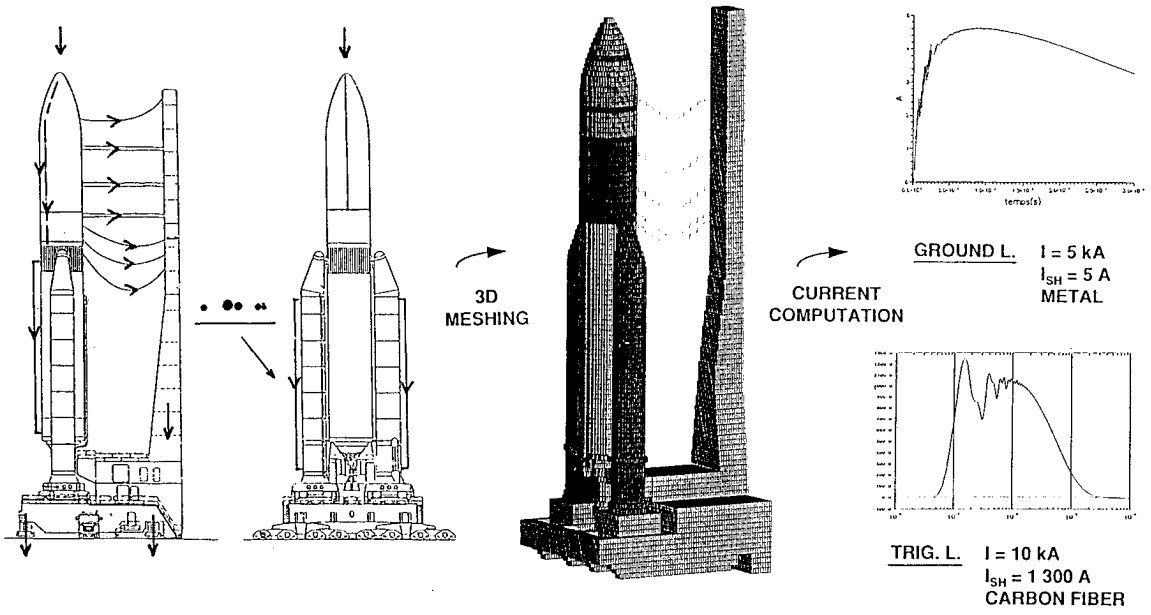



FIGURE 2 - CURRENT COMPUTATION PROCESS

Launcher top could be hit by lightning on ground and perhaps in flight (appropriate launch rules will avoid the risk). Currents flowing along structure may have different shapes, according to relevant phenomenology: on ground lightning pulse features a few microseconds rise time, whereas in flight the phenomenon leads to tens of microsecond.

Cables of concern are located outside lower stages which are made of metal, or inside upper fairing, the structure of which is made of carbon fiber.

2. EED input impedances measurement in order to derive an electrical model.

3. Cable shield transfer impedance measurement (required as input for transmission line code).

4. Tests of EDD susceptibility to lightning pulse.

5. EED line coupling modelling with transmission line code, its output being ligthning pulse characteristics in EED filament.

6. Susceptibility assessment.

An example of cable bundles arrangement over a booster structure is shown in figure 1.

Then, 3D FDTD modelling requires a meshing, the dimensions of which being linked to time step through the well known stability condition.

Cable current can be computed by two methods:

- in case of simple configuration (typically 2 to 3 cables or bundles) cables can be introduced in 3D modelling according to thin wire formalism,
- for more complex configuration, electromagnetic topology concepts can be used; this requires the electromagnetic fields calculated by 3D code as an input.

Two examples of results are given in figure 1:

- ground lightning of peak level 5 kA and 6 µs time to peak induces a peak shield current of about 5 A for a cable over a metal ground plane,
- if the ground plane is made of carbon fiber, and for a 10 kA triggered lightning strike having a time to peak of 100 ns the induced peak current reaches 1,3 kA.

## EED ELECTRICAL MODEL

Differential and common mode impedances have been measured by a reflectometry method, on five samples of each type of EDD, in order to set-up electrical models.

Results are very similar for every samples of each type.

Internal design and electrical models are given in figure 3.

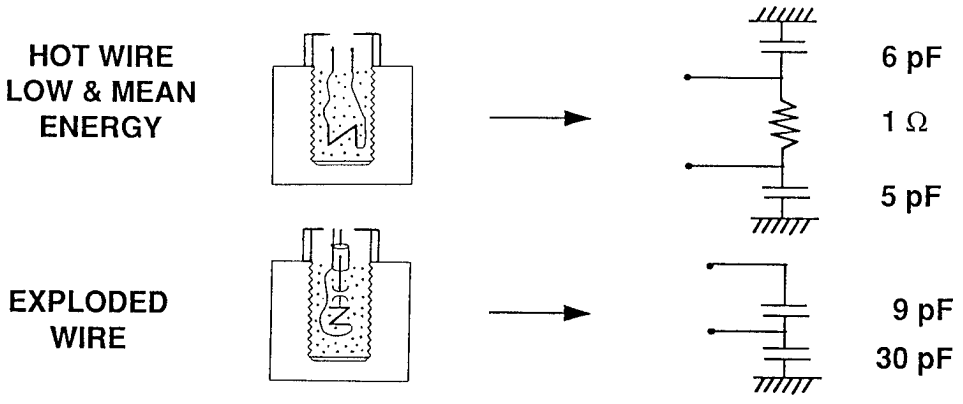



FIGURE 3 - ELECTRICAL MODELS OF EED

The hot wire model is the same for low and mean energy. Common mode impedances are small capacitors having almost the same value. Filament resistance is 1 Ω.

The exploded wire model is not symetrical, because its connector is coaxial. The differential mode impedance is due to the spark gap connected in series with the wire. The validity domain of these models reaches 50 MHz.

## CABLE TRANSFER IMPEDANCE

Cable shield transfer impedance and also cable geometry over the ground plane, are required inputs for the transmission line code. The first data is given in figure 4, for a AWG 22 twisted/shielded double wire cable, the length of which being 33 cm.

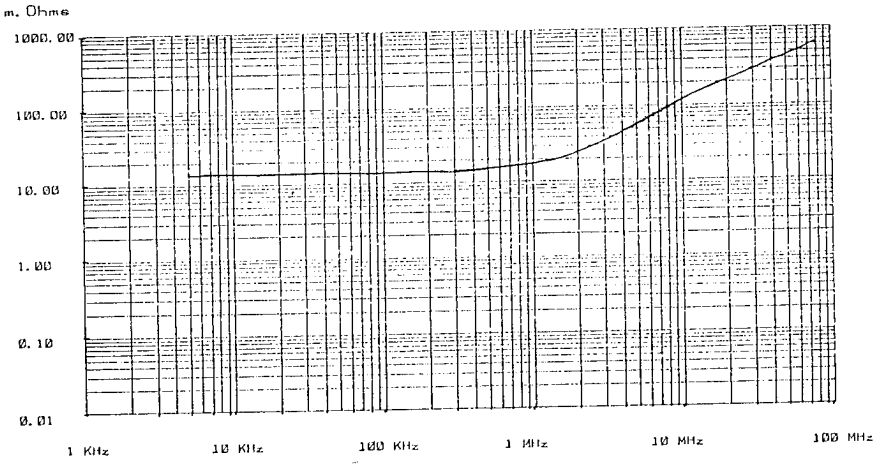



FIGURE 4 - CABLE TRANSFER IMPEDANCE

The following transfer impedance model can be derived from this curve:

$$Z_t = R_t + j\omega L_t \quad \begin{cases} R_t = 42\ m\Omega/m \\ L_t = 2.10^{-8}\ H \end{cases}$$

## EED SUSCEPTIBILITY

Susceptibility tests have been performed only on hot wire EED.

Two pulse durations have been applied: 10 and 100 µs (FWHM).

Results are given in table 1

| PULSE DURATION (FWHM) | SUSCEPTIBILITY LEVEL (A) (99%) | | | |
|---|---|---|---|---|
| | LOW | | MEAN | |
| | $I_F$ | $I_{NF}$ | $I_F$ | $I_{NF}$ |
| 10 µs | 10 | 6 | 24 | 13 |
| 100 µs | 5 | 3 | 6 | 5 |

TABLE 1 - EED SUSCEPTIBILITY

Firing and no-firing currents ($I_F$ and $I_{NF}$) have been determined, according to Bruceton methodology (probability 0.99, confidence level 0.95).

No statistical data are available for exploded wire EED, nevertheless it is known that its firing requires about a 1 kV, 1 µs pulse.

## COUPLING ANALYSIS

## MODELLING

Former established data allow to sep-up the coupling model (see figure 5) for hot wire EED.

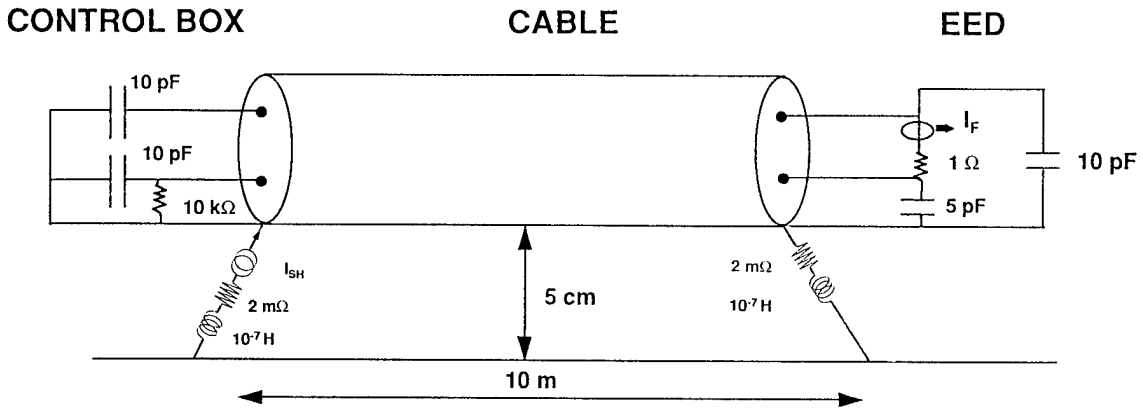



FIGURE 5 - COUPLING MODEL

Control Box relay contact model is a 10 pF capacitor (measured); EED common mode capacitors dissymetry has been increased.

Pigtails are modelized by a 2 mΩ, $10^{-7}$ H series dipole.

The height of the shield above the ground plane is 5 cm.

The current calculated by 3D code is injected into the shield by a source put in a pigtail (the current is approximately constant along the shield).

The tool used for coupling simulation is a transmission line code (multi-wire) called CRIPTE, developed by french O.N.E.R.A. according to electromagnetic topology concepts (BLT equation). This code works in frequency domain, thus time domain applications require Fourrier transform computation.

Outputs of the code may be every desired parameter such as currents in wires, in terminal loads, and voltages versus shield potential.

## RESULTS

Main results are given in figure 6 which shows filament current in frequency and time domains - EED common mode voltage is also shown.

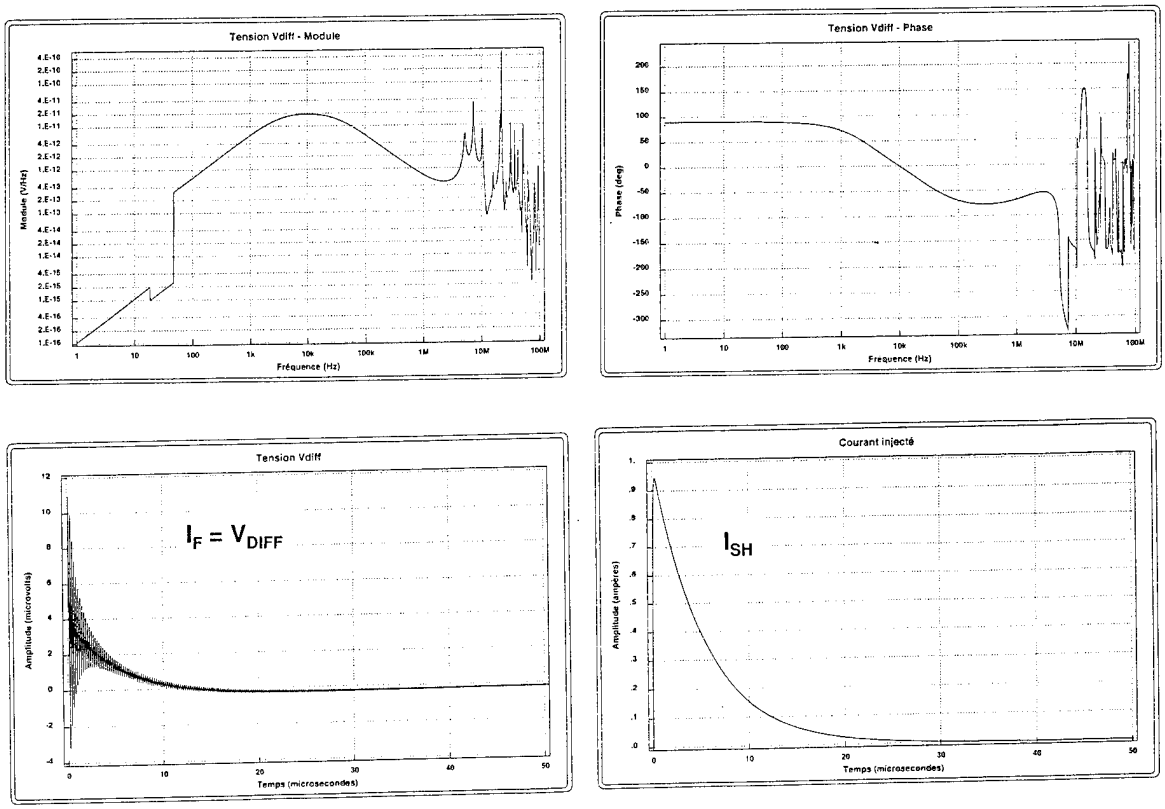



FIGURE 6 - COUPLING RESULTS

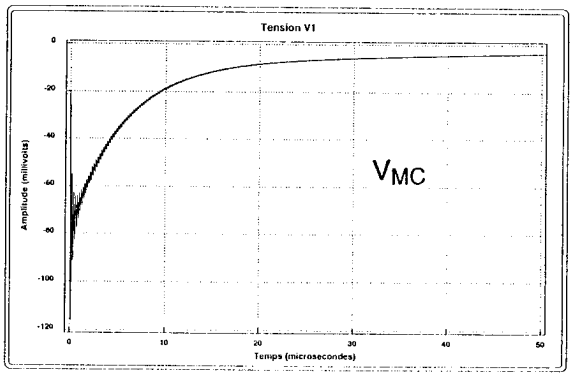



FIGURE 6 - COUPLING RESULTS

The injected current corresponds to triggered ligthning.

It is modelized by the double exponential equation:

$$I_{SH} = I_0 (e^{-\alpha t} - e^{-\beta t}) \quad \begin{cases} I_0 = 1\ A \\ \alpha = 1{,}9.10^5 \\ \beta = 19.10^6 \end{cases}$$

The filament response current features the same shape with a surimposed high frequency oscillation (~ 8 MHz). Its peak value is 12 µA. For a shielding current of 1 300 A, filament current reaches 16 mA and common mode EED voltage 156 V.

## CONCLUSIONS

## SUSCEPTIBILITY

For hot wire EED, in a severe coupling case (triggered lightning, carbon fiber structure), current induced in filament is 16 mA for a 10 kA threat, when low energy susceptibility threshold is 6 A (10 µs pulse).

On the other hand, common mode voltage of 156 V cannot produce the ignition of EED.

So at 10 kA the risk is negligible. At 100 kA, there still remains a margin of about 30 dB.

Modelling has not been performed for exploded wire, but due to required ignition pulse characteristics (1 kV, 1 μs), the risk is assessed to be negligible.

## FURTHER DEVELOPMENT

The remaining work consists in modelling validation by a global test performed in a strip line with, however, some difficulties (no access to filament current, differential mode measurement).

After this validation, a system tool able to deal with every ligthning threat and coupling configuration will be available.

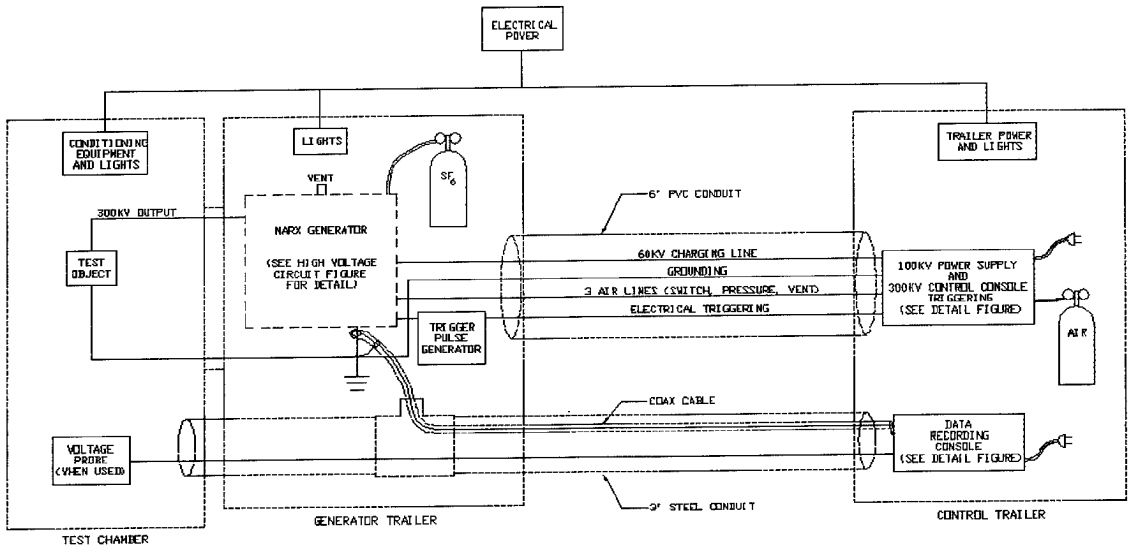
# A TEST FACILITY FOR DETERMINING WEAPON SYSTEMS VULNERABILITY FROM THE ELECTROSTATIC DISCHARGE (ESD) PHENOMENON

Nickolas Kaloterakis, Joseph Dulcey, John A. Nial, T. William Ammons
Electronic Systems Development Branch, Code 6720
Indian Head Division, Naval Surface Warfare Center,
Indian Head, MD 20640-5035
Telephone (301) 743-4466 FAX (301) 743-4004

**ABSTRACT**: This report describes the test facility built at Naval Surface Warfare Center, Indian Head Division (NSWC/IHDIV) to determine weapons systems' vulnerabilities to helicopter borne Electrostatic Discharge (ESD). The Navy's ESD research and development test facility provides the environment(s) for testing ordnance sensitivities in many environments. An ESD pulse can follow an electrical path directly to an Electroexplosive (EED) component or to a sensitive explosive component. This report discusses the design, development, and implementation of the NSWC/IHDIV test facility and the problems encountered. This report details the instrumentation and test verification processes. The NSWC/IHDIV test system consists of a Marx generator a high voltage transmission line and data acquisition system. The Marx generator provides the ESD pulse by charging a set of capacitors in parallel and discharging them in series.

**INTRODUCTION:** After installing a facility to test for helicopter ESD vulnerability of weapons systems, we thought a paper was appropriate to communicate to our colleagues the challenges we encountered and the methods by which we met these challenges. The challenges stemmed from our desire to perform 300 kilovolt ESD testing on weapons with live explosive components. Since we were dealing with the mixture of explosives and high voltage, our first concern was the safety of the operation. Our second concern was to verify the specified capacitive discharge pulse is delivered to the test item. The ESD test specified in MIL-STD-331 is for fuzes. The reason we built a facility that would be capable of testing weapons instead of just fuze components is we did not feel that verifying the fuze was adequate in determining a weapon's vulnerability to ESD. The subject of weapon vulnerability to ESD merits consideration in a separate paper in this conference.

**Figure 1**




ELECTROSTATIC DISCHARGE TEST EQUIPMENT SCHEMATIC

**FACILITY SAFETY DESIGN AND OVERVIEW:**

Figure 1 depicts the layout of the facility. The facility was designed in three sections: the explosion hardened test chamber, the Marx generator section, and the control room. The explosion hardened test chamber is adjacent to the Marx generator trailer. The control room is approximately 60 feet from the Marx generator trailer. The instrumentation trailer is where operation personnel are located during the test. The

explosion hardened test chamber and the standoff distance from the control room to the test chamber reinforce personnel safety during a test. To protect the Marx generator, we located it in a separate trailer and not inside the test chamber. This way we can keep most of the high voltage components away from explosives. A high voltage coaxial output line transfers the pulse to the test object inside the test chamber.

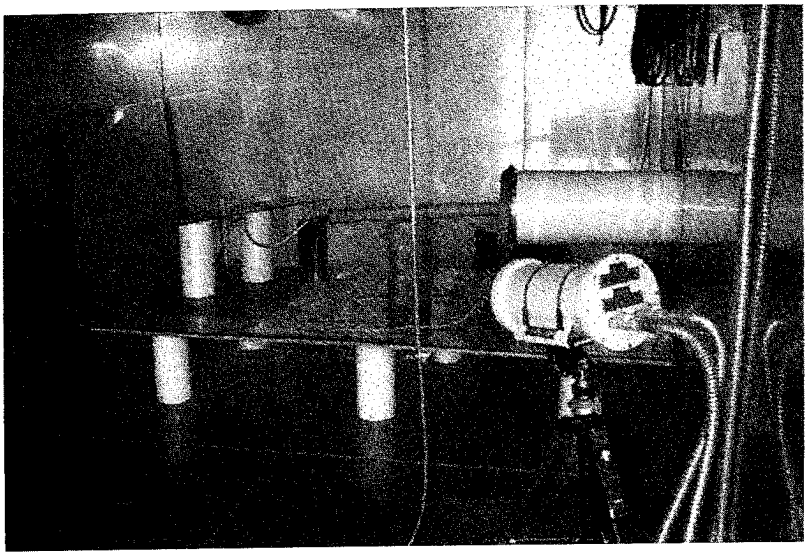
Marx generator high voltage components are enclosed in a tank that must be filled with Sulfur-hexafluoride ($SF_6$) gas. $SF_6$ gas is used for its dielectric strength. Since, the gas is five times denser than air, it displaces air, and is an asphyxiator. To mitigate the asphyxiation hazard, we installed ventilation ports at the bottom of the trailer. Prior to electrically charging the Marx, the 100 kilovolt air switches in the Marx are pressurized to 50 psi. Pressurized synthetic air (79% Nitrogen- 21% Oxygen) is routed from the control trailer to the Marx generator trailer and is controlled by electrical solenoids in the control console. The Marx air switches can be pressurized, purged or "dumped". Purging is used to rid the switches of ionized air. Dumping can be used to lower the pressure in the air switches to "erect", or discharge at the Marx generator. The 60 kilovolt charging line runs from the control console in the instrumentation trailer to the Marx generator trailer. The charging line is shielded, with the shield connected to ground at the Marx generator to prevent electrocution if the high voltage line dielectric breaks down. A separate air line is used to control a capacitor bleed (shorting) switch inside the Marx generator. This switch bleeds (discharges) the Marx capacitors and is automatically in the "Bleed" position at shut down so the capacitors do not self-charge. As a result of dielectric polarization, the capacitor dielectric has memory. The fall time (90% discharge time) of the bleed circuit is 15 seconds. We require a wait time of 30 seconds prior to an operator leaving the instrumentation trailer after a test. This way, we can be assured the Marx is discharged when the operator enters the Marx trailer or the test chamber.

Charging of the Marx generator is not possible unless five electrical interlocks are engaged. The first interlock is the operating console key. Without the key the facility is inoperable. There are two interlock switches in the Marx generator trailer, one for the door and one for the grounding staff. The grounding staff must be in its cradle and the door closed for the Marx to charge. The grounding staff is located across the doorway so it blocks the entrance (once the door is opened). The grounding staff tip is a grounded brass hook isolated from the operator by a long insulated handle. The staff must be picked up by the person approaching the Marx and used to ground the Marx. The remaining two interlocks are the test chamber door switch and the test chamber grounding staff switch. The test chamber door must be closed and the grounding staff must be placed in a cradle at the doorway closing a switch before the Marx can be charged.

The output of the Marx generator is always grounded when test items are being handled at the test chamber. Personnel do not leave the instrumentation room without the operating console key. The explosive operators are required to wear conductive shoes and are preceded by a test engineer who safely shorts the output of the Marx by first using the grounding staff to ground the output line of the Marx and then connects a

grounding cable. The area is sealed off and all personnel must remain inside the control trailer during a test with live ordnance. The area is completely enclosed by a fence. A second outside gate is monitored. A yellow rope designates the high voltage area and a flashing red light functions when the facility enable (interlock) key is inserted in the operation console.

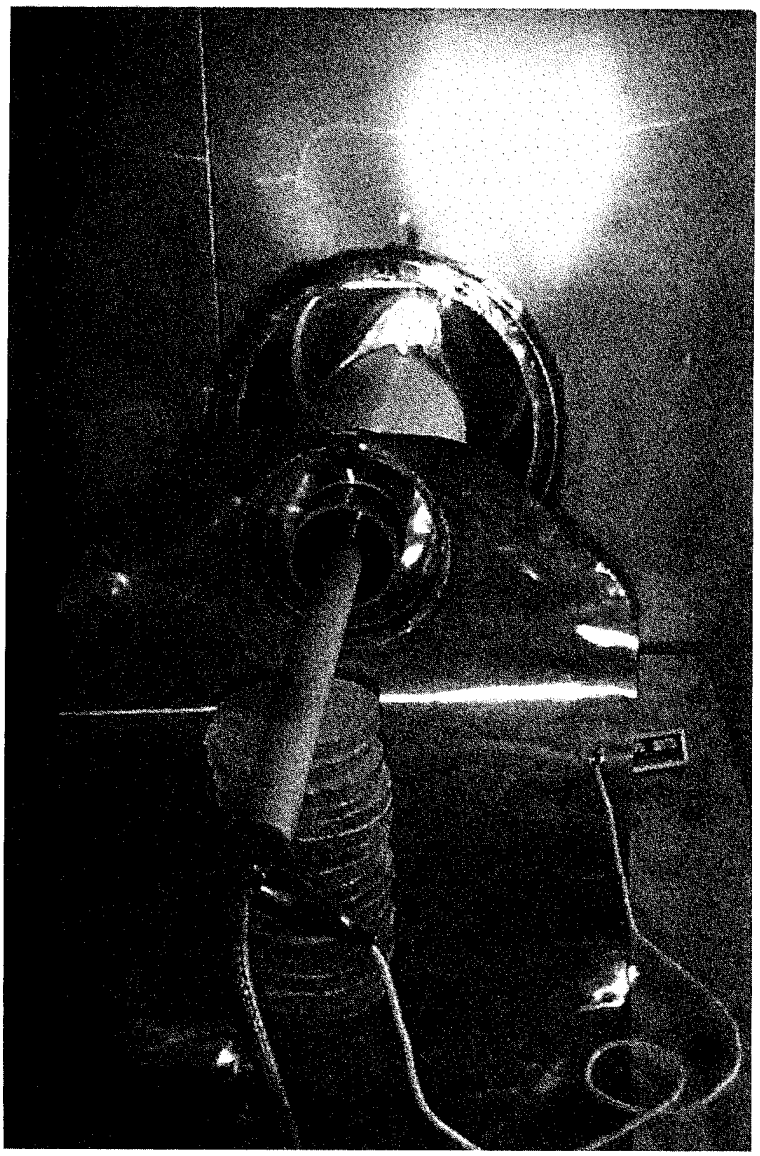
**Figure 2**



**EXPLOSION HARDENED TEST CHAMBER**-- Figure 2 is an image of the explosion hardened environmentally controlled test chamber. It is a walk-in box that is capable of stable temperatures in the range of -65 to +165 °F. This temperature range is much wider than necessary for MIL-STD-331 testing, however, it lends itself to explosive sensitivity research for hot and cold environments. The chamber is equipped with a video camera in an explosion hardened enclosure.

The high voltage Marx output line is brought to the test chamber by a tube that connects the Marx to the output chamber. The high voltage discharge output is carried by a 0.5 inch coaxial center conductor connected to the output of the Marx generator located in a trailer approximately 2 feet away from the test chamber. The return path of the high voltage discharge is the copper inner lining of a 12 inch PVC pipe. A 3 inch and 6 inch PVC pipe, (as well as the air) isolate the signal line from the outer (return) coaxial conductor. The coaxial line is further shielded on the outside of the test chamber by a 2 ft. diameter stainless steel tube reaching from the stainless steel test chamber to the Marx trailer. To mitigate safety and radio emission problems we eliminated large potential (voltage) differences between the Marx generator trailer and the test chamber. We accomplished this by isolating the Marx output and return lines from the stainless steel chamber. The copper plane that is part of the return path rests on a polycarbonate bed approximately 2 feet off the chamber floor and supported by PVC pipe legs.

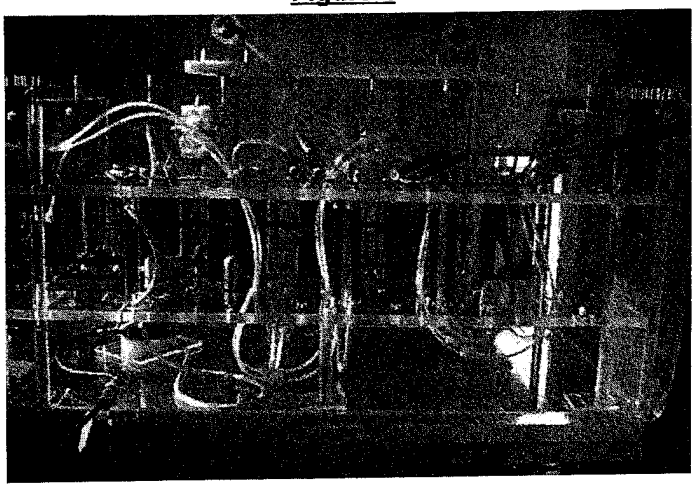
**Figure 3**



Approximately 50 inches from the output of the Marx, 24 inches inside the test chamber, the 12 inch outer coaxial return line changes into a copper "ground" plane. The line above the ground plane carries the discharge signal to the test item. This line is grounded when not in use. The coaxial output line makes a transition to a ground plane and a parallel conductor. Figure 3 illustrates the system output line in detail. The capacitance of the coaxial line is calculated to be 28 picofarad. The capacitance of the (parallel) line to the ground plane is calculated to 26 picofarad. This closely matches the 60 picofarad of capacitance we measured with the impedance analyzer. These parameters were used in our computer models.

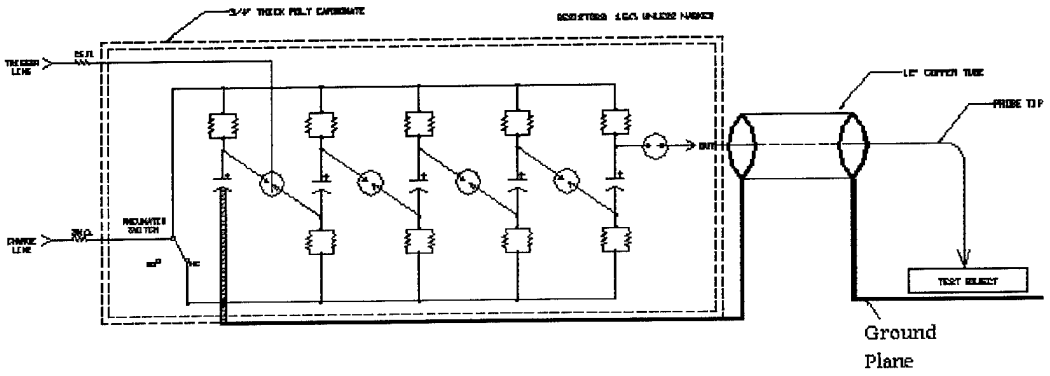
The length of the coaxial output line is approximately 1.37 meters which means transmission line effects become applicable at frequencies greater than 21 MHz, and are prevailing after 76 MHz. The measured frequency bandwidth is 1 Hz to 20 MHz. The primary signal being measured is under 20 MHz.

**Figure 4**



**MARX GENERATOR--** The Marx generator, shown in figure 4, is the heart of the ESD facility and it is located in the Marx generator trailer next to the test chamber. The Marx generator is filled with $SF_6$ gas prior to functioning. The Marx generator simplified schematic is shown in figure 5. It is composed of five 100 kilovolt, 5 nanofarad, capacitors charged in parallel and discharged in series. We measured the overall capacitance of the Marx generator by installing shorting bars across the high voltage switches and measuring the capacitance of the five capacitors in series using the HP 4194 analyzer. The capacitance value was 1.02 nanofarad. The switching is accomplished by 100 kilovolt air gap switches.

**Figure 5**



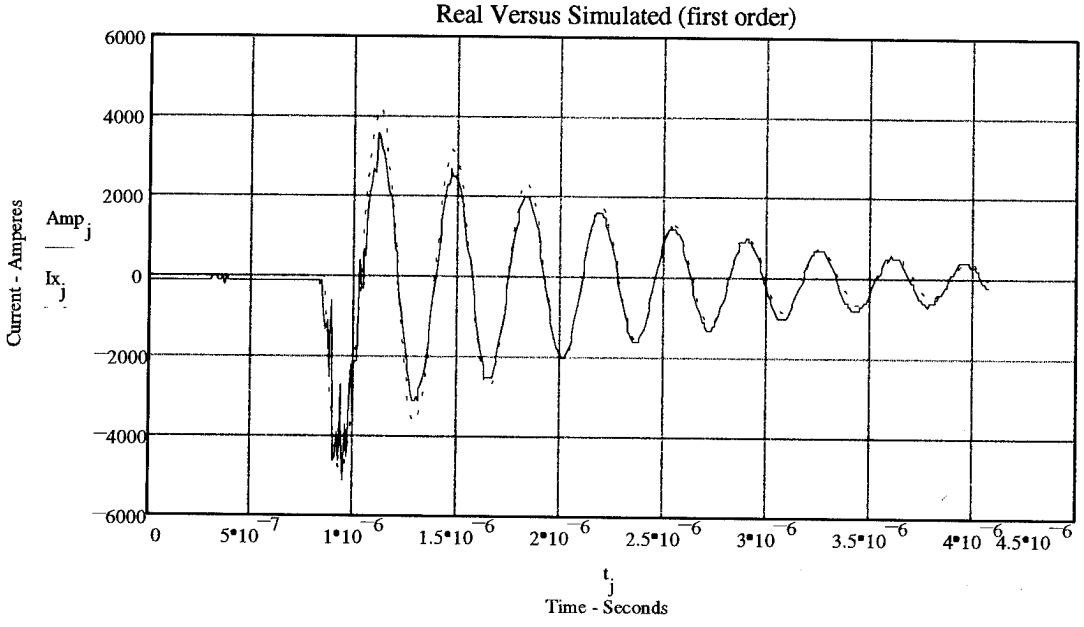

The air switches will only hold about 20 kilovolts at standard atmospheric pressure. The Marx may be triggered by applying a high voltage pulse to the switches' center plate or by lowering air pressure. During a test the air switches are typically pressurized to 50 psi. Dropping the pressure on the switches erects the Marx generator. Earth grounding of the generator is accomplished at the return entry point of the Marx generator. That point is directly beneath the last capacitor as shown in figure 5. Earth grounding is required by safety regulations.

**TEST MEASUREMENTS AND SYSTEM IMPROVEMENTS:** When we originally tested the generator, we observed the peak current amplitude was low, approximately 2

kiloamperes, during a normal short circuit discharge. This meant the inductance of our Marx generator was high. The reason was the high voltage switches were to the left or right of the capacitors. In fact the wiring of the Marx formed a coil. To determine the Marx inductance, we circumvented the air switches by installing a flat copper bar across each switch. Then, we measured the impedance using a HP 4194A phase gain analyzer and found the inductance of our original generator was in the order of 7.2 microhenries. MIL-STD-331 allows up to 20 microhenries. To reduce the inductance we changed the current path through the Marx by locating the air switches to minimize the length of the path. The result was the alignment of the capacitors and air switches on one (vertical) plane as shown in figure 4 and in the simplified schematic, figure 5. The reduction in inductance gives the test engineer the ability to test at higher frequencies and higher current amplitudes while maintaining his option to add inductance for the purpose of testing at lower frequencies and lower current amplitudes. The improved Marx inductance is in the order of 1 microhenry. The output line adds approximately 2 microhenries of inductance.

We can model the high voltage discharge as a series resistive-inductive-capacitive (R-L-C) circuit. R is 5 ohms L is 3.2 microhenries and C is 1.02 nanofarad charged to 300,000 volts. Figure 6 shows the ideal "simulated" discharge as a dotted (blue) line, overlapped with actual current data from a Marx discharge into the test a short circuit in the test chamber at the end of the output line. The actual current trace data is shown in figure 6 as a solid (red) line. The "ringing" on the peaks of the sinusoid is caused by the distributed capacitance/ inductance in the system. The current is detected by a Pearson 20 MHz bandwidth current probe. The bandwidth is adequate for the major harmonic; however, the higher harmonics are attenuated.

**Figure 6**



The simulated waveform shows a 5 ohm loss in the discharge system. This loss is due to the dielectric loss of the capacitors. This loss was confirmed by the HP 4194A impedance analyzer. MIL-STD-331 does not address losses in the capacitors. MIL-STD-331 only addresses the DC resistance of the RLC circuit. The measured circuit resistance of our system is 0.026 ohms. We have discussed the issue of dielectric loss with capacitor vendors. We have been told we can trade a decrease in loss with an increase in inductance. We have not completed our trade-off study at this time.

MIL-STD-331 requires a "calibration" test of the discharge circuit. The calibration test requires using a 100 ohm resistor as the "test load". When we first observed the 100 ohm discharge we noticed the waveform was not as clean as we expected. The waveform is depicted in figure 7.

The reason for the distortion is the distributed capacitance and inductance resulting from the Marx and output line geometries. We can use computer circuit simulations to illustrate the source of the distortion or "ringing" found in the measured discharge of figure 7.

**Figure 7**

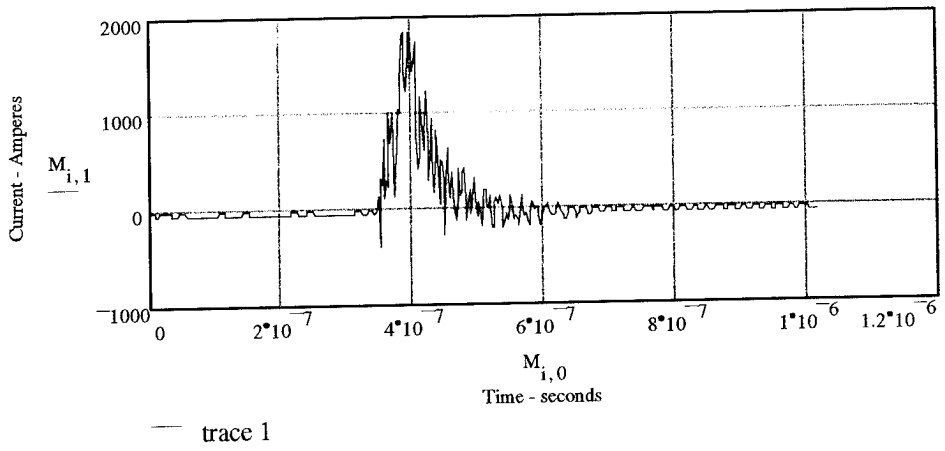
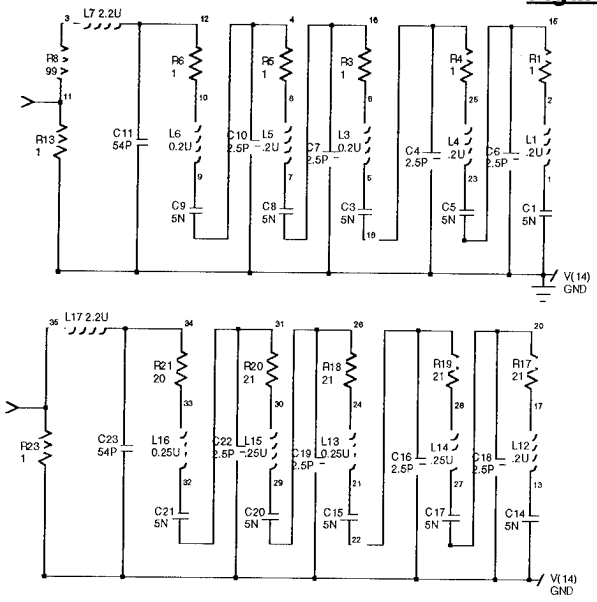
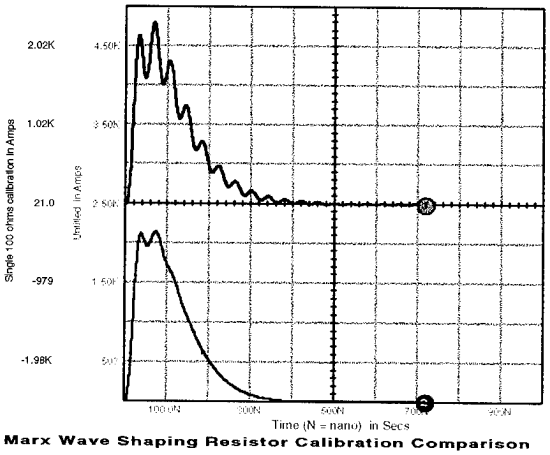



Figure 8 depicts two circuit models of our discharge circuit and their current traces (simulations). The current is "measured" by the computer monitoring the voltage measured across a 1 ohm resistor that is part of the calibration load. The top model represents our current calibration method where a single 100 ohm load is substituted for the test item. The bottom circuit model on figure 8 has five 20 ohm loads that are distributed to dampen each RLC subcircuit in the discharge path. It is obvious from figure 8 the distributed resistances would damp the "stray" RLC circuits in the discharge path, resulting in a cleaner waveform. Figure 9 Illustrates the current of the single and distributed Marx circuits at the return point of entry of the ground plane into the last capacitor of the Marx generator. The effect of the multiple return paths through the stray capacitors is more pronounced. One consequence of the high frequency ringing is it can further distort our measurements since our current probe is nonlinear at

frequencies above 20 MHz. We are now working on improving the current measurements by incorporating a different current probe.

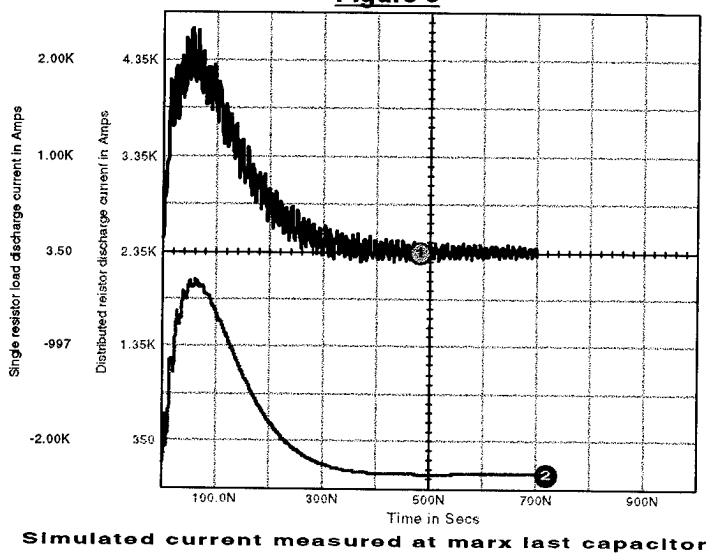
**Figure 8**




**Marx Wave Shaping Resistor Calibration Comparison**

**Figure 9**




**Simulated current measured at marx last capacitor**

The Marx was furnished with a high voltage probe. The probe was functional, however it presented a 1 nanofarad capacitive load to the measuring point. This was not acceptable. We were forced to purchase a second voltage probe that is basically a copper sulfite voltage divider currently calibrated by the manufacturer for a 800:1 voltage divider ratio.

**Future instrumentation**: We have experienced a need for instrumentation that will permit us to monitor current and voltage signals across electroexplosive devices. We do not think these measurements will be a substitute for live ordnance testing. However, we do feel it can provide us with the margin of safety for an EED that is experiencing energy transfer from ESD. In addition, voltage and current data will be useful for evaluating prototype designs.

**Data Records**: We record data for every discharge in a test sequence. This is accomplished by retrieving the voltage data from a HP54110 oscilloscope through the IEEE-488 instrumentation bus. The voltage data is scaled to account for the attenuators in the measurement transmission line. Traces of every test shot on a test specimen are recorded and maintained in permanent memory or disk.

**SUMMARY:** This paper presents the operating design of a facility for high voltage explosive testing. Three fundamental safety hazards were addressed in the design: electrocution, asphyxiation, and explosive mishaps. The test chamber and Marx generator electrical parameters were modeled. Design improvements to the Marx generator and their effects were discussed. Improvements were done to decrease system inductance and to affect a wider frequency bandwidth. This allows for the inductance to be increased by the test engineer. The ESD test facility is a tool that should be used in conjunction with analysis to bring out weapon system vulnerabilities. Calibration measurements and suspected distortions were explained and improvements proposed. One of the improvements we considered involved incorporating distributed damping resistors to smooth the measured distortions. After rethinking the proposed improvement we decided incorporating wave shaping resistors changes the output of any real-world Marx generator so it "smoothes" imperfections caused by multiple RLC circuits. A Marx is a tool of engineering practicality because it is extremely difficult to hold and direct 300,000 volts. Since a Marx is an imperfect tool that approximates a single capacitor being discharged, it is best to measure its true output. Ongoing improvements to the facility include pulse voltage measurements and EED instrumentation.

# EXPLOSION PROOFING THE "EXPLOSION PROOF" VACUUM CLEANER

R. D. Jones, K. C. Chen, and S. W. Holmes
Electromagnetic Analysis and Test Department
Sandia National Laboratories
Albuquerque, New Mexico 87185-0865, USA
Telephone (505)845-8647 FAX (505)844-7857

## ABSTRACT

Because of the low humidity environments required in the fabrication of nuclear explosives, assembly technicians can be charged to tens of kilovolts while operating, for example, compressed air, venturi-type, "explosion proof" vacuum cleaners. Nuclear explosives must be isolated from all sources of, and return paths for, AC power and from any part of the lightning protection system. This requirement precludes the use of static ground conductors to drain any charge accumulations. Accordingly, an experimental study of the basic charging mechanisms associated with vacuum operations were identified, the charge generation efficacy of various commercial cleaners were established, and a simple method for neutralizing the charge was devised.

## INTRODUCTION

The electrostatic discharge (ESD) from a person or an object that has become electrically charged is a very real and practical potential threat environment to the safe handling and reliable operation of advanced weapons. Personnel routinely become charged to and maintain voltage levels of 6 to 12 kV or more from triboelectric processes associated with normal daily activity. Under conditions of low humidity, an individual operating a vacuum cleaner can develop substantially higher voltage with respect to the surroundings.

Perhaps the most widely used American utility vacuum cleaner in both light industry and the home workshop is the "wet/dry" vacuum. Because of its popularity, and those features that make this device almost a workshop necessity, it has found a place in many maintenance facilities. It is durable, reliable, inexpensive (typically, less than $40.00 with attachments) and easy to use. Unfortunately, it is a very effective electrostatic charge generator. In a series of laboratory measurements, the hose attachment attained voltages in excess of 50 kV resulting from intake of abrasive sand, causing a corona discharge that apparently limits the charge.

An evaluation of the wet/dry vacuum from the standpoint of nuclear and personal safety is informative. The Underwriters Laboratory (UL) requires that a three-conductor grounding cord and plug be used to provide power to these devices. The power head, that is, the motor including the fan, is usually "grounded" by means of the "green" lead. The green lead presumably reaches an "earthed counterpoise." It is likely that the third

or "neutral" wire eventually reaches the center tap of the 220-V pole transformer in a typical power distribution system. Any surge on the line induced by a nearby lightning stroke, for example, after some attenuation depending on the effectiveness of the counterpoise, could pass on to the power head. However, nuclear explosives must be isolated from all sources of, and return paths for, ac power. In particular, nuclear explosives must be isolated from what is commonly referred to as "green ground," which could be connected to the grounded, neutral portion of an ac power distribution system. This requirement precludes the use of any "explosion proof" vacuum cleaner that contains a low resistance path from the working end of the hose to "green ground."

The power head of a conventional, UL-approved vacuum cleaner is doubly insulated to protect the operator. Therefore, a surge on the line cannot be propagated to an assembly undergoing maintenance; that is, nuclear safety is not compromised.

"Explosion proof" industrial-type vacuum cleaners approved for use in UL class I or II environments have motors that are totally enclosed so that commutator sparking provides no threat when operated in those environments associated with flour milling, refinery operations, or any activity resulting in accumulations of ignitable dust or vapors. Typically, heat exchangers cool the totally enclosed, high-powered (3 to 4 HP) motors used and electrical continuity is maintained from the grounding plug at the end of the power cord to the metallic attachments to the conducting vacuum hose. Although this arrangement eliminates the hazards associated with electrostatic discharges (ESD), unfortunately, nuclear safety is compromised because the ground for the power distribution system becomes connected to an explosive device. If non-conductive vacuum attachments or pneumatic extensions are used to circumvent the nuclear safety hazard, these modifications introduce an ESD hazard.

It should be noted here that maintenance operations on electroexplosive devices (EEDs) are never performed in UL class I or II environments. The explosives themselves are always contained, that is, enclosed in a metallic, plastic, or ceramic shell.

Figure 1 shows a typical EED. A fine bridgewire, imbedded in a sensitive explosive mix, serves as an electrothermal converter. When an electrical current passes through the bridgewire, its temperature rises. If the temperature is great enough, the sensitive mix is initiated; it explodes and detonates the secondary explosive.

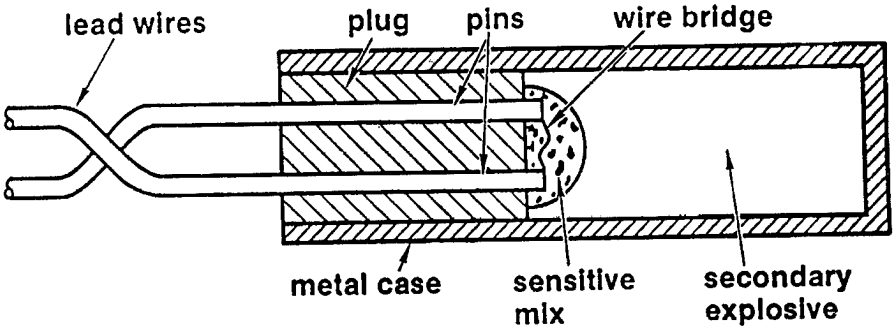



Figure 1. Typical electroexplosive device (EED)

Initiation of the explosive mix can also result inadvertently if an electrical arc occurs between either pin and the metal case, that is, a pin-to-case discharge. This can be avoided by shunting the pin and case by either a spark gap or large resistance. Most modern EEDs are protected this way. However, some of the older EEDs are not protected and an arc path can be established through the primary explosive by inadvertent application of only a few kilovolts. The electrostatic charge required to produce the arc is generated very efficiently by the vacuum. The resulting hazard can be mitigated by either attenuating the charge induced by the vacuum process or by ensuring that the attachments, operator, and EED (leads and case) are all at the same electrical potential. Elaboration on both options are presented in this paper.

The question addressed next is whether or not a shop-type vacuum cleaner may be used safely to clean loose dirt, dust, or other foreign matter from weapon assemblies in view of the ESD hazard introduced by these cleaners. The answer is yes, provided a simple electrical modification is made on the cleaner.

## NON-CONDUCTING HOSE TESTS

Figure 2 shows two vacuum/system test configurations using a non-conducting hose. The system on the right side is the "victim," and as the hose attachment approaches or touches the system, charge on the hose is transferred to it. The resistance between a conducting point on the tank and laboratory ground was found to be greater than 10 GΩ. For all the tests described here, the resistance between the tank and ground can be considered infinite. All voltage and resistance measurements are referenced to laboratory ground, which is the copper pipe system used to distribute cooling water to various laboratory power supplies. The block labeled *System* is some conductive object bonded to an EED. This system makes physical contact with the hose by means of an accessory attachment, for example, a crevice tool or gulper nozzle. In all tests, abrasive sand was used to simulate dust. However, little difference was noted between observed electric field intensities resulting from ingestion of either abrasive sand or ordinary desert sand.

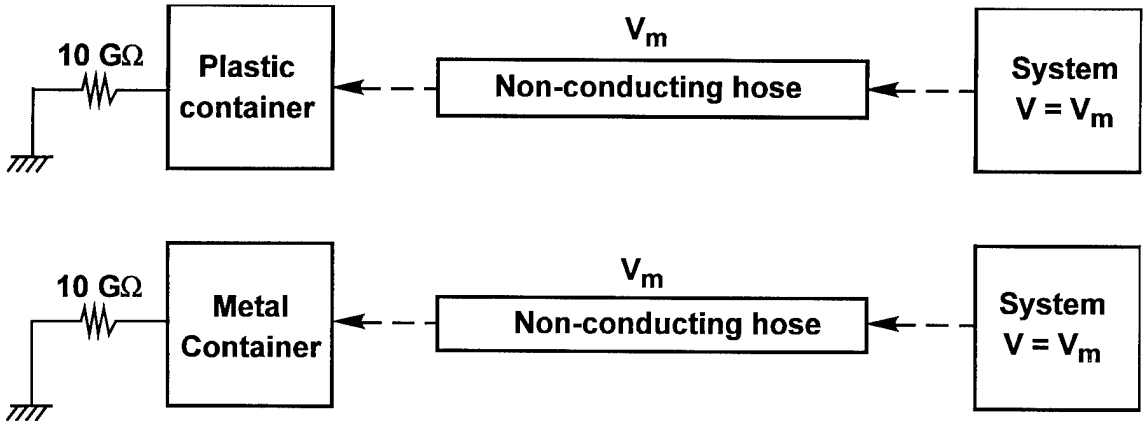



Figure 2. Vacuum cleaner/system configured with non-conducting hose. (Dashed lines indicate pneumatic continuity.)

All tests were performed in the Sandia EM Analysis and Test Department ESD laboratory. Electrostatic fieldmeters were used to detect charge buildup on the plastic container and non-conducting hose resulting from the uptake of a small amount of sand. The hose attachment (and hose) attained a maximum voltage in excess of 50 kV, negative, while the container attained a voltage of 8 kV, positive; that is, as the non-conducting hose becomes negatively charged, the tank becomes positively charged. Although the physics is probably much more complex, it may be postulated that a dust particle colliding with the vacuum hose loses an electron to the hose in a triboelectric exchange. The dust particle, which is now positively charged as a result of loss of an electron, is propelled by the high-velocity air stream into the container where it gives up its positive charge to the container.

Tests performed using sand clearly were designed for maximum charge buildup. However, hose charging occurred even with ambient air particulate uptake. The maximum voltage attained by the hose was -6 kV at the attachment end; the minimum voltage was zero at the container end of the hose. The container itself charged to 2-kV positive maximum. It is notable that the charge distribution along the hose does not decrease uniformly to zero. Instead, successive maximum and minimum occur in the unipolar charge distribution along the hose.

## CONDUCTING HOSE TESTS

Normally, vacuum hose and attachment accessories are non-conducting. Separate conducting hoses priced under $50 are available from a number of vendors. The hose used in these tests consisted of a plastic hose reinforced by a steel helix. A "pig-tail" at the female end of the hose provides an electrical connection with the helix. The other end of the helix was connected electrically to a metallic male termination.

Figure 3 shows schematically the experimental arrangement for the conducting hose tests. In the first setup, the conducting hose was electrically isolated from the container. The maximum voltage attained by the hose from sand uptake was -8 kV; the container charged to +800 V.

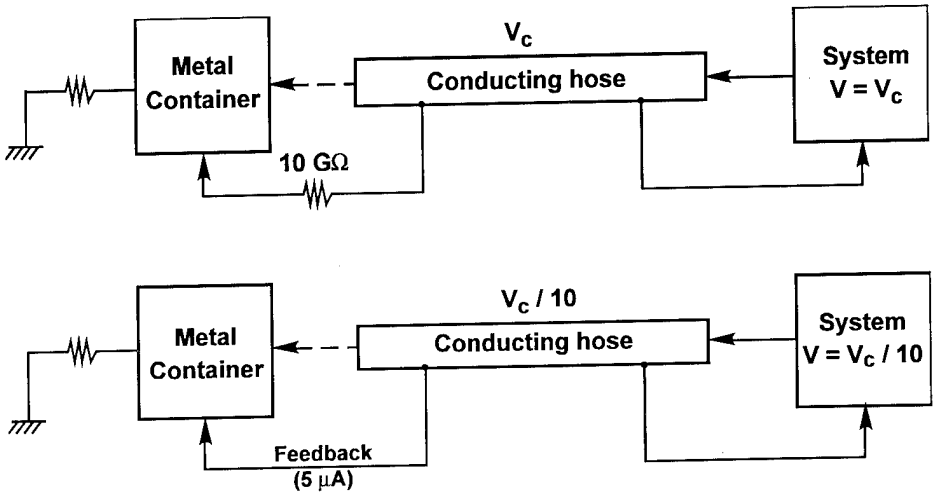



Figure 3. Vacuum cleaner/system configurations (conducting container, conducting hose).

Proceeding on the assumption that the negative charge on the hose could be neutralized by the positive charge on the container, an ammeter was placed electrically in series between hose and container. A current of 5 μA was observed during sand uptake and the voltage on the hose decreased to 800 V.

Because the electrostatic energy stored in a capacitor is proportional to the square of the voltage, the energy constituting the ESD hazard is attenuated by a factor somewhere between four and six orders of magnitude.

The capacitance of the conducting hose was determined to be 50 pF. The total electrostatic energy threat to a victim system ($CV^2/2$) is only 16 μJ if a conducting hose attachment is electrically connected to the conducting tank. Details of the modification to a typical vacuum cleaner are shown in Figures 4 and 5. Without the modification, that

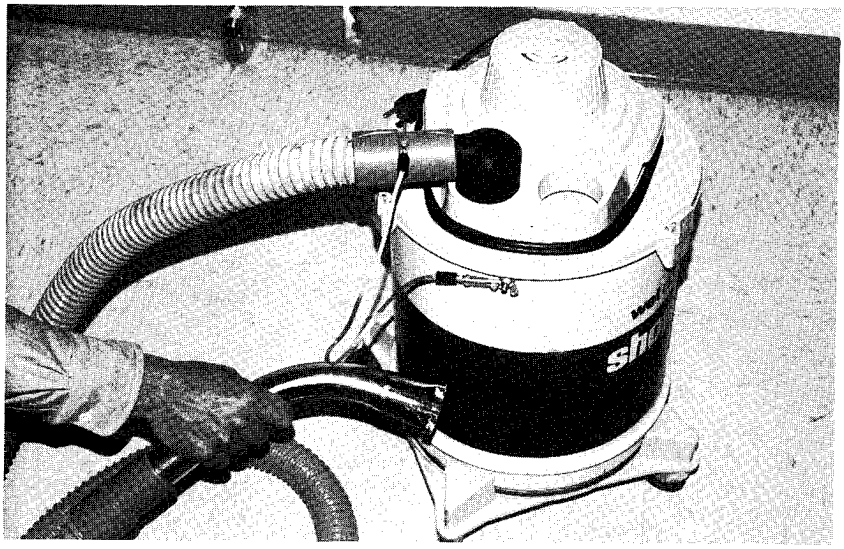


Figure 4. Modified shop vacuum

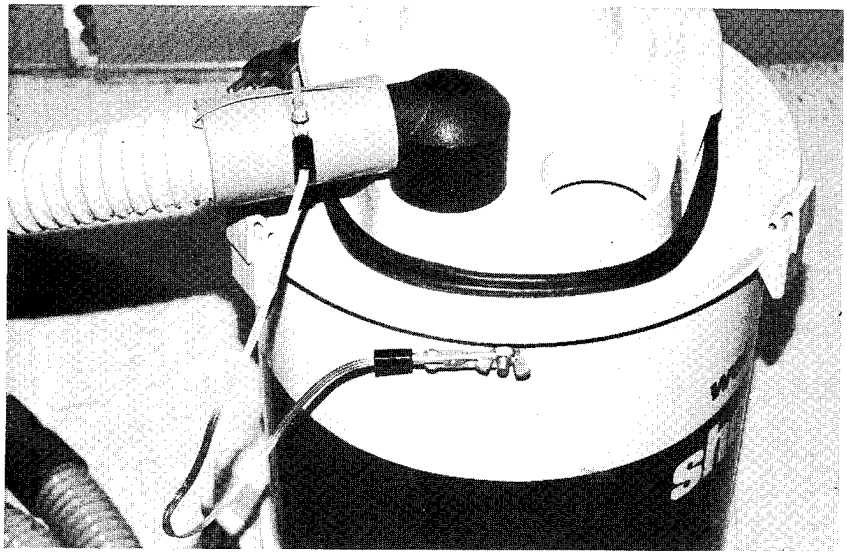


Figure 5. Feedback wiring detail

is, the same vacuum with a non-conducting hose, threat energies as high as 60 mJ are possible. Even higher threat energies (of the order of tenths of a joule) would result if the more powerful vacuum systems are used.

## VENTURI VACUUMS

From a nuclear safety standpoint, the venturi vacuum cleaner is unsurpassed. The device is driven by compressed air, has no moving parts, and has no electrical connections. Essentially, a venturi cleaner consists of a short tube with a tapered constriction in the middle that causes an increase in the flow velocity of air in the constriction with a corresponding decrease in air pressure thereby creating a suction. The air exhausts through a porous canvas bag that retains debris taken in by a conventional vacuum hose with attachments.

An ESD evaluation was made of a venturi-type cleaner along with a non-conducting hose attachment. The same test procedure used with the electric cleaners was followed with the same results. Uptake of abrasive sand led to several tens of kilovolts negative charge on the hose while the bag charged to a positive one kilovolt.

Following the reasoning described above, a conducting hose was substituted for the non-conducting hose and the bag was made conducting by an inner lining of hardware cloth and an outer layer of copper screen (see Figure 6). Electrical contact was established between the aluminum venturi tube, inner and outer screen, and the conducting hose to provide a mechanism whereby electrons from the hose would be neutralized by the positively charged screen. With these modifications the electrostatic potential of the conducting vacuum system was reduced to zero. The experimental arrangement is shown in Figure 7. Therefore, the system may be considered both ESD hazard free and explosion proof.

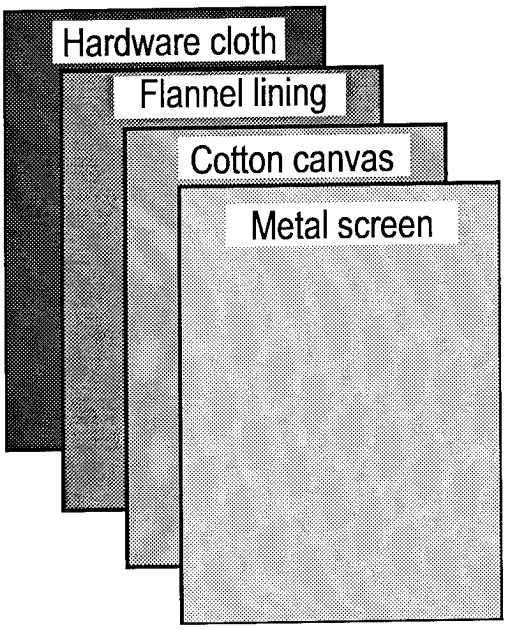



Figure 6. Laminated bag modifications for use with venturi vacuum cleaner

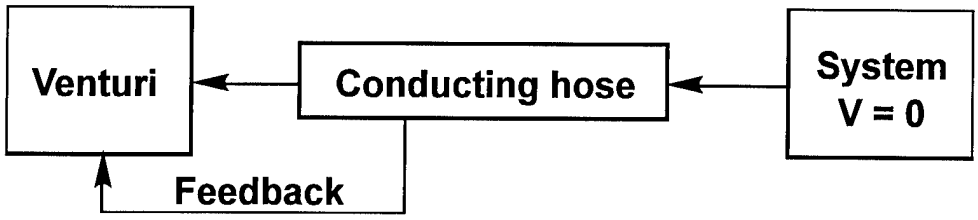



Figure 7. Experimental arrangement for conducting bag venturi vacuum evaluation

Subsequently, the complex bag was replaced by one fabricated from a conductive fabric, consisting of a polyester fabric that is plated with either copper, nickel, or a combination of both. Surface resistivity measurements were made (surface resistivity of a material is the ratio of the potential gradient parallel to the current along its surface to the current per unit width of the surface and is numerically equal to the surface resistance between two electrodes forming opposite sides of a square. The size of the square is immaterial.) The surface resistivity of the fabric used in the test was 5 ohms per square using the criteria specified by the American Society for Testing Materials, *ASTMD257*.

Figure 8 shows the venturi cleaner with a metallized vacuum bag. The mechanical durability of the bag is unknown. It should be noted, however, that normal use of the vacuum would be only for very short duration periods that would occur very rarely. It is assumed that the cleaner will be dedicated to only those operations involving subsystems incorporating EEDs.

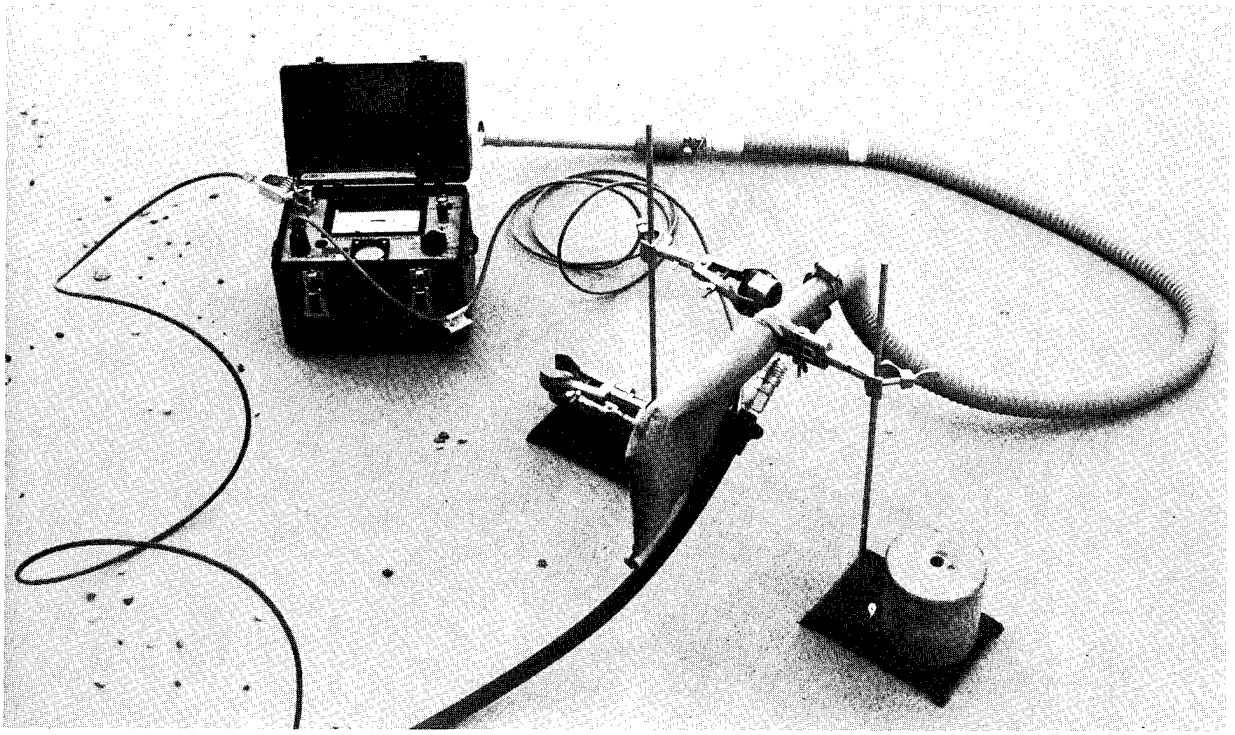


Figure 8. Venturi cleaner with metallized vacuum bag (note vibrating reed sensor)

## ATTACHMENT CHARGING

To avoid compromise of nuclear safety when using an "explosion proof" vacuum cleaner, it has been suggested that non-conducting attachments be used with a conducting hose. The acceptability of this approach depends on the extent to that the attachment acquires a charge. Accordingly, a series of measurements were made to determine the efficacy of this process.

An "explosion proof" vacuum system was simulated by a shop vacuum cleaner with a conducting hose that was connected to laboratory ground. The attachment used was a 10-inch-long plastic crevice tool, an accessory supplied with the cleaner. A fieldmeter was used to determine that a copper foil wrap on the outer surface of the crevice tool attained a voltage in excess of 10 kV negative from the uptake of abrasive sand.

The external foil wrap on the crevice tool was electrically connected to an aerodynamic shape that charged to 1 kV by sand uptake (see Figure 9). The capacitance of the system referenced to laboratory ground was 2 nF and the corresponding charge (Q = CV) was 2 μC, that corresponds to a stored energy of 1 mJ. The relative humidity at the time of the test was 25 percent. Again, it should be noted that much larger threat energies are possible at a lower relative humidity, especially if the more powerful vacuum systems are used. Therefore, plastic vacuum attachments should not be used in the vicinity of EEDs.

By use of the setup shown schematically in Figure 10, it was demonstrated that the same aerodynamic shape charged to 0.8 kV when a non-conducting hose and a conducting attachment were used. This illustrates the charge build up that results if an "explosion proof" vacuum cleaner is made "nuclear safe." Accordingly, "explosion proof" vacuum cleaners modified to satisfy the nuclear safety requirement should not be used in weapon assembly or maintenance areas unless the conducting attachment is electrically bonded to the assembly.

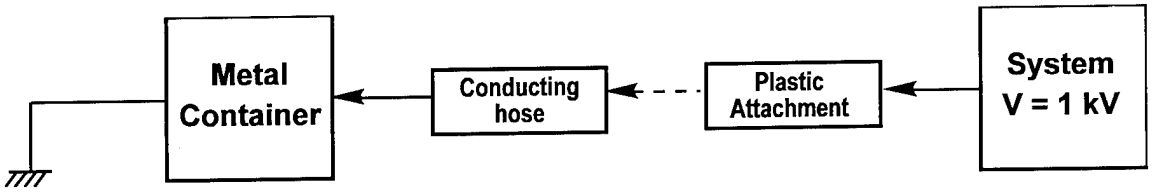



Figure 9. System charging resulting from use of plastic attachment

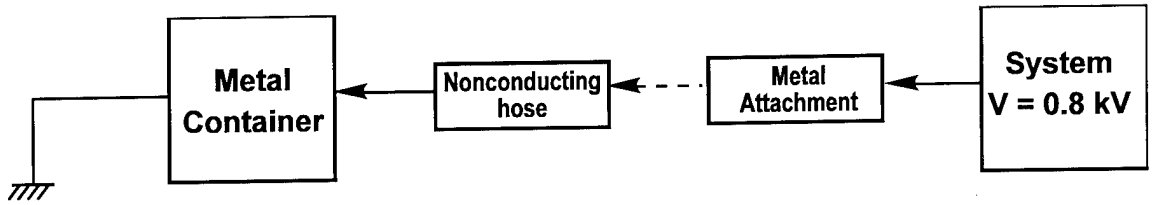



Figure 10. System charging resulting from use of non-conducting hose and conducting attachment

## CONCLUSION AND RECOMMENDATIONS

An evaluation of representative, commercially available vacuum cleaners commonly used in weapon assembly and maintenance areas has been made. Significant differences between these representative cleaners were found. The so-called "explosion proof" machines were excluded from the study because their use compromises nuclear safety; indeed, "explosion proof" cleaners should not be used. All models tested were found to be effective generators of electrostatic energy, typically 60 mJ at voltages in excess of 50 kV. Even greater energies and voltages would be expected in production environments where extremely low atmospheric humidity must be maintained. These energy sources could lead to the inadvertent initiation of sensitive electroexplosive devices. Accordingly, it is recommended that a standard cleaner design be designated as the most suitable for use in operations involving nuclear systems.

The threat posed by pneumatic devices can be mitigated by simple modifications to commonly available types of commercial utility vacuum cleaners. Conducting hoses and conducting attachments should be used exclusively in vacuuming operations. Canvas dust collecting bags used in venturi-type cleaners should be replaced by metallized fabric bags; the venturi assembly itself should be metallic. Venturi-type vacuum cleaners are preferred to electrically powered cleaners because the venturi cleaner is isolated from the electrical supply system and the facility ground. However, if compressed air is unavailable and electrical shop-type cleaners must be used, these should be doubly insulated and the tank, that should be conducting must be isolated from the "green ground." Provision should be made to ensure that electrical contact between the tank, hose, and attachments is made automatically when these machines are in use. On some models of tank cleaners, the required modification consists simply of replacing a non-conducting rubber gasket by one that conducts. It should be emphasized that issues relative to radiation safety have not been addressed in this study; modifications recommended here are restricted to issues relevant to ESD safety. Suitability of modifications recommended here should be endorsed by a radiation safety study.

## ACKNOWLEDGMENT

This work was supported by the U.S. Department of Energy under Contract DE-AC04-94AL85000.

# SESSION 09A
# MEASUREMENTS
# CHAIRPERSON: VLADISLAV MAZUR

# MEASURED ENVIRONMENTS WITHIN 20 METERS OF THE STRIKE POINTS OF TRIGGERED LIGHTNING

R.J. Fisher, G.H. Schnetzer, and M.E. Morris
Electromagnetic Analysis and Testing Department
Sandia National Laboratories
Albuquerque, NM 87185, USA
Telephone (505) 845-8647 FAX (505) 844-7857

## ABSTRACT

Vertical electric fields, azimuthal magnetic fields, and earth voltages developed over 0.5-m radial step distances have been measured at 10 and 20 m from the ground attachment point of triggered lightning. The magnetic fields are found to follow Ampere's law closely. The relationship between maximum vertical electric field change due to a descending dart leader and the peak of its associated return-stroke current is linear. Recorded earth step voltages have the same waveforms as the incident return-stroke currents, and, for distances between 10 and 20 m from the strike point, their amplitudes exhibit a 1/r dependence. Statistics are given for observed radial filamentary arcing from the ground attachment point.

## INTRODUCTION

A detailed knowledge of the electromagnetic environment very close to the ground strike point of lightning is of both general phenomenological interest and considerable importance in designing and assessing the effectiveness of protection systems. Using triggered lightning to produce real lightning strikes to designated points on the earth, the electromagnetic environments at ground-level stations located 10 and 20 m from the channel bases were measured. The quantities that were recorded included vertical electric field ($E_V$), horizontal (azimuthal) magnetic field ($H_a$), and earth step potential differences ($V_S$) developed over 0.5-m radial increments. During the summer of 1993, seven flashes were triggered in support of these experiments. Data were acquired on a total of 31 individual return strokes, with a range of peak return-stroke current amplitudes from 3.3 to 30 kA. The experiments were carried out at Ft. McClellan, Alabama at a flat test site that had been freshly cleared of vegetation 45 days prior to the beginning of the testing. The soil composition was heavy red clay, with an average conductivity of $1.8 \times 10^{-3}$ S/m, the mean value derived from standard four-probe resistivity measurements conducted daily at five different locations throughout the 50-day fielding period. The general site layout is shown in Figure 1. Rocket launching and data recording operations were carried out using the Sandia Transportable Triggered Lightning Instrumentation Facility (SATTLIF), the details of which have been described elsewhere (1).

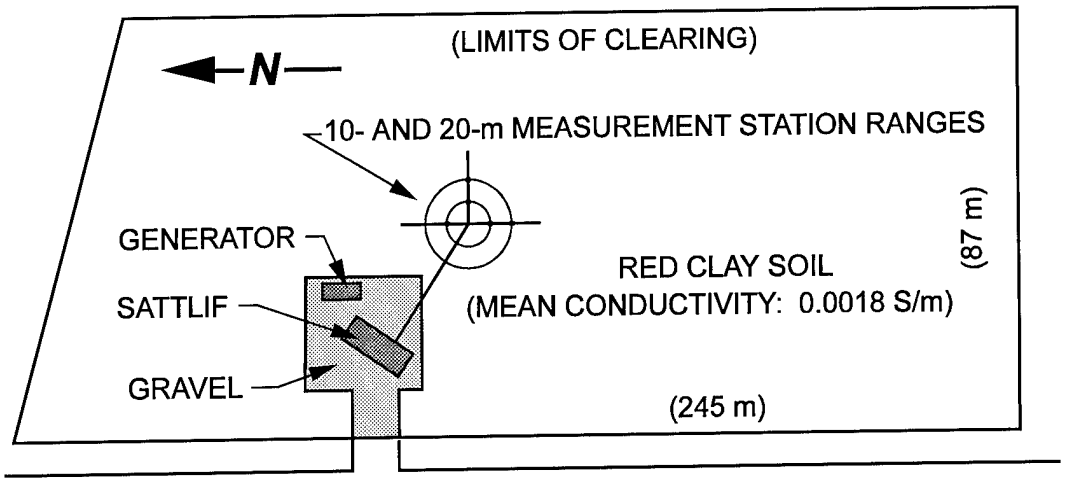



Figure 1. Overview of the 1993 triggered lightning experiment site

## EXPERIMENTAL PROCEDURES

A total of five monitoring stations were arrayed at 10- and 20-m radial distances from the base of the rocket launcher assembly (RLA), which served as the designated strike point for the triggered flashes. It was arranged that flash currents striking the RLA would flow to earth through the coaxial current monitor mounted below the main supporting frame of the launcher. The earthing point consisted of a zinc-coated steel ground rod below the steel instrumentation box that contained the current sensor and its associated fiber optic transmitter electronics. The ground rod depth was intentionally kept to a minimal length to simulate closely a strike to raw earth. Data were acquired during four separate storms. During the first two storms, the ground rod depth was 0.3 m, while for the last two, it was changed to 1.3 m.

Over the course of the summer, data were obtained at each of the monitoring stations indicated in Figure 2. During the first and second storms, identical complements of sensors were deployed at stations 1 through 3. Each consisted of a commercial magnetic field derivative detector (plus in-line active integrator), a flat plate vertical electric field sensor, and an earth step potential sensor with its two 0.3-m long probes separated by a distance of 0.5 m. Stations 1, 2, 4, and 5, comprised of different combinations of sensors as defined in Figure 2, were activated during storms 3 and 4. In this way, data were obtained as functions of radial distance (10 and 20 m) and of azimuth at the multiple monitoring positions around the 10- and 20-m arcs.

With the exception of the earth step potential measurement, the sensors, signal conditioning, data transmission links, and recording instrumentation were all substantially the same as were employed previously during the triggered lightning test of a munitions storage bunker that was conducted during 1991 (2). The technique used in measuring the earth step potentials is described below in the discussion of the experimental results. All of the data presented herein were recorded digitally with a 40-ns sampling interval. The 3-dB upper frequency limit of the incident stroke current measurement was 6 MHz, which was set by the frequency response of the current sensor. The upper frequency limit of the rest of the measurements was 10 MHz.

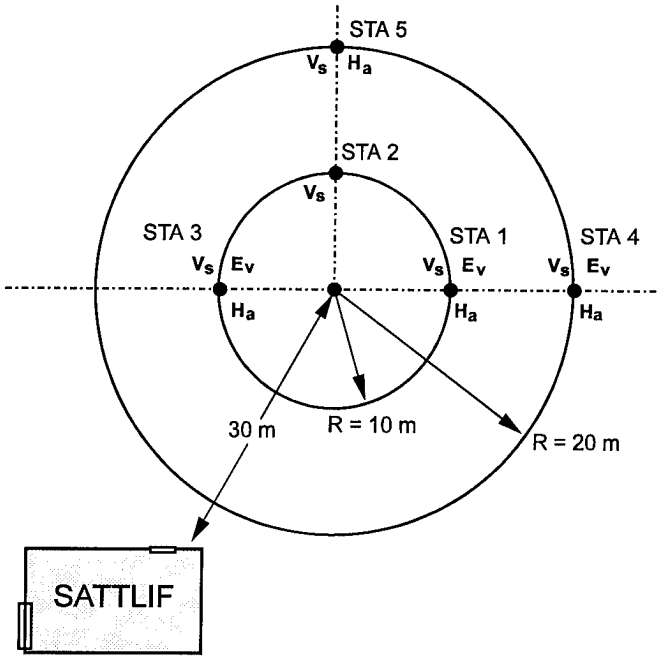



Figure 2. Measurement locations and assigned sensor groups. (Station 2 consisted of $V_S$ sensor only during Storms 3 and 4; otherwise it was comprised of the full set of sensors.)

DATA

MAGNETIC FIELDS–Plotted in Figure 3 are the peak values of the azimuthal magnetic fields measured at 10.7 and 20.7 m as a function of the peak amplitudes of their associated return-stroke currents. Linear regression lines are displayed for the data set corresponding to each distance. Ampere's law applied to this situation is given by the relationship

$$H(t) = I(t)/(2\pi r) \qquad (1)$$

where H(t) is the magnitude of the azimuthal component of the magnetic field, I(t) is the current flowing in the lightning channel, and r is the radial distance from the strike point. In the figure, curves corresponding to Eqn. 1 are plotted as solid lines for each distance. As can be seen, there is very close agreement between this relationship and the experimental data. The correspondence between the waveshapes of the incident stroke currents and their associated magnetic fields is virtually exact in most of the data, although instrumentation effects are evident at times beyond the peaks in some cases.

VERTICAL ELECTRIC FIELDS–Figure 4 is a plot of a typical vertical electric field change recorded at 9.3 m from the base of a stroke that was initiated by a dart leader. The V shape of the waveform is characteristic of electric field changes out to well beyond 500 m (3). The rate of change and peak amplitude of the wavefront preceding the bottom of the V is associated with the propagation velocity and linear charge density, respectively, of the descending dart leader. The rapid change following the peak corresponds to neutralization of leader charge as the return-stroke wavefront propagates up the channel from the ground.

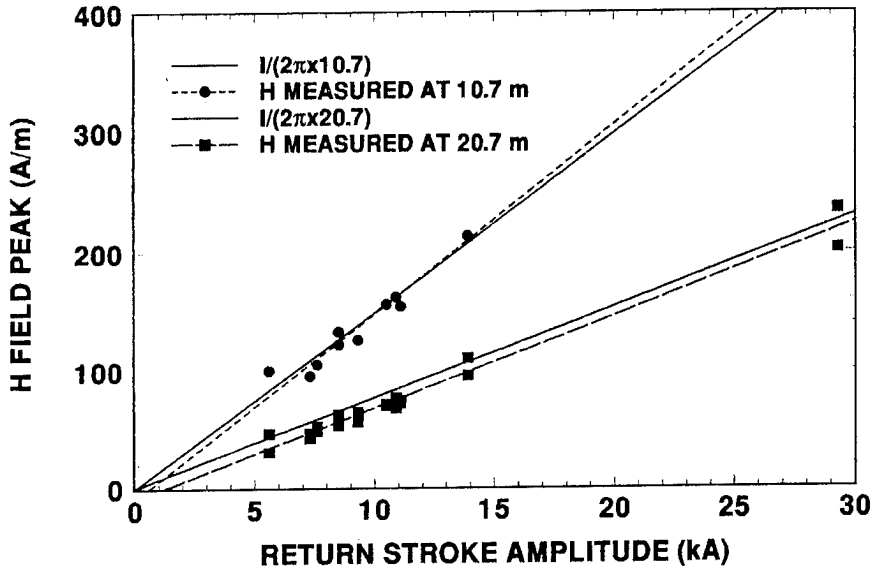



Figure 3. Comparison of Ampere's law with peaks of magnetic fields measured at 10.7 and 20.7 m from the strike point

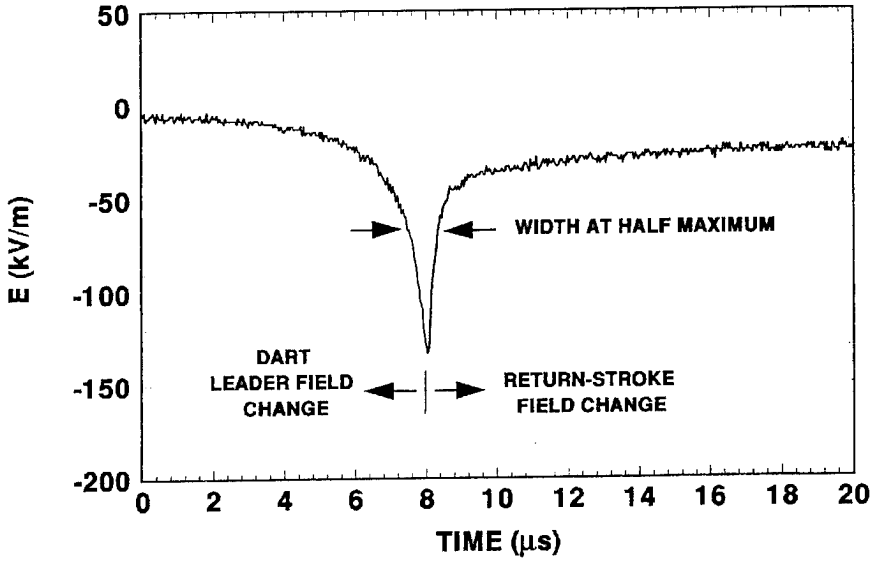



Figure 4. Typical electric field change recorded 9.3 m from the base of a return stroke preceded by a dart leader

Presented in Figure 5 is a plot of recorded peak return-stroke currents against their preceding dart leader electric field changes, as measured at 9.3 and 19.3 m from the channel. The evident linearity (correlation coefficients of 0.7 and 0.95 at the 9.3 and 19.3-m stations respectively) is presumably a consequence of the fact that peak return-stroke current amplitude is proportional to the charge per unit length deposited by the dart leader over the last 100 m or so of its channel. Assuming a linear charge distribution, the proportionality constant is the return-stroke propagation velocity.

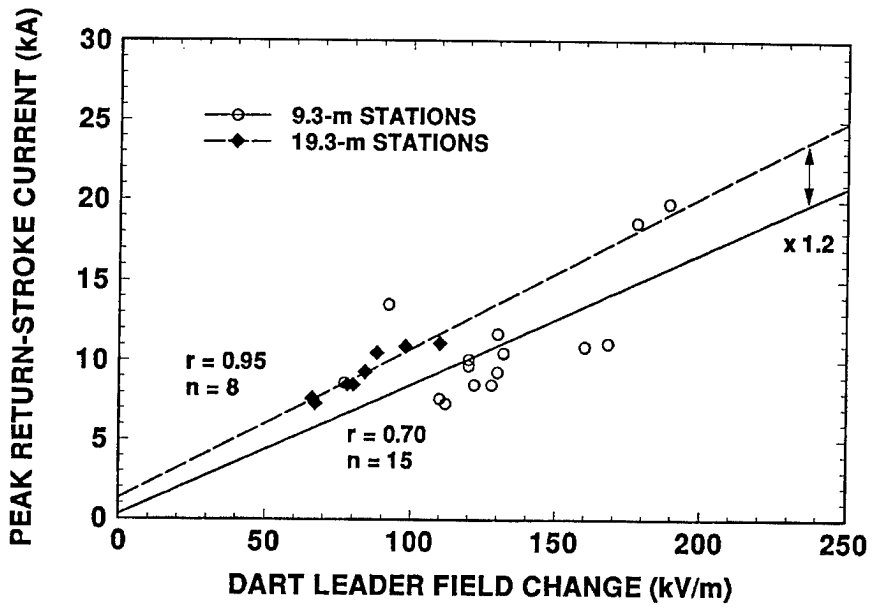



Figure 5. Peak return-stroke current as a function of peak dart leader electric field changes recorded at 9.3 and 19.3 m from the ground strike point

On two occasions, measurements were obtained of electric field changes on strokes preceded by dart-stepped leaders. One example is given in Figure 6. In both instances, the strokes were the final ones in their respective flashes, and both were preceded by extraordinarily long interstroke intervals, namely 345 and 290 ms, respectively. (The median value interstroke interval in triggered flashes in Florida and Alabama is 48 ms (4).) The mean interval between steps in the two examples that were obtained is

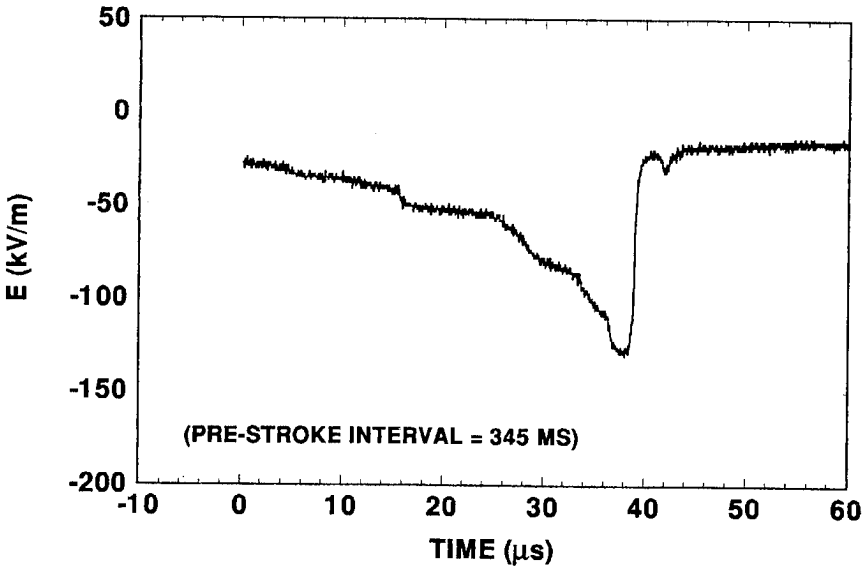



Figure 6. Example of an electric field change recorded 9.3 m from the base of a return stroke preceded by a dart-stepped leader

6.3 μs, a value consistent with data for dart-stepped leaders during the last tens of microseconds prior to return strokes in naturally initiated lightning in Florida, 6.5 μs, and Arizona, 7.8 μs, (5).

RADIAL EARTH STEP VOLTAGES–The technique employed in measuring voltages developed by return-stroke currents injected into the earth at the base of the rocket launcher is shown in Figure 7. An adequate equivalent circuit of this measurement is shown in Figure 8. Because the impedance of the instrumentation circuit is so much higher than the source impedance presented by the earth at the probe terminals, the earth voltage is unperturbed by the presence of the measurement circuit. Stray magnetic or electric field coupling into the measurement circuit was not found to be a problem.

The major results from these measurements are summarized in Figure 9, in which the peak voltages recorded at the 10- and 20-m stations are plotted against peak return-stroke current. As is evident, the voltages are highly linear with respect to the stroke currents that produced them (correlation coefficients of 0.97 at 10 m and 0.98 at 20 m). In those cases for which multiple-station data are available, the voltages from the different stations agree very closely in both amplitude and waveshape. From this it is inferred that the spatial distribution of current density flowing within the earth outward from the injection point must be essentially uniform. Perhaps more precisely stated, there appear to be no significant net effects from any local nonuniformities in that current distribution. This result would, of course, not hold in the presence of any buried

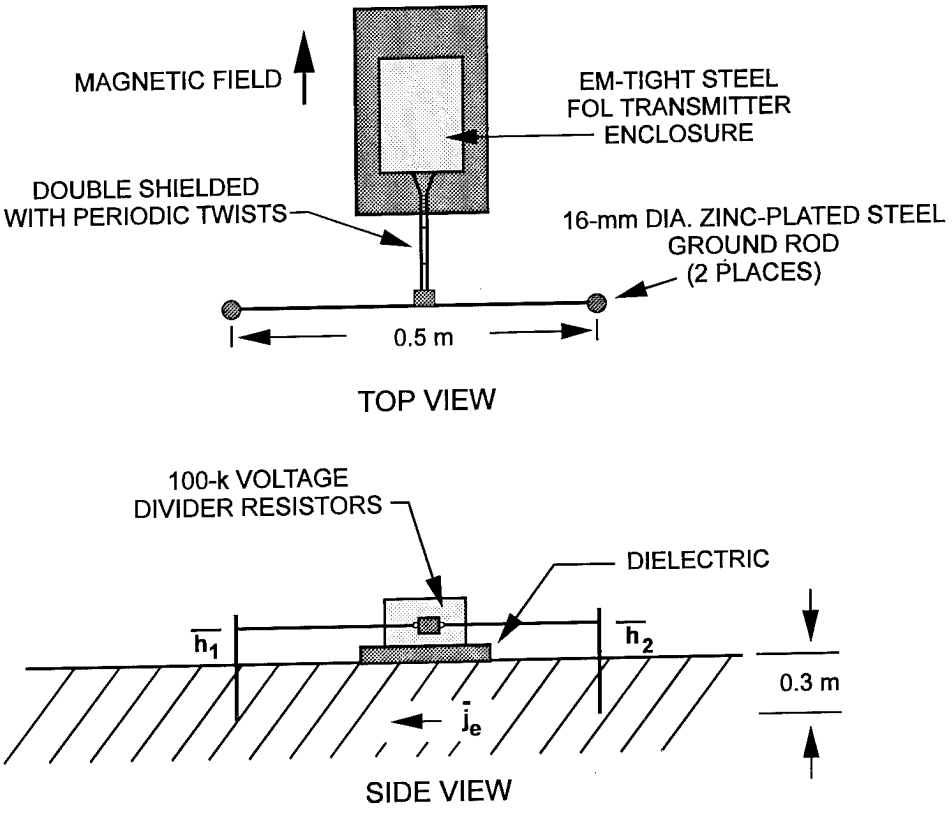



Figure 7. Technique used to measure radial earth step voltages

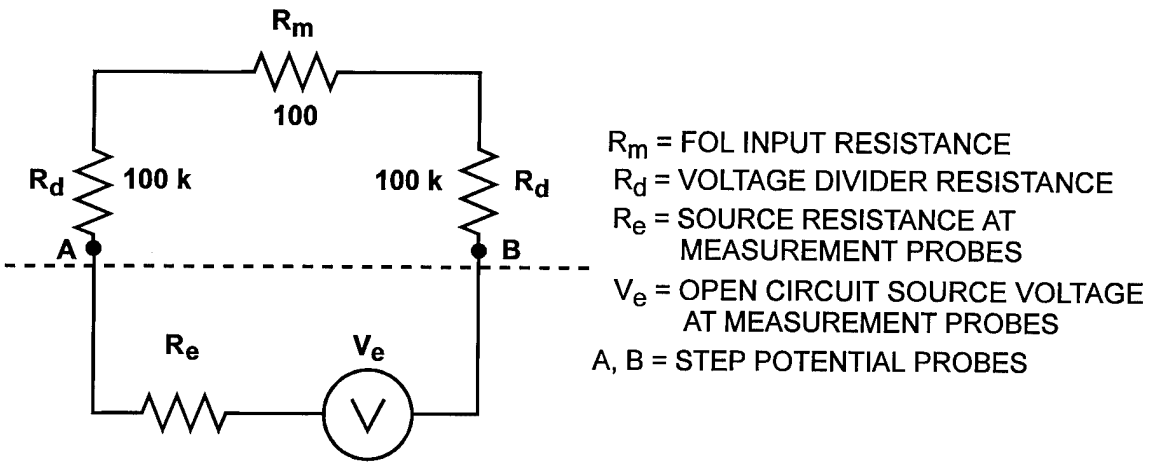



Figure 8. Equivalent circuit model of earth step measurement in Figure 7

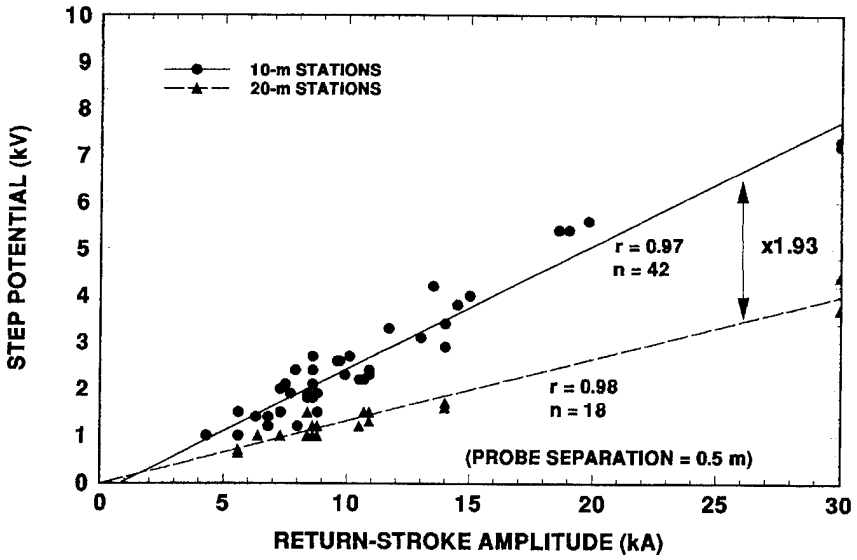



Figure 9. Peak earth voltages developed over 0.5-m step distances measured at 10 and 20 m from triggered lightning strike points plotted against peak return-stroke current

conductors, such as pipes, cables, or even major tree roots; but this situation was intentionally avoided during the present experiments. The waveshapes of the recorded voltages are virtually identical to those of their associated stroke currents.

Perhaps the most interesting feature of the step voltage data is the rate at which they scale with distance from the strike point. Based on the fitted regression line in Figure 10, this dependence is very close to 1/r between the 10 and 20-m stations. This is contrary to the expectation of a $1/r^2$ functionality that would be predicted by the uniform hemispherical model of current density that is often employed to estimate earth potentials close to a strike point to earth. An alternative model has been proposed that produces very good agreement with the limited present data (6). The model involves

the assumption of a thin surface layer of much higher conductivity than that of the bulk of the earth below it. The high conductivity layer is ascribed to standing rain water, which existed more or less uniformly over the test site during the triggering sessions. Unfortunately, with the limited amount of presently available data, it is not yet possible to validate definitively this or any other model for explaining the observed behavior.

RADIAL SURFACE ARCING–In addition to the active electrical measurements described above, numerous video records were taken from various angles and with different fields of coverage. Sixteen-millimeter high speed movies with 5-ms time resolution were also obtained on 5 of the 7 triggered flashes. These records revealed the frequent occurrence of substantial radial surface arcing outward from the ground attachment point. As indicated in Figure 10, significant arcing was detected on 100 percent of all strokes with peak currents of 15 kA or greater, as well as on a significant fraction of strokes with currents below that level. The arcing appeared to be random in direction. Not every stroke in the same flash produced a detectable arc, and during some flashes, arcs occurred in one direction on one stroke and in another direction on some other stroke. Following each storm the area around the base of the RLA was carefully examined for residual evidence of arcing. With the exception of localized occurrences of splintering of pieces of plywood, which were placed on the ground to avoid standing in mud when working around the launcher, no such evidence was observed. Nor were any fulgurites found when the earthing rod was either removed or changed. What was observed, however, was distinct evidence of discrete, concentrated current exit points at several spots along the length of the steel ground rods after they were removed from the earth.

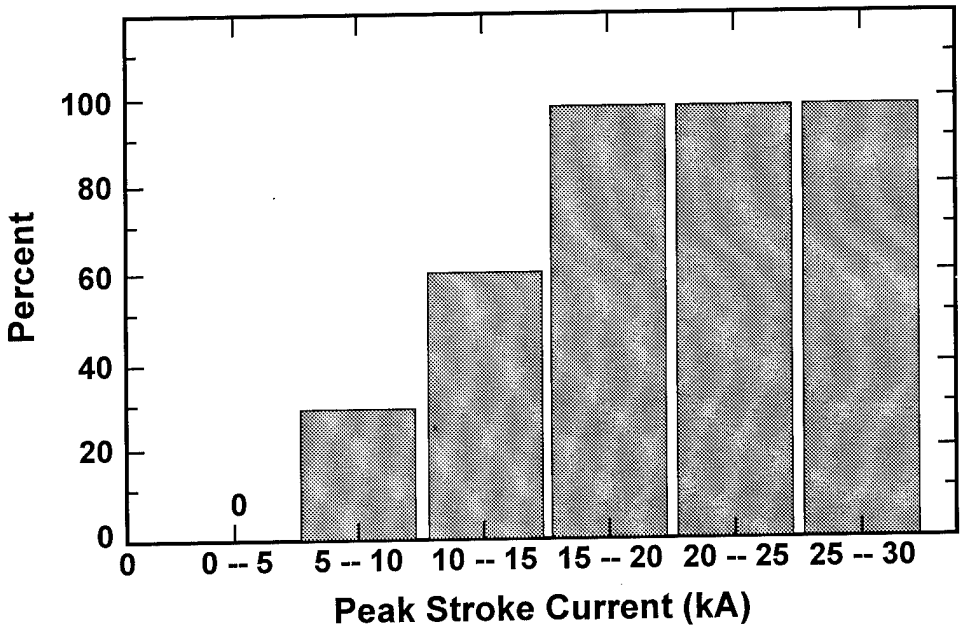



Figure 10. Frequency of detected surface arcing from the base of a poorly grounded triggered lightning termination mast as a function of peak return-stroke current amplitude

During one particular stroke of 20-kA peak amplitude, the Station 1 instrumentation was contacted by one branch of a surface arc. Analysis of the behavior of the various sensors at that station indicated that the arc carried approximately 1 kA, or about 5 percent of the peak current of that stroke. The most impressive photograph of this arcing phenomenon that was obtained is shown in Figure 11. The right edge of the photograph represents a distance of 10 m from the strike point under the RLA. The horizontal branch of the arc can be seen to have reached this range. As deduced from excursions in the signals recorded at one or more of the 20-m station sensors on two other occasions, a range of at least 20 m was attained by some of the arcs. Whether this distance was ever exceeded cannot be determined with certainly from the present data.

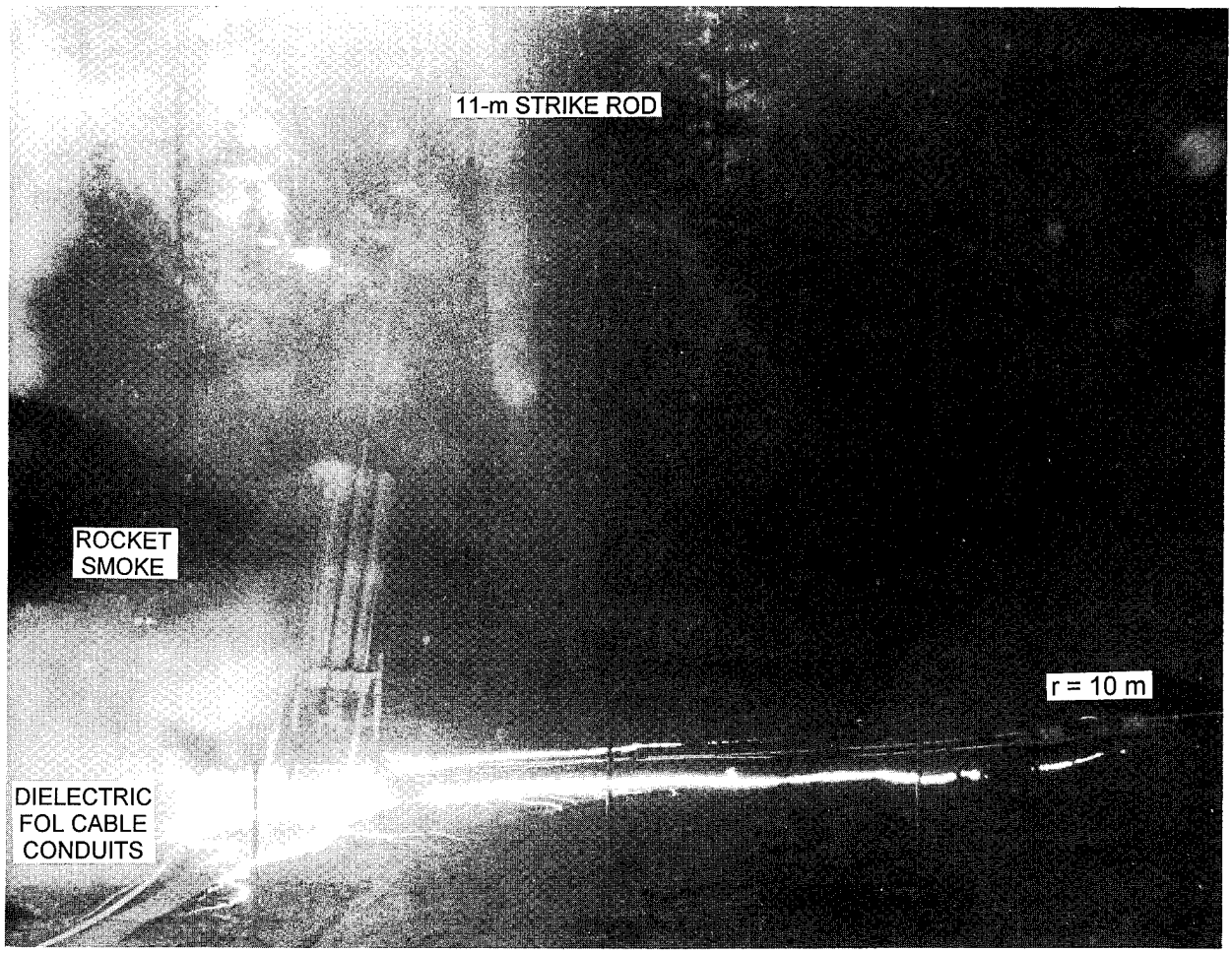



Figure 11. Still photograph of radial branched surface arcing from the base of a triggered lightning channel; the observed arcing occurred on the second stroke (peak current of 29.4 kA) of Flash 93-12. (Attachment of the return stroke to the top of the strike rod is outside the field of view.)

## CONCLUSIONS

Analysis of the data performed to date has resulted in the following conclusions:

1. The magnetic field at ground level out to a range of at least 20 m from the base of a lightning channel is well described by Ampere's law.
2. Subsequent return-stroke current amplitudes are linear with respect to the peak electric field changes produced by the dart leaders that initiate them.
3. Vertical electric field change amplitudes as high as 300 kV/m, occurring with rise times of the order of a few microseconds, can be experienced at a range of 20 m from a lightning channel that is carrying a return-stroke current of 30 kA.
4. Earth step potentials measured at 10 and 20 m from the strike point are linear with return-stroke current and have the same waveshape as their associated return-stroke currents. Over the range of 10 to 20 m, their peak magnitudes were observed to fall off as 1/r.
5. The likelihood of significant radial surface arcing out to ranges well in excess of 20 m must be considered to be part of the hazardous environment close to the base of a lightning channel, even in areas of relatively high earth conductivities. Individual branches of such arcs can carry appreciable fractions of the peak value of return-stroke current.

## ACKNOWLEDGMENTS

This work was supported by the U.S. Department of Energy under Contract DE-AC04-94AL85000 and by the U.S. Department of the Army, Armament Research, Development and Engineering Center, Picatinny Arsenal.

## REFERENCES

1. Schnetzer and R.J. Fisher, "The Sandia Transportable Triggered Lightning Instrumentation Facility," Int. Aerospace and Ground Conf. on Lightning and Static Electricity, Cocoa Beach, April 16-19, 1991.
2. Schnetzer and R.J. Fisher, "Rocket-Triggered Lightning Test of an Earth-Covered Munitions Bunker," Int. Aerospace and Ground Conf. on Lightning and Static Electricity, Atlantic City, October 2-5, 1992.
3. Rubenstein, M., F. Rachidi, M.A. Uman, R. Thottappillil, V.A. Rakov, and C.A. Nucci, "Characterization of Vertical Electric Fields 500 m and 30 m from Triggered Lightning," *J. Geophys. Res.*, 100, 8863-8872, May 20, 1995.
4. Fisher, G.H. Schnetzer, R. Thottappillil, V.A. Rakov, M.A. Uman, and J.D. Goldberg, "Parameters of Triggered Lightning in Florida and Alabama," *J. Geophys. Res.* 98, 22,887-22,902, 1993.
5. Krider, C.D. Weidman, and C.R. Noggle, "The Electric Fields Produced by Lightning Stepped Leaders," *J. Geophys. Res.*, 82, 951-960, 1977.
6. Fisher, G.H. Schnetzer, and M.E. Morris, "Measured Fields and Earth Potentials at 10 and 20 m from the Base of Triggered Lightning Channels," 22nd Int. Conf. on Lightning Protection, Budapest, September 19-23, 1994.

# STATISTICS OF LIGHTNING STRIKES TO THE CN TOWER OBSERVED DURING 1978-1994

W. Janischewskyj
University of Toronto
Toronto, Ontario, Canada
Telephone (416) 978-3116 Fax (416) 971-2325

A.M. Hussein
Ryerson Polytechnic University
Toronto, Ontario, Canada
Telephone (416) 979-5000 x6108 Fax (416) 979-5280

J-X. Li
Xi'an Jiaotong University
Xi'an, China

I. Rusan
University of Western Ontario
London, Ontario, Canada

J-S. Chang
McMaster University
Hamilton, Ontario, Canada
Telephone (905) 525-9140 x24924 Fax (905) 527-5222

## ABSTRACT

The unique site of the 553-m high CN Tower has been used since 1978 to carry out observations and measurements of lightning events. Video records of flashes to the CN Tower during the intervening lightning seasons, up to and including 1994, have been analyzed and statistical findings are presented in the paper. In the first place, flash durations, multiplicity of strokes in a flash and interstroke intervals are analyzed and compared with other observations. Information derived will be relevant to lightning protection of tall structures, and of power line and substation components.

## 1. INTRODUCTION

The 553-m high CN Tower situated in Toronto offers a unique opportunity for measurements of lightning parameters and for studies of lightning characteristics at tall structures. While the local lightning flash density in Toronto is 2.5 flashes per square kilometre per year, the tower receives many tens of lightning flashes during a lightning

season. Utilizing this unique site, waveshapes of lightning currents have been digitized at the tower, characteristics of electric and magnetic fields radiated in its vicinity by these lightning events have been simultaneously measured, and video records of the lightning path as well as the return-stroke velocity have been observed at the same time (1). This information is of primary significance for such areas of study as insulation coordination of power lines and substations, and for protection of tall structures against lightning. Figure 1 shows the details of instrumentation used to obtain enumerated data.

In contrast to lightning in the open country (2), lightning occurring at tall structures has certain peculiarities (3-5). In the first place, because of the increased strength of the electric field at the top of a slim and more than 500-m tall structure, such as the CN Tower, more than 90% of flashes are initiated by an upward-directed leader (6). Nevertheless, in many cases the final jump takes place only few hundred meters above the top of the tower. Figure 2 is an example of such an event, where the lightning channel is eventually vertical. At the same time, there are lightning flashes to the tower where the channel is nearly horizontal, as shown in Figure 3. Furthermore, as documented already in early reports on CN Tower lightning (7), the multiplicity of strokes to the CN Tower is higher than that to flat country. In all these respects, characteristics of lightning observed at the CN Tower resembles somewhat the lightning occurring in high mountains (8).

In this paper video data related to 460 lightning flashes, collected from 1978 to 1994, will be utilized to provide statistical information on the frequency of occurrence and on time parameters associated with lightning observed at the CN Tower. Flash and stroke statistics of these events are compared with observations of lightning at other tall structures and in flat country. Seasonal variations as well as changes with time of the day are presented. Accumulated data on stroke multiplicity, interstroke intervals and flash durations should be of particular interest to designers of protection equipment such as lightning arresters. These units are often used for protection of power lines against overvoltages in areas with high ground resistivities. In its turn, high ground resistivity usually occurs in mountainous terrains where lightning characteristics are not much different from those occurring at tall structures. For that reason, CN Tower data are especially relevant for protection of power lines in mountains.

## 2. VIDEO RECORDING OF LIGHTNING EVENTS

CN Tower lightning flashes have been observed and recorded using a pair of video measuring and recording systems. Each of the two video recording systems used, consists of a video camera (Hitachi VM-3100A) and a set of video recorders (RCA VR250, Hitachi VT-3050A) which permits continuous 24-hour operation. As shown in Figure 1, the two video cameras are located in such a way as to view the CN Tower from almost perpendicular directions (82.5 degrees). This arrangement will permit construction of a three-dimensional image of the lightning path. One video system is positioned on the roof of the main building of Ontario Hydro Technologies (OHT), 11.8 km west of the tower, and the other is situated at the Rosebrugh Building of the University of Toronto located 2.0 km north of the tower. Both video systems operate at a rate of 60 frames per second with 2:1 interlace which gives a time resolution of 33.3 ms.

The horizontal line drawn through the location of the camera at OHT would intersect the CN Tower 129.5 m above ground level (AGL), while that in case of the University of Toronto (U of T) camera would land at the 124.7 m AGL. The inclination of the first camera with respect to this horizontal line is 3.0° and of the second is 15.5°. The field of view for the OHT camera has the CN Tower somewhat off center and extends vertically from the 481 m AGL to the 1004 m AGL, and horizontally from 270 m left of the tower (north) to 500 m right of it (south). The field of view for the U of T camera covers vertically the space from 543 m to 820 m AGL and horizontally from 165 m on its left (east) to 220 m on its right (west).

As will be described later, 460 lightning flashes to the CN Tower, recorded by the U of T video system between 1978 and 1994, are analyzed in this paper. Video records at the OHT site are available only since 1991 and have been used to verify U of T video records. It should be also pointed out that, contrary to limitations on the number of strokes in a flash recorded by both the current and the field measuring systems, when a video system is used, there is no such restriction (1). As will be shown in Section 4, the largest observed stroke multiplicity was 10. These video records will be presented in two separate segments. Statistical data on occurrence of lightning flashes and that on detailed characteristics of each flash will be discussed in subsequent sections.

## 3. STATISTICS OF LIGHTNING OCCURRENCES

Global statistics on yearly distribution of lightning flashes reaching the CN Tower and those on their diurnal variation will be offered first. It will be seen that these observations, although somewhat different, are consistent with information collected by other investigators in North America. Pierce (9) indicates the yearly peak of lightning activities as occurring in May at Austin, Texas, in June at Grand Forks, North Dakota and in July at Orlando, Florida. Similarly, in diurnal variation of thunderstorm activity, Pierce shows hours from 16:00 to 18:00 as corresponding to maxima during various months of the year at the Kennedy Space Centre in Florida.

STATISTICS OF THE MONTHLY LIGHTNING RATE--Figure 4 presents the distribution of the number of flashes reaching the CN Tower during each of the 12 months of the year. In Toronto, about 58% of observed lightning events occur during the months of July and August. During the winter, November to February, lightning events hardly take place. However, statistical data of Figure 4 imply that lightning events may also occur as early as March and as late as October even in areas above the 40° latitude. One implication of this observation is the fact that electrical maintenance and repair of lightning protection equipment for electrical power lines and substations ought to take place during the winter. In that way it will be ready for reliable operation and protection of electrical installations during the summer months.

DIURNAL DISTRIBUTION OF FLASHES--Figure 5 shows the distribution of the number of flashes that occurred at a given hour in a day. During the lightning season, lightning events may take place at any time of the day. However, statistical data of the seventeen years indicate that the largest number of lightning events at the CN Tower is clustered around eight o'clock in the evening. It is very interesting that the least number of lightning flashes is found 12 hours later, at eight o'clock in the morning. About 66% of

lightning flashes occur during the night, from eight o'clock in the evening to seven o'clock of the morning, while during the 12 hours of day-time only 34% of lightning events take place. Note that in Figure 5, information on midnight events is repeated for the sake of comparison. It is first given under the abscissa of 0 hr and is again plotted in the 24 hr slot .

## 4. STATISTICS OF LIGHTNING PARAMETERS

The continuous nature of video records permits a detailed time analysis of events involved in each individual lightning flash. Because of two to one interlacing and the 60 pictures per second camera, the time interval between two successive frames is 33.3 ms. Thus to determine flash duration in milliseconds, we count the number of frames from the first appearance of the lightning channel to the last frame of the flash and multiply that number by 33.3. Similarly, interstroke interval is computed from the number of frames between adjacent peaks of channel luminosity. Finally, stroke multiplicity is found as the number of subsequent luminosity maxima within the flash.

MULTIPLICITY OF STROKES IN A FLASH--A lightning flash must contain at least one, but may have several strokes. As far as exposure of installations and systems to lightning is concerned, this fact implies that struck entities on occasion may be required to withstand the effects of the discharge in a series of strokes within a short interval of time. Their own design and that of their protective systems must be capable of withstanding severe heating caused by closely spaced repetition of lightning strokes. For their effective protection, therefore, adequate knowledge of the probability of occurrence of multiple stroke flashes is clearly required. Figure 6 gives the global information on this aspect of lightning flashes endured by the CN Tower from 1978 to 1994. Among the 460 flashes recorded by the University of Toronto video camera, 211 contain only one stroke. On that basis, single stroke incidence is observed to constitute 46% of CN Tower flashes. Within the 460 records, the largest observed stroke number per flash is 10. The two 10 stroke flashes occurred on September 2, 1980 and on August 10, 1992. It is worth mentioning that the system time resolution of 33.3 ms may have prevented discerning more strokes when interstroke times were comparable to system time resolution. A high speed camera of 1 ms time resolution is being presently acquired to overcome this limitation.

FLASH DURATION--Although instantaneous values of lightning current are responsible for the heating effect, lightning flashes of longer durations will in general cause more severe stresses. Figure 7 presents statistical results of flash durations observed at the CN Tower over the last seventeen years. The longest flash duration among the accumulated data is 1433 ms, which occurred on July 27, 1978. This flash contained 8 strokes. Figure 7(a) shows that about 10% of flashes have durations of at least 1000 ms. It is also of interest to observe that, in general, the flashes with long durations have a larger number of strokes. For example, the 10% of flashes of more than 1000 ms duration contain at least 4 strokes each, and durations of the two 10-stroke flashes are 900 ms and 1267 ms. Undoubtedly, flashes with longer durations and with a larger multiplicity of strokes constitute a more severe threat to electrical power installations and tall structures.

INTERSTROKE INTERVAL--Figure 8 presents the statistical results of interstroke intervals. As already explained, interstroke intervals are determined from the number of video frames between the occurrence of brightest lightning channel pictures of two adjacent strokes. It is important to stress that in view of the different ways in which interstroke intervals and flash durations are determined, flash duration is not simply equal to the sum of interstroke intervals; it is normally larger than this sum. Analysis of data used for construction of Figure 8 indicates that the 50% value of the interstroke interval is roughly 120 ms, and some 67% of intervals are clustered between 66 and 200 ms. There are only 14% of intervals with durations shorter than 65 ms. As will be shown later, this information, is of interest for testing of lightning arresters.

## 5. COMPARISON WITH OTHER DATA

In order to better evaluate collected data, a comparison is made with results obtained by other investigators. As benchmarks, two tall structures are chosen, the Empire State Building (ESB) (3) and the tower on the San Salvatore's Mountain (SSM) (4), where extensive lightning studies have been conducted in the past. The height of the ESB reaches 410 m above the New York City Street level and the two masts (70 m high) on the San Salvatore's Mountain are situated 640m above Lake Lugano. Additionally, data for lightning occurring in open country (2) is also included in the comparison so as to better judge the effect of CN Tower's height.

Figure 9 shows the statistics concerning the number of strokes in a flash. It indicates that the relative occurrence of flashes with large number of strokes is, in general, higher for tall objects than for the open country. As seen from Figure 9, the 50% values of stroke multiplicity for the CN Tower, the ESB, the SSM, and open country are 2.3, 2.7, 1.8, and 2.5, respectively. At the same time, on the basis of the 460 flashes recorded from 1978 to 1994, single stroke incidence for the CN Tower was calculated to be 46% and for the combined observation of 6428 flashes world wide it is 45%. These values underscore the difference between incidence of single-stroke flashes and the mean number of strokes within a flash.

The findings clearly indicate that tall structures and equipment installed in them are exposed to a larger number of flashes with multiple strokes than low-height installations in the open country. Furthermore, since it is observed that lightning events in mountains (8) are similar to those at tall structures, information collected at the CN Tower should be applicable to lightning protection of power lines crossing mountain ridges.

For geological reasons, resistivity of terrain in mountains is normally very high. This fact requires, for effective control of line overvoltages, the use of special measures, such as counterpoise, to reduce the footing resistance of power-line support structures. Installation of lightning arresters in such regions often becomes an additional necessity. When lightning strikes the line, these devices take the brunt of stresses and thereby protect the line from excessive overvoltages. In order to be effective they themselves must be so designed as to withstand overvoltages and safely conduct the current down to ground. Full information on characteristics of the lightning current is therefore essential. This paper provides part of that essential information, and indicates that in mountains, where upward initiated lightning is prevalent, flashes with multiple strokes

would be more frequently expected than in the open country. That circumstance implies that exposure to multiple flashes must be an integral part of arrester design and testing.

Figure 10 shows that, generally, flash duration increases with the height of the struck object. While 50% of CN Tower flashes exceeded 480 ms, the corresponding 50% values for ESB, SSM and the open country, are 300 ms, 200 ms and 140 ms, respectively. For the CN Tower, 95% of flashes have exceeded 80 ms and 5% exceeded 1150 ms. These average values, as well as the more complete statistical information on flash duration provided by Figure 10, point again to significantly increased stresses when lightning strikes tall structures.

Figure 11 presents interstroke time intervals. For the affected structure or the device under consideration this means the time available for its recovery until the next lightning stroke. The 50% values for this time interval are 120 ms and 90 ms, respectively, for the CN Tower and open country. While these two times differ by 30%, the full statistical variation in interstroke times between the two extremal cases of lightning, as presented by Figure 11, does not seem to be as one sided. At very high probabilities both cases are identical, the 90% probability being 50 ms for both. However at 67% probability the interstroke interval is 110 ms for the CN Tower and 75 ms for open country, and the 33% probability is 145 ms and 120 ms respectively for the two. The 10% probability starts the reversal, being 240 ms for the CN Tower and 250 ms for open country, but the real difference occurs at 5% probability where CN Tower case shows 270 ms while that of open country 360 ms. All this means that, in general, lightning in the open country shows a higher probability of shorter time intervals. For assessing severity of lightning events, this fact should, of course, be combined with the lower probability for stroke multiplicity of lightning in the open country (Figure 9).

## 6. CONCLUSIONS

Extensive video records of lightning strikes to the Toronto CN Tower, accumulated between 1978 and 1994, permit the following assessment of collected data:

(1) In Toronto, lightning events take place usually from April to October each year. They occur mostly in July and August. During the winter months lightning is rare.

(2) During the lightning season, lightning flashes may occur in Toronto at any time of the day, although the number of those occurring at night is about two times larger than those taking place during daytime. A distinct minimum is observed from 7 to 9 a.m.

(3) As for stroke multiplicity, the proportion of flashes with multiple strokes is seen to increases with the height of the struck object. This fact indicates that equipment installed on tall structures or in mountains is exposed to more severe stresses from lightning.

(4) Tall structures are also found to be responsible for flashes of longer durations. Comparison between flat country and structures of various heights indicates that flash duration increases as the height of the structure is increased. This again means, in case of tall structures and in mountainous regions, a more severe exposure to lightning.

(5) When interstroke intervals observed at the CN Tower are compared with those in the open country, it is found that most often they are shorter for lightning in the latter case. However, in rare cases (about 5% of occurrence) interstroke intervals are

shorter for CN Tower lightning. Whenever the interstroke intervals are short stresses on equipment are high since there is little time for cooling and for stress recovery.

(6) In general, lightning flashes with long durations may present high level of threat to structures and equipment. A lightning flash with both long duration and with multiple strokes will present an even higher threat level. CN Tower video records show that about 10% of flashes have extremely long flash durations (at least equal to 1000 ms). It is significant that these same flashes also contain a large number of strokes, at least 4 strokes per flash. Careful attention should be paid to this coincidence in the assessment of lightning protection for power systems and for tall structures.

## ACKNOWLEDGEMENTS

Throughout the years, the Federal Government, Canadian Power Utilities and the Ontario Provincial Government have been the major supporters of CN Tower Lightning Studies at the University of Toronto through their agencies, Natural Sciences and Engineering Research Council (NSERC), Canadian Electrical Association (CEA), and the University Research Incentive Fund (URIF), respectively. Support of these agencies is hereby acknowledged with appreciation.

## REFERENCES

1. A.M. Hussein, W. Janischewskyj, J-S. Chang, V. Shostak, W.A. Chisholm, P. Dzurevych and Z-I. Kawasaki, "Simultaneous Measurements of Lightning Parameters for Strokes to the Toronto CN Tower", Journal of Geophysical Research-Atmosphere, vol. 100, no. 5, pp. 8853-8861, May 1995.

2. H. Linck and M.A. Sargent, "Lightning Performance of Modern Transmission Lines", CIGRE Paper 33-09, Paris, 1974.

3. J.H. Hagenguth and J.G. Anderson, "Lightning to Empire State Building", AIEE Transactions, vol. 71, pp. 641-649, 1952.

4. K. Berger, "Novel observations on lightning discharges: results of research on Mount San Salvatore ", Journal of the Franklin Institute, vol. 283, no. 13, June 1967.

5. J.S. Chang, T.G. Beuthe, L. Seto, A. Duft, N. Hayashi, W.A. Chisholm, and W. Janischewskyj, "An investigation of the possible relationship between thundercloud electric fields and the lightning parameters for tall structures", Journal of Geophysics Research, 94, pp. 13,197-13,205, 1989.

6. R. B. Anderson and A. J. Eriksson, "Lightning Parameters for Engineering Application", Electra, no. 69, pp. 65-102, March 1980.

7. T. R. McComb, H. Linck, E. A. Cherney and W. Janischewskyj, "Preliminary Measurements of Lightning Flashes to the CN Tower in Toronto", Canadian Electrical Engineering Journal, vol. 5, no. 4, pp. 3-9, October 1980.

8. W. Janischewskyj, A.M. Hussein, V. Shostak, P. Dzurevych and W.A. Chisholm, "Use of CN Tower Lightning data for Assessment of Power Line Protection in Mountainous Terrain", Lightning and Mountains, International Conference and Exhibition, Chamonix, France, Paper A.1.3, June 6-9, 1994.

9. E.T. Pierce, "Lightning Warning and Avoidance", in "Lightning". Vol. 2. Edited by R.H. Golde, Academic Press, 1977.

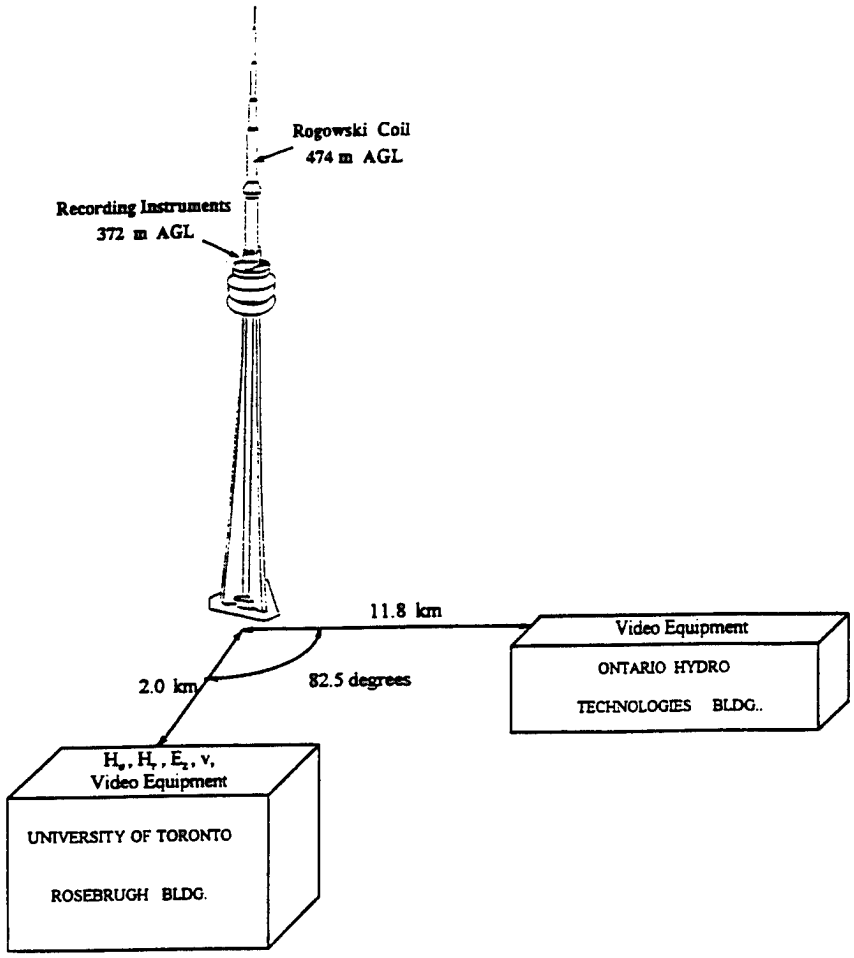



FIGURE 1. LOCATION OF INSTRUMENTATION



FIGURE 2. TYPICAL VERTICAL FLASH TO THE CN TOWER



FIGURE 3. TYPICAL HORIZONTAL FLASH TO THE CN TOWER

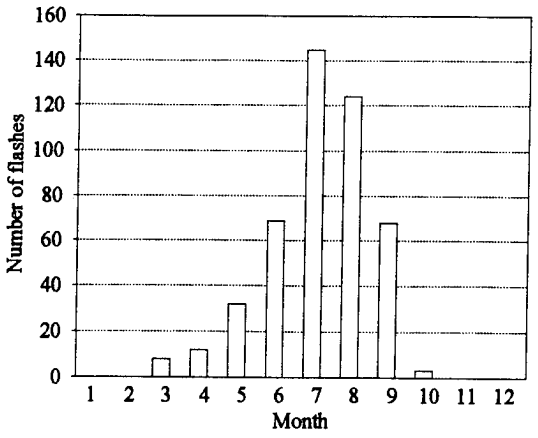



FIGURE 4. MONTHLY DISTRIBUTION OF FLASHES

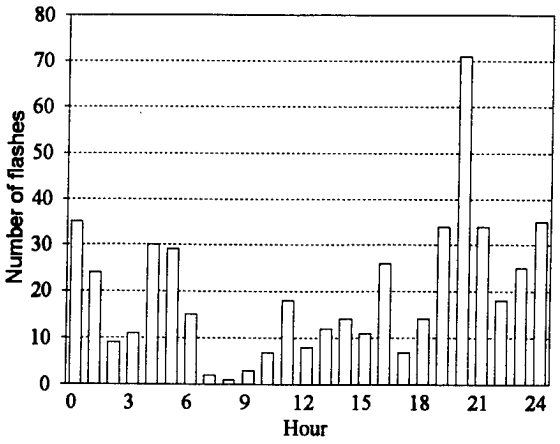
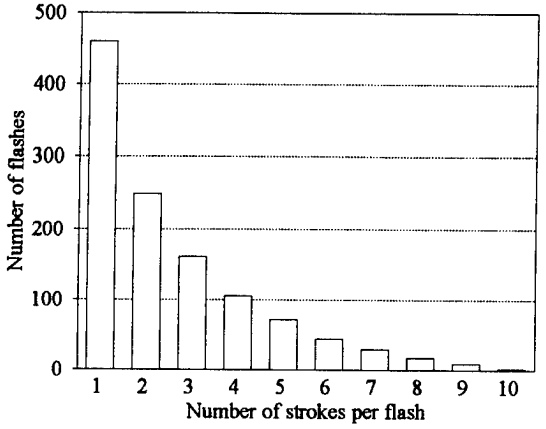
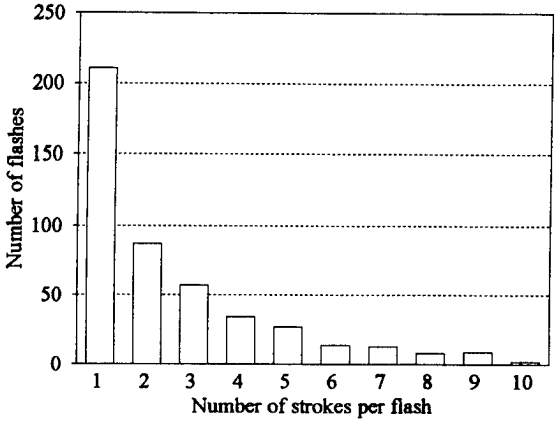



FIGURE 5. HOURLY DISTRIBUTION OF FLASHES

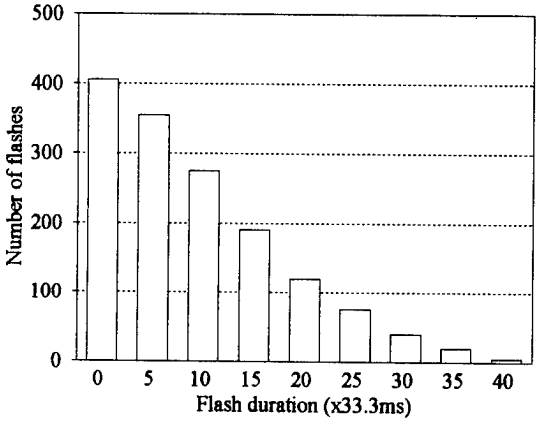



(a) Cumulative distribution

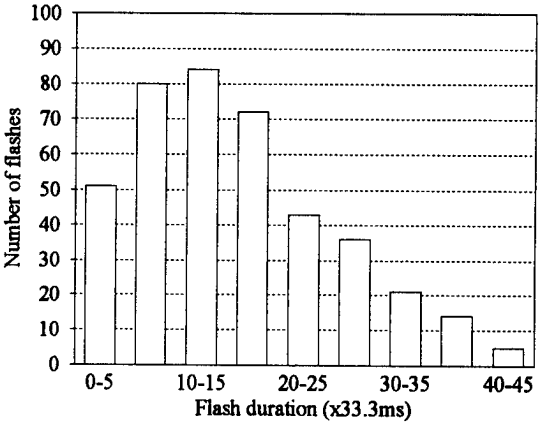



(b)Frequency distribution

FIGURE 6. MULTIPLICITY OF STROKES IN A FLASH

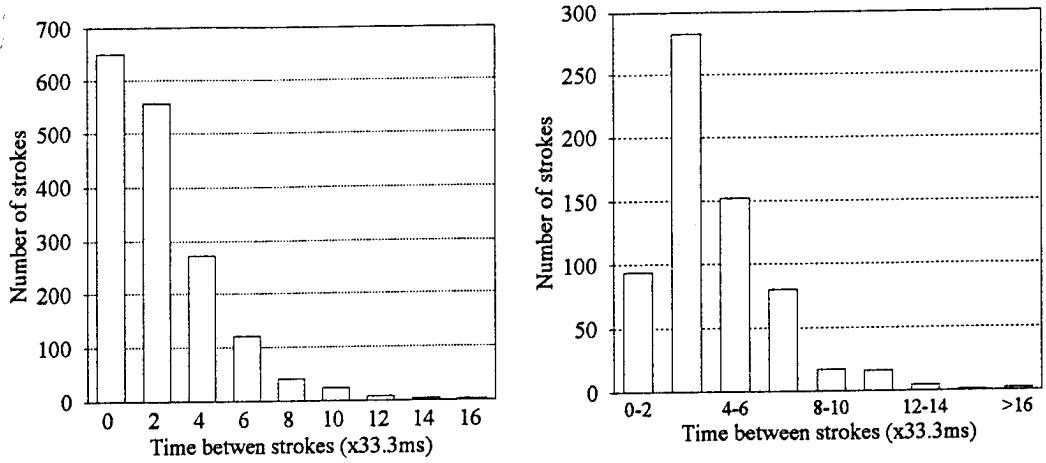



(a) Cumulative distribution




(b) Frequency distribution

FIGURE 7. FLASH DURATION




(a) Cumulative distribution (b) Frequency distribution

FIGURE 8. INTERSTROKE INTERVALS

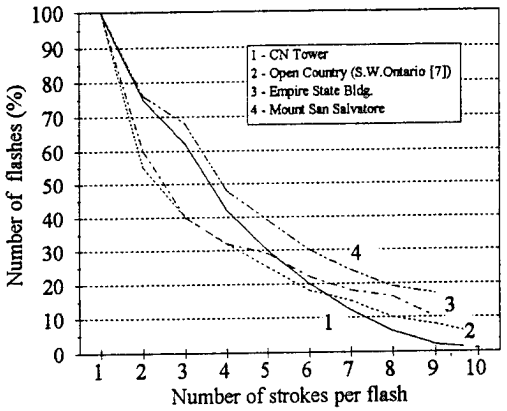



FIGURE 9. CUMULATIVE DISTRIBUTION OF STROKE MULTIPLICITY

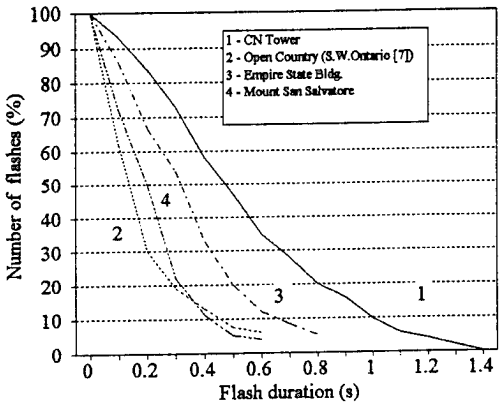



FIGURE 10. CUMULATIVE DISTRIBUTION OF FLASH DURATION

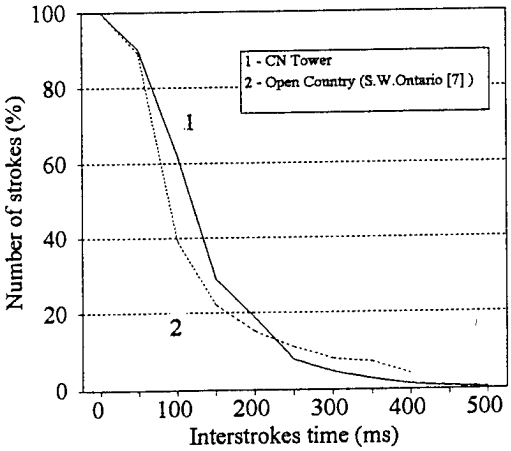



FIGURE 11. CUMULATIVE DISTRIBUTION OF STROKE INTERVALS

# REVIEW OF 15 YEARS LEMP MEASURING ACTIVITIES IN THE SOUTH OF GERMANY

F. Heidler and Ch. Hopf

Federal Armed Forces University Munich
ET 7, Werner-Heisenberg-Weg 39
D-85577 Neubiberg, GERMANY
Telephone +49/89/60043736 FAX +49/89/60043723

## ABSTRACT

Since about 15 years the lightning electromagnetic impulses (LEMP) were measured in the region of Munich. Especially very near lightnings in the distance range of the audible thunder were examined to avoid attenuation effects related to the wave propagation along the non-ideal conducting earth's surface. Up to now the LEMP measuring station was equipped with four different instrumentations. The aim was to capture mainly the field derivatives radiated at the beginning of the return stroke period. The paper gives a review about the basic instrumentations. The experimental data are discussed differing between stepped leaders, cloud-to-cloud discharges, long duration currents, positive or negative return strokes.

## 1. INTRODUCTION

In the year 1980 at the High Voltage Institute of the Federal Armed Forces University Munich a measuring campaign was started especially for the LEMP registration of nearby lightnings in the distance range of the audible thunder. The LEMP station was located in the region nearby Munich, where the soil conductivity is in the order of about $5 \cdot 10^{-3}$ S/m. Because of this high conductivity the attenuation effects related to the wave propagation over lossy earth can be neglected advantageously /1/. The first results were obtained in 1981. Meanwhile the LEMP measuring station was equipped with 4 different instrumentations, where generally the thunder sound was used for the distance determination.

The first measurements were performed by ***Feuerer*** with instrumentation 1 in 1981 /2/. The magnetic field derivative $\dot{H}(t)$ was measured with two crossed loop antennas (loop area 1 $m^2$). For the registration two digitizers (biomation 8100) were used having a minimum scanning rate of 10 ns and a memory capacity of 2000 points. The upper bandwidth limit of the complete analogue measurement equipment including the loop antennas, the cables and the digitizers was better than $f_g = 7{,}7$ MHz.

Because with instrumentation 1 return strokes couldn't be separated from predischarges, instrumentation 2 was equipped by ***Heidler*** in 1982 /3, 4/. The $\dot{E}$-signatures were measured with a vertical electrical rod antenna having an upper bandwidth limit $f_g \approx 35$ MHz. The $\dot{H}$-signatures were registered simultaneously with a crossed loop antenna consisting of two independent loops with an upper bandwidth limit $f_g \approx 25$ MHz. For the registration the same digitizers were used as in instrumentation 1 (biomation 8100). At the earth's surface the superposition of an incident plane wave and the reflected wave leads to the following relationship for the total field ($\alpha$: reflection angle) /3/:

$$\frac{E(t)}{H(t)} = \frac{dE/dt}{dH/dt} = \Gamma_o \frac{\sin\alpha}{\sqrt{1 + \tan^2\beta \cos^2\alpha}} \quad , \qquad \Gamma_o = 377\ \Omega \tag{1}$$

The polarization angle ß is defined to be zero for a vertical polarization of the incident electric field.

Equation (1) becomes $\dot{E}_{max}/\dot{H}_{max} = \Gamma_o$ for low altitudes ($\alpha \approx 90°$) and $\dot{E}_{max}/\dot{H}_{max} < \Gamma_o$ for increasing altitudes ($\alpha < 90°$). For radiation sources located directly over the reflection point ($\alpha = 0$) the electric field vanishes completely resulting in $\dot{E}_{max}/\dot{H}_{max} = 0$. Therefore in very near distances cloud-to-cloud strokes can be excluded triggering on the $\dot{E}$(t)-amplitudes. Especially up to s = 4 km the registration of cloud-to-cloud discharges was reduced.

In 1986 by ***Heidler*** instrumentation 3 was installed for the registration of multiple lightning discharges including the predischarges and the return stroke processes /5, 6, 7/. The $\dot{E}$-signatures were measured with the vertical rod antenna and the digitizer (biomation 8100) used in instrumentation 1. Generally the sample rate was chosen to 10 ns. The digitizer was used like an oscilloscope in the non-storage mode. The $\dot{E}$(t)-signatures presented at the monitor screen were scanned by a video camera with 25 pictures per second. Since the video system had a horizontal resolution of only about 200 points, the effective bandwidth decreases. Impulses with a time duration of 100 ns however could still be resolved. With the method the whole $\dot{E}$(t)-signatures of a thunderstorm higher than the trigger level could be recorded. Generally a cloud-to-cloud stroke was excluded for s < 4 km (see above).

In 1988 ***Hopf*** started with the installation of instrumentation 4 /1, 8, 9, 10, 11/. The $\dot{E}$(t)-signatures and E(t)-fields were measured with two rod antennas with a rod length l = 1,2 m. The LEMP station was triggered whenever the output signature of the 4th order Butterworth lowpass filter with a cutoff frequency of 500 kHz exceeded a positive or negative preset threshold corresponding to an $\dot{E}$-amplitude of $\pm$ 10 V/(m*$\mu$s). The bandwidth limitation of the trigger channel lead to an increase of the number of captured return stroke $\dot{E}$(t)-signatures from 1% to 25% relative to all recorded $\dot{E}$(t)-signatures. The $\dot{E}$(t)-signatures and the analogue integrated E(t)-fields however were recorded without this bandwidth limitation. The analogue bandwidth of the complete equipment was always better than 40 MHz. The digitizers were sampled with a rate of 10 ns. The LEMP station was capable to trigger up to 10 times within one flash. Thus it was possible to record the $\dot{E}$(t)-signatures and the E(t)-fields from multiple strokes. Earth strokes could clearly be detected by the use of an all sky camera. For the registration of multiple earth strokes a 'slow' field measurement system was installed in addition.

## 2. CHARACTERISTICS OF THE MEASURED FIELD AND FIELD DERIVATIVES

The 'slow' electric field shown in fig. 1 was captured with instrumentation 4. The fast rise portions stem from 6 return strokes to earth. Between the 5th and 6th return stroke the slow rise portion is typical for a long duration current. With instrumentation 4 10 different types of E(t)-fields or $\dot{E}$(t)-signatures could be separated shown in fig. 2 or fig. 3 (definitions see clause 3). The negative E(t)-field of a positive return stroke has normally an initial peak followed by a ramp (fig. 2a). The E(t)-fields of negative first and subsequent strokes are quit similar except of the inverse polarity (fig. 2b, c). Corresponding to the initial field peak the $\dot{E}$(t)-signatures have typical bipolar waveforms with duration times on half value of about $T_{50}$ = 0,2 ... 2 $\mu$s just being opposite to measurement results presented in /14/ (fig 3a, b, c).

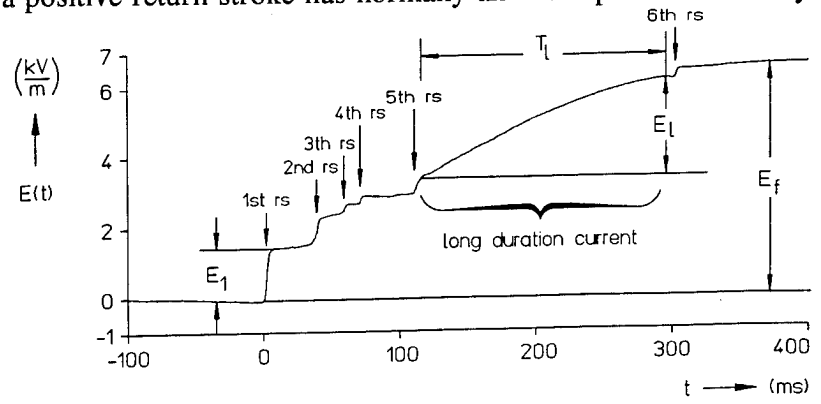
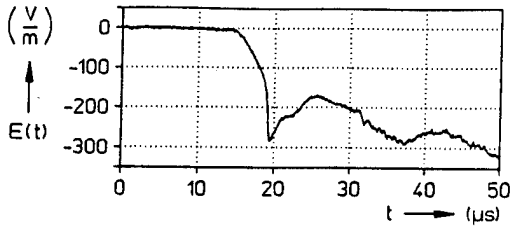


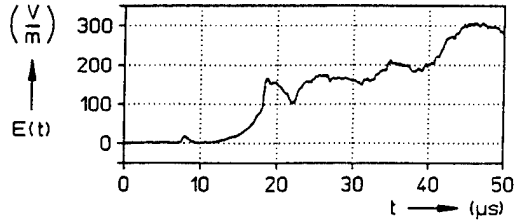

Fig. 1: 'Slow' electric field of a multiple lightning discharge to earth

Normally the $\dot{E}(t)$-signatures of stepped leaders and return strokes are very similar, but the duration time is reduced to $T_{50} \lesssim 100$ ns for the stepped leaders (fig. 3d, e). The electric field amplitudes are also reduced by about one order of magnitude compared to the initial peaks of the return strokes (fig. 2d, e).

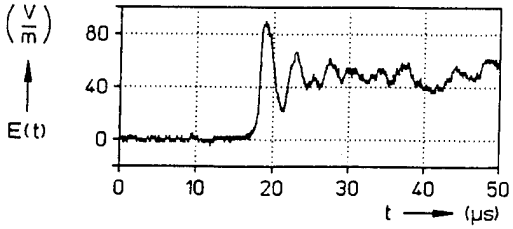
Long duration currents have very fast $\dot{E}(t)$-signatures (fig. 2f, 3f). Thus for $f \gtrsim 1$ MHz the electric field amplitude density spectra are normally higher compared to the spectra of return stokes /10/.



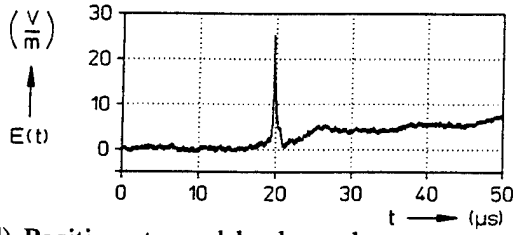

a) Positive earth stroke



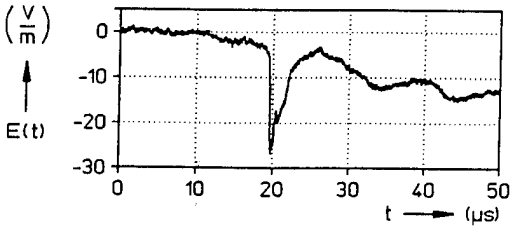

b) Negative first earth stroke



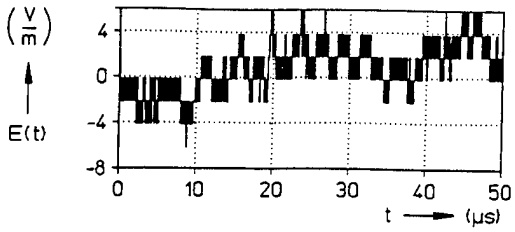

c) Negative subsequent earth stroke



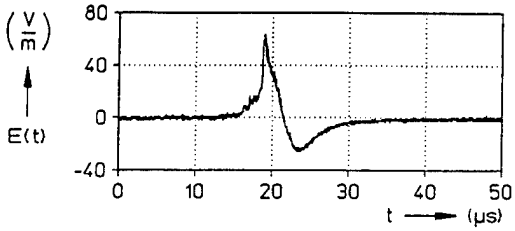

d) Positive stepped leader pulse



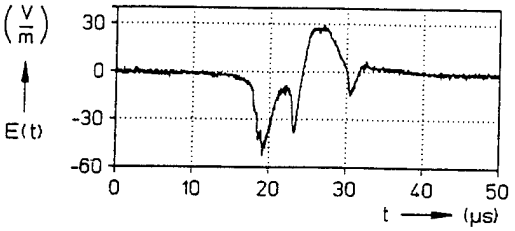

e) Negative stepped leader pulse



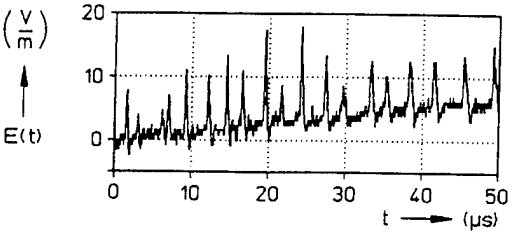

f) Long duration current



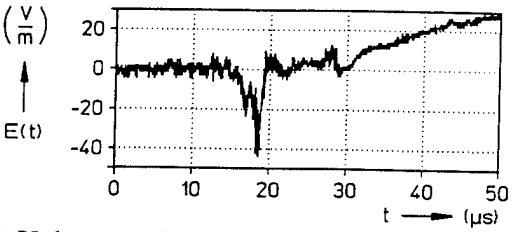

g) Positive cloud-to-cloud discharge




h) Negative cloud-to-cloud discharge



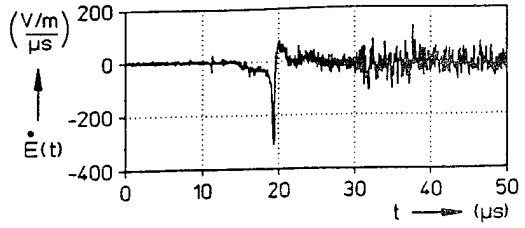

i) Cloud-to-cloud discharge with multiple pulses



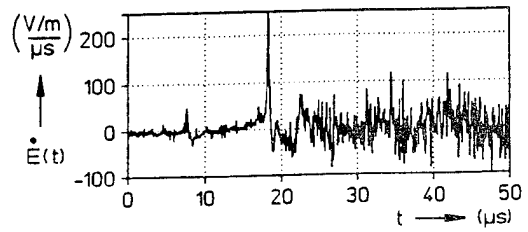

k) Unknown signatures

Fig. 2: Types of E(t)-fields stemming from different lightning sources in about 4 km distance.

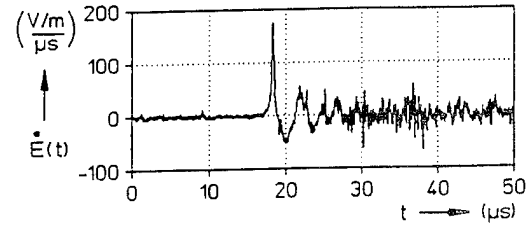
From cloud-to-cloud discharges positive and negative $\dot{E}(t)$-signatures were measured, which are quite similar to the $\dot{E}(t)$-signatures of positive or negative return strokes (fig. 3g, h). But opposite to the return strokes the E(t)-field of cloud-to-cloud discharges have normally no typical ramp even at near distances (fig. 2g, h). Besides that from cloud-to-cloud discharges a second type of E(t)-fields was captured consisting of very fast multiple E(t)-pulses in time intervals of some microseconds (fig. 2i). The $\dot{E}(t)$-signatures are very similar to the step leaders having values of $T_{50}$ in the order some 10 ns (fig. 3i).



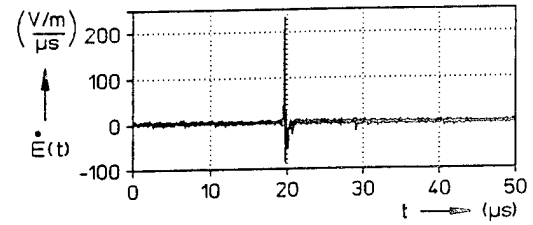

a) Positive earth stroke



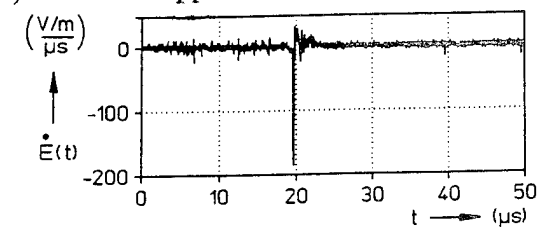

b) Negative first earth stroke



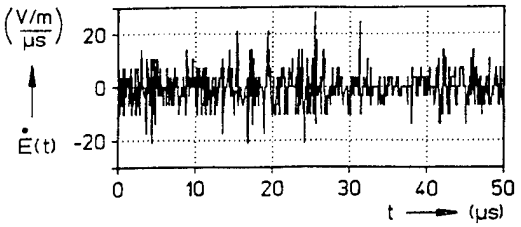

c) Negative subsequent earth stroke



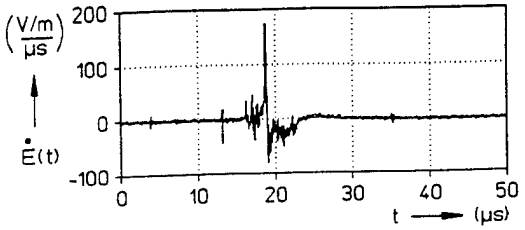

d) Positive stepped leader



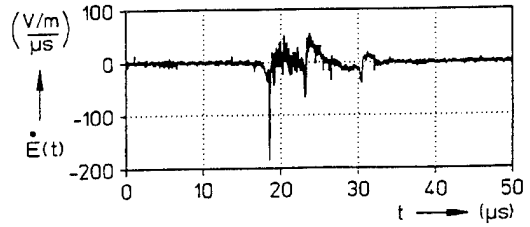

e) Negative stepped leader



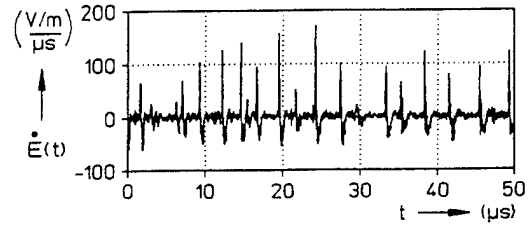

f) Long duration current



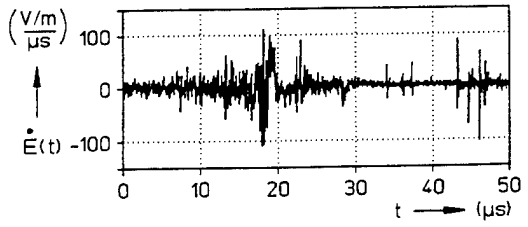

g) Positive cloud-to-cloud discharge




h) Negative cloud-to-cloud discharge




i) Cloud-to-cloud discharge with multiple pulses

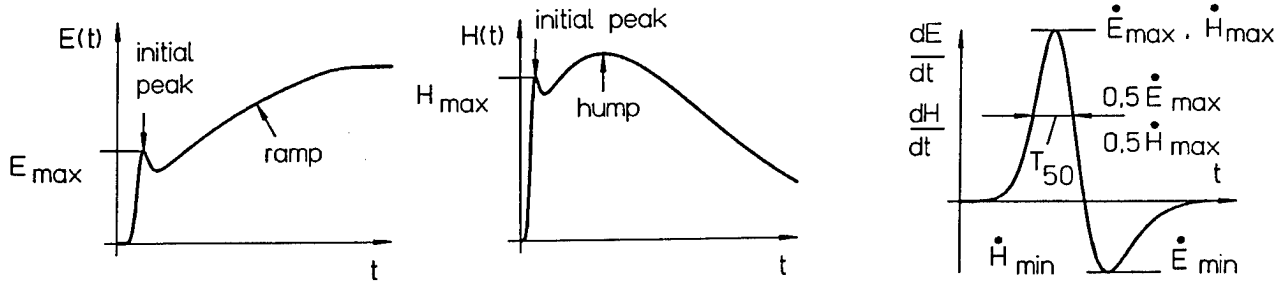



k) Unknown signatures

Fig. 3: Types of $\dot{E}(t)$-signatures stemming from different lightning sources in about 4 km distance.

## 3. EXPERIMENTAL RESULTS FROM RETURN STROKES TO EARTH

Fig. 4 shows schematically the E(t)- and H(t)- fields and the corresponding $\dot{E}(t)$- and $\dot{H}(t)$-signatures of a negative return stroke to earth. Except of the inverse polarity the field of positive earth strokes has the same characteristics. The electric and magnetic fields have typical initial peaks $E_{max}$ and $H_{max}$. In near distances up to some kilometers typically the E(t)-field has a ramp and the H(t)-field a hump. With increasing distance the ramp and the hump vanish. For very far distances (greater some 10 km) the E(t)- and H(t)-field show a typical zero crossing. Caused by the initial field peak the field derivatives have a bipolar waveform with a first maximum $\dot{E}_{max}$, $\dot{H}_{max}$ and a second maximum of inverse polarity $\dot{E}_{min}$, $\dot{H}_{min}$. The duration on half value $T_{50}$ is normally used to characterize the fast field rise /13, 14/.




a) Electric field b) Magnetic field c) Electromagnetic field derivative

Fig. 4: LEMP characteristics of near return strokes to earth

### 3.1 Field derivatives

Table 1 shows the statistics about the maxima of the bipolar $\dot{E}(t)$-signatures $\dot{E}_{max}$ or $\dot{H}_{max}$ resulting from instrumentation 1 and 2. The values are scaled to s = 100 km by the inverse distance relationship: $\dot{E}_{max}$, $\dot{H}_{max} \sim 1/s$. The signatures with a positive $\dot{E}_{max}$-value may stem from stepped leaders or negative earth strokes and the signatures with a negative $\dot{E}_{max}$-value may stem from stepped leaders or positive earth strokes. Related to s = 100 km table 2 shows the mean values of $\dot{E}_{max}$ stemming from the bipolar $\dot{E}(t)$-signatures at the beginning of the return stroke period. With instrumentation 2 the signatures of 19 negative and 3 positive return strokes given by $\dot{E}_{max}/\dot{H}_{max} \approx \Gamma_o$ were measured. On average they are given by $\dot{E}_{max}$ = 6,5 V/(m*$\mu$s), $\sigma$ = 4,5 V/(m*$\mu$s) for negative strokes and $\dot{E}_{max}$ = -12,6 V/(m*$\mu$s), $\sigma$ = 9,6 V/(m*$\mu$s) for positive strokes. With instrumentation 3 the bipolar $\dot{E}$-signatures of 39 negative first and 76 negative subsequent strokes were recorded within a maximum distance of s $\leq$ 4 km. For the first strokes the mean value results in $\dot{E}_{max}$= 3,0 V/(m*$\mu$s), $\sigma$ = 1,5 V/(m*$\mu$s) and for the subsequent strokes in $\dot{E}_{max}$= 3,0 V/(m*$\mu$s), $\sigma$ = 1,3 V/(m*$\mu$s). With instrumentation 4 the bipolar $\dot{E}(t)$-signatures of 73 negative first strokes (mean value: $\dot{E}_{max}$ = 4,70 V/(m*$\mu$s), with $\sigma$ = 3,40 V/(m*$\mu$s)), 86 negative subsequent strokes (mean value: $\dot{E}_{max}$ = 4,40 V/(m*$\mu$s), with $\sigma$ = 2,16 V/(m*$\mu$s)) and 23 positive strokes (mean value: $\dot{E}_{max}$ = -6,10 V/(m*$\mu$s), with $\sigma$ = 2,44 V/(m*$\mu$s)) could be recorded.

| instrumentation | recorded by | maximal field derivatives | number | mean value | standard deviation $\sigma$ |
|---|---|---|---|---|---|
| 1 | Feuerer | $\dot{H}_{max}$ | 90 | 0,03 A/(m*$\mu$s) | - |
| 2 | Heidler | positive $\dot{E}_{max}$<br>negative $\dot{E}_{max}$ | 483<br>11 | 3,6 V/(m*$\mu$s)<br>4,3 V/(m*$\mu$s) | 1,7 V/(m*$\mu$s)<br>3,0 V/(m*$\mu$s) |

Table 1: $\dot{E}_{max}$, $\dot{H}_{max}$ of bipolar $\dot{E}(t)$-signatures related to 100 km by the inverse distance relationship.

| instrumentation | recorded by | stroke | number | mean $\dot{E}_{max}$ | $\sigma$ | remark |
|---|---|---|---|---|---|---|
| 2 | Heidler | negative<br>positive | 19<br>3 | 6,5 V/(m*$\mu$s)<br>-12,6 V/(m*$\mu$s) | 4,5 V/(m*$\mu$s)<br>9,6 V/(m*$\mu$s) | $\dot{E}/\dot{H} \approx$ 377 $\Omega$ |
| 3 | Heidler | negative first<br>negative subsequent | 39<br>76 | 3,0 V/(m*$\mu$s)<br>3,0 V/(m*$\mu$s) | 1,5 V/(m*$\mu$s)<br>1,3 V/(m*$\mu$s) | s $\leq$ 4 km |
| 4 | Hopf | negative first<br>negative subsequent<br>positive | 73<br>86<br>23 | 4,70 V/(m*$\mu$s)<br>4,40 V/(m*$\mu$s)<br>-6,10 V/(m*$\mu$s) | 3,40 V/(m*$\mu$s)<br>2,16 V/(m*$\mu$s)<br>2,44 V/(m*$\mu$s) | observed channel |

Table 2: $\dot{E}_{max}$ of return strokes to earth related to s = 100 km by the inverse distance relationship

Table 3 shows the statistics for the duration on half value $T_{50}$. For the negative return strokes the mean values vary between 0,489 $\mu$s $\leq \bar{T}_{50} \leq$ 0,67 $\mu$s. Remarkably there are nearly no differences between the first and subsequent negative strokes, whereas the mean values are somewhat higher for positive return strokes. From instrumentation 2 the mean value of positive strokes results in $\bar{T}_{50}$ = 1,4 $\mu$s with $\sigma$ = 0,87 $\mu$s and from instrumentation 4 it is given by $\bar{T}_{50}$ = 0,712 $\mu$s with $\sigma$ = 0,299 $\mu$s.

| instrumentation | recorded by | stroke | number | mean $\bar{T}_{50}$ | $\sigma$ | remark |
|---|---|---|---|---|---|---|
| 2 | Heidler | negative<br>positive | 19<br>3 | 0,67 $\mu$s<br>1,4 $\mu$s | 0,34 $\mu$s<br>0,87 $\mu$s | $\dot{E}/\dot{H} \approx$ 377 $\Omega$ |
| 3 | Heidler | negative first<br>negative subsequent | 39<br>76 | 0,63 $\mu$s<br>0,52 $\mu$s | 0,29 $\mu$s<br>0,23 $\mu$s | s $\leq$ 4 km |
| 4 | Hopf | negative first<br>negative subsequent<br>positive | 73<br>86<br>23 | 0,489 $\mu$s<br>0,505 $\mu$s<br>0,712 $\mu$s | 0,226 $\mu$s<br>0,179 $\mu$s<br>0,299 $\mu$s | observed channel |

Table 3: $T_{50}$ of negative and positive return strokes

Although for negative first and subsequent return strokes the values of $\bar{T}_{50}$ are nearly identical, with instrumentation 4 a little bit greater differences were found, if the rise time of the bipolar $\dot{E}$(t)-signature $T_{r/\dot{E}}$ is considered. $T_{r/\dot{E}}$ is defined to be the time between the 10% and the 90% value of $\dot{E}_{max}$ multiplied by the factor 1,25. On average the 73 negative first return strokes had $\bar{T}_{r/\dot{E}}$ = 0,522 $\mu$s ($\sigma$ = 0,426 $\mu$s) and the 86 negative subsequent return strokes had $\bar{T}_{r/\dot{E}}$ = 0,412 $\mu$s ($\sigma$ = 0,217 $\mu$s). For the 23 positive return strokes the average value is given by $\bar{T}_{r/\dot{E}}$ = 0,845 $\mu$s ($\sigma$ = 0,508 $\mu$s).

## 3.2 Initial peaks of positive and negative return strokes to earth

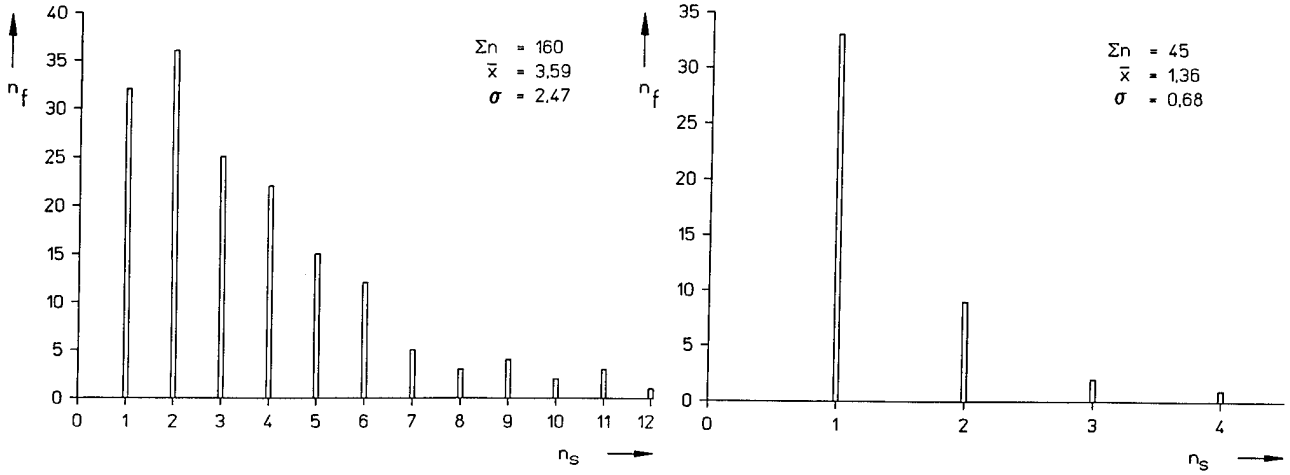
For return strokes to earth table 2 contains the results of the initial peak scaled to s = 100 km. With instrumentation 2 the electric field of 19 negative and 3 positive earth strokes could be recorded. On average the initial peak amounts to $\bar{E}_{max}$ = 6,5 V/m with $\sigma$ = 4,0 V/m for negative strokes and $\bar{E}_{max}$ = -21,6 V/m with $\sigma$ = 6,3 V/m for positive strokes. With instrumentation 4 the electric fields of 73 negative first, 86 negative subsequent and 23 positive return strokes could be measured. The mean values of the initial peaks are given by $\bar{E}_{max}$ = 4,30 V/m with $\sigma$ = 2,87 V/m for the negative first strokes, $\bar{E}_{max}$ = 3,23 V/m with $\sigma$ = 1,70 V/m for the negative subsequent strokes, and $\bar{E}_{max}$ = -8,58 V/m with $\sigma$ = 5,08 V/m for the positive strokes.

| instrumentation | recorded by | stroke | number | mean $E_{max}$ | $\sigma$ | remark |
|---|---|---|---|---|---|---|
| 2 | Heidler | negative<br>positive | 19<br>3 | 6,5 V/m<br>-21,6 V/m | 4,0 V/m<br>6,3 V/m | $\dot{E}/\dot{H} \approx 377\ \Omega$ |
| 4 | Hopf | negative first<br>negative subsequent<br>positive | 73<br>86<br>23 | 4,30 V/m<br>3,23 V/m<br>-8,58 V/m | 2,87 V/m<br>1,70 V/m<br>5,08 V/m | observed channel |

Table 4: Initial peak $E_{max}$ of return strokes related to s = 100 km by the inverse distance relationship

### 3.3 Number of positive or negative strokes in a earth flash

Table 5 shows the statistics about the number of single strokes in an individual earth flash. With instrumentation 3 81 negative earth flashes were measured in the distance range up to s = 4 km. On average an individual negative earth flash consists of 2,4 single return strokes ($\sigma$ = 1,8). With instrumentation 4 160 negative earth flashes could be registered. On average 3,59 single negative return strokes were observed in an individual negative earth flash ($\sigma$ = 2,47). Fig. 5a shows the distribution of the number of negative strokes per earth flash. With instrumentation 4 45 positive earth flashes could be measured with on average 1,36 single positive strokes in an individual earth flash ($\sigma$ = 0,679). Fig. 5a shows the distribution of the number of positive strokes per earth flash. In the distance s = 6 km one positive earth flash was measured having 3 positive subsequent strokes !




a) Negative earth flash

b) Positive earth flash

Fig. 5: Number of single strokes in an individual negative or positive earth flash
($n_s$: number of single strokes in a flash; $n_f$: number of flashes)

| instrumentation | recorded by | type of earth flash | number of flashes | mean | $\sigma$ | remark |
|---|---|---|---|---|---|---|
| 3 | Heidler | negative | 81 | 2,4 | 1,8 | s ≤ 4 km |
| 4 | Hopf | negative<br>positive | 160<br>45 | 3,59<br>1,36 | 2,47<br>0,679 | observed |

Table 5: Number of single strokes in an individual earth flash

### 3.4 Number of interstroke intervals between single strokes in an individual earth flash

Table 6 contains the statistical results about the number of interstroke intervals $T_s$ between two single strokes in an individual positive or negative earth flash. With instrumentation 3 116 interstroke intervals between two single negative strokes could be measured. On average the interstroke interval results in $\bar{T}_s$ = 87 ms with $\sigma$ = 80 ms. With instrumentation 4 414 interstroke intervals between two negative strokes could be registered. The mean value is given by $\bar{T}_s$ = 87,1 ms with $\sigma$ = 95,8 ms. For the measured 16 interstroke intervals between two single positive strokes the mean value results in $\bar{T}_s$ = 120 ms with $\sigma$ = 96,9 ms.

| instrumentation | recorded by | type of earth flash | interstroke intervals | mean $\bar{T}_s$ | $\sigma$ | remark |
|---|---|---|---|---|---|---|
| 3 | Heidler | negative | 116 | 87 ms | 80 ms | s ≤ 4km |
| 4 | Hopf | negative<br>positive | 414<br>16 | 87,1 ms<br>120 ms | 95,8 ms<br>96,9 ms | observed |

Table 6: Interstroke interval $T_s$ between two single strokes in an individual earth flash

Table 7 shows the statistical outcome for the total duration of an individual flash $T_f$. For an individual flash with more than one single stroke $T_f$ is defined to be the time interval between the first and last stroke. With instrumentation 4 the total duration of 128 negative and 12 positive flashes to earth could be registered. The mean values are given by $\bar{T}_f$ = 282 ms with $\sigma$ = 233 ms for the negative flashes and $\bar{T}_f$ = 160 ms with $\sigma$ = 135 ms for the positive flashes.

| instrumentation | recorded by | type of earth flash | number of flashes | mean $\bar{T}_f$ (ms) | $\sigma$ (ms) | remark |
|---|---|---|---|---|---|---|
| 4 | Hopf | negative<br>positive | 128<br>12 | 282<br>160 | 233<br>135 | observed |

Table 7: Duration $T_f$ of an individual earth flash having more than one single stroke.

## 4. LONG DURATION CURRENT

Table 8 contains the statistics about the long duration currents stemming from the field data of 47 negative earth flashes captured with instrumentation 4 (see fig. 1). Although for 15 flashes the distance could not clearly be evaluated, the maximum distance is less than about 12 km. Generally the lightning discharge was starting with a return stroke. An individual negative earth flash had $n_s$ = 4,79 (standard deviation $\sigma$ = 2,08) return strokes on average, $n_s$ = 11 return strokes on maximum and $n_s$ = 1 return stroke on minimum. 95% of the flashes had 2 or more return strokes, whereas the 5%-value is given by 8,54 return strokes per flash. The long duration current lasted $T_l$ = 221 ms ($\sigma$ = 103 ms) on average, $T_l$ = 551 ms on maximum and $T_l$ = 67 ms on minimum. 95% of the long duration currents exceeded $T_l$ = 82,7 ms and 5% $T_l$ = 391 ms. Totally the flash duration amounted to $T_f$ = 440 ms ($\sigma$ = 180 ms) on average, $T_f$ = 837 ms on maximum and $T_f$ = 148 ms on minimum. 95% of the flashes had a longer duration than $T_f$ = 193 ms and 5% of the flashes a longer duration than $T_f$ = 755 ms.

The discharge process of the first stroke is characterized by $E_1$, of the long duration current by $E_l$ and of the total flash by $E_f$ (fig. 1). For the long duration current it resulted $E_l$ = 3,01 kV/m ($\sigma$ = 3,92 kV/m) on average, $E_l$ = 15 kV/m on maximum and $E_l$ = 185 V/m on minimum. In a rough approxi-

mation the ratio $E_l$ to $E_1$ is equal to the ratio of the charge of the long duration current to the charge of the first return stroke. This ratio resulted in $E_l/E_1 = 5{,}67$ ($\sigma = 4{,}66$) on average, $E_l/E_1 = 25{,}5$ on maximum and $E_l/E_1 = 1{,}13$ on minimum. The ratio $E_l$ to $E_f$ is approximately equal to the ratio of the charge of the long duration current to the charge of the whole flash. It resulted in $E_l/E_f = 0{,}471$ ($\sigma = 0{,}178$) on average, $E_l/E_1 = 0{,}833$ on maximum and $E_l/E_1 = 0{,}113$ on minimum.

The fields of 67 flashes could be recorded successfully, where the distance is absolutely known amounting to s = 6,36 km on average. In 32 cases long duration currents could be separated. This result means, that 48% of the flashes contained a long duration current. The data shown in table 9 are quit similar to the data of table 8. By 18 flashes the long duration current was followed by one or more return strokes, but by 14 flashes the long duration current occurred at the end of the lightning discharge.

| | $n_s$ | $T_l$ | $T_f$ | $E_l$ | $E_l/E_1$ | $E_l/E_f$ |
|---|---|---|---|---|---|---|
| mean | 4,79 | 221 ms | 444 ms | 3,01 kV/m | 5,67 | 0,471 |
| $\sigma$ | 2,08 | 103 ms | 180 ms | 3,92 kV/m | 4,66 | 0,178 |
| maximum | 11 | 551 ms | 837 ms | 15 kV/m | 25,5 | 0,833 |
| minimum | 1 | 67 ms | 148 ms | 185 V/m | 1,13 | 0,113 |
| 5%-value | 8,54 | 391 ms | 755 ms | 13,7 kV | 15,6 | 0,757 |
| 95%-value | 2 | 82,7 ms | 193 ms | 291 V/m | 1,30 | 0,174 |

Table 8: Data of long duration currents from the fields of 47 negative earth flashes recorded by *Hopf* with instrumentation 4.

| | $n_s$ | $T_l$ | $T_f$ | $E_l$ | $E_l/E_1$ | $E_l/E_f$ | s |
|---|---|---|---|---|---|---|---|
| mean | 5,16 | 218 ms | 476 ms | 3,43 kV/m | 4,21 | 0,467 | 6,36 km |
| $\sigma$ | 2,08 | 96,9 ms | 191 ms | 4,4 kV/m | 3,71 | 0,168 | 1,19 km |
| maximum | 11 | 435 ms | 837 ms | 15 kV/m | 19,6 | 0,815 | 10 km |
| minimum | 2 | 82 ms | 180 ms | 185 V/m | 1,13 | 0,164 | 3,3 km |
| 5%-value | 10 | 193 ms | 477 ms | 14,8 kV/m | 4,16 | 0,432 | 10 km |
| 95%-value | 2 | 83 ms | 198 ms | 307 V/m | 1,31 | 0,178 | 3,99 km |

Table 9: Data of long duration currents from the fields of 32 negative earth flashes recorded by *Hopf* with instrumentation 4.The distance s is known.

## 5. CONCLUSION

During about 15 years the field and the field derivatives were measured with 4 various equipments up to now. Pre-discharges as stepped leaders (fig. 3d, e), cloud-to-cloud discharges (fig. 3g, h) as well as positive (fig. 3a), negative first (fig. 3b) and negative subsequent return strokes (fig. 3c) have bipolar $\dot{E}(t)$-signatures with maximum values in the same order of magnitude. Typically for the stepped leaders the duration on half value is in the order of $T_{50} \leq 100$ ns, whereas for return and cloud-to-cloud

strokes this value is higher and lies in the order of about $T_{50} \approx 0{,}5\ \mu s$. According to the bipolar $\dot{E}(t)$-signatures the corresponding electric fields show typical initial peaks. For the positive (fig. 2a), negative first (fig. 2b) and negative subsequent return strokes (fig. 2c) the electric field remains typically on a relatively high level after the initial peak. Opposite that the electric field of cloud-to-cloud strokes shows normally a bipolar waveform (fig. 2g, h), whereas the electric field of stepped leaders showing an unipolar waveform is reduced by about one order of magnitude (fig. 2d, e).

With instrumentation 4 return strokes to earth could clearly be detected by the use of an all sky video camera. It was found, that even positive earth flashes may have subsequent return strokes. At maximum a single positive earth stroke with 3 subsequent positive return strokes was registered! The following data of long duration currents could be evaluated successfully from the measured field:

- Nearly 50% of the negative earth flashes had long duration currents.
- About 44% of the long duration currents occurred at the end of the flash.
- Compared to the first return stroke the charge of the long duration current is typically 5 times higher.
- Typically the charge of the long duration current is as high as the summarizing charge of the return strokes in a flash.
- Compared to a multiple flash without a long duration current the flash lasted about 2 times longer.
- Typically a flash with a long duration current contains about 1 ... 3 return strokes more than a flash without a long duration current.

## REFERENCES


/1/ Hopf, Ch.: Effects of propagation on the electric fields radiated by return strokes in distances up to 15 kilometers. 22nd International Conference on Lightning Protection (ICLP), Budapest (1994), rep. R 1a-01.

/2/ Feuerer, R.: Zeitliche Änderung der magnetischen Induktion bei negativen Erdblitzen. Phil. Thesis University of Armed Forces Munich, 1984.

/3/ Heidler, F.: Lightning electromagnetic impulse - Theorie und Messungen. Phil. Thesis University of Armed Forces Munich, 1987.

/4/ Heidler, F.: Results of simultaneous dE/dt- and dH/dt- measurements. 22nd International Conference on Lightning Protection (ICLP), Budapest (1994), 1c-04.

/5/ Heidler, F.: E-dot measurement by video tape recorder. 7th International Symposium on EMC, Zurich (1987), report 14D2, p. 69 - 74.

/6/ Heidler, F.: Results of $\dot{E}(t)$-measurements using video tape recorder. International Aerospace and Ground Conference on Lightning and Static Electricity (1994), Mannheim, Germany, p. 45 - 54.

/7/ Heidler, F.: $\dot{E}(t)$- signals of near lightning strokes using video tape recorder. 22nd International Conference on Lightning Protection (ICLP), Budapest (1994), R 1c-03.

/8/ Hopf, Ch.: dE/dt-measurements and simultaneous all sky video camera observations. 9th International Symposium on EMC, Zurich (1993), report F4.

/9/ Hopf, Ch.: Parameters and spectra of return stroke fields in the short distance range. 21nd International Conference on Lightning Protection ICLP (1992), Berlin, report 1.01, p. 7 - 12.

/10/ Hopf, Ch.: Parameters and spectra of lightning radiated electric fields in the short distance range. International Conference on Lightning and Static Electricity ICOLSE (1992), Atlantic City, New Jersey.

/11/ Hopf, Ch.: Characteristics of return stroke electric fields produced by lightning flashes at distances of 1 to 15 kilometers. International Aerospace and Ground Conference on Lightning and Static Electricity (1991), Cocoa Beach, Florida.

/12/ Hopf, Ch.: Transiente elektrische Feldänderungen und Felder naher Blitzentladungen. Phil. Thesis University of Armed Forces Munich, submitted to the Faculty of Electrical Engineering.

/13/ Heidler, F.; Wiesinger, J.: Survey of actual Lightning-EMP measurement and analysis activities. 10th International Symposium on EMC, Zurich (1993), report 29F1, p. 139 - 144.

/14/ Uman, M: The lightning discharge. 1st edition, Orlando, USA: Academic Press, 1987.

/15/ Weidman, C; Krider, E: The submicrosecond structure of electromagnetic field radiated by lightning. 17th International Conference on Lightning Protection (ICLP), The Hague (1983), p. 65 - 72.

# SYNCHRONIZED MULTIPOINT MEASUREMENTS OF LIGHTNING ELECTRIC FIELD CHANGES

T. Ushio, D. Wang, Z-I. Kawasaki, K. Matuura
Department of Electrical Engineering, Osaka University
Yamadaoka 2-1, Suita, Osaka, 565, Japan
Telephone +81-6-879-7691 FAX +81-6-875-0506
E-mail ushio@pels.pwr.eng.osaka-u.ac.jp

## ABSTRACT

We have developed a system with 4 stations to locate sources of electromagnetic pulses(E-M pulses) from lightning discharge processes in a 8km ×8km at Hokuriku district area. In this system, we exploit GPS systems to synchronize four wideband (0.2Hz-2MHz) slow antennas with the time accuracy of 1μs. With this system, we had many occasions to record lightning flashes at Hokuriku district area from December 2, 1993 to January 28, 1994. Almost all lightning flashes show consecutive pulses superimposing on their slow field changes with the time intervals of tens microseconds. We measured the difference in the time of arrival of E-M pulses and succeeded in locating the sources of the pulses which are from PB(Preliminary Breakdown), L(Leader), R(Return stroke), and C(Continuing current) stage for a positive cloud to ground discharge, and from so-called recoil streamer for a cloud discharge. Furthermore the lowered charge amount and its location for a return stroke are determined. Since we combine the functions of traditional slow antennas with lightning location method, this system would be a significant tool to study lightning physics, especially the physics of the initiation of lightning.

## INTRODUCTION

Initiation process of lightning discharge has been the subject of numerous studies. According to the measurements of the electric field change caused by downward lightning discharges, a breakdown process with its duration from a few milliseconds to a few hundred milliseconds usually exist prior to the first return stroke in a negative cloud-to-ground flash(1, 2, and 3). This process, referred as preliminary breakdown, is thought to be very important not only to understanding the initiation of lightning discharges but to forecasting when and where lightning discharges would occur. Unfortunately, because this process occurs only inside thunderclouds, it is very difficult to make a direct measurement of its characteristics and consequently, a little has been known of this process. In the previous literatures, the following three approaches have been taken to study the preliminary breakdown: (1) the measurement at a single station of the preliminary-breakdown electric field change(4, 5, 6, 7, 8, 9, and 10) the simultaneous measurement of the electric field change of the preliminary breakdown at multi ground stations(11, 12, 13, and 3) location of its VHF radiation sources by the technique of the time-of-arrival and interferometry(14, 15, 16, 17, and 18). Each of these approaches has its advantages and disadvantages. To overcome these disadvantages, we combined all of these three approaches into one system by synchronizing in microsecond order the multi-point observation of the electric field change of lightning discharges. This paper is to report our new system and some preliminary results obtained with this system.

## SETUP OF SLOW ANTENNA SYSTEMS

The slow antenna system (19), as shown in Figure 1, consists of a disk antenna, optical triggering unit , GPS unit (20) and recording system. The induced voltage on the antenna by electrostatic field change of lightning discharges is amplified by a wide band operation amplifier and then sampled and memorized temporally by an A/D board with 12 bit resolution and 1 MHz frequency. Since lightning discharges generally last less than 1 second, the recording time of 1 second for each lightning is assured by the temporal memory. After the sampling for one event of lightning is completed, the data in the temporal memory is transferred into hard disk. Lightning caused electric field change can be deduced from the induced voltage because they have positively linear relations (11).

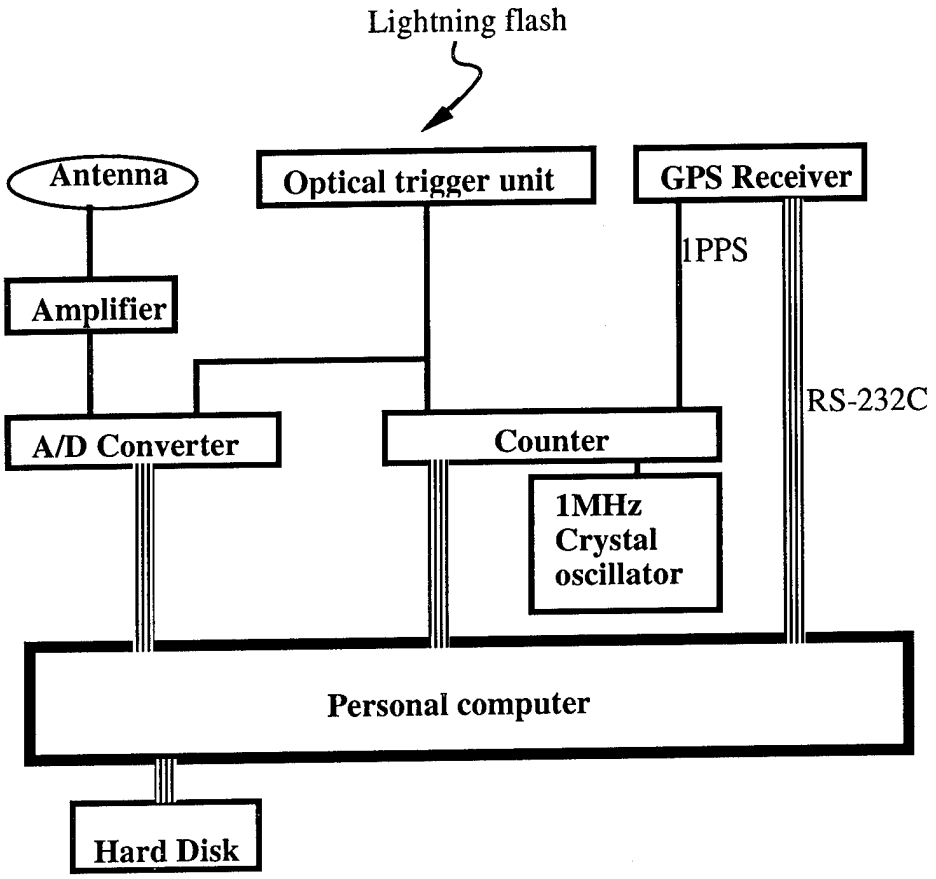



Figure 1 Schematic setup of a slow antenna system.

A photo-diode is used to sense the optical signal radiated by lightning and its output is served as the external triggering signal of the A/D board. A commercially available GPS unit provides a standard square pulse every second with the time accuracy of 500 nsec, which is used to reset a 1 MHz counter. At each time when the A/D board is triggered, the memory of the counter will be hold and then its value is sent to the recording system as the absolute time of the triggering. By this way, the absolute time of any pulses which might appear in the lightning caused electric field change could be determined with the time accuracy of 1 $\mu$ s. Table 1 lists the specification of the slow antenna system. To record simultaneously the slow electric field

change, the time constant of the system was set to 5s and as a result, the frequency bandwidth of the whole system is 0.2Hz to 2MHz. To do multi-point observation, three sets of this system have been accomplished with the same characteristics.

Table 1 Specification of slow antenna system

| Sensor | Disk antenna |
|---|---|
| Bandwidth | 0.1Hz～2MHz |
| Time constant | 5 seconds |
| Sampling time | 1 microsecond |
| Recording time | 1 second |
| A/D converter | ADH-12LM(Sun System Co.) |
| GPS | GN-72(Furuno Electric Co.) |

Before multi-point lightning observation, three sets of these systems were installed side by side at same place 2.7 km away from the site of rocket triggered lightning experiment and a great number of electric field changes caused by lightning discharges were recorded to confirm the accuracy of these systems. Figure 2 gives a recorded pulse waveform which was identified as a return stroke in a positive cloud to ground discharge. All the three different systems present entirely same waveforms. The absolute times of the pulse peak which is pointed with an arrow in Figure 2 could be read, respectively, from the three systems. It was found that although the triggering time of each system is different from each other and the absolute times of the pulse peak calculated from different systems are same with the time accuracy of 1 microsecond. This proved the correct performance of the systems.

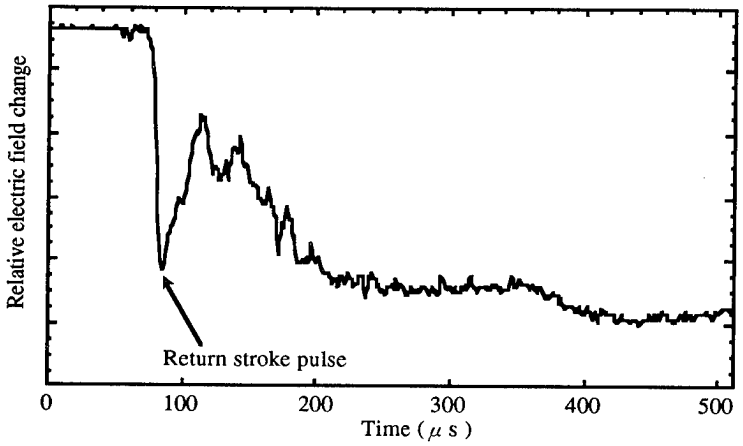



Figure 2 The observed return stroke pulse for confirming the performanceof the observation systems.

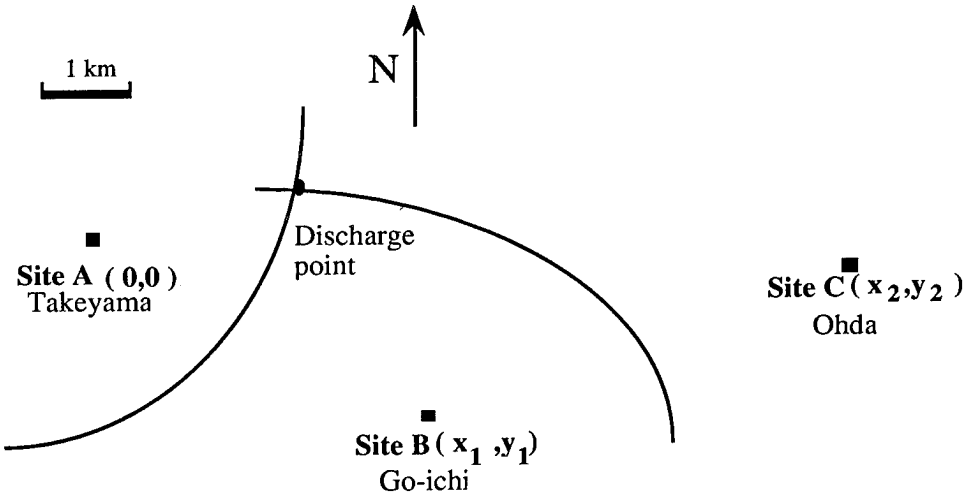



Figure 3 Map of multi-point lightning observation setup.

Multi-point slow antenna observation of lightning was carried out at the Hokuriku district area facing the sea of Japan. Considered that winter thunderstorms are generally very lower than summer thunderstorms, slow antenna systems were set up with the distances of about several kilometers from each other. Figure 3 shows the map of observation sites and as well as the operational principle of the slow antenna systems. Since the absolute time of all pulses superimposed in electric field change of lightning discharges can be determined by the observation system, the difference in time of arrival ( $\Delta t_1$, $\Delta t_2$ ) of each pulse to site A, B and C can be obtained. Based on relations (1) and (2),

$$\sqrt{x^2+y^2+z^2}-\sqrt{(x-x_1)^2+(y-y_1)^2+z^2}=c\Delta t_1 \qquad (1)$$

$$\sqrt{(x-x_2)^2+(y-y_2)^2+z^2}-\sqrt{(x-x_1)^2+(y-y_1)^2+z^2}=c\,\Delta t_2 \qquad (2)$$

the sources of all the pulses can be located by assuming height z to be constant.

On the other hand, for the well-known point charge model(3, and 11) the electric field change of cloud to ground flash observed at the ground is given by

$$\Delta E_i=\frac{1}{4\pi\varepsilon_0}\left[\frac{2\Delta Q z}{\left\{ x-x_i{}^2+(y-y_i)^2+z^2\right\}^{\frac{3}{2}}}\right] \qquad (3)$$

where x, y, z are the coordinates of the charge $\Delta Q$, $x_i$, $y_i$ is the location of the observer. Since x and y are the function of z, $\Delta E$ becomes the function of z and $\Delta Q$ by substituting (1) and (2) to (3). Consequently, measurements of $\Delta E_i$ at three locations are sufficient for determining the four variables x, y, z, $\Delta Q$ by performing a nonlinear least squares fit of the data to a point-charge model. The function minimized is the reduced chi-square

$$\chi_i^2=\sum_{i=1}^{3}\frac{\left[\Delta E_i-\Delta E_i(z,\ \Delta Q)\right]^2}{\sigma_i^2} \qquad (4)$$

where $\Delta E_i$ is the field change measured at the ith location, $\Delta E_i(z, \Delta Q)$ is the fitted value of the field change, and $\sigma_i^2$ is the variance of the measurement $\Delta E_i$ due to experimental error.

With four or five stations, the amount of charge neutralized by cloud to cloud flash and the locations of these charge centers can be derived. Unfortunately due to an accident, we can operate only three antennas.

## LOCATIONS OF THE PRELIMINARY BREAKDOWN PULSES IN LIGHTNING DISCHARGES

The field multi-point observation of lightning discharges were performed from December 1th, 1993 to January 31th, 1994 and more than 100 lightning discharges were recorded. Figure 4 gives an example of electric field change waveform observed at site A. The total field change is negative and thus is considered to be caused by a positive cloud-ground flash discharge. Preliminary breakdown pulses appear suddenly without any precursor in the waveform. A slow change with its duration of about 10 ms follows these pulses and then an abrupt change appears at the end of the slow change. Another slow field change succeeds with its duration of about several milliseconds. The first slow change, the rapid change and the second slow change are identified as leader, return stroke and continuous current.

To see more detail of the preliminary breakdown, the initial part of Figure 4 is expanded as shown in Figures 5, and 7 for three sites, respectively. Compared Figures 5, and 7, it is apparent that the preliminary pulses observed in different sites have similar appearances. About ten of bipolar pulses superimposed on the field change waveforms and their amplitudes increased with time. The initial polarities of the pulses are the same as the return stroke-caused electric field change that follows. The bipolar pulses appear regularly with their intervals of about 40 $\mu$ s and lasting time of about 20 $\mu$ s.

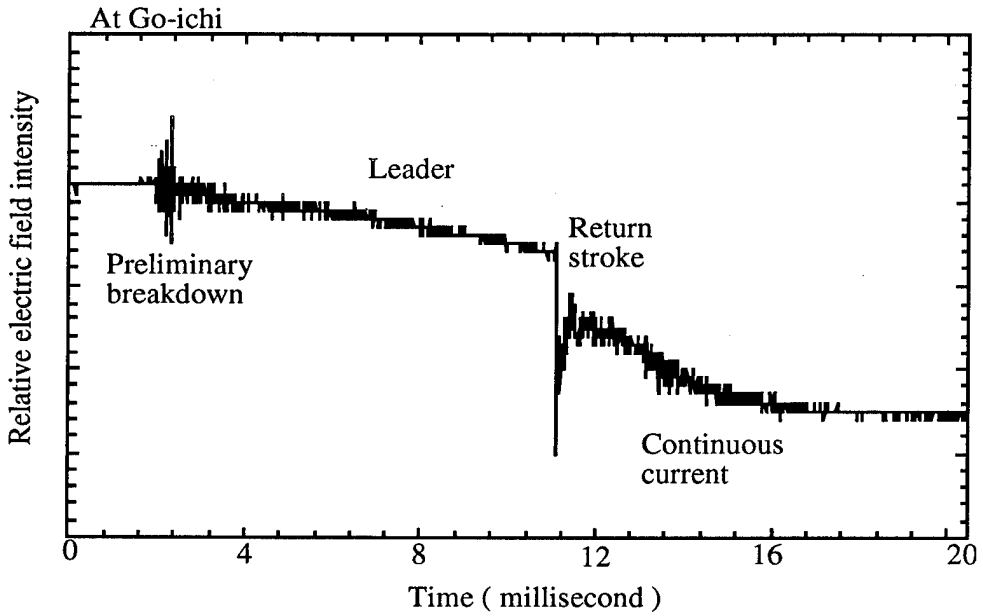



Figure 4 One example of electric field change of positive lightning discharge.

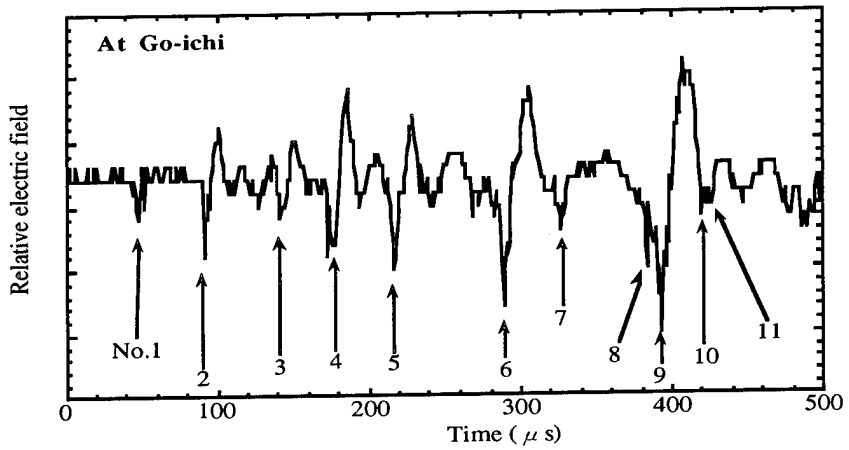



Figure 5 The preliminary breakdown pulses of Figure 4 discharge at site Go-ichi.

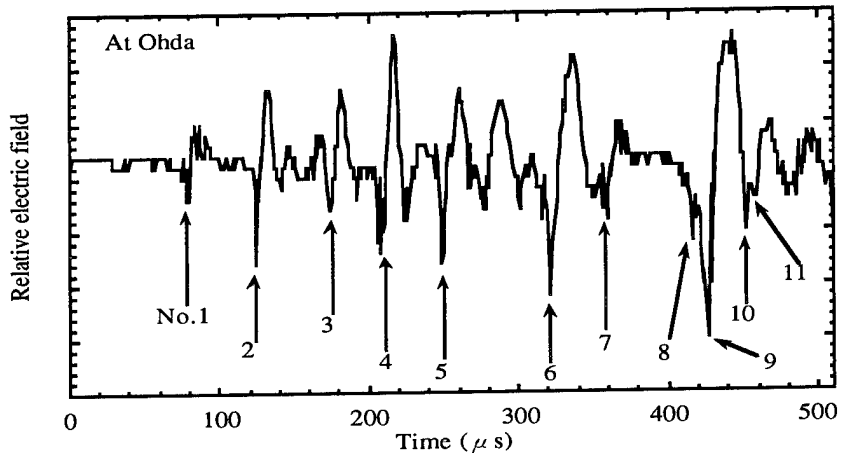



Figure 6 The preliminary breakdown pulses of Figure 4 discharge at site Ohda.

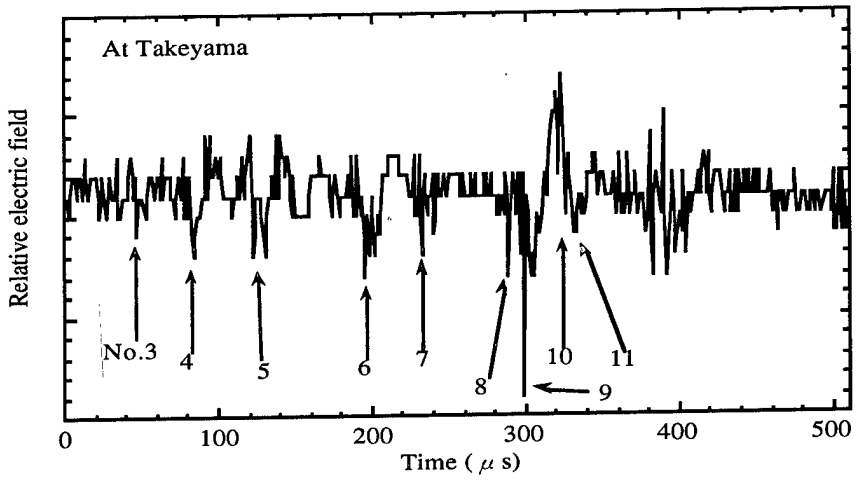



Figure 7 The preliminary breakdown pulses of Figure 4 discharge at site Takeyama.

To show the whole process of the Figure 4 lightning discharge, the following return stroke pulse and the pulses during continuous current are also presented which are found in Figures 8 and 9, respectively.

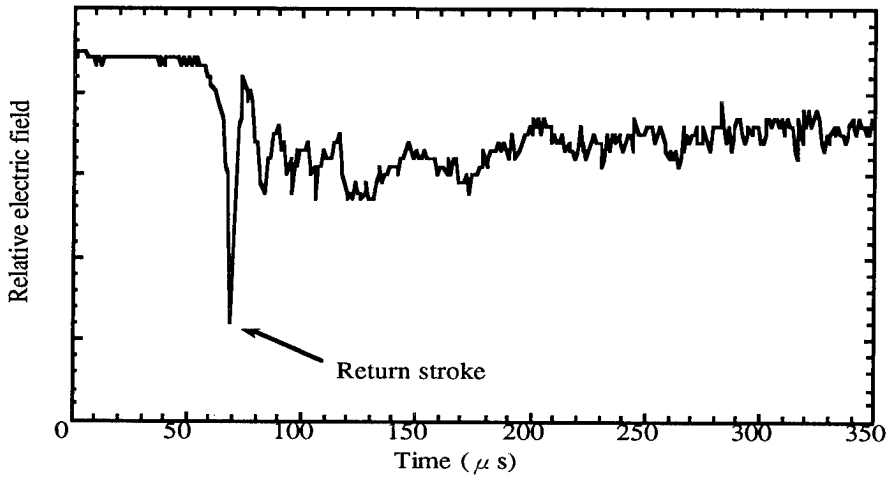



Figure 8 The return stroke pulse of Figure 4 discharge.

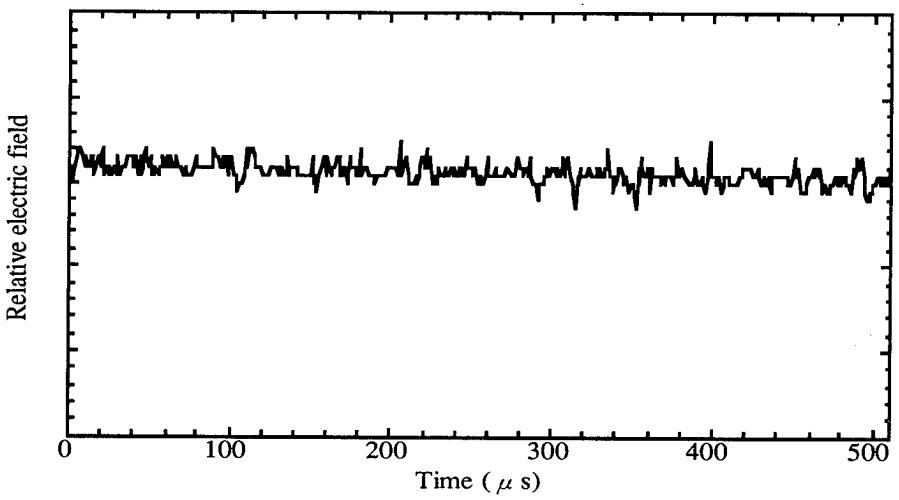



Figure 9 Microsecond scale pulses during continuous current of Figure 4 discharge.

Based on equations (1), (2), the sources of all the preliminary breakdown pulses, together with the following return stroke and the pulses in continuous current process are located in two dimensions, which are shown in Figure 10. The small circle around each located point indicates the location error for each pulse.

Based on the equation (3) and (4), the lowered charge amount and its height for a return stroke are determined. The result is shown in Table 2. Here, the experimental error $\sigma_i^2$ is estimated at 30% in the calculations.

Based on Figure 10 and the time sequences of the pulses, it was proposed that the lightning develops itself as shown in Figure 11. The leader which might be initiated by the preliminary breakdown progressed over a horizontal distance of about 2 km away from its initiation place before going to the ground and then triggered the return stroke. The pulses during the continuous current appeared around the preliminary breakdown pulses in the opposite side of the leader. This suggests that the pulses during the continuous current might be caused by J processes(21, 22, and 23) which neutralize the cloud charge far away from the region of the initiation of the leader.

The height of charge center, 5.4 km, is thought to be the that of the upper positive region of the cloud. It's height is lower than that in summer. Because the tropopause comes down about 10 km altitude in winter, while it stays about 16 km altitude in summer. The amount of charge neutralized in this flash is smaller than that of Brook et al.(12)'s results. The flash analyzed in this paper is thought to occur in electrically very weak thunderstorm cell.

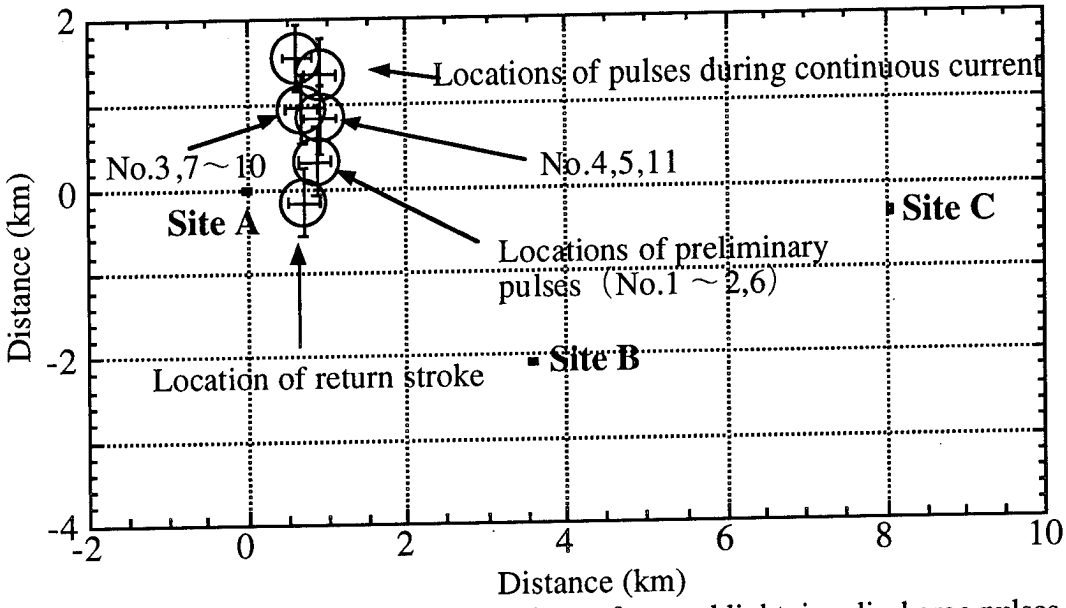



Figure 10 One example of projected locations of ground lightning discharge pulses.

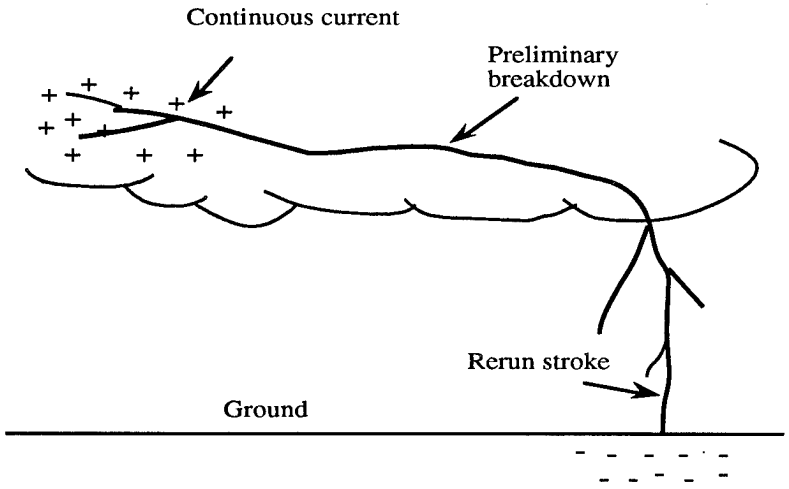



Figure 11 The proposed progression of a positive ground lightning discharge based on Figure 10.

Table 2 Height and magnitude of ground stroke charge

| | |
|---|---|
| Z [km] | $5.4 \pm 0.5$ |
| Q [c] | $1.9 \pm 0.1$ |
| Chi-square | 0.24 |

**SUMMARY**

A synchronized slow antenna systems have been accomplished and applied successfully to locate two dimensionally the microsecond scale pulses and to determine the amount of charges neutralized in lightning discharges.

This technique can be used not only in studying the initiation processes but in studying the whole process of lightning discharges.

**Reference**

(1) ND.Clarence and D.J.Malan : "Preliminary discharge processes in lightning flashes to ground", *Q.J.R.Meteorol.Soc.*, 83, 161, 1957

(2) Beasley, W.H., M.A.Uman, and P.L. Rustan , "Electric fields preceding cloud-to-ground lightning flashes", *J.Geophys.Res.*, 87, 4883-4902, 1982

(3) Uman, M. A. , The lightning discharge, *Academic, San Diego, Calif.*,71,1987.

(4) Clarence, N. D., and D.J. Malan, Preliminary discharge processes in lightning flashes to ground, Q. J. R. Meteorol. Soc., 83, 161-172, 1957.

(5) M.A.Uman, et al. : "An unusual lightning flash at Kennedy Space Center", *Science*, 201, 9, 1978

(6) M. Ishii, et al. : "Statistics on fine structure of cloud-to-ground lightning field waveforms", *J.Geophy.Res.*, 94, 13267, 1989

(7) Mazur, V., and L. Ruhnke, "Common physical processes in natural and artificialy triggered lightning", *J.Geophy.Res.*, 98, 12913, 1993
(8) Z.Kawasaki, et al. : "The electric field changes and UHF radiation caused by the triggered lightning in Japan", *Geophy.Res.Lett.*, 19, 1711, 1991
(9) C.D.Weidman and E.P.Krider : "The radiation field waveforms produced by intracloud lightning discharge processes", *J.Geophy.Res.*, 84, 3157, 1979
(10) Kawasaki, Z-I, and V. Mazur "Common physical processes in natural and triggered lightning in winter storms in Japan", *J.Geophy.Res.*, 97, 12935-12945, 1992
(11) Krehbiel, P.R., M. Brook, and R. A. McCrory, "An analysis of the charge structures of lightning discharges to ground" , *J.Geophy.Res.* , 84 , 2432 , 1979
(12) Brook, M., M.Nakano, P.Krehbiel, and T. Takeuti, "The electrical structure of the Hokuriku winter thunderstorms" , *J.Geophy.Res.* , 87 , 1207-1215 , 1982.
(13) Liu, X., P.R. Krehbiel, "The initial streamer of lightning flashes" , *J.Geophys.Res.* , 90 , 6211-6218, 1985
(14) D.E.Proctor : "A hyperbolic system for obtaining VHF radio pictures of lightning" , *J.Geophy.Res.* , 76 , 1478 , 1971
(15) Rustan, P.L., M.A. Uman, D.G. Childers, W.H. Beasley, and C.L. Lennon, "Lightning source locations from VHF radiation data for a flash at Kennedy Space Center", *J.Geophy.Res.*, 85, 4893-4903, 1980
(16) P.Richard,et al. : "VHF-UHF interferometoric measurements application to lightning discharge mapping" , *Radio Science* , 20 , No.2 , 171, 1985
(17) Proctor, D.E., R. Uytenbogaardt, and B. M. Meredith, "VHF radio pictures of lightning flashes to ground", *J.Geophy.Res.*, 93, 12683-12727, 1988
(18) Hayega, C.O., and J.W. Warwick, "Two-dimensional interferometic positions of VHF lightning sources", *J.Geophy.Res.*, 86, 7451-7462, 1981
(19) Kawasaki, Z-I., K. Matsuura, K. Yamamoto, M. Nagatani, H. Nakada, M Nakano, and T. Takeuti, Design of the transient memory of extremely large size for electric field changes due to the lightning discharge and observation results during summer and winter thunderstorms, Trans. IEE of Japan, Vol. 111 - B, No.5, 1991.
(20) Hofmann-wellenhof, B., H.Lichtenegger, and J.Collins:"GPS theory and practice", *Springer-Verlag* , 1992.
(21) Brook, M., and B. Vonnegut, Visual confirmation of the junction process in lightning discharges, J. Geophys. Res., 65, 1302 - 1303, 1960.
(22) Kitagawa, N., M. Brook and E.J. Workman, Continuing currents in cloud to grond lightning discharges, J. Geophys. Res., 67, 637 - 647, 1962.
(23) Brook, M., N. Kitagawa, and E.J. Workman, Quantitive study of strokes and continuous currents in lightning discharges to ground, J. Geophys. Res., 67, 649-659, 1962.

# SESSION 09B
# LIGHTNING PROTECTION
# CHAIRPERSON: EDWARD F. ROBERTS, JR.

# LIGHTNING PROTECTION OF RF-SYSTEMS

K. Borgeest, J.L. ter Haseborg
Technical University of Hamburg-Harburg
Dept. of Measurement Engineering/EMC
Harburger Schloss-Strasse 20, D-21071 Hamburg
Tel. +49/40/7718-2873 FAX +49/40/7718-2382
Email borgeest@tu-harburg.d400.de

F. Wolf
C. Plath GmbH
Company for Nautical Electronics
Gotenstrasse 18, D-20097 Hamburg

## ABSTRACT

In many cases the grounding of RF-systems for lightning protection impairs the function of these systems. It is desirable to realize a grounding which is highly impedant for RF-signals, but not for lightning surges. Such an impedance can be realized with a grounding cable covered with ferrites. In case of steeply rising lightning surges the ferrite gets slowly into the saturated state and so the induced voltage is limited. The paper describes the measurement setup which has been used to investigate this kind of grounding and presents the obtained results. Theoretical considerations explain the results. Finally practical consequences are discussed.

## INTRODUCTION

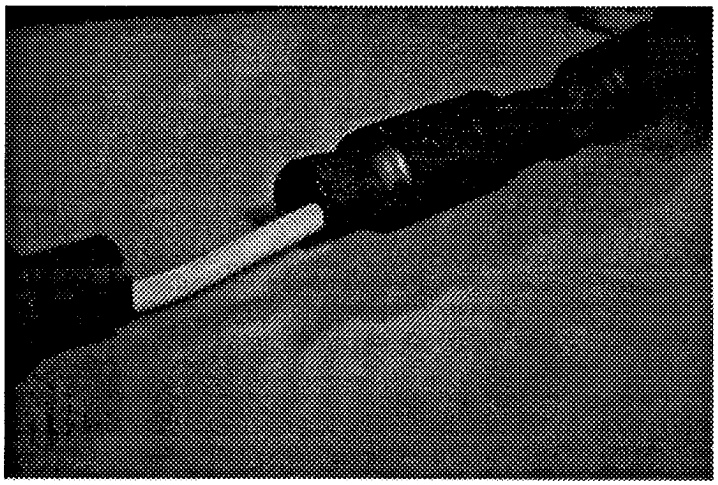


FIGURE 1:
THE INVESTIGATED GROUND CABLE WITH FERRITE RINGS UNDER SHRINK-ON-SLEEVES

In some RF-applications grounded metallic structures as used for lightning protection could influence the operation of these systems in an inadmissible manner. Antennas of radio direction finders are an example case in which grounding may cause problems. They should be mounted on isolating masts. On the other hand lightning protection measures are necessary to protect human lives and the equipment and also to fulfill legal requirements. So a grounded cable must be connected via a spark gap to the antenna. In these cases lightning protection systems with little effect on the RF-signals must be developed. The problem is to block high frequencies on a lightning arrester without increasing its impedance to lightning surges.

The approach presented in this paper combines a high impedance to RF-signals with a low impedance to surges. Between the lightning currents and the signals there are differences in amplitude and in steepness. So the idea was to use a component with a low impedance for high currents, which requires any kind of saturation effect, and for steep pulses, which requires any kind of inertia. These properties can be realized with ferrite cores, which are put over the grounding cable as shown in Fig. 1.

The behavior of the ferrites is represented by its magnetization curve which is shown in exemplary way in Fig. 2. The magnetic quantities $B$ (flux density) and $H$ (field strength) correspond to the electric quantities $V$ (voltage) and $I$ (current) by Ampère´s law (equation 1) and Faraday´s law (equation 2):

$$I = c_1 \cdot H . \tag{1}$$

$$U = c_2 \cdot \frac{\partial B}{\partial t} . \tag{2}$$

The constant factor $c_1$ depends on the distance of a certain point in the ferrite from the conductor center and $c_2$ could be determined experimentally if necessary. Since the magnetic values are not constant over the volume of the ferrites a mean value must be assumed. With the used ferrites and a medium radius of about 2 cm $c_1$ can be estimated to 0.1 m. An estimation of $c_2$ would be more difficult, but is not necessary here.

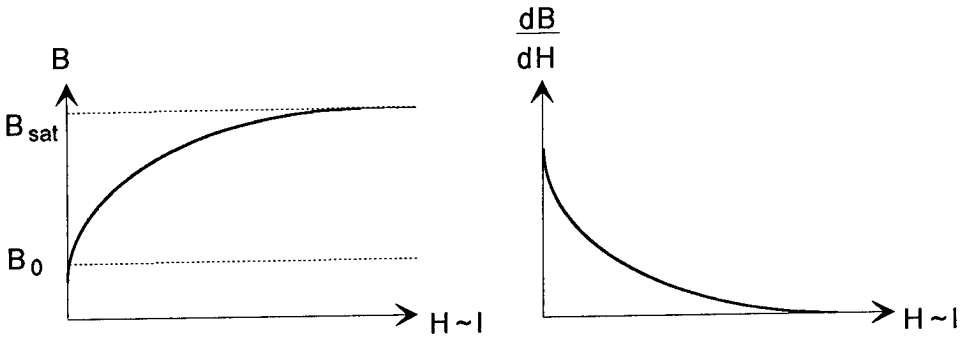



FIGURE 2:
MAGNETIZATION CURVE OF FERRITE MATERIAL (LEFT) AND ITS DIFFERENTIAL (RIGHT), AFTER THE MATERIAL HAS BEEN ONCE SATURATED.

If the protected structure is struck by lightning, a current pulse is imposed on the ground cable. So a magnetic flux H is imposed on the ferrite. Approaching the lightning current coarsely by a linearly rising front followed by a constant current, the curves in Fig. 2 are passed with a constant velocity from 0 to the right until H stops at a certain level. One recognizes easily that the induced voltage at each time depends on the actual steepness of the magnetization curve. The peak voltage which is to be minimized for this application depends on the maximum value of the right curve.

The magnetization curve in Fig. 2 can approximately be described by the function

$$B(H) = B_0 + \left(1 - e^{-\frac{H}{c_H}}\right)(B_{sat} - B_0), \tag{3}$$

where $c_H$ is a constant with the dimension of a magnetic field strength. Accordingly the right differential curve is

$$B'(H) = \frac{1}{c_H} e^{-\frac{H}{c_H}} (B_{sat} - B_0). \tag{4}$$

For the induced voltage follows:

$$u(t) = \frac{c_2}{c_H} e^{-\frac{H(t)}{c_H}} (B_{sat} - B_0). \tag{5}$$

If the front of the lightning pulse is also assumed exponential with equation 1 H(t) can be written

$$H(t) = c_1 \left(1 - e^{-\frac{t}{\tau}}\right) \hat{I}. \tag{6}$$

Insertion into equation 5 yields

$$u(t) = \frac{c_2}{c_H} e^{\frac{c_1 \left(e^{-\frac{t}{\tau}} - 1\right) \hat{I}}{c_H}} (B_{sat} - B_0) \quad . \tag{7}$$

The maximum of the induced voltage is reached at t=0 and amounts to

$$u(t = 0) = \frac{c_2}{c_H} (B_{sat} - B_0) \quad . \tag{8}$$

In this expression $(B_{sat}-B_0)/c_H$ is a measure of steepness.

One can see that the saturation flux density does not influence directly the peak voltage, but, of course, the steepness of the magnetization curve depends on it. For a good protection effect the steepness must be as low as possible. On the other hand a high inductance for small signals requires a high initial steepness, because

$$\mu_{r0} = \left.\frac{\partial B}{\partial H}\right|_{H=0} \tag{9}$$

So the static magnetic characteristic shown in Fig. 2 is not suitable to combine low surge voltages with a high RF-impedance, but in case of highly rising currents the dynamic properties of ferrimagnetic materials get important.

Generally there are three dynamic effects in ferrites known:

- Polarization delay due to finite propagation velocity of the magnetic domain walls (1),
- Gyromagnetic resonance (1),
- Eddy currents (2).

A ferrimagnetic (like ferrites) or ferromagnetic material consists of several magnetic domains with a spontaneous orthogonal magnetic polarization (3). These domains form spontaneously in an energetically favorable way, which means in particular that the ferrite does not generate external magnetic fields. If an increasing external magnetic field is applied the walls between the domains move in favor of those domains which have already a polarization similar to the direction of the external field. This process goes on till the best directed domain has extended over the whole volume close to $B_{sat}$. Finally the elementary dipoles in the domain align totally with the external field. Now $B_{sat}$ is definitely reached. The propagation velocity of the domain walls is limited to about 100 m/s (1) in case of ferrites with little impurity. With increasing impurity the maximum velocity decreases. Considering the domain extensions from some μm up to some 100 μm, one can coarsely estimate the minimum time to reach the saturation inductance in the order of a μs or more and so the maximum steepness of the slope in Fig. 2. So with increasing current through the cable the induced voltage grows first proportionally than the contribution of the ferrites to the induced voltage should stay constant and the slow remaining increase is due to the constant line inductance. Calling $T$ the time to reach saturation this can be expressed as a proportionality relation

$$\mathrm{Max}(U_F) \sim \mathrm{Max}(\frac{\partial B}{\partial t}) \approx B_{sat} / T. \qquad (10)$$

where $U_F$ is the ferrite contribution to the induced voltage. The measurements will confirm these theoretical considerations.

The gyromagnetic resonance has been without effect in these measurements, because the resonant frequency has not been reached. Closely around this frequency the flux density falls rapidly and remains low at higher frequencies, whereas the ohmic losses show a peak at this point. Concerning the RF-behavior this resonance frequency must be taken into consideration, because a resonant frequency below the signal range would make almost disappear the desired blocking effect.

The increasing magnetic field in the ferrite induce voltages in the material which cause eddy currents. The effect of the eddy currents are ohmic losses and a reduction of inductance. So they support the magnetic delay effect, but due to the low conductivity of the ferrite their effect is inferior.

## THE MEASUREMENT SETUP

For all measurements the setup in Fig. 3 has been used to measure the voltage across the cable with and without ferrites. Ohmic and inductive losses in the ground had to be kept as small as possible. The instrumentation must be free from ground loops, because the current surges produce a quickly rising magnetic field which would induce voltages in loops.

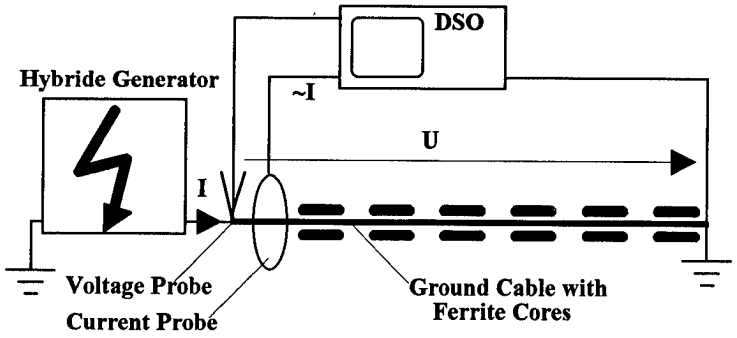



FIGURE 3:
THE MEASUREMENT SETUP FOR THE SURGE CURRENT FED INTO THE GROUND WIRE AND THE CORRESPONDING VOLTAGE.

For the measurement it is irrelevant how the cable is geometrically aligned. It can be stretched or installed in waves. The only arrangement to be avoided are closed loops as demonstrated in Fig. 4. This is also interesting for the practical application.

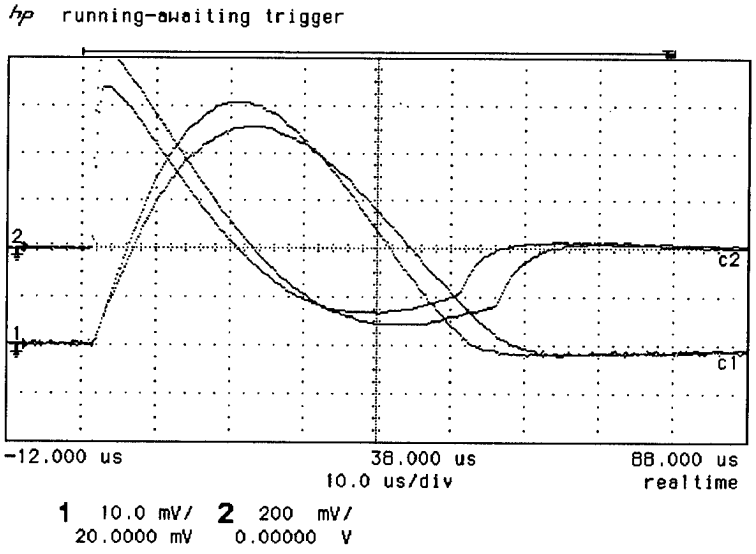



FIGURE 4:
INFLUENCE OF CABLE ARRANGEMENT IN TWO EXTREME CASES, STRAIGHT AND ROLLED UP.

## RESULTS

The figures 5 and 6 demonstrate the course of the current through the cable and the caused voltage across the cable without and with ferrites.

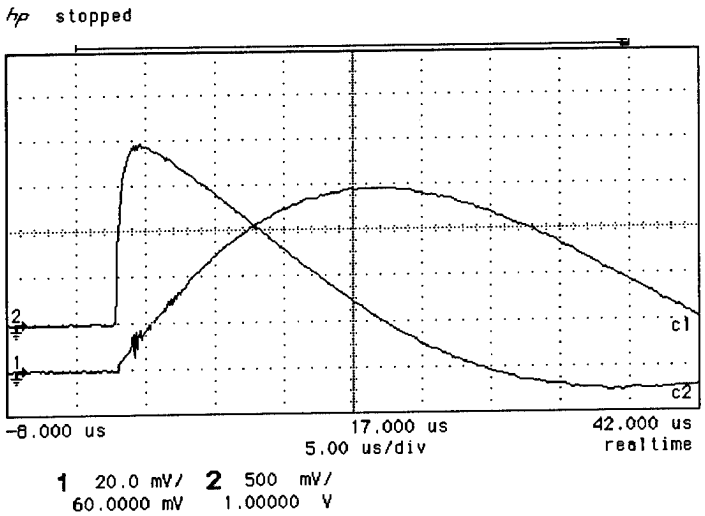



FIGURE 5:
CURRENT (TRACE 1) AND VOLTAGE (TRACE 2) WITHOUT FERRITE CORES.
Trace 1: 400A/DIV, Trace 2: 500V/DIV

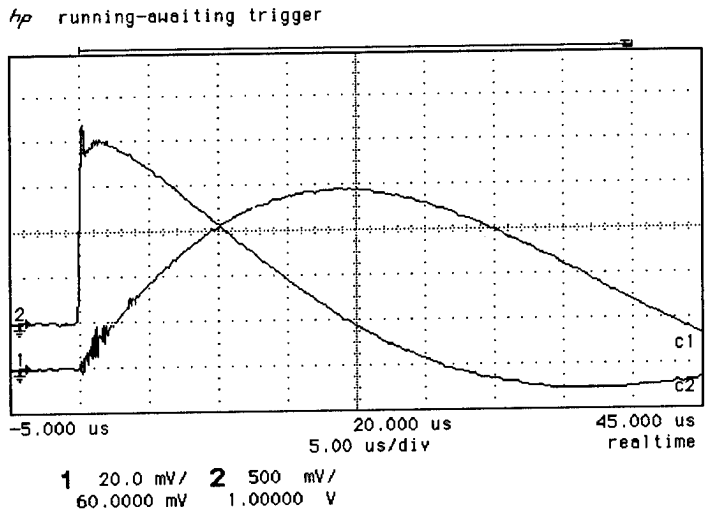



FIGURE 6:
CURRENT (TRACE 1) AND VOLTAGE (TRACE 2) WITH FERRITE CORES.
Trace 1: 400A/DIV, Trace 2: 500V/DIV

In Fig. 5 one recognizes well that the voltage curve is the time differential of the current curve, so the behavior is almost purely inductive. From the cable data (copper, length 8m, cross section 16 $mm^2$) a resistance of 9 mΩ and an inductance of 14 μH can be computed without consideration of the skin effect. The computed inductance agrees well with that one computed from the measurements in Fig. 8

With the ferrites the voltage waveform is nearly the same except a short peak at the beginning. Fig. 7 shows such a peak in a higher time resolution. This peak is additively superimposed on the curve obtained without the ferrites and represents the ferrite contribution $U_F$. After the ferrite has reached its saturation induction , which means that the ferrites do not contribute anymore to the induced voltage, the two curves are equal. It is interesting that the saturation induction effects on the duration of the peak, but not directly on its amplitude. If $B_{sat}$ is low the saturation is reached quickly and the overvoltage pulse remains short. If the applied pulses are steeper than the magnetization can follow, the waveform of the peak depends only on the way in which the material admits an increase of flux density. The peak is not influenced anymore by the steepness or amplitude of the pulse.

Due to the limited bandwidth of the measurement setup and to the generator waveform which does not reach immediately its maximum steepness, the peak does not occur at *t=0* as predicted in equation 7, but about 1 μs later. The ferrite has already been magnetized before, so the magnetization curve as in Fig. 2 has no slowly rising area for small amplitudes, which otherwise could have been a reason of a delay.

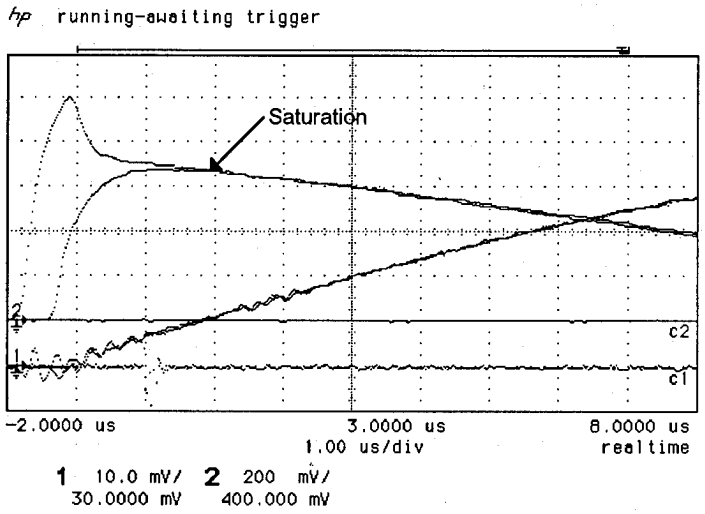



FIGURE 7:
HIGHLY RESOLVED INDUCED PEAK WITH FERRITES.
TO PROVIDE A COMPARISON THE CORRESPONDING CURVE
WITHOUT FERRITES IS ALSO SHOWN.
Trace 1: 100A/DIV, Trace 2: 200V/DIV

The figures 8 and 9 show the induced peak voltages across the cable depending on the steepness of the current surge. The rise time has been kept constant while the current amplitude has been varied. Without the ferrite cores the linear dependence is obvious. With the ferrite rings the induced voltage first rises steeply (marked by the first straight line in the figure) till the steepness finally reaches a similar characteristic as without ferrites as marked by the second straight line in the same figure. The peak of the superimposed voltage $U_F$ does not change anymore, so above 100 kA/µs only a constant shift between the figures 8 and 9 is observable.

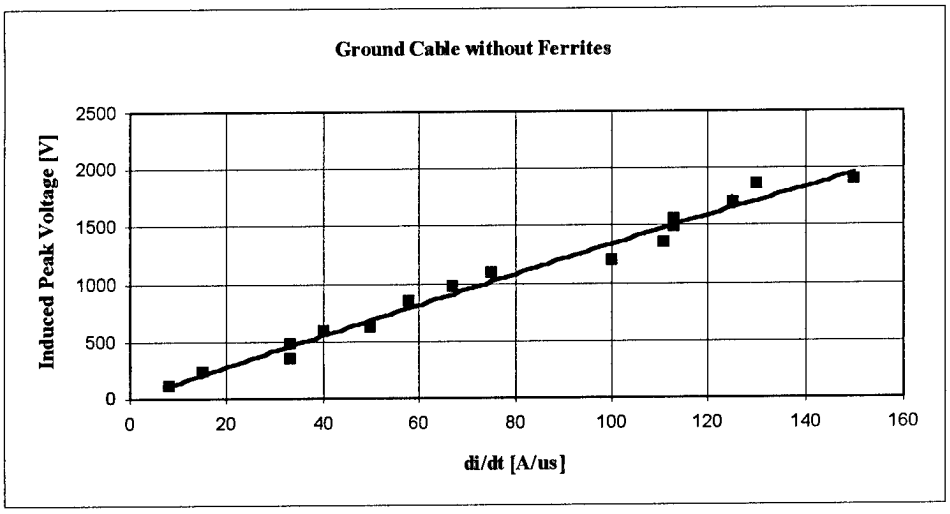



FIGURE 8:
INDUCED PEAK VOLTAGE DEPENDING ON CURRENT STEEPNESS WITHOUT FERRITES

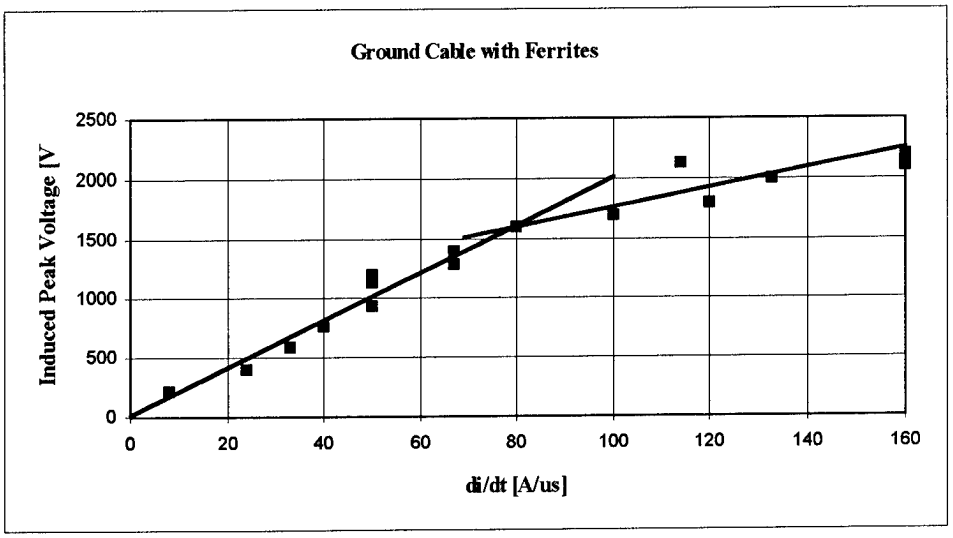



FIGURE 9:
INDUCED PEAK VOLTAGE DEPENDING ON CURRENT STEEPNESS WITH FERRITES

## SUMMARY AND CONCLUSION

1. The measurements have shown that the dynamic properties of ferrites can be used to block radiofrequent currents on ground cables of lightning protection systems without the risk of significantly increased induction voltages due to the lightning currents. The scope of this paper has been to present this idea and to demonstrate its feasibility. Nevertheless, for practical application improvements are possible. For these measurements only one ferrite type has been used, but based on this experience one can chose the ferrite which complies best with the demands of a certain application.

2. To obtain a maximum delay and this way a slowly increasing flux density and low induction voltage, one should choose a ferrite material with a high impurity. A good conductivity would allow high eddy current which support this effect, but on the other hand also the RF-blocking effect would decrease, so the ferrite should have a low conductivity. Another criterion is the gyromagnetic resonant frequency which must be far enough above the signal frequency range. The permeability is not a criterion, because after the ferrite has once been driven into saturation it is not valid anymore. Depending on the polarity of lightning it could assume two states on the hysteresis curve after the surges and so the initial permeability can assume three different values including the original one. Even if there was only one value for the permeability, a high value would improve RF-blocking, but would also cause a higher induction voltage for slow surges. If a material with a low saturation induction is chosen, the duration of the induced peak can be minimized. Since ferrites show a different magnetic behavior in different directions (anisotropy) geometrical aspects should be also considered.

3. An aspect which has not been considered is the dynamic behavior of the ferrites during a steep decay. It is not approximately as steep as the rise, but the question if an analogue behavior can be observed also in this case is interesting from a theoretical point of view. A further interesting item for future research is the influence of the heat generated by the surge on the ferrites. In case of extremely high currents the decrease of $\mu$ at higher temperatures can support the desired behavior.

4. The presented concept diverts a great share of the lightning energy into ground. Nevertheless, an overvoltage in the order of some kV can remain and would be still destructive for sensitive RF equipment. So an additional nonlinear protection circuit is highly recommended (Fig. 10). This nonlinear protection circuit consists of two or three stages. It must be designed to protect the input stages of the connected electronic apparatus reliably even from smallest overvoltages (4). On the other hand the influence of the protection circuit on the signal (attenuation, reflections, nonlinear distortions) has to be considered. The network analysis program SPICE (5) has been proven useful for an efficient design combining the requirements in time domain (6), linear frequency domain (7) and can also be used in the nonlinear large-signal frequency domain (8). The designer and user must take care that all transmission lines are well screened and as short as possible, otherwise the lightning current induces overvoltages in the lines. This effect can also be predicted during the design phase with SPICE (9).

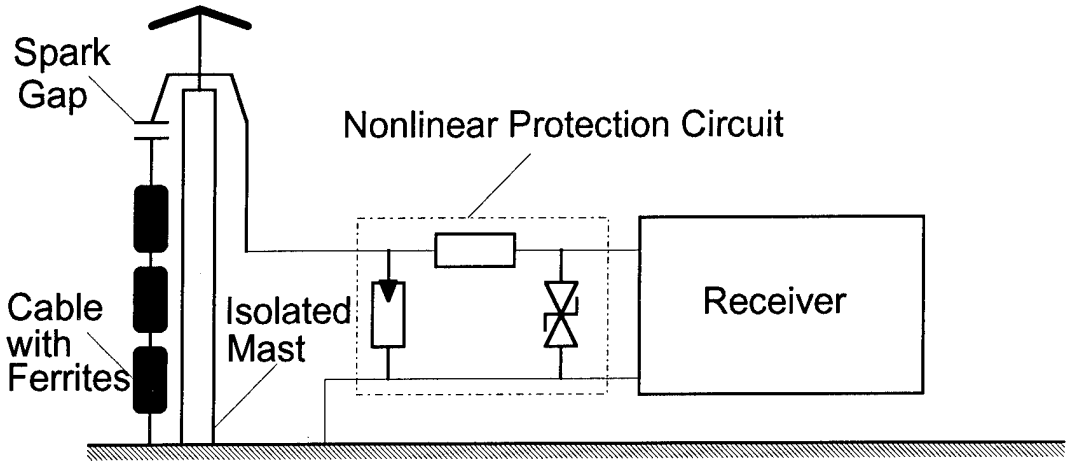



FIGURE 10:
A COMPLETE APPLICATION EXAMPLE: RADIO DIRECTION FINDING SYSTEM

## REFERENCES

1. W. v. Münch, "Elektrische und magnetische Eigenschaften der Materie", (Electrical and Magnetic Properties of Matter), B.G. Teubner, Stuttgart, 1987.

2. H. Kaden, "Wirbelströme und Schirmung in der Nachrichtentechnik", (Eddy Currents and Screening in communication engineering", Springer, Berlin, 1959.

3. B.I. Bleaney, B. Bleaney: "Electricity and Magnetism", Oxford University Press, Oxford, 1976.

4. R.B. Standler, "Protection of Electronic Circuits from Overvoltages", J. Wiley & Sons, NY, 1989

5. L.W. Nagel, D.O. Pederson: "SPICE (**S**imulation **P**rogram with **I**ntegrated **C**ircuit **E**mphasis)", University of California, Berkeley, 1973

6. K. Borgeest, J.L. ter Haseborg, "A Gas Arrester SPICE Model considering the Voltage/Time Characteristics", International Symposium on Electromagnetic Compatibility, Roma, September 13-16, 1994

7. K. Borgeest, J.L. ter Haseborg, F. Wolf, "Simulating the Frequency Response of non-linear Protection Circuits with SPICE", EUROEM, Bordeaux, May 29 - June 3, 1994

8. K. Borgeest, J.L. ter Haseborg, "Measurement and Modeling of Nonlinear Components for SPICE Simulation of Signal Distortions by Protection Circuits", 11th International Symposium on Electromagnetic Compatibility, Zurich, March 7-9, 1995

9. C.R. Paul, "Analysis of Multiconductor Transmission Lines", J. Wiley & Sons, NY, 1994

## BIBLIOGRAPHY

M. Cyrot, "Magnetism of Metals and Alloys", North Holland Publ. Comp., 1982,

R.L. Gardner, "Lightning Electromagnetics", Hemispherer Publ. Corp., NY, 1990

# LIGHTNING SAFETY EVALUATION OF LAUNCH COMPLEXES FOR PERSONNEL SAFETY

Ronald J. Wojtasinski, PE

Science and Technology Corporation
400 West Central Boulevard
Cape Canaveral, Florida 32920
Phone 407 799 0667
Fax 407 799 9164

ABSTRACT

The threat of lightning constrains work activities on the launch complexes and the processing of a aerospace vehicles for flight. During the summer months, sixty percent of the work time can be lost because of thunderstorms within five miles of the launch complex. A systematic engineering approach is used to evaluate direct and induced effects of lightning on aerospace launch systems at Cape Canaveral Air Force Station. An analysis identifies hazards caused during lightning strikes, the adequacy of facilities to conduct lightning currents safely, and the effectiveness of lightning protection and grounding of facilities. Lightning interceptor systems are considered in this application and there effectiveness is compared to the inherent electrical capacity of the structures. The 200 kA lightning wave form is applied to electric models of the launch structures. Using detailed electrical models of structures and geometric lightning attachment models, lightning hazards are determined for the manned operating areas. Coupling mechanisms by induction and through the earth and grounding system introduce lightning currents into other systems and structures. Locations of hazardous voltages to personnel were derived from the analysis. Voltage hazards were identified around the structure and mitigated by conventional construction practice. Effects on telephone, video and control systems was analyzed for personnel and equipment hazard. Personnel hazards were identified on the structures, control, telephones and camera systems. Power and lightning systems because of overhead wire and multiple grounds and earth conductors provided gratuitous protection. The probability distributions of magnitude and frequency of the threat are applied to a hazard analysis of the operations. The operational requirement of systems which must function during a lightning event and personnel functions required provides the criteria for investment in lightning mitigating techniques. The possible benefits are derived by the reduction of lightning effects as a consequence of the interceptor systems but there parasitic effects remain. Voltage hazards were created at the peripheral grounding locations of lightning down conductors and transmitted along the security fence and other inadvertent conductors. The direct current component of the lightning strike current was eliminated from the launch structure but effects effects from fast di/dt rise times remained along with high EM fields. The conclusion is that lightning protection design must be evaluated with respect to the operations that are to be protected. The launch facilities are over twenty-five years old and changing construction practice increases the sensitivity of new facilities to lightnings detrimental effects and high speed data systems function at lower voltages. The use of PVC conduit to replace metallic conduit increases induced and potential drop effects. The sensitvity of people to lightning shock is poorly understood, however, direct attachment of lightning or side strikes are the lethal hazard.

## INTRODUCTION

Installation of Lightning Mitigation Systems begged the question "What operations may be allowed during a lightning advisory?". Increased operations during a lightning advisory could be allowed if risk could be assessed for those operations. To answer these questions the 45th Space Wing Safety Director commissioned a study to evaluate lightning hazards to personnel on space launch facilities. This evaluation considers the design of the facility, lightning effects, and the hazards engendered during the operations that may be in processes. The primary concern of the study is the safety of personnel. The analysis was performed on the Air Force space launch complexes at Cape Canaveral Air Force Station supporting the Delta, Atlas and Titan launch systems. The Titan launch complexes have a Lightning Mitigation System (LMS) that is an over head lightning interceptor and grounding system protecting an entire launch facility. The data prented in this report is from the Atlas facility because of contrasting designs betweeb Pad A and B. The methods of analysis have been applications of previously presented computer modeling systems. The approach to the evaluation is guided by referenced military and civilian specifications: MIL HBK 419A, MIL-STD-1542A, NFPA 780, NEC 250-81C and with regard to the present knowledge of lightning phenomena. Since the facilities were built in the 1960's, lightning currents over 200 kA have been reported and the concept of the striking distance of lightning leaders has modified the assessment of lightning protection and risk. The statistical properties reported in The Transmission Line Reference Book, EPRI EL-2500 were used. The codes do not address the probability of occurrence of lightning nor the magnitude of the lightning event to which the code applies; these topics are partially addressed in AF-HND-419A. A comprehensive reference for grounding and the human physiology of electrical shock is in ANSI/IEEE Standard 80, IEEE Guide for Safety in Substation Grounding and analysis by Dalziel[1] from which the electrical impulse criteria is utilized for personnel shock tolerance. The lightning safety evaluation for personnel is performed in three parts: the Facility Evaluation, the Lightning Hazard Analysis, and the Operational Hazard Analysis (OHA). These three analysis define the environment envelope for lightning hazards within a facility based upon its use.

## FACILITY EVALUATION

The Facility Evaluation is a review of the design of facilities and systems and an inspection to confirm the physical attributes of the overall facility. In cases where individual designs and modification drawings were not available, the attributes were derived by inspection and construction practice. Characteristics of the construction affecting the exposure of personnel to hazardous voltages, the conduction of lightning currents and, lightning attachments are included in a risk assessment. The Facilities Lightning Risk Analysis qualitatively rates the relative lightning risk for each structure. The risks of lightning hazards to personnel and operating systems is presented in Table 3. The hazard from lightning to personnel, sensitive commodities and systems within an operating area, and the protective features of the facility are given relative numerical grades that allow a comparative assessment of risk within the facility. The assessment is based on configuration of the structure, conductivity of the structural material, presence of personnel and sensitivity of contained commodities or systems housed in the facility. The ranking

progresses in relative severity from the least severe (ranking 10) to the most severe (ranking 1). The lightning effects are developed from the electrical model of the structure and the response of the structure to a 200-kA peak lightning strike. The numeric value defining terms for the risk analysis are:

Structure type (S)
- 5 All metal
- 4 Structural metal frame
- 3 Steel reinforced concrete
- 2 Poor electrical conductivity materials
- 1 None

Walking surface materials (W)
- 4 Metal
- 3 Steel reinforced concrete
- 2 Asphalt
- 1 Grass-soil

Lightning Hazard (H)
- 5 Step voltage on walking surface
- 4 Insulated conductor from other locations
- 3 Contact voltages from conducting surfaces
- 2 Flash over
- 1 Lightning attachment

Operation sensitivity (O)
- 5 None
- 4 Intermittent operation allowable
- 3 Loss of control of a major process
- 2 Catastrophic failure
- 1 Personnel

The highest risk number is assigned depending on the analysis of facility construction, function, and personnel hazard. The facility risk number (FRN)=.5(S+W+H+O) is a relative risk number to compare the lightning risk at each facility. The range of the FRN is 1 to 10, 1 being the most severe risk. This analysis is similar to the risk assessment developed in the NFPA 780 but tailored specifically for structures within launch facilities with numerical values scaled to correspond with the Operational Hazard Analysis developed later.

LIGHTNING HAZARDS ANALYSIS

The Lightning Hazards Analysis is the analysis of lightning attachment and the induced effects from nearby lightnings to the structures to quantify the electrical hazards to which personnel are exposed. The lightning effects are quantified with mathematical models for structures and calculated values for contact voltage, step voltage, and flash over. A qualitative analysis of the relative risk is developed for each facility based on the nature of the construction. The computer models used are FLASH an electro geometric model for the termination of lightning strikes on ground objects, attachment locations and statistical properties; CYLINDER a derivative of FILAMENT[2] for determining lightning current distribution, voltage gradients, and induced effects within structures and specific deterministic models[3] are used to calculate step voltages on walking surfaces and voltages generated between different locations at the space launch complexes.

ROLLING BALL TECHNIQUE The lightning protection codes for the location of protective masts and towers are based on the "rolling ball" model. Radii of 100 and 150 ft for the rolling ball are used in the lightning protection codes; these distances respectively correspond to strike currents of 7.8 kA and 14.6 kA in peak magnitude, and to 97 percent and 83 of all lightning strikes. Using the 50-ft rolling ball clearance around structures corresponds to 2.7 kA peak magnitude and 99 percent of all lightning strikes The justification for such distances comes from the observation of lightning step leaders

(LaForest, 1987, p. 568)[4]. The areas safe from direct strike and hazardous areas are shown on Figure 1 summarized in Table 3.

The FLASH program is used to estimate the probability of lightning strikes to tall structures. The program propagates a lightning leader down in a random fashion until an

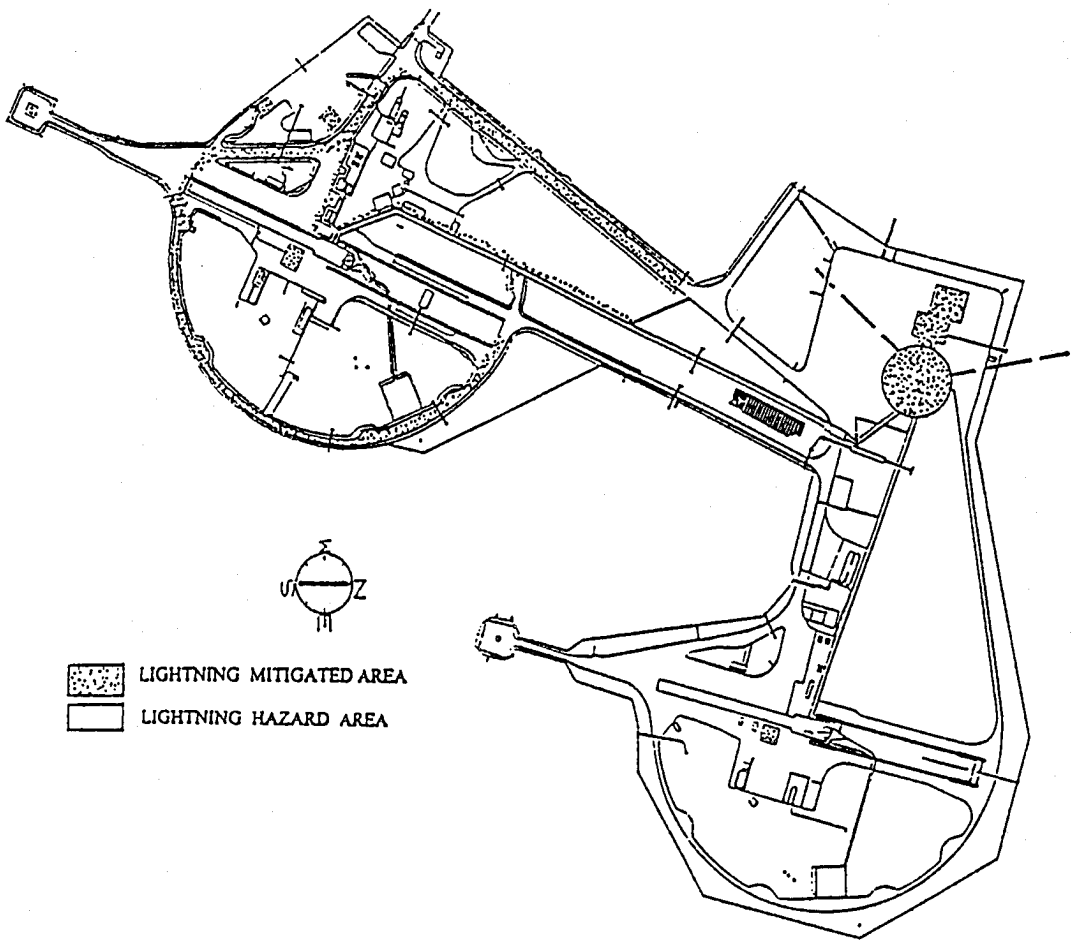



**Figure 1. Safe and Hazardous Areas at SLC 36A and SLC 36B**

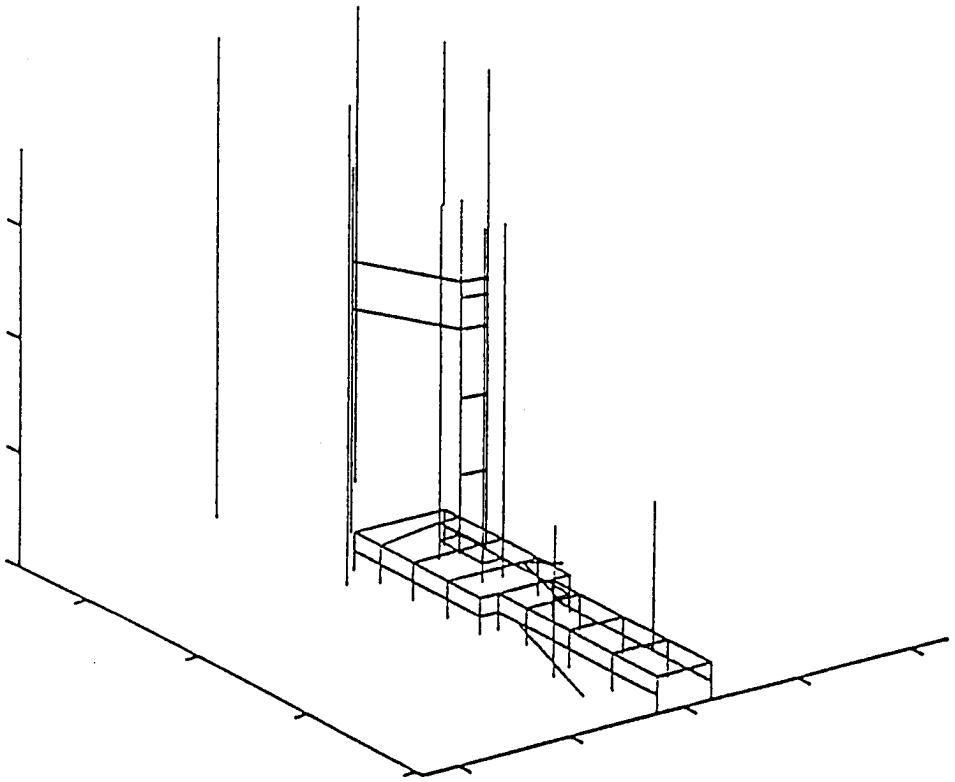


**Figure 2 CYLINDER model of UT, MST, LSB light poles and Atlas Vehicle**

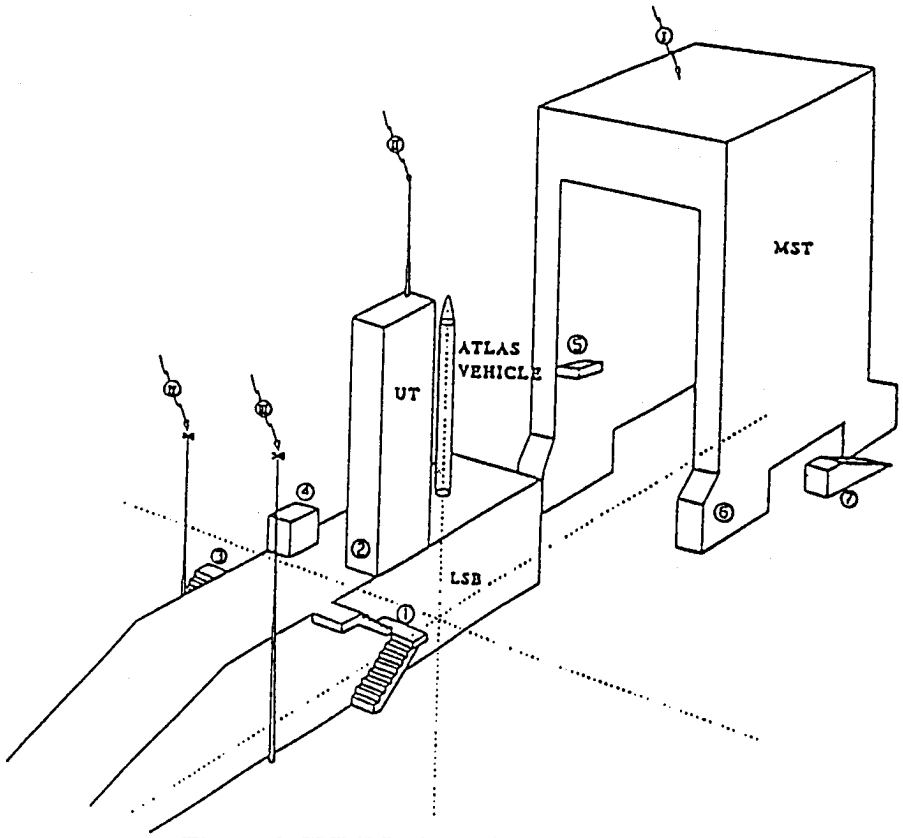



**Figure 3 CYLINDER strike attachment points**

object is within striking distance.. The log normal probability distribution of lightning currents is according to Anderson (LaForest, 1987, p. 549). The base striking distance (the distance determined by the lightning current) is 80 percent of Love's formula, as reported by Anderson. The leader steps down 50 ft in altitude to random locations on a 50-ft square centered beneath the present leader position until an object is contacted. An enhancement effect is included for sharp objects (pointed objects have longer striking distances than blunt objects) with the initial striking distance determined from peak current leader. The process continues until one or more objects are within striking distance and the closest object is hit. The number of lightning flashes and the number of hits to each object are tallied. An estimate of an object's probability of being hit, given that a lightning event occurred within the 2000-ft by 2000-ft square centered on the vehicle, is the ratio of the total object hits to the total number of lightning flashes. The confidence interval for the estimate is reduced by increasing the number of lightning flashes. The program simulates more than 100 million lightning flashes, or 20 million years, in order to establish the confidence interval of 5%. Attachments to the MST, UT, and other objects on the ground have been assessed and summarized in Table 3.

FILAMENT is a program that performs transient analysis of interconnected wires. The program was developed by Fisher (1992). The program determines the electrical characteristics of structures, develops an equivalent electrical filament network for the structures, and determines the distribution of currents in the structures from a modeled lightning strike. The CYLINDER program incorporates the same principles outlined in FILAMENT, which allows greater flexibility and more detail.

The CYLINDER PROGRAM operates by determining the electrical characteristics of the structures being analyzed. The self-inductance and mutual inductance of interconnected cylinders, that represent the various physical members of the structures, are calculated and creates an input file for Pspice (a commercially available circuit simulation software). The circuit simulation software allows for the selection of points of concern within the model and displays the resulting voltage gradient associated with the member(s). Figure 2 depicts the SLC 36B model for the CYLINDER analysis. The results of the CYLINDER analysis are shown in Tables 1 and 2. The tables consist of two sets of data. The first set was modeled with the MST at the LSB position (Table 1) and then with a LMS over the launch pad. With the MST in the park position (Table 2). Both sets of data contain the voltage gradients at areas of concern for four different strike attachment positions. The four attachment points used for the analysis are indicated in Fig.3. A future LMS consisting of overhead catenary wires supported by insulated towers was modeled to investigate areas for improved protection. The dimensions of the array are 150 ft long by 150 ft wide by 250 ft high. The results of the model are summarized in column WITH LMS Table 1. This table shows the voltage gradients for the locations of concern associated with a strike to the LMS. The response of the protected structure is dependent on the relative position of the LMS to launch facility features. Specific features can be protected such as swing arms can enhance varying the LMS. The induced effects of lightning are demonstrated with the MST in the park position shown in table 2. The induced effects have an inverse response with distance of lightning channel from the structures.

**Table 1.Voltage Gradients at Areas of Concern for Four Hit Locations (kV/m) with the Mobile Service Tower in LSB Position, with and without Lightning Mitigation System**

| | | Lightning Attachment Location | | | | WITH LMS |
|---|---|---|---|---|---|---|
| No | | I | II | III | IV | |
| | Area of Concern | MST 200 kA | UT 200 kA | West Light Pole 30 kA | East Light Pole 30 kA | NW TOWER LMS |
| 1 | East LSB Stairs (top)<br>(bottom) | 19.5<br>24.7 | 20.8<br>27.6 | 3.6<br>3.45 | 3.93<br>3.60 | 16.8<br>18.6 |
| 3 | West LSB Access Stairs | 26.3 | 27.9 | 5.64 | 4.88 | 22.4 |
| 2 | UT Base | 80.4 | 101 | 9.40 | 9.53 | 51.9 |
| 6 | Lower Corner of MST | 88.0 | 86.2 | 9.44 | 9.47 | 54.6 |

**Table 2.Voltage Gradients at Areas of Concern for Four Hit Locations (kV/m) with the Mobile Service Tower in Park Position**

| | | Lightning Attachment Location | | | |
|---|---|---|---|---|---|
| No | | I | II | III | IV |
| | Area of Concern | MST 200 kA | UT 200 kA | West Light Pole 30 kA | East Light Pole 30 kA |
| 1 | East LSB Stairs (top)<br>(bottom) | 14.8<br>17.4 | 21.9<br>29.9 | 3.72<br>3.60 | 4.0<br>3.78 |
| 3 | West LSB Access Stairs | 20.1 | 29.0 | 5.76 | 5.0 |
| 2 | UT Base | 51.3 | 119 | 10.0 | 10.3 |
| 6 | Lower Corner of MST | 88.6 | 43.0 | 5.94 | 5.94 |

RISK ASSESSMENT AND OPERATIONAL HAZARD ANALYSIS

The process of risk assessment and operational hazard analysis provides a technique for establishing priorities for the improvement of facilities and operational procedures. This process quantifies the lightning risk to personnel from the hazards of lightning based on the operation. It addresses personnel exposure during facility maintenance and vehicle operational activities in support of launch. The risk assessment classifies the identified hazards, the probabilities of occurrences, and the urgency of mitigation and by assigning an arbitrary risk assessment code establishes a priority system for corrective action. The lightning effects resulting from a lightning strike are:

Direct Strike
Side Strike
Conducted Strike Current
Structure Voltage Gradient
Induced Effects
Streamer Conductor
Step Voltage
Surface Arcing Around Grounds
Sequelae

Operational Hazard Analysis (OHA) was conducted on the prelaunch and launch operations at a space launch complex. The facilities analyses are listed in Table 2 in descending order of the Risk Assessment Code (RAC). The individual RAC is developed in the OHA for the facility as previously discussed using operations hazards analysis methods. The result of ordering by RAC emphasizes the areas with increased risk, the lower the rank number the higher the risk. This alternative perspective of the process allows low profile sensitivities to be uncovered. Notably, the security gates have the highest risk because of the lack of mitigation from other high structures, the small size of the enclosure, and the continuous presence of personnel and the increased number of personnel exiting the complex lightning advisories.

**Table 3. Facilities Risk Avoidance Matrix—SLC 36B Lightning Analysis**

| OPERATING AREA | CONCERN | ANALYSIS | FRN 1 TO 10 | OHA RAC 1 TO 10 |
|---|---|---|---|---|
| Launch Control | Ref. of no concern<br>Lightning attachment<br>Protected area<br>Roof<br>Parking Lot<br>Probability | (Pcr=$8x10^{-5}$=1: 12,500 yr)<br>Lt. Mast 1:4 yr<br>Inside Protected<br>1:140 yr<br>Exposed<br>1:45 yr | 5.5 | 10 |
| Umbilical Tower (UT) | Lightning attachment<br>Probability<br>Gradient stairway<br>Gradient at LSB | wo/MST 1:3.5 yr<br>w/MST 1:5.8 yr<br>Outside 110 kV/m<br>Outside 119 kV/m | 5 | 7 |

| | | | | |
|---|---|---|---|---|
| Vehicle:<br>Access from MST: | Contact potential<br>Station 0-MST 18 ft<br>Station–MST 139 ft<br>Station–MST 70 ft | 61 kV (bond to work platform)<br>125 kV<br>10 kV | 7 | 7 |
| EM to vehicle | Current across umbilical:<br>Level 92 ft<br>Level 102 ft | 140 kA<br>55 kA | | |
| Contact voltage from MST | Potential across:<br>damper, Level 122 ft<br>ECS duct, level 152 ft | 125 kV | | |
| Mobile Service Tower (MST) | Lightning attachment Probability | 1:3.5 yr | 6 | 7 |
| Crane Operations Voltage to LSB | MST 100, LSB<br>MST 200, LSB | 190 kV<br>380 kV | | |
| Personnel Egress: | Contact voltage<br>Apron<br>LSB<br>Bridge UT, Lv. 35 ft<br>Bridge UT, Lv. 69 ft<br>Bridge UT, Lv. 99 ft<br>Bridge UT, Lv.113 ft<br>Bridge UT, Lv.120 ft | 13 kV/m<br>5 kV/m<br>10 kV/m<br>6 kV/m<br>15 kV/m | | |
| MST Tracks, Operations on Apron, MST Park 100 $ft^2$ Midway | Lightning attachment Probability<br>Step voltage | 15 kA<br>1:55 yr<br>Low | 6.5 | 7 |
| Launch Service Building (LBS) and Ramp Area | Contact voltage<br>Gradient east stair<br>Gradient west stair<br>Lightning attachment<br>Extent of safe area<br>UT SRB parking<br>Light poles | 30 kV/m<br>30 kA max<br>Between light poles and within 50 ft of LSB<br>1:140,000 yr<br>1:140 yr | 6 | 4 |
| LH Area | Lightning attachment<br>Firex Overhead<br>Step voltage<br>Light poles | 1:120 yr<br>mitigated wire reinforced concrete<br>1:4.5 yr | 4.5 | 7 |

| | | | | |
|---|---|---|---|---|
| Liquid Oxygen ($LO_2$) Area | Lightning attachment<br>Tank<br>Step voltage | <br>1:750 yr<br>Low | 4.5 | 7 |
| Mechanics Shop | Lightning attachment<br>Exterior wall (inside)<br>Contact voltage | 1:320 yr<br>Lightning protected<br>High<br>80 kV/m exterior gradient | 5 | 7 |
| Security Posts Gates (Pads A and B) | Lightning attachment<br>Step potential<br>Contact voltages | 1:22 yr<br>High within 90 ft. | 2 | 2 |
| Fencing | Lightning attachment<br>Main gate<br>Contact voltage<br><br>Step potential | 1:44 yr/100 ft<br>1:22 yr<br>18.5 kV/m (10 kA inject from power pole)<br>90 ft to safe distance | 3.5 | 4 |
| Poles, Lighting, Pad Apron Peripheral Road (protected by lights w/ aerial wires)<br>TV Towers | Lightning attachment<br>Magnitude<br>Probability<br>Magnitude<br>Safe distance<br>Probability<br>Safe distance | 1:140 yr<br>30 kA<br><1:140,000 yr<br>200 kA<br>30 ft<br>1:4.5 yr<br>90 ft | 4 | 4 |
| Camera System and sites | Lightning attachment<br>Voltage | 1:8,000 yr<br>Limited to 1000 V by cable insulation and terminals | 3.5 | 4 |
| Communications:<br><br>Telephones<br><br>Transistorized Operational Phone System (TOPS) | Lightning attachment to all towers<br><br>Cable contact voltage | <br>1:4.5 yr<br><br>Over voltage protection is 300 V otherwise limited by cable to 1000 V or failure of equipment | 7 | 5 |

## REFERENCES


1. Dalziel, C., 1953: A study of the hazards of impulse currents. *Amer. Inst. Electr. Eng. Transactions*. IEEE, New York, **72**, 1032–1042.
2. Fisher, F., 1992: FILAMENT—A program for transient analysis of interconnected wires. *Proc., International Aerospace and Ground Conference on Lightning and Static Electricity, Atlantic City, New Jersey, 6–8 October 1992*, Vol. 1, Ch. 10, 1–12.
3. Institute of Electrical and Electronics Engineers, 1986. *IEEE Guide for Safety in AC Substation Grounding,* New York.
4. La Forest, J.J. (ed.), 1987: *Transmission Line Reference Book*, second edition, revised, Electric Power Research Institute (EPRI), Palo Alto, California, 625 pp.

# INSURED PROPERTY DAMAGE DUE TO LIGHTNING IN THREE WESTERN US STATES

Ronald L. Holle and Raúl E. López
National Severe Storms Laboratory, NOAA
Norman, Oklahoma

Lowell J. Arnold[1] and John Endres[2]
State Farm Fire and Casualty Company
Denver[1] and Greeley[2], Colorado

## ABSTRACT

Insurance claims resulting from lightning-caused damage in Colorado, Utah, and Wyoming were analyzed. Most claims were from personal accounts, while some were commercial. Lightning damage in the three states resulted in an annual average of 6755 claims being filed. Most claims were from Colorado and more than half from the Denver Metropolitan area. Over $7 million a year in lightning losses occurred in the three states for these types of insurance policies when a $150 deductible is included; most losses were in Colorado. The average value paid per claim was $916 for all three states and types of claims; commercial claims averaged $1369 and personal claims, $873. Annual US totals of 307,000 claims and $332 million in losses were extrapolated from the three-state sample.

One lightning insurance claim is estimated to occur in this region for every 55 cloud-to-ground lightning flashes recorded by detection networks. Nearly all lightning claims were from May through September. Largest numbers of claims were in counties with the largest populations. However, claim rate per population and dollar loss per claim were not well related to county population. A rate of 4.7 claims per 10,000 people applied to Colorado, 1.4 for Utah, and 3.9 for Wyoming. The dataset had 367 times as many claims as similarly insurable damage reports in NOAA's *Storm Data* during the same years in Colorado, Utah, and Wyoming. This publication is widely used as the basis for lightning and other storm-related casualty and damage information.

## INTRODUCTION

Cloud-to-ground (CG) lightning flashes cause a large amount of material damage, as well as many deaths and injuries. Statistics that are commonly quoted are taken from the NOAA publication *Storm Data,* which lists lightning as a relatively small cause of property damage (Table 1). To assess the impact of lightning more completely, an insurance claim database was made available covering significant damage done by lightning to dwellings, small businesses, and their contents in the area of Figure 1.

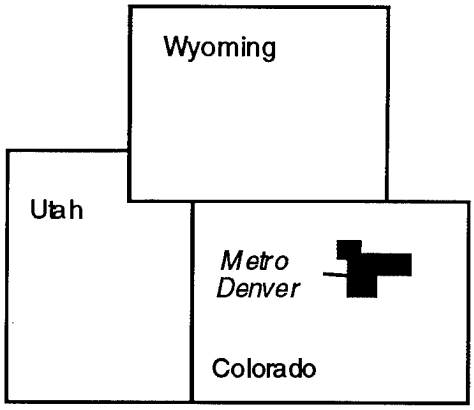



*FIGURE 1. Region of lightning claim study.*

TABLE 1. Summary of 1990, 1991, and 1992 property damage costs from *Storm Data*.

| Weather type | Damage in $ million | | | |
|---|---|---|---|---|
| | 1990 | 1991 | 1992 | Average |
| Hurricane | 0 | 1164 | 33,611 | 11,592 |
| Winter weather | 621 | 514 | 28 | 775 |
| Tornado | 668 | 798 | 765 | 744 |
| Extreme temp. | 1317 | 224 | 480 | 674 |
| Drought | 2 | 157 | 1780 | 646 |
| River flood | 1125 | 418 | 263 | 602 |
| Other high wind | 163 | 1564 | 44 | 590 |
| Hail | 716 | 412 | 533 | 554 |
| Flash flood | 625 | 429 | 428 | 494 |
| Thunderstorm wind | 425 | 294 | 266 | 328 |
| **Lightning** | **41** | **25** | **16** | **27** |
| Other | 319 | 204 | 140 | 221 |
| Total | 6022 | 6203 | 38,354 | 16,860 |

Data on lightning damage are generally quoted from the monthly publication *Storm Data* that describes damaging and severe weather during the year. *Storm Data* includes deaths, injuries, and material damage reports from the phenomena in Table 1, and is available from NOAA in Asheville, North Carolina. Reports in *Storm Data* usually contain date, time, location, type of casualty or damage, age and gender of victims, and a verbal description of the event and the type of property or object that was impacted. For lightning in particular, entries in *Storm Data* are compiled primarily from newspaper reports provided to the National Weather Service (NWS) by contracted clipping services (1). Information from each NWS office is sent to the National Climatic Data Center in Asheville where *Storm Data* is compiled and published. *Storm Data* was shown by López et al. (1) to underestimate lightning-caused deaths by 22% and injuries by 42%; Mogil et al. (2) found similar rates. The underreporting of lightning casualties has some unique features relative to other weather phenomena, especially for injuries:

- Most cases affect one person or object.
- Events may not be part of widespread storms such as floods or tornadoes.
- The event may be considered minor, and few people may be made aware of the event.
- When the event is brought to the attention of the media, the news may not survive the assembly of the daily or weekly paper.

The problem is greatly amplified for property damage. The media usually do not report a house or other object damaged by lightning unless there is a casualty, a large dollar loss, or multiple buildings or objects struck in the same storm. It must be emphasized that there is no effective way for NWS staff assembling *Storm Data* to reconstruct a database of all lightning cases when they were rarely reported to emergency agencies or covered by the media, and involved no injuries.

Damage due to lightning during the last three years in the US is reported in Table 1 as $27 million a year by *Storm Data*. However, previous estimates of lightning damage, not documented in the formal meteorological or climatological literature, show that *Storm Data* greatly underestimates the losses by a highly variable and large amount. For example, Uman (3) estimates the frequency of lightning strikes to a house in a region with moderate thunderstorm frequency and a flat residential lot on a quarter acre of land to be "about once every 100 years. Saying the same thing another way, one in every hundred houses is hit each year".

Recent studies of the lightning threat to people and property in Colorado using *Storm Data* have been made by López et al. (1, 4) and Holle et al. (5). Intercomparison of the present study with results from those publications will allow better characterization of the lightning claim record.

## INSURANCE DATABASE

Lightning-caused damages that led to insurance claims being paid by a large insurer were obtained through the Colorado Chapter of Chartered Property and Casualty Underwriters. Data were divided into Colorado, Utah, Wyoming, and the Denver Metropolitan area (Figure 1). Policies are divided into two categories:

•Personal lines are issued to occupants of homes, farms, apartments, and condominiums. These policies include contents of the house.
•Commercial lines are issued for offices, mercantile stores, contractors, hotels, motels, churches, apartments, and condominiums. Not included are schools, warehouses, refineries, manufacturing, agricultural, and similar facilities.

Lightning damage for a claim is determined by several methods summarized by Dye (6). It is difficult to separate a claim resulting from lightning or electrical disturbance from maintenance-related claims. Dye categorizes the effects into two groups:
♦Direct effects of lightning striking an object. These are generally obvious, and accompanied by burning of materials and evidence of damage. Such effects may be found on a building, television antenna, or an outdoor air conditioning unit.
♦Indirect effects where the flash hits elsewhere and its effects are transmitted to another location, typically through power or telephone lines. Most insurance claims are of this type. The flash may directly strike the lines or something connected to them, or effects may result from a power surge induced by lightning striking close to the lines. Such effects include damage to television sets, well pumps and sprinkler systems, and air conditioning units, or a sudden failure of other appliances.

Dye (6) lists the following questions for the insurance adjuster to ask when investigating a claim reported as due to lightning:
- Was there visible lightning damage?
- Were fuses blown or circuit breakers tripped?
- Were other appliances also damaged?
- Was there evidence of lightning damage to the building?
- Was lightning in the immediate area?
- Do National Weather Service records confirm that lightning strikes were observed or recorded in the area?

## EXTRAPOLATION TO ALL INSURERS

The information available for this study was provided by one insurer for Colorado, Utah, and Wyoming. The share of this insurer in the total market was known on a state by state basis, so the data were extrapolated to the total claims and losses for each state by assuming that the entire market was represented by the data provider. Since the market share was available only for homeowner claims, the commercial information was assumed to be the same. Information in subsequent sections refers to the total claims and losses after extrapolation is made to the total insurance market from the single data source.

## CLAIMS AND LOSSES IN COLORADO, UTAH, AND WYOMING

The annual frequencies of personal and commercial claims attributed to lightning from 1987-1991 (Figure 2), when extrapolated to all insurers, show Colorado to have much higher numbers than Wyoming or Utah. The annual rate is 6755 lightning claims for the three states. In Colorado, there were more claims from the six Denver Metropolitan counties (Figure 1) than from the rest of Colorado. The ratio of personal to commercial claims was 11:1 in Colorado, 16:1 in Utah, and 7:1 in Wyoming; the variation is probably due to the small sample sizes of commercial claims. Lightning accounted for 2.1% of all insurance claims in these states from 1989-1993. Details for these and most other subsequent statistics are in Holle et al. (5).

Annual dollar losses from these claims due to lightning from 1987-1991 over the three

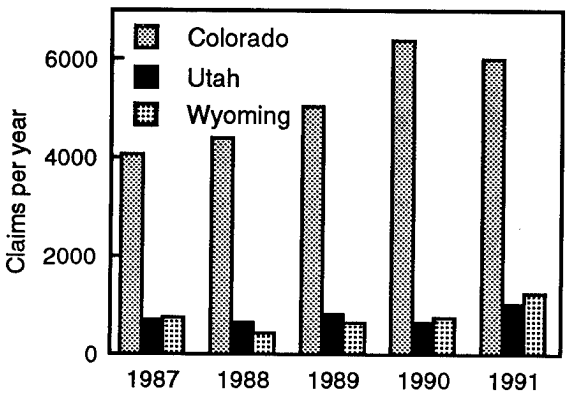



*FIGURE 2. Annual number of personal and commercial lightning claims in Colorado, Utah, and Wyoming from 1987-1991, extrapolated to all insurers.*

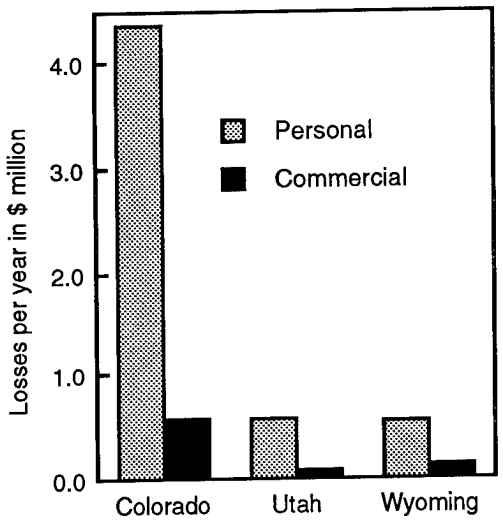



*FIGURE 3. Losses from lightning insurance claims per year in Colorado, Utah, and Wyoming from 1987-1991, extrapolated to all insurers. Additional costs of deductibles paid by policyholders not included.*

states, when extrapolated to all insurers, totaled over $6 million (Figure 3); $5 million was from personal and commercial accounts in Colorado. Commercial losses were 14% of personal losses. Lightning accounted for 1.4% of all insurance losses in the three states from 1989-1993.

## NATIONAL EXTRAPOLATION

The dataset is from three western states whose combined population of 5,470,832 was 2.2% of the US total in 1990. The insurance claim database was only compiled for these states. National frequencies were found by extrapolation on the basis of population with the assumption that claim experiences in the three states are representative of the entire country. When total claims and annual dollar losses for Colorado, Utah, and Wyoming are applied on a national basis (Table 2), the result is 307,000 lightning-related claims for a total of $286 million annually in paid insurance.

This method does not include lightning-caused losses to objects and facilities in the following categories; there are no doubt many others:

- Other insured losses in addition to the homeowners and smaller commercial facilities in the database.

TABLE 2. Annual national extrapolation of the number of lightning claims and costs based on 1987-1991 frequencies in three western states. Deductibles not included.

| | Colo.-Utah-Wyo. | United States |
|---|---|---|
| Claims | 6755 | 307,000 |
| Losses | $6,292,000 | $286,000,000 |

- Situations where no insurance coverage is purchased.
- Federal, state, and other governmental losses that are self insured.
- Forest and range fire losses to timber and other related infrastructure.
- Utility and communication losses.

The preceding results do not take into account the deductible amount of the loss paid directly by the policyholder before insurance takes effect. Most policyholders had deductibles on the order of $100 to 250 during the time of the database; an amount of $150 was used. Figure 4 shows that for the entire United States, the total of $286 million (Table 2) for the insurance industry increases to $332 million when the $46 million first paid by policyholders is included.

## FLASHES PER CLAIM

Comparisons can be made between insurance claims and lightning frequency by two methods. The first method uses a lightning climatology for the Denver region that has 123,663 flashes during June, July, and August of 1983 (7). When extrapolated to the total market share, there were 2401 claims per year made to all insurance providers from 1987-1991 in the Denver Metro-

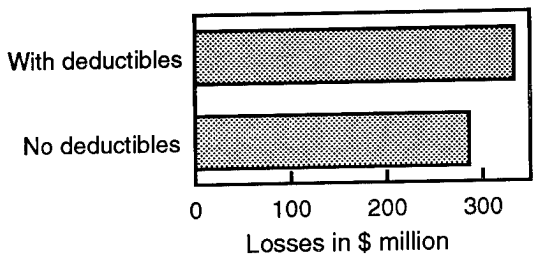



*FIGURE 4. Annual costs of lightning claims for the US with and without deductibles from 1987-1991 based on three western states.*

politan area over 5 years. Assuming that the number of lightning flashes that occurred each year is comparable, the conclusion from this method is a rate of one lightning-caused insurance claim for every 52 CG flashes in the Denver area.

The other method uses the average of 17,600,000 CG flashes detected by the National Lightning Detection Network across the US from 1989-1993 (8). The annual total of national lightning claims was 307,000 based on the 3-state sample (Table 2). The conclusion from this method is one lightning-caused insurance claim for every 57 CG flashes in the US.

Considering the disparity in sources of data, these two methods give close values. More reliable results can be expected if the insurance claims and flash datasets were better matched in time and space.

A similar calculation for dollar amounts can be made. The total loss is $332 million a year for the US, including deductibles, based on the three states (Figure 4). Given the 17,600,000 flashes per year in the US (8), the result is an insured loss of $18.86 for each flash that strikes the country.

## LOSSES PER CLAIM

The average loss for personal and commercial claims combined is $916 per claim. Distributions of amounts of lightning costs per claim in Figures 5 and 6 are for the period from 1987 through June 1992. Results are the following:

- There was no payment for 12% of the claims. A claim for lightning damage was filed by the policyholder but the deductible exceeded the costs. The insurer paid nothing to the insured for this incident, although the deductible was partially met if a loss would occur later in the policy's yearly cycle.
- Another 10% of the losses is in the $1-100 range.
- The next four categories have similar frequencies of 16 to 19%. The categories span increasing ranges of losses.
- 4% of the losses are from $2501-5000.
- A few claims are over $5000.

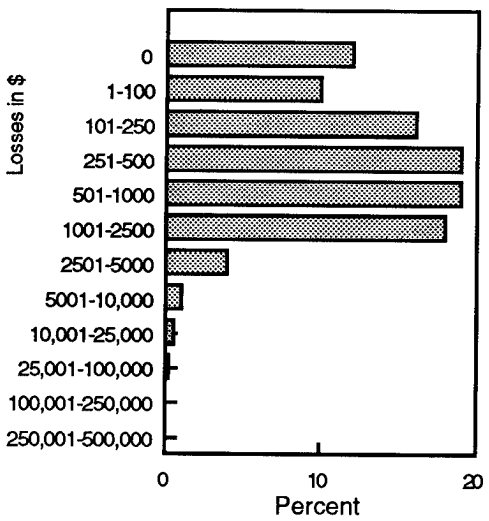



*FIGURE 5. Distribution by amount of losses from lightning claims in Colorado, Utah, and Wyoming from 1987 through June 1992. Deductibles not included.*

- When losses are shown in a cumulative format (Figure 6), it is apparent that almost half of all claims are under $500, and more than three quarters are under $1000.

With regard to location, Figure 7 shows that for personal claims, the highest average loss is $1071 in Denver. Other locations have smaller losses around $750. The larger amount for the Denver Metropolitan area could reflect higher values of homes in that region.

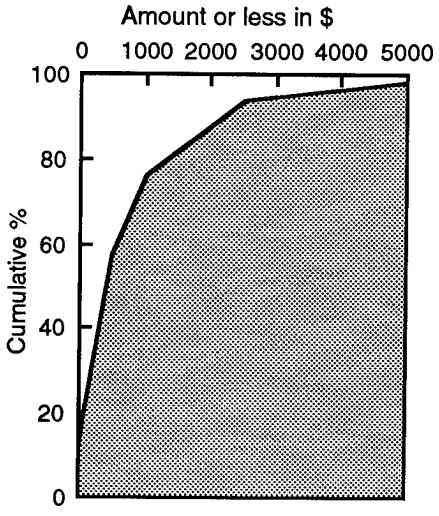



*FIGURE 6. Cumulative amounts of losses due to lightning in Figure 5.*

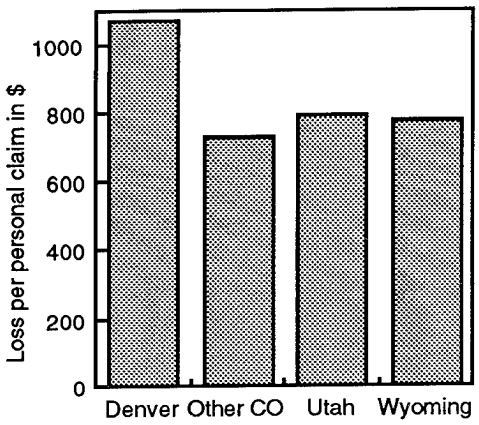



*FIGURE 7. Average loss per personal lightning insurance claim from 1987-June 1992 in Denver, the rest of Colorado, Utah, and Wyoming. Deductibles not included.*

There are differences according to type of claim (5). Commercial claims average $1369 and personal average $873. Personal claims are more frequent in the $0-250 range (38%) than commercial (30%). However, commercial claims are more frequent from $2501-25,000 (13%) than personal (5%).

## MONTHLY DISTRIBUTION

Monthly distributions of claims for Colorado (Figure 8) show that lightning losses occur primarily in summer. There is a dramatic increase in lightning claims from April to May, then values are high during summer months until September when claims are half of the August number.

Comparison in Figure 8 with *Storm Data* lightning damage reports from 1950-1991 in Colorado (4) shows very similar monthly percentages of cases. However, lightning victims in *Storm Data* are more sharply clustered from June through August than damage reports from either source. The differences may be due to more people involved in outdoor recreation during the summer months, while reports of damage to inanimate objects are more representative of actual lightning activity.

Utah has fewer insurance claims in June than during May and July; June is after the winter and spring disturbances in the westerlies and before the summer monsoon for Utah (5). Wyoming lightning claims start later and end

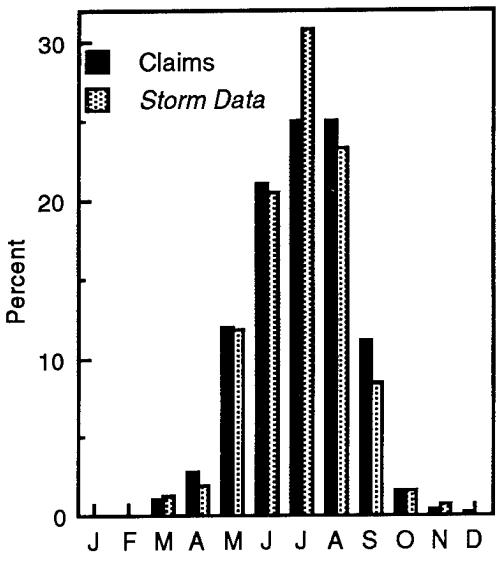



*FIGURE 8. Claims: Monthly Colorado insurance claims due to lightning from 1987-1991.* Storm Data: *Monthly Colorado property damage reports from 1950-1991 (from 6).*

earlier than in Colorado since it is at a higher latitude and altitude, and has a cooler spring and fall than most of Colorado and Utah.

## CLAIMS BY COUNTY

The geographical distribution of lightning claims by county in Colorado, Utah, and Wyoming is shown in Figure 9. Information was not available in the insurance database by city. The highest numbers of claims are in the counties with the largest populations in and near cities of Figure 9. In Utah, most people live in Salt Lake City and surrounding cities, towns, and populous unincorporated portions of counties. In Wyoming, the southeast county includes the state capital of Cheyenne. Most people in Colorado live in a north-south region along the eastern slope of the Rocky Mountains that includes Denver, Colorado Springs, and other cities and counties with large populations.

Claims are graphed in Figure 10 according to county population in Colorado, Utah, and Wyoming from the insurance database. In general, the most populous counties have more claims and least populous counties have fewer claims. The same result applies for each state separately.

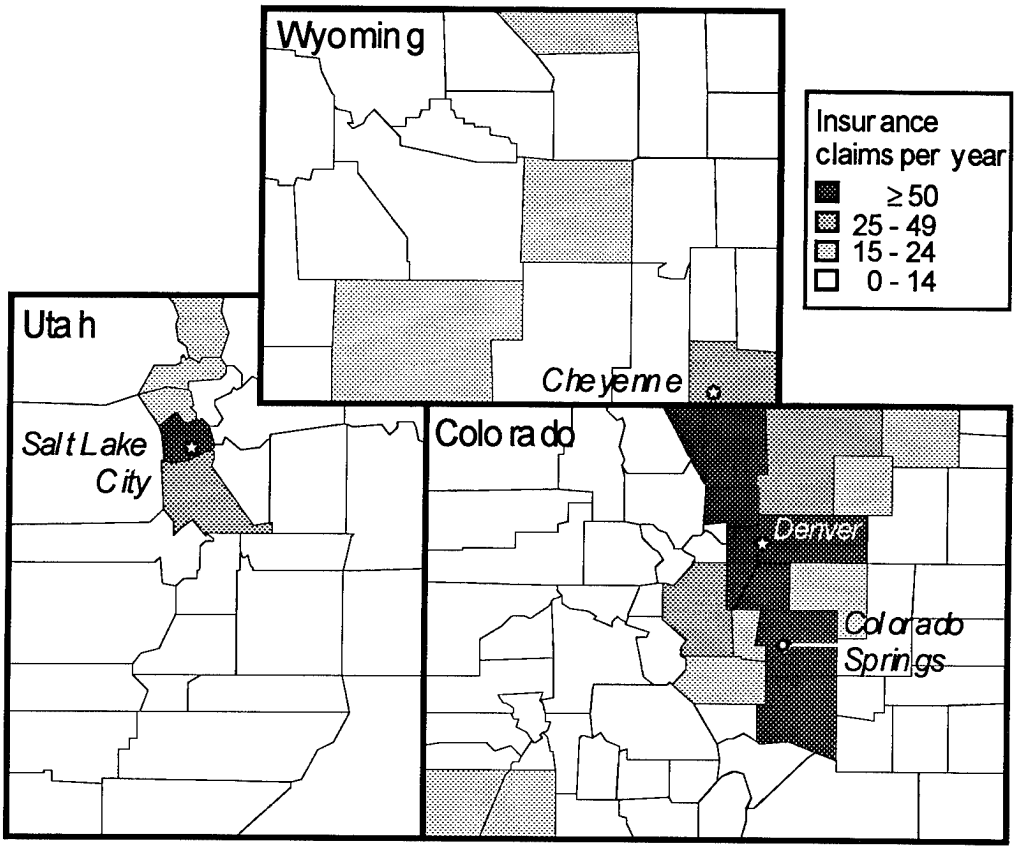



*FIGURE 9. Number of insurance claims per year due to lightning by county in Colorado, Utah, and Wyoming from 1989-1993.*

When the claim rate per 10,000 people is calculated by county (Figure 11), most counties have a rate of less than 7. Maps for each state (5) indicate that highest claim rates are away from the most populous regions; high rates usually occur when the sample size is small in a less populous county, and the natural variability of only a few claims raises the rate to large values. However, high rates may not be entirely due to small sample size; a concentration of high rates extends from north to south through the middle of Colorado along the highest mountains near the Continental Divide. This region was identified by López and Holle (7) to have more lightning than areas on the plains to the north and east. López et al. (4) also found a higher rate of lightning casualties per population and area in these high-mountain counties.

When loss per claim is plotted against population (Figure 12), there is a vertical band for all sizes of county populations around $500

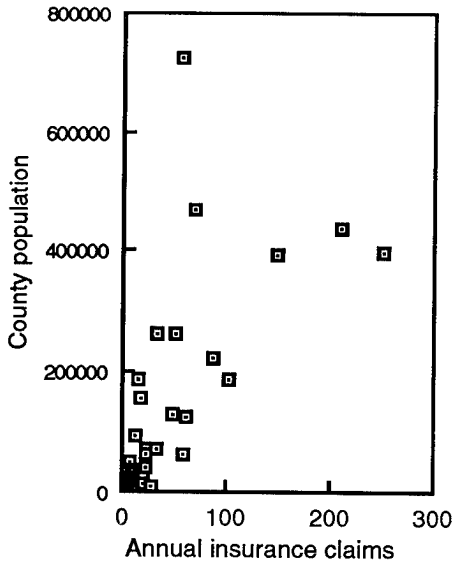



*FIGURE 10. Population of each county in Colorado, Utah, and Wyoming plotted against annual number of lightning claims in the database from 1989-1993.*

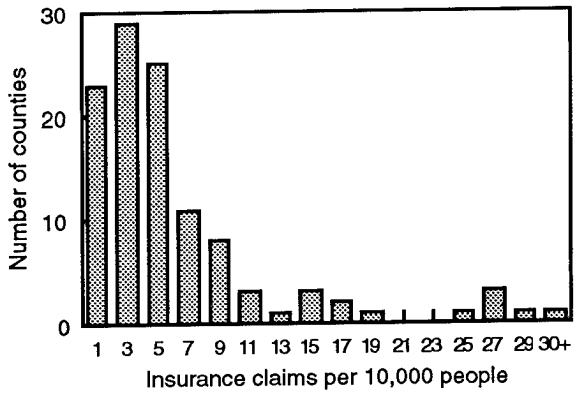



*FIGURE 11. Distribution of county rates of lightning insurance claims per 10,000 people in Colorado, Utah, and Wyoming.*

to $750. Highest average losses are in less populous counties and scattered with no obvious organization across Colorado, Utah, and Wyoming (5). Since one large loss raises the average in a county with few claims, little meaning should be attributed to a high average loss in a small county. Factors that can affect the average loss include differences among counties in housing costs, amount of buried utility lines, proportion of multi-family housing, vulnerability of structures to lightning, extent and type of agricultural facilities, and other factors not identifiable with the present dataset.

The rate of claims per 10,000 people in Utah is 1.4 compared to 4.7 for Colorado. The lower Utah rate is not clearly due to less lightning compared to Colorado, since Reap (9) for 1983-1984 and Orville (10) for 1989-1991 showed no significant differences between flash densities for these states. The rate in Wyoming is 3.9, almost the same as the 4.7 for Colorado. However, Reap (9) and Orville (10) showed a lower lightning frequency for Wyoming compared to Colorado. Better understanding could result if flashes on a county by county basis were directly compared with claims.

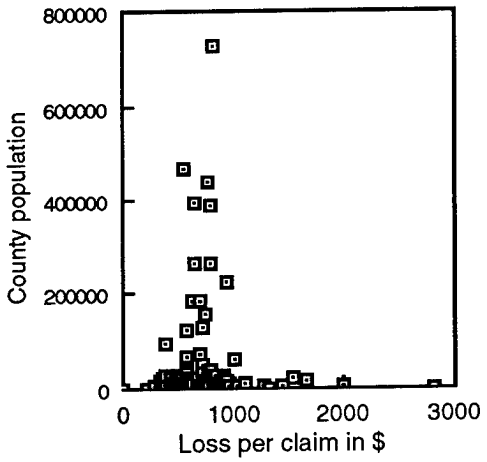



*FIGURE 12. County population for Colorado, Utah, and Wyoming plotted against dollar loss per lightning insurance claim from 1989-1993.*

## CLAIMS COMPARED TO *STORM DATA*

On the state level, the number of claims was compared with numbers of lightning victims in *Storm Data*. There is no close relationship for a single state and year for Colorado and Utah (5). The number of claims is a larger, more constant number than casualties. There were no Wyoming lightning victims during the period.

On the county level for Colorado, López et al. (4) lists the number of lightning-caused deaths, injuries, and damage reports from 1950-1991 in *Storm Data*. Figure 13 shows a general trend that large numbers of claims in a county from 1989-1993 are related to many casualties and damage reports; however, this applies only to counties with highest frequencies.

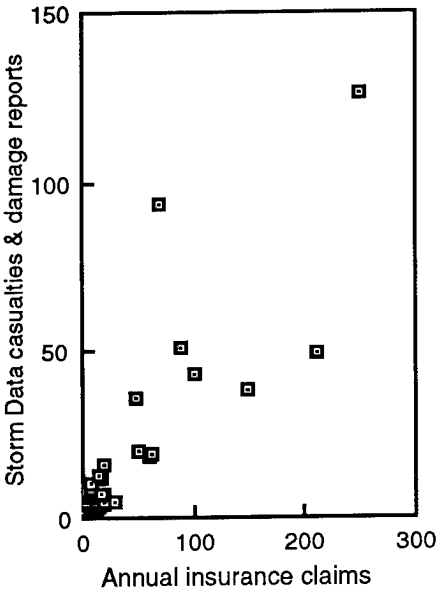



*FIGURE 13. Annual lightning insurance claims (1989-1993) plotted against combined* Storm Data *lightning casualty and damage reports (1950-1991) by county in Colorado.*

TABLE 3. Annual lightning insurance claims compared to damage reports in *Storm Data* from 1987-1991.

| State | Insurance claims | *Storm Data* reports | Ratio |
|---|---|---|---|
| Colorado | 5188 | 15.2 | 341:1 |
| Utah | 774 | 2.2 | 352:1 |
| Wyoming | 793 | 1.8 | 610:1 |
| All | 6755 | 18.4 | 367:1 |

Table 3 compares damage reports in *Storm Data* with total lightning insurance claims by state. *Storm Data* was used to find the number of property-related lightning damage reports that could have resulted in a personal or commercial insurance claim. Ratios range from 341 insurance claims to one *Storm Data* report in Colorado to 610:1 in Wyoming. The overall ratio is 367 claims per *Storm Data* report.

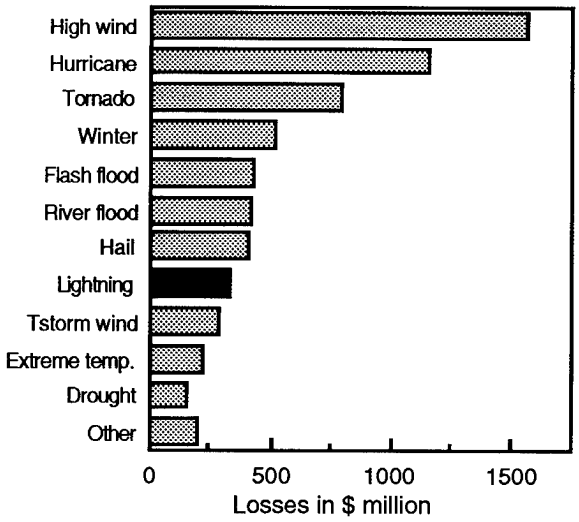



*FIGURE 14. 1991 weather-related property damage in the US from Table 1, except showing $332 million for lightning insurance claims found in current study.*

## SUMMARY AND CONCLUSIONS

A total of 6755 insurance claims per year was found from 1987-1991 in Colorado, Utah, and Wyoming when the database from one large insurer was extrapolated to all companies. Annual losses were $5,000,000 a year in Colorado, and $650,000 a year each in Utah and Wyoming. The database did not include the type of damage to buildings or their contents, but it is possible that the widespread use of delicate electronics such as computers, VCRs, and microwave ovens is increasing the claim rate. All but one year between 1987 and 1991 had more claims than during the previous year for the three states together, but population also increased during these years and lightning frequency varies.

A national estimate of the insurance risk from lightning was based on the three-state database by assuming that the population and lightning risk are representative of the whole country. The extrapolated totals for the US are 307,000 lightning claims and a total cost of $332,000,000 when a $150 deductible is taken into account. When this amount is plotted (Figure 14) rather than the $25 million for 1991 from *Storm Data* in Table 1, lightning becomes as significant a source of loss as most other weather phenomena.

Maps of claims by county showed that largest numbers were always in counties with the largest populations. The dollar loss per claim was not well related to the population, and tended toward large numbers in counties with less population; both claim rate and loss per claim vary widely in less populous counties due to the natural variability caused by a few claims. A rate of 4.7 claims per 10,000 people applied to Colorado, 1.4 for Utah, and 3.9 for Wyoming. These differences were not attributable to known differences in state lightning frequency. Other factors are important, such as type and cost of housing and agricultural facilities, the portion of dwellings that are apartments or has buried utility lines, and other influences that could not be resolved with the data.

There were 367 times as many claims as insurable damage reports in *Storm Data* during the same years in Colorado, Utah, and Wyoming. Losses in the US from 1990-1992 averaged $27 million according to *Storm Data*, but personal and commercial losses alone ($332 million) from this study of insurance claims were extrapolated to be more than 10 times that amount.

*Acknowledgments.* Members of the Colorado Chapter of the Society of Chartered Property Casualty Underwriters, Underwriting Subsection, supported the concept of this study. They are David Storhaug and Rich Madison of The Traveler Companies in Denver, Wido Wundt of State Farm in Denver, Stephen Woods of Travelers in Englewood, Ronald Gardner of SAFECO Insurance in Lakewood, and Pat Holohan of State Farm in Greeley.

## REFERENCES

1. R.E. López, R.L. Holle, T.A. Heitkamp, M. Boyson, M. Cherington, and K. Langford. "The underreporting of lightning injuries and deaths in Colorado." Bulletin of the American Meteorological Society, Vol. 74, 2171-2178, 1993.

2. H.M. Mogil, M. Rush, and M. Kutka. "Lightning—An update." Preprints, 10th Conference on Severe Local Storms, Omaha, Nebraska, American Meteorological Society, 226-230, 1977.

3. M.A. Uman. "All about lightning." Dover Publications, New York, p. 22, 1986.

4. R.E. López, R.L. Holle, and T.A. Heitkamp. "Lightning casualties and property damage in Colorado from 1950 to 1991 based on Storm Data." Weather and Forecasting, Vol. 10, 114-126, 1995.

5. R.L. Holle, R.E. López, L.J. Arnold, and J. Endres. "Insured property damage from lightning in Colorado, Utah, and Wyoming." NOAA Technical Memorandum ERL NSSL-104, 47 pp., 1995.

6. Dye, W., 1995: Lightning: Cause, effect, control, and insurance. *CPCU Journal* [submitted].

7. R.E. López and R.L. Holle. "Diurnal and spatial variability of lightning activity in northeastern Colorado and central Florida during the summer." Monthly Weather Review, Vol. 114, 1288-1312, 1986.

8. GeoMet Data Services. "1989-1993 measured lightning flash density." One-page poster available from Global Atmospherics, Inc., 2705 E. Medina Rd., Tucson, AZ 85706, 1994.

9. R.M. Reap. "Evaluation of cloud-to-ground lightning data from the western United States for the 1983-1984 summer seasons." Journal of Climate and Applied Meteorology, Vol. 25, 785-799, 1986.

10. R.E. Orville. "Cloud-to-ground lightning flash characteristics in the contiguous United States: 1989-1991." Journal of Geophysical Research, Vol. 99, 10,833-10,841, 1994.

*1995 INTERNATIONAL AEROSPACE AND GROUND CONFERENCE ON LIGHTNING AND STATIC ELECTRICITY*

# PROTECTION OF A COMPUTER CENTER

**F. J. van der Hooft** **Stork** **Einhoven** **Netherlands**
**P.A.Konings** **S.W.I.F.T.** **La Hulpe** **Belgium** **32.2/6553639**

## 1. INTRODUCTION

This presentation will explain how **S.W.I.F.T.** (Society for Worldwide Interbank Financial Telecommunication) is improving it's protection level for buildings and facilities against lightning strikes. The improvement takes into account the damage that can be caused by direct hits of lightning and by nearby lightning strikes whereby induction plays a key role.

S.W.I.F.T. supports the financial data communication and processing needs of international financial institutions. Worldwide, S.W.I.F.T. provides a dedicated network and an unequalled range of financial messaging services and interface and application software. Our services are renowned for security and reliability.
Our Customers are banks, broker-dealers, investment managers, securities exchanges, central securities depositories and clearing organisations. They exchange up to two and a half million messages a day using S.W.I.F.T.
Our Markets are financial institutions conducting business in payments, forex and money markets, securities and trade finance benefit from our wide-ranging services.
S.W.I.F.T. guarantees secure, reliable and competitively priced financial data communication and exchange by means of standardised message as were developed by S.W.I.F.T. and it's customers.

In the process of message transfer the reliability of facilities plays a key role. It is this reliability that can be influenced in a negative way by lightning discharges.
Swift connects more then 100 countries through a telecommunication network with our 2 operating centres, one in the Netherlands and one in Virginia USA. Because of the impact of lightning on our operating centres we will present the way the 2 centres are protected and which problems we faced during the project and how the feasibility phase and the installation phase were approached.

## 2 PROBLEM DEFINITION

The last 20 years most companies changed drastically, centralisation and specialisation have led to the increased usage of electronics and electronic control equipment. All these changes made companies vulnerable, especially companies like S.W.I.F.T. that depend completely on electronics. Also we see that electronics become more and more sensitive for overvoltages, caused by lightning hits and induction. In S.W.I.F.T. 's situation there are 5 reasons to improve on protection :

1 Experience.
2 Insurance companies start to ask for extra protection.
3 Indirect cost and risks are of such a magnitude that senior management recognise today the risks of lightning. Lightning protection today is part of our **disaster avoidance en recovery plans.**
4 Electronics are becoming more and more sensitive for overvoltages.
5 The market provides components for protection at reasonable prices.

ad 1 The only concrete input we have today is experience with some damage caused by direct lightning hits in our US centre and damage caused by induction in our Dutch operation centre. The cost of a several hundred thousand dollars is not enough to justify heavy investments.

ad 2 In the past reporting of damage caused by lightning in electronics was hardly done. Today every thunderstorm causes many damage claims as can be concluded from the tabulation below .

paid claims by Dutch insurance company

| | | | |
|---|---|---|---|
| theft | 8.2 % | sabotage | 0.9% |
| water | 7.1 % | negligence | 27.5% |
| fire | 6.5 % | overvoltages | 28.7% |
| theft + damage | 4.0 % | others | 16.5% |

Figures for Germany and Austria are comparable.
So if no protection will be installed in the future with the increased usage and increased sensitivity of electronics increase of damage can be expected. S.W.I.F.T. is now requested / demanded by our insurers to improve our lightning and overvoltage protection. The level of protection is however defined by S.W.I.F.T..
Limiting ourselves to insurance only would not be enough, because the consequences of a damage would be disastrous.

ad 3 Companies that work seriously on a disaster avoidance and recovery plan will have to include the risk of lightning in these plans. Insurance is not enough ( see item 2 ) , protection will be very difficult to cover 100% so a company like S.W.I.F.T. always has to take into account the "unexpected" from lightning. This means protection for lightning

strikes for an intensity that is only passed in 1% , provide back-up systems in other locations etc. .

ad 4 The fact that electronics get more and more sensitive is considered as a fact of life.

ad 5 S.W.I.F.T. wants to be prepared for lightning strikes at the best reasonable and possible way. A balance between investment and level of protection need to be found. Today, components exist that give a high level of protection at a reasonable price. The investment part needs however constant analysis of what to protect and maybe more important of what not to protect. It is practically impossible to cover a whole computer centre for 100% at a reasonable price.

As this looks like an easy objective the question can be raised :
Why participating on this conference as a speaker?
Because different codes and technical approaches are leading to different technical installations and we wonder what is the best solution for us.

Looking for solution we will deal in the following with Norm driven and Technology driven solutions. Differences between locations (US-NL) and Norms and Technology will be highlighted and hopefully ideas and answers will be generated .

## 3 PROTECTION NECESSITY

On one site demands of equipment for protection increased ( increased sensitivity) and on the other site protection technology improved. CENELEC at a European level develops norms that ask for a more extended protection installation.
S.W.I.F.T. has to deal for this protection with several national and international codes as show in the tabulation.

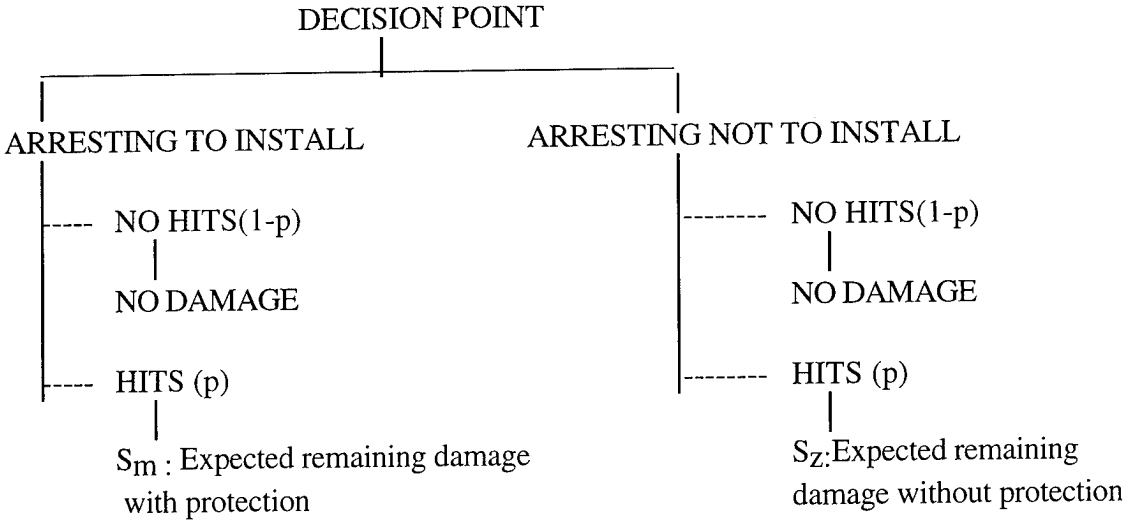
| | | |
|---|---|---|
| **Belgium codes:** | | NBN C18-100 2 edition may 1985 |
| | | NBN C18-100 supplement 1991 |
| | | BEC (Belgium Electrical Committee) |
| **Dutch codes** | : | NEN 1014 edition November 1992 |
| | | NEC (Dutch Electrical Committee) |
| **European** | : | CENELEC Expected 1998, in line with IEC |
| **American** | : | NFPA 75 August 14, 1992 |
| | | Protection of electronics Computer/Data Processing Equipment. |
| | | NFPA 780 August 14, 1992 |
| | | Lightning protection. |
| **International** | : | International standard CEI/IEC 1024-1 (1990) |
| | | Protection of structures against lightning, general principles. |
| | | International standard CEI/IEC 1024-1-1 (1993) |
| | | Protection of structures against lightning, general principles |

Selection of protection levels for lightning protection systems.
IEC 1312-1 (1995) General principles, protection against lightning electromagnetic impulse.

Not needed to state that S.W.I.F.T. is confused as lightning is a Worldwide phenomena and codes and technologies are different.
Besides the codes we are confronted with the questions if it is necessary to protect and how far should we go with the protection. In order to get a realistic approach a Dutch code committee ( NEC group 81) studied these questions and they looked into :

- The change to get a lightning strike on the building.
- The change that overvoltage occurs.
- The risk of damage and operational interruptions.
- How much to invest in prevention.
- Is the insurance solving our problem.

A cost balance exists with on one site the expected damage without protection and on the other site the protection cost plus the remaining risk. Normally the protection cost must be lower then the risk against which they protect. This means that protection of a piece of equipment can be more expensive as the equipment itself.
Based on these points a model has been developed in order to evaluate the need of lightning protection. The model requires a number , practical chosen , Building related factors and is built as follows.




First decision to take is to protect or not as shown in the figure. In each branch the consequences are evaluated with or without lightning hits with the related expected damage. The tree construction leads to 4 branches. The change of having lightning hits is indicated with p, so no hits is (1-p). The expected damage value in a period is p.S, the change of a hit multiplied by the expected average

damage. Branch 1 gives an expected damage value of $p.S_Z$, branch 2 $p.S_m$. The decision to install a lightning arresting system is positive if the expected damage without a lightning arresting system is larger as the sum of the expected damage plus the cost (K) of installation of an arresting system :

$$p.S_Z > p.S_m + K$$

Practically it is assumed that $S_m = S_Z$, but that only the change of damage is different between a protected and a non protected installation. It is supposed that in a minor amount of cases the arresting installation is not working properly or insufficient. The formula becomes :

$$p.S_Z > p.(1-n).S_m + K$$

n = the protection level of the lightning arresting installation.
A practical value for n = 0.95 (95 %).

For $S_m = S_Z$ we get : $K < n.p.S_Z$

So no lightning arresting system will be installed if the cost of installation is higher as the expected damage value multiplied by the protection degree of the lightning arresting system. If n is smaller or if there is little risk for lightning hits a lightning arresting system is not needed. Same if the installation is poorly executed.

A high value for the average damage will lead to a positive recommendation for installation. This is quickly the case in computer centres.
When a risk acceptation factor is added to the formula this leads to:

$$K < n.p_1.p_2.\Sigma\, f_i.f'_i.S_i$$

- K = cost of external and internal lightning protection installation
- n = protection level of the lightning arresting installation
- $p_1$ = change of lightning hits per year
- $p_2$ = change of damage
- $f_i$ = weigh factor related to total damage
- $f'_i$ = weigh factor related to internal protection
- $S_i$ = replacement costs
  - S1 = replacement cost for building
  - S2 = replacement cost for equipment in the building
  - S3 = immaterial damage

In a case like S.W.I.F.T.'s operating centres the factor S3 in extremely high so the decision to install is relatively easy as shown in the case study below.

## 4 EXAMPLE

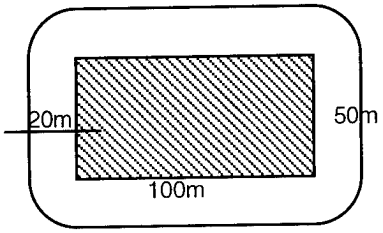



figure 1

| | | |
|---|---|---|
| Construction concentration | | = 1.0 |
| $A_{eff}$ = 100.50+ 2.(20.100)+ 2.(20.50)+ $\pi$.20$^2$ | | =12,256 m$^2$ |
| $N_f$ | | = 2,5.10$^{-6}$ per m$^2$ /per year. |
| $P_1$=12,256.0.0025 | | = 30.64 |
| Change of building damage | $P_2$ | = 0.4 (reference VDE ) |
| Size of the damage | $f_1$ | = 0.7 |
| Damage reduction | $f_i$ | = 0 |
| Replacement value of building | S1 | = 1,000,000 NLG |
| Replacement value of equipment | S2 | = 5,000,000 NLG |
| Replacement value of consequences | S3 | = 100,000,000 NLG |
| Investment cost external and internal | | = 400,000 NLG |
| Amortisation period | | = 25 year |
| Annual maintenance cost | | = 5,000 NLG |
| Cost K | | = 21,000 NLG/y |
| Protection degree | | = 0.95 |
| n damage expectation | | = 10 |

$$K < n.p_1.p_2.\Sigma\, f_i.f'_i.S_i$$

$$21{,}000 < 10.\ 30.64.\ 0.4.\Sigma\ 0.07.\ 106{,}000{,}000$$

$$21{,}000 < 60{,}542$$

So S.W.I.F.T. decided install based on these figures an external and internal lightning protection installation. Also other interesting conclusions were drawn from the approach and the calculation results. The investment of 400,000 NLG as done sofar are well below the calculated limits, when all data connections are also protected it is still expected we will stay well below the maximum calculated investment limit. The figure for S3 must be considered low for the company. So this fact gives even more room to move, but it is at the end also the technical evaluation that will be part of the decision process.

## 5 TECHNICAL EVALUATIONS

As said above technical evaluations are considered in our case a important as financial evaluations. What are the technical evaluations:

5.1 External installation

The lightning current is conducted to earth via an external installed lightning arresting system.

5.2 Overcurrent protection

All direct entering lightning currents or via induction created currents on power, data etc. must be lead to earth

5.3 Overvoltage protection

All induced voltages will be lead to earth via the fine protection systems. The sensitivity of the equipment and the peak voltages must be taken into account.

Schematically the protection looks as follows:

| | | |
|---|---|---|
| zone 0 | Outside | External installation |
| zone 0/1 | From outside to inside | Overcurrent protection |
| zone 1/2 | Inside | Overvoltage protection |
| zone 2/3 | Equipment protection | Overvoltage protection |

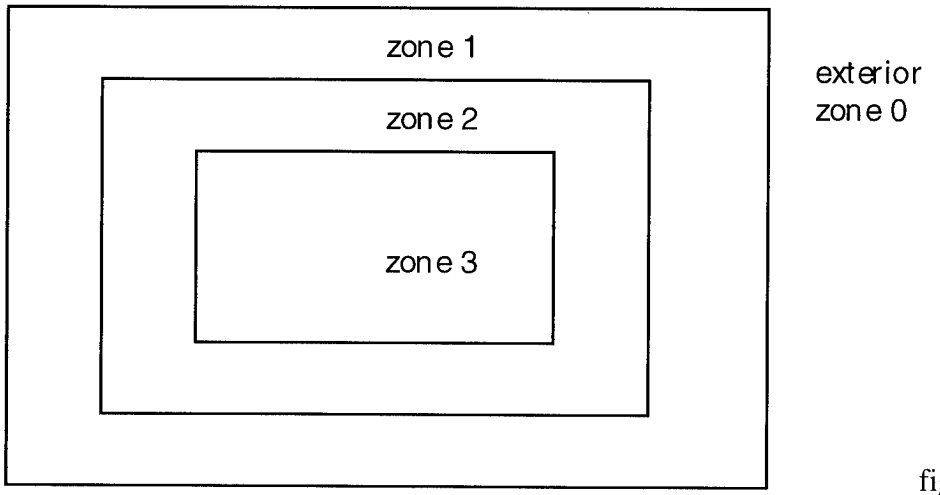



figure 2

5.1 External lightning protection

The external lightning protection will provide ways for the main discharge to go directly to the ground without causing damage to the object and to persons. Even if the discharge reaches up to 500 ft above the ground or the building the arresting system can positively influence the routing of the discharge.

In case a properly grounded lightning arresting system is installed a high concentration of positive ions will "jump" from the copper wires to the lightning and create a good way to earth.
The efficiency of the protection can be increased by installing a grid with smaller dimensions on the roof. The smaller the grid is the earlier the lightning can be "catched".

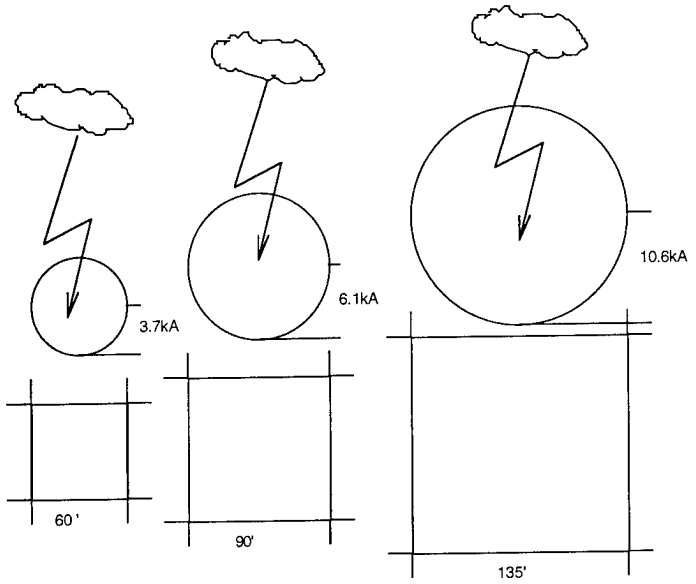



figure 3

A good external lightning arresting system forms a cage around the building to guide the lightning to earth. This cage of Faraday results that the full discharge current is split in numerous part currents, so external damage to the building is avoided. This requires a perfect installed and maintained installation.

In figure 4 we find :
$U_S$(loop A) = $a.\mu_o.\mu_a./ (2\pi).\ln (R+b)/R$ . di/dt . $10^9$ = 38.18 kV
$U_S$(loop B) = 12.65 kV
Induced voltages depend on location of strike and di/dt

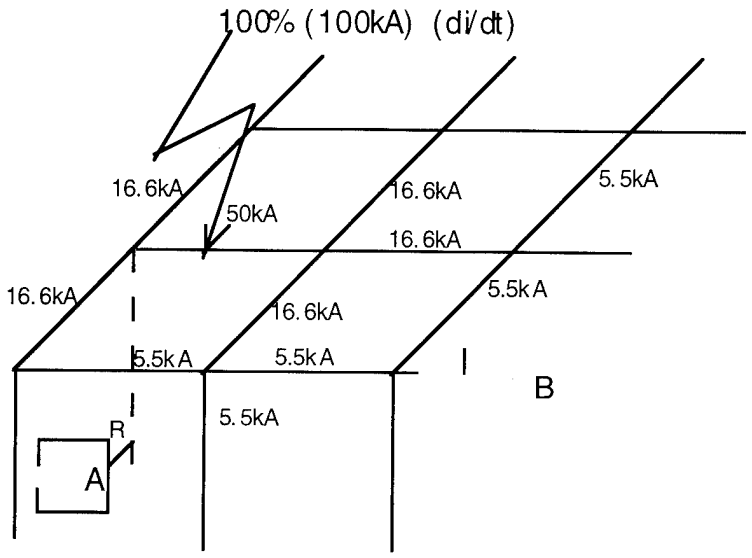



figure 4

As S.W.I.F.T. is present in many countries different codes are experienced per country. Combining these codes we are questioning what protection to install and whether the installation should be based on codes or on technical knowledge. Experience shows some differences between US and EU, like the principle of the free standing arresting for protection of roof units.

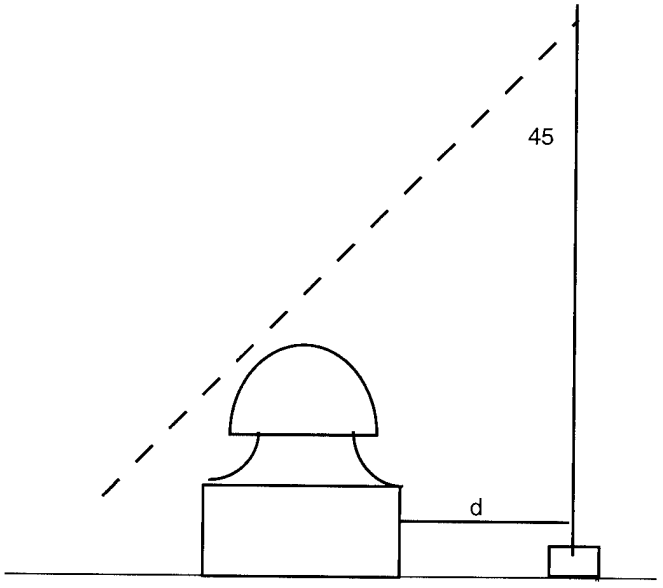



figure 5

d= l/ 7.N

As indicated the EU installation accepts a protection zone under a free standing lightning arrestor. As long as the exhaust fan in this case is completely installed in the 45$^{o}$ protection zone lightning will not hit the fan. Advantage is that the lightning current is not reaching the component to protect. The US installation demands still the direct connection of all components. The lightning current will in this

case use also the safety ground as conductor to earth, so the current will enter the building. In some cases upto 80% of the lightning current. As resistance will only slightly differ between the routes the routing of the current through the building is not defined.
S.W.I.F.T. decided to prepare the lightning arresting installation according to code and for the highest peak currents and the most heavy wave form (10/350 µs). Investigation in the US showed too many difficulties in case we deviate from the code, for what ever technical reasons.
Maybe with this introduction some attention to the subject will be given.

5.1.1 equipotential.

All conductive parts of the building like roof parts, structural steel all safety grounding will be solid connected to one point. Also shielding of data cabling will be included. In case of a discharge the complete voltage level of the building will go upto and voltage differences will remain as before between conductors in the building. This avoids damage to any parts and almost guarantees damage to each part overlooked.
In our installation only one earth is used, split between a clean and a dirty earth is considered as not needed and in some cases even dangerous.

5.2 Overcurrent protection.

As lightning might strike the power supply to the building a high current can flow into the building and cause problems. Especially in the US this is very realistic with the great amount of overhead distribution power lines. This protection is the transfer from zone 0 to 1.
The current has been measured and standardised, but is differently evaluated in different countries and as such differently treated in the codes.

The US uses still the 8/80µs wave form will in EU the 10/350µs wave form is used.
As our computer centre is considered to be protected at the highest level S.W.I.F.T. decided to protect its centre against the lightning wave form 10/350µs. This turns out to be very difficult in the US as no components exist to protect against this wave form and the high currents. The Dehn components we used in EU do comply with the wave form and the peak current, but for the US the didn't have the UL listed label. After review of the situation first S.W.I.F.T. decided to install these overcurrent arrestors on top of the normal local standards and take the risk related to the code as it was stated no UL label could be obtained as the 10/350 µs wave form is unknown in the US. Market developments however changed the situation. UL listing will be obtained by testing the components on the 8/80µs wave form, the fact that the component will accept also the 10/350µs is considered as an extra.
The Overcurrent component are installed in an existing building , this lead to several installation problems. Most serious is the fact that selectivity is a problem in power panels of small size.

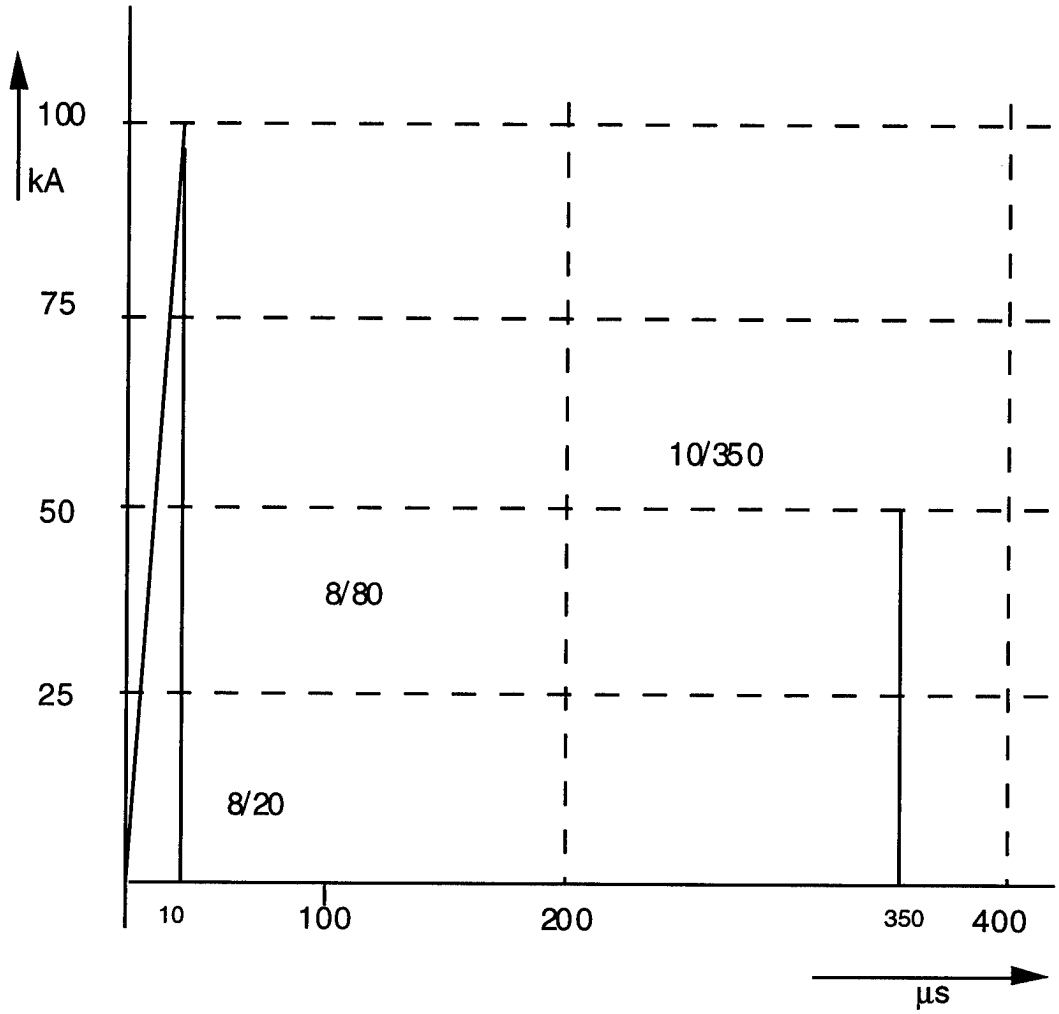



Figure 6

Lack of selectivity has to be accepted if no major installation changes are made, as the supply to the Overcurrent protection needs to be over 60 A protected. If chosen lower the lightning current will switch of the device from the power panel and no protection exists for following strikes even in the same strike. For new constructions it is necessary to limited the amount of places where feeders are entering and leaving the building to avoid selectivity problems and to keep the Overcurrent protection limited.

5.3 Overvoltage protection.

In the transfer from zone 1 to 2 and from 2 to 3 the remaining Overcurrent and the overvoltage that has been built up most be further reduced to a level that finally can be accepted by the end users. The standard voltage wave form 8/20µs has been accepted as a reference for the protection device design.

As we go deeper and deeper in the installation the amount of places to protect increase enormously. S.W.I.F.T. follows therefor 2 ways to define his protection strategy.

1 The zone 2 will be completely protected on the power panel level.
The protection of security and safety installations is done selectively.

2 The data installation will be protected selectively, a first step to take is reduce the risk by using alternate technologies like fiberoptics and investigate if buying spare parts is in some cases not cheaper as protecting.

After these points have been evaluated we came to a protection that can be managed and most important in the area's with many changes can be followed up.
The protection of zone 2 for power panels and security and safety installations has been completed. Zone 3 protection has not been foreseen sofar. The protection of data is in the inventory status of all cabling. As soon as this information is available with the information for the signal type we can investigate the protection possibilities. Especially in the US we are not so much pouched as the wires are mostly installed in metal conduct and as such forms already a protection on its self.

## **Referenties** :


* Dutch codes

* Belgium codes

* American codes

* Overvoltage protection of low voltage systems
IEE power series 12
P. Hasse

* Handbuch fur Blitzschutz und Erdung
Hasse/Wiesinger

* EMV Blitzschutzzonenkonzept
Hasse/Wiesinger
Including the Dutch transalation that includes some exemples

# SESSION 10A
# GROUND SITE LIGHTNING PROTECTION
# CHAIRPERSON: JACK R. LIPPERT

# ROCKET TRIGGERED LIGHTNING -KENNEDY SPACE CENTER AND BEYOND

William Jafferis
**BJC**
4140 Hickory Hill Blvd.
Titusville, Florida 32780
Telephone 407-269-6943

**Introduction:** The Kennedy Space Center covers an area of 100 $Km^2$, and is in one of the highest isokraunic levels in the country. Outdoor operations involving space vehicles, towers, explosives and fuel storage, aerial and buried cabling and piping connecting widely distributed sensitive electronic and mechanical equipment; all subjected to critical schedules making lightning a serious hazard. This hazard was recognized in the very early days of space center by Dr. Kurt Debus, the center director. To eliminate effects to operations and assure maximum safety to all personnel, flight and ground support equipment Dr. Kurt Debus recommended the development of a lightning protection system for all launch critical processing facilities and a system to detect charged clouds capable of producing lightning within the operational area. Both systems, lightning protection and detection where considered *STATE OF THE ART* and as such, the advice Dr. Debus recommended was to use the best experts and research scientist available and develop local instrumentation capable of measuring lightning events so that the effectiveness of these systems could be verified. A center wide lightning committee was formed to develop lightning protection and measuring system for all critical launch processing facilities and a system to detect charged clouds capable of producing lightning within the operational areas. Experience has shown that solutions to these problems are very difficult and time consuming. Through the years the lightning protection system was verified and were deficiencies were noted , by use of the measuring system corrections were made.

This concern for lightning effects to launch operation and a request by United States Air Force, Navy and Federal Aviation Administration to participate in an international program to study the effects of lightning on aircraft started a project that would use rocket triggering to create natural lightning in a laboratory enviroment. Permitting accurate time correlated measurement of pertinent data to verify *the adequacy of the lightning protection systems* and *the extensive meteorological instrumentation systems* used to satisfy operational requirements These data would be available to researchers in a time correlated fashion enabling in-depth studies

This research facility was called **KSC Atmospheric Science Field Laboratory (ASFL)** and was active from 1984 through 1991. The facility was closed for budgetary reasons. This paper will discuss some of the results of these operations as well of the resulting rocket triggering facilities located in north central Florida and north central Alabama.

**BACKGROUND: The** Kennedy Space Center's awareness of lightning hazards to both the launch vehicles and facilities was renewed because of the lightning incidents during the Apollo 15 processing flow; manned Apollo 12 liftoff to the moon; recommendations from lightning scientists; impact of work stoppages due to lightning warnings and sensitivity of the ASTP launch. A number of KSC lightning committee review meetings and studies pertaining to the adequacy of the lightning protection system, as installed, resulted in; the addition of an insulated mast, lightning rod, catenary wire system to the top of the Launch Umbilical Tower (LUT); an improved system to measure the direct and indirect lightning effects to the launch facilities.

**APOLLO, SKYLAB and ASTP** model testing; insulated lightning mast design verification; computer analyses (using ECAP and/or SPICE) of current distribution in the vehicle and structures using worst case lightning current (200ka) resulted in major improvements to the lightning protection system used for the STS program. Lightning susceptibility (Hazard analysis) studies were performed on all critical STS ground processing facilities using worst case stroke to the EXTERNAL tank (ET) and Fixed Service Structure. Induced voltages were calculated and compared with component voltages failure. Similar analyses were perform on the Flight Vehicles, ORB, ET and SRBs. Criteria were developed which would require vehicle retest if lightning induce voltages were excessive and/or lightning had attached to the vehicle.

**STS LIGHTNING PROTECTION & MEASURING SYSTEM (LPMS)**: In the Apollo program lightning protection started with the conducting mast (lightning rod) connected to the LUT, good bonding, grounding, and shielding practices backed up with modeling and simulated lightning testing, validation procedures, and semiannual preventative maintenance of all bonding and grounding systems. The insulated mast supported the lightning rod which was connected to either side of the pad to ground. The STS LPMS design involved from the Apollo, Skylab and ASTP programs and was improved through *Lessons Learned Technique* provided improvement in shielding and terminating shields ($360^{0}$) and routed most vehicle to ground power and signal lines entering the vehicle via the tail service mast or tail plugs rather than upper service arms.

The measuring system consisted of three major systems; the Catenary Wire Lightning Instrumentation System (CWLIS)[1] , which measures lightning wave form and peak current; Lightning Induced Voltage Instrumentation System (LIVIS which measures induced voltages of the orbiter buses(3) and Astronaut intercom circuit(1); and current flowing through each Tail Service Mast T-0(2) and the ET vent arm shields(1); an optical system (OTV)[1] three or more video camera/recorder system to determine the attachment point of lightning. All data is collected in one report and is used to assess damages to STS vehicles and/or launch facilities.

**Lightning Events To KSC Launch Complexes:** The lightning data collected during these event have verified the KSC launch complex lightning protection systems in terms of safety and cost. the lightning mast/catenary wire system has successfully protected the APOLLO, SKYLAB, ASTP and STS vehicles from direct lightning strikes. There had been no death, injuries or significant damages to the space vehicles or processing facilities to date. Lightning damage during the Apollo program prompted studies involving lightning effects on ground support cable systems at launch complexes 39 A&B, principally induced effects to external cables; improvements to methods to measure and analytically calculate the direct and indirect effects of lightning flashes striking a launch facility. Methods to calculate, by computer analyses, current distribution in the vehicle and structure with strokes to various parts of the structure were developed. Results of this effort indicated; induced currents and voltages from nearby lightning were of one third the magnitude of a direct lightning flash; direct strikes to the structure passed forty-five percent of lightning current through the Apollo vehicle.

Experience gained during the Apollo, Skylab and ASTP programs during which many of the eighteen vehicles, thirteen Saturn V (ten manned) where exposed to a lightning environment and the ability to measure and perform hazard analyses of all critical launch processing facilities provided the rational for KSC Safety policy which permits selected operations to continue during thunderstorms thereby minimizing work stoppages. Similar experiences were gained during the on-going SHUTTLE program.

**Kennedy Space Center** became envolved in **Rocket Triggered Lightning** for a number of reasons; to provide support for the Air Force, Navy, FAA and ONERA C-580 Aircraft test Program ie triggered lightning through a flying aircraft and a simulated fuslage (10mx0.5 m cylinder)at the rocket triggered lightning site; to be recognized as a center of knowledge and experience with lightning and other severe weather; the need for additional information to overcome potential problems posed by the increased frequency of future launch and landing operations; and as a research facility (ASFL) would use triggered lightning to create natural lightning in a laboratory setting, permitting acurate correlated measurement of pertinent data enabling in-depth studies of all meteorological systems supporting launch and landing operations.

During the eight years of operations the program fired 377 rockets during 65 storms into eight strike objects on the ground developing 545 lightning strikes. The maximum peak current of 99 kilkoamperes and a peak current derivative of 518 kiloamperes per microsecond. A total of 67 airborne missions were conducted exposing either aircraft, Aerostat or elavated rocket launch platform to 52 natural lightnings and 5 triggered lightnings. These projects were supported by about 20 government agencies and universities , foreign and domestic. All of the projects have been reported to lightning conferences around the world .The need exists to develop the operational capability to provide the means to further develop a triggered lightning model to include the following: conductive lengths of aerospace vehicles; dielectric strength of air at various altitude; speed of aerospace vehicles; electric field at various altitudes.

Kennedy Space Center is an operational center, and as such research must compete for funds . For this reason the Rocket Triggered Lightning Program, as well as ASFL were shut down, KSC encouraged continuation of rocket triggered lightning and loan/provided EPRI launching equipment and all remaining rocket and motors for use at Camp Blanding , Florida.

Rocket Triggered Lightning Program at Camp Blanding , Florida: The **Electric Power Research Institute** and **Power Technology Incorporated** particapated in ASFL/RTLP 87,88 studies of power equipment. The results were very successful and **EPRI/PTI** requested a large scale experiment involving aerial and buried electric power transmission cables. When KSC closed down ASFL the center director agreed to loan the necessary equipment and material to **EPRI** if a suitable site was found. The State of Florida agreed to lease a portion of Florida State Army property, which has the necessary air clearance and rocket storage facility. The site, 0.3 $Km^2$ located on the western edge of Camp Blanding or 10 Km east of Starke, Florida and has been operational during the summers of 1993 and 1994. Operations were conducted by **PTI** assisted by the Fench group from CEA at Grenoble.**EPRI** , because of lack of funds was no longer able to fund **PTI**

and has agreed to the University of Florida use of **EPRI** equipment. The Florida State Army has agreed to support **UF.** Dr Martin A. Uman , with **UF** students operates the facility.

**Rocket Triggered Lightning Program** at Pelham Range, Fort McClellan, Alabama: The **SANDIA NATIONAL LABORATORY** supported by the **U.S. ARMY** participated in **ASFL/RTLP 1990.** Studies of materials and field testing their rocket triggering system to be used at facilities located at Fort McClellan Anniston, Alabama. The site, 0.02 $Km^2$ in area is on Pelham Range located north west of Anniston and has been operational during the summers of 1991 and 1992. Air space is not a problem as operations can be conducted at any time.

## REFERENCES:

(1)Twenty Fourth Space Congress Proceedings, Apr.1987 Atmospheric Science Field Lab.- A feasibility Study. William Jafferis Kennedy Space Center 32899.

(2) NASA-10-7871 Final Report, Mar 1973 Lightning effects on ground support cable systems at Launch Complex 39A-KSC, F.A. Fisher, General Electric High Voltage Lab, Pittsfield, Massachusetts

(3) NASA 10-11020; Final Report, Sep. 1985, Studies of Lightning Strikes To Launch Complexes 39 A&B-KSC. M.A.Uman & E.M.Thompson University of Florida, Gainsville Florida

# ROCKET TRIGGERED LIGHTNING - KENNEDY SPACE CENTER AND BEYOND

| | | KSC | PELHAM RANGE | CAMP BLANDING |
|---|---|---|---|---|
| LOCATION | | | | |
| | STATE | FLORIDA | ALABAMA | FLORIDA |
| | LAT | 28.7N | 33.65N | 29.9 |
| | LONG | 80.7W | 85.83W | 81.8 |
| | ELEV (asl) | 4,98meter | 200meter | 37.77meter |
| | Closet City | 2 kmSW Titusville | 130 kmSE Huntsville | 40kmNE Gainesville |
| RANGE | | | | |
| | CONTROL | 5km X 5 km | 87M X 245M | 460M x 820 M |
| | OPS | 100M X100M | 5M X5M | 100M X100M |
| | AIR SPACE | 1640 Meter | YES | 1640Meter |
| FLASH DENSITY | | 1.6 fl/km-2 3month ave over 6 yrs | 0.895 fl/km-2 annual ave over 4 yrs | 1,25 fl/km-2 3 month ave over 3 yrs |
| OPERATION | | | | |
| | PERIOD | 1984-1991 | 1991-1993 | 1993 |
| | SITE MGR | W. Jafferis KSC Ret. | G.H. SCHNETZER, SNL Ret.* | M, A, UMAN UF |
| | SPONSOR | NASA | DOD-ARMY | UF/NSF EPRI FL ARM |
| | CONTACT | John Madura | P. MacNotti ARMY | MARTIN A UMAN |
| | Phone | 407-867-2666 | 201-724-2595 | 904-392-0931 |
| | FAX | 407-867-3720 | 201-724-5461 | 904-392-8671 |

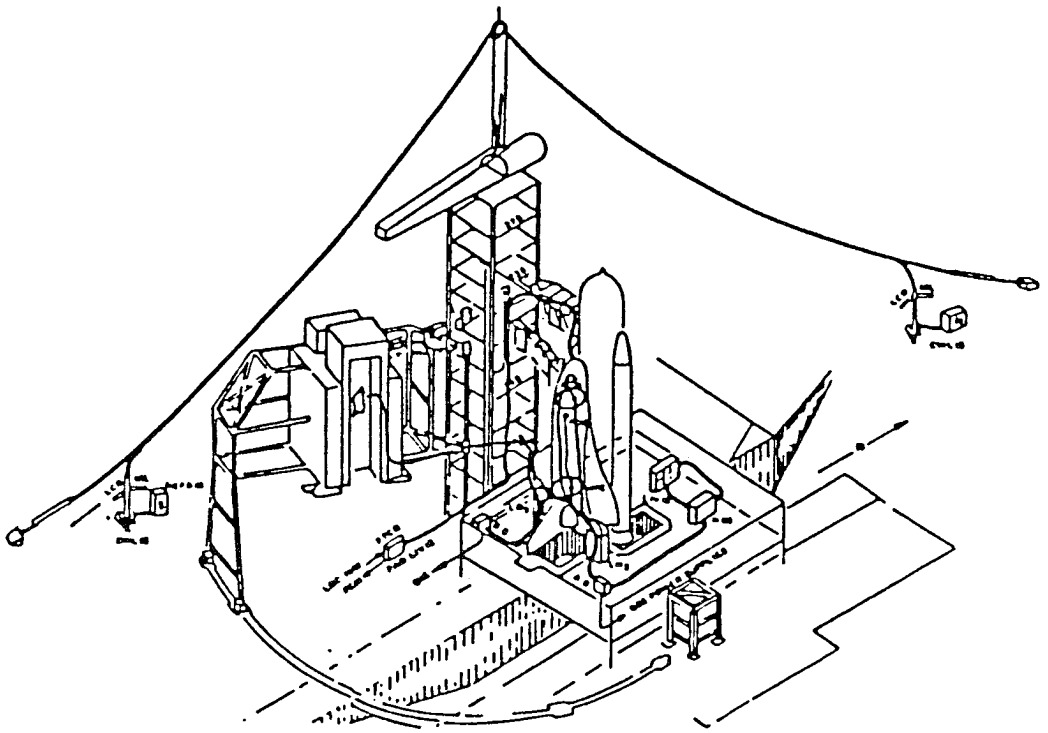
R. FISHER FONE 412- 663-500 *EX SUPV DR. MARVIN MORRIS 505-845-8647

1994 WAS SLOW FOR ROCKET TRIGGERED LIGHTNING
CAMP BLANDING ABOUT 24 FLASHES-PTI POWER EQUIP EXP ACCOMPLISHED
FRENCH (ANDRE) HAD EXCITING RESULTS WITH THE LIGHTNING ROD EXP
E 2000 COLLECTED SOME E FAR FIELD DATA.
PELHAM MANAGED 10 FLASHES ( 4-5 STRIKES/ FLASH AND COLLECTED DATA ON ORDNAN
SOME DATA WAS OBTAINED ON THE STEP VOLTAGE EXP

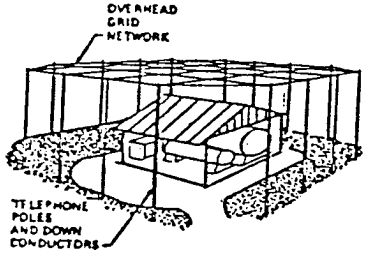
1995 MANAGEMENT CHANGES
CAMP BLANDING UNIV OF FL M. UMAN, PTI IS NO LONGER ENVOLVED
PELHAM RANGE G. SCHNETZER (RETIRED) TO MANAGE SITE FOR THE ARMY AND CONTIN
ON ORN OPS BLDG. THE ARMY HAS EXPRESSED INTEREST IN EXP WITH EXPLOSIVE

# AREA LIGHTNING PROTECTION SYSTEM

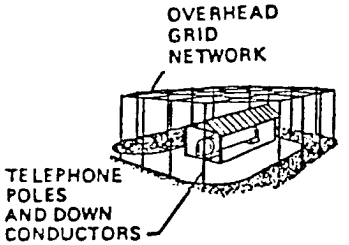




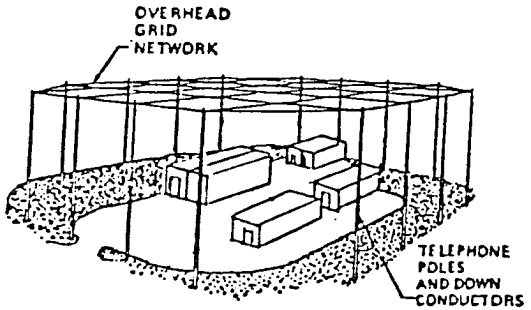
STS COMPLEX ALPS




FUEL ALPS




OXIDIZER ALPS




SCAPE REST ALPS

# ROCKET TRIGGERED LIGHTNING - KENNEDY SPACE CENTER AND BEYOND

## O WHY KENNEDY SPACE CENTER

- O PROVIDE SUPPORT FOR AIRFORCE, NAVY, FAA, & ONERA C-580 AIRCRAFT TEST PROGRAM - Triggered Lightning Through Aircraft and Simulated Fuselage (10x.5 meter cylinder) at the Launch Site
- O RECOGNITION OF KSC AS A CENTER OF KNOWLEDGE AND EXPERIENCE WIT H LIGHTNING AND OTHER SEVERE WEATHER
- O RECOGNITION BY KSC OF THE NEED FOR ADDITIONAL INFORMATION TO OVERCOME THE POTENTIAL PROBLEMS POSED BY THE INCREASED FREQUENCY OF FUTURE SHUTTLE LAUNCH AND LANDING OPERATION - Lightning Protection and Detection System improvements
- O AS A RESEARCH FACILITY (ASFL) WOULD USE ROCKET TRIGGERED LIGHTNING TO CREATE NATURAL LIGHTNING IN A LABORATORY SETTING, PERMITTING ACCURATE TIME CORRELATED MEASUREMENT OF PERTINENT DAT A ENABLING IN-DEPTH INTEGRATED STUDIES

# ROCKET TRIGGERED LIGHTNING - KENNEDY SPACE CENTER AND BEYOND

## RTLP - GROUND RESULTS

| YEAR<br>DURATION | 1984<br>7/10-8/20 | 1985<br>6/15-8/20 | 1986<br>7/18-8/20 | 1987<br>7/15-8/30 | 1988<br>7/15-8/30 | 1989<br>7/24-9/26 | 1990<br>3/30-6/5<br>7/15-8/25 | 1991<br>7/25-8/25 | TOTAL |
|---|---|---|---|---|---|---|---|---|---|
| STRIKE OBJECT | - | AFWAL-LSC<br>KSC-ALPS | LLNL-LIDS<br>KSC-ALPS | BAC-RADOME<br>EPRI<br>KSC-ALPS | BAC RADOME<br>EPRI<br>KSC-ALPS | LLNL-CP<br>ANL-CHEM<br>KSC-ALPS | ANL-CHEM<br>AF-REFS<br>KSC-ALPS | AF-REFS<br>KSC-ALPS | |
| STORMS DAYS | 3 | 13 | 7 | 6 | 16 | 10 | 9 | 11 | 65 |
| ROCKETS LAUNCHED | 19 | 40 | 39 | 82 | 56 | 53 | 52 | 36 | 377 |
| STRIKE DATA | 31 | 103 | 112 | 137 | 72 | 89 | 65 | 61 | 545 |
| PEAK I MAX (KILO AMPERE) | 30.00 | 49.40 | 32.00 | 89.00 | 33.00 | 99.00 | 37.50 | 36.00 | 99.00 |
| PEAK DI/DT<br>(KILOAMPER/MICROSECOND) | | | | 411 | 271 | 518 | 186 | 96 | 518 |

PARTICIPANTS- KSC, ESMC, AFWAL, NRL, ONERA, CENG, CENS, CNET, LLNL, NSSL
SNL, ANL, BELL LABS, ATT, EPRI, UA, UF, UM, SUNYA, & UCLA

# KSC ROCKET TRIGGERED LIGHTNING PROGRAM-AIRBORNE RESULTS

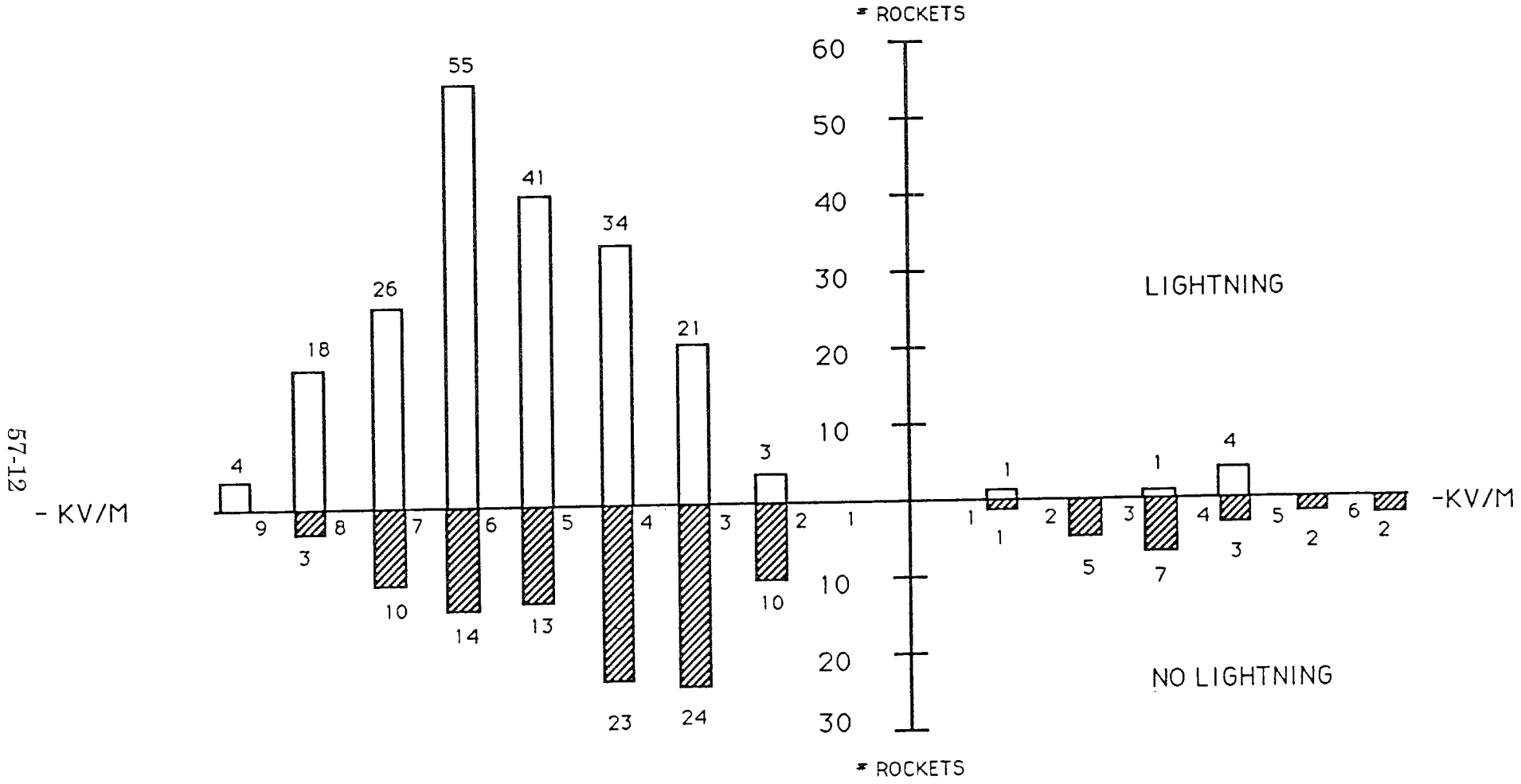
| YEAR<br>DURATION | 1984<br>6/11-9/28 | 1985<br>6/15-8/28 | 1986<br>7/15-8/30 | 1987<br>7/15-8/30 | 1988<br>7/15-8/30 | 1989<br>7/24-9/30 | 1990<br>7/15-8/25 | 1991<br>7/25-8/26 | TOTAL |
|---|---|---|---|---|---|---|---|---|---|
| OBJECTIVE | C-580 | C-580 | DNA | DNA | LSO ALOFT<br>E ALOFT<br>AEROSTAT | LSO ALOFT<br>E ALOFT<br>E ROCKET<br>AEROSTAT | LSO ALOFT<br>E ALOFT<br>E ROCKET<br>AEROSTAT | LSO ALOFT<br>E ALOFT<br>E ROCKET<br>AEROSTAT | |
| MISSIONS FLOWN | 27 | 17 | DNA | DNA | 17 | 5 | ? | 1 | 67 |
| NATURAL LIGHTNING | 21 | 27 | DNA | DNA | 1 | 0 | 2 | 1 | 52 |
| TRIGGERED LIGHTNING | 6 NEARBY | 1 NEARBY | DNA | DNA | 1 WIREBURN | 5 | 0 | 0 | 5 |

PARTICIPANTS- KSC, ESMC, AFWAL, NRL, FAA, ONERA, CENG, CENS, CNET, LLNL, SNL, ANL, , ATT, EPRI, UA, UF, UM, SUNYA, & UCLA

# 1991 ROCKET TRIGGERED LIGHTNING PROGRAM

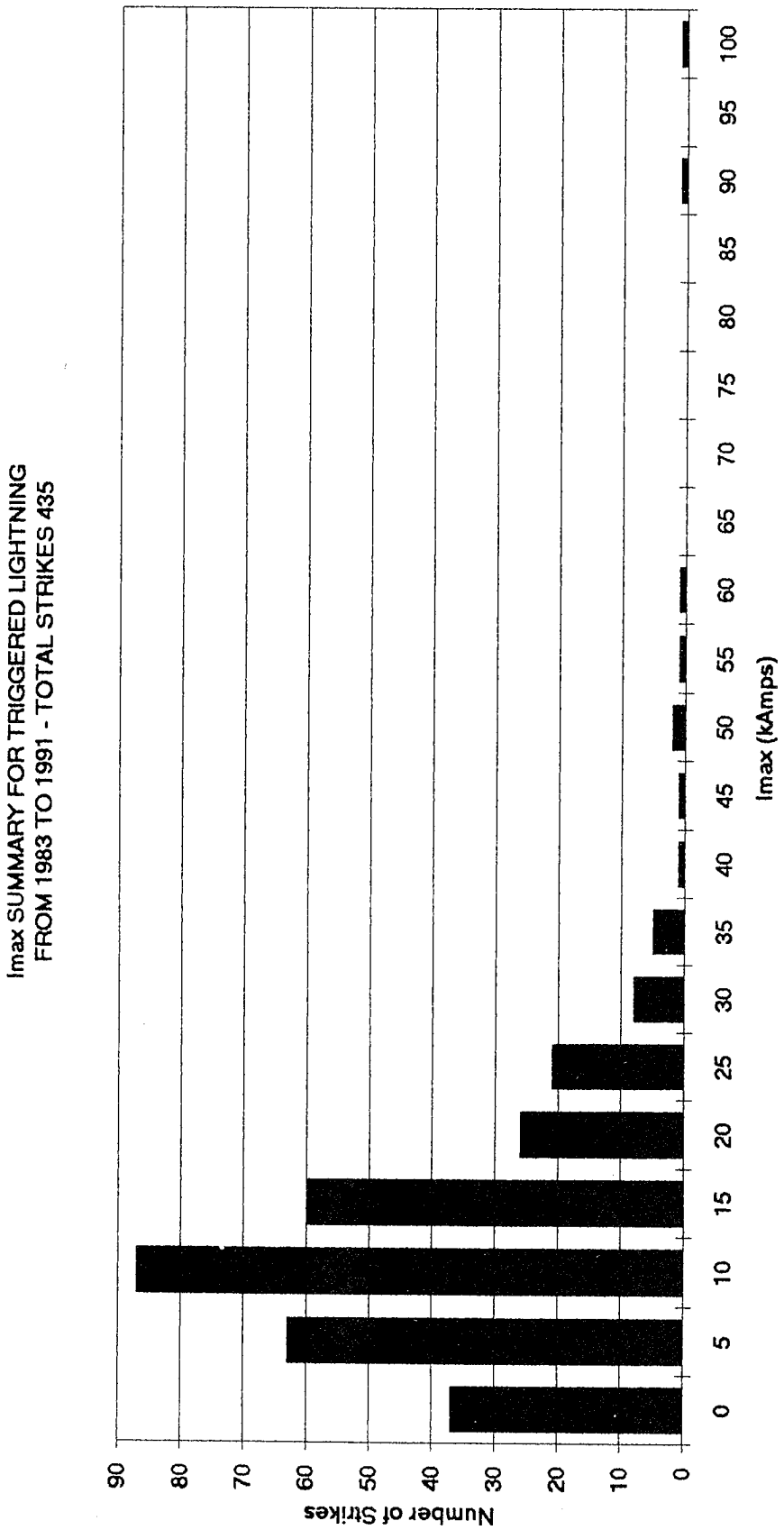
| RESEARCH | PARTICIPANTS |
|---|---|
| MEASURE VERTICAL ELECTRIC FIELD USING AEROSTAT | *SERGE CHAUZY* - LABORATORY AEROLOGIE; France<br>*CHRISTOPER PHELPS* - EMBRY-RIDDLE |
| MEASURE VERTICAL ELECTRIC FIELD USING ROCKET | *JOHN WILLET* - AF GEOPHYSICAL LAB<br>*JEAN-LOUIS, ANDRE EYBERT-BERARD* - ONERA France |
| PHOTO OF UPWARD PROPAGATING LEADER | *VINCE IDONE* - STATE UNIVERSITY OF NY, ALBANY |
| LIGHTNING INTRACLOUD DEVELOPMENT INFRARED FILM HIGH SPEED CAMERA | *VLAD MAZUR* - NATIONAL SEVERE STORM LAB |
| WIDEBAND ELECTRIC FIELD MEASURING SYSTEM DIGITALLY RECORDING ENTIRE FLASH | *MARX BROOKS* - NEW MEXICO INSTITUTE OF TECHNOLOGY |
| MEASURE SLOW ELECTRIC FIELD WITH 3 STATION SYSTEM | *LOTHAR RUHNKE* - NAVY RESEARCH LAB |

# TRIGGERED LIGHTNING SUMMARY AT KSC FROM 1983 TO 1991

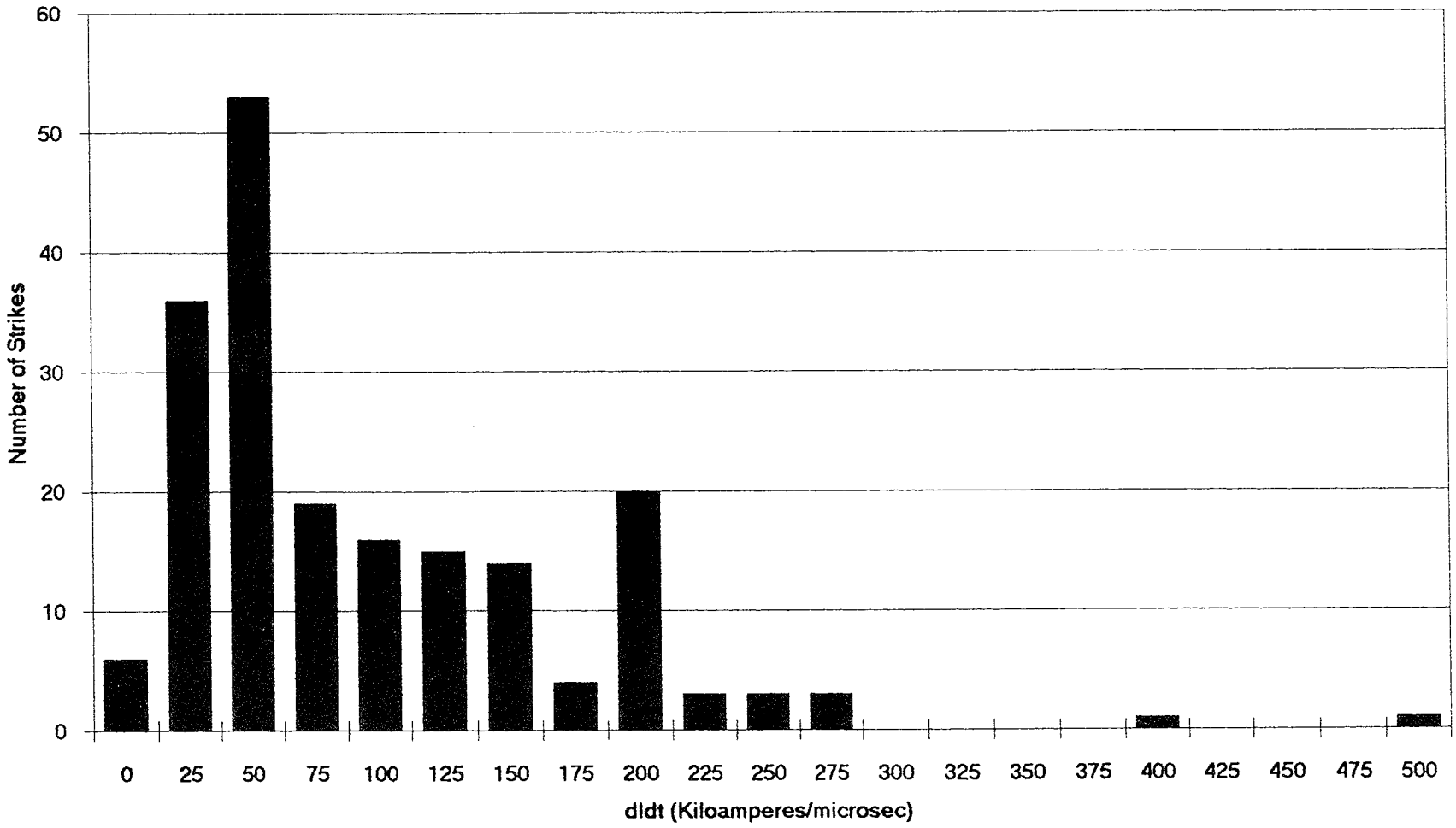


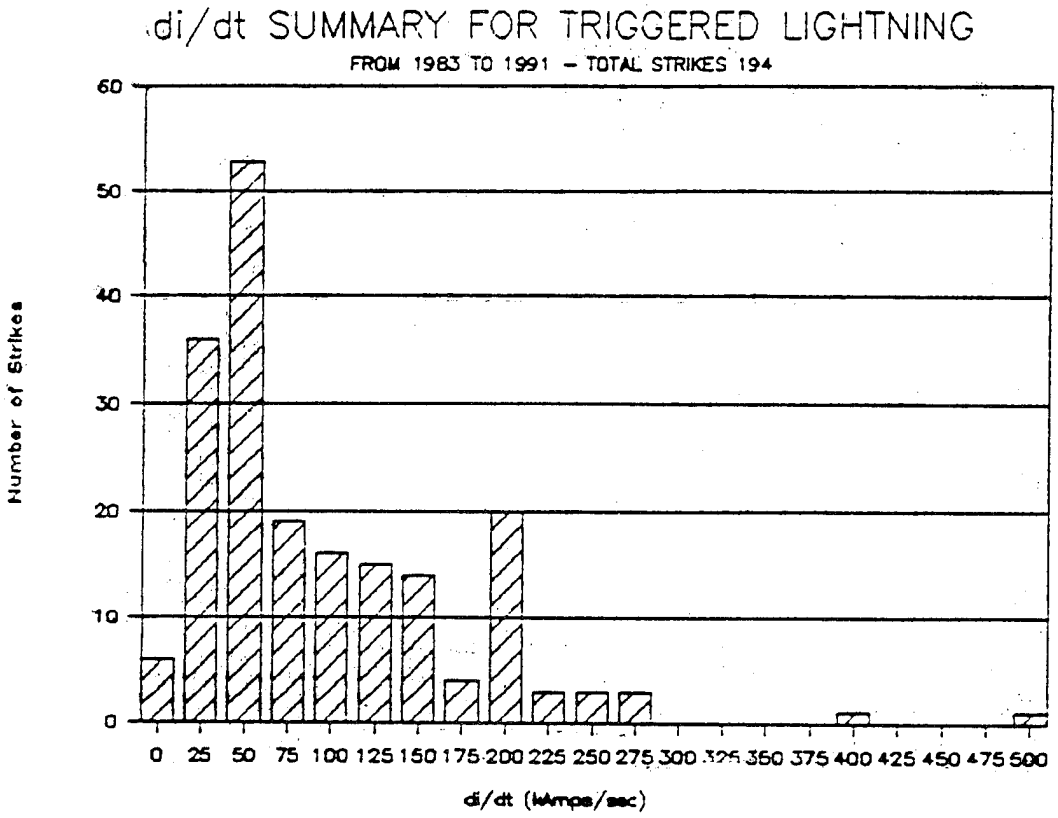

242 ROCKETS TRIGGERED LIGHTNING ( READINGS NOT AVAILABLE FOR 34)

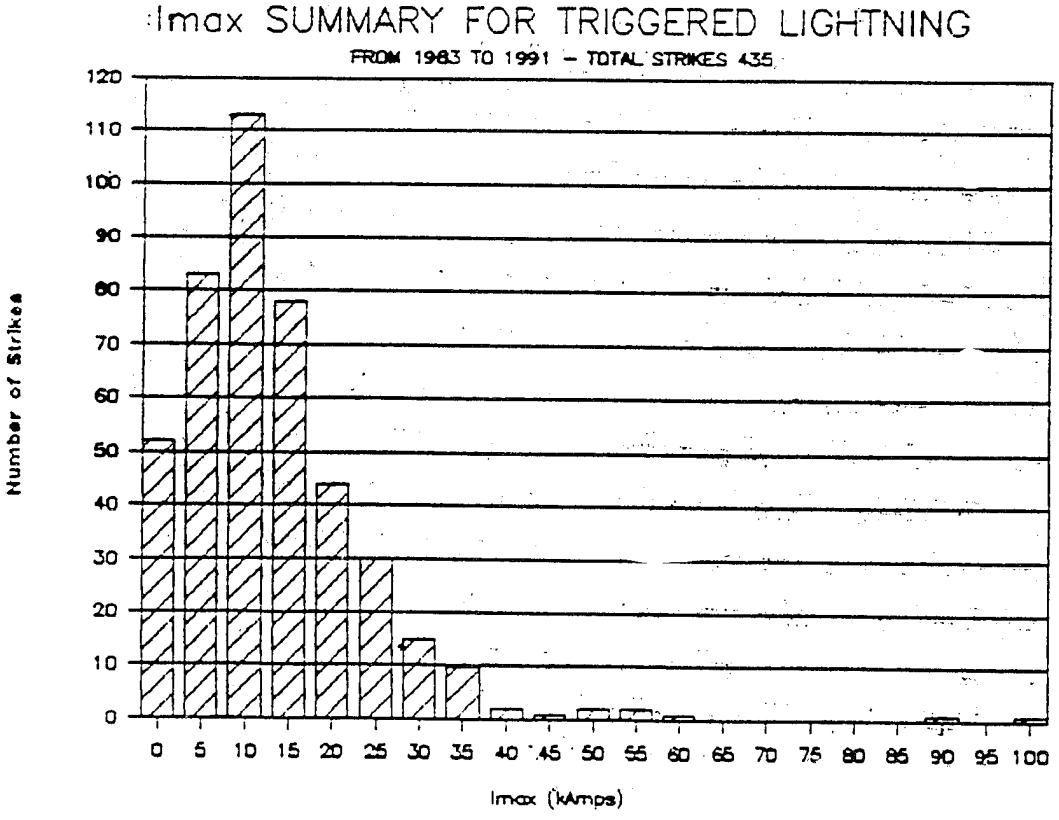
167 ROCKETS DID NOT TRIGGER LIGHTNING (READINGS NOT AVAILABLE FOR 50)


Imax SUMMARY FOR TRIGGERED LIGHTNING
FROM 1983 TO 1991 - TOTAL STRIKES 435
Number of Strikes
0
10
20
30
40
50
60
70
80
90
Imax (kAmps)
0
5
10
15
20
25
30
35
40
45
50
55
60
65
70
75
80
85
90
95
100

di/dt SUMMARY FOR TRIGGERED LIGHTNING
FROM 1983 TO 1991 - TOTAL STRIKES 194




di/dt SUMMARY FOR TRIGGERED LIGHTNING
FROM 1983 TO 1991 – TOTAL STRIKES 194
Number of Strikes
0
10
20
30
40
50
60
0 25 50 75 100 125 150 175 200 225 250 275 300 325 350 375 400 425 450 475 500
di/dt (kAmps/sec)


Imax SUMMARY FOR TRIGGERED LIGHTNING
FROM 1983 TO 1991 – TOTAL STRIKES 435
Number of Strikes
0
10
20
30
40
50
60
70
80
90
100
110
120
0 5 10 15 20 25 30 35 40 45 50 55 60 65 70 75 80 85 90 95 100
Imax (kAmps)

# ROCKET TRIGGERED LIGHTNING - KENNEDY SPACE CENTER AND BEYOND

## 1991 RTLP FINDINGS

- CIRCULAR POLARIZED RADAR DETECTED ALIGNMENT OF ICE CRYSTALS-
  This correlated with high electric fields capable of producing lightning

- LINEAR POLARIZATION RADAR DETECTED BRIGHT BANDS -
  Indicating sources of electric charge.Tested with triggered lightning.

- OPTICALLY VERIFIED TRIGGERED LIGHTNING POS LEADER PROPAGATION-
  From ground up to the cloud

- ROCKET TRIGGERED LIGHTNING IS A FUNCTIONAL TOOL-
  Can be used to simulate the electrical atmosphere to produce lightning in a controlled manner

# ROCKET TRIGGERED LIGHTNING - KENNEDY SPACE CENTER AND BEYOND

## RTLP CLOSURE

- KSC NOT A RESEARCH CENTER - Funds required for operations
- KSC ENCOURAGED CON'T OF ROCKET TRIGGERED LIGHTNING
- LOAN/PROVIDED EQUIPMENT TO EPRI - For Camp Blanding start
- VALIDATED/TRAINED SNL SYSTEM & PERSONNEL-For Pelham range

# ROCKET TRIGGERED LIGHTNING - KENNEDY SPACE CENTER AND BEYOND FUTURE WORK

- THE NEED EXISTS TO DEVELOPE THE OPERATIONAL CAPABILTY TO provide the means to further develop a triggered lightning model to include:
  - CONDUCTIVE LENGTHS OF AEROSPACE VEHICLES
  - DIELECTRIC STRENGTH OF AIR AT VARIOUS ALTITUDES
  - SPEED OF AEROSPACE VEHICLES
  - ELECTRIC FIELD AT VARIOUS ALTITUDES

# ROCKET TRIGGERED LIGHTNING - KENNEDY SPACE CENTER AND BEYOND

## SUMMARY

### o 1993 RTLP CAMP BLANDING

- o PHIL BARKER. LIGHTNING TECHNOLOGIES INC SUCCESSFULLY TESTED BURIED HIGH VOLTAGE TRANSMISSION LINE.-
  Will conduct RTLP 1994 for electric utility company
- o MARTIN A UMAN, UNIV OF FLA MEASURED EM FIELDS
- o A. EYBERT-BEDARD, CENG MEAS LIGHTNING EFFECTS TO LIGHTNING ROD
  Will support 1994 RTLP during August

**EPRI UNABLE TO CON'T SPONSORING RTL-LACK OF FUNDS**
*BEYOND 1994 FINANCIAL SUPPORT IS REQUIRED*

### o 1993 RTLP PELHAM RANGE

- o FACILITY TO BE TESTED NOT COMPLETED FOR 93 RTL-
  Step voltage,EM Field and lightnig protection test successfully completed
- o DICK FISHER RETIRES- will support 1994 RTLP during July and August

**ARMY CONCERN FOR FUTURE DOD SUPPORT -**
*TEST FACILITY UNDER UTILIZED*

# ROCKET TRIGGERED LIGHTNING - KENNEDY SPACE CENTER AND BEYOND

| | | KSC | PELHAM RANGE | CAMP BLANDING |
|---|---|---|---|---|
| LOCATION | | | | |
| | STATE | FLORIDA | ALABAMA | FLORIDA |
| | LAT | 28.7N | 33.65N | 29.9 |
| | LONG | 80.7W | 85.83W | 81.8 |
| | ELEV (asl) | 4,98meter | 200meter | 37.77meter |
| | Closet City | 2 kmSW Titusville | 130 kmSE Huntsville | 40kmNE Gainesville |
| RANGE | | | | |
| | CONTROL | 5km X 5 km | 87M X 245M | 460M x 820 M |
| | OPS | 100M X100M | 5M X5M | 100M X100M |
| | AIR SPACE | 1640 Meter | YES | 1640Meter |
| FLASH DENSITY | | 1.6 fl/km-2 3month ave over 6 yrs | 0.895 fl/km-2 annual ave over 4 yrs | 1,25 fl/km-2 3 month ave over 3 yrs |
| OPERATION | | | | |
| | PERIOD | 1984-1991 | 1991-1993 | 1993 |
| | SITE MGR | W. Jafferis KSC Ret | G.H. SCHNETZER, SNL Ret.* | M, A, UMAN UF |
| | SPONSOR | NASA | DOD-ARMY | UF/NSF EPRI FL ARM |
| | CONTACT | John Madura | P. MacNotti ARMY | MARTIN A UMAN |
| | Phone | 407-867-2666 | 201-724-2595 | 904-392-0931 |
| | FAX | 407-867-3720 | 201-724-5461 | 904-392-8671 |

R. FISHER FONE 412- 663-50( *EX SUPV DR. MARVIN MORRIS 505-845-8647

1994 WAS SLOW FOR ROCKET TRIGGERED LIGHTNING
CAMP BLANDING ABOUT 24 FLASHES-PTI POWER EQUIP EXP ACCOMPLISHED
FRENCH (ANDRE) HAD EXCITING RESULTS WITH THE LIGHTNING ROD EXP
E 2000 COLLECTED SOME E FAR FIELD DATA.
PELHAM MANAGED 10 FLASHES ( 4-5 STRIKES/ FLASH AND COLLECTED DATA ON ORDN/
SOME DATA WAS OBTAINED ON THE STEP VOLTAGE EXP

1995 MANAGEMENT CHANGES
CAMP BLANDING UNIV OF FL M. UMAN, PTI IS NO LONGER ENVOLVED
PELHAM RANGE G. SCHNETZER (RETIRED) TO MANAGE SITE FOR THE ARMY AND CONT
ON ORN OPS BLDG. THE ARMY HAS EXPRESSED INTEREST IN EXP WITH EXPLOSIVE

# ELECTROMAGNETIC RESPONSES OF LV/SV UNDER THE CATENARY WIRES ARRAY LIGHTNING PROTECTION SYSTEM TO NEAR-BY LIGHTNING STRIKES

J.C. Chai
The Aerospace Corporation
P.O. Box 92957, M4-179
Los Angeles, CA 90009, USA
Telephone (310) 336-8341 FAX (310) 336-5581

## ABSTRACT

The responses of a LV/SV system under the Catenary Wires Array Lightning Protection System to the frequently occurring *near-by* lightning strikes at SLC40/41 of CCAS, Florida, USA are found by using the method of moments model simulations. The results present an answer to the often-asked question: how effective is an overhead lightning protection system in protecting electronic hardware against the induced electromagnetic effects on the LV/SV system from near-by lightning strikes.

## INTRODUCTION

The Catenary Wires Array Lightning Protection System (CWALPS, Figure 1)

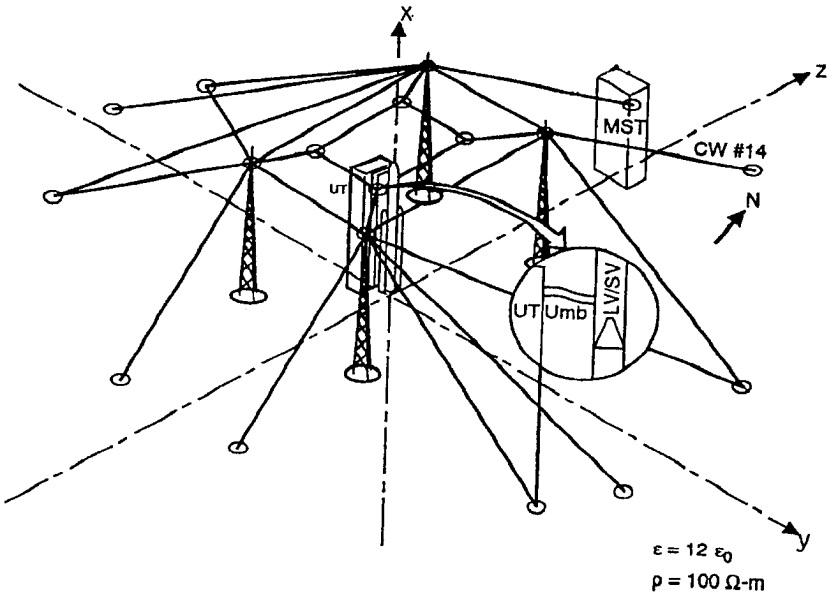



FIGURE 1. THE CATENARY WIRES ARRAY LIGHTNING PROTECTION SYSTEM (CWALPS) AT SLC40/41.

have been built for space launch complexes 40 and 41 (SLC40/41) at Cape Canaveral Air Station (CCAS) in Florida, USA. The CWALPS is designed to attract and divert direct lightning strikes in a controlled manner to achieve the main objective of protecting the launch vehicle/space vehicle (LV/SV) system and personnel on the launch pads. The CWALPS consists of four self-standing 260-ft (80-m) metal towers with four 76-ft (23-m) insulators on top of each tower. Lightning rods are attached to the array wires above each insulator. The protection structure covers the entire launch pad with 26 stainless steel cables, 14 of which are grounded at various points surrounding the launch pad periphery. On top of the array structure, there is a rectangular opening to allow the LV/SV to launch through.

Although the CWALPS is to protect the LV/SV system from being struck directly by lightning, the existence of such a gigantic metal structure may significantly alter the electromagnetic (EM) environment for the LV/SV system. In other words, due to the illumination of the CWALPS by frequent near-by lightning strikes at CCAS, the radiated fields created by the array wires and towers at close proximity may pose a worse EM environment for the LV/SV than without the presence of the CWALPS. Weather data* shows that within a radius of five-mile from SLC40 (or SLC41), direct attachments to the objects located within the boundaries of the launch pads are much rarer than near-by strikes, although the direct strikes tend to have more severe effects on the LV/SV system than strikes near by. In previous papers [1,2] the authors showed the effects of a *direct* lightning attachment to the CWALPS for the LV/SV system and personnel on the pad . This paper deals with the more frequent lightning events, i.e., the cloud-to-ground strike occurrences near-by the launch pad. In this scenario, the LV/SV responses with and without the CWALPS can then be meaningfully compared.

## MATHEMATICAL MODEL FOR THE ANALYSIS

To include correct interaction physics and essential geometry for a complex system in a lightning analysis, scattering/coupling computer codes are needed. The Numerical Electromagnetic Code (NEC) [3] has been chosen for this paper for the reasons discussed in Reference [1].

NEC: - PLANE WAVE INCIDENCE-- The supporting towers, the catenary array wires, the LV/SV system, the T-0 umbilical cable, Umbilical Tower (UT) and the Mobile Service Tower (MST) at the parked position, and personnel are modeled as segments of wires/cylinders according to the rules discussed in Reference [1]. The marked difference of this analysis from the previous one is the source term: in a direct attachment as in [1] the current source is placed at one of the lightning rods, while in this analysis for near-by strikes, the source term is the incident plane EM wave generated by a vertical lightning channel at a selected distance. In the NEC model of this analysis, there is no need to model the ionized return path and no need to find the system impedance due to the presence of the ground plane for a current source. The outputs from NEC runs are the impulse responses to delta impulse stimuli on the surfaces of any segments which characterize the wave scattering/coupling to the particular structure. In concert with a conservative attitude, two incident scenarios are

---

* Such as the data collected by Weather Service at CCAS, using the Lightning Location and Protection System (LLPS).

run to maximize the possible coupling to structures by the vertical and horizontal E-field components. These impulse response functions with and without the CWALPS are therefore indicative of the effects of the CWALPS on LV/SV responses to near-by lightning strikes, regardless of the severity of a particular lightning strike.

NEC: - GROUND EFFECTS-- The presence of a ground plane (i.e., the earth ground) changes the LV/SV responses in the following ways: (a) by modifying the current distribution through near-field interaction; (b) by changing the field illuminating the LV/SV system; and (c) by changing the re-radiated field.

Perfect Ground-- An idealized situation is to model the real earth ground as a perfectly conducting plane. This method is used by many to calculate the EM field generated from near-by lightning strikes. Examples are the dipole fields in Master, Uman, Lin and Standler [5], and Heidler and Hopf [6] papers, whose results can be convoluted with the impulse response functions to yield the surface responses of the LV/SV. The reason for this idealization is its simplicity since now the ground can be replaced by the perfect image of the currents above it, using the theory of images. Results from many calculations indicate that the perfect ground idealization tends to give much worse (larger) responses for the LV/SV system in complex geometry. Realistically, the earth ground is far from a perfect conducting plane. However, for worse-case analyses, the perfect ground treatment provides a conservative upper bound for the LV/SV system responses.

Finite Ground-- The earth ground at SLC40/41 has been realistically modeled as a finite-conducting ground with the relative permittivity equal to 12, and a resistivity of 100 ohms-m, as was done in Reference [1]. NEC provides two options for treating the finite ground: (1) the more accurate Sommerfeld solution for interaction distances less than one wavelength and an asymptotic expansion for larger distances, and (2) a modified image method using the Fresnel plane-wave reflection coefficients (RCM). The first method's computation is very time consuming because of evaluation of the Sommerfeld integrals, while the second method is more attractive because of its numerical simplicity which provides reasonable approximations for structures that are not too near the ground. Since the SV and T-0 umbilical cable are high above the earth ground, the RCM is chosen for all these analyses. Our limited comparative study shows that in the major resonance region, RCM *over*-estimates the LV/SV response by a margin of a few dBs. Therefore, our analytical results are on the conservative side. Figure 2 shows the sample frequency spectra of horizontal incident electric fields (vertically polarized components), due to Heidler & Hopf's traveling current source [6] and Component A of MIL-STD-1795A, over the finite ground defined in this analysis.

## INDUCED ELECTROMAGNETIC RESPONSES OF LV/SV SYSTEM

In a near-by lightning strike scenario, the entire LV/SV system is bathed in the EM environment created by incident, scattered, as well as re-radiated EM waves.

IMPULSE RESPONSES OF LV/SV-- The surface response of the LV/SV to this environment is the NEC solution called the impulse response function in the frequency domain. In order to determine the EM effect of the CWALPS on the LV/SV responses, NEC runs are carried out for the LV/SV system with and without the CWALPS.

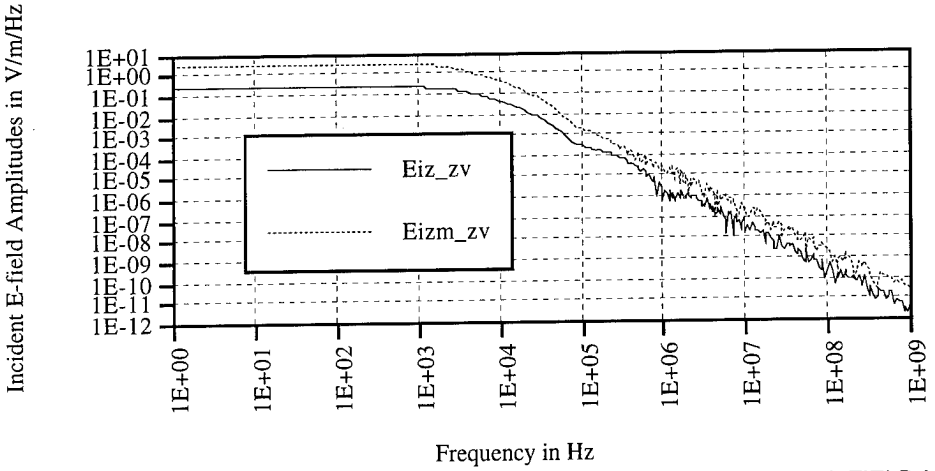



**FIGURE 2.** THE SAMPLE FREQUENCY AMPLITUDE SPECTRA OF INCIDENT ELECTRIC FIELD HORIZONTAL COMPONENTS WITH VERTICAL POLARIZATION, FOR THE CURRENT SOURCES FROM REFERENCE [6] (Eiz_zv) AND FROM COMPONENT A, MIL-STD-1795A (Eizm_zv), OVER THE FINITE GROUND USED IN THIS ANALYSIS.

Because of NEC limitations on segment lengths with respect to wavelengths of interests in a wide frequency spectrum such as the one for lightning, many segment models of the structures with different segment lengths have to be made. Figure 3 (a) shows, for the broad-side incidence (with the propagation vector **k** perpendicular to the LV/SV)#, the current density (thus, the H-field) ratio, in dB, of the SV impulse response functions with and without the CWALPS, while Figure 3 (b) shows the charge density (i.e., E-field) ratio. As previously mentioned, this ratio quantity is an indication of the effect of the CWALPS on the LV/SV response. It is interesting to note that each ratio plot divides itself approximately into three regions: below 1 MHz, between 1 MHz and 10 GHz, and above 10 GHz. Below 1 MHz, the effect of the CWALPS on the SV is to cause a reduction of the surface response by 10 to 20 dB . This agrees with the intuitive physical picture of the CWALPS as a quasi-Faraday (somewhat leaky) cage, because in the long wavelength region the CWALPS appears to be a more continuous metal sheet to the EM waves. The 'shielding' effect provided by the CWALPS is therefore evident in this frequency region below 1 MHz. However, between 1 MHz and 10 GHz where many resonances of the system occur, the CWALPS seems to have some adverse effect on the SV system: the induced surface EM field ratios vary greatly, and tend to show the amplification of the induced fields on the SV. Although the systems with and without the CWALPS have different 'total effective lengths', the worsening (enlarging) of the SV response due to the CWALPS is unmistakable. This suggests that in the resonance region, the re-radiated field dominates, and there is definitely no 'shielding' advantage offered by the CWALPS. Above 10 GHz, the ratio plots show that there is no significant difference between the SV response with or without the CWALPS. This again can be easily understood as a statement of the fact that in the short wavelength region, the CWALPS is of no significance as far as the SV response is concerned. This is so because to the short wavelength waves, the CWALPS appears extremely distant, therefore the effect of the CWALPS on the SV response becomes insignificant.

---

# It is chosen because it has been shown, by analyses and by system level tests in the electromagnetic-pulse community, that this incidence is likely to represent the worst-case coupling to the LV/SV system.

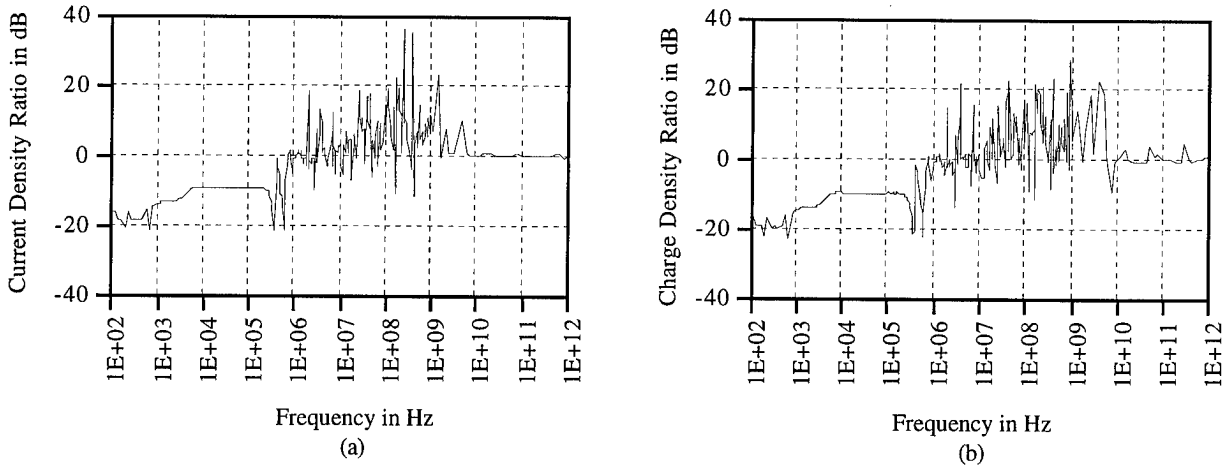



**FIGURE 3.** THE IMPULSE RESPONSE AMPLITUDE RATIOS (IN dB) OF THE SV (NEAR TOP OF LV/SV SYSTEM) FOR THE BROAD-SIDE INCIDENCE WITH AND WITHOUT THE CWALPS, IN THE FREQUENCY DOMAIN. A POSITIVE dB MEANS AN AUGMENT OF THE RESPONSE, WHILE A NEGATIVE dB INDICATES A REDUCTION. **(a)** IS FOR THE CURRENT DENSITY RATIO, AND **(b)** IS THE CHARGE DENSITY RATIO.

The shielding effectiveness, as defined in the traditional way, is in reference to the environments at *empty* spatial points inside and outside the enclosure in question. Distinction must be made between the EM environment and the induced response on an object. The environment needs to be scattered/coupled to the object to involve the object where the characteristics of the object enters into the picture; otherwise, a severe or benign environment may not be used as an indication of how an object /system would respond to the environment.

SURFACE RESPONSES OF LV/SV-- To obtain the LV/SV response to the near-by lightning strike, the delta impulse response function discussed in the last section has to be convoluted with the EM field generated by the near-by lightning strike. In this paper, the responses of the SV (near the top of the LV/SV system) and the umbilical cable need be calculated as examples. In order to do this, the EM field generated by near-by lightning strikes has to be characterized. The one that has been widely used and referenced is the dipole model of the lightning channel for the first return strike in Reference [5], and then, one of its variation (with current reflections) as recently done in Reference [6]. In addition to these, as illustrated and compared to the results in Reference [1], Component A of MIL-STD-1795A is also used in the convolution. The obvious difference is that the former dipole fields represent average lightning events for the LV/SV system, while MIL-STD-1795A's waveform can be considered as the worst-case lightning current for whatever/wherever the lightning strike may be.

Dipole Model of Lightning Channel-- Uman, et al. [4] first calculated the EM fields of a finite dipole antenna with a current pulse propagating up the antenna in the time domain. This calculation was later utilized and refined by Master, et al. [5] to model the lightning channel to calculate the return stroke EM fields above ground, which yields good predictions of measured ground-based fields up to 100 micro-seconds. In order to account for the realistic current reflections from the ground and from the channel, Heidler, et al. [6] performed the calculation of vertical electric field and traverse magnetic field for an ideal conducting ground. In this paper, the horizontal E-field component is also included for observation points above a finite

conducting ground treated by the reflection coefficient method (RCM). Using the travel current source (TCS) model and field expressions derived therein, the EM fields in the time domain at 1 km (as illustrating examples) from the LV/SV are calculated. These fields are then Fourier-transformed to the frequency domain by an integral Fourier transform algorithm** in order to convolute with the impulse response functions of the SV and the T-0 umbilical cable in the frequency domain. Figures 4 (a) and (b) show the E- and H-field *component* responses due to E- and H- field coupling to the SV, using the current source given in Reference [6], with the horizontal component normal to the SV surface. The sample *resultant* surface E-field response of the SV and the surface H-field response of the umbilical cable in the frequency domain, as shown in Figures 5 (a) and (b), are then inverse-Fourier-transformed back to the time domain to obtain the time domain SV and T-0 umbilical cable responses in Figures 6 (a) and (b). Note that the source current ($i_Q$) is as defined in Equation (28) of Reference [6], with the current maximum at 30 kA, which represents typical and *average* lightning events frequently encountered at CCAS. These sample results can then be regarded as the typical LV/SV responses to the average near-by lightning events at CCAS.

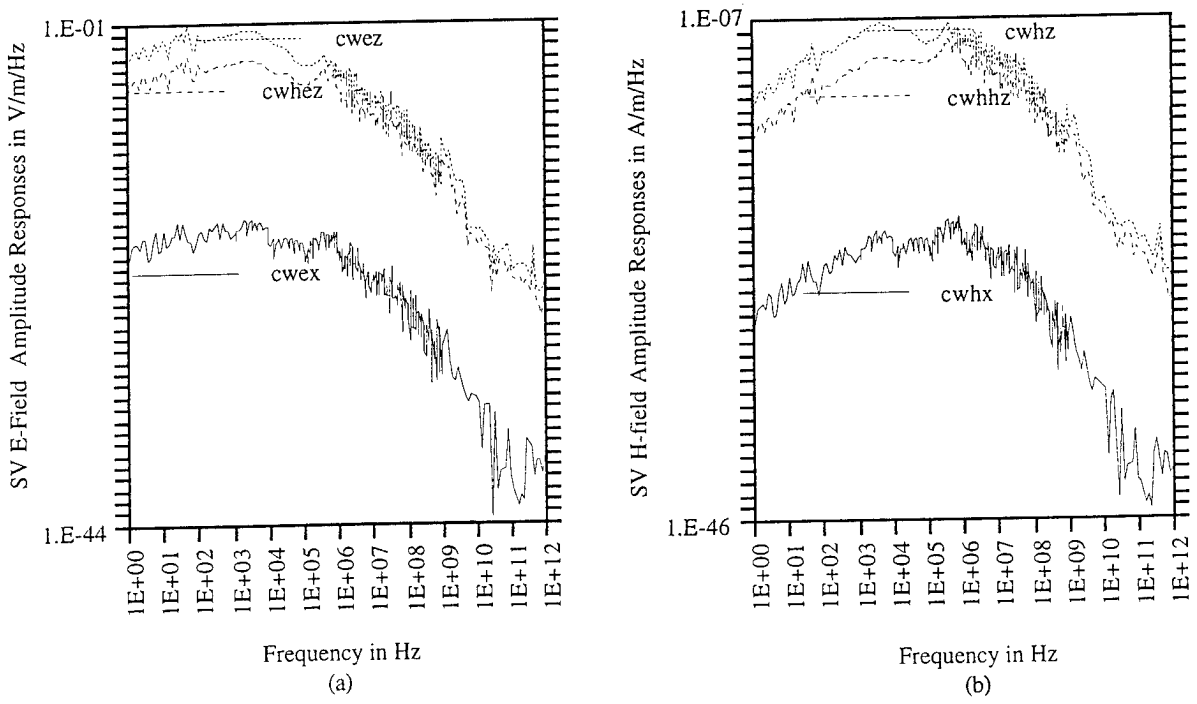



**FIGURE 4.** SV FIELD COMPONENT AMPLITUDE RESPONSES TO THE BROAD-SIDE INCIDENCE WITH THE CURRENT SOURCE GIVEN IN REF. [6]. **(a)** IS THE VERTICAL (cwex, LOWER CURVE) AND HORIZONTAL (cwez, UPPER CURVE) E-FIELD RESPONSE DUE TO E-FIELD COUPLING, AND HORIZONTAL (cwhez, MIDDLE CURVE) E-FIELD DUE TO H-FIELD COUPLING, WHILE **(b)** SHOWS THE VERTICAL (cwhx) AND HORIZONTAL (cwhz) H-FIELD RESPONSE DUE TO E-FIELD COUPLING, AND HORIZONTAL (cwhhz) H-FIELD DUE TO H-FIELD COUPLING.

** The integral Fourier Transform codes are provided by R. Andre.

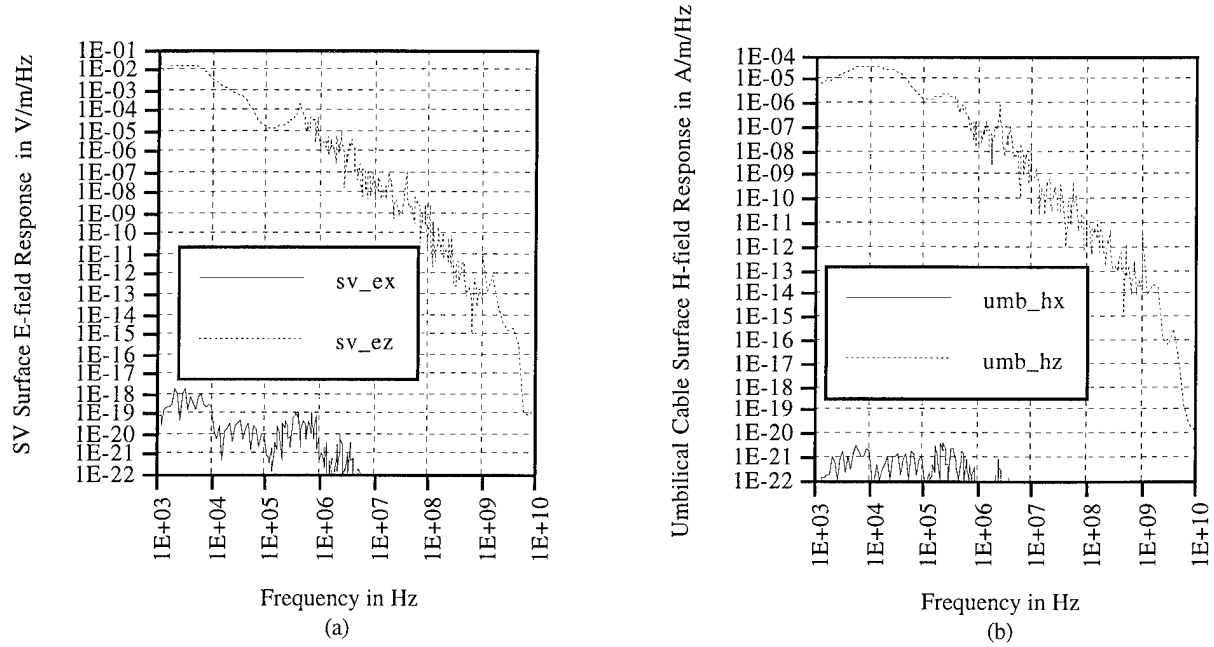



**FIGURE 5.** SURFACE AMPLITUDE RESPONSES TO THE BROAD-SIDE INCIDENCE WITH VERTICAL (x-) & HORIZONTAL (z-) COMPONENTS IN THE FREQUENCY DOMAIN. TRAVEL CURRENT SOURCE OF PEAK AMPLITUDE OF 30 KA IN HEIDLER & HOPF'S MODEL [6] IS USED WITH A FINITE GROUND. **(a)** IS THE SV E-FIELD RESPONSE, WHILE **(b)** IS THE T-0 UMBILICAL CABLE'S H-FIELD RESPONSE.

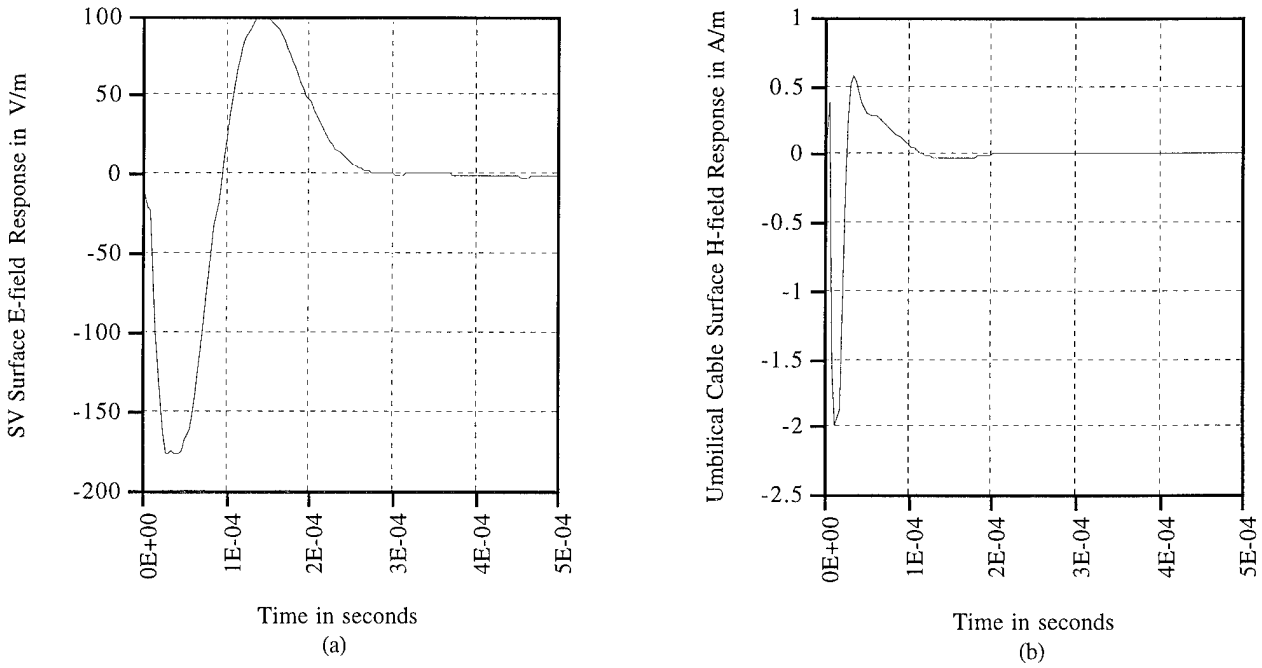



**FIGURE 6.** SURFACE RESPONSES TO THE BROAD-SIDE INCIDENCE WITH VERTICAL & HORIZONTAL COMPONENTS IN THE TIME DOMAIN. TRAVEL CURRENT SOURCE OF PEAK AMPLITUDE OF 30 KA IN HEIDLER & HOPF'S MODEL [6] IS USED WITH A FINITE GROUND. **(a)** IS THE SV E-FIELD RESPONSE, WHILE **(b)** IS THE T-0 UMBILICAL CABLE'S H-FIELD RESPONSE.

Component A, MIL-STD-1795A-- The waveform defined in this military standard is used as the driving current source ($i_Q$) traveling up the lightning channel. It probably represents one of the worst-case scenarios with peak current amplitude at 200 kA. The EM field components with this source current in Heidler and Hopf's model [6] of the lightning channel at the sample distance of 1 km are calculated in the time domain to yield the EM waves incident on the LV/SV system. These dipole fields are first Fourier-transformed to the frequency domain to convolute with the impulse response functions obtained earlier from the NEC runs. Figures 7(a) and (b) show the E-field and H-*field component* responses to the broad-side incidence due to E- and H-couplings to the SV, respectively. The *resultant* surface E-field response of the SV (Figure 8 (a)) and the surface H-field response of the umbilical cable (Figure 8 (b)) are then inverse-Fourier-transformed back to the time domain, and are shown in Figures 9 (a) and (b). When compared to the results obtained for direct attachments to the CWALPS in Reference [1], it is found that the LV/SV surface responses in near-by lightning scenarios are about 40 dB weaker in *amplitude* than those of direct CWALPS attachments. Note that they also have quite different characteristics in frequency spectra and temporal behaviors: in direct attachments, the CWALPS is driven by the return stroke current and the LV/SV is the responding resonator, while in near-by strikes, both the CWALPS and the LV/SV system are the responding resonators, thereby with longer pulse widths. Since it is found in Reference [1] that careful, traditional mitigation techniques are adequate to prevent burn-out damage for the sample LV/SV system studied, these mitigation techniques should be sufficient to protect the same LV/SV system in the EM environment induced by the more frequent near-by lightning strikes.

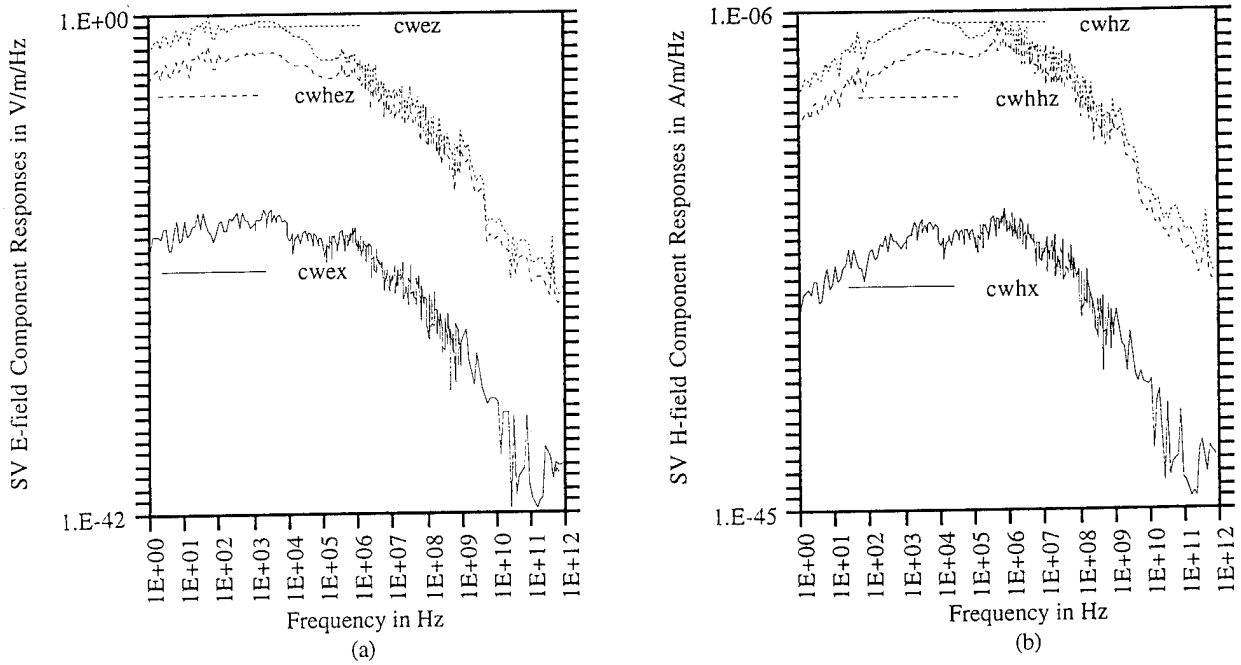



**FIGURE 7.** SV FIELD COMPONENT AMPLITUDE RESPONSES TO THE BROAD-SIDE INCIDENCE WITH COMPONENT A IN MIL-STD-1795A. **(a)** IS THE VERTICAL (cwex, LOWER CURVE) AND HORIZONTAL (cwez, UPPER CURVE) E-FIELD RESPONSE DUE TO E-FIELD COUPLING, AND HORIZONTAL (cwhez, MIDDLE CURVE) E-FIELD DUE TO H-FIELD COUPLING, WHILE **(b)** SHOWS THE VERTICAL (cwhx) AND HORIZONTAL (cwhz) H-FIELD RESPONSE DUE TO E-FIELD COUPLING, AND HORIZONTAL (cwhhz) H-FIELD DUE TO H-FIELD COUPLING.

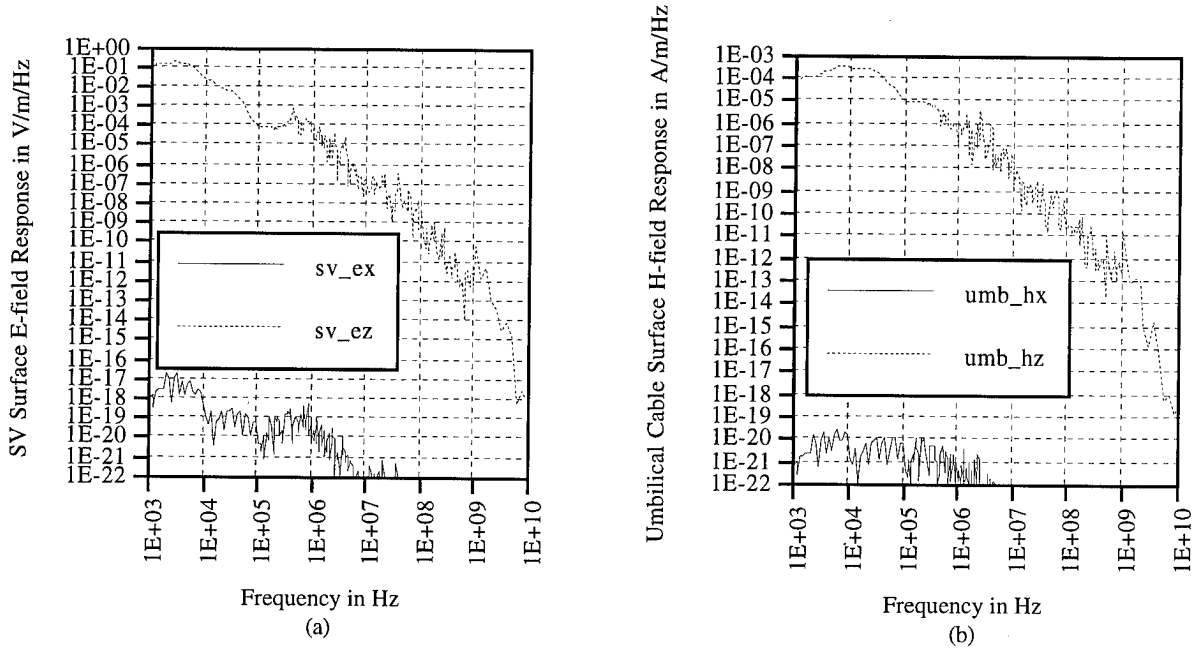



**FIGURE 8.** SURFACE AMPLITUDE RESPONSES TO THE BROAD-SIDE INCIDENCE WITH VERTICAL (x-) & HORIZONTAL (z-) COMPONENTS IN THE FREQUENCY DOMAIN. COMPONENT A WITH PEAK AMPLITUDE OF 200 KA IN MIL-STD-1795A IS USED AS THE TRAVELING CURRENT SOURCE IN HEIDLER & HOPF'S MODEL [6] IMPLEMENTED FOR A FINITE GROUND. **(a)** SHOWS THE SV E-FIELD RESPONSES, WHILE **(b)** SHOWS THE T-0 UMBILICAL CABLE H-FIELD RESPONSES.

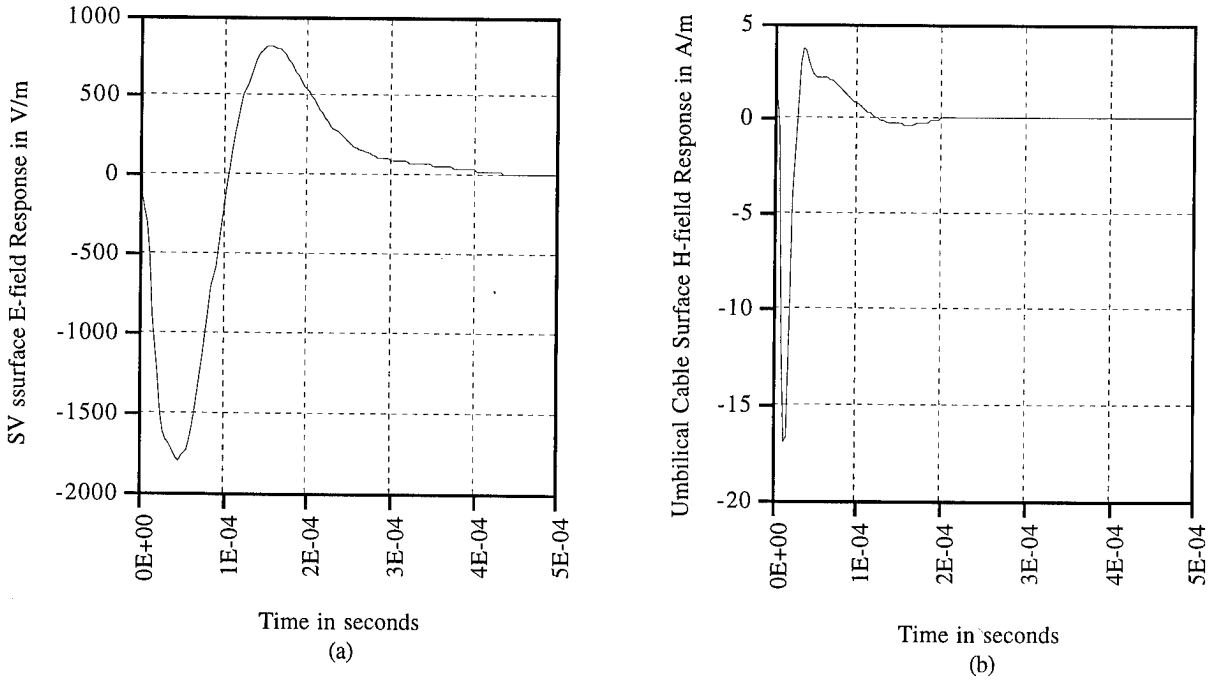



**FIGURE 9.** SURFACE RESPONSES TO THE BROAD-SIDE INCIDENCE WITH VERTICAL & HORIZONTAL COMPONENTS IN THE TIME DOMAIN. COMPONENT A WITH PEAK AMPLITUDE OF 200 KA IN MIL-STD-1795A IS USED AS THE TRAVELING CURRENT SOURCE IN HEIDLER & HOPF'S MODEL [6] IMPLEMENTED FOR A FINITE GROUND. **(a)** SHOWS THE SV E-FIELD RESPONSE, WHILE **(b)** SHOWS THE T-0 UMBILICAL CABLE'S H-FIELD RESPONSE.

## SUMMARY AND DISCUSSION

The surface responses of the SV and the T-0 umbilical cable under the CWALPS at SLC40/41 are found for the more frequent near-by lightning events. They are less severe in amplitudes with longer pulse widths, but more frequently occurring, than those induced by direct attachments to the CWALPS found in a previous analysis.

The EM effect of the CWALPS on the LV/SV system is expressed in terms of the surface response of the SV and of the T-0 umbilical cable in three distinct regions of the frequency. While it is generally believed that the CWALPS will divert direct attachments away from the LV/SV system, it could worsen the EM environment in the *mid* (resonance) region of the frequency for the LV/SV system because of the re-radiated fields. The CWALPS appears to provide some shielding for the LV/SV in the *low* frequency region, and its presence seems to have no significant effect on the shielding of the LV/SV at the *high frequency* end. However, due to different scattering/coupling mechanisms and characteristics, the combined CWALPS effects on LV/SV system for near-by lightning strikes seem quite benign, when compared to those from direct attachments.

To mitigate the EM effect induced by near-by lightning, traditional mitigation techniques such as shielding, grounding, and transients protection devices are deemed sufficient, provided they are sized and implemented correctly and potential side-effects carefully traded and prevented.

## REFERENCES


[1] J.C. Chai, H.A. Heritage and R. Briët, "Electromagnetic Effects of the Four-Tower Supported Catenary Wires Array Lightning Protection System," Proceedings of the 1994 International Conference on Lightning and Static Electricity, p. 377, Mannheim, Germany, May 24-27, 1994.

[2] J.C. Chai, H.A. Heritage and H.Z. Wilson, "Lightning Energy Absorption in Humans and Personnel Safety," Proceedings of the 1994 International Conference on Lightning and Static Electricity, p. 483, Mannheim, Germany, May 24-27, 1994.

[3] G.J. Burke, and A.J. Poggio, "Numerical Electromagnetic Code (NEC) - Method of Moments," Lawrence Livermore National Laboratory, UCID-18834, January 1981.

[4] M.A. Uman, D.K. McLain, and E.P. Krider, "The Electromagnetic radiation from a Finite Antenna," Am. J. Phys., Vol. 43, p. 33, 1975.

[5] M.J. Master, M.A. Uman, Y.T. Lin and R.B. Standler, "Calculation of Lightning Return Electric and Magnetic Fields above Ground," J. Geophys. Res., Vol. 86, N0. C12, December 20, 1981.

[6] F. Heidler, and Ch. Hopf, "Influence of the Lightning Channel Termination on the Lightning Current and Lightning Electromagnetic Impulse," Proceedings of the 1994 International Conference on Lightning and Static Electricity, p.65, Mannheim, Germany, May 24-27, 1994.

# PROBABILITY CALCULATION OF DIRECT LIGHTNING ATTACHMENTS TO STRUCTURES AT SLC40/41

W.M. Jackson, H.E. Eley, J.C. Chai, and R. Briët

The Aerospace Corporation, P.O. Box 21205, Kennedy Space Center, Fl., 32815, USA.
Tel. (407) 853-6666; FAX (407) 853-3690

## ABSTRACT

A computer program designed to calculate the probability of direct lightning attachment to structures at Cape Canaveral Air Station's Space Launch Complex 40 and 41 (SLC40/41) is described. The program uses the striking distance concept and Monte Carlo techniques to simulate lightning attachments. Examples are given to illustrate the utilization of such a program, and the potential of extensions to other similar applications.

## INTRODUCTION

The Air Force's Titan-IV/Centaur launch pads are located in a high thunderstorm activity area on the east coast of Florida. These launch pads are large fenced areas with many tall structures which are potential attraction points for a lightning strike. The Titan-IV/Centaur vehicle varies in height, depending on payload configuration, from approximately 180 feet to 210 feet. The fixed-position umbilical tower is approximately 171 feet tall. A very large, 260 foot tall, mobile service tower (MST) surrounds the entire vehicle until a few hours before launch. The final preparation of the Titan-IV/Centaur vehicle involves moving the MST from the service position to a parked position (approximately 600-feet from the vehicle), and fueling the Centaur upper stage. Once the MST moves from the service position, the vehicle is virtually unprotected from lightning strikes. To reduce the risk of a lightning strike to the vehicle and reduce lost work time due to lightning evacuations which occur frequently during the summer months, a lightning protection system was installed on each of the two pads. The SLC40/41 lightning protection system design evolved from a simple single tower system to a very complex six-tower system. The system eventually installed was composed of four 264-foot steel towers topped by 76-foot insulators which support 26 individual catenary wires.

To guide the design of the lightning protection system and assess the systems effectiveness, a method to easily calculate the probability of direct lightning attachment to the proposed protection system and the objects the system protects was urgently needed. In this paper we describe the computer program that was developed to model the complexity of the Titan-IV launch pad lightning protection system, vehicle, and ground facilities. The program utilizes a Monte Carlo simulation technique to estimate attachment probabilities. Using this program, many years of lightning strike experience can be simulated within minutes. With simple modifications this program can be applied to any structure or installation for estimating the probability of direct lightning attachment.

## AVAILABLE STATISTICS

Meteorological personnel have studied the frequency of lightning strikes to the launch pad area. They were able to derive a number which quantified the probability that lightning would strike the pad area within a 24 hour period given that lightning was within 5-nautical miles at any time during that 24 hours. The forecaster also provides probability estimates that lightning will be within 5-nautical miles of the pad area. It was still necessary to know the conditional probability that a specific object would be struck, given the probability that lightning will strike somewhere in the pad area in order to determine the probability of striking the missile, a possibility which we had to avoid because of the severity of the consequences.

J.R. Stahmann, in support of the U.S. Space Shuttle program, presented papers at previous International Aerospace and Lightning Conferences addressing lightning attachment to grounded objects. A manual implementation of Stahmann's approach is extremely difficult if more than a few grounded points are considered. D. Downs of the Lockheed Martin Company first used a computer based algorithm to calculate lightning attachment probability, using the selection rules formulated by Stahmann. Inspired by Downs work and with many enhancements over his original version, this paper vividly demonstrates the utility of using a computer to sort out attachment statistics by mechanizing Stahmann's manual method.

## SUMMARY OF STAHMANN'S APPROACH

The approach used by Stahmann to estimate the probability that lightning would strike a point on a structure, as opposed to some other nearby point, was based on the striking distance theory. This theory assumes that lightning will progress toward earth and strike the first grounded object or the earth on one final jump. The height before the final jump to earth is defined as the striking distance. For a single grounded point, for example the tip of a tower, if the stroke gets within striking distance 'Sd' of the point before reaching the striking distance to the earth, the strike will be to the grounded point. Stahmann described the striking distance around a grounded point on a structure (called a structural node) in terms of a *spherical shell* about the point. This sphere forms a sphere of attraction with a radius of attraction equal to the striking distance. That is, if a lightning stroke contacts the surface of this imaginary sphere, the stroke is by definition within the striking distance of the grounded point and will jump to that point. Figure-1 shows this geometry in detail.

The strike will be to the tower if the distance 'd' is greater than the striking distance to earth. The node of interest is the tip of a tower of height 'z' located at coordinates (x, y). The stroke earth-intercept point is at coordinates (sdx, sdy). The vertical distance 'd' from the tip of the last leader to earth is easily calculated as follows.

$$d = \sqrt{(Sd)^2 - (sdx - x)^2 - (sdy - y)^2} + z = \sqrt{\arg} + z$$

If the value 'arg' is less than zero, the stroke is not within striking distance of the tower and will strike the earth. If the value of 'arg' is equal to or greater than zero, the stroke is within striking distance of the tower and will penetrate the sphere at distance 'd' from earth and jump to the tip of the tower.

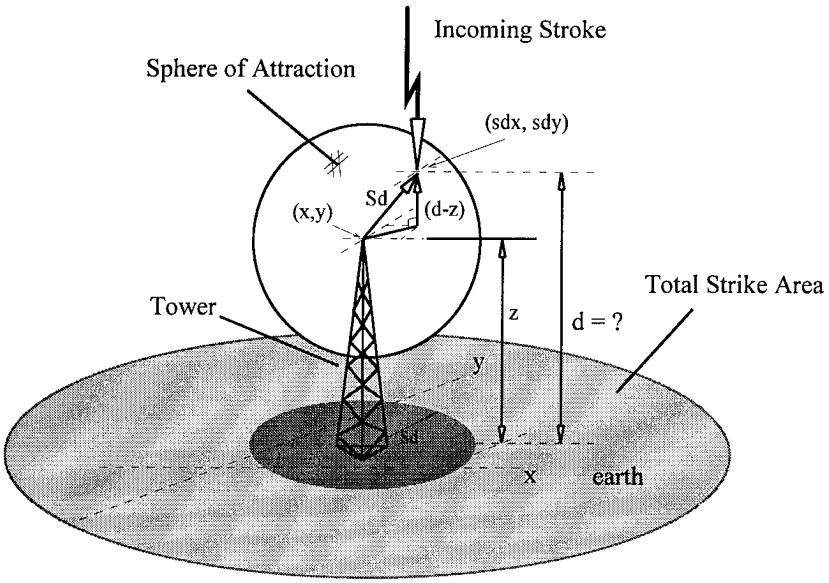



FIGURE-1 SPHERE OF ATTRACTION

## MONTE CARLO TECHNIQUE

A projection of the sphere onto a horizontal plane forms a circular area having a radius equal to the radius of attraction. This area, called the area of attraction, is shown in figure-1. The ratio of the area of attraction to the total strike area equals the conditional probability that lightning will strike the tower given that a strike occurs somewhere in the total strike area. A complication arises when structural points of interest are in the presence of other structural points. In this more complex case the projected area of attraction for a structural point will not be circular but will be irregularly shaped because of the likelihood that a nearby structure will attract the stroke. Competing structures, in effect, steal away strikes from the original structure node. This is shown in figure-2 for the case of one additional node, the tip of a second tower.

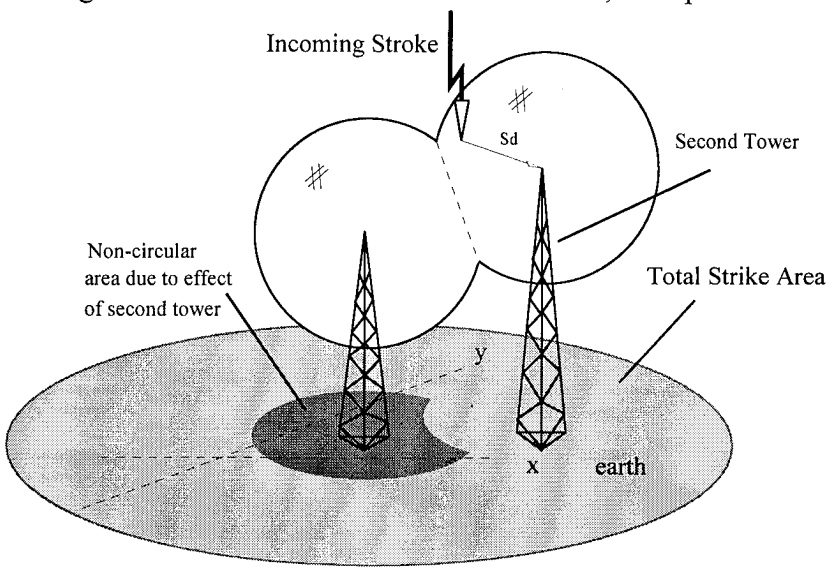



FIGURE-2 TWO INTERSECTING SPHERE'S OF ATTRACTION

The irregular area, shown in figure-2, represents that portion of the total strike area attracting strikes to the tip of the first tower. The ratio of the irregular area to total area represents the conditional probability that lightning will strike the tip of the first tower given that lightning strikes somewhere in the total strike area.

The problem of determining this probability reduces simply to a problem of determining the ratio of areas. Computing the ratio of areas is easily solved by using a direct Monte Carlo simulation technique. Consider an idealized case where all strokes give rise to the exact same strike distance. If strokes are dropped randomly within the total strike area it is only necessary to keep track of the *number* of strokes landing within the irregularly shaped area to the total *number* of strokes generated. The *ratio of strokes which attach* to the tower to the total number of strokes randomly dropped into the strike area in effect *equals the ratio of the two areas*. The more strokes randomly dropped into the strike area the better will be the desired area ratio. This ratio represents the conditional probability that *these fixed amplitude strikes* will attach to the tower. If the *strike current amplitude* for each randomly dropped stroke is not fixed but randomly selected from a *representative probability distribution* then the area of attraction will not only be irregular but the area boundary will blur. This blurring represents the composite of all possible irregular areas due to all possible strike amplitudes as strikes attach to the earth, other grounded objects, or to the tower. The area ratio is nevertheless developed over time and will represent the conditional probability that lightning will strike the tower during an *actual* lightning storm, given that lightning strikes somewhere in the total pad area.

## IMPLEMENTATION

The computer program implements Stahmann's geometrical approach and utilizes many of his assumptions such as the relationship between strike current and strike distance. The specific formulas and probability distributions could, however, be *easily modified* to account for *different* theories and assumptions. The utility of the Monte Carlo implementation is relatively *independent* of the specific distribution or mathematical relationship used.

During the simulation the program generates a configuration vector which defines each lightning stroke. The program generates one stroke after another until the desired number of strokes is reached. A configuration vector defines the following parameters, (1) the (x, y) coordinate location on a plane orthogonal to the incoming stroke direction, (2) the stroke compass angle (azimuth angle), (3) the stroke tilt angle (from zenith), and (4) stroke current intensity converted to strike distance. Lightning strike intensities, and strike directions toward the pad area (defined by the compass and tilt angle) are randomly selected from specific probability distributions. Currently the (x, y) coordinate stroke aim point and compass direction are selected from uniform random distributions, strike intensity levels are selected from either a distribution developed by Stahmann[1] or Maier[2], and strike tilt angles are selected from a $\cos^2$ density function. The compass angle, tilt angle, and strike intensity level can also be set to fixed values in any combination. Each generated stroke drops toward earth and the program determines the strike attach point based on the geometry developed by Stahmann. This process

[1]J.R. Stahmann, "Launch Pad Lightning Protection Effectiveness," Proceedings of the 1991 International Lightning Conference, 31-1, Cocoa Beach, Fl., April 16-19, 1991.
[2]M. Maier, of Computer Science/Raytheon, private communication, 1991.

is repeated over and over, and after each stroke a conditional probability is calculated for the vehicle, pad facilities and the lightning protection system. The SLC40/41 pad area with structures are shown three dimensionally on the computer screen for each incoming stroke. The components which make up the lightning protection system are user definable and easily modified. The program automatically positions the required number of nodes needed to model each tower and wire, taking wire sag into account.

Several enhancements were made to the program to increase execution speed and decrease required simulation time. The program determines, for each randomly generated stroke, if any portion of a tower or wire is within striking distance. If not, none of the nodes representing that tower or wire are tested. Another enhancement was to implement a form of Latin Hypercube Sampling[3]. As an example, strike current is selected from a custom probability distribution. Although the distribution function is sampled randomly during the simulation, it may take many samples before the entire range is covered. In this case we divided the distribution into 100 equal probability intervals. We then generate 100 uniform random numbers to represent probability levels. These 100 numbers are scaled such that exactly one probability value will fall within each of the 100 intervals. These scaled numbers are used with the cumulative probability density function to produce the desired strike current samples. One hundred strike current values at a time are selected this way and stored for program use. To avoid undesired correlation, these 100 samples are not used in the order of generation but are used in random order. Once these 100 samples are used another 100 samples are generated.

## STRIKE GEOMETRY

Early in the development of the program it was desired to provide for side strikes to the pad area. The program was implemented to randomly vary the angle of the incoming strike toward the pad. The basic geometry is shown in figure-3.

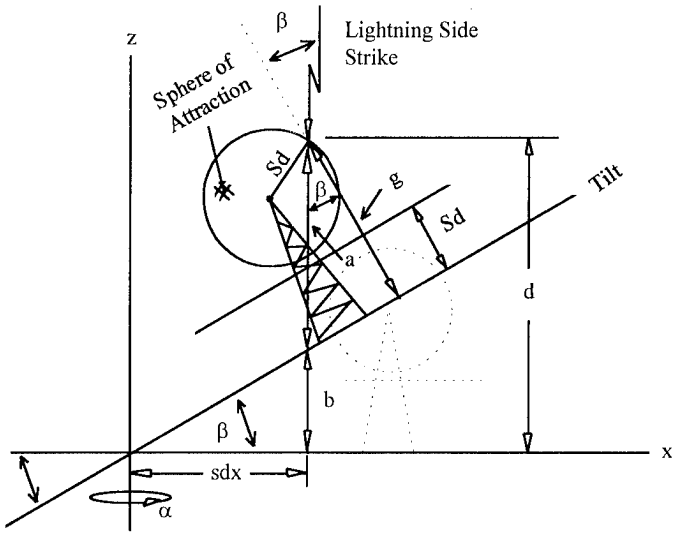



FIGURE-3 SIDE STRIKE GEOMETRY

[3]R.L. Iman, J.M. Davenport, D.K. Zeigler, "Latin Hypercube Sampling (Program User's Guide)," Report SAND79-1473, Sandia Laboratories, Albuquerque, New Mexico, January 1980.

The compass angle '$\alpha$' was allowed to vary uniformly random over the range from 0 to 360 degrees. The tilt angle '$\beta$' of the incoming strike (from zenith) was allowed to vary according to a custom probability distribution ($\cos^2$). Other distributions can easily be substituted.

Our implementation picks an incoming strike direction toward the pad (compass and tilt angle) and holds this orientation for 100 strikes. The exact aim point toward earth for each individual stroke is randomly selected as is the stroke current from the specified distribution. After 100 strikes a new strike angle toward the pad is selected and the process is repeated. The geometry is changed to account for each new strike angle by rotating every point in the model by the appropriate amount.

The nature of the problem remains the same as was described for figure-1. In the case where side strikes are allowed, it is only necessary to calculate the distance 'g' (shown in figure-3) for the node of interest. If 'g' is greater than the striking distance to earth then it is assumed that the strike is to the node otherwise the strike is to earth. Again it is necessary to first calculate the value 'g' for every node in the model. The node corresponding to the largest value of 'g' will be the attach point unless this value is less than the striking distance to earth, in which case the strike will be to the earth. The value 'g' is calculated as follows.

$$g = a\cos(\beta)$$

$$a = d - b$$

$$b = sdx\tan(\beta)$$

$$d = \sqrt{(Sd)^2 - (sdx - x)^2 - (sdy - y)^2} + z = \sqrt{\arg} + z$$

where:

$(x, y, z)$ represent the initial node location

$\beta$ = the side strike angle (from zenith)

## EXAMPLE COMPUTER PROGRAM OUTPUT

During program execution, primary output is to the computer color screen. The screen provides a three dimensional graphics display of the launch pad area including the lightning protection system. Also shown on the screen is the list of the conditional probabilities (in percent) associated with the modeled structures, information on the selected stroke current probability density function, location of the MST, and the analysis mode, either fixed or random.

The fixed analysis mode allows the user to specify a specific compass and tilt angle of the strike toward the launch pad. In the random analysis mode the program automatically picks compass and tilt angles from specific probability distributions. The screen display updates after each 100 strikes to the pad area. After program termination there is an option to store the last color graphic image (containing the summary of results) and a option to print the final results. The printed output contains the same data provided on the screen display in addition to a list of tower and wire locations and wire sag. A typical screen display is shown in figure-4.

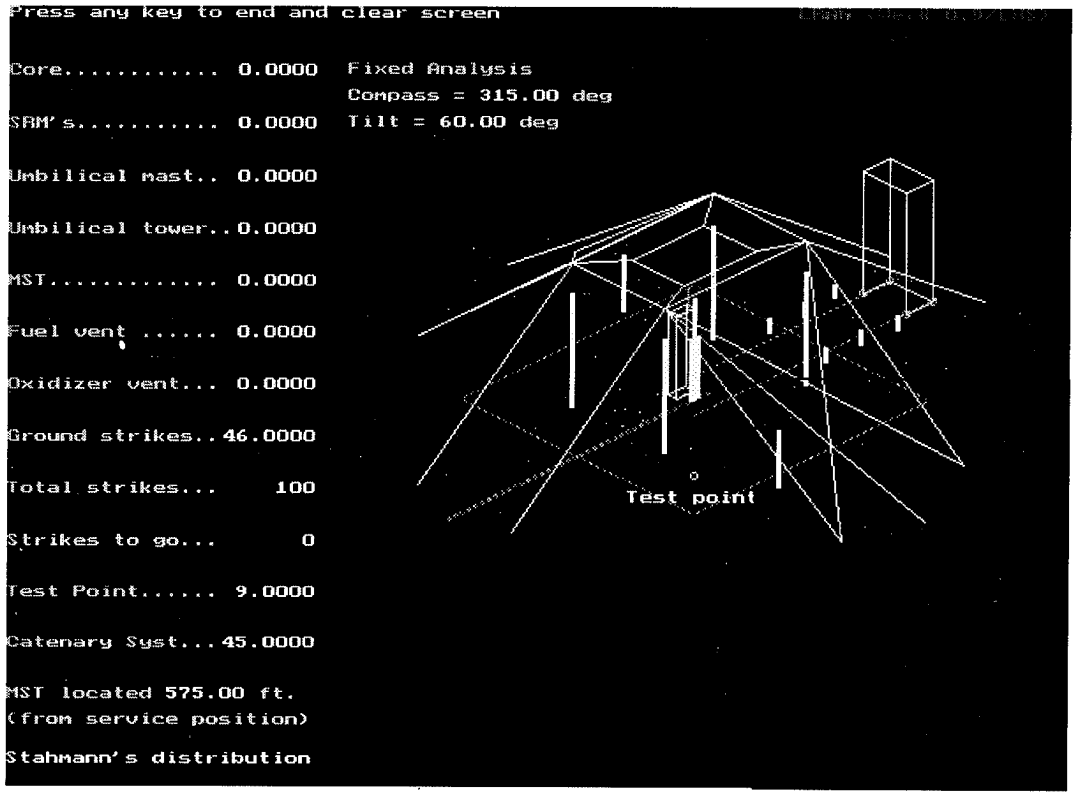



FIGURE-4 SAMPLE SCREEN DISPLAY

## PROGRAM UTILIZATION

Before the lightning protection system design was finalized, our program was used extensively to investigate numerous arrangements of towers and wires making up various proposed lightning protection systems; and after the four-tower system was built, to investigate the relevant lightning attachment probabilities in various situations. The following section presents several examples of the use made of this program. Although these examples address the SLC40/41 launch area, direct lightning attachment concerns for any facility or installations can be addressed by this program with simple modifications.

In the following examples a minimum of 500,000 lightning events were simulated during program execution. In the first example, the MST is in the service position while the other examples place the MST is in the parked position. The actual computer time required depends on the type of computer used and the complexity of the lightning protection system. When run on a 90 MHz Pentium based system the required time to complete 10,000 strikes to the pad area varied from 15 seconds (no lightning protection system) to 58 seconds (for the full four tower 26 wire system installed at SLC40/41).

Note that the results predicted by this program are purely analytical. The SLC40/41 lightning protection system is not instrumented. As a result, actual performance data is not verifiable at this time.

(1) Evaluation of various lightning protection system configurations (probability of attachment to MST at center of launch pad). Use of the program enabled us to thoroughly evaluate the effectiveness of the SLC40/41 lightning protection system. The probability of lightning penetrating the system reduced to an evaluation of the probability of striking the 260 foot tall MST which stood at the center of the launch pad. We therefore used the probability of striking the MST per year as the unit of measure for this effectiveness. If the probability of striking this large steel structure was acceptability low, then the concern over safety of personnel at the launch pad would be greatly reduced.

The complete lightning protection system is supported by four 264 foot tall steel towers each topped with 76-foot insulators. These towers form a rectangle 262 feet by 378 feet. Twelve horizontal catenary wires supported by the insulators are used to intercept lightning and fourteen down conductors conduct current to earth. A simpler lightning protection system was used, before completion of the final system, which consisted of four 290 foot tall steel towers without insulators with only two horizontal wires stretched between towers.

As explained above, we had statistical data which gave the probability of lightning striking the launch pad within a 24 hour period, given that lightning was within 5 nautical miles at any time within that 24 hour period. We used the normal expectancy of 3.32 strikes per year based on launch pad area and flash density of 20 strikes per square kilometer per year. Computer runs were made using the various configurations of the catenary wires and towers of the lightning protection system. Each configuration was tested by simulating 500,000 strikes to the launch pad area. This is the equivalent of approximately 150,000 years of actual lightning strike experience.

This simulation utilized all of the capabilities of the computer program; random strike amplitudes, random azimuth angles, random tilt angles, and random strike locations toward the pad area. Figure-5 shows the results of this study.

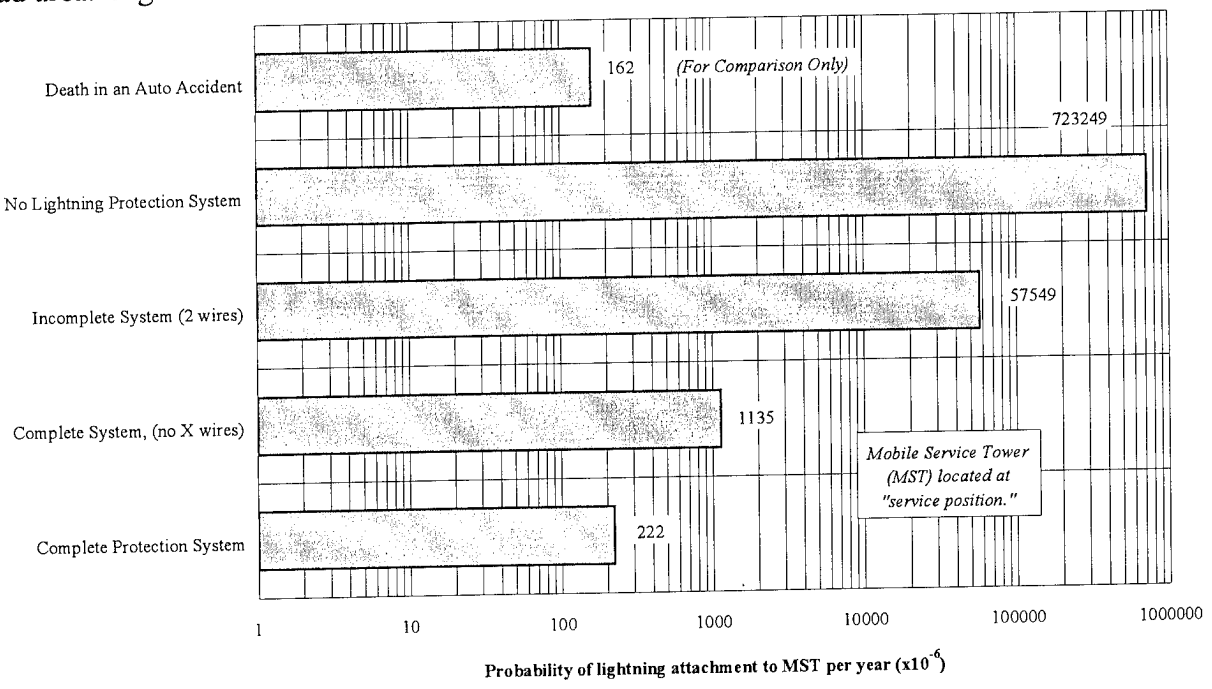



FIGURE-5 SLC40/41 STUDY RESULTS

The short bar on the bottom of the chart shows that the probability of striking the 260 foot MST while it is under the umbrella of the protection system is 222 x $10^{-6}$ per year on the average. The second bar from the bottom shows that building the complete array except for the cross wires on the sloped open sides (see figure-4) degrades the effectiveness by admitting many side strikes which causes the yearly probability of strikes to the MST to rise about five fold.

Protection to the launch pad afforded by the partially completed towers with only two horizontal wires was calculated and is shown on the center bar. It can be readily seen that even this limited protection helped by a factor of twelve fold over the risk realized by operating with no lightning protection system at all. In the latter case the probability of striking the structure is 723,249 x $10^{-6}$.

In order to give meaning to the statistics, a bar is added to the chart giving the probability of a person dying in an auto accident in a year. This number is 162 x $10^{-6}$. The chart thus clearly portrays the effectiveness of lightning protection by comparison with a more familiar everyday statistic.

(2) Attachment probability as a function of lightning forecast. In actual launch situations, Weather Services at Cape Canaveral Air Station (CCAS) provide forecasts (in percent) that lightning will occur within 5 nautical miles of the launch pad within the next 24 hour period. It has been found[4] that the probability that lightning will strike within an area typical of the SLC40/41 perimeter size, within the 24 hour period, is 0.0374 (3.74%). Using the program described in this paper, with the MST in the parked position, the probability of lightning attachment to a Titan-IV booster (two stage core vehicle plus the two SRMs) is found to be 0.000014 (0.0014%) given that lightning strikes somewhere in the pad area. Using simple scaling, the following table can then be generated for assessing the likelihood of vehicle strikes under the present four tower protection system.

Table-1. PROBABILITY OF TITAN-IV STRIKE AT SLC40/41 FOR VARIOUS LIGHTNING FORECASTS WITH MST IN PARKED POSITION

| Forecast (24 hours) ≤ 5 nmi | Probability of Strike ≤ 230 meters | Probability of Vehicle Strike (24 hours) |
|---|---|---|
| 20% | 0.0075 | 1.05 x $10^{-7}$ |
| 40% | 0.0150 | 2.09 x $10^{-7}$ |
| 60% | 0.0224 | 3.14 x $10^{-7}$ |
| 80% | 00299 | 4.19 x $10^{-7}$ |
| 100% | 0.0374 | 5.24 x $10^{-7}$ |

The second column is obtained by multiplying the first column by 0.0374, and the third column is obtained by multiplying the second column by 0.000014, the Titan-IV strike probability obtained by the computer program.

[4]M. Maier, "Update Estimate of the Probability of Cloud-to-Ground Lightning within 230 meters of SLC41", Memorandum for the Record, Computer Sciences/Raytheon, 27 January 1992.

(3) Probability of direct attachments inside SLC40/41 with the MST in the parked position. In this example, the probabilities of Titan-IV strikes are calculated with and without the SLC40/41 protection system. The probability of direct attachment to any object can be obtained from the product:

$$p = p_1 p_2 f_d$$

where $p_1$ is the frequency of occurrence of a flash with a particular amplitude and is equal to unity if all current amplitudes are included. The value $p_2$ is the probability of a strike, given one flash falling within the area in question. This probability is what our program provides, and is found to be 0.000014 with the protection system in place, and equal to 0.0139 without the protection system. The value $f_d = 3.32$ is the flash density per year falling within SLC40/41, based on 20 strikes per year per square kilometer for this area. The example shows that the annual probability of lightning hitting a Titan-IV is 0.046 (4.6%) before the protection system was installed. Another way of realizing the benefit of the protection system is to say that the probability of strike to a Titan-IV has been reduced from once in about 22 years to about once in 21,500 years with the protection system in place.

(4) Probability of induced current/EM field reaching a predetermined level. Many payloads have pre-determined levels of tolerance for sensitive parts, derived from scattering/coupling analysis and circuit susceptibility analyses. Although the probability of direct strike to a Titan-IV under the protection system is very small, the induced EM environment from re-radiated emissions following a direct strike to the protection system must be assessed. Separate analysis has determined that a direct strike of 74 kA peak current to the SLC40/41 protection system induces the maximum tolerable stress on selected circuits. It is highly desirable to know the probability of this occurrence for risk management. The same probability expression ( $p = p_1 p_2 f_d$ ) is used with different component probability values. The probability of a 74 kA strike occurring at CCAS, based on Maier's summer 1990 LLPS data is $p_1 = 0.01$. The probability calculated by our program that a 74 kA strike will hit the SLC40/41 protection system is $p_2 = 0.677$ (with the MST in the parked position), given that one flash falls in the SLC40/41 pad area. The flash density per year falling within the SLC40/41 area is $f_d = 3.32$ based on 20 strikes per year per square kilometer for this area. Therefore $p = 0.0225$ in one year, which can be translated to about once in 44 years.

## CONCLUSIONS

The usefulness of the computer program described in this paper and the benefit of the protection system at SLC40/41 are shown through examples, and the easy extension of this program to any facility is evident from the description of this program. However, the validity of the program and the effectiveness of the protection system have to be verified with actual lightning measurements.

# SESSION 10B
# LIGHTNING, GENERAL
# CHAIRPERSON: JOHN C. WILLETT

# COMPARISON OF LIGHTNING MAPPING WITH OPERATIONAL TIME-OF-ARRIVAL AND INTERFEROMETRIC SYSTEMS

Vladislav Mazur
NOAA/National Severe Storms Laboratory, Norman, OK 73069
Telephone (405) 366-0406 FAX (405) 366-0472

Earle Williams
Massachusetts Institute of Technology, Cambridge, MA 02139
Telephone (617) 981-3744 FAX (617) 981-0632

Robert Boldi
Massachusetts Institute of Technology/Lincoln Lab., Lexington, MA 02173
Telephone (617) 981-2293 FAX (617) 981-0632

Launa Maier
NASA/ Kennedy Space Center, FL 32899
Telephone (407) 867-4409 FAX (407) 867-2848

David E. Proctor
P.O. Box 193, Honeydew 2040 Republic of South Africa

## ABSTRACT

The comparison of lightning mapping with operational Time of Arrival (NASA/LDAR) and the Interferometric (French ONERA-3D) systems is made both on a storm scale and for individual flashes using lightning observations in central Florida. Although somewhat limited in scope, the analysis shows a significant difference in representation of lightning radiation with each mapping technique, especially noticeable in the radiation duty cycle and spatial structures. On the time scale of the entire flash, the LDAR data show high duty cycle of radiation sources translated into spatial continuity and a three-dimensional structure of the lightning flash. The ONERA-3D data show low duty cycle translated into spatial discontinuity and more of a two-dimensional structure. The most striking distinction between radiation sources mapped by the two systems is in propagation velocities which range between $10^4$ and $10^5$ m $s^{-1}$ for LDAR system, and $10^7$ and $10^8$ m $s^{-1}$ for ONERA-3D. We infer that the difference in results is due to the fact that most of the radiation sources mapped with LDAR were associated with negative breakdown processes typical of slowly propagating leaders, while most of the radiation mapped by ONERA-3D is produced by fast intermittent processes typical of dart leaders and K-changes. Thus each operational system emphasizes different parts of the lightning flash, and neither of them maps the entire flash.

## INTRODUCTION

Lightning studies historically have advanced primarily through the results of various field observations. Starting nearly two decades ago, Time-Of-Arrival (TOA) and interferometric (ITF) radiation mapping techniques presented the opportunity to study the dynamics of lightning with a high degree of spatial and temporal resolution by mapping it initially in two-dimensions and later three-dimensionally. These techniques are responsible for the significant progress achieved in identifying lightning radiation processes. This together with the new results obtained from in-situ measurements of aircraft- and rocket-triggered lightning have further stimulated the search for the physical concepts that bridge experimental results with models of lightning discharge.

With heavy reliance on experimental data in lightning research, concern arises about an instrument-biased approach in interpretations of physical processes resulted from the limitations of observational techniques. The objective of this paper is to demonstrate the possibilities of the operational TOA and ITF mapping systems in representation the entire lightning flash. This is done through analysis of simultaneous measurements of the same lightning flashes, and identification of these observations with specific physical processes.

## TIME OF ARRIVAL AND INTERFEROMETRIC TECHNIQUES

The TOA uses this difference in arrival times of electromagnetic waves at different antennas to calculate the position of the radiation source at the intersection of hyperbolic surfaces. Maximum precision in defining a time difference is achieved if the source impulses are delta functions. The preservation of approximate delta function behavior is achieved through the use of wide bandwidth radio receivers. In radio interferometry, the differential phase at pairs of antennas is used to calculate the arrival angle of an electromagnetic wave radiated from the source. The accuracy in determining the phase difference desired for arrivals at two receivers is best defined for narrow band CW signals with approximate delta function behavior in the frequency domain.

In TOA, the antennas are positioned on a base line of tens of km, in order to obtain the time of arrival difference greater than the sampling interval of the system [1]. In ITF, the baseline is set up in wavelengths and half-wavelengths in order to resolve the ambiguity of the arrival angle [2].

From observations obtained with the research quality TOA [3] and ITF systems (e.g., Richard et al. [4]), we know that UHF-VHF lightning radiation exhibits two modes of signals: (1) a discontinuous series of pulses at low repetition rate (1-100 pulses $ms^{-1}$), with individual pulses of approximately 1μs duration; and (2) a more continuous noise-type radiation lasting tens to hundreds of μs, also called Q-trains (Fig. 1). These observations and the principles of operation of the two systems discussed above suggest the following. The TOA system (1) is best suited for mapping the individual, spaced pulses of short duration (a few μs long) in a low rate radiation process, (2) resolves pulses widely separated in space and occurring at time intervals greater than the sampling period, but (3) can not discern individual pulses

in noise-like Q-trains. The ITF system (1) is best suited for mapping the Q-train sequences (they are characterized by continuity of phase), but (2) cannot resolve two simultaneous processes separated in space (e.g., two Q-train sequences or one Q-train and a discontinuous sequence of pulses) [5]. Illustrations of the concepts of the TOA and the ITF systems are presented in Figs. 2 and 3.

## LIGHTNING MAPPING OF THE SAME STORM WITH THE KSC/LDAR AND THE ONERA/3D SYSTEMS

The only data set of lightning measurements from the same storm using both techniques was obtained by the 3-dimensional TOA system called Lightning Detection and Ranging (LDAR) [1] at NASA/KSC, and by the French interferometer, ONERA-3D [6], during the summers of 1992 and 1993 near Orlando, Florida. The LDAR is an operational system with real time display of 3-dimensional locations of lightning radiation sources. The ONERA-3D is an experimental system that calculates 3-dimensional locations in post analysis, but works like an operational system for 2-dimensional locations of radiation sources (we conditionally identify the ONERA-3D as an operational system ). Both systems have data acquisition schemes much cruder (e.g., greater data window, higher signal threshold) than that suitable for scientific studies, in order to decrease the amount of data processed in real time.

The measurements we analyze here, therefore, although indicating important differences in the lightning processes detected by the two systems (TOA and the interferometer), fall short of exploring the full capabilities of each technique. The technical characteristics of both operational systems are summarized in Table 1.

Table 1. Specifications of LDAR and ONERA 3D systems

| *Parameter* | *LDAR* | *ONERA 3D* |
|---|---|---|
| Operating frequency | 63 MHz | 110-118 MHz |
| Data band width | 6 MHz | 1 MHz |
| Data window | 82 μs | 23 μs |
| Data collection rate (maximum) | $10^4$ events/second | $4x10^3$ events/second |
| Number of stations | 6 remote, 1 central | 2 remote |
| Minimum detectable signal | -79 dBm | -75 dBm |
| Baseline | 8-9 km average | 40 km |

Operational characteristics of each system are chosen to take advantage of a given technique, e. g., the amplitudes of single pulses are higher at 63 MHz than at 110 MHz which makes 63 MHz preferable for the TOA system.

The height/time plots of lightning radiation sources from the storm on August 14, 1992 are presented in Fig. 4, with height increments dz = 500 meters and time increments dt = 90 seconds, the same for both data sets. The comparison

reveals that (1) radiation sources mapped by LDAR do not reach the ground, while those mapped by ONERA-3D do; (2) the altitudes of radiation sources in the LDAR data extend up to 20 km, while those in ONERA-3D remain below 15 km; and (3) the region of greater source density in the LDAR data is between 6 and 12 km, with its maximum at approximately 9 km, while the same region in the ONERA-3D data is situated between the ground and 7 km, with its maximum at approximately 5 km. A similar conclusion emerges from plots for the storm on August 31, 1992 (Fig. 5). The locations of regions with a high radiation source density in the X-Y plane plots are different for both data sets as well (Fig. 6).

We may understand the differences in the height-time and X-Y plane plots described above through comparison of the radiation maps of individual flashes. The LDAR and ONERA-3D records, with synchronized timing and positions for each radiation source, were available for the storm near Orlando, Florida on August 28, 1993, between 18:00 and 19:15 UT. Without available correlated ground-based electric field and optical measurements that are essential for interpretation of the nature of radiation sources, we are able to make only a qualitative comparison of two sets of observations. However, even this limited analysis is valuable in view of the simultaneous observations with both mapping systems.

Out of 41 flashes detected both by LDAR and ONERA-3D during the period of 1 hour and 15 min, nine are identified as cloud-to-ground (CG) flashes by the National Lightning Detection Network (NLDN). The first noticeable feature in all height-time plots is the contrast between the persistent radiation mapped with LDAR and the rather sporadic radiation mapped with ONERA-3D (Figs. 7, 8, 9). LDAR also systematically detects radiation before ONERA-3D. The short-lived (a few ms) radiation sequences in the ONERA-3D plots are separated by intervals lasting from several ms up to tens of ms. Some radiation sequences extend toward the ground, e.g., in CG flashes (Fig. 8). In most sequences for this storm, the ONERA-3D system shows the vertical extent of this radiation to altitudes up to 20 km, which is unusual for LDAR data. (We cannot provide an explanation of this effect.) LDAR maps the radiation sources from the same lightning flashes contained inside the cloud and not reaching the ground. The plots in the X-Y plane for LDAR data show tree-like structures, while the interferometric images look like clusters of sources that are only occasionally organized into channels.

The LDAR plots the radiation sources of most lightning flashes, both intracloud (IC) and CG types, as stratified within one or two horizontal layers. Eight CG flashes and four non-CG flashes have radiation sources between 5 and 7.5 km altitude, and one CG flash had sources descending from 10 to 5 km. Among other non-CG flashes we found that (1) 10 flashes had radiation sources within two layers at altitudes of 5-7.5 km and 10-13 km, (2) 13 flashes had radiation only at a higher layer, between 7.5 and 10 km, and (3) 3 flashes show radiation sources descending from 10 km to 5 km.

## INTERPRETATION OF RADIATION MAPPING OBTAINED WITH TWO TECHNIQUES

NATURE OF VHF LIGHTNING RADIATION- VHF lightning radiation is, in general, a superimposition of impulsive and noise-like emissions (see Figure 1).

These two types of emission occur either concurrently or separately within the life cycle of a flash. As shown by Friel [7], the concept of the duty cycle of a radar is well suited for describing lightning radiation. (Friel identified the radiation duty cycle as the number of intervals above a given signal power threshold divided by the total number of intervals, thus making the duty cycle a function of power.) Friel calculated that with a 100 μs integration time, the duty cycle for IC and CG flashes varies from 60 to 65%, indicating that lightning at VHF radiates energy throughout a significant portion of the duration of the flash (Fig. 10, 11). The distant flashes show a much smaller duty cycle at the same power level (usually less than 5%) (Fig. 12), which indicates that much of the energy radiated by lightning at VHF is weak and will not be detected unless a high gain antenna is used. The LDAR depicts lightning flash as high duty cycle radiation similar to that shown in Figs. 10-11. As opposed to this, the ONERA-3D depicts lightning as a sequence of intermittent processes, i.e. as low duty cycle radiation similar to that shown in Fig. 12.

Let us examine what is known about the nature of lightning radiation processes from previous studies. Among the sources of strong VHF radiation detectable with the interferometer are (1) fast negative breakdown processes such as stepped and dart leaders, and K- changes, and (2) positive breakdown processes that follows return strokes in negative CG flashes and exhibits RF signature of Q-trains [8]. Continuously propagating positive leaders do not emit sufficiently strong VHF radiation to be detected by either the TOA system [9] or the interferometer [10]. TOA systems do not map well radiation of the Q-train type associated with fast leaders, but locate radiation sources of slow negative breakdown processes at the tip(s) of propagating negative leaders [9]. This radiation is in a form of sequences of separated pulses and is weaker than that of fast negative breakdown processes. This fact is confirmed by the airborne records of current pulses with a characteristic rate of pulses in slow negative leaders during the lightning attachment to aircraft [11]: current pulses during lightning initiation on an aircraft (slow negative breakdown) have average amplitudes twice smaller than that from fast streamers (fast negative breakdown) occurring much later and traversing the channel in intervals of tens of ms.

DOUBLE-ENDED "LIGHTNING TREE" - In order to interpret the difference in the data sets obtained with two systems, we shall examine the nature of lightning radiation by applying the concept of a bi-directional "lightning tree" consisting of a positive branched leader on one end and a negative branched leader on the other [12, 13, 14]. Mazur and Ruhnke [15] speculate that the "lightning tree" develops asymmetrically because of the difference in the physical mechanisms of propagation for positive and negative leaders. During lightning initiation in the region of maximum potential gradient, both positive and negative leaders progress quasi-simultaneously (within milliseconds) into cloud regions with ambient electric fields of a polarity opposite to that of each leader. Mazur and Ruhnke [15] suggest that in the later stages of a lightning flash, development may become uni-directional as a result of current cutoff in the conductive channel that connects the positive and negative ends of the lightning tree. The leader extension ceases when it enters a cloud region where the potential gradient at the leader's tip is less than that required for sustained propagation. A negative breakdown at the dormant end (as opposed to

active end) of the positive leader initiates a recoil streamer traversing the old leader channel toward its origin. For a few milliseconds, this constitutes a renewal of bi-directional leader development.

The essential factor in maintaining a lightning discharge is a continuing breakdown, at the tip of positive, negative, or both ends of the lightning tree, that extends the channel and its branches into new cloud regions. Owing to the different natures of positive and negative leader breakdown, lightning radiation may also differ significantly in the signal type, power, and frequency band. However, radiation of some kind (impulsive, noise-like, or both) is always present during the entire flash; so, in a wide frequency band and at close range, lightning radiation should have a duty cycle close to 100%. (We realize, however, that because of a limited speed of data processing, depicting the 100% duty cycle in radiation sources mapped with any technique is not possible.)

## DISCUSSION

We are well aware that both the TOA and interferometric systems, in their scientific versions and under favorable circumstances may produce more detail in images of lightning processes than those obtained with operational systems like the LDAR and ONERA-3D. The comparison attempted here of data sets obtained simultaneously with the two techniques is the first of its kind and is limited one. The general topic of technical possibilities of the TOA and interferometric mapping techniques is out of the scope of this paper. A limited analysis of two data sets shows a significant difference in the representation of lightning with each mapping system, especially noticeable in the radiation duty cycle. The main contributor to this difference in lightning representation is the difference in two mapping techniques.

The duty cycle concept has been found to be important in understanding the behavior of lightning. A continuous duty cycle in time (in RF time series) translates to a continuous duty cycle in space (in RF maps). On the time scale of the entire lightning flash (hundreds of milliseconds) the LDAR data show more persistence and continuity than the ONERA interferometric data.

A research grade TOA system with a large dynamic range (e.g., Proctor[3]) is capable of mapping radiation associated with a breakdown at the tip of a negative leader. Such negative breakdown emits pulses slowly, usually less than 1,000 per second, and constitutes either (1) a progression of the negative end of the lightning tree into the region above 7.4 km in the case of IC flashes, or (2) an initial breakdown in negative CG flashes near 5.3 km [16]. Speeds of negative leader progression range from $3.0 \times 10^4$ m $s^{-1}$ to $4.2 \times 10^5$ m $s^{-1}$, with median value of $1.3 \times 10^5$ m $s^{-1}$ [9]. By Proctor's estimate, almost half of all flashes have their origins higher than 7.4 km AMSL. From numerous in-situ measurements of the ambient electric field in thunderstorms (see review in Williams, [17]), we know the region above 7.5 km corresponds to the upper positive charge region. Therefore, we infer that horizontally stratified radiation sources at altitudes above 7.5 km depicted by LDAR (its dynamic range is the same as Proctor's system) are produced by emission from

the tips of the negative leader extending at low speed (~ $10^5$ m $s^{-1}$, see Fig. 13) on a continuous basis.

The nature of radiation sources shown by the LDAR as propagating between 5 and 7.5 km altitude is not as obvious as the nature of those at greater altitude (Fig. 4a). At the mature stage of a storm, the main negative space charge is situated between 5 and 7.5 km (see Williams [17]). Therefore, any continuing radiation process in this layer and during this storm stage that propagates away from the flash origin should be associated with a positive leader. On the other hand, during storm decay, a layer of a positive space charge forms near the melting level and the radar "bright band", at 4-5 km of altitude [18]. (From observations with the interferometer, "spider lightning" was found to be a negative leader propagating horizontally in the vicinity of the radar bright band [5], i.e., within a positive space charge region.)

Extensive studies of CG flashes (e.g., Krehbiel [19]) have shown that the intra-cloud development of CG flashes between return strokes is associated with the horizontal progression of the flash away from its origin. This has been interpreted as the progression of a positive leader into new regions of negative space charge. Radiation sources depicted by the LDAR at the 5-7.5 km layer seem to be behaving similarly to positive leaders, because they move away from the flash origin. However, we do not have evidence, supported by ground electrical measurements, to draw a definite conclusion. In addition, although the TOA system does map the radiation burst of the positive breakdown at the end of the return stroke [Proctor, 1988], there is no indication that it maps the continuing positive breakdown at the tip of the positive leader. Thus, our analysis raises a question, which remains unresolved, about the nature of radiation sources stratified between 5 and 7.5 km altitudes and depicted by LDAR. We expect that future synchronized lightning observations with both systems, conducted to minimize the effect of different locations of each system and to obtain complementary electrical and optical measurements will be able to provide some answers.

The intermittent radiation bursts (Q-trains) seen with ONERA-3D occur in time intervals typical for dart leaders and K-changes (< 100 ms), propagate at high speed (>$10^7$ m $s^{-1}$, see Fig. 13), and are interpreted as fast negative streamers traversing ionized channels developed earlier in the flash by slow extension. It is well documented that these processes are mapped by research grade interferometric systems [20].

The most striking distinction between radiation sources mapped by the two systems is illustrated by the plot of propagation velocities in Figure 13. Velocities ranging $10^4$-$10^5$ m $s^{-1}$ correspond to leaders with slow negative and positive breakdown at their tip, while those between $10^7$ and $10^8$ m $s^{-1}$ are signatures of Q-train in fast negative streamers and dart leaders.

According to the picture of the bi-directional lightning tree [13], fast negative streamers originate somewhere at the positive end of the tree and traverse previously established channels of positive leaders toward the lightning origin. It is therefore likely that the ONERA-3D system depicts the lightning flash as an intermittent radiating process of low duty cycle that occurs mainly in the middle

and low parts of the storm. None of the interferometers, however, has produced maps of flashes that emit pulses slowly, up to 1,000 pulses per second, which is characteristic of the breakdown at the tip of the propagating negative leader. There is also no evidence that either the interferometric or the TOA systems map radiation from positive leaders, probably because of the low amplitude of their emission in the VHF band, as indicated by the measurements of long gap sparks [21].

We conclude, therefore, that an operational interferometer, like ONERA-3D, maps fast intermittent processes in negative CG flashes, but does not map the continuously developing intracloud processes in IC and CG flashes. Since Q-trains appear only in a subset of previously formed channels, it seems that an operational TOA system is better suited for comprehensive maps of the lightning tree.

We consider the analysis presented here only as a preliminary one. Additional experiments in comparison of TOA and interferometric techniques in lightning representation are still necessary.

**Acknowledgments.** This work was supported in part by the MIT/Lincoln Laboratory Grant CX-16576 F19628-90-C-0002. We are grateful to Mark Weber for this support. We also appreciate illuminating discussions with Pat Friel and assistance from Pierre Laroche with ONERA-3D data used in this work.

**References**

1. Lennon, C. L, and L. Maier, Lightning mapping system, Proc. 1991 International Aerospace and Ground Conference on Lightning and Static Electricity, Cocoa Beach, Florida, April 16-19, 1991, NASA Conference publication 3106, pp. 89-1 to 89-10.

2. Rhodes, C. T., Interferometric observations of VHF radiation from lightning, Ph.D. Thesis, New Mexico Institute of Mining and Technology, Socorro, 1989.

3. Proctor, D. E., A hyperbolic system for obtaining VHF radio pictures of lightning, J. Geophys. Res., 76, 1478-1489, 1971.

4. Richard, P. , A. Delannoy, G. Labaune, and P. Laroche, Results of spacial and temporal characterization of the VHF-UHF radiation of lightning, J. Geophys. Res., 91, 1248-1260, 1986.

5. Mazur, V., X. M. Shao, and P. R. Krehbiel, "Spider" intracloud and positive cloud-to-ground lightning in the late stage of a Florida storm, Proc. 1994 Intl. Aerospace and Ground Conference on Lightning and Static Electricity, May 24-27, 1994, Mannheim, Germany, pp. 33-41, 1994.

6. Laroche, P., A. Bondiou, P. Blanchet, J. Pigere, 3D VHF mapping of lightning discharge within a storm, Publication ONERA, N° 1994-127.

7. Friel, P. J., VHF lightning sensors and field measurements: an application to airport weather monitoring, Ph.D. dissertation, Tufts University, June 1993.

8. Shao, X. M., P. R. Krehbiel, R. J. Thomas, W. Rison, Radio interferometric observations of cloud-to-ground lightning phenomena in Florida, J. Geophys. Res., 100, 2749-2783, 1995.

9. Proctor. D. E., R. Uytenbogaardt, and B.M. Meredith, VHF radio pictures of lightning flashes to ground, J. Geophys. Res., 93, 12,683-12,727, 1988.

10. Krehbiel, P. R., X. M. Shao, M. Stanley, G. Gray, S. McCrary, R. Scott, J. Lopez, C. Rhodes, and D. Holden, Interferometer observations of natural and triggered lightning at Langmuir Laboratory, oral presentation at 1994 Fall AGU meeting, San Francisco, Dec. 5-9, 1994.

11. Burket, H. D., L. C. Walko, J. Reazer and A. Serrano, In-flight lightning characterization program on a CV-580 aircraft, Report of AF Wright Aeronautical Lab., AFWAL-TR-88-3024, June 1988.

12. Kasemir, H. W., Qualitative Uebersicht ueber Potential-, Feld, und Ladungsverhaltnisse bei einer Blitzentladung in the Gewitterwolke, in Das Gewitter, edited by H. Israel, Akad. Verlags. Ges. Geest und Portig K. -G., Leipzig, Germany, 1950.

13. Mazur, V. A physical model of lightning initiation on aircraft in thunderstorms, J. Geophys. Res., 94, 3326-3340, 1989.

14. Moreau, J. P., J. C. Alliot, and V. Mazur, Aircraft lightning initiation and interception from in-situ electric measurements and fast video observations, J. Geophys. Res., 97, 15,903-15,912, 1992.

15. Mazur, V. and L. H. Ruhnke, Common physical processes in natural and artificially triggered lightning, J. Geophys. Res., 98, 12,913-12,930, 1993.

16. Proctor, D. E., Regions where lightning flashes began, J. Geophys. Res., 96, 5099-5112, 1991.

17. Williams, E, The tripole structure of thunderstorms, J. Geophys. Res., 94, 13,151-13,167, 1989.

18. Stolzenburg, M., T. C. Marshall, W. D. Rust, B. F. Smull, Horizontal distribution of electrical conditions across the stratiform region of a mesoscale convective system, Monthly Weather Review, 122, 1777-1797, 1994.

19. Krehbiel, P. R., M. Brook, and R. A. McCrory, An analysis of the charge structure of lightning discharges to ground, J. Geophys. Res., 84, 2432-2456, 1979.

20. Rhodes, C. T., X. M. Shao, P. R. Krehbiel, R. J. Thomas, and C. O. Hayenga, Observations of lightning phenomena using radio interferometry, J. Geophys. Res., 99, 13,059-13,082, 1994.

21. Bondiou, A. , personal communication, 1992, unpublished article "Electromagnetic characterization of intracloud lightning. Comparison with laboratory experiments."

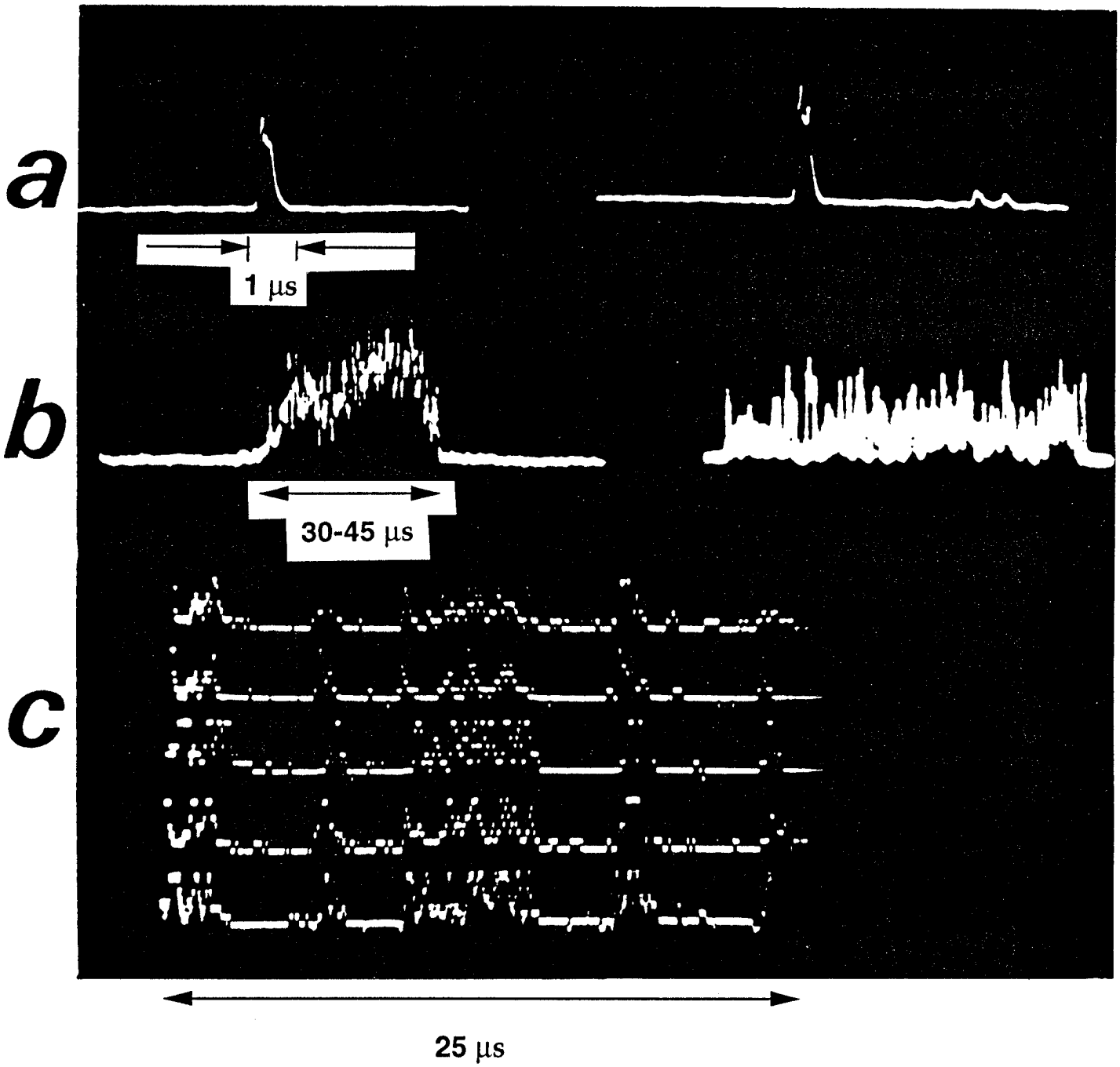
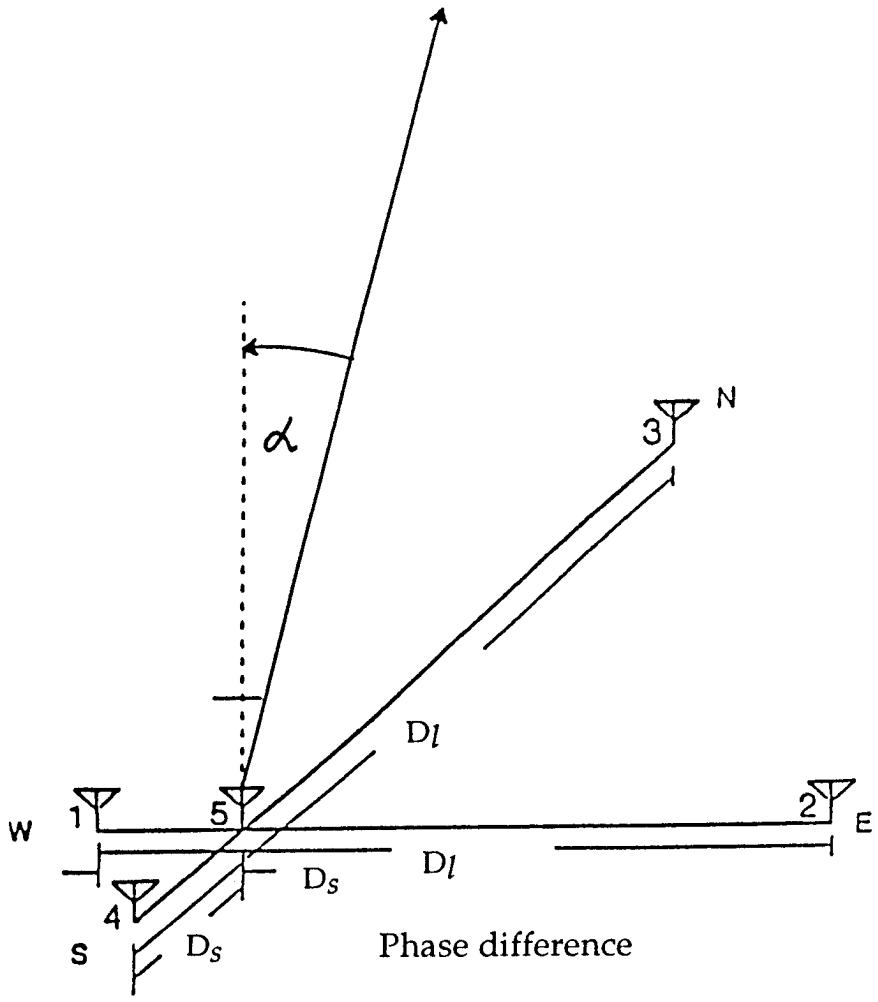



Figure 1. Types of VHF lightning radiation signals (adapted from Proctor, 1988) (a) individual pulse or one in a slow rate pulse series, (b) noise-type radiation, also called Q-train, and (c) series of slow-rate pulses recorded at five different antennas.




Phase difference

Closest antenna: $\Delta\phi_{short} = \frac{2\pi D_s}{\lambda} Sin\alpha$

Farthest antenna: $\Delta\phi_{long} = \frac{2\pi D_l}{\lambda} Sin\alpha$

Figure 2. The concept of interferometric system for lightning mapping with expressions for phase differences at one of two orthogonal antennas.

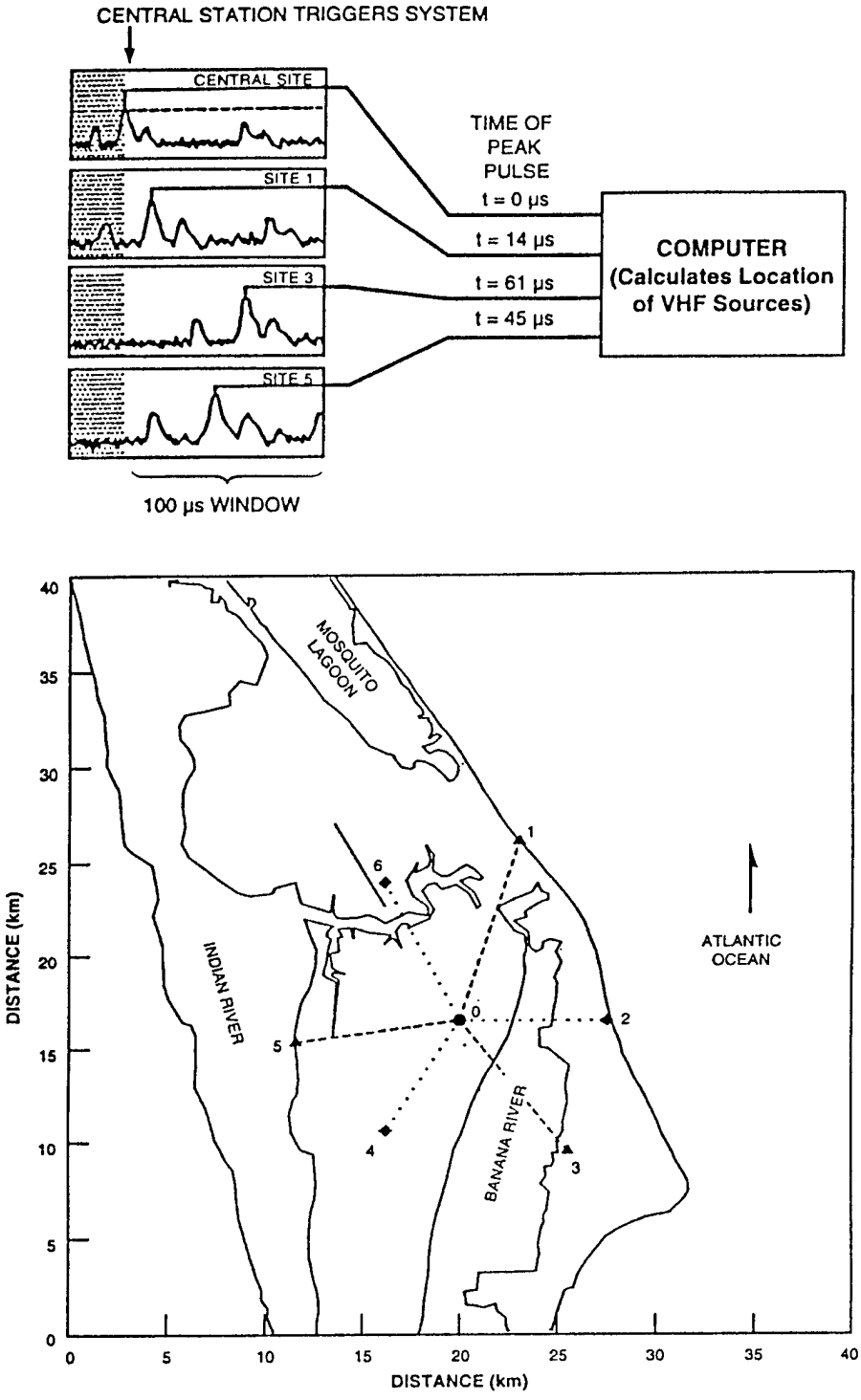



Figure 3. The concept of the Time-Of-Arrival system for lightning mapping. Signal processing scheme and antenna locations for LDAR system at NASA/Kennedy Space Center.

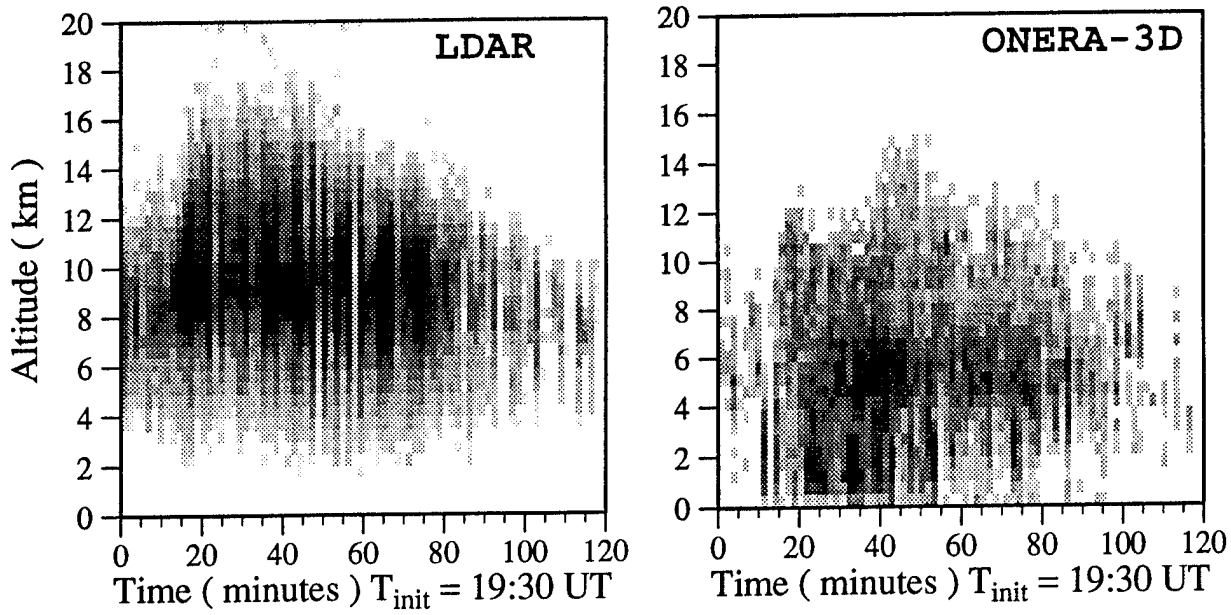



Figure 4. The height-time plot of radiation sources mapped by (a) the LDAR, and (b) the ONERA-3D systems for the storm on Aug. 14, 1992. Here and in Figs. 5 and 6, the gray scale of source density per dz=500m and dt=90 s, with different incremental values for ONERA-3D and LDAR, covers the range of radiation sources obtained by each system.

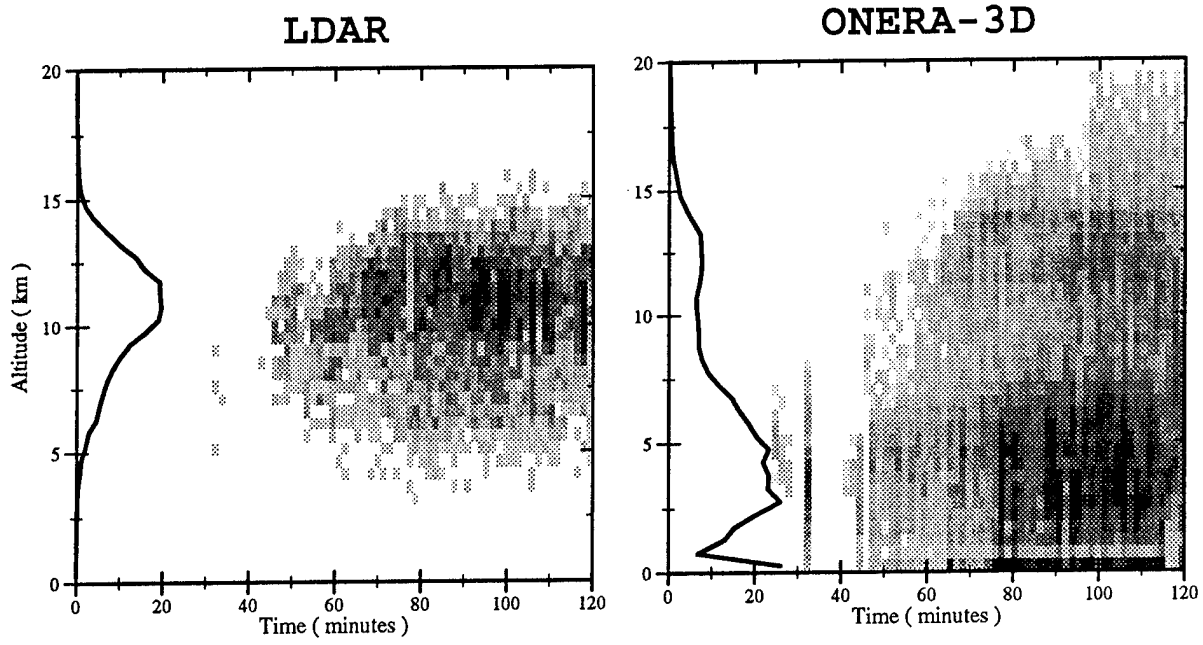



Figure 5. The height-time plot of radiation sources mapped by (a) the LDAR, and (b) the ONERA-3D systems for the storm on Aug. 31, 1992.

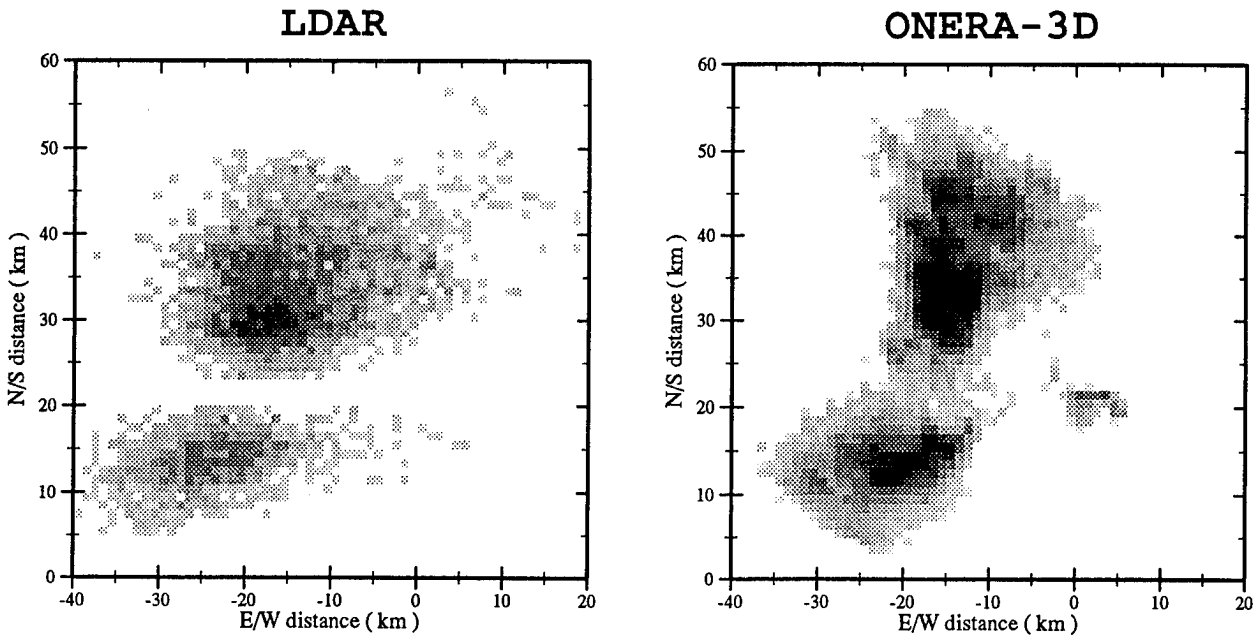



Figure 6. The X-Y plane plots of radiation sources mapped by (a) the LDAR, and (b) the ONERA-3D systems for the storm on Aug. 31, 1992.

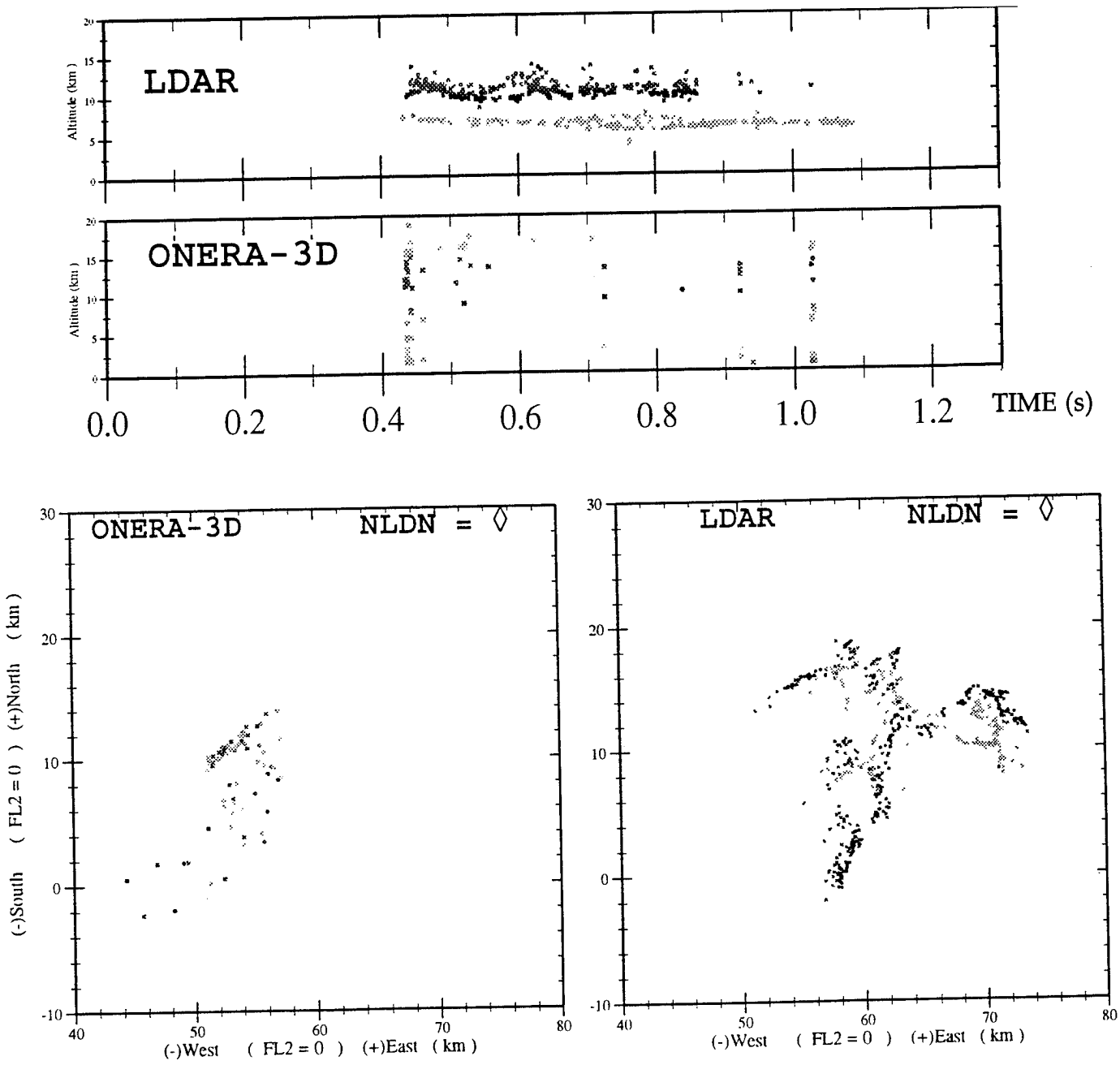



Figure 7. The height-time and X-Y plane plots of radiation sources by the LDAR and ONERA-3D systems for the intracloud flash at 18:04:32 UT, August 28, 1993. Dark and light dots mark sources located at the upper (above 10 km) and lower (5-7 km) layers, respectively.

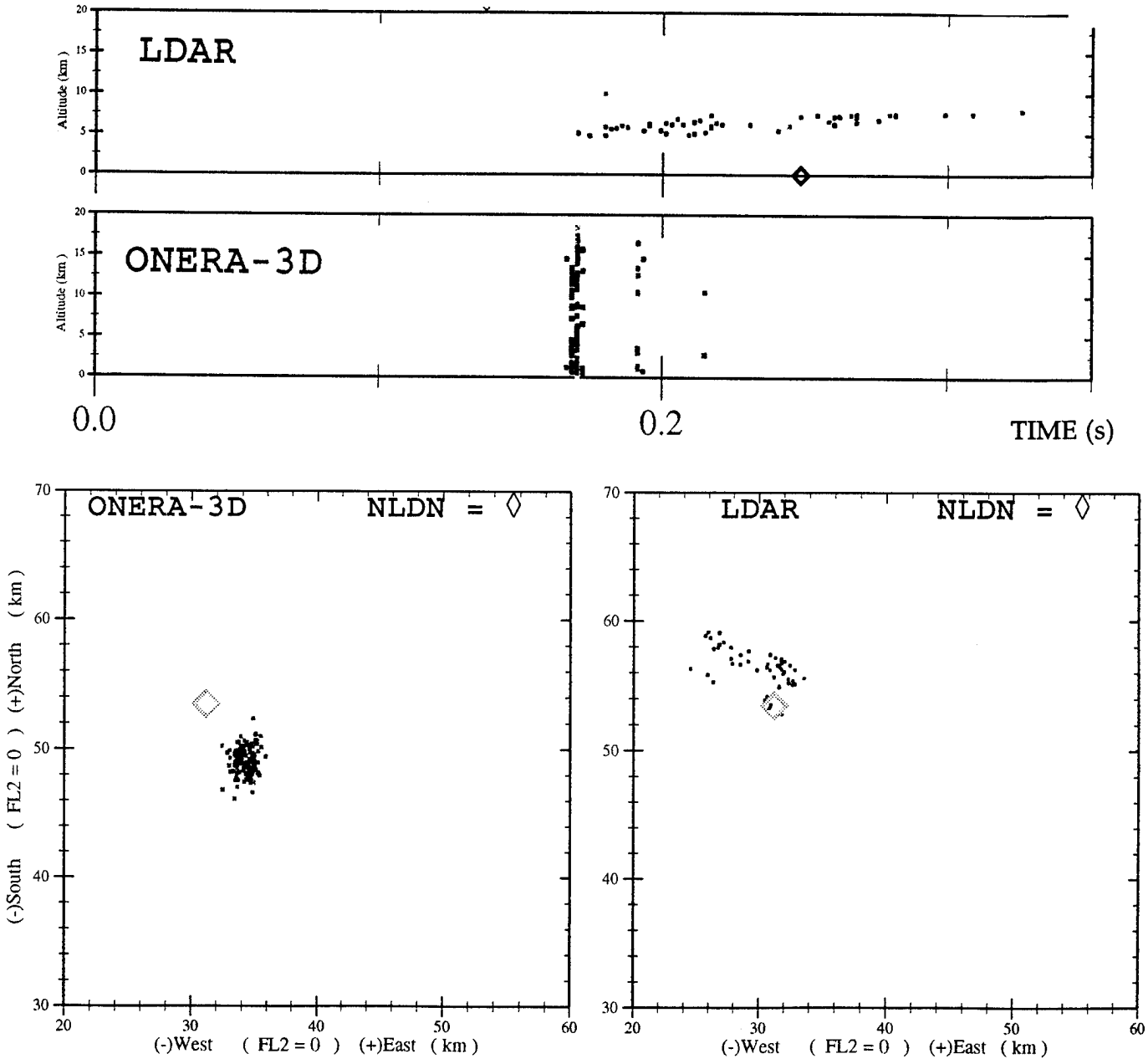



Figure 8. The same as Fig. 7, but for the cloud-to-ground flash at 18:56:43 UT, August 28, 1993.

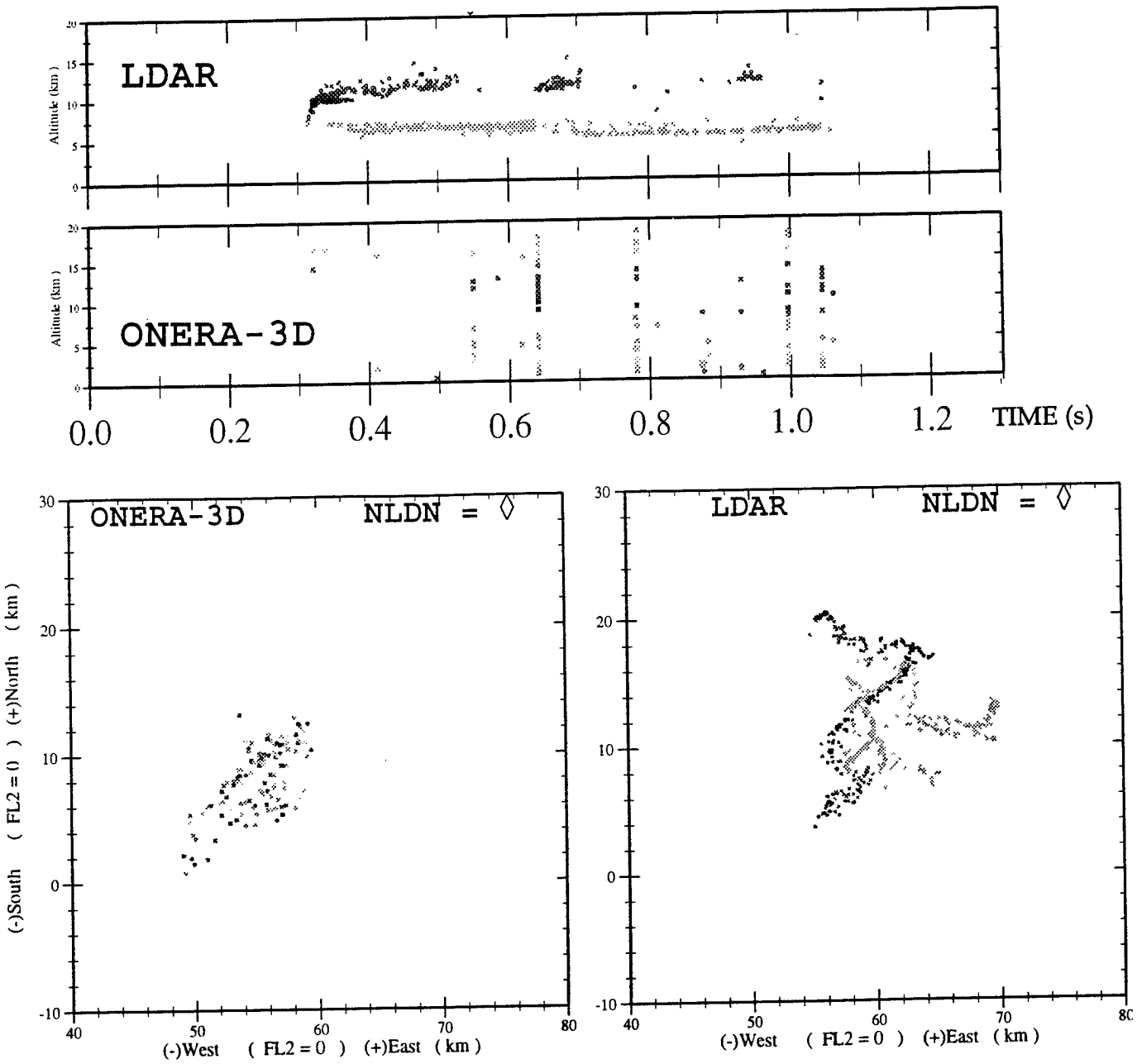



Figure 9. The same as Fig. 7, but for the intracloud flash at 18:05:53 UT, August 28, 1993.

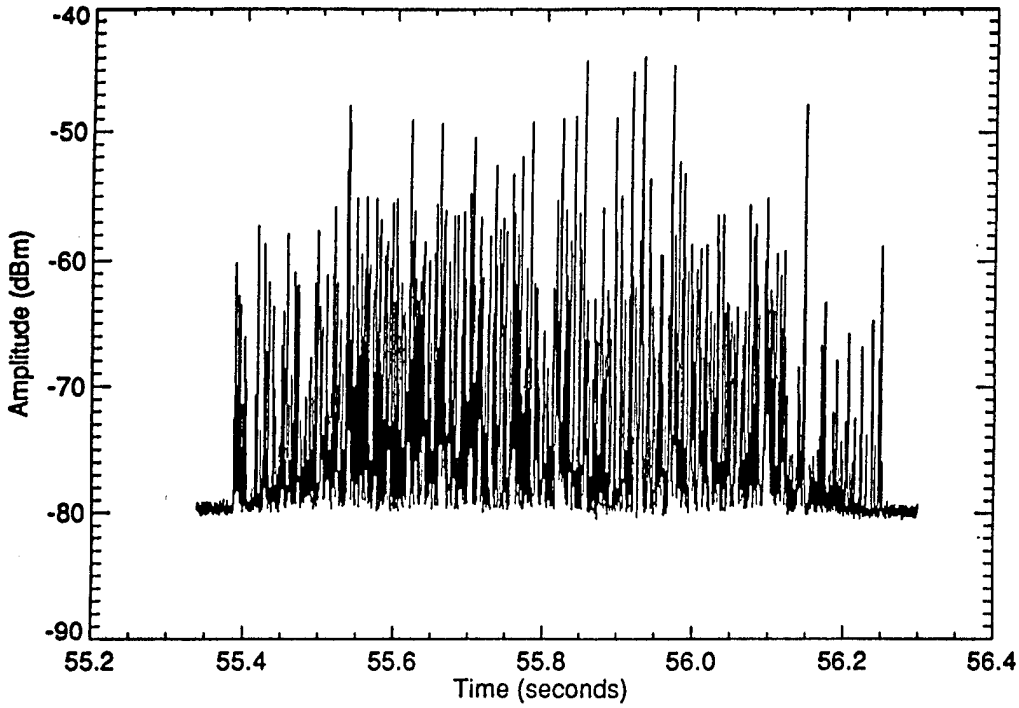



Figure 10. VHF radiation of an intracloud discharge at range of 8.1 km from the receiver (adapted from Friel, 1993). Here and in Figs 11 and 12, lightning radiation was received with a VHF antenna (3 dB beam width in azimuth and elevation planes of 45$^{o}$ and 71$^{o}$, respectively.)

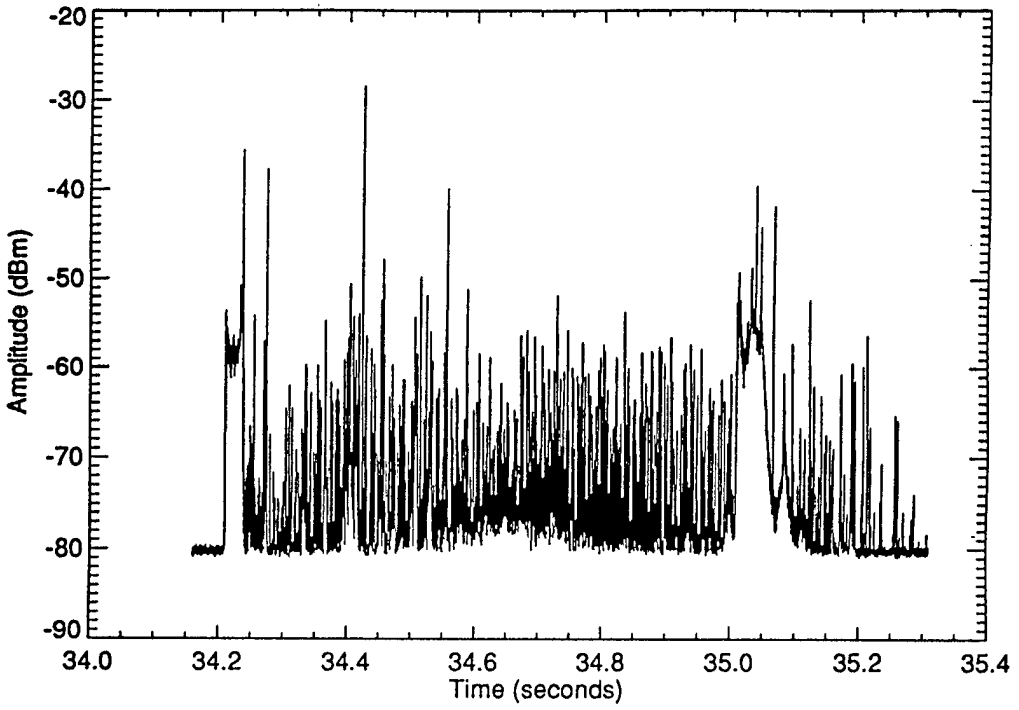



Figure 11. VHF radiation of a cloud-to-ground discharge at range of 9.8 km from the receiver (adapted from Friel, 1993).

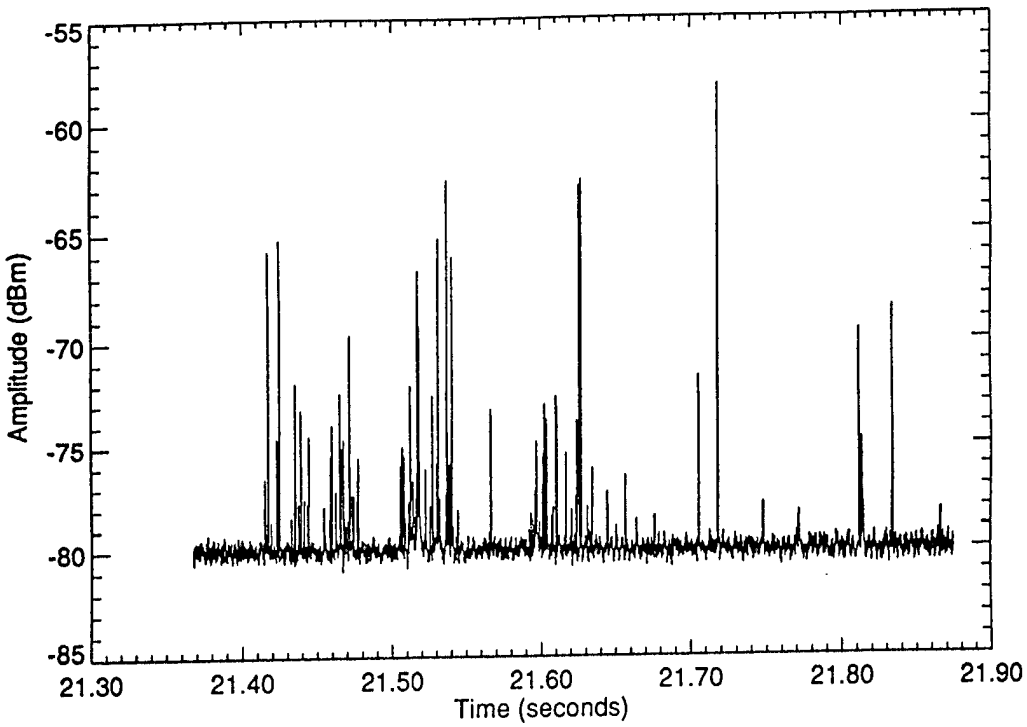



Figure 12. VHF radiation of a discharge at 68.3 km (adapted from Friel, 1993).

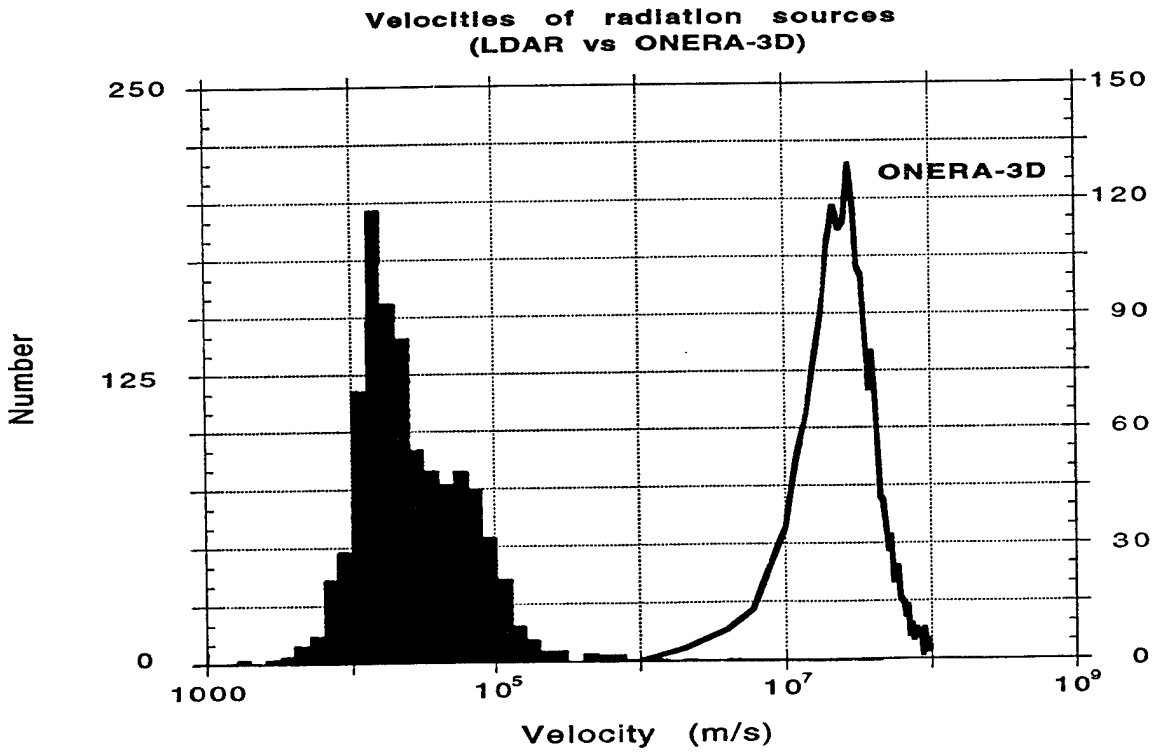



Figure 13. Propagation velocities of radiation sources mapped by ONERA-3D, one hour of observation (adapted from Laroche et al., 1994), and by LDAR, two hours of observations.

# The Measurement and Use of Lightning Ground Flash Density

Leon G. Byerley III, Kenneth L. Cummins,
Jeff Tuel, D.J. Hagberg, Jr.
Global Atmospherics, Inc.
Tucson, Arizona, U.S.A.
Telephone (520) 741 2838

William Bush
Telecomputer Reliability Services
Southern Pines, North Carolina, U.S.A.
Telephone (910) 692 4787

## ABSTRACT

The number of times that lightning strikes ground in a specified area over some period of time is called *lightning ground flash density* or "flash density". This parameter is important because it allows, among other things, the prediction of the frequency of lightning interactions with complex systems. For almost a century, human observations of thunderstorms have been used to derive "thunderstorm day" maps of the United States. Since the 1950's, electronic lightning flash counters have been used for the direct measurement of flash density. In recent years and in lieu of flash density measurements, contour maps of "thunderstorm hours" derived from human observations have been used to obtain approximations to regional flash density. Today, large-area lightning locating networks are used to directly measure flash density. The U.S. National Lightning Detection Network allows scientists and engineers to use historical lightning location data not just for flash density studies based on ground flash occurrence, but also for flash density analyses using parameters such as flash polarity. The lightning data base of the United States from 1989 to the present allows flash density to be analyzed over long and short time periods, and for large and small grid sizes and areas. We review and compare the different ways of evaluating flash density and we discuss uses for flash density information. We give examples of these analyses and we suggest that it is no longer valid, useful or necessary to use the thunderstorm day for engineering purposes in the United States.

## INTRODUCTION

Perhaps the most ubiquitous figure in the literature of lightning and thunderstorms in the United States is the contour map of mean annual thunderstorm days or

thunderdays. In the United States, a thunderday is recorded by weather observers when one or more peals of thunder are heard during a calendar day (1).

The thunderday map of the United States appears in electrical engineering texts, meteorology texts, books about thunderstorms and lightning, technical reports, manufacturer's sales literature, lightning protection codes and the protection engineering standards of the telecommunications and electric power industries. The thunderday map of the United States has become a paradigm of power and protection engineering and thunderday data are frequently used for meteorological studies. In this paper we look at the ways of measuring where and how often lightning occurs (with emphasis on the United States) and we consider the properties and usefulness of these data.

## HISTORICAL BACKGROUND, HUMAN OBSERVATIONS

Centuries before Christ, the Chaldeans of Babylonia developed a system of weather prediction (2) that involved counting thunder. People in medieval Europe followed the Chaldean practice, and created brontologies or thunder almanacs which listed "signa tonitrui" which were used to make weather predictions based on historical records of thunder heard on specific days.

In 1873, the International Meteorological Committee (IMC) met in Vienna and adopted a resolution (3) stating:

> "In order to obtain results which admit of comparison, it is recommended to enumerate only Days of Thunderstorm ... Only days on which both thunder and lightning are observed should be counted as days of thunderstorm."

This instruction to weather observers was further refined by the IMC in 1896 to define three types of thunderstorm observations and the symbols to be used for recordkeeping:

T to indicate days on which distant thunder is heard,

to indicate the observation of distant or diffused lightning,

to indicate all observations of thunder and lightning.

Lightning without thunder was excluded to prevent the recording of very distant thunderstorms.

"Isobronts" or lines drawn on a chart connecting places at which the first thunder from a storm was heard simultaneously were plotted in the late 1870's (2). Isobront (lines of equal thunder) records evolved into plots of "isochromes" which included first thunder, loudest thunder and the beginning of rain. Isobront charts provided a way of looking at the movement of a thunderstorm over a large area. The term *isoceraunic* (meaning equal thunder and lightning) refers to a line or isogram of equal thunderday frequency. This term came into use in the 1920's (4) and is now usually spelled *isokeraunic*.

Thunderday data based on human observation allowed the first quantitative comparisons of thunderstorm occurrence for regions of a country, at different times of year and for different places around the world. Early investigators noted that thunderday data showed year-to-year variations and data from different observing sites showed a lack of uniformity in quality over time partly due to the scarcity of observers and also due to the quality of instructions to observers and the diligence of observers (4). Of particular interest to early investigators were the patterns of thunderstorm occurrence by month when averaged over many years. In 1924, Alexander (4) showed average "isoceraunics" for the previous twenty years (see Figure 1) on a monthly basis for the United States. Figure 2 shows a more recent plot of annual mean thunderdays using data through 1969. These two data sets are quite similar, although the more recent thunderday map (Figure 2) provides somewhat more detail in the western states.

## HISTORICAL BACKGROUND, LIGHTNING FLASH COUNTERS

Since the 1950's, electronic lightning *flash counters* have been used to make direct measurements of lightning ground flash density over limited areas in various regions of the world. Flash counters are electric field change sensors that are biased to respond primarily to the electrostatic components of ground discharges. Uman (5) gives an excellent summary of flash counters and flash density measurements using flash counters.

Because flash counters are short-range sensors, many are needed to cover a large area. Due to the cost and logistical problems of communicating data from many stations, flash counter flash density measurements have traditionally been limited to small regions. Despite sensor limitations, flash counter data can give excellent measurements of flash density. Janischewskyj and Chisholm (6) discuss the difficulties and benefits of using modern flash counters for flash density studies. Prentice (7) showed a variation of two orders of magnitude between measured ground flash density using flash counters and the average number of thunderdays for a region in Australia. Clearly, even crude, direct measurements of flash density give protection engineers vastly better information about the frequency of lightning risks than do thunderday data.

Numerous attempts (5,7,8) have been made to find some relationship between flash counter-based flash density and thunderdays but the variability of thunderstorms in frequency, duration and intensity throughout the world renders these efforts primarily academic. It appears that the thunderday map of the United States in general greatly underestimates the frequency of thunderstorms and lightning (7,8,9). The thunderday simply has a highly variable, non-linear relationship to lightning ground flash density.

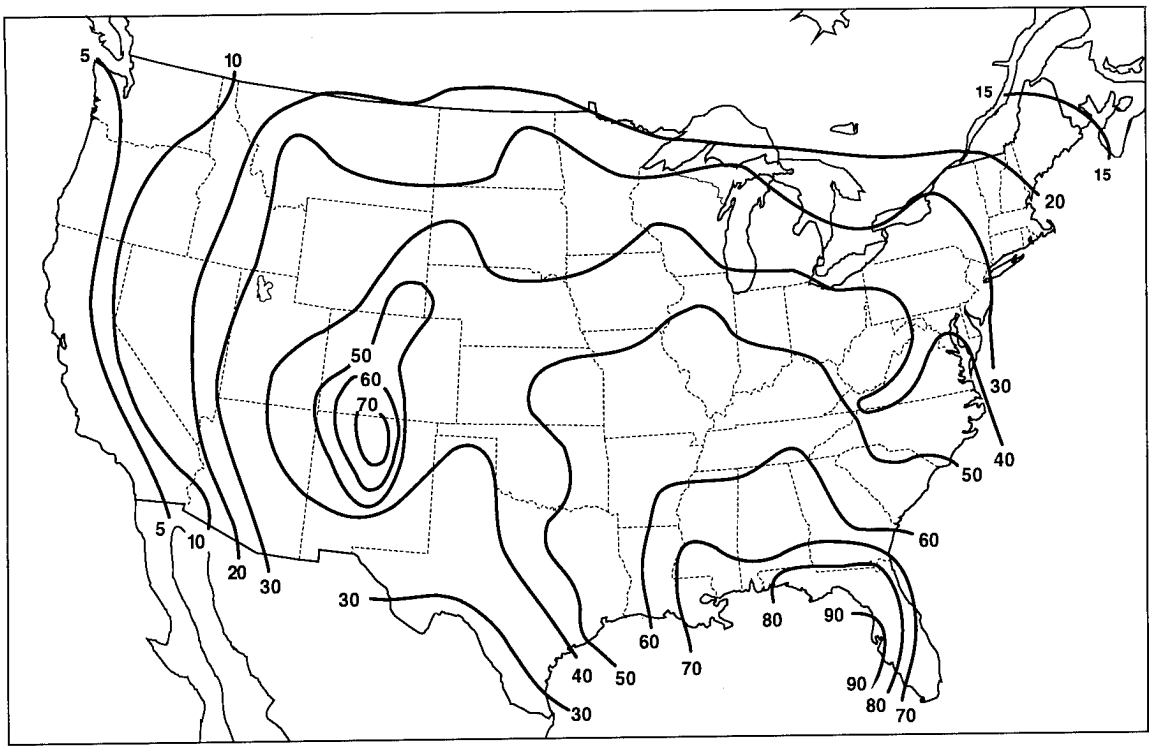



**Figure 1** An early thunderday map of the United States showing the average number of thunderstorm days from 1904 to 1923. Adapted from Alexander, 1924.

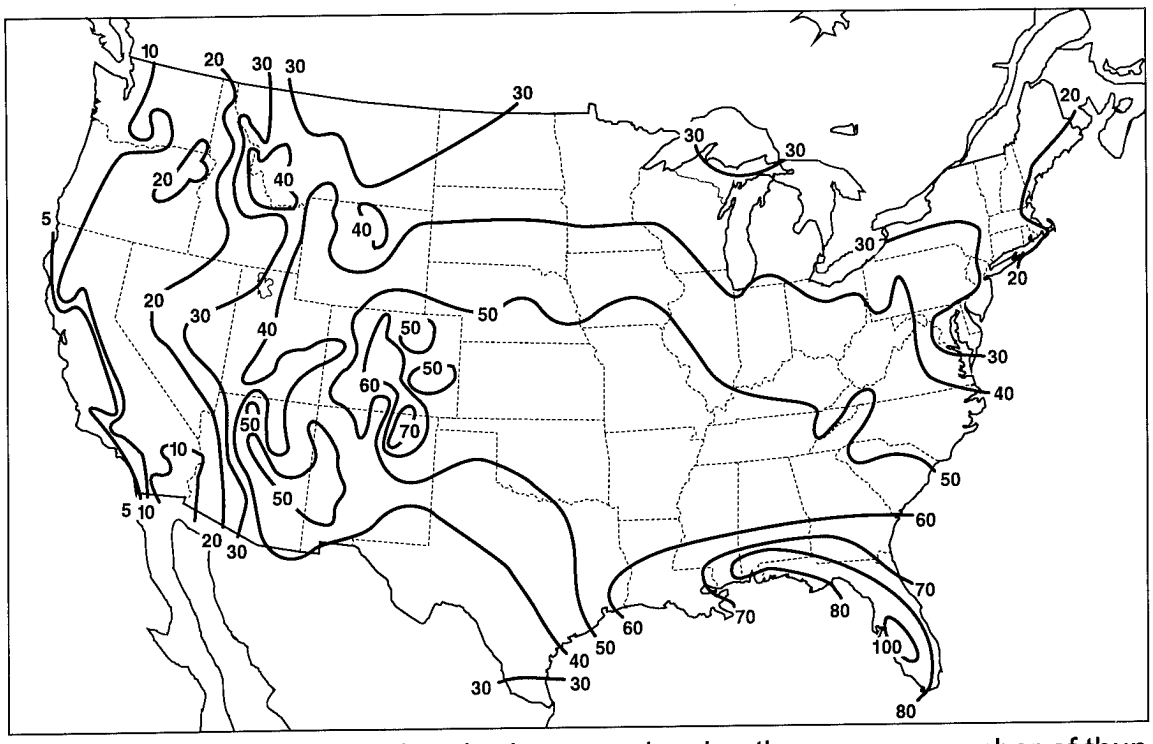



**Figure 2** A contemporary thunderday map showing the average number of thunderstorm days through 1969. Adapted from U.S. Dept. of Commerce data.

## HISTORICAL BACKGROUND, THUNDERSTORM DURATION STUDIES

Although lightning locating and mapping systems appeared in the late 1970's (10,11), sensors were initially too sparsely deployed to give nationwide flash density measurements. However, human thunderstorm *duration* observations of good quality were available from approximately 400 manned aviation weather stations operated throughout the United States. These two facts prompted MacGorman *et al.* (8) to look for a relationship between thunderstorm duration (hereafter referred to as thunderhour) data for the United States and measured flash density to allow inference of nationwide flash density for protection engineering purposes.

MacGorman *et al.* showed that human observations of thunderstorm duration give better correlation than thunderday data with flash density. Figure 3 shows a mean annual thunderhour map of the United States with lines of equal thunderstorm duration in hours. These thunderstorm data were used by MacGorman *et al.* to produce an "inferred" flash density for the United States using a non-linear mapping of thunderhour to flash density. The resulting thunderhour contour map represented a significant improvement in information for lightning risk assessment. This approach might have seen widespread acceptance had a nationwide lightning locating network not been under development, with the prospect of giving directly measured flash density for the United States.

## HISTORICAL BACKGROUND, LIGHTNING LOCATING NETWORKS

The widespread use of lightning locating networks (12) from the late 1970's to the present allowed direct measurements of lightning ground flash density over large areas. Maier and Boulanger (13) performed the first flash density study in 1979 using a lightning locating network in south Florida with the significant finding that measured flash densities can vary more than an order of magnitude over distances of tens of kilometers due to orographic, geographic and meteorological factors. Such interesting fine detail cannot be shown in a national-scale plot of flash density. Orville (14) published the first nationwide annual summary of measured lightning ground flash density in 1991 using lightning location data from a combination of large independent networks that were operating in the United States. Orville used a grid size of 30 by 50 kilometers.

Since 1991, the National Lightning Detection Network™ (NLDN) originated by Orville and associates at the State University of New York at Albany (12) has been operated by GeoMet Data Services, now a division of Global Atmospherics, Inc., in Tucson, Arizona. A paper by Cummins *et al.* (15) presented at this conference discusses the evolution and present status of the NLDN.

The NLDN has measured the time and location of flashes throughout the contiguous United States since 1989. Between 1989 and 1995, this flash information was archived along with estimates of the peak current of the first stroke, the polarity of the first stroke and the number of strokes in the flash (multiplicity). Since January 1, 1995, the archive lightning location data has included the time, location, peak current

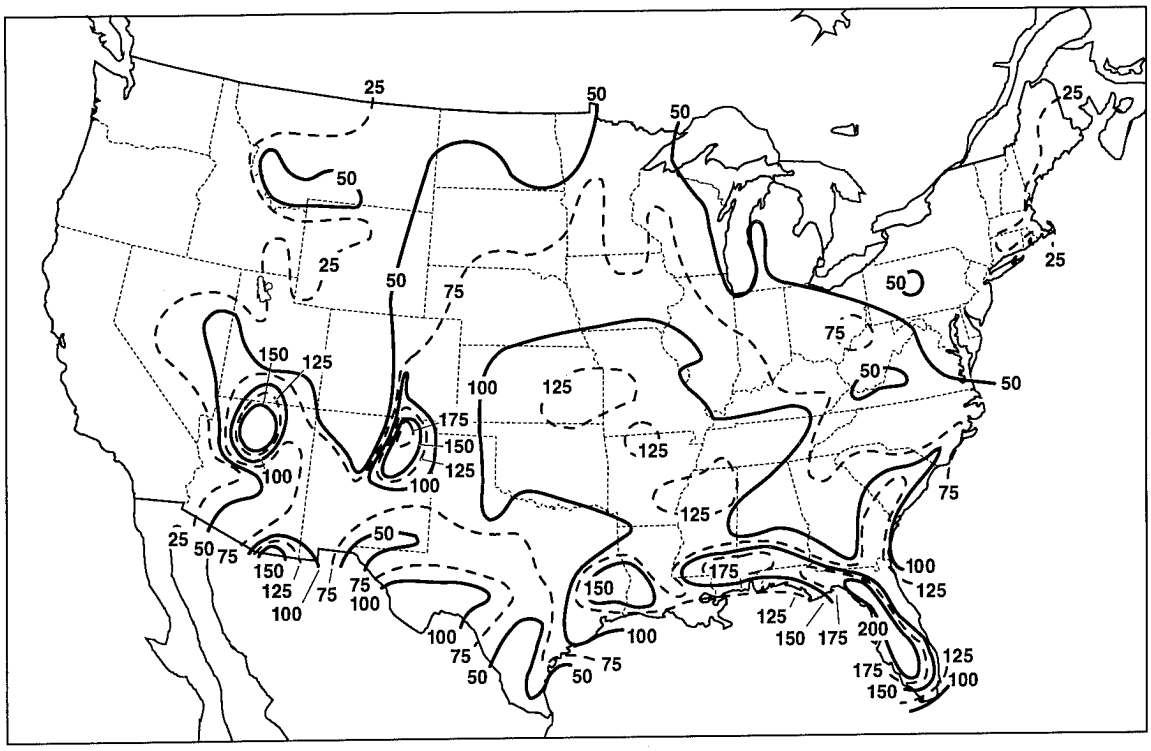



**Figure 3** Mean annual thunderhour map of the United States showing lines of equal thunderstorm duration in hours. Adapted from MacGorman *et al.*, 1984, with permission.

and polarity of all cloud-to-ground return strokes detected by the NLDN. Details of the method for grouping strokes into flashes is described by Cummins *et al.* (15).

The availability of these lightning location data and lightning parameter data over a period of many years allows flash density studies which are not possible with traditional flash counters. For example, Reap and MacGorman (16) showed the first maps of flash density for negative flashes and for positive flashes for the same storm using data from the National Severe Storms Laboratory lightning locating network. Orville (17) plotted flash density for positive flashes as well as contours of percentage of positive flashes for the United States for 1989 through 1991.

## GRIDDING, CONTOURING, AND SAMPLING PERIOD

Flash density is defined as the number of flashes occurring in a specified area per unit time. It is typically represented as flashes/km$^2$/yr. Flash density data produced by a lightning locating network is significantly more uniform than data produced from human thunderhour observations or from flash counters, both of which are measurements from sparse individual observation locations. Flash density derived from lightning location data is computed by dividing the region of interest into small rectangles, and accumulating the total number of flashes occurring in each rectangular "grid cell" over

the time interval of interest. In order to convert this gridded data to flash density contours, these data must first be smoothed, in order to remove local variations. An example of such a grid plot for all of 1993 is shown in Figure 4. The gridded data shown in this figure were smoothed by averaging the eight "nearest neighbor" points prior to encircling the regions with density contours. Each grid cell has an approximate size of

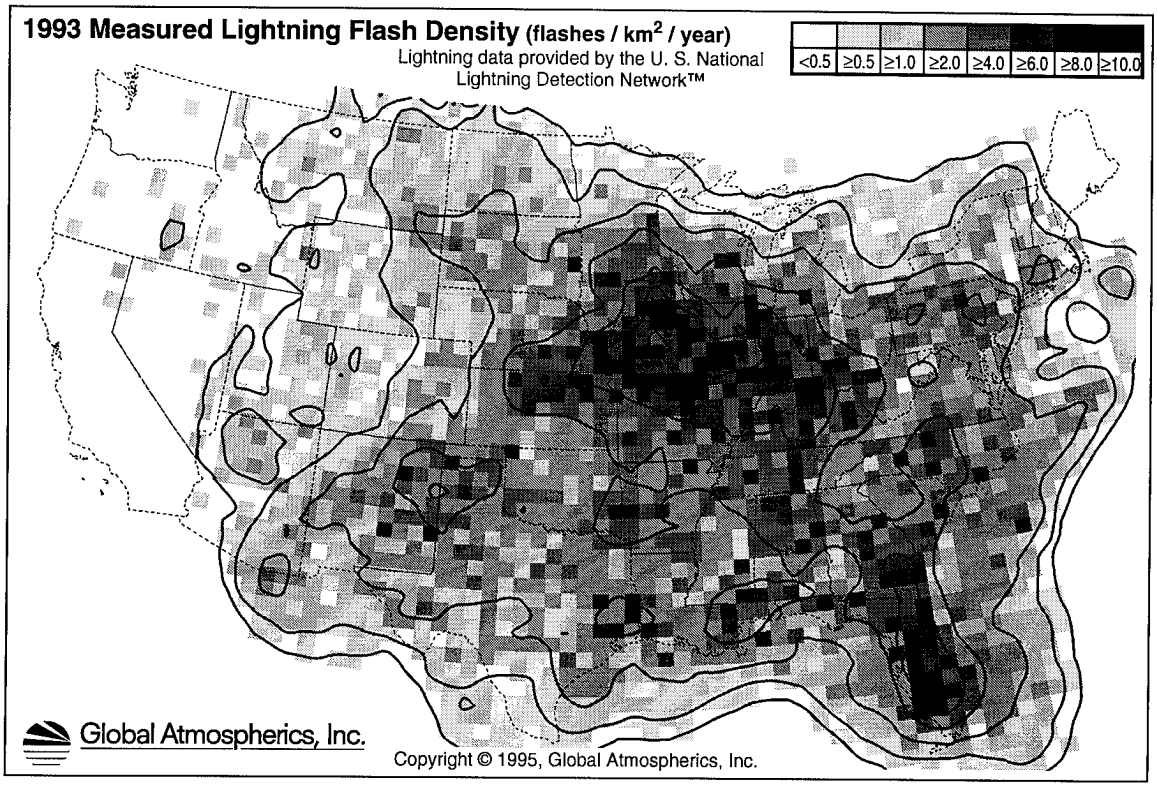



**Figure 4** Grid plot and related contours of mean annual flash density for the United States in 1993 using data from the NLDN. Flash density units are flashes/km$^2$/year.

60 by 60 kilometers. This "grid method" for representing flash density information shows the data in its most direct and fundamental form. Small regional variations in flash density can easily be seen in these grid maps.

## LONG-TERM NATIONAL FLASH DENSITY

A five-year flash density contour map for the United States (1989-1993) is shown in Figure 5. The contour resolution was selected to be similar to the resolution of the thunderhour data shown in Figure 3. For this map, the United States was gridded at 88 by 50 and the data were smoothed using three nearest-neighbors with uniform weighting. Contour lines for this map were then found using a line-following algorithm and drawn

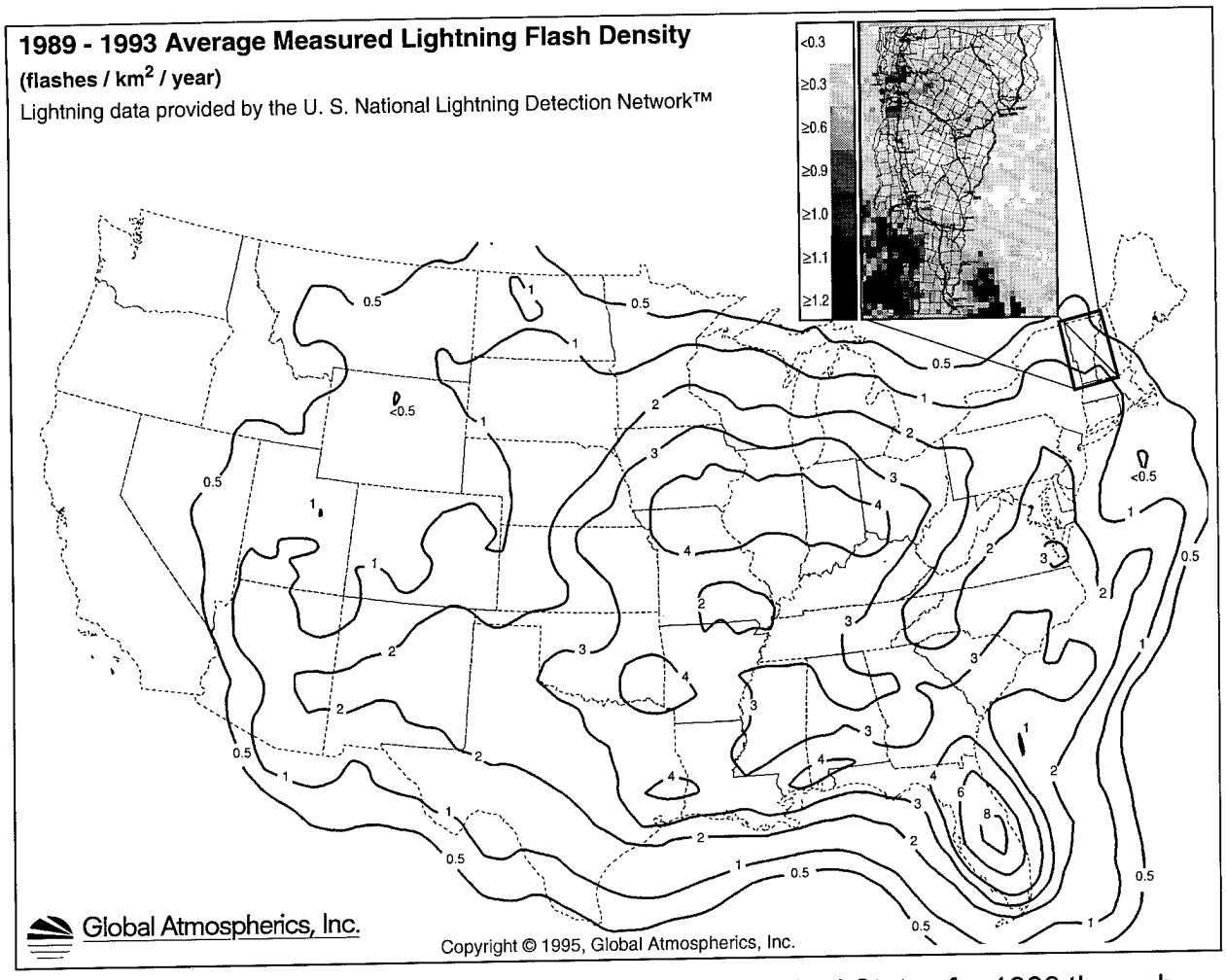



**Figure 5** Annual flash density contour map for the United States for 1989 through 1993. Inset shows grey scale grid of flash density for the state of Vermont.

as Bezier splines. The inset of Vermont is shown as an approximate 5 $km^2$ grid and then shaded according to the scale shown.

It is interesting to compare the non-linear mapping of thunderday and thunderhour to flash density by comparing similar regions in Figures 2, 3 and 5. For example, note that southeastern Nebraska has 50 thunderdays, 100 thunderhours and a flash density of 3 flashes/$km^2$/year while southwestern Montana has 40 thunderdays, 50 thunderhours and .5 flashes/$km^2$/year.

Flash density contours for 1992 and 1993 are shown in Figure 6. Note the significant variability in flash density for these two years. In 1992, only 16 million flashes were detected by the NLDN, whereas more than 24 million were detected in 1993. The NLDN was stable over this two-year period, in terms of instrumentation and algorithms. The major differences are in the Ohio valley and east-central United States. These differences are probably correlated with the extensive flooding that occurred in the summer of 1993.

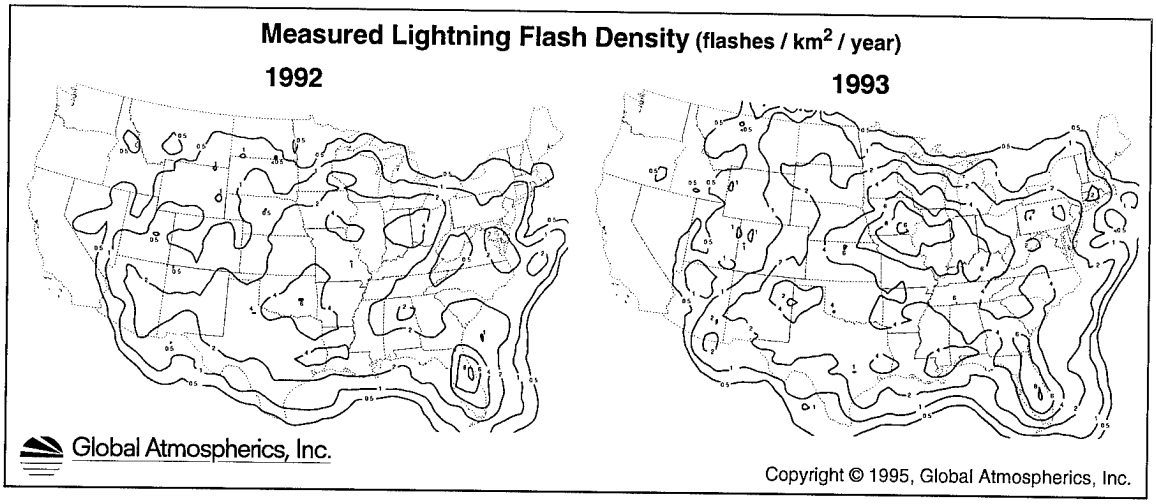



**Figure 6** Yearly flash density contours for 1992 and 1993.

The one-year flash density contours in Figure 6 were produced with fewer contour lines than the five-year average shown in Figure 5 to eliminate some of the variability. Averages over several years as in Figure 5, will tend to reduce random variations of flash density from year to year. While seasonal and random variations of flash density occur on short time scales, non-random variations in regional thunderstorm activity as measured by thunderday appear to span decades (18, 19). Flash density data are not available for any region of the world for much more than a decade.

## REGIONAL FLASH DENSITY GRIDS

It is not possible to present a legible contour map of the United States that properly shows the fine structure of the variation of lightning ground flash density for a given region. Differences of an order of magnitude in flash density can occur in adjacent areas of tens to hundreds of square miles. Such variations cannot be shown clearly on a national scale map for which contouring using large grids and smoothing are required. The best method to represent the local variability of flash density seems to be in the form of regional flash density grids, as shown in Figure 7.

Figure 7 shows the average annual gridded flash density for the state of Vermont for the years 1989 through 1994. Note the unusually high average flash density in the Burlington region in the northwestern part of the state. The flash density we see in this presentation is about four times greater than what is shown in Figure 4. The anomalous flash density in the Burlington region may be due to the relatively flat surrounding terrain which can promote convection of moisture from Lake Champlain.

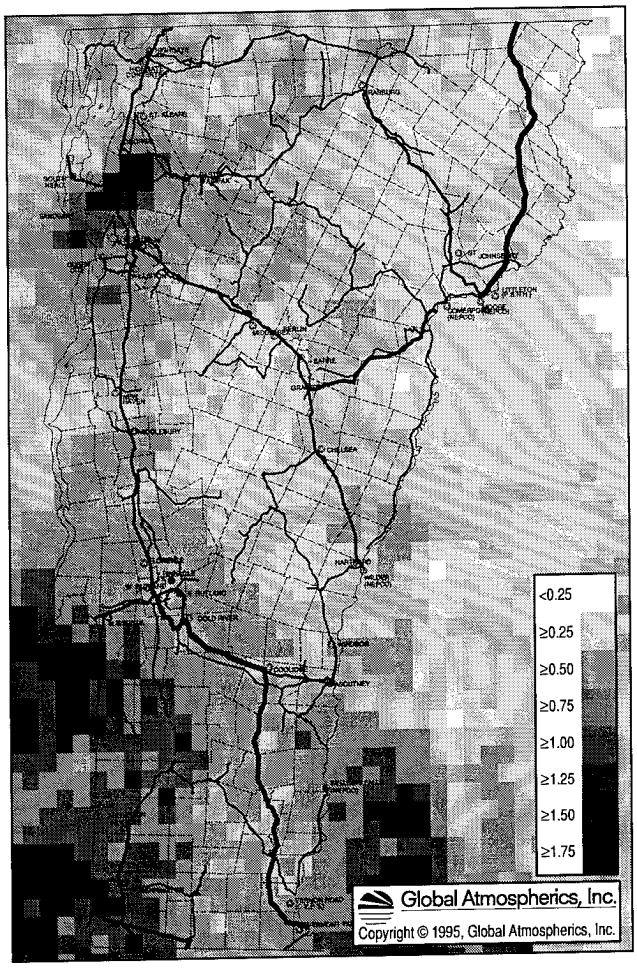



**Figure 7** Flash density grid plot for the state of Vermont superimposed on local municipal boundaries and power transmission lines.

## CONCLUSIONS

Although of great historical significance and still of some meteorological significance, the thunderday is not a measure of the incidence of lightning in a given area which is a variable of great importance to lightning protection engineers. Since the thunderday has no meaningful relationship to flash density, thunderday data should not be used for lightning risk assessment. Attempts to relate thunderday records to *inferred* flash density are of academic interest only in view of the availability of measured flash density data. Thunderhour data for the United States provide a significant improvement over the thunderday measure and show a better correlation with actual flash density. However, thunderhour data are a poor indicator of the frequency of ground discharges in a region.

We have known for 50 years or so that direct measurement of ground flash density using electronic sensors provides meaningful and useful information for lightning risk assessment. Lightning locating networks are now in common use throughout the world and the operational lifetime of some of these networks is approaching twenty years. Because of ready availability in the United States, measured lightning flash density should be used in place of thunderday or thunderhour data for lightning risk assessment.

National-scale maps of flash density are useful for general purpose lightning risk assessment. For serious problems, where characterization of local flash density is required, it is necessary to look at flash density in high resolution. Because of short- and long-term random and systematic variations in thunderstorm occurrence, it is important to look at the extremes of flash density as well as the mean for many years. For protection of complex systems, it is rarely good practice to design for the minimum or average expected incidence of lightning.

It is now possible to plot ground flash density by specific lightning parameters such as flash density for positive flashes only or flash density of negative flashes having strokes with peak currents greater than 100 kA. Lightning data from the NLDN enable many types of lightning risk assessment that are not possible with human observations or with traditional lightning flash counters.

We find no reason to continue to use the thunderday map of the United States for lightning risk assessment and we recommend that all concerned authoritative bodies consider amending codes and standards to require the use of direct measurements of lightning ground flash density.

## ACKNOWLEDGEMENTS

The authors are indebted to Ron Holle and Raul Lopez of the National Severe Storms Laboratory in Norman, Oklahoma for a multitude of contributions to this paper.

## REFERENCES

1. U.S. Dept of Commerce, Weather Bureau, "History of Observation Instrumentation as Applied to Thunderstorms." Key Meteorol. Rec. Doc. 3.12, 11 pages, Supt. of Documents, Washington, D.C., 1958.

2. R. Hardy, "The Weather Book." Michael Joseph Limited, London, pp. 185-186, 1982.

3. C.E.P. Brooks, "The Distribution of Thunderstorms Over the Globe." Air Ministry Meteorological Office, Geophysical Memoirs, No. 24, His Majesty's Stationary Office, 1925.

4. W.H. Alexander, "The Distribution of Thunderstorms in the United States." Monthly Weather Review, American Meteorological Society, Vol. 52, No. 7, pp. 337-343, July 1924.

5. M.A. Uman, "The Lightning Discharge." Academic Press, pp. 37-40, 1987.

6. W. Janischewskyj, W.A. Chisholm, Report (179 T 382) for the Canadian Electrical Association: "Lightning Ground Flash Density Measurements in Canada, March 1, 1984 to December 31, 1991." University of Toronto Department of Electrical Engineering, Toronto, Ontario, August 1992.

7. S.A. Prentice, "Frequency of Lightning Discharges." in "Lightning, Vol. 1, Physics of Lightning," edited by R.H. Golde, Academic Press, p. 7, 1977.

8. D.R. MacGorman, M.W. Maier, W.D. Rust, "Lightning Strike Density of the Contiguous United States From Thunderstorm Duration Records." NUREG/CR-3759, prepared for the U.S. Nuclear Regulatory Commission under contract no. NRC-01-79-007, May 1984.

9. S.A. Changnon, D. Changnon, R.B. Pyle, "Thunder Events and Cloud-to-Ground Lightning Frequencies." Journal of Geophysical Research, vol. 93, No. D8, pp. 9495-9502, 1988.

10. E.P. Krider, R.C. Noggle, M.A. Uman. "A Gated, Wideband Magnetic Direction Finder for Lightning Return Strokes." Journal of Applied Meteorology, Vol. 15, pp. 301-306, 1976.

11. E.P. Krider, R.C. Noggle, A.E. Pifer, D.L. Vance, "Lightning Direction Finding Systems for Forest Fire Detection." Bulletin of the American Meteorological Society, Vol. 61, pp. 980-986, 1980.

12. R.E. Orville, R.W. Henderson, L.F. Bosart, "An East Coast Lightning Detection Network." Bulletin of the American Meteorological Society, Vol. 64, pp. 1029-1037, 1983.

13. M.W. Maier, A.G. Boulanger, R.I. Sax, "An Initial Assessment of Flash Density and Peak Current Characteristics of Lightning Flashes to Ground in South Florida." USNRC Report NUREG/CR-1024, 43 pages, Sept. 1979.

14. R.E. Orville, "Lightning Ground Flash Density in the Contiguous United States -1989." Monthly Weather Review, Feb., pp. 573-577, 1991.

15. K.L. Cummins, E.A. Bardo, W.L. Hiscox, R.B. Pyle, A.E. Pifer, "A Combined TOA/MDF Technology Upgrade of the U.S. National Lightning Detection Network." Presented at the 1995 International Aerospace and Ground Conference on Lightning and Static Electricity, Williamsburg, Virginia, Sept. 26-28, 1995.

16. R. Reap, D. MacGorman, "1989: Cloud-to-Ground Lightning: Climatological Characteristics and Relationships to Model Fields, Radar Observations, and Severe Local Storms." Monthly Weather Review, Vol. 117, pp. 518-535, 1989.

17. R.E. Orville, "Cloud-to-Ground Lightning Characteristics in the Contiguous United States: 1989-1991." Journal of Geophysical Research, Vol. 99, No D5, pp. 10,833-10,841, May 20, 1994.

18. S.A. Changnon, Jr, "Secular Trends in Thunderstorm Frequencies." Electrical Processes in Atmospheres: Proceedings of the International Conference on Atmospheric Electricity, Garmisch-Partenkirchen, W. Germany, Sept. 2-7, 1974, Darmstadt, Dietrich Steinkopff, Verlag, pp. 482-487, 1977.

19. N. Kitagawa, "Long-Term Variations in Thunder-Day Frequencies in Japan." Journal of Geophysical Research, Vol. 94, No. D11, pp. 13,183-13,189, 1989.

# EVALUATION OF LIGHTNING PERFORMANCE OF 115 kV TRANSMISSION LINES WITH SPLINE BALL IONIZERS BASED ON MODEL TESTS

S. Grzybowski
Mississippi State University
High Voltage Laboratory
Department of Electrical & Computer Engineering
Mississippi State, MS USA
Telephone (601) 325–2148 FAX (601) 325–2298

## ABSTRACT

This paper presents the experimental results of an investigation of the lightning performance of a 115 kV transmission lines with spline ball ionizers (dissipators). The evaluation was based on the measurements of CFO voltage between transmission lines and cloud models. The investigation was conducted on a scale model of a charged cloud (without and with leader) and transmission lines. The investigation was conducted on single transmission line models and two transmission line models tested simultaneously. The CFO voltages were measured for both negative and positive polarities. The discussion of the results follows the presented data.

## INTRODUCTION

Lightning phenomena have been studied for many years, and several theories have been developed to explain the mechanisms involved. As more sophisticated instruments have become available, considerably more has been learned about this most interesting physical occurrence. Satellites have been particularly effective in recording lightning strikes between clouds and from clouds to the ground. A reasonable understanding of the lightning mechanism may be dated back to 1930. Since that time, considerable work has been devoted to a more thorough understanding of the electrical discharge. A relatively recent comparison of several of these investigations on discharge mechanisms and lightning parameters was presented by M.N. Uman (1).

There appears to be good agreement that the bottom part of a thundercloud will typically become negatively charged while the upper part is charged positive. If positive charge does appear in the bottom part of the cloud, it is localized usually in a very small region. Therefore, most lightning strokes (e.g., 90–95%) that hit transmission lines, distribution lines, or other objects on the ground are usually from the negative charge (1, 2, 3).

Even the lightning phenomena, lightning discharge mechanism are in some way known, it is impossible to eliminate the lightning strokes. It is a natural phenomena which humanity still does not control. Therefore, the place, the object, time, where and when the the lightning strokes may and will hit are still more or less unpredictable. We may use different types of shielding to protect the selected objects from direct lightning

strokes, but we could not eliminate the lightning strokes.

It has been observed that lightning will often strike towers for overhead transmission and distribution lines as well as the midspan of the lines. This may result in a flashover around the line insulation. Shielding wires have been found effective in avoiding flashover when they are attached to the top of tower structures above the phase conductors. Transmission and distribution systems which employ shielding wires according to established guidelines have been found to have relatively low lightning outages (3, 4, 5, 6).

Several different concepts have been employed by electric utilities to protect transmission lines and towers from direct lightning strokes. One concept which has attracted some attention in recent years is the use of an element to enhance the dissipation of charge from the structure (7). The effectiveness of such devices has been the subject of discussion for several years. Unfortunately, no test data was available regarding the effectiveness of such dissipators nor are we aware of any previous use of the devices on transmission lines.

One particular type of charge dissipator was evaluated in the MSU High Voltage Laboratory in 1992 and 1993; the results have been presented (8, 9). The effectiveness of the spline ball ionizers was evaluated by determining the CFO voltage between the models of the transmission lines and the cloud and the results were previously published (10, 11). One would deduce that the line has a higher probability of being struck by lightning relative to another configuration if the CFO voltage is lower. So as to make a relative comparison, two different models were simultaneously tested where one of the models included a charge dissipator.

In an initial investigation conducted in 1992, no effort was made to simulate a lightning leader with a conducting element. As it was later determined, the experimental model needed improvement. This investigation (11) reports on the use of a conducting rod to simulate the lightning leader. The tip of the rod was located at different distances above the transmission line models and moved out of lines. The tip of the rod was also located at different positions in the span between the tower models.

## OBJECTIVE OF THE STUDY

The lightning strokes have appeared also in the area where experimental transmission lines are installed with spline ball ionizers. Therefore, the spline ball ionizers do not eliminate the lightning strokes, as some people tried to persuade. To eliminate the impact of any other object on the lightning protection, the models of the transmission lines need to be evaluated as separate lines or two lines simultaneously.

As previously noted, the objective of this study is to evaluate the lightning performance of a 115 kV transmission lines with spline ball ionizers. More specifically, spline balls of 1.2 m diameter were studies for use on a H–frame tower of a 115 kV transmission line.

The effectiveness of the device was evaluated by determining the CFO voltage between the models of the transmission lines and clouds without and with a simulated lightning leader. For the spline balls to be effective, the electrical withstand (strength) between the transmission lines with ionizers and the surrounding clouds must be greater than the electrical withstand of the lines without the spline balls.

Two basic types of experiments were conducted. In the first, single models of a transmission line were studied for various combinations of lightning protection devices which included shielding wires and spline balls. The second group of experiments involved the simultaneous comparison of two different transmission lines. In these experiments, various combinations of lines were likewise tested with different protection devices.

The following configurations of single line models were investigated:

a) Transmission line without shielding wires and spline ball ionizers
b) Transmission line with two spline ball ionizers on the tower structure
c) Transmission line with two shielding wires
d) Transmission line with two shielding wires and two spline ball ionizers mounted on the tower structure.

The first group of experiments, using a simulated cloud with leader and a transmission line, was conducted on single transmission line models as shown in Fig. 1.

The second group of experiments where two transmission lines were simultaneously evaluated (Fig. 2), were conducted for the following two sets of lines:

1) First set of evaluated lines
   a) One transmission line with two spline ball ionizers located on the tower structure
   b) The second transmission line with two shielding wires
2) Second set of evaluated lines
   a) One transmission line with two shielding wires and two spline ball ionizers,
   b) The second transmission line with only two shielding wires

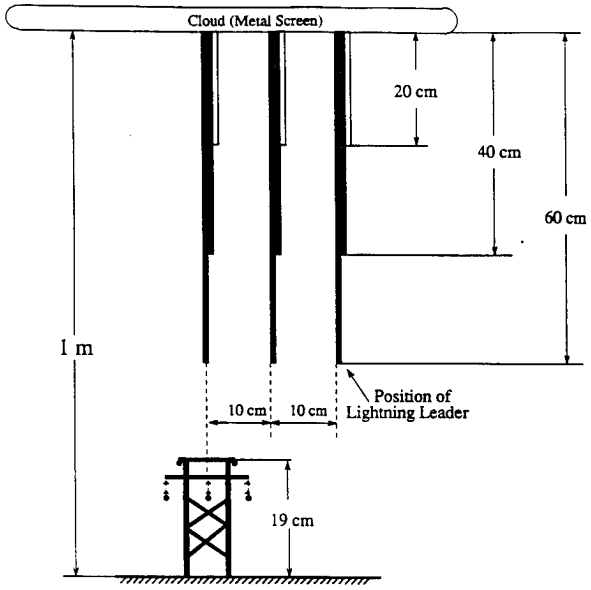



Fig. 1 The lightning leader tip (metal rod) location at three different levels above the line models and moved out from the line models

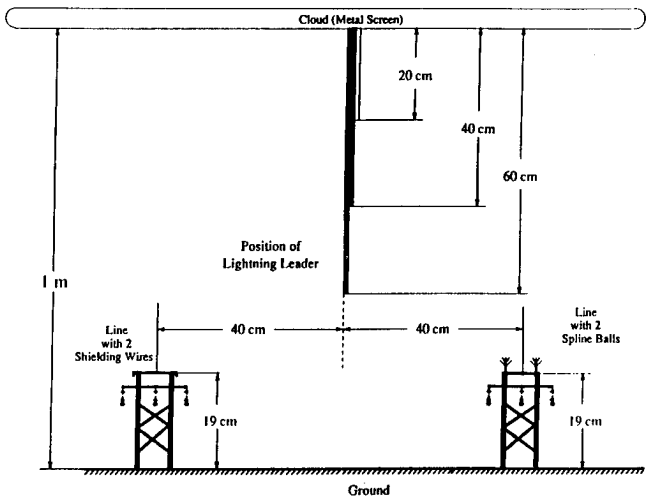



Fig. 2 The lightning leader tip location for two transmission line models investigated simultaneously

EXPERIMENTAL ARRANGEMENT

Models of the transmission lines were built on a scale of 1:100. As the standard span for these transmission lines is 183 m, the distance between the towers of the model was selected as 1.83 m. The metal screen (2.5 m x 5 m) which represented a cloud, was secured a distance of 1 m from the model ground. The spline ball ionizers were represented by the wires of the control cable. The end of the cable was spread out so that the wires of 6 mm in length were sprayed. The towers were assembled on the metal board, which simulated the ground. All phase conductors, shielding wires and spline ball ionizers were connected with metal board of the model line. The metal board was grounded.

For single line model, when the metal rod which simulated a lightning leader was used, it was located at the positions shown in Fig. 1. It means the rod was located above the line and moved out a distance of 10 cm and 20 cm from the line. The data were acquired at three different heights as shown in Fig. 1. Data was also acquired with the rod at five different points, ($P_1$, A, B, C and $P_2$), Fig. 3.

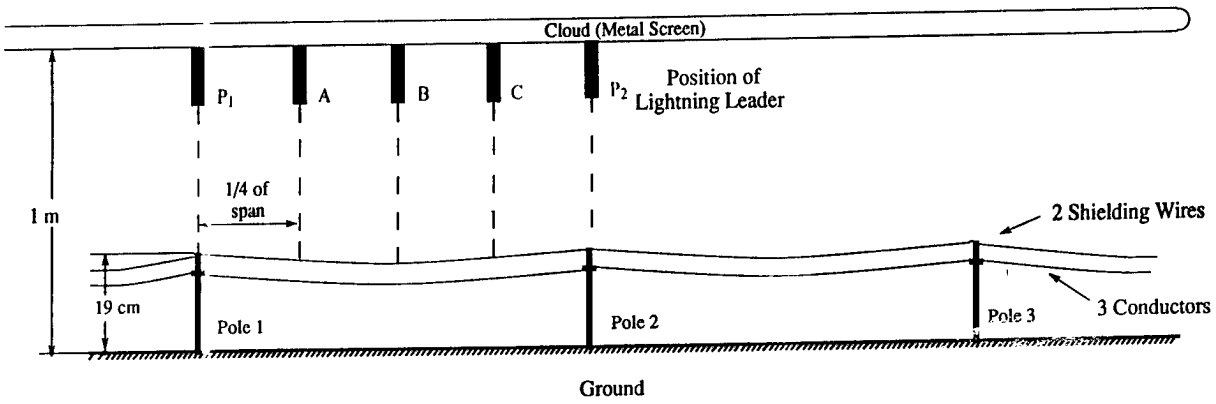



Fig. 3 Position of the lightning leader (metal rod) at the 5 points along the line models

When two transmission lines were used in the second group of experiments, the lines were located parallel to each other and in the same horizontal plane as shown in Fig. 2. The centers of the towers for the two lines were spaced a distance of 40 cm, and the rod used to simulate a lightning leader was located midway between the lines. Data was acquired also with the rod at five different points ($P_1$, A, B, C and $P_2$) in a direction parallel with the lines.

The electrical impulse to the cloud and leader, which are simulated by the metal screen and rod, was provided by a 3000 kV, 56 kJ impulse generator. The standard lightning impulse and switching impulse, as well as the steep front pulse, were formed by means of a Marx circuit impulse generator. The lightning impulse used in all of the laboratory investigations was a 1.2/50 μs standard lightning impulse as described in IEEE Standard #4, Techniques for High Voltage Testing. To study the impact of impulse duration, also 300/2500 μs switching impulse and a short 0.14/11 μs steep front impulse were used in the investigation.

Both negative and positive polarity impulses were applied. The second terminal of the generator was grounded to the model ground. As the line conductors were likewise

grounded, the polarity of the conductors was opposite of the metal screen or lightning leader which were energized by the impulse generator. In this paper, the polarity presented refers to the metal screen (cloud) or lightning leader relative to the ground plane.

## EXPERIMENTAL RESULTS

The dissipated charge from the spline ball ionizers will be larger and therefore, stronger impact on lightning protection, when the test impulse will have longer front and tail.

There was not any difference in spline ball ionizers's behavior of the 300/2500 μs switching, 0.14/11 μs steep front impulse and 1.2/50 μs standard impulses. For specific configuration of the line and cloud. The lowest CFO voltage was for switching impulse and the highest CFO voltage for 0.14/11 μs steep front impulse. The ratio of negative and positive CFO voltage magnitude for specific configurations of lines and clouds were the same for all types of impulses. Using the standard lightning impulse, the spline balls are able to emit more charge than when the 0.14/11 μs was applied. The only difference was in the CFO voltage magnitudes, therefore, the data for this paper will be presented for standard lightning impulse.

SINGLE TRANSMISSION LINE MODELS—Measured results of CFO voltages with negative and positive polarities of the lightning impulse for the transmission line models and cloud without leader are presented in the paper (10).

The CFO voltages with negative polarity of the lightning impulse are much lower than the CFO voltages with positive polarity, respectively, for each model line configuration.

As mentioned before, the charge concentrated in the bottom part of the cloud is in majority negative. The CFO voltage is lower for negative polarity of the cloud. Therefore, it is especially important to discuss the magnitudes of CFO voltages when a lightning stroke from the cloud carries a negative charge.

According to the value of CFO voltages for negative polarity of the cloud, two groups of configurations may be distinguished. To the first group belong transmission lines without spline balls on the tower. For these lines, the CFO voltage is 451 kV and is higher than 437 kV, the CFO voltage of the second group of lines. To the second group of line configurations belong the transmission line with 2 spline ball ionizers.

Instantly, the conclusion is rising in this case, the spline balls are reducing the CFO voltage, i.e., decreasing the electrical withstand of the gap between the line and the cloud. This is caused by the fact that when cloud has negative charge and the line dissipates the positive charge which creates the positive space charge around the line. The transmission lines with spline balls dissipate (emit) more positive charge at the tower, at the same condition, than the lines without spline balls. The positive space charge is moving slowly in the direction of the cloud and creates a positive charged upward streamer above the tower which reduces the negative lightning withstand of this configuration. Therefore, the spline balls on the towers at negative polarity of the cloud (approximately 90% of the thunderclouds) and positive polarity of the spline balls are attracting the lightning strokes.

Fig. 4 represents the photographs of the electrical arc channels for the negative lightning strokes to the line model with 2 spline ball ionizers. Most of the strokes hit the towers. It may be observed that an additional streamer from the transmission line model was also created above other towers. It is an upward leader from line to cloud model. The negative lightning stroke to the span was registered only in approximately 5% of total negative strokes.

Fig. 5 represents the channels of the positive lightning strokes from the cloud to the line model with 2 spline ball ionizers. The negative space charge around the spline ball ionizers on the tower caused that the lightning strokes appeared to the span of the line.

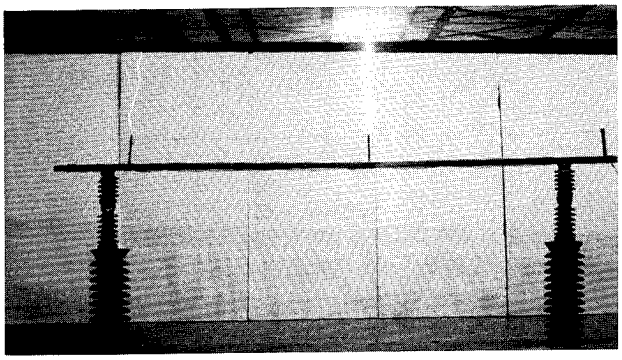


Fig. 4 Electrical arc channels for negative lightning strokes from cloud without leader to the line model with 2 spline balls

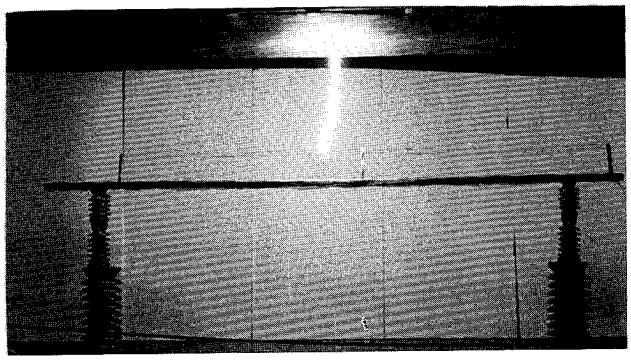


Fig. 5 Electrical arc channels for positive lightning strokes from cloud without leader to the line model with 2 spline balls.

The CFO voltage for positive lightning strokes (for approximately 10% of total lightning strokes, when the bottom of the cloud has positive charge) is 756 kV, the lowest value for line with 2 shielding wires. The spline balls ionizers have negative polarity and dissipate the negative charge. The negative charge dissipated by spline ball ionizers is moving very fast in all directions and creates more uniform field distribution around the tower and the line. That reduces the electrical field stress around the tower and the line, and that increases the CFO voltage. In this case, i.e., when the lightning stroke from the cloud carries the positive charge and the line has the negative polarity, the spline ball ionizers are improving the field distribution mainly around the towers and the lightning strokes hit to the spans of the lines.

For lines without spline ball ionizers and without shielding wires, as well as line with shielding wires, the positive lightning strokes were in approximately 80% to the tower and 20% to the spans.

Several general observations can be made that apply to configurations with leader from the cloud. With a leader rod of 20 cm, the CFO voltages with negative polarity are lower than with positive polarity. This was also observed in an earlier study without the use of a simulated leader. It is interesting to note, however, that with a longer rod (e.g., 40 cm and 60 cm) this trend is reversed, and the CFO voltage is lower for positive polarity than for negative polarity of the cloud (11).

The above observations can be explained by considering changes in the electric field distribution as a function of the rod length. Without a rod or when the rod is short (e.g., 20 cm), the electric field is more uniform at the "cloud" in comparison to the high field regions of the transmission line model. As the rod is further extended, the opposite becomes true and the highest field regions occur at the rod attached to the screen. The experimental observations can now be interpreted as breakdown most easily occurs where the high field regions are at a positive polarity.

It is further noted that for all leader rod lengths considered when positioned directly above the towers (locations $P_1$ and $P_2$), the CFO voltage is higher with models employings shielding wires than with spline ball ionizers for the case of negative polarity at the cloud. For positive polarity, the CFO voltage is approximately the same for these configurations. The reduction in CFO voltage for line with spline balls at negative polarity at the cloud with leader can again be interpreted as resulting from the high positive electric field regions surrounding the transmission line with spline ball ionizers.

On the other hand, when the negative lightning leader was located along the transmission line span (points A, B or C), the CFO voltage was higher for the line model without shielding wires and with spline balls than with shielding wires. This occurs because of field disturbances due to the shielding wires. In this case, the lightning stroke is to the phase conductors, so that the transmission line is unprotected. It thus appears

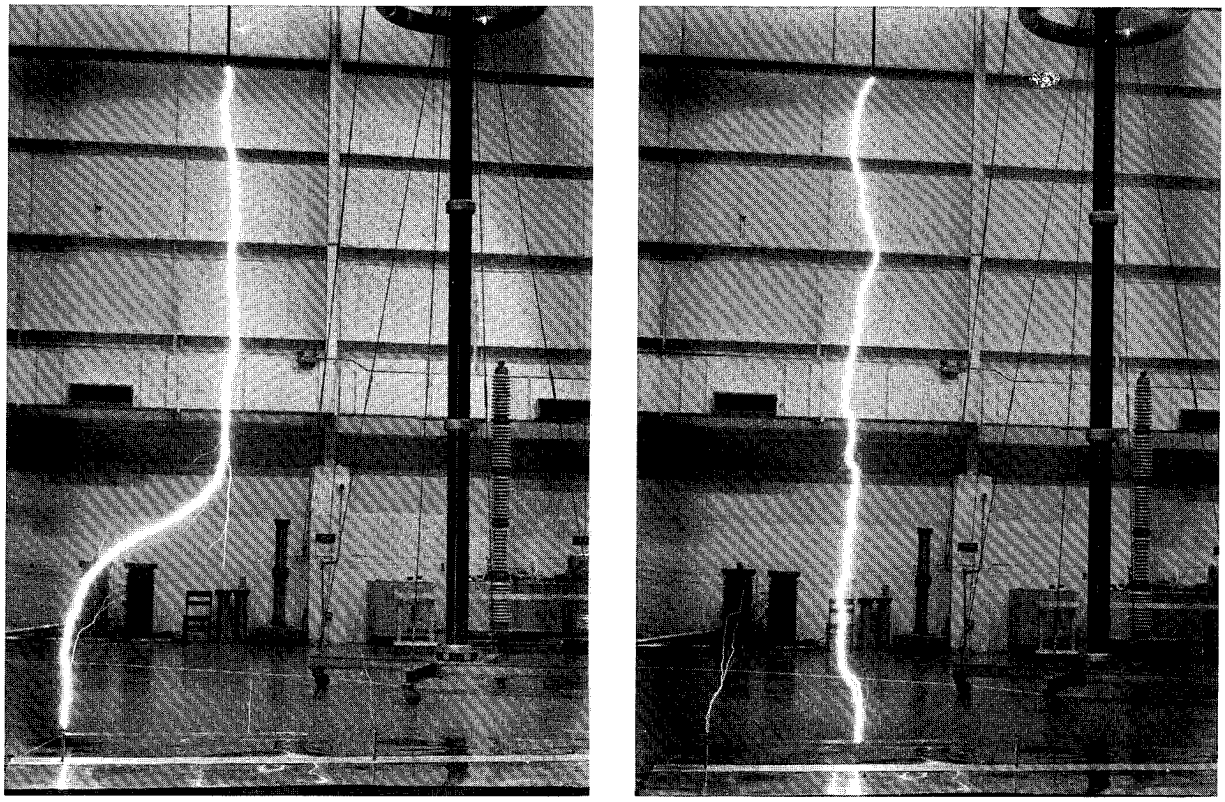


Fig. 6 Lightning impulse flashes to transmission line model with spline ball ionizers from the rod simulating leader. Air gap 4.2 m. Positive polarity:
a) Stroke to spline ball on tower b) Stroke to phase conductor

that the spline ball ionizers do not protect the line, and they only attract the lightning stroke at tower so serve as a lightning collector at the tower.

When the lightning leader was located along the transmission line span (points A, B or C) with a positive leader, the CFO voltage was higher for the line model without the shielding wires and the stroke hits the phase conductors of the line. Again, the spline balls did not protect the phase conductors from the lightning strokes.

The same phenomena was observed when the distance from the rod to ground was increased up to 3.2 m and 4.2 m. The spline balls did not protect the transmission line (Fig. 6) when the leader developed in the middle of the span.

For positive leader, 50% of strokes hit the spline ball and the second 50% of strokes hit the phase conductor. For negative leader, 70% of strokes hit the spline ball ionizers and 30% to the phase conductor in the middle of the span.

TWO TRANSMISSION LINE MODELS TESTED SIMULTANEOUSLY—For cloud model without leader (rod), two pairs of line configurations were selected for simultaneously evaluation of CFO voltages. One compared pair of lines contained the transmission line model without shielding wires and the second line model with two spline ball ionizers. The second compared pair of lines contained the transmission line model with two shielding wires and the second transmission line model with two spline ball ionizers. The spline ball ionizers behaviour in both cases are identical.

When the cloud was energized with negative charge, all lightning strokes hit to the towers with 2 spline ball ionizers. When the cloud was energized with positive charge, all lightning strokes hit to the shielding wires at span, not far away from the towers.

Once again, the previous phenomena for lightning strokes was observed. For negative lightning strokes from cloud to the transmission line, the spline ball ionizers attracted the lightning stroke, so behaved as a collector of lightning strokes.

On the other hand, with a positive cloud polarity, the negative charge from the spline ball ionizers disperse relatively widely and rapidly, so the negative space charge around the spline ball ionizers and lines become more uniform, distributed, reducing the electrical stress in the region of the spline ball ionizers.

For cloud with leader (rod) model, data are presented in paper (11). It was found that independent of the leader length and location of the leader along the span, the CFO voltages were higher for negative lightning leaders than for positive polarity. The difference between the CFO voltages for negative and positive polarities increased as the leader rod increased in length.

In addition to measuring the actual CFO voltages, it was most interesting to note which of the two models was struck by the lightning impulse. For negative polarity of the leader (rod) when positioned above the tower (locations $P_1$ and $P_2$), all strikes were to the tower with the spline balls. independent of the leader length. It was further observed that for negative polarity, strikes occurred to the spline ball ionizers at $P_1$, $P_2$, or $P_3$ from the cloud and not from a 20 cm leader when positioned along the span (locations A,B and C). For longer leaders (e.g., 40 cm and 60 cm) along the span, most strikes were to the model which used shielding wires. This occurs because of the

reduced distance between the shielding wires and the leader (rod) and the minimal influence of the spline balls at some distance from the towers.

When the lightning leader had a positive polarity, the location of the strike depended strongly on the length and position of the simulated leader. Approximately 60% of the strikes were to the spline ball ionizers when the leader was 20 cm long and located at the tower structures ($P_1$ and $P_2$). For a 40 cm rod, 80% of the strikes were to the line with shielding wires for locations along the span (locations A, B and C). It was further observed that with a 60 cm rod, the strikes were to the ground instead of the transmission line structure. In addition, a few strikes to the ground were recorded when the leader was 20 cm and 40 cm long.

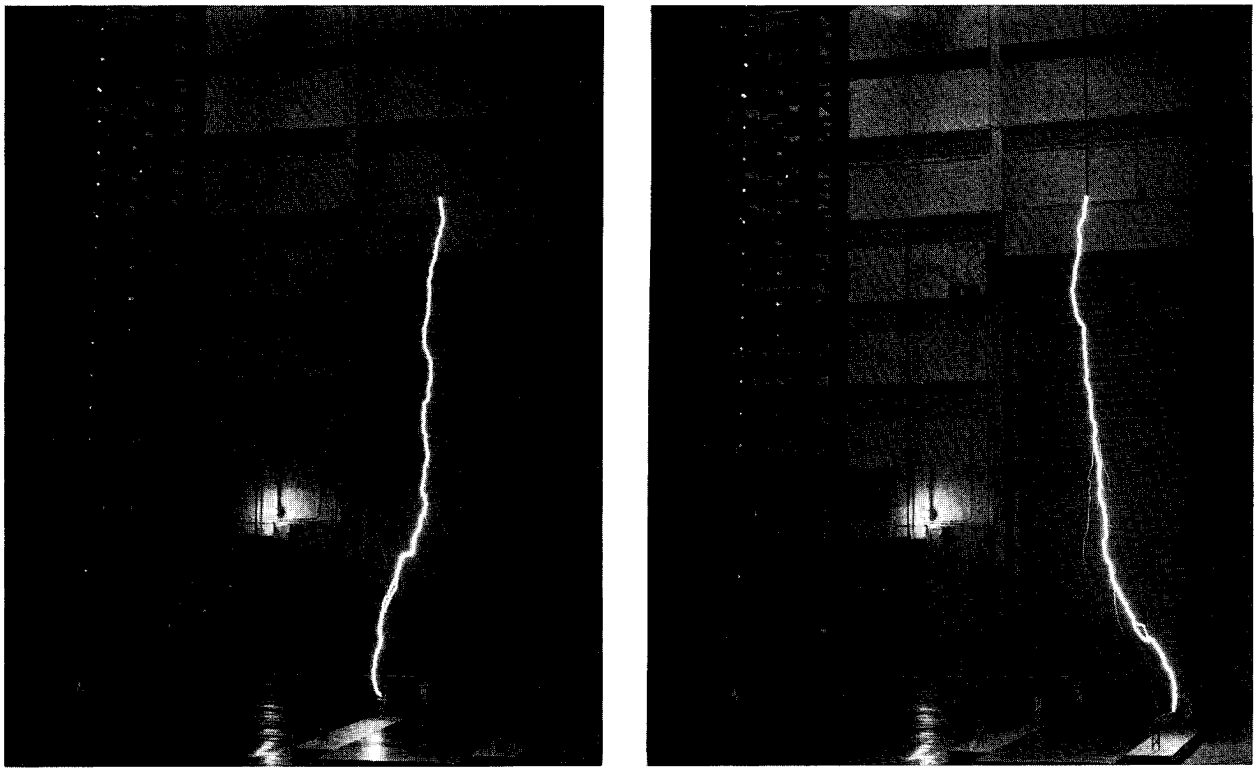


Fig. 7 Lightning impulse flashes two transmission lines tested simultineously. Rod simulated the leader was energized with positive polarity and located in the middle of splan. Air gap to ground 4.2 m. Distance between the lines was 90 cm.
On the right, line without spline ball ionizers
On the left, line with spline ball ionizers

## CONCLUSIONS

Reviewing the results from the measurement of the CFO voltages at negative and positive lightning impulses, switching impulses and steep front pulses for different transmission line models and cloud, with and without spline ball ionizers, several general conclusions can be stated:

1) The CFO voltages are lower for a transmission line model employing spline ball ionizers as compared with a model using shielding wires.

2) For a negative leader polarity when the leader is positioned at the tower, the lightning discharges were to the tower with spline balls rather than the transmission line with shielding wires.

3) For a positive leader, lightning strikes occurred to both transmission line models.

4) When the leader is positioned at space (A, B, C), the lightning discharge was to the line conductor or ground.

5) The spline ball ionizers are improving the electrical field distribution mostly around towers and in some part around line conductors only when the cloud is energized with positive charge. That happened in approximately 10% of the lightning strokes

6) It was further observed that the spline ball ionizers attracted the lightning leader and served as collectors of lightning strikes when the cloud has a negative charge as is typically the case.

7) The spline ball ionizers do not appear to provide any degree of protection for the phase conductors from lightning strikes.

REFERENCES


1. M.N. Uman, *Lightning*, Dover Publications, Inc., New York, 1984.

2. B.F.J. Schonland, "Progressive Lightning, IV. The Discharge Mechanism," Proc. Roy. Soc., Series A, 164, 1938, p. 132.

3. F.S. Young, J.M. Clayton, A.R. Hileman, "Shielding of Transmission Lines," IEEE Transaction on PAS, Special Supplement, Paper No. 63–640, 1963, pp. 134–154.

4. W.W. Lewis, *The Protection of Transmission Systems Against Lightning*, Dover Publication, Inc., New York, 1965.

5. J.G. Anderson, "Lightning Performance of Transmission Lines," Chapter 12 of the *Transmission Line Reference Book: 345 kV and Above*, Second Edition, EPRI, 1982.

6. EPRI, "Lightning Performance," Section 6 of the *Transmission Line Reference Book: 115–138 kV Compact Line Design*, EPRI, 1978.

7. B.A. Kaisen, "Lightning Protection Systems," Broadcast Engineering, May 1992, pp. 42–47.

8. S. Grzybowski, "Effectiveness of Dissipators Used for Lightning Protection on 115 kV Transmission and 13 kV Distribution Lines," MSU Research Report for MP&L, January 1992.

9. S. Grzybowski, "Influence of Spline Balls Ionizers on Lightning Protection of 115 kV Transmission Lines," MSU Research Report for Entergy Services, Inc., December 1993.

10. S. Grzybowski, E.B. Jenkins, "Estimation of Lightning Performance on Models of 115 kV Transmission Lines," 8th International Symposium on High Voltage Engineering, Yokohama, Japan, Vol. 3, 1993, pp. 324–328.

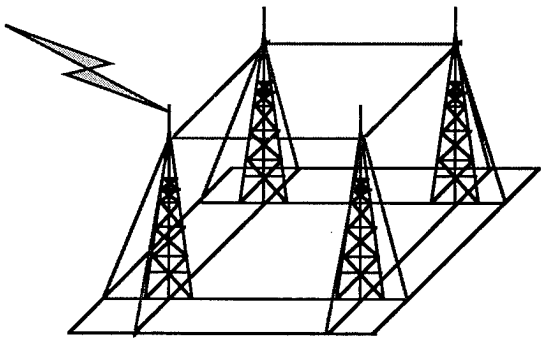
11. S. Grzybowski, G.M. Molen, C.R. Davis and E.B. Daigle, "Effectiveness of Spline Ball Dissipators Used for Lightning Protection on 115 kV Transmission Lines – Model Tests," 22nd International Conference on Lightning Protection, Budapest, Hungary, 1994, Paper R2–03.

# SESSION 11A
# LIGHTNING PHENOMENOLOGY
# CHAIRPERSON: WILLIAM JAFFERIS

# FUNDAMENTAL PRINCIPLES OF GROUND-BASED LIGHTNING PROTECTION SYSTEMS

## PART II

## Multiple cable Lightning Protection Systems (Catenoid Lightning Protection Systems)



**Richard Briët, Ph.D.**
LT-MP Applications
5661 Citrus Court
Cypress, CA 90630
Phone/Fax: (714)-826-8490

ABSTRACT

This is the second of two companion papers about the theory of lightning protection systems: it contains the general theory. The special theory was introduced in **Part I**, where we showed that the propagation of lightning is governed by the fundamental LT-MP principle. For the user, the most important information from the first paper is that the lightning protection zone of a Franklin rod collapses as a function of the inclination angle of the inclined Franklin rod. This could have catastrophic consequences. The result is easily explained both from the perspective of the LT-MP principle (least time), and from the perspective of Ohm's law (least impedance).

Most practicing engineers are more familiar with Ohm's law than with Fermat's principle of Least Time, and so, in this paper the expression for the equivalent length of a structure is obtained with the help of Ohm's law. However, once the expression for the equivalent length is obtained, the remainder of the theoretical description of lightning interactions with structures reverts back to the LT-MP principle.

This paper shows that there are three distinct interaction modes, and three distinct types of catenary lightning protection systems. The closed-form solutions significantly simplify trade-off studies, and enable us to obtain closed-form expressions for optimal lightning protection systems: they yield the optimal dimensions for the most suitable LPS configuration. To demonstrate its utility, this paper concludes with an example trade-off study.

GENERAL INTERACTION EQUATIONS

The general expression for calculating the time for the last step leader to reach the ground by way of a building or some other structure is given by:

$$\tau(p) = \left(\frac{1}{\mu_o}\right) \cdot \left(a(p) + S_{EQ}(p) \cdot \cos\beta\right) \qquad (01)$$

where $S_{EQ}(p)$ is the generalized equivalent electrical length of the structure that is struck by lightning, and $p$ is a length parameter, measured along the structural member which receives the lightning stroke. This allows us to find the minimum time by applying Fermat's principle of least time. In terms of its horizontal and vertical components, the general expression for the air channel is:

$$a(p) = \sqrt{a_h(p)^2 + a_v(p)^2} \qquad (02)$$

From the first derivative of **Equations (01)**, and **(02)** we obtain the general expression for the angle of incidence: (d/dp)[a(p)]=cosγ. Using the standard notation $f'(x) = df(x)/dx$, it is:

$$\cos\gamma = S_{EQ}'(p) \bullet \cos\beta = \frac{-\left(a_h(p) \bullet a_h'(p) + a_v(p) \bullet a_v'(p)\right)}{|a(p)|} \qquad (03)$$

The general expression for the minimum travel time is obtained by solving **Equation (03)** for the length of the air channel, $a(p)$, and substituting the result into **Equation (01)**. The result is:

$$\boxed{\tau(p)_{\min} = \frac{-\left(a_h(p) \bullet a_h'(p) + a_v(p) \bullet a_v'(p)\right) + S_{EQ}(p) \bullet S_{EQ}'(p) \bullet \cos^2\beta}{S_{EQ}'(p) \bullet \cos\beta}} \qquad (04)$$

DERIVATION OF THE EQUIVALENT ELECTRICAL LENGTH, $S_{EQ}$.

Unlike the single grounded lightning rod discussed in the first paper, most catenary lightning protection systems have a complicated structure. In this paper, we assert without formal proof that there is an equivalency relationship between Ohm's law and the LT-MP principle, and that the equivalent electrical length of any structure, $\mathbf{S_{EQ}}$, can be calculated either from the analog of its over-all network impedance, or admittance, where *the equivalent electrical length of each conducting structural member is its impedance divided by its characteristic impedance per unit length.* In this way, a closed-form expression can be derived for the equivalent electrical length, $\mathbf{S_{EQ}}(p)$, for any structure from the analog of the impedance matrix, $\mathbf{M}(p)$, or the admittance matrix, $\mathbf{W}(p)$. The equivalent length matrix is obtained from the impedance matrix by replacing each lumped element in the equivalent circuit model by the equivalent electrical length of the corresponding structural component. Thus, using Cramer's rule, we can solve the matrix equation:

$$\bar{\mathbf{V}} = \underline{\underline{\mathbf{M}(p)}} \bullet \bar{\mathbf{I}}, \qquad (05)$$

and write the solution in the form:

$$\mathbf{I}_1 = \left(\frac{1}{S_{EQ}(p)}\right) \cdot \mathbf{V}_1 \qquad (06)$$

Alternatively, $\mathbf{S_{EQ}}(p)$ can be obtained from the analog of the admittance matrix. This matrix, $\mathbf{W}(p)$, is obtained by replacing each admittance term by the inverse of the equivalent electrical length of the corresponding structural components between nodal points. $\mathbf{S_{EQ}}(p)$ is obtained from the solution for the voltage at the network node, that corresponds to the point where lightning is assumed to strike the structure. Thus, $\mathbf{S_{EQ}}(p)$ can be obtained from the solution of the matrix equation:

$$\bar{\mathbf{I}} = \underline{\underline{\mathbf{W}(p)}} \bullet \bar{\mathbf{V}} \qquad (07)$$

where the matrix $\mathbf{W}(p)$ is the inverse of the matrix $\mathbf{M}$, i.e.:

$$\underline{\underline{\mathbf{W}(p)}} = \underline{\underline{\mathbf{M}^{-1}(p)}} \qquad (08)$$

If we assume that the last step leader strikes a structure at an attachment point $\mathbf{A_x}(p)$, then the general solution for $\mathbf{S_{EQ}}(p)$ is:

$$\boxed{S_{EQ}(p) = \frac{\|\mathbf{W}_{xx}(p)\|}{\|\mathbf{W}(p)\|} = m_{xx}} \qquad (09)$$

where the determinant "$\|\mathbf{W_{xx}}(p)\|$" is the cofactor of the matrix element $w_{xx}$: $\mathbf{S_{EQ}}(p)$ is the element $m_{xx}$ in the matrix $\mathbf{M}$. Whether we choose to start the derivation of the expression for $\mathbf{S_{EQ}}(p)$ from **Equation (05)**, or from **Equation (07)** is a matter of personal preference. We chose to start with **Equation (07)**. To keep it simple, let us assume that each structural member has the same impedance per unit length. This assumption is not necessary, in general, but it will simplify our discussion in the following way: (1) Each diagonal element in the admittance matrix, $w_{ii}$, is replaced with the sum of the inverse of the lengths of the structural components connected to the $(i+1)^{st}$ node in the equivalent circuit diagram, and (2) each off-diagonal element in the admittance matrix is replaced with the inverse of the length of the structural member that connects adjacent nodes. For catenary LPSs, the matrices $\mathbf{M}$, and $\mathbf{W}$ are symmetrical, and with the assumption that the impedance per unit length is the same for all structural members, each element in the impedance matrix is replaced with the actual length of a structural member. In the admittance matrix, after the appropriate substitutions are made, the element $w_{00}$ is the sum of all inverse lengths of the structural members that are connected to the first node; the element $w_{01} = w_{10}$ is 1/(length of the structural member connecting node 1 with node 2). It is conventional to assign the index "0" to the node representing the reference ground. However, before we calculate the equivalent length, $\mathbf{S_{EQ}}(p)$, we must say something about the three types of Lightning Protection Structures.

## TYPE-I, TYPE-II, AND TYPE-III LPS STRUCTURES

For catenary lightning protection systems, $\mathbf{M}$ and $\mathbf{W}$ are sparsely populated symmetrical matrices: They show symmetry properties that are characteristic for self-standing, grounded lightning rods, and for primary structures[1], configured in a string, or a ring of interconnected, individually grounded lightning rods, which are usually mounted on separate support towers (See **Figures 1 through 3**). For this reason we call the self standing grounded lightning rod a "**Type-I**" (or "Type-A") structure; we call the **string** configuration a "**Type-II**" (or "Type-S") structure, and we call the **ring** configuration a "**Type III**" (or "Type-R") structure. All primary structures exhibit symmetry features

[1]We introduced the term " primary structure" for a LPS in **Part I** of these papers: it refers to structures whose primary function is to attract lightning away from objects that are protected against direct strikes. A new LPS, not to be discussed here (invented by this author), will also mitigate induced effects.

which can be identified with one or more types. A ladder configuration is an example of a hybrid (or "Type-H") structure which exhibits Types II, and III symmetry features[1]. We will now introduce a short-hand notation to describe lightning interactions with specific types of primary structures on the ground, i.e. we will use

- a left-superscript, m, for the number of support towers or masts,
- a right-subscript I (or A), II (or S), III (or R), H, or T for the type of structure, and
- a left-subscript, n, for the number of down conductors used to ground each lightning rod.

The third of these indices is practical only if each air terminal is grounded by the same number of down conductors. For example, the cryptograms:

$$ {}^{m}_{n}S_{III}(p) = S_{EQ}(p) \qquad (10) $$

and

$$ {}^{m}_{n}\tau_{III}(p) = \left(\frac{1}{u_o}\right)\left(a(p) + {}^{m}_{n}S_{III}(p)\cdot\cos\beta\right) \qquad (11) $$

are expressions for the equivalent electrical length, and the traveling time of the last step leader of lightning, that reaches the ground by way of a Type-III lightning protection system, which has an air terminal on each of $m$ masts, each of which has $n$ grounding cables. The grounded Franklin rod is an example of a Type-I structure, where both $m$, and $n$ are *one*. We will use the right-hand subscript $H$ to identify a hybrid structure, and we will use the right-subscript $T$ when there is no need to identify a specific type of primary structure. When the discussion is of a general nature, we may leave off all subscripts, and/or superscripts. Furthermore, it is found that the expressions for the equivalent electrical length of a structure is unique for each one of three interaction modes, which will be discussed below. These modes depend on the location of the lightning attachment point on the structure.

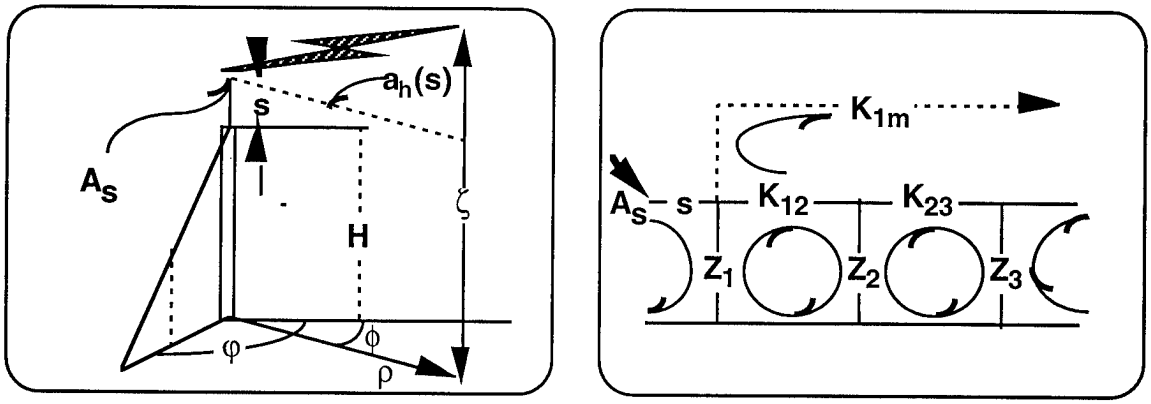
## LIGHTNING INTERACTION MODES

Lightning may strike a catenary lightning protection structure at any one of three clearly identifiable locations. Based on the location of the lightning attachment point, we list all three interaction modes. When lightning strikes a primary structure at:

(1) a point on the lightning rod, we call it a "Mode-1 Interaction";
(2) a point on a down conductor, we call it a "Mode-2 Interaction"; or
(3) a point on a cable connecting two rods, we call it a "Mode-3 Interaction".

The diagrams in the figures on the following page show the interaction modes in the order of ascending complexity. In each diagram $Z_i$ is the equivalent length of the network of grounding cables for the $i^{th}$ lightning rod; $K_{ij}$ is the cable length between the $i^{th}$ , and $j^{th}$ rod. **Figure 1** shows the attachment point, $\mathbf{A_S}$, where $p$ :=> **s** measures the length of the conducting segment of the lightning rod. The second diagram in **Figure 1** shows the equivalent circuit diagram: this diagram is used to construct the equivalent impedance, or admittance matrix.

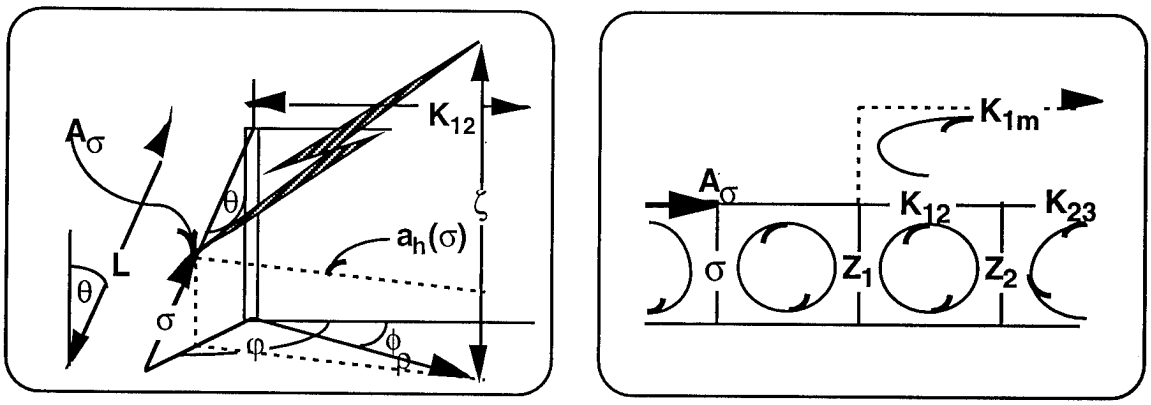
[1]The two four-tower lightning protection systems at LC-40, and at LC-41 at Cape Canaveral, in Florida are examples of hybrid LPS structures.




Lightning striking a lightning rod  Equivalent Circuit Diagram

**FIGURE 1.** THIS IS A DIAGRAM OF A "MODE-1 INTERACTION" WHERE $S_{EQ}={}_n^m S_T(\mathbf{s})$.

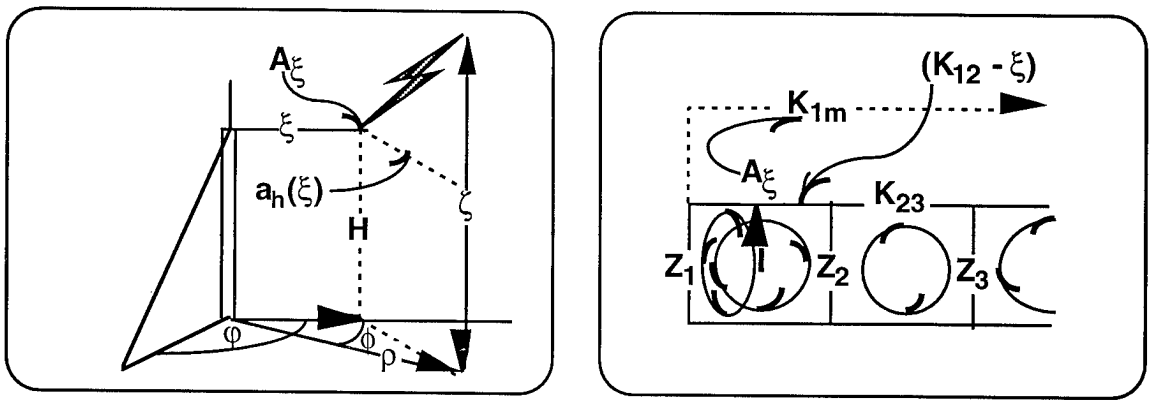
**Figure 2** shows a Mode-2 interaction, and the corresponding equivalent circuit diagram. The length $p$ :=> $\sigma$ is measured between the ground, and the attachment point, $\mathbf{A}_\sigma$.




Lightning striking a down conductor  Equivalent Circuit Diagram

**FIGURE 2.** THIS IS A DIAGRAM OF A "MODE-2 INTERACTION" WHERE $S_{EQ}={}_n^m S_T(\sigma)$.

**Figure 3** shows a "Mode-3 interaction", and the corresponding equivalent circuit diagram, where $\xi$ measures the distance between a reference tower, and the attachment point $\mathbf{A}_\xi$.




Lightning striking a cable $K_{12}$  Equivalent Circuit Diagram

**FIGURE 3.** THIS IS A DIAGRAM OF A "MODE-3 INTERACTION" WHERE $S_{EQ}={}_n^m S_T(\xi)$.

PARAMETRIC TRADE STUDIES

*Example of Mode-1 interactions with Type II primary structures*

As defined in the last section, when lightning strikes an air terminal at a point $\mathbf{A_S}$, it is called a *Mode-1* interaction (See **Fig. 1**). Here, the general equation for the travel time is:

$$ {}^{m}_{n}\tau_{\mathrm{T}}(\mathbf{s}) = \left(\frac{1}{u_o}\right)\left(a(\mathbf{s}) + {}^{m}_{n}S_{\mathrm{T}}(\mathbf{s})\cdot\cos\beta\right) \qquad (12) $$

where the horizontal and vertical components of the lightning air channel, respectively, are given by:

$$ a_{\mathrm{h}} = \rho\,, \quad \text{and} \quad a_{\mathrm{v}} = (\zeta - \mathbf{z}) \qquad (13) $$

We assume that the source region for the last step leader is located at an elevation $\zeta$ above the ground, where $\zeta$ is a function of the peak lightning current, $I_{pk}$. It is given by an equation due to Love[1]: $\zeta=10.(I_{pk})^{0.65}$. The attachment point, $\mathbf{A_S}$, on a rod is located at $\mathbf{z=s+}H$ above the ground. With the help of the equivalent circuit diagram in **Figure 1**, it can be shown that for a Mode-1 lightning interaction with primary structures, the solution in **Equation (09)** for the equivalent electrical length, $\mathbf{S_{EQ}(s)}$ is:

$$ S_{EQ}(\mathbf{s}) = {}^{m}_{n}S_{\mathrm{T}}(\mathbf{s}) = \mathbf{s} + {}^{m}_{n}F_{\mathrm{T}}\left(\{Z_i\};\{K_{ij}\}\right), \qquad (14) $$

where ${}^{m}_{n}F_{\mathrm{T}}\left(\{Z_i\};\{K_{ij}\}\right)$ is a **Form Function**: it depends only on the network of grounding cables for each lightning rod, $Z_i$, and the interconnecting cables between two lightning rods, $K_{ij}$ (Some of the details of the derivation are shown at the end of this paper). For example, for regular[2] structures:

$$ \begin{aligned} {}^{1}_{n}F_{\mathrm{I}}\left(\{Z_1\};\{\mathbf{no}\cdot K_{ij}\}\right) &= Z_1 = \frac{L}{n} = \frac{H}{n\cdot\cos\theta} \\ {}^{2}_{n}F_{II}\left(\{Z_1,Z_2\};\{K_{12}\}\right) &= \frac{Z_1\cdot(K_{12}+Z_2)}{(Z_1+K_{12}+Z_2)} = \frac{(\kappa\cdot n\cdot\cos\theta+1)}{(\kappa\cdot n\cdot\cos\theta+2)}\cdot H \end{aligned} \qquad (15) $$

where $L$ is the length of one of the $n$ grounding cables for each lightning rod, $K_{12}$ =k.H is the length of the cable between the first, and the second grounded rod, $\theta$ is the inclination angle of a grounding cable, measured with respect to the vertical direction, and $H$ is the height of a support tower, or mast, on which a lightning rod is mounted.

From **Equation (14)** it follows that $S'(s)=1$. Substituting this result into **Equation (03)** shows that the angle of incidence, $\gamma$, equals the *constant* angle, $\beta$. We can apply this result to obtain the minimum time directly from the first diagram in **Figure 1**, or we can substitute **Equations (13)**, and **(14)** into **Equation (12)** to derive the expression for the minimum time. Either way, the result is the same:

---

[1]Ref.: "Lightning," Vol. 2, Lightning Protection, p. 560.

[2]We call a structure "regular" if every lightning rod is grounded in exactly the same way, every support mast has the same height, H, and the distance between any two masts, K, is the same.

$$
\begin{aligned}
{}^{m}_{n}\tau_{\mathrm{T}}(\mathbf{s}) &= \left(\frac{1}{u_o}\right)\left(\frac{(\zeta-\mathbf{z})}{\cos\beta}+{}^{m}_{n}S_{\mathrm{T}}(\mathbf{s})\cdot\cos\beta\right) = \\
&= \frac{\zeta-\mathbf{z}\cdot\sin^2\beta-\left(H-{}^{m}_{n}F_{\mathrm{T}}\left(\{Z_i\};\{K_{ij}\}\right)\right)\cdot\cos^2\beta}{u_o\cdot\cos\beta} = \\
&= \frac{\zeta-\mathbf{s}\cdot\sin^2\beta-\left(H-{}^{m}_{n}F_{\mathrm{T}}\left(\{Z_i\};\{K_{ij}\}\right)\cdot\cos^2\beta\right)}{u_o\cdot\cos\beta}
\end{aligned}
\qquad (16)
$$

where we have made a substitution:

$$\mathbf{z} = \mathbf{s} + H \qquad (17)$$

For design purposes it is important to calculate the optimal height of the support towers used in a particular LPS configuration. This is accomplished by equating **Equation (16)** with $\zeta/\mathbf{u_o}$, and solving for $H_{\mathrm{B}}$. A useful format for writing the solution is:

$$H_B-{}^{m}_{n}F_{\mathrm{T}}\left(\{Z_i\};\{K_{ij}\}\right)\cdot\cos^2\beta = H_B\cdot\left(1-{}^{m}_{n}f_{\mathrm{T}}\cdot\cos^2\beta\right) = \sin^2\beta\cdot\left(\frac{\zeta}{1+\cos\beta}-\mathbf{s}\right) \qquad (18)$$

where

$${}^{m}_{n}f_{\mathrm{T}} = \frac{{}^{m}_{n}F_{\mathrm{T}}\left(\{Z_i\};\{K_{ij}\}\right)}{H_B} \qquad (19)$$

is called the **Form Factor** for the given type of lightning protection system. Thus, the optimal height for any type of lightning protection system in a *Mode-1* interaction, can be calculated from **Equation (20):**

$$H_{\mathrm{B}} = \frac{\sin^2\beta}{\left(1-{}^{m}_{n}f_{\mathrm{T}}\cdot\cos^2\beta\right)}\cdot\left(\frac{\zeta}{1+\cos\beta}-\mathbf{s}\right) \qquad (20)$$

For example, for a grounded Franklin rod, ${}^{1}_{1}F_{1}\left(\{Z_1\};\{no\cdot K_{ij}\}\right) = H$, and so ${}^{1}_{1}f_{1} = 1$. By substituting these expressions into **Equation (20)**, the optimal height for a **Type-I** lightning protection system, such as a grounded Franklin rod is:

$$H_{\mathrm{F}} = \left(\frac{\zeta}{1+\cos\beta}-\mathbf{s}\right) = \left(\mathbf{z}_{\mathrm{x}}-\mathbf{s}\right) \qquad (21)$$

This result was first obtained in **Part I**, using a very different method. Since the form factor, ${}^{m}_{n}f_{T}(p)$, is *usually* less than *one*, a comparison of **Equation (20)** with **Equation (21)** shows that *usually* $H_B < H_F$ . However, this is not true if (n.cosθ) < 1.

*It is always true that the effectiveness of a catenoid lightning protection system is degraded if the grounding cables are spread apart in an umbrella like fashion to cover a larger area!*

The simplest explanation is that according to Ohm's Law, the act of spreading the grounding cables apart increases the network impedance, and therefore decreases its effectiveness to attract lightning. The tables at the end of this paper show this effect in the numerical results of a trade study of **Mode-I** lightning interactions with **Type-I**, and **Type-II** LPSs.

SUMMARY OF ANALYSIS RESULTS

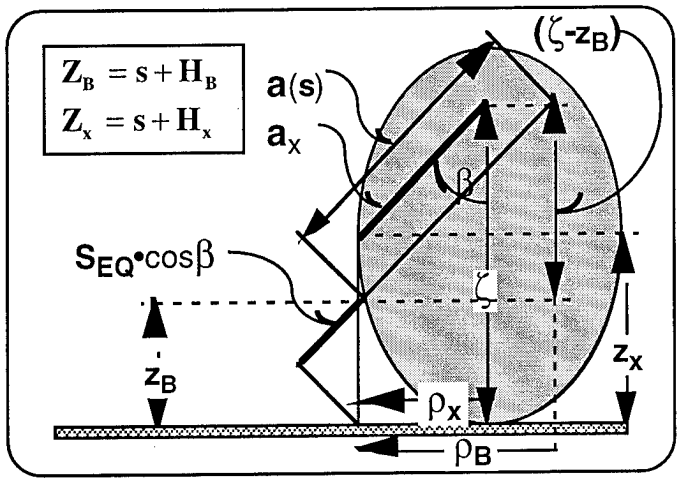



FIGURE 4. GEOMETRICAL RELATIONSHIPS BETWEEN $\zeta$,, $S_{EQ}$, $Z_B$, $\rho_B$, $Z_X$,AND $\rho_X$. FOR REFERENCE,THE COMPANION LETHAL ZONE OF AN ERECT **TYPE-I** STRUCTURE. IS ALSO SHOWN.

**Figure 4.** shows the interrelationship of the parameters $\beta$, $\mathbf{a_X}$, $\mathbf{a(s)}$, $\mathbf{z_X}$, $\mathbf{Z_B}$, $\rho_X$, and $\rho_B$. For a **Mode-1** interaction, the critical angle of incidence, $\beta$, is independent of the location of the point of attachment on the lightning rod. This makes it possible to obtain all equations in the text by inspection. For example, we substitute $\mathbf{a(s)=(\zeta - Z_B)/\cos\beta)}$ into **Equation (11)** to derive **Equation (15)**. Likewise, by inspection, the critical range $\rho_B$ is given by $\rho_B=(\zeta - \mathbf{Z_B}).\tan\beta$. When compared with the critical range, $\rho_X$, for a grounded Franklin rod, the relationship is $\rho_B=\rho_X.(\zeta - \mathbf{Z_B})/(\zeta - \mathbf{z_X})$. This means that it is possible to build low profile lightning protection systems that are effective in attracting lightning away from taller secondary structures, even if the secondary structure and the source region are on the same side of the primary structure! The converse is also true:

*It is possible that the effectiveness coefficient of a tall lightning protection system is less than that of the shorter structure it is supposed to protect.*

If this happens, then the role of primary vs. secondary structures is reversed, and the protection system is said to fail. This explains some of the reports of incidents where people were struck by lightning when they were walking between, or near tall structures.

ANNOTATED REFERENCES

LIGHTNING, Volume 2, Lightning Protection, Edited by R.H. Golde, Academic Press, 1977, is a compilation of articles by various lightning experts. In Chapter 17, *The lightning Conductor,* Golde shows that there are many opinions about the shape, and size of lightning protection zones, all of which are based on observations of artificial, and natural lightning.

"The Lightning Protection Code," in NFPA 780, Section 3-10, 1992., is issued, and periodically updated by the National Fire Protection Association. It is a "How-to" document, which contains descriptions of lightning protection zones, which varies as a function of the criticality of the protected assets (Compare, for example, Section 3 with Section 6).

The International Standard, CEI/IEC 1024-1: 1990, "Protection of Structures," Part 1: General Principles is a living document, written and maintained by an international committee, which includes members from the American National Standards Institute, ANSI.

Fermat's Principle of Least Time, and the Principle of Least Action is described in many physics books. The Feynman LECTURES ON PHYSICS is one of my favorite references.

"Lightning Protection of Aircraft," F.A. Fisher, and J.A. Plumer, Lightning Technologies Inc., and R.A. Perala, Electro Magnetic Applications Inc., 1990, published by Lightning Technologies Inc., 10 Downing Parkway, Pittsfield, MA 01201, USA. Lightning attachment zones on aircraft are described in Chapter 3.

APPENDIX: DERIVATION OF THE FORM FUNCTION/FORM FACTOR

The only example discussed in this paper concerns a Mode-1 interaction, where lightning is assumed to strike a primary catenoid structure at an air terminal. For such interactions,

$$w_{00} = w_{01} = w_{10} = \left(\frac{1}{s}\right); \qquad w_{11} = \left(\frac{1}{s} + \frac{1}{K_{12}} + \frac{1}{Z_1} + \left[\frac{1}{K_{1m}}\right]\right); \qquad w_{12} = w_{21} = \left(\frac{1}{K_{12}}\right) \tag{A-1}$$

$$w_{1m} = w_{m1} = \left(\frac{1}{K_{1m}}\right) \qquad w_{ii} = \left(\frac{1}{K_{(i-1),i}} + \frac{1}{Z_i} + \frac{1}{K_{i,(i+1)}}\right); \text{ and } \; w_{i,(i\neq j)} = \left(\frac{1}{K_{i,(i\neq j)}}\right) \tag{A-2}$$

for $i$ greater than 1. It can be shown that the general form for the equivalent electrical length, $S_{EQ}$, is given by:

$$ {}^{m}_{n}S_T(s) = s + {}^{m}_{n}F_T(s) \tag{A-3}$$

where ${}^{m}_{n}F_T(s)$ is called the "**Form Function**" of a Type-T primary structure in a Mode-1 interaction. The "Form Function" depends exclusively on the lengths of the structural components of a lightning protection system. Furthermore, if we limit our discussion to Type I, and II structures, where $w_{1m}=w_{m1}=0$, it is found that if the LPS configuration is:

a grounded Franklin rod, then: $$ {}^{1}_{1}F_I = H \tag{A-4}$$

a one-mast LPS, then: $$ {}^{1}_{n}F_I = \frac{H}{n \cdot \cos\theta} \tag{A-5}$$

a two-mast, Type-II LPS, then: $$ {}^{2}_{n}F_{II} = \left[\frac{1}{{}^{1}_{n}F_I} + \frac{1}{K + {}^{1}_{n}F_I}\right]^{-1} \tag{A-6}$$

a three-mast, Type-II LPS, then: $$ {}^{3}_{n}F_{II} = \left[\frac{1}{{}^{1}_{n}F_I} + \frac{1}{K + {}^{2}_{n}F_{II}}\right]^{-1} \tag{A-7}$$

an $m$ -mast, Type-II LPS, then: $$ {}^{m}_{n}F_{II} = \left[\frac{1}{{}^{1}_{n}F_I} + \frac{1}{K + {}^{(m-1)}_{n}F_{II}}\right]^{-1} \tag{A-8}$$

*It is worth to note the recursion relationship!* For convenience we express the equivalent lengths in terms of the height of a support tower, or mast, i.e. :

$$K_{rb} = \kappa \cdot H_B, \quad \text{and} \quad Z_b = \left(\frac{L_b}{n}\right) = \left(\frac{1}{n \cdot \cos\theta_b}\right) \cdot H_B \tag{A-9}$$

The Form Function can now be written as:

$$ {}^{m}_{n}F_T(s) = H_B \cdot {}^{m}_{n}f_T\left(\{Z_i / H_B\}, \{K_{ij} / H_B\}\right) \tag{A-10}$$

where ${}^{m}_{n}f_T\left(\{Z_i / H_B\}, \{K_{ij} / H_B\}\right)$ is called the "**Form Factor**" of a Type-T LPS structure.

NUMERICAL RESULTS OF MODE-I INTERACTIONS WITH TYPES I, & II STRUCTURES

This study shows how the inclination angle, $\theta$, affects the normalized optimal height of a catenary LPS, $H_B/z_X$. The index "j" locates $\mathbf{A_S}$. The study assumes: **n=1**; **K = H**, and $\beta$**=45**.

**$\theta$ = 00 degrees**

| j :=> | 1 | 2 | 3 | 4 | 5 | 6 | 7 |
|---|---|---|---|---|---|---|---|
| \m/ | | | | | | | |
| 1 | 1.00 | | | | | | |
| 2 | 0.75 | 0.75 | | | | | |
| 3 | 0.73 | 0.67 | 0.73 | | | | |
| 4 | 0.72 | 0.66 | 0.66 | 0.72 | | | |
| 5 | 0.72 | 0.65 | 0.65 | 0.65 | 0.72 | | |
| 6 | 0.72 | 0.65 | 0.65 | 0.65 | 0.65 | 0.72 | |
| 7 | 0.72 | 0.65 | 0.65 | **0.64** | 0.65 | 0.65 | 0.72 |

**$\theta$ = 30 degrees**

| j :=> | 1 | 2 | 3 | 4 | 5 | 6 | 7 |
|---|---|---|---|---|---|---|---|
| \m/ | | | | | | | |
| 1 | ***1.18*** | | | | | | |
| 2 | 0.80 | 0.80 | | | | | |
| 3 | 0.77 | 0.69 | 0.77 | | | | |
| 4 | 0.76 | 0.68 | 0.68 | 0.76 | | | |
| 5 | 0.76 | 0.68 | 0.67 | 0.68 | 0.76 | | |
| 6 | 0.76 | 0.68 | **0.66** | **0.66** | 0.68 | 0.76 | |
| 7 | 0.76 | 0.68 | **0.66** | **0.66** | **0.66** | 0.68 | 0.76 |

**$\theta$ = 45 degrees**

| j :=> | 1 | 2 | 3 | 4 | 5 | 6 | 7 |
|---|---|---|---|---|---|---|---|
| \m/ | | | | | | | |
| 1 | ***1.71*** | | | | | | |
| 2 | 0.90 | 0.90 | | | | | |
| 3 | 0.84 | 0.74 | 0.84 | | | | |
| 4 | 0.83 | 0.72 | 0.72 | 0.83 | | | |
| 5 | 0.83 | 0.71 | 0.70 | 0.71 | 0.83 | | |
| 6 | 0.83 | 0.71 | **0.69** | **0.69** | 0.71 | 0.83 | |
| 7 | 0.83 | 0.71 | **0.69** | **0.69** | **0.69** | 0.71 | 0.83 |

**$\theta$ = 60 degrees**

| j :=> | 1 | 2 | 3 | 4 | 5 | 6 | 7 |
|---|---|---|---|---|---|---|---|
| \m/ | | | | | | | |
| 1 | ***1432.8*** | | | | | | |
| 2 | ***1.25*** | ***1.25*** | | | | | |
| 3 | ***1.05*** | 0.88 | ***1.05*** | | | | |
| 4 | ***1.01*** | 0.82 | 0.82 | ***1.01*** | | | |
| 5 | 1.00 | 0.80 | 0.78 | 0.80 | 1.00 | | |
| 6 | 1.00 | 0.80 | 0.77 | 0.77 | 0.80 | 1.00 | |
| 7 | 1.00 | 0.80 | **0.76** | **0.76** | **0.76** | 0.80 | 1.00 |

These results show that increasing the inclination angle, $\theta$, degrades the effectiveness of a catenary LPS. This effect is especially noticeable for the single tower, which is consistent with the collapsing zone of protection as discussed in **Part I**.

# USING LASERS TO TRIGGER/GUIDE LIGHTNING

Arnold A. Barnes, Jr.
Phillips Laboratory
Geophysics Directorate
Hanscom Air Force Base
Massachusetts, USA 01731-3010
Telephone (617) 377-2939 FAX (617) 377-8892

Matthew A. Kozma
Physics Department
United States Air Force Academy
Colorado, USA 80841-2922

ABSTRACT

One way to protect high value assets and reduce losses due to lightning strikes would be to provide a preferential path for the lightning to follow or to discharge clouds by triggering lightning prior to the occurrence of natural lightning. One mechanism to accomplish this would be to use a laser to create an ionized path in the atmosphere. Initial attempts with powerful $CO_2$ laser were defeated due to plasma quenching which limited the length of the ionized path.

Three methods of circumventing this problem have been investigated recently. Work in Japan has concentrated on multiple foci of the laser beams to create ionized line segments. They also intend to launch the laser beam from the top of a 50 m or 100 m tower where the electric field would be stronger than at the ground.

The United States Air Force and NASA have in the recent past funded two programs to look into the possibility of ionizing specific constituents of the atmosphere to create a conducting path.

Ophir Corporation investigated the use of a laser to ionize argon (which composes 0.94% of the air in the troposphere) by means of multiple photon absorption. Their model calculations predict that an ionized column a couple of hundred meters in length could be created, and initial laboratory experiments indicated that this method would work without producing inverse bremsstrahlung.

A second approach being pursued by the University of New Mexico is to ionize atmospheric oxygen and nitrogen by multi-photon absorption. Their laboratory experiments have shown that this technique works, and they have actually produced a spark (triggered lightning) between two charged plates in the laboratory. In order to extend the lifetime of the ionized column they have proposed to use a second laser, co-axial with the first laser. This second laser needs to be shorter than 800 nm.

In these latter two techniques, the laser wavelengths are in the visible and ultraviolet parts of the spectrum where the single photon absorption is small. The particular frequencies were carefully chosen so that either the argon or oxygen and nitrogen would be ionized by multi-photon absorption.

## INTRODUCTION

The Air Force is interested in protecting high value asset, explosives etc. from lightning strikes. Laser lightning rods (LLR) have the potential to guide natural lightning near the ground to provide protection. LLRs might also have the potential to initiate (trigger) lightning from charged clouds which are not producing natural lightning. Triggered lightning is a major concern for missile launches from Kennedy Space Center/Cape Canaveral Air Force Station. (See Barnes and Willett (1) in these proceedings.)

Since the 1970's the Air Force and others have attempted to use lasers to create an ionized path in the atmosphere for use as a lightning rod. Most of these efforts were done with $CO_2$ lasers without success. In 1988 it was suggested (2, 3) to us that more energetic photons in the 200-300 nm range be used so that only a few photon would be required to ionize atmospheric constituents. A basic research, high risk/high payoff contract was let by the Air Force to investigate one of the approaches. One of the other approaches was funded as a Small Business Innovative Research (SBIR) contract by NASA/KSC.

## IONIZATION OF OXYGEN AND NITROGEN

Under the Air Force contract, Professor Diels of the Physics Department at the University of New Mexico developed a 248 nm laser in order to ionize atmospheric oxygen with three photon and atmospheric nitrogen with four photons (4, 5). The laser pulse was compressed to ~200 femtoseconds ($200 \times 10^{-15}$ seconds) to create a high density of photons to enhance the ionization. In addition, the pulse was to be chirped (swept in frequency) so that the rear of the pulse would travel faster through the atmosphere than the front of the pulse. This would compress the pulse and hence increase the photon density while photons were being decreased due to capture and ionization of the $O_2$ and $N_2$. Laboratory experiments have confirmed and theoretical calculations have shown that the ionization provides a preferred path between two charged plates. The reader is referred to (4, 5), funded by EPRI, for details.

Recently Deals, et al, (5, 6) found that the intense pulse is self-focusing, a process called self-filamentation. This will also help to slow the decrease in the density of the photons being depleted by the ionization process.

In order to enhance and maintain the ionization of the column they have suggested the use of a second laser with wavelength less than 800 nm. This work continues to be funded by the Electric Power Research Institute (EPRI).

## IONIZATION OF ARGON

Argon is a minor, well mixed constituent of the atmosphere. In the troposphere is composes 0.94% of the atmosphere. Ophir Corporation did some theoretical modeling calculations on ionizing Argon with a 314.5 nm laser which looked very promising for creating an ionized column of a couple of hundred meters in length. The initial modeling work was done under a Department of Energy contract (3). More recently they were funded by NASA/KSC under a Small Business Innovative

Research (SBIR) contract but were never able to get definitive laboratory results primarily due to problems with the laser equipment from Germany. Their model calculations and initial laboratory experiments indicated that this technique would work without producing inverse bremsstrahlung which defeated earlier $CO_2$ laser experiments.

The selective ionization of Argon might be considered as an alternative to the University of New Mexico approach if the University of New Mexico approach produces too much ionization.

Currently this work is not continuing.

## USING A POWERFUL $CO_2$ LASER

The Japanese are interested in protecting their high voltage electric power lines from lightning strikes. Their approach (7, 8) has been to extend the length of the ionized path created by a powerful $CO_2$ laser. So far they have created paths up to 12 meters in length in the laboratory. This is accomplished by use of specially constructed optics which focus the dispersed laser beam at a number of points along the beam axis. Laboratory experiments have also created zigzag ionized paths between two electrodes. Laboratory lightning was then created along the zigzag path.

Wang, et al, (8) have found during periods of thunderstorms that the electric fields at the top of one 50 meter tower ran 100 times as intense as the fields at the ground. In addition, their laboratory experiments indicate that 200 kV/m are necessary to initiate lightning and 170 kV/m are required to maintain the path between the electrodes. Increased ionization from the laser might reduce these figures.

Their plan seems to be to propagate the laser beam from the top of a 50 m or 100 m tower, in order to start the path in a high ambient field, and to aim the beam towards lightning breakdown pulses or downward propagating lightning. Location of the preliminary lightning breakdown pulses would be detected by a slow antenna.

## DISCUSSION

Progress is being made towards developing a functional laser lightning rod to protect high value assets. We would look to the combinations of the University of New Mexico femtosecond UV approach combined with the elevated tower approach suggested by the Japanese to achieve this goal. A lightning mapper might be a better choice than a slow antenna for detection of the breakdown pulses. A fast response, computer driven beam mounted on a tower would provide improved protection from cloud to ground strikes over a radius of perhaps a half a kilometer.

The use of a laser lightning rod to trigger lightning in charged clouds which are not producing lightning is more problematical. First the fields at the top of the tower might not be large enough to initiate a leader. Second, if the ionized column near the cloud does initiate a leader, the cloud-to-ground stroke might not follow the path to the tower. Obviously this scenario needs more thought and research.

It has been suggested that a LLR be used to harvest the energy in lightning. Dr. Stan Heckman has shown that this is not presently economical and his calculations are contained in Appendix A of (9).

The use of laser lightning rods would indeed be a dual use technology. Besides being used to protect DoD high value assets (10), it could be used to protect commercial assets including high voltage electric power lines.

REFERENCES


1. A. A. Barnes, and J. C. Willett, "Cost Benefit of an ABFM at KSC," Paper presented at the 1995 International Aerospace and Ground Conference on Lightning and Static Electricity, Williamsburg, Virginia, September 26-28, 1995.

2. G. J. Fetzer, J. E. Stockley, and L. J. Radziemski, "Perturbation of the local charge concentrations in the atmosphere due to high irradiance laser beams," Proceedings of SPIE Symposium on Innovative Science and Technology for Government and Civilian Applications O/E Lase Conference, Los Angeles, Jan. 1989.

3. G. J. Fitzer, "Geophysical Amplified Directed Energy Weapon," New & Innovative Concepts Program, Summary Report, U.S. Department of Energy, Oakland, California, October 1989.

4. X. M. Zhao, J.-C. Diels, "How Lasers Might Control Lightning Strikes," Laser Focus World, November 1993.

5. X. M. Zhao, J.-C. Diels, C. Y. Wang, J. M. Elizondo, "Femtosecond Ultraviolet Laser Pulse Induced Lightning Discharges in Gases," IEEE Journal of Quantum Electronics, Vol. 31, No. 3, 1995, pp 599-612.

6. X. M. Zhao, P. Rambo, J.-C. Diels, J. M. Elizondo, "Effect of Oxygen on Laser Triggering of Lightning," Proceedings of CLEO, Baltimore, Maryland, 1995.

7. D. Wang, "Preliminary Study on Laser Triggered Lightning," thesis, Osaka University, Osaka, Japan, 1995, vi + 97.

8. D. Wang, T. Ushio, Z.-I. Kawasaki, K. Matsuura, Y. Shimada, S. Uchida, C. Yamanaka, Y. Izawa, Y. Sonoi, N. Simokura, "A Possible Way to Trigger Lightning Using a Laser," Journal of Atmospheric and Terrestrial Physics, Vol. 57, No. 5, 1995.

9. M. A. Kozma, "A Brief History of Laser Guided Lightning Discharge Models and Experiments," Environmental Research Papers, No. 1153, PL-TR-94-2193, AD A 290 349, Phillips Laboratory, Hanscom Air Force Base, MA, 1994, vii + 17.

10. A. A. Barnes, R. O. Berthel, "A Survey of Laser Lightning Techniques," Proceedings of the 1991 International Aerospace and Ground Conference on Lightning and Static Electricity, Vol. 1, NASA Conference Publication 10058, Cocoa Beach, Florida, 16-19 April 1991, 53-1 to 52-6.

# THUNDERSTORM LOCALIZATION USING MUSIC

**Timothy M. Rynne, John Robinson, Kim Olszewski, & Christof Berthold**
**Scientific Applications and Research Associates, Inc.**
**Huntington Beach, CA, USA**
**Telephone (714) 373-5509 FAX (714) 373-4771**
**and**
**Launa Maier**
**National Aeronautics and Space Administration**
**Kennedy Space Center**
**Florida, USA**
**Telephone (407) 867-4409 FAX (407) 867-2848**

ABSTRACT

This paper describes a novel application of the Multiple Signal Characterization (MUSIC) algorithm which enables localization of thunderstorm activity and prestrike prediction and location of lightning strikes. The capability to predict the occurrence of lightning strikes, not simply detect the presence of lightning, is now possible. The need for this capability is underscored by the tremendous costs each year in the loss of life, property, and operational productivity.

Under a Phase II Small Business Innovation Research contract with the NASA, SARA, Inc. has developed a workstation that will track storm centers based on electric field data, animate the storm tracks, establish system errors, and predict the on set of lightning strikes. The workstation performs and displays the results of two analyses of the electric field mill data. One analysis, based on MUSIC eigenanalysis, utilizes a model of the thunderstorm and calculates model parameters while efficiently searching the entire parameter space. The other analysis, in which a least squares algorithm has been implemented, utilizes the same thunderstorm model as the MUSIC algorithm but only searches a subset of the model space. The storm centers are displayed in color and looped to depict storm movement and charge locations.

In this paper, the analysis techniques will be discussed briefly and the results of the analyses using data from electric field mills installed at the KSC will be presented on a workstation display. Also, comparisons of MUSIC products and Lightning Detection and Ranging (LDAR) products will be presented for several thunderstorms. These comparisons confirm the reliability of the analytical techniques incorporated in the workstation. In fact, for the initial cases studied, the MUSIC product predicts where lightning activity will occur. The subsequent presence of lightning is confirmed by the LDAR data.

## INTRODUCTION

Due to the deleterious effects lightning can produce, and has produced, on aerospace equipment and personnel, launch and ground operations at the KSC are suspended whenever atmospheric conditions associated with thunderstorm activity are observed. There are always significant cost impacts as a result of these suspensions, and frequently, there are even lost launch opportunities. Therefore, the KSC has developed and implemented several techniques for observing and correlating atmospheric conditions associated with hazardous thunderstorm activity for the purpose of reducing unnecessary suspensions. However, the utility of these techniques is limited because they function on the occurrence of lightning rather than on the conditions immediately preceding the occurrence of lightning. There still remains a need to predict where lightning will occur before it actually does and when it will occur unexpectedly under apparent conditions of fair weather.

Under a Phase II SBIR effort, a Thunderstorm Localization Workstation (TLW) which can predict where lightning will occur has been developed. The TLW utilizes, for atmospheric condition sensory input, the data from the existing field mill array installed at the KSC. This array has been installed for several years and data from it has provided some, but not definitive, indication of thunderstorm activity. Through application of advanced signal processing techniques it is now possible to significantly enhance the utility of these field mill data.

The TLW uses the MUSIC inversion method to localize charge centers, from which the lightning strike emanates, based on field mill output. The TLW displays the field mill strip charts, the existing Launch Pad Lightning Warning System (LPLWS) contours, and the localization contours simultaneously. The output uses the CINE loop format familiar to weather operations personnel for visually predicting charge speed and direction. The resulting data product has been validated against simulated and LDAR videos. The localization contours appear prior to lightning strikes, and therefore can be used to predict the location of imminent lightning.

The TLW overcomes the limitation in setting better field mill criteria for launch and ground operations due to the need for objective interpretations of the array output. The advanced signal processing techniques utilized promise better integration of the interpretation of field mill data into real-time operations, such that unnecessary operational halts can be avoided. Any wide area which has a lightning safety concern will also benefit from the methods described herein. With the TLW it is now possible to predict where lightning will occur because the magnitude and geographical coordinates of electrical charge accumulation can be determined very precisely.

## LAUNCH PAD LIGHTNING WARNING SYSTEM DESCRIPTION

Currently, KSC uses a network of accurate electric field sensors, called field mills, to determine potential threats to vehicles due to atmospheric charge. A lightning strike on Apollo 12 in 1969 led to the development of the electric field mill network operated by KSC. Data from the network are used by Range Operations Control Center (ROCC) personnel to identify potential range safety threats due to possible electric field discharges (lightning) on a vehicle during launch. The network actually measures the local vertical electric field at 31 points around the Cape Canaveral area [1].

The LPLWS was upgraded in 1992-1993, with the new field mills providing greater dynamic range at finer quantization levels, a self monitoring and reporting feature, and rain protection. The field mill array comprises 31 field mills in a network across the cape. Figure 1 presents the location of the sensors, numbered 1 to 34; sensor numbers 3, 24, and 31 are not used. The outputs of the sensors are gathered in the ROCC by the LPLWS Base Station running a real-time operating system. Some of the data presented in this report came from an earlier network which was still functional in the Spring of 1995, although the newer network has replaced the older one as an operational tool. The locations of the old mills are the same, to within one or two meters, as the locations of the network described above. The data stream from all sensors is time-tagged and recorded continuously.

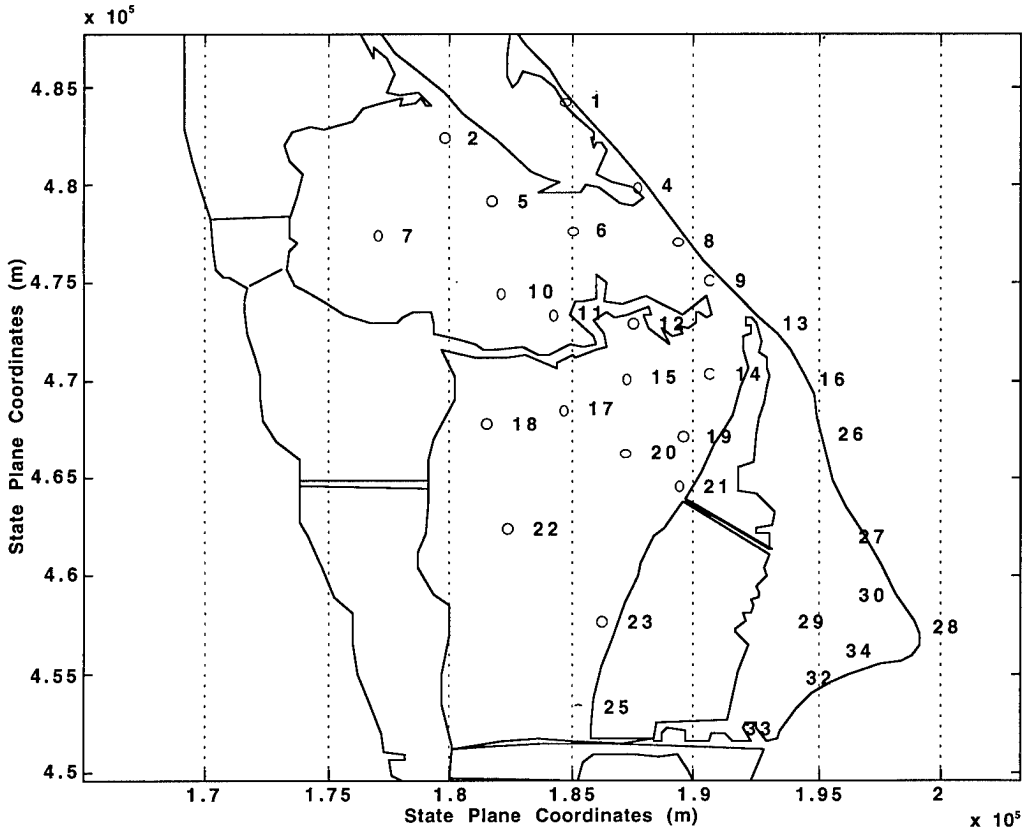



FIGURE 1.LPLWS FIELD MILL MAP.

## MUSIC BACKGROUND

Data from the electric field mill array over the KSC/Cape Canaveral regions can be mathematically inverted to determine the location of charges, assuming the number of charges. Non-linear least squares methods have been utilized in the past to attempt to localize charges, but, being

recursive in nature, occasionally they require long periods of time to converge, and may converge on a "local" minimum, yielding misleading results. Modern signal processing methods, not subject to these limitation, can be brought to bear to localize the charges and determine their number.

The MUSIC algorithm was first developed in the late-1970s as an array signal processing technique for direction finding [2]. MUSIC belongs to a class of methods known as inverse methods, and a subclass called the parametric spectrum approach [3]. It is also sometimes referred to in the context of eigenanalysis methods - those methods which exploit the eigenvalues, eigenvectors, and subspaces thereof, associated with a data matrix. It has been successfully applied as a frequency estimation technique [4], and as a method to localize magnetic encephalogram sources in three dimensions [5]. MUSIC's advantages include robustness, predictable processing requirements, and ability to utilize data from non-uniform arrays of sensors. Its disadvantages include reduced accuracy compared to recursive least squares approaches. However, this disadvantage has been found to be inconsequential in localizing charge centers.

## STORM CHARGE MODELS

The contour map presently generated at KSC is implicitly based on a point charge model, albeit 31 charges in a fixed pattern about the Cape. These contour patterns generated are still subject to quite a degree of interpretation, and the patterns vary significantly in the presence of minor fluctuations. The model presented in this section is also based on a point charge, but interpretation of the model is more straightforward. Any complex distribution of static charges can be simplified to a point charge, if viewed from a distance relatively large compared to the diameter of the charge distribution [6]. The primary drawback of simplicity is the increased modeling error, but the MUSIC procedures presented in this research provide means of solving this simple model even under less than ideal conditions.

We assume a point charge source of intensity Q coulombs located at position $(x_q, y_q, z_q)$. The observer position is on the ground at position $(x, y, 0)$. We use the sign convention that a positive electric field indicates that a positive charge would move upwards (i.e., the negative of the potential gradient). In weather related terms, our sign convention is "fair weather negative." Representing the earth as a perfect ground plane, the electric field at the surface has only a non-zero vertical component:

$$E = \frac{-Qz_q}{2\pi\varepsilon\left((x-x_q)^2 + (y-y_q)^2 + z_q^2\right)^{3/2}} = QF\{x_q, y_q, z_q, x, y\} \qquad \text{(EQ 1)}$$

where $\varepsilon$ is the permittivity of the medium, here assumed to be free space. We note that this point charge model is a quite common starting point in most thunderstorm models and thus represents a potential basis upon which the more sophisticated models may be built.

The above formulas were for a single charge and a single sensor. The extension to multiple charges and sensors follows directly. We can arrange our data into spatiotemporal matrix as:

Each vector $\boldsymbol{e}\,(t)$ represents the electric field signal for $m$ sensors (e.g. $m = 31$) at a single time instance$t$ due to $p$ sources:

(EQ 2)

$$e_1 = \left( \sum_{(i=1)}^{p} Q_i F\{x_{qi}, y_{qi}, z_{qi}, x_1, y_1\} \right)$$

$$e_2 = \left( \sum_{(i=1)}^{p} Q_i F\{x_{qi}, y_{qi}, z_{qi}, x_2, y_2\} \right)$$

$$\cdots$$

$$e_m = \left( \sum_{(i=1)}^{p} Q_i F\{x_{qi}, y_{qi}, z_{qi}, x_m, y_m\} \right)$$

Because of the form of this equation, each element $e_i$ above can be computed as the inner product of a charge intensity vector $\boldsymbol{Q} = [Q_1\, Q_2 \ldots Q_p]^t$ and a spatial transfer function vector or gain $\boldsymbol{g_i}$, where each element of $\boldsymbol{g_i}$ is of the form

$$\frac{z_{qr}}{2\pi\varepsilon\left( (x_i - x_{qr})^2 + (y_i - y_{qr})^2 + z_{qr}^2 \right)^{3/2}}$$

Thus, we can combine all such vectors $\boldsymbol{g_i}$ into a gain matrix $\boldsymbol{G}$ whose columns are the gain vectors for each sensor-source combination to obtain

$$\boldsymbol{e} = \boldsymbol{G}^t\boldsymbol{Q}. \qquad \text{(EQ 3)}$$

Over a fixed interval of time, we acquire $n$ such vectors of data. We observe that this data is changing as a function of time, and we therefore need some sort of time dependent parameter. The reduced sampling interval of 10 samples/second is relatively fast compared to the ground speed of the thunderstorm, and we will process the data in relatively short time segments. During these intervals, we can approximate the position of the storm as relatively fixed in space and *assume that only the intensity Q is changing as a function of time*. Therefore, the gain matrix G is assumed to be time-independent, and the only variation is due to the sources themselves, yielding the time-dependent forward model

$$(t) = [\boldsymbol{e}\,(t_1), \ldots, \boldsymbol{e}\,(t_n)] = \boldsymbol{G}[\boldsymbol{q}\,(t_1), \ldots, \boldsymbol{q}\,(t_n)] = \boldsymbol{GQ}\,(\tau). \qquad \text{(EQ 4)}$$

Continuing with superposition, a dipole model can be constructed as the superposition of 3 co-located orthogonal dipoles, and adding associated terms to the gain matrix.

MUSIC LOCALIZATION - THEORY

In this section the application of the MUSIC algorithm to the thunderstorm localization problem is summarized. Much of the discussion here is adapted from [5] to the point charge model. The MUSIC algorithm can be summarized as:

1. Given the $m \times n$ data matrix $\boldsymbol{E}$f or $m$ sensors and $n$ time samples, perform the eigendecomposition of the estimate $\hat{\boldsymbol{R}}_E = (1/n)\boldsymbol{E}\boldsymbol{E}^T = \hat{\Phi}\hat{\Lambda}\hat{\Phi}^T$. Here, $\hat{\Phi}$ is the matrix of eignenvectors, $\hat{\Lambda}$ the diagonal matrix of eigenvalues, $\boldsymbol{R}$ is the autocorrelation matrix form from the data matrix $\boldsymbol{E}$. Order the eigenvalues, such that $\lambda_1 \geq \lambda_2 \geq \ldots \geq \lambda_m$. Equivalently, perform the singular value decomposition (SVD) of $\boldsymbol{E}$, where the eigenvalues are the square of the singular values (svd is a single built in function call in MATLAB).

2. Select the separation point (rank) $1 \leq r < m$ between the signal and noise subspace eigenvalues. The rank r is assumed to equal the number of sources. While theoretically $\lambda_{min} = \sigma^2$, the random variance in the data, repeats with multiplicity $(m\text{-}r)$, in practice there is some spread among the smaller eigenvalues, depending on the number of time slices $n$ used to estimate $\boldsymbol{R}_E$. If the signals are of sufficient strength and sufficiently uncorrelated during the time interval, then a distinct drop in the magnitude of eigenvalues will occur between $\lambda_r$ and $\lambda_{r+1}$. (A more detailed treatment of the order determination problem is given in (7).) Form the estimated matrices $\hat{\Phi}_s$ and $\hat{\Phi}_o$ from the corresponding signal and noise eigenvectors.

3. Over a fine grid of three-dimensional locations $\{(x, y, z)_p\}$, calculate the corresponding $m \times 1$ gain matrix $\boldsymbol{G}_p$ for each location, obtain the principal left eigenvectors $\boldsymbol{U}_{Gp}$ of $\boldsymbol{G}_p$, using an SVD such that $G_p = \boldsymbol{U}_{Gp}\Sigma_{Gp}\boldsymbol{V}_{Gp}^T$, and evaluate the cost function $I(p) = \boldsymbol{U}_{Gp}^T\hat{\Phi}_o\hat{\Phi}_o^T\boldsymbol{U}_{\boldsymbol{C}}$ Form two-dimensional slices through the three-dimensional space, e.g., $(x, y)$ planes for constant $z$, and plot the function $Z\{(x, y, z)_p\} = 1/J_h(p)$ as contours, images, or oblique mesh plots. The peaks of this function give the locations of the $p$ sources.

We now state the assumptions necessary for proving some of the MUSIC assertions.

- [AH] (Gain Matrix Assumption)-- The $m \times r$ hybrid gain matrix $\boldsymbol{G}$, $m > r$, is of full column rank $r$ for $p$ point charges. In other words, the gain columns of the source components cannot be combined to simulate the gain columns of a third source component. For $p$ point charges, the rank $r = p$.
- [AS] (Asynchronous Assumption)-- The time series for different charge strengths $Q_i(t)$ components are asynchronous or linearly independent, i.e., the time series of one component is not simply a scalar multiple of the time series from another component, nor can any combination of time series form another time series. Thus the time series matrix $\boldsymbol{Q}$ is also of full rank $r$.

- [AW] (Noise Whiteness)-- The additive noise is considered temporally and spatially zero-mean white noise with variance $\sigma^2$, such that the expectation of the outer product of the $m \times n$ noise matrix is $E\{\boldsymbol{N}(n)\,\boldsymbol{N}(n)^T\} = \sigma^2\boldsymbol{I}$, where $n$ is the number of time slices, and $E\{\}$ is the expectation operator. This requirement may be eased by prewhitening of the data, if the noise statistics are known.

The key assumption is that spatially distinct sources have linearly independent time series over the measured time segment.

Our model for noiseless data with $m$ sensors, $n$ time slices, and $r = p$ point sources is $\boldsymbol{E} = \boldsymbol{GQ}$, where E is $m \times n$ , $\boldsymbol{G}$ is $m \times p$ , $m > p$, and $\boldsymbol{Q}$ is $p \times n$ , $p < n$. Consider the model for the noisy data under the assumption AW of zero mean white noise, $\boldsymbol{E} = \boldsymbol{GQ} + \boldsymbol{N}$. The spatial autocorrelation of the data is then

$$\boldsymbol{R}_F \equiv E\{\boldsymbol{E}(n)\,\boldsymbol{E}(n)^T\} = E\{[\boldsymbol{GQ}(n) + \boldsymbol{N}(n)][\boldsymbol{GQ}(n) + \boldsymbol{N}(n)]^T\} = \boldsymbol{GR}_Q\boldsymbol{G}^T + \sigma^2\boldsymbol{I} \qquad \text{(EQ 5)}$$

where $E\{\}$ is the expectation operator, and $\boldsymbol{R}_Q = E\{\boldsymbol{Q}(n)\,\boldsymbol{Q}(n)^T\}$, and $I$ is the $m \times m$ identity operator. By assumption AS, the correlation matrix $\boldsymbol{R}_Q$ is of full rank. The square symmetric matrix $\boldsymbol{R}_E$ may be written in terms of its eigendecomposition as

$$\boldsymbol{R}_E = \Phi\Lambda\Phi^T = [\Phi_s\Phi_o]\begin{bmatrix}\Lambda_s & \\ & \Lambda_o\end{bmatrix}[\Phi_s\Phi_o]^T \qquad \text{(EQ 6)}$$

where we define $\Lambda_s$ as the diagonal matrix containing the $p$ largest eigenvalues and $\Phi_s$ as the matrix containing the corresponding eigenvectors. By our assumptions, it is well known that the eigenvalue equal to the variance of the noise, $\lambda = \sigma^2$, repeats with multiplicity $m - p$ [2]. Accordingly, $\Lambda_o = \sigma^2\boldsymbol{I}$, and $\Phi_o$ is the matrix containing the corresponding $m - p$ eigenvectors.

Comparing Equation (5) and Equation (6) and using assumptions AH and AS, it is straightforward to show that the space spanned by $\Phi_s$ is identical to that spanned by $\boldsymbol{GR}_Q\,\boldsymbol{G}^T$; therefore, $\Phi_s$ is said to span the *signal* subspace (hence the subscript $s$). The space spanned by $\Phi_o$ is the orthogonal complement of the signal subspace and is referred to as the *orthogonal* or *noise* subspace (hence the subscript $o$). Based on these observations, it can be shown that the quantity

$$\boldsymbol{U}_{Gp}^T\Phi_o\Phi_o^T\boldsymbol{U}_{Gp} \qquad \text{(EQ 7)}$$

is zero for any matrix $G_p = \boldsymbol{U}_{Gp}\Sigma_{Gp}\boldsymbol{V}_{Gp}^T$ corresponding to a true source location [2]. Thus we can determine the source locations exactly using Equation (7) provided $\boldsymbol{R}_E$, and hence $\Phi_o$, is known exactly.

In practice, MUSIC approximates $\boldsymbol{R}_E$ by $\hat{\boldsymbol{R}}_E = (1/n)\,\boldsymbol{EE}^T$. Estimates of the signal and noise subspaces, $\hat{\Phi}_s$ and $\hat{\Phi}_o$, are formed using an eigendecomposition of $\hat{\boldsymbol{R}}_E$.

ORDER SELECTION--To successfully apply MUSIC, a determination of the MUSIC order (i.e. rank of the data matrix, which is assumed to be equal to the number of sources) is critical. The intuitive method of order determination is to plot the sorted eigenvalues of the data matrix on a logarithmic scale, and select only those which are high and are not in the "flat" tail of the plot, where the supposed noise eigenvalues occur. Typical objective measures of the order can be determined by the Akaike Information Criterion (AIC)(8), the Minimum Description Length (MDL) Criterion(9), and a modified version of the AIC due to Wax and Kailath (10). For this research both the AIC and modified AIC were tried, but typically overestimated the order. A heuristic order determination based on a simple statistical F-test was found to be more fruitful at correctly estimating the order of the data matrix. An upper bound on the order was set at 4, this being equal to the number sources which could be located by classical least squares techniques while still allowing almost one extra degree of freedom in the data per independent variable (16 unknowns with 31 observations). The steps in estimating the order are

- Compute the SVD of the data matrix and sort the singular values (a $m$ by $m$ matrix, where m = 31).
- Compute a test value by taking the maximum of (the mean of eigenvalues 5-10) and (the uniform quantization error).
- Compare eigenvalues 1,2,3, and 4 to the maximum of the test value using an F-test with a significance of 0.05.
- Count the eigenvalues which, based on the F-test, differ significantly from the test value - this is the order.

MUSIC LOCALIZATION - STUDIES

The results of several studies performed with MUSIC are presented herein.

SINGLE POINT CHARGE--Validation runs were made for a single point charge at 2km in height and 10C in strength - a very well defined source. By placing the sources at various locations over the field mill area, a visual determination of the efficacy of MUSIC was made. It was determined that the horizontal error can be up to 3km at points just inside the array, but it's below 100m well inside the array; the vertical error stays below 60m inside the array. Based on this observation and a grid spacing of 1km, the actual MUSIC peak detector does not scan for peaks in the corners of the grid; the actual scan space follows the parallelogram shape of the electric field mill array as shown in Figure 2.

TWO POINT CHARGES--Several studies were conducted in order to determine the ability of MUSIC to resolve two spatially separated charges when the order was directly assumed. For the case of two charges of 5C each at 5km height, and separated by roughly 2km, and a grid at 1km resolution, MUSIC could not resolve the two charges (i.e. only one peak was detected). For a separation of 6 km, it was found that MUSIC resolves the two quite well. For an intermediate value of 4km in the x and y directions, MUSIC resolves both charges nicely over the array and near the edges of the useful space shown in Figure 1. It should also be noted that in most cases, where MUSIC was unable to resolve two charges, it gave the centroid between the two charges as the likely location and a magnitude of almost the sum of the two. Thus a good estimate of the centroid, modeled as a point charge, results.

ORDER DETECTION--For the two-charge case, the order F-test had little difficulty correctly selecting the correct value of 2 for the 6km charge separation, but could not, even at the higher threshold of 0.1, correctly obtain the order for two charges for close-in spacing. This is a limitation on the resolution capability of the existing array, and is independent of the MUSIC grid. Figure 3 shows the results of the F-test analysis.

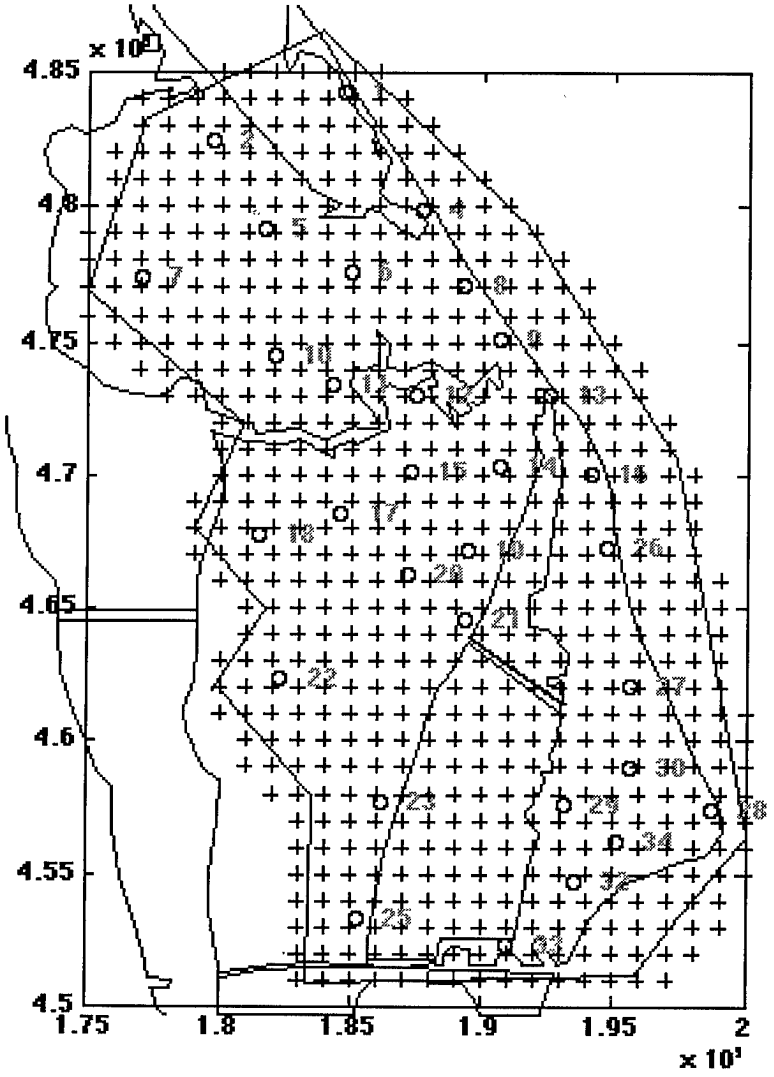
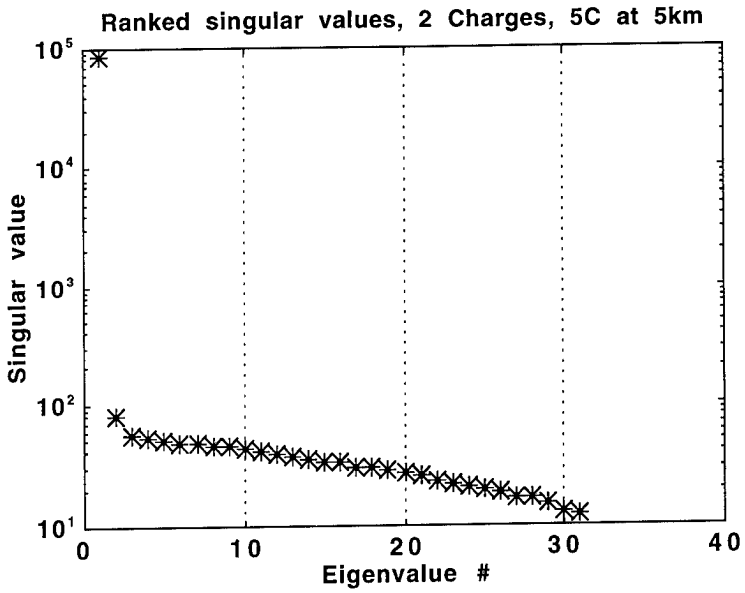
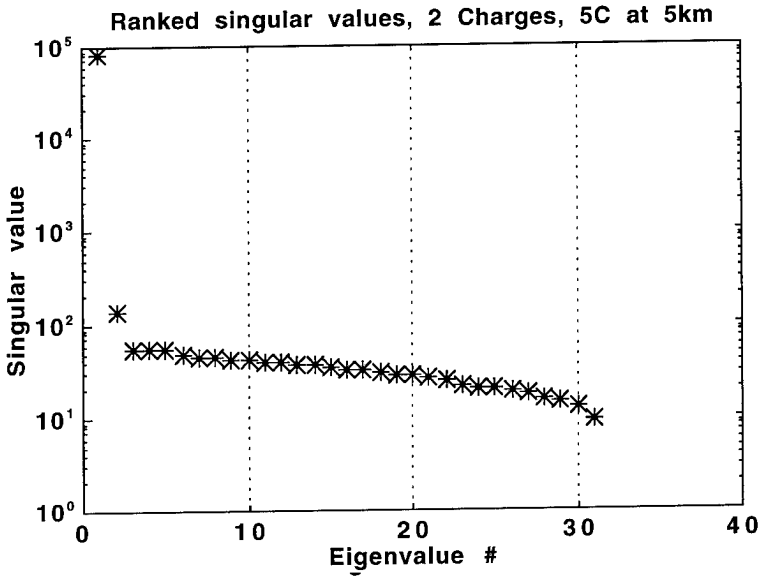



FIGURE 2: USEFUL GRID FOR RESOLVING CHARGES.

COMPARISON WITH LPLWS CONTOURS AND LDAR--Besides performing simulated studies of the ability of MUSIC to identify, localize, and estimate the charge of cells above the KSC, we also performed investigations of the temporal estimation of charge cell location with actual data from the field mill. In order to provide a visual validation for the MUSIC process, the charge cell localization three dimensional projections were contrasted directly against data from the LDAR system. These comparisons showed excellent agreement between the MUSIC estimation of charge buildup location and the subsequent lightning discharge location as determined by




a) 2km Separation




b) 6km Separation

FIGURE 3: F-TEST ASSESSMENT OF ORDER ESTIMATION.

the LDAR system. In fact the sequential observation shows that MUSIC was able to determine the existence of a strong charge cell prior to initiation of the lightning event. Figures 4 and 5 show an example of this in which two frames of MUSIC and LDAR system displays separated by 1 minute are shown. These figures are overlaid with the MUSIC display and the associated ground level electrical field contours in the upper left hand corner and the LDAR display on the lower and

right hand sides. The MUSIC display is in a gray scale with the lighter grays indicating highest probability of localization. The LDAR system display is a large set of dots which represent detected locations for step leader formation. Please note that the scales of these two displays is quite different in that the MUSIC plots concentrate on the immediate area of the KSC and Cape Canaveral Air Force Station (CCAFS). In Figure 4, MUSIC is showing a strong cell existing off the False Cape at the KSC while no lightning events are shown for this cell. Subsequently, as indicated in Figure 5, LDAR system is showing a number of discharges off the False Cape area.

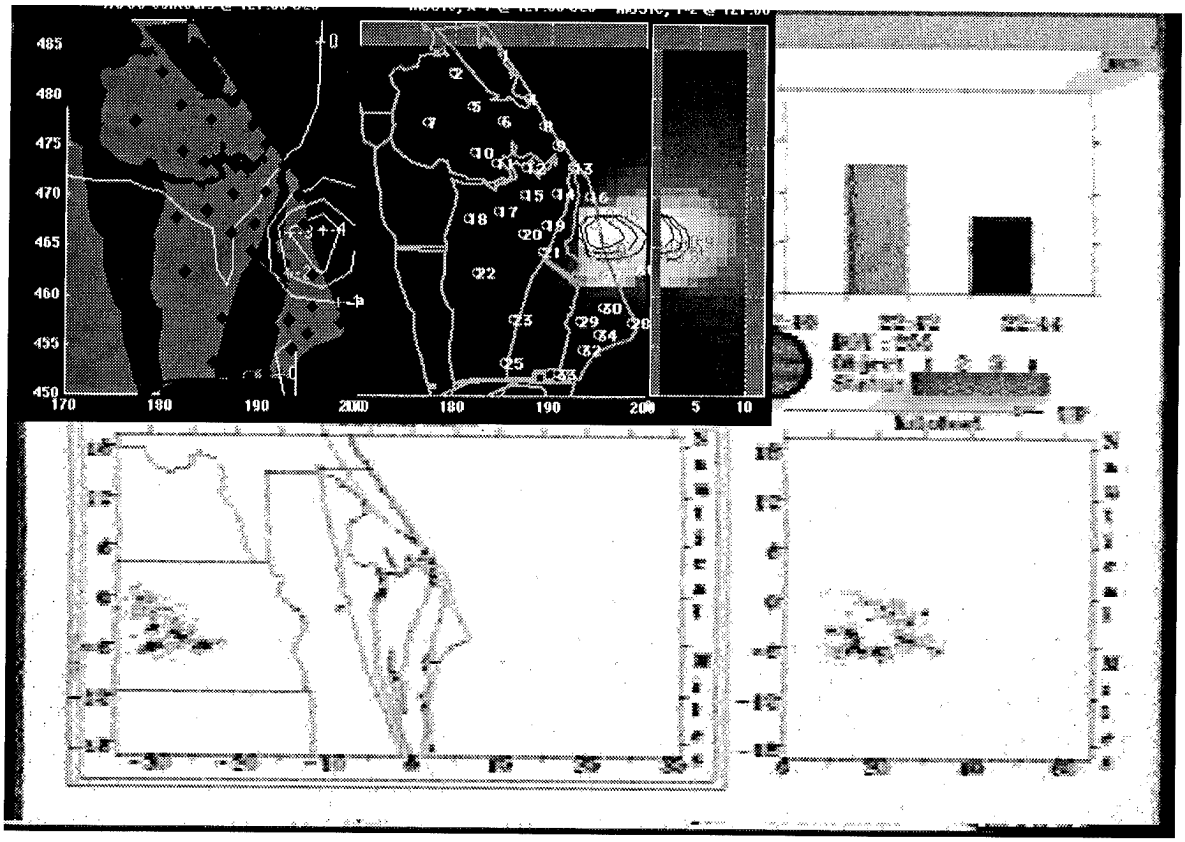



FIGURE 4: MUSIC ESTIMATION OF STRONG CHARGE CELL WITH LDAR SYSTEM NOT SHOWING ACTIVITY IN CHARGE CELL LOCATION.

## CONCLUSIONS

The main conclusions from the thunderstorm model and MUSIC studies are

- vertical dipole models significantly improved localization
- eliminating a small number of mills during a localization procedure will not significantly affect error, and may be desirable if corona effects are detected at some mills

- addition of a few mills around the perimeter of the existing array (e.g., a mill anchored in the sandbars False Cape), is the an effective for improving storm detection for launch operations.

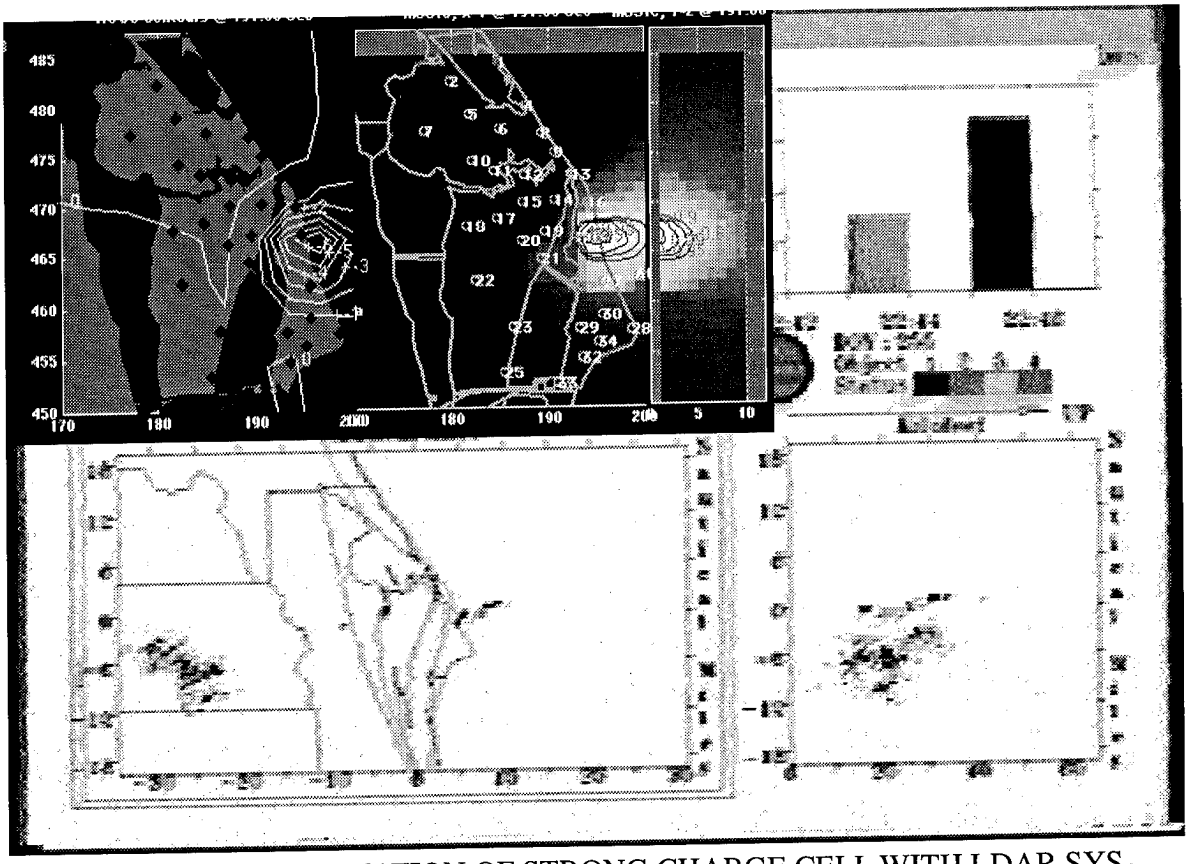



FIGURE 5: MUSIC ESTIMATION OF STRONG CHARGE CELL WITH LDAR SYSTEM NOW SHOWING ACTIVITY AT 1 MINUTE LATER TIME THAN IN FIGURE 4.

- over estimation of order by a small number may still result in a well defined MUSIC spectrum;
- charge center detection from MUSIC spectra that are high (as indicated by red or brighter on the MUSIC display, and as visually determined) over the entire array should be treated with caution
- charge center detection outside a parallelogram roughly 5km outside the array should be treated with caution
- MUSIC and LDAR show good correlation.

REFERENCES

[1] Maier, L. M., and T. R. Strange, "Electric Field Mill Training Handbook," *Computer Sciences Corporation* Kennedy Space Center, Contract NAS10-11400, January 1988.

[2] R. O. Schmidt, "Multiple emitter location and signal parameter estimation", IEEE Transactions on Antennas and Propagation, vol. AP-34, pp. 276--280, March 1986. Reprint of the original 1979 paper from the RADC Spectrum Estimation Workshop.

[3] S. Haykin et al, "Some Aspects of Array Signal Processing", IEE Proceedings-F, vol. 139, no. 1, February 1992.
[4] S. L. Marple, Jr., "Digital Spectral Analysis with Applications", 1987 Prentice-Hall, New Jersey.
[5] J.C. Mosher, "Localization from Near-Source Quasi-Static Electromagnetic Fields", Ph.D. Thesis no. LA-12622-T, Los Alamos National Laboratories, NM.
[6] Lorrain & Corson
[7] W. Chen, K. M. Wong, and J. P. Reilly, "Detection of the number of signals: A predicted eigen-threshold approach", IEEE Transactions on Signal Processing, vol. 39, pp. 1088--1098, May 1991.
[8] Akaike, H., "A New Look at the Statistical Model Identification", IEEE Trans. Autom. Control, vol AC-19, pp. 716-723, December 1974.
[9] Rissanen, J., "A Universal Prior for the Integers and Estimation by Minimum Description Length", Ann. Stat., vol. 11, pp 417-431, 1983.
[10] Wax, M. and Kailath, T., "Detection of Signals by Information Theoretic Criteria", IEEE Trans. Acoust. Speech and Signal Process., vol. ASSP-33, pp 387-392, April 1995.

# THE FORMATION OF SUPERBOLTS IN THUNDERCLOUDS

by Anton Pühringer
Central Institute for Meteorology and Geodynamics
Hohe Warte 38, PO Box 342
A - 1191 Vienna, Austria.

**ABSTRACT**

Superbolts can be dangerous for aviation because their high power may damage airplanes. The thunderstorm theory based on the electromagnetic induction (e.m.i.) can indicate the dangerous zones. As a result, we can instruct the pilots of airplanes where they have to keep a greater safety distance from the thundercloud.

**INTRODUCTION**

In June 1983, I could present the thunderstorm theory with the e.m.i. at the 8th International Aerospace and Ground Conference on Lightning and Static Electricity (session 12, A 3) in Fort Worth. At this conference, I have already warned of the danger threatening by the superbolts. Since this was 12 years ago, I will repeat the principle of this theory in a shorter form.

## THE THUNDERSTORM THEORY WITH ELECTROMAGNETIC INDUCTION

The law of e.m.i. was discovered in 1831 by Michael Faraday. This method of producing electricity, which became most important for humankind, requires an electric conductor that is moved into a magnetic field. It is quite curious that the e.m.i. has never been used as a basis for a thunderstorm theory, because all we need for the application of the e.m.i. to thunderclouds, is available.

We have cloud particles as electric conductors which are moved by the wind into the magnetic field of the earth. Therefore, all cloud particles become undirected electric dipoles. Now you will perhaps say that the induced electric field is too weak to generate the high voltage of a thunderstorm. But the space intervals between the cloud particles form little electrical capacitors, and we get a cumulative effect. The more cloud particles are present, the more dipole charges will be separated in each cloud particle. Therefore, the electrification process will only be effective in a very big cloud.

The dimension of the cloud in the direction of the induced electric field should be at least 12 km (36.000 feet). The electrostatic forces between cloud particles cause the formation of a space lattice, reminiscent to crystals. This makes the thundercloud build up and stabilize. On the other hand, the Coulomb forces between the dipoles can advance the contact; water droplets may coalesce. This leads to

electric discharges between the could particles. Werner Naumann (Dresden) assumed that such discharges can propagate within the cloud similar to a domino effect or a chain reaction. The sequence is an electric current going through the cloud - always in the same direction. The high-voltage charges appear as area charges at two opposite edges of the cloud and keep growing until a lightning discharge may occur.

The production of the superhigh voltages is only possible because the electric charges are conducted according to the principle of the *van de Graaf*-generator: from the inside of the electric conductors to its surface.

## EXAMPLES OF LIGHTNING DISCHARGES AT DIFFERENT PLACES.

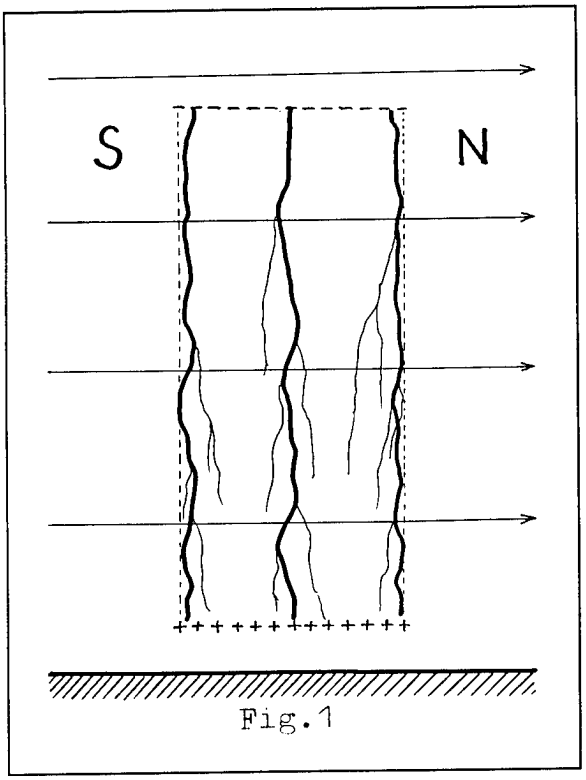


Fig. 1

Fig. 1 shows a thundercloud at the magnetic equator. Here, only the horizontal-intensity of the magnetic field exists. The electric field that is induced by the e.m.i. is vertically orientated. The thunderclouds at the magnetic equator are therefore vertical columns.

In all figures from No. 1-7 we are looking into the drift direction of the cloud; in fig. 1. it is from E to W. When we apply the "three-finger-rule" of the e.m.i., the top of the cloud becomes a negative, the bottom a positive charge. ("Three-finger-rule": Put the forefinger of the right hand into the direction of the magnetic field, the middle finger into the drift direction of the cloud, then the thumb points to the negative charge.) The height of the cloud is at least 12 km (36.000 feet).

The e.m.i. can only separate the charges. The negative charge is an excess, the positive charge a lack of electrons. As a result, the amounts of the charges are equal. This cloud at the magnetic equator represents a closed system similar to a condenser. Here, the electric force lines between the high electric tensions exist only within the pillar cloud. There is no electrostatic induction between the cloud and the soil; therefore no lightnings between the could and the earth can occur. In this zone, the buildings need no lightning-conductors. The lightnings only take place within the cloud, they are vertically orientated and all superbolts (i.e. the current intensity amounts of several hundreds of kA). Tornadoes may not occur here, either.

When the cloud is moving from E to W like in fig. 1, it is prepolarised from the normal electric field of the atmosphere in the right direction, negative above and positive below. "Normal field" means the vertical electric field between the ionosphere and the earth, where the bottom of the ionosphere has a positive, and the earth a negative charge. The electrification of the cloud by the e.m.i. can therefore begin at a lower drift velocity as if the cloud drifts from W to E. If this is the case, the e.m.i. must first invert the prepolarisation of the cloud.

A thunderstorm in the vicinity of the magnetic equator can never arise when the cloud is drifting into the direction of a magnetic meridian.

Summing up, we can assume for all thunderstorms around the world that they need a horizontal wind velocity. When the cloud formation is bound to a mountain chain or a volcano, we can get the impression of a thunderstorm that is not moving at all. Nevertheless, these cloud particles must also be moved by a horizontal wind. Updrafts and downdrafts can be useful for the production of a great cloud volume, but they are rather hindering the fully developed thunderstorm. All thunderstorms must have a minimum drifting velocity that depends on the place, the strength of the magnetic field and the drifting direction. No thunderstorms can occur when their drifting velocity is smaller than this minimum.

The energy balance of a thunderstorm is very simple because a part of the kinetic energy of the cloud is transformed into electric energy. Therefore, the cloud is moving slower than the air surrounding it. The power of a common thunderstorm can be about 300 MW, thus it is similar to the capacity of a major river power plant.

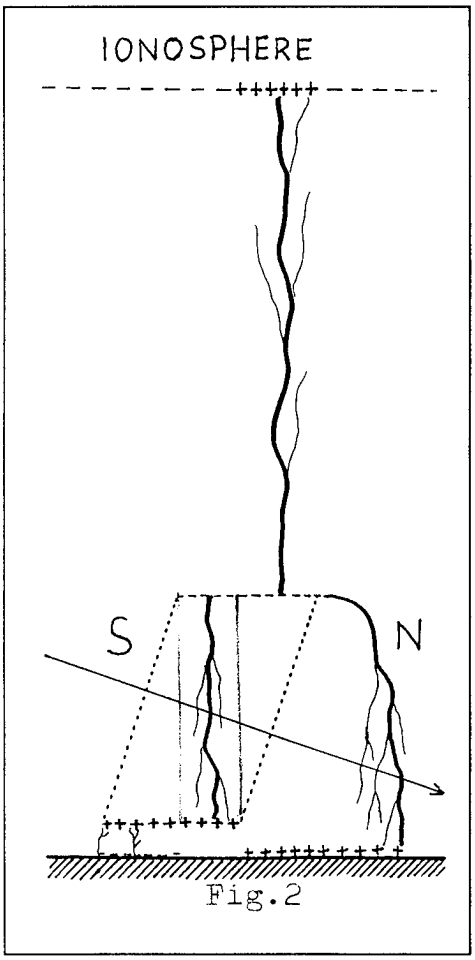


Fig.2

Fig. 2 shows a thundercloud with its lightning discharges at the northern hemisphere. The magnetic inclination is approximately 20°. This could be e.g. in South America in Quito, Ecuador, or on the east coast Pelém, Brazil, the second is southerly to the geographic equator. We recognize that in the theory with e.m.i. the hemispheres are separated by the geomagnetic, not by the geographic equator.

In the middle of the cloud, there exists again a rest of the closed system similar to fig. 1. But on the left southern bottom of the could free positive charges appear which can come into contact with the electricly conducting earth. Here, under the southern side of the cloud, normal lightnings may occur which are mostly harmless to airplanes because the metal skin works like a Faraday cage, protecting the interior.

At the northern upper side of the cloud (on the right side in fig. 2), the superhigh negative

voltage may also come in contact with the earth through electrostatic induction. The cloud forms an anvil here. The lightnings from this charge situated high up are very strong superbolts that can severely damage airplanes. Due to the repulsive Coulomb forces, these negative superbolts can catapult more than 5 km away from the cloud before they strike the ground.

This can perhaps be the famous lightning from the blue sky.

On fig 2. we can also see that there exists one more electric leading stratum, the ionosphere, which can also come into electrostatic induction with the upper charge of the thundercloud. Owing to the long distance between cloud and ionosphere, the discharge must be a titanic bolt. It will change into a red colored discharge - similar to polar lights - in the rarefield gases of the upper region. This phenomenon was named "red sprite".

"Blue jets", another lightning phenomenon, that jumps up like fountains, are maybe produced by the Lorentz forces. An electric charge moves into a homogenous field where it starts moving in a circle. In the case of fig. 2, the negative electric charge will get an upward acceleration. These blue jets produce an extremely high ionization of the air, and this can help to prepare the gigantic discharge between the cloud and the ionosphere.

The most favorable conditions for the production of such a titanic bolt exist when

1. the thundercloud is very high (20 km and more),
2. when the cloud is moving from E to W, because the bottom of the ionosphere has already got a positive charge from the normal atmospheric electric field,
3. when the power of the thunderstorm is intense enough; this requires a higher wind velocity,
4. when the life duration of the cloud is long enough so that the extremely high electric tension can develop.

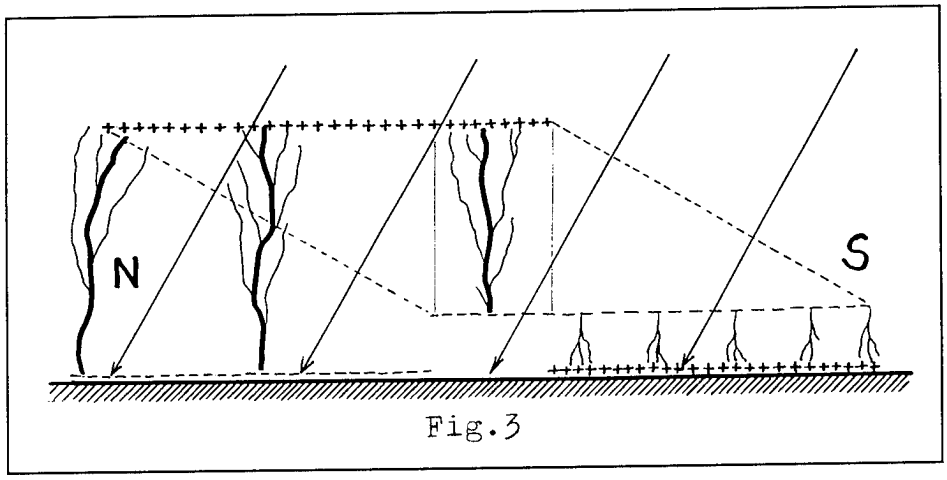


Fig.3

Fig. 3 shows a thunderstorm in the northern hemisphere. The magnetic inclination is 60°. Such a thunderstorm could appear e.g. near Fort Worth. The cloud

is moving from W to E. There is still a rest of the closed system like in fig 1. in the middle of this cloud. Negative charges appear under the left bottom of the cloud. Here common lightnings may occur. When the power of the thunderstorm is high enough, we can also get tornadoes under the right side of the cloud.

On the left, the northern side, the cloud forms and anvil. The superhigh voltage at the top of the cloud is positive. The dangerous superbolts are at the northern side of the cloud. This thundercloud is no longer as high as the thunderstorms near the magnetic equator; and the superhigh voltage and the current intensity of the superbolts is weaker. Nevertheless, the superbolts of this cloud are still very dangerous.

Looking at the direction of the magnetic field in fig. 4, we recognize that we are now on the southern hemisphere. The magnetic inclination is -60°. This thunderstorm could occur for example in Johannesburg, South Africa, or in Sydney, Australia, but not in South America. The closed system is lacking here; however, this must not always be the case. The positive charge is here under the northern bottom of the cloud. That's where the normal lightnings and tornadoes appear.

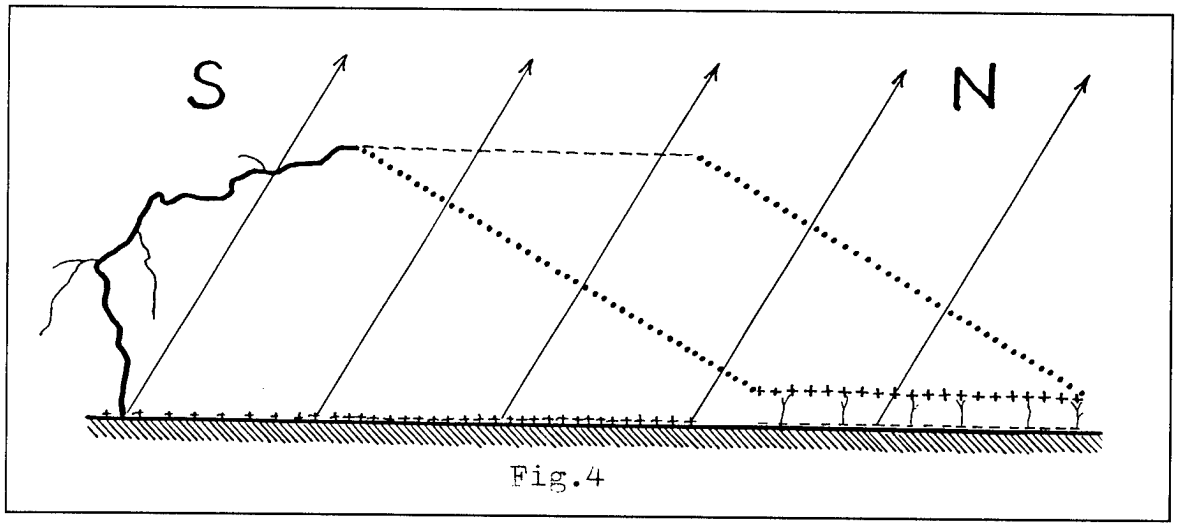


Fig.4

In 1963 I predicted an orientation law for tornadoes which was proved in 1971 by many reports from Europe, America and Australia. This orientation law says that the tornadoes at the northern hemisphere are always under the southern, those of the southern hemisphere always under the northern border of the thundercloud. This law would make it possible to warn people more precisely and effectively of tornadoes.

Tornadoes are also a danger to airplanes, which break to pieces when they strike them.

Here the question may arise why the United States are tormented so often by severe thunderstorms, tornadoes and hail. This is possible because here the total intensity of the magnetic field is considerably strong.

In fig. 4 we see that the superhigh negative voltage in the southern hemisphere is situated on the southerly upper border of the cloud when it moves from E to W.

The superbolt can here jump out like a snake nearly 6 km of the anvil cloud. Therefore, the safety distance for airplanes should be 7 km.

In both hemispheres, the thunderstorms moving from E to W are particularly dangerous.

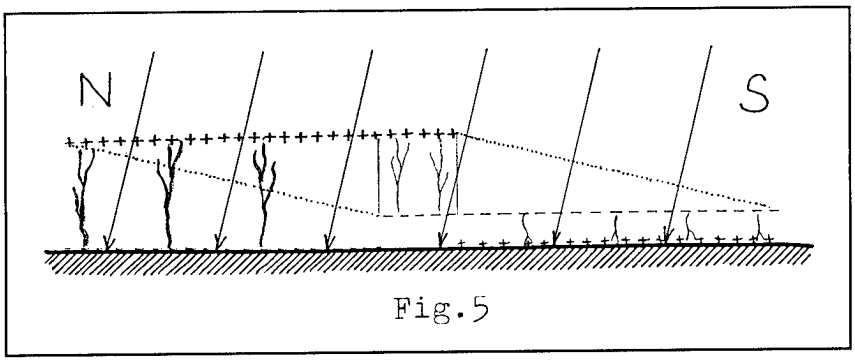



Fig.5

Fig. 5 shows a thunderstorm on the northern hemisphere. The magnetic inclination is about 75°. Such a thunderstorm may occur for example near Winnipeg, Canada. The cloud is moving from W to E, and he height of the cloud is very small. There can be again a closed system in the middle of the cloud, in this case with upwards lightnings. Under the southern part of the cloud we get negative lightnings, and from the upper northern side positive ones. The heights of the charges do not differ much. Accordingly, the differences in voltages and current intensities are insignificant, too. Therefore, this thunderstorm has no superbolts.

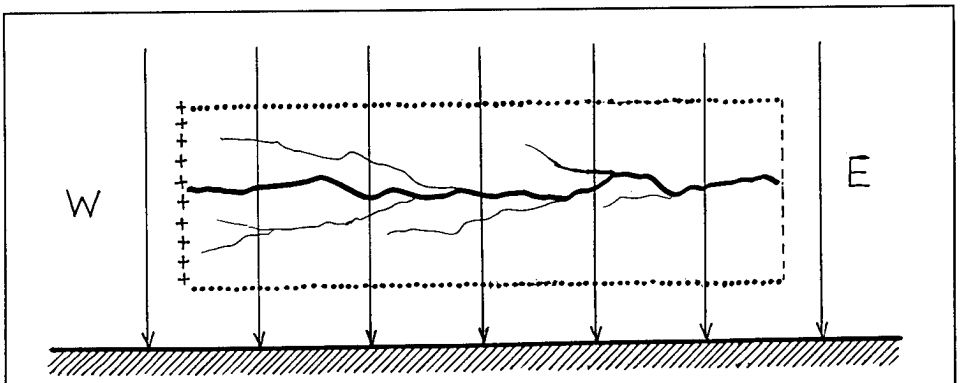



Fig.6

Fig. 6 shows a thunderstorm on the northern hemisphere moving in direction of a magnetic meridian from S to N. Here only the vertical intensity of the geomagnetic field is at disposal for the e.m.i. The induced electric field lies horizontally, and we get a closed system again for high tensions; i.e. in this case we get mostly lightnings from the cloud. This would also be the case for thunderstorms directly on the magnetic north pole.

When the motion of the cloud deviates slightly from the magnetic meridian, (e.g. when it is drifting from SSE to NNW), we can get lightnings inside and outside of the cloud as illustrated in fig. 7. Only the lightnings inside of the cloud are superbolts. The discharges between the cloud and the ground (on both the left and the right side) are normal lightnings.

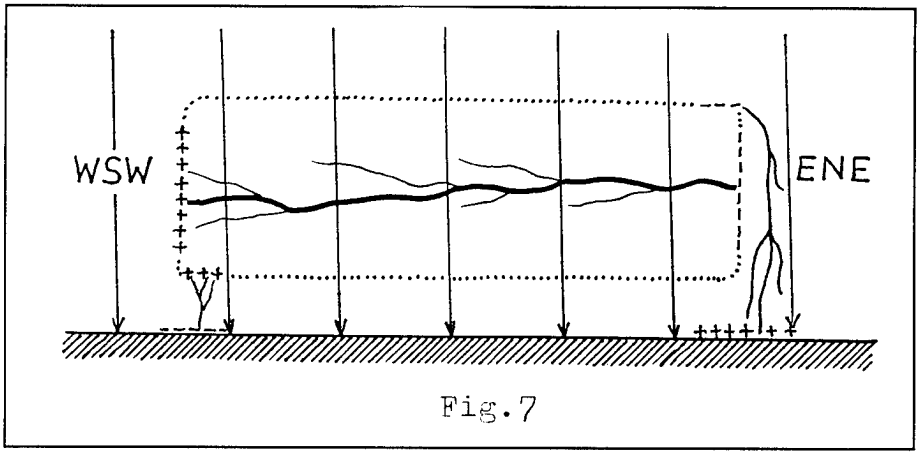



Fig.7

## HOW CAN WE AVOID DISASTERS DUE TO SUPERBOLTS?

Airplanes should never fly into a thundercloud, because the lightnings inside of the cumulonimbus are mostly superbolts. When it is not possible to fly over a thundercloud, the aircraft should bypass it. On the northern hemisphere it is better to avoid the dangerous northern side of thunderclouds and to fly via a southern route. If this alternation of the route should not be possible and the aircraft must pass the northern side of the cloud, the pilot has to observe a horizontal safety distance of at least 7 km from the northern top of the cloud. - Vice versa, the southern tops of the clouds are dangerous on the southern hemisphere.

We get an orientation law for the superbolts similar to the orientation law for tornadoes and common lightnings.

Here we should point out once more that the magnetic equator separates the hemisphere.

When an airplane has come too close to the dangerous zone of a thundercloud, it should not change its height. The plane carries its own electric charge and when it is starting or landing, it can disturb the electric field and thereby trigger a lightning.

What is more, the meteorologist(s) of the airport should have the right to postpone starts or landings until the danger is over.

# SESSION 11B
# LIGHTNING MODELING
# CHAIRPERSON: ROD A. PERALA

# INFLUENCE OF TALL TOWERS ON THE RETURN STROKE CURRENT

F. Heidler and T. Zundl

Federal Armed Forces University Munich
ET 7, Werner-Heisenberg-Weg 39
D-85577 Neubiberg, GERMANY
Telephone +49/89/60043736 FAX +49/89/60043723

## ABSTRACT

In the last years more than 100 lightning currents could be registered successfully at the telecommunication tower Peissenberg, which is located nearby Munich in Germany. During the first microseconds the impulse currents show typical reflections, which were analyzed with an electrodynamic computer program based on the Method of Moment (MOM)- theory in the frequency domain. In this program the structure of the tower and the lightning channel were modelled by wires and ideal conducting patches. The MOM- solutions were compared to the results of a transmission line approach.

## 1. INTRODUCTION

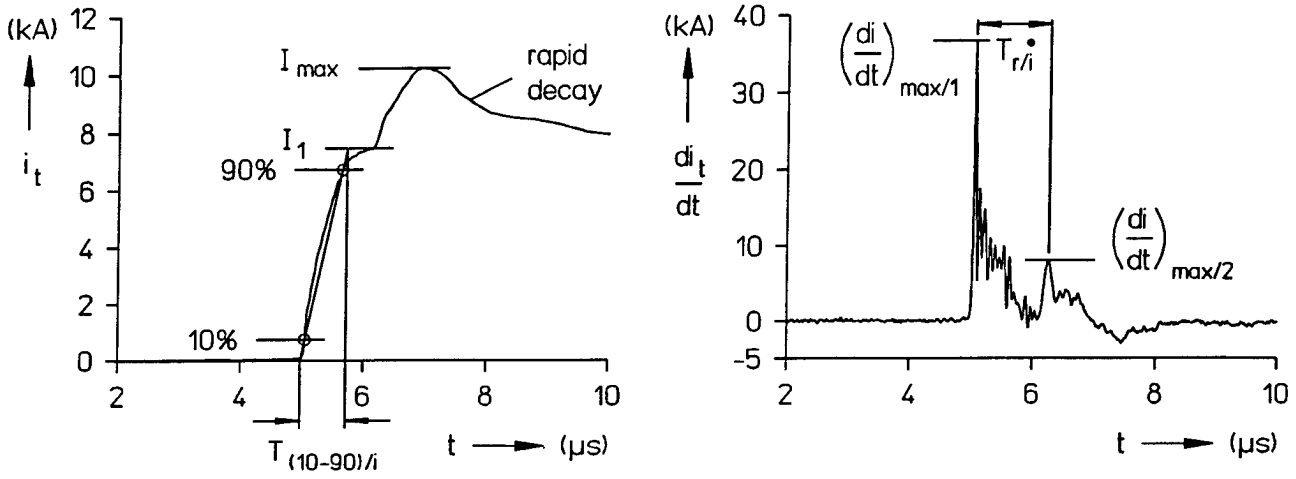
In the past the most essential data of natural lightning currents were captured by Prof. *Berger* at the Monte San Salvatore in Switzerland with an upper bandwidth limit of about 1 MHz /1/. To resolve the current rise and the current steepness more in detail a new measuring campaign was started at the Peissenberg tower in Germany. The tower is located about 100 km away from Munich close to the Alps in a region, where the lightning activity is relatively high with more than 30 thunder days per year. The measurements were realized by the High Voltage Institute of the Federal Armed Forces University Munich and the High Voltage Institute of the Technical University Munich.

The currents and the current derivatives were measured simultaneously at the tower top with two independent sensors. The current sensor is a commercial current transformer from Pearson (type 2093) with an upper bandwidth limit of 200 kHz and a lower bandwidth limit of 0,15 Hz. With the current transformer the amplitudes and the decays of the impulse currents as well as long duration currents could be resolved. For the fast current rise a di/dt-sensor with an upper bandwidth limit better than 20 MHz was developed /2/. A numerical integration routine and in addition an active integrator installed in the measuring cabin were used for the evaluation of the current rise from the registered di/dt-waveforms. The measuring station is operating completely automatically. Up to now the currents and current derivatives of more than 100 lightning strikes to the Peissenberg tower could be registered successfully /3, 4/.

Fig. 1 shows an example of the captured current and the current derivative stemming from a negative stroke. The tower reflections lead to a characteristic current amplitude $I_1$ = 7,4 kA and a current maximum $I_{max}$ = 10,3 kA (fig. 1a). The characteristic current amplitude $I_1$ is given by the point, where the current steepness is increasing strongly. The waveform of the current derivative shows two maxima given by $(di/dt)_{max/1}$ = 36,7 kA/$\mu$s and $(di/dt)_{max/2}$ = 8,1 kA/$\mu$s (fig. 1b). The rise time of the current amounts to $T_{(10\text{-}90)/i}$ = 0,58 $\mu$s. For currents with a rise time in the microsecond range $I_1$ is not clearly resolvable. Otherwise, if the rise time decreases the first maximum is becoming more significantly.

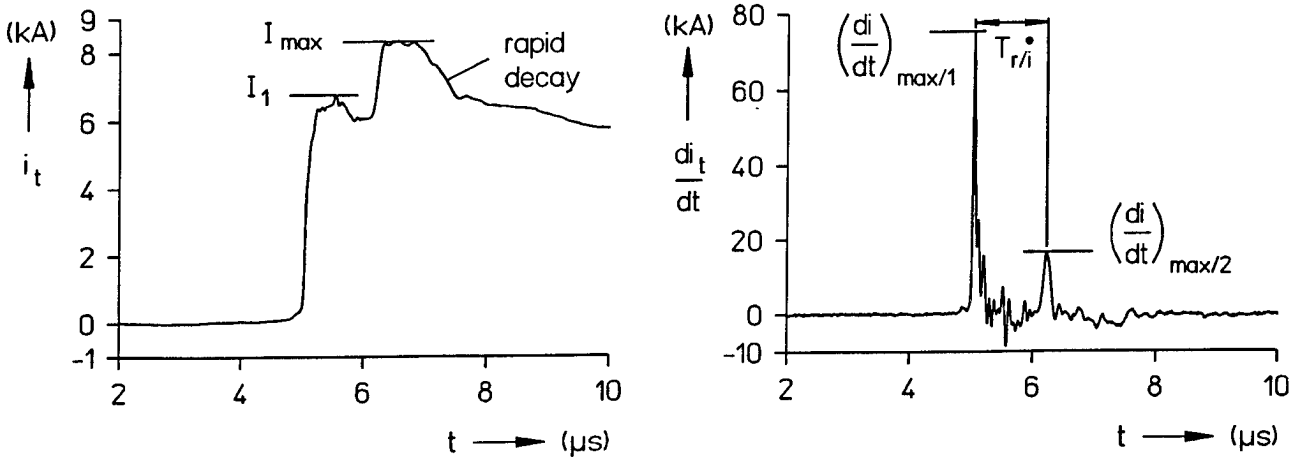
Exemplarily fig. 2a shows a current with a rise time $T_{(10\text{-}90)/i} = 0{,}20\ \mu s$ having a very strong characteristic current amplitude $I_1 = 6{,}8$ kA followed by a current maximum $I_{max} = 8{,}3$ kA. The reduced rise time leads to an increase of the current steepness. In fig. 1b the maximal current derivatives are given by $(di/dt)_{max/1} = 75{,}4$ kA/$\mu$s and $(di/dt)_{max/2} = 16{,}6$ kA/$\mu$s.

The current fed into the tower top is reflected at the basement of the tower. Considering a tower height $h_t = 168$ m the current arrives at the tower top after the reflection time $T_{r/i} = 2 \cdot h/c_o = 1{,}12\ \mu s$, where the speed of light is given by $c_o = 300$ m/$\mu$s. Opposite that the reflection time is measured to $T_{r/i} = 1{,}18\ \mu s$ in fig. 1b and to $T_{r/i} = 1{,}17\ \mu s$ in fig. 2b. The difference can be explained by the fact, that the foundation of the tower is some meters below ground level resulting in an increase of the effective tower height.




a) Current b) Current derivative

Fig. 1: Lightning current and current steepness of a negative stroke with a current rise time $T_{(10\text{-}90)/i} = 0{,}58\ \mu s$ measured at the Peissenberg tower




a) Current b) Current derivative

Fig. 2: Lightning current and current steepness of a negative stroke with a current rise time $T_{(10\text{-}90)/i} = 0{,}20\ \mu s$ measured at the Peissenberg tower

Typically the current maximum $I_{max}$ is about 30% higher than the characteristic current amplitude $I_1$. In fig. 1a and fig. 2a the current waveforms show a rapid decay immediately after the current maximum $I_{max}$. Especially for impulse currents with relatively short rise times this rapid decay is very typical leading to a reduction of $I_{max}$ by about 20% within a time of some microseconds.

In the TCS- and DU- model a current source is postulated moving from the striking point in the direction of the thunder cloud /5, 6/. In addition to the tower reflections therefore reflections at the current source have also to be considered. Because the current source is moving and thus the geometry of the lightning channel is varied by time, the reflections at the current source superpose continuously the tower reflections. To enable a separation of the different reflections, opposite to the postulations of the TCS- model the movement of the current source was neglected replacing the traveling current source by a stationary current source in a certain height above the tower.

## 2. ELECTRODYNAMIC MODEL OF THE PEISSENBERG TOWER

### 2.1 Geometry of the Peissenberg tower

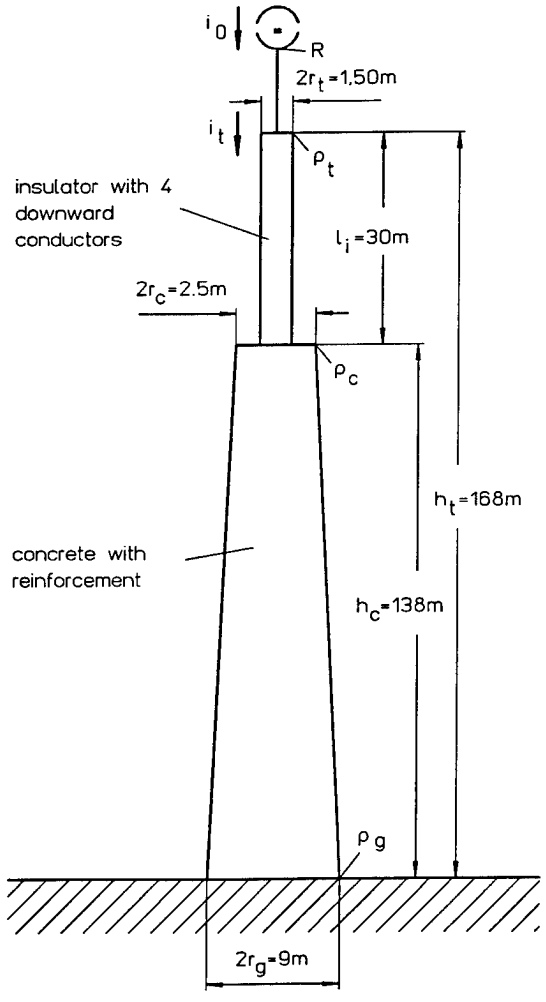



Fig. 3: Geometry of the Peissenberg tower

Fig. 3 shows the geometrical dimensions of the Peissenberg tower with a total height $h_t$ = 168 m. From the basement to the height $h_c$ = 138 m the tower is built up by concrete with reinforcement. This lower part of the tower has the shape of a cone with a diameter $2 \cdot r_g$ = 9 m at the basement and $2 \cdot r_c$ = 2,5 m in the height $h_c$.

The upper part of the tower is built up by an cylindrical isolator tube, which contains the transmitting antennas. The isolator tube has a length $l_i$ = 30 m and a diameter $2 \cdot r_t$ = 1,50 m. The top of the tube is covered by a metal disc with the same diameter $2 \cdot r_t$ = 1,50 m as the isolator tube. For the lightning protection 4 downward conductors with a radius $r_w$ = 4,5 mm are installed along the isolator tube. The downward conductors are connected to the metal disc at the tower top and to the reinforcement of the lower tower part in the height $h_c$.

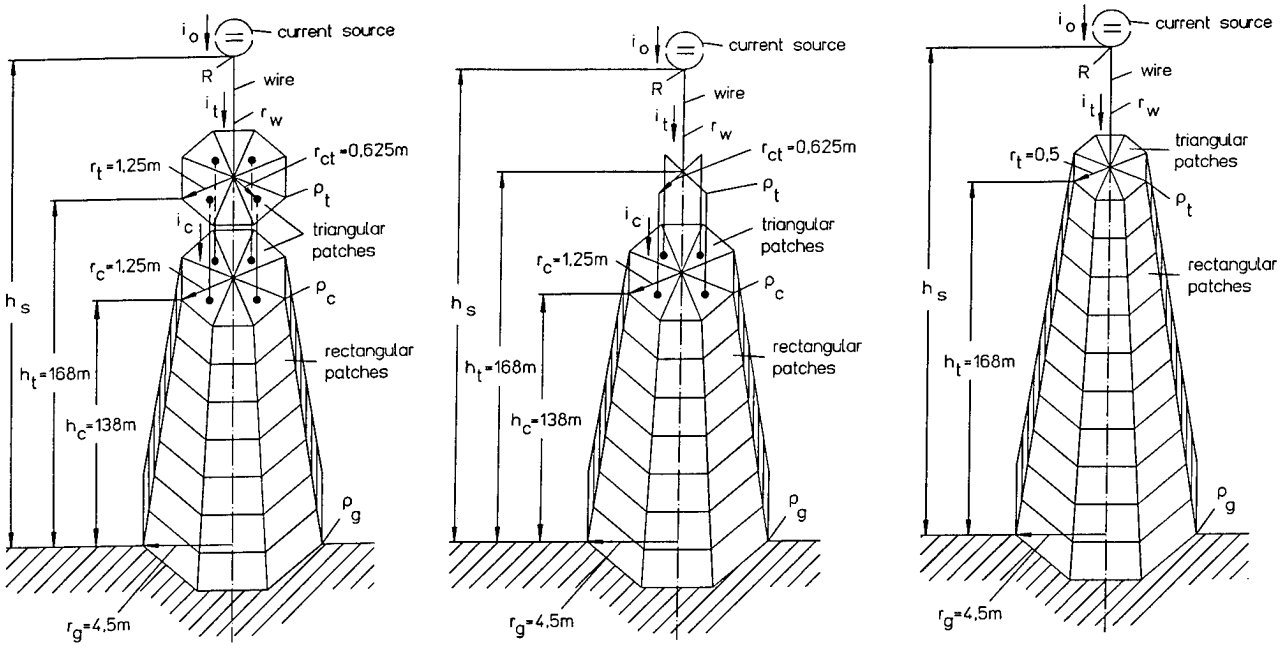
The current transformer and the di/dt-sensor are installed on the metal disc at the tower top. For the measurements coaxial cables are used for transmitting the measuring signals from the tower top to a shielded cabin, which is located inside the tower in a height of about 5 m over ground level. The cabin is equipped by the data acquisition system consisting a. o. in 3 digital oscilloscopes.

2.2 Electrodynamic models of the Peissenberg tower

The reflection behavior of the tower and the attached lightning channel was examined with the computer program CONCEPT /7/. CONCEPT based on the MOM- theory in the frequency domain allows the electrodynamic examination of metal structures, which are excited e.g. by a current source. The calculations were performed with a lowest frequency of 100 Hz and a highest frequency of about 7,5 MHz. The frequency steps were chosen to $\Delta f$ = 200 Hz between 100 Hz and 1,9 kHz. Between 1,9 kHz and 0,2 MHz the frequency steps were chosen to $\Delta f$ = 2 kHz. Between 0,2 MHz and 7,5 MHz the frequency steps were increased to $\Delta f$ = 10 kHz. The time domain solution was obtained by a numerical inverse Fourier's transformation.

The electrical structure of the Peissenberg tower including the attached lightning channel was modelled by patches and wires according to the simulation conditions of CONCEPT. In CONCEPT ideal conducting triangular and rectangular patches are used advantageously for the simulation of voluminous electrical bodies. Thin cylindrical structures as the lightning channel are modelled by wires, which are subdivided into segments. The segments may be ideal conducting or loaded e.g. by a finite conductivity. The length of a segment should be limited to $\lambda/8$, where $\lambda$ is the wavelength of the highest considered frequency.

3 different tower models were examined, where opposite to the schematic drawings shown in fig. 4 up to nearly 300 patches were used. Generally the tower was built up by octagonal pyramids having a maximum diameter $2 \cdot r_g$ = 9 m at the basement. The sides of the pyramids were modelled by rectangular patches and the top of the pyramids by triangular patches. The lightning channel was assumed to be vertical attaching the tower in the middle of the tower top.




a) Model A b) Model B c) Model C

Fig. 4: Schematic drawings of the tower models used in CONCEPT

Current reflections occur at points, where the diameter of the structure is changing rapidly. Therefore current reflections are expected at the tower top, at ground level and in the height $h_c$. The reflections are described by the reflection factors $\varrho_t$, $\varrho_g$ and $\varrho_c$. As mentioned above an additional current reflection is expected at the end of the lightning channel in the height of the current source. This reflection is described by the reflection factor R.

In model A shown in fig. 4a only the lower tower part is modelled by an octagonal pyramid. The tower top is modelled by a disc, which consists of 8 triangular patches. The disc and the top of the pyramid are connected by 4 ideal conducting wires representing the downward conductors of fig. 3. Model A is the most realistic tower model, although the diameter of the insulator tube was lowered to $2 \cdot r_{ct}$ = 1,25 m and a greater disc radius was chosen as in reality. This modifications were necessary to improve the calculation results. Especially the attachment of the wires at the edges of the triangular patches had to be avoided. The decrease of the diameter of the insulator tube was compensated by the increase of the wire radius to $r_w$ = 5 mm.

In model B the disc is replaced by 4 ideal conducting wires with a radius of 5 mm connecting the downward conductors to the lightning channel. With model B the influence of the disc at the tower top was studied. In model C the whole tower is modelled by an octagonal pyramid (fig. 4c). In this model the reflection $\varrho_c$ is neglected in the height $h_c$.

2.3 Current of the current source $i_o$

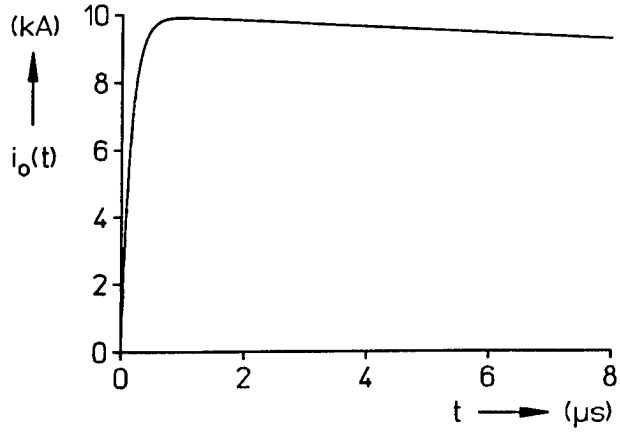



Fig. 5: Current of the current source

The current of the current source is defined by:

$$i_o(t) = \frac{i_{o/max}}{\eta}(e^{-t/\tau_1} - e^{-t/\tau_2}) \qquad (1)$$

($\eta$ : correction factor of the current maximum $i_{o/max}$)

Generally the current maximum $i_{o/max}$ = 10 kA was considered. The decay and rise time parameters were chosen to $\tau_1$ = 100 $\mu$s and $\tau_2$ = 0,15 $\mu$s. Fig. 5 shows the front of the defined source current. The rise time (definition see fig. 1a) results in $T_{(10\text{-}90)/i}$ = 0,40 $\mu$s. The decay time to half value amounts to 70 $\mu$s.

## 3. COMPUTER RESULTS OF THE ANALYSIS WITH CONCEPT

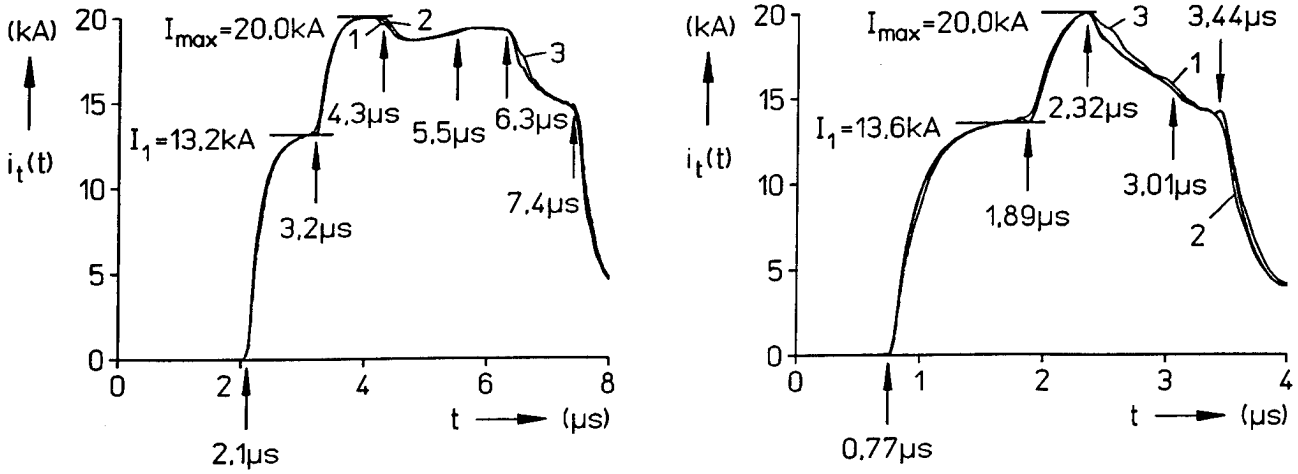
3.1 Comparison between the model A, B and C

The lightning channel is simulated by an ideal conducting cylindrical wire with a radius of 1,00 cm. Considering the height of the current source to $h_s$ = 800 m fig. 6a shows the currents $i_t$ calculated with the different models at the tower top. It is remarkable, that no significant difference could a be found in the reflection behavior, if the metal disc at the tower top (model A) is replaced by 4 wires (model B). The same result was obtained reducing the height of the current source to $h_s$ = 400 m (fig. 6b).

From the current waveforms captured with model A and model B no current reflection in the height $h_c$ could be detected. Probably the rise time of the current was not short enough to resolve the reflection. On the other hand in a frequency domain analysis of the measured currents no corresponding resonant frequency could be detected /3/. Therefore in model C the structure of the tower was simplified building up the whole tower by an octagonal pyramid. As demonstrated in fig. 6 for $h_s$ = 800 m and $h_s$ = 400 m a very good agreement to the currents of model B and C could be achieved considering the diameter of the tower top to $2 \cdot r_t$ = 1,00 m. In the following only model C is considered.

The current of the current source is switched on at t = 0. For $h_s$ = 800 m it arrives at the tower top ($h_t$ = 168 m) after 2,1 $\mu$s. Here the current is split up in a current wave, which is reflected toward to the current source, and a current wave, which is transmitted to ground. The reflected current wave is reflected at the current source and arrives as negative current wave at the tower top after 6,3 $\mu$s. The transmitted current wave is reflected at the tower basement and arrives at the tower top after 4,3 $\mu$s. Here one portion of the current is transmitted toward to the current source and the other portion is reflected toward to ground. The transmitted portion is reflected at the current source and arrives at the tower top as negative current wave after 7,4 $\mu$s. The reflected current portion is reflected again at the tower basement arriving at the tower top after 5,5 $\mu$s.

In fig. 6b the height of the current source is reduced to $h_s$ = 400 m. The current arrives at the tower top after 0,77 $\mu$s. The transmitted current wave is reflected at the tower basement and arrives at the tower top after 1,89 $\mu$s, where it reflected to earth arriving again at the tower top after 3,01 $\mu$s. The reflected current wave is reflected at the current source and arrives at the tower top as negative current wave after 2,32 $\mu$s. Because the tower height is reduced to $h_s$ = 400 m, the reflection at t = 3,01 $\mu$s cannot be resolved. The reflection after 3,44 $\mu$s results from the current portion, which was reflected firstly at the tower basement and then at the current source.



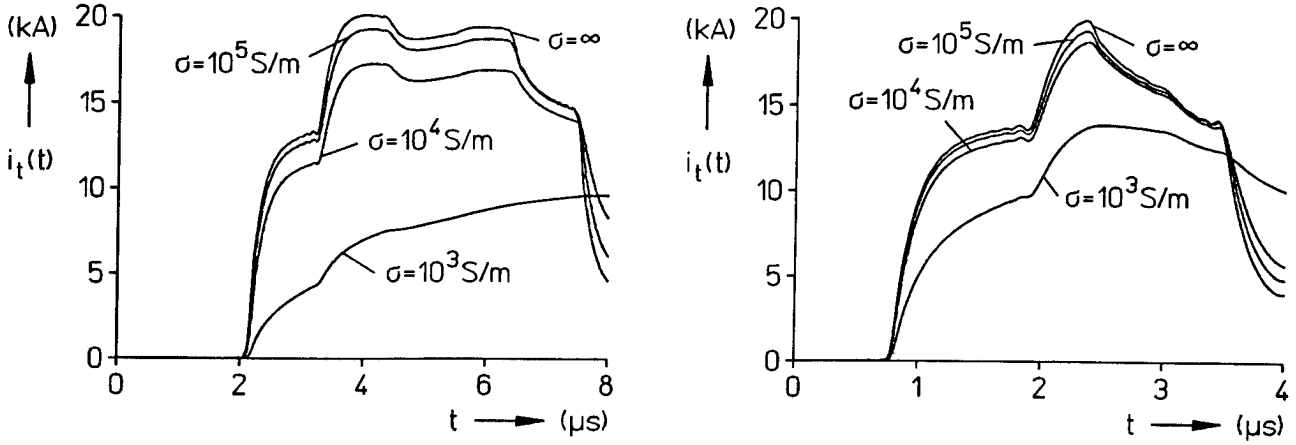

a) Height of the current source $h_s$ = 800 m

b) Height of the current source $h_s$ = 400 m

Fig. 6: Comparison of the lightning currents at the tower top calculated with the tower models A, B and C. The arrows indicate the times, when the different current portions arrive at the tower top.
1: model C, 2: model A, 3: model B

3.2 Influence of a finite lightning channel conductivity

The radius of the lightning channel (model C) is chosen to $r_w$ = 1,00 cm. Considering the skin effect the conductivity was chosen to $\sigma = \infty$, $\sigma = 10^5$ S/m, $\sigma = 10^4$ S/m and $\sigma = 10^3$ S/m. For $h_s$ = 800 m fig. 7a shows the calculated currents at the tower top $i_t$. For $\sigma \geq 10^4$ S/m the conductivity had only a weak influence on the current waveforms, but the amplitudes were reduced, if the conductivity is lowered. Compared to $\sigma = \infty$ for $\sigma = 10^5$ S/m the current maximum is reduced by 3,7 % and for $\sigma = 10^4$ S/m by 14,1 %. For $\sigma = 10^3$ S/m the waveform is changed very strongly. Fig. 7b shows the corresponding calculations for h = 400 m. For $\sigma \geq 10^4$ S/m the conductivity had only a very weak influence on the current waveforms. Compared to $\sigma = \infty$ for $\sigma = 10^5$ S/m the current maximum is reduced by 3,1 % and for $\sigma = 10^4$ S/m by 6,3 %. For $\sigma = 10^3$ S/m the waveform is changed very strongly.




a) Height of the current source $h_s$ = 800 m

b) Height of the current source $h_s$ = 400 m

Fig. 7: Influence of the conductivity $\sigma$ on the current at the tower top

3.3 Influence of the lightning channel diameter on the current at the tower top

The arc diameter $d_{arc}$ of the hot core of an impulse current can be estimated by *Bellaschi's* formula given in /8/:

$$\frac{d_{arc}}{[cm]} \approx 0{,}16 \sqrt{\frac{i}{[kA]}} \qquad (2)$$

E.g. it results $d_{arc}$ = 16 mm for i = 100 kA or $d_{arc}$ = 2,3 mm for i = 2 kA.

Based on this formula the radius of the lightning channel assumed to be an ideal conducting wire was chosen to $r_w$ = 10 mm, $r_w$ = 5 mm, $r_w$ = 2 mm and $r_w$ = 1 mm. The relatively great height of the current source $h_s$ = 800 m was necessary to avoid disturbing current reflections from the current source during the first microseconds. With the tower model C fig. 8a shows the calculated currents at the tower top $i_t$. For $r_w$ = 10 mm the characteristic current amplitude and the current maximum result in $I_1$ = 13,2 kA and $I_{max}$ = 20,0 kA. With decreasing radius the characteristic current amplitude increases resulting in $I_1$ = 13,5 kA for $r_w$ = 5 mm, $I_1$ = 13,9 kA for $r_w$ = 2 mm and $I_1$ = 14,2 kA for $r_w$ = 1 mm. The increase of the current maximum is not strong with $I_{max}$ = 20,2 kA for $r_w$ = 5 mm, $I_{max}$ = 20,4 kA for $r_w$ = 2 mm and $I_{max}$ = 20,5 kA for $r_w$ = 1 mm.

The reflection factor at the tower top $\varrho_t$ can be calculated from the characteristic current amplitude $I_1$ and the corresponding current value $I_{1/0}$ of the incident current wave:

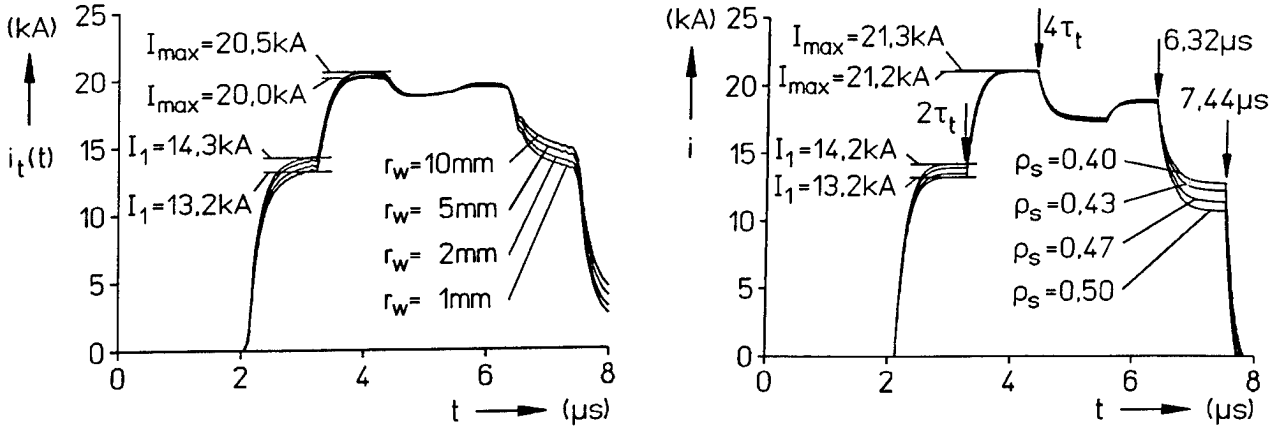
$$\varrho_t = \frac{I_1}{I_{1/0}} - 1 \tag{3}$$

$I_{1/0}$ was calculated with CONCEPT replacing the tower by an ideal conducting wire with the same diameter as the lightning channel. Caused by the radiation resistance the current amplitude decreases, when the current is running on the lightning channel. Especially the current maximum of the source current amounting to 10 kA in $h_s$ = 800 m is lowered to $I_{1/0}$ = 9,45 kA in the height $h_t$ = 168 m independently from the radius of the lightning channel $r_w$.

Table 1 gives an overview of the calculation results. With decreasing radius of the lightning channel $r_w$ the ratio of $I_1$ to $I_{1/0}$ increases resulting in $I_1/I_{1/0}$ = 1,40 for $r_w$ = 10 mm, $I_1/I_{1/0}$ = 1,43 for $r_w$ = 5 mm, $I_1/I_{1/0}$ = 1,47 for $r_w$ = 2 mm and $I_1/I_{1/0}$ = 1,50 for $r_w$ = 1 mm. With equation (3) the reflection factor at the tower top follows to $\varrho_t$ = 0,40 for $r_w$ = 10 mm, $\varrho_t$ = 0,43 for $r_w$ = 5 mm, $\varrho_t$ = 0,47 for $r_w$ = 2 mm and $\varrho_t$ = 0,50 for $r_w$ = 1 mm. The ratio of the current maximum to the incident current results in $I_{max}/I_{1/0}$ = 2,12 for $r_w$ = 10 mm, $I_{max}/I_{1/0}$ = 2,14 for $r_w$ = 5 mm, $I_{max}/I_{1/0}$ = 2,16 for $r_w$ = 2 mm and $I_{max}/I_{1/0}$ = 2,19 for $r_w$ = 1 mm. This result is very interesting meaning, that the tower reflection increases the amplitudes of the incident current waves at the tower top by more than a factor of 2 !

| $r_w$ | $I_{1/0}$ | $I_1$ | $I_{max}$ | $I_1/I_{1/0}$ | $I_{max}/I_{1/0}$ | $\varrho_t$ |
|---|---|---|---|---|---|---|
| 10 mm | 9,45 kA | 13,2 kA | 20,0 kA | 1,40 | 2,12 | 0,40 |
| 5 mm | 9,45 kA | 13,5 kA | 20,2 kA | 1,43 | 2,14 | 0,43 |
| 2 mm | 9,45 kA | 13,9 kA | 20,4 kA | 1,47 | 2,16 | 0,47 |
| 1 mm | 9,45 kA | 14,2 kA | 20,5 kA | 1,50 | 2,19 | 0,50 |

Table 1: Parameters of the lightning current at the tower top for different values of the radius $r_w$.




a) Calculation results of CONCEPT

b) Results of a transmission line approach

Fig. 8: Influence of the channel radius on the current at the tower top for $h_s$ = 800 m.

## 4. COMPARISON BETWEEN CONCEPT AND TRANSMISSION LINE RESULTS

Fig. 9 shows the model of the Peissenberg tower used in a transmission line approach. In $h_s$ = 800 m an ideal current source assumed. The maximum of the source current is chosen to $i_{o/max}$ = 9,45 kA for the comparison to the CONCEPT results (see above). At the current source the current is totally reflected as negative current wave (R = -1). The Peissenberg tower is simulated by an ideal transmission line with a characteristic impedance $\Gamma_t$ and a transit time $\tau_t = h_t/c_o$ = 0,56 $\mu$s. The lightning channel is also simulated by an ideal transmission line with a characteristic impedance $\Gamma_l$ and a transit time $\tau_l = (h_s - h_t)/c_o$ = 2,11 $\mu$s. The tower is well grounded and therefore the earth resistance is chosen to $R_e$ = 0 resulting in a total current reflection at ground level given by $\varrho_g$ = 1.

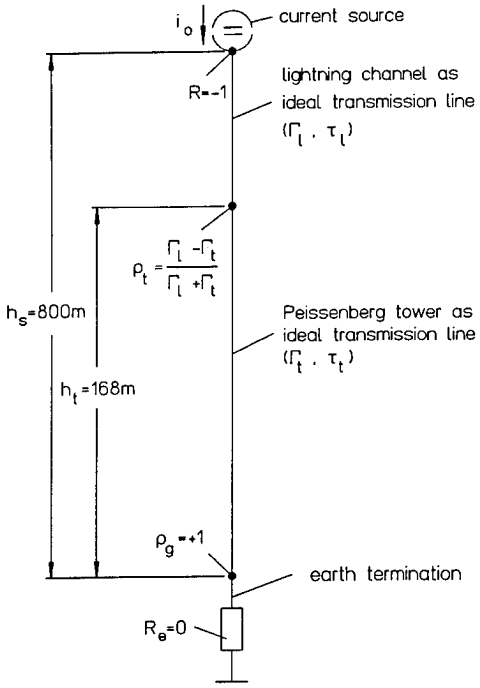



Fig. 9: Transmission line approach of the Peissenberg tower

At the tower top the reflections factor is given by:

$$\varrho_t = \frac{\Gamma_l - \Gamma_t}{\Gamma_l + \Gamma_t} \tag{4}$$

The values of the reflection factor $\varrho_g$ are given in table 1. With equation (4) the ratio of the characteristic impedances follows to:

$$\frac{\Gamma_t}{\Gamma_l} = \frac{1 - \varrho_t}{1 + \varrho_t} \tag{5}$$

In the calculations the characteristic impedances may be chosen arbitrarily, but equation (5) must be fulfilled.

For the different values of $r_w$ fig. 8b shows the currents resulting at the tower top. In comparison to the results of CONCEPT (fig. 8a) the current maximum is somewhat higher with $I_{max} \approx$ 21 kA and the reflected current portions are a little bit more significant. This behavior can be explained by the fact, that the transmission line approach neglects the radiation effects. Besides that the transmission line and the CONCEPT results are in a very good agreement.

The current wave arrives at the tower top after $\tau_l$ = 2,11 $\mu$s, where the current is reflected to the current source or transmitted to the tower basement. The maximum of the transmitted wave is given by $(1 + \varrho_t) \cdot i_{o/max}$, whereas the maximum of the reflected wave is given by $\varrho_t \cdot i_{o/max}$. The transmitted current wave is reflected totally at the tower basement arriving at the tower top after $2 \cdot \tau_t$, where it is transmitted with a current maximum $(1 + \varrho_t) \cdot (1 - \varrho_t) \cdot i_{o/max}$ or reflected arriving again after $4 \cdot \tau_t$ at the tower top. The current maximum $I_{max}$ results from the sum of the source current maximum $i_{o/max}$, the maximum of the reflected wave $\varrho_t \cdot i_{o/max}$ and the maximum of the transmitted current portion $(1 + \varrho_t) \cdot (1 - \varrho_t) \cdot i_{o/max}$. It follows:

$$\frac{I_{max}}{i_{o/max}} = 2 + \varrho_t - \varrho_t^2 \tag{6}$$

E.g. for $\varrho_t$ = 0,5 and with $i_{o/max}$ = 9,45 kA the current maximum results in $I_{max}$ = 21,3 kA (see fig. 8b).

## 5. CONCLUSION

With the computer program CONCEPT and in comparison with an transmission line approach the reflection behavior of the Peissenberg tower was examined. The main results are as follows:

- At the tower basement the current is approximately reflected totally ($\varrho_g \approx 1$).
- At the tower top the reflections depend on the arc diameter of the lightning channel and therefore on the current amplitude. For typical impulse currents the reflection factor is given by $\varrho_t = 0{,}4 \ldots 0{,}5$.
- At the current source the current is totally reflected as negative current (R = -1). For a moving current source the reflection factor will be reduced /9/.
- If the current source is not high enough over the tower top the tower reflections are superposed by the reflections from the current source. According to the TCS- model possibly the reflections cannot be resolved in detail. Therefore a 'decontamination' of the measured currents from reflections due to the presence of the strike object as proposed in /10/ seems to be difficult.
- If an ideal conducting lightning channel is assumed, during the first microseconds the CONCEPT and the transmission line results agree very well, although the radiation resistance leads to a decrease of the current amplitudes in CONCEPT.
- Compared to an ideal conducting lightning channel for $\sigma \geq 10^4$ S/m the conductivity had only a very weak influence on the current waveforms, but the amplitudes were reduced with decreasing conductivity. For $\sigma \leq 10^3$ S/m the current waveforms were changed strongly.

The tower reflection increase the amplitudes of the incident current waves by more than a factor of 2. Therefore possibly the current amplitudes of lightnings to a tower are higher than the current amplitudes of return strokes to earth. In a transmission line approach the ratio of the maximum current at the tower basement $i_{b/max}$ to the maximal current of the current source $i_{o/max}$ is given by:

$$\frac{i_{b/max}}{i_{o/max}} = 2 + 2 \cdot \varrho_t \qquad (7)$$

E.g. with $\varrho_t = 0{,}5$ the current amplitude at the tower basement is 3 times higher than the maximum current $i_{o/max}$ of the current source!

## REFERENCES


/1/ Berger, K.; Anderson, R.B.: Parameters of lightning flashes. Electra 41 (1975), p. 23 - 37.

/2/ Trapp, N.: Erfassung des zeitlichen Verlaufes und der Wirkungsparameter von Blitzströmen in automatisch arbeitenden Blitzmeß - Stationen. Phil. Theses, Technical University Munich, 1985.

/3/ Beierl, O.: Elektromagnetische Verträglichkeit beim Blitzeinschlag in ein Gebäude. Phil. Theses, Technical University Munich, 1985.

/4/ Zundl, T.: First results of the coordinated lightning current and LEMP measurements at the Peissenberg tower. 22nd Intern. Conf. on Lightning Protection ICLP (1994), Budapest, report R 1c-09.

/5/ Heidler, F.: Traveling current source model for LEMP calculation. 6th EMC Symp. (1985), Zurich, p. 157 - 162.

/6/ Diendorfer, G.; Uman, M.A.: An improved return stroke model with specified channel-base current. JGR (1990), vol. 95, no. D9, p. 13621 - 13644.

/7/ Singer, H.; Bruens, H.-D.; Mader, T.; Freiberg, A.: CONCEPT II - Anleitung zum Programmsystem. University Hamburg-Harburg, 1994.

/8/ Brocke, R.; Noak, F.; Schönau, J.: Stresses of parts of external lightning protection systems by the first stroke. 22nd Intern. Conf. on Lightning Protection ICLP (1994), Budapest, report R 3b-00.

/9/ Heidler, F.; Hopf, Ch.: Lightning current and lightning electromagnetic impulse considering current reflection at the earth's surface. 22nd Intern. Conf. on Lightning Protection (1994), Budapest, R 4-05.

/10/ Guerrieri, S.; Nucci, C. A.; Rachidi, F.; Rubinstein, M.: On the influence of elevated strike objects on the lightning return stroke current and the distant electric field. Int. Conf. on EMC (1994), Rome, p. 13 - 16.

# FINITE DIFFERENCE CALCULATIONS OF LIGHTNING EFFECTS AT THE SPACE SHUTTLE LAUNCH PAD

Richard S. Collier
Electromagnetic Applications Inc
7655 West Mississippi Ave, Suite 300
Lakewood CO 80226-4332
Phone (303)980-0070 FAX (303)980-0836

Dr. Garland Thomas
RT-SRD-1
Kennedy Space Center, FL 32899
Phone (407)867-4493 FAX (407)867-8038

## ABSTRACT

Three Dimensional Finite Difference (3DFD) computer models have been created to calculate potential effects of lightning at the Space Shuttle Launch Pad. These models include situations with the Orbiter in place on the Pad both with and without mating to the Payload Changeout Room (PCR). Models also include the case with the Orbiter absent and the PCR retracted to the Park position. Lightning attachments for Standard NSTS and other waveforms are considered to the catenary Lightning Protection cable over the Launch Pad and also to parts of the Launch Pad stucture.

## 1.0 INTRODUCTION

In a previous conference paper, Collier and Fisher (1) report the technical basis for experimental modeling and three dimensional computerized finite difference modeling (3DFD) of lightning effects in and around the Space Shuttle Launch Pad. Lightning strikes will normally attach to the Catenary Lightning Protection Cable which is above the Launch Complex. Occasionally, lightning will attach to various parts of the Launch Pad structure itself.

It was found by Collier and Fisher (1) that both experimental and theoretical 3DFD models reasonably predict lighting simulator data reported by Eckhoff, Fisher, Medelius, Nguyen and Thomas (2). Typically the modeling values are within about a factor of 2 of the experimentally determined results.

3DFD models have been created to simulate natural lightning events and also to predict lightning effects for Launch geometries which are less amenable to experimental lightning simulation. Two specific uses of these models which are reported here are:

1. A simulation of a natural lightning attachment to the PCR (Payload Changeout Room) frame structure which occured on June 24, 1994. In this case, the Orbiter is absent and the PCR is retracted to its Park position.

2. A simulation of a 1 percent NSTS Component A attachment to the top of the catenary wire above the Launch Complex. In this case, the Orbiter is present in launch position. Calculations are performed for the two cases where the PCR is retracted to the Park position and where the PCR is mated to the Orbiter.

In these computer simulations Electric and Magnetic fields are calculated in and around critical areas of the PCR and the Orbiter Cabin access port. Voltages and currents are calculated across major component interfaces. An example is given here for various grounding cable configurations between the Orbiter Cabin and the White Room at the end of the Orbiter Access walkway. Various cable grounding configurations can have a large effect on the voltage and currents which were calculated.

## 2.0 FINITE DIFFERENCE ANALYSIS

It was shown in Reference (1) that finite difference analysis is performed by constructing a space filling rectangular grid of cells which contain the structure and the immediate problem space around the structure. There are typically about 1 million cells in the problem space. The space exterior to the Structure of the Launch Pad contains cells which are 1 meter cubes. Examples are shown in Figures 1, 2, 3 and 4 showing grids of the the Launch Pad Structure with the PCR in the Park Position and in a Mate Position with the Orbiter. Details of the Orbiter and PCR are also shown.

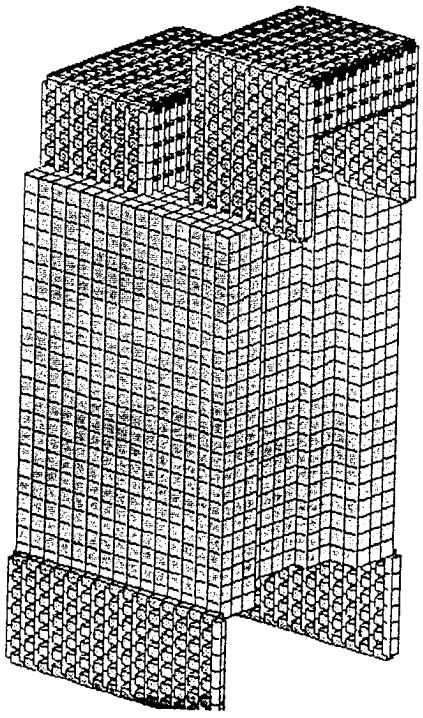


Figure 1. PCR - Doors Closed

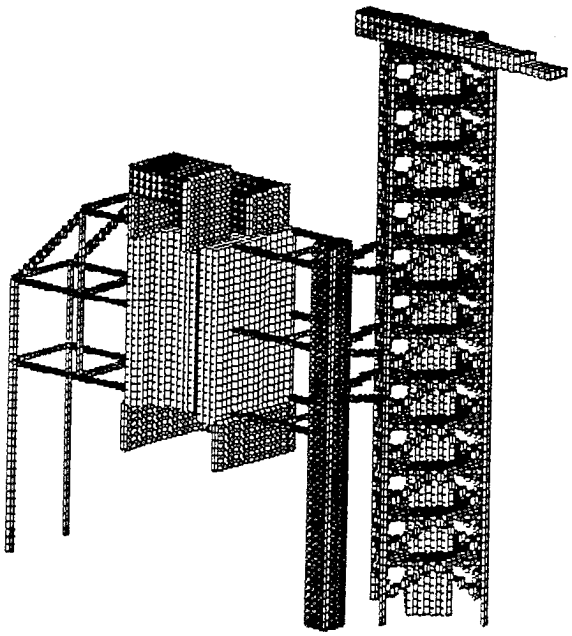


Figure 2. PCR in Park Position

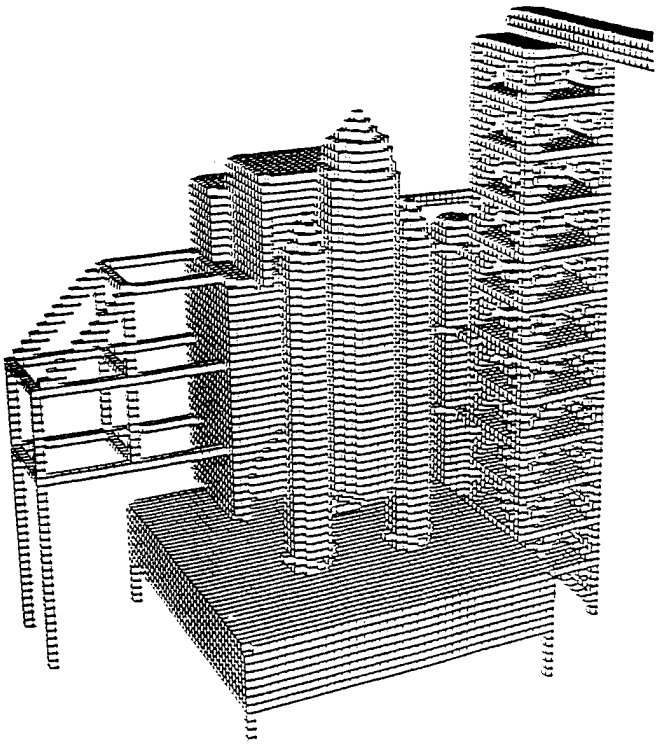


Figure 3. PCR - Mate Position

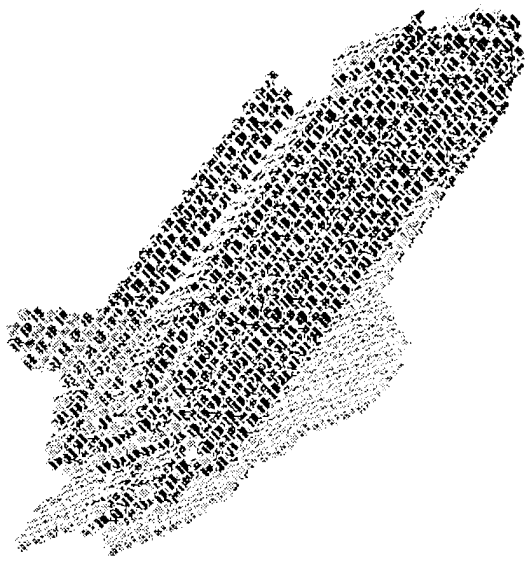


Figure 4. Orbiter - Doors Open

Each cell contains a staggered vector grid of electric and magnetic field which are assumed to be the average values of these field components over the grid size. Material properties which are dielectric constant, magnetic permeability and conductivity are assigned to each cell. Metals are included by requiring that the electric field tangential to the metal be zero at all times. The electric and magnetic fields are propagated numerically in both space and time according to a finite difference formulation of the Maxwell curl equations. The maximum time step is determined by the Courant Condition which requires that the numerical propagation of the solution be faster than the speed of light. The time step for the external solutions calculated herein is 1.8 nsec. The grid size for the PCR interior is taken to be .5 meter or .25 meter cubes. The time step for these solutions is .9 nsec and .45 nsec respectively.

The time domain solutions at each cell location are explicit and accurate to second order in both space and time. The upper limit of frequency resolution is determined by the cell size and is approximately 60 MHz for these calculations. This is thought to be well sufficient to calculate the response of most lightning waveforms.

Lightning is introduced into the problem space by increasing the current along a line of zero electric field from the edge of the problem space to the assumed point of attachment. The current is time dependent according to a definite time dependent waveform. Figures 5, 6 show waveforms which are used for these calculations.

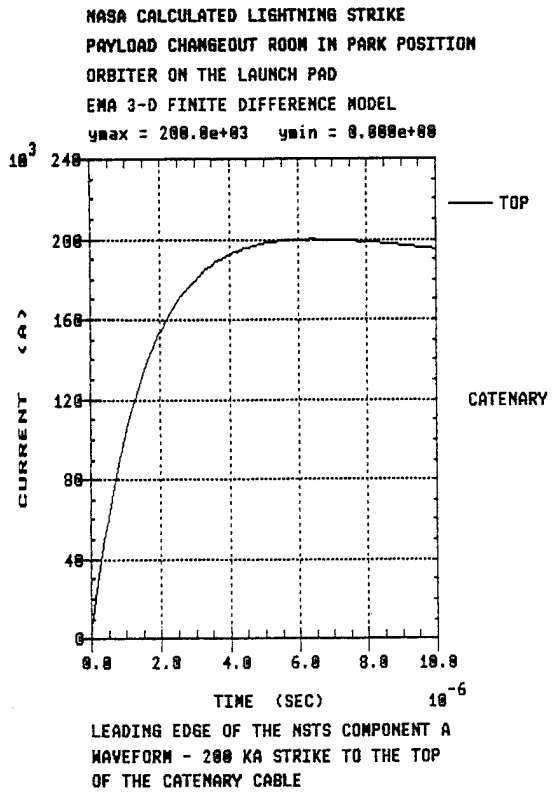



Figure 5. NSTS - A Waveform

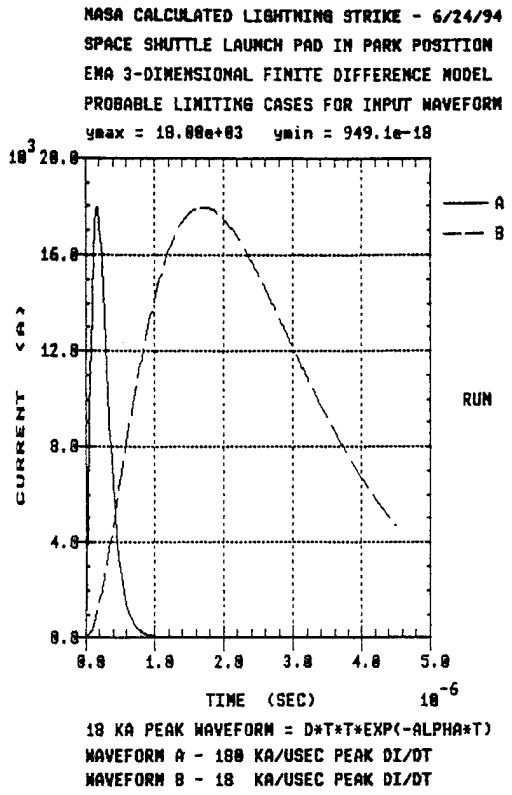



Figure 6. Simulated Waveforms

## 3.0 LIGHTNING STRIKE WAVEFORMS AND ATTACHMENT

Figure 5 shows the leading edge of the NSTS Component A waveform. The amplitude of 200 KA, assumed to be a 1 percent strike, peaks at about 6 usec. The waveform is a double exponetial which decreases exponentially at longer times. It is seen that the time derivative of this waveform is non-zero at time zero. This waveform was assumed to attach at the top of the catenary wire.

Figure 6 shows two waveforms which were used to simulate the natural lightning attachment of June 24, 1994. This attachment was photographed and later determined to be located on an angle corner of the RSS (Rotating Service Structure) near the top back outside corner of the PCR. The amplitude of this strike was determined by remote measurement to be about 18 KA. The risetime, from zero to peak, was estimated statistically to be bounded below by 18 KA/usec and be bounded above by 180 KA/usec; these are shown by curves A and B respectively in Figure 6. Thus the natural lightning event is assumed to be somewhere between curves A and B in Figure 6.

Both waveforms in Figure 6 are decreasing exponential at long times which is multiplied by a time-squared factor. The advantage of this waveform is that the time derivative is zero at zero time. This corresponds more closely to natural lightning. Also, for the numerical calculation, the zero derivative provides less of a shock to the system at time-zero than does the double exponetial waveform as found in the NSTS Component A.

## 4.0 CALCULATIONS AT THE ORBITER-WHITE ROOM INTERFACE

For these calculations, the Orbiter is in the Launch position on the Pad as shown in Figure 3; the PCR on the RSS is rotated back to the Park position as shown in Figure 2. The walkway access to the Orbiter Cabin extends from the Fixed Service Structure (FSS) at the level of the Orbiter Cabin. This walkway terminates at the White Room which interfaces with the Orbiter Cabin. There is an electrically insulating seal between the White Room and the Cabin. Except for the time of the intial contact, there is a grounding cable about 3 meters long connecting the White Room to the Orbiter. On the floor of the White Room is a Slide or "walk-bridge" about 24 inches wide and 44 inches long which extends into the Orbiter to support personnel access into the Orbiter cabin. This slide is made of metal but is not normally grounded on both ends to the White Room and the Orbiter.

The lightning attachment is at the top of the Catenary Wire which is above and insulated from the FSS. The waveform is taken to be the 1 percent strike shown in the NSTS Component A waveform of Figure 5. It should be noted that this does not represent a direct lightning attachment to any part of the Orbiter or Launch Pad structure. All the direct lightning current is going down the catenary cable to north and south grounding points about 1000 feet from the FSS. All currents and voltages calculated result from currents which are induced by the time varying electromagnetic fields emanating from the lightning channel and the catenary wire.

Calculated voltages between the Orbiter and White Room are shown in figures 7 and 8. Figure 7 shows a comparison of voltage between the Orbiter and White Room for cases where there are no ground strap connections. The comparison shows the difference between the PCR being present in the Mate position and being removed from the calculation; this shows that the PCR in the Mate position provides some shielding for the interface. The interface peak voltage is about 50 KV when shielded by the PCR and the peak voltage is about 100 KV when the Orbiter is free standing in the launch position.

Figure 8 shows the effect of grounding across the interface first with a 3 meter long ground strap and secondly if the walk-bridge has solid connection to both the White Room and the Orbiter. In this case the Orbiter is free standing. Thus the peak voltages range from 100 KV to 24 KV to 4 KV for no ground, a 3 meter ground strap and an additional solid connected metal sheet respectively. The metal sheet provides a much lower inductive path across the interface. Additional calculations with a shorter 2 meter ground strap shows peak voltages decreasing in approximate proportion to the length (and hence inductance) of the ground strap, Figure 9.

Figure 10 shows the currents calculated in the ground strap under various conditions. The 2 and 3 meter ground strap both carry the same current, about 750 Amps, showing that the impedance effect of the ground strap is negligible. The current in the cable is reduced to about 130 Amps when the walk-bridge is connected. In this case the bridge will carry most of the current.

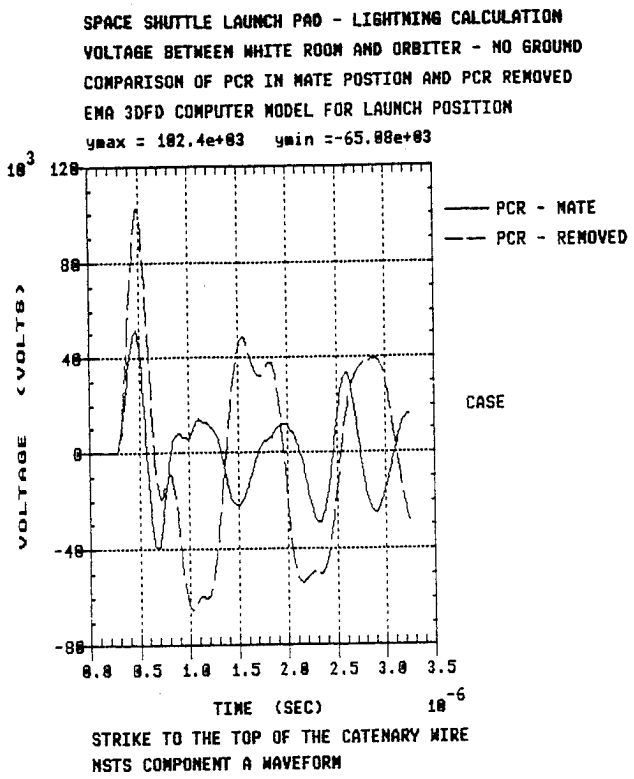



Figure 7. Interface Voltage

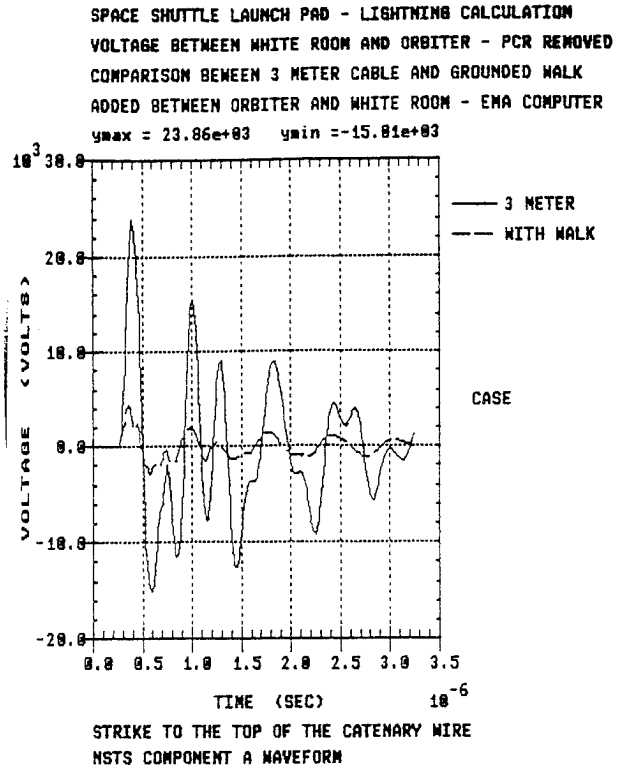



Figure 8. Interface Voltage

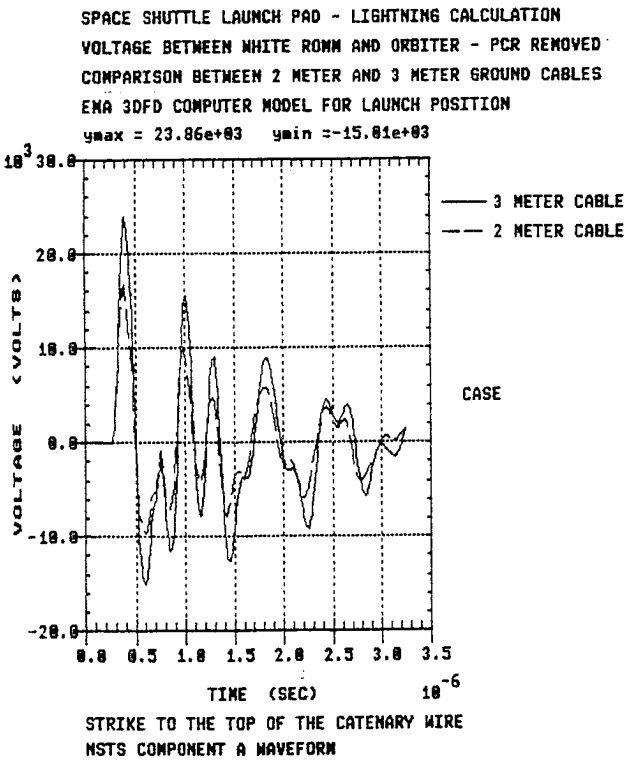



Figure 9. Interface Voltage

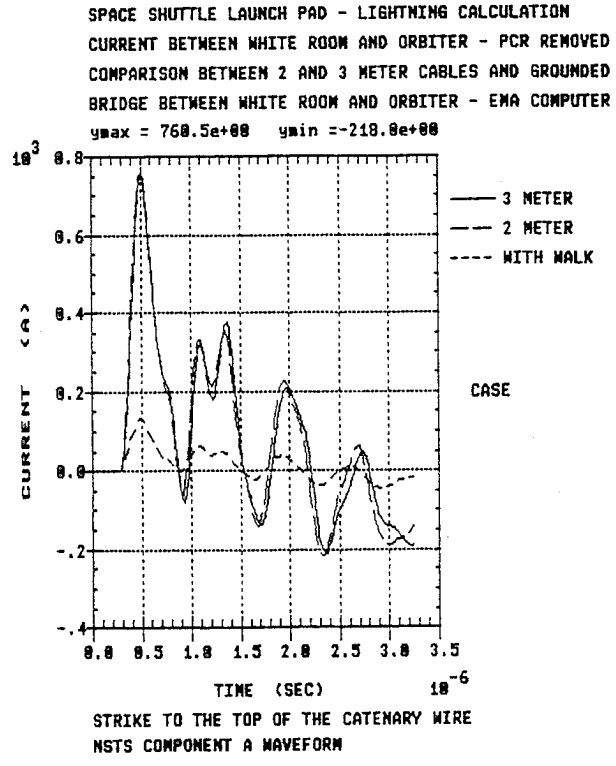



Figure 10. Cable Currents

It is observed in Figures 7 through 10 that there are strong resonance oscillations, on the order of 1-2 MHz and higher, in both the current and voltage waveforms at the interface. The observed oscillations are due to structural resonances of the larger parts of the launch pad structure. For example, there is a large loop formed by the Orbiter Cabin walkway, the FSS, the Launch Pad and the Obiter-Solid Rocket Booster assembly; the weak link in this loop is the Orbiter-White Room interface where the calculations have been made. This loop will have a resonance frequency on the order of 1 MHz. Resonance reflections can also occur at places where there is a large dissimilarity in the size and shape of the structural elements; for example, the connection of the walkway with the FSS and the connection interface of the Launch Pad and the Solid Rocket Boosters. The existance of resonances could provide an additional hazard or threat if there are assets such as cables, electronics, or personnel which may have components which could resonate in sympathy with the driving oscillations. It is noted that all of these effects are indirect inductive effects and do not represent, in this case, any direct conduction of the main lightning current.

## 5.0 SIMULATION OF THE JUNE 24, 1994 LIGHTNING STRIKE

In this case the Orbiter is absent, and the PCR and RSS are rotated back to the Park position; the PCR doors are closed. In this case the primary interest is in electric and magnetic fields which may propagate to the PCR interior, primarily through seams formed by insulating gaskets around the main doors. These seams are approximately 1 inch wide and are treated as apertures. The vertical seams are interrupted at 3 meter intervals by door hinges and buckles. The horizontal seams, at the top and bottom of the doors, are 11 meters long and are not interrupted by metal jumpers. The apertures are represented by equivalent polarizabilities Pe and Ph which multiply the time derivatives of the electric and magnetic fields at the exterior of the seam, and give equivalent electric and magnetic dipole currents at the interior door seam locations. These interior dipoles are then used as source currents to drive a completely different 3DFD interior problem. The interior PCR grid in these calculations are .5 meter cubes and include elements of structure inside the PCR. The structure and locations of test test points interior to the PCR are shown in Figure 11.

It is also of interest to calculate some of the direct external currents due to the direct lightning attachment to the RSS. There are three points of contact of the RSS with the ground which provide the primary gounding points for the lightning charge. Two of these are at the wheel-track interface at the end of the two exterior legs of the RSS. The third is at the pivot point of the RSS. Figure 12 shows calculated currents in each of the legs and at the pivot point. There are two sets of curves corresponding to the limiting input waveforms A and B shown in Figure 6. In either case the current in each of the exterior legs is about 5 KA and about 3 KA at the pivot point. This accounts for 13 of the 18 KA

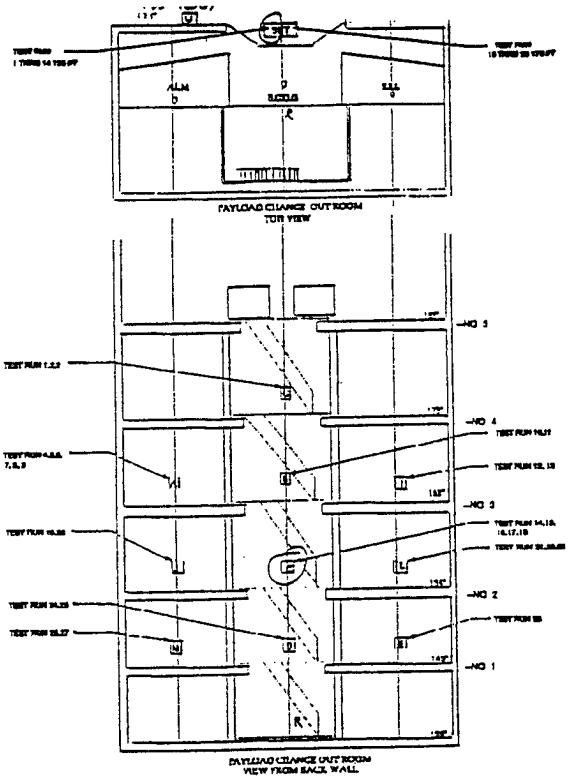


Figure 11. Interior of PCR

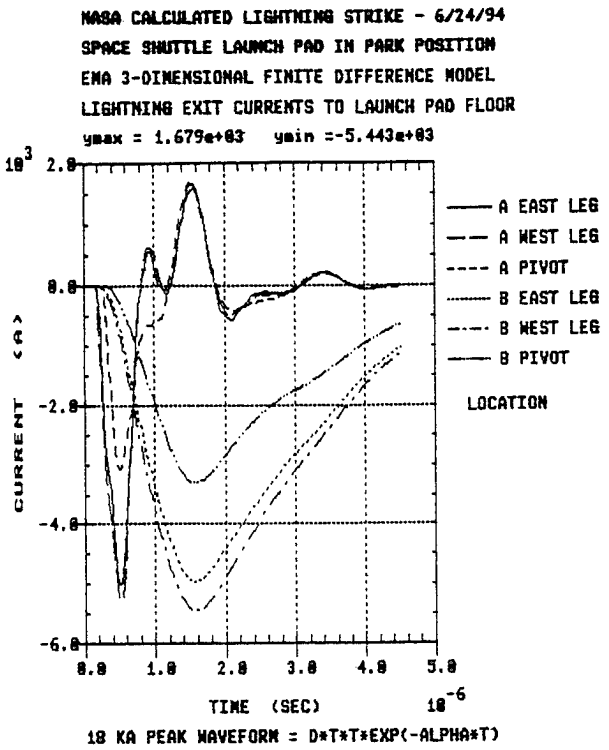



Figure 12. Direct Lightning

input. The other 5 KA goes into the FSS. From the 5 KA current there was apparently some damage to a switch box on the west leg.

The electric and magnetic fields at the PCR door center are shown in Figures 13 and 14; the time derivatives of these fields are shown in Figures 15 and 16. The time derivatives are obtained at each door seam location, thirty 3-meter vertical seam segments and two 11-meter horizontal seam segments. The internal fields are shown in Figures 17 - 20. The largest internal fields are due to magnetic field coupling to the horizonal door seams because the polarizability is proportional to the cube of the seam length. Here, again, it is inferred that coupling could be significantly reduced by using additional ground straps across horizontal seams. Also, it is seen again that higher frequency resonances appear in the interior responses which could possibly couple to assets.

## 6.0 REFERENCES

1. R.S. Collier, F.A. Fisher, "Lightning Induced Electromagnetic Environment of the Space Shuttle Payload Changeout Room-Modeling" 16th International Aerospace and Ground Conference on Lightning and Static Electricity, p.417-426, May 24, 1994 Mannheim, Germany

2. A.Eckhoff, F.A.Fisher, P.Medelius, Nguyen, G.Thomas, "Lightning Induced Electromagnetic Environment of the Space Shuttle Payload Changeout Room-Measuring", 16th International Aerospace and Ground Conference on Lightning and Static Electricity, p.407-416, May 24, 1994 Manheim, Germany

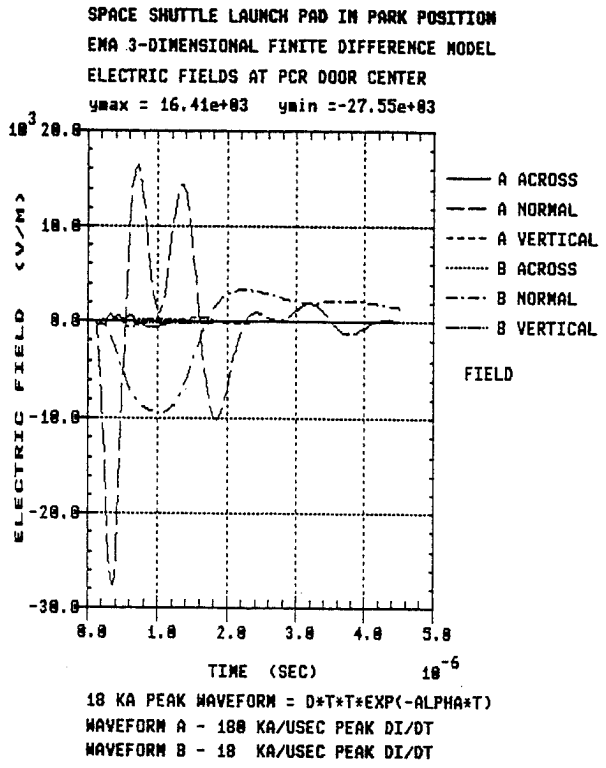



Figure 13. Exterior E-Fields

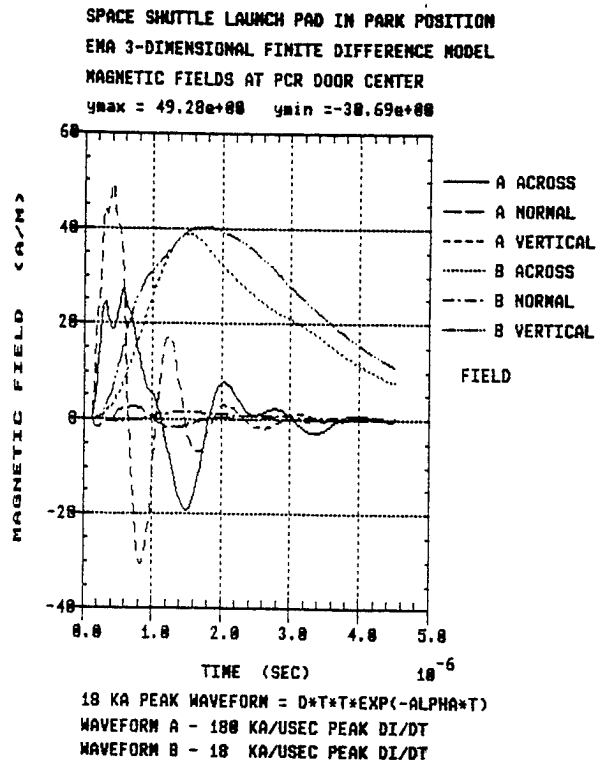



Figure 14. Exterior H-Fields

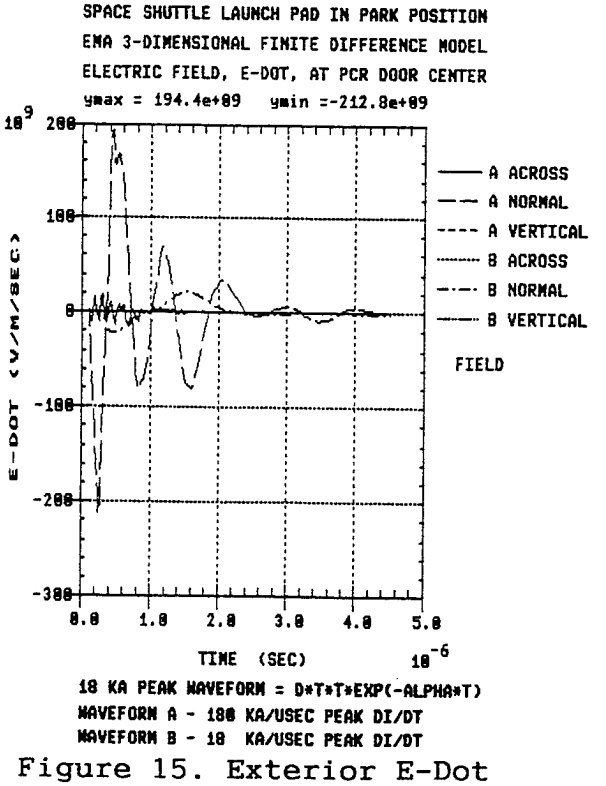



Figure 15. Exterior E-Dot

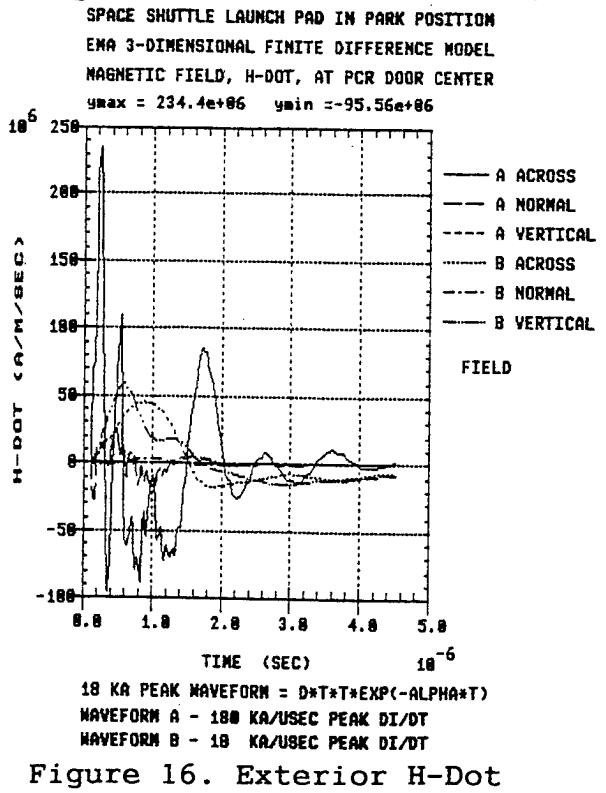



Figure 16. Exterior H-Dot

Figures 13 through 16, 3DFD Computer Simulation of June 24, 1994 Natural Lightning Strike to RSS - PCR was in the Park Position

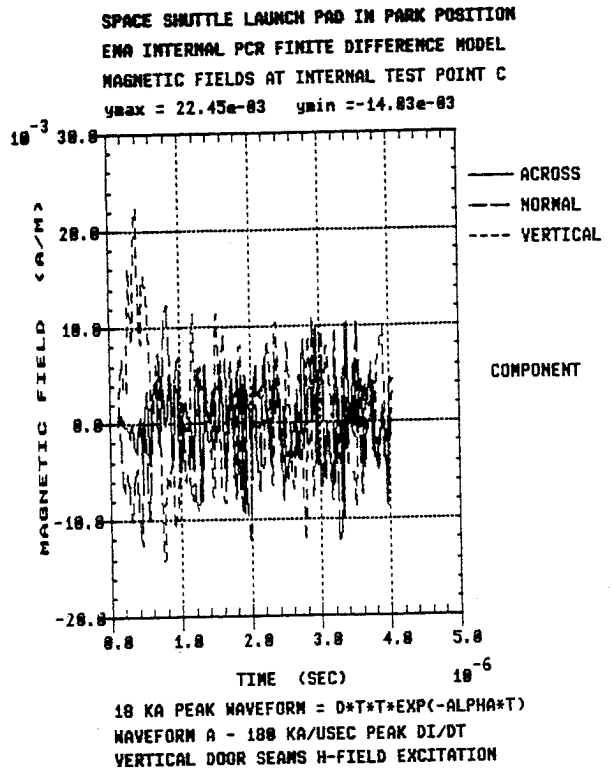



Figure 17. Interior H-Fields at C

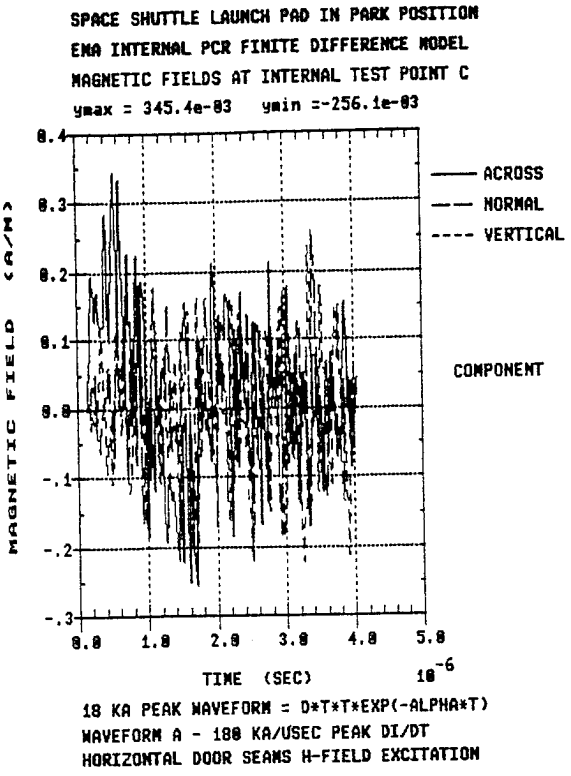



Figure 18. Interior H-Fields at C

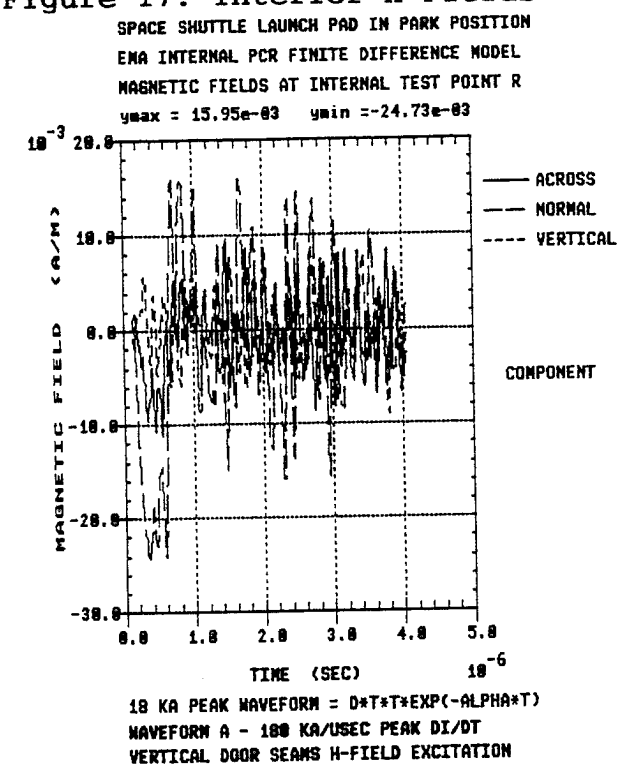



Figure 19. Interior H-Fields at R

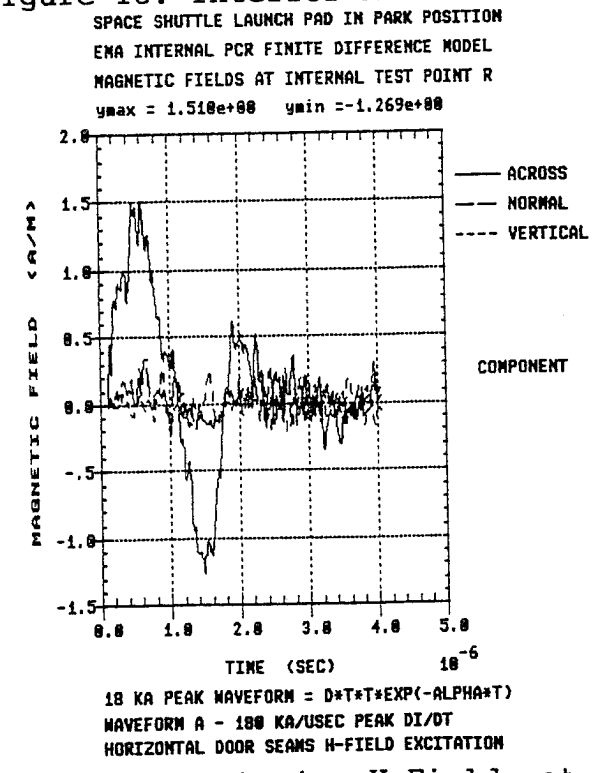



Figure 20. Interior H-Fields at R

Figures 17 through 20, 3DFD Computer Simulation of June 24, 1994 Natural Lightning Strike to RSS - PCR was in the Park Position

# MD-90 TRANSPORT AIRCRAFT LIGHTNING INDUCED TRANSIENT LEVEL EVALUATION BY TIME DOMAIN THREE DIMENSIONAL FINITE DIFFERENCE MODELING

B. D. Sherman, T. He, B. Nozari
Douglas Aircraft Company
Long Beach, California, USA
Telephone (310) 593-9514 Fax (310) 982-5030

T. Rudolph
Electro Magnetic Applications Inc.
Denver, Colorado, USA
Telephone (303) 980-0070 Fax (303) 980-0836

## ABSTRACT

The Time Domain Three Dimensional Finite Difference (T3DFD) technique was used to model the MD-90 transport aircraft electromagnetic response to a lightning strike in a free space environment. The objective was to determine the peak lightning induced transient levels at the critical/essential equipment interfaces for the purpose of transient control level (TCL) verification. These data together with the equipment transient design levels (ETDL) were used to qualify the McDonnell Douglas MD-90 transport aircraft for the FAA/JAA certification. This is the first known application of T3DFD for modeling and coupling analysis of a complex transport aircraft for formal lightning certification.

## INTRODUCTION

The transient level evaluation had to be performed accurately, inexpensively and in a timely manner. The TCL level determination by lightning simulation tests is effective and yet expensive, and the setup conditions inflexible and sometimes not totally realistic. It is difficult to overcome the ground effects. It is also expensive and time consuming to conduct parametric measurements; such as transient level evaluations for different attachment points, current waveforms, structural configurations, and wire routes. In contrast, an analysis similar to T3DFD does not encounter any of these limitations.

Lightning induced transient level evaluation of an aircraft for the purpose of certification has usually been performed by lightning simulation tests or continuous wave testing. Commercial transport aircraft have never (or at least rarely) been certified for lightning indirect effects purely on the basis of analysis, T3DFD included. This has been mainly due to the lack of comprehensive validation data with sufficient accuracy.

The analysis had to be completed on time for aircraft certification in spite of budget limitations. Every effort had to be streamlined for efficiency, and unnecessary sophistication and complexity avoided. All aspects of methodology had to be validated against test data (1) to make the analysis acceptable for the FAA and JAA Certification. The required resolution to model all the necessary details was approximated to be 2 to 3 inches (50.8 to 76.2 mm) which, with the available computer resources, made the complete aircraft too large to model in one piece. The reasonable solution was to partition the aircraft into largest sections possible without exceeding the computer memory capacity. To avoid unrealistic resonances, equivalent surface formalism could have been used; however, initial studies showed that this approach not only would have increased the spread between the test and calculated data, but would have involved a lengthier validation effort which could not have been afforded. The artifactitious resonances are due to small size of the model compared to actual aircraft, and staircase approximation of wire routes. The most efficient approach was to model the sections without equivalent surfaces and then to minimize the resonances by terminating the long or less stable models at the boundary on one side, terminating the wires at their characteristic impedances, and further reducing the artifactitious frequency components consistent with model size and limitations by using filters or moving average operation. The sectionalized modeling allowed using lightning simulation test data already available for the nose and engine-pylon sections of the MD-80 aircraft for validation. Due to similarity of these sections to their corresponding MD-90 sections, the validation was proper and no further analysis was necessary to link the validation to the actual analysis.

This paper presents the analysis approach, model description and visualization, method of sectional model analysis data transformation to complete wire route transient waveforms, and final analysis data.

## APPROACH

The analysis approach parallels the lightning simulation test approach which has been used at Douglas Aircraft Company. The aircraft was partitioned (figure 1) into a minimum number of sections which were modeled independently. The dimensions of each problem space were bound by the available computer resources and required resolution. The resolution for each particular section was dictated by its smallest dimension of apertures and wire route spacing from the closest structure. Each division was modeled using a validated T3DFD technique.

The models consisted of the nose, fuselage, wing/wheel well/landing gear, engine/pylon, aft accessory compartment, and horizontal/vertical stabilizer sections. Some of the sections, such as the nose section, were subdivided due to the structural and wire route separation within the section. All the models except the nose and empennage sections were gridded at a 3-inch step size. The nose and empennage were gridded at 2-inch step size. To preserve the code stability, the Courant criterion, equation 1, was used to calculate the models time step ($\Delta t$) upper limit. The time step was different for each model but was in the range indicated in equation 2.

$$\Delta t \le \sqrt{\varepsilon\mu} \Big/ \sqrt{\frac{1}{\Delta x^2} + \frac{1}{\Delta y^2} + \frac{1}{\Delta z^2}} \tag{1}$$

$$0.08\ ns \le \Delta t \le 0.13\ ns \quad \text{for} \quad \Delta x = \Delta y = \Delta z = 2\ in \text{ or } 3\ in \tag{2}$$

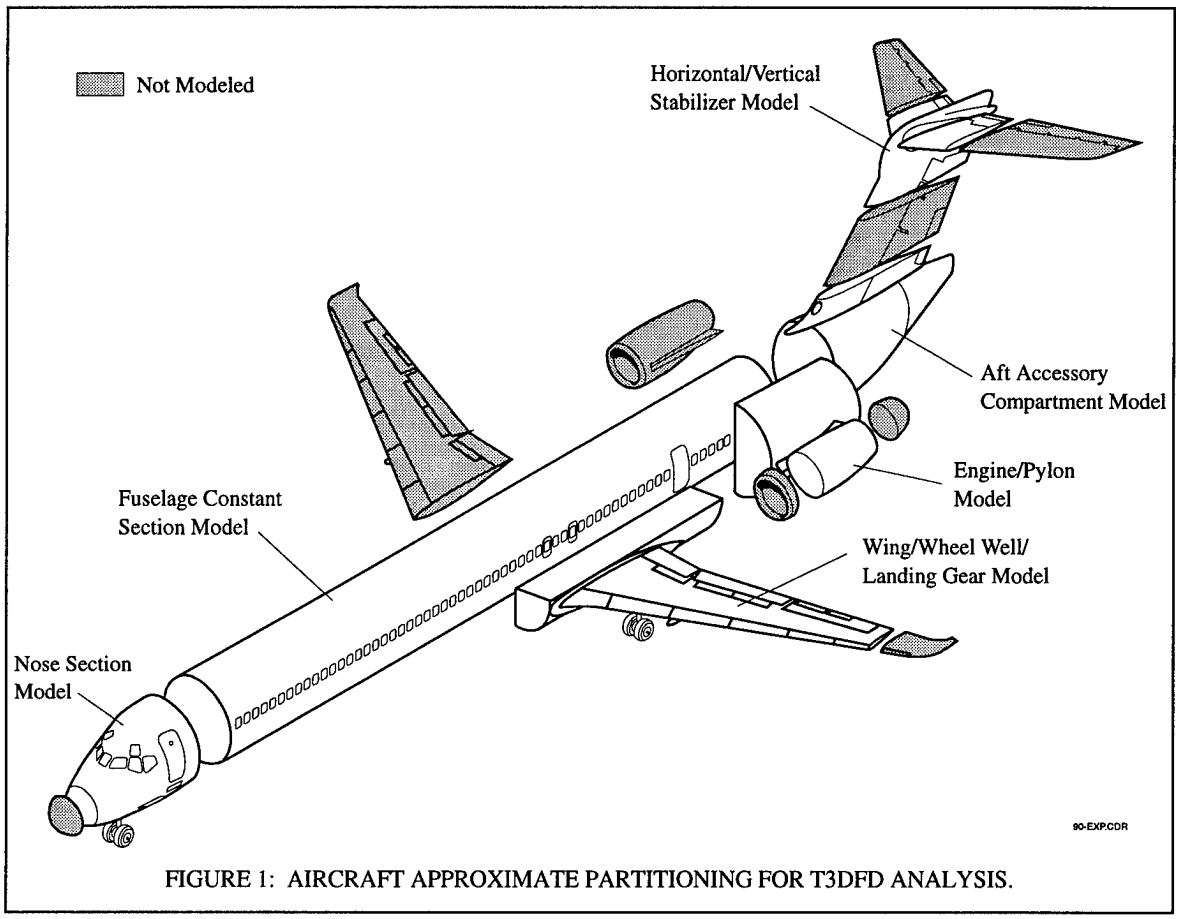



FIGURE 1: AIRCRAFT APPROXIMATE PARTITIONING FOR T3DFD ANALYSIS.

**STRUCTURE**— In simulating the structure, the external structure such as skin and doors was modeled completely, while the internal structure was modeled selectively. All the internal structural elements that were estimated to have significant effect on the field intensity in the areas of interest were simulated. The internal structure was not modeled if (a) it was estimated to have no effect or small reduction on the local field, or (b) it was located in a protected area and was not significantly affecting the field intensity. Each section, with the exception of the engine-pylon, was modeled assuming perfect conducting skin and structure. This was a safe assumption since voltage drops along the aluminum structure next to the subject wire routes are insignificant during a severe lightning strike, even with the most imposing lightning attachment configuration. However, this condition is not true in the engine-pylon section where the fuselage skin surrounding the pylon area is made of titanium alloy which has a resistivity approximately 17 times that of aluminum.

**Apertures/Doors/Slots**—Windows were modeled using T3DFD basic techniques. Most of the windows, grouped together such as fuselage and cockpit windows, were equal or larger than 3 cells wide, while a few isolated windows were 2 cells wide, and thin slots less than one cell wide. The doors were modeled by using two different techniques. The resistive thin slot formalism (2) was used for one of the doors, while others were simulated by a 3-dimensional structure, instead of the more common two dimensional geometry. In this design, due to a structural overhang (see figure 2) at the door jamb, the internal area exposure is more similar to

that of the aircraft, in spite of the gap being larger than the actual one by an order of magnitude. The structural aperture model was more flexible and allowed many variations such as changes in the door thickness, or different shapes of contacts between the door and the surrounding structure.

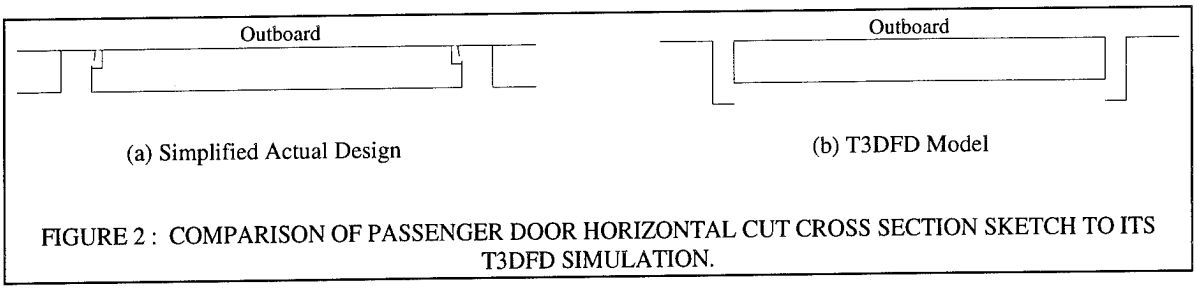



FIGURE 2 : COMPARISON OF PASSENGER DOOR HORIZONTAL CUT CROSS SECTION SKETCH TO ITS T3DFD SIMULATION.

**Structural Caps**—Open ends of every model (where cross sectional cutting occurred) were capped with a perfectly conducting surface. This was to close any aperture that was an artifact of sectionalized modeling. For example the aft end of the nose, forward end of the fuselage, and inboard end of the wing sections were capped in their respective models.

**WIRING**—Representative samples of different wire routes in each section, including the routes in the highly exposed areas, were modeled using the thin wire technique (3). Wires were modeled singly, not in bundles as assembled in production. Wire spacing from the structure was based on a conservative average value (this was one of the factors determining the cell size). The model's wiring loop area formed between the interface wiring, aircraft skin/structure, and the terminations at both ends of the wire was always larger than the actual one. Wires were terminated at their transmission line characteristic impedance (360Ω—based on empirically weighted average spacing) at both ends to minimize reflections.

The shields of shielded wires were the only part of this type of wiring that were modeled by T3DFD. The shields in moderately exposed areas were simulated as wires except their diameter was equivalent to the shield diameter. The shielded wires in highly exposed areas were modeled as a wire with a diameter equivalent to that of their bundle to take advantage of current sharing between wires. The voltage and current calculations for these wires required additional steps beyond those taken for the unshielded wire transient level calculations. The computations shall be discussed later in the "Calculations" section.

Mixed wire runs (part of the length shielded and part unshielded) were modeled as if they were different wire routes; i.e., the shielded and unshielded sections were terminated at both ends independently.

**SETUP**—The boundary of each problem space was separated 20 cells from the nearest model surface on each side. The exceptions were the models of fuselage, aft accessory compartment, and horizontal/vertical stabilizer sections which extended into the boundary at one end. This was due to the large sizes of these sections and the fact that the end running to the boundary minimized the reflections at that end, as the initial studies showed. A specially developed boundary condition (4) for low frequency applications was used for improved performance of quasi-magnetostatic coupling of lightning current to the interior of aircraft. Each attached lightning channel was modeled by a line of single cells. The current entered the model

through the single-cell line representing a current source between the boundary and the model, and exited either through the end extending to the boundary, or another single-cell line representing a current drain. In either case, the boundary became part of the current return path.

## COMPUTING RESOURCES

**WORKSTATIONS & COMPUTER CODE**—All computations were performed on Hewlett Packard 9000 series work stations. The stations used for this modeling had the CPU speed of 75 to 100 MHz, RAM capacity of 64 to 136 MB, and hard disk capacity of 600 MB to 1 GB. The basic computer code was developed by Electro Magnetic Applications, Inc.

**VISUALIZATION**— A computer program titled, "TSAR" from Lawrence Livermore Laboratory was adapted to the system to visualize the constructed models. This program represents each null electric field by a line segment equal to the step size. The effect is a collection of see-through cubicles which represent the shape of the subject T3DFD model. All the model representations in this paper are the results of this visualization.

## MODELS

**NOSE**—The nose section consisted of the foremost 16-foot conductive section of the aircraft (figure 1). The nose section has the highest density of electronic equipment and wire bundles; therefore, its electromagnetic exposure level affects more systems than any other section of aircraft. The most significant exposure path for this model is through the cockpit windows and aft cockpit doors (forward passenger & service doors). The model setup is shown in figure 3. The most severe lightning strike configuration, nose radome area to an extremity point aft of the nose section such as wing tip or tail, was modeled. The lightning channel attachment severity was determined by previous lightning simulation tests. Figure 4 shows all the significant structural elements that were modeled. The model was internally divided, by conductive surfaces as in production aircraft, into four subsections of cockpit, electrical/electronic compartment, forward accessory compartment, and nose landing gear/wheel well. The subdivision was performed since each section is structurally separated from the rest, and has a different level of electromagnetic exposure, in addition to being illuminated through a different path. A total of 11 wire routes in the cockpit, 8 in the electrical/electronic compartment, 3 in the forward accessory compartment, and one in the wheel well area were modeled. In addition, 23 wire route subsections were modeled in the cockpit. The purpose was to simulate the significant common subsections of all the cockpit wire routes, and therefore, to identify the common high exposure areas. The high exposure subsections were then used to construct some of the most exposed wire routes. Figure 5 shows some of the typical modeled cockpit wire routes.

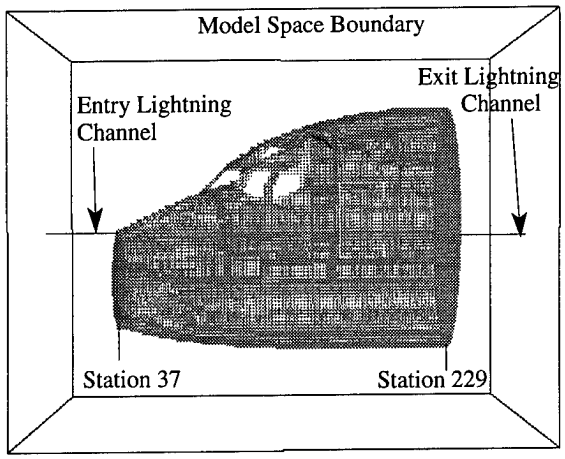



FIGURE 3: NOSE SECTION MODEL SETUP.

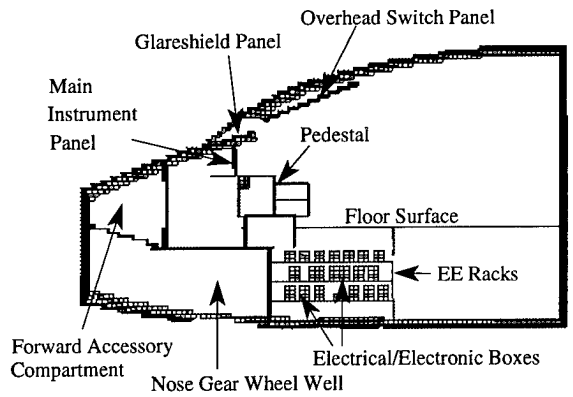



FIGURE 4: MODELED SIGNIFICANT STRUCTURAL ELEMENTS OF NOSE SECTION.

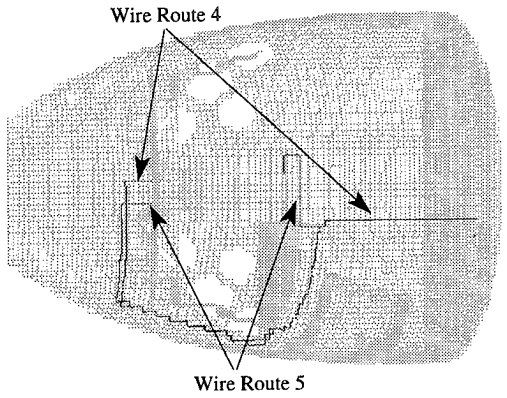



FIGURE 5: TWO TYPICAL MODELED COCKPIT WIRE ROUTES.

**FUSELAGE—** The constant section of fuselage, with quasi-cylindrical cross section, in addition to some of the tapered sections on both ends, from aft of the nose section for 1200 inches (30.48 m) was modeled. To simplify the modeling, the total length was modeled as a constant section. The most significant electromagnetic exposure path is through the 58 windows on either side of the fuselage. The most severe lightning attachment configuration, nose to an extremity point on the tail was simulated. Figure 6 shows a longitudinal cut-away section of the fuselage in the respective setup. A total of 9 typical wire routes were modeled below the floor, right and left side, and overhead at the center. Figure 7 shows the modeled wires in front, inside, perspective view.

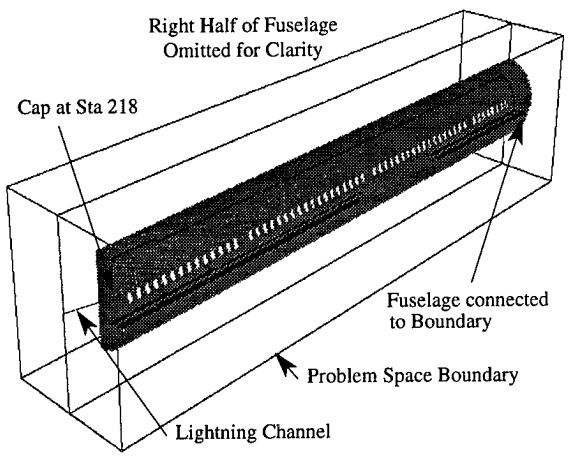



FIGURE 6: OVERALL PERSPECTIVE VIEW OF FUSELAGE MODEL IN ITS SETUP.

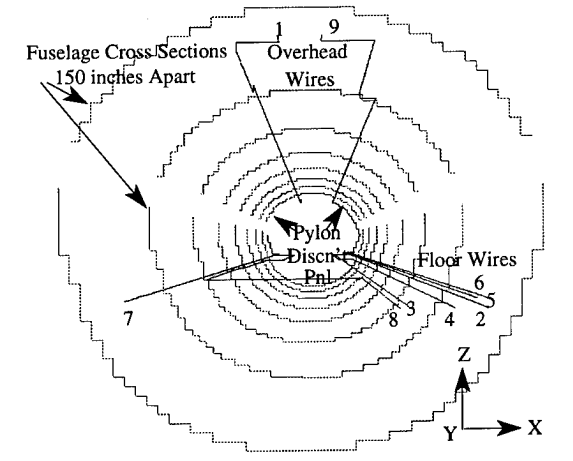



FIGURE 7: FRONT INSIDE PERSPECTIVE VIEW OF FUSELAGE MODEL WITH SIMULATED WIRE ROUTES.

**WING / WHEEL WELL / LANDING GEAR** —This section consisted of the left wing, main landing gear and wheel well, and the wing immediate area of the fuselage (cut-away section of fuselage), as shown in figures 1 & 8. The wing was modeled fully except for the deletion of 81 inches (2 m) at the wing tip. The wing upper and lower skins, front and rear spars, leading edge, and some of the trailing edge panels were simulated. All of the fuel tank access doors were simulated as part of the upper/lower skin, with no apertures, due to their good all-around bonding. The most significant exposure for this model is at the wing trailing edge (aft of rear spar), forward wing root, wheel well, and around the landing gear main strut. Two most severe lightning strike configurations, nose to wing tip and landing gear to tail, were simulated. A total of 9 wire routes were modeled, 2 at the wing leading edge, 3 at the trailing edge, 3 in the wheel well area, and one on the landing gear. Figure 8 shows the leading and trailing edge wire routes, and figure 9 illustrates the wheel well wire routes.

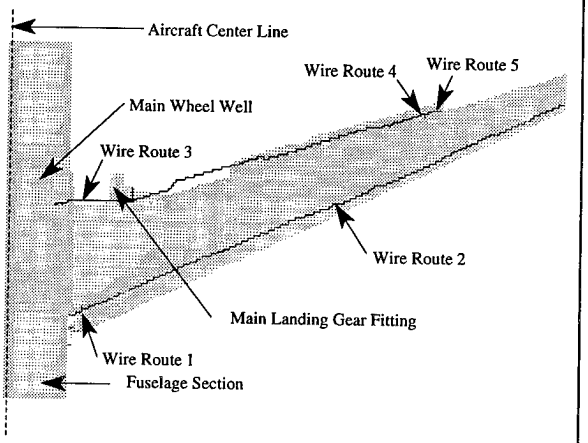



FIGURE 8: WING LEADING AND TRAILING EDGE WIRE ROUTES.

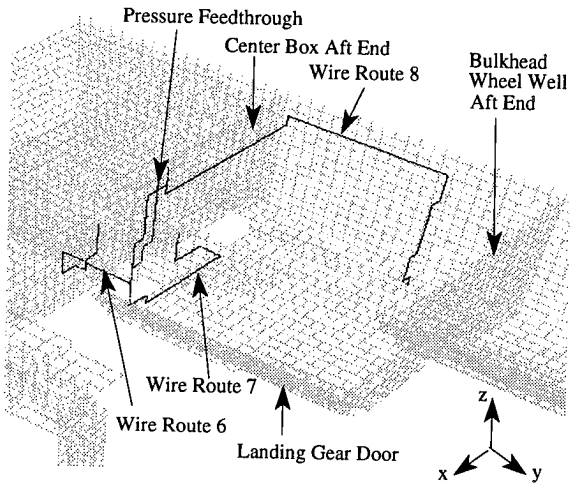



FIGURE 9: WHEEL WELL WIRE ROUTES.

**ENGINE/PYLON**—The right engine fan case and core, pylon, and a 25-foot (7.62 m) long right cut-away side of fuselage around the pylon attachment were modeled (figure 1). The engine part of the model did not include the nacelle, inlet, reverser assembly, or nozzle assembly. The modeled fuselage section, unlike the actual aircraft, did not taper, for simplicity. Two most severe lightning strike configurations were modeled, engine nose to an extremity in the aircraft tail, and engine exhaust nozzle to an aircraft extremity forward of the model such as the wing tip or the nose. Figure 10 shows the conductive elements between the engine and pylon that were simulated. The lightning current is distributed amongst these elements inversely proportional to their inductance, resistance, and other higher order effects. This results in a dynamic field configuration, in the engine and pylon area, which induces transients on the equipment interface wires. The gap between the forward pylon and fuselage is exaggerated; the actual gap is 0.3 to 1.75 inches (7.62 to 44.45 mm) compared to 3 inches (76.2 mm), one cell wide, in the model. The reason for exaggeration was the 3-inch cell size limitation of this model. Four power feeder wires and a total of 9 intra- and inter-engine wires were modeled. Figure 11 illustrates some of the modeled wires.

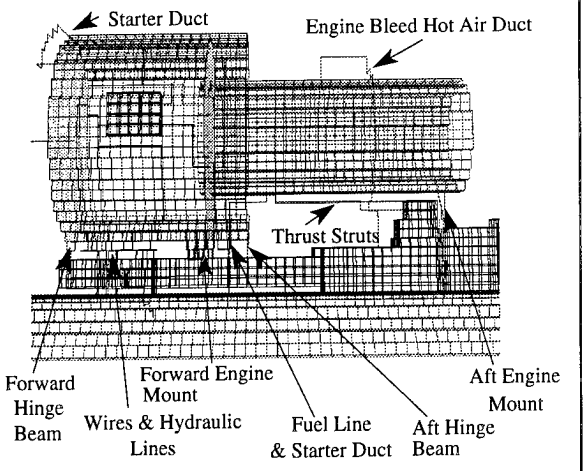



FIGURE 10: CLOSEUP OF ENGINE-PYLON MODEL SHOWING CONDUCTIVE CONNECTIONS ACROSS THE ENGINE / PYLON GAP.

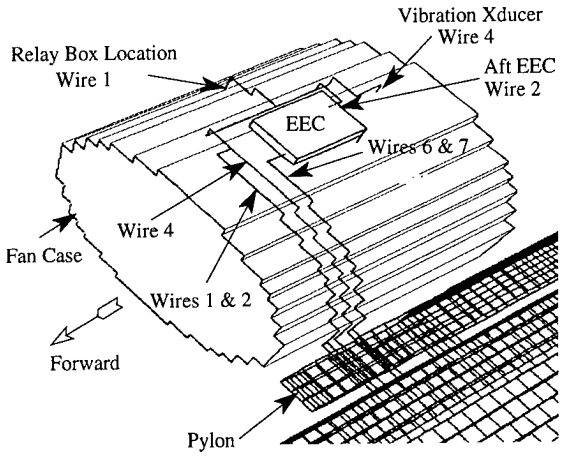



FIGURE 11: ENGINE / PYLON TYPICAL WIRE ROUTE MODELS.

**AFT ACCESSORY AND APU COMPARTMENTS**—This model consists of the aft accessory compartment (AACC), vertical stabilizer and rudder stub, auxiliary power unit (APU) compartment, and the conductive section of the composite tailcone, as shown in figure 1, and in figure 12 with more detail. The modeled section is the aft tapered part of fuselage, behind the aft pressure bulkhead, without the control surfaces. Figure 13 shows the details of modeled internal structural sections. The most significant exposure path is through the tailcone interface and ventral staircase door gap. Some of the wire bundles are routed close to the tailcone attach frame and therefore are highly exposed. Two most severe lightning channel attachment configurations were modeled, the tailcone cap to an extremity at the forward fuselage (such as nose or wing tip), and a horizontal/vertical stabilizer extremity to a forward fuselage extremity. The forward section of this model is terminated at the boundary. A total of 11 wire routes in the AACC and one route in the APU compartment were modeled. Figure 14 shows some of the simulated wire routes for this section, and continuation of some of the horizontal/vertical stabilizer wiring.

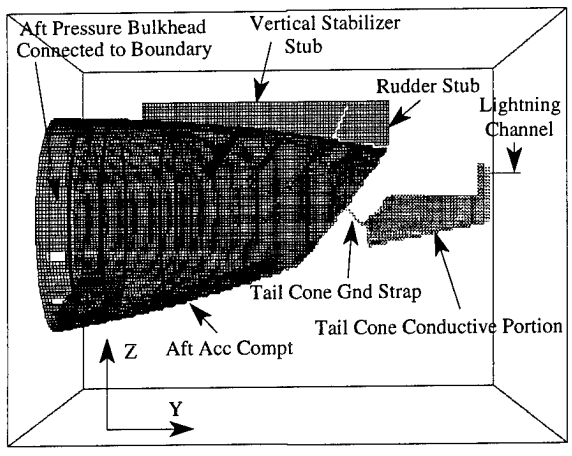



FIGURE 12: AFT ACCESSORY AND APU COMPARTMENT MODELS.

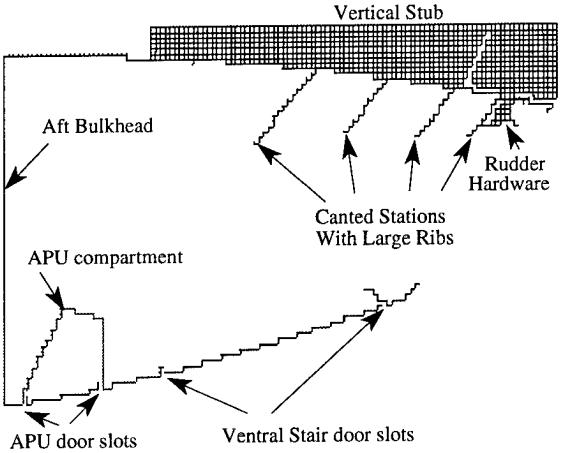



FIGURE 13: MODELED INTERNAL STRUCTURE DETAILS OF AFT ACCESSORY & APU COMPARTMENTS.

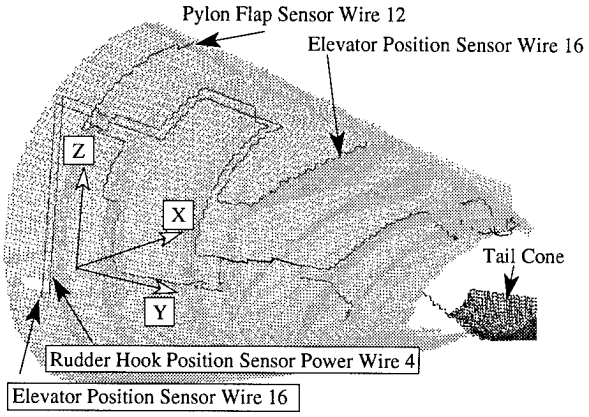



FIGURE 14: TYPICAL AFT ACCESSORY COMPARTMENT SIMULATED WIRE ROUTES.

**HORIZONTAL / VERTICAL STABILIZERS**—This model consists of truncated vertical and horizontal stabilizers (figures 1, 15 & 16). The sections were truncated to lower the requirement for computing resources and the length of run time. The horizontal stabilizer was shortened by 180 inches ($\Delta x \cong 161$", 4.1 m) each side, and the vertical stabilizer by approximately 73 inches ($\Delta z \cong 45$", 1.14 m) at the lower end. This was justified since none of the simulated wiring extends to the outboard (not-modeled) sections of the horizontal stabilizer, and the wire bundles in the lower and mid sections (not-modeled) of the vertical stabilizer all lie behind the stabilizer's leading edge which is an electromagnetically protected area and, therefore, does not allow the external fields to affect the wires, regardless of their length. The primary exposure sources for this model are at the vertical stabilizer fin cap (very top of the vertical stabilizer) and horizontal-vertical stabilizer joint cavity area. A total of 3 wire routes, which were divided into shielded and unshielded portions, were modeled to evaluate the maximum exposure of wiring exposed to the primary sources. Two most severe lightning strike configurations were modeled; aft top of the vertical stabilizer, and outboard tip of the horizontal stabilizer, to an extremity forward of the aft pressure bulkhead, such as the nose or the wing tip.

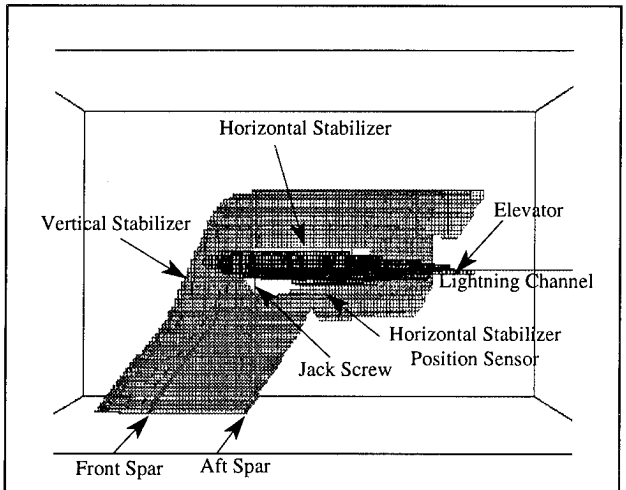



FIGURE 15: LEFT PERSPECTIVE VIEW OF HORIZONTAL/VERTICAL STABILIZER MODEL.

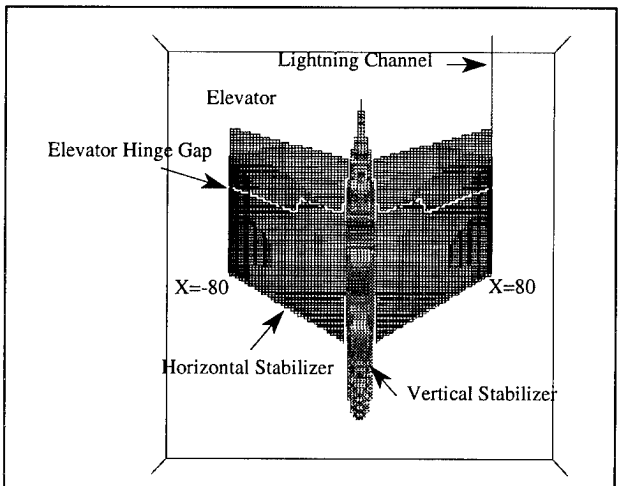



FIGURE 16: TOP PERSPECTIVE VIEW OF HORIZONTAL/VERTICAL STABILIZER MODEL.

## RUNS/EXECUTION

**CODE SIZE & RUN TIME**—Each model required a different RAM capacity and took a different length of time to run for a fixed amount of simulation time. Table 1 shows approximate size of the memory used for each section, and the time it took to acquire the results. The real

time necessary to reach the 1st peak was in the range of 50 ns to 1 μs for the voltage waveforms, and 5 to 12 μs, for the current waveform.

TABLE 1: REQUIRED RAM SIZE & RUN TIME FOR MODELS

| MODEL IDENTIFICATION | CELL SIZE (INCHES) | REQUIRED RAM SIZE (MB) | REQUIRED RUN TIME FOR 6-μs REAL TIME (HRS/DAYS) |
|---|---|---|---|
| Nose | 2 | 40 | 36/1.50 |
| Fuselage | 3 | 86 | 180/7.50 |
| Wing/M Lndng Gr/wheel Well | 2 | 73 | 72/3.00 |
| Engine-Pylon | 3 | 25 | 60/2.50 |
| Aft Acesry & APU Cmprt | 2 | 55 | 96/4.00 |
| Hrzntl-Vrtcl Stabilizer | 2 | 40 | 78/3.25 |

**EXCITATION**—Each model was excited by the most severe lightning current component applicable to the section's assigned lightning zone, as defined by the FAA requirements. Since each section (wholly or partly) can be classified to be located in lightning zone 1 or 3, a lightning current component A should be applied for induced effect studies. All models were exposed to a slightly modified current component A. The following equation identifies the drive current:

$$i(t) := \kappa \cdot Io \cdot \left[ \frac{1}{\kappa - \alpha} \cdot \exp(-\alpha \cdot t) - \frac{1}{\kappa - \beta} \cdot \exp(-\beta \cdot t) + \frac{\beta - \alpha}{(\kappa - \alpha) \cdot (\kappa - \beta)} \cdot \exp(-\kappa t) \right] \quad (3)$$

where:

$$Io = 224.22 \cdot 10^3 \qquad \alpha = 16.164 \cdot 10^3 \qquad \beta = 685.878 \cdot 10^3 \qquad \kappa = 41.617 \cdot 10^6$$

The waveform and its expanded leading edge is shown in figure 17. The important difference between this current waveform and Lightning Current Component A is that the slope of this waveform does not change abruptly from $t=0^-$ to $0^+$. Since aperture coupling is a function of current first derivative (inductive), if the derivative is discontinuous, it would have destabilizing effects. This modified waveform still retained the required FAA parameters of 200 kA peak current and $1.4*10^{11}$ A/s current rate of rise.

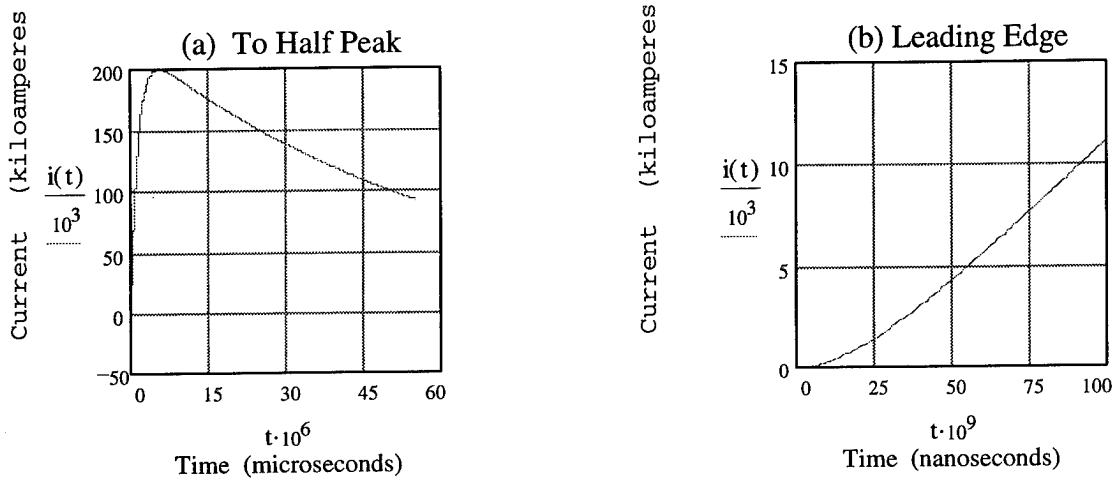



FIGURE 17: DRIVE CURRENT WAVEFORM.

For wire routes spanning more than one section, the voltage and current waveforms were integrated/transformed to acquire the total high impedance voltage and short circuit current waveforms.

**CALCULATIONS**—The following formulation was used to approximate the total transient level for the entire length of each modeled wire route. Since each wire was terminated at both ends with a 360-Ω resistor, to determine the total voltage waveform of a wire route, the waveforms of the two terminations were added. The short circuit current was calculated through the code, using the thin wire formalism, when both ends of the wire were shorted to ground.

For shielded wires, the shield current was computed by shorting both ends of the shield through the pigtails, if present. Then, since the shield voltage capacitively couples to the wire, the wire voltage was calculated by conservatively equating it to the sum of developed voltages across the shield and pigtails (which is the maximum voltage the wire could develop when it is terminated at the high impedances). This was accomplished by writing the following equation into the code:

$$V_{SW} = V_{Sh} + V_{PT} = i_{Sh} * R_{Sh} + L_{PT} * \frac{di_{Sh}}{dt}, \tag{4}$$

where,

$V_{SW}$: Shielded wire voltage, $V_{Sh}$: Shield voltage, $V_{PT}$: Pigtail voltage,
$i_{Sh}$: Shield current, $R_{Sh}$: Shield resistance, $L_{PT}$: Pigtail inductance.

The shield resistance, $R_{Sh}$=6 mΩ/ft (20 mΩ/m), and pigtail inductance $L_{PT}$=65 nH/inch (not linear with respect to length), which were evaluated from independent measurements, were set in the code.

In this equation the pigtail resistance and shield inductance are ignored. The pigtail resistance is insignificant in comparison to the shield resistance, and the voltage across the shield resistance is a conservative evaluation of the voltage that would develop inside the shield. The operations performed by equation 4 are valid only if the shielded wires are contained within a section, and when the effect of the wire's resistance is insignificant compared to its inductance. For wire routes extending beyond one section, a different approach was used and will be discussed in the "Integration" section.

To calculate the developed voltage on a shield of one of the wires in a bundle, the following empirical equation was used:

$$V_{Sh} = \frac{k}{N} * i_B * R_i, \tag{5}$$

where,

$k$=2.0 (for bundles up to 30 wires) N: Number of wires in bunble
$i_B$: Bundle current $R_i$: Individual wire shield resistance.

The constant $k$ varies slowly in the same direction as the number of wires in a bundle; i.e., for a bundle of a few hundred wires, $k$ can be as large as 3.0; however, for our application the value we used was a conservative number. The bundle current ($i_B$) was calculated by T3DFD, and the resistance was directly measured from the actual installation.

For mixed shielded-unshielded wires, the shielded and unshielded lengths of wire were considered as independent wire routes and induced voltages were calculated separately per the

corresponding procedure delineated above, and then the waveforms were added. The current calculations were performed on the basis of total voltage and inductance of the wire route as described in the next section, "Integration", since the procedure is identical to what is done for calculating the current of a wire extended through several sections.

**Integration**—A simplified model was used to process the transient waveforms from different sections to acquire the complete wire route voltage and current waveforms. Although this was not a complete electromagnetic model but comparing to an alternative, using transmission line formulation, had the advantage of being efficient, and not needing the computational resources beyond what was available to us, considering the number of time steps, wires and models, and the length of wires.

The voltage waveform for a complete wire route was obtained by simply adding all the voltage waveforms from different lengths of wire routes in different models regardless of their type, as shown by equation 6,

$$V_T = V_1 + V_2 + \ldots V_n, \tag{6}$$

and figure 18, for a typical voltage waveform addition. These waveforms could have different shapes, depending mostly on whether they are from shielded or unshielded portions. The unshielded route waveforms are similar to the derivative of the drive current with slightly slower rise, while shielded portion waveforms generally follow the shape of the drive current.

The current waveform processing is somewhat more complex. The inductance of each length of wire can be approximated from the current and voltage relation, when the wire's characteristics are approximated as those of a non-resistive wire, and its inductance is assumed to be constant with respect to time. This is a safe assumption since dominant lightning frequencies are low. Therefore,

$$i(t) = \frac{1}{L_i}\int V(t)*dt \quad \Rightarrow \quad L_i = \frac{1}{i(t)}\int V(t)*dt, \tag{7}$$

where,

$L_i$ : a wire route inductance in a model.

The voltage and current waveforms are known for each section, and since equation 7 holds for any positive value of 't', including the voltage waveform zero crossing time which is coincident with the current waveform peak time, then the integral is evaluated between zero time and zero voltage crossing time, and the current peak value is used to calculate the inductance of each wire section,

$$L_i = \frac{1}{i_P}\int_0^{\tau} V(t)*dt. \tag{8}$$

where, $\tau$ : Voltage zero crossing time.

Then the inductance for the entire wire run is

$$L_T = L_1 + L_2 + \ldots L_n, \tag{9}$$

and the short circuit current waveform and peak current are

$$i_{SCP} = \frac{1}{L_T}\int_0^{\tau} V_T(t)*dt. \tag{10}$$

For the mixed combination of shielded and unshielded sections in different models, once the voltage is known for each model, the total voltage is the sum of all voltage waveforms. The

current is also calculated as described above with some subtle peculiarities. The inductances of shielded sections (between the shield and center wire) were approximated by using the transmission line equations. The shielded section voltage contribution is not only relatively low, but due to high source impedance (capacitance between the shield and the center wire) the voltage does not contribute significantly to the total voltage for the short circuit current calculations, and therefore was not included. Figure 19 shows comparison of a complete wire run current waveform with those of its sections. Figure 20 compares the typical voltage

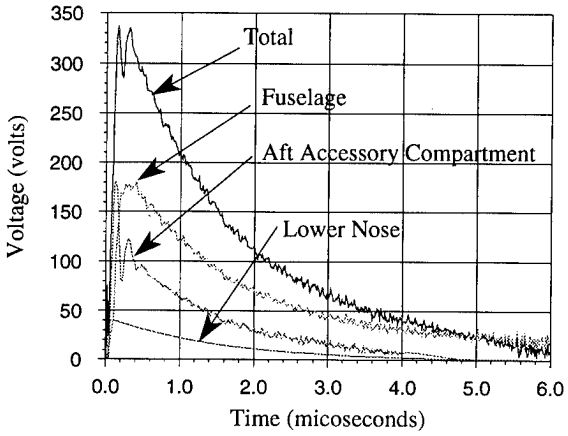



FIGURE 18: COMPARISON OF VOLTAGE WAVEFORMS FOR A COMPLETE WIRE ROUTE & ITS PARTITIONED INDIVIDUAL SECTIONS.

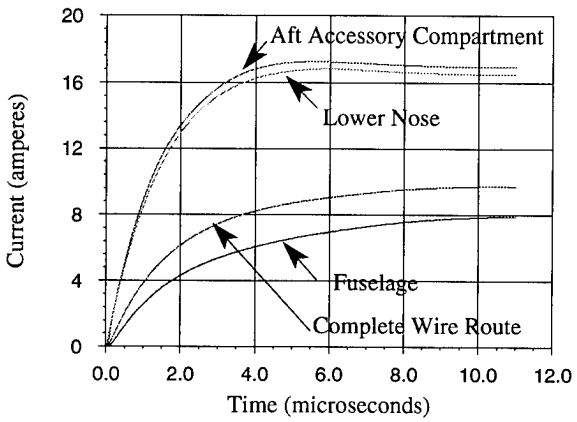



FIGURE 19: COMPARISON OF CURRENT WAVEFORMS FOR A COMPLETE WIRE ROUTE & ITS PARTITIONED INDIVIDUAL SECTIONS.

waveforms of various routes, exposures and strike configurations in the aircraft. The waveform (a) was calculated during a nose to Engine nozzle strike, (b), during a nose to horizontal stabilizer strike, (c), during a nose to tailcone strike, and (d) during a nose to wing tip strike.

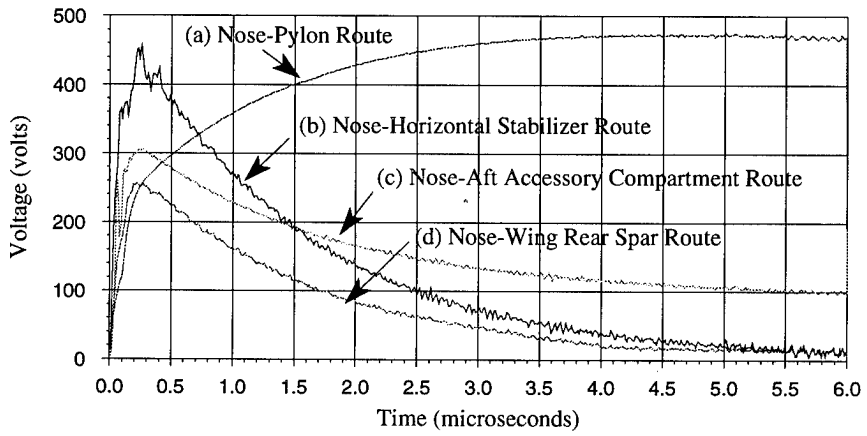



FIGURE 20: TYPICAL SAMPLE OF TOTAL VOLTAGE WAVEFORMS FOR DIFFERENT EXPOSURE LEVEL WIRE ROUTES AND LIGHTNING STRIKE CONFIGURATIONS.

## RESULTS

A sample of the total peak voltage and current levels in all modeled lightning strike configurations for the MD-90 aircraft critical/essential equipment interface wiring is shown in table 2. Some of the transient levels are from totally or partially shielded wires. The shield current and open shield voltage in highly exposed areas could be as high as 14 kA and 10 kV.

TABLE 2: SAMPLE OF PEAK TRANSIENT LEVELS FOR CRITICAL/ESSENTIAL EQUIPMENT INTERFACE WIRING IN ALL STRIKE CONFIGURATIONS

| STRIKE CONFIGURATION | WIRE ROUTE | PEAK VOLTAGE (V) | PEAK CURRENT (A) |
|---|---|---|---|
| Nose Radome to Engine's Aft | Upper Nose to Engine | 326 | 8.00 |
| Nose Radome to Main Landing Gear | Lower Nose to Main Landing Gear | 572 | 6.00 |
| Nose Radome to An Extremity Aft of Nose | Lower Nose to Lower Nose | 62.0 | 25.0 |
| Nose Radome to Wing Tip | Lower Nose to M Wheel Well/Wing Tr E | 538 | 6.10 |
| Nose Radome to Tailcone | Lower Nose to Aft Stair | 323 | 10.1 |
| Nose Radome to Horiz/Vertical Stab/Elevator | Lower Nose to Tailcone Interfaces | 335 | 15.0[1] |
| Wing Tip to Tail | Wing Trailing Edge to Engine | 523 | 6.10 |

## CONCLUSION AND DISCUSSION

The subject was broad and space to discuss somewhat limited. The option was made to present an overall view of the total project without in depth discussion of various modeling, and theoretical issues. Many sections of this paper could have been the subjects of independent papers.

The lightning induced voltage and current transient waveforms were calculated for all the MD-90 aircraft individual sections using the T3DFD technique. A minimum of 95 wire routes in 6 models were simulated, and a total of 181 complete wire route peak transient levels were evaluated. Total transient levels were computed on the basis of T3DFD analysis output data, by using basic engineering techniques. The project showed that T3DFD can be successfully used for large transport aircraft with a high confidence level even without using some of the more advanced techniques of T3DFD. The savings are estimated to be a minimum of 1.5 million dollars with respect to building the same number of physical models of reasonable size and subjecting them to impulse testing.

The sectionalized analysis provided the necessary resolution without exceeding the computer resources or pushing the run times to unreasonable lengths. The most exposed areas of the aircraft were main landing gear, wheel well, engine/pylon, wing root area, and tailcone interface of aft accessory compartment. The least exposed area was forward accessory compartment.

All the new system transient levels were evaluated and, with few exceptions, were lower than the equipment transient design levels with safe margins. For the exceptions, the respective wires were further shielded to create a safe margin between the tested levels and transient levels.

[1] Estimated Maximum Value

Simultaneous test and analysis should be performed to provide more control and reliability in the output data, and therefore, raise the confidence level in the analysis, and with some luck provide tighter correlation. Further investigation is desirable to validate usage of equivalent surface formalism for large aircraft transient level analysis. This would enable one to carry the full aircraft analysis with moderate computer resources and reduced artifactitious resonances. In addition, automation of problem area gridding, including the wiring, and using equivalent surfaces for increasing the resolution at areas of interest would make the analysis much more efficient, especially if the structural assemblies and wiring installation data are digitally available to be directly used for T3DFD analysis.

## REFERENCES


1. T. He, B.D. Sherman, T. Rudolph, and B. Nozari, "Time Domain Finite Difference Validation For Transport Aircraft Lightning Induced Effects Studies." Presented at the IEEE International Symposium on EMC, Atlanta, Georgia, August 14-18, 1995.

2. T. Rudolph, "Time Domain Finite Difference Technique For Coupling Of Electromagnetic Fields To Resonant Apertures," Electro Magnetic Applications Inc., Denver, Colorado, Tech. Rep. EMA-91-R-36, August 1991, p. 91.

3. T. Rudolph, "Application Of Finite Difference Technique To Electromagnetic Scattering Problems," Electro Magnetic Applications, Inc., Denver, Colorado, Tech. Rep. EMA-93-R-009, December 1992, pp. 7.2-7.4.

4. T. Rudolph, T. He, B. D. Sherman, and B. Nozari, "Low Frequency Boundary Condition For The Time Domain Finite Difference Technique." Presented at the IEEE International Symposium on EMC, Atlanta, Georgia, August 14-18, 1995.

# Can a Transmission Line model predict the lightning current pulse?

G.Vecchi and F.Canavero
Dipartimento di Elettronica, Politecnico, I-10129 Torino
fax: 39 11 5644015; e-mail: vecchi@polito.it

**Abstract** — We examine the discharge process of an initially charged, linear lossy transmission line (TL), in order to assess its validity as a model for the formation, and upward propagation, of the return stroke pulse. Approximate and exact (numerical) solution to the problem are obtained, that indicate that the model yields meaningful results. A double-exponential pulse form is obtained from the approximate solution, with rise time dictated by the grounding inductance and decay time related to the TL relaxation time. Upward propagation is also examined, and a physical explanation is provided of the obtained solutions; the role of loss-related diffusion in channel charge removal is discussed.

## Introduction

A wide literature exists on on the modeling of the lightning base current pulse, either based on direct current measurements or on inference from the waveform of the electromagnetic fields generated by the return stroke (e.g. [1]). On the other hand, the (lossy) Transmission Line (TL) model is widely and successfully used to predict the upward propagation of the discharge current pulse, as needed in the evaluation of the radiated field (e.g. [2]); in it, the current at a given height $z$ along the channel is obtained as solution of the equations that represent an initially uncharged TL at whose end a prescribed current (the base current pulse) is forced.

It is therefore legitimate to speculate whether the same transmission line model, under appropriate physical assumptions, could serve to predict also the early phase of the return stroke, where the base current pulse originates from the connection of the stepped leader with the upward streamers (or rocket driven wire).

Although some work exists on the early phase of the return stroke, based on linear and non-linear transmission line theory [3, p. 101-114], to the best of our knowledge no open literature has yet addressed the following simple, but practically important question:
*does the discharge of a charged transmission line predict a meaningful base current pulse?*
This is the question that we will try to answer in this paper, confining ourselves to the linear case. It appears that, under reasonable assumptions, the answer is mostly affirmative, and a simple yet useful model emerges therefrom.

## Statement of the problem

In the physical process we are trying to model, a fast current pulse is generated by the connection of the charged, leader generated, down-propagating conducting channel with a grounded conducting body, typically a (shorter) conducting channel (streamer) originating either from

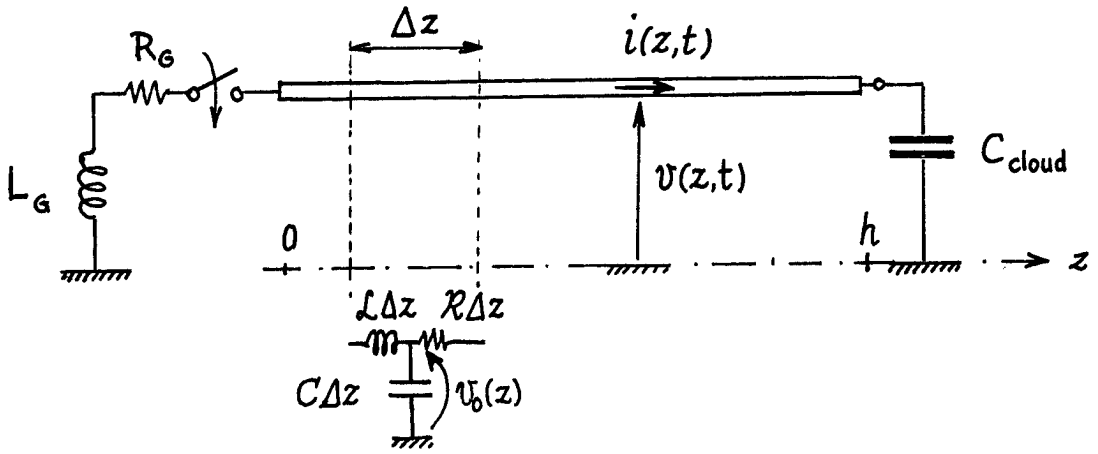



Figure 1: *Approximate TL model for pulse formation.*

ground or an elevated (grounded) structure. The corresponding model (see Fig. 1) is a charged transmission line terminating at one end on a charged capacitance $C_{\text{cloud}}$ that represents the cloud, and at the other end onto an (ideal) switch closing at $t = 0$. At the opposite end of the switch there is a network that represents the grounding structure. Of this latter, we retain in this model only a self-inductance $L_{\text{G}}$ associated to the magnetic field produced by the current flowing along the (short) streamer and/or elevated grounding structure, and into the ground, along with a grounding resistance $R_{\text{G}}$ that takes into account the finite conductivity along the current path. While the above parameters parameters are necessary to account for the physics of the phenomenon, a more sophisticated network will merely act as a refinement on the solution.

Losses in the transmission line cannot be neglected a priori, as apppears from recent studies on the pre-connection channel properties [4]. Consistently, the per-unit-length (pul) equivalent circuit of the line will include the pul capacitance $\mathcal{C}$ and (self)inductance $\mathcal{L}$, and a series p.u.l. resistance $\mathcal{R}$ is retained, as representative of the channel finite conductivity; the shunt conductance $\mathcal{G}$ (free flow of charge carriers from channel to ground through air) is negelected. The transmission line (TL) equations describing the time evolution of the voltage $v(z,t)$ and current $i(z,t)$ along the line will have initial conditions

$$i(z,0) = 0, \quad v(z,0) = v_0(z) \tag{1}$$

that represent a *charged* ($v_0 \neq 0$) line with stored pul charge $q(z,0) = \mathcal{C}v_0(z)$; accordingly, the initial charge in the line (channel) is $Q_l = \mathcal{C}\int_0^h dz v_0(z)$ and the total charge in the system is $Q = Q_l + Q_{\text{cloud}}$, where $Q_{\text{cloud}} = C_{\text{cloud}}v_0(h)$ is the charge in the cloud. Note that these (simplifying) steady-state type initial conditions are physically meaningful because of the negligible shunt conductance ($\mathcal{G} = 0$) assumption.

The boundary conditions are specified by the circuit equations at the line terminations $z = 0$ and $z = h$.

On introduction of the "differential" voltage $u$,

$$u(z,t) \equiv v(z,t) - v_0(z) \tag{2}$$

one has a driven problem with homogeneous initial conditions for the state variables $(u, i)$,

$$\begin{cases} -\dfrac{\partial}{\partial z}u(z,t) = (\mathcal{L}\dfrac{\partial}{\partial t} + \mathcal{R})i(z,t) + \dfrac{d}{dz}v_0(z) \\ -\dfrac{\partial}{\partial z}i(z,t) = \mathcal{C}\dfrac{\partial}{\partial t}u(z,t) \\ u(z,0) = 0, \quad i(z,0) = 0 \end{cases} \tag{3}$$

with boundary condition at $z = 0$ modified by the presence of (lumped) DC voltage generator $v_0(0)$, since $u(0,t) = v(0,t) - v_0(0)$. In the following, we will restrict ourselves to the simplest initial charge condition, that of constant initial charge $q_0(z)$ =const., or $v_0(z) = -V_0 = \text{const.}_z$ which cancels the distributed driving term $\frac{d}{dz}v_0(z)$ from (3). In this case, one has a standard problem involving an initially uncharged TL, driven at the ground end by a network with a step-like voltage generator (DC voltage plus switch). In the Fourier trasform (FT) domain $\omega$, here denoted by capital letters, the boundary conditions read

$$\begin{aligned} &U(0) = -(V_g + Z_{\text{G}}I(0)), \quad V_g = V_0[PV\tfrac{1}{j\omega} + \pi\delta(\omega)]; \\ &U(h) = \frac{1}{j\omega C_{\text{cloud}}}I(h) \end{aligned} \tag{4}$$

where $PV$ indicates a principal-value integral (in the inverse transform) and $\delta$ is a Dirac's delta; in our case, $Z_{\text{G}} = R_{\text{G}} + j\omega L_{\text{G}}$, but more complex networks could be used. The characteristic impedance $Z_\infty$, and the wavenumber $k$ of the (lossy) line will be given by

$$Z_\infty(\omega) = \sqrt{\frac{\mathcal{R} + j\omega\mathcal{L}}{j\omega\mathcal{C}}}, \quad k(\omega) \equiv \beta(\omega) - j\alpha(\omega) = \sqrt{-(\mathcal{R} + j\omega\mathcal{L})(j\omega\mathcal{C})} \tag{5}$$

The solution of the transformed pair (3) with the boundary conditions (4) is straightforward; it is immediate to see that the presence of the capacitor $C_{\text{cloud}}$ yields zero DC (final), current on the line, so that one can do away with $\omega = 0$ and related $\delta$ and $PV$ sign in (4).

**Typical values of parameters.** We shall try to estimate the model parameters from "observable" quantities that are most commonly found in the literature.

For early enough times, i.e. for not too low frequencies (in the sense that $\omega\mathcal{L}/\mathcal{R} \gg 1$), the pul attenuation $\alpha$ attains the frequency-independent value $\alpha \approx \alpha_0 = \frac{1}{2}\mathcal{R}/Z_0$, so that the altitude-dependent attenuation is $A(z) \approx \exp(-z/\ell_c)$ with

$$\ell_c = 1/\alpha_0 = 2\frac{Z_0}{\mathcal{R}}, \quad \alpha_0 = \frac{1}{2}\mathcal{R}/Z_0 \tag{6}$$

which in fact corresponds to the modified TL model (MTL) [1]). With the same assumptions, for the characteristic impedance $Z_\infty$ and the propagation speed $v$ one has

$$Z_\infty \approx Z_0, \quad Z_0 \equiv \sqrt{\mathcal{L}/\mathcal{C}} \qquad v \approx c_0, \quad c_0 \equiv 1/\sqrt{\mathcal{L}\mathcal{C}} \tag{7}$$

For the line parameters, using essentially the TL model and estimates in [3, pp. 17-41], one finds characteristic impedances on the order of a few hundred Ohm; here we take $Z_0 = 400\,\Omega$ as an example. On the other hand, a typical propagation speed on the TL model of the return stroke is $c_0 \approx 10^8\,\mathrm{ms}^{-1}$. With these values one finds typical values for $\mathcal{L}$, $\mathcal{C}$; with our values, $\mathcal{C} = 25\,\mathrm{pF/m}$, $\mathcal{L} = 4\,\mu\mathrm{H/m}$. By further assuming a charge density on the channel as in [3, pp. 14,19], $q_0 \sim 10^{-4}\,\mathrm{C/m}$, one obtains an electric potential $V_0 \sim 10^7\,\mathrm{V}$, which is coherent with the estimate in [2, p.12]; we take here $q_0 = 2\cdot 10^{-4}\,\mathrm{C/m}$, which yields $V_0 = 0.88\cdot 10^7\,\mathrm{V}$. We consider an attenuation length $\ell_c = 1000\,\mathrm{m}$ (typical, [1]), that yields a pul resistance $\mathcal{R} = 0.2\,\Omega/\mathrm{m}$.

As to the grounding, we take here $R_\mathrm{G} = 10\,\Omega$; as to the inductance, we may consider the example of a (short) streamer: for a length of 10m, using the same pul $\mathcal{L}$ as above, one finds a value $L_\mathrm{G} = 4\cdot 10^{-5}\,\mathrm{H/m}$.

The reader may try other values, without much change.

## Base current

For the FT of the base current $I(0)$, one obtains

$$I(0) = -\frac{V_G}{2Z_\mathrm{G}}\frac{(1-\Gamma_\mathrm{G})(1+\Gamma_0)}{1-\Gamma_\mathrm{G}\Gamma_0}, \quad \Gamma_0 = \Gamma_h e^{-2jk(\omega)h} \tag{8}$$

where $\Gamma$ indicates (current) reflection coefficients,

$$\Gamma_h = \frac{j\omega C_\mathrm{cloud} - Y_\infty}{j\omega C_\mathrm{cloud} + Y_\infty}, \quad \Gamma_\mathrm{G} = \frac{Y_\mathrm{G} - Y_\infty}{Y_\mathrm{G} + Y_\infty}, \tag{9}$$

and $Y = 1/Z$. Since $|\Gamma_\mathrm{G}| < 1$ (because of $R_\mathrm{G}$), one can expand the denominator of (8) in a geometric series, whose terms can be intepreted easily as successive reflections (at both ends) of upward ($e^{-jkz}$) and downward ($e^{+jkz}$) traveling pulses, damped ($\alpha \neq 0$) by the losses on the line and distorted by the loss-related dispersion ($\beta(\omega)/\omega \neq$const.). The total path loss on the line $\alpha h \approx h/\ell_c$ appears from most observations to be large enough as to render all reflections from the cloud negligible, so we can stop the above geometric series to its first term, and write

$$I_0(\omega) \equiv I(0;\omega) \approx -\frac{V_0/j\omega}{Z_\infty + Z_\mathrm{G}} \tag{10}$$

We should however remember that because of this approximation the equation (10) represents an infinitely extended line; our assumption $v_0(z)$ =const. implies an associated infinite total charge, so we cannot use (10) for assessing global charge conservation and the like.

**Approximate solution.** The pulse shape in time $i_0(t)$ can be obtained numerically via conventional FFT of the samples of (10). It is however significative to attempt an approximate solution valid for early and moderate times (that correspond to high frequencies), whose extraction from the global solution also renders the FFT easier.

For $\omega \gg \mathcal{R}/\mathcal{L}$, one can approximate

$$Z_\infty \approx Z_a \equiv Z_0 + \frac{1}{j\omega C_\infty}, \quad Z_0 \equiv \sqrt{\mathcal{L}/\mathcal{C}}, \quad C_\infty \equiv \mathcal{C}\ell_c \tag{11}$$

and $I_0(\omega) \approx I_a(\omega)$ where $I_a$ is obtained from (10) by replacing $Z_\infty$ by $Z_a$; from the above one has

$$I_a = \frac{V_0}{L_G} \frac{1}{-\omega^2 + j(\omega/\tau_G) + \Omega^2}, \quad \tau_G \equiv L_G/(R_G + Z_0), \quad \Omega^2 \equiv 1/(L_G C_\infty) \tag{12}$$

which can be readily back-transformed in time via residue integration about the poles at $\omega = \omega^\pm$ obtained from the roots of the denominator. For typical values of the parameters, one has $\Omega \ll 1/2\tau_G$ (in the case examined above $\Omega\tau_G \sim 10^{-2}$) and both solutions $\omega^\pm$ are purely imaginary,

$$\omega^\pm = j\alpha^\pm, \quad \alpha^\pm = \frac{1}{2}(1/\tau_G) \pm \frac{1}{2}\sqrt{(1/\tau_G)^2 - 4\Omega^2} \tag{13}$$

($\alpha^\pm > 0$) so that one readily obtains

$$i_a(t) = I_p(e^{-\alpha^- t} - e^{-\alpha^+ t}), \quad I_p = \frac{V_0}{\sqrt{(R_G + Z_0)^2 - 4L_G/C_\infty}} \tag{14}$$

Clearly, (14) describes a double-exponential pulse, whose rise time is proportional to $t_r = (1/\alpha^+)$, while the decay time is proportional to $t_f = (1/\alpha^-)$. Since $(1/\tau_G)^2 \gg 4\Omega^2$ one can approximate $\alpha^+ \approx 1/\tau_G$, $\alpha^- \approx \Omega^2\tau_G$, and $\alpha^- \ll \alpha^+$. It then follows that $t_r \ll t_f$ and

$$t_r = (1/\alpha^+) \approx \tau_G, \quad t_f = (1/\alpha^-) \approx \tau_{TL}, \quad \tau_{TL} \equiv C_\infty(R_G + Z_0); \tag{15}$$

so that the rise time is essentially the due to the time constant of the grounding circuit closed on the "initial" line impedance $Z_0$ (i.e its high-frequency limit), while the decay time appears as the relaxation time of the TL. Straightforward calculations show that the maximum of the pulse is attained for $t_p \approx (1/\alpha^+) \ln \frac{\alpha^+}{\alpha^-}$, where the sum of the two exponentials is approximately 1, so that $I_p$ in (14) is actually the peak current of the pulse, which can be further approximated as

$$I_p \approx \frac{V_0}{R_G + Z_0} \tag{16}$$

With our parameter estimate, on has $t_r = 9.8 \cdot 10^{-8}$ s, $t_f = 4 \cdot 10^{-5}$ s; using the value $V_0 = 0.88 \cdot 10^7$ V, one finds from (14) a peak current $I_p = 21.2$ kA.

All the values listed above seem to fall in the average of most estimate in the literature [1], [2, Ch. 7]; on the other hand, a double-exponential pulse well models the actual base current, except for the derivative in the origin.

It should be noted that the approximation (11) can easily be extended to consider three (or more) terms in $1/\omega$, which improves the approximation to later times. With three terms one has three time exponentials, which is another pulse model used in the literature; the solution can be obtained directly by solving a cubic equation (exactly or by perturbation), or through direct numerical evaluation of the time constants; in the latter case one can include virtually any numer of exponentials, with the coefficients obtained directly from the frequency domain solution. Here, we confined ourselves to the two-exponential level.

Using the relationship between the parametrs of the model and those of the pulse waveform ($I_p$, $t_r$, $t_f$), we can try to relate these latter to global macroscopical quantities in a direct manner, at least on an order-of-magnitude base. Right before the offstart of leader formation,

the charge $Q$ stored in the cloud is tied to the cloud-to-ground potential $V_c$ and the cloud capacitance $C_{\rm cloud}$ by $Q = C_{\rm cloud}V_c$; right before the return stroke initiation, assuming an at-rest condition, both the cloud ($C_{\rm cloud}$) and the leader (TL) will be at the same potential, $V_0$, and the TL stores a charge $Q_{\rm TL} = \mathcal{C}V_0 h$, so that total charge conservation yields $V_0(C_{\rm cloud} + \mathcal{C}h) = C_{\rm cloud}V_c$. We can assume that the cloud-to-ground electric field at the leader offstart was the breakdown field $E_b$, and thus $V_c \approx E_b h$; at this point $V_0$ can be expressed either in terms of the cloud charge or of its capacitance; chosing the former way, for $h = 1\,\mathrm{km}$ and $E_b = 2 \cdot 10^6\,\mathrm{V/m}$ one finds $C_{\rm cloud} = 1\,\mathrm{nF}$, while $\mathcal{C}h = 25\mathrm{nF}$; hence

$$V_0 \approx \frac{Q}{C_c + \mathcal{C}h} \sim \frac{Q}{\mathcal{C}h} \tag{17}$$

Furthermore, from (16) and the consideration that typically $Z_0 > R_{\rm G}$, one can approximate

$$I_p \approx \frac{V_0}{R_{\rm G} + Z_0} \sim \frac{V_0}{Z_0} = \frac{Q}{h/c_0} \tag{18}$$

and likewise,

$$t_r \sim \frac{L_{\rm G}}{Z_0}, \quad t_f \sim Z_0 C_\infty = \frac{\ell_c}{c_0} \tag{19}$$

**Numerical solution.** Because of the diverging behaviour of $I_0(\omega)$ for $\omega \to 0$ in (10), one cannot apply the FFT directly. Instead, one can obtain $i_0(t)$ as $i_0(t) = \int_0^t dt'\, h(t)$ where $h(t)$ is the FT of the trasfer function $H(\omega) = 1/(Z_{\rm G} + Z_\infty)$ which has $H(0) = 0$. Furthermore, one can extract the asymtotic approximation $I_a(\omega) = H_a(\omega)V_0/(j\omega)$ of which we know the FT in closed form, so that the difference $H_d \equiv H - H_a$ will have a largely reduced bandwitdh, with strongly beneficial effects on the numerical implementation. The results are reported in Fig. 2, where it is seen that for the most relevant part of the pulse $i_a$ is a good approximation, while at later times the difference $i_d(t)$ provides a more important correction. As noted above, should one wish to have a better approximation for later times, it is sufficient to insert more terms in (11).

On insertion of the parameter values as above, one finds pulse duration (from 2kA to half peak value), total deposited charge, and integral $\int dt\, i^2(t)$ well within the most likely values reported in [2].

## Upward pulse propagation.

Along the TL the charge stored in an elemental length $\Delta z$ is $\Delta Q = q(z,t)\Delta z = v(z,t)\mathcal{C}\Delta z$; therefore, the propagation of voltage along the TL will yield direct information on the discharge process. Within the same assumptions used to derive $i_a(t)$, inspection of (11) reveals that the "differential" voltage $u_0(t)$ at the channel base is obtained from

$$u_0(t) \approx u_a(t) = Z_0 i_a(t) + (1/C_\infty)\int_0^t dt'\, i_a(t') \tag{20}$$

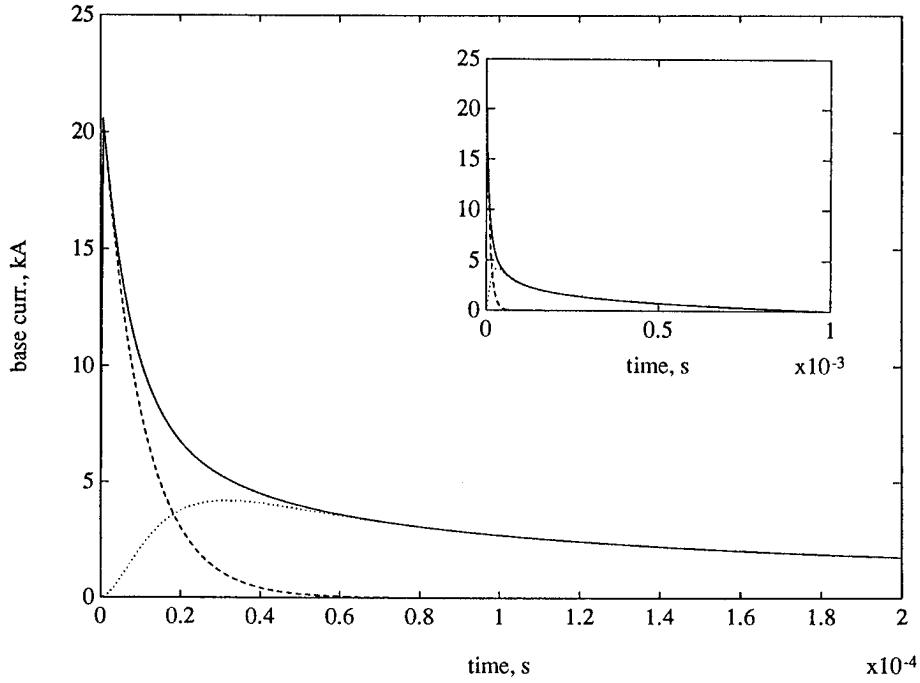



Figure 2: *Base current pulse. Solid line: total current $i_0(t)$, dashed line: asymptotic approximation $i_a(t)$, dotted line: difference $i_d = i_0 - i_a$; same parameters as in the text: $\mathcal{C} = 25\,pF/m$, $\mathcal{L} = 4\,\mu H/m$, $\ell_c = 1000\,m$, $V_0 = 0.88 \cdot 10^7\,V$, $L_G = 4 \cdot 10^{-5}\,H/m$, $R_G = 10\Omega$.*
*Inset: overall behaviour up to extinction.*

which yields

$$u_a(t) = Z_0 i_a(t) + (I_p/C_\infty) r(t), \quad r(t) \equiv \frac{1}{\alpha^-}(1 - e^{-\alpha^- t}) - \frac{1}{\alpha^+}(1 - e^{-\alpha^+ t}) \tag{21}$$

From (21) it is clear that $u_a$ rises to a value close to $V_0$ with the same rise time as $i_a$ ($t_r$), while the term in $r(t) \approx (1/\alpha^-)(1 - e^{-t/t_f})$ enters on a much slower time scale ($t_f$), essentially correcting the final value to $V_0$. The actual voltage $v_a(t) = -V_0 + u_a(t)$, initially at $-V_0$, drops fastly to an almost zero value and is thus a (negative) sharp pulse.

For a qualitative appreciation of the pulse propagation along the channel, we can approximate $k(\omega) \approx (\omega/c_0) - j\alpha_0$, which corresponds to the standard MTL approximation (as discussed above), so that one can write

$$u(z,t) \sim e^{-z/\ell_c} u_a(t - z/c_0), \quad i(z,t) \sim e^{-z/\ell_c} i_a(t - z/c_0) \tag{22}$$

Within these approximations, the qualitative altitude distribution of the current and of the charge density $q(z,t) = q_0 + \mathcal{C}u(z,t)$ is shown in Fig. 3 for different times $t$.

One can note an incomplete charge removal in Fig. 3; it is due to the non-dispersive approximation on $k(\omega)$. In fact, within the framework of the initial approximations of this work, the exact shape of the upward propagating pulse can be obtained by time convolution with the impulse-response $h(z,t)$ of the (lossy, and thus dispersive) transmission line. It is a

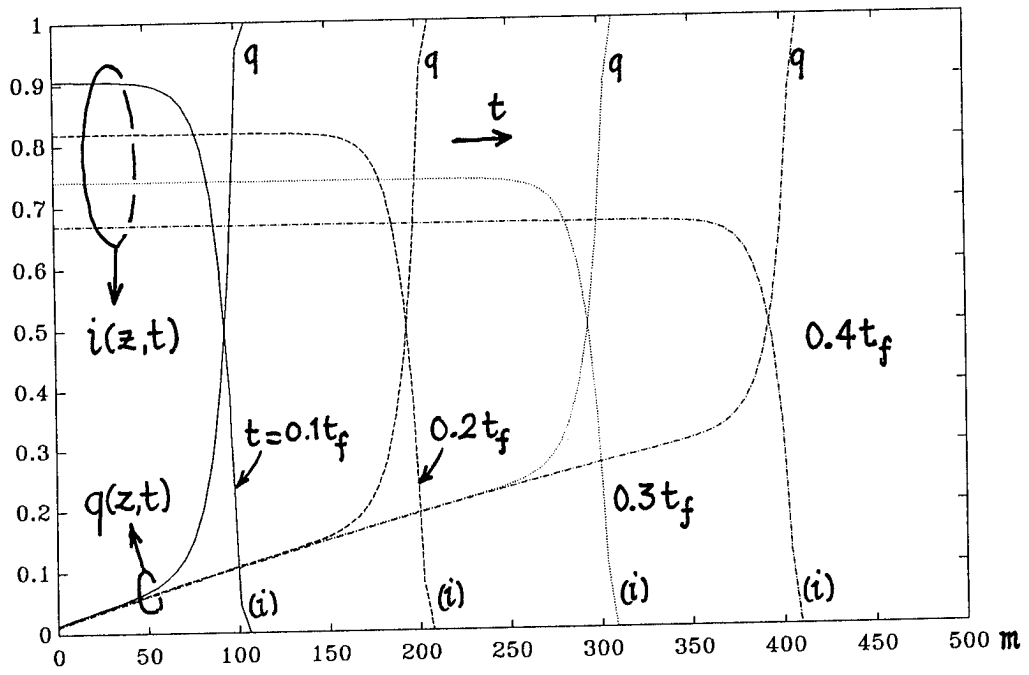



Figure 3: *Altitude evolution of return stroke pulse in the MTL approximation. The graph shows "snapshots" of the current and charge density along the TL for times* $t = 0.1t_f, ..., 0.4t_f$ *($t_f$ is the pulse decay time, see text). Charge and current ar normalized to* $q_0 = CV_0$ *and* $I_p$*, respectively; only the MTL approximate behaviour in (22) are reported here.*

classic result of Laplace transforms (eg. [5]) that

$$\begin{aligned} h(z,t) &= e^{-\alpha_0 z}\left\{\delta(t - z/c_0) + h_{\text{diff}}(z,t)\right\} H(t - z/c_0), \\ h_{\text{diff}}(z,t) &= \frac{z/\ell_c}{T(z,t)} I_1(T(z,t)/t_c) e^{-t/t_c}, \\ T(z,t) &= \sqrt{t^2 - (z/c_0)^2}, \quad t_c \equiv \ell_c/c_0 \end{aligned} \tag{23}$$

where $H(t)$ is the Heaviside unit step function, and $I_1(x)$ is the modified Bessel function of order 1. In (23), the first term is precisely the traveling term associated to early times and high frequencies; we will call this wavefront the traveling breakdown pulse, because of its analogy with the omonimous term in the literature [2]. On the other hand, the term $h_{\text{diff}}(z,\theta)$ represents a diffusion (drift) tail due to losses, and generated by diffusively delayed (RC) charge release initiated by the passage of the traveling breakdown pulse. When this term is taken into account, the solution is written as

$$f(z,t) = \int_{-\infty}^{\infty} dt' h(z, t - t') \cdot f(0,t'), \tag{24}$$

where $f$ stands for both $i$ or $u$. The effect of the diffusion can be appreciated in Fig.4; although $i(0,t)$ and $u(0,t)$ are approximated by their asymptotic counterparts $i_a(t)$ and $u_a(t)$), one can note an almost-complete charge removal as also the diffusion wave has passed.

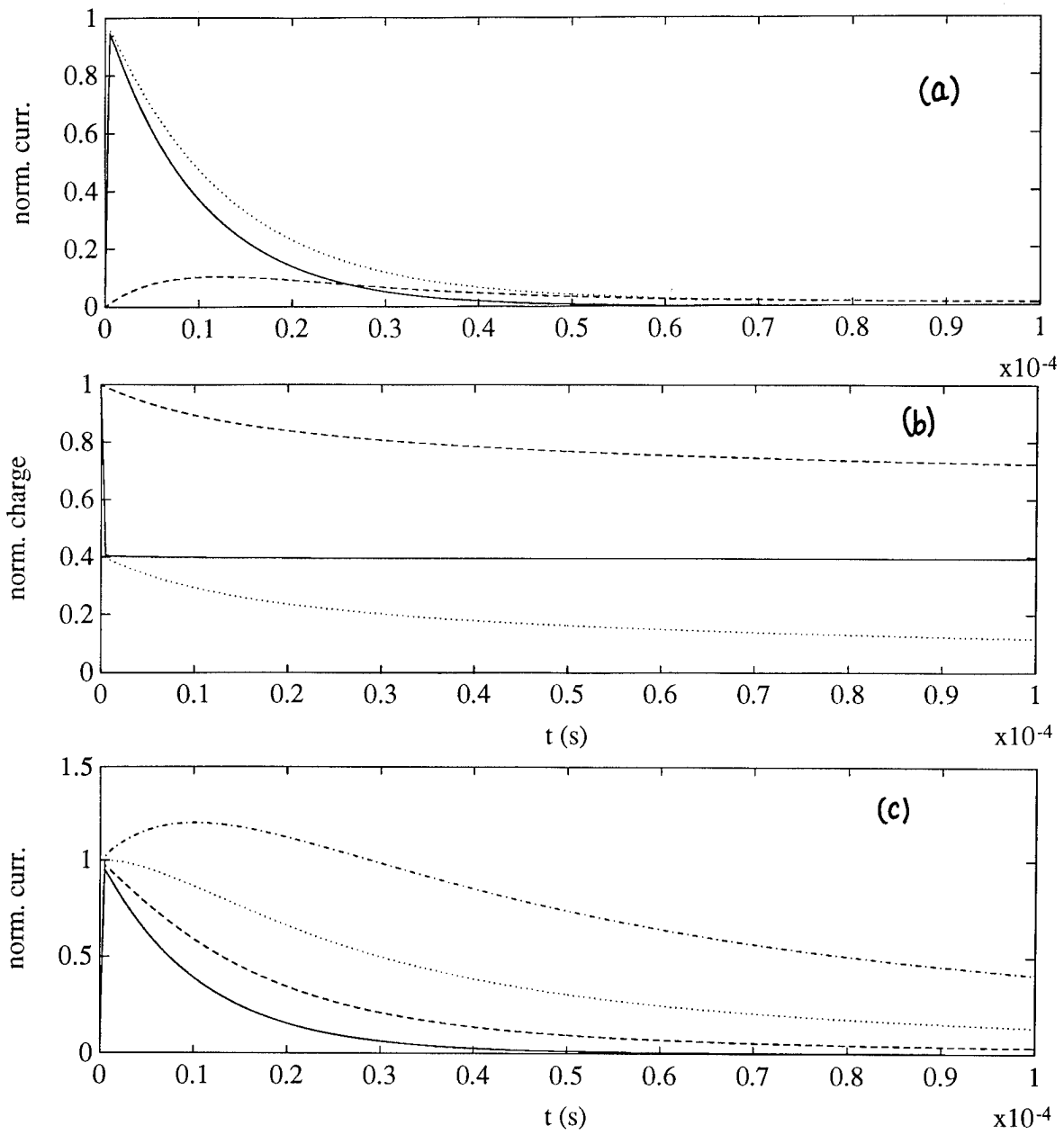



Figure 4: *Altitude evolution of return stroke pulse, with diffusion terms. The graphs are time-histories: a) current pulse, b) charge (voltage) normalized as in Fig. 3; solid line: traveling term, dashed line: diffusion term, dotted line: total. The altitude here is* $z = 500\,\mathrm{m}$. *Note the almost-complete charge removal as the diffusion term passes. Graph (c) shows the total normalized current pulse at altitudes* $z = 100, 500, 2000, 3000\,\mathrm{m}$. *The origin of time axis corresponds here to* $z/c_0$.

Also, one notes the altitude-increasing trend of $h_{\text{diff}}$, and its slow time decay (for large arguments, $I_1(x) \approx \exp(x)/\sqrt{2\pi x}$); for late enough times, or high enough altitudes, compared to losses, the diffusion term will dominate over the traveling pulse: this generates a waveform whose overall rise time (defined in the usual way, and not as the time derivative) will be larger than that of the breakdown pulse; an example of this is shown in Fig. 4c. This might explain the experimental observation of changing rise time with altitude.

**Interpretation.** From (22) and Fig. 3, ie. neglecting the diffusion, we ascertain that at height $z$, the voltage $v(z,t)$ remains fixed to the initial value $-V_0$ until time $t \approx z/c_0$ when the pulse reaches height $z$; at that point, the (fast) voltage drop causes charge release, and current flow, from the local elemental capacitor $\Delta C = \mathcal{C}\Delta z$; that is, the voltage pulse "triggers" removal of the charge stored in the vicinty of the channel. On the other hand, the base current is due to the charge that descends along the channel. The discharge initiation at $z = 0$ drains current from the charge deposited around the channel in the vicinity of $z \approx 0$; this corresponds to a voltage drop that "releases" charge from immediately higher locations $z$, and so on following the voltage pulse propagation. The charge released at height $z$ takes about a time $t(z) \approx z/c_0$ to reach the base, and thus the base current at time $t$ is due to charges that have left their location $z < c_0 t$ on the channel at times earlier that $t$.

Most of the charge stored in a portion $[z, z + \Delta z]$ of the channel is released in a time $T_r \sim t_r$, and is proportional to the voltage drop; note that energy dissipation (on $\mathcal{R}$) decreases the amplitude of the up-traveling pulse: as a result, the charge released "immediately" as the pulse reaches height $z$ is lower and lower (exponentially) at increasing heights. This explains the (slow) reduction with time of the base current.

On the other hand, the diffusion mechanism associated with losses amounts to delaying the charge release, as detailed above and in Fig. 4. In a lossless line, the charge stored in the elemental capacitor $\Delta C$ is released immediately as the "triggering" voltage breakdown pulse passes, while the presence of resistence delays the discharge, ie. the charge removal. Along the same line, it is suggestive to note that the slow component $i_d(t)$ of the base current (due to downward diffusion) resembles the so-called "corona" current [2].

# References


[1] Nucci, C.A., G. Diendorfer, M.A. Uman, F. Rachidi, M. Ianoz, and C. Mazzetti: "Lightning return stroke current models with specified channel-base current: A review and comparison", *J. Geophys. Res.*, *95*, pp. 20,395-20,408, 1990.

[2] Uman, M. A., *The Lighting Discharge*, Academic Press, New York, 1987.

[3] Baum, C. E.: various contributions in *Lightning Electromagnetics*, edited by R. L. Gardner, pp. 101-114, Hemisphere, New York, 1990.

[4] J.E.Borowsky: "An electrodynamic description of the lightning return stroke and dart leaders: guided-wave propagation along conducting cylindrical channels", *J. of Geoph. Res.*, to be published; and: Los Alamos Nat. Lab. Techn. Rep. LA-UR-93-3177.

[5] A. Ghizzetti, A. Ossicini, *Trasformate di Laplace e Calcolo Simbolico*, UTET, Torino, 1971; Ch. 7.

# POSTER PRESENTATIONS

# *The Origin of Electric Charge*

Swen Alfas
ELKRAFT, Innovation Dept.
Lautruphøj 5, DK - 2750 Ballerup, Denmark
Telephone (+45) 44 66 00 22 FAX (+45) 44 65 61 04

ABSTRACT The old fashioned view of electric charge as quantified, conserved, supreme mystery is updated and its origin explained on the basis of realising the fundamental state of matter - FIELD - and electromagnetic fields as certain spectrum of FIELD's fluctuations through vortexes. Quantitative description of FIELD divergence through vortical motion shows why the natural forces are inversely proportional to the square of the distance.

## 1. Introduction

Charge is the oldest idea about electricity. It has been defined as a quantified and conserved quantity of electricity particles can carry. This definition is from the time when the view of material world was limited to atoms, particles and empty space between them, Fig. 1a. Within such a view the origin of charge is conceived as the "supreme mystery",[1].

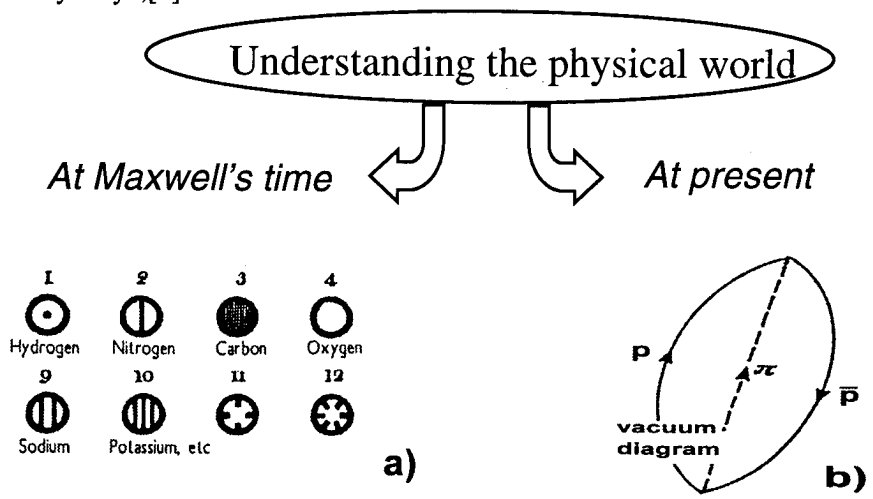



Fig. 1a In 19th century: matter consists ultimately of indivisible, discrete particles.
Fig. 1b Today: Particles come into being and vanish without end.

Since the observation and definition of electric charge, it has become known that the smallest possible quanta of matter - particles - undergo interactions and thus, do not last for ever. cf. vacuum diagram, Fig. 1b. Particles through interactions come to annihilate each other's shapes. After particles annihilation, the matter within particles' shape spreads throughout space as wavy field until the amplitudes die away and matter reaches a state of complete unification called FIELD (or vacuum), Fig. 2. Illustratively, FIELD can be considered as vaporized particles. From FIELD particles come into being and vanish into it without end. Today it is realized that not only particles, but particles and FIELD compose the physical world. "The FIELD exists everywhere; it can never be removed. It is the carrier of all material phenomena,"[2]. Since Maxwell's time the background on which the basic definitions of electricity were defined has changed. Einstein in

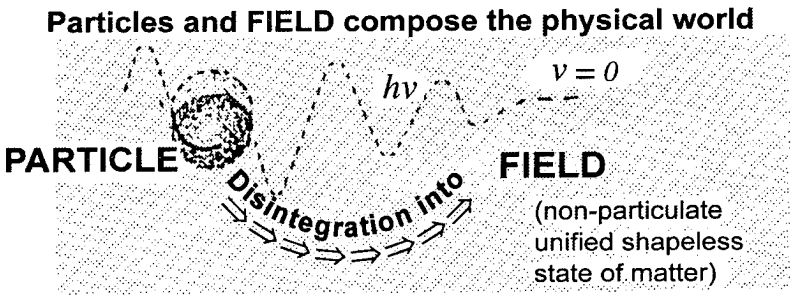



Fig. 2 Particles and FIELD compose the physical world.

December 1954 remarked that matter:" is to be regarded itself as a part, in fact the principal part, of the electromagnetic field." and added, "It is only the circumstance that we have no sufficient knowledge of the electromagnetic field,"[3].

**The aim** is to introduce the origin of electric charge based on the up to date broadened knowledge of all states of matter, particularly FIELD. The introduction will be based on present understanding of electromagnetic field as a part of matter, [4]. The knowledge of electromagnetic field as part of matter provides the physical foundation on which the "supreme mystery" of charge can be unravelled.

## 2. Electromagnetic Field as Part of Matter

After particles' disintegration, the resultant wavy FIELD - gamma rays - are today recognised to be electromagnetic field of the shortest observable wave lengths, cf. Fig 2. But not only gamma rays, the whole spectrum of wavy FIELD down to the stationary state is electromagnetic field spectrum.

The latest progress in electromagnetics research shows that what are supposed as waves of FIELD are actually vortexes of FIELD [4]. The vortexes of FIELD are recognised as electromagnetic vortexes the components of which are electric and magnetic field, Fig 3a.

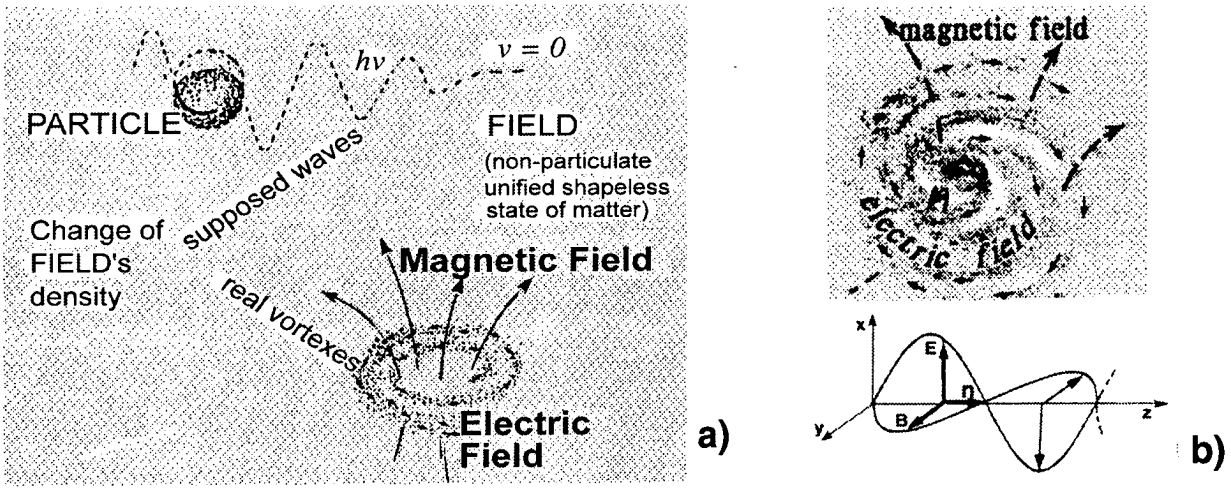



Fig. 3a Vortex of FIELD is electromagnetic field.
Fig. 3b Electromagnetic waves - a floor projection of FIELD vortex.

In particular, what is electric and what is magnetic field of FIELD vortex, is that:

- Field in vortex condition is what is called dynamic electric field **E**.

- Initially, vortex occurs in a plane and its effect arises on both sides of the vortex plane. The bipolar regions of FIELD in which FIELD vortex exerts its effect are recognised as magnetic field **B**. Magnetic field is polarised state of FIELD caused by FIELD vortex. Thus, it is important to realise that the physical entity, FIELD, and magnetic field are basically one and the same.

Electromagnetic waves in the present description of non-stationary state of FIELD are floor projections of the actual state of electromagnetic vortexes, Fig. 3b.

If we look at the electromagnetic spectrum, electromagnetic waves of a short wave-length behave like particles and end up as particles. Understanding electromagnetic fields as part of the matter provides the information that *particles are small intensive vortexes of FIELD*. As a structure of FIELD, particles can naturally emit and absorb a quantum of electromagnetic field. This explains Planck's law. Naturally, particles can disintegrate into FIELD and be created out of FIELD, vacuum diagram.

## 3. Creation of Matter's Shape - Particles

The shape of matter undergoes disintegrations from solid form to shapeless state, FIELD. Creation of matter's shape, particles, is a reversible process, an event in which an intangible amount of FIELD becomes tangible entity. About such reversible processes it has already been indicated, that:" Being and fading of particles are merely forms of motion of the FIELD", cf. [2].

Electromagnetics shows that the natural way for FIELD to acquire motion is by turning into whirling motion. Such FIELD circulation creates an overall shape, which, when viewed from the outside, can look like a spherical body, as schematically shown in Fig 4 below. For the time being, this FIELD formation will be called here, a "SHAPE".

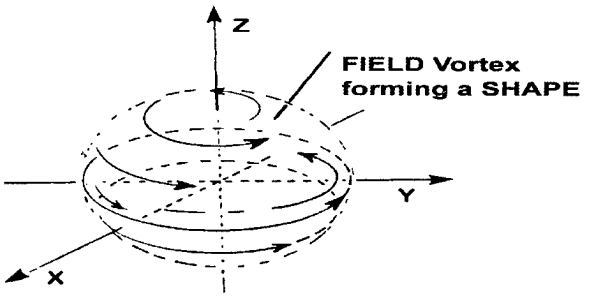



Fig. 4 SHAPE - created by FIELD Vortex.

The formation of a SHAPE is the result of an expansion or contraction of FIELD from a supposed higher density to a lower density. The created SHAPE is the result of a difference in the FIELD density inside and outside the SHAPE. Such difference of FIELD density can be designated by a decreasing function, curve **'a'** in Fig. 5. The derivative of curve **'a'** is illustrated in Fig. 5 by the dotted line. The value of the derivative displays the local difference of FIELD density, i.e. the local intensity of the FIELD expansion through circulation. The highest value of the derivative indicates the greatest or the most intensive circulation. As the value of the derivative approaches zero, the amount of FIELD in circulation approaches zero as well.

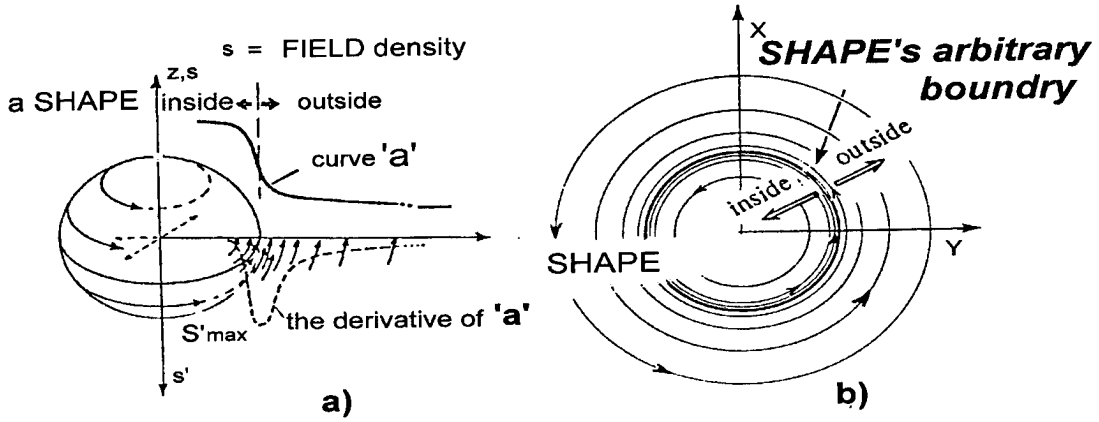



Fig. 5 SHAPE's boundary just after the most intensive FIELD circulation.

Thus, the created SHAPE has no sharp boundaries to distinguish precisely inside from outside. Therefore, the region, where the most intensive circulation of FIELD has just passed is designated as the arbitrary boundary of the SHAPE, sectionally viewed in Fig. 5b. Hence, "outside" the created SHAPE, a less intensive circulation of FIELD continues to exist. One or more SHAPES can be created within the region where the density of FIELD decreases (or increases). In case of more than one SHAPE created in a region with uniform change of density, FIELD circulations with all SHAPES move in the same direction. The outward circulations of FIELD, then, combine to form one outward circulation round the group of SHAPEs. The outer FIELD circulation of a compact group of SHAPES is identical to that of one SHAPE. This point to the fact that shapes behave similarly on a small scale (one SHAPE) as well as on a large scale (group of SHAPES).

## 4. Forces Between SHAPES

Suppose that one SHAPE or group of SHAPES is larger than another one. The SHAPES are situated in a way that the outward FIELD circulation of the larger one permeates the space of the smaller one, Fig. 6a.

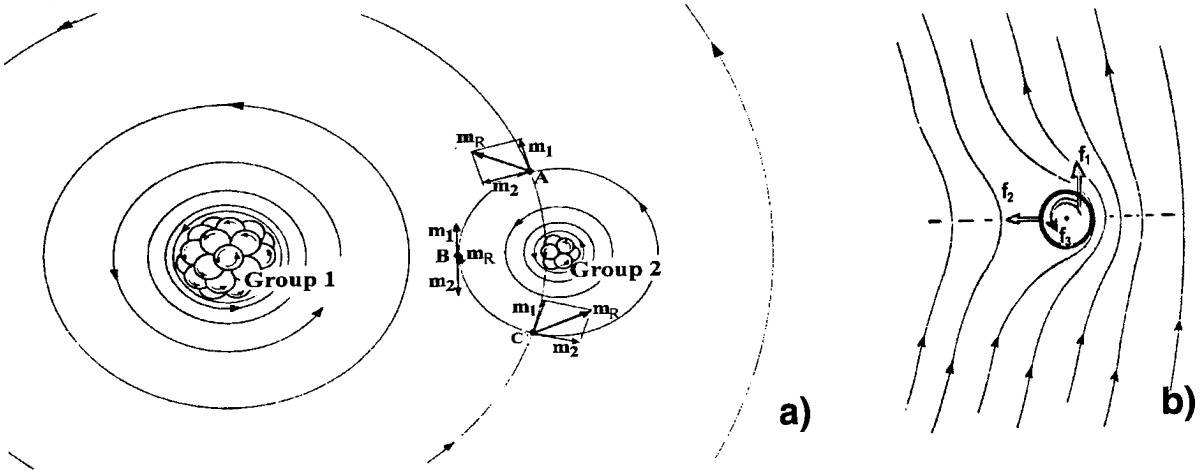



Fig. 6a The collision between the outward FIELD circulations estimated at three arbitrary points.
Fig. 6b The resultant FIELD motion with two SHAPES.

The circulations of these outward FIELDS collide with each other. FIELD circulations carry a pushing momentum and such collision yields a result. The result of such collision is shown in Fig. 6a. at three arbitrary points A, B and C. At these points, $\mathbf{m_1}$ stands for the pushing momentum carried by FIELD circulation of the larger SHAPE, $\mathbf{m_2}$ stands for the momentum of smaller one, and $\mathbf{m_R}$ for the point-resultant momentum of the two. The actual FIELD motion is in the direction of this point-resultant $\mathbf{m_R}$.

The resultant momentum can be estimated or calculated at any point within the space of the two influencing FIELDS. Such estimations of point-resultant reveal an overall FIELD motion in space outlined by full lines in Fig. 6b. The FIELD circulation of the smaller SHAPE forces the FIELD circulation of the larger SHAPE to make detour around the smaller one. This increases the density of FIELD towards the outside of the smaller SHAPE. The result is a force, in Fig. 6b denoted as $\mathbf{f_2}$ acting on the smaller SHAPE and directed towards the larger one. The outward FIELD motion of the larger SHAPE permeates the space of the smaller one, and therefore, it exerts a pushing force $\mathbf{f_1}$ on the smaller SHAPE to drive it out tangentially. More precisely, since the whirling FIELD motion of the larger SHAPE is amassed more on one side, the pushing force $\mathbf{f_1}$ acts eccentrically on the smaller SHAPE. This produces a torque $\mathbf{f_3}$ on it.

The force $\mathbf{f_1}$ pushes the smaller SHAPE out tangentially. The force $\mathbf{f_2}$ pulls the smaller SHAPE towards the larger one. The actual effect of these two forces $\mathbf{f_1}$ and $\mathbf{f_2}$ makes the smaller SHAPE orbit around the larger one. And due to the torque $\mathbf{f_3}$, the smaller SHAPE rotates on its own axis while orbiting around the larger one, Fig. 7.

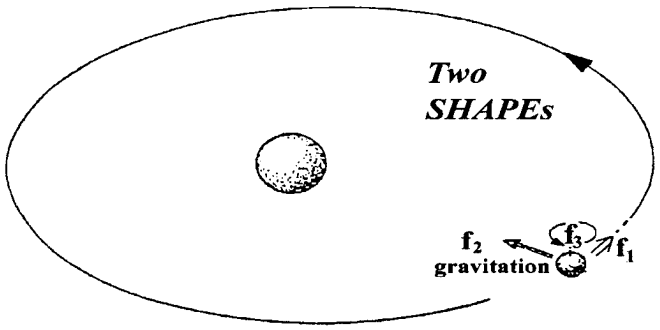



Fig. 7 The natural forces causing the orbital motion of two SHAPES.

All motions in the physical world are due to these forces arising out of interactions between outward FIELD circulations of two SHAPES or two groups of SHAPES. The two motions of the earth, one around the sun and one upon its own axis, are patterns of the motions of the smaller group of SHAPES under the influence of a larger group. And on a smaller scale, atoms exemplify these same motions. The explained attracting force $\mathbf{f_2}$, termed gravity, has been traditionally given prominence. But, besides $\mathbf{f_2}$, there are also the pushing force $\mathbf{f_1}$ and the twisting force $\mathbf{f_3}$ which are concomitant with it. Gravitational force is not isolated force in universal motions.

Understanding the origin of natural forces causing the orbital motions in nature points to the SHAPE (Fig. 4) as being a particle. A particle is a structure of FIELD, a specific FIELD-vortex. Further investigation into the origin of electric charge provides additional verification of SHAPE being a particle.

## 5. The Quantitative Approach of the Origin of Natural Forces

Newton mathematical expression of mutual attraction between particles, masses, offers no explanation of the origin of gravity and why it is inversely proportional to the square of the distance, $1/\mathbf{r}^2$, between them.

Vortex approach of particles offers a qualitative explanation based on kinematical principles of mutual interaction between two vortexes. This qualitative understanding can be improved now quantitatively. As shown previously the physical entity of FIELD and magnetic field are basically the same state of matter. Therefore the magnetic field density **B** can denote FIELD density as well.

FIELD density outside of a vortex-shape falls with the distance, **r**. This decrease is assumed as $B_r = B_0/r$, (cf. curve **'a'** in Fig. 5a). $B_0$-FIELD density inside the FIELD-vortex can stand for expression of particle's mass. The FIELD expansion through vortex expressed by divergence of **B** in spherical co-ordinates is:

$$\mathrm{div}\,\mathbf{B} = \frac{1}{r^2}\frac{\partial}{\partial r}(r^2 B_r) + \frac{1}{r\sin\vartheta}\frac{\partial}{\partial \vartheta}(B_\vartheta \sin\vartheta) + \frac{1}{r\sin\vartheta}\frac{\partial B_\varphi}{\partial \varphi}$$

With expansion through vortex, it can be assumed that:

$$\sin\vartheta = 1\,,\quad \frac{\partial B_\vartheta}{\partial \vartheta} = 0\,,\quad \frac{\partial B_\varphi}{\partial \varphi} = 0\,,$$

The equation about become reduced to: $\mathrm{div}\,\mathbf{B} = \frac{1}{r^2} B_0$

FIELD expansion through vortex falls inversely proportional to the square of the distance. Consequently, the gravitational force, and the related electric forces shown below are inversely proportional to the square of the distance.

## 6. Particles in Motion - The Origin of Electric Charge

Today it is an observable fact that when particles are in motion, they become charged. Thus, a particle can become charged and in this state it exerts a force towards its environment. If we want to look at the origin of this force, we have to look at particles structure. Particle is a vortex of FIELD and as previously explained, the FIELD density from inside to outside of FIELD vortex decreases by a continuous function, curve **'a'** in Fig. 8 below.

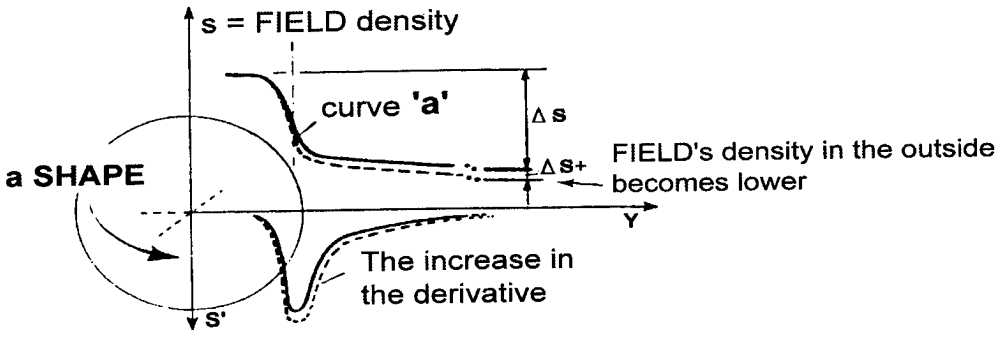
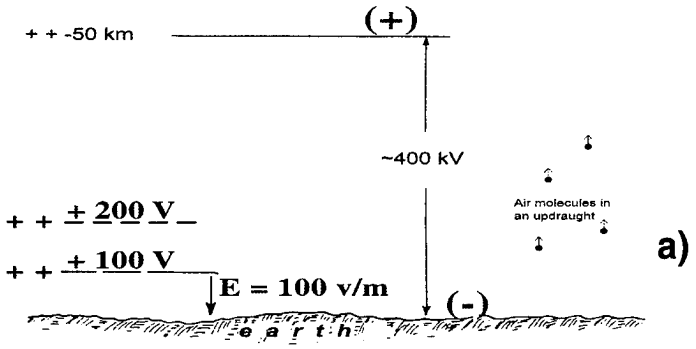



Fig. 8 A change of SHAPE's neutral state.

The qualitative understanding of the derivative of the function **'a'** introduced previously shows the distribution (intensity) of FIELD in circulation. When the circulation corresponds fully to the value of the derivative, this condition presents a state qualified as a ***neutral*** state.

Now we can examine what happens when a particle, or small group of particles, is leaving a larger group of particles, for example when molecules of air are in updraught, fig. 9a.



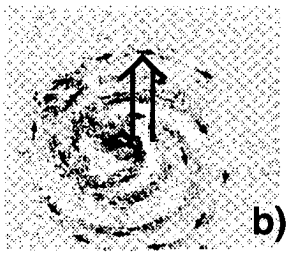




Fig. 9a Particles in an updraught become charged.
Fig. 9b In motion FIELD vortex collides with surrounding FIELD.

The outward FIELD density of the earth falls with the distance according to the curve **'a'**, Fig.8. The molecules (particles) in the updraught get the density of the FIELD on the outside changed, it becomes lower. The difference between FIELD density inside and outside the leaving particles increases. This result in an increased amount of FIELD in circulation of the leaving particles.

When particles move rapidly away from the big group, the change of particles' FIELD circulation has to happen very fast. If the FIELD circulation has not yet changed correspondingly to the change of FIELD density outside, then this exerts a *deviation* from the neutral state. Such deviation happens also due to the motion of FIELD vortex in space of FIELD. When in motion, FIELD vortex collides with surrounding FIELD, cf. Fig. 9b.

A frontal collision occurs on one side of the vortex and a parallel motion on the other side. The collision slows down the whirling motion of FIELD vortex. Therefore, in motion, particles FIELD circulation will deviate from the neutral state. The consequence of such deviation is that the resulting force $\mathbf{f_2}$ (cf. Fig. 7, 8) deviates from the neutral state too. To show such deviation schematically by lines, we suppose a particle in space of FIELD with an average density of, say 5 units, shown by vertical lines in Fig. 10a. The average density of particle's FIELD circulation is , say 7 units, shown by a circular line.

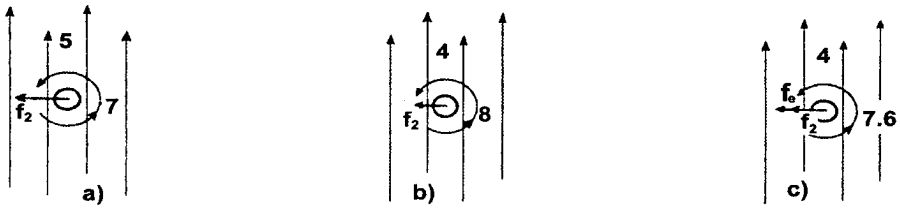



Fig. 10 The electric force $f_e$

The particle then moves into a space of lower FIELD density of, e.g. 4 units, Fig 10b. The result of this is that the particle's FIELD circulation has to increase, say to 8 units in order to obtain a new neutral state. On the particle's right side, Fig. 10b, where both FIELD's circulations have same directions, the resultant FIELD's density is, for the sake of argument, 8 + 4 = 12 units. On the particle's left side, where FIELD's circulations have opposite direction, we get 8 - 4 = 4 units. The difference between the left and the right side is that on the right side we get a three time stronger FIELD density corresponding to the gravitational force at this new distance in the neutral state.

Now, we suppose that the particle's FIELD circulation has not only reached a density of 7.6 units instead of 8 units due to its motion in space, Fig. 10c. That is to say, the neutral state is not obtained. On the particle's right side the resultant density is 11.6 units and on the left side 3.6 units. On the right side we now get a 3.22 times stronger FIELD density than on the left side. The increase of the difference from 3 to 3.22 times means an increase of the gravitational force. Such increase exists until the new neutral state is obtained, and it can therefore be recognised as an additional force $\mathbf{f}_e$ on the line of the gravitational force.

The deviation of particle's FIELD circulation from the neutral state is the origin of electric charge. This deviation can be "positive" or "negative" and the result - changed gravitational force - can be shown as an electric force, $\mathbf{f}_e$ added to gravitational force. This electric force has, as described, logically the same origin, and the same characteristics as gravitational force.

Materials (various groups of particles)are normally observed in neutral state. When a particle is in motion or removed from a group of particles, it can then become charged. But in principle, particles are not observed charged when they are part of a group. Finding particles being charged when they are in motion or removed from a group of particles, and postulating that they also carry this charge when they are part of a group, can be a misleading hypothesis.

## 7. Kikuchi's Velocity

When FIELD vortex (particle) is in motion in the space of FIELD, this effects its circulation, and particles appear as electrically charged. Basically the same expression we find in the work concerning critical velocities, pointing to particles becoming charged. [cf. 5]. The kinetic energy of particles can be transformed to the ionization energy. This conversion of energy is experimentally verified and the velocity, at which a particle or a group of particles becomes fully ionised is known as Kikuchi's velocity, [6].

## 8. SUMMARY

The disintegration processes of matter's shape end with the state of matter reaching integration and homogeneity called FIELD. The creation of matter's shape, particles, occurs in the space of FIELD. The basic state of matter is FIELD having only one parameter, FIELD density. The change of FIELD density occurs by FIELD turning into vortex. Different extent of FIELD density change, arises different sizes of FIELD vortexes (from galaxies to the smallest possible particles or strings). In this spectrum of FIELD vortexes there is a region identified in particular as electromagnetic vortexes. The physical entity FIELD and magnetic field are basically one and the same. Understanding electromagnetic field as part of matter - certain FIELD vortexes - provides the background for understanding and verifying, what particles are - small intensive vortexes of FIELD.

Analyzing interactions between two vortexes discloses the origin of natural forces. FIELD density change through vortex is the first physical law from which all other laws can be found to derive, e.g. the enigma of charge. It is an observable fact that when particles are in motion they become charged. Looking at the structure of particles as particular FIELD vortexes in motion, a deviation of FIELD-vortex circulation from the neutral state occurs. This deviation can be positive or negative and it is the origin of electric charge.

The amount of FIELD which turns into vortex, diverges from the area encircled by the vortical motion. Initially the phenomenon of a vortex occurs in a plane and consequently, the divergence here is a surface divergence which in spherical co-ordinates can be reduced as:

$$\mathrm{div}\,\mathbf{B} = \frac{1}{r^2} B_0$$

This provides the explanation why the gravitational and electric forces are inversely proportional to the square of the distance.

When FIELD vortexes (particles) are in motions, a part of the kinetic energy can be viewed as converted into a form of electric field. Particles become fully ionized when they reach their specific Kikucki's velocity.

Knowledge about the origin of charge can be used for appropriate protection against the hazards caused by static electricity and lightning.

## 9. References:


1. H. Aspden, *Gravitation*, Sabberton publications, Southhampton, 1975, p. 69.
2. W. Thirring, *Urbausteine der materie*, Almanach der österreichischen Akademie der Wissenschaften, Vol. 118,168, p. 153.
3. A. Einstein, *The Meaning of Relativity*, Princeton University Press, 1955, p. 82.
4. S. Alfas, *Einstein's Approach to Understanding Electromagnetic Field as Part of Matter in EMC*, EMC Proceedings, Tel Aviv, 1992, p. 3.3.2 - 7.
5. H. Kikuchi, *Electric Reconnection, Critical Velocity and triggered Lightning,* Reprint, Springer-verlag New York, 1989.
6. S. Alfas, S. Ipavec, *The State of Matter FIELD and Its Property: A New Basic Approach to the Understanding of Terrestrial and Extraterrestrial Electromagnetic Environment,* Dusty and Dirty Plasma, Noise, and Chaos in Space and in the Laboratory, Edited by H. Kikuchi, Plenum Press, New York, 1994, p. 177 - 196.

# NLDN'95: A COMBINED TOA/MDF TECHNOLOGY UPGRADE OF THE U.S. NATIONAL LIGHTNING DETECTION NETWORK

Kenneth L. Cummins, Edward A. Bardo, William L. Hiscox
Richard B. Pyle, Alburt E. Pifer

Global Atmospherics, Inc.
Tucson, Arizona, U.S.A.
Telephone (520) 573 0090 FAX (520) 741-2848

## ABSTRACT

The U.S. National Lightning Detection Network™ (NLDN) has provided lightning data covering the continental U.S. since 1989. Using information gathered from more than 100 sensors, the NLDN provides both real-time and historical lightning data to the electric utility industry, the National Weather Service, and other Government and commercial users. It is also the primary source of lightning data for use in research and climatological studies in the United States. In this paper we discuss the design, implementation, and data from the network following a recent system-wide upgrade. The location accuracy has been improved by a factor of 4-8, resulting in an average accuracy of 500 meters. The expected flash detection efficiency ranges between 80-90 percent, varying slightly by region.

## INTRODUCTION

The growing uses of lightning information over the last six years have led to the demand for performance improvements in the NLDN, in terms of the location accuracy, the percentage of lightning discharges that are detected (detection efficiency), and the locations and peak current data on all the component strokes. These demands have been met through a recently completed upgrade of the network that was co-funded by the Electric Power Research Institute (EPRI) and GeoMet Data Services (GDS). This upgrade, based on a new lightning location methodology combining time-of-arrival and direction-finding techniques, uses sensors manufactured by Atmospheric Research Systems (ARS) and Lightning Location and Protection (LLP). The resulting "hybrid" network substantially outperforms the original NLDN, and is designed for higher reliability and redundancy. Preliminary validation of performance is also reviewed, based on multi-camera video studies of storms in New York and on rocket-triggered lightning measurements in Florida. A summary of the network coverage and performance improvements over the last 5 years is presented, and the effects of lightning locating system performance on reported lightning parameters is discussed.

## BACKGROUND

HISTORY--The NLDN began as a research program at the State University of New York at Albany (1), employing commercially available direction-finding sensors (2,3,4,5). This initial 10-sensor network covered the east coast of the United States between North Carolina and the Canadian border, as discussed by Orville *et al.* (1). The electric utility industry recognized the research and operational potential of lightning locating systems, and consequently funded the expansion and operation of this "SUNYA Network" through EPRI, on behalf of its member utilities. By 1989, the network was expanded and experimentally combined with existing lightning

detection networks operated by the U.S. Bureau of Land Management in the western U.S. and by the NOAA National Severe Storms Laboratory in Oklahoma and Kansas (6). By 1991, it was proposed that there was sufficient commercial interest in national-scale lightning information to justify the establishment of a commercial data service. EPRI and LLP formed Geomet Data Services, Inc. (GDS), which serves as the commercialization arm for the NLDN. Today, GDS, ARS, and LLP form the three operating entities of Global Atmospherics, Inc., a wholly owned subsidiary of Sankosha Corporation.

BASIC LIGHTNING TERMINOLOGY--A Cloud-to-Ground (CG) *flash* is typically composed of a sequence of individual *return strokes* that transfer significant electrical charge from the cloud to ground. Each stroke exhibits peak currents in the range of 5ka to 300ka and has a nominal duration of 20-50 microseconds. The return strokes comprising a flash are typically separated in time by 20 to 100 msec. A flash will on average be comprised of 2-3 strokes, but may contain as few as one and as many as twenty strokes. The number of strokes in a flash is frequently referred to as the *multiplicity*. For most flashes, the *subsequent strokes* (i.e. strokes that occur after the first stroke) will contact the earth at the same *strike point* as the first stroke because they travel through the same *channel* that was established by the first stroke. However, nearly one half of all flashes can contain strokes with different ground strike points, separated by a few hundred meters to several kilometers. More information regarding these concepts can be found in Uman (7), Uman and Krider (8), and Thottappillil *et al.* (9).

In addition to CG lightning, there are numerous types of cloud discharges which do not find their way to ground (7). Some cloud discharges initiate individual CG lightning flashes, whereas others are large inter- and intra-cloud discharges that have no specific relation to CG lightning. These discharges are currently rejected by the NLDN sensors because the primary objective of the NLDN is to identify and locate CG lightning.

APPLICATIONS--The NLDN currently provides real-time lightning data to the utility industry, several government agencies, airlines, and other commercial users. It has been the primary research tool used to provide key data on the historical trends of cloud-to-ground lightning in the United States (10,11,12). An emerging application of lightning data is its use by the insurance industry to verify the presence of lightning for damage claim verification.

As noted above, there has been a continuous demand for performance improvements in the NLDN. These demands have been addressed through a recently completed upgrade which was co-funded by EPRI and GDS. This upgrade is based on a new lightning location technology employing both time-of-arrival and direction-finding methods.

The following sections of this paper provide a summary of the design, implementation, and performance of the upgraded network. Information about performance during the early years of the network is also provided. The final section discusses the effects of lightning locating system performance on reported lightning parameters. Our hope is to assist our users in the analysis and interpretation of lightning data provided by the NLDN.

## DESIGN OVERVIEW

This section describes the NLDN system and its component elements, and provides a summary of the upgrade design objectives. A graphical representation of real-time network operation and data flow is shown in Figure 1. Ground-based sensors detect the electromagnetic signals produced by lightning discharges {1} and transmit salient information to the Network Control Center (NCC) in Tucson, Arizona via a two-way satellite system {2-3}. This "raw" data from the remote sensors is processed in the NCC {4} to provide the time, location and peak current of each detected discharge. This processed information is sent back out the

communications network for satellite broadcast dissemination {5} to real-time users {6}. All this takes place within 30-40 seconds of the lightning discharge.

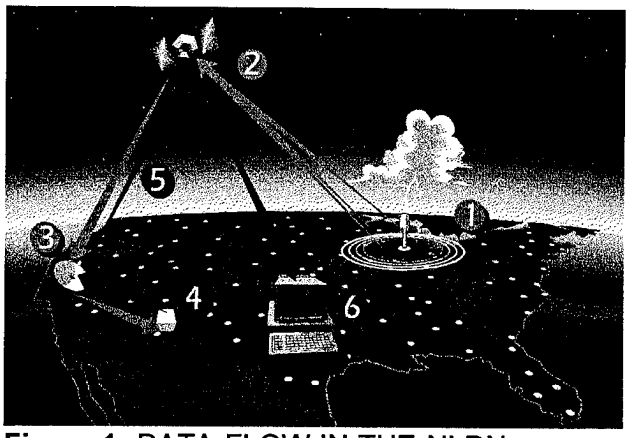


**Figure 1** DATA FLOW IN THE NLDN

OBJECTIVES OF THE NLDN UPGRADE--There were four principal objectives of the NLDN upgrade. The primary objective was to improve location accuracy of the network for CG lightning, in order to meet the growing demands of emerging applications in the electric utilities. The second objective was to provide the infrastructure to process and deliver both stroke and flash information in real-time. The third objective was to improve detection efficiency for low peak current events, down to 5 ka. The final objective was to accomplish these first three objectives while improving long-term reliability. The major network performance specifications set by EPRI were as follows:

* Flash Detection Efficiency: 70% +/- 5%
* Lightning Location Accuracy: 50% within 0.5 Km
* Peak Current Accuracy: 30% (RMS)
* Absolute Stroke Timing: 1 mSec or better
* Cloud Discharge Contamination: less than 2%

The mechanism for achieving these improvements while controlling equipment costs was to employ the forty-five existing IMPACT sensors from the NLDN and sixty of the LPATS timing sensors from the ARS National Network (13). Specific details regarding the sensor, communications system and NCC design are discussed below.

THE SENSOR--The NLDN is comprised of 105 sensors divided roughly evenly between timing-only and timing/angle sensors. The reliability of the network in terms of its detection efficiency (DE) -- the percentage of all C-G discharges that are reported by the network -- is primarily a function of the number of sensors that are available to detect the discharge. Availability in this context means that the sensor is operational and communicating, and that the lightning discharge is within the range of the sensor. Further details regarding sensor design is provided in the section on Sensor Performance.

The topology of the network was selected such that the failure of any one sensor would not compromise the DE of the network in the area influenced by that single sensor. "Compromise" in this context means the reduction of DE below the value agreed upon between Global Atmospherics and EPRI, as listed above. Network DE is, however, effected by the failure of more than one sensor in a region.

The sensor sites themselves have no backup communications systems or hardware redundancy. There is a 15 minute uninterruptable power supply (UPS) available at each location to carry the site through most power outages. Detailed sensor diagnostics are performed in terms of each sensors individual health, their communications path and the quality of the data each sensor is contributing to the network. Using this diagnostic information, NCC operators are able to determine quickly if a particular sensor needs attention.

INBOUND COMMUNICATIONS--Very Small Aperture Satellite Terminals (VSATS) are used to provide a communications path between the remote sites and the NCC in Tucson, Arizona. The VSAT network utilizes a Star topology where a master "Hub" communicates with each of the remote VSATS. The Hub in turn communicates via a terrestrial link to the NCC. Each terrestrial link is backed up with an alternate carrier's switched digital facility. Two separate VSAT vendors are used. Each vendor uses a different satellite, different Hub, and different Land Line communications mechanism from their respective Hubs to the NCC.

The primary failure mode for a VSAT remote unit is "rain fade". Since the VSATS utilize the KU satellite band, which is attenuated by rain, outages will periodically occur on those sites over which intense rainfall is occurring. The sites will recover after the passage of the event. NLDN depends on adjacent redundant sites to detect the lightning in this event. The other primary failure mode is what is termed a "sun-outage". This occurs when the sun aligns with the satellite as seen by various VSATS. This occurs twice per year for about 1 hour over a three day period.

Each Hub is fully redundant in its network hardware. Single points of failure include the satellites that each use and the antenna assembly at each Hub. From the Hub antenna to Tucson all mechanisms are backed up with redundant hardware and power supplies. Both carriers must provide 99.7% or better network uptime by contract.

NETWORK CONTROL CENTER (NCC)--The Network Control Center (NCC) is the hub of all communications, computation and archiving activity for the NLDN. At the core of the NCC are redundant, multiprocessor UNIX systems that command, control and manage all sensors in the field. These UNIX processors run a set of processes, each one of which are responsible for a subset of the command and control of the lightning sensors as well as calculation of lightning solutions and data storage. The processes communicate with each other using standard UNIX interprocess communications methods that allow the processing to be distributed among one or more hardware processors. Uninterruptable power supplies feed conditioned power to these processors and to all support communications, storage and monitoring equipment.

Data arrives at the control center via multiple, digitally backed up, 56 kilobit/second digital lines from the VSAT hubs located in Denver and Los Angeles. The data is presented to the NCC utilizing the X.25 communications protocol and is fed into redundant X.25 switches which are responsible for providing multiple data paths to the redundant UNIX processor. If one path is blocked due to a processor failure, the data is automatically routed to another UNIX processor. The data, having passed through the X.25 switches, is presented to the UNIX processors.

Lightning records and status messages from the sensors are then translated from the X.25 protocol into a User Datagram Protocol / Internet Protocol (UDP/IP) by the UNIX processors and are immediately sent to dual redundant Magneto Optical Recording Media. In this way all data and network status is stored on a removable archive media for any post analysis that is necessary. The data from different sensor types is then translated into a consistent internal format for downstream processing.

The lightning data, having been archived, is then forwarded to the core lightning location calculation processes. This sequence of procedures first sort sensor reports by time, then a location is calculated for time coincident sensors. Quality checks are then done on the location and inconsistent sensor reports are sent back to the time sorting algorithm for possible inclusion in other lightning location calculations.

From this point, the lightning solutions are forwarded to three distinct processes, i) to the archiving mechanisms; ii) to the network data quality monitors, and iii) to the subscribers of the real time data stream. Lightning location archiving is accomplished utilizing the Sybase$^{tm}$ Relation Database Management System (RDBMS). This system allows network access via Transmission Control Protocol / Internet Protocol (TCP/IP) to all lightning solutions via standard

System Query Language (SQL) requests. Utilizing this data access mechanism, derivative data products are produced such as FALLS™, StrikeFAX™, CDA™ and others.

DATA DELIVERY SYSTEM--Global Atmospherics utilizes the California Microwave C-100 broadcast mechanism to distribute the NCC results in real time. This mechanism utilizes C-Band spread spectrum technology to deliver a 1200 bit/sec stream from the NCC to the end users who typically run PC-based THUNDER or VIS displays. The delivery of data to the end user starts on a terrestrial circuit originating at the NCC and terminated at the C-100 hub in California. This terrestrial circuit is backed up through switched digital service provided by alternate carriers and automated switching equipment.

The C-100 Master Earth Station broadcasts the data via satellite using the C-Band. This frequency range is not effected by rain attenuation but is affected by sun outage as previously described in the Inbound Communications Section.

Single points of failure for the Data Delivery Mechanism include the satellite and antennas used by the Master Earth Station. All terrestrial communications and Master Earth Station Components are backed up with redundant hardware. Alternate modem-based dial-in mechanisms are available for users who have failure of their C-100 equipment, or who do not employ the satellite delivery mechanism.

## LIGHTNING LOCATION METHODS

Most existing methods for determining the position of individual C-G lightning strokes or flashes are based either on direction-finding or time-of-arrival methods, or a combination of these methods. Early work in applying time-of-arrival for locating lightning was performed by Lewis *et al.* (14) and Oetzel and Pierce (15). U.S. Patents on various implementation of hyperbolic methods for locating lightning date back to the early 1950's. This methodology is currently in use in commercially available systems developed and patented by ARS.

Work in applying magnetic direction finding for locating lightning dates back to the 1920's (16). As with time-of-arrival, there are several U.S. Patents on specific methods for location by direction-finding. LLP developed modern commercial systems employing wide-band peak-gated direction finding (2,3). The basic principles for these two methods are discussed in Cummins *et al.* (17) and Holle and Lopez (12).

Another current commercial system for lightning detection and location, employing VHF interferometric techniques, is described by Richard *et al.* (18). A more complete summary of lightning location techniques is contained in a paper by Lee (19).

IMPACT:"IMPROVED PERFORMANCE FROM COMBINED TECHNOLOGY"--By 1992, LLP had completed the development of a method for combining direction-finding and time-of-arrival to produce yet another lightning location method which is referred to as the IMPACT method. In this approach, direction finding provides azimuth information and absolute arrival time provides range information. These data are employed in a generalization of the LLP optimization method (20) to obtain estimates of the CG discharge location, employing all available data. This approach does not suffer from the problems inherent with each of the methods when they are used separately. As an example, a discharge which occurs between two sensors along their baseline will be precisely located by the intersection of the azimuth "vectors" and range "circles", as shown in Figure 2. In this figure, the azimuth information for sensor S1 is the angle $\theta 1$, and the range value (based on absolute arrival time) is r1. It is important to note that in this example there are four measured parameters -- two angles and two arrival times. These measurements produce three estimated parameters -- latitude, longitude, and discharge time. Thus the IMPACT method has redundant information which allows for an optimized

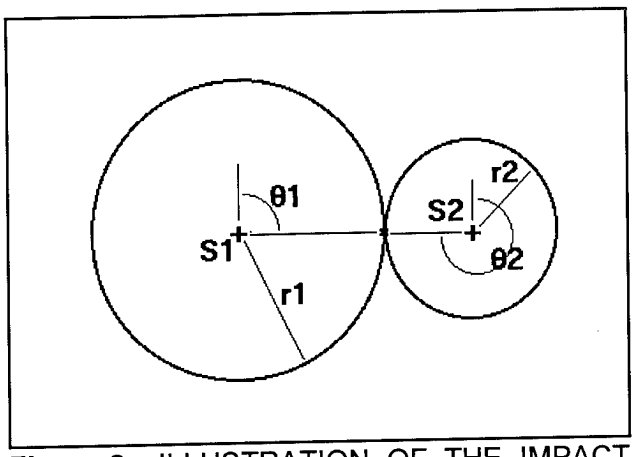



**Figure 2** ILLUSTRATION OF THE IMPACT METHOD FOR LOCATING LIGHTNING ON THE BASELINE BETWEEN TWO SENSORS.

estimate of location even in the minimal situation where a discharge is detected by only two sensors. Evaluations of this method have shown that this combined method outperforms either method by itself, both in its location accuracy and in its probability of detection.

NLDN: A HYBRID TOA-MDF IMPLEMENTATION--The IMPACT location algorithm is a sufficiently general approach to allow arbitrary combinations of timing-based and angle-based sensors. The only constraint for a location solution is that there are more independent observations of angle and/or time than there are variables to estimate (latitude, longitude, and stroke time). A representative minimal example is an optimized location derived from three sensors -- one providing both angle and time information, and two others providing time information. Figure 3 shows a stroke located in Florida by five sensors -- three IMPACT sensors contributing both timing and angle information, and two LPATS sensors providing timing. The angle information is represented by the straight-line "vectors" emanating from the sensors, and the timing information is represented by "timing circles" which are centered around each sensor. This event is typical of strokes detected by the NLDN, which is designed to have an average of 6-8 sensors contributing to the location of a 30 ka stroke.

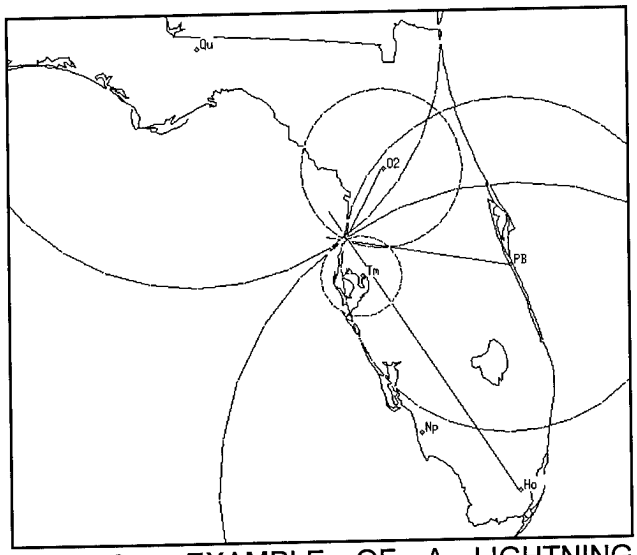



**Figure 3** EXAMPLE OF A LIGHTNING STROKE LOCATED BY TWO LPATS SENSORS AND THREE IMPACT SENSORS.

SENSOR PERFORMANCE

Both sensor types employed in the NLDN upgrade -- IMPACT and LPATS -- required modifications in order to improve their sensitivity and reliability. Prior to implementing the upgrade, both sensor types were evaluated in terms of sensitivity, quality of signal strength measurement, and waveform classification. The fundamental metric which determined the maximum spacing between adjacent sensors was the "Network Relative Detection Efficiency" (NRDE) vs. range. NRDE is defined as the percentage of events reported by the network that are detected by an individual sensor, computed as a function of range from the sensor. Sample results for a typical sensor are shown in Figure 4. A standard-gain IMPACT sensor (before upgrade) is shown as the solid curve, having a nominal NRDE of 70-75 percent out to 300 Km, and falling off to less than 30 percent beyond 450 Km. In order to improve these sensor's performance, the overall gain was increased by 50 percent, the threshold was reduced, and waveform criteria were modified to improve detection efficiency in the 400-600 Km range. The resulting NRDE after modifications

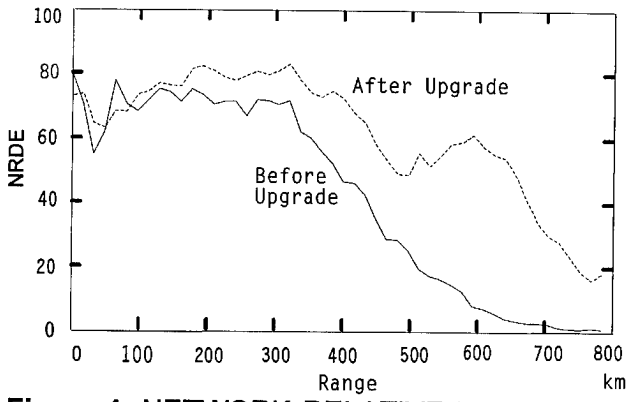



**Figure 4** NETWORK RELATIVE DETECTION EFFICIENCY FOR AN IMPACT SENSOR BEFORE AND AFTER MODIFICATION.

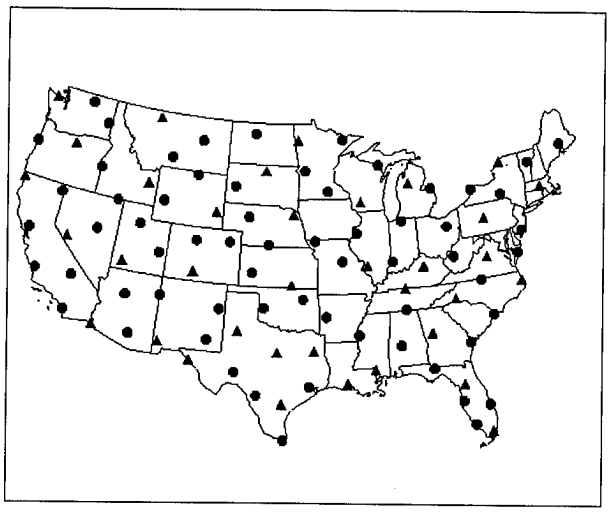


**Figure 5** NLDN SENSOR LOCATIONS. TRIANGLES REPRESENT IMPACT SENSORS; CIRCLES REPRESENT LPATS SENSORS.

for the same sensor is plotted as a dashed curve, showing the useful range of the sensor extending beyond 650 Km.

The LPATS sensors were initially too sensitive, in that as stroke rates increased and storms approached the sensor location, the CG stroke detection efficiency fell rapidly due to triggering on nearby cloud discharges and leader pulses, and due to the use of adaptive gain reductions which were required to control communications rates. Based on these findings and due to our focus on CG lightning, the LPATS sensors were modified by reducing their gain by a factor of 2 and adding waveform criteria to provide rejection of noise, leader pulses and cloud discharges. In addition, the effective communications bandwidth was increased by a factor of 3 to allow higher stroke rates, and all LPATS sensors were upgraded with GPS-based timing similar to the IMPACT sensors. These changes resulted in an overall performance which is similar for the two sensor types.

By producing a useful range for all sensors out to 650 Km it was possible to increase the nominal baseline between sensors to about 350-400 Km. This design constraint led to a final network configuration requiring 100 sensors in order to meet the EPRI requirements. This upgrade was a significant task in which nearly 200 sites were visited for upgrades, relocation, new installation, or decommissioning. The final sensor locations are shown in Figure 5. The triangles represent IMPACT sensor sites which provide both timing and angle information, and the circles represent LPATS sites which provide timing information. An additional five IMPACT sensors are included as part of the network in Tennessee and South Carolina, placed there by the Tennessee Valley Authority and Duke Power Company in order to further enhance performance in their operating areas.

## NLDN NETWORK PERFORMANCE PROJECTIONS

The NLDN has undergone a series of extensions and upgrades over the last four years. In this section, we summarize the evolution of the network, and discuss its effect on network performance.

LOCATION ACCURACY PROJECTIONS--The most informative means to represent location accuracy is to describe it in terms of the expected region of possible locations (confidence region), given a specific probability, or confidence level (21). When location errors are Gaussian,

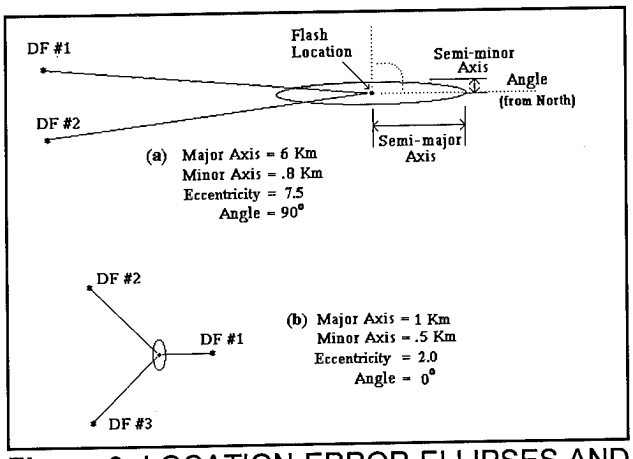



**Figure 6** LOCATION ERROR ELLIPSES AND RELATED PARAMETERS.

these confidence regions are elliptical, allowing them to be fully described by their semi-major axis, semi-minor axis, and angle of orientation. Figure 6 illustrates the error ellipses for two lightning strokes located using direction finding methods. In order to represent location accuracy of a specific network, a contour plot of the semi-major axis of the error ellipse at the 50% confidence interval is employed. This value is equivalent to the median semi-major axis. The resulting "Location Accuracy Projections" are used to represent estimated performance in LLP and ARS lightning networks worldwide.

In early 1992 when GDS assumed responsibility for the network, a complete calibration of sensor sites was carried out resulting in a fairly uniform location accuracy (50th percentile semi-major axis) of 2-4 Km throughout the Network (22). Prior to that time, GDS estimates the average location accuracy to be 8-16 Km, based on observations by users of the network and on the assumption that uncorrected site errors were typically 1-3 degrees. During the summer of 1992, 34 new sensors were installed

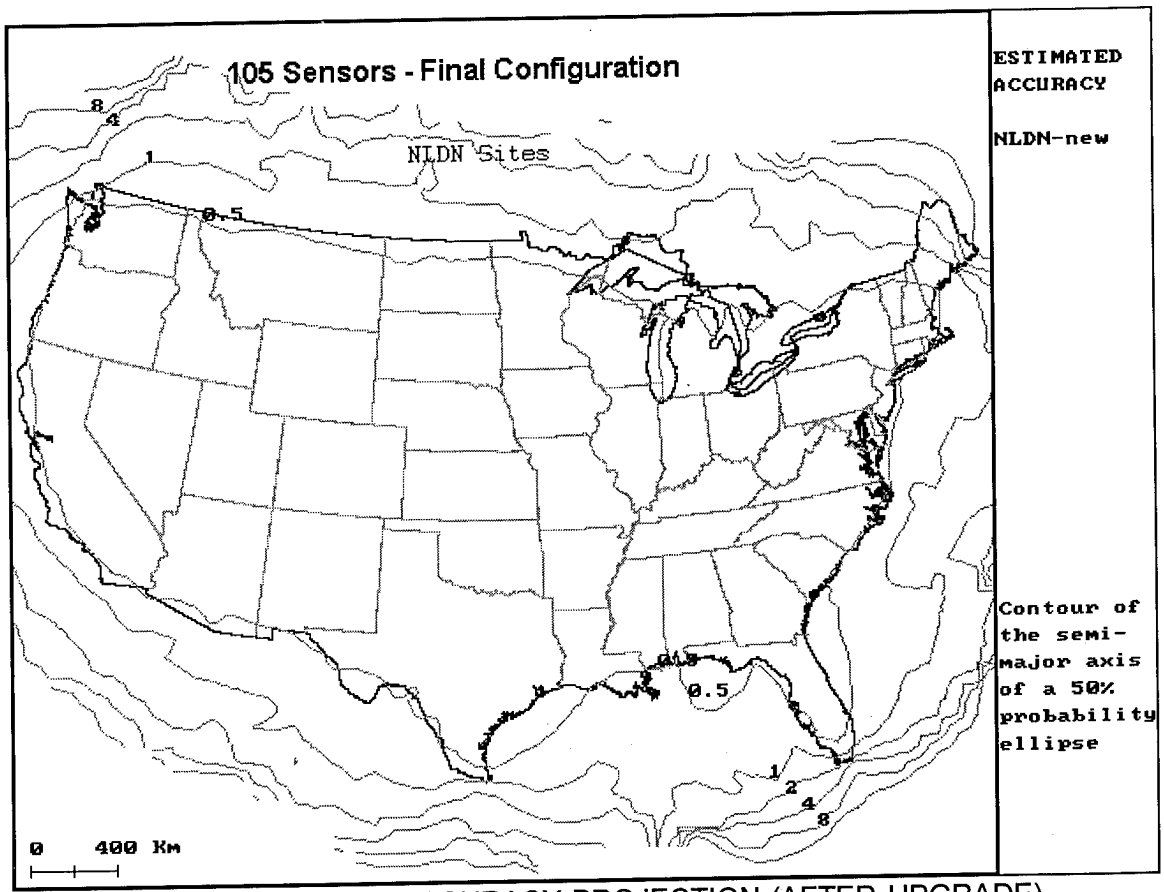



**Figure 7** NLDN LOCATION ACCURACY PROJECTION (AFTER UPGRADE).

in the western U.S., eliminating the reliance on lightning sensors operated by the U.S. Bureau of Land Management. In 1993, GDS experimented in parts of the network with the new IMPACT location technology developed by LLP, demonstrating average location accuracies of approximately 500 meters in the upgraded areas (17). Between July and December of 1994, GDS upgraded the NLDN using the LPATS and IMPACT sensors described above. The projected average location accuracy for this upgraded network is shown in Figure 7, drawn as contours of constant median accuracy in km. Note that most of the continental U.S. has a median accuracy of 500 meters.

DETECTION EFFICIENCY PROJECTION--Like location accuracy, network detection efficiency (DE) has also improved over the last few years. Between 1992 and 1994, the DE for CG flashes with first-stroke peak currents above 10 ka is estimated to be between 65 and 80 percent. This means that 7-8 out of 10 CG flashes were typically detected and reported. This range of values is approximately 10 percent less than was projected in an earlier report by Cummins *et al.* (22). The revised estimates of DE for this period are the result of DE model improvements implemented during the design phase of the current NLDN upgrade. Global Atmosphercis now employs a more accurate signal propagation model (exponential, with a space constant of 1000 Km), a more accurate model of sensor behavior derived from direct field measurements, and a model peak current distribution which includes events with peak currents

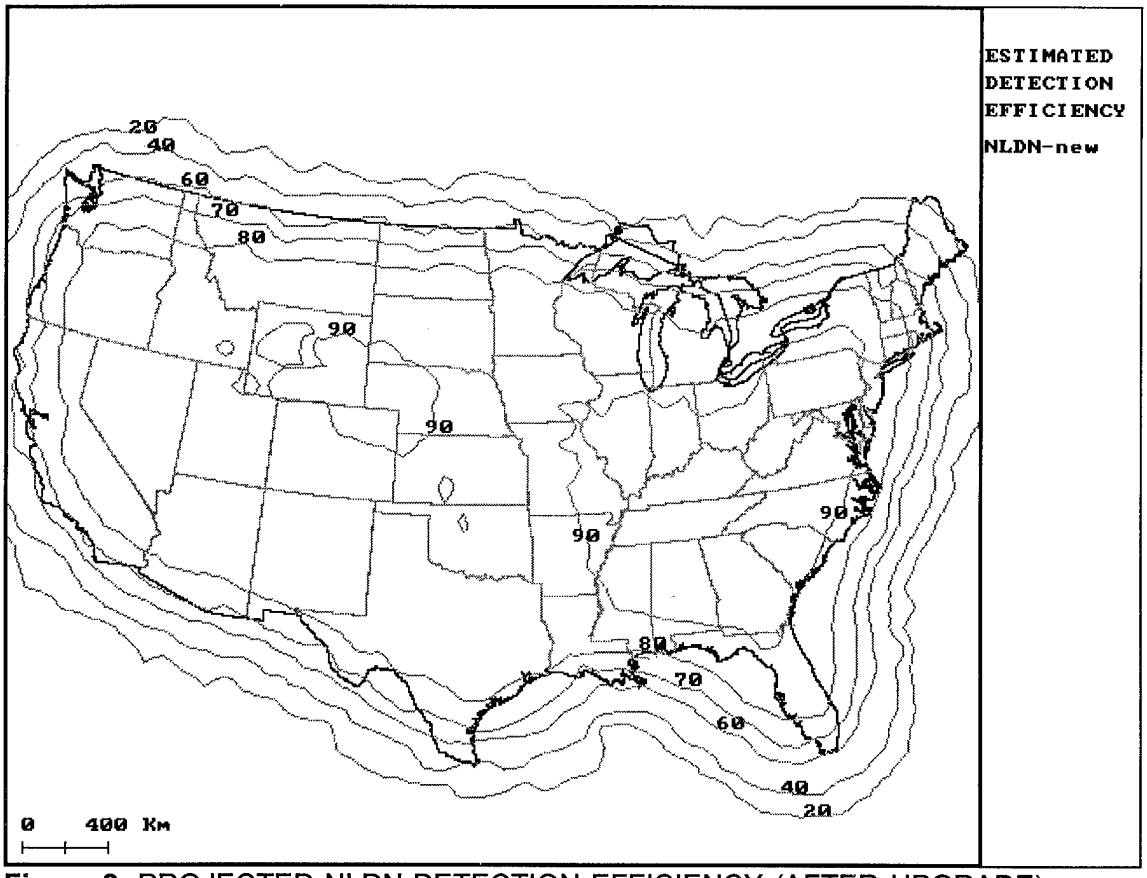



**Figure 8** PROJECTED NLDN DETECTION EFFICIENCY (AFTER UPGRADE).

down to 5 ka. The 1992 model had been limited with a minimum peak current of 10 ka. Commencing in 1995, the NLDN upgrade was designed to provide typical flash detection

efficiencies in the range of 80 to 90 percent, as shown in Figure 8. Note, however, that DE falls of rapidly as the continental borders are approached.

Table 1 summarizes the estimated location accuracy and detection efficiency achieved by the NLDN since 1989. The location accuracy estimates are provided as the semi-major axis of the error ellipse (confidence interval) for both the 50th percentile (median) and 95th percentile.

**Table 1** Estimated location accuracy and detection efficiency for the NLDN between 1989 and 1995.

| YEAR | 50% Semi-major axis | 95% Semi-major axis | Detection Efficiency |
|---|---|---|---|
| 1995 | 0.5-1.0km | 1-2km | 80-90% |
| 1994 | 2-4km | 4-8km | 65-80% |
| 1993 | 2-4km | 4-8km | 65-80% |
| 1992 | 2-4km | 4-8km | 65-80% |
| 1991 | 4-8km | 8-16km | 70%[a] |
| 1990 | 4-8km | 8-16km | 70%[a] |
| 1989 | 4-8km | 8-16km | 70%[a] |

[a] Network detection efficiency was not well characterized during this period (Orville, 1994)

FLASH AND STROKE INFORMATION--The NLDN has historically reported the first stroke of a flash, and a count of the number of subsequent strokes (multiplicity). The multiplicity was computed as the largest number of strokes reported by any of the sensors that participated in the flash, where the Direction Finding (DF) sensors determined their stroke counts by accumulating all events that occurred in a +/- 2.5 degree interval for a one second period after the first stroke. This approach can overestimate the multiplicity, due to the potential for concurrent flashes having similar angles from one or more sensors. This method for determining multiplicity became a practical problem when the number of DF sensors in the NLDN network was decreased and the spacing between these sensors was increased. Due to these issues, multiplicity for flashes in the upgraded NLDN is now determined by applying a spatial and temporal clustering algorithm (discussed below) to all stroke locations. This change to all-stroke processing was implemented in the real-time data stream as of June 15, 1995. All archived lightning data since January 1, 1995 have been reprocessed using this algorithm. Both flash and stroke data are currently available to our customers. The flash information provides sufficient detail to detect and track thunderstorms. The stroke information includes the latitude, longitude, peak current and stroke time for each detected stroke, along with several parameters which characterize the accuracy of the location estimate which are referred to as "Location Quality Parameters" (GDS Applications Note #3). Stroke data are used when point-specific information is required.

Flash data are derived from stroke data as follows. Upon locating a stroke which cannot be associated with a "current" flash (see below), the first stroke of a new flash is identified. Additional strokes may be added to any "current" flash for a period of up to one second after the time of its first stroke, as long as the stroke occurs within 10 Km of the first stroke. In the unlikely case of a stroke qualifying as part of more than one flash, it is associated with the flash with the closest first stroke. Additionally, if for any reason the location quality parameters for a given stroke are such that its location is not clearly distinguishable from the location of a first stroke, it will be included in that flash even if the locations differ by more than 10 Km.

## PERFORMANCE VALIDATION STUDIES

As with all physical measurements in nature, the parameters reported for each stroke or flash have some uncertainty. The stroke times for the NLDN are now accurate to a few microseconds, due to the use of absolute timing in the IMPACT optimization procedure. The

peak current estimates are estimated to be accurate to approximately 25-30% (22,23). Due to the importance of stroke location and DE in electric utility applications, several "ground truth" evaluations of these system performance factors have been carried out over the last two years. Results of three such studies are briefly summarized below. The details of these experiments will be reported separately.

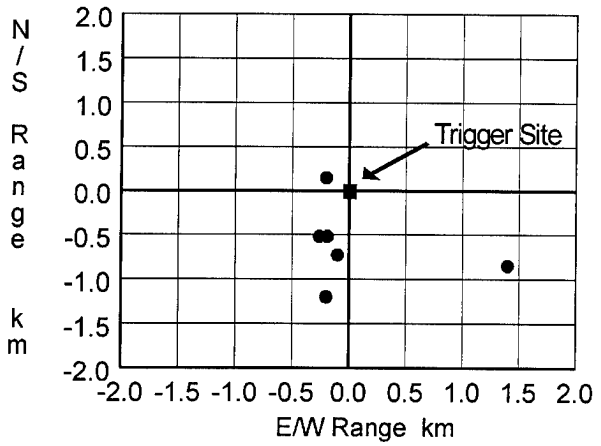



**Figure 9** COMPUTED GROUND STRIKE POINTS FOR ROCKET TRIGGERED LIGHTNING.

Location accuracy for the IMPACT technology has been studied in a variety of ways. The most direct means to validate location accuracy of the system is to compare computed locations with known ground-strike locations. The rocket triggered lightning studies carried out each year at Camp Blanding near Gainesville, Florida provide an ideal data set for this analysis. Figure 9 shows the computed ground strike point for six rocket-triggered strokes located by the NLDN in 1993, positioned relative to the triggering site. At that time, the NLDN in this area had been partially upgraded to the IMPACT technology, in that about two-thirds of the sensors reporting in the Gainesville area included timing information. Three of seven located events were placed within 600 meters of the launch site, and all six were within 1.5 Km.

In order to obtain estimates of location accuracy over a larger area, position differences have been computed between the NLDN and the short baseline network at Kennedy Space Center operated by the U.S. Air Force on three separate occasions in the last three years, as first described in Cummins *et al.* (22). Since upgrading the NLDN in Central Florida, an average location difference of 600-700 meters between these two networks has consistently been achieved, suggesting an average location accuracy for the NLDN of better than 500 meters.

An independent evaluation of NLDN location accuracy was also carried out by researchers at the State University of New York at Albany (SUNYA), as part of the upgrade program. This study provided clear evidence that the error-ellipse model and related parameters employed in our accuracy projections provide conservative estimates of the actual location accuracy. During the summer of 1994, CG strokes were located in the Albany area using a multi-camera precision video intersection method developed at SUNYA. The 190 "best accuracy" video locations, estimated to have better than 1 Km accuracy, were compared in position to the locations determined by the NLDN. This "Video derived location error" was plotted as a function of the error ellipse semi-major axis, which was computed using the NLDN location algorithm. The resulting scattergram is shown in Figure 10. For the error ellipse estimates to be correct, approximately 50 percent of the strokes must be located to the "left" of the "Y = X" line. In this example, 58 percent of the events were in this category. Similarly, approximately 92 percent of the events need to fall to the left of the "Y = X/2" line -- in this case 89 percent meet this criterion. This result supports the use of error ellipses to estimate location accuracy. For this study, the median "video derived location error" was 2 Km. Assuming an average error in the video system of about 500-1000 meters, the remaining error was consistent with our estimated median accuracy of just over one Km for the partially-upgraded Albany area during the test period. This study is being repeated in 1995 for the fully-upgraded NLDN, employing an improved video locating system. This study will also include a detailed evaluation of stroke and flash detection efficiency.

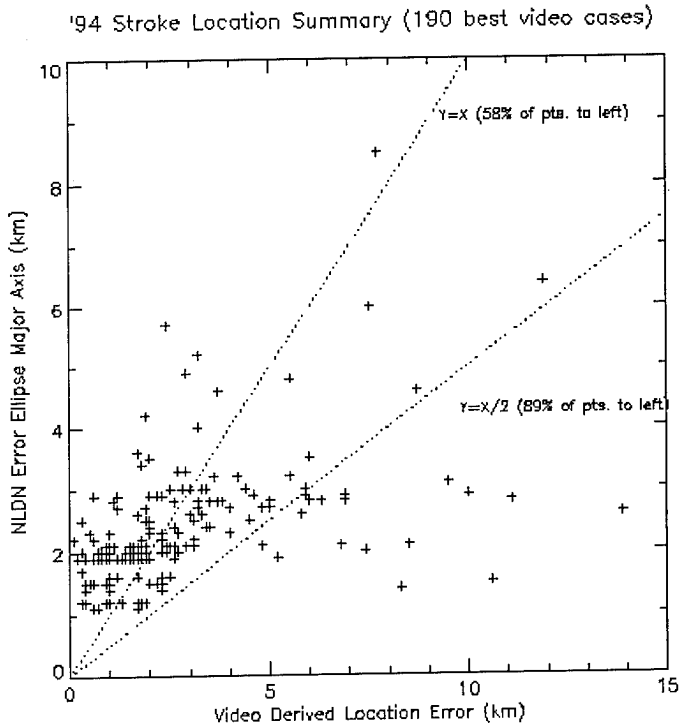



**Figure 10** SCATTERGRAM ILLUSTRATING RELIABILITY OF THE ERROR ELLIPSE MODEL FOR LOCATION ACCURACY.

This 1994 SUNYA study discussed above also included a video-based assessment of flash detection efficiency. A CG flash was considered to be detected when at least one of its strokes, as identified in individual video frames, was also detected by the NLDN. Although the DE percentage varied significantly between storms, the average flash DE of 76 percent determined from 7 storms, was consistent with the "70-80 percent" which was predicted by our DE model for the Albany area at that time. This variability in DE will be re-examined in the 1995 study.

## INTERPRETATION OF LIGHTNING DATA

Anyone employing lightning data derived from locating systems in any quantitative way should first understand the limitations of the technology behind the data in order to avoid misinterpretation of the information. Although a detailed discussion of this subject is beyond the scope of this paper, Global Atmospherics requests that our technical and scientific users keep the following issues in mind.

VARIABILITY IN DETECTION EFFICIENCY--As discussed above, DE can vary with location (due to network geometry) and with time (due to network status and the nature of the thunderstorm). Because of these facts, care must be taken in the interpretation of changes in stroke or flash densities over space and/or time. This fact is illustrated in a paper by Lopez *et al.* (24) which discusses the impact of DE and signal strength on the observed dynamics of a storm. In addition, variations in DE can seriously affect the measured peak current distribution, as well as the measured percent of events that have a positive polarity. In the NLDN, we have strived for a uniformly high DE throughout the U.S. The DE projection shown in Figure 7 can be used as a "first order" correction for DE variation with region, although one should be careful at the "edges" of the network. Global Atmospherics will continue to carry out characterizations of actual performance in various regions of the U.S.

VARIABILITY IN PEAK CURRENT ESTIMATES--The primary use to date for peak current information is in the design and assessment of lightning protection for electric power utilities. In this application, the distribution of peak currents, depicted as a cumulative distribution, provides the basic data set for determining the theoretical "risk" for faults on transmission and distribution lines, and for assessing the cause of lightning damage to substations and other utility equipment. In this application, errors in peak current estimates on the order of 25-30 percent are not too significant. At this time, it can only be stated that lightning networks are capable of estimating negative subsequent stroke peak currents to this level of accuracy, based on rocket-

triggered lightning studies (23). At this time, direct calibration of peak current for positive CG strokes has not been achieved.

DETERMINATION OF FLASH MULTIPLICITY--The method for estimating flash multiplicity is inherently different for systems based on direction-finding and systems based on time-of-arrival, as noted above. The original LLP method based on direction-finding reliably produced an average multiplicity of 2.4 to 2.7 in the U.S., when averaged over long periods of time. The absolute accuracy of this estimate is affected by numerous factors related to sensor spacing, sensor detection efficiency, spatial separation of subsequent strokes, and overall flash rate. It is generally thought that the "true" average multiplicity is actually 3-4 (25).

The new multiplicity estimate used in the NLDN, which is required when timing is the primary method for locating strokes, will be inherently lower because it is directly related to the overall stroke detection efficiency of the network. In preliminary evaluations involving about 40,000 strokes in the NLDN, it appears that the average multiplicity determined in this manner typically ranges between 1.9 and 2.1. This result is consistent with a subsequent stroke DE of about 60 percent. Due to the fact that subsequent strokes typically have smaller peak currents than first strokes, this finding is not inconsistent with our projected overall flash DE of 80-90 percent. A detailed analysis of the stroke/flash relationship is currently in progress. It should not be overlooked that there is a distinct advantage in locating the individual strokes of a flash. The advantage is clear for applications where individual ground strike points are critical, such as electric power line reliability analysis. Additionally, it enables the scientific study of specific spatial and temporal relationships between first and subsequent strokes.

## CONCLUDING REMARKS

Over the last 6 years, the NLDN has undergone a number of modifications and upgrades which have improved both its detection efficiency and location accuracy for cloud-to-ground lightning. These changes have mirrored the demands of our customers, and have parallelled the technological advances in instrumentation and information processing developed by Global Atmospherics. These advances are not without problems, in that along with improved performance comes changes in the way the data should be interpreted. It is our intention to manage any negative impact to our user community which results from these improvements by maintaining an active dialogue with our users and by collaborating with the scientific community in the assessment of our systems. It is our hope that this paper moves both of these intentions forward.

*Acknowledgements.* A number of people have directly or indirectly contributed to the NLDN upgrade and to the content of this paper. The NLDN upgrade was funded by GDS and by EPRI on behalf of its member utilities. We would like to thank the following scientists for their support, their insights, and their constructive criticisms: Martin Uman, E. Philip Krider, Rodney Bent, Marx Brook, Ralph Bernstein, Bill Chisholm, John Cramer, Ron Henderson, Ron Holle, Vince Idone, Raul Lopez, Don MacGorman, Fred Mosher, and Tom Rodby.

## REFERENCES

1. R.E. Orville, R.W. Henderson, and L.F. Bosart, "An East Coast Lightning Detection Network." Bull. Amer. Meteor. Soc., 64, 1983, pp. 1029-1037.

2. E.P. Krider, R.C. Noggle, and M.A. Uman, "A Gated, Wide-band Magnetic Direction Finder for Lightning Return Strokes." J. Appl. Meteorol., 15, 1976, pp. 301-306.

3. E.P. Krider, R.C. Noggle, A.E. Pifer, and D.L. Vance, "Lightning Direction-finding Systems for Forest Fire Detection." Bulletin of the American Meteorological Society, 61, No. 9, 1980, pp. 980-986.

4. M.W. Maier, R.C. Binford, L.G. Byerley, E.P. Krider, A.E. Pifer, and M.A. Uman, "Locating Cloud-to-ground Lightning with Wideband Magnetic Direction Finders." Fifth Symposium on Meteorological Observations and Instrumentation, 1983, pp. 497-504.

5. M.W. Maier, L.G. Byerley, R.C. Binford, W.L. Hiscox, E.P. Krider, A.E. Pifer, and M.A. Uman, "Gated, Wide-band Magnetic Direction-finders for Locating Cloud-to-ground Lightning." Conference on Atmospheric Electricity, Albany, New York, 1984, pp. 305-310.

6. R.E. Orville, "Lightning Ground Flash Density in the Contiguous United States - 1989." Mon. Wea. Rev. 119, 1990, pp. 573-577.

7. M.A. Uman, "The Lightning Discharge." New York, New York: Academic Press, Inc. 1987.

8. M.A. Uman and E.P. Krider, "Natural and Artificially Initiated Lightning." Science, 246, 1989, pp. 457-464.

9. R. Thottappillil, V.A Rakov, M.A Uman, W.H. Beasley, M.J. Master, and D.V. Shelukhin, "Lightning Subsequent-stroke Electric Field Peak Greater than the First Stroke Peak and Multiple Ground Terminations." Journal of Geophysical Research, 97, 1992, pp. 7503-7509.

10. R.E. Orville (Editor), "Thunderstorm Electrification and Lightning." Mon. Wea. Rev., 122, No. 8, 1994a.

11. R.E. Orville, "Cloud-to-ground Lightning Flash Characteristics in the Contiguous United States: 1989-1991." J. Geophysical Research, 99, 1994b, pp. 10833-10841.

12. R.L. Holle and R.E. Lopez, "Overview of Real-time Lightning Detection Systems and Their Meteorological Uses." NOAA Technical Memorandum ERL NSSL-102, 1993.

13. P.W. Casper and R.B. Bent, "Results from the LPATS U.S.A. National Lightning Detection and Tracking System for the 1991 Lightning Season." Paper presented at 21st ICLP International Conference on Lightning Protection, Berlin, Germany, 1992.

14. E.A. Lewis, R.B. Harvey, and J.E. Rasmussen, "Hyperbolic Direction Finding with Sferics of Transatlantic Origin," Journal of Geophysical Research, 63, No. 7, 1960, pp. 1879-1905.

15. G.N. Oetzel and E.T. Pierce, "VHF Techniques for Locating Lightning." Radio Sci., 4, 1969, pp. 199-201.

16. F. Horner, "Very-low-frequency Propagation and Direction Finding." Proceedings of the IEEE, 101B, 1957, pp. 73-80.

17. K.L. Cummins, R.O. Burnett, W.L. Hiscox, and A.E. Pifer, "Line Reliability and Fault Analysis Using the National Lightning Detection Network." Paper presented at Precise Measurements in Power Conference, Arlington, Virginia, 1993.

18. P. Richard, A. Soulage, P. Laroche, and J. Appel, "The SAFIR Lightning Monitoring and Warning System, Application to Aerospace Activities." Int. Aerospace and Ground Conf. on Lightning and Static Electricity, 1988, pp. 383-390.

19. A.C.L. Lee, "Bias Elimination and Scatter in Lightning Location by the VLF Arrival Time Difference Technique." Meteorological Office, Bracknell, Berkshire, United Kingdom, 1990.

20. W.L. Hiscox, E.P. Krider, A.E. Pifer, and M.A. Uman, "A Systematic Method for Identifying and Correcting 'Site Errors' in a Network of Magnetic Direction Finders." Paper presented at Int. Aerospace and Ground Conference on Lightning and Static Electricity, 1984.

21. R.G. Stansfield, "Statistical Theory of D. F. Fixing." J. IEE, Part IIA, 1947, pp. 762-770.

22. K.L. Cummins, W.L. Hiscox, A.E. Pifer, and M.W. Maier, "Performance Analysis of the U.S. National Lightning Detection Network." Paper presented at 9th International Conference on Atmospheric Electricity, St. Petersburg, Russia, June, 1992.

23. V.P. Idone, A.B. Saljoughy, R.W. Henderson, P.K. Moore, and R.B. Pyle, "A Reexamination of the Peak Current Calibration of the National Lightning Detection Network." Journal of Geophysical Research, 98, No. D10, 1993, pp. 18,323-18,332.

24. R.E. Lopez, R.L. Holle, R. Ortiz, and A.I. Watson, "Detection Efficiency Losses of Networks of Direction Finders Due to Flash Signal Attenuation with Range." Paper presented at Proceedings of the 1992 International Aerospace and Ground Conference on Lightning and Static Electricity, Atlantic City, 1992.

25. E.M. Thomson, M.A. Galib, M.A. Uman, W.H. Beasley, and M.J. Master, "Some Features of Stroke Occurrence in Florida Lightning Flashes." J. Geophys. Res., 89, 1984, pp. 4910-4916.

# TEST REQUIREMENTS AND SCIENCE OF DETERMINING THE ELECTROSTATIC DISCHARGE (ESD) VULNERABILITIES OF WEAPON SYSTEMS

J. DULCEY
AND
N. KALOTERAKIS

INDIAN HEAD DIVISION
NAVAL SURFACE WARFARE CENTER
INDIAN HEAD, MD 20640-5035

## ABSTRACT

The purpose of this paper is to review the present requirements for determining the electrostatic discharge sensitivity of weapon systems and the methods available to perform the analysis and testing needed. The intent of the authors is not to criticize the present requirements, but to assess the electrostatic analysis and test methods currently in use versus the ordnance products being designed and manufactured today. Some work is being done to address some issues raised in this paper, but an overall concerted effort by the ESD community is needed to establish new ESD test requirements.

## INTRODUCTION

The need for a specification to cover testing of weapon assemblies is increasing every year. The weapons and their shipping/handling containers are changing both internally and externally. This paper will explore the current situation and point out possible solutions to address the problem. The need for reform is well known to the ESD testing community.

## REVIEW OF CURRENT REQUIREMENTS

The current requirements for ESD testing are covered by various documents. The main documents are as follows:

Mil-Std-331: *"Fuze and Fuze Components, Environmental and Performance Tests for"* [1]

Test F1 covers the testing of packaged and unpackaged fuzes at both 25,000 volt (human body) and 300,000 volt (air replenishment) ESD testing. The human body test also has two models represented by series resistances of 500 and 5000 ohms. The relative humidity during testing is to be 50% or less.

Mil-Std-1512: "*Electroexplosive Subsystems, Electrically Initiated, Design Requirements and Test Methods*"[2]

This Air Force standard covers all electroexplosive subsystems and component parts. Test method 205 covers 25,000 volt ESD testing. The Human body model is 5000 ohms series resistance. Humidity is not listed as a requirement.

Mil-I-23659: "*Initiators, Electric, General Design Specification for*"[3]

The specification covers the testing of electric initiators and electric initiator subassemblies at 25,000 volts. The human body model is a series resistance of 5000 ohms. The relative humidity during testing is to be 50% or less.

STANAG 4239: (Draft)"*On Electrostatic Discharge, Munitions Test Procedures*"[4]

The testing pattern on this review is very similar to Mil-Std-331. The relative humidity limit has been raised to 60% maximum.

These testing specifications do not require the all up round or issued form of weapons to be tested. The mechanism currently requiring weapon assembly testing is the Weapons System Explosive Safety Review Board. The issue of complete weapon testing is particularly important for the 300,000 volt ESD testing of items subjected to vertical replenishment. The typical form of many weapons during vertical replenishment is all up or completely assembled. Some weapons are fuzed after replenishment.

The need exists to specifically require that complete weapon systems be covered by ESD requirements. Not all systems require ESD testing. Some systems can be analyzed or partially tested without all the explosives and/or propellants installed.

The Navy typically uses Mil-Std-331 to address ESD testing. This fuze specification works for complete weapons, because provision is made for testing both containerized (packaged) and bare (unpackaged) fuzes. The tests for both 300,000 volt (vertical replenishment) ESD and 25,000 (human body) ESD are delineated. The human body ESD also has two models, 500 and 5000 ohm series resistances.

Most weapon systems that are vertically replenished are packaged in shipping containers. Mil-Std-331 contains reasonable post test requirements on packaged weapons. The tested item must be safe to handle and use. The tested item must also remain fully functional.

Mil-Std-331 also requires the bare test item be subjected to both 300,000 and 25,000 volt ESD. This requirement is something of a penalty test for some weapons. The post test requirement is not as stringent as the containerized test. The fuze must be safe to handle and use, but it is required to function only after the 25,000 volt ESD test. Since all possible ESD exposure scenarios cannot be anticipated, the bare ESD test is a reasonably conservative test approach. A real life example of the need to test bare is one weapon that is exposed to ESD hazard in an unusual manner. The weapon is normally transported in the shipping container. The unusual hazard is created when

the item is reloaded. The bare unit is sometimes reloaded when the helicopter is on the ground with the helicopter rotors still turning and building up ESD charge. This reload scenario is done in dry areas without a proper ground being available.

Mil-I-23659 is often used to test the electroexplosive devices inside a weapon. The results from Mil-I-23659 are sometimes used instead of the 25,000 volt test in Mil-Std-331. The direct application of the 25,000 volt potential to the leads of the EED is considered a worst case scenario.

Some specifications are fairly consistent on the issues of humidity and temperature. The humidity is usually set at 50% maximum. The temperature requirements are in the 70-80 degree F range. The ramifications of the temperature and humidity requirements will be discussed further in the engineering analysis section.

## THE MATCH BETWEEN ORDNANCE AND ESD REQUIREMENTS

Weapon systems have been evolving rapidly from an ESD perspective. The specifications being used today were devised when the weapons world was far simpler. Thirty years ago, the typical weapon consisted of a nonmetallic explosive or propellant contained in a metal case or chamber. The igniter or detonator used a metal bridge wire. The trend for years has been to add more metallic ingredients to the propellants and explosives. Weight, cost and sometimes stealth have required the increased use of nonmetallic cases, chambers and shipping containers. The effects on ESD sensitivity can be disastrous and apparently unexpected.

The accidental ignition of a Pershing II rocket in Germany in 1985 was attributed to ESD.[5] Cold temperatures made the problem more severe. The propellant in the Pershing is more sensitive at cold temperatures. No requirement exists to test at cold temperatures. No specific requirement exists to test or evaluate a complete weapon system.

The conventional wisdom is that to dissipate ESD, the volume resistivity of a propellant should be as low as is practical. Unfortunately, if 300,000 volts is impressed on a low volume resistivity propellant, the greater the probability the discharge will find a path to ground through the propellant. There is a large difference between 25 and 300kV in terms of energy delivery. The energy from the capacitive ESD test equipment is calculated from $^1/_2CV^2$. C is the system capacitance and V is the voltage of the test. The required series resistance in the 25 kV test is 5000 ohms versus 1 ohm in the 300 kV test. The 300 kV tests can deliver as much as 1,440,000 times more energy than the 25 kV test for test samples with very low resistivity. For test samples with high resistivity, the difference between the 300 kV and 25 kV tests can drop as low as 288 times as much energy.

One helicopter transported item tested by the Electronic Systems Development Branch illustrates the evolutionary changes in weapons that have been occurring. The initiator was a common percussion primer. The explosive contained about 30% aluminum. The body was made of polyurethane foam. Ordinarily, percussion initiated devices would not be ESD tested. The fuze with the percussion primer was metal encased and was not sensitive to ESD at either 25 or 300 kV. The urethane foam body

exploded on the first 300 kV discharge to the body. The wall thickness of urethane foam protecting the explosive charge was about one centimeter. The dielectric strength of polyurethane foams is about 50-100 kV/cm. The path of least resistance was clearly through the foam wall and explosive and not around the circumference of the body. The item withstood intensive 25 kV testing. The outside of the item was modified with the addition of a metallic shield and retested successfully.

The present requirement specifications have centered on electroexplosive devices (EED) in the weapons. The EED world has been dramatically changing. The choices for ignition and detonation are now many. Examples are, exploding foil (slapper), semi conductor bridge (SCB), laser, and exploding bridgewire to name a few. Some devices are now hybrids of several initiation methods. The changes are not inherently bad, in fact some new methods are much less ESD sensitive. The traditional patterns and test sequences may not adequately expose ESD vulnerability. The old "weak" link may no longer be the EED. For example, SCB devices are particularly sensitive to polarity. Bridgewire devices are not polarity sensitive.

The 300,000 volt ESD test is considered to be a worst case helicopter discharge. Some devices may be susceptible to lower voltages because of physical configuration or break down paths. Mil-Std-331 mentions the lower voltages for "informational testing" only. The linearity of the response of various devices has not been established. Hazards of Electromagnetic Radiation to Ordnance (HERO) testing is performed over a range of frequencies to look for excitation levels or a response. Vibration testing looks for resonance responses. ESD testing does not require consideration of or search for responses at different voltages.

The current requirements allow a wide range of pulse characteristics. The ESD pulse can vary from underdamped to overdamped decaying exponential waveforms. The wave forms can occur in a wide band of frequencies. Additional work is necessary to determine the characteristics of a helicopter borne discharge and transform the information into a repeatable test. If the helicopter discharge characteristics vary, the ESD test characteristics should also be varied.

## ANALYSIS

A proper ESD engineering analysis should require review of several factors. The first is the geometry of the item under consideration. The shape and wall thickness of a test object are very important. Discontinuities, joints and fasteners merit special attention. The construction materials and the electrical properties of the materials must always be considered. Since the Pershing incident, the need to better understand the electrostatic discharge phenomena in solid rocket motors was recognized.[6] Five electrical properties are getting particular attention. The most interesting is percolation breakdown coefficient. The coefficient has been extensively measured by the French Societe National Des Poudres Et Explosifs (SNPE). The French have now adopted a refined "P breakdown percolation" coefficient equation. The refined equation considers density, % weight, diameter of finest fraction of conducting and non-conducting

particles. The density, volume resistivity and percent weight of the binder are also considered. The second electrical property test is the RC discharge-test. The RC test is performed with 30 kV on a propellant cylinder. If any of the 90 firings react, the propellant is considered sensitive. The third property is surface and volume resistivity as a function of temperature. The fourth electrical property is dielectric constant. The last property of propellants is dielectric breakdown strength.[6] The electrical properties mentioned are typically measured at 30-40kV. The effects due to the much higher and far more powerful 300 kV test are not known.

The implementation of any analysis requirements must consider the lack of data for certain properties. Because the electrical properties in question are not commonly used, they are typically not measured. The formulation of propellants and explosives is not enough information. The ESD related data available for explosives and propellants is typically an overall test result such as ESD sensitivity. Even the ESD data is not determined at the same temperatures or relative humidity. The electrical or ESD results are very variable relative to particle size, temperature and humidity. The loading facility environmental conditions may greatly influence the ESD sensitivity of a particular propellant or explosive. The use of salients during ESD testing needs to be standardized.

## TEST METHODS

The test methods required currently need to be reviewed. The most obvious starting point is the requirement to test at two set voltages, either 25,000 or 300,000 volts. There is provision to test at other voltages for informational purposes in Mil-Std-331, but no requirement exists. The ESD tests are typically performed as a go or no/go test. The relative factor of safety or closeness to passing or failing is not determined. The current and/or voltage that is passing through the EED is not measured. Some items tested by the Electronic Systems Development Branch pass the ESD test, but the change in the resistance in some of the EEDs after testing shows that the test is very stressful to the bridge wires in the EEDs. The change is a small but consistent drop in resistance through the initiator bridgewire. One initiator manufacturer has noted the change in their own ESD testing and have attributed the change to reheating of the bridgewire tack welds. The all fire and no fire data of a specific EED may be of very limited use since the ESD pulse duration is very short. The firing times are measured in milliseconds, the ESD pulse time is in microseconds.

No measurement of the current or voltage in the EEDs undergoing testing is required at this time. Voltage and current readings should be in conjunction with but never instead of explosive testing. No model and/or sufficient data exists to extrapolate the voltage and current data to the real world response of a multicomponent explosive device.

## CONCLUSIONS

A specification mandated requirement to test or at least analyze complete weapon systems is needed. The push to reinvent government, eliminate unfunded mandates and regulation has created a hostile environment for Military Standard requirements. Unfortunately safety test requirements are not always distinguished from item purchase description type military specifications. The requirement for analysis should be strengthened and standardized. Test instrumentation should be standardized. The test environment parameters should be standardized. Propellants with heightened sensitivity at temperature extremes should also be tested at those extremes.

ESD testing must be more than a go or no/go test. The current and or voltage flow to the EEDs should be measured as it is done for HERO testing in order to determine a relative factor of safety. Go or no/go testing gives very little information in this regard, especially with the small sample sizes required. A formal check list of potential problem areas should be established to require all testing facilities to address the same issues on each item evaluated. A form with the words 'not applicable' written next to a potential concern is far preferable to the present vague and open-ended requirements.

The most logical means of implementing these requirements would be to add them to an existing specification. Mil-Std-331 is the most comprehensive specification and the best vehicle to move forward as needed.

## REFERENCES


1. Military Standard, "Fuze and Fuze Components, Environmental and Performance Tests for" Mil-Std-331B, Notice 3, 1 December 1992.

2. Military Standard, "Electroexplosive Subsystems, Electrically Initiated, Design Requirements and Test Methods" Mil-Std-1512 , 21 March 1972.

3. Military Specification, "Initiators, Electric, General Design Specification for" Mil-I-23659C , 31 August 1972.

4. Standard NATO Agreement, "Electrostatic Discharge, Munitions Test Procedures" STANAG 4239 Draft Edition 1

5. P. W. Gibson, "Air Force Solid Rocket Motor Electrostatic Hazard Assessment" AFRPL-TR-86-075, October 1986, Air Force Rocket Propulsion Laboratory.

6. J. Covino and F. E. Hudson, III " Dielectric Breakdown and Dielectric Strength Measurements for Propellants and Propellant Ingredients". Dec 1987 Meeting Paper; CPIA-PUB-480-VOL-5

# DEMONSTRATION OF THE USER-FRIENDLY FAA RESEARCH ELECTROMAGNETIC DATABASE

*D. J. Grush, E. L. Webb, D. E. Evans
Idaho National Engineering Laboratory
P.O. Box 1625, Idaho Falls, ID 83415

The FAA Research Electromagnetic Database (FRED) is available with a greatly improved user interface, new capabilities, and additional data. FRED now uses the power of the user's PC and the capabilities within Windows to provide a point-and-click interface. An overview plot of each waveform is stored in the database and is displayed automatically when the electromagnetic parameters for the waveform are viewed. The entire waveform or a subset of the data points can be plotted, manipulated through FRED's analysis capabilities, or downloaded to the user's PC for use in local analysis programs. The interface allows multiple windows to be open simultaneously, and therefore data on different strikes or waveforms can be compared easily. The Windows' printer drivers, display color and font selections, and PC applications are available for use with the data. Many other new features have also been incorporated.

In addition to the new capabilities and improved user interface, FRED contains new data. The CV-580 data has been supplemented with NASA F-106 digital data. The conversion of the French C-160 Transall data is in progress. The expanded base of data means the user can access gigabytes of data to perform safety analyses and research. All data conversion to FRED is validated by the FAA through the original research organization that collected the data.

The online demonstration of FRED will provide an overview of all the capabilities and data sources. Hands-on use by the conference attendees will also be encouraged. FRED is a valuable tool for the lightning research community. Its new capabilities, new look, and expanded data set make it an even greater asset to the researcher.

# AUTOMATIC LIGHTNING WARNING SYSTEM FOR INDIAN HEAD DIVISION, NAVAL SURFACE WARFARE CENTER: A CASE STUDY

Mr. Christopher R. Karabin
United States Navy Technical Center for Explosives Safety
Indian Head Division, Naval Surface Warfare Center
Indian Head, Maryland 20640

## ABSTRACT

The United States Navy Technical Center for Explosives Safety at Indian Head Division, Naval Surface Warfare Center, Indian Head, Maryland (IHD/NSWC) is the technical agent for lightning warning system policy for all Naval and Marine Corps explosives areas. In support of this function, an automatic lightning warning system utilizing National Lightning Detection Network™ data was implemented at IHD/NSWC. This paper discusses the design, implementation, performance, and lessons learned. Many of these experiences will be developed into new Navy policy.

## 1.0 Introduction

The intent of this paper is to (1) review existing lightning warning system regulations, (2) discuss the design of the alarm delivery system, (3) provide a description of Indian Head's automatic lightning warning system (current configuration), and (4) discuss the system's performance, lessons learned, and modifications. The data presented was acquired during an analysis period beginning 10 May 1995 and ending 8 August 1995.

## 2.0 Lightning Warning System Regulations

The following paragraphs provide background information about existing lightning warning system regulations and Indian Head's local Thunderstorm Action Plan.

### 2.1 Department of Defense Standard 6055.9

DOD-STD-6055.9 - Ammunition and Explosives Safety Standards requires lightning protection for ammunition and explosives facilities but does not *require* lightning warning systems. 6055.9 permits omission of physical lightning protection systems for facilities when the facility has a "local lightning warning system to permit operations to be terminated before the incidence of an electrical storm if all personnel can and will be evacuated... and the damage from a lightning strike is acceptable to the Military Service." This exception permits activities to secure a facility and evacuate personnel rather than design and construct an external lightning protection system for the facility. This is often the most reasonable plan especially for relatively small explosives operations taking place in relatively large facilities.

However, no specific design or performance requirements for lightning warning systems are given.

## 2.2 Naval Sea Systems Command OP 5

NAVSEA OP 5 - Ammunition and Explosives Ashore, Safety Regulations for Handling, Storing, Production, Renovation, and Shipping reiterates the 6055.9 exception and provides additional information about lightning warning system technology. The Navy requires the lightning warning system be "adequate". NAVSEA OP 5 requires planning and specific actions when thunderstorm conditions are issued but provides no minimum requirements for the design or performance of the lightning warning system itself:

1) Installations with lightning warning systems shall establish a specific criteria in their destructive weather plan, destructive weather bill, etc., detailing how the lightning warning hardware will be used in terminating ordnance operations at the approach of a thunderstorm.

2) Facilities that use the electric field gradient indication as their only storm warning system shall immediately terminate ordnance operations when the electric field gradient exceeds 2,000 volts per meter and remains at that level or continues to increase in magnitude.

3) In cases where the facility has in place other storm warning systems, the indications from these systems together with the electric field gradient indication will be used to determine when to terminate ordnance operations.

4) The hazardous weather plan shall detail specific criteria for the evacuation of personnel.

5) In no case shall a storm approach closer than five miles before an ordnance operation is terminated.

## 2.3 Indian Head Instruction 3006.23 - Thunderstorm Action Plan

Indian Head's local Thunderstorm Action Plan implements the requirements of NAVSEA OP 5. The plan contains a description of the lightning warning system components and the specific actions required upon receipt of thunderstorm conditions.

The Thunderstorm Action Plan maps lightning warning system range alarms into operational requirements for securing and shutting down explosives operations. Previous procedures required termination of explosives operations as quickly and safely as possible after lightning is seen or heard. Personnel are not to rely solely on the lightning warning system. However, when lightning warnings are issued, the following specific actions are required:

Thunderstorm Condition III - Lightning occurring within thirty-five miles

1) Departments prepare/plan to cease explosives operations.

2) Ordnance handling operations that will take more than three hours are postponed and rescheduled.

3) Careful consideration should be given to starting any explosive loading cycle.

Thunderstorm Condition II - Lightning occurring within ten miles

1) Handling or processing explosives should proceed to a completion point.

2) Secure open magazines.

3) Do not start any explosive mixing cycle not already in progress.

Thunderstorm Condition I - Lightning occurring within five miles

1) Cease all explosives operations, except those identified in each department's plans. Secure all main power switches in facilities without lightning surge protection, and evacuate personnel to the designated safe locations.

2) Operations shall not be shut down for processes where the shut down creates a greater risk to the facility and personnel than the thunderstorm. These facilities are identified in each department's safety approved evacuation plan.

3) Motor vehicles containing ammunition shall, if possible, be placed in an area equipped with primary lightning protection. Loading or unloading is prohibited.

4) The destruction of ammunition, explosives and other hazardous materials as well as explosives tests and operations incidental thereto shall cease.

5) Cease all fueling operations.

6) Cease all high work (such as electrical power line work, tree cutting/trimming, water tower painting, etc.)

Thunderstorm Condition All Clear - No lightning within thirty-five miles in last 15 minutes

1) Operations may resume.

**3.0 Performance Specification (Ideal)**

The ideal lightning warning system for Indian Head would have the following performance specifications and features:

1) Predict with 100% reliability when cloud-to-ground lightning will and will not occur within the perimeter of Indian Head.

2) Predict with 100% reliability the location of the cloud-to-ground lightning with a prescribed location error so specific planning of explosives operations can occur.

3) Provide sufficient warning time so safe termination of explosives operations and efficient planning of new explosives operations can occur.

4) Provide 100% coverage with 100% reliability so all personnel receive all lightning warnings without the need for exposed human messengers. Provide an acknowledgment feature so receipt of new thunderstorm conditions can be documented and verified.

5) Provide continuous service. Be automatic so human resources are not required for the operation of the system.

6) Be reasonably affordable so the system can be used throughout the Navy and Marine Corps.

While no lightning warning system can offer all of these features today, the continuous improvement of the system is directed toward these goals.

## 4.0 System Design Issues

Of the many design issues were encountered during the design and implementation of the lightning warning system, the design of the alarm delivery system was most difficult.

## 4.1 Alarm Delivery System Design

Indian Head contains many explosives manufacturing facilities where flammable gases, vapors, fumes, and combustible dusts normally exist. It is critical explosives personnel working in these areas have direct and immediate access to lightning warnings.

Selecting a medium for delivering thunderstorm conditions was extremely difficult because of the variety of people, locations, explosives operations, and facilities involved. Indian Head decided on a signaling system consisting of a combination of the telephone and paging systems to obtain the most effective and economical lightning warning delivery system. The telephone system is used to transmit area alarms to specific buildings and areas. The paging system transmits individual alarms to specific personnel independent of location. Indian Head combined these two methods to provide personnel complete, timely, and economical coverage. The telephone system is preferable wherever personnel are centrally located. The paging system is preferable wherever personnel are mobile, remote, or otherwise inaccessible by telephone. The paging system delivers thunderstorm conditions much faster than the telephone system and is therefore recommended wherever urgent notification is required.

During system design, many different delivery systems were considered before the combination system was selected. Below is a description of all systems considered.

### 4.1.1 Sirens

A siren has the capability of reaching everybody in a short amount of time but has no provision for acknowledgment. At Indian Head, an analysis showed two sirens would not be heard by all personnel in all facilities during all explosives operations. Distance (remoteness), attenuation (due to facility construction), and local equipment (background) noise would prevent complete coverage. Also, a siren would have to transmit different signals for each of the different lightning warnings. These signals would be susceptible to misinterpretation.

### 4.1.2 Fire Alarm System

Existing fire alarm system wiring at most explosives facilities could be used in lieu of telephone service installation but only at great expense. The fire alarm system could be used to broadcast area alarms and receive acknowledgments. However, the reliability of both the fire alarm system and the lightning warning system would be reduced because of shared wiring. Also, it is not cost

effective to provide area alarming for magazines because of the large number of magazines and relatively few (infrequent) magazine operations. It is much more cost effective to provide individual alarms for the personnel performing magazine operations.

### 4.1.3 Radios

Radios provide individual coverage because radios are normally associated with specific personnel independent of personnel location or mobility. Like sirens, radios have a broadcast capability allowing all personnel to be contacted quickly. Radios provide two-way communication capability which permits warning signal acknowledgment. Indian Head's radio system provides complete signal coverage but radios are not permitted in most explosives facilities because of the hazards of initiating explosives from emission of radio frequency energy. Also, it is very costly to equip all personnel with two way radios.

### 4.1.4 Telephone System

The base telephone system cannot reach everybody with a need-to-know because of the lack of telephone service and the mobile nature of many explosives operations. Since personnel are at storage facilities infrequently and for relatively short periods of time (during loading, unloading, and inspection operations), installation of telephone service is not cost effective. Secondly, many explosives operating areas require intrinsically safe or explosion proof equipment because of the hazardous (explosive) atmospheres normally present. Explosion proof telephone equipment is prohibitively expensive. Even if telephone service was installed in all explosives facilities, mobile or in-transit personnel would not receive coverage. Like radios, cellular telephone equipment is not permitted in most explosives areas because of the hazards of initiating explosives from emission of radio frequency energy. Also, the telephone system cannot normally broadcast a message to multiple parties. Therefore, multiple simultaneous calls are required or the call list must be kept very short or unnecessary warning delays will result.

### 4.1.5 Human Messengers

Human messengers were considered but quickly dismissed because of the obvious shortcomings of sending personnel out during the approach of thunderstorms. Also, the spatial extent of Indian Head is large enough that multiple messengers would be necessary or unnecessary warning delays would result.

### 4.1.6 Paging System

Indian Head personnel operate and support a Motorola based paging system providing local coverage extending over the entire perimeter of the station. The transmitter is located on top of a water tower, one of the highest points on the station. In the past, the transmitter has been disabled by lightning activity. Today, new cabling techniques, surge suppression hardware, and proper bonding and grounding have increased the reliability of the system.

It is critical all paging equipment (indeed all electrical equipment) be suitable for use in all explosives areas with hazardous

(classified) location designations. Indian Head has performed an analysis which shows the Motorola Director II pagers in use at Indian Head are intrinsically safe (as defined by the National Electrical Code and the Instrument Society of America) for all explosives areas at Indian Head. This means the pagers are not capable of delivering sufficient energy to ignite any of the hazardous atmospheres that may be present in any of Indian Head's explosives areas.

Another concern was the time it would take to sequentially page over one hundred pagers. To reduce pager delay time, a 'group call' (broadcast) was created. This permits the paging system to contact over one hundred pagers simultaneously. Unfortunately, the pager hardware necessary to create a group call was not present in pagers procured before the development of the lightning warning system. The cost of parts and labor to modify the existing pagers was comparable to the cost of procuring new pagers. This prompted the decision to procure new pagers for all personnel requiring lightning warning notifications and transfer existing pagers to personnel not requiring lightning warning notifications.

Pagers do not have acknowledgment capability so the lightning warning system has no means of verifying all pager alarms are received. Pagers with acknowledge capability are essentially radios and have all of the problems of radio equipment described above. The benefits of paging equipment (individual alarms, complete coverage, very short delay times, high reliability) are more critical than the lack of acknowledgment problem. The search for pager acknowledgment methods will continue as the warning system is continuously improved.

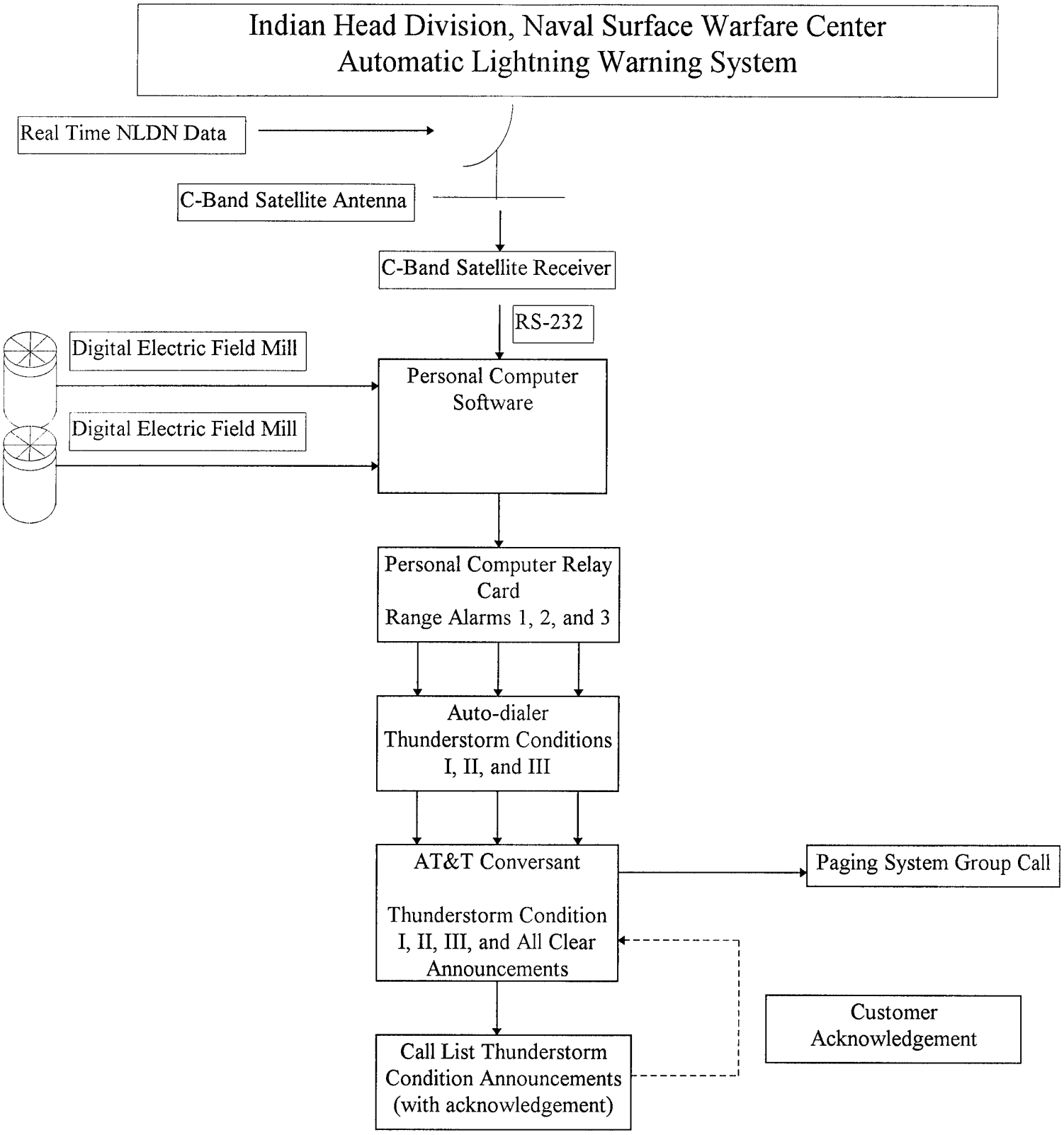
Generally, pagers are carried so tlightning warnings are received regardless of location. However, the benefits of area alarming can be realized by "stationing" pagers in facilities or vehicles. "Stationed" pagers can be installed in facilities and attached to signal lights or audible alarms so all personnel in the area receive the area alarm without having to provide all facility personnel with pagers. An electrical explosives safety analysis must be performed to ensure the pager and associated apparatus are not an electrical hazard to the explosives operations and personnel located in the facility.

## 5.0 Lightning Warning System Description

The following paragraphs describe the components of Indian Head's lightning warning system.

### 5.1 National Lightning Detection Network™ (NLDN) Station

The heart of Indian Head's lightning warning system is an NLDN station consisting of a satellite antenna and receiver, personal computer, software, and personal computer relay card. The station receives NLDN data and closes one or more range alarm relays when lightning occurs within one or more of the preprogrammed range boundaries surrounding Indian Head. The relay closures start the auto-dialer described above.


Indian Head Division, Naval Surface Warfare Center
Automatic Lightning Warning System
Real Time NLDN Data
C-Band Satellite Antenna
C-Band Satellite Receiver
RS-232
Digital Electric Field Mill
Digital Electric Field Mill
Personal Computer Software
Personal Computer Relay Card
Range Alarms 1, 2, and 3
Auto-dialer
Thunderstorm Conditions
I, II, and III
AT&T Conversant
Thunderstorm Condition
I, II, III, and All Clear
Announcements
Paging System Group Call
Customer Acknowledgement
Call List Thunderstorm Condition Announcements (with acknowledgement)

### 5.1.1 Secondary NLDN Display Station

The Test and Evaluation Department performs outdoor explosives operations that cannot easily be terminated once initiated. These operations take place along the southwest station perimeter along the Potomac River and involve many personnel. (Thunderstorms usually approach from the southwest and are usually first observed by Test Department personnel). The duration of these operations can be ninety minutes or more. Because the lightning warning system issues warnings only when lightning occurs within thirty-five miles, sufficient warning time is not provided.

The Test and Evaluation Department decided to procure an NLDN display terminal to assist in daily explosives operations planning. The Test and Evaluation Department may not use the NLDN data to make operational decisions that conflict with the required actions contained in Indian Head's Thunderstorm Action Plan. I.e. the NLDN display terminal provides additional information that may only be used for planning. The terminal may not be used to override, exempt, or supersede the requirements of the Thunderstorm Action Plan.

### 5.1.2 Satellite Antenna and Receiver and "Rain Fade"

The satellite antenna and receiver receive real-time NLDN data under licensed agreement from GDS Incorporated, Tucson, Arizona. The satellite receiver delivers lightning data to the personal computer via the computer's 9-pin, RS-232 serial communications port.

Originally, the satellite system technology (KU-band) was susceptible to "rain fade". Rain fade occurs during heavy precipitation and causes temporary signal loss. Rain fade occurred several times during heavy rainfall before the analysis period. The duration of the outage was usually no more than a few minutes. Rain fade had little effect on warning system performance because rain fade usually would not occur until after Thunderstorm Condition I had been issued. Today the satellite system utilizes "C-band" technology which is not susceptible to rain fade.

## 5.2 Personal Computer, Software, and Relay Card

The personal computer is a 386 based machine with standard options. The computer receives real time lightning data from the satellite system. The software displays, archives, prints lightning data and closes the appropriate range alarm relay whenever lightning flashes occur within one or more of the range alarms.

## 5.3 Range Alarms

An inactive range alarm is asserted immediately after the NLDN detects and reports a lightning flash inside of the range. The range alarm remains asserted until there are no new flashes inside the range for fifteen minutes. Indian Head's lightning warning system has three range alarms as shown below. Range alarm three is intended to indicate atmospheric instability in the region and to provide early warning of the possibility of local instability. Range alarms two and one indicate local instability.

**Lightning Warning System Range Alarms**

| Range Alarm Number | Width of Range Alarm (Nautical Miles) |
|---|---|
| III | 35 |
| II | 10 |
| I | 5 |

### 5.4 Auto-dialer

A Kaye Instruments "Dialog™ Plus" auto-dialer inputs relay closure signals from the relay card in the NLDN station and starts the AT&T Conversant™ system by dialing the Conversant™ system on a dedicated telephone line. After Conversant™ answers the call, the auto-dialer transmits the new thunderstorm condition with a sequence of touch tones. Conversant™ then acknowledges the auto-dialer with an acknowledge sequence of touch tones. The auto-dialer will terminate only if the acknowledgment tones are received ensuring new thunderstorm conditions are never forgotten, missed, or ignored by Conversant™.

### 5.5 AT&T Conversant™

AT&T's Conversant™ is a programmable telephone voice system normally used to implement various automatic, interactive telephone services including auto-attendants, voicemail, and menu driven financial information and transaction systems. At Indian Head, Conversant™ was selected to automate the signaling mechanism of the warning system. When triggered to issue a new thunderstorm condition, Conversant™ performs the following functions to transmit the warning to all pagers in the group call, and all personnel on the predetermined call list.

1) Conversant™ answers the auto-dialer call. Conversant™ accepts the new thunderstorm condition code from the auto-dialer. The condition code is simply a sequence of four touch tones. Conversant™ validates the thunderstorm condition code and then acknowledges the auto-dialer with a sequence of touch tones. The acknowledge tones disable the auto-dialer until the next thunderstorm condition is asserted.

2) Conversant™ calls the paging system and announces the new thunderstorm condition to all pagers in the group call as described above.

3) Conversant™ calls the next primary telephone number on the predetermined call list starting with the first primary telephone number.

4) Conversant™ determines the result of the phone call. Possibilities are answered, no answer (maximum of three rings), busy, or error.

5) If the primary telephone call is answered, the prerecorded thunderstorm condition is announced and # (pound) key acknowledgment is requested. If acknowledgment is received, the call list telephone number is marked "successful" and the next primary telephone number is called (Step 3).

6) If acknowledgment is not received, or if the telephone call is not answered, busy, or in error, the secondary telephone number is called and Steps 4 and 5 are repeated. If the secondary call is not completed, the

number is skipped and Conversant™ continues with the next telephone number on the call list. (Step 3).

7) When all calls have been completed, Conversant™ terminates and remains inactive until the next call from the auto-dialer.

### 5.6 Paging System

The group call pagers are activated with a single telephone call to the paging system. After the paging system answers the call, the group call identification number is entered to tell the paging system the announcement is intended for all pagers in the group call. Next, a spoken announcement is recorded by the paging system. After recording is complete, the paging system transmits signals via the paging system transmitter to activate all group call pagers. Finally, the recorded announcement is transmitted to all activated pagers for all users to hear. The paging system is called automatically from the AT&T Conversant™ system.

### 5.7 Lightning Warning System Call List

The call list contains of a wide variety of organizations at Indian Head with a need for thunderstorm condition information. The organizations are called sequentially from top to bottom. The intent is to follow the pager group call with telephone calls to administrative personnel. The telephone calls allow management to plan for shutdown of current operations and startup of new operations in accordance with the Thunderstorm Action Plan. These calls also provide a second means of delivering thunderstorm condition information to explosives workers. These calls are not to be used as the primary method of receiving thunderstorm conditions. Pagers are to be used wherever quick and reliable information is required.

The Ordnance Department is first on the call list because most of the highly susceptible explosives manufacturing and handling operations are performed by the Ordnance Department. The Research and Technology Department handles relatively small quantities of explosives in a laboratory environment without elaborate external or internal lightning protection systems. The Test and Evaluation Department performs outdoor ballistic testing of various size explosives devices. The Public Works Department has a large number of exposed work

**Lightning Warning System Call List**

| Call Sequence Number | Organization |
|---|---|
| 1 | Paging System (Group Call) |
| 2-7 | Ordnance Department |
| 8-9 | Research and Technology Department |
| 10-14 | Test and Evaluation Department |
| 15 | Cartridge Actuated Devices Department |
| 16-18 | Public Works Department |
| 19 | Security Department |
| 20 | Safety Department |
| 21 | Morale, Recreation, and Welfare |
| 22 | Swimming pool |

crews and contractors with a clear need for thunderstorm condition information. The Security department has personnel stationed at entry gates and on patrol. The Safety Department evaluates system performance and inspects for compliance with the Thunderstorm Action Plan. Morale, Recreation, and Welfare manages various outdoor activities including the golf course, softball league, volleyball league, outdoor concerts, a daycare center, and the swimming pool.

### 6.0 Performance Evaluation

The following paragraphs describe several observations of the lightning warning system during the evaluation period.

### 6.1 Alarm Bouncing

Frequently during the evaluation period, an alarm was asserted, released, and reasserted again within a short amount of time. We refer to these occurrences as "bounces". The "reassertion time" is the time between the alarm is released and then reasserted. Bounces are a side effect of thunderstorm conditions generated automatically and solely from range alarms. Bounces reduce user confidence in the system because the system appears uncertain or unstable. Bounces occur when lightning activity occurs along the edge of a range alarm boundary or when numerous thunderstorms occur in the region. The shorter the reassertion time, the more unstable the system appears to be. During the analysis period, the following bouncing statistics were obtained.

**Bouncing Statistics**

| Bounce Sequence | Number of Occurrences with Reassertion Time of Twenty Minutes or Less | Number of Occurrences with Reassertion Time of Fifteen Minutes or Less |
|---|---|---|
| III, All Clear, III | 33 | 30 |
| II, III, II | 5 | 3 |
| I, II, I | 5 | 4 |

If the maximum undesirable reassertion time is added to the minimum range alarm assertion time, all undesirable bouncing is eliminated. Currently, the minimum range alarm assertion time is fifteen minutes. If increased to thirty minutes, virtually all undesirable bouncing is eliminated. Increasing the minimum assertion time also increases the minimum operations shutdown time. Thirty minutes is not expected to significantly impact operations at Indian Head although further consultations are necessary before implementation.

### 6.2 Repeated Alarms

Repeated alarms are a form of bouncing where the reassertion time is so short, the reasserted alarm is reissued before the released alarm. This often confuses the user because the same alarm is issued twice. Numerous repeated alarms were issued during the analysis period and are shown below.

**Repeated Alarm Statistics**

| Repeated Alarm | Number of Repeated Alarms During the Analysis Period |
|---|---|
| III | 22 |
| II | 5 |
| I | 3 |

Repeated alarms can be prevented with Conversant™ programming. Conversant™ merely needs to compare the new alarm with the current alarm. If the alarms are the same, then a new thunderstorm condition need not be issued. This modification will ensure every thunderstorm condition issued is different from the current condition.

### 6.3 Range Skipping

Ideally, the transition of thunderstorm conditions follows the following pattern: III, II, I, II, III, All Clear. During the analysis period, one or two range alarms were skipped numerous times as shown in the table below:

**Multiple Range Transitions**

| Range Alarm Transition | Number of Occurrences During the Analysis Period |
|---|---|
| All Clear - II | 2 |
| All Clear - I | 1 |
| III - I | 6 |
| I - III | 5 |
| I - All Clear | 1 |
| II - All Clear | 3 |

The value of electric field mill data is clearly demonstrated in the above table. Lightning activity originated over Indian Head once with no warning. Thunderstorm Condition I was entered six times with a prior Thunderstorm Condition III warning and without a prior Thunderstorm Condition II warning. Thunderstorm Condition II was entered twice without a prior Thunderstorm Condition III warning. The All Clear to Thunderstorm Condition I transition clearly demonstrates the inability of NLDN data to consistently predict lightning activity. The need for an additional prediction capability is clear. Indian Head will utilize electric field mill data to help fill this void.

## 7.0 Lessons Learned

### 7.1 Uninterruptible Power Supply

The design of the lightning warning system included plans for uninterruptible power supplies but the system was activated before supplies were installed. On the very first evening of activation, the Conversant™ system was disabled by a power failure due to lightning. Records indicate the failure duration was one hour and occurred seventeen minutes after Thunderstorm Condition I was issued.

### 7.2 Termination of Lightning Warning "All Clear" Alarms

Soon after the warning system was activated, most weekend alarm calls were unanswered until the following Monday morning. Shutting off the warning system on weekends was not practical because some explosives operations take place on weekends. Occasional second and third shift explosives operations and twenty-four hour security patrols require twenty-four hour thunderstorm condition reporting. So deactivating the system

during certain periods is not a viable option.

To solve the problem, Conversant™ programming was modified to self terminate after ten passes through the call list when the thunderstorm condition is "All Clear". This change allows the Conversant™ to terminate when one or more of the telephone numbers is not answered for a long period of time and the thunderstorm condition is known to be "All Clear". During thunderstorm conditions other than "All Clear", Conversant™ endlessly calls all unanswered and unacknowledged telephone numbers remaining on the call list.

### 7.3 Answering Machines

Soon after the lightning warning system was activated, an unexpected anomaly was discovered. Two of the telephone numbers on the call list were connected to answering machines during non-office hours. When thunderstorm conditions are issued during non-office hours, the lightning warning system persistently and relentlessly calls all telephone numbers on the call list until acknowledgment is received from every number. The answering machines were not able to acknowledge the alarm calls. By morning, the answering machine tapes were full of thunderstorm condition announcements. Two solutions were employed to solve the problem. The lightning warning system disconnects the call if unanswered after three rings. If answering machines are configured to answer after four rings, the alarm call will never be answered and never recorded.

The other solution is simply to change the telephone number to a number not connected to an answering machine. Most facilities at Indian Head contain multiple telephone extensions and changing to an alternate number is usually not a problem. However, in some facilities, incoming telephone calls are automatically routed to the next available extension making it impossible to separate incoming telephone calls from the attached answering machine. In these cases, the answering machine must be reconfigured to answer after four rings.

### 7.4 Rotary Telephones

One of the customers on the call list used a rotary telephone. The first activation of the warning system proved to be a very frustrating afternoon for the rotary phone customer. After announcing the new thunderstorm condition, Conversant™ requests acknowledgment by asking the customer to press the pound key (#). The rotary telephone customer, of course, could not "press" pound and thus could not acknowledge the call. After the first half hour of repeated thunderstorm condition calls, the customer placed his receiver "off hook". Fortunately, the customer had an alternate touch tone telephone number. The lightning warning system call list was modified appropriately.

## 8.0 Proposed Modifications

### 8.1 Range Alarm II Expansion

During the period 10 May 1995 to 15 June 1995, the minimum time for a thunderstorm to progress from range two to range one was 6 minutes 18 seconds.

This time is inadequate for explosives operations to be terminated and for personnel to evacuate explosives areas. Consequently, on 6 June 1995, range two was expanded from 20 nautical miles to 27.5 nautical miles. For the period 6 June 1995 to 1 August 1995, the minimum time for a thunderstorm to progress from range two to range one was 16 minutes 10 seconds. We do not expect 16 minutes to be the new minimum. However, we do expect the average minimum time to increase.

**Range Alarm Boundaries**

| Range Alarm Number | Width of Range Alarm (Naut. Miles) |
|---|---|
| III | 35 |
| II | 10 |
| II (adjusted 6/15/95) | 13.35 |
| I | 5 |

### 8.2 Multiple Simultaneous Alarm Calls

Conversant™ has the capability of issuing multiple alarm calls simultaneously. Clearly, optimal performance is obtained when all numbers are called simultaneously. At this time, sufficient hardware is present for three to five simultaneous calls. However, a significant amount of programming overhead is involved with multiple simultaneous calls making the expected performance gains unclear. Testing is required before this option can be fully evaluated.

### 8.3 Lightning Warning System Service Review

Regulations currently do not require explosives personnel to test or evaluate the "adequacy" of their lightning warning system service. Currently under review is a proposed addition to explosives safety regulations to require a record (log) of all issued and received thunderstorm conditions. The log could be used to evaluate the "adequacy" of the lightning warning system. The review would be a relatively short affair and could be scheduled to coincide with required annual electrical explosives safety inspections. Each explosives area would be responsible for determining the adequacy of the service. Unsatisfactory evaluations could be forwarded to the local Safety Office or Commanding Officer for resolution.

### 8.4 General Condition Alarm System

At Indian Head, discussions are underway to utilize the lightning warning system's signaling system to transmit other important information directly to personnel in an efficient and controlled manner. Department of Defense and National Weather Service weather watches and warnings and other urgent information could be transmitted directly to personnel via the signaling system. These additional functions could be automated to a great degree by utilizing the flexible features of Conversant™.

### 8.5 Reminder Calls and the Thunderstorm Condition Hot Line

Currently, the lightning warning system signals a thunderstorm condition whenever a thunderstorm condition transition occurs. During the analysis period, many thunderstorm conditions were asserted for one hour or longer. If a thunderstorm condition is asserted before normal work hours, arriving

explosives personnel might not learn of the condition until the condition changes and a new condition is signaled.

The Conversant™ system could be programmed to periodically retransmit the current thunderstorm condition. Since Thunderstorm Condition III occurs much more frequently then Conditions II and I, it seems reasonable to retransmit Condition III less frequently than Conditions II and I. For example, perhaps it would be appropriate to retransmit Condition III alarms every thirty minutes and Condition II and I alarms every ten or fifteen minutes.

The Conversant™ system could also be programmed to establish a Thunderstorm Condition Hotline. The Hotline could handle multiple (three to five) incoming telephone calls. Callers could listen to a short prerecorded announcement of the current (real time) thunderstorm condition. With this capability, explosives personnel could obtain timely thunderstorm condition information before starting explosives operations.

Further consultations with users will be conducted before any modifications are implemented.

### 8.6 Electric Field Mills

The lightning warning system currently has two (inactive) electric field mills connected to the NLDN station personal computer. Indian Head agreed to perform a one year evaluation of the electric field mills to determine suitable alarm thresholds before inclusion in the system proper.

The first field mill is located on the southwest perimeter of the station where storms normally approach. The second field mill is located in the center of the station along a roadside. Proper calibration and enhancement procedures were performed at installation.

During the field mill evaluation period, the roadside electric field mill reported electric field levels over 2000 volts per meter on several occasions while the perimeter mill reported low levels. Since the second field mill is installed along a roadside and near a parking lot, diesel fuel exhaust can contaminate the local atmosphere and cause false alarms although this was never proven by observation.

Further data analyses are needed before the two electric field mills are incorporated into the lightning warning system.

# THE SELECTION OF PARAMETER VALUES OF NEGATIVE AND POSITIVE LIGHTNING FOR COMBINATION IN THE COMPOSITE TEST WAVEFORM

R H Evans and G A M Odam
GAO Consultancy, Barmouth, Gwynedd, UK
(Consultants, previously employed at RAE Farnborough)

## ABSTRACT

When tests to simulate the direct effects of lightning are being formulated it is common practice to base them on the published statistics of negative flashes to ground, with some increase in severity to allow for the more severe but much less frequent positive flashes. This paper proposes a more systematic method of combining the published parameters of negative and positive flashes in a way that takes into account any given relative frequency of occurrence that may be considered appropriate.

After establishing the combined statistical distribution of the three main parameters significant for direct effects (peak current, charge transfer and action integral), assuming a typical relative frequency of occurrence of negative and positive flashes, they are then discussed in relation to present specifications, particularly the composite test waveform. It is suggested that there is a case for increasing the values of charge transfer and action integral for ground and sea applications, but no changes are suggested for air applications.

## INTRODUCTION

The four parameters of lightning flashes which are the most important from the point of view of the hazards they present to aircraft and other materiel are:-

a) Peak current amplitude

b) Maximum rate of current rise

c) Charge transferred ($\int i\,dt$ coulomb)

d) Action integral or specific energy ($\int i^2.dt$ $A^2$ s, or J/ohm)

When lightning tests are being formulated it is necessary to decide what numerical level of these parameters should be incorporated in the current waveforms. Evidently the test parameters should bear some relation to those of real lightning flashes but these fall into several categories, such as:-

a) Natural or triggered by airborne vehicle

b) Inter-cloud, intra-cloud or ground flash

c) If a ground flash, is it positive or negative, and are the significant parameters those at ground level or at altitude.

This paper is mainly concerned with the direct effects of lightning and in particular the contribution of positive ground flashes, and it therefore does not enter into discussion concerning the maximum rate of current rise likely to be found in the various categories. It is generally agreed that the most severe direct effects are likely to be produced by parameters based on those of ground flashes measured at ground level, and of these the positive flashes are likely to be the most severe. However, since positive flashes are much less frequent than negative they must not be allowed unduly to influence decisions on test parameters. The present paper gives a method of combining the published parameters of positive and negative flashes in a way that takes into account any given relative frequency of occurrence that may be considered appropriate.

After establishing the combined statistical distribution of the three parameters significant for direct effects, assuming a typical relative frequency of occurrence of negative and positive flashes, they are then discussed in relation to present specifications, particularly the composite test waveform. It is suggested that there is a case for increasing the values of charge transfer and action integral for ground and sea applications.

## SUMMARY OF PARAMETER STATISTICS

The parameters of lightning flashes vary widely from flash to flash and are therefore best described in statistical terms, usually as a set of curves each plotting the percentage of flashes which are above a particular value for the parameter concerned. To accommodate a wide spread of values a logarithmic scale is often used for the parameter, and if a 'normal probability' scale is employed for the percentages then the curves take on the convenient form of straight lines, thus facilitating a small degree of extrapolation. However, the relationship is essentially empirical and it has to be remembered that the published graphs represent the best linear fit to the recorded data and are therefore surrounded by a zone of uncertainty even within the observed range. The statistical distributions employed here are largely based on the ground measurements of Berger, as analysed by Cianos and Pierce (1, 2), by Berger, Anderson and Kroninger (3), and by Phillpott (4). Some of the statistical distribution curves are reproduced in Reference 5.

Log normal plots for peak current and rate of rise are given in Fig 1, for negative and positive flashes. For the peak current in negative flashes, separate curves are given for the first return stroke and subsequent strokes; it is seen that the latter values are lower. It is also seen that there are more very high values of peak current in positive flashes than in negative flashes, but also more very low values (the two curves cross each other near the middle of the scale); thus positive flashes contain more extremes at both ends, or in other words, the standard deviation is higher. Charge transfer and action integral are plotted in Fig 2; it is seen that both these parameters are higher for positive flashes.

The median level (50% above) may be taken as typical but it is necessary for design and test purposes to decide what is the most severe level to be considered; usually the 2% level is chosen. Table 1 shows the 50% and 2% levels for the parameters of negative flashes. It also includes the typical (50%) level for the parameters of positive flashes. As mentioned above, the choice of the maximum level to be considered for positive flashes is complicated by the fact that positive flashes are much rarer than negative flashes, the proportion varying between 1% and 20% dependent on geographical location, the average being about 10%. For this reason it would be unrealistic to give the same weight to positive as negative flashes when devising design or test criteria, but on the other hand positive flashes cannot be ignored. As explained below, the 18% level for positive flashes has been included in Table 1.

TABLE 1 PARAMETERS OF GROUND FLASHES

| Parameter | Negative | | Positive | |
|---|---|---|---|---|
| | Typical 50% above | Extreme 2% above | Typical 50% above | Extreme 18% above |
| Peak current (kA) | 20 | 140 | 25 | 100 |
| Max rate of rise (kA/μs) | 22 | 100 | 2.5 | 10 |
| Charge transfer (coulomb) | 15 | 200 | 70 | 200 |
| Action integral (MJ/ohm) | 0.02 | 0.8 | 0.5 | 3.8 |

The inclusion of the 18% level for positive flashes is based on the argument by Phillpott (4) that there is a certain severity level of positive flashes (say m) which will give the same probability of aircraft loss as the 2% severity level of negative flashes, and the airworthiness authorities have in effect accepted the 2% negative level as giving an acceptable loss probability. Taking the ratio of negative to positive flashes as 9:1 (90% against 10%), the probability of loss for negative and positive strikes is 0.9 x 0.02 x s and 0.1 x m x s respectively, where s is the probability of loss given a strike to the aircraft. Equating the two expressions for equal probability of loss yields m = 0.18, that is 18% is the appropriate `severe` level for positive flashes.

## COMBINING THE PARAMETER STATISTICS

The above argument for using the 18% level for positive flashes is not entirely convincing and it is suggested that a more logically consistent method of combining the two sets of statistics is as follows. If for the parameter of interest, say peak current, we have the curves for the statistical distribution of negative and positive flashes respectively then we may take a particular value, say 100 kA, and read off the corresponding percentage levels from the two curves, say n% and p% respectively. For purposes of illustration we may take the proportion of positive flashes to be 10%, although the same method applies for any chosen figure. Then in 100 flashes there will be 90 negative flashes and of these 90 x n/100 will exceed 100 kA; there will be 10 positive flashes of which 10 x p/100 will exceed 100 kA. Of the 100 flashes therefore the total number exceeding 100 kA will be 0.9n + 0.1p. This therefore defines a point on the new combined statistical distribution curve, and we may repeat for other chosen values of current until sufficient points have been obtained to draw the curve. The `severe` level is now defined by the 2% point on this combined curve. Any change in the accepted statistics for lightning as a result of further measurement programmes will of course not affect the method of constructing combined curves, although the numerical results will be different. The process has been carried out for peak current, charge and action integral in Table 2 below and the results plotted in Fig 3. A linear scale has been employed for the parameter value because of the narrow range involved for the present purpose, but a logarithmic scale used for the percentages (a normal probability scale could have been used).

TABLE 2 DERIVATION OF COMBINED CURVES

| Current (kA) | 100 | 150 | 200 | 250 |
|---|---|---|---|---|
| Negative flashes (n%) | 5.0 | 1.8 | 0.85 | 0.48 |
| Positive flashes (p%) | 18.0 | 11.0 | 8.00 | 6.00 |
| 0.9n + 0.1p | 6.3 | 2.7 | 1.57 | 1.03 |

| Charge (coulomb) | 100 | 200 | 250 | 300 | 400 |
|---|---|---|---|---|---|
| Negative flashes (n%) | 7.0 | 2.0 | 1.40 | 1.0 | 0.60 |
| Positive flashes (p%) | 40.0 | 18.0 | 14.00 | 11.0 | 6.00 |
| 0.9n + 0.1p | 10.3 | 3.6 | 2.66 | 2.0 | 1.14 |

| Action int (MJ/ohm) | 0.5 | 1.0 | 2.0 | 3.0 | 4.0 |
|---|---|---|---|---|---|
| Negative flashes (n%) | 3.7 | 1.6 | 0.5 | 0.3 | 0.15 |
| Positive flashes (p%) | 49.0 | 37.0 | 27.0 | 21.0 | 17.5 |
| 0.9n + 0.1p | 8.2 | 5.1 | 3.15 | 2.4 | 1.9 |

The di/dt values are not included since these are small for positive flashes and we may therefore consider the values for negative flashes only. The 2% levels for the combined curves are given in Table 3 below together with the 2% levels for negative flashes and the 18% levels for positive flashes. The levels given in the internationally accepted composite test waveform are also included for comparison.

TABLE 3 `SEVERE` LEVELS OF LIGHTNING PARAMETERS

| Parameter | 2% neg | 18% pos | 2% combined | Test W/Fm |
|---|---|---|---|---|
| Peak current (kA) | 140 | 100 | 180 | 200 |
| Charge (coulomb) | 200 | 200 | 300 | 210 |
| Action int (MJ/ohm) | 0.8 | 3.8 | 3.7 | 2.25 |

If a smaller proportion than 10% was assumed for the occurrence of positive flashes then the combined curves would of course approach more closely to the curves for negative flashes. We may also note the special cases when n% or p% is small. If for a particular parameter (for example, action integral) the value is comparatively small for negative flashes (n% small) then 0.9n + 0.1p becomes

nearly 0.1p and the 2% level on the combined curve is the same as the 20% level on the positive curve. This corresponds nearly to the Phillpott 18% criterion. If on the other hand for a particular parameter (for example, di/dt) the value is small for positive flashes then p% is small and 0.9n + 0.1p becomes nearly 0.9n and the 2% level on the combined curve is the same as the 2.2% level on the negative curve. Thus we may then take the 2% level on the negative curve for practical purposes.

## DISCUSSION OF PARAMETER LEVELS RELEVANT TO DIRECT EFFECTS

PEAK CURRENT--The 2% level for negative flashes is 140 kA and for the combined curve is 180 kA. The commonly employed composite test waveform has a higher peak than this, namely 200 kA, and the derivation of this figure is rather obscure, although it possibly includes a safety factor to take into account the occasional very severe positive flash. There seems no good reason to change it, while recognising that it is probably more severe than the 2% level which as a general rule is considered to be the appropriate level.

CHARGE TRANSFER--Because both the 2% negative level and the 18% positive level give 200 coulomb this value of charge is usually accepted for test purposes. However, the combined curve of the present paper gives a 2% level of 300 coulomb, and it is thought that at least for ground applications a case can be made out for an increase in the design/test level for this parameter.

ACTION INTEGRAL--It is usually considered that the composite test waveform essentially represents a negative flash but with an increase in action integral to take some account of positive flashes. However, still further enhanced values are often advocated, and it seems that there may be some justification for this, at least for ground applications, since both the 18% positive level and the 2% combined level are about 3.7 MJ/ohm.

APPLICATION TO STANDARDS--The lightning statistics quoted in this paper are the published results of ground measurements and it is recognised that the parameters appropriate to airborne vehicles may be less severe. A draft NATO Standard (6, 7) which is at present under discussion takes this into account by retaining the presently accepted composite waveform for airborne applications but increasing the values of charge transfer and action integral for ground and sea applications in the light of such considerations as those discussed in the present paper. A comparison of the three parameters in the composite waveform would then be as follows. The peak current would be unchanged at 200 kA for all applications, while the charge transfer and action integral would be 200 coulomb and 2.0 MJ/ohm for air application, 300 coulomb and 3.5 MJ/ohm for ground/sea application.

## ACKNOWLEDGMENT

This paper is based on work performed for the UK Ministry of Defence.

REFERENCES

1 N Cianos and E T Pierce, 'A Ground Lightning Environment for Engineering Usage', Tech Report 1, SR1 Project 1834, Stanford Research Institute, August 1972.

2 E T Pierce, 'Natural Lightning Parameters and their simulation in Laboratory Tests', Lightning and Static Electricity Conference, Oxford, UK, 1975.

3 K Berger, R Anderson and H Kroninger, 'Parameters of Lightning Flashes', CIGRE Journal Electra No 41, July 1975.

4 J Phillpott, 'Simulation of Lightning Currents in relation to Measured Parameters of Natural Lightning', Lightning and Static Electricity Conference, Oxford, UK, 1975.

5 F A Fisher, J A Plumer and R A Perala, 'Aircraft Lightning Protection Handbook', FAA Report DOT/FAA/CT-89/22, September 1989.

6 NATO/CNAD, 'Lightning Environmental Conditions Affecting the Design of Materiel for Use by the NATO Forces', Second Draft STANAG 4236, Edition 2, February 1994.

7 G A M Odam and M Richardson, 'The Rationale of Proposed NATO STANAGS Describing the Lightning Environment for Land, Sea and Air Use and Defining Lightning Assessment Procedures for Munitions and Associated Systems', Williamsburg Lightning Conference, September 1995.

British Crown Copyright 1995/MOD
Published with the permission of the Controller of Her Britannic Majesty's Stationery Office

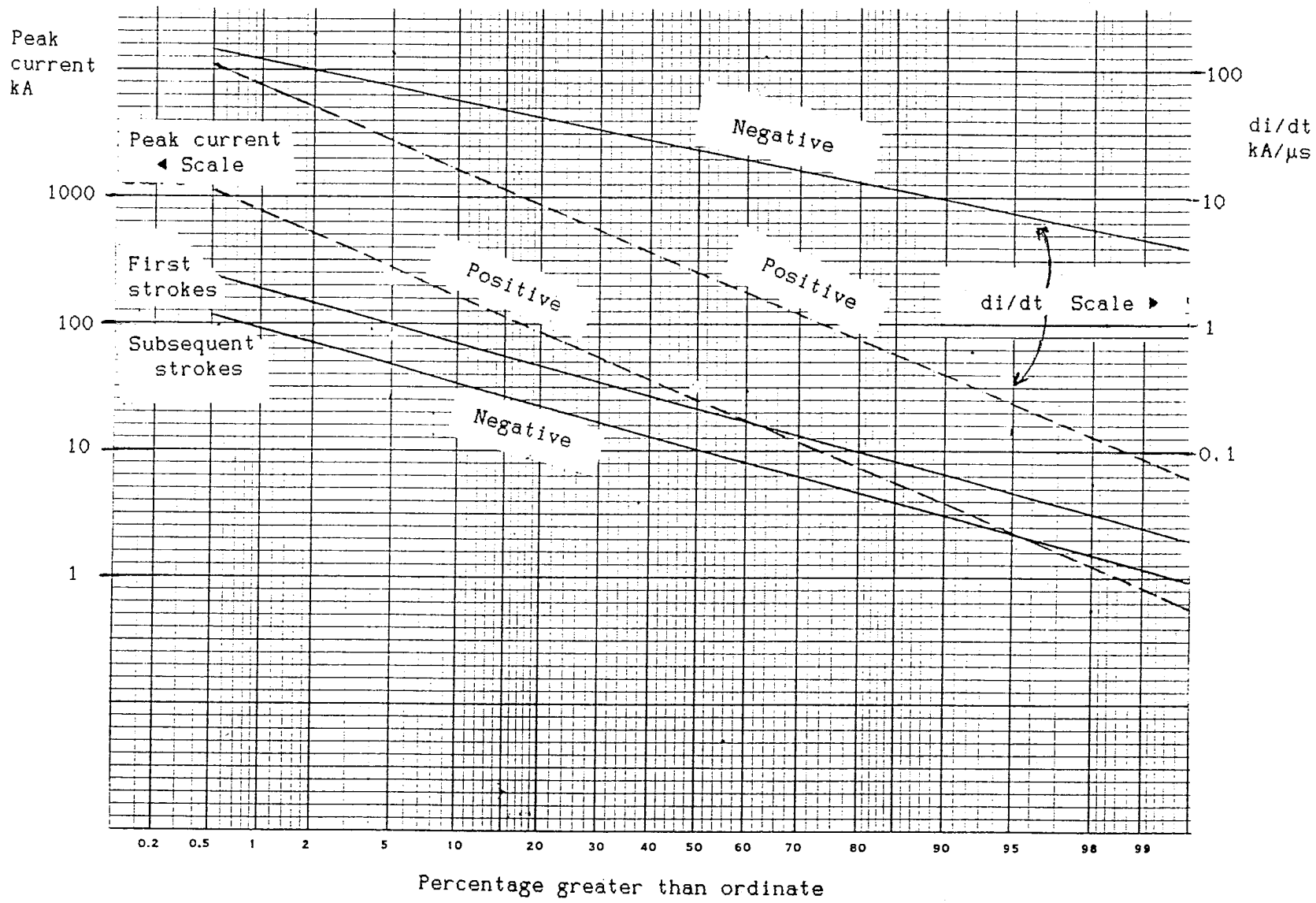



FIGURE 1 STATISTICAL DISTRIBUTION OF PEAK CURRENT AND MAXIMUM di/dt

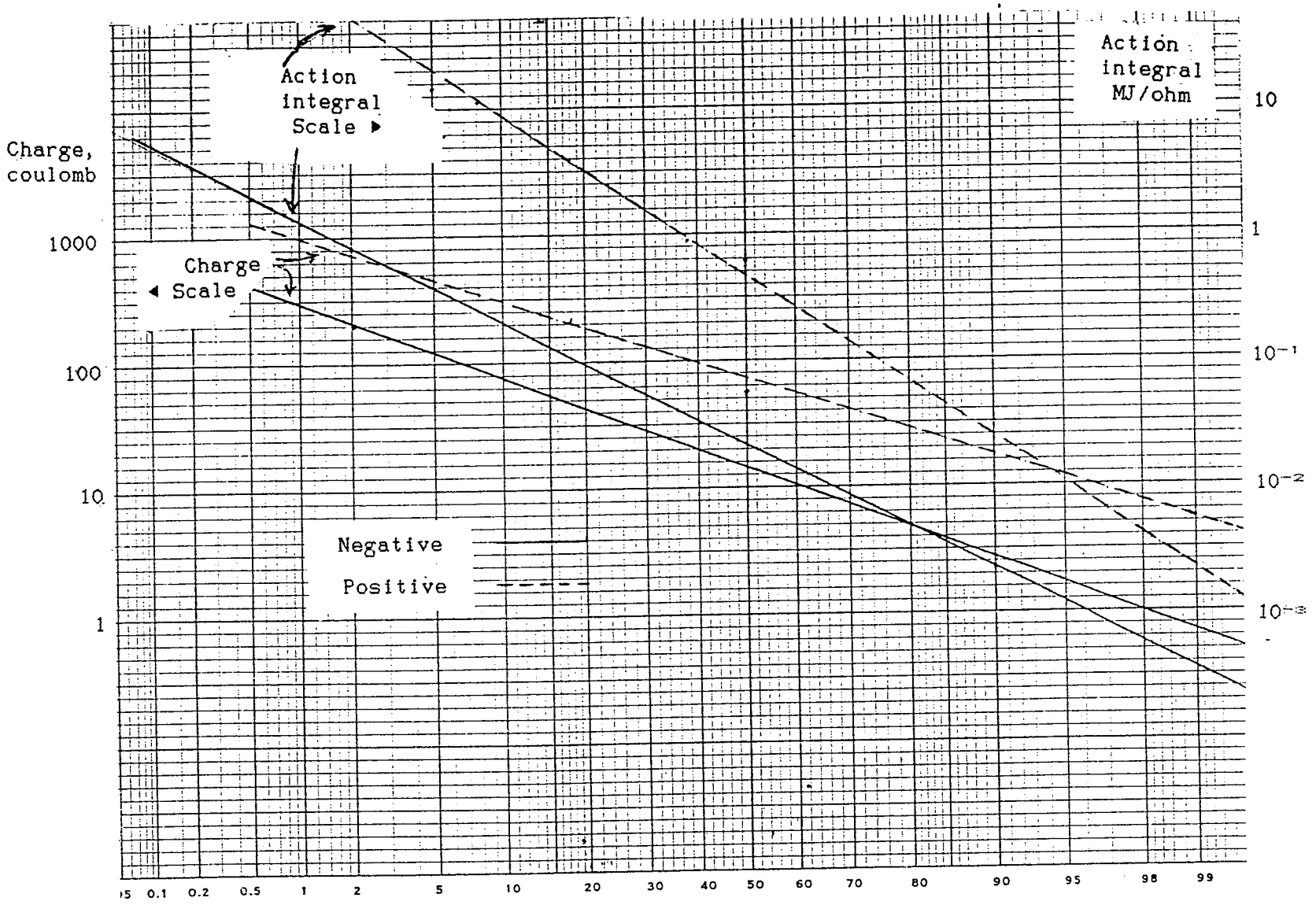



FIGURE 2 STATISTICAL DISTRIBUTION OF CHARGE TRANSFER AND ACTION INTEGRAL

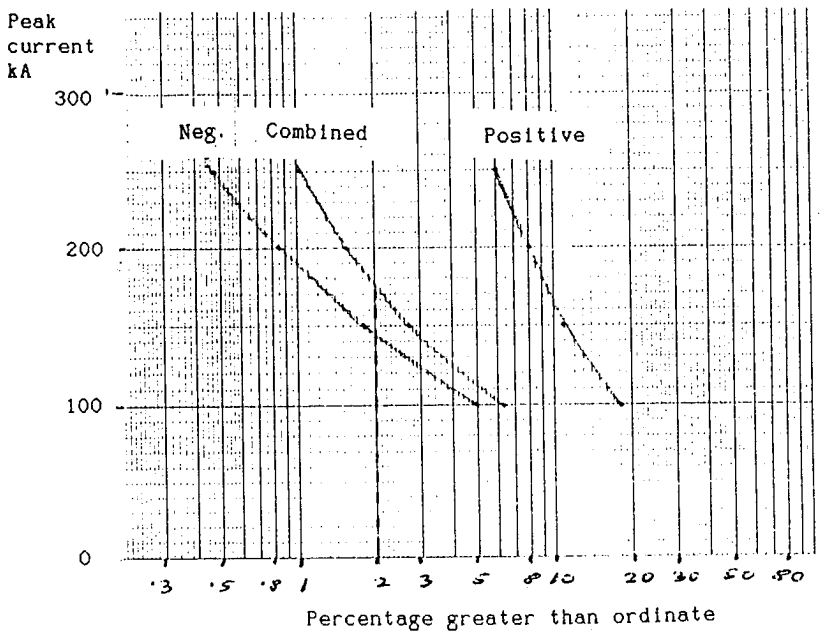



FIGURE 3a COMBINED CURVE - PEAK CURRENT

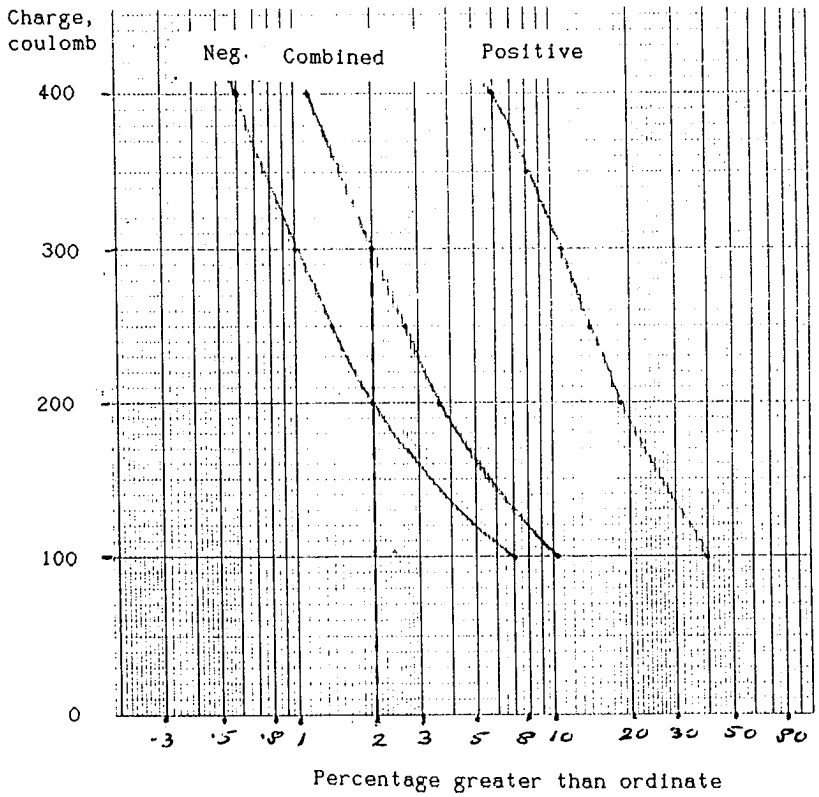



FIGURE 3b COMBINED CURVE - CHARGE TRANSFERRED

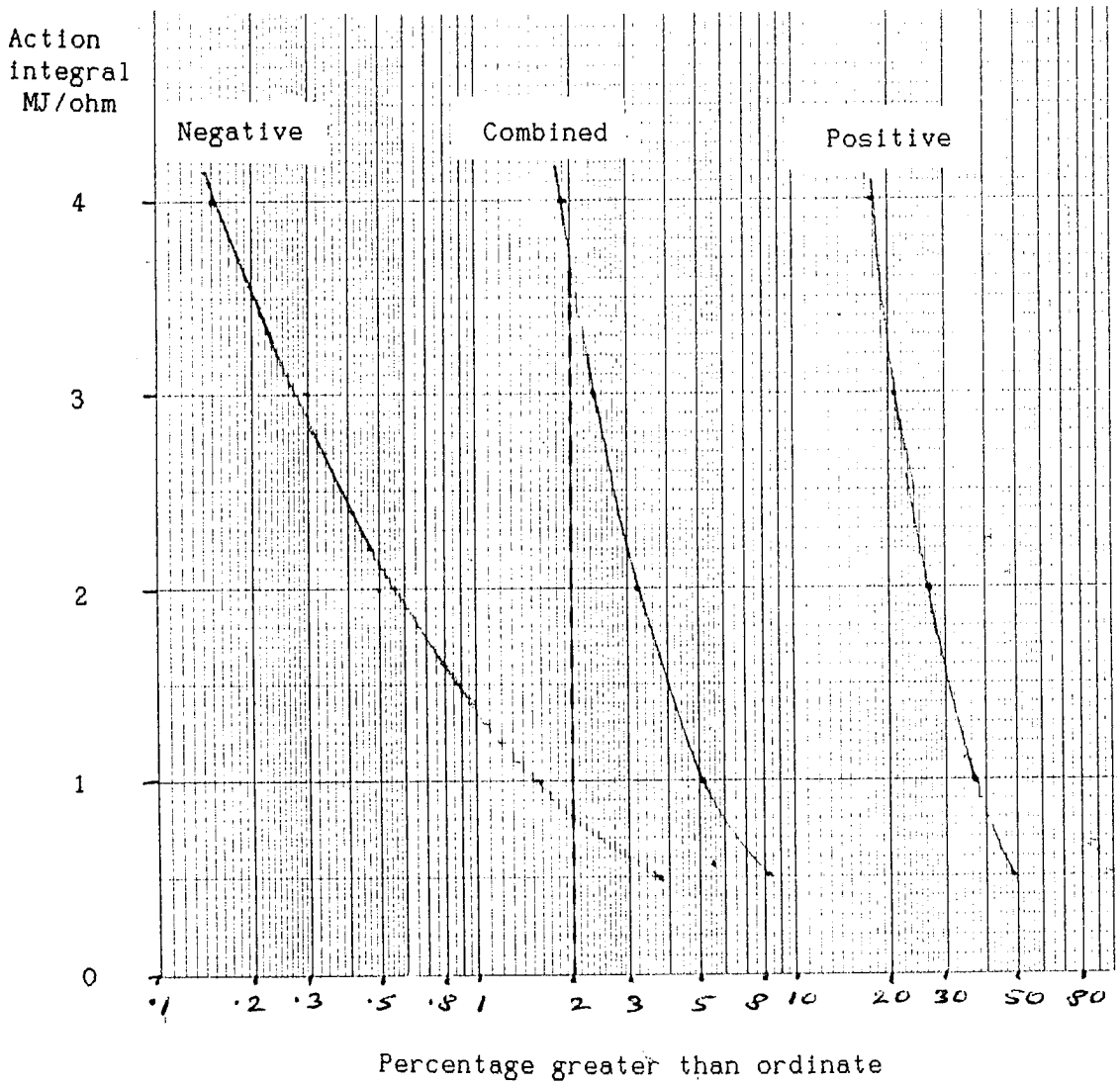



FIGURE 3c COMBINED CURVE - ACTION INTEGRAL

# LIGHTNING IMPLICATIONS OF DECREASING CIRCUIT CARD TRACE SIZE AND SPACING

Sadegh M. Vakil
Rockwell International
Collins General Aviation Division
Cedar Rapids, Iowa USA
Telephone (319) 395-8902 FAX (319) 395-3661

## ABSTRACT

Present circuit card designs used in avionics equipment provide enough design features and devices to withstand lightning threats. As trace size and spacing decrease, lightning protection techniques become a major concern. This paper discusses the implications of using smaller trace dimensions and spacing. In particular, it demonstrates how the lightning protection device or component input impedances, which are imposed on the circuit cards for protection, may cause the common mode lightning induced voltages to appear as potential differences between the circuit board neighboring traces.

## INTRODUCTION

Circuit card designs are moving toward saving cost and size by reducing the circuit card dimensions. This dimension reduction is accomplished by reducing trace width and spacing between the lines on circuit cards. The idea of trace lines with smaller dimensions and finer spacing is gaining more attention since it reduces the total circuit card area and limits the number of layers. These savings ultimately result in a cost reduction for producing circuit cards.

With the technology advancements in circuit card designs, soon circuit cards with smaller dimensions will find broad applications in personal computers, home appliances, and many other industrial applications. The broad range of possible applications for small circuit cards include many critical areas. A few examples of critical applications are: military equipment performing critical functions, equipment used for the exploration of space, and avionics equipment where the safety of flight depends on properly functioning critical equipment.

The smaller trace dimension and finer spacing in circuit cards will be primarily designed to carry electrical source voltages limited to a maximum of 33 volts, signal voltages not exceeding 3 to 15 volts, and trace currents limited to a few amperes. Special attention and considerations in the circuit card design will be necessary to ensure the ability of the card circuits to perform their functional operations in adverse environments. There are many environments in which the circuit cards have been employed to perform critical category functional operations. One of these areas is high altitudes in which the lower dielectric strength may increase the probability of inter trace dielectric breakdown in the circuit cards. In the lightning environment, which may exist at both ground level and in the inter cloud spaces at higher elevations, high voltages which are induced in the equipment cable wiring and carried to the circuit card traces are considered the main causes of spark overs between the traces. These spark overs may contribute to the inter trace electro-migration in the circuit card dielectric medium (1). High relative humidity, smog, dust, and other pollution in the air surrounding circuit cards can easily increase the chance of breakdown, facilitate the triggering of inter trace and trace to ground spark overs, and contribute to worsening

effects of electro-migration. This would result in component damage and shortening of the circuit card mean time between failures (MTBF).

In particular, the circuit cards used in avionics equipment which operate in high altitudes, and are exposed more often to the lightning environments, should be designed such that no adverse effects on the circuit card electronic components and operational functions are produced by the lightning environment. The lightning implications of smaller trace dimensions and finer spacing on the circuit card stems from the fact that the electric fields in the inter trace spacing due to the lightning induced voltages can be substantially increased. The stronger electric field could enhance and expedite the formation of conductive filaments within the card dielectric substrates with the immediate effect of causing dielectric breakdown or an end effect of shortening the MTBF of the circuit card dielectric substrate. With shorter distances between the traces and between the trace and ground plane, the probability of a spark flash occurrence triggered by stronger lightning induced electric fields will be substantially increased. Therefore, the emphasis on the effects of lightning induced pulse voltages on circuit cards with smaller trace and finer pitch/spacing is based on the realization that these circuit card size reduction methods can have an immediate influence on component damage due to possible spark generation and insulation breakdown, and a prolonged effect leading to the circuit card substrate failure through electro-migration.

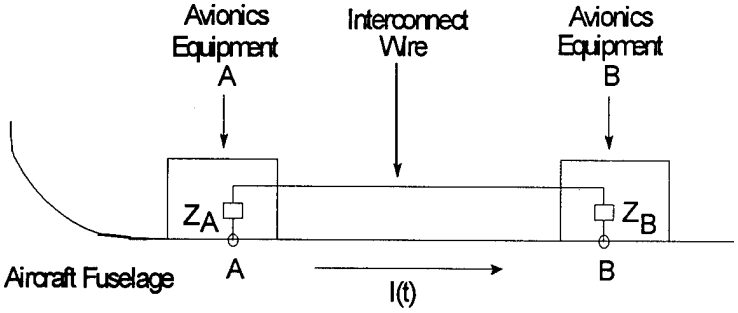
In present circuit card design technology, it is assumed that the pitch and trace dimensions can be designed and made as fine and small as possible. The technology established for the circuit card trace spacing design has also taken into account the fact that trace distance and insulation dielectric strength are sufficiently large enough that they inhibit the arc initiation and the breakdown of the insulation material. Voltages as large as 600 volts DC are established between the circuit card traces or between the traces and the circuit card layers of buried and surface laid ground planes.

In circuit card designs for applications in avionics equipment, trace widths of about 12 mils and trace spacing of 13 mils (25 mils pitch) have proved to be compatible with moderate lightning requirements specified by maximum peak voltages of 600 Volts. However, failure leading to component damage on the circuit cards was observed when pulse peak voltages exceeding 900 volts were injected between the card trace lines and the ground plane. Investigation of the failure cause revealed that spark over originating from the injected trace lines was responsible for damage to several components in a neighboring trace circuit. This neighboring circuit was inherently vulnerable to lightning damage and was electrically isolated from the injected trace line. In contrast, the interface components which were directly connected to the injected trace, were found to be immune from damage as the injected trace circuitry was designed to be inherently immune to lightning damage. Verification of the component damage in the neighboring isolated circuits, in addition to the visual observation of arcing between the traces, proves the importance of trace spacing in the design of circuit cards.

Recent research (1, 2) on electro-migration within the dielectric medium in the space between traces or between traces and ground, has confirmed the relationship between electro-migration and circuit card MTBF. It also concludes that the migration is expedited by an increase in the electric field and the moisture level in the surrounding environments. This leads to a reduced MTBF as the electric field and the moisture level in the surrounding medium are increased.

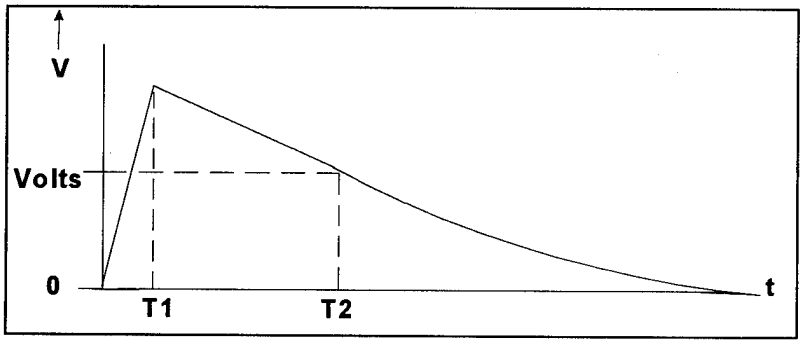
LIGHTNING ENVIRONMENT AND CIRCUIT PROTECTION CONCEPT

LIGHTNING INDUCED TRANSIENT WAVEFORMS AND PEAK AMPLITUDES - Electronic equipment operating in the lightning environments must be hardened against the lightning induced transients. Hardening is necessary to insure that components on the equipment circuit cards remain immune from damage and the equipment operational functions are protected from upset. A good example of such equipments are those installed in an aircraft at locations A and B with the aircraft fuselage used as a ground plane (Figure 1). Experimental observations of transients recorded when the aircraft are struck by lightning indicate that transient voltages resulting from potential differences between points on the fuselage and those resulting from fuselage/cabling electrical oscillations, have waveforms which can be approximated by the waveforms in Figures 2, 3, and 4 for the various levels of the lightning category.



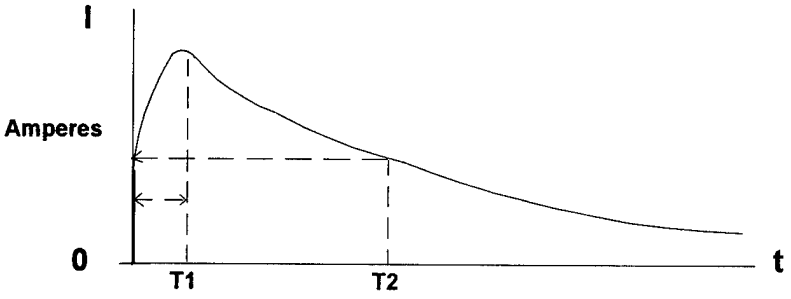

I(t)R
$V(t)$ = IR
$V(t)$ = Induced voltage surge
$I(t)$ = Lightning current passing through fuselage
$Z_A$ = Load impedance at $A$
$R$ = Fuselage resistance
$Z_B$ = Load impedance at $B$

FIGURE 1 USING A FUSELAGE AS A GROUND PLANE IN AVIONICS INSTALLATIONS



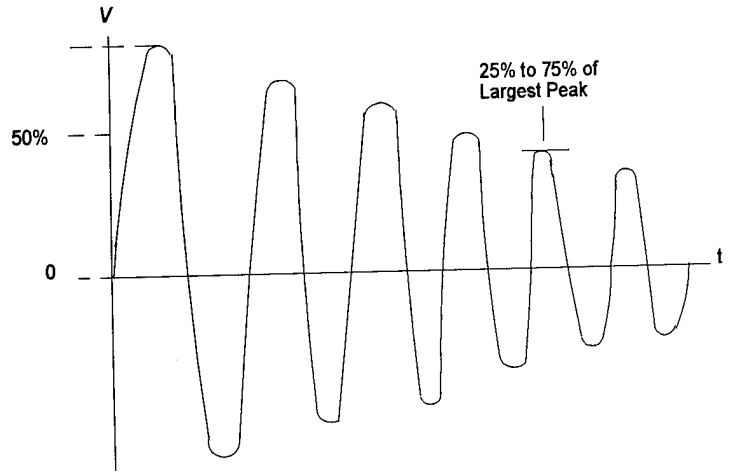

$V_p$ = 50 to 1600 volts
$T_1$ = 6.4 μS ± 20%
$T_2$ = 70 μS ± 20%

FIGURE 2 VOLTAGE WAVEFORM 4




$I_p$ = 50 to 1600 amperes
$T_1$ = 50 μS ± 20%
$T_2$ = 500 μS ± 20%

FIGURE 3 VOLTAGE/CURRENT WAVEFORM 5




$V_p$ = 100 V/4 Amp. To
3200 V/128 Amp.

FIGURE 4 VOLTAGE/CURRENT WAVEFORM 3

LIGHTNING PROTECTION, INTERFACE HARDENING CONCEPT AND DEVICES - Interconnect wiring loops are formed when the cable wiring entering the equipment cable receptacle terminate on the circuit card interface traces which are connected to the circuit card impedances of electronic and electrical components (Figure 5a). The lightning induced voltage waveforms described in the previous section then become the loop driving source which inject the lightning currents into the circuit card through the interface trace impedance (Figure 5b). Protection of sensitive circuit components from the lightning adverse effects can be accomplished (in addition to the wire shielding practices) by limiting the lightning current in the loop or to curb the lightning energy from reaching the circuit card. In Figure 6a, the transorb D (which limits the lightning voltage, diverts and absorbs a large portion of the lightning current away from entering the circuit card), and in Figure 6b, the large resistor R (which limits the lightning current and is able to dissipate a significant portion of the lightning generated heat), are examples of modern lightning protection design techniques and devices.

As shown in Figures 6a and 6b, the transorb imposes a new impedance at the circuit card trace when lightning strikes. In the case of the protective device such as transorb D, impedance $z_i$ is replaced by $Z_i$ which is equal to the transorb forward impedance (usually a small resistance equal to $R_\epsilon = 0.1\Omega$) for the negatively induced lightning pulse. When the lightning induced voltage in Figure 5 is positive, the transorb input voltage is clamped at $V_i = i_b \; x \; r_b + V_{BD}$ , where $r_b$ is the reverse breakdown resistance and $V_{BD}$ is the device breakdown voltage. The input impedance $Z_i$ then becomes equal to $r_b$ (which is approximately equal to $0.5\Omega$) in parallel with impedance $z_i$. In the case of series $R$ added as a protection component, $z_i$ is replaced by $Z_i = R + z_i$ as the new trace impedance imposed by the protective component $R$.

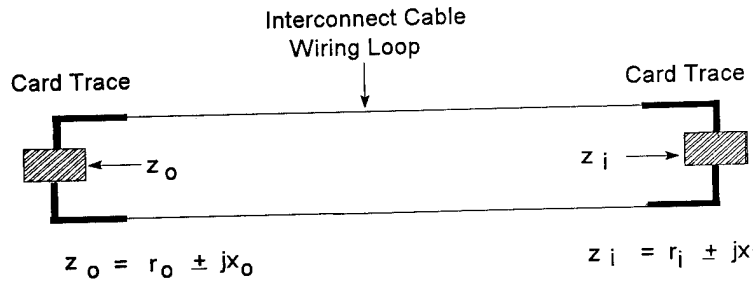



Figure 5a Prior to protection of interface card, circuits $z_i$ and $z_o$ are the impedances which are different from the lightning imposed impedances of Figure 5b.

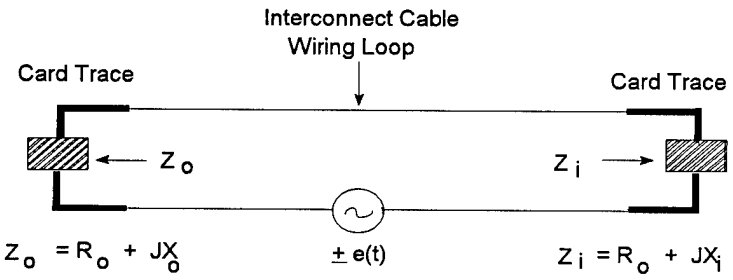



Figure 5b $Z_i$ and $Z_o$ are impedances presented to the lightning induced *e(t)*.

FIGURE 5 INTERFACE TRACE IMPEDANCE

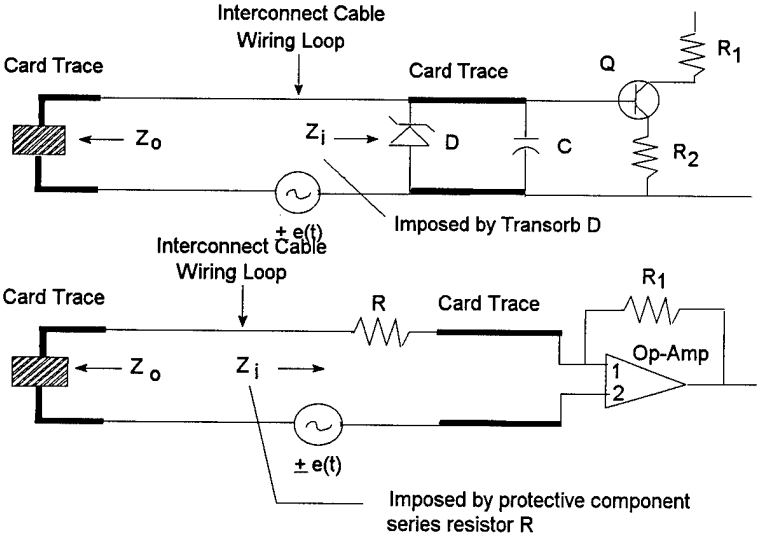



Figure 6a Lightning protection device D impose new input impedance as induced *e(t)* causes breakdown in diodes, transorbs, varistors, or other semiconductor junctions.

Figure 6b Lightning protection device R impose new input impedance as induced *e(t)* causes breakdown in diodes, transorbs, varistors, or other semiconductor junctions.

FIGURE 6 INTERCONNECT WIRING LOOPS WITH TERMINATING INPUT AND OUTPUT IMPEDANCES $Z_I$ AND $Z_O$ IMPOSED BY LIGHTNING

INTERFACE, BURIED, AND ISOLATED CIRCUITS - For the sake of lightning effect analysis, circuit layouts in cards are classified into three distinct categories; interface, buried, and isolated circuits (Figure 7). The interface circuits can be defined as a combination of network loop elements and impedances which are directly connected to interface traces. On card circuits, the interface traces are realized as those traces which carry power, command, control, and data signals to or from the connector pins of the input and output receptacles. These are considered to be the up-front or the front guard circuits, which could be directly affected by the lightning induced voltages in the cable wiring loops. Buried circuits are referred to as elements and impedances in cascaded loops which follow the interface circuits. Such circuits are less affected by the cable wiring loop induced voltages as the lightning energy is mostly dissipated in lightning protection devices or in the elements and impedances of the interface circuit. Isolated circuits are not a part of the cascaded network conductively connected to the interface circuitry of the circuit card. They are isolated in the sense that under normal conditions they are not electrically connected to the interface circuits although loose connections due to capacitive, inductive, or high resistive coupling may exist. Although at higher frequencies the inductive and capacitive coupling could respond to the energy transfer from the interface circuits to such isolated circuits in the form of cross-talk, the amount of energy transferred from lightning induced sources at lightning specified frequencies can be considered as insignificant. Small card circuits with circuit traces laid

out at distances close to the interface circuit traces, are examples of the circuits which are isolated from the interface traces under normal conditions that may receive a large portion of the lightning energy in the case of spark over or arcing between the neighboring interface and isolated circuit board traces.

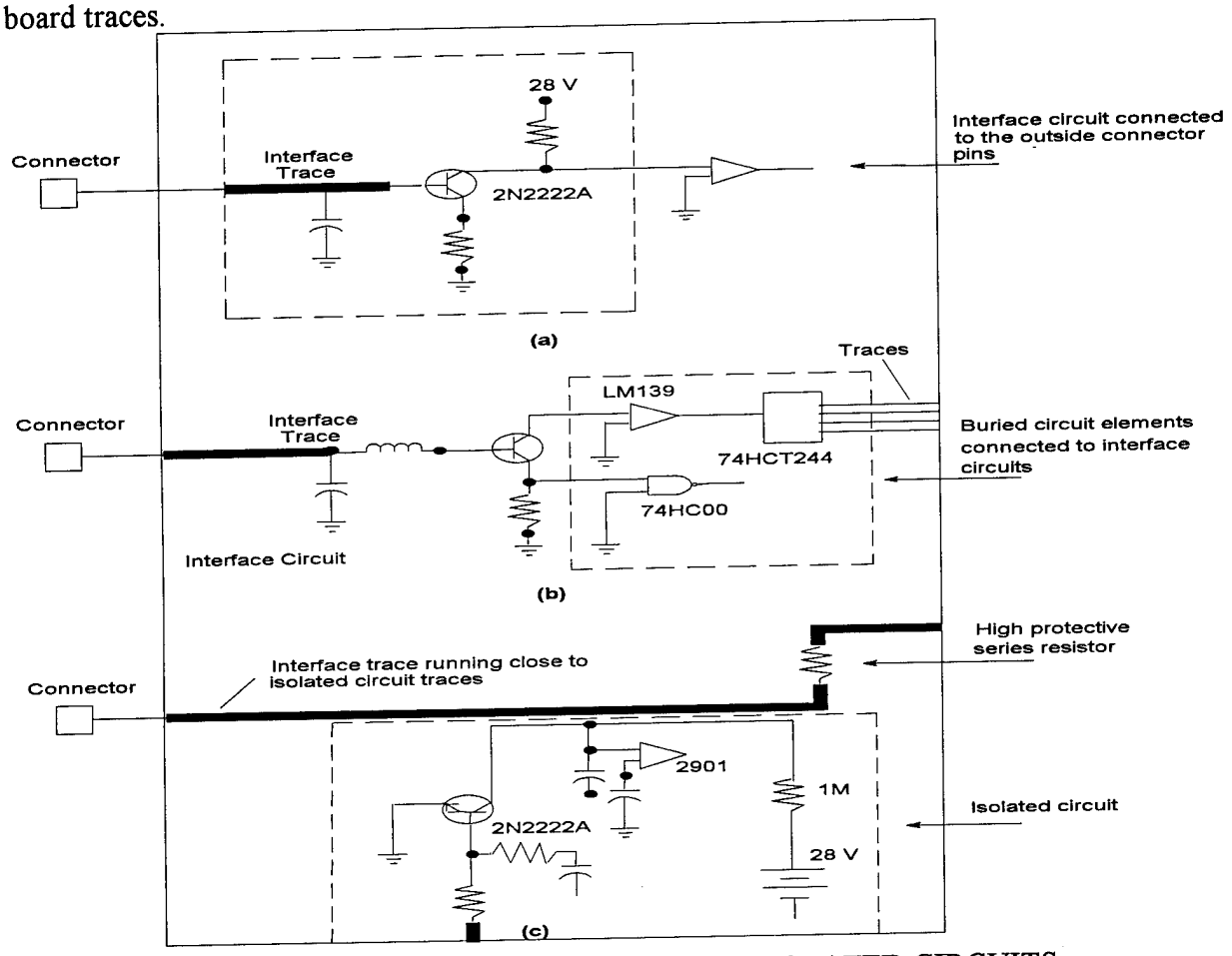



FIGURE 7 INTERFACE, BURIED, AND ISOLATED CIRCUITS

STATE OF THE ART CIRCUIT CARD DESIGN WITH 12 MILS TRACE LINE SPACING - For moderate lightning environments, the 12 mils circuit card line spacing is sufficient to circumvent spark triggering and inhibit arcing in the inter-trace spacing, and in the dielectric medium and spaces between traces and the layers of ground planes. 12 mils spacing immunity from circuit card spark over and arcing implies that the lightning induced voltages shall be confined to 300 volt and 600 volt ranges for double exponential waveform and the damped sinusoidal waveform respectively. In the absence of inter trace sparking, and the insulation breakdown of the substrate layers, both isolated and buried circuits will remain immune from the effect of immediate damage and failures. Only the interface circuits must be hardened whenever damage and upset prevention for a typical equipment functioning in the lightning environment is desirable or is required. Following the state of the art design hardening techniques against lightning, and adhering to the lightning protection design guidelines, devices such as transorbs can be deployed to limit the lightning voltage and absorb the lightning energy (Figure 8a). The use of transorbs as lightning protection devices becomes mandatory when the total impedance of the

loops terminating on interface pins can not be increased to limit the lightning current, or the lightning energy can not be diverted by using passive low shunt impedances at the interface pins.

However, because of the higher component and maintainability cost for transorbs, higher priority and preference is given to the addition of passive shunt elements at interface pins, or passive series components in the interface circuit loops, in order to reduce and limit the effects of lightning.

Figures 8b and 8c depict the deployment of series resistors and inductors terminating in interface traces and the addition of shunt capacitors and small resistors at pins which may carry the lightning induced voltage and currents. The series and shunt passive elements are effective and useful in reducing and limiting the lightning induced currents and voltages below the failure levels of circuit card sensitive components, provided that they will not affect the circuit design characteristics and functional performance specification of the circuit card.

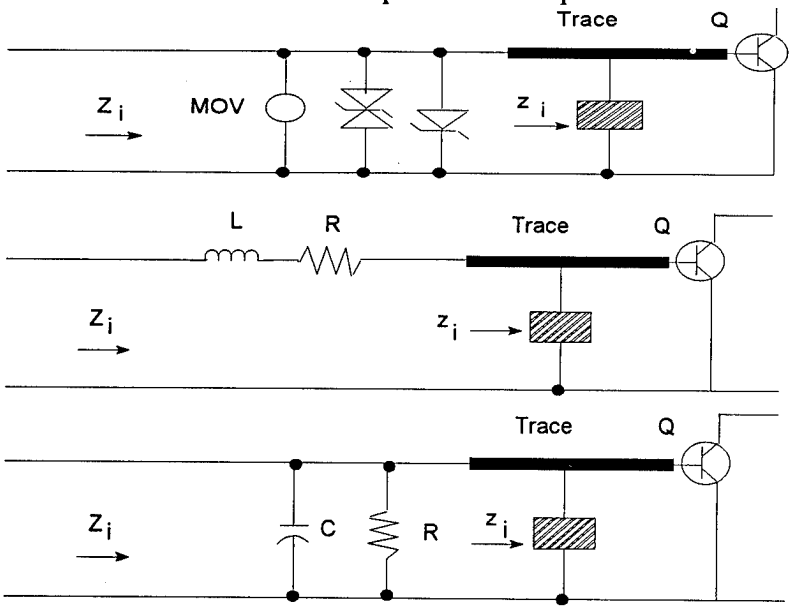



Figure 8a Protective semi-conductor Zener diodes and transorbs or metal oxide varistors

Figure 8b Protective passive elements series resistor $R$, and series inductance $L$

Figure 8c Protective passive element shunt resistor $R$

FIGURE 8 PROTECTIVE COMPONENTS

REDUCTION IN TRACE SPACING

LIGHTNING IMPACT AND PROTECTION DESIGN GOALS - It has been observed that cost saving trends are looking toward reducing the circuit board size (area and the number of board layers). This in turn mandates the use of smaller circuit board spacing in order to accommodate the same number of electronic circuits and components on the circuit cards. As the distance between trace lines and ground planes/traces decreases, the possibility of sparks and arcing in the inter line spacings and the chances of breakdown in the board substrates increases. The main concerns are arcing between the circuit board traces and breakdown in the insulation substrates which could be detrimental to components and circuit boards used in electronic equipment circuit cards.

In the analyses and discussions that follow, it will be assumed that in pursuit of new trends in circuit board technology, the line spacing and the inter layer substrate thickness have decreased such that the threat of inter trace arcing and inter substrate breakdown exists. The intent of the analyses and discussions is to address the interface and buried circuit configurations and to offer

solutions to the problems arising from the lightning effect. For each case, the conditions of the circuits to be hardened and the various techniques to be used for lightning hardening can be reviewed and evaluated. Since using circuit boards crowded with smaller line spacings will find extensive application in the foreseeable future, the ultimate goal is to provide these circuit boards with protection from lightning induced transients. That is, to protect the circuit board and the circuit card components from failure and permanent damage, to immune the functional operations of the circuit cards to upset, and to safeguard the MTBF of the circuit board from degradation.

CIRCUIT BOARD TRACE INDUCED VOLTAGE THEORY

Single Trace Common Mode Lightning Induced Voltages - It is well known that the lightning induced voltages in the interconnect wiring loops are predominantly common mode voltages. These voltages appear between the board interface traces and the ground planes through connector pins in the equipment input and output cable receptacles. In general, a common mode lightning transient voltage *e(t)* is induced in a wiring loop of inductance $L$, which is terminated in input and output load impedances between the circuit board traces and the ground plane (Figure 9). For analysis simplicity, impedances $Z_i$ and $Z_o$ are assumed to be resistive loads $R_i$ and $R_o$ as are found in most circuit card designs. However, even in cases where they may have inductive or capacitive components, it can be proved that such complex impedances are irrelevant to the results of analysis. In a wiring loop with induced lightning transient voltage *e(t)*, the lightning induced current *I(t)* is described by equation (1).

$$e(t) = R_i I(t) + R_o I(t) + L\frac{dI(t)}{dt} \tag{1}$$

For small loads where, $R_i I(t) + R_o I(t) \ll L\frac{dI(t)}{dt}$, the lightning induced current becomes independent from the loop input and output terminating load impedances. The lightning induced current is solely determined by the wiring loop inductance $L$.

$$e(t) = L\frac{dI(t)}{dt}, \qquad I(t) = \frac{1}{L}\int e(t)dt \tag{2}$$

$$V_i(t) = R_i I(t), \qquad V_o(t) = R_o I(t), \qquad \text{where } V_i(t),\ V_o(t) \ll e(t) \tag{3}$$

For large loads where, $R_i I(t) + R_o I(t) \gg L\frac{dI(t)}{dt}$, the lightning induced voltage *e(t)* becomes equal to the total input and output voltages $V_i$ *(t)* and $V_o$ *(t)* across the terminating loads.

$$e(t) = V_i(t) + V_o(t) = R_i I(t) + R_o I(t) \tag{4}$$

$$I(t) = \frac{e(t)}{(R_i + R_o)}, \qquad V_i(t) = \frac{R_i\, e(t)}{(R_i + R_o)}, \qquad V_o(t) = \frac{R_o\, e(t)}{(R_i + R_o)} \tag{5}$$

For input loads $R_i \ll R_o$, $R_i + R_o \approx R_o$, and,

$$V_i(t) = \frac{R_i\, e(t)}{R_i + R_o} \approx \frac{R_i\, e(t)}{R_o} \tag{6}$$

For:

$$R_i \gg R_o, \frac{R_i}{R_i + R_o} \approx \frac{R_i}{R_i}, \text{ and, } V_i(t) = e(t) \tag{7}$$

If $R_i$ and $R_o$ are large and approximately of the same order of magnitude, $R_i + R_o \approx 2R_i$, then,

$$V_i(t) = \frac{R_i\ e(t)}{R_o + R_i} = \frac{R_i}{2R_i} e(t) = \frac{e(t)}{2} \tag{8}$$

Equations (2) through (7) clearly demonstrate that the input impedance $R_i$ plays an important role in carrying the lightning induced voltages to the circuit card traces and electronic components. For very large values of $R_i$, almost all the lightning induced common mode voltage is carried to the circuit card traces. Whereas for small $R_i$ compared to $R_o$, and for $R_i$ and $R_o$ both being small, only a fraction of the lightning induced voltage $e(t)$ appears at the circuit trace reaching its maximum value of $\frac{e(t)}{2}$ when $R_i$ and $R_o$ are both large and approximately of the same size.

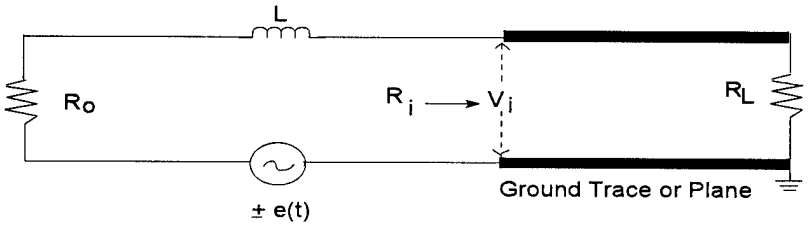



FIGURE 9 SINGLE INTERFACE TRACE INDUCED LIGHTNING VOLTAGE THEORY

Lightning Induced Voltages Between Two Neighboring Traces - As the dependence of common mode induced voltages on the loop termination impedances are well understood by considering equations (2) through (8), the relation between lightning induced voltages at neighboring traces $A$ and $B$ (Figure 10), the equations for trace induced voltages $e_a(t)$ and $e_b(t)$ due to lightning can be expressed as;

$$e_a(t) = L_a \frac{dI_a(t)}{dt} + I_a(t)R_{ia} + I_a(t)R_{oa} \pm M_{ab} \frac{dI_b}{dt} \tag{9}$$

$$e_b(t) = L_b \frac{dI_b(t)}{dt} + I_b(t)R_{ib} + I_b(t)R_{ob} \pm M_{ab} \frac{dI_a}{dt} \tag{10}$$

where, $L_a$ and $L_b$ are the self inductance of the cable wiring loops connected to traces $A$ and $B$ respectively. $R_{ia}$ and $R_{oa}$ are the input and output impedances at trace $A$, and $R_{ib}$ and $R_{ob}$ are the input and output impedances at trace $B$. $M_{ab}$ is the mutual inductance of the wiring loops terminating on traces $A$ and $B$.

For sufficiently small input and output loop terminating impedances $R_{ia}$, $R_{oa}$, $R_{ib}$,, and $R_{ob}$, at adjacent traces $A$ and $B$ the self inductance and the mutual inductance terms in equations (9) and (10) become dominating factors in determining the trace currents and voltages. The voltage drops, $I_a(t)\ (R_{ia} + R_{oa})$, and $I_b(t)\ (R_{ib} + R_{ob})$, become negligible with respect to the inductance terms $L_a \frac{dI_a(t)}{dt} \pm M_{ab} \frac{dI_b(t)}{dt}$ and $L_b \frac{dI_b(t)}{dt} \pm M_{ab} \frac{dI_a}{dt}$ respectively resulting in the following relations:

$$V_{ia}(t) = I_a(t)R_{ai} \ll e_a(t)$$
$$V_{ib}(t) = I_b(t)R_{bi} \ll e_b(t) \tag{11}$$

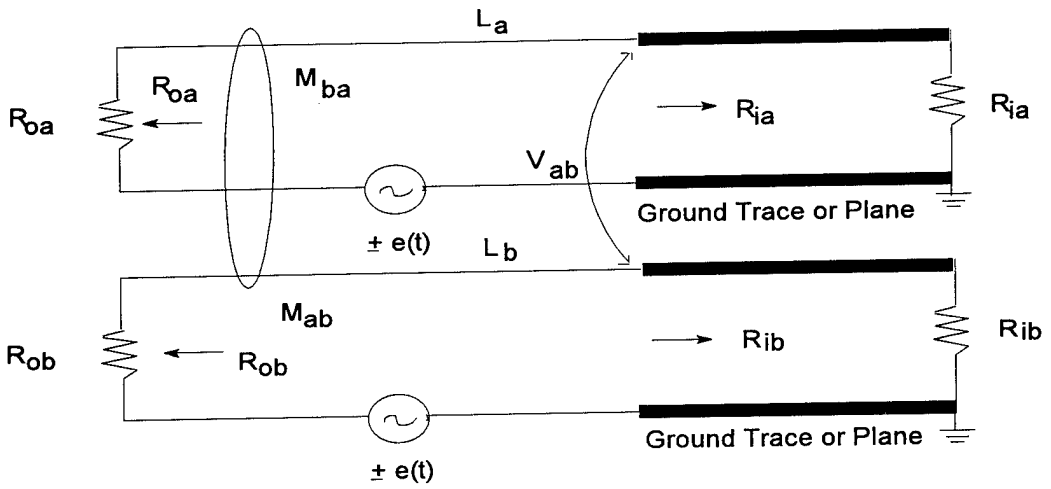



FIGURE 10 TWO TRACE INDUCED LIGHTNING VOLTAGE THEORY

In general, $e_a\ (t)$ and $e_b\ (t)$ may vary for wiring loops of different dimensions and for different categories of lightning environments. However, when the two cable interconnect wiring loops terminating on traces $A$ and $B$ are in the same lightning environments and have equal loop dimensions $e_a\ (t)$ and $e_b\ (t)$ can be considered to be equal or to be limited by the lightning threshold specification levels. In particular, when $e_a\ (t) = e_b\ (t) = e(t)$:

$$V_{ia} = R_{ia}\, I_a(t) \ll e_a(t) = e(t)$$
$$V_{ib} = R_{ib} I_b(t) \ll e_b(t) = e(t) \qquad (12)$$

The difference between trace voltages $V_{ia}$ and $V_{ib}$ at adjacent traces $A$ and $B$ remains noticeably small with respect to the lightning induced voltages $e_a\ (t)$ and $e_b\ (t)$.

$$V_{ab}(t) = V_{ia} - V_{ib} = R_{ia}\, I_a(t) - R_{ib} I_b(t) \ll e_a(t) \text{ and } e_b(t) \qquad (13)$$

For large values of the total loop terminating input and output impedances, both self and mutual inductance terms in each loop equation have insignificant effect in limiting the induced lightning currents. The loop currents $I_a\ (t)$ and $I_b\ (t)$ are considered to depend mostly on input and output trace impedances yielding to the following loop voltage equations:

$$e_a(t) = R_{ia} I_a(t) + R_{oa} I_a(t)$$
$$e_b(t) = R_{ib} I_b(t) + R_{ob} I_b(t) \qquad (14)$$

For the input impedance $R_{ia}$ and $R_{ib}$ much smaller than the output impedances $R_{oa}$ and $R_{ob}$, from equation (6), the trace voltage $V_{ia}\ (t)$ and $V_{ib}\ (t)$ becomes equal to a small fraction of the lightning induced voltages $e_a\ (t)$ and $e_b\ (t)$.

$$R_{ia} \ll R_{oa} \qquad R_{ib} \ll R_{ob}$$
$$R_{ia} + R_{oa} \approx R_{oa} \qquad R_{ib} + R_{ob} \approx R_{ob}$$
$$V_{ai}\ (t) = \mathrm{I_a}(t)\ R_{ia} = \frac{e_a(t)\, R_{ia}}{R_{ia} + R_{oa}} \approx e_a(t) \frac{R_{ia}}{R_{oa}}$$
$$V_{bi}\ (t) = \mathrm{I_b}(t)\ R_{ib} = \frac{e_b(t)\, R_{ib}}{R_{ib} + R_{ob}} \approx e_b(t) \frac{R_{ib}}{R_{ob}} \qquad (15)$$

The difference in trace voltage will still remain small and equal to a fraction of wiring loop lightning induced voltages $e_a\ (t)$ and $e_b\ (t)$.

$$V_{ab}(t) = V_{ai}(t) - V_{bi}(t) = e_a(t)\frac{R_{ia}}{R_{oa}} - e_b(t)\frac{R_{ib}}{R_{ob}} \tag{16}$$

for $e_a(t) = e_b(t) = e(t)$,

$$V_{ab}(t) = V_{ai}(t) - V_{bi}(t) = e(t)\left[\frac{R_{ia}}{R_{oa}} - \frac{R_{ib}}{R_{ob}}\right] \tag{17}$$

For the trace input impedances much larger than the output impedances, $R_{ia} \rangle\rangle R_{io}$ and $R_{ib} \rangle\rangle R_{ob}$ , using equation (7), the voltage at traces $A$ and $B$ approaches the lightning loop induced voltages $e_a(t)$ and $e_b(t)$ respectively.

$$V_{ia}(t) = \frac{e_a(t)\ R_{ia}}{R_{ia} + R_{oa}} \approx \frac{e_a(t)\ R_{ia}}{R_{ia}} = e_a(t)$$

$$V_{ib}(t) = \frac{e_b(t)\ R_{ib}}{R_{ia} + R_{oa}} \approx \frac{e_b(t)\ R_{ib}}{R_{ib}} = e_b(t) \tag{18}$$

The difference between trace voltages becomes equal to:

$$V_{ia}(t) - V_{ib}(t) = e_a(t) - e_b(t) \tag{19}$$

For the case where $e_a(t) = e_b(t) = e(t)$:

$$V_{ab}(t) = V_{ia}(t) - V_{ib}(t) = e(t) - e(t) = 0 \tag{20}$$

The results obtained from equations (11) through (20) conclude that for neighboring traces $A$ and $B$ which have identical input impedances, the voltage difference between the traces remains reasonably insignificant as long as the wiring loop terminating impedances are kept small or one terminating impedance is sufficiently large and has a dominant influence on the trace circuit. Only in the cases where trace $A$ has an input impedance large enough to have a significant influence on the wiring loop trace current, and trace $B$ has an input impedance sufficiently small with no predominate influence on the loop trace current, the voltage difference between the traces approaches a maximum approximately equal to $e_a(t)$. Using the equation (6) for trace $B$, and equation (7) for trace $A$, the maximum potential difference between the traces $A$ and $B$ becomes:

$$V_{ab}(t) = V_{ia}(t) - V_{ib}(t) = e_a(t) - e_b\frac{R_{ib}}{R_{ob}} \approx e_a(t) \tag{21}$$

The concept of potential differences between two adjacent traces can be extended to circuit boards with multiple interface traces. An analysis similar to the above can clearly demonstrate that the potential difference between the neighboring traces may approach the peak trace voltages $e_a(t)$ or $e_b(t)$.

## SUMMARY

State of the art circuit card operational function design so far has been concerned with the common mode voltages most often limited to 30 Vdc and differential voltages varying between -15 to +15 volts. Lightning induced voltages generated by the lightning environment result in common mode voltages up to 1500 volts peak which have often been suppressed to a maximum of 50 volts peak using semiconductors, transistors, or varistors deployed as voltage clamping devices. Differential mode voltages induced between the circuit card traces have been of little concern with respect to clamping, design safety, or component reliability evaluation.

This paper proves that as a result of the new input and output impedances imposed on the circuit cards by the lightning protection devices and components in the lightning environment, the differential mode voltages which appear between the traces are significant and large enough that they should be clamped or their resulting electric field reduced. The results of the analysis indicate that inter trace voltages can easily approach the magnitude of the loop voltages induced by the lightning. As the wiring loop peak lightning voltages in high lightning environment may reach 1500 volt peak levels, carefully designed trace spacings are required in order to prevent the adverse effects of spark over between the circuit card traces as well as between the circuit card traces and the ground planes.

REFERENCES

1. David Jennings, Balu Rudra, "Failure Mechanism Models for Conductive Filament Formations." IEEE Transactions on Reliability, Vol. 43, No. 3, September 1994, pp. 354-360.

2. Michael Pecht, Balu Rudra, "Assessing Time-To-Failure Due to Conductive Filament Formation in Multi-Layer Organic Laminates." IEEE Transactions on Components, Packaging, and Manufacturing Techniques, Part B, Vol. 17, No. 3, August 1994, pp. 269-276.

# Field Experiments On Laser Triggered Lightning

D. Wang*, T. Ushio, Z-I. Kawasaki, S. Uchida**, Y. Shimada**, H. Yasuda**, T. Yamanaka, C. Yamanaka**, K. Matuura, Y. Ishikubo***, M. Adachi***

Osaka University, Osaka, Japan
*Gifu University, Gifu, Japan
**Institute for Laser Technology, Osaka, Japan
***Kansai Electric Power Co.

International Aerospace and Ground Conference on Lightning and Static Electricity
September 28, 1995
Williamsburg, Virginia, USA

## ABSTRACT

A series of laboratory experiments has been conducted to investigate the initiating and guiding effects of laser plasma channel on electrical discharge. It was confirmed that the plasma channels have strong guiding effects and reduce the required electrical field strength for electrical discharges to occur. A field experimental site targeting natural lightning is being prepared to develop the thunder storm monitoring system and to test the laser and optical systems against various weather conditions. The results from the laboratory experiments and laser transmission in snowy conditions as well as attempt of initiating electrical leader will be discussed.

## 2. INTRODUCTION

### 2.1 The motivations

Approximately two-thirds of the power line accidents are caused by lightning. Once the accident takes place the damages toward the power company and the society could be very serious. These problems have been coped with using passive measures. However, these measures are not sufficient for the highly computerized society since even a small power surge causes a fatal damage to the system. Thus active methods for neutralize the thunderstorm activities before they hit the important facilities.

### 2.2 Overview of artificially triggered lightning

In recent ten years, several schemes for artificially triggering lightning have been proposed and tested against natural thunderstorm conditions. These schemes use rockets, water jet, flame and lasers. Among them, only the rocket method has gone to field experiments successfully.

In Japan the method has been studied for ten years and succeeded in triggering natural lightning more than a hundred times. The scheme uses rockets developed for marine distress signal attached to a piano wire. When the velocity of the rocket exceeds ~100 m/s, an electrical leader starts extending from the rocket since the wire brings the ground potential and enhances the electrical field strength at the tip of the wire. If the field strength of the thunderstorm is strong enough, the leader propagates beyond the wire extension and reaches thunderclouds leading a return stroke, the main discharge phenomenon in thunderbolt, takes place.

Although the rocket method has been successful, it has certain restrictions. 1) The method launches flying objects in air and therefore cannot be used in any place and requires permissions from local aviation control for each attempt. This

makes it difficult to respond to a quick change of thunderstorm. 2) After an unsuccessful attempt, recovery of debris has to be done. Because of this, the method cannot be used near town.

On the other hand, the method using laser beam to trigger lightning clears the above restrictions and has even certain advantages in terms of response time and residual debris such as rocket itself and grounded wire. These factors become important when the method is applied to protect live power facilities. The method produces plasma in air and uses it electrical conductivity to trigger lightning. Since lasers can produce plasmas within microseconds and the entire process of lightning usually lasts over few hundreds millisecond, one can irradiate laser beam after detecting a precursor of thunderbolt. This could lead to very high successful rate.

Due to the recent developments of high power laser systems, the application of such laser systems toward the lightning protection becomes feasible. The scheme was first proposed by Ball in 1974.[1] A US research group unsuccessfully made attempts to trigger lightning using a few meters of laser produced plasmas at 500 m altitude in New Mexico, USA in 1978.[2] The cause of their failure is considered to be using short isolated plasmas that are floating both electrically and spatially in the middle of air and hence have no reference potential nor inducing effects. Recently Japanese research groups found that some thunderstorms in Japan have certain advantage for laser triggered lightning (LTL), that is, the height of the clouds is relatively low which leads to the high electric fields under the clouds. The high electric fields ease the initiation of a leader propagation in plasma channels.

Two schemes for LTL are under investigation. One uses a high power $CO_2$ laser to generate strongly ionized plasmas to induce electrical discharges. The other uses short wavelength lasers such as eximar lasers to produce weakly ionized plasmas. Since a high power $CO_2$ lasers are readily available, a number of experimental studies have been carried out based on the "strong ionization scheme". The authors' group uses a high power $CO_2$ laser to study the strong ionization scheme.

### 2.3 Japan's winter thunderstorm

The principal mechanism of the thunderstorm development is considered to be convecting air flows in thunderclouds. In the air flow, small ice particles are brought upward, on the other hand, large ice balls, i. e. hail, fall against the convecting upward flow due to gravitation. Friction between these particles causes charge separation which occurs most significantly at -15 °C. The temperature of atmosphere decreases 0.65 degree every 100 m, therefore, the height of the -15 °C point is determined by the temperature on the ground. In winter season of south shore of Sea of Japan, Hokuriku region, the ground temperature is below 0 °C and thus the charge separation in thundercloud takes place at a few km above ground. This height is relatively low compared to that of summer thunderstorms. Therefore, the electric field strength is very large in winter thunderstorms.

This strong fields cause rather unique phenomenon called triggered lightning. Since the field strength under thunderclouds is very large, the enhanced electric field at the top of power transmission line tower could be as high as few hundreds of kV/m. These fields are strong enough for corona currents to be significant so that a electrical leader initiates and propagates toward the clouds and finally trigger return strokes. In fact, many thunderbolts starting from ground objects have been observed. These naturally occurred triggered lightning suggests the possibility of artificially triggered lightning.

### 2.4 Concept of laser triggered lightning

The schematic of laser triggered lightning system is depicted in Fig. 1. The system consists of a pulsed high power $CO_2$ laser, a lightning tower, and a focusing mirror. The laser beams are focused by multi-focusing reflecting mirrors to produce a long plasma channel in air near the top of the lightning tower. The top of the lightning tower distorts the uniform ambient electric fields between the thunderclouds and the ground and enhances fields around it. When the laser plasma is sufficiently close to the top, an electric leader starts from the top to the plasma. Due to good conductivity of plasmas, leader extends along the laser plasma while it brings the earth potential with it. The end point of the laser plasma does not have to reach the thunderclouds but an electrical streamer keeps extending toward the clouds and triggers a main

discharge like the natural triggered lightning. Since the discharge path is already made by the plasma, the energy of the lightning is safely guided to the lightning tower not to the power line.

The laser triggered lightning requires (1) producing a long scale laser plasma in atmosphere, (2) knowledge of the conditions for the laser plasma to induce discharges, (3) characterization of the laser transmission in air, and (4) lightning fore-casting. This paper reviews a series of laboratory experiments to produce long scale plasmas and to obtain the conditions for laser plasmas to induce lightning. The design of our field experimental site was based on the conditions for the plasmas and field strength in laboratory scale. Methods have to be developed to produce sufficiently long and effective plasmas in air using a feasible laser system and optics. A new type of focusing optics with a multi-focusing function has been developed. For field experiments aiming triggering natural lightning, high output power laser system and large aperture focusing optics have been developed. The field experimental site is equipped with a number of thunderstorm and lightning diagnostic system. These systems will be described in detail. Finally some results from the field experiments such as producing a long plasma channel, measurements of field strength of thunderclouds and laser transmission in thunderstorms will be described.

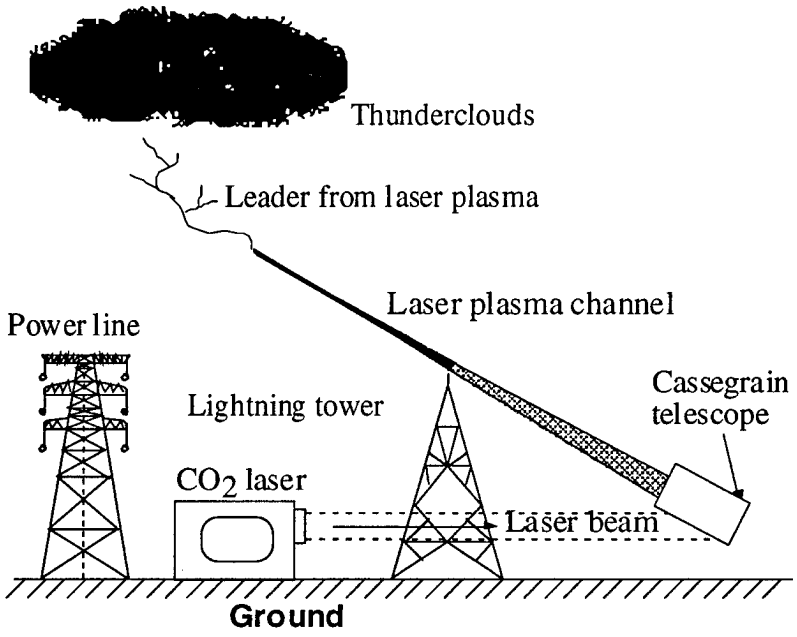



Figure 1. Schematic diagram of laser triggered lightning system

## 3. PRELIMINARY LABORATORY EXPERIMENTS

### 3.1 Characteristics of laser plasma channel

When an intense laser beam is focused in air, two kind of breakdown processes will take place; 1) air molecule breakdown and 2) aerosol breakdown. The air molecule breakdown process has threshold intensity of $10^{10}$ W/cm$^2$, two orders of magnitude higher threshold than that of aerosol breakdown. Thus plasma channel usually consists of a number of plasma beads made from aerosols as a seed. A blown up photograph of a plasma channel is shown in Fig. 2. Approximately 100J of 10 μm laser energy was focused in 1 m long region. The focused laser intensity was ~$10^9$ W/cm$^2$.

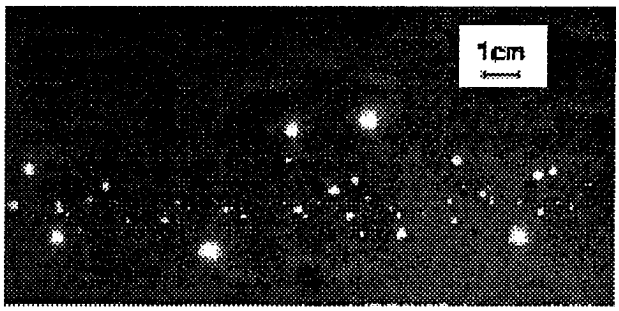



Figure 2. Plasma channel consists of plasma beads due to aerosol ionization

The density of the plasma beads is approximately 0.3 cm$^{-3}$. This number agrees to the measured aerosol distribution in our laboratory. Given the focused laser intensity of $10^9$ W/cm$^2$ and referring to the measurements by Lencioni [3], aerosols larger than 1 μm can be attributed to plasma production. The plasma bead density increases as the absorbed laser energy increases.

### 3.2 Leader initiating conditions

To realize laser triggered lightning, it is crucial to initiate a leader in plasma channel. We measured the

leader initiating field strength as a function of laser energy. A pair of 1.5m×2.0m plane electrodes with a 0.5-m separation was used to give uniform electric fields. Each electrode had a 50 mm diameter hole to let the laser beam go through into the gap. Negative high voltages were applied on an electrode where laser beam is incident. An impulse generator (1 MV maximum output in 50 ms pulse width (FWHM:Full Width at Half Maximum)) was used for voltage source. The minimum electric field for flashover to occur was measured as a function of laser energy, i. e. the plasma beads density. We assume that whenever a leader initiates, it leads to a flashover. Thus the minimum flashover fields are identical to the leader initiating fields.

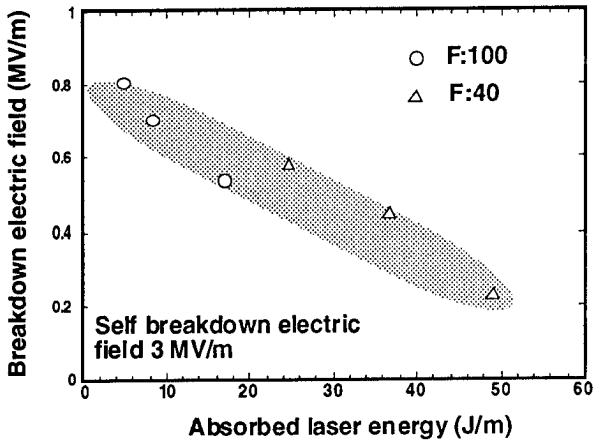



Figure 3. The breakdown electric fields decres as the laser energy or plasma density decreases

Uniform laser energy absorption over the entire plasma was assumed for calculating the abscissa. The initiating electric fields decrease as the input laser energies increase. A numerical calculation shows that the electrical field at 10 cm from the top of a 50-m lightning tower under typical thunderstorm reaches as high as 0.6 MV/m. These data interrelate the laser energy, the position of the laser beam and the height of the tower for initiating a leader from the tower into the plasma.

### 3.3 Verification of discharge guiding effects

To verify the strong guiding effects of plasma channel on electrical discharge, a folded plasma path was formed between a pair of rod electrodes. The plasma channel was formed in zig-zag shape or "Z" shape so that the discharge path is parallel to the equi-potential surface. A total laser energy of 100 J was divided into 3 parts. The total length of the path was 4 m.

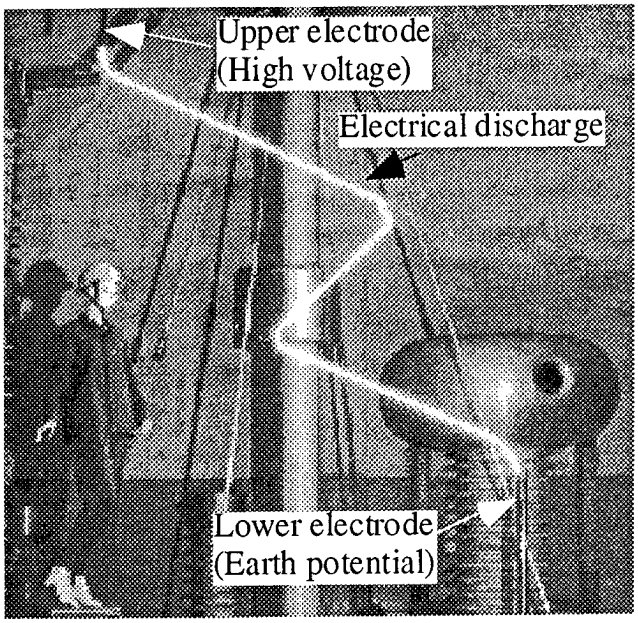



Figure 4. Electrical discharge is guided by plasma in "Z" shape

Figure 4 is a time integrated photograph of an electrical discharge triggered and guided by a laser plasma. Negative high voltage was applied on the upper rod electrode. Note that the middle portion of the plasma path is near parallel to the equi-potential surface and therefore, a natural discharge won't take place. This fact indicates that once leader initiates and starts propagating in a plasma channel, the leader brings the electrode potential with it and distorts and enhances the electric field at the tip The leader keeps propagating due to the enhanced fields and the guiding effect of plasma channel.

### 3.4 Multi-focusing mirror

In the real laser triggered lightning, laser plasma channels with a sufficient length have to be produced at the top of a 50-m tower. Focusing optics with a single focal point cannot be used because of the fact that the 10-μm laser light does not propagate beyond the plasma produced in air (cut-off density of the 10-μm light is $10^{19}$ $cm^{-3}$ which is two orders of magnitude less than air plasma). This prohibits a long plasma channel to be produced. To circumvent the difficulty, a new type of mirror with multiple focuses has been developed.

Figure 5 shows the principle of the mirror. The mirror consists of multiple concave surfaces so that each surface focuses laser light at different position and produces relatively long plasma. In this sense the mirror is called MACH (Multi Active CHannel) mirror. Since the laser light through the outer surface of the mirror goes round the plasmas made by other focuses, a very long plasma can be produced. An 8.5 m of laser plasma triggered discharge has been achieved which had not been possible with single-focus mirrors.

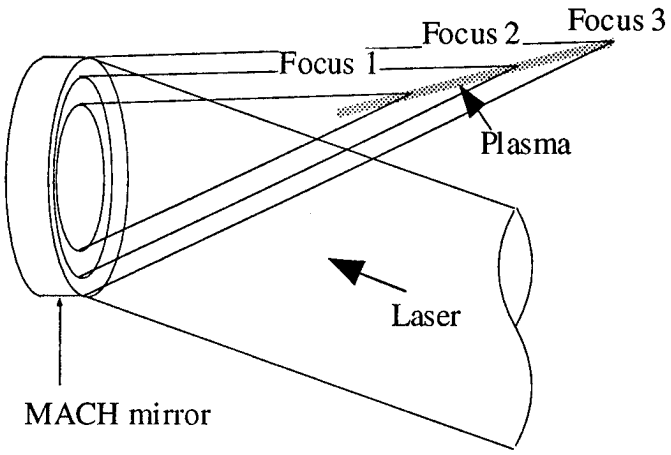



Figure 5. A multi-focus mirror focuses energies along laser axis

## 4. LASER TRIGGERED LIGHTNING SYSTEM

### 4.1 Overview of the field experimental site

Based on the results of the laboratory experiments, field experimental site was designed to test the idea of LTL. The purpose of the experiments were as follows. 1) Establishing LTL system which works in various weather conditions under thunderstorms. 2) Testing laser and focusing optics for producing sufficiently dense and long plasma channels at the top of a lightning tower. 3) Developing thunderstorm diagnostics systems for lightning forecasting and characterization of thunderstorms. And finally 4) verifying the initiation and propagation of electrical leader in plasma channel and triggering natural lightning. The system consists of four principal elements: 1) laser system, 2) focusing optics, 3) thunderstorm and lightning diagnostics and 4) operation and monitoring room.

Figure 6 depicts our field experimental site. The main facilities were built at the top of a 200-m high hill, called Dake-yama. The laser and focusing optics are in the buildings at the foot of the lightning tower. The laser control is 60 m away from the tower and connected with the laser system and diagnostics through optical fibers to avoid electrical hazards to personnel. The control building also functions as a terminal of thunderstorm diagnostics so that the timing of the laser irradiation is determined according to the thunderclouds' conditions.

Beside the thunderstorm diagnostics on the hill, there are three satellite observation stations equipped with various EM wave detectors 4 to 10 km away from the main site.

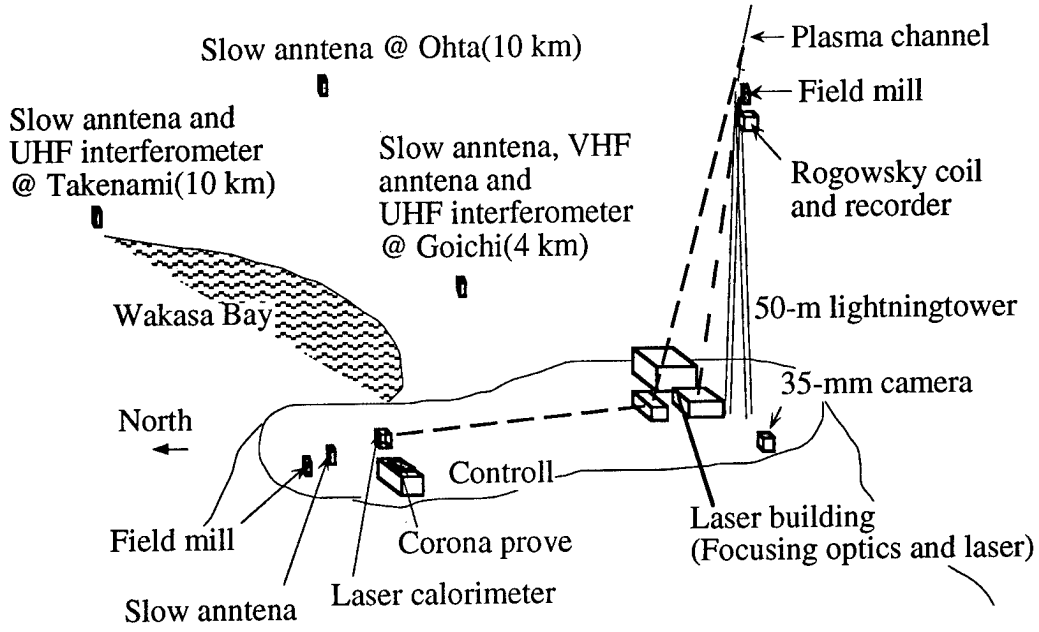



Figure 6 LTL field experimental site has been established on a 200-m high "Dake-yama"

**4.2 Laser system**

The laser system used for the experiment has a double beam configuration. It delivers 1-kJ output per beam in 50 ns pulse width (FWHM) from normal oscillations. The oscillator is configured to an unstable resonator with a beam aperture of 20 cm in diameter. The laser gas consisting of $CO_2$ and $N_2$ (4:1) is pumped by electron beam controlled discharge. Using electron beams, one can easily sustain discharges across the laser gas with relatively low voltages.

**4.3 Focusing system**

Making a dense plasma channel at the top of the 50-m tower, a same f number has to be kept in designing focusing optics. From laboratory experiments f numbers of 50 to 100 were found to be suitable. Cassegrain type focusing telescopes were designed to obtain such large f numbers from 20 cm beam diameter. The principal mirrors are 100 cm and 50 cm in diameters and polished spherically. To reduce the weight of the mirror, "bubble quartz" is used for the principal mirror. The secondary mirror surfaces were aspherically processed so that the system has multiple focusing points to produce long plasma channels or concentrate laser energies in a small region.

**4.4 Lightning tower**

The height of the tower was determined according to the laboratory experiments which suggest that around 500 CV/m of field strength is necessary to initiate a leader with the present laser capacity. Assuming that typical thunderclouds give 10 kV/m uniform field strength between the ground, the 50-m high tower enhances the field to 500 kV/m within 20 cm from the top. The tower foot is grounded with less than 10 Ω.

The tower is equipped with a Rogowsky coil and a field sensor (field mill) at the top. Rogowsky coil is used to measure the current wave forms when lightning hits the tower. Up to 10 wave forms are stored in an IC card and post-processed. The field sensor detects the locally enhanced field strength at the tower top. The signal is sent to the control room through an optical link so that a real time field strength can be monitored for laser irradiation.

# 5. THUNDERSTORM DETECTION SYSTEM

## 5.1 Field mills (Electric field sensor)

The field mill detects ambient DC fields produced between thunderclouds and the ground which are considered to directly determine the laser irradiation timing since, contrary to other diagnostics, it doesn't depend on the thundercloud discharges and therefore, could give precursor to lightning. Two detectors were located at the top of the lightning tower and on the ground, 80 m away from the tower top.

The measurement of the field mill is sometimes disturbed by falling snow even though it is equipped with a heater. This is a severe problem since winter thunderstorms are always accompanied by snow or hail. One of the field mills on the ground is set up up side down so that snow won't build up on the detector.

## 5.2 Corona prove

Corona prove measures currents induced by enhanced electric fields at the tip of a sawing needle. It is the simplest field sensor and yet gives important information for laser irradiation timing. The prove measures corona current which appears when ambient electric fields exceed certain value ( corona threshold ). Since it shows threshold characteristics, it gives distinguishable signal for laser irradiation timing.

## 5.3 Slow antenna

Slow antenna can detect from nearly DC field to 100 MHz field variation. From the amplitude of the signals, one can determine the amount of charges neutralised in a discharge. To do this, four slow antennas are distributed with 4 to 10 km separations. Each antenna is equipped with a GPS (Global Positioning System) to obtain synchronised GMT from satellites. Thus both strength and the location of lightning discharges can be obtained.

## 5.4 Interferometer

The principle of interferometer is same as that of EM-wave telescope, that is, the direction of the incident EM waves is obtained by measuring the phase difference of the wave between two closed by antennas. One system is equipped with a long range and a short range arm. Since the EM waves are emitted at the tip of leader propagation, time and spatial resolved measurements give the information of the thunderbolt dynamics. By using multiple interferometer systems, one can map out the lightning discharge path in three dimensions.

## 5.5 SAFIR

"SAFIR" is the similar technique as the interferometer and has much wider range of detection. The system consists of three antennas with a span of 100 km and traces thunderstorm discharge activity. All the antennas are linked with dedicated telephone lines to synchronise. The system can be used as a long term storm monitoring.

## 6. RESULTS FROM THE FIELD EXPERIMENTS

### 6.1 Electric field measurements

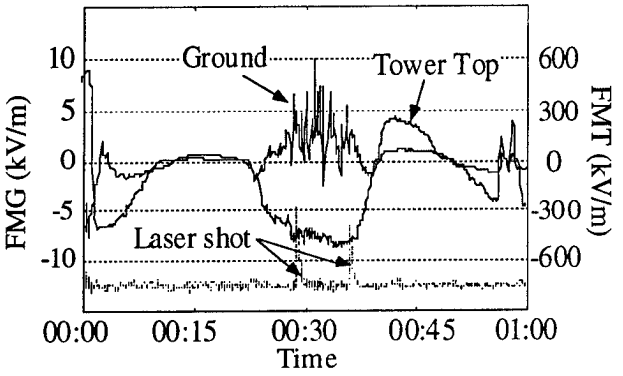



Figure 7. Time elapse of the electric fields at the top of the tower and on the ground

Figure 7 shows the time elapse of the field mill measurements on the ground and at the tower top. The left and the right vertical axis corresponds to the ground fields and the tower top fields respectively. It is clearly shown that the fields at the tower top is approximately two orders of magnitude larger than that on the ground, the enhancements predicted by electrostatic calculation.

In general, the tower-top and on-the-ground field mills indicate the similar field trends. However, in this particular measurement, polarity of the fields reversed between the tower top and on the ground, phenomenon observed once in a while during the experiments. This polarity-reverse phenomenon can be due to a space charge distribution of small scale structure of the order of a few tens of meters. When such a space charge structure exists, the electric field of the thundercloud will be shielded or even the polarity reverse takes place. In other incidence when several lightning strikes took place near the site (the closest one was 350 m away), the field mills observed the polarity reverse. In this particular case, the tower top field was over 500 kV/m while the on-the-ground field was near zero. These observations indicate that the determination of the laser irradiation timing cannot depend on the field mill measurement alone.

### 6.2 EM wave measurements

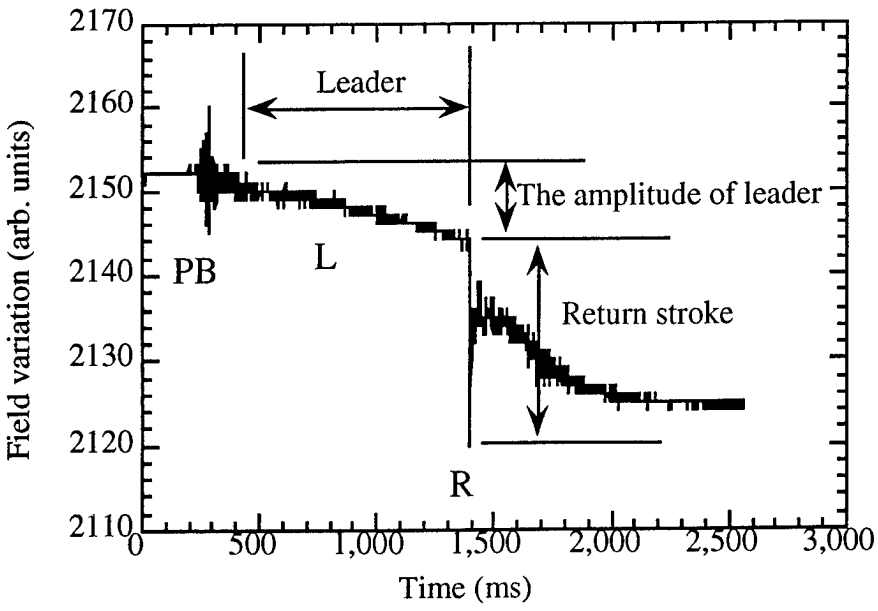



Figure 8. EM wave from lightning discharge exhibits a preliminary breakdown (PB) and leader propagation

The wide band slow antenna detects EM waves generated due to lightning discharge development. The wave form is typically divided into three phases; (1) Preliminary Break-down (PB), (2) leader propagation, and (3) return stroke. As shown in the figure, there is a time lag of the order of 100 ms between the PB and the return stroke. If the leader propagation occurs near the field experimental site, one can expect the field enhancement on the ground due to the approach of the leader. Therefore, the possibility of triggering could be increased if plasma is formed with the PB signal.

Figure 9 shows the plasma channel produced at the top of the tower using the 2-kJ laser system and two Cassegrain focusing telescopes. The total length of the plasma in this case is 13 m (a combination of an 8-m and a 5-m long plasma channels). The 5-m long plasma was formed so that the plasma density is very high By replacing the

secondary mirror of the focusing telescope with a mirror for multiple focusing mode, forming up to 20 m of plasma channel using a single beam was demonstrated.

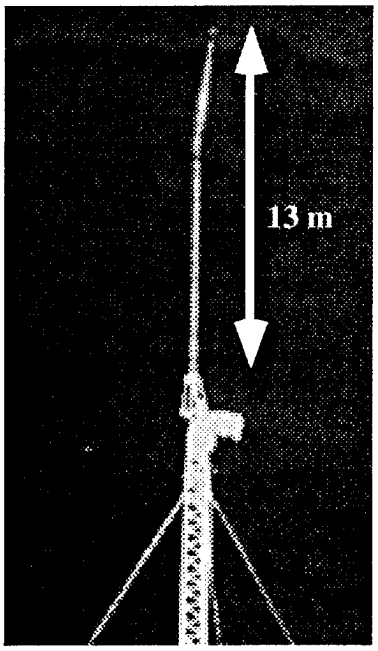
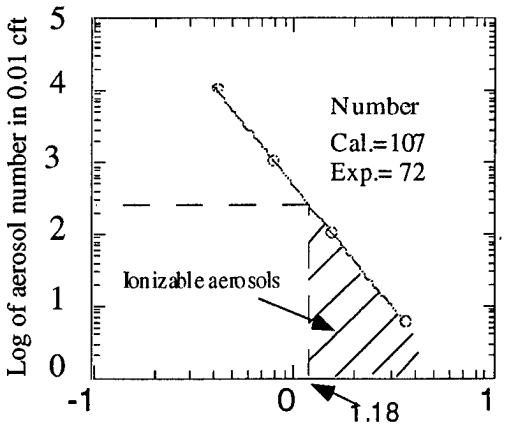



Figure 9. Two plasma channels are connected at the tower top

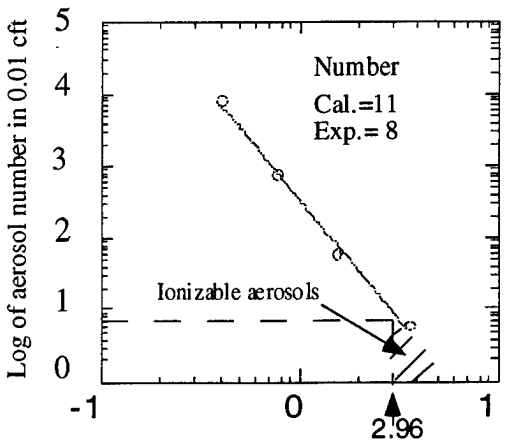
The plasma channel shown in Fig. 9, however, was taken in fine weather. The plasma density decreases to 20 % at most in very heavy snow falling. This is attributed to decrease of aerosols in air and laser energy reduction. The cause of decreasing aerosol density is considered to be snow sweeping effects and repelling effects due to corona discharge. Since smaller aerosol won't be ionized as laser intensity decreases, the above mechanisms reduces the plasma density significantly. Figure 10 shows the aerosol distributions in fine and snow weather conditions. The aerosols which can be ionized are indicated by hatched region. Since the threshold diameter of aerosols for plasma generation is determined by laser intensity, it is indicated on the ordinate after Lencioni.[3]

The plotted data were measured by a dust counter as the plasma channel was generated. The calculated values of aerosols decrease from 107 to 11 while experimental values decrease from 72 to 8, reasonably in good agreement.

The remedies for the problem are to increase the laser intensity and to deliver aerosols artificially near the tower top. The methods for increasing laser intensity include the improvement of the laser focusing characteristics and shortening of the laser pulse width.




a) Fine




b) Snow

Figure 10 Number of plasma beads depends on the aerosol distribution

## 7. CONCLUSIONS

The research of LTL has passed two stages so far; (1) preliminary laboratory experiments and (2) laser and focusing system development and their installation into the field experimental site.

In the laboratory experiments, mechanism of plasma channel formation in air was studied. It was shown that the plasma channel consists of a number of plasma beads and does not have a very good conductivity like metals. However, it was verified that such plasma has both leader initiating effect and discharge guiding effect. The conditions for laser plasma to trigger leader propagation were measured in terms of laser energies and electric field strength. In the field measurements, the conditions do exist at the top of 50-m high lightning tower when thunderclouds are overhead.

A 2-kJ $CO_2$ laser system and large aperture Cassegrain type focusing telescopes were developed for field experiments. It has been confirmed that the system produces long dense plasma channel at the top of the lightning tower. However, in snowy conditions, it was found that the density of the plasma channel decreases due to aerosol reduction and laser energy attenuation.

## 8. REFERENCES


1. L. M. Ball, Appl. Opt. 13 pp. 2292, 1974.

2. C. W. Schubert, "Investigation into Triggering Lightning with a Pulsed Laser", presented at IEEE Int. Pulse Power Conf., 1979.

3. D. E. Lencioni, "The effect of dust on 10.6-μm laser-induced air breakdown", Appl. Phys. Lett., 23, 1, pp. 12, 1973

# CONFERENCE PARTICIPANTS

| Name | Affiliation | Telephone |
|---|---|---|
| Adamo, Richard C. | SRI International - Bldg. 408/62<br>333 Ravenswood Avenue<br>Menlo Park, CA 94025<br>USA | TEL: (415) 859-2370<br>FAX: (415) 859-6259 |
| Adang, Tom, Colonel | USAF<br>1201 Minuteman St.<br>Patrick AFB, FL 32925<br>USA | TEL: (407) 494-7426<br>FAX: (407) 853-4315 |
| Albright, David L. | U.S. Army Aviation and Troop Command<br>2967 Westminster Drive<br>Florissant, MO 63033<br>USA | TEL: (314) 263-1648<br>FAX: (314) 263-1622 |
| Alfas, Swen | ELKRAFT, Innovation Dept.<br>Lautruphoj 5<br>2750 Ballerup<br>Denmark | TEL: (+45) 44 66 00 22<br>FAX: (+45) 44 65 61 04 |
| Antley, Mike | Scientech, Inc.<br>6121 Indian School Road, N.E.<br>Suite 232<br>Albuquerque, NM 87110<br>USA | TEL: (505) 881-9139 |
| Arellano, Joe | Sandia National Labs<br>P.O. Box 5800, MS 1157<br>Albuquerque, NM 87185<br>USA | TEL: (505) 845-7204<br>FAX: (505) 845-7602 |
| Bagwell, David W. | AMTEC Corp.<br>1309 Quarry Road<br>Union Grove, AL 35175<br>USA | TEL: (205) 876-1798<br>FAX: (205) 842-9637 |
| Barnes, Arnold A. | Phillips Lab/GPA<br>29 Randolph Road<br>Hanscom AFB, MA 01731-3010<br>USA | TEL: (617) 377-2939<br>FAX: (617) 377-2984 |
| Baseley, Dennis | USAF ASC/EHAI<br>2450 D Street<br>Wright Patterson AFB, OH 45433-7630<br>USA | TEL: (512) 255-5078 |

| Name | Affiliation | Telephone |
|---|---|---|
| Bassett, David | Army Research Lab<br>AMSRL-SL-I<br>Aberdeen Proving Ground, MD 21005<br>USA | TEL: (410) 278-8624<br>FAX: (410) 278-7254 |
| Benson, Barry | R&B Enterprises<br>Naval Air Warfare Center Aircraft Division<br>EMT Branch<br>Bldg. 2100<br>Patuxent River, MD 20670<br>USA | |
| Bérger, Gerard | Laboratoire de Physique des Gaz ete des Plasmas<br>Décharges Electriques et Environnement<br>CNRS-SUPELEC, Plateau de Moulon<br>91990 GIF sur YVETTE<br>France | TEL: 33 169851777<br>FAX: 33 169410334 |
| Bergman, Carl W. | Carl Bergman & Assoc.<br>P.O. Box 549<br>Ranier, WA 98576<br>USA | TEL: (360) 446-7750<br>FAX: (360) 446-7750 |
| Bernstein, Ralph | EPRI<br>3412 Hillview Avenue<br>Palo Alto, CA 94304<br>USA | |
| Binford, Ronald C. | Mission Instruments Co.<br>5937 East Pima Street<br>Tucson, AZ 85712-4353<br>USA | TEL: (602) 721-9242<br>FAX: (602) 721-6697 |
| Blackwell, H. | NAVAVN MSAS CP<br>AV8BISST-2<br>Cherry Plaza<br>Havelock, NC 28532<br>USA | |
| Blanks, Wayne, CWO4 | Naval Safety Center<br>375 A Street<br>ATTN: Code 125<br>Norfolk, VA 23511-4399<br>USA | TEL: (804) 564-206 |
| Blundell, Russell | Commander,<br>US Army White Sands Missile Range<br>ATTN: STEWS-DATS-O<br>White Sands Missile Range, NM 80002<br>USA | |

| Name | Affiliation | Telephone |
|---|---|---|
| Borgeest, K. | Technical University of Hamburg - Harburg<br>Dept. of Measurement Engineering/EMC<br>Harburger Schloss-Strasse 20, D-21071<br>21071 Hamburg<br>Germany | TEL: 49-40-7718-2873<br>FAX: 49-40-7718-2382 |
| Boulay, Jean-Louis | ONERA<br>BP72<br>92322 Châtillon Cedex<br>France | TEL: 33 1 66736855<br>FAX: 31 166736168 |
| Bowly, Tim | British Aerospace Dynamics Ltd.<br>FPC 065<br>EMC Test Facility<br>Filton, Bristol BS 125RY<br>England | |
| Brehm, Ernst H. | ABB Management Services GmbH<br>P.O. Box 100351<br>D 68128 Mannheim<br>Germany | TEL: (01149)6213813518<br>FAX: (01149)6213817480 |
| Briët, Richard | LT-MP Applications<br>5661 Citrus Court<br>Cypress, CA 90630<br>USA | TEL: (714) 826-8490<br>FAX: (714) 826-8490 |
| Britting, Al | Aerospace Corp.<br>P.O. Box 92957<br>Los Angeles, CA 90009<br>USA | TEL: (310) 336-9253<br>FAX: (310) 336-7681 |
| Brooks, John | U.S. Air Force<br>205 WD Ste 318<br>Eglin AFB, FL 32578<br>USA | |
| Brooks, Michael W. | INET<br>INI-4<br>Kennedy Space Center, FL 32899<br>USA | TEL: (407) 867-4879<br>FAX: (407) 867-7534 |
| Brown, Jeffrey C. | NASA Lewis Research Center<br>21000 Brook Park Road<br>MS 86-5<br>Cleveland, OH 44135<br>USA | TEL: (216) 433-3888<br>FAX: (216) 433-6382 |

| Name | Affiliation | Telephone |
|---|---|---|
| Burrows, Brian | 5 Willow Lane<br>Milton, Abingdon, Oxon OX144EG<br>United Kingdom | TEL: +44 1235 821620<br>FAX: +441235 817994 |
| Busse, Heinrich | BAKWVT<br>Seckenheimer Landstr 8-10<br>Mannheim 68163<br>Germany | TEL: 49 621 418091<br>FAX: 49 621 41843 |
| Calabria, Joseph A. | CSC<br>200 Lakeside Drive<br>Suite 248<br>Horsham, PA 19044-2316<br>USA | TEL: (215) 957-8905<br>FAX: (215) 957-2890 |
| Carmona, Carlos E. | REN<br>AV. E.U.A. 55 - 1700 LISBOA<br>Portugal | TEL: (351) 01-8470180<br>FAX: (315) 01-809444 |
| Chai, J. C. | The Aerospace Corporation<br>P.O. Box 92957<br>M4-179<br>Los Angeles, CA 90009<br>USA | TEL: (310) 336-8341<br>FAX: (310) 336-5581 |
| Chen, K. C. | Sandia National Laboratories<br>Electromagnetic Analysis and Test Dept.<br>P.O. Box 5800<br>Albuquerque, NM 87185-0865<br>USA | TEL: (505) 845-8647<br>FAX: (505) 844-7857 |
| Chen, Yung G. | Maxwell Laboratories, Inc.<br>8888 Balboa Avenue<br>San Diego, CA 92123<br>USA | TEL: (619) 576-7852 |
| Clark, Bill | Clark-MXR, Inc.<br>3349 Monroe Avenue<br>Rochester, NY 14618<br>USA | |
| Clelland, Michael | Naval Air Warfare Center Aircraft Division<br>EMT Branch<br>(Code 5.1.7.2 - MS3)<br>22633 Joyce Road<br>Patuxent River, MD 20670<br>USA | TEL: (301) 342-3872<br>FAX: (301) 342-3786 |

| Name | Affiliation | Telephone |
|---|---|---|
| Clerc, Jean-Pierre | CEAT<br>23, Avenue H. Guillaumet<br>31056 TOULOUSE CEDEX<br>France | TEL: (33)61.58.73.22<br>FAX: (33)61.58.73.39 |
| Cline, Jay | Dayton Granger, Inc.<br>P.O. Box 350550<br>Ft. Lauderdale, FL 33335<br>USA | TEL: (305) 463-3451<br>FAX: (305) 761-3172 |
| Cohen, Richard L., Dr. | PANAMAX<br>150 Mitchell Boulevard<br>San Raffael, CA 94903-2057<br>USA | TEL: (800) 472-555 ex. 3<br>FAX: (415) 472-5540 |
| Collier, Richard S. | Electromagnetic Applications, Inc.<br>7655 West Mississippi Ave.<br>Suite 300<br>Lakewood, CO 80228-4332<br>USA | TEL: (303) 980-0070<br>FAX: (303) 980-0836 |
| Cooper, Mary Ann | The University of Illinois at Chicago,<br>Department of Emergency Medicine<br>M/C 724, Room 618, College of Med. West<br>1819 West Polk Street<br>Chicago, IL 60612-7354<br>USA | TEL: (312) 413-7480<br>FAX: (312) 413-0289 |
| Corbett, David | Short Brothers<br>Airport Road<br>Belfast BT39DZ<br>Northern Ireland | TEL: 011441232462576<br>FAX: 011441232733427 |
| Crain, Bruce | Lockheed Martin<br>1250 Rockcrest Dr.<br>Marietta, GA 30062-3018<br>USA | TEL: (404) 494-7411 |
| Craven, Jeff | U.S Army Redstone Technical Center<br>ATTN: STERT-TE-E-EM<br>Redstone Arsenal, AL 35898-8052<br>USA | |
| Crouch, Keith | Lightning Technologies, Inc.<br>10 Downing Parkway<br>Pittsfield, MA 01201<br>USA | TEL: (413) 499-2135<br>FAX: (413) 499-2503 |

| Name | Affiliation | Telephone |
|---|---|---|
| Crowley, Tom | Commander, US Army ARDEC<br>Building 61 South<br>Picatinny Arsenal, NJ 07806<br>USA | TEL: (201) 724-3124 |
| Cummins, Kenneth | Global Atmospherics<br>2705 E. Medina Road<br>Tucson, AZ 85706<br>USA | TEL: (520) 741-2838<br>FAX: (520) 741-2848 |
| Daehne, Armin R. | Bundesaunt fuer Wehrtechnik und Beschaffung<br>LG 1112<br>Postfach 7360<br>D 56057 Koblenz<br>Germany | |
| Davis, Michael | Naval Air Systems Command<br>1421 Jefferson Davis Highway<br>Arlington, VA 22243<br>USA | |
| Dawson, John | Naval Air Warfare Center Aircraft Division<br>E3 Division<br>M.S. 3, Hangar 144<br>48158 Standley Road<br>Patuxent River, MD 20670<br>USA | TEL: (301) 342-4681 |
| Douay, Arnauld | Aerospatiale<br>12 rue Pasteur B.P. 76<br>Suresnes 92152<br>France | TEL: (415) 859-3853<br>FAX: (415) 859-2260 |
| Doyle, Jack | JP Doyle Enterprises<br>8600 Bound Brook Lane<br>Alexandria, VA 22309<br>USA | |
| Dubovoy, Edward I. | 2/11 Chertanovskaja<br>Ap. 2<br>113208 Moscow<br>Russia | TEL: 311-59-57 |
| Dulcey, Joseph | Naval Surface Warfare Center<br>Indian Head Division<br>Electronic Systems Development Branch<br>(Code 6720)<br>Indian Head, MD 20640<br>USA | TEL: (301) 743-4466<br>FAX: (301) 743-4004 |

| Name | Affiliation | Telephone |
|---|---|---|
| Dunkley, Vernon | AEA Technology Lightning Test & Technology<br>D1 Culham, Abingdon<br>Oxfordshire<br>OX14 3DB<br>United Kingdom | TEL: 0235 464243<br>FAX: 0235 464325 |
| Farfal, Patrick | Aerospatiale Espace & Défense<br>Boîte postale no 2<br>78133 Les Mureaux Cedex<br>France | TEL: 33 1 34 92 23 70<br>FAX: 33 1 34 92 13 11 |
| Fellin, David E. | Naval Air Systems Command<br>(AIR-4.1.7)<br>1421 Jefferson Davis Highway<br>Arlington, VA 22243<br>USA | TEL: (703) 604-6060 |
| Field, Charlie | Sandia National Labs<br>P.O. Box 5800, MS 1157<br>Albuquerque, NM 87185<br>USA | TEL: (505) 845-7204<br>FAX: (505) 845-7602 |
| Fisher, Bruce | NASA<br>Langley Research Center<br>MS247<br>Hampton, VA 23681-0001<br>USA | |
| Fisher, Franklin A. | Lightning Technologies<br>10 Downing Parkway<br>Pittsfield, MA 01201<br>USA | TEL: (413) 499-2135<br>FAX: (413) 499-2503 |
| Fisher, Richard J. | 1797 Pleasant Grove Rd.<br>Claysville, PA 15323<br>USA | TEL: (412) 663-5006<br>FAX: (412) 663-5006 |
| Foegelle, Michael | EMCO<br>2205 Kramer Lane<br>Austin, TX 78758<br>USA | TEL: (512) 835-4684 x650 |
| Frazier, Samuel J. | Naval Air Warfare Center Aircraft Division<br>Building 966<br>Patuxent River, MD 20670-5304<br>USA | TEL: (301) 342-3868<br>FAX: (301) 342-3871 |
| Garmon, John | USAF OC-ALC/LCRE<br>Tinker Air Force Base<br>Oklahoma City, OK 73145<br>USA | TEL: (405) 736-3832<br>FAX: (405) 736-5604 |

| Name | Affiliation | Telephone |
|---|---|---|
| Garry, John | FAA<br>FAATC, ACT-330<br>Atlantic City, NJ 08405<br>USA | TEL: (609) 485-6734<br>FAX: (609) 485-6809 |
| Gazzale, Jim | SENTEL Corp.<br>225 Reinekers Lane<br>Suite 500<br>Alexandria, VA 22314<br>USA | TEL: (703) 739-0084 |
| George, Stan | US Navy<br>NSWCDL Code F54<br>17320 Dahlgren Road<br>Dahlgren, VA 22448-5100<br>USA | TEL: (540) 653-8481 |
| Geradt, R. | ABB-Germany<br>P.O. Box 100351<br>Mannheim 68128<br>Germany | TEL: 011-49-621-381-3655<br>FAX: 011-49-62-381-7480 |
| Glynn, Michael S. | FAA<br>ACD 230<br>Atlantic City Airport, NJ 08405<br>USA | TEL: (609) 485-4138<br>FAX: (609) 485-4005 |
| Goebel, David | US Army CECOM<br>AMSEL-RD-C2-PP-PA<br>8713 Standish Road<br>Alexandria, VA 22308<br>USA | TEL: (703) 704-1859<br>FAX: (703) 704-3333 |
| Goldblum, Charles | R&B Enterprises<br>20 Clipper Road<br>West Conshohocken, PA 19428-2721<br>USA | |
| Gondot, Pascal | Aerospatiale<br>12, rue Pasteur B.P. 76<br>92152 Suresnes Cedex<br>France | TEL: 33 1 46 97 33 79<br>FAX: 33 1 46 97 30 08 |
| Grace, Andrew | BT Laboratories<br>B54 Room 74<br>Martlesham Heath<br>Ipswich, Suffolk, IP5 7RE UK<br>United Kingdom | TEL: +44-1473-644257<br>FAX: +44-1473-640929 |

| Name | Affiliation | Telephone |
|---|---|---|
| Graves, Chuck | TRW<br>12229 Dalewood Drive<br>Wheaton, MD 20902<br>USA | |
| Grenis, Matthew | Naval Air Systems Command<br>1421 Jefferson Davis Highway<br>Arlington, VA 22243<br>USA | TEL: (703) 604-6060 |
| Grush, Donna J. | INEL<br>P.O. Box 1625<br>MS 3730<br>Idaho Falls, ID 83415-3730<br>USA | TEL: (208) 526-9406<br>FAX: (208) 526-9908 |
| Grzbowski, Stanislaw | Mississippi State University, Electrical &<br>Comp. Eng. Dept.<br>Box 9571<br>Mississippi State, MS 35762<br>USA | TEL: (601) 325-2148<br>FAX: (601) 325-2298 |
| Hardwick, John | AEA Technology, Lightning Test & Technology<br>Building D1, AEA Culham<br>Abingdon, Oxfordshire, OX14 3DB<br>United Kingdom | TEL: (44)-1235-464278<br>FAX: (44)-1235-464325 |
| Harrison, Steve | W. J. Furse & Co., Ltd.<br>Electronic Systems Protection Division<br>Wilford Road, Nottingham, NG2 1EB<br>United Kingdom | TEL: 011441159863471<br>FAX: 011441159860538 |
| Harwood, Theodore L. | CSC Professional Services Group<br>1215 Jefferson Davis Highway<br>Suite 1209<br>Arlington, VA 22202<br>USA | TEL: (703) 416-0966<br>FAX: (703) 416-0885 |
| Hash, George | FAA<br>DOT/FAA<br>Fort Worth, TX 76193-0150<br>USA | TEL: (817) 222-5139<br>FAX: (817) 222-5960 |
| He, Terri | Douglas Aircraft Co.<br>3855 Lakewood Blvd.<br>Long Beach, CA 90846<br>USA | TEL: (310) 593-8459<br>FAX: (310) 982-5030 |

| Name | Affiliation | Telephone |
|---|---|---|
| Heather, Fred | Naval Air Warfare Center Aircraft Division<br>Electromagnetic Systems (Code 5.1.7.1)<br>MS 3, 48158 Standley Road<br>Patuxent River, MD 20670-5304<br>USA | TEL: (301) 342-4681 |
| Heidler, Fridolin | Federal Armed Forces University Munich<br>Fakultat Elektrotechnik/Institut 7<br>Werner-Heisenberg-Weg 39<br>D-85577 Neubiberg<br>Germany | TEL: 0879 6004 3721<br>FAX: 089 6004 3723 |
| Hellman, Adrian | NSWC<br>17320 Dahlgren Rd.<br>Code F54<br>Dahlgren, VA 22448-5100<br>USA | |
| Hillyar, Charles C., Dr. | 4700 Ortega Blvd.<br>Jacksonville, FL 32210<br>USA | |
| Ho, Son | EG&G<br>BOC-329<br>Kennedy Space Center, FL 32815<br>USA | TEL: (407) 861-0626 |
| Holle, Ronald L. | National Severe Storms Lab<br>1313 Halley Circle<br>Norman, OK 73069<br>USA | TEL: (405) 366-0516<br>FAX: (405) 366-0472 |
| Holmes, S.W. | Sandia National Laboratories<br>Electromagnetic Analysis and Test Dept.<br>Albuquerque, NM 87185-0865<br>USA | TEL: (505) 845-8647<br>FAX: (505) 844-7857 |
| Hooper, Art | US Navy (SP27346)<br>Strategic Systems Programs<br>1931 Jefferson Davis Highway<br>Arlington, VA 22241-5362<br>USA | |
| Hopf, Christian | Federal Armed Forces University Munich<br>Et 7, Werner-Heisenberg - Weg 39<br>D-85577 Neubiberg<br>Germany | TEL: 49-89-60043736<br>FAX: 49-89-60043723 |

| Name | Affiliation | Telephone |
|---|---|---|
| Iacono, Anthony J. | Naval Air Systems Command<br>(AIR 4.1.7)<br>1421 Jefferson Davis Highway<br>Arlington, VA 22243-5200<br>USA | |
| Jacquette, Jim | NESCO Service<br>23 Roberts Street<br>Farmingdale, NY 11735<br>USA | TEL: (516) 224-2490<br>FAX: (516) 224-2499 |
| Jafferis, William | BJC<br>4140 Hickory Hill Blvd.<br>Titusville, FL 32780<br>USA | TEL: (407) 269-6943<br>FAX: (407) 264-0876 |
| Jones, Christopher | EW & Stealth Facilities Dept. W7G, British Aerospace<br>Warton Aerodrone, Preston<br>Lancs PR4 1AX<br>United Kingdom | TEL: 1772 854799 |
| Jones, Richard D. | Electromagnetic Analysis & Test Department<br>Sandia National Laboratories<br>P.O. Box 5800<br>Albuquerque, NM 87185-0865<br>USA | TEL: (505) 844-5662<br>FAX: (505) 844-7857 |
| Jue, Les | Naval Air Warfare Center Weapons Division<br>Code 41700E<br>Building 735<br>Pt. Mugu, CA 93042-5001<br>USA | |
| Junghans, Kay | NAVCOMSYSTEMS, Inc.<br>600 Maryland Ave., S.W.<br>Suite 300E<br>Washington, DC 20024<br>USA | TEL: (202) 863-0780 |
| Kaloterakis, Nickolas | Naval Surface Warfare Center<br>Indian Head Division<br>Electronic Systems Development Branch<br>(Code 6720)<br>Indian Head, MD 20640<br>USA | TEL: (301) 743-4466<br>FAX: (301) 743-4004 |

| Name | Affiliation | Telephone |
|---|---|---|
| Karabin, Christopher R. | Naval Surface Warfare Center<br>Indian Head Division<br>Code 6720R<br>101 Strauss Avenue<br>Indian Head, MD 20640<br>USA | TEL: (301) 743-4466<br>FAX: (301) 743-4004 |
| Kikuchi, Hiroshi | Nihon University, College of Science & Technology<br>8, Kanda Surugadai, 1-chome, Chiyodaku<br>Tokyo, 101<br>Japan | TEL: +813 3917 9418<br>FAX: +81-3-5275-8326 |
| King, Charles | 27030 40th Avenue South<br>Kent, WA 98032<br>USA | TEL: (206) 852-1449 |
| Kithil, Richard | National Lightning Safety Institute<br>891 North Hoover Avenue<br>P.O. Box 778<br>Louisville, CO 80027<br>USA | TEL: (303) 666-8817<br>FAX: (303) 666-8768 |
| Konings, Piet | S.W.I.F.T.<br>Avenue Adele 1<br>La Hulpe B1310<br>Belgium | TEL: +32 2 655 31 11<br>FAX: +32 2 655 32 26 |
| Krider, E. Philip | Institute of Atmospheric Physics, Room 542<br>PAS Bldg #81<br>University of Arizona<br>Tuscon, AZ 85721<br>USA | TEL: (602) 621-6831<br>FAX: (602) 621-6833 |
| Kroll, James T. | AFOSR/NM<br>110 Duncan Avenue<br>Suite B115<br>Bolling AFB<br>Washington, DC 20332<br>USA | TEL: (202) 767-5026 |
| Kuhlman, Brian | Douglas Aircraft<br>3855 Lakewood Boulevard 800-21<br>Long Beach, CA 90846<br>USA | TEL: (310) 496-9638 |
| Kuras, John | Boeing Helicopters, Mail Stop P24-51<br>P.O. Box 16858<br>Philadelphia, PA 19142-0858<br>USA | TEL: (610) 591-2384<br>FAX: (610) 591-8238 |

| Name | Affiliation | Telephone |
|---|---|---|
| Lessard, Briand J. | Lockheed Martin<br>86 S. Cobb Drive<br>Marietta, GA 30063-0982<br>USA | TEL: (770) 793-0693<br>FAX: (770) 793-0760 |
| Lie, T. J. | (M4/935) The Aerospace Corporation<br>P.O. Box 92957<br>Los Angeles, CA 90009<br>USA | TEL: (310) 336-8341<br>FAX: (310) 336-5581 |
| Lippert, Jack R. | Computer Science and Applications, Inc.<br>2 Clifford Drive<br>Shalimar, FL 32579<br>USA | TEL: (904) 651-4991<br>FAX: (904) 651-2816 |
| López, Raúl E. | National Severe Storms Laboratory/NOAA<br>1313 Halley Circle<br>Norman, OK 73069<br>USA | TEL: (405) 366-0416<br>FAX: (405) 366-0472 |
| Ludwar, Gerhard | BUNDESFORSCHUNGS-UND<br>PRUFZENTRUM ARSENAL<br>A-1031 Wien, Faradaygasse 3<br>Austria | TEL: 222-876-8804 |
| Luteran, Frank | R&B Enterprises<br>Naval Air Warfare Center Aircraft Division<br>EMT Site<br>Bldg. 2100<br>Patuxent River, MD 20670<br>USA | |
| Magyar, Ernest A. | Magyar & Associates, Inc.<br>1925 Clifford Street 301<br>Ft. Myers, FL 33901<br>USA | TEL: (813) 332-2075 |
| Maier, Launa | NASA<br>TE-ISD-3A<br>Kennedy Space Center, FL 32899<br>USA | TEL: (407) 867-4409<br>FAX: (407) 867-2848 |
| Maneuvrier, J. | NUCLETUDES<br>5 Avenue De Hoggar - BP 117<br>Les Ulis 91944<br>France | TEL: 69 071020<br>FAX: 69 072101 |
| Martin, Billy | Cessna Aircraft Co.<br>P.O. Box 7704<br>Witchita, KS 67277<br>USA | TEL: (316) 941-7895 |

| Name | Affiliation | Telephone |
|---|---|---|
| Mazur, Vladislav | National Severe Storms Laboratory<br>1313 Haley Circle<br>Norman, OK 73069<br>USA | TEL: (405) 366-0406<br>FAX: (405) 366-0472 |
| McClure, Bruce | United International Engineering, Inc.<br>EMT Site, Bldg. 2100<br>Patuxent River, MD 20670<br>USA | TEL: (301) 342-3872<br>FAX: (301) 342-3786 |
| McCormack, Jerry | McDonnell Aircraft Company<br>P.O. Box 516<br>St. Louis, MO 63166-0516<br>USA | |
| McDowall, Rosemarie L. | Galaxy Scientific Corporation<br>2500 English Creek Avenue<br>Pleasantville, NJ 08323<br>USA | TEL: (609) 485-5228<br>FAX: (609) 485-4005 |
| Mills, J. P., Jr. | FAA<br>P.O. Box 20636<br>ASO 471<br>Atlanta, GA 30320<br>USA | TEL: (404) 305-6588 |
| Mohd, Magsood | Sverdrup<br>P.O. Box 1935<br>Building 260<br>Eglin Air Force Base, FL 32542<br>USA | TEL: (904) 678-2001 |
| Moreau, J. P. | Dassault<br>Z.A. Villacoublay Velizy<br>Uelizy 78<br>France | |
| Nagabhushana, G. R. | High Voltage Engy Dept.<br>Indian Institute of Science<br>Bangalore 560012<br>India | TEL: 33-444-11 |
| Nguyen, Cuong C. | NASA<br>Kennedy Space Center<br>DF-ELD<br>Kennedy Space Center, FL 32899<br>USA | TEL: (407) 867-6566 |

| Name | Affiliation | Telephone |
|---|---|---|
| Nguyen Truong | NASA Langley<br>Bldg. 1220, MS 130<br>Hampton, VA 23681<br>USA | TEL: (804) 864-7528<br>FAX: (804) 864-4234 |
| Nial, Jack | Naval Surface Warfare Center<br>Indian Head Division<br>Electronic Systems Development Branch<br>(Code 6720)<br>101 Strauss Avenue<br>Indian Head, MD 20640<br>USA | TEL: (301) 743-4466<br>FAX: (301) 743-4004 |
| Nobis, Wolfgang | D-91171 Greding<br>WTB81<br>Germany | |
| Nozari, Bahman | McDonnell Douglas Corporation Douglas Aircraft<br>3855 Lakewood Boulevard<br>Long Beach, CA 90846<br>USA | TEL: (310) 593-0648<br>FAX: (310) 982-5030 |
| O'Neill, Mike | Telematic<br>Alban Park, Stalbans<br>AL4 OXY<br>United Kingdom | TEL: 44-1727833<br>FAX: 44-1727850687 |
| Oda, J. A. | Lockheed Martin Aeronautical<br>D7305 Z0199<br>86 South Cobb Drive<br>Marietta, GA 30063<br>USA | TEL: (404) 494-1097<br>FAX: (404) 494-5207 |
| Odam, Gerry AM | GAO Consultancy<br>Grantham House, 5 Kings Crescent<br>Barmouth<br>Gwynedd LL42 IRB<br>United Kingdom | TEL: 44 341-281012<br>FAX: 44 341-23403 |
| Olson, C. | Beech Aircraft Corp.<br>P.O. Box 85<br>Witchita, KS 67201<br>USA | |
| Olson, Glenn | The Boeing Co.<br>108 N. 67th Street<br>Seattle, WA 98103<br>USA | TEL: (206) 662-3119<br>FAX: (206) 662-2025 |

| Name | Affiliation | Telephone |
|---|---|---|
| Olson, Lee | SARA, Inc.<br>15262 Pipeline Lane<br>Huntington Beach, CA 92649<br>USA | TEL: (714) 373-5509 |
| Orsatti, Louis G. | Electronic Space Systems Corporation<br>Old Powder Mill Road<br>Concord, MA 01742<br>USA | TEL: (508) 369-7200<br>FAX: (508) 369-7641 |
| Parimuha, Edward M. | Naval Air Warfare Center Aircraft Division<br>22467 Millstone Road<br>Code 517200A, MS 3<br>Patuxent River, MD 20670-5304<br>USA | TEL: (301) 342-3872<br>FAX: (301) 342-3781 |
| Perala, Rod A. | EMA, Inc.<br>7655 W. Mississippi Avenue<br>Suite 300<br>Lakewood, CO 80228-4332<br>USA | TEL: (303) 980-0070<br>FAX: (303) 980-0836 |
| Peterson, James M. | FAA, Witchita Aircraft Certification Officer<br>1801 Airport Road, Room 100<br>Witchita, KS 67209<br>USA | TEL: (316) 946-4131<br>FAX: (316) 946-4407 |
| Pfeffer, Robert A. | U.S. Army Nuclear and Chemical Agency<br>7150 Heller Loop, Suite 101<br>ATTN: MONA-NU (R. Pfeffer)<br>Springfield, VA 22150-3198<br>USA | TEL: (703) 806-7860<br>FAX: (703) 806-7900 |
| Pitts, Felix | Retired NASA<br>506 Piney Point Road<br>Grafton, VA 23692<br>USA | TEL: (804) 898-8069 |
| Powers, Ed | KTAADN, Inc.<br>1320 Centre Street<br>Suite 201<br>Newton, MA 02153<br>USA | TEL: (617) 527-0056 |
| Press, James L. | R&B Enterprises<br>20 Clipper Road<br>West Conshohocken, PA 19428-2721<br>USA | TEL: (610) 825-1960<br>FAX: (610) 825-1684 |

| Name | Affiliation | Telephone |
|---|---|---|
| Primeau, Margaret | The Chicago Medical School<br>Department of Psychology<br>3333 Green Bay Road<br>North Chicago, IL 60064<br>USA | TEL: (708) 578-3305<br>FAX: (708) 578-3015 |
| Pühringer, Anton, Dr. | Zentralanstalt fur Meterologie<br>Gorgengasse 9-11/10<br>A 1190 Wien.<br>Austria | TEL: (011431) 36-60544 |
| Ragland, John | Naval Air Warfare Center Aircraft Division<br>Hangar 144<br>Patuxent River, MD 20670<br>USA | |
| Rasch, Nick | NICG Alumni, Triangle Consulting & Engineering Co.<br>18310 Candice Drive<br>Triangle, VA 22172<br>USA | TEL: (703) 321-5239 |
| Revay, Andrew W., Jr. | Florida Institute of Technology<br>150 West University Boulevard<br>Melbourne, FL 32901<br>USA | TEL: (407) 768-8022<br>FAX: (407) 984-8461 |
| Roberts, Edward F., Jr. | FAA/DOT<br>800 Independence Avenue, S.W.<br>ANS-520<br>Washington, DC 20591<br>USA | TEL: (202) 267-9382<br>FAX: (202) 267-5784 |
| Roy, Thomas | AMTEC Corp.<br>92 Rabbit Ridge Put Dr.<br>Danville, AL 35619<br>USA | TEL: (205) 876-3263<br>FAX: (205) 842-9637 |
| Rynne, Tim | SARA, Inc.<br>15262 Pipeline Lane<br>Huntington Beach, CA 92649<br>USA | TEL: (714) 373-5509 x220<br>FAX: (714) 373-4771 |
| Sakate, Fred | McDonnell Douglas Transport Aircraft<br>25591 Golden Spring<br>Dana Point, CA 92629<br>USA | TEL: (310) 497-5142 |

| Name | Affiliation | Telephone |
|---|---|---|
| Sandip, Lal | Kennedy Space Center<br>BOC-130<br>Kennedy Space Center, FL 32899<br>USA | |
| Saraceni, Pete | FAA<br>FAA Technical Center<br>AAR-421<br>Atlantic City Int'l Arpt, NJ 08405<br>USA | TEL: (609) 485-5577<br>FAX: (609) 485-4005 |
| Sargent, Noel B. | NASA - Lewis<br>21000 Brookpark Road<br>Cleveland, OH 44135<br>USA | |
| Schaffar, André | Aerospatiale<br>Espace & Défense<br>BP no96<br>78133 Les Mureaux Cedex<br>France | TEL: 33 1 34 92 27 45<br>FAX: 33 1 34 92 17 34 |
| Schnetzer, G. H. | 10509 Moontree Court<br>Albuquerque, NM 87111<br>USA | TEL: (505) 845-8647<br>FAX: (505) 844-7857 |
| Schroeder, Jack E. | Lightning Diversion Systems<br>17851 Jamestown Lane<br>Huntington Beach, CA 93647<br>USA | TEL: (714) 841-1080<br>FAX: (714) 841-5095 |
| Schultz, John | Naval Air Systems Command<br>10405 Karmich Ct.<br>Fairfax Station, VA 22039<br>USA | TEL: (703) 250-609 |
| Schweickart, Daniel L. | Wright Laboratory<br>WL/POOX-2/Bldg. 450<br>2645 Fifth Street, Rm. D101<br>Wright Patterson AFB, OH 45433<br>USA | |
| Setchell, Richard H. | Wisconsin Electric Power Co.<br>333 West Everett Street<br>Milwaukee, WI 53203<br>USA | TEL: (414) 221-2407<br>FAX: (414) 221-2318 |
| Shapiro, Seth | R&B Enterprises<br>20 Clipper Road<br>West Conshohocken, PA 19428<br>USA | TEL: (610) 825-1684<br>FAX: (610) 825-1960 |

| Name | Affiliation | Telephone |
|---|---|---|
| Shostak, Volodymyr | University of Toronto, Dept. of Electrical & Computer Eng.<br>10 King's College Road<br>Toronto, Ontario<br>Canada M5S 1A4 | TEL: (416) 978-3116<br>FAX: (416) 971-2325 |
| Sirola, Brien | Shore Acres Enterprises, Inc.<br>POJ1PO RR NO. 3<br>10 Appaloosa Drive, New Liskeard<br>Ontario, Canada<br>Canada | TEL: (705) 647-4548 |
| Sirola, Todd | Shore Acres Enterpriese, Inc.<br>53 Darren Drive<br>Angus Ontario<br>LOMIBO<br>Canada | TEL: (705) 424-2526<br>FAX: (705) 424-7121 |
| Soteropoulos, George | FAA/AIR-120<br>800 Independence Ave, SW<br>Washington, DC 20591<br>USA | TEL: (202) 267-9796<br>FAX: (202) 267-5340 |
| Soule, Michael R. | McDonnell Douglas Aerospace West<br>Mail Stop 12-2<br>5301 Bolsa Ave.<br>Huntington Beach, CA 92647<br>USA | TEL: (714) 896-5408<br>FAX: (714) 896-6995 |
| Spiller, Olaf | Daimler-Benz Aerospace Airbus<br>D-28183 Bremen<br>Germany | TEL: ++49 421 538 4423<br>FAX: ++49 421 538 5031 |
| Squires, Mike | Naval Air Warfare Center Aircraft Division<br>EMT Branch<br>Code 517200A, MS 3<br>Bldg. 2100<br>Patuxent River, MD 20670<br>USA | TEL: (301) 342-4598<br>FAX: (301) 342-3786 |
| Stewart, Bill | Milliken & Co.<br>920 Milliken Road; MS 405<br>Spartanburg, SC 29303<br>USA | TEL: (803) 503-2676<br>FAX: (803) 503-2417 |
| Straehle, Ulf D. | Bundesministerium der Verteifdigung -<br>Rue IV3<br>Postfach 1328<br>53003 Bonn<br>Germany | TEL: 0228 124218<br>FAX: 0228 126784 |

| Name | Affiliation | Telephone |
|---|---|---|
| Sutton, Jeff | The Boeing Co.<br>6534 26th Ave., N.E.<br>Seattle, WA 98115<br>USA | TEL: (206) 662-3138<br>FAX: (206) 655-7965 |
| Tam, Edward | Naval Air Warfare Center Weapons Division<br>521 9th Street<br>Code 521500E<br>Pt. Mugu, CA 93042-5001<br>USA | TEL: (805) 989-7986<br>FAX: (805) 989-7184 |
| ter Haseborg, Jan-Luiken | Arbeitsbereich MeBtechnik TU<br>Harburger Schlosstr. 20<br>21071 Hamburg<br>Germany | TEL: 040/7718 3013<br>FAX: 040/7718 2382 |
| Thomas, G. L. | Kennedy Space Center<br>RT-SRD-1<br>Kennedy Space Center, FL 32899<br>USA | TEL: (407) 867-4493<br>FAX: (407) 867-8038 |
| Thomas, Yvette | Naval Air Systems Command<br>1421 Jefferson Davis Highway<br>Arlington, VA 22243<br>USA | TEL: (703) 604-6060<br>FAX: (703) 604-2051 |
| Timms, Murray S. | Helikopter Service<br>PO Box 522<br>Stavanger Lufthavn N-4055<br>Norway | TEL: 45-51653885<br>FAX: 47-51651860 |
| Turner, Danny | Northrop Grumman B-2 Division<br>8900 East Washington Boulevard<br>Pico Rivera, CA 90660-3737<br>USA | TEL: (310) 942-5297<br>FAX: (310) 948-8146 |
| Ushio, Tomoo | University of Osaka, Electrical Engineering Dept.<br>Yamadaoka 2-1, Suita<br>Osaka 565<br>Japan | TEL: 81-6-879-7691 |
| Vakil, Sadegh M. | Collins General Avionics, Rockwell International<br>400 Collins Road NE, M/S 106-113<br>Cedar Rapids, IA 52498<br>USA | TEL: (319) 395-8902 |

| Name | Affiliation | Telephone |
|---|---|---|
| van der Hooft, F. J. | Stork Installatietechniek Eindhoven B.V.<br>Daalakkersweg 2, 5641 JA<br>Eindhoven<br>Netherlands | TEL: 00 31 40829224 |
| Vaughn, Richard L. | FAA ASW-150<br>2601 Meacham Boulevard<br>Fort Worth, TX 76193<br>USA | |
| Vecchi, Giuseppe | Dip. Elettronica, Politecnico<br>Corso Duca degli Abruzzi, 24<br>I-10129 Torino<br>Italy | TEL: +39 11 564 4000<br>FAX: +39 11 564 4015/4099 |
| Verma, T. S. | Department of Physics<br>University of Roorkee<br>Roorkee-247667<br>India | TEL: (01332)-74108<br>FAX: (091)-1332-73560 |
| Vidakovits, Louis | Raychem<br>300 Constitution Drive<br>Menlo Park, CA 44025<br>USA | TEL: (415) 361-5068<br>FAX: (415) 361-7385 |
| Wada, Atsushi | Central Research Institute of Electric<br>Power Industry<br>11-1, Iwado Kita 2-Chome<br>Komae-shi, Tokyo 201<br>Japan | TEL: (81-3) 3480-2111<br>FAX: (81-3) 3488-6697 |
| Walker, Bill | VEDA<br>300 Exploration<br>Lexington Park, MD 20653<br>USA | TEL: (301) 737-2611<br>FAX: (301) 737-1498 |
| Walko, Lawrence C. | U.S. Air Force<br>WL/POOX-2, Bldg. 450<br>2645 Fifth Street, Suite 13<br>Wright-Patterson AFB, OH 45433-7919<br>USA | TEL: (513) 255-9634<br>FAX: (513) 476-4095 |
| Welch, John S. | ASC/YC-ASIPT (C-17 SPO)<br>2600 Paramount Place<br>Fairborn, OH 45324<br>USA | TEL: (513) 255-4720 x410<br>FAX: (513) 255-3207 |

| Name | Affiliation | Telephone |
|---|---|---|
| Whitaker, Mike | Naval Air Warfare Center Aircraft Division<br>EMT Branch<br>M.S. 3, Bldg. 2100<br>22633 Joyce Road<br>Patuxent River, MD 20670<br>USA | TEL: (301) 342-3873<br>FAX: (301) 342-3876 |
| Wild, Ed | USAF<br>8 Southwind Ct.<br>Niceville, FL 32578<br>USA | TEL: (904) 897-1542<br>FAX: (904) 882-5101 |
| Willett, John C. | PL/GPAA<br>29 Randolph Road<br>Hanscom AFB, MA 01731-3010<br>USA | TEL: (617) 377-5954<br>FAX: (617) 377-2984 |
| Willis, Kenneth E. | Quantic Industries, Inc.<br>990 Commercial Street<br>San Carlos, CA 94070-4084<br>USA | TEL: (415) 637-3074<br>FAX: (415) 637-3093 |
| Wilson, Tony | FAA<br>Bldg. 201 AAA-421<br>Atlantic City Int'l Airport, NJ 08405<br>USA | |
| Wojtasinski, Ronald | Science and Technology Corp.<br>400 W. Central Boulevard<br>Cape Canaveral, FL 32920<br>USA | TEL: (407) 799-0667 |
| Zaepfel, Pete | NASA Langley Research Center<br>MS 490<br>Hampton, VA 23681<br>USA | |
| Zischank, Wolfgang J. | Universitat der Bundeswehr Munchen<br>Fakutat fur Elektrotechnik, ET 7<br>Werner-Heisenberg - Weg 39<br>D-85 579 Neubiberg<br>Germany | TEL: +49 89 6004 3721<br>FAX: +49 89 6004 3723 |
| Zoro, Reynaldo | ELPATSINDO<br>Jalan Hasanudin No. 9<br>40132 Bandung<br>Indonesia | TEL: + 62 22-2507315<br>FAX: + 22-2500918 |

# INDEX OF AUTHORS


| Name | Title | Page No. |
|---|---|---|
| Adachi, M. | Field Experiments on Laser Triggered Lightning | 78-1 |
| Alfas, S. | The Origin of Electric Charge | 71-1 |
| Ammons, T. | A Test Facility for Determining Weapon Systems Vulnerability from the Electrostatic Discharge (ESD) Phenomenon | 47-1 |
| Arnold, L. | Insured Property Damage Due to Lightning in Three Western US States | 55-1 |
| Avenet, J-P. | Lightning-Induced Damage Phenomenology in Carbon Fiber Composite Materials | 39-1 |
| Baldwin, R. | A Review of Progress on the Joint Programme on Improving the Lightning and Static Protection of Radomes | 3-1 |
| Bardo, E. | A Combined TOA/MDF Technology Upgrade of the U.S. National Lightning Detection Network | 72-1 |
| Barnes, A., Jr. | Cost Benefit of an ABFM at KSC | 8-1 |
| | Using Lasers to Trigger/Guide Lightning | 64-1 |
| Berger, G. | Inception Electric Field of a Laboratory Simulated Lightning Upward Leader Emitted from a Franklin Rod | 28-1 |
| Berthold, C. | Thunderstorm Localization Using MUSIC | 65-1 |
| Boldi, R. | Comparison of Lightning Mapping with Operational Time-of-Arrival and Interferometric Systems | 60-1 |
| Borgeest, K. | Lightning Protection of RF-Systems | 53-1 |
| Bostock-Smith, M. | Visualising the Correlation Between Telecommunication Faults and Lightning Activity | 5-1 |
| Boulay, J. | Triggered and Intercepted Lightning Arcs on Aircraft | 22-1 |
| Bourne, N. | Stress Wave Visualisation in Aluminium and CFC Plates Subject to Simulated Lightning Strikes | 36-1 |

| Name | Title | Page No. |
|---|---|---|
| Briët, R. | Lightning Threat Probability for Space Launch Operations | 10-1 |
| | Fundamental Principles of Ground-Based Lightning Protection Systems | 41-1 |
| | Probability Calculation of Direct Lightning Attachments to Structures at SLC40/41 | 59-1 |
| | Fundamental Principles of Ground-Based Lightning Protection Systems | 63-1 |
| Brooks, M. | JRS Magnetic Lightning Current Detector | 13-1 |
| Bush, W. | The Measurement and Use of Lightning Ground Flash Density | 61-1 |
| Byerley, L. III | The Measurement and Use of Lightning Ground Flash Density | 61-1 |
| Calabria, J. | Electrical Bonding Resistance Variations in CFC Panels | 38-1 |
| Canavero, F. | A Fractal Model of the Fine Structure of Lightning Radiation | 16-1 |
| | Can a Transmission Line Model Predict the Lightning Current Pulse? | 70-1 |
| Cantaloube, M. | Improvement of Lightning Attachment Tests | 31-1 |
| | The Electrostatic Hazards Under an Hovering Helicopter | 33-1 |
| Chai, J. | A Retest Criterion for Space Launch Processing Following Lightning Storms | 11-1 |
| | Electromagnetic Responses of LV/SV Under the Catenary Wires Array Lightning Protection System to Near-By Lightning Strikes | 58-1 |
| | Probability Calculation of Direct Lightning Attachments to Structures at SLC40/41 | 59-1 |
| Chambert, G. | EMC Specifications for Modular Avionics | 21-1 |
| Chang, J-S. | Statistics of Lightning Strikes to the CN Tower Observed During 1978-1994 | 50-1 |
| Chen, K. | Explosion Proofing the "Explosion Proof" Vacuum Cleaner | 48-1 |
| Chin, T. | A Retest Criterion for Space Launch Processing Following Lightning Storms | 11-1 |

| Name | Title | Page No. |
|---|---|---|
| Clelland, M. | E-6A Precipitation Static Assessments | 34-1 |
| Clerc, J-P. | A Review of Progress on the Joint Programme on Improving the Lightning and Static Protection of Radomes | 3-1 |
| | Improvement of Lightning Attachment Tests | 31-1 |
| Collier, R. | Finite Difference Calculations of Lightning Effects at the Space Shuttle Launch Pad | 68-1 |
| Cooper, M. | Chronic Pain Syndrome in a Lightning Victim | 43-1 |
| | Psychological Sequelae of Lightning Injury | 44-1 |
| Crouch, K. | Aircraft Fuel System Lightning Protection Design and Qualification Test Standard | 25-1 |
| | Detection of Fuel System Ignition Sources Using Hydrogen Vapor | 30-1 |
| Cummins, K. | The Measurement and Use of Lightning Ground Flash Density | 61-1 |
| | A Combined TOA/MDF Technology Upgrade of the U.S. National Lightning Detection Network | 72-1 |
| Davoise, C. | The Electrostatic Hazards Under an Hovering Helicopter | 33-1 |
| DePasquale, W. | E-6A Precipitation Static Assessments | 34-1 |
| Douay, A. | Lightning-Induced Damage Phenomenology in Carbon Fiber Composite Materials | 39-1 |
| Drumm, F. | Reliable Simulation of Metal Surface Penetration by Lightning Continuing Currents | 40-1 |
| Dubovoy, E. | Lightning Energy Release Remote Measurement by Means of Radar | 15-1 |
| Dulcey, J. | A Test Facility for Determining Weapon Systems Vulnerability from the Electrostatic Discharge (ESD) Phenomenon | 47-1 |
| | Test Requirements and Science of Determining the Electrostatic Discharge (ESD) Vulnerabilities of Weapons Systems | 73-1 |
| Dunkley, V. | Susceptibility of Equipments to Multiple Strike Threats | 19-1 |

| Name | Title | Page No. |
|---|---|---|
| Eley, H. | Probability Calculation of Direct Lightning Attachments to Structures at SLC40/41 | 59-1 |
| Endres, J. | Insured Property Damage Due to Lightning in Three Western US States | 55-1 |
| Engelstatter, G. | Psychological Sequelae of Lightning Injury | 44-1 |
| Evans, D. | Demonstration of the User-Friendly FAA Research Electromagnetic Database | 74-1 |
| Evans, R. | Electromagnetic Environments and Test Methods for the Assessment of Indirect Hazards Due to Lightning Strikes | 2-1 |
| | Methods of Determining the Electrostatic Potential and Charging Current of a Hovering Helicopter | 35-1 |
| | The Selection of Parameter Values of Negative and Positive Lightning for Combination in the Composite Test Waveform | 76-1 |
| Farfal, P. | EMC Specifications for Modular Avionics | 21-1 |
| Fisher, R. | Reliable Simulation of Metal Surface Penetration by Lightning Continuing Currents | 40-1 |
| | Measured Environments Within 20 Meters of the Strike Points of Triggered Lightning | 49-1 |
| Frazier, S. | Data Acquisition for System Level Indirect Effects of Lightning | 12-1 |
| Glynn, M. | Comparison of Electric Current Data from the FAA Research Electromagnetic Database with the Proposed Environment Standard | 4-1 |
| Grace, A. | Visualising the Correlation Between Telecommu-nication Faults and Lightning Activity | 5-1 |
| Gondot, P. | Lightning-Induced Damage Phenomenology in Carbon Fiber Composite Materials | 39-1 |
| Grush, D. | Demonstration of the User-Friendly FAA Research Electromagnetic Database | 74-1 |
| Grzybowski, S. | Evaluation of Lightning Performance of 115 kV Transmission Lines with Spline Ball Ionizers Based on Model Tests | 62-1 |

| Name | Title | Page No. |
|---|---|---|
| Hagberg, D., Jr. | The Measurement and Use of Lightning Ground Flash Density | 61-1 |
| Haines, J. | E-6A Precipitation Static Assessments | 34-1 |
| Hardwick, C. J. | A Review of Progress on the Joint Programme on Improving the Lightning and Static Protection of Radomes | 3-1 |
| | Susceptibility of Equipments to Multiple Strike Threats | 19-1 |
| | Stress Wave Visualisation in Aluminium and CFC Plates Subject to Simulated Lightning Strikes | 36-1 |
| Harwood, T. | USN/USA/USAF Aircraft Lightning Strike Survey | 26-1 |
| He, T. | MD-90 Transport Aircraft Lightning Induced Transient Level Evaluation by Time Domain Three Dimensional Finite Difference Modeling | 69-1 |
| Heidler, F. | Influence of Channel-Base Current and Current Reflections on the Initial and Subsidiary Lightning Electromagnetic Field Peak | 18-1 |
| | Review of 15 Years LEMP Measuring Activities in the South of Germany | 51-1 |
| | Influence of Tall Towers on the Return Stroke Current | 67-1 |
| Hiscox, W. | A Combined TOA/MDF Technology Upgrade of the U.S. National Lightning Detection Network | 72-1 |
| Holle, R. | Recent Trends in the Number of Lightning Deaths and Injuries in the United States | 45-1 |
| | Insured Property Damage Due to Lightning in Three Western US States | 55-1 |
| Holmes, S. | Explosion Proofing the "Explosion Proof" Vacuum Cleaner | 48-1 |
| Hopf, Ch. | Influence of Channel-Base Current and Current Reflections on the Initial and Subsidiary Lightning Electromagnetic Field Peak | 18-1 |
| | Review of 15 Years LEMP Measuring Activities in the South of Germany | 51-1 |
| Hussein, A. | Statistics of Lightning Strikes to the CN Tower Observed During 1978-1994 | 50-1 |
| Ishikubo, Y. | Field Experiments on Laser Triggered Lightning | 78-1 |

| Name | Title | Page No. |
|---|---|---|
| Jackson, W. | Probability Calculation of Direct Lightning Attachments to Structures at SLC40/41 | 59-1 |
| Jafferis, W. | Rocket Triggered Lightning - Kennedy Space Center and Beyond | 57-1 |
| Janischewskyj, W. | Statistics of Lightning Strikes to the CN Tower Observed During 1978-1994 | 50-1 |
| Jones, R. | Explosion Proofing the "Explosion Proof" Vacuum Cleaner | 48-1 |
| Kaloterakis, N. | A Test Facility for Determining Weapon Systems Vulnerability from the Electrostatic Discharge (ESD) Phenomenon | 47-1 |
| | Test Requirements and Science of Determining the Electrostatic Discharge (ESD) Vulnerabilities of Weapons Systems | 73-1 |
| Karabin, C. | Automatic Lightning Warning System for Indian Head Division, Naval Surface Warfare Center: A Case Study | 75-1 |
| Kawasaki, Z-I. | Synchronized Multipoint Measurements of Lightning Electric Field Changes | 52-1 |
| | Field Experiments on Laser Triggered Lightning | 78-1 |
| Kikuchi, H. | A New Model of Cloud-to-Ionosphere Discharge - In Terms of a Ground-Cloud-Ionosphere Capacitor Derived from EHD (Electrohydrodynamics) on the Basis of New Physical Concepts of Critical Velocity and Electric Reconnection | 42-1 |
| Kithil, R., Jr. | A Risk Management Approach to Lightning Safety | 9-1 |
| Konings, P. | Protection of a Computer Center | 56-1 |
| Kozma, M. | Using Lasers to Trigger/Guide Lightning | 64-1 |
| Krider, E. | Submicrosecond Fields Radiated by First Return Strokes in Cloud-to-Ground Lightning | 1-1 |
| Kuras, J. | Electromagnetic Joint Integrity of the V-22 | 37-1 |
| Labate, D. | A Fractal Model of the Fine Structure of Lightning Radiation | 16-1 |
| Lehmann, M. | Techniques for Producing Unipolar MIL-STD-1757A Waveforms Using Unique Resistor Banks | 32-1 |

| Name | Title | Page No. |
|---|---|---|
| Leteinturier, C. | Submicrosecond Fields Radiated by First Return Strokes in Cloud-to-Ground Lightning | 1-1 |
| Li, J-X. | Statistics of Lightning Strikes to the CN Tower Observed During 1978-1994 | 50-1 |
| Lie, T. | Lightning Threat Probability for Space Launch Operations | 10-1 |
| Lippert, J. | Scaling Algorithm for C-17A Simulated Lightning Test | 14-1 |
| López, R. | Recent Trends in the Number of Lightning Deaths and Injuries in the United States | 45-1 |
| | Insured Property Damage Due to Lightning in Three Western US States | 55-1 |
| Lubosch, B. | E-6A Precipitation Static Assessments | 34-1 |
| Lumsden, P. | Data Acquisition for System Level Indirect Effects of Lightning | 12-1 |
| Maier, L. | Three-Dimensional Lightning Structure in a Summer Florida Thunderstorm | 17-1 |
| | Comparison of Lightning Mapping with Operational Time-of-Arrival and Interferometric Systems | 60-1 |
| | Thunderstorm Localization Using MUSIC | 65-1 |
| Matuura, K. | Synchronized Multipoint Measurements of Lightning Electric Field Changes | 52-1 |
| | Field Experiments on Laser Triggered Lightning | 78-1 |
| Mazur, V. | Comparison of Lightning Mapping with Operational Time-of-Arrival and Interferometric Systems | 60-1 |
| McClam-Brown, N. | Electromagnetic Joint Integrity of the V-22 | 37-1 |
| McClure, B. | Data Acquisition for System Level Indirect Effects of Lightning | 12-1 |
| McDowall, R. | Comparison of Electric Current Data from the FAA Research Electromagnetic Database with the Proposed Environment Standard | 4-1 |
| Mebar, Y. | Stress Wave Visualisation in Aluminium and CFC Plates Subject to Simulated Lightning Strikes | 36-1 |

| Name | Title | Page No. |
|---|---|---|
| Morris, M. | Reliable Simulation of Metal Surface Penetration by Lightning Continuing Currents | 40-1 |
| | Measured Environments Within 20 Meters of the Strike Points of Triggered Lightning | 49-1 |
| Nawawi, Z. | Lightning Protection System for Telecommunication Relay Station Design and Maintenance, A Field Experience in Tropical Country | 7-1 |
| Nial, J. | A Test Facility for Determining Weapon Systems Vulnerability from the Electrostatic Discharge (ESD) Phenomenon | 47-1 |
| Nozari, B. | MD-90 Transport Aircraft Lightning Induced Transient Level Evaluation by Time Domain Three Dimensional Finite Difference Modeling | 69-1 |
| Odam, G. | Electromagnetic Environments and Test Methods for the Assessment of Indirect Hazards Due to Lightning Strikes | 2-1 |
| | The Rationale of Proposed NATO STANAGS Describing the Lightning Environment for Land, Sea and Air Use and Defining Lightning Assessment Procedures for Munitions and Associated Systems | 23-1 |
| | Methods of Determining the Electrostatic Potential and Charging Current of a Hovering Helicopter | 35-1 |
| | The Selection of Parameter Values of Negative and Positive Lightning for Combination in the Composite Test Waveform | 76-1 |
| Olszewski, K. | Thunderstorm Localization Using MUSIC | 65-1 |
| Parimuha, E. | Data Acquisition for System Level Indirect Effects of Lightning | 12-1 |
| Passi, R. | Recent Trends in the Number of Lightning Deaths and Injuries in the United States | 45-1 |
| Perala, R. | The Physics of Zoning | 24-1 |
| Pifer, A. | A Combined TOA/MDF Technology Upgrade of the U.S. National Lightning Detection Network | 72-1 |
| Plumer, J. | A Review of Progress on the Joint Programme on Improving the Lightning and Static Protection of Radomes | 3-1 |
| Press, J. | Techniques for Producing Unipolar MIL-STD-1757A Waveforms Using Unique Resistor Banks | 32-1 |

| Name | Title | Page No. |
|---|---|---|
| Primeau, M. | Psychological Sequelae of Lightning Injury | 44-1 |
| Proctor, D. | Comparison of Lightning Mapping with Operational Time-of-Arrival and Interferometric Systems | 60-1 |
| Pyle, R. | A Combined TOA/MDF Technology Upgrade of the U.S. National Lightning Detection Network | 72-1 |
| Pühringer, A. | The Formation of Superbolts in Thunderclouds | 66-1 |
| Richardson, M. | The Rationale of Proposed NATO STANAGS Describing the Lightning Environment for Land, Sea and Air Use and Defining Lightning Assessment Procedures for Munitions and Associated Systems | 23-1 |
| Rigden, G. | The Physics of Zoning | 24-1 |
| Robinson, J. | Thunderstorm Localization Using MUSIC | 65-1 |
| Rudolph, T. | The Physics of Zoning | 24-1 |
| | MD-90 Transport Aircraft Lightning Induced Transient Level Evaluation by Time Domain Three Dimensional Finite Difference Modeling | 69-1 |
| Rusan, I. | Statistics of Lightning Strikes to the CN Tower Observed During 1978-1994 | 50-1 |
| Rynne, T. | Thunderstorm Localization Using MUSIC | 65-1 |
| Schaffar, A. | Lightning Coupling to EED Lines | 46-1 |
| Schneider, J. | Scaling Algorithm for C-17A Simulated Lightning Test | 14-1 |
| Schnetzer, G. | Reliable Simulation of Metal Surface Penetration by Lightning Continuing Currents | 40-1 |
| | Measured Environments Within 20 Meters of the Strike Points of Triggered Lightning | 49-1 |
| Sherman, B. | MD-90 Transport Aircraft Lightning Induced Transient Level Evaluation by Time Domain Three Dimensional Finite Difference Modeling | 69-1 |
| Shimada, Y. | Field Experiments on Laser Triggered Lightning | 78-1 |
| Shindo, T. | Lightning Measurement System Using Remote Control by Telephone Line and Electric Field Observations of Lightning in Winter | 6-1 |

| Name | Title | Page No. |
|---|---|---|
| Shockey, D. | Lightning-Induced Damage Phenomenology in Carbon Fiber Composite Materials | 39-1 |
| Spencer, R. | Susceptibility of Equipments to Multiple Strike Threats | 19-1 |
| Spiller, O. | Lightning Protection for and Qualification Testing of Modular Avionics | 20-1 |
| ter Haseborg, J. | Lightning Protection of RF-Systems | 53-1 |
| Thomas, G. | Finite Difference Calculations of Lightning Effects at the Space Shuttle Launch Pad | 68-1 |
| Tuel, J. | The Measurement and Use of Lightning Ground Flash Density | 61-1 |
| Uchida, S. | Field Experiments on Laser Triggered Lightning | 78-1 |
| Ushio, T. | Synchronized Multipoint Measurements of Lightning Electric Field Changes | 52-1 |
| | Field Experiments on Laser Triggered Lightning | 78-1 |
| Vakil, S. | Lightning Implications of Decreasing Circuit Card Trace Size and Spacing | 77-1 |
| van der Hooft, F. | Protection of a Computer Center | 56-1 |
| Vecchi, G. | A Fractal Model of the Fine Structure of Lightning Radiation | 16-1 |
| | Can a Transmission Line Model Predict the Lightning Current Pulse? | 70-1 |
| Verma, T. | Charge Deposition on Ice Crystals and Drops After Lightning | 29-1 |
| Wada, A. | Lightning Measurement System Using Remote Control by Telephone Line and Electric Field Observations of Lightning in Winter | 6-1 |
| Walker, W. | Electrical Bonding Resistance Variations in CFC Panels | 38-1 |
| Wang, D. | Synchronized Multipoint Measurements of Lightning Electric Field Changes | 52-1 |
| | Field Experiments on Laser Triggered Lightning | 78-1 |
| Webb, E. | Demonstration of the User-Friendly FAA Research Electromagnetic Database | 74-1 |

| Name | Title | Page No. |
|---|---|---|
| Whitaker, M. | Data Acquisition for System Level Indirect Effects of Lightning | 12-1 |
| | E-6A Precipitation Static Assessments | 34-1 |
| Willett, J. | Submicrosecond Fields Radiated by First Return Strokes in Cloud-to-Ground Lightning | 1-1 |
| | Cost Benefit of an ABFM at KSC | 8-1 |
| Williams, E. | Comparison of Lightning Mapping with Operational Time-of-Arrival and Interferometric Systems | 60-1 |
| Willis, K. | The Use of Magnetically Coupled Power Sources to Protect Ordnance and Electronics from Lightning and Static Electricity | 27-1 |
| Wojtasinski, R. | Lightning Safety Evaluation of Launch Complexes for Personnel Safety | 54-1 |
| Wolf, F. | Lightning Protection of RF-Systems | 53-1 |
| Yamanaka, C. | Field Experiments on Laser Triggered Lightning | 78-1 |
| Yamanaka, T. | Field Experiments on Laser Triggered Lightning | 78-1 |
| Yasuda, H. | Field Experiments on Laser Triggered Lightning | 78-1 |
| Zischank, W. | Reliable Simulation of Metal Surface Penetration by Lightning Continuing Currents | 40-1 |
| Zoro, R. | Lightning Protection System for Telecommunication Relay Station Design and Maintenance, A Field Experience in Tropical Country | 7-1 |
| Zundl, T. | Influence of Tall Towers on the Return Stroke Current | 67-1 |

# REPORT DOCUMENTATION PAGE

*Form Approved*
*OMB No. 0704-0188*

Public reporting burden for this collection of information is estimated to average 1 hour per response, including the time for reviewing instructions, searching existing data sources, gathering and maintaining the data needed, and completing and reviewing the collection of information. Send comments regarding this burden estimate or any other aspect of this collection of information, including suggestions for reducing this burden, to Washington Headquarters Services, Directorate for Information Operations and Reports, 1215 Jefferson Davis Highway, Suite 1204, Arlington, VA 22202-4302, and to the Office of Management and Budget, Paperwork Reduction Project (0704-0188), Washington, DC 20503.

| 1. AGENCY USE ONLY *(Leave blank)* | 2. REPORT DATE | 3. REPORT TYPE AND DATES COVERED |
|---|---|---|
| | 26-28 SEP 1995 | CONFERENCE PUBLICATION |

**4. TITLE AND SUBTITLE**
1995 INTERNATIONAL AEROSPACE AND GROUND CONFERENCE ON LIGHTNING AND STATIC ELECTRICITY

**5. FUNDING NUMBERS**

**6. AUTHOR(S)**

**7. PERFORMING ORGANIZATION NAME(S) AND ADDRESS(ES)**
U.S. NAVY
NAVAL AIR WARFARE CENTER AIRCRAFT DIVISION
PATUXENT RIVER, MARYLAND 20670-5304

**8. PERFORMING ORGANIZATION REPORT NUMBER**
NAWCADPAX--95-306-PRO

**9. SPONSORING/MONITORING AGENCY NAME(S) AND ADDRESS(ES)**
U.S. NAVY
NAVAL AIR SYSTEMS COMMAND (AIR 4.1.7)
1421 JEFFERSON DAVIS HIGHWAY
ARLINGTON, VIRGINIA 22243

**10. SPONSORING/MONITORING AGENCY REPORT NUMBER**

**11. SUPPLEMENTARY NOTES**

**12a. DISTRIBUTION/AVAILABILITY STATEMENT**
APPROVED FOR PUBLIC RELEASE; DISTRIBUTION IS UNLIMITED.

**12b. DISTRIBUTION CODE**

**13. ABSTRACT** *(Maximum 200 words)*
This publication reports the proceedings of the 1995 International Aerospace and Ground Conference on lightning and static electricity, which was held at the Williamsburg Cascades Conference Center, Williamsburg, Virginia, on 26-28 September 1995. The conference was sponsored by the Naval Air Systems Command (AIR 4.1.7) and the National Interagency Coordination Group (NICG), which consists of research experts from NASA, DOD, NOAA in concert with the Florida Institute of Technology.

**14. SUBJECT TERMS**
LIGHTNING
ELECTROSTATICS
NICG

**15. NUMBER OF PAGES**
828

**16. PRICE CODE**

| 17. SECURITY CLASSIFICATION OF REPORT | 18. SECURITY CLASSIFICATION OF THIS PAGE | 19. SECURITY CLASSIFICATION OF ABSTRACT | 20. LIMITATION OF ABSTRACT |
|---|---|---|---|
| UNCLASSIFIED | UNCLASSIFIED | UNCLASSIFIED | SAR |